Observational Asteroseismology

Habilitationsschrift
eingereicht von
Mag. Dr. Gerald Handler

an der Fakultät für
Geowissenschaften, Geographie und Astronomie
der Universität Wien

Wien, im November 2007

Institut für Astronomie
Türkenschanzstrasse 17
A-1180 Wien, Österreich

Contents

Chapter 1

Introduction

Nearly all the physical processes that determine the structure and evolution of stars occur in their (deep) interiors. The production of nuclear energy that powers stars takes place in their cores for most of their lifetime. The effects of the physical processes that modify the simplest models of stellar evolution, such as mixing and diffusion, also predominantly take place in the inside of stars.

The light that we receive from the stars is the only information that astronomers can use to study the universe. However, the light of the stars originates from their surfaces. Therefore it would seem that there is no way that the analysis of starlight tells us about the physics going on in stellar interiors.

1.1 Variable stars

However, there are stars that reveal more about their physics than others. For instance, variable stars are objects for which we can measure a time-dependent light output, on a time scale shorter than that of evolutionary changes. There are two major groups of variable stars, extrinsic and intrinsic variables.

Extrinsic variables do not change their light output directly. For example, the light changes of eclipsing binary stars are caused by two stars passing in front of each other, so that light coming from one of them is periodically blocked. The component stars of eclipsing binaries do not need to be variable themselves. By analysing the temporal light variations and orbital motion of eclipsing binaries, one can determine their fundamental properties, and by assuming that their components are otherwise normal stars, determine fundamental properties of all stars, such as their mass. In this way, stars and stellar systems can be understood better.

Intrinsic variables, on the other hand, change their light output physically. Supernovae can become brighter than their host galaxies because of the ejection of large amounts of material. Even more revealing are stars that can change their physical size: pulsating variables.

1.2 Pulsating stars

How can a star change its size? Under some special physical conditions, stars can store energy in some particular interior layers for some time. This would for instance be a zone where a certain chemical species becomes (partly) ionised. Many stars have such ionisation regions in their interiors as a natural consequence of the gradual increase of temperature and pressure from the stellar surface to the core.

If a (partial) ionisation region is located in a region where the thermal time scale is of the same order of magnitude as the dynamic time scale, stellar pulsations can develop (Cox 1980). The energy that is stored during a contraction of the star, is released when it tries to reach its equilibrium state by expanding. Therefore, the star actually expands beyond its equilibrium radius. When the material recedes, energy is again stored in the stellar interior, and the whole cycle repeats: a periodic stellar pulsation evolves. This is a rough description so-called kappa mechanism (Baker & Kippenhahn 1962 and references therein) that drives many different groups of pulsators.

There are other mechanisms that can cause a star to pulsate, for instance stochastic excitation by turbulence in surface convection zones of solar-like stars, or excitation by dust formation in red (super)giant stars. As the existence of stellar pulsations is always linked to some excitation mechanism that requires certain physical conditions, several types of pulsating stars exist in certain regions of the HR Diagram. An overview of many types of pulsating variables is shown in Fig. 1.1.

The previous argument can also be reversed: if the instability region of some class of pulsating variables is accurately known, its excitation mechanism must be able to account for it. This is already a first constraint on the interior structure of a pulsating variable. However, some types of pulsators are suitable for much more detailed studies: multiperiodic radial and nonradial pulsators. The research field that deals with such studies is called asteroseismology.

1.3 Asteroseismology

We start with a definition: asteroseismology is the study of the interior of (nonradially) pulsating stars by means of their normal mode spectrum. This technique is analogous to the determination of the Earth's inner structure using earthquakes: we use stellar pulsations as "starquakes" or, more scientifically, we use stellar pulsation modes as seismic waves.

What is a pulsation mode? It is nothing more than an individual stellar oscillation. The latter come in many different flavours, and we do not intend to give a complete overview of pulsation modes. Instead, we refer the reader to the excellent monograph by Unno et al. (1989) for more detailed information. For the present purpose, it is most important to know that there are two main groups of pulsation modes, the pressure (p) and the gravity (g) modes. These modes are classified after

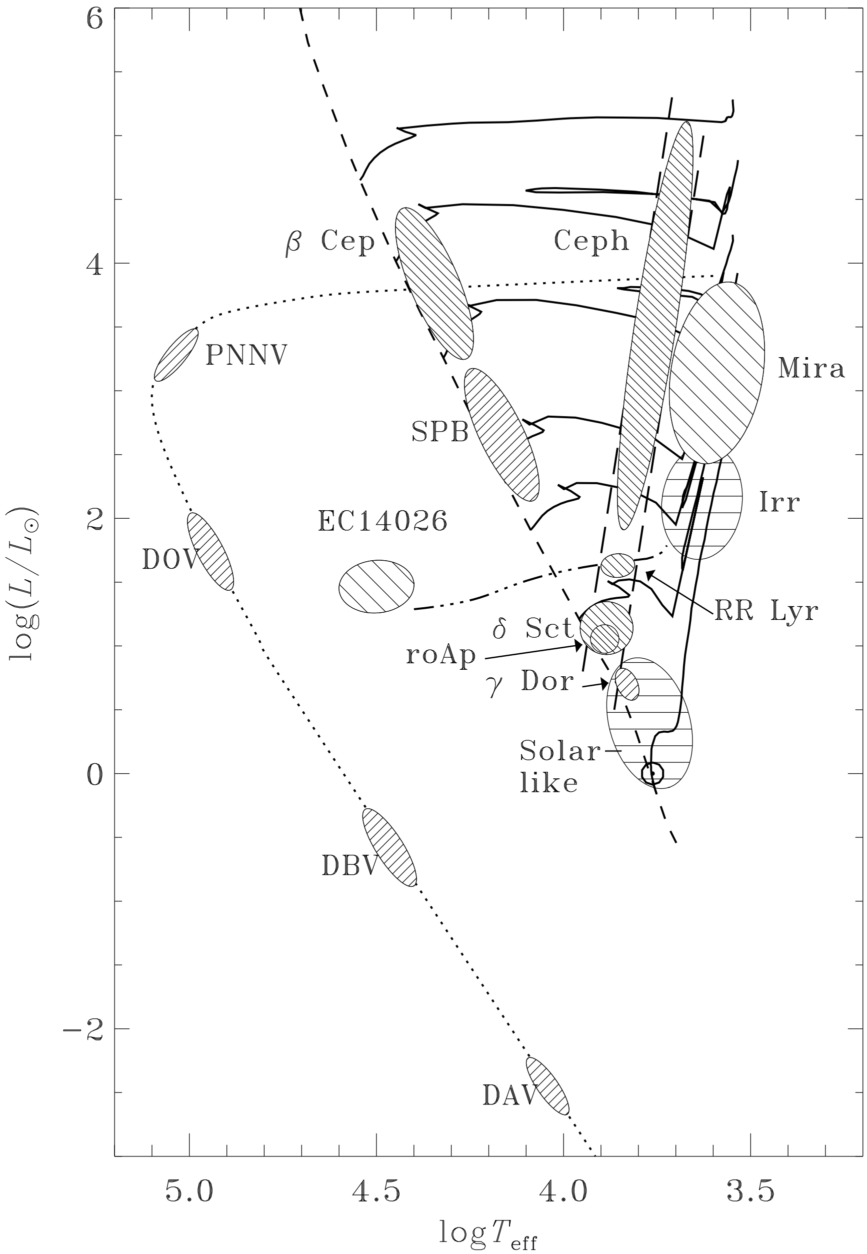

Figure 1.1: Theoretical HR diagram with many classes of pulsating stars indicated. The dashed line is the theoretical main sequence, the dotted line the white dwarf cooling track and some evolutionary tracks are also indicated. Used with permission from J. Christensen-Dalsgaard.

the force that restores the stellar equilibrium shape following the motion caused by pulsation, either pressure or buoyancy.

Pulsation modes are additionally defined by the shape of the distortions they create on the stellar surface and interior. In general, the pulsations separate the stellar surface into expanding and receding as well as heating or cooling areas. The shape of these distortions can be quantified with (combinations of) spherical harmonics; an example of these is shown in Fig. 1.2.

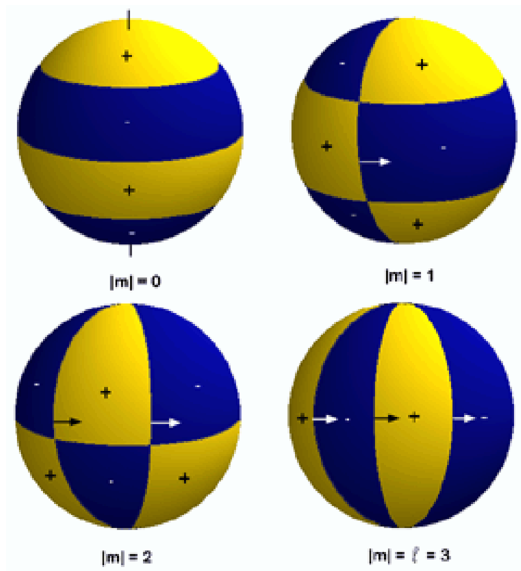

Figure 1.2: Schematic description of the surface distortions produced by pulsation modes with a spherical degree $\ell = 3$. Whilst the brighter areas of the star are moving outward, the darker parts move inward, and vice versa. Graphics courtesy by W. Zima.

Between the expanding and receding surface areas, no motion takes place. The lines along which this is the case are called the node lines. The number and direction of these node lines are used for the classification of the pulsation modes. The total number of node lines on the stellar surface is the spherical degree ℓ, which must in all cases be larger than or equal to zero. The number of node lines that are intersected when travelling around the stellar equator is the azimuthal order m. Pulsation modes with $m \neq 0$ are travelling waves, and as they can run either with or against the rotation of the star, m can lie in the interval $-\ell, \ell$. Finally, the number of node lines in the stellar interior is called the radial overtone k (or sometimes n).

In this framework, radial pulsations can just be seen as modes with $\ell = 0$; all other modes are called nonradial oscillations. A mode with $k = 0$ is called the fundamental mode, a mode with $k = 1$ is named the first overtone, etc. Pulsation modes with periods longer than that of the radial fundamental mode are usually g modes, whereas p modes have periods equal or shorter than that; radial pulsations are always p modes.

Now, asteroseismology takes advantage of the fact that some stars can oscillate in many of these radial and/or nonradial modes simultaneously. This is the key for asteroseismology, as each pulsation mode carries information about the region in which it propagates, its pulsation cavity. Every single pulsation mode has a different cavity, and its oscillation frequency is determined by the physical conditions in its cavity.

Therefore, interior structure models of the stars can be refined by measuring the oscillation frequencies of pulsating stars and by reproducing them with stellar models. The prerequisite for successful seismic modelling, however, is that the observer provides the largest possible number of intrinsic pulsation frequencies with a correct identification of all the underlying modes to the theorist. Should the observer fail to do so, for instance by over-interpreting the observational results or by providing incorrect mode identifications, any seismic model computations will lead to incorrect results.

Asteroseismology can go even beyond an improved understanding of stellar structure. For instance, some of the most massive pulsating stars will become Type II Supernovae in the future. Supernova explosions are mostly responsible for the enrichment of the interstellar medium. If we know the interior structure of an immediate supernova progenitor, we will be able to constrain the chemical evolution of galaxies. Asteroseismology of pulsating white dwarf stars teaches us about nuclear reaction rates, neutrino physics and the history of the object's evolution on the Asymptotic Giant Branch. It is therefore clear that asteroseismology has a large impact on astrophysics in general.

1.3.1 Success stories and challenges

The greatest successes of asteroseismology were obtained for the star closest to us, the Sun. The interior structure of the Sun was modelled to fine detail (e.g., see Christensen-Dalsgaard 2002 for an extensive review) because millions of pulsation modes can be used for seismic analyses. Since the solar surface can be resolved in two dimensions, even local asteroseismology (e.g., dealing with subsurface and meridional flows) can be carried out. However, the recent revisions in the solar elemental abundances (Asplund et al. 2004) suggest that our present solar model needs some modifications.

Comparing the Sun and the distant stars, two major problems for asteroseismology are immediately obvious: asteroseismologists have to work with integrated light as stellar surfaces cannot be (sufficiently) resolved and much less light is available. This means that only a restricted range of modes, depending on their ℓ values, is available for analysis, and that the accuracy of asteroseismic observations will be poorer than helioseismic data.

Nevertheless, asteroseismology of some pulsating white dwarf stars (e.g., see Winget et al. 1991, 1994) was quite successful, resulting in exact determinations of masses, rotation periods, luminosities, and chemical element layer masses, as well as in estimates of magnetic field strengths.

Why was this possible? The frequencies of the pulsation modes of these stars were arranged in clear patterns. Pulsating white dwarfs oscillate in g modes of high radial order. Asymptotic theory then predicts that consecutive overtones are equally spaced in period (Tassoul 1980). Consequently, the pulsation modes of these stars could be identified by just examining their frequency spectra.

Regrettably, this mode identification method does not work for all pulsating stars. Even in cases where a sufficient number of pulsation modes was observed, so that patterns within their frequencies were to become visible, they escaped detection (e.g., see Handler et al. 2000). A second problem that is common in the analysis of asteroseismic data is that only a small percentage of the theoretically predicted number of pulsation modes is observed in reality, and that it is not clear which particular set of modes the star chooses to excite to measurable amplitude.

As a result, additional observational methods that allow an identification of the stellar pulsation modes are required. The interplay of the different surface distortions and the changes in gravity and temperature caused by a given mode combined with limb darkening effects give us this possibility. Therefore, amplitude ratios or phase shifts between different photometric passbands, also in combination with radial velocity data, can reveal the pulsation mode (Dziembowski 1977). The line profiles of an oscillating star will also reflect the pulsations (Ledoux 1951) and can thus be used to identify the mode. The shape of the mode can be reconstructed by Doppler Imaging (Hatzes 1998). We conclude that one can derive, or at least constrain, the ℓ and m values for at least the strongest pulsation modes of a given star.

However, some words of caution are necessary here: unless the identifications from any individual technique are unambiguous, extreme care must be taken when applying such methods. If possible, cross-checks between different techniques must be made, but it must also be checked whether they are indeed (mostly) independent. We refer to the discussion by Balona (2000) who showed that the agreement of the mode identifications derived from one photometric and one spectroscopic technique were not due to their reliability, but resulted from the two methods being basically sensitive to the same quantities.

In planning an observational project one should therefore take care that mode identification methods can be applied. However, their limitations must be kept in mind and must be critically examined.

Another observational challenge for asteroseismology is that pulsational signals of extremely low amplitude (less than 1 millimagnitude or a few centimetres/second) need to be detected reliably, requiring the acquisition of large amounts of high-quality measurements. Finally, the observer should be careful to measure stars not only have identifiable pulsation modes, but also can be treated by theory within its current limitations. Close interaction between observers and theorists is therefore required. In fact, the subfields of asteroseismology where the first successes were obtained, benefited from just this interaction.

1.3.2 Multisite observing campaigns

To detect the required number of pulsation frequencies of a star with the necessary reliability, measurements from a single site are usually not sufficient. The regular daytime breaks caused by the Earth's rotation leave too many gaps in the data. As a consequence, ambiguities in the identification of the intrinsic frequencies arise. These become worse the closer one comes to the observational noise level, because the relative effect of the interference of intrinsic variations with noise becomes stronger.

Therefore, an asteroseismic data set should have gaps as few and as small as possible. There are two basic strategies to reach this goal, observations from space satellites, or multisite campaigns. The latter involve collaboration of colleagues interested in the matter over the whole globe. Each group applies for observing time at their home observatory for the same time slot, observers are sent to sites where no local collaborators are available, and then the whole network measures the same target. In this way, daytime gaps can often be minimised, and nighttime gaps only occur at geographical longitudes covered by few sites and suffering from unfortunate weather conditions.

This type of observing has been done more than 50 years ago for the first time, when communication between the different collaborators was much less efficient than nowadays (de Jager 1963). However, worldwide campaigns were carried out regularly within the last 20 years with collaborations such as the Delta Scuti Network, founded by Michel Breger in 1983 (e.g., see Breger et al. 1987) or the Whole Earth Telescope (Nather et al. 1990). The latter network is particularly well known not only for its scientific success but also for its real-time communication between a headquarters staffed 24 hours per day and the individual observers at the remote sites.

We would like to stress that these campaigns are not organised to minimise the work of each individual involved in such a collaboration; they are required to reach the scientific goal of the team. Therefore, the amount and complexity of the data sets obtained during a multisite observing campaign is considerably larger than for single-site observations: all observers carry out a full single-site study, and the principal investigator has to reduce, combine and analyse the whole set, often needing the help of co-investigators. Therefore, the naive assumption that the amount of work put into such an effort (as far as the ones where the present author is/was involved) by each individual co-author of the resulting paper is equal to $1/n$, where n is the number of paper authors, or the more sophisticated view that it is $\sim 1/k!$, where k is the position in the author's list, is plainly wrong: each author contributes much more than that.

1.3.3 Conclusions and outlook

We believe that the future of asteroseismology is a bright one. Some classes of pulsating stars recently became available for seismic modelling. Mode identification methods are maturing and will become more and more reliable. Several interesting individual objects were discovered recently ("hybrid" pulsators showing both low-order p and g modes as well as high-order g modes). Because of the construction of giant mirrors, telescopes of the 2 – 4 metre class are becoming more easily available for stellar astronomy, which will be particularly helpful for the application of spectroscopic mode identification methods. Present asteroseismic satellite missions (in particular MOST, Walker et al. 2003) are already delivering data of unprecedented quality, and it is hoped that other space projects such as the recently launched COROT satellite (Baglin 2003) will open further dimensions in precision asteroseismology.

1.4 Structure of the following chapters

The following parts of this work are based on 43 refereed papers in major astronomical journals. They are ordered in sections after the groups of pulsators that were studied, starting with three groups of variables just a little more massive than the Sun, moving up the main sequence to B stars and then making an excursion to the stellar graveyard along the white dwarf cooling track. The sections themselves are split into subject groups, following an order that should help the reader understand the development within each subject group. It is therefore hoped that less experienced colleagues can use this work as an introductory reference.

Chapter 2

Delta Scuti stars

2.1 Introduction

These A/F-type pulsators (with periods between 30 minutes and 6 hours) located around the intersection of the classical instability strip with the main sequence were among the first groups of stars to be seismically explored. It is not yet possible to determine details of their interior structure, but some progress has been made.

Section 2.2 presents a case study for a δ Scuti star. CD$-$24 7599 = XX Pyx was serendipitously discovered to pulsate during a Whole Earth Telescope (WET) run (Sect. 2.2.1) and turned out to be an unevolved multiperiodic variable. Consequently, it was observed during another WET campaign (Sect. 2.2.2) that revealed the presence of 13 independent pulsation modes, a record at the time. Repetitive structure within the mode frequencies was discovered and was used to derive the mean stellar density and the distance to XX Pyx - the first such determinations for a nonradially pulsating δ Scuti star. Section 2.2.3 is devoted to the study of the temporal variations of the pulsation frequencies and amplitudes of XX Pyx. Section 2.2.4 reports on a massive theoretical survey to find a seismic model for the star. This survey essentially confirming the findings of Sect. 2.2.2, but it was not possible to find the desired seismic model. A subsequent extended multisite campaign (Sect. 2.2.5) again increased the number of known pulsation frequencies to a new record by then, and showed that the amplitude variability of XX Pyx occurs on time scales down to three weeks, still the shortest such time scale known for a δ Scuti star. Section 2.2.6 reports additional light variability of the star on a longer time scale than the pulsation, already suspected and discussed by Handler (1994), who was however unable to prove the presence of slow variability because the observing technique used in the earlier studies of the star was unsuitable for these purposes. Finally, Sect. 2.2.7 proves that XX Pyx is located in a close binary system, which complicates its seismic modelling considerably. Therefore, progress must be made on the theoretical side to account fully for the physical environment of this star, before new observations would be justifiable.

Section 2.3 is devoted to another thoroughly studied δ Scuti pulsator, FG Virginis. As for XX Pyx, its initial study revealed a large number of pulsation frequencies (Sect. 2.3.1) from an extended multisite campaign. The capabilities of the WET network are used to search for the presence of roAp-like oscillations in FG Vir (Sect. 2.3.2). This is interesting because both types of oscillation have never been seen to co-exist in the same star, and it gives some constraints on the physical conditions under which rapid oscillations in A stars become excited, and what the driving mechanism would be. Further multisite campaigns on FG Vir not included here (Breger et al. 1998, 2004) increased the number of known pulsation frequencies further, culminating in the detection of more than 60 mode frequencies for the star (Sect. 2.3.3), which is still exemplary in the field.

Section 2.4 deals with some additional δ Scuti stars that are interesting candidates for seismic studies. The star 4 CVn is an evolved pulsator and should, according to theory, have many more modes excited than main sequence stars such as FG Vir and especially XX Pyx. However, it does not (Sect. 2.4.1), given a similar detection level as for the other stars. This raises the important question of the existence of a pulsational mode selection mechanism in δ Scuti stars and if so, what it would be. Section 2.4.2 reports on an extended study of the star BI CMi that also has 20 pulsation modes detected, putting it into an exclusive club of only four δ Scuti stars with more than 15 mode frequencies known; all four of them are discussed in the present work. AV Ceti (Sect. 2.4.3) is interesting for another reason: it rotates at least twice as fast as all the other δ Scuti stars discussed in detail here. This should complicate the identification of the pulsation modes, and likely does.

Finally, Sect. 2.5 takes a look at the question of how the chemical surface abundances of δ Scuti stars affect their pulsational behaviour. It is well known that metallic-line and magnetic A stars do not show pulsation of the δ Scuti type, with a few exceptions - two of them reported in Sect. 2.5.1. The spectroscopically peculiar stars of λ Bootis type are briefly introduced in Sect. 2.5.2; they are discussed in detail by Paunzen (2003). Many of these objects are located in the δ Scuti instability strip and do pulsate, perhaps differently than their chemically "normal" counterparts, which may suggest that chemical peculiarity would be more than just a stellar "skin disease".

2.2 CD−24 7599 = XX Pyxidis

2.2.1 Nonradial pulsation of the unevolved hot δ Scuti star CD−24 7599 discovered with the Whole Earth Telescope

Original paper:

G. Handler, M. Breger, D. J. Sullivan, A. J. van der Peet, J. C. Clemens, D. O'Donoghue, A.-L. Chen, A. Kanaan, C. Sterken C. F. Claver, K. Krisciunas, S. J. Kleinman, D. T. Wickramasinghe, B. J. Wills, J. L. Provençal, R. E. Nather, D. E. Winget, T. K. Watson, M. A. Barstow, D. A. H. Buckley, 1996, A&A 307, 529

Astron. Astrophys. 307, 529–538 (1996)

ASTRONOMY AND ASTROPHYSICS

Nonradial pulsation of the unevolved hot δ Scuti star CD-24°7599 discovered with the Whole Earth Telescope

G. Handler[1,2], M. Breger[1], D.J. Sullivan[3], A.J. van der Peet[3], J.C. Clemens[4,5,6], D. O'Donoghue[7], A.-L. Chen[7], A. Kanaan[4,8], C. Sterken[9]*, C.F. Claver[4,10], K. Krisciunas[11], S.J. Kleinman[4,12], D.T. Wickramasinghe[13], B.J. Wills[4], J.L. Provençal[4,14], R.E. Nather[4], D.E. Winget[4], T.K. Watson[4], M.A. Barstow[15], and D.A.H. Buckley[7,16]**

1 Institut für Astronomie, Universität Wien, Türkenschanzstraße 17, A-1180 Wien, Austria
2 INTERNET:HANDLER@ASTRO.AST.UNIVIE.AC.AT
3 Department of Physics, Victoria University of Wellington, P. O. Box 600, Wellington, New Zealand
4 Department of Astronomy and McDonald Observatory, University of Texas, Austin, TX 78712, USA
5 Guest Astronomer, Cerro Tololo Inter-American Observatory
6 Current Address: Department of Physics and Astronomy, Iowa State University, Ames, IA 50211, USA
7 Department of Astronomy, University of Cape Town, Rondebosch 7700, South Africa
8 Instituto de Fisica, Universidade Federal do Rio Grande do Sul, 90049 Porto Alegre-RS, Brazil
9 Faculty of Sciences, Vrije Universiteit Brussel, Pleinlaan 2, B-1050 Brussels, Belgium
10 Guest Astronomer, Mauna Kea Observatory
11 Joint Astronomy Center, 660 N. A'ohōkū Place, University Park, Hilo, Hawaii 96720, USA
12 Guest Astronomer, Siding Spring Observatory
13 Department of Mathematics, Australian National University, Canberra, Australia
14 Current Address: Department of Physics and Astronomy, University of Delaware, Newark, DE 19716, USA
15 Physics and Astronomy Department, University of Leicester, Leicester, LE1 7RH, UK
16 South African Astronomical Observatory, P.O. Box 9, Observatory 7935, South Africa

Received 3 February 1995 / Accepted 15 July 1995

Abstract. We report a frequency analysis of the δ Scuti star CD-24°7599 and the discovery that it pulsates nonradially with at least 7 frequencies between 27.01 and 38.11 cycles per day (312 to 441 μHz). These results are based on 116.7 hours of photometric data obtained with the Whole Earth Telescope network. New $uvby\beta$ photometry implies that the star is unevolved and located near the observed hot border of the classical instability strip. We give arguments for interpreting the pulsation periods in terms of low-order low-degree nonradial p-modes. Rotational m-mode splitting is likely. Few radial modes could also be present. The rich modal content and unevolved state of CD-24°7599 emphasize its importance for δ Scuti star asteroseismology.

We detect linear combination frequencies of the pulsation modes with the highest photometric amplitudes and suggest they are not normal modes excited by resonance.

Key words: stars: variables: δ Sct – stars: oscillations – stars: individual: CD-24°7599 – techniques: photometric

Send offprint requests to: G. Handler

* Belgian Fund for Scientific Research (NFWO)
** Science and Engineering Council Advanced Fellow

1. Introduction

The seismological investigation of stellar objects by measuring their pulsation frequencies and amplitudes is an extremely powerful tool for obtaining information about the interior structure of stars. Successful studies have already been undertaken for a number of objects and considerable theoretical and observational effort is expended on the process of asteroseismology applied to various classes of pulsating stars.

The most commonly used observing technique in variable star work is time-series photometric monitoring of the target objects. Subsequent extraction as well as analysis of the pulsation frequencies and amplitudes (temporal spectroscopy) allows the detection of low-degree ($l \leq 3$) modes. However, studies from only a single site are confronted with the problem of spectral leakage. Consequently, a number of multisite campaigns have been organized by various groups. The most spectacular results have been achieved via the WET (Whole Earth Telescope, Nather et al. 1990) network.

More than 100 pulsation modes in the pre-white dwarf star PG 1159-035 (Winget et al. 1991), and about 60 in the variable DB white dwarf GD 358 (Winget et al. 1994) could be identified. The observational data, in combination with accompanying model calculations, yielded both information about the stellar interior (compositional stratification and/or differential rotation data) and quality data on masses, luminosities and magnetic field strengths (see e.g. also Bradley & Winget 1994).

This success became possible not only due to the rich modal content in the light curves of the variable white dwarfs; an important factor here is also the range of the pulsation frequencies. In practice, high frequencies, as found in white dwarfs (around 200 cycles per day or 2500 μHz) are easier to study photometrically than are low frequencies around 10 c/d (120 μHz), e.g. as found in δ Scuti stars. One of the reasons for the considerable amount of observing time needed for detecting low frequencies lies in the requirement of measuring (two) comparison stars with the same channel in order to eliminate atmospheric and instrumental effects. Regrettably, this procedure causes gaps in the coverage of the target star and decreases the signal-to-noise ratio of the observations.

Despite these difficulties, asteroseismological studies are also undertaken for stars on and close to the Main Sequence. The most favorable cases are the rapidly oscillating Ap (roAp) stars (e.g. Kurtz et al. 1989), which show pulsation frequencies comparable to those found for the white dwarfs, and the more slowly pulsating δ Scuti stars (e.g. Breger et al. 1990, 1995).

Most of the well-studied δ Scuti stars are evolved objects. However, theoretically calculated frequency spectra for δ Scuti stars become very dense as the objects leave the Main Sequence (Dziembowski & Królikowska 1990). Still, the richness of *observed* frequency spectra for evolved stars does not seem to differ from that of their younger counterparts. Dziembowski & Królikowska speculated that among the possible pulsation modes, only those trapped in the envelope are preferentially excited to visible amplitudes. They found that trapping is essentially absent at $l = 2$ and $l = 3$, and therefore only modes with $l = 0$ and $l = 1$ should be seen in amplitude spectra of evolved δ Scuti stars. This is in disagreement with the mode identification for the evolved star 4 CVn, for which Breger et al. (1990) and Breger (1990a) found the pulsation modes to be consistent with $l = 2$. This problem has not yet been solved due, in part to the many degrees of freedom in mode identification procedures for δ Scuti stars, but also because of the lack of commonly available results of recent model calculations. An additional difficulty is represented by the sparseness of observational data for unevolved objects, as e. g. pointed out by Dziembowski (1990). For these stars, theoretical frequency spectra are simple, and there is a good chance that reliable mode identifications can be made, in turn allowing the models to be tested.

Consequently, a suitable way of overcoming this mode-identification dilemma is the concentrated study of a few selected evolved stars as well as a number of stars in an early phase of core hydrogen burning. The main difficulty in such studies is the need to obtain large amounts of high-quality photometric data to detect the expected very low-amplitude pulsation modes. In this paper we report the light-curve analysis of an unevolved δ Scuti star.

2. Data acquisition and reduction

2.1. WET observations

During an observing run of the WET network devoted to the recently discovered dwarf nova 1H0857-242, the observers were instructed to choose either CD-24°7599 or CD-24°7605 as their comparison star. However, CD-24°7599 was soon discovered to be variable. Since the time scale of these variations (tens of minutes) appeared to be significantly longer than those in the faint main target, it was decided that this comparison could still act as an adequate sky transparency monitor, in spite of its variability.

Consequently, CD-24°7599 was used as a second target object. The participating sites and the journal of the observations are given in Table 1 and Table 2, respectively. After performing data reduction as described below, 116.7 hours of high-speed photometry remained, resulting in a duty cycle of 40% (including overlaps).

In this campaign, high-speed photometric measurements with an integration time of 5 seconds were obtained with a number of two-star photometers. CD-24°7599 was always observed with a Johnson B-filter, while 1H0857-242 was observed in white light. Observations in both channels were interrupted at irregular intervals to obtain measurements of the sky brightness.

This paper will be based upon the data acquired for CD-24°7599; the analysis of the photometric observations of 1H0857-242 will be reported elsewhere (Buckley et al. 1995).

2.2. Reduction of the high-speed photometry and preliminary analysis

At first glance, the light curves (Figs. 1 and 2) show modulation with a time scale of about 40 minutes. Amplitude variations from cycle to cycle are clearly visible. A low-resolution spectrogram obtained by BJW suggests spectral type A without peculiarities. The time scale of the light variations and the spectral type strongly support the idea that CD-24°7599 is a δ Scuti variable. Because δ Scuti stars can show periods up to 0.3 days, we did not adopt the standard reduction technique for WET photometry developed to detect periods of about 15 minutes or shorter (Nather et al. 1990, Winget et al. 1991). We first had to examine whether or not variations intrinsic to the star with periods of some hours are present in the data. We, therefore, adopted the following reduction scheme:

We first performed sky subtraction using a piecewise linear fit and discarded bad data (e.g. integrations made while moving the telescope). Where the data set contained gaps longer than 15 minutes, we treated both parts as if they were different runs. In order to investigate the low-frequency domain in our power spectra, we had to carefully examine the light curves for possible sky transparency irregularities, instrumental drifts and similar phenomena not caused by the target star. Indeed, some small instrumental (SAAO) and atmospheric (MKO) problems became apparent. Consequently, we omitted the data from these two sites for the analysis of the lowest frequencies, corrected the remainder for extinction by fitting a straight line to the Bouguer plot

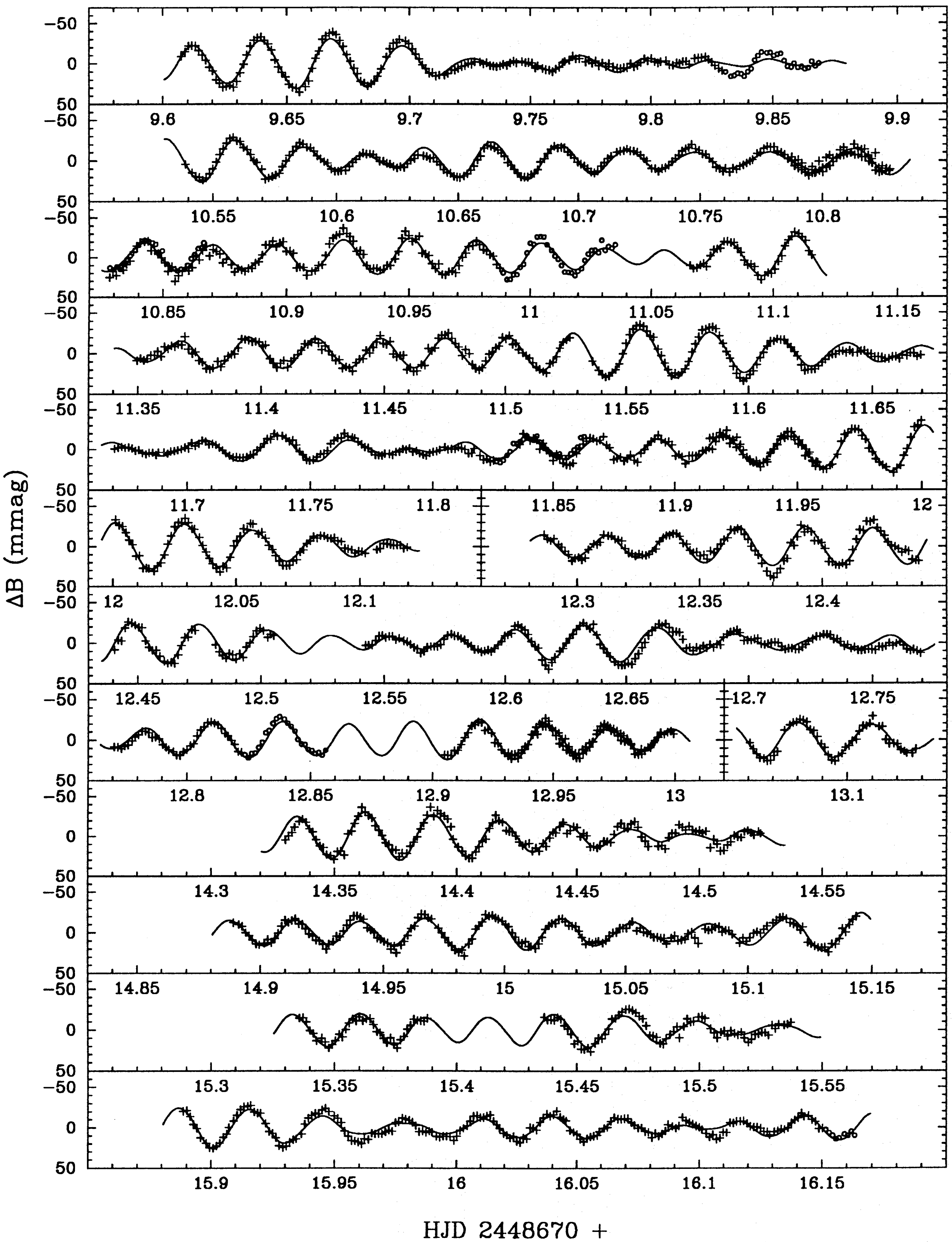

Fig. 1. B-light curves and the corresponding (7+1)-frequency fit (derived in Sect. 3) for the WET data on CD-24°7599. Plus signs represent data taken at air mass values smaller than 2, open circles are data taken at air mass values larger than 2

Table 1. Participating sites

Observatory	Location	Longitude	Latitude	Telescope
South African Astronomical Observatory (SAAO)	Sutherland, South Africa	+20°49′	-32°22′	0.75 m
Siding Spring Observatory	Siding Spring, Australia	+149°04′	-31°16′	1.0 m
Mount John University Observatory (MJUO)	Lake Tekapo, New Zealand	+170°28′	-43°59′	1.0 m
Cerro Tololo Interamerican Observatory (CTIO)	La Serena, Chile	-70°49′	-30°09′	1.0 m
McDonald Observatory	Fort Davis, Texas	-104°01′	+30°40′	0.9 m
Mauna Kea Observatory (MKO)	Hilo/Mauna Kea, Hawaii	-155°28′	+19°50′	0.6 m

Table 2. Journal of the observations

Run Name	Observatory	Observer(s)	Date (UT)	Start (UT)	Start (HJD 2448670 +)	Length (hrs)
JCC-0195	CTIO	JCC	27 Feb 92	2:21:00	9.607	4.1
JCC-0196	CTIO	JCC	27 Feb 92	6:25:01	9.773	2.4
JCC-0197	CTIO	JCC	28 Feb 92	0:48:00	10.539	7.9
CFC-0074	MKO	CFC, KK	28 Feb 92	6:15:20	10.788	6.7
FE2892	MJUO	DJS	28 Feb 92	12:33:20	11.066	3.8
S5454	SAAO	ALC	28 Feb 92	20:10:04	11.350	4.5
JCC-0198	CTIO	JCC	29 Feb 92	0:44:00	11.536	7.9
CFC-0077	MKO	CFC, KK	29 Feb 92	7:39:10	11.836	3.3
DJS-0002	MJUO	DJS	29 Feb 92	9:45:40	11.914	6.0
S5456	SAAO	ALC	29 Feb 92	18:39:55	12.286	5.7
JCC-0199	CTIO	JCC	1 Mar 92	0:47:00	12.542	7.8
DJS-0003	MJUO	DJS	1 Mar 92	9:27:50	12.905	5.6
SJK-0195	Siding Spring	SJK, DTW	1 Mar 92	10:14:00	12.931	1.5
S5459	SAAO	ALC	2 Mar 92	19:36:54	14.330	4.9
DJS-0007	MJUO	AJvdP	3 Mar 92	8:59:50	14.889	7.2
S5461	SAAO	DOD	3 Mar 92	19:45:00	15.336	5.1
DJS-0008	MJUO	AJvdP	4 Mar 92	9:00:00	15.889	7.0
S5462	SAAO	DOD	4 Mar 92	18:44:00	16.295	5.8
JCC-0206	CTIO	JCC	5 Mar 92	6:40:30	16.791	1.7
S5463	SAAO	DOD	5 Mar 92	18:39:00	17.300	1.6
RA273	McDonald	AK	6 Mar 92	2:20:00	17.672	6.5
RA275	McDonald	AK	7 Mar 92	2:18:10	18.608	6.0
DJS-0010	MJUO	DJS, AJvdP	7 Mar 92	8:55:30	18.882	7.3
DJS-0011	MJUO	DJS, AJvdP	8 Mar 92	8:44:30	19.887	3.3
DJS-0012	MJUO	DJS, AJvdP	8 Mar 92	12:59:20	20.046	3.2
S5471	SAAO	DOD	8 Mar 92	19:39:00	20.329	4.5

of the Channel 2 data, and calculated the amplitude spectrum shown in Fig. 3 using the program PERIOD (Breger 1990b) described in Sect. 3.

The effects of extinction, arbitrary zeropoint adjustments and possible intrinsic stellar variability cannot be separated for frequencies lower than about 7 c/d (80 μHz). Therefore, we cannot use our data to search for pulsation frequencies between 0–7 c/d.

If we consider the range between 7 and 20 c/d (80–230 μHz) in Fig. 3, we see that the amplitude of the noise peaks decreases towards higher frequencies. We conclude that if the data are carefully reduced, then the detection of pulsation frequencies between 7 to 20 c/d is possible. Numerical simulations show that the corresponding amplitudes cannot be assumed to be reliable. As a "detection level" for modes in this domain we estimate pulsations with amplitudes down to 2.5–3 mmag could be discovered in our 73 hr subset. Within these limitations we did not find evidence for low-frequency oscillations in CD-24°7599.

It may be useful to compare our noise level in the low-frequency domain with the results of similar studies of δ Scuti stars using multi-channel high-speed photometry. Examining Figs. 2a and 2b in Belmonte et al. (1994), we find that our noise level is half as high, although we could not use a comparison star in our reduction procedures. This suggests that the WET data are of very high quality.

In order to prepare the data for the multiple-frequency analysis, we explored the feasibility of averaging data because of the large amount of closely-spaced data points. We calculated power

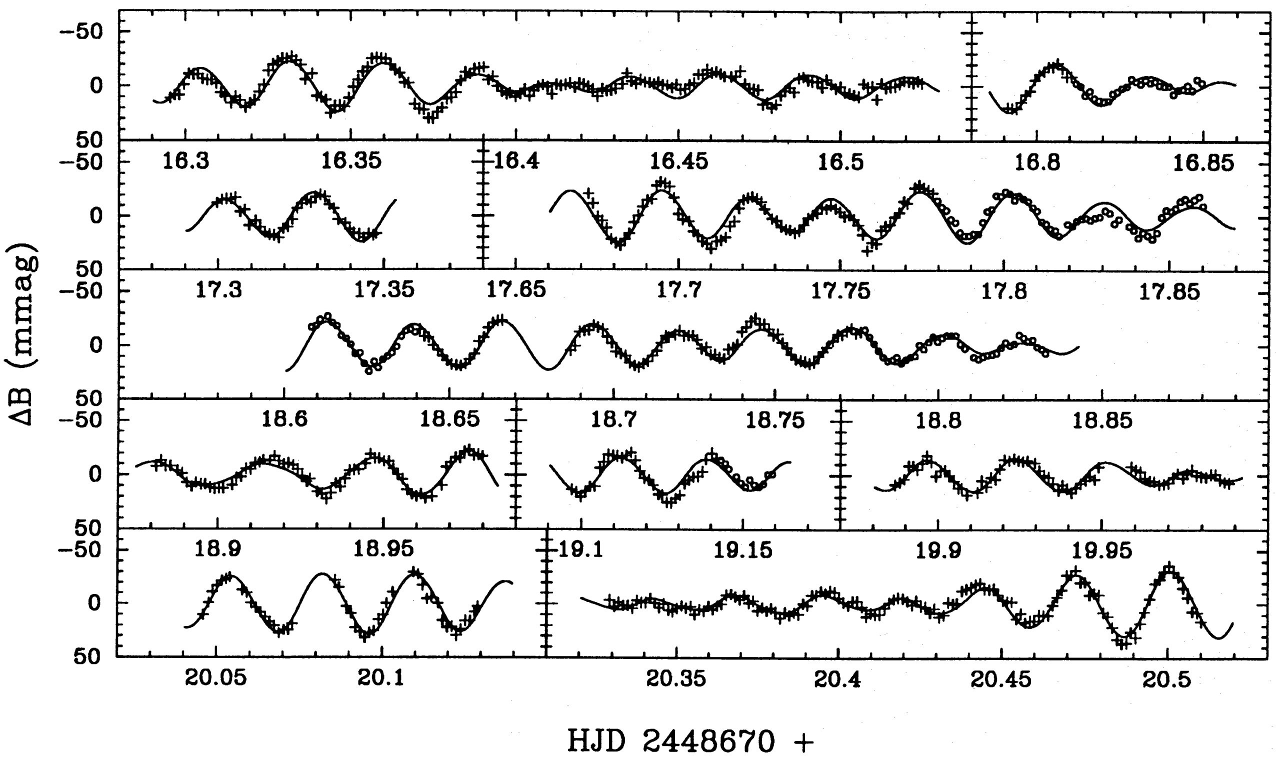

Fig. 2. Further light curves of CD-24°7599. The meaning of the symbols is the same as in Fig. 1

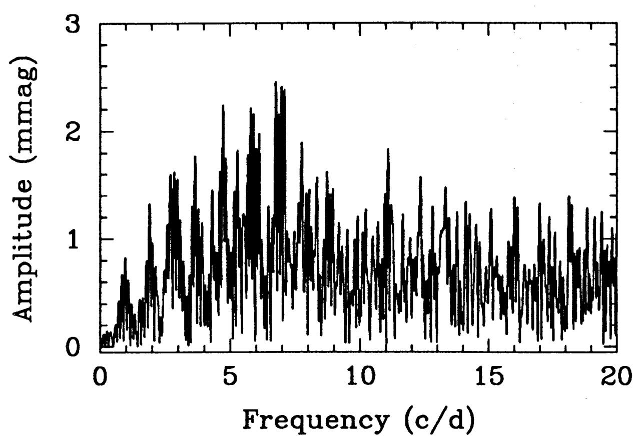

Fig. 3. Amplitude spectrum for the subset of data where no atmospheric or instrumental effects were detected. An artificial drop in the noise level for frequencies lower than 7 c/d caused by the reduction technique is visible (see text)

spectra up to the Nyquist frequency of 8640 c/d (100 mHz) for every single run and for the combined data. Our spectra did not show any peak with an amplitude signal-to-noise (S/N) ratio larger than four[1] in the range where periods are found for roAp stars or solar-like oscillations may be suspected (80–1000 c/d). We were also unable to find a regular frequency spacing indicating the presence of high-order p-modes.

At frequencies higher than 1000 c/d, the power spectrum also contains only noise. Therefore, we averaged the data into 2 minute bins for further analysis. The resulting decrease in the calculated amplitude of the signal is not extensive, as can be seen from the easily inferred formula (e. g. see Michel 1993):

$$A_{\mathrm{calc}} = A_{\mathrm{true}} \frac{\sin \pi/n}{\pi/n}, \qquad (1)$$

where A_{calc} and A_{true} are the calculated and the true amplitude of the signal, respectively, and n is the number of data points contained in one cycle after averaging.

Anticipating the later result that the shortest pulsation period found in CD-24°7599 is 37.78 minutes, we estimate that the decrease in amplitude caused by averaging the data is less than 0.5% of the amplitude for every mode. Consequently, we consider this effect to be negligible.

In order to be able to use also the data from SAAO and MKO for the analysis (a larger data sample decreases the noise at higher frequencies), and in order to decrease the noise at low

[1] The noise level is defined as the average amplitude in an oversampled ($\Delta f = 1/20\Delta T$, where Δf is the sampling interval in the spectrum and ΔT is the length of the data set) amplitude spectrum in the domain where the suspected frequency is located. The empirical criterion proposed by Breger et al. (1993a), that an amplitude S/N ratio larger than 4 usually corresponds to a peak intrinsic to the target, proved to yield a useful guideline where to stop a period search in cases where no further constraints on the value of a suspected frequency are available. However, we emphasize that this criterion should not be taken as a strict limit to decide whether a frequency is not real or is. Every doubtful case should be critically examined on its own merits.

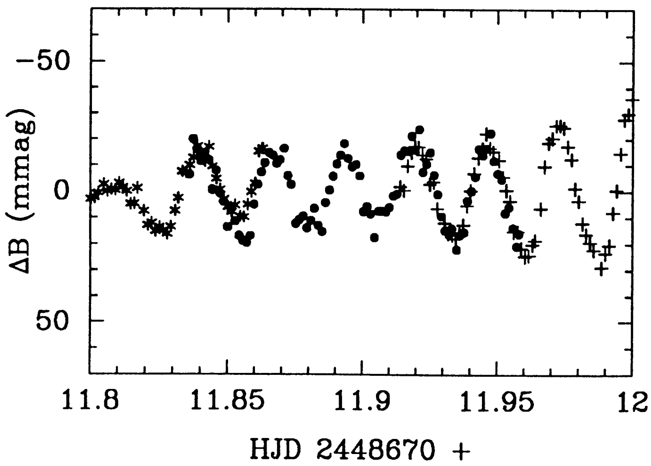

Fig. 4. Overlap of the runs JCC-0198 (asterisks), CFC-0077 (dots) and DJS-0002 (plus signs)

frequencies, we finally reduced the data by removing extinction with the coefficient derived from the longest run at each site. We then fitted low-order polynomials to the data (the order of the polynomial depending on the length of the run) and subtracted this fit to remove residual sky transparency variations and instrumental drifts. This is necessary since we did not have measurements of constant comparison stars available. After subtracting the frequencies found in Sect. 3, we again re-examined the zeropoints by fitting the residuals with a straight line. Combining all the data sets, we found very good agreement for overlapping data. An example is displayed in Fig. 4.

2.3. Strömgren photometry

In February 1993, CS carried out *uvbyβ* observations of CD-24°7599 with the 50 cm Danish telescope at the European Southern Observatory (ESO). The transformation matrix (see Sterken et al. 1993) was calculated from about 170 measurements of more than 80 standard stars. Additional observations of CD-24 7599 with β filters were acquired by GH with the 90 cm telescope at McDonald Observatory on Nov. 28, 1994, using 9 standards with spectral type A.

Consequently we determined $y = V = 11.49 \pm 0.02$, $(b-y) = 0.214 \pm 0.008$, $m_1 = 0.160 \pm 0.013$, $c_1 = 0.956 \pm 0.015$, and $\beta = 2.880 \pm 0.02$ for CD-24°7599. The error sizes were estimated from photon statistics as well as from transformation errors.

3. Determination of the individual frequencies

In order to calculate a reliable synthetic light curve, we used single-frequency Fourier and multiple-frequency least-squares techniques implemented in the program PERIOD (Breger 1990b). This analysis does not depend on successive prewhitening, but calculates the best fit to the data with all given frequencies simultaneously by minimizing the residuals between light curve and fit. Using PERIOD, one can also improve the frequencies estimated from a visual inspection of the corresponding power spectrum by nonlinear least-squares fits.

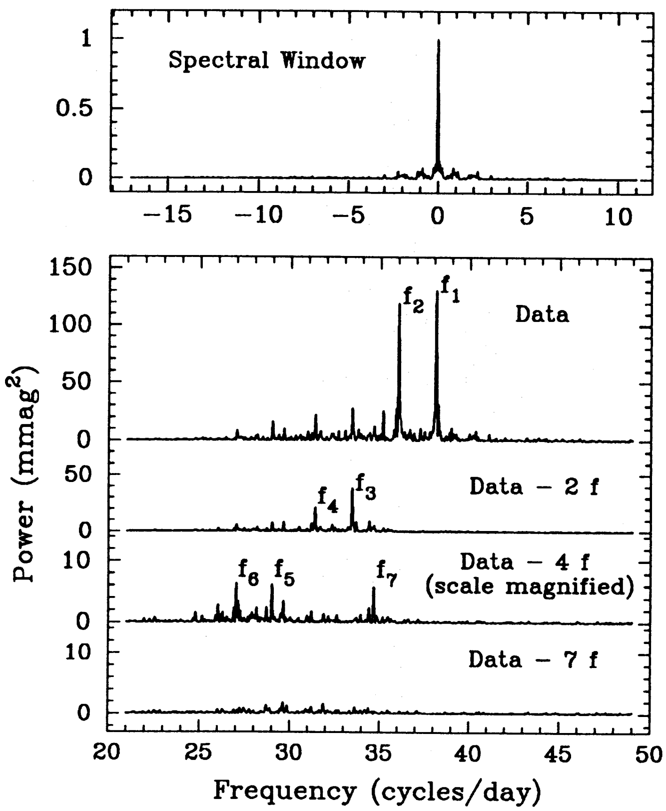

Fig. 5. Spectral window and power spectra for the WET data on CD-24°7599. Note the different scales of the power-axis

The top panel of Fig. 5 shows the spectral window pattern of the data. Due to the multisite coverage, aliases are quite low in power. The panels below show the results after subsequent removal of the variations due to two, four and seven simultaneously optimized frequencies.

In order to investigate whether our seven frequencies are intrinsic to the star or not we divided the data into two partitions of equal size and repeated the analysis for each subset. The results were consistent with each other as well as with the overall solution. However, when removing a seven-frequency fit from the data and calculating a power spectrum of the residuals, we do not see white noise. Therefore, we suspect that further pulsation modes with frequencies around 30 c/d exist. The most interesting peaks are located at 28.7, 29.6, 31.9 and 34.4 c/d, respectively (332, 343, 369 and 398 μHz). These peaks were present in both subsets, however with variable amplitudes from data set to data set. They also do neither improve the residuals significantly nor have amplitude signal-to-noise ratios larger than 4. Consequently, these frequencies were not included in our final frequency solution. The noise level between 25 and 40 c/d (290–460 μHz) is 0.37 mmag.

During the data analysis we noticed that the height of the peaks in the power spectrum in the range of 60 to 80 c/d (690–930 μHz) did not decrease towards higher frequencies, as would be expected for noise peaks originating from residual transparency variations. A more careful examination of this domain showed that the frequency values of several of the higher peaks could be matched with sums or harmonics of pulsation frequencies already found (Fig. 6). The peak at $2f_1$ exceeds the noise level (0.17 mmag between 60–80 c/d) by more than a factor of 4, and could consequently also be included in the final multi-frequency solution of the light curve obtained for CD-24°7599. Although the peaks at the linear combination frequencies are not significant in the sense of our amplitude signal-to-noise criterion, their systematical occurrence at "expected" frequencies suggests that most of them are real.

We also performed the frequency analysis using intensity units as the expression of the amplitudes. The unit "millimodulation amplitude" (mma) corresponds to a modulation of 1/1000 of the total intensity of the star's light. Anyway, the results were the same as those obtained using magnitudes. This agreement is not surprising because of the small amplitudes of the pulsation modes. All information about the (7+1)-frequency fit, which reflects the observed light curve well within 5 mmag per single measurement, can be found in Table 4. Error bars of the frequencies are 1σ values determined following Kovacs (1981); for further information we refer to the excellent review by Cuypers (1993).

4. Discussion

4.1. The range of 25–40 c/d: pulsation mode identification

The first step to identify the pulsation modes of δ Scuti stars can be made via an estimate of the radial orders $k_{\rm i}$. We therefore rewrite the period-mean density relation $Q_{\rm i} = P_{\rm i}\sqrt{\rho_*/\rho_\odot}$ in the form

$$\log Q_{\rm i} = C + 0.5\log g + 0.1M_{\rm bol} + \log T_{\rm eff} + \log P_{\rm i} \qquad (2)$$

adopting $T_{\rm eff,\odot} = 5780$ K, $\log g_\odot = 4.44$, $M_{\rm bol,\odot} = 4.75$ (Allen 1976) and thus $C = -6.456$.

The numerical values of $M_{\rm bol}$, $\log g$ and $T_{\rm eff}$ can be derived by applying calibrations for *uvbyβ* photometry. Using dereddening formulae and calibrations given by Crawford (1979), leads to $(b-y)_0 = 0.068$, δm_1 = -0.007, δc_1 = -0.003 and $M_{\rm v}$ = 2.3. From model-atmosphere calculations of Kurucz (1991) we find $\log T_{\rm eff} = 3.935 \pm 0.010$ and $\log g = 4.3 \pm 0.05$.

This leads to pulsation constants between $0\overset{\rm d}{.}018$ and $0\overset{\rm d}{.}025$ for the various modes which are not unexpected for hot δ Scuti stars (cf. Table 2 of Breger & Bregman 1975). From calculations of error propagation by Breger (1989) we estimate the errors of the $Q_{\rm i}$ values to be $\pm\, 0\overset{\rm d}{.}004$. Now we can constrain the nature of the pulsation modes in CD-24°7599:

– purely radial pulsation can immediately be ruled out due to the large ratio of the values of consecutive frequencies
– the $Q_{\rm i}$ values and the unevolved state of the star suggest pulsation with nonradial and possibly radial p modes
– since we have shown that the star is well described with a ZAMS model we can neglect mixed modes, compare our Q values with theoretical values calculated by Dziembowski (private communication) and find CD-24°7599 is pulsating with $p_{2\pm1}$ modes
– it can be shown that the observed frequencies cannot be identified with only one l value. However, the presence of differential or rapid rotation could affect this conclusion
– the observed frequency differences $\Delta f_{\rm A} = f_1 - f_2 = 2.10$ c/d (24.3 μHz), $\Delta f_{\rm B} = f_3 - f_4 = 2.05$ c/d (23.7 μHz) and $\Delta f_{\rm C} = f_5 - f_6 = 1.99$ c/d (23.0 μHz) can be interpreted in terms of nonradial m–mode splitting. Due to the small total range of observed frequencies, they are very unlikely to be attributed to the difference between $l = 1$ and $l = 2$ modes of consecutive radial overtones.

We also tried to derive more specific mode identifications using models of Dziembowski (priv. comm.), but were not successful. Since we can only rely on the values of our pulsation frequencies, we conclude there are too many degrees of freedom in our mode identification attempts. For instance, we lack a measurement of the projected rotational velocity of the star and also time-series color photometry.

Dziembowski & Pamyatnykh (1991) proposed the existence of so-called $g_{\rm c}$ modes for δ Scuti stars in the middle of their Main-Sequence evolution. The detection of these particular modes would allow a determination of the amount of overshooting from the convective core, and is – for this reason – asteroseismologically valuable. We could not find convincing evidence that such modes are excited in CD-24°7599 but we mention that the star may be insufficiently evolved for $g_{\rm c}$ modes to appear.

4.2. The range of 60–80 c/d: linear combinations of excited frequencies?

In Sect. 3 we found some peaks at frequencies corresponding to sums of already detected pulsation frequencies. Such peaks can be artifacts. If we assume a strictly sinusoidal intensity modulation, then the transformation into a logarithmic scale (i.e. magnitudes) distorts the shape of the light curve, and results in the appearance of harmonics in a power spectrum. The amplitude of such a spurious harmonic frequency at $2f$ can be calculated using

$$a_{\rm h} = 0.625A^2\log e + O(A^4), \qquad (3)$$

where $a_{\rm h}$ is the amplitude of the spurious harmonic frequency, and A is the amplitude of the signal itself. In Fig. 6, the only high-amplitude harmonic can be found at $2f_1$. If it were due to the effect described above, its amplitude should be about 34 μmag, well below our detection limit, and much less than 0.8 mmag we have found for that peak. We conclude that the sum and harmonic frequencies in our power spectrum cannot originate from the choice of magnitudes as the unit of the photometric amplitude.

Consequently, three ways of explaining the peaks coinciding with sum and harmonic frequencies appear to be reasonable:

1. They are due to chance agreements.

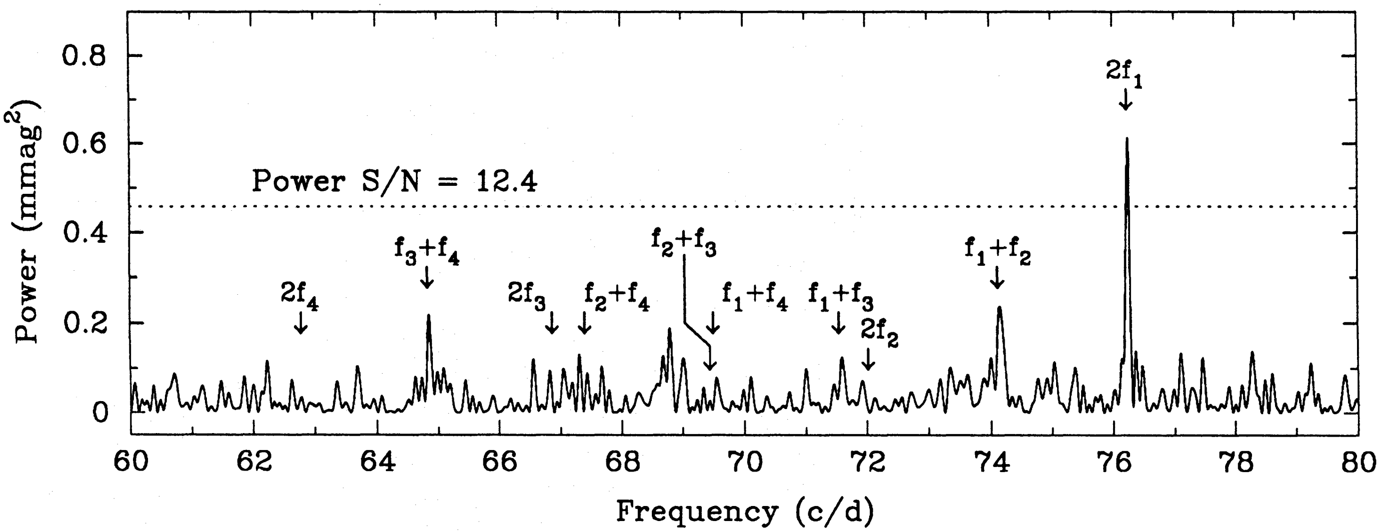

Fig. 6. Power spectrum of the domain where possible linear combination and harmonic frequencies can be found. All possible combinations and harmonics of f_1, f_2, f_3 and f_4 are indicated and several agreements are visible. A power S/N ratio of 12.4 corresponding to an amplitude S/N ratio of 4 (see text) in this domain is indicated

Table 3. Frequencies of the δ Scuti star CD-24°7599 with an amplitude S/N ratio larger than 4

Designation	Frequency (cycles/day)	Frequency (μHz)	Epoch (HJD) 2448670 +	B Amplitude (mmag)	B Amplitude (mma)	S/N
f_1	38.111 ± 0.001	441.10 ± 0.01	14.1263 ± 0.0001	11.2 ± 0.2	10.3 ± 0.2	30.1
f_2	36.013 ± 0.001	416.81 ± 0.01	14.1407 ± 0.0001	10.1 ± 0.2	9.3 ± 0.2	27.2
f_3	33.435 ± 0.001	386.98 ± 0.02	14.1273 ± 0.0002	6.1 ± 0.2	5.6 ± 0.2	16.3
f_4	31.392 ± 0.002	363.33 ± 0.02	14.1304 ± 0.0003	4.3 ± 0.2	4.0 ± 0.2	11.7
f_5	28.997 ± 0.002	335.61 ± 0.03	14.1509 ± 0.0005	2.6 ± 0.2	2.4 ± 0.2	7.3
f_6	27.011 ± 0.002	312.63 ± 0.03	14.1436 ± 0.0005	2.7 ± 0.2	2.5 ± 0.2	6.9
f_7	34.662 ± 0.003	401.18 ± 0.03	14.1304 ± 0.0005	2.3 ± 0.2	2.1 ± 0.2	6.1
$f_8=2f_1$	76.235 ± 0.008	882.34 ± 0.10	14.1365 ± 0.0006	0.8 ± 0.2	0.7 ± 0.2	4.6

2. They are normal modes, near combination frequencies, and excited by resonant mode-coupling (Dziembowski 1982).
3. The light curve is harmonically distorted, because the propagating material cannot exhibit a totally elastic response to the full acceleration caused by pulsation.

Peaks at linear combinations and harmonics of known frequencies are not uncommon in power spectra of δ Scuti stars. They are found in both Population I and Pop. II high-amplitude multi-mode pulsators (e.g. Walraven et al. 1992, Rodriguez et al. 1992, Rolland *et al.* 1991) as well as in medium-amplitude Pop. I δ Scuti stars (Mantegazza & Poretti 1992). The most common interpretation for those frequencies, so far, was that resonant modes in some δ Scuti stars are excited (see also Antonello et al. 1985).

However, Winget et al. (1994) discussed the same phenomenon observed in the variable DB white dwarf GD 358, and they were able to show that harmonic distortion is the reason for the combination frequencies. For CD-24°7599 we can – under the preliminary assumption that our combination frequencies are not chance agreements – argue as follows:

If the peaks at frequency sums are caused by normal modes due to resonant mode coupling, they should have similar amplitudes in all subsets of data, since growth rates for modes in δ Scuti stars are small (of the order 10^{-4} and smaller, Lee 1985). This means that the contribution of any cycle of the driving modes to the resonating mode is very small, even if the actual growth rates of the driven modes were higher by a factor of 10 or more. Moreover, if the driving of the resonant mode would be stopped somehow, this mode would still be observable for a long time (compared to its period).

Following this prediction, we divided the data into two subsets of almost the same size. One subset contained data with large light variations, the other set had the data with less extensive modulation. This choice was made arbitrarily in order to avoid spurious spectral window effects caused by systematic selection of data. The variations due to the 7 pulsation frequencies were removed, and power spectra were calculated for each subset (Fig. 7).

In Fig. 7, the peaks corresponding to linear combination frequencies of the seven pulsation frequencies considerably in-

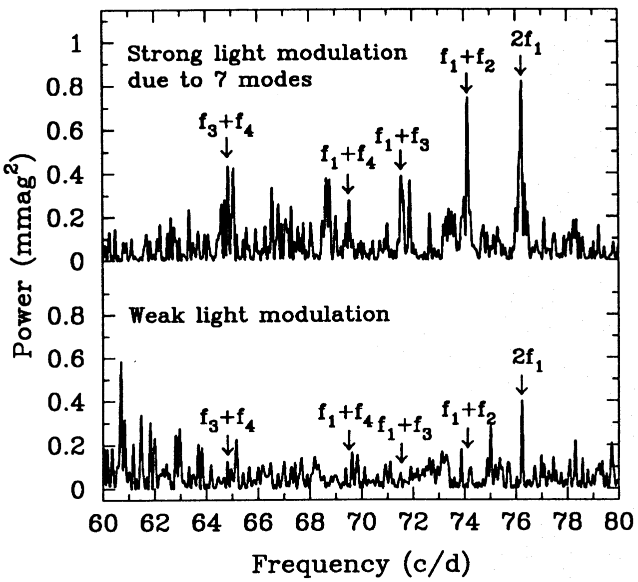

Fig. 7. Power spectra of subsets of data chosen with respect to the amplitude of the light modulation. Upper panel: data with strong modulation caused by the 7 pulsation modes. Lower panel: data with weak light variations. Peaks at sum and harmonic frequencies are indicated by arrows

crease in power when the star shows larger light modulations. The reality of this effect was additionally tested by multiple non-linear least squares analysis, variance reduction techniques (Mayr 1994), and numerical simulations. Of course, some of the peaks in the top panel of Fig. 7 can be chance agreements, but certainly not all are. We, therefore, suggest that resonant mode coupling is not the reason for the sum and harmonic frequencies we detected during our analysis of the light curves of the δ Scuti star CD-24°7599. The most promising idea is that these peaks represent nonlinearities originating in the outer part of the star's envelope, where the pulsation amplitude is highest.

Unlike the peaks at sum frequencies, the size of the peak at $2f_1$ is, however, not conspicuously decreased in the lower panel of Fig. 7. It is also the *only* harmonic we could detect. Consequently, we suspect that this harmonic is caused by strong driving of the mode with frequency f_1 (producing a non-sinusoidal pulse shape), whose photometric amplitude is decreased by projection or geometric cancellation effects.

Finally, we also note that CD-24°7599 is the lowest-amplitude δ Scuti star in whose light curves nonlinearities were found. In the present stage we cannot judge whether this detection was simply favored by the high pulsation frequencies of CD-24°7599 (compared to other well-studied δ Scuti stars) or whether the star is unique in this context. Also, some roAp stars (see Kurtz 1990) and pulsating white dwarfs show harmonics and linear combination frequencies in their power spectra, but some do not. More detailed theoretical investigations of the nonlinearities would be desirable.

5. Summary and perspectives

In this paper we reported the serendipitous discovery of a short-period δ Scuti star. Our data obtained with the WET technique allowed us to search for potential oscillation frequencies higher than 7 c/d (80 μHz).

We found 7 independent pulsation frequencies and interpreted them to be mainly due to nonradial $p_{2\pm1}$ modes. Rotational m-mode splitting is probable. Few radial modes could be present, but not necessarily. We also found some peaks at linear combination frequencies of already detected normal pulsation modes and suggested they are due to harmonic distortion of the light curve.

A definite mode identification is presently not possible but we are optimistic that additional measurements as well as model calculations will allow an identification. For instance, a measurement of the star's rotational velocity would be very helpful to constrain m-mode splitting. New extensive photometric observations utilizing both the WET technique and a method using comparison stars would help to detect possible further pulsation and combination frequencies (especially frequency differences). Multicolor observations should allow a determination of the l value of at least the 4 modes with the highest photometric amplitudes excited in CD-24°7599 by examination of phase shifts and amplitudes of color variations (Garrido *et al.* 1990, Watson 1988, Balona & Stobie 1979). A substantial improvement compared to the present study would require more than 200 hours of time-series photometry obtained on telescopes of the 1-meter class at excellent photometric sites, but we are confident that, despite the faintness of the star, the scientific outcome will justify this effort.

Acknowledgements. This work has been partially supported by the Austrian Fonds zur Förderung der wissenschaftlichen Forschung under grant P8543–GEO, and by grant AST-9217988 from the National Science Foundation, U.S.A. C. S. acknowledges support from the Belgian Fund for scientific research (NFWO). DJS and AJvdP thank the University of Canterbury for the allocation of observing time at MJUO, and the VUW Internal Research Committee for financial support. We are grateful to Wojtek Dziembowski for kindly supplying results of his model calculations.

References

Allen, C. W., 1976, in *Astrophysical Quantities*, London: Athlone Press, p. 161 f.
Antonello, E., Guerrero, G., Mantegazza, L., Scardia, M., 1985, A&A 146, 11
Balona, L. A., Stobie, R. S., 1979, MNRAS 189, 649
Belmonte, J. A., Michel, E., Alvarez, M. et al., 1994, A&A 283, 121
Bradley, P. A., Winget, D. E., 1994, ApJ 430, 850
Breger, M., 1989, Communications in Asteroseismology 7, 1 (University of Vienna)
Breger, M., 1990a, A&A 240, 308
Breger, M., 1990b, Communications in Asteroseismology 20, 1 (University of Vienna)
Breger, M., Bregman, J. N., 1975, ApJ 200, 343

Breger, M., McNamara, B. J., Kerschbaum, F. et al., 1990, A&A 231, 56
Breger, M., Stich, J., Garrido, R. et al., 1993a, A&A 271, 482
Breger, M., Martin, B., Garrido, R. et al., 1993b, A&A 281, 90
Breger, M., Handler, G., Nather, R. E. et al., 1995, A&A, 297, 473
Buckley, D. A. H. et al., 1995, MNRAS, in preparation
Crawford, D. L., 1979, AJ 84, 1858
Cuypers, J., 1993, Proc. International Conference on Applications of Time Series Analysis in Astronomy and Meteorology, Universitá di Padova, p. 139
Dziembowski, W. A., 1982, Acta Astron. 32, 147
Dziembowski, W. A., 1990, Lect. Notes Phys. 367, 359
Dziembowski, W. A., Królikowska, M., 1990, Acta Astron. 40, 19
Dziembowski, W. A., Pamyatnykh, A. A., 1991, A&A 248, L11
Garrido, R., Garcia-Lobo, E., Rodriguez, E., 1990, A&A 234, 262
Kovacs, G., 1981, Ap&SS 78, 175
Kurtz, D. W., 1990, ARA&A 28, 607
Kurtz, D. W., Matthews, J. M., Martinez P. et al., 1989, MNRAS 240, 881
Kurucz, R. L., 1991, Van Vleck Obs. Contr. 11, 27
Lee, U., 1985, PASJ 37, 279
Mantegazza, L., Poretti, E., 1992, A&A 255, 153
Mayr, B. J., 1994, unpublished diploma thesis, University of Vienna
Michel, E., 1993, Delta Scuti Star Newsletter 6, 19 (University of Vienna)
Nather, R. E., Winget, D. E., Clemens, J. C., Hansen, C. J., Hine, B. P., 1990, ApJ 361, 309
Rodriguez, E., Rolland, A., López de Coca, P., Garcia-Lobo E., Sedano, J. L., 1992, A&AS 93, 189
Rolland, A., Rodriguez, E., López de Coca, P., García-Pelayo, J. M., 1991, A&AS 91, 347
Sterken, C., Manfroid, J., Anton, K. et al., 1993, A&AS 102, 79
Walraven, Th., Walraven, J., Balona, L. A., 1992, MNRAS 254, 59
Watson, R. D., 1988, Ap&SS 140, 255
Winget, D. E., Nather, R. E., Clemens, J. C. et al., 1991, ApJ 378, 326
Winget, D. E., Nather, R. E., Clemens, J. C. et al., 1994, ApJ 430, 839

This article was processed by the author using Springer-Verlag LaTeX A&A style file version 3.

2.2.2 New Whole Earth Telescope observations of CD−24 7599: steps towards δ Scuti star seismology

Original paper:

G. Handler, H. Pikall, D. O'Donoghue, D. A. H. Buckley, G. Vauclair, M. Chevreton, O. Giovannini, S. O. Kepler, P. R. Goode, J. L. Provencal, M. A. Wood, J. C. Clemens, M. S. O'Brien, R. E. Nather, D. E. Winget, S. J. Kleinman, A. Kanaan, T. K. Watson, A. Nitta, M. H. Montgomery, E. W. Klumpe, P. A. Bradley, D. J. Sullivan, K. Wu, T. M. K. Marar, S. Seetha, B. N. Ashoka, H. S. Mahra, B. C. Bhat, V. C. Babu, E. M. Leibowitz, S. Hemar, P. A. Ibbetson, E. Mashal, E. G. Meištas, W. A. Dziembowski, A. A. Pamyatnykh, P. Moskalik, S. Zola, G. Pajdosz, J. Krzesinski, J. E. Solheim, S. Bard, C. M. Massacand, M. Breger, M. J. Gelbmann, E. Paunzen, P. North, 1997, MNRAS 286, 303

Mon. Not. R. Astron. Soc. **286,** 303–314 (1997)

New Whole Earth Telescope observations of CD−24 7599: steps towards δ Scuti star seismology

G. Handler,[1⋆] H. Pikall,[1] D. O'Donoghue,[2] D. A. H. Buckley,[3] G. Vauclair,[4] M. Chevreton,[5] O. Giovannini,[6†] S. O. Kepler,[6] P. R. Goode,[7] J. L. Provencal,[8] M. A. Wood,[9‡] J. C. Clemens,[10‡] M. S. O'Brien,[10] R. E. Nather,[11] D. E. Winget,[11] S. J. Kleinman,[11§] A. Kanaan,[11] T. K. Watson,[10,11] A. Nitta,[11] M. H. Montgomery,[11] E. W. Klumpe,[11] P. A. Bradley,[12] D. J. Sullivan,[13] K. Wu,[14] T. M. K. Marar,[15] S. Seetha,[15] B. N. Ashoka,[15] H. S. Mahra,[15] B. C. Bhat,[15] V. C. Babu,[15] E. M. Leibowitz,[16] S. Hemar,[16] P. A. Ibbetson,[16] E. Mashal,[16] E. G. Meištas,[17] W. A. Dziembowski,[18] A. A. Pamyatnykh,[18,19] P. Moskalik,[18] S. Zola,[20] G. Pajdosz,[20] J. Krzesinski,[20] J. E. Solheim,[21] S. Bard,[21] C. M. Massacand,[21] M. Breger,[1] M. J. Gelbmann,[1] E. Paunzen[1] and P. North[22]

[1] *Institut für Astronomie, Universität Wien, Türkenschanzstraße 17, A-1180 Wien, Austria*
[2] *Department of Astronomy, University of Cape Town, Rondebosch 7700, South Africa*
[3] *South African Astronomical Observatory, PO Box 9, Observatory 7935, South Africa*
[4] *Observatoire Midi-Pyrenees, 14 Avenue E. Belin, 31400 Toulouse, France*
[5] *Observatoire de Paris-Meudon, F-92195 Meudon, Principal Cedex, France*
[6] *Instituto de Fisica, Universidade Federal do Rio Grande do Sul, 91501-970 Porto Alegre-RS, Brazil*
[7] *Department of Physics, New Jersey Institute of Technology, Newark, NJ 07102, USA*
[8] *Department of Physics and Astronomy, University of Delaware, Newark, DE 19716, USA*
[9] *Department of Physics and Space Sciences, Florida Institute of Technology, 150 W. University Blvd, Melbourne, FL 32901, USA*
[10] *Department of Physics and Astronomy, Iowa State University, Ames, IA 50211, USA*
[11] *Department of Astronomy and McDonald Observatory, University of Texas, Austin, TX 78712, USA*
[12] *Los Alamos National Laboratory, XTA, MS B220, Los Alamos, NM 87545, USA*
[13] *Physics Department, Victoria University of Wellington, PO Box 600, Wellington, New Zealand*
[14] *Department of Mathematics, Australian National University, Canberra, Australia*
[15] *Indian Space Research Organization, Technical Physics Division, ISRO Satellite Centre, Airport Road, Bangalore 560 017, India*
[16] *Wise Observatory, Sackler Faculty of Exact Sciences, Tel Aviv University, Tel Aviv 69978, Israel*
[17] *Institute of Theoretical Physics and Astronomy, Goštauto 12, Vilnius 2600, Lithuania*
[18] *Copernicus Astronomical Center, ul. Bartycka 18, 00-716 Warsaw, Poland*
[19] *Institute of Astronomy, Pyatnitskaya Street 48, Moscow 109017, Russia*
[20] *Mount Suhora Observatory, Krakow Pedagogical University, ul. Podchorążych 2, 30-084 Cracow, Poland*
[21] *Institutt for Matematiske Realfag, Nordlysobservatoriet, Universitet i Tromsø, 9000 Tromsø, Norway*
[22] *Institut d'Astronomie de l'Université de Lausanne, CH-1290 Chavannes-des-Bois, Switzerland*

Accepted 1996 October 5. Received 1996 September 27; in original form 1996 August 16

ABSTRACT

92 h of new Whole Earth Telescope observations have been acquired for the δ Scuti star CD−24 7599. All the seven pulsation modes reported by Handler et al. are confirmed. However, significant amplitude variations which are not caused by beating of closely spaced frequencies occurred within two years. Analysing the combined data of both WET runs, we detect six further pulsation modes, bringing the total number up to 13. We also examine our data for high-frequency pulsations similar to those exhibited by rapidly oscillating Ap stars, but we do not find convincing evidence for variability in this frequency domain.

⋆E-mail: gerald@procyon.ast.univie.ac.at
†Guest observer, Laboratorio Nacional de Astrofisica/CNPq, Brazil.
‡Guest observer, Institute for Astronomy, Honolulu, Hawaii, USA.
§Guest observer, Mount Stromlo and Siding Spring Observatory, NSW, Australia.

From new colour photometry and spectroscopy we infer that CD−24 7599 is a hot main-sequence δ Scuti star with approximately solar metallicity and $v \sin i = 52 \pm 2$ km s^{-1}. We cannot yet propose a definite pulsation mode identification, but we report the detection of a characteristic frequency spacing between the different modes. We ascribe it to the simultaneous presence of $\ell = 1$ and $\ell = 2$ modes of consecutive radial order. A comparison of this frequency spacing with frequencies of solar-metallicity models, as well as stability analysis, allows us to constrain tightly the evolutionary state of CD−24 7599. It is in the first half of its main-sequence evolution, and has a mass of 1.85 ± 0.05 M$_\odot$ and a mean density of $\bar{\rho} = 0.246 \pm 0.020\,\bar{\rho}_\odot$. This yields a seismological distance of 650 ± 70 pc, which is as accurate as distance determinations for δ Scuti stars observed in clusters.

Most of the pulsation modes are pure p modes of radial order $k = 4$–6, but the g_1 mode of $\ell = 2$ is likely to be excited and observed as well. Since a significant contribution to this mode's kinetic energy comes from the outer part of the convective core, CD−24 7599 becomes particularly interesting for testing convective overshooting theories.

Key words: techniques: photometric – stars: fundamental parameters – stars: individual: CD−24 7599 – stars: oscillations – δ Scuti.

1 INTRODUCTION

The variability of CD−24 7599 was discovered during observing run XCOV 7 of the Whole Earth Telescope (WET, Nather et al. 1990). To increase the scientific output of this WET run, the star was chosen as a second target and a high-quality data set was acquired, allowing the extraction of seven pulsation frequencies as well as the first harmonic of one of these modes. Applying calibrations to subsequent *uvbyβ* photometry allowed the estimation of the position of CD−24 7599 in the Hertzsprung–Russell (HR) diagram: according to these results, this δ Scuti star is located near the hot border inside the instability strip on the lower main sequence. The unevolved nature of CD−24 7599 is confirmed by the star's high pulsation frequencies between 312 and 441 μHz.

The excitation of many pulsation modes with relatively high photometric amplitudes in an unevolved δ Scuti star is extremely important for seismology of this type of pulsator: theoretically predicted frequency spectra are simpler than for evolved objects, making the task of mode identification much easier.

Moreover, linear combination frequencies were detected in the power spectrum of the XCOV 7 data; their properties were not consistent with the 'usual' explanation of such phenomena: resonant mode coupling. Their detection was somewhat surprising, because linear combination frequencies have so far only been reported for high-amplitude δ Scuti stars. The analysis was published by Handler et al. (1996, hereafter Paper I), and the reader is referred to this paper for more information.

After removing an eight-frequency solution from the XCOV 7 light curves, the power spectrum of the residuals did not consist of white noise. The presence of a number of further pulsational modes with frequencies similar to those already detected was strongly suspected. Regrettably, due to their similar amplitudes and close spacing, we could not be confident which of the peaks were due to intrinsic stellar variability. It was therefore decided to re-observe the star with the Whole Earth Telescope. For a star as faint as CD−24 7599, with such high pulsation frequencies, and with such a complicated frequency spectrum, WET observations are required (for more details see Handler 1995a).

2 DATA ACQUISITION AND REDUCTION

2.1 WET observations

CD−24 7599 was included as third priority target, mainly for observatories located in the southern hemisphere, in WET observing run XCOV 10. High-speed photometry with an integration time of 10 s was obtained with two-star and three-star photometers (the latter have recently been described by Kleinman, Nather & Philips 1996). Johnson *B* filters were used. Whenever possible, the channel 2 comparison star was observed in channel 1 before and after the time series of CD−24 7599 was acquired. Cross-calibrations of all channels by measuring the sky brightness were done at the beginning of each run with a three-channel photometer. The participating sites and an observing log are given in Tables 1 and 2, respectively.

Two further data sets acquired during XCOV 7, which were overlooked during the busy last hours of this run, will also be

Table 1. Sites participating in the observations of CD-24 7599.

Observatory	Location	Longitude	Latitude	Telescope
South African Astronomical Observatory (SAAO)	Sutherland, South Africa	+20°49′	−32°22′	0.75 m
Wise Observatory	Mount Zin, Israel	+35°46′	+30°36′	1.0 m
Siding Spring Observatory	Siding Spring, Australia	+149°04′	−31°16′	0.6 m
Mount John University Observatory	Lake Tekapo, New Zealand	+170°28′	−43°59′	1.0 m
Mauna Kea Observatory	Hilo/Mauna Kea, Hawaii	−155°28′	+19°50′	0.6 m
McDonald Observatory	Fort Davis, Texas	−104°01′	+30°40′	2.1 m
Observatório do Pico dos Dias (OPD)	Itajubá, Brazil	−45°34′	−22°31′	1.6 m

Table 2. Journal of the WET observations.

Run Name	Observatory	Observer(s)	Comparison	Date (UT)	Start (UT)	Start (HJD 2448670 +)	Length (hrs)
sjk-0320	Siding Spring	SJK	C3	2 May 94	9:46:30	804.908	2.5
DB002	SAAO	DAHB	C1	3 May 94	18:08:30	806.257	2.5
sjk-0324	Siding Spring	SJK	C3	4 May 94	8:58:30	806.875	2.5
sjk-0325	Siding Spring	SJK	C3	4 May 94	11:27:30	806.978	0.7
DB007	SAAO	DAHB	C1	4 May 94	17:42:00	807.238	3.0
jcc-0230	Mauna Kea	JCC	C3	5 May 94	6:03:00	807.753	1.3
sjk-0330	Siding Spring	SJK	C3	5 May 94	8:56:30	807.873	3.6
DB012	SAAO	DAHB	C1	5 May 94	17:24:00	808.226	3.8
jcc-0232	Mauna Kea	JCC	C3	6 May 94	6:06:00	808.755	1.4
sjk-0335	Siding Spring	SJK	C3	6 May 94	8:40:30	808.862	3.8
DB014	SAAO	DAHB	C1	6 May 94	16:58:30	809.208	4.2
jcc-0234	Mauna Kea	JCC	C3	7 May 94	6:07:00	809.756	1.1
sjk-0339	Siding Spring	SJK	C3	7 May 94	8:55:30	809.873	2.9
DB016	SAAO	DAHB	C1	7 May 94	17:06:20	810.213	3.9
jcc-0236	Mauna Kea	JCC	C3	8 May 94	6:07:30	810.756	1.1
sjk-0343	Siding Spring	SJK	C3	8 May 94	8:43:30	810.864	3.8
DB018	SAAO	DAHB	C1	8 May 94	16:57:10	811.207	4.1
ro053	OPD	OG	C2	8 May 94	22:55:30	811.456	2.2
sjk-0347	Siding Spring	SJK	C3	9 May 94	10:18:30	811.930	2.2
DB021	SAAO	DAHB	C1	9 May 94	18:37:30	812.277	2.4
jcc-0239	Mauna Kea	JCC	C3	10 May 94	6:02:00	812.752	1.0
S5725	SAAO	DOD	C1	10 May 94	17:15:00	813.219	1.8
maw-0131	Mauna Kea	MAW	C3	11 May 94	6:01:00	813.751	1.0
S5727	SAAO	DOD	C1	11 May 94	17:06:00	814.213	3.4
maw-0133	Mauna Kea	MAW	C3	12 May 94	6:02:50	814.752	1.0
sjk-0354	Siding Spring	SJK	C3	12 May 94	8:45:00	814.865	3.7
S5729	SAAO	DOD	C1	12 May 94	17:11:00	815.216	3.3
maw-0135	Mauna Kea	MAW	C3	13 May 94	6:00:50	815.751	0.9
MY1394	Mt. John	DJS	C1	13 May 94	7:50:10	815.827	4.3
sjk-0356	Siding Spring	SJK, KW	C3	13 May 94	9:45:30	815.907	2.6
S5731	SAAO	DOD	C1	13 May 94	17:04:00	816.211	3.6
maw-0139	Mauna Kea	MAW	C3	14 May 94	6:03:20	816.753	0.8
MY1494	Mt. John	DJS	C1	14 May 94	7:12:20	816.800	4.4
sjk-0360	Siding Spring	SJK, KW	C3	14 May 94	9:20:30	816.889	2.8
S5733	SAAO	DOD	C1	14 May 94	17:07:00	817.213	2.6
maw-0141	Mauna Kea	MAW	C3	15 May 94	6:01:00	817.751	0.8
sjk-0365	Siding Spring	SJK, KW	C3	15 May 94	8:41:00	817.862	3.6
tkw-0048	McDonald	TKW, MSO	C2	16 May 94	3:04:10	818.628	0.8
sjk-0370	Siding Spring	SJK, KW	C3	16 May 94	9:05:30	818.879	3.2
S5734	SAAO	DOD	C1	16 May 94	17:41:00	819.237	1.4
ra277	McDonald 0.9 m	AK	–	8 Mar 92	3:41:20	19.667	4.5
ra279	McDonald 0.9 m	AK	–	9 Mar 92	2:24:20	20.620	5.6

Observers: SJK = S. J. Kleinman, DAHB = D. A. H. Buckley, JCC = J. C. Clemens, OG = O. Giovannini, DOD = D. O'Donoghue, MAW = M. A. Wood, DJS = D. J. Sullivan, KW = K. Wu, TKW = T. K. Watson, MSO = M. S. O'Brien.

included in this study. They were reduced as described in Paper I, and we list them in Table 2 for completeness. Re-analysing the XCOV 7 data with those two runs made only small changes (within the quoted errors) to the published results.

2.2 Comparison stars

In typical WET observations, the comparison stars serve to monitor the quality of the photometric conditions, and their data are not necessarily used during the reductions. This is possible since the periods of the light variations of typical WET targets, i.e. white dwarfs, are (except in the presence of clouds) significantly shorter than the time-scales of variations of sky transparency. However, this is not the case for CD−24 7599, whose pulsation periods found in Paper I were between 38 and 53 min. Therefore we intended to make use of the comparison star data to compensate for atmospheric effects as often as possible; however, since this can introduce errors, we proceeded with caution, as follows.

We selected three possible comparison stars: C1 = SAO 176755 was chosen to be the primary comparison object, since its spectral type of F0 suggests that it has similar colours to the target. Hence it could also be a δ Scuti star and its photometric constancy must be checked carefully. SAO 176755 can only be observed in channel 2 for telescopes with apertures of about 1 m. Consequently, we further selected the star GSC 6589−0348 as C2 for larger telescopes and C3 = CD−24 7591 for smaller telescopes. We did not have spectral types for C2 and C3 available, but a comparison of their

Table 3. $UBV(RI)_c$ photometry for the comparison stars.

Star	V	B−V	U−B	V−R	V−I
C1	10.17	0.416	0.008	0.241	0.479
C2	12.97	0.707	0.181	0.444	0.879
C3	11.26	1.093	1.015	0.670	1.254

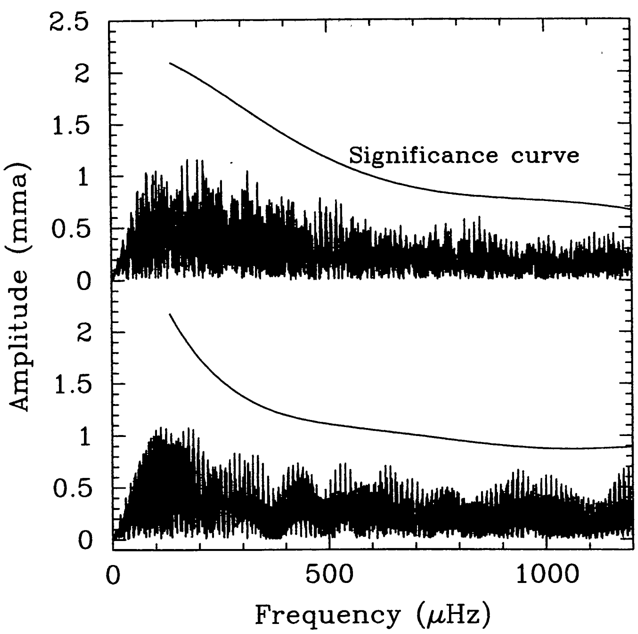

Figure 1. Amplitude spectra of the reduced channel 2 star data. Upper panel: C1 = SAO 176755; lower panel: C3 = CD−24 7591. There is no evidence for variability of either of these stars in the investigated frequency range, as can be judged by comparison with the curve, above which we regard a peak to be significant.

magnitudes on the Palomar plates suggested that they are neither extremely hot nor very cool objects.

Still, it was felt desirable to obtain colour photometry of the comparison stars. In 1995 March, GH acquired $UBV(RI)_c$ photometry of the three stars as well as of a number of faint E-region standards at the 0.5-m telescope of the South African Astronomical Observatory. The results are summarized in Table 3, from which we can estimate that C1 is an early to mid-F star, C2 has early to mid-G spectral type and C3 is a mid-K dwarf. C2 and C3 are clearly too cool to be inside the instability strip. On the other hand, reddening might put C1 inside the instability strip. Therefore, $uvby\beta$ photometry was also obtained for C1 (Handler 1995b), showing that it is not likely to be a short-period pulsating variable.

2.3 Constancy of the comparison stars

Before reducing the programme star data, we examined the comparison stars for variability. A search for variations with time-scales of a day or longer, as well as for possible variations occurring on time-scales of several hours, gave negative results. Moreover, we only found occasional small (< 3 per cent) signs of photomultiplier tube drift, suggesting high long-term stability of the instruments used.

It is most important to check the constancy of the comparison stars in the frequency range of interest for the programme star before constructing differential time series. Therefore we first examined the extinction-corrected data for transparency variations by comparing the channel 1 and 2 measurements. Those runs where we found transparency variations superposed on both the variable and comparison star data were set aside. For the remaining runs, we summed the channel 2 data in 120-s bins (as we will do later with the variable star data), converted the time of measurement into Heliocentric Julian Date (HJD), and calculated amplitude spectra for these data (Fig. 1).

We only plotted the amplitude spectra for comparison stars C1 and C3, since C2 was observed only for about 3 h during the WET run. Consequently, C2 was *not* used further in our reductions. C1 and C3 are constant. No peak in Fig. 1 even approaches the level at which we would consider it to be real (amplitude signal-to-noise ratio of 4); for the definition of this criterion see Breger et al. (1993). The shape of the significance curves is typical for variations in sky transparency ($1/f$-component) plus scintillation noise.

The unit that we usually adopt in this study to express intensity amplitudes is milli-modulation amplitude (mma); it corresponds to a fractional modulation of 10^{-3} of the mean intensity. Power spectra are labelled in micro-modulation power (μmp), where 1 μmp = $(1\ \mathrm{mma})^2$.

We should comment on the noise level that we achieved in the low-frequency domain: in Paper I we showed that WET performs very well for frequencies lower than 1000 μHz. We found the observing technique to become unreliable for frequencies lower than 80 μHz, but capable of discovering variability with amplitudes of about 2.5 milli-modulation amplitudes (mma) between 80 and 230 μHz. Examining Fig. 1, we note that the noise level achieved here is even lower than that in Paper I. We can now confidently assert that our detection limit between 100 and 250 μHz for the present data set is around 1.5 mma (note that each panel in Fig. 1 contains only about 30 h of measurement). The low-frequency cut-off can be estimated to be near 120 μHz. Not surprisingly, this is somewhat higher than in Paper I, since the runs analysed here are shorter on the average.

2.4 Reduction of the programme star time series

Owing to the low count rates no correction for coincidence losses was required. Sky subtraction was performed by fitting polynomials or splines to the sky measurements of the two-channel instruments, and subtracting those fits from the data. For three-channel data, the sky measurements were multiplied by a gain ratio determined from the cross-calibrations for each of the channels. Then they were subtracted from the channel 1 and 2 data on a point-by-point basis. However, the time series of the sky measurements was smoothed whenever possible, in order not to introduce additional scatter to the data.

Having shown that our comparison stars are constant in light, we can finally construct the time series of our measurements of CD−24 7599. Extinction corrections were performed by fitting a straight line to the magnitude versus air mass plot of the data in both channels. The intensity time series were normalized by dividing by the average count rate.

Whenever necessary, transparency variations were compensated for by dividing the time series for CD−24 7599 by that of C1 or C3. Depending on the time-scale of the transparency variations, some smoothing of the comparison star data was applied. The degree of smoothing was chosen to give the lowest scatter in the variable star light curve. In this way it is sometimes also possible to correct carefully for thin clouds. Special care was taken not to introduce artefacts during these corrections.

Finally, all the measurements were summed into 120-s bins, and the times of measurement of CD−24 7599 were converted into HJD. The resulting light curves are shown in Fig. 2 together with a 14-frequency fit that we derive in the next section. The two additional runs acquired in 1992 are included in Fig. 2 with the 14-frequency fit for the XCOV 7 data. The light curves are plotted exactly on the same scale and by using the same units as in Paper I.

In total, 92 h of photometric data were acquired during this run, corresponding to a duty cycle of 27 per cent. Considering that CD−24 7599 was only the third priority object, and that the coverage for the first priority target during this run was the best ever achieved (Nather 1995), this number of data is remarkable and emphasizes one particular strength of the Whole Earth Telescope operation: the ability to obtain good results for multiple targets.

2.5 Colour photometry of CD−24 7599

Since mode identification for δ Scuti stars depends critically on the estimation of the radial order of the excited modes and thus depends on the star's luminosity, gravity and temperature, the latter values must be well known. Therefore we carried out additional colour photometry of CD−24 7599.

GH acquired Strømgren as well as Johnson–Cousins photometry with the 0.5-m telescope at SAAO (see also Section 2.1 and Handler 1995b), while EP and PN obtained measurements of the star in the Geneva system with the 0.7-m Swiss telescope at the European Southern Observatory. The results of the new Strømgren photometry were combined with those reported in Paper I and are summarized together with the other colour photometry in Table 4.

2.6 Spectroscopy

Further constraints for pulsational models and for mode identification of a δ Scuti star can be gathered from the object's rotational velocity and from its metal abundance. Consequently, GH took high-resolution spectra of CD−24 7599 with the Cassegrain Echelle spectrograph attached to the McDonald Observatory 2.1 m telescope on 1996 March 28 and 30. A wavelength range of 4290–4790 Å was covered with an effective resolution of $R \approx 50\,000$.

The spectra were reduced using the standard IRAF procedures and were added together into a 120-min exposure. The rotational and the radial velocity of CD−24 7599 were determined by using the program ROTATE (Piskunov 1992) which yielded $v \sin i = 52 \pm 2$ km s^{-1} and $RV = +72 \pm 2$ km s^{-1}. Furthermore, from an abundance analysis of the elements Fe, Ti and Mg, carried out with the program package Abundance Analysis Procedure (Gelbmann 1995), we estimate [M/H] $= 0.0 \pm 0.2$.

3 FREQUENCY ANALYSIS

Our frequency analysis was performed using the program PERIOD (Breger 1990), the main features of which were described in Paper I. We first calculated a spectral window of our data (shown in the uppermost panel of Fig. 3). This spectral window is not as good as usually achieved by WET, but we keep in mind that CD−24 7599 had only third priority during this run, so we regard the window to be more than satisfactory.

We then computed power spectra of the original data as well as of pre-whitened light curves (Fig. 3). Pre-whitening was done by subtracting a synthetic light curve from the data by simultaneously optimizing the frequencies, amplitudes and phases of previously identified periodicities.

In Fig. 3 we have indicated the seven pulsation frequencies reported in Paper I. As can easily be seen from a comparison with fig. 5 of Paper I, conspicuous amplitude variations occurred within the two years between the two WET runs. However, all pulsation modes found earlier are still present, although we would not have been able to detect unambiguously more than four of these modes based only on the new data set. Moreover, f_4 and f_6 have very low amplitudes in the new data. On the other hand, the lowest panel of Fig. 3 clearly shows that the residuals and the shape of the significance curve are by no means consistent with noise caused by variations in sky transparency and by scintillation. Further pulsation frequencies must be present, a conclusion that we already reached in Paper I.

Since our available data set is now larger, we can attempt to determine at least some of the additional frequencies. Because of the amplitude variations we need to be careful. Thus we calculated synthetic light curves by first optimizing the frequencies for the whole data set, and then subtracting these fits by locking the values and the phases of the frequencies over the two years, but allowing the amplitudes to be different in the two data sets. This results in somewhat higher formal residuals between light curve and fit, but it increases the reliability of the result by reducing the number of free parameters. We note that allowing the amplitudes in the solution to vary avoids the problem of picking up spurious frequencies caused by the amplitude variations. Moreover, fixing the phases in the pre-whitening procedure of the combined data set will also not cause artefacts. In case of (small) frequency/phase variations between the two WET runs a 'mean' frequency will be obtained, completely accounting for such effects.

Consequently, we removed such an eight-frequency fit from the data. However, severe aliasing is present, since the two data sets are of 11- and 14-d duration, respectively, spaced by about 800 d. Therefore we determined the residuals between the light curve and our fit for several trial frequencies, and adopted the value that yielded the lowest residuals. Although such an approach can only result in formal frequency values, we believe that it is much more credible than other procedures (especially in the presence of amplitude variations), e.g. simply adopting the highest peak in the original or pre-whitened power spectra.

We calculated the power spectrum of the residuals and discovered several significant peaks. Following the procedure above, we determined the values of these frequencies step by step (checking whether new frequencies affect the other values and adjusting them, if necessary) by calculating a simultaneous n-frequency fit to the data, until no new frequencies could be identified with confidence. Some steps of the pre-whitening process are shown in Fig. 4; the significance curve in the lowest panel clearly confirms our detections. The resulting 14-frequency fit to the data of both WET runs is listed in Table 5. The amplitude variations of f_1, f_2, f_3, f_4 and f_9 are considered to be significant, and f_6, f_{11} and f_{14} are also likely to have changed their amplitudes within the two years between the two WET runs. We shall discuss the amplitude variations in detail elsewhere (Handler et al., in preparation), including additional time-series photometry. It should also be noted that the signal-to-noise ratio of the modes (determined following Breger et al. 1993) detected in Paper I is now larger (resulting in 12 formally significant peaks), since part of the

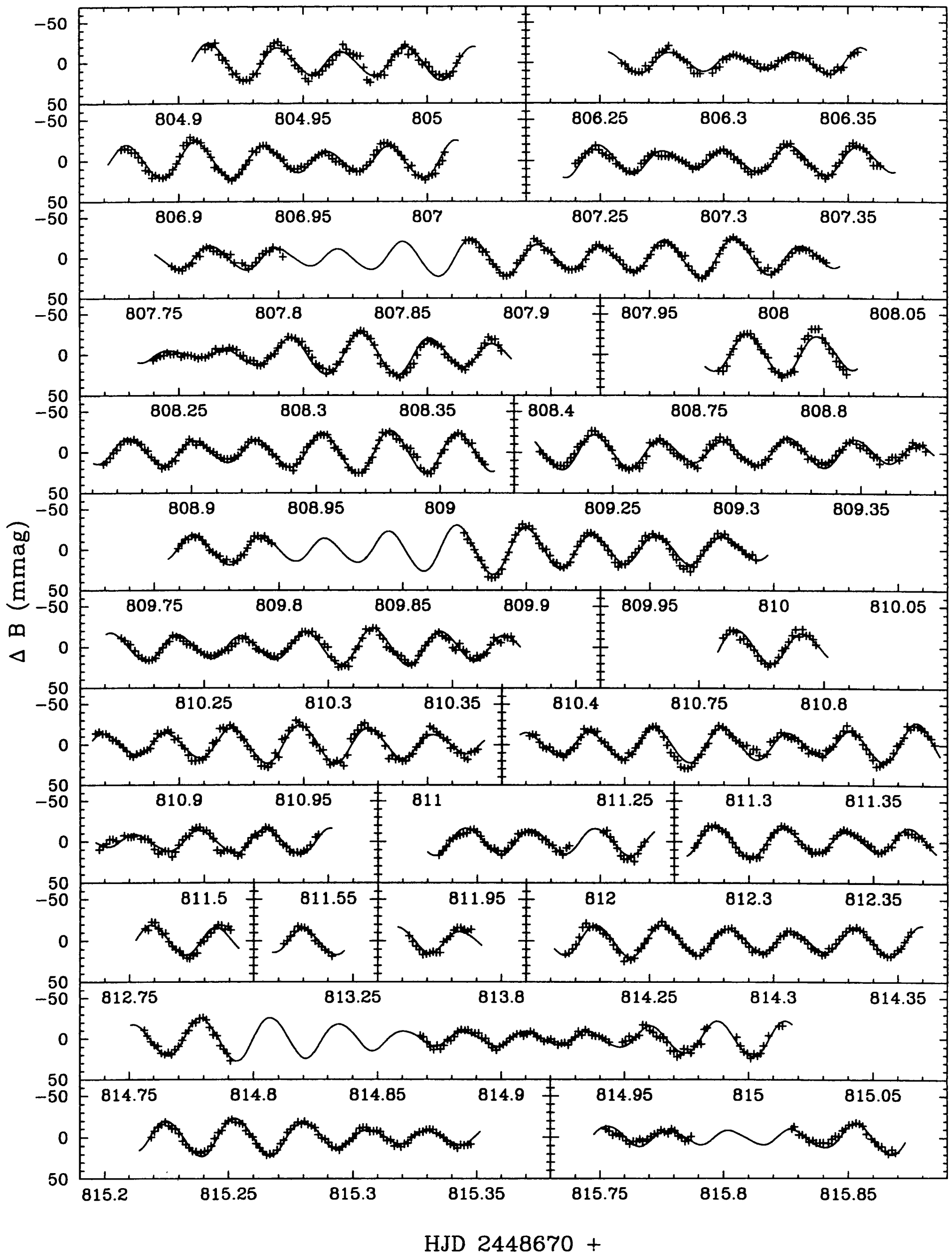

Figure 2. *B* light curves and the corresponding 14-frequency fit (derived in Section 3) for the new WET data on CD−24 7599. The two older runs plus the 14-frequency fit taken from Paper I are also shown.

residual 'noise' left in the old solution is due to frequencies intrinsic to CD−24 7599.

After removing our new 14-frequency solution from the data, the residual power spectra are still not consistent with white noise. Although non-white noise could in part be generated as an artefact of pre-whitening, we think that there are still intrinsic frequencies left in the residuals. Our new frequency solution leaves an rms residual of 4.0 mma per single measurement in the XCOV 7 data and 3.5 mma per single measurement in the XCOV 10 data. The better quality of the new data is attributable to a number of reasons: the use of three-star photometers at some sites, the ability to correct carefully for transparency variations, the facts that CD−24 7599 was observed in channel 1 (less bad points), that the measurements were taken at lower average air mass, etc.

In the second lowest panel of Fig. 4, we can identify a peak near 340 μHz, which is significant according to our convention. However, this peak is only prominent in the 1992 data, while there seems to be just a normal noise peak at this frequency in the 1994 data. This prevents us from suggesting that the 340-μHz peak is real. It should also be noted that this peak is very near to aliases of f_3 and f_4 and could therefore be affected during pre-whitening, since the new data have a more complicated window pattern. The same comment applies to a peak near 398 μHz, which was already regarded to be promising in Paper I. We hasten to add that we would not have been able to detect all frequencies in Table 5 without pre-whitening. We consider pre-whitening to be a very useful method, but only when applied carefully.

In Paper I, we reported the detection of linear combination frequencies in our power spectra. Consequently, we also examined

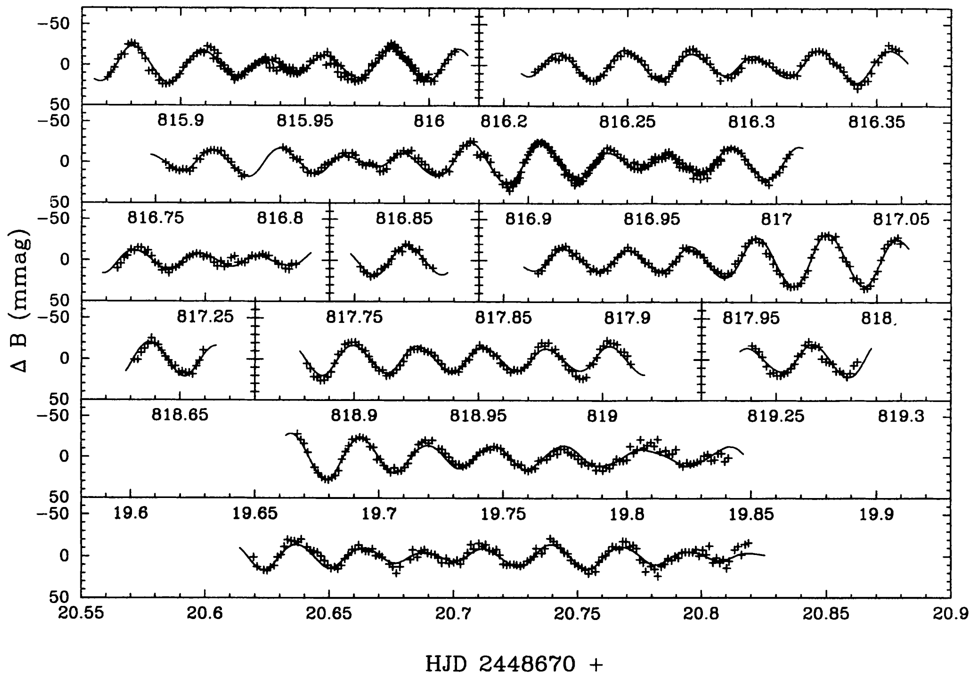

Figure 2 – *continued*

Table 4. Johnson–Cousins, updated Strømgren–Crawford and Geneva photometry of CD−24 7599.

V	B−V	U−B	V−R	V−I	
11.50	0.343	0.228	0.204	0.436	
±0.01	±0.007	±0.010	±0.007	±0.010	
V	b−y	m_1	c_1	β	
11.50	0.225	0.150	0.982	2.871	
±0.01	±0.008	±0.013	±0.013	±0.015	
m_V	B2−V1	d	m_2	g	Δ
11.47	0.144	1.318	-0.504	0.089	0.455
±0.01	±0.008	±0.014	±0.014	±0.014	±0.014

this data set for such peaks. The power spectrum in the respective frequency range is shown in Fig. 5 (after pre-whitening of the 14-frequency solution in order to avoid spectral leakage into the high-frequency domain: see Breger et al. 1996), and some linear combination frequencies can again be discerned, although they are not significant. We note, however, that the noise in this frequency region is not white as well (which can best be seen by examining the shape of the significance curve), suggesting that intrinsic frequencies are present in this domain. We regard this as a confirmation of the presence of linear combination frequencies in the light curves of CD−24 7599.

We also analysed the behaviour of the star at high frequencies. In Paper I, we briefly reported a null result for a search for frequencies similar to those of rapidly oscillating Ap stars or solar-like oscillations. Recently, Breger et al. (1996) examined the high-frequency domain for the δ Scuti star FG Vir in detail. They did not find evidence for variability with frequencies between 1 and 10 mHz.

In Fig. 6, we show a power spectrum of the combined, unbinned XCOV 7 and XCOV 10 data at high frequencies. Pre-whitening in the low-frequency domain was again performed to avoid spectral leakage to higher frequencies. In the 1992 data from SAAO, a spurious periodicity due to a periodic tracking error was removed before this analysis was performed. This tracking error was also found in other studies and has been corrected (see Martinez 1993). Consequently, no such effect was found in the 1994 SAAO data. There is no evidence for high-frequency variability intrinsic to CD−24 7599.

Finally, we searched for a characteristic frequency spacing between the modes of CD−24 7599, as this could indicate either rotational splitting or the excitation of consecutive radial overtones.[1] To search for such a splitting, we performed a Fourier analysis of our pulsation frequencies, assuming unit amplitude for all peaks. The latter makes the method insensitive to effects of mode driving, amplitude variations, inclination, etc. Consequently, we will obtain information about possible regular frequency spacings present, in analogy to the spectral window of photometric time series: if the data points are equally spaced, the window has maxima at the sampling frequency and its harmonics (see Kurtz 1983 for an illustration). The result of this analysis is shown in Fig. 7.

The highest peak in Fig. 7 corresponds to a frequency spacing of 26 μHz, and the two peaks next to it represent spacings near 18 and 14 μHz. To assess the significance of this detection, we created artificial power spectra consisting of 13 random frequencies between 310 and 445 μHz and searched them for characteristic spacings between 20 and 35 μHz with the same method as described above. In less than 3 per cent of all trials we obtained peaks at least as high as the 26-μHz peak in Fig. 7. Therefore we consider the detection of a characteristic frequency spacing of 26 μHz in the power spectra of CD−24 7599 to be statistically significant. The meaning of this result will be discussed in Section 4.2.

[1]Of course, for low-overtone pulsators such as δ Scuti stars, one cannot expect to find the asymptotic frequency spacing. However, the deviations from a regular frequency spacing are small even for low radial overtones, and so some regularity in the power spectrum can be expected if a large number of possible pulsation modes are excited to visible amplitude.

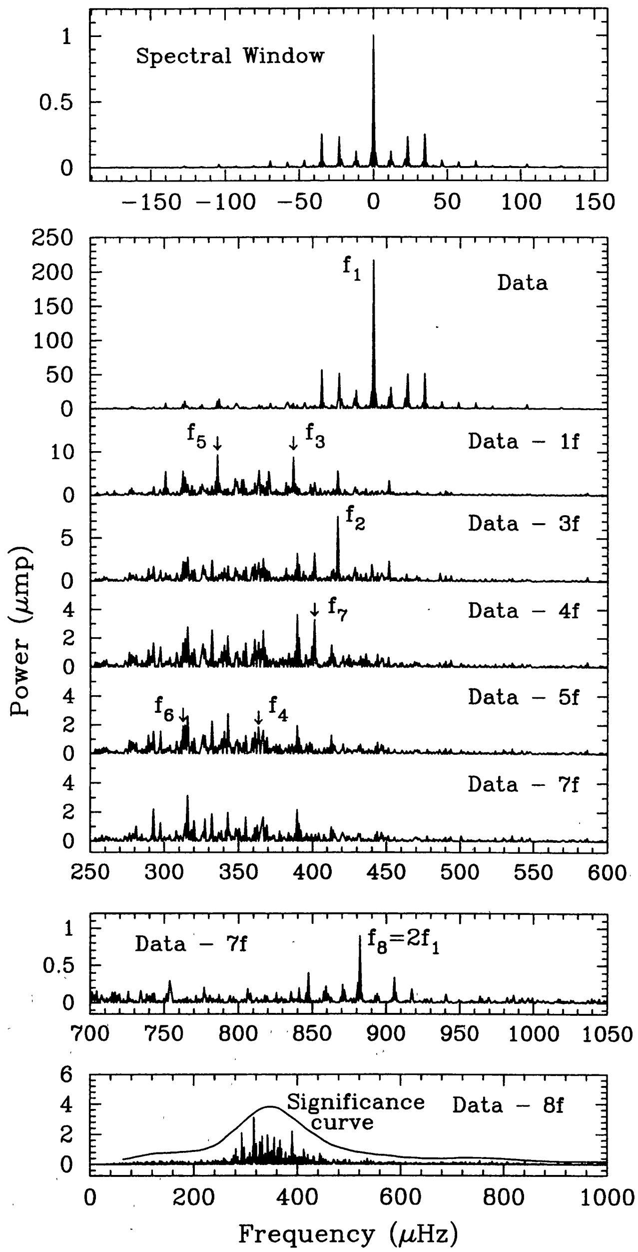

Figure 3. Spectral window and power spectra for the XCOV 10 data of CD−24 7599. The peaks already identified in Paper I are indicated with the same designations as in the first paper.

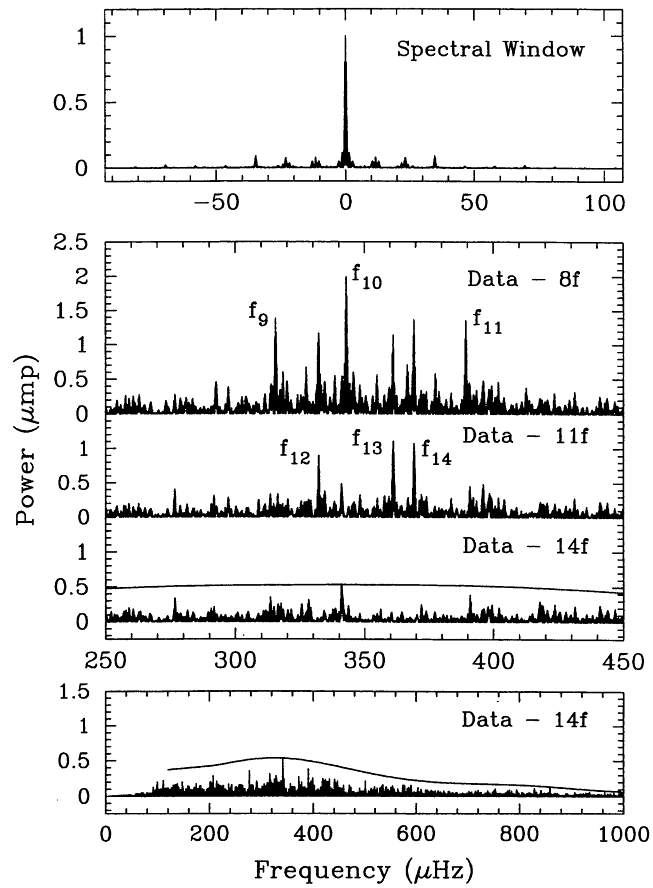

Figure 4. Spectral window and power spectra for the combined XCOV 7 and XCOV 10 residuals of CD−24 7599. Six new pulsation frequencies are found.

4 THE POSITION OF CD−24 7599 IN THE HR DIAGRAM

4.1 Colour photometry

With the new colour photometry at hand (Table 4), we can revise the position of CD−24 7599 in the HR diagram. We start with a check of the consistency of the Strømgren–Crawford and Johnson–Cousins data.

Applying the calibrations of Crawford (1979) to the Strømgren–Crawford photometry, we determine $E(b-y)=0.154$, $(b-y)_0=0.071$, $\delta m_1=0.003$ and $\delta c_1=0.039$. This also yields $M_v=1.97$. A comparison of $(b-y)_0$ and $E(b-y)$ with the $UBV(RI)_c$ photometry of Table 4 by using the relations of Caldwell et al. (1993) suggests that the measurements in these two systems are consistent with each other within the observational uncertainties.

Now we can use Kurucz's (1991) model atmospheres to estimate $T_{\rm eff}=8400\pm150$ K and $\log g=4.25\pm0.15$ for CD−24 7599, which correspond to a slightly more evolved evolutionary state than suggested in Paper I (however, also with the new data, the star is still close to the zero-age main sequence, or ZAMS). Furthermore, Smalley's (1993) calibration supplies $[M/H]=0.05\pm0.15$.

Making use of the Geneva photometry, we can deredden $B2-V1$, since $E(b-y)$ is known (all other Geneva indices listed in Table 4 are reddening-free). With a ratio $E(B2-V1)/E(b-y)=1.146$, this yields $(B2-V1)_0=-0.032$. Next, we apply the new calibrations of Künzli (1994) and derive $T_{\rm eff}=8250\pm150$ K and $\log g=4.25\pm0.15$. From the reference sequence of Hauck et al. (1991), we infer $\Delta m2=-0.041$. Berthet's (1990) calibration then provides $[M/H]=-0.19\pm0.14$.

Thus the colour photometry suggests that CD−24 7599 is a main-sequence star with $T_{\rm eff}=8300\pm200$ K and $\log g=4.25\pm0.15$, and with approximately solar metal abundance. The error bars given here were chosen to yield best agreement between the different determinations and are therefore conservative. According to the results above, the values for the pulsation constants Q_i of the different modes, as derived and listed in Paper I, decrease by 19 per cent (or 1σ).

Table 5. Frequencies of the δ Scuti star CD−24 7599 with an amplitude signal-to-noise ratio larger than 4. The frequencies given yield the lowest residuals between observed light curve and fit, but can only be seen as formal values. The frequency errors are estimated from our trial fits and should be realistic; they are integer multiples of the spacing of the aliases (1/799 d).

	Frequency		Amplitude (1992)		S/N	Amplitude (1994)		S/N
	(μHz)	(cycles/day)	(mma)	(mmag)	1992	(mma)	(mmag)	1994
f_1	441.090 ± 0.014	38.1101 ± 0.0013	10.6 ± 0.2	11.5 ± 0.2	51.1	14.7 ± 0.2	15.9 ± 0.2	52.8
f_2	416.808 ± 0.029	36.0122 ± 0.0025	9.2 ± 0.2	10.0 ± 0.2	41.6	3.0 ± 0.2	3.3 ± 0.2	10.5
f_3	386.982 ± 0.029	33.4353 ± 0.0025	5.9 ± 0.2	6.4 ± 0.2	25.1	3.5 ± 0.2	3.8 ± 0.2	12.0
f_4	363.339 ± 0.029	31.3925 ± 0.0025	3.5 ± 0.2	3.8 ± 0.2	14.6	1.7 ± 0.2	1.9 ± 0.2	6.1
f_5	335.590 ± 0.029	28.9950 ± 0.0025	2.2 ± 0.2	2.4 ± 0.2	9.5	2.5 ± 0.2	2.7 ± 0.2	8.3
f_6	312.533 ± 0.029	27.0028 ± 0.0025	2.2 ± 0.2	2.4 ± 0.2	9.5	1.5 ± 0.2	1.6 ± 0.2	5.3
f_7	401.224 ± 0.043	34.6657 ± 0.0038	2.1 ± 0.2	2.2 ± 0.2	8.9	1.9 ± 0.2	2.0 ± 0.2	6.3
$f_8 = 2f_1$	882.180 ± 0.043	76.2203 ± 0.0038	0.7 ± 0.2	0.8 ± 0.2	5.0	1.0 ± 0.2	1.1 ± 0.2	8.2
f_9	315.550 ± 0.159	27.2635 ± 0.0138	0.9 ± 0.2	1.0 ± 0.2	3.8	1.7 ± 0.2	1.9 ± 0.2	6.1
f_{10}	342.820 ± 0.087	29.6196 ± 0.0075	1.4 ± 0.2	1.5 ± 0.2	5.8	1.2 ± 0.2	1.3 ± 0.2	4.1
f_{11}	389.313 ± 0.145	33.6367 ± 0.0125	1.1 ± 0.2	1.2 ± 0.2	4.5	1.6 ± 0.2	1.7 ± 0.2	5.4
f_{12}	332.153 ± 0.159	28.6980 ± 0.0138	1.0 ± 0.2	1.1 ± 0.2	4.2	1.3 ± 0.2	1.5 ± 0.2	4.7
f_{13}	361.150 ± 0.188	31.2033 ± 0.0163	1.3 ± 0.2	1.4 ± 0.2	5.3	1.0 ± 0.2	1.1 ± 0.2	3.4
f_{14}	369.285 ± 0.116	31.9062 ± 0.0100	0.9 ± 0.2	1.0 ± 0.2	3.8	1.5 ± 0.2	1.7 ± 0.2	5.3

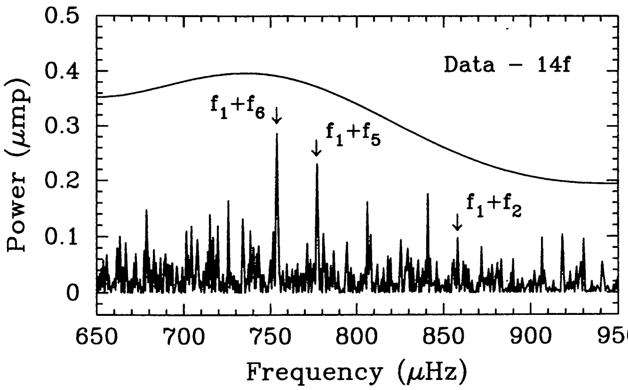

Figure 5. Power spectra for the XCOV 10 data of CD−24 7599 in the range where linear combination frequencies can be found. Some of these frequencies are again present.

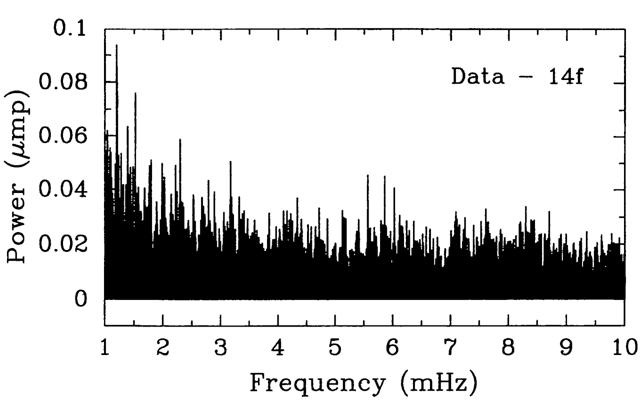

Figure 6. Power spectra of the combined XCOV 7 and XCOV 10 data of CD−24 7599 in the high-frequency domain. No convincing evidence for high-frequency oscillations of the star can be found.

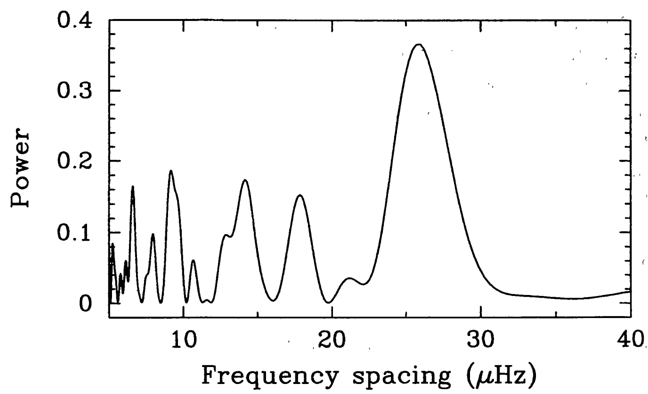

Figure 7. Search for the presence of a regular frequency spacing within the 13 pulsation modes of CD−24 7599. The highest peak corresponds to a frequency spacing of 26 μHz and is statistically significant (see text).

4.2 Model calculations

Given the observed pulsation frequencies, temperature, surface gravity and metallicity, we now face the theoretical challenge of trying to construct stellar models that will satisfy the observationally derived constraints. To compute the models, we have used the standard stellar evolution code which was developed in its main parts by B. Paczynski, M. Kozlowski and R. Sienkiewicz. The same code was applied previously in the study of FG Vir (Breger et al. 1995a). We used the latest versions both of the OPAL opacity tables (Iglesias et al. 1995) and of the OPAL equation of state (Rogers, Swenson & Iglesias 1996) which were copied from Lawrence Livermore National Laboratory by file transfer protocol (FTP). The effects of slow solid-body stellar rotation were taken into account together with the assumption about conservation of the global angular momentum during the evolution of the star from the ZAMS.

We calculated the models assuming an initial hydrogen abundance $X = 0.70$ and a heavy element abundance $Z = 0.02$. We used the standard mixing-length formalism for convection adopting the parameter $\alpha = 1$. This choice has a negligible effect on the model's parameters (see also Audard & Provost 1994). Stellar masses from 1.75 to 2.05 $M_\odot$ were considered in steps of 0.05 $M_\odot$. Since we only have a lower limit to the rotational velocity of CD−24 7599, we computed three sequences with $v_{rot} = 75$, 125 and 175 km s^{-1} on the ZAMS. For this choice of parameters, the models that fit the values of T_{eff} and log g derived in Section 4.1 are in the main-sequence stage of stellar evolution. We note that the assumption of global angular momentum conservation results in only a small change of the rotational velocity during main-sequence evolution: the model with $v_{rot} = 100$ km s^{-1} on the ZAMS will have $v_{rot} = 93$ km s^{-1} at the end of the main-sequence stage.

For the models considered we performed a linear non-adiabatic analysis of low-degree oscillations ($\ell \leq 2$). The effects of slow rotation on the oscillation frequencies were calculated up to second order in the rotational velocity using the method developed by Dziembowski & Goode (1992). In these oscillation calculations we neglected the Lagrangian perturbation of the convective flux. The choice of α has again a negligible effect on mode frequencies in the frequency range of interest, but has a non-negligible effect on mode stability. For the models used here an increase of α promotes instability and results in some increase of the frequency range of the unstable modes.

We are now in a position to apply two different methods to determine the position of models matching CD−24 7599 in the HR diagram. First, we performed a stability analysis of the pulsation modes: as a δ Scuti star model evolves from the ZAMS, instability first occurs at high p-mode frequencies (and high overtones). As the radius of the star increases, the excited p-mode spectrum shifts to lower frequencies. Additionally, lower radial overtones become excited as well (this is illustrated, for example, by Dziembowski 1995).

Consequently, we can compare the unstable model frequencies with the modes actually excited to observable amplitude (assuming that there are no further modes outside the range of pulsation frequencies detected so far) as the model evolves, and we can derive a range of possible effective temperatures for given mass. We performed this procedure for models in the range of 1.75–2.00 $M_\odot$. For more massive models the theoretically expected and observed frequency ranges did not match anymore; most of the modes between 312 and 441 μHz were stable. To account for the unknown rotation rate of CD−24 7599, we averaged the results of the stability analysis over the different rotational velocities of the models and increased the error bar in the effective temperature accordingly.

For lower mass models, the range of unstable model frequencies becomes larger than the observed one, and therefore the error size of the determination of possible model effective temperatures increases. Moreover, this comparison can only be done for model frequencies of $m = 0$. Thus rotational splitting may affect the result. We incorporated this in our error estimate. The position of models matching the observed frequency range of CD−24 7599 will be displayed in Fig. 9 below.

The second method to determine the position of the star in the HR diagram uses the frequency spacing derived in Section 3. Let us first explain its origin. If it were caused by rotational splitting, CD−24 7599 would need to rotate with $v \approx 190$ km s^{-1} (adopting the values of T_{eff} and log g determined in Section 4.1 and $M = 1.85\,M_\odot$). However, at such large rotation rates the rotationally split pattern becomes asymmetric due to second-order effects of rotation. Therefore the detection of a 26-μHz spacing due to rotational splitting is not expected.

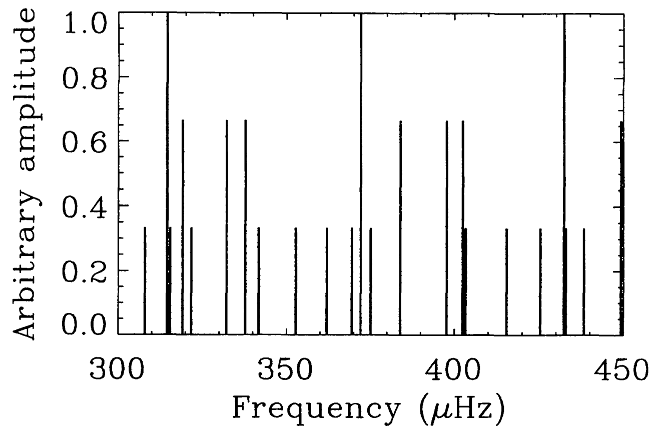

Figure 8. Schematic amplitude spectrum of $\ell = 0$–2 and $|m| \leq \ell$ pulsation frequencies for one possible model of CD−24 7599 (see text for its parameters). The modes are of radial order $k = 3$–5. Peaks with an amplitude of 1.0 represent radial modes, those with 0.67 amplitude correspond to dipole mode frequencies, while peaks with amplitudes of 0.33 are at frequencies of quadrupole modes.

Another possibility is that this frequency spacing is caused by the presence of consecutive radial overtones of the same ℓ. For illustration, we computed a model of CD−24 7599 with parameters close to those inferred in Section 4.1 ($M = 1.85\,M_\odot$, log $T_{eff} = 3.920$, log $L = 1.147$, thus log $g = 4.20$) with $v_{rot} = 75$ km s^{-1}, and plot its pulsation frequencies in Fig. 8.

As can be seen, consecutive modes of equal ℓ and m have approximately the same frequency spacing even at low overtones. However, a spacing of 26 μHz would correspond to a post-main-sequence evolutionary state of the star (e.g. Heller & Kawaler 1988), even though we do not measure the asymptotic value. Modes of consecutive radial order in Fig. 8 have a spacing of about 60 μHz.

On the other hand, the $m = 0$ components of $\ell = 2$ modes are approximately intermediate in frequency compared with the $\ell = 1$ modes of the same k and $k - 1$. Consequently, if modes of both $\ell = 1$ and $\ell = 2$ were excited in CD−24 7599, we would expect to see half of the spacing of consecutive overtones of the same ℓ (a suspicion which already emerges from a close look at Fig. 8). To check this idea, we performed the Fourier analysis described at the end of Section 3 for the model frequencies. The considered model frequency range matched the range actually excited in the star.

The resulting power spectra closely resembled Fig. 7. By comparing the location of the highest peaks in the spectral window with the model frequencies, we verified that this analysis indeed returns a value for half the frequency spacing of modes of consecutive radial overtones with the same ℓ and m. Now we can also explain the peaks at spacings of 18 and 14 μHz in Fig. 7: they are harmonics of the basic spacing of 54.0 μHz, like the 26-μHz peak.

We performed several further tests to verify the validity and applicability of this analysis tool. For instance, we determined the location of the highest peak for several trial model frequency spectra when we assumed different rotation rates (which change the 'noise properties'). We found that the method is reliable when carefully applied.

Finally, we determined the error size for a frequency spacing of 54.0 μHz. We considered a number of model frequency spectra, randomly selected 13 modes in the range of 310–445 μHz and analysed them in the same way as the observed frequencies. From these simulations we estimate that the accuracy of our determination is ±2.3 μHz. We would like to make a technical comment here: the frequency spacing analysis performed above seems to be a very powerful tool to investigate the frequency spectrum of δ Scuti stars and other multimode pulsators. However, it must be noted that the frequency spectrum of CD−24 7599 is particularly well suited to this method: the star has a large number (about 40 per cent) of all possible ($\ell \leq 2$) modes excited (cf. Fig. 8), and pulsates in only a few radial overtones. For stars with only a few observed modes or for objects whose theoretical frequency spectra are very dense, we do not expect this technique to be very helpful.

As the mean frequency spacing of 54.0 ± 2.3 μHz found for CD−24 7599 is a measure of the sound crossing time through the object, we can use it to determine its mean density. To be as objective as possible, we decided to adopt the following procedure: we selected a sequence of five models along their main-sequence evolutionary track in the HR diagram in steps of 0.005 in log $T_{\rm eff}$, roughly centred on a frequency spacing of 54 μHz in the 300–450 μHz range. The same mass and rotational velocity ranges as for the stability analysis were considered. The pulsation modes were then searched for equal frequency spacings with the Fourier technique described above. We used all modes in the frequency range excited in CD−24 7599. This is a worst case assumption: rotationally split modes as well as g modes introduce 'noise', and therefore the error bars that we obtain are conservative. As in the stability analysis, we found a dependence of the resulting frequency spacing on the star's rotation rate. This was again taken into account when estimating the error size.

As the model evolves along the main sequence, the sound traveltime across the object increases and thus the spacing of consecutive overtones of the same ℓ and m decreases. Consequently, we can, at given mass, infer the effective temperature of the model matching the 54.0-μHz spacing best by fitting a straight line to a frequency spacing versus effective temperature plot.[2] With these parameters in hand, we can easily calculate the mean density of the best matching model.

We found no dependence of the mean density of the best matching models on mass, as may be suspected. This allows us to determine the mean density of the most promising models of CD−24 7599 to be $0.246 \pm 0.020\,\bar{\rho}_\odot$. The main contribution to the size of this error comes from the uncertainty of the mean frequency spacing of the observed modes. We note that there could be systematic errors in this determination, e.g. the star may have a metallicity different from the assumed $Z = 0.02$. Then the evolutionary tracks of the models would change and the instability would shift to (slightly) different overtones. Therefore the ratio of the determined frequency spacing to the asymptotic value and thus to the mean density would change. However, some tests (like employing a different equation of state in the models) suggest that this would alter our results only within the quoted errors. Anyway, the results of model calculations reported here are only a first step in the seismological investigation of the star; a more complete account will be given by Pamyatnykh et al. (in preparation).

Before we start to point to a definite mode identification, we will compare and discuss our constraints on the position of CD−24 7599 in the HR diagram. They are summarized in Fig. 9.

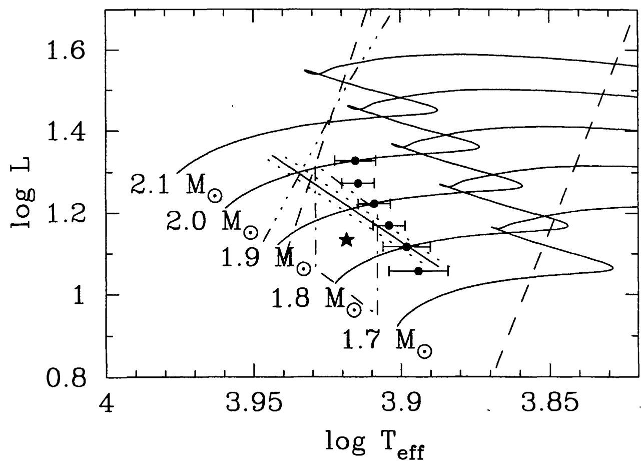

Figure 9. Determination of the position of CD−24 7599 in the HR diagram. Full lines correspond to some of our evolutionary tracks for $Z = 0.02$. The star symbol denotes the position of the star determined from colour photometry, while the dashed-dotted box represents the corresponding error size. The dots with the horizontal error bars are possible positions of the star determined from our stability analysis. The straight line connects models with mean densities of $0.246 \pm 0.020\,\bar{\rho}_\odot$. Finally, the observed red and blue edges of the instability strip taken from Breger (1995, dashed lines) as well as the theoretical blue edge of our models (dashed-triple dotted line) are indicated.

The results of our different independent analyses agree well. The model calculations suggest a slightly more evolved evolutionary state for the star than does the colour photometry, but this is well within the errors. Taking all our constraints together, we infer that CD−24 7599 is in the first half of its main-sequence evolution and is best represented by a model with $Z = 0.02$, $M = 1.85 \pm 0.05\,{\rm M}_\odot$ and $\bar{\rho} = 0.246 \pm 0.020\,\bar{\rho}_\odot$. This yields $R = 1.96 \pm 0.07\,{\rm R}_\odot$ and $L = 14.7 \pm 1.6\,{\rm L}_\odot$, allowing us to infer a distance to the star of 650 ± 70 pc. This seismological distance to CD−24 7599 is as accurate as distance estimates that one can derive for δ Scuti stars in clusters. We also note that independent model calculations by Bradley & Guzik (1996) give results consistent with those presented in this paper.

Now we can compare our pulsation frequencies with those of our best matching models. We define the fundamental radial mode to be $k = 1$. Most of the excited modes are pure p modes, for which three overtones ($k = 4$–6) are present. Consequently, we cannot explain all 13 modes with only $\ell = 0$ and $\ell = 1$. Moreover, it is also impossible that exclusively $\ell = 0$ and $\ell = 2$ modes are seen: otherwise the frequency spacing analysis would have revealed the 54-μHz spacing (and not only its harmonics), since the $m = 0$ component of $\ell = 2$ modes has a frequency only a few μHz different from that of the radial mode with the same k. Thus both $\ell = 1$ and $\ell = 2$ modes must be present.

Turning to rotational splitting, we can infer a lower limit to the star's rotational frequency from its $v \sin i$ and its radius determined above. This yields $\nu_{\rm rot} \gtrsim 5.9$ μHz. Even at this low rotation rate, second-order effects of rotation become important and destroy the frequency symmetry of the rotationally split peaks in the power spectrum. Without any further constraint on the ℓ values of the individual modes, we did not find clues for deciding which modes belong to the same rotationally split multiplets. In this context it should be noted that non-linear calculations for $\ell = 1$ modes (Buchler, Goupil & Serre 1995) predict equal frequency spacings

[2] This assumes that the model evolves along a track described by a straight line in the theoretical HR diagram. For the small temperature range that needs to be considered and for stellar evolution on the main sequence, this is correct within the errors of the determination of the frequency spacing.

within the triplets independently of the stellar rotation rate; an observational examination of this effect has to await definite mode identifications.

Interestingly, in models with mean densities matching that inferred for CD−24 7599, one g mode for $\ell = 2$ is excited at a frequency of about 350 μHz. This mode originates as the g_1 mode on the ZAMS and, since a significant fraction of its kinetic energy comes from the outer part of the convective core, it can be taken as a test for convective overshooting theories (Dziembowski & Pamyatnykh 1991). It is interesting to note that the observed frequency spectrum of CD−24 7599 is denser around 350 μHz than at higher frequencies. This can be taken as evidence that this g_1 mode is actually observed in CD−24 7599. If so, the star becomes particularly interesting for seismology.

5 SUMMARY AND CONCLUSIONS

The δ Scuti star CD−24 7599 has been re-observed with the Whole Earth Telescope. At least 13 pulsation modes are excited in this object. With the help of new colour photometry as well as model calculations, we have shown that the star is best represented by models of solar metallicity with mass $1.85 \pm 0.05\,M_\odot$ and $\bar{\rho} = 0.246 \pm 0.020\,\bar{\rho}_\odot$. We have inferred a seismological distance of 650 ± 70 pc. The star is in the first half of its main-sequence evolution and it pulsates mainly with p modes of $k = 4$–6. Both $\ell = 1$ and $\ell = 2$ modes are present and about 40 per cent of all the possible modes have been detected by us. However, one g_1 mode for $\ell = 2$ may be excited as well, thus making CD−24 7599 an excellent candidate to test convective core overshooting, one of the most important parameters for stellar evolution calculations.

Therefore it is of considerable importance to continue to study the star comprehensively. Detailed theoretical investigations are underway (Pamyatnykh et al., in preparation). Another extended photometric campaign [similar to that for the δ Scuti star FG Vir, for which Breger et al. (1995b) acquired about 550 h of data] to detect even more pulsation modes ought to be undertaken. As already pointed out in Paper I, the observations should be done in more than one filter to be able to determine the ℓ values of the pulsation modes of the highest amplitudes, thus increasing our chances of finding a secure mode identification. Then precision asteroseismology of a normal main-sequence star should be possible.

ACKNOWLEDGMENTS

This work was partially supported by the Austrian Fonds zur Förderung der wissenschaftlichen Forschung under grant S-7304. GH thanks Nathalie Audard for useful comments on a draft version of this paper.

REFERENCES

Audard N., Provost J., 1994, A&A, 282, 73
Berthet S., 1990, A&A, 236, 440
Bradley P. A., Guzik J. A., 1996, BAAS, 27, 1430
Breger M., 1990, Commun. Asteroseism., 20, 1
Breger M., 1995, in Stobie R. S., Whitelock P. A., eds, ASP Conf. Ser. Vol. 76, Astrophysical Applications of Stellar Pulsation. Astron. Soc. Pac., San Francisco, p. 596
Breger M. et al., 1993, A&A, 271, 482
Breger M. et al., 1995a, A&A, 297, 473
Breger M. et al., 1995b, Commun. Asteroseism., No. 83
Breger M. et al., 1996, A&A, 309, 197
Buchler J. R., Goupil M.-J., Serre T., 1995, A&A, 296, 405
Caldwell J. A. R., Cousins A. W. J., Ahlers C. C., van Wamelen P., Maritz E. J., 1993, S. Afr. Astron. Obs., Circ., 15, 1
Crawford D. L., 1979, AJ, 84, 1858
Dziembowski W. A., 1995, in Stobie R. S., Whitelock P. A., eds, ASP Conf. Ser. Vol. 76, Astrophysical Applications of Stellar Pulsation. Astron. Soc. Pac., San Francisco, p. 586
Dziembowski W. A., Goode P. R., 1992, ApJ, 394, 670
Dziembowski W. A., Pamyatnykh A. A., 1991, A&A, 248, L11
Gelbmann M. J., 1995, Commun. Asteroseism., 89, 1
Handler G., 1995a, Baltic Astron., 4, 434
Handler G., 1995b, Inf. Bull. Variable Stars, 4216
Handler G. et al., 1996, A&A, 307, 529 (Paper I)
Hauck B., Jaschek C., Jaschek M., Andrillat Y., 1991, A&A, 252, 260
Heller C. H., Kawaler S. D., 1988, ApJ, 329, L43
Iglesias C. A., Wilson B. G., Rogers F. J., Goldstein W. H., Bar-Shalom A., Oveg S., 1995, ApJ, 445, 855
Kleinman S. J., Nather R. E., Philips T., 1996, PASP, 108, 356
Künzli M., 1994, Master's thesis, University of Lausanne
Kurtz D. W., 1983, Inf. Bull. Variable Stars, 2285
Kurucz R. L., 1991, Van Vleck Obs. Contrib., 11, 27
Martinez P., 1993, PhD thesis, University of Cape Town
Nather R. E., 1995, Baltic Astron., 4, 321
Nather R. E., Winget D. E., Clemens J. C., Hansen C. J., Hine B. P., 1990, ApJ, 361, 309
Piskunov N. E., 1992, in Glagolevskij Y. V., Romanyuk I. I., eds, Stellar magnetism. Nauka, St Petersburg, p. 92
Rogers F. J., Swenson F. J., Iglesias C. A., 1996, ApJ, 456, 902
Smalley B., 1993, A&A, 274, 391

This paper has been typeset from a TEX/LATEX file prepared by the author.

2.2.3 On the frequency and amplitude variations of the δ Scuti star CD−24 7599 (=XX Pyx)

Original paper:

G. Handler, A. A. Pamyatnykh, W. Zima, D. J. Sullivan, N. Audard, A. Nitta, 1998, MNRAS 295, 377

Mon. Not. R. Astron. Soc. **295,** 377–385 (1998)

On the frequency and amplitude variations of the δ Scuti star CD$-$24 7599 (=XX Pyx)

G. Handler,[1★†‡] A. A. Pamyatnykh,[1,2,3] W. Zima,[1§] D. J. Sullivan,[4] N. Audard[5,6†] and A. Nitta[7]

[1] *Institut für Astronomie, Universität Wien, Türkenschanzstraße 17, A-1180 Wien, Austria*
[2] *Copernicus Astronomical Center, ul. Bartycka 18, 00-716 Warsaw, Poland*
[3] *Institute of Astronomy, Pyatnitskaya Street 48, Moscow 109017, Russia*
[4] *Physics Department, Victoria University of Wellington, PO Box 600, Wellington, New Zealand*
[5] *Observatoire de Nice, BP 4229, F-06304 Nice Cedex 4, France*
[6] *Institute for Astronomy, Madingley Road, Cambridge CB3 0HA*
[7] *Department of Astronomy and McDonald Observatory, University of Texas, Austin, TX 78712, USA*

Accepted 1997 October 4. Received 1997 September 29; in original form 1997 August 13

ABSTRACT

We present 132 h of new time-series photometric observations of the δ Scuti star CD$-$24 7599 acquired during 86 nights from 1993 to 1996 to study its frequency and amplitude variations. By using all published observations we demonstrate that the three dominating pulsation modes of the star can change their photometric amplitudes within one month at certain times, while the amplitudes can remain constant within the measurement errors at other times. CD$-$24 7599 also exhibits frequency variations, which do not show any correspondence between the different modes.

The typical time-scale for the amplitude variations is found to be several hundred days, which is of the same order of magnitude as the inverse linear growth rates of a selected model. We find no evidence for periodic amplitude modulation of two of the investigated modes (f_2 and f_3), but f_1 may exhibit periodic modulation. The latter result could be spurious and requires confirmation. The observed frequency variations may either be continuous or reflect sudden frequency jumps. No evidence for cyclical period changes is obtained.

We exclude precession of the pulsation axis and oblique pulsation for the amplitude variations. Beating of closely spaced frequencies cannot explain the amplitude modulations of two of the modes, while it is possible for the third. Evolutionary effects, binarity, magnetic field changes or avoided crossings cannot be made responsible for the observed period changes. Only resonance between different modes may be able to explain the observations. However, at this stage a quantitative comparison is not possible. More observations, especially data leading to a definite mode identification and further measurements of the temporal behaviour of the amplitudes and frequencies of CD$-$24 7599, are required.

Key words: techniques: photometric – stars: individual: CD$-$24 7599 – stars: individual: XX Pyx – stars: oscillations – δ Scuti.

1 INTRODUCTION

Frequency and amplitude variations have been discovered in various classes of pulsating star. Several different causes can be distinguished.

Amplitude variability may simply be produced by beating of independent close pulsation frequencies. The different pulsation modes of rapidly oscillating Ap (roAp) stars vary in amplitude over the rotation period because these stars are oblique pulsators (Kurtz 1982). Some RR Lyrae stars change their amplitudes as well as the shape of their light curves: the Blazhko effect (Blazhko 1907). The peculiar Cepheid HR 7308 exhibits periodic amplitude variations attributed to a resonance (Van Hoolst & Waelkens 1995). Several objects belonging to different classes of pulsators have been reported to switch their mode spectrum on short time-scales: e.g.

★E-mail: gerald@procyon.ast.univie.ac.at
† Guest Observer, McDonald Observatory, University of Texas at Austin.
‡ Guest Observer, South African Astronomical Observatory.
§ Guest Observer, Cerro Tololo Interamerican Observatory.

the δ Scuti star 21 Mon (Stobie, Pickup & Shobbrook 1977) or pulsating central stars of planetary nebulae (Ciardullo & Bond 1996). For other stars, some pulsation modes only seem to be excited at certain times; they come and they go (e.g. Matthews, Kurtz & Wehlau 1987 for a roAp star; Kleinman 1995 for cool DA white dwarfs). Some further objects seem to change their amplitudes slowly compared with their pulsation periods (e.g. Breger 1990a and Poretti, Mantegazza & Bossi 1996 for δ Scuti stars; Jerzykiewicz & Pigulski 1996 for a β Cephei star; Nather 1995 for a DB white dwarf), but most of the pulsation modes are detected all the time.

Frequency changes are also attributable to several causes. In case of binarity, periodic frequency modulation owing to the orbital motion of the pulsating star is generated (e.g. Kleinman et al. 1994; Kiss & Szatmary 1995). Stellar evolution predicts variations of pulsation frequencies because of temperature and radius changes. Evolutionary frequency changes seem to have been detected for AHB1 variables (Diethelm 1996) and for the hot DA white dwarf G117-B15A (Kepler et al. 1991, 1995), but the cool DA G29-38 (Kleinman 1995) exhibits frequency modulations on much shorter time-scales.

Cyclic frequency variability has been found for the roAp star HR 3831 as well as for a number of related objects (see Martinez & Kurtz 1995). Because of the similarity to the frequency changes of solar p modes during a solar cycle, Kurtz et al. (1994) suggested that the frequency variability of HR 3831 may be caused by a magnetic cycle of roAp stars.

For δ Scuti stars, the situation is also difficult. Breger (1990b) noted that evolved stars show decreasing periods, which is in conflict with their expected evolutionary period change. Rodriguez et al. (1995) recently updated this study and confirmed the results for evolved δ Scuti stars. Moreover, they pointed out that main-sequence δ Scuti stars show period variations that are much too large to be attributed to stellar evolution alone. It may also be the case that period changes of some δ Scuti and SX Phe stars are not smooth, but that period jumps occur at certain times (Powell, Joner & McNamara 1995).

Photometric variability of the δ Scuti star CD−24 7599 was discovered during an observing run of the Whole Earth Telescope (WET: Nather et al. 1990) network. The star was included as a second target in this campaign, and seven frequencies of pulsation were detected (Handler et al. 1996, hereafter Paper I). Follow-up WET observations revealed the presence of at least six more pulsation modes, and by undertaking a preliminary seismological analysis, Handler et al. (1997b, hereafter Paper II) showed that the star is a 1.85-$M_\odot$ object in the first half of its main-sequence evolution. Recently, CD−24 7599 has been given the variable star designation XX Pyx (Kazarovets & Samus 1997).

It was noted in Paper II that significant amplitude variations occurred within the two years between the two WET runs. Since this time-scale for amplitude variations of a δ Scuti star appeared to be very short, it was decided to monitor the star more often in order to constrain this time-scale. Of course, such long-term monitoring also allows us to look for possible frequency variations. In this paper we report the results of the first three years of this programme.

2 DATA ACQUISITION AND REDUCTION

New time-series photometric observations of CD−24 7599 were acquired with various instruments and observing techniques at several sites; a summary of these observations is given in Table 1. Data were acquired at McDonald Observatory (MD) in Texas, USA, with the 0.8-, 0.9- and 2.1-m telescopes, at the South African Astronomical Observatory (SA) with the 0.5-m telescope, at the Cerro Tololo Interamerican Observatory (CT) in Chile with the 0.6-m telescope, and at Mt John University Observatory (MJ), New Zealand, with the 1.0-m telescope. Our codes for the instruments are as follows: P1D denotes differential photometry with a single-channel photometer, P1H stands for high-speed photometry with a single-channel photometer, P2H is high-speed photometry with a two-channel instrument, and P3H represents high-speed photometry with a three-channel photometer. Some time-series CCD photometry was also acquired.

All photoelectric observations were obtained through a Johnson *B* filter, since generally (except for the SA data) blue tubes were used. This maximizes the number of photons counted for this rather faint (V=11.50 mag) star by simultaneously producing highest signal-to-noise ratio data (for a discussion see Breger 1992). Because of the much more numerous photoelectric measurements, we also used the *B* filter for the CCD observations. Regrettably, the CCD run from 1995 December 20 was acquired through a *V* filter because of minor technical problems.

Integration times were 5 or 10 s, respectively, for the photoelectric measurements, while we integrated for 25 s with the CCD, which had a readout time of 15 s.

Since some pulsation modes of CD−24 7599 have low photometric amplitudes, we could not expect to be able to monitor the frequency and amplitude variations of all modes. Consequently, we restricted ourselves to the modes that showed relatively high amplitudes in most of the data sets. Moreover, due to the multiperiodic nature of the light variations, we had to be careful not to run into aliasing ambiguities.

Therefore we decided to monitor the star whenever possible for a time span of at least 12 nights. The (usually) dominating pulsation modes of CD−24 7599 have frequencies of 33.44, 36.01 and 38.11 cycle d^{-1} (387.0, 416.8 and 441.1 μHz, respectively) and can therefore be separated from each other and from the further known pulsation frequencies together with their alias structure when observing for 12 nights or more.

2.1 Photometric reductions

The two- or three-channel photoelectric measurements were reduced as described in Paper II. SAO 176755 was always used as Channel 2 comparison star; in Paper II we showed this object to be constant in light. It is also outside the δ Scuti star instability strip (Handler 1995). In a few cases, we used the Channel 2 data to correct for sky transparency variations or thin clouds.

Single-channel high-speed measurements were sky-subtracted and corrected for extinction. Whenever doubts about the good photometric quality of the nights occurred, the respective runs were discarded.

The differential observations were also corrected for sky background and extinction, and a differential light curve of CD−24 7599 relative to the comparison stars SAO 176755 and HD 76912 (the latter showing no evidence for variability) was generated.

Our CCD data were processed and reduced as described by Handler, Kanaan & Montgomery (1997a); none of the eight selected comparison stars was discovered to be intrinsically variable. The single run acquired through the *V* filter was also used in the analysis after increasing the measured amplitude by a factor of 1.32, adopting the theoretical *B*/*V* amplitude ratio given by Watson (1988). The possible phase shift introduced by including this run is

Table 1. New photometry of CD−24 7599.

Telscp.	Inst.	Obs.	Date (UT)	Start (UT)	Δt (hrs)
MD 0.8	P1D	GH, ES	17 Mar 93	2:32:47	1.11
MD 0.8	P1D	GH, ES	20 Mar 93	2:16:43	0.73
MD 0.8	P1D	GH	26 Mar 93	2:23:02	0.97
MD 0.8	P1D	GH	27 Mar 93	2:29:58	0.55
MD 0.8	P1D	GH	28 Mar 93	2:29:20	0.74
MD 0.8	P1D	GH	31 Mar 93	2:34:36	0.77
MD 0.9	P2H	GH	24 Nov 94	11:51:30	0.79
MD 0.9	P2H	GH	26 Nov 94	11:11:00	1.50
MD 0.9	P2H	GH	27 Nov 94	11:25:15	1.28
MD 0.9	P2H	GH	29 Nov 94	9:03:25	0.91
MD 0.9	P2H	GH	30 Nov 94	11:27:20	1.27
MD 0.9	P2H	GH	1 Dec 94	11:15:30	1.11
MD 0.9	P2H	GH	2 Dec 94	11:10:15	1.56
MD 0.9	P2H	GH	3 Dec 94	10:47:05	1.90
SA 0.5	P1H	GH	2 Mar 95	18:10:39	2.11
SA 0.5	P1H	GH	3 Mar 95	18:22:45	2.03
SA 0.5	P1H	GH	4 Mar 95	18:18:10	1.89
CT 0.6	P1H	WZ	5 Mar 95	0:30:05	1.60
CT 0.6	P1H	WZ	6 Mar 95	0:25:03	1.99
SA 0.5	P1H	GH	6 Mar 95	18:00:52	2.19
CT 0.6	P1H	WZ	7 Mar 95	1:14:56	1.37
CT 0.6	P1H	WZ	8 Mar 95	0:14:41	2.27
SA 0.5	P1H	GH	8 Mar 95	17:56:18	1.99
CT 0.6	P1H	WZ	9 Mar 95	0:10:43	2.16
CT 0.6	P1H	WZ	10 Mar 95	0:15:18	2.06
CT 0.6	P1H	WZ	11 Mar 95	0:10:59	1.87
SA 0.5	P1H	GH	11 Mar 95	18:00:32	1.63
CT 0.6	P1H	WZ	12 Mar 95	0:04:17	2.04
CT 0.6	P1H	WZ	13 Mar 95	0:00:57	1.90
SA 0.5	P1H	GH	13 Mar 95	17:57:00	1.63
SA 0.5	P1H	GH	14 Mar 95	17:59:09	1.57
SA 0.5	P1H	GH	19 Mar 95	17:56:00	1.66
CT 0.6	P1H	WZ	19 Mar 95	23:51:25	1.71
SA 0.5	P1H	GH	20 Mar 95	17:51:20	1.61
CT 0.6	P1H	WZ	20 Mar 95	23:49:35	1.57
MD 0.9	P3H	AN	21 Mar 95	1:24:00	1.74
CT 0.6	P1H	WZ	21 Mar 95	23:43:22	1.67
MD 0.9	P3H	AN	22 Mar 95	2:17:00	1.26
SA 0.5	P1H	GH	22 Mar 95	23:12:19	0.53
SA 0.5	P1H	GH	23 Mar 95	17:39:59	1.47
CT 0.6	P1H	WZ	23 Mar 95	23:40:42	1.41
MD 0.9	P2H	GH	17 Oct 95	10:31:50	1.51
MD 0.9	P2H	GH	18 Oct 95	10:41:30	1.36
MD 0.9	P2H	GH	19 Oct 95	10:37:45	1.46
MD 0.9	P2H	GH	20 Oct 95	10:24:20	1.65
MD 0.9	P2H	GH	21 Oct 95	10:20:10	1.78

Table 1 – *continued*

Telscp.	Inst.	Obs.	Date (UT)	Start (UT)	Δt (hr)
MD 0.9	P2H	GH	22 Oct 95	10:24:15	1.73
MD 0.9	P2H	GH	24 Oct 95	11:17:05	0.84
MD 0.9	P2H	GH	25 Oct 95	10:28:15	1.72
MD 0.9	P2H	GH	27 Oct 95	10:00:10	2.14
MD 0.9	P2H	GH	28 Oct 95	9:50:25	2.36
MD 0.9	P2H	GH	30 Oct 95	9:36:15	0.92
MD 2.1	P2H	GH	12 Dec 95	8:47:30	1.14
MD 2.1	P2H	GH	14 Dec 95	9:11:50	3.28
MD 2.1	P2H	GH	15 Dec 95	8:30:50	2.67
MD 0.9	CCD	GH, MM	16 Dec 95	11:47:30	1.16
MD 0.9	CCD	GH	20 Dec 95	10:53:18	1.57
MD 0.9	CCD	GH	21 Dec 95	10:14:26	1.21
MD 0.9	P2H	GH	25 Dec 95	9:13:50	2.90
MD 0.9	P2H	GH	27 Dec 95	10:43:50	2.07
MD 0.9	P2H	GH	28 Dec 95	10:47:00	2.08
MD 0.9	P2H	GH	29 Dec 95	6:09:10	1.03
MD 0.9	P2H	GH	30 Dec 95	10:26:35	1.39
MD 0.9	P2H	GH	8 Feb 96	3:13:10	1.32
MD 0.9	P2H	GH	11 Feb 96	3:47:40	1.06
MD 0.9	P2H	GH	12 Feb 96	6:53:40	1.33
MD 0.9	P2H	GH	14 Feb 96	3:59:30	0.73
MJ 1.0	P2H	DJS	16 Feb 96	14:39:20	2.08
MJ 1.0	P2H	DJS	17 Feb 96	14:01:40	2.13
MJ 1.0	P2H	DJS	20 Feb 96	14:52:10	1.22
MJ 1.0	P2H	DJS	21 Feb 96	14:45:00	2.07
MD 0.9	P2H	JG, GH	22 Feb 96	6:40:29	1.46
MD 0.9	P2H	GH	6 Mar 96	1:50:00	1.14
MD 0.9	P2H	GH	10 Mar 96	1:45:20	1.08
MD 0.9	P2H	GH	11 Mar 96	3:27:20	2.68
MD 0.9	P2H	GH	12 Mar 96	1:55:35	0.78
MD 0.9	P2H	GH	13 Mar 96	1:52:20	1.33
MD 0.9	P2H	GH	15 Mar 96	1:56:10	1.22
MD 0.9	P2H	GH	16 Mar 96	1:57:30	1.18
MD 0.9	P2H	GH, NA	18 Mar 96	2:02:15	1.17
MD 0.9	P2H	GH, NA	19 Mar 96	2:07:20	1.13
MD 0.9	P2H	GH, NA	21 Mar 96	2:11:04	1.04
MD 0.9	P2H	NA, GH	24 Mar 96	2:04:40	2.42
MD 0.9	P2H	NA, GH	25 Mar 96	2:10:13	1.00
MD 0.9	P2H	NA	26 Mar 96	2:17:28	1.38
MD 0.9	P2H	NA	28 Mar 96	2:05:07	1.36
Total			86 nights		132.40

Observers: GH = G. Handler, ES = E. Serkowitsch, WZ = W. Zima, AN = A. Nitta, MM = M. H. Montgomery, DJS = D. J. Sullivan, JG = J. A. Guzik, NA = N. Audard.

small compared with the accuracy of our O−C values to be derived in the next section.

The reduced data were summed into 120-s bins to give all the observations equal weight and to decrease the number of data points to a reasonable amount. Finally, the times of measurement were converted into Heliocentric Julian Date (HJD). Neither barycentric nor leap-second corrections were applied; they simply were not necessary.

3 ANALYSIS

3.1 Amplitude variations

Our frequency analysis was performed with an updated version of the program PERIOD (Breger 1990c). First, amplitude spectra were calculated for all the monthly subsets of data. It was found that $f_1 = 441.1$ μHz is prominent in all data sets, except 1993 March. We prewhitened that frequency by fitting a synthetic light curve to the monthly data sets and calculated amplitude spectra of the residuals. The result is displayed in Fig. 1.

Fig. 1 shows several remarkable features. The amplitude of f_1 dropped to half its value from 1994 May to November. Afterwards, it grew again to decrease by about 40 per cent from 1995 October to 1996 February. Moreover, the amplitude of f_2 was dramatically reduced between 1993 March and 1994 May. Since then, the amplitudes of f_2 and f_3 seem to have increased slowly.

To quantify the amplitude variations better, we simultaneously fitted, whenever unambiguously detected, f_1, f_2 and f_3 as well as any further pulsation frequency (if clearly present in the amplitude

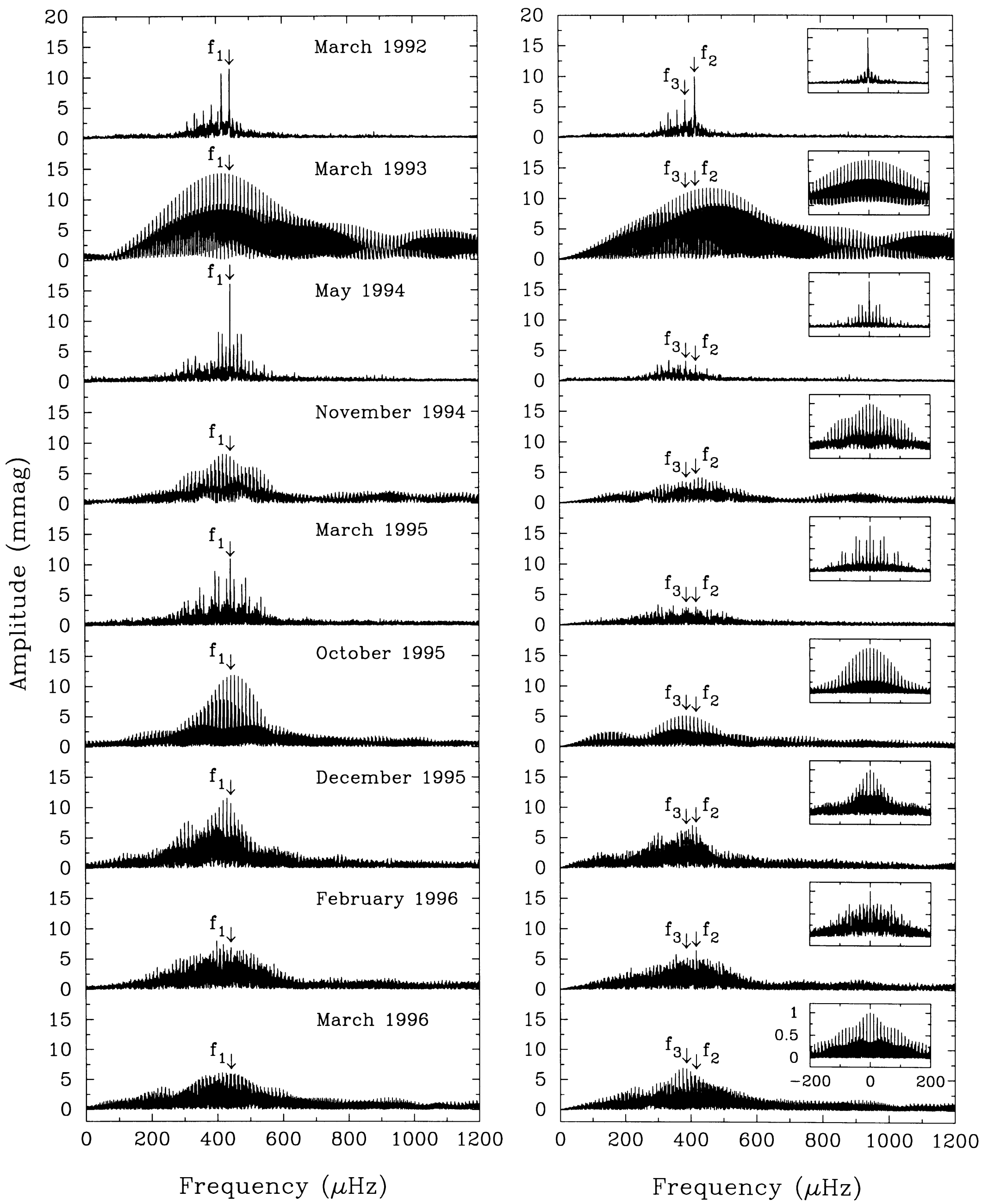

Figure 1. Monthly amplitude spectra of CD−24 7599 before (left-hand panels) and after pre-whitening f_1=441.1 μHz (right-hand panels). Spectral windows are inserted in the right-hand panels. The locations of f_1, f_2=416.8 μHz and f_3=387.0 μHz are indicated. Amplitude variations on time-scales down to 2 months are clearly visible.

spectra and if identified in Paper II) to the data and derived the amplitudes for these frequencies. We note that because of the small 1993 March data set we could only fit f_2, and because of the short time baseline for 1994 November, we only considered f_1 and f_3. On the other hand, we also included f_6=312.5 μHz in the synthetic light curves for 1995 March and December. f_{13}=361.2 μHz was detected in 1995 October. We note that we did not attempt to quantify the amplitude variations of f_6 and f_{13}: these frequencies are close to aliases of f_5=335.6 μHz and f_9=315.6 μHz, respectively. Amplitude variations of f_6 and f_{13} may therefore simply be caused by beating with such aliases and cannot be considered to be reliably determined.

The results of our analysis are summarized in Table 2; the amplitudes for the two WET data sets were taken from Paper II. A graphical representation of the amplitude variations is displayed in Fig. 2. We have also indicated 1σ error bars determined following Kovacs (1981). Because of the probable presence of further low-amplitude pulsation frequencies, these error bars may be underestimates owing to correlated noise: e.g. see Kepler et al. (1995). However, since our considered pulsation modes always dominate the amplitude spectra and since we checked that our frequency solutions are stable, correlated noise should neither systematically nor significantly influence our analysis.

Table 2. Monthly amplitudes of CD−24 7599 (in mmag).

	$f_1 = 441$ μHz	$f_2 = 417$ μHz	$f_3 = 387$ μHz
Mar 1992	11.5 ± 0.2	10.0 ± 0.2	6.4 ±0.2
Mar 1993	< 5	14.5 ± 1.8	< 5
May 1994	15.9 ± 0.2	3.3 ± 0.2	3.8 ± 0.2
Nov 1994	7.4 ± 0.4	< 2.5	4.1 ± 0.4
Mar 1995	10.8 ± 0.3	2.8 ± 0.3	2.8 ± 0.3
Oct 1995	12.0 ± 0.4	2.7 ± 0.4	5.4 ± 0.4
Dec 1995	8.6 ± 0.4	5.8 ± 0.4	4.0 ± 0.4
Feb 1996	7.3 ± 0.5	6.5 ± 0.5	4.1 ± 0.5
Mar 1996	7.5 ± 0.5	3.2 ± 0.5	7.8 ± 0.5

From Fig. 2 it turns out that some pulsation modes of CD−24 7599 can change their photometric amplitudes on time-scales down to one month. We looked for amplitude variations on even shorter time-scales by subdividing the two WET data sets as well as the three-site data from 1995 March, but we could not find evidence for such short-term amplitude variability.

We also searched for possible periodicities in the amplitude variations. The uppermost panel of Fig. 2 indeed indicates some cyclic variability of the monthly amplitudes of f_1. We quantified this by calculating a sinusoidal fit to these data. Our best fit (yielding a period of 446 d, a mean amplitude of 11.5 mmag and an amplitude of the amplitude variations of 4.3 mmag) leaves a surprisingly low residual scatter of only 0.11 mmag per monthly data point, which is smaller than the smallest error of each individual determination of the amplitude of f_1.

Therefore one may be inclined to believe that f_1 indeed shows periodic amplitude variations. However, we keep in mind that we had to determine four independent parameters (frequency, amplitude, phase and zero-point) from only eight data points for our sinusoidal fit, which leaves ample room for spurious results. We also note that our fit fails to predict the low amplitude of f_1 (< 5 mmag) for 1993 March: the fit suggests an amplitude of about 15 mmag for this data set.

An examination for possible periodic amplitude variations of f_2 and f_3 yielded negative results. Most of the promising modulation frequencies were near the Nyquist frequency of the data set, and those clearly below the Nyquist frequency gave residuals much higher than those of the individual measurements. We conclude that there is some evidence for periodic amplitude variation of f_1 (but confirmation is needed), and no evidence for periodic amplitude variability with constant modulation amplitude of f_2 and f_3 with time-scales between 4 months and 4 yr.

On the other hand, we may estimate the time-scale on which the amplitude variations occur from examining Fig. 2: it is about 450 d for f_1, approximately 250 d for f_2 and about 350 d for f_3.

3.1.1 *Pulse shapes*

Owing to non-linearities (e.g. the Blazhko effect in RR Lyr stars), the pulse shapes of the different modes may vary when their amplitudes change. However, only f_1 has large enough amplitude in most data sets to allow a meaningful comparison.

Therefore we determined its pulse shapes in the following way: we fitted the best n-frequency solution to the 1992 March, 1994 May, 1994 November, 1995 March, 1995 October, 1995 December and 1996 February + March subsets of data. Then we calculated a synthetic light curve from all the frequencies except f_1 and its harmonic (if detected). This synthetic light curve was subtracted

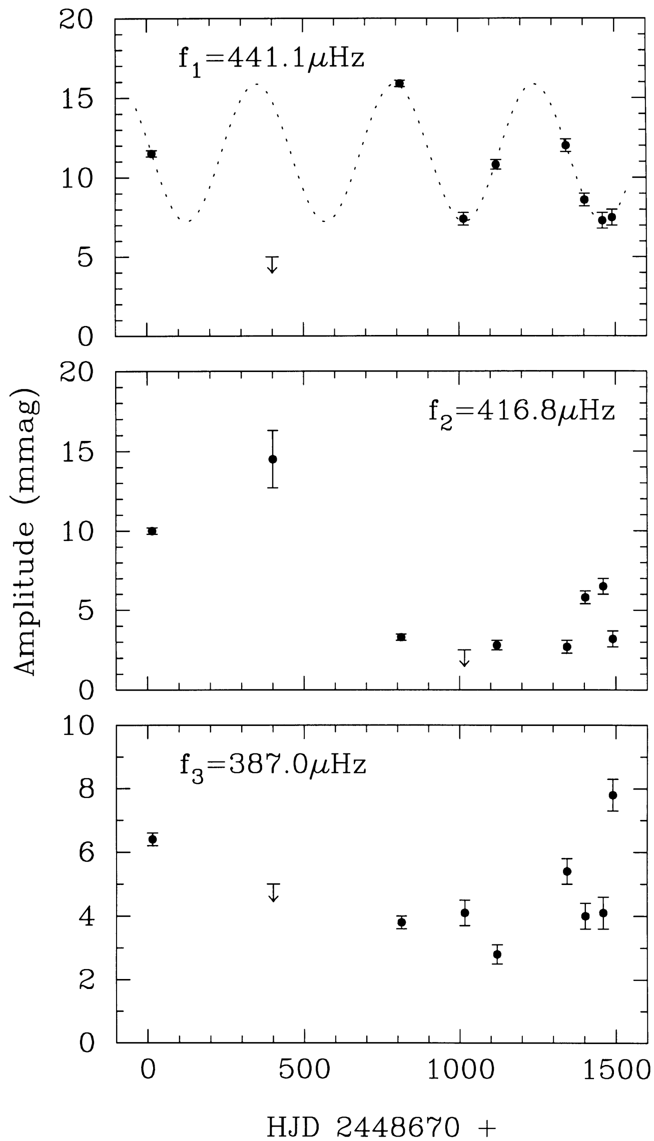

Figure 2. Time-dependent variation of the amplitudes of the three strongest modes of CD−24 7599. The error bars are of 1σ size. The downward arrows denote data sets for which we could only infer upper limits of the amplitudes. A possible sinusoidal fit to the amplitudes of f_1 is also shown (see text). Note the larger scale of the lowest panel.

from the data, so that only the modulation of f_1 plus noise remained. Consequently, we constructed phase diagrams with respect to f_1, consisting of 25 normal points. Some of them are shown in Fig. 3.

There seems to be no significant change in the pulse shape of f_1 when the amplitude of the pulsation changes. To quantify this suspicion further, we applied the following test. We aligned the phases of our pulse shapes and normalized the amplitudes to the same value. We generated differential phase diagrams by subtracting these normalized pulses from each other. Then we Fourier analysed the differential pulse shapes and looked for power at harmonic frequencies. To judge the significance of such peaks, we generated pulse shapes consisting of Gaussian noise sampled in the same way as the differential phase diagrams and having the same standard deviation (as determined when calculating the normal points). Even with this procedure, we could not detect any significant change in the pulse shape of f_1 dependent on its amplitude.

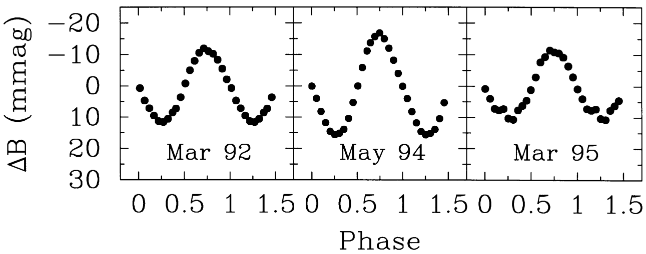

Figure 3. Phase diagrams for f_1 for different subsets of data. The errors have at worst the size of the dots. No change in the pulse shape seems to accompany the amplitude variations.

Table 3. O−C values of CD−24 7599 (in seconds).

	$f_1 = 441$ μHz	$f_2 = 417$ μHz	$f_3 = 387$ μHz
Mar 1992	+138 ± 9	−104 ± 10	+30 ± 18
Mar 1993		+45 ± 91	
May 1994	−118 ± 8	+500 ± 46	−39 ± 40
Nov 1994	−209 ± 40		+274 ± 81
Mar 1995	−115 ± 13	+461 ± 55	−73 ± 56
Oct 1995	+5 ± 23	+289 ± 107	−129 ± 56
Dec 1995	+88 ± 28	+51 ± 45	+37 ± 67
Feb 1996	+54 ± 45	−39 ± 58	+16 ± 94
Mar 1996	+19 ± 45	−283 ± 106	+60 ± 53

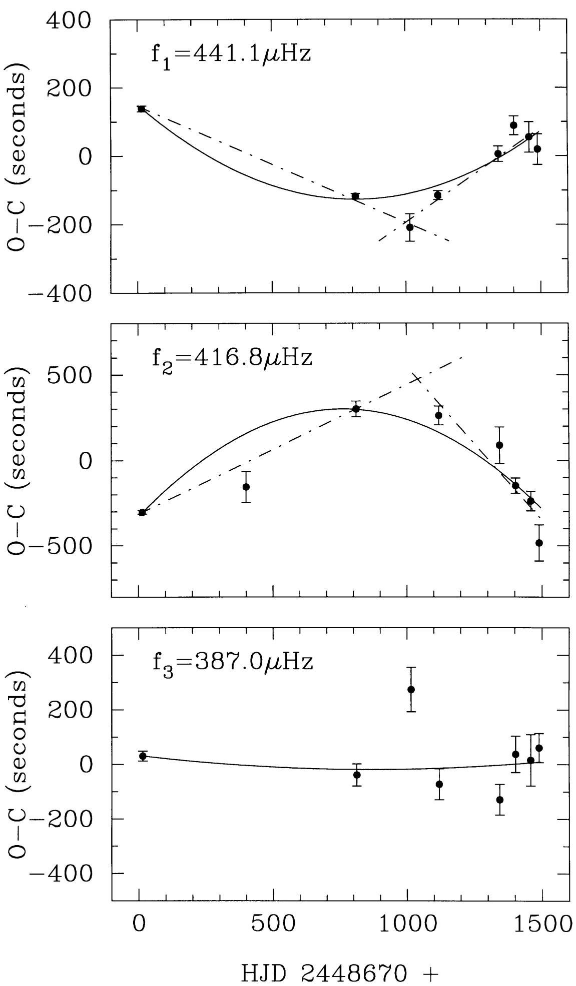

Figure 4. O−C diagrams for the three strongest modes of CD−24 7599. The error bars are 1σ. Some possible fits are shown: the full line assumes a constant period change, while the dash–dotted lines correspond to sudden changes of otherwise constant pulsation frequencies.

3.2 Frequency variability

To search for possible frequency variations in our data set, we first have to determine the best frequency values for the three modes under consideration. Yearly or monthly aliasing may prevent a correct determination of the pulsation frequencies. However, since our data sets often comprise a good fraction of a month or of a year, this problem is not severe.

We first took the frequencies from Paper II as accurate starting values. Afterwards, we refined these frequencies by fitting them to the combined 1996 February/March data set. Consequently, we could also incorporate the 1995 December and October data, further refining our frequencies. This allowed us to bridge to the 1995 March data, and with the frequency values from this combined data set it was easy also to include the 1994 data and to improve our frequencies once more. Finally, also the 1993 and 1992 data could be used. With this procedure we finally determined $f_1 = 441.088$ μHz, $f_2 = 416.797$ μHz and $f_3 = 387.011$ μHz. There is no aliasing ambiguity for any of these values.

We simultaneously fitted the frequencies listed above to the whole data set as well as to the monthly subsets, and constructed ‘observed minus calculated (O−C) diagrams for each of the pulsation modes. These are displayed in Fig. 4, while the O−Cs for the monthly data subsets are listed in Table 3. We note again that the 1σ errors may be underestimates, but the basic shape of the O−C diagrams is not expected to be influenced. We are careful to point out that there is no aliasing ambiguity in the O−C diagrams themselves. Examining Fig. 4, we find no correspondence between the behaviours of the frequency variations of the different modes.

We show possible fits to the O−C diagrams. Following Kepler et al. (1995), we calculated a parabolic fit of the form

$$O - C = \Delta E_0 + \Delta P \times E + \frac{1}{2} \times P \times E^2 \times \frac{\mathrm{d}P}{\mathrm{d}t}$$

to the data, where ΔE_0 is a possible shift in the zero-epoch, E stands for the epoch, ΔP represents a possible inaccuracy in the adopted period, P is the period itself and dP/dt is the secular period change. The individual data points were weighted inversely proportionally to their error size. This yields values of dP/dt of $+2.55 \pm 0.31 \times 10^{-10}$ s s^{-1} for f_1, $-6.9 \pm 1.2 \times 10^{-10}$ s s^{-1} for f_2 and $+0.5 \pm 1.1 \times 10^{-10}$ s s^{-1} for f_3. While f_1 and f_2 show formally very significant changes, f_3 can be assumed to have constant frequency throughout the whole data set.

We also computed piecewise linear fits to the O−C values of f_1 and f_2 to illustrate that the parabolic fits are not unambiguous. One could as well claim that f_1 and f_2 were constant from the beginning of our observations until the end of 1994, and then they suddenly decreased by 0.0039 μHz and increased by 0.0149 μHz, respectively. No such statement about f_3 is possible. Finally, we note that the present data set is too small to look for eventual cyclic frequency changes. We can only state that the time-scale for such cyclical changes cannot be shorter than ≈1000 d, and that the shape of the O−C diagram for f_1 should not be interpreted in this way with the current number of data available.

4 DISCUSSION

4.1 Amplitude variations

The simplest explanation for amplitude variability is beating of closely spaced pulsation frequencies, where the beat period is not resolved in our data sets. Beating would result in periodic, sinusoidal amplitude modulation. This cannot be the case for f_2 and f_3, but is possible for f_1. This would require at least two close frequencies. Since it has been shown in Paper II that CD−24 7599 is a main-sequence star, its theoretical frequency spectrum is simple and therefore the occurrence of closely spaced frequencies with high photometric amplitudes is unlikely. Beating of unresolved frequencies would generate phase variations on the same time-scale as the amplitude variations. Since the dominant contribution to the O−C diagram of f_1 in Fig. 4 does not occur on that time-scale, we cannot examine this hypothesis in more detail. We conclude that beating of multiple modes is not the cause for the amplitude variations of f_2 and f_3, while it is possible, but not probable, for f_1.

Balona (1985) suggested that precession of the pulsation axis could explain the amplitude variations of some binary β Cephei stars. This is also conceivable for non-radially pulsating δ Scuti stars. However, the short time-scales of the amplitude variations of CD−24 7599 and their complicated nature argue against such an interpretation; the latter also provides strong evidence that possible oblique pulsation is not responsible for the amplitude variations. Furthermore, low- (Paper I) and high-resolution (Paper II) blue spectra as well as a low-resolution red spectrum (Kerschbaum, private communication) obtained for CD−24 7599 showed no trace of a binary companion to the star. We conclude that precession of the pulsation axis or oblique pulsation of CD−24 7599 does not generate the observed amplitude variations.

Another possible explanation for amplitude variability in multimodally pulsating stars is non-linear interaction between the different modes. In this case, their amplitude variations should occur on time-scales of the order of the reciprocal of their linear growth rates.

To allow a qualitative comparison of the temporal behaviour of the star's pulsation amplitudes with theory, we computed a number of pulsational models (see Paper II for more details) for CD−24 7599. We tried to match the observed frequency range of the star with the unstable mode domain of our models, but did not focus too much on reproducing the location of the star in the Hertzsprung–Russell (HR) diagram as inferred in Paper II. Finally, we chose a 1.95-$M_\odot$, log T_{eff} = 3.907 model, which exhibits a pulsationally unstable frequency range of 285–468 μHz; the (so far) detected pulsation modes of CD−24 7599 lie within 312–441 μHz. Moreover, this model has two radial modes at the same frequencies as the observed f_1 and f_{10}. Linear growth rates of this model are shown in Fig. 5.

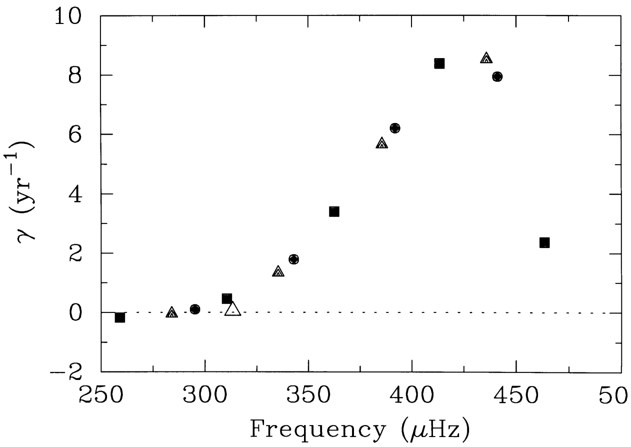

Figure 5. Growth rates for a 1.95-$M_\odot$, log T_{eff} = 3.907 model for CD−24 7599. Circles represent radial modes, squares are dipole modes, and triangles correspond to quadrupole modes. Open symbols denote mixed modes, and only $m = 0$ modes are displayed. The pulsationally unstable frequency range is 285–468 μHz.

The growth rates of our model in the frequency range of interest are about 4–9 yr^{-1}. Their reciprocal is of the same order of magnitude as the time-scales of the amplitude variations. It is also interesting that the predicted time-scales of amplitude variation become much smaller for modes near the high-frequency cut-off compared with modes at somewhat lower frequencies. This resembles the observed behaviour of CD−24 7599 well. Therefore we consider the qualitative agreement between theory and observations to be very encouraging.

Of course, we cannot quantify this result further, since we do not (yet) have definite mode identifications for CD−24 7599 available. Therefore our model is rather ill-constrained and the growth rates of a final model of the star may be different from those calculated here. However, they are expected to be of the same order of magnitude. It should also be noted that more observations of the temporal behaviour of the modes are required to constrain the observed time-scales of the amplitude variations better. For more details on this kind of amplitude modulation we refer to the discussion by Jerzykiewicz & Pigulski (1996).

We may also compare the shape of the amplitude modulations with those predicted by non-linear theory. Moskalik (1985) studied resonant coupling of an unstable mode to two lower frequency stable modes. This can lead to periodic amplitude modulation with a slow exponential increase followed by a rapid drop in amplitude, accompanied by a large phase jump. Our observed amplitude variations do not show such features; phase jumps are not present in our O−C diagrams.

Buchler, Goupil & Hansen (1997) investigated resonances in non-radial pulsators by means of the amplitude equation formalism. They obtained solutions with constant and variable amplitudes. In the case of 2:1 resonances they found periodic (but not necessarily sinusoidal) amplitude modulations. This may be observed for f_1, but not for f_2 and f_3. On the other hand, Van Hoolst (1995) studied 1:1 resonances and showed that irregular amplitude variations, resembling those of f_2 and f_3, are possible.

4.2 Frequency variability

One of the most interesting branches of pulsating star research utilizes period changes to infer the evolutionary speed of stars in several parts of the HR diagram. However, it has turned out that for many objects the observed period changes do not unambiguously reflect effects of stellar evolution. For main-sequence δ Scuti stars, evolutionary period changes of the order $\mathrm{d}P/\mathrm{d}t \approx +7 \times 10^{-14}$ s s^{-1} are expected (e.g. see Rodriguez et al. 1995). However, the measured period changes of two of the examined modes of CD−24 7599 are 3–4 orders of magnitude too large, and one has even negative sign. The period variability of CD−24 7599 can therefore not solely be caused by its evolutionary temperature and radius changes.

With two modes having different signs of dP/dt, a binary origin can also be ruled out for (a large fraction of) the observed period changes. Furthermore, as noted above, there is no trace of a secondary in any spectrum that we have available for the star.

Possible magnetic field changes are also very unlikely to cause the frequency variations of CD−24 7599. It is a rather hot δ Scuti star (Papers I and II), and can therefore only possess a very shallow surface convection zone (even compared with most roAp stars). Moreover, we have no spectroscopic evidence for the presence of a magnetic field in CD−24 7599.

Another possibility for generating frequency variations would be avoided crossing (Aizenman, Smeyers & Weigert 1977). In cases where g and p modes are very close in frequency, large period changes are expected. However, we consider this to be unlikely for two reasons. First, it would be surprising if two of the three modes that we monitored were just in the short-lived stage where avoided crossing occurs. Secondly, in the evolutionary stage of CD−24 7599 as inferred in Paper II, only one g mode of $\ell = 2$ will be excited. Following Dziembowski & Pamyatnykh (1991), this mode would be expected to have a frequency of about 315 μHz. The two modes observed to show significant period variations have frequencies of 417 and 441 μHz, respectively.

Considering resonances (as investigated by e.g. Buchler et al. 1997) between different modes as the explanation of the observed behaviour, one would expect the frequency variations to occur on similar time-scales to the amplitude variations. While this may be the case for f_1 during the late 1995 and 1996 observations, it is not seen for the other two modes. The dominating part of the frequency variations should then be the result of some other effect.

5 SUMMARY AND CONCLUSIONS

We have studied the amplitude and frequency variations of the δ Scuti star CD−24 7599 over a time span of four years. The three dominating pulsation modes of the star can change their photometric amplitudes within a month. The associated time-scales are about 450 d for f_1, approximately 250 d for f_2 and $\sim$ 350 d for f_3. No changes in the pulse shapes accompany the amplitude variations of f_1. There is some evidence that the amplitude variations of this mode may be periodic, but confirmation is needed.

Precession of the pulsation axis in a possible binary system or oblique pulsation cannot explain the observations. Beating between closely spaced pulsation modes is only possible, but not probable, for f_1. The time-scale of the amplitude variations is of the same order of magnitude as the reciprocal of the growth rates of the modes, which points towards resonant mode coupling as the origin of the amplitude variations. However, the few possible quantitative comparisons between observation and theory give inconclusive results.

The frequency changes of CD−24 7599, if interpreted as being continuous, show very discrepant behaviour among the three modes under consideration. dP/dt values of $+2.55 \pm 0.31 \times 10^{-10}$ s s^{-1} for f_1, $-6.9 \pm 1.2 \times 10^{-10}$ s s^{-1} for f_2 and $+0.5 \pm 1.1 \times 10^{-10}$ s s^{-1} for f_3 can be derived. It is, however, also possible that sudden frequency jumps of f_1 and f_2 occurred, while f_3 remained constant within the errors of measurement over the whole four-year data set.

Evolutionary effects, binarity, magnetic field variations or avoided crossing cannot be made responsible for the observed period changes. Resonant coupling of the modes may explain part of the observations.

To conclude, a better quantification of the amplitude and frequency variations of CD−24 7599 can only be given when definite mode identifications are available. For this star this seems to be possible, considering its unevolved stage and its therefore simple theoretical frequency spectrum (Paper II). A large multisite campaign allowing us to achieve definite mode identifications for the star will be undertaken at the beginning of 1998.

Further observations of the temporal behaviour of δ Scuti stars (or pulsating white dwarfs) exhibiting amplitude and frequency changes are needed. CD−24 7599 gives us a unique opportunity to study these effects, since they occur on time-scales long enough to be conveniently monitored, but short enough that a valuable data set can be acquired within a few years.

ACKNOWLEDGMENTS

This work was partially supported by the Austrian Fonds zur Förderung der wissenschaftlichen Forschung under grant S–7304. NA acknowledges partial support by the Fonds zur Förderung der wissenschaftlichen Forschung under grant S–7303 (Lise Meitner Fellowship, project M00323-AST) and by the PPARC in Cambridge. GH received partial support by the Austrian Zentrum für Auslandsstudien, and thanks Joyce Guzik, Mike Montgomery and Eddi Serkowitsch for assistance during a few of the observations. Franz Kerschbaum kindly provided an unsolicited red spectrum of our programme star.

REFERENCES

Aizenman M., Smeyers P., Weigert A., 1977, A&A, 58, 41
Balona L. A., 1985, MNRAS, 217, 17P
Blazhko S., 1907, Astron. Nachr., 175, 325
Breger M., 1990a, A&A, 240, 308
Breger M., 1990b, in Cacciari C., Clementini, G., eds, ASP Conf. Ser. Vol. 11, Confrontation between stellar pulsation and evolution. Astron. Soc. Pac., San Francisco, p. 263
Breger M., 1990c, Commun. Asteroseism. 20, 1
Breger M., 1992, in Percy J. R., Mattei J. A., Sterken C., eds, Variable Star Research: An international perspective. Cambridge Univ. Press, Cambridge, p. 171
Buchler J. R., Goupil M.-J., Hansen C. J., 1997, A&A, 321, 159
Ciardullo R., Bond H. E., 1996, AJ, 111, 2332
Diethelm R., 1996, A&A, 307, 803
Dziembowski W. A., Pamyatnykh A. A., 1991, A&A, 248, L11
Handler G., 1995, Inf. Bull. Variable Stars, 4216
Handler G. et al., 1996, A&A, 307, 529 (Paper I)
Handler G., Kanaan A., Montgomery M. H., 1997a, A&A, 326, 692
Handler G. et al., 1997b, MNRAS, 286, 303 (Paper II)
Jerzykiewicz M., Pigulski A., 1996, MNRAS, 282, 853
Kazarovets E. V., Samus N. N., 1997, Inf. Bull. Variable Stars, 4471
Kepler S. O. et al., 1991, ApJ, 378, L45
Kepler S. O. et al., 1995, Baltic Astron., 4, 221
Kiss L. L., Szatmary K., 1995, Inf. Bull. Variable Stars, 4166
Kleinman S. J., 1995, PhD thesis, University of Texas
Kleinman S. J. et al., 1994, ApJ, 436, 875
Kovacs G., 1981 Ap&SS, 78, 175
Kurtz D. W., 1982, MNRAS, 200, 807
Kurtz D. W., Martinez P., van Wyk F., Marang F., Roberts G., 1994, MNRAS, 268, 641
Martinez P., Kurtz D. W., 1995, in Stobie R. S., Whitelock, P. A., eds, Proc. IAU Colloq. 155, ASP Conf. Ser. Vol. 83, Astrophysical Applications of Stellar Pulsation. Astron. Soc. Pac., San Francisco, p. 58
Matthews J. M., Kurtz D. W., Wehlau W. H., 1987, ApJ, 313, 782
Moskalik P., 1985, Acta Astron., 35, 229

Nather R. E., 1995, Baltic Astron., 4, 321
Nather R. E., Winget D. E., Clemens J. C., Hansen C. J., Hine B. P., 1990, ApJ, 361, 309
Poretti E., Mantegazza L., Bossi M., 1996, A&A, 312, 912
Powell J. M., Joner M. D., McNamara D. H., 1995, PASP 107, 225
Rodriguez E., Lopez de Coca P., Costa V., Martin S., 1995, A&A, 299, 108
Stobie R. S., Pickup D. A., Shobbrook R. R., 1977, MNRAS, 179, 389
Van Hoolst T., 1995, A&A, 295, 371
Van Hoolst T., Waelkens C., 1995, A&A, 295, 361
Watson R. D., 1988, Ap&SS, 140, 255

This paper has been typeset from a TEX/LATEX file prepared by the author.

2.2.4 Towards a seismic model of the δ Scuti star XX Pyxidis

Original paper:

A. A. Pamyatnykh, W. A. Dziembowski, **G. Handler,** H. Pikall, 1998, A&A 333, 141

Astron. Astrophys. 333, 141–150 (1998)

ASTRONOMY
AND
ASTROPHYSICS

Towards a seismic model of the δ Scuti star XX Pyxidis

A.A. Pamyatnykh[1,2,3], **W.A. Dziembowski**[1,2], **G. Handler**[2], **and H. Pikall**[2]

[1] N. Copernicus Astronomical Center, Polish Academy of Sciences, Bartycka 18, PL-00716 Warszawa, Poland
[2] Institute of Astronomy, University of Vienna, Türkenschanzstraße 17, A-1180 Wien, Austria
[3] Institute of Astronomy, Russian Academy of Sciences, Pyatnitskaya 48, 109017 Moscow, Russia

Received 26 November 1997 / Accepted 26 January 1998

Abstract. Frequencies of 13 oscillation modes in the star XX Pyxidis (CD–24 7599) are accurately measured but for none of the modes the spherical harmonic degree (ℓ) is known. We present results of an attempt to construct the model whose low–ℓ mode frequencies reproduce possibly close the observations. Models are constrained by the mean photometric and spectroscopic data for the star. However, the strongest constraint on the effective temperture is from the requirement that the modes excited in the star fall into the range of the modes driven by the opacity mechanism.

Our models are built with the standard stellar evolution code allowing no overshooting from the convective core. Effects of rotation are taken into account both in stellar evolution and in linear nonadiabatic oscillation calculations. Uniform rotation rate and conservation of the global angular momentum during evolution are assumed.

We find several distinct mode identifications and associated stellar models leading to frequency fits of similar quality. Determination of the ℓ values for some of the modes could remove the ambiguity. None of the fits is satisfactory: the mean departures exceed the mean observational frequency error by at least one order of magnitude. The fits could be improved by means of adjusting model parameters that were kept fixed. However, such effort will be meaningful only after improving accuracy in calculation of the effects of rotation in oscillation frequencies.

Key words: stars: oscillations – stars: evolution – δ Scu – stars: individual: CD–24 7599 = XX Pyx

1. Introduction

Long–time network observations of Delta Scuti stars resulted in establishing truly multimodal character of oscillations in a few objects of this type. The four objects with the largest number of modes detected are FG Virginis with 24 modes (Breger et al. 1997), 4 Canum Venaticorum with at least 17 modes (Breger 1997), XX Pyxidis with 13 modes (Handler et al. 1997a) and BH Piscium with 13 modes (Mantegazza et al. 1996). Though these numbers of modes in comparison with the Sun or certain oscillating white dwarfs may appear small, reproducing mode frequencies with model calculation represents a challenge.

What makes our task more difficult than in the solar and white–dwarf cases, is the fact that the observed spectra do not reveal patterns enabling mode identification. Modes detected in δ Scuti stars are of low radial order and their frequencies do not obey simple asymptotic relations. Further, these stars are rather rapid rotators and rotational splitting is not equidistant. Multicolor photometry may be used to determine the spherical harmonic degree, ℓ. Spectroscopy allows, in addition, to determine the azimuthal order, m. In practice, however, reliable ℓ and m values are only seldom available. Thus, mode identification in δ Scuti stars cannot be done independently of calculations involving construction of equilibrium models and their oscillation properties. The aim is to construct a stellar model with frequencies of low–degree modes which fit the observed ones. In analogy to helioseismology we use the name *seismic model*.

The ultimate purpose of seismic model construction is testing the ingredients of stellar evolution theory: its basic assumptions and the input microscopic physics. Stellar evolution theory has reached an advanced level some 20 to 30 years ago. However, important questions concerning convection and rotation remain unanswered. For instance, is the mixing–length theory sufficient for describing convective flux in subphotospheric layers? If so, what is the best choice for the mixing length parameter, α, depending on stellar parameters? What is the extent of element penetration, $d_{\rm over}$, from the convective to the radiative regions? What is the law of the angular momentum evolution? What is the role of rotationally induced instabilities in chemical element mixing?

In recent years considerable progress has been made in treatment of the equation of state and opacity for stellar interiors (see Christensen–Dalsgaard & Däppen 1993 and references there, Rogers et al. 1996, Rogers & Iglesias 1994 and references there, Iglesias & Rogers 1996, Seaton 1996). The uncertainties, however, are difficult to estimate. It is therefore important to use possibly diversified sets of observational data for testing. Observers provide us very accurate frequency measurements but a major effort is needed to connect these quantities to other stellar characteristics and to parameters used in model construction.

In the next section we will outline methodology of constructing seismic models, which, we believe, is applicable to all

Send offprint requests to: W.A. Dziembowski multimode δ Scuti stars in the Main Sequence phase of evolution. We should stress that our work is not the first effort aimed at reproducing observed frequencies in objects of this type. Goupil et al. (1993) modelled GX Pegasi for which five frequencies have been measured. Breger et al. (1995) and Guzik and Bradley (1995) constructed models of FG Virginis, which approximately reproduced observations. Our target accuracy is much higher – we want to approach the level of the observational error.

The rest of this paper concerns XX Pyxidis (CD–24 7599), which seemed to be a good choice for the first attempt in accurate reproducing observed spectrum. Amongst most multimode δ Scuti stars it is the hottest and least evolved. In such stars the predicted spectrum of unstable modes is relatively simple. With the progress of stellar evolution the instability extends to mode of mixed pressure/gravity (p/g) character and to pure g–modes. Separations in frequency between modes of the same $\ell > 0$ decrease, which complicates mode identifcation. In post Main Sequence stars the density of predicted spectra is so high that the task of mode identification will remain impossible unless we discover the clue to mode selection. Furthermore, the uncertainty in the description of the subphotosperic convection is less severe in this relatively hot star.

After presenting data in Sect. 3, we discuss in Sect. 4 constraints on mean parameters of the star. The methodology of the simultaneous search for mode identification and refinement of model parameters is described in Sect. 5. In the same section several alternative solutions are presented. In Sect. 6 we explain why these are unreliable and in the last section we discuss prospects for construction of a still improved seismic model of the star.

2. Construction of seismic stellar models

2.1. Principles

The number of modes detected in individual δ Scuti stars is far too small to attempt to determine radial structure directly from measured frequencies. Everything we may hope to achieve is to use the observed frequencies to determine global parameters characterizing the star and certain parameters of the theory. The equations of problem are obtained by equating observed and calculated frequencies,

$$f_{j,\mathrm{obs}} = f_{j,\mathrm{cal}}(\ell_j, m_j, n_j, \boldsymbol{P}_S, \boldsymbol{P}_T), \qquad (1)$$

where j labels measured frequencies, ℓ_j, m_j, n_j are numbers identifying the mode, $\boldsymbol{P}_S$ gives the set parameters characterizing the model, and $\boldsymbol{P}_T$ gives the set of free parameters of the theory.

A comment is needed about n_j. Nonradial modes excited in δ Scuti stars could be p–modes, g–modes, and modes of mixed character. In the present application, continuity of f as function of $\boldsymbol{P}$ for specified (ℓ, m, n) is essential. The avoided crossing effect causes that the continuity is guaranteed if we define the n values at ZAMS where the g– and p–mode spectra are separated in frequency. Following Unno et al. (1989) we will denote with $n < 0$ and $n > 0$ modes which in ZAMS models are consecutive g– and p–modes, respectively. For $\ell > 1$ there is the fundamental mode which is denoted with $n = 0$. With this choice, in evolved models some of modes denoted with $n > 0$ will have predominatly g–mode properties and *vice versa*.

The parameters given by $\boldsymbol{P}_S$ are those characterizing the evolutionary sequence like initial mass M, chemical composition, X_0 and Z_0, and the angular momentum. In addition, there is a single parameter identifying the model within the evolutionary sequence. The age is always a good choice. In the present application we use the initial equatorial velocity $V_{\mathrm{rot},0}$ instead of the angular momentum and $\log T_{\mathrm{eff}}$ instead of the age. The latter choice is acceptable because XX Pyx is certainly in the expansion phase of the Main Sequence evolution and T_{eff} is a monotonic function of the age. In any case there are five parameters in $\boldsymbol{P}_S$.

The quantities one may include in $\boldsymbol{P}_T$ are mixing–length parameter α, overshooting distance d_{over}, as well as parameters characterizing angular momentum evolution and mass loss. None of these will be included in the present work. Constraining these parameters is certainly the most important application of asteroseismology. However, as we will see later in this paper, we are not yet at this stage.

2.2. Tools

2.2.1. Evolution code

Stellar evolution code we use was developed in its original version by B. Paczyński, R. Sienkiewicz and M. Kozlowski. It is in fact a modern version of B. Paczyński's code (Paczyński 1969, 1970), which is now written in a modular form enabling an easy implementation of microscopic physics data from various sources. In the present application we use most recent versions of OPAL opacity (Iglesias & Rogers 1996) and equation of state (Rogers et al. 1996) data. The nuclear reaction rates are the same as used by Bahcall and Pinsonneault (1995).

The effect of averaged centrifugal force is taken into account in the equation for hydrostatic equilibrium. We assume uniform rotation and conservation of global angular momentum. These are the simplest assumptions which we are prepared to abandon if this is required for a successful seismic model construction. Similarily, we are prepared to introduce overshooting and/or rotationally induced mixing of the chemical elements outside of the convective core, but these effects are ignored in the present work. With these assumptions the input parameters for sequences are total mass, M, initial values for hydrogen abundance, X_0, metal abundance, Z_0, and the equatorial velocity $V_{\mathrm{rot},0}$. Initial heavy element mixture is that of Grevesse & Noels (1993). The assumed parameters for convection are $\alpha = 1$, $d_{\mathrm{over}} = 0$. The choice of α is unimportant in the present application.

For selected values of T_{eff} the code returns all needed parameters of the model such as $\log g_{\mathrm{eff}}$, V_{rot} or Ω and the matrix of the coefficients needed for calculation of linear nonadiabatic oscillation properties.

2.2.2. Nonadiabatic oscillation code

The code we use is a modified version of the code developed long ago by one of us (Dziembowski 1977). The important modification is taking into account the effect of the averaged centrifugal force. Modified equations for adiabatic oscillations are given by Soufi et al. (1997). The corresponding change in the full nonadiabatic set is trivial. The input to this code specifies the range of frequencies and the maximum value of ℓ. The standard output are the following characteristics of the $m = 0$ modes: complex dimensionless frequencies σ, modified growth rates, η, and the complex ratio of the flux to displacement eigenfunctions at the surface, $\mathcal{F}$.

The frequency, f, which we compare with observations is given by the real part of σ:

$$f = \Re(\sigma)\sqrt{\frac{G\bar{\rho}}{\pi}}. \tag{2}$$

For higher order p–modes beginning with, say, $n = 5$ or 6, the nonadiabatic effects are important at the level of the accuracy of frequency measurements. The growth rate is given by $-\Im(\sigma)$. A more convenient measure of mode stability is η which varies from –1, if damping occurs everywhere in the stellar interior, to +1, if driving occurs everywhere. At neutral stability we have $\eta = 0$. Values of η are important as constraints on modes and models. We will use them in the next sections. Also $\mathcal{F}$'s have applications in asteroseismology, especially, in determination of ℓ–values (see Cugier et al. 1994). However, we do not have neccesary observational data on XX Pyx to make use of this quantity.

2.2.3. Calculation of the rotational splitting

Rotation has an important effect on the structure of oscillation spectra. Even at modest equatorial velocities such as 50–100 km/s the effect of rotation can not be reduced to the linear splitting $\propto m\Omega$. Our code calculating the rotational splitting is accurate up to Ω^2. It is a version of the code by Dziembowski and Goode (1992) modified by two of us (WAD, AAP) and M.–J. Goupil. It uses the adiabatic approximation. The same nonadiabatic correction evaluated with the the code described in the previous subsection is added to all modes within the multiplet.

3. Frequency data

More than 350 hours of time–series photometric observations of XX Pyx are available. These include two Whole Earth Telescope runs (Handler et al. 1996, 1997a) as well as follow–up measurements to study the star's amplitude and frequency variations (Handler et al. 1997b).

Analysis of the two WET data sets allowed the extraction of 13 pulsation frequencies plus one 2f–harmonic. These frequencies are summarized in Table 1, and mostly taken from Handler et al. (1997a, hereafter HPO). Moreover, from an examination of the follow–up data, the values of frequencies f_1, f_2 and f_3 could be refined. The three revised frequencies are also listed in Table 1. Their error sizes differ from those listed in HPO, since these frequencies are now known without alias ambiguity. However, these three frequencies are slightly variable (Handler et al. 1997b). Therefore the error bars have been modified to account for the latter effect.

Table 1. Frequencies of the 13 pulsation modes and the $2f_1$–harmonic of the δ Scuti star XX Pyx unambiguously detected by HPO

	Frequency (cycles/day)	Ampl. (1992) (mmag)	Ampl. (1994) (mmag)
f_1	38.1101 ± 0.0004	11.5 ± 0.2	15.9 ± 0.2
f_2	36.0113 ± 0.0010	10.0 ± 0.2	3.3 ± 0.2
f_3	33.4370 ± 0.0002	6.4 ± 0.2	3.8 ± 0.2
f_4	31.3925 ± 0.0025	3.8 ± 0.2	1.9 ± 0.2
f_5	28.9950 ± 0.0025	2.4 ± 0.2	2.7 ± 0.2
f_6	27.0028 ± 0.0025	2.4 ± 0.2	1.6 ± 0.2
f_7	34.6657 ± 0.0038	2.2 ± 0.2	2.0 ± 0.2
f_8=$2f_1$	76.2203 ± 0.0038	0.8 ± 0.2	1.1 ± 0.2
f_9	27.2635 ± 0.0138	1.0 ± 0.2	1.9 ± 0.2
f_{10}	29.6196 ± 0.0075	1.5 ± 0.2	1.3 ± 0.2
f_{11}	33.6367 ± 0.0125	1.2 ± 0.2	1.7 ± 0.2
f_{12}	28.6980 ± 0.0138	1.1 ± 0.2	1.5 ± 0.2
f_{13}	31.2033 ± 0.0163	1.4 ± 0.2	1.1 ± 0.2
f_{14}	31.9062 ± 0.0100	1.0 ± 0.2	1.7 ± 0.2

4. Constraints

4.1. Mean surface parameters from observations

To estimate the position of XX Pyx in the H–R diagram, color photometry and high–resolution spectroscopy of the star have been carried out by HPO. Applying calibrations to the photometric data, they infer that XX Pyx is a main–sequence δ Scuti star with $T_{\rm eff} = 8300 \pm 200$ K, log $g = 4.25 \pm 0.15$. From their spectroscopy HPO determined the star's projected rotational velocity with $v \sin i = 52 \pm 2$ km/s and that the object has approximately solar metal abundance: $[M/H] = 0.0 \pm 0.2$.

4.2. Structures in the power spectra

An important constraint for identifying the different pulsation frequencies of XX Pyx with the corresponding quantum numbers was found by HPO. They searched for characteristic spacings within the 13 pulsation frequencies with a Fourier technique: they assumed unit amplitude for all the individual pulsations they detected and Fourier analysed the resulting signal. This is analogous to a spectral window: the power spectrum of such a signal has maxima at the sampling frequency and its harmonics (see Kurtz 1983). With this method it is possible to find regular frequency spacings in an objective way.

There are two physical reasons why regular frequency spacings can be present: in case of slow (rigid) rotation the members of different multiplets are approximately equally spaced in frequency. Since the measured $v \sin i$ of XX Pyx is 52 km/s (HPO), rotational splitting could, under favourable circumstances, be

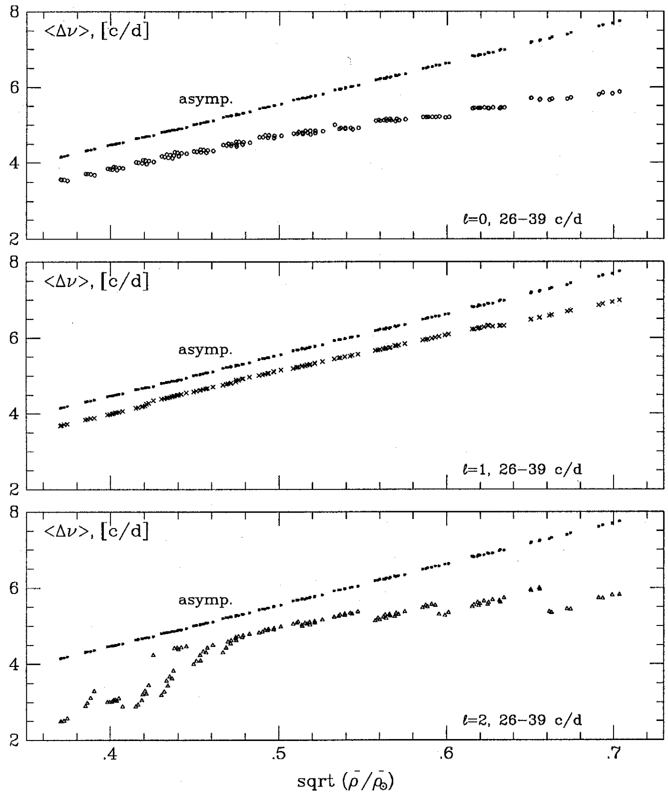

Fig. 1. Asymptotic frequency spacing of high-order p–modes of our main–sequence models compared to the mean spacing of $\ell = 0, 1, 2$ modes in the frequency range excited in XX Pyx. Only axisymmetric ($m = 0$) modes are shown. Rightmost points correspond to stellar models of lowest mass and highest effective temperature. The higher mass and/or the lower effective temperature the higher overtones of p–modes are appeared in a fixed frequency range, therefore the mean frequency spacing is approaching the asymptotic value. The scatter of the datapoints, most pronounced for $\ell = 0$ modes, reflects the different rotation rates of our models. The discontinuities of $\ell = 2$ modes at $\sqrt{(\bar{\rho}/\bar{\rho}_\odot)} \leq 0.46$ are due to intruding g–modes, while more regular level shifts of $\ell = 1$ and $\ell = 2$ modes are caused by different overtones (and different number of these overtones) appearing in the frequency range of interest.

detected. The second possibility is that consecutive modes of the same ℓ are excited. Even for low–overtone pulsations such modes are approximately equally spaced in frequency.

To illustrate this second possibility, we used our basic grid of the main–sequence models and their oscillation frequencies (see Subsect. 5.2): $M = 1.75 - 2.05\ M_\odot$ with a step of $0.05\ M_\odot$, $\log T_{\rm eff} = 3.905 - 3.925$ with a step of 0.05, $V_{\rm rot,0} = 50 - 125$ km/s with a step of 25 km/s. For each of these models, we compared the asymptotic frequency spacing with the mean spacing between frequencies of consecutive modes of a given ℓ value. We restrict to the observed frequency range of XX Pyx. The results are shown in Fig. 1. (Remember that the asymptotic frequency spacing for high overtone p–modes is determined by the following formula, see Unno et al. 1989, Eq. (16.36): $\Delta\nu = 0.5/(\int_0^R \frac{dr}{c})$, where c is the sound speed, — i.e. it is proportional to the square root of the star's mean density.)

As can easily be seen from Fig. 1, the assumption that regular frequency spacings are present even at relatively low overtones is justified. The frequency spacings of the different ℓ's are very similar. Consequently, HPO carried out the Fourier analysis described above and discovered a regular frequency spacing within the pulsation modes of XX Pyx, with a probability of less than 3% that this detection was caused by chance. Because of the value of this spacing ($\approx 26\ \mu$Hz ≈ 2.25 c/d), HPO suggested that it cannot reflect rotational splitting (since the second–order terms would destroy any frequency symmetry at such high rotation rates).

From a comparison of the Fourier analyses of the observed and of several model frequency spectra, HPO concluded that this spacing is caused by the presence of modes corresponding to consecutive overtones of $\ell = 1$ and $\ell = 2$ modes. HPO determined the spacing of consecutive overtones of the *same* ℓ with $54.0 \pm 2.3\ \mu$Hz ($= 4.67 \pm 0.20$ c/d). This frequency spacing is a measure of the sound crossing time through the object, and thus it can be used to determine the mean density of the star. For a model sequence with solar metallicity, HPO determined $\bar{\rho} = 0.246 \pm 0.020\ \bar{\rho}_\odot$.

HPO performed several tests to verify the validity of this method and the correct interpretation of its result (see their paper for more details) and found their Fourier technique to be reliable, since the frequency spectrum of XX Pyx is very well suited for such an analysis: only a few overtones are excited, but a large number of possible pulsation modes are photometrically observed.

Actually, one can use this Fourier method to test a common assumption in mode identification attempts from photometric (and radial velocity) data: with increasing degree ℓ of the pulsations, geometrical cancellation (Dziembowski 1977, Goupil et al. 1996) decreases the photometric amplitude of the modes. Therefore, it is usually assumed that only modes with $\ell < 3$ can be detected using photometric data. The photometric amplitude of an $\ell = 3$ mode with the same intrinsic amplitude as an $\ell = 1$ mode is only about a factor of 12 smaller, which is approximately the range of photometric amplitudes of the different pulsation modes detected for XX Pyx. However, when considering rotational splitting, seven modes of $\ell = 3$ can be present, but only three $\ell = 1$ modes. Therefore it can not be ruled out that a non–negligible number of $\ell = 3$ modes is excited to observable amplitude.

Consequently, we applied HPO's Fourier technique to model frequencies, incorporating modes with $\ell = 3$ and/or $\ell = 4$. In cases where many of these high ℓ modes were present, no significant frequency spacing could be found, since their rotationally split patterns "masked" the regular spacing of the $\ell = 0 - 2$ modes. Only with a few of the high ℓ modes the typical frequency spacing could be revealed. This suggests that most of the pulsation modes of XX Pyx are indeed of $\ell = 0 - 2$.

4.3. Implication from the stability survey

XX Pyx is a hot δ Scuti star located near the blue edge of the instability strip. In such an object the opacity mechanism driving

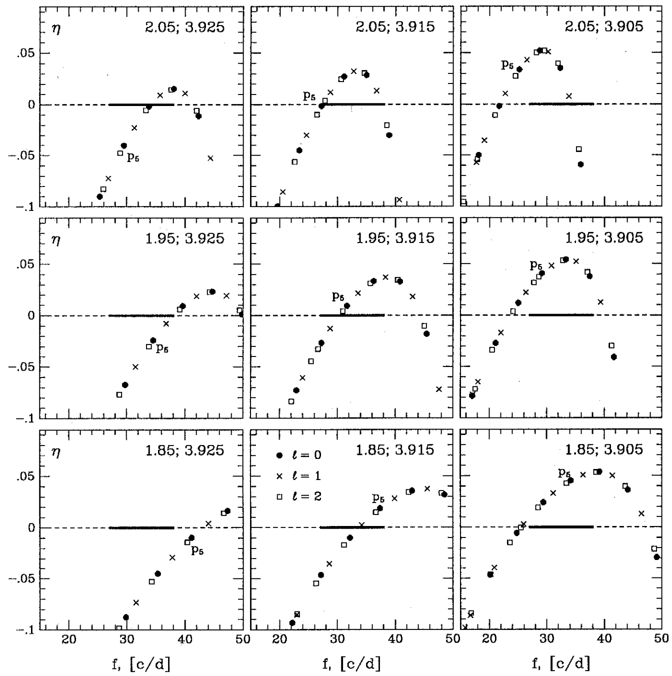

Fig. 2. Normalized growth rates, η, plotted against frequency, f, in selected models spanning the allowed ranges of M and $\log T_{\rm eff}$. The values of M (in solar units) and $\log T_{\rm eff}$ are given in each panel. Models were calculated with $X_0 = 0.7$, $Z_0 = 0.02$ and $V_{\rm rot} = 0$. The symbol $\rm p_5$ is plotted near the corresponding radial overtone. The thick horizontal line shows the range of frequencies measured in XX Pyx.

is confined to modes in a narrow range of frequencies and the driving effect is marginal. This is seen in Fig. 2. Values of η never exceed 0.05. The range of f where $\eta > 0$ never spans more than three radial orders for radial modes. In models considered the lowest values of n is 4 and the highest is 8. The behaviour of $\eta(f)$ in several models is shown in Fig. 2. The selected models have the surface parameters in the range consistent with the data on XX Pyx. The independence on ℓ and occurence of a single maximum are typical features for the opacity driven modes.

Values of η do not have the same reliability as those of f. Our treatment of the optically thin layers and the convective flux is crude. Therefore we will regard identifications with modes of small negative η's as admissible. However, we can exclude identifications involving radial modes with $n < 4$ and $n > 8$ as well we can exclude all models with, approximately, $\log T_{\rm eff} > 3.925$ and the low mass models with $\log T_{\rm eff} > 3.92$ (see Fig. 2).

5. A search for best parameters and mode identification

We have no observational information about the ℓ and m values for the modes detected in XX Pyx. The assignment of these two quantum numbers as well as n may only be done together with model parameter determination. The basis is Eq. (1) applied to the 13 measured frequencies. We only assume that all modes are of low degree. Most of the results we will present here were obtained with the assumption $\ell \leq 2$ for all modes. We carried out also calculation allowing one of the mode to have $\ell = 3$. Some of the results for such a case will be discussed at the end of this section.

At this stage we allow no free theoretical parameters $\boldsymbol{P}_T$ and we fix X_0 and Z_0 at the values 0.7 and 0.02, respectively. Thus, we allow only three free model parametres: M, $V_{\rm rot,0}$, and $T_{\rm eff}$. For each model the modes are assigned to minimize

$$\chi^2 = \tfrac{1}{j} \textstyle\sum_{i=1}^{j} (f_{{\rm obs},i} - f_{{\rm calc},i})^2, \qquad (3)$$

where $j = 13$ or 12. The first value was used in the case when we assumed $\ell \leq 2$ for all modes. In the alternative version we search for the minimum of χ^2 relaxing the fit for one of measured frequency. In the automatic fitting routine we made sure that each of the model frequencies was assigned at most to one of the stellar frequencies.

5.1. *Uncertainties in stellar and model frequencies*

In our search for best models and mode identification we use unweighted observational data. The reason is that the errors in the frequency measurements are smaller than the uncertainities in the theoretical values. In Table 1 we may see that the errors range from 4×10^{-4} for f_1 to 163×10^{-4} for f_{13}. Thus the relative accuracy of frequency is, at worst, $\sim 5 \times 10^{-4}$, which is by one order of magnitude less than the theoretical uncertainty.

The main problem on the side of theory is in the treatment of rotation. We found that at equatorial velocities ~ 100 km/s the second order perturbation treatment yields relative accuracy in frequencies $\sim 5 \times 10^{-3}$.

5.2. *Tabulation of model frequencies*

With the codes described in Subsect. 2.2 we prepared tables with frequencies for modes with $\ell = 0$, 1, 2 covering the range of the stellar pulsation frequencies. At this stage we neglected the effects of near–degeneracy which we discuss in Sect. 6, because it complicates calculations and it is not essential at this stage. The range of $\log T_{\rm eff}$ values was $[3.905 - 3.925]$ with a step of 0.05. The lower limit is somewhat less than the lower limit allowed by the photometry (Subsect. 4.1) while the upper limit follows from the stability consideration (Subsect. 4.3). The range of equatorial velocities was $[50 - 125]$ km/s with a step of 25 km/s. Here the lower limit follows from the $v \sin i$ measurement (Subsect. 4.1). The upper limit was adopted to avoid large errors in treatment of rotation. The adopted mass range was $[1.75 - 2.05] M_\odot$ with a step of $0.05 M_\odot$. The implied range of the mean density is significantly larger than that inferred in Subsect. 4.2. We consider models in the wider range of mean densities because there is a nonzero probability that the HPO spacing is caused by chance.

5.3. *Properties of* $\chi^2(M, V_{\rm rot,0}, T_{\rm eff})$

We calculated values of χ^2 according to Eq.(3) with $j = 13$ for nearly 40000 models interpolating model parameters and frequencies from the three–dimensional basic grid described

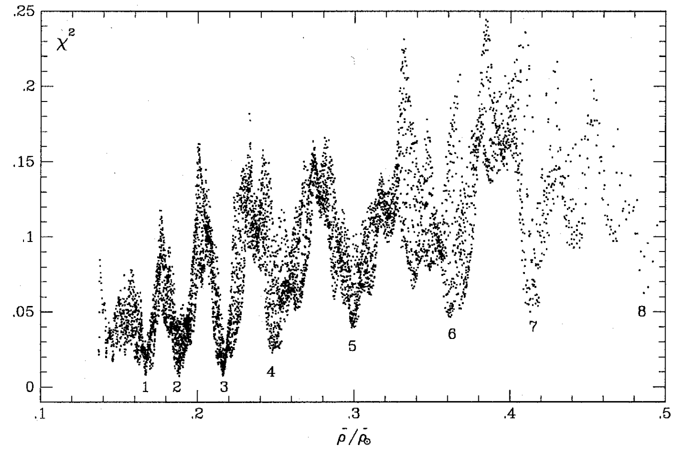

Fig. 3. Values of χ^2 evaluated for frequencies in ~ 7000 models in the ranges $M = 1.75 - 2.05\ M_\odot$, $V_{\rm rot,0} = 50 - 110$ km/s, $\log T_{\rm eff} = 3.905 - 3.925$. The patterns are the same (but less dense) as in the case of ~ 40000 models used to choose best identifications.

above. At this stage we confined the upper limit of the equatorial rotational velocity still more, to the value of 110 km/s. In Fig. 3 we plot the values of χ^2 against mean density, which is the most important parameter determining p–mode spectra. We see several dips in χ^2 which allows us to isolate potential mode identification. One of the dips occurs close to $\bar{\rho} = 0.246$, which was the preferred value from the observational frequency spacing. The present analysis shows that there are few alternative "good" values. We stress that a good fit may occur even if there is no preferred spacing. The coincidence however speaks in favor of identfications corresponding to this particular dip. The dips become shallower with the increasing $\bar{\rho}$ which merely reflects the fact that in less evolved models there are fewer modes in the specified frequency range.

At this stage we have to consider the identifications associated with the dips located near the following eight values of $\bar{\rho}$: 0.17, 0.19, 0.22, 0.25, 0.30, 0.36, 0.41 and 0.49. It should be noted, however, that all the minimum values of χ^2 are still far larger than the measurement errors.

Next important parameter is the equatorial velocity of rotation which determines the m–dependence. The plot of χ^2 against $V_{\rm rot,0}$, which we do not reproduce here, shows two shallow minima around the values 60 and 100 km/s.

5.4. *Possible models and identifications*

There is no doubt that if all (or almost all) 13 modes detected in XX Pyx are of $\ell \leq 2$ degree then the mode identification and model must correspond to one of the dips in χ^2. At each dip we chose a number of identifications with nearly the same lowest values of χ^2. All such identifications are listed in Table 2. They are grouped according to the dips. For each specified identification the three model parameters – M, $V_{\rm rot,0}$, $\log T_{\rm eff}$ – are determined through the χ^2 minimalization. These and other model characteristics are listed in Table 3.

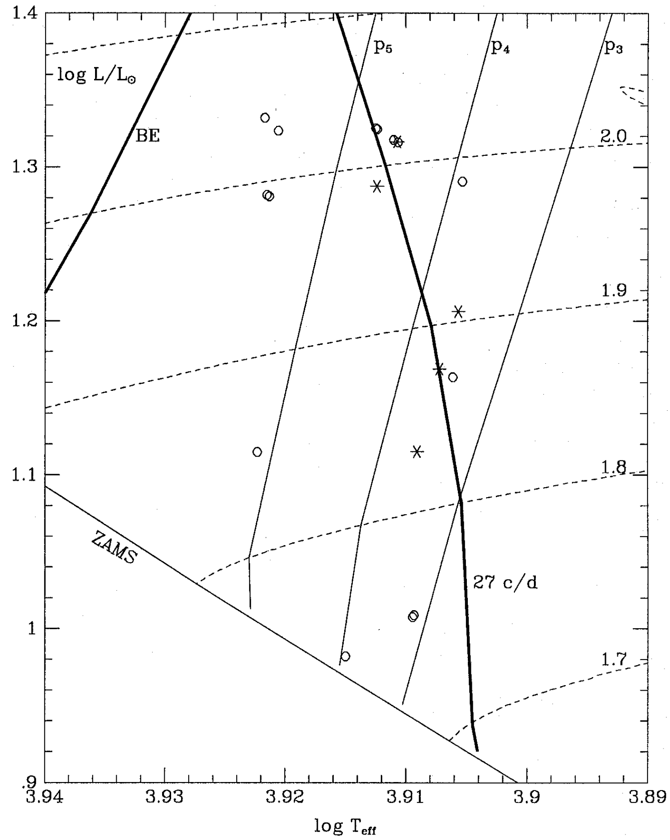

Fig. 4. Position (symbols) of the best models in the H–R diagram. The asterisks show the models used in Fig. 5. The evolutionary tracks for models with indicated mass and $V_{\rm rot} = 0$ are shown with dashed lines. The line denoted with BE shows the absolute blue edge; there are no unstable modes in models to the left of this line. The lines denoted with p$_n$ are the blue edges for the corresponding radial overtones and the line denoted with 27 c/d is the blue edge for modes with the corresponding frequency.

Not all models listed in Table 3 are consistent with the requirement that the identified modes are pulsationally unstable. Thus far we made a limited use of the constraint following from the stability considerations.

In fact, the stability argument may be used to eliminate some of the models listed in Tables 2 and 3 as candidates for the seismic model of XX Pyx. A comparison of the model positions with the blue edges in the H–R diagram, shown in Fig. 4, facilitates the elimination. We see that all the models with $M \leq 1.9 M_\odot$ and hotter than some $\log T_{\rm eff} = 3.91$ lie rather far from the blue edge for modes with $f \leq 27$ c/d, which is the lowest frequency observed in XX Pyx. At higher masses the upper limit of $\log T_{\rm eff}$ should be moved to 3.914. In this way we may eliminate models D2B, D2C, D3B, D3C and D8A.

Perhaps model D1A may be eliminated with the opposite argument because it lies far to the red of the 27 c/d blue edge. This means that there are unstable modes in the model with lower frequencies that are not seen in the star. This is, however, a much weaker argument because it is not an uncommon situation that unstable modes are not excited with detectable amplitudes.

Table 2. Possible identifications of the 13 modes detected in XX Pyx. Horizontal lines separate groups of the identifications associated with the consecutive dips of χ^2 seen in Fig. 3. Note that within the group most of the identifications are identical. Models corresponding to each identification are determined by minimalization of χ^2.

	f_6	f_9	f_{12}	f_5	f_{10}	f_{13}	f_4	f_{14}	f_3	f_{11}	f_7	f_2	f_1
	27.003	27.264	28.698	28.995	29.620	31.203	31.392	31.906	33.435	33.637	34.666	36.012	38.110
Model	l n m	l n m	l n m	l n m	l n m	l n m	l n m	l n m	l n m	l n m	l n m	l n m	l n m
D1A	2 3-1	2 3-2	1 5 1	2 4-1	1 5-1	2 5 0	2 5-1	2 5-2	1 6 0	1 6-1	2 6 1	2 6-2	2 7 2
D1B	2 3-1	2 3-2	1 5 1	2 4-2	1 5-1	2 5 0	0 6 0	2 5-2	1 6 0	1 6-1	2 6 1	2 6-2	2 7 2
D1C	2 3-1	2 4 2	1 5 1	2 4-2	1 5-1	2 5 0	2 5-1	2 5-2	1 6 0	1 6-1	2 6 1	2 6-2	2 7 2
D1D	2 3-2	2 4 2	1 5 1	2 4-2	1 5-1	2 5 0	2 5-1	2 5-2	1 6 0	1 6-1	2 6 1	2 6-2	2 7 2
D1E	2 3-1	2 4 2	1 5 1	2 4-2	1 5-1	2 5 0	0 6 0	2 5-2	1 6 0	1 6-1	2 6 1	2 6-2	2 7 2
D1F	2 3-2	2 4 2	1 5 1	2 4-2	1 5-1	2 5 0	0 6 0	2 5-2	1 6 0	1 6-1	2 6 1	2 6-2	2 7 2
D2A	1 4-1	2 3-1	2 4 0	0 5 0	1 5 1	1 5 0	1 5-1	2 5 1	2 5-1	1 6 1	2 6 2	2 6 1	2 6-2
D2B	1 4-1	2 3-2	2 4 0	0 5 0	2 4-2	1 5 0	1 5-1	2 5 1	2 5-1	1 6 1	2 6 2	2 6 1	2 6-2
D2C	1 4-1	2 3-2	2 4 0	2 4-1	2 4-2	1 5 0	1 5-1	2 5 2	0 6 0	2 5-1	1 6 1	2 6 2	2 6-2
D3A	2 3 0	1 4 1	2 4 2	1 4-1	2 4 1	0 5 0	2 4-1	1 5 1	1 5 0	1 5-1	2 5 1	2 5-1	1 6 0
D3B	2 3-1	1 4 1	1 4 0	1 4-1	2 4 1	0 5 0	2 4-1	1 5 1	1 5 0	1 5-1	2 5 1	2 5-1	1 6 0
D3C	2 3-1	1 4 1	2 4 2	1 4-1	2 4 1	0 5 0	2 4-1	1 5 1	1 5 0	1 5-1	2 5 1	2 5-1	1 6 0
D4A	2 3 2	2 3 1	0 4 0	2 3-2	1 4 1	1 4-1	2 4 2	2 4 1	0 5 0	2 4-2	1 5 1	1 5-1	0 6 0
D4B	2 3 2	2 3 1	2 3-1	2 3-2	1 4 1	1 4-1	2 4 2	2 4 1	0 5 0	2 4-2	1 5 1	1 5-1	0 6 0
D5A	1 3 1	2 2-2	1 3-1	2 3 2	2 3 1	2 3-1	0 4 0	2 3-2	1 4 0	2 4 2	2 4 1	2 4 0	1 5 1
D6A	2 2 2	2 2 1	2 2-1	2 2-2	1 3 1	1 3 0	1 3-1	2 3 2	2 3 0	2 3-1	2 3-2	1 4 1	2 4 2
D7A	2 1-2	1 2-1	2 2 2	2 2 1	2 2 0	0 3 0	2 2-2	1 3 1	1 3 0	1 3-1	2 3 1	2 3 0	1 4 1
D7B	2 1-2	1 2-1	2 2 2	2 2 1	2 2 0	0 3 0	2 2-2	1 3 1	1 3-1	2 3 2	2 3 1	2 3 0	1 4 1
D8A	2 1 0	0 2 0	2 1-2	1 2 0	1 2-1	2 2 2	2 2 1	2 2 0	2 2-2	0 3 0	1 3 1	1 3 0	2 3 1

Table 3. Parameters of models determined by the χ^2 minimalization. N_m is the total number of modes with $\ell \leq 2$ within the frequency range of modes detected in XX Pyx. The number decreases with mean density which explains increase of the χ^2 minima. Note that the difference in mean radial mode degree between consecutive groups is close to 0.5. Models used in Fig. 5 are marked with asterisks in the last column.

Model	$M/M_\odot$	$V_{\rm rot}$(ZAMS)	$V_{\rm rot}$	$\log T_{\rm eff}$	$\log L$	$\bar\rho/\bar\rho_\odot$	χ^2	N_m	$\Sigma(n+l/2)/13$	
D1A	1.9869	57.50	51.92	3.90533	1.2906	.16692	.006876	30	5.92	
D1B	2.0181	61.82	55.92	3.91101	1.3175	.16717	.006217	29	5.92	
D1C	2.0160	60.18	54.43	3.91063	1.3158	.16710	.006224	29	6.00	
D1D	2.0266	59.38	53.69	3.91247	1.3249	.16708	.007508	29	6.00	
D1E	2.0165	61.55	55.69	3.91072	1.3161	.16715	.006108	29	6.00	$*$
D1F	2.0260	60.59	54.79	3.91235	1.3243	.16711	.007646	29	6.00	
D2A	1.9953	108.01	99.30	3.91241	1.2876	.18680	.008070	27	5.73	$*$
D2B	2.0477	110.35	101.56	3.92169	1.3320	.18681	.007450	26	5.62	
D2C	2.0333	66.67	61.20	3.92056	1.3233	.18842	.007387	26	5.62	
D3A	1.9122	95.00	88.65	3.90567	1.2064	.21608	.007856	24	5.23	$*$
D3B	1.9986	97.64	91.16	3.92154	1.2819	.21614	.007181	23	5.23	
D3C	1.9972	95.40	89.09	3.92132	1.2809	.21605	.007530	23	5.23	
D4A	1.8722	66.67	63.00	3.90611	1.1635	.24711	.019895	20	4.77	
D4B	1.8782	67.27	63.60	3.90723	1.1688	.24732	.020005	20	4.77	$*$
D5A	1.8367	81.32	78.62	3.90907	1.1149	.29872	.036899	19	4.23	$*$
D6A	1.8527	60.28	59.07	3.92234	1.1148	.36149	.045757	18	3.69	
D7A	1.7556	75.00	74.63	3.90944	1.0074	.41550	.050614	17	3.27	
D7B	1.7562	74.13	73.72	3.90933	1.0086	.41368	.048300	17	3.31	
D8A	1.7500	61.11	61.17	3.91500	0.9819	.48689	.061828	18	2.85	

In Fig. 5 the frequencies determined for XX Pyx are compared with frequencies of low degree modes in selected models. These are not all acceptable but they cover the whole range. The common pattern of the model frequency spectra is the large departure from the equidistant pattern of the rotational splitting. This is particularly well seen in the case of the $\ell = 1$ triplets. One may see that with the increasing radial order the triplet becomes more and more asymmetric, so that the prograde mode $m = -1$ almost overlap the centroid mode $m = 0$ at the high frequency end. There is a near equidistant separation between the consecutive centroid modes at each ℓ in most of the cases. The exception is the low frequency part of the $\ell = 2$ spectrum

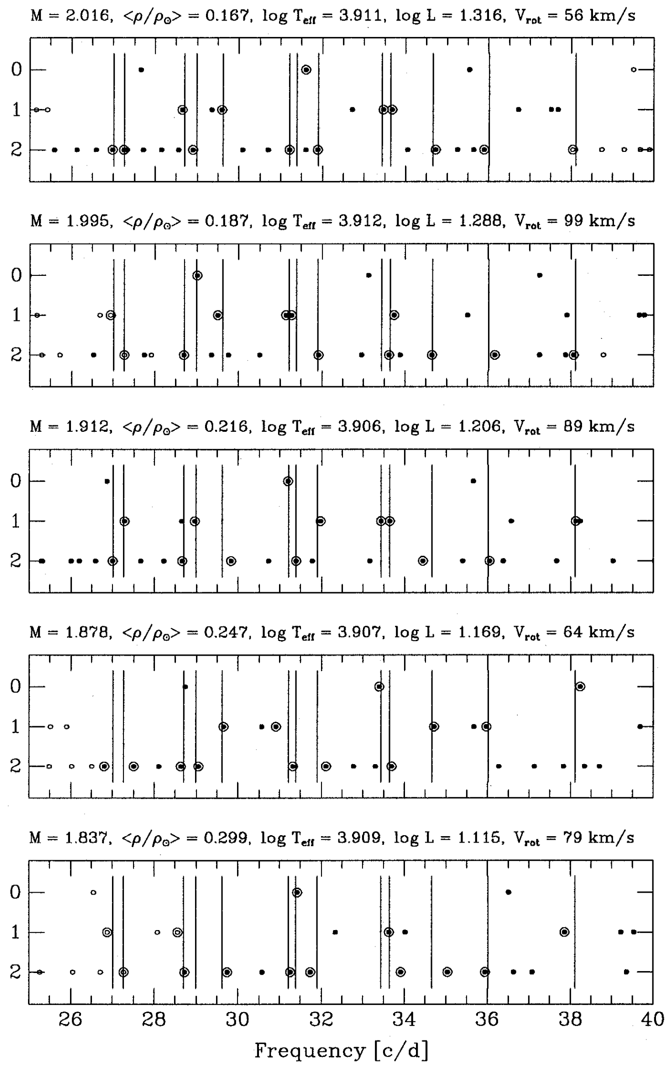

Fig. 5. Comparison of the XX Pyx frequencies (vertical lines) with model frequencies (symbols) for $\ell = 0$ (top row), $\ell = 1$ (middle row), $\ell = 2$ (bottom row). The encircled symbols denote the modes identified with those excited in the star. Small open circles denote the stable modes (always very close to instability $\eta \approx 0$. Positions of the selected models in the H–R diagram are denoted with asterisks in Fig. 4. In Tables 2 and 3 these models (from top to bottom) are denoted as D1E, D2A, D3A, D4B, and D5A.

in all, but the lowest mass models. Here we see the effect of *avoided crossing* between two multiplets. Modes in this range have mixed (p– and g–) character. Their frequencies are sensitive to the structure of the deep interior and therefore these modes are of special interest for seismic sounding.

5.5. Fitting 12 modes

Naturally, if we demand fitting for only 12 of the measured frequencies we may attain significantly lower values of χ^2. To estimate the effect we looked for the minimum of χ^2 considering all possible choices of 12 modes for each model. As expected, the general patterns of the χ^2 dependence on $\bar{\rho}/\bar{\rho}_\odot$ were found very much like those in Fig. 3. In particular, the dips occured at the same locations. For the same set of models the absolute minimum of χ^2 (0.00254) was reached at dip 3 ($\bar{\rho}/\bar{\rho}_\odot = 0.216$). The minimum value was nearly three times smaller than the absolute minimum in the previous 13-mode case. The implied mean frequency mismatch of 0.05 c/d is close to the estimated uncertainty in calculated frequencies. It is, thus, clear that improvement on the side of theory is needed before we will be able to produce a credible seismic model for this star. In the next section we discuss two most needed improvements.

6. Problems

One important effect in the treatment of rotational frequency perturbation which we did not include so far in our calculation was the near–degeneracy of certain modes which may be coupled by rotation. The effect is discussed in details by Soufi et al. (1997). Here we will present selected results for our model D3A.

Uniform (more generally, spherical) rotation couples modes if their azimuthal numbers (m) are the same and their degrees (ℓ) are the same or differ by 2. If the frequency difference between the two (or more) coupled modes is of the order of the rotation frequency one has to use the version of the peturbation formalism appropriate for the case of degeneracy i.e. to consider as a zeroth order basis a linear combination of the nearly degenerate modes. The relative contributions of the components are determined from the second order (in Ω) perturbation equations.

In application to XX Pyx a systematic near–degeneracy occurs between the $\ell = 0$ and 2 modes and between the $\ell = 1$ and 3 modes. In the latter case, for each multiplet we have three coupled modes corresponding to $m = -1$, 0, 1. These near–degeneracies follow from rather high values of n and, hence, approximate validity of the p–mode asymptotics. We also considered coupling involving three modes, e.g. $\ell = 0$, 2, 4 or $\ell = 0$, 2, 2, in the case of avoided crossing. In none of the cases considered the inclusion of the third mode was essential.

Model D3A and its oscillation frequencies were obtained by means of interpolation described in the previous section. In order to evaluate the effect of the degeneracy we had to recalculate the model and its frequencies. A comparison of the two upper panels of Fig. 6 clearly shows that the grid of models was not sufficiently dense. The differences between interpolated and calculated frequencies are easily seen, especially for the $\ell = 2$ modes near the avoided crossing. This inadequacy of our grid is not essential at this stage but must be kept in mind in more advanced efforts. In the top panel one may see how the fit is improved if the $\ell = 2$ identification for $f_7 = 34.7$ c/d is replaced with the $\ell = 3$. The value of χ^2 is then lowered by some 30 %. No fit improvement is achieved by allowing the $\ell = 3$ identification for another poorly fit frequency $f_{10} = 29.6$ c/d. One may see, however, in the mid panel that the situation changes if instead of the interpolated frequencies one uses the calculated ones.

A comparison of the mid and bottom panels shows the effect of the coupling between nearly degenerate modes. The effect is

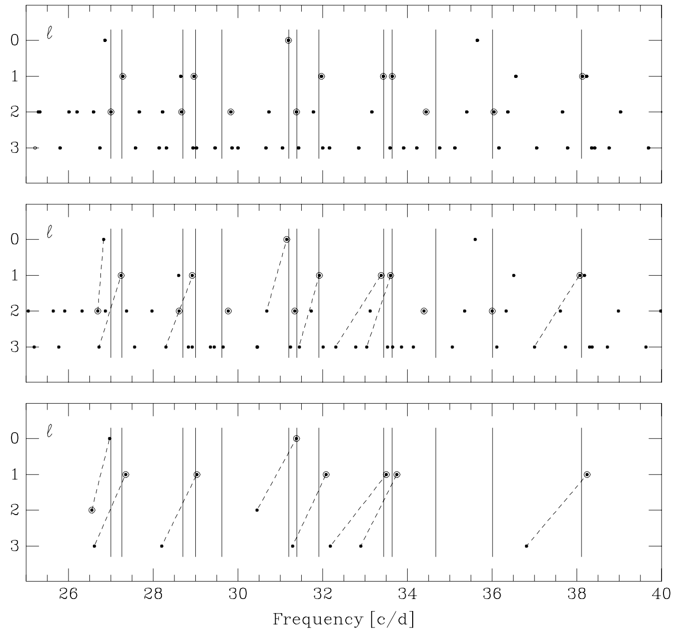

Fig. 6. Effects of inadequate grid density and near degeneracy shown for one of the best models (D3A). The upper panel shows interpolated frequencies which are the same (except that $\ell = 3$ modes are added) as in the mid panel in Fig. 5. The mid panel here shows frequencies of the same modes for the recalculated model. Frequencies of the modes coupled by rotation are connected with dashed lines. The resulting frequencies of these modes are shown in the lower panel.

Table 4. Effects of coupling between nearly degenerate modes

$f_{\rm obs}$	ℓ	n	m	f_0	δf	$A_{\rm low}$	$A_{\rm high}$
f_6	0	4	0	26.832	0.139	0.923	-0.385
	2	3	0	26.686	-0.139	0.761	0.649
f_9	1	4	1	27.239	0.112	0.935	-0.356
	3	3	1	26.720	-0.112	0.422	0.906
f_5	1	4	-1	28.932	0.096	0.951	-0.308
	3	3	-1	28.293	-0.096	0.374	0.927
f_{13}	0	5	0	31.153	0.226	0.881	-0.474
	2	4	0	30.678	-0.226	0.513	0.858
f_{14}	1	5	1	31.923	0.153	0.915	-0.403
	3	4	1	31.443	-0.153	0.481	0.877
f_3	1	5	0	33.374	0.122	0.962	-0.275
	3	4	0	32.302	-0.122	0.337	0.942
f_{11}	1	5	-1	33.613	0.137	0.931	-0.365
	3	4	-1	33.038	-0.137	0.441	0.897
f_1	1	6	0	38.064	0.174	0.944	-0.329
	3	5	0	36.988	-0.174	0.370	0.929

best seen in the case of $\ell = 2$ and 0 modes. The frequency distance between the modes increases when the coupling is taken into account. In Table 4 we give the values of the frequency shifts (δf) caused by the mode coupling as well as the amplitudes of the spherical harmonic components ($A_{\rm low}$ is corresponding to $\ell = 0$ or 1 and $A_{\rm high}$ is corresponding to $\ell = 2$ or 3). One may see that the mutual contamination of the $\ell = 0$ and 2 components is quite strong. This is bad news for prospects of mode discrimination by means of two–color photometry because such contaminated modes may appear in the *amplitude ratio – phase difference* diagrams (Watson 1988, Garrido et al. 1990) in the $\ell = 0$, 1 or 2 domains depending on the inclination of the rotation axis. Fortunately, modes with $m \neq 0$ are not affected. The mutual contamination is also significant for the $\ell = 1$ and 3 pairs. In all the cases the nominal $\ell = 3$ modes will be most likely observable through their $\ell = 1$ contaminations.

7. Discussion

Clearly, we have not succeeded in constructing the seismic model of XX Pyx. Models regarded as plausible, such as those in Fig. 5, do not reproduce the frequencies within the observational errors. In fact, we are quite far from the $10^{-3} - 10^{-2}$ c/d error range seen in Table 1. The departures from the fit for some of the identifications are in fact easily visible in Fig. 5. The problem proved more difficult than we have anticipated. We believe that we learned something in the process and that this knowledge should be shared with other groups undertaking similar efforts.

Undoubtedly, an improvement of the fits could be accomplished by allowing adjustment of the chemical composition parameters. The overshooting distance and parameters in the radial dependence of rotation rate should also be regarded as adjustable quantities. These degrees of freedom affect primarily the positions of the mixed modes relative to pure p–modes. In this application the mixed modes exist for $\ell = 2$ at the low frequency end. Such modes extend to higher frequencies for higher ℓ's. However, the freedom allows also a fine tuning of the distances between pure p–modes. One could hope that there is just one mode identification and one corresponding model of the star for which the frequency fit within the measurement errors is possible.

The reason why we cannot yet proceed this way is that our treatment of rotation is not adequate. We used here a perturbation theory which is accurate up to some 0.05 c/d, much worse than the measurement accuracy. We are not yet sure that the recently developed cubic theory (Soufi et al. 1997) would yield a sufficient accuracy.

Observational determination of the ℓ values for some of the excited modes could significantly change the situation. Imagine, for instance, that we find that the photometric data place the f_1 mode into the $\ell = 0$ domain of an *amplitude ratio – phase difference* diagram (see Watson 1988, Garrido et al. 1990). We may see in Table 1 that this mode has far the highest amplitude and certainly it will be the first for which we will have the required data. As we have discussed in Sect. 6, the possibility that this is not a $\ell = 0$ mode but rather a $\ell = 2, m = 0$ mode must be considered. Fortunately, we do not see such an identification for f_1 in Table 2. Thus, we are left with only two models, D4A and D4B, with very similar parameters and the same identification for almost all modes excited in XX Pyx. We could discriminate between the two if we knew ℓ for f_{12} which is the only mode with different identification. If, however, the

f_1 position in the diagram corresponds to an $\ell = 1$ domain, we are less lucky. The possible models are not only six models with $\ell = 1$ for f_1 but also models D4A and D4B with $\ell = 0$ because radial modes contaminated with a $\ell = 2$ component may appear in the $\ell = 1$ domain. The ambiguity implies a wide range of admissible model parameters.

Acknowledgements. Pamyatnykh and Dziembowski enjoyed the hospitality during their stays in Vienna and express their thanks to Mike Breger and his collaborators for it. We all thank Bohdan Paczyński, Maciej Kozlowski and Ryszard Sienkiewicz for the stellar evolution code. We thank also Marie–Jo Goupil for her contribution to development of the code calculating the rotational splitting. This work was supported in part by the Austrian Fonds zur Förderung der wissenschaftlichen Forschung, project number S7304, and also by the grants AFOSR–95–0070, NSF–INT–93–14820, RFBR–95–02–06359 and KBN–2P304–013–07.

References

Bahcall, J. N., Pinsonneault, M. H. 1995, Rev. Mod. Phys, 67, 781
Breger, M., 1997, in *New eyes to see inside the Sun and stars: pushing the limits of helio– and asteroseismology with new observations from ground and from space*, Proc. IAU Symp. 185, Kyoto, in press
Breger, M., Handler, G., Nather, R. E., et al. 1995, A&A, 297, 473
Breger, M., Zima, W., Handler, G., et al. 1997, A&A, in press
Christensen–Dalsgaard, J., Däppen, W. 1993, A&AR, 4, 267
Cugier, H., Dziembowski, W. A., Pamyatnykh, A. A. 1994, A&A, 291, 142
Dziembowski, W. A. 1977, Acta Astron., 27, 203
Dziembowski, W. A., Goode, P. R. 1992, ApJ, 394, 670
Garrido, R., Garcia–Lobo, E., Rodriguez, E. 1990, A&A, 234, 262
Goupil, M.–J., Michel, E., Lebreton, Y., Baglin, A. 1993, A&A, 268, 546
Goupil, M.–J., Dziembowski, W. A., Goode, P. R., Michel, E. 1996, A&A, 305, 487
Grevesse N., Noels A. 1993, in *Origin and Evolution of the Elements*, eds. Pratzo N., Vangioni-Flam E., Casse M., Cambridge Univ. Press., p. 15
Guzik, J. A., Bradley, P. 1995, Baltic Astronomy, 4, 442
Handler, G., Breger, M., Sullivan, D. J., et al. 1996, A&A, 307, 529
Handler, G., Pikall, H., O'Donoghue, D., et al. 1997a, MNRAS, 286, 303 (HPO)
Handler, G., Pamyatnykh, A. A., Zima, W., et al. 1997b, MNRAS, in press
Iglesias, C. A., Rogers, F. J. 1996, ApJ, 464, 943
Kurtz, D. W., 1983, IBVS 2285
Mantegazza, L., Poretti, E., Bossi, M. 1996, A&A, 308, 847
Paczyński, B. 1969, Acta Astron., 19, 1
Paczyński, B. 1970, Acta Astron., 20, 47
Rogers, F. J., Iglesias, C. A. 1994, Sci, 263, 50
Rogers, F. J., Swenson, F. J., Iglesias, C. A. 1996, ApJ, 456, 902
Seaton, M. J., 1996, MNRAS, 279, 95
Soufi, F., Goupil, M.–J., Dziembowski, W. A., 1997, A&A, submitted
Unno, W., Osaki, Y., Ando, H., Saio, H., Shibahashi, H. 1989, Nonradial oscillations of stars, University of Tokyo Press
Watson, R. D. 1988, Ap&SS, 140, 255

2.2.5 Delta Scuti Network observations of XX Pyx: detection of 22 pulsation modes and of short-term amplitude and frequency variations

Original paper:

G. Handler, T. Arentoft, R. R. Shobbrook, M. A. Wood, L. A. Crause, P. Crake, F. Podmore, A. Habanyama, T. Oswalt, P. V. Birch, G. Lowe, C. Sterken, P. Meintjes, J. Brink, C. F. Claver, R. Medupe, J. A. Guzik, T. E. Beach, P. Martinez, E. M. Leibowitz, P. A. Ibbetson, T. Smith, B. N. Ashoka, N. E. Raj, D. W. Kurtz, L. A. Balona, D. O'Donoghue, J. E. S. Costa, M. Breger, 2000, MNRAS 318, 511

Mon. Not. R. Astron. Soc. **318**, 511–525 (2000)

Delta Scuti Network observations of XX Pyx: detection of 22 pulsation modes and of short-term amplitude and frequency variations

G. Handler,[1,2]★ T. Arentoft,[3] R. R. Shobbrook,[4,5] M. A. Wood,[6] L. A. Crause,[7] P. Crake,[8] F. Podmore,[9]† A. Habanyama,[10]† T. Oswalt,[6] P. V. Birch,[8] G. Lowe,[8] C. Sterken,[3] P. Meintjes,[11] J. Brink,[11]† C. F. Claver,[12] R. Medupe,[2,7] J. A. Guzik,[13]‡ T. E. Beach,[14]‡ P. Martinez,[2] E. M. Leibowitz,[15] P. A. Ibbetson,[15] T. Smith,[8] B. N. Ashoka,[16] N. E. Raj,[16] D. W. Kurtz,[7] L. A. Balona,[2] D. O'Donoghue,[2] J. E. S. Costa[17]§ and M. Breger[1]

[1]*Institut für Astronomie, Universität Wien, Türkenschanzstraße 17, A-1180 Wien, Austria*
[2]*South African Astronomical Observatory, PO Box 9, Observatory 7935, South Africa*
[3]*Vrije Universiteit Brussel, Pleinlaan 2, B-1050 Brussels, Belgium*
[4]*PO Box 518, Coonabarabran, NSW 2357, Australia*
[5]*Research School of Astronomy and Astrophysics, Australian National University, Weston Creek PO, ACT 2611, Australia*
[6]*Department of Physics and Space Sciences & SARA Observatory, Florida Institute of Technology, 150 W. Univ. Blvd., Melbourne, FL 32901, USA*
[7]*Department of Astronomy, University of Cape Town, Rondebosch 7700, South Africa*
[8]*Perth Observatory, Walnut Rd., Bickley, Western Australia 6076, Australia*
[9]*Department of Physics, University of Zimbabwe, PO Box MP167, Mount Pleasant, Harare, Zimbabwe*
[10]*Department of Physics, University of Zambia, PO Box 32379, Lusaka, Zambia*
[11]*Physics Department, University of the Orange Free State, Bloemfontein 9300, South Africa*
[12]*National Optical Astronomy Observatories, PO Box 26732, Tucson, Arizona 85726-6732, USA*
[13]*Los Alamos National Laboratory, X-2, MS B220, Los Alamos, NM 87545-2345, USA*
[14]*Department of Natural Sciences, University of New Mexico, Los Alamos, 4000 University Drive, Los Alamos, NM 87544, USA*
[15]*Wise Observatory, Sackler Faculty of Exact Sciences, Tel Aviv University, Tel Aviv 69978, Israel*
[16]*Indian Space Research Organisation, Technical Physics Division, ISRO Satellite Centre, Airport Road, Bangalore 560017, India*
[17]*Instituto de Fisica, Universidade Federal do Rio Grande do Sul, 91501-970 Porto Alegre-RS, Brazil*

Accepted 2000 June 5. Received 2000 May 26; in original form 2000 March 15

ABSTRACT

We report multisite observations devoted to the main-sequence δ Scuti star XX Pyx, conducted as the 17th run of the Delta Scuti Network. Over 125 nights a total of 550 h of usable time-series photometric *B*- and *V*-filter data were acquired involving both photoelectric and CCD measurements at eight observatories spread around the world, which represents the most extensive single time-series for any pulsating star other than the Sun obtained so far.

We describe our observations and reduction methods, and present the frequency analysis of our new data. First, we detect six new pulsation and five new combination frequencies in the star's light curves. We also discover evidence for amplitude and/or frequency variations of some of the modes during the observations. These can occur on time-scales as short as 20 d and show quite diverse behaviour. To take them into account in the frequency analysis, a so-called non-linear frequency analysis method was developed, allowing us to quantify the temporal variability of the modes and to compensate for it. Following that we continue the frequency search and we also incorporate published multisite observations. In this way, we reveal three more pulsation and two more combination frequencies. In the end, we report a total of 30 significant frequencies – 22 of which correspond to independent pulsation modes. This is the largest number of independent modes ever detected in the light curves of a δ Scuti star.

★ E-mail: gerald@saao.ac.za
† SAAO Summer School student.
‡ Guest observer, McDonald Observatory, University of Texas at Austin, USA.
§ Guest observer, Laboratorio Nacional de Astrofisica/CNPq, Brazil.

The frequencies of the modes show preferred separations as already suggested by previous work on this star; they are also arranged in clear patterns. These results lead to a refinement of the stellar mean density ($\bar{\rho} = 0.241 \pm 0.008\,\bar{\rho}_{\odot}$) and to a new constraint on the rotation rate of XX Pyx ($\nu_{\mathrm{rot}} = 1.1 \pm 0.3\,\mathrm{d}^{-1}$). However, our attempts to identify the modes by pattern recognition failed. Moreover, mode identification from multicolour photometry failed as well because the high pulsation frequencies make this method unfavourable. The diverse behaviour of the amplitude and frequency variations of some of the modes leaves resonances as the only presently known possibility for their explanation.

Key words: techniques: photometric – stars: individual: CD-24 7599 – stars: individual: XX Pyx – stars: oscillations – δ Scuti.

1 INTRODUCTION

Asteroseismology is the study of the interior structure of multiperiodically pulsating variable stars by identifying all the observed pulsation modes and by reproducing the observed frequency spectra via model calculations. With this method a good understanding of the interior structure of the Sun and of pulsating white dwarfs has been obtained. However, the application of asteroseismological techniques to main-sequence pulsators other than the Sun has proven to be difficult.

The most promising candidates for exploring the deep interior of main sequence stars through asteroseismology are the δ Scuti stars. These are spectroscopically (mostly) normal A–F stars of luminosity classes III–V; most of them are multiperiodic non-radial pulsators. Regrettably, seismological studies of these objects are not straightforward. The main problems are:

(i) Most of the excited pulsation modes have low photometric amplitude; a large amount of data is required to detect them (e.g. see Breger et al. 1999).

(ii) δ Scuti stars are low radial order p- and g-mode pulsators; asymptotic theory in general cannot be applied to decipher the pulsation spectra.

(iii) Many well-observed δ Scuti stars are in the phase of shell hydrogen burning; theoretical frequency spectra of such evolved δ Scuti stars are very dense. It is therefore difficult to identify the pulsation modes correctly as only a small percentage of unstable modes is actually observed (Dziembowski & Krolikowska 1990).

(iv) Most multiperiodic δ Scuti stars are fast rotators: rotationally split multiplets may overlap in frequency and second-order effects destroy equal frequency splittings (see Templeton, Bradley & Guzik 2000 for an illustration). Differential rotation would result in a further complication of the frequency spectrum.

(v) Mode identification methods usually have different sensitivities for different types of mode; they are therefore hard to cross-calibrate. Their reliability is often questionable and depends on the physical parameters of the target star (e.g. Balona & Dziembowski, private communication).

One possible way to overcome all these difficulties is to select stars with the simplest interior structure, slow rotation, and a large number of excited and detectable pulsation modes for in-depth studies. This idea is based on an examination of models of δ Scuti stars in the beginning of main-sequence evolution: the unstable mode spectrum of such models only comprises p-modes and is therefore relatively simple. If a sufficient number of these modes is detected in a real star, and if several consecutive radial overtones are excited, obvious patterns within the mode frequencies should appear, even if rotationally split multiplets of modes of different degree, ℓ, overlap. These patterns will allow an assignment of the pulsational quantum numbers ℓ and m to the modes (if the star obeys the same physics as the models). This method has been tested successfully (Handler 1998). Furthermore, photometric colour information could be used to check these mode identifications.

An ideal target for the application of this strategy is XX Pyx. Using 220 h of measurement during two Whole Earth Telescope (WET, Nather et al. 1990) campaigns, Handler et al. (1996, 1997) detected 13 pulsation frequencies in the light curves; this corresponds to approximately 40 per cent of the theoretically predicted number of modes with $\ell \leq 2$. For this low $v \sin i$ ($52\,\mathrm{km\,s^{-1}}$) δ Scuti star, Handler et al. (1997, hereafter HPO) managed to obtain some initial seismological results despite the lack of definite mode identifications: XX Pyx is a 1.85-$M_{\odot}$ star in the first half of its main-sequence evolution. A first seismological distance to a δ Scuti star of 650 ± 70 pc has been derived for this object. Pamyatnykh et al. (1998) attempted to obtain a 'best seismic model' for the star, but they could not find even one model that matched all the observed frequencies acceptably well. The reason for this result was suspected to be due to deficiencies in the model physics; the detection of more pulsation modes is hoped to point towards the cause of the problem.

XX Pyx is just sufficiently evolved that it may have one (and only one!) mode with g-mode properties in the interior excited. This particular mode can be used to determine the star's interior rotation rate and to measure the amount of convective core overshooting (Dziembowski & Pamyatnykh 1991), because a large fraction of this mode's kinetic energy originates from the outer part of the convective core. The size of the overshooting parameter is one of the most ill-determined quantities in stellar model calculations: it is 'found small if supposed small, large if supposed large' (Renzini 1987). A determination of this parameter is of crucial importance for the understanding of stellar structure and evolution, in particular for modelling open cluster HR diagrams (some people need convective overshooting to explain them), solar and stellar activity (the underlying dynamo mechanism) and, of course, stellar interiors.

Finally, XX Pyx has been reported to exhibit amplitude variations on time scales as short as one month, as well as frequency variability detectable over a few years (Handler et al. 1998, hereafter HPZ). This behaviour can make different sets of normal modes detectable at different times. Then the combined ensemble of modes can be used for an asteroseismological investigation. Such a strategy has been applied successfully already (Bond et al. 1996, Kleinman et al. 1998).

For all the reasons stated above, we deemed it worthwhile to devote a large observational effort to XX Pyx. A major multisite campaign has therefore been organized by the Delta Scuti Network (see Zima 1997); the initial results of that campaign are the subject of this paper.

2 OBSERVATIONS

Our multisite photometry was carried out between 1998 January 15 and April 5; the total time-base of our data set is therefore 81 d. We used 13 different telescope/detector combinations at nine observatories suitably spread in geographic longitude, and we obtained data during 125 clear nights at the different sites. We utilized both charge-coupled devices (CCDs) and photomultipliers (PMTs) as detectors, taking advantage of their different wavelength sensitivities: CCD measurements were taken through the Johnson (or Bessell) V filter whereas the PMT observations were acquired through the Johnson B filter. A brief synopsis of our measurements is given in Table 1, where PMT1 denotes a single-channel photometer, PMT2 a two-channel photometer and PMT3 a three-channel photometer.

The photoelectric observations were taken as high-speed photometric measurements, i.e. continuous 10-s integrations on the target star were performed. Because of the faintness of XX Pyx ($V = 11.50$ mag) and its short periods, this is the observing technique which promises the best results (see Handler 1995 for a more detailed discussion) in the case of photoelectric observations. The integrations on the target star were only interrupted to acquire measurements of sky background. If single-channel photometers were employed, additional observations of a close comparison star (SAO 176755) were obtained at hourly intervals. For multi-channel photometers, the latter object served as a sky-transparency monitor in Channel 2.

Our CCD measurements were obtained with a number of 512×512 and 1024×1024 chips, resulting in fields of view between 3×3 and 11×11 arcmin^2. The telescopes were pointed to acquire the maximum number of possible comparison stars on the frames, and care was taken to minimize drifts of the images over the chip. Integration times were chosen to yield one image every 60–120 s. Bias and dark frames as well as sky or dome flat fields were also taken every night (whenever possible).

3 REDUCTIONS

3.1 Initial CCD reductions; variable stars in the field

The reduction of the CCD frames was started by correcting for bias and flat field using standard routines. For the SARA observations, a correction for dark current was also useful. The extraction of the stellar time series was mainly accomplished using the MOMF package (Kjeldsen & Frandsen 1992), which combines point spread function (PSF)-fitting and aperture photometric techniques and gives excellent results. Under some circumstances (e.g. slow image rotation during a run) this needed to be supplemented by IRAF aperture photometry. The MOMF routines allow an easy choice of optimal aperture sizes, whereas we followed Handler, Kanaan & Montgomery (1997) for determining the best aperture radii for the IRAF results. The SAAO CCD measurements were analyzed using a modified version of DoPhot; the results were compared to those obtained by MOMF and found to be of similar quality.

We took special care in checking the constancy of the CCD comparison stars; we found two new variable stars in the field. A finding chart for those stars is given in Fig. 1. Variability of Star A ($V = 15.1$, no identification found in the literature) was discovered on the SAAO CCD frames. It varied sinusoidally with a time-scale of about 20 d and an amplitude of about 0.1 mag. The new variable B (GSC 6589-0555, $V = 14.5$) showed slow drifts of a few hundredths of a magnitude during the two nights of observation from Wise Observatory. These light variations were subsequently confirmed with the SARA data; the star was not present on any of the other observatories' frames. We note that it has a close companion which might affect the photometry, but this is unlikely owing to the applied MOMF photometry algorithm and because the magnitude changes were not correlated with seeing variations. The light variations of GSC 6589-0555 are rather complicated with a time-scale of about 20 h; no satisfactory multifrequency solution could be found.

To pinpoint the nature of these two variables, classification spectra were taken at the 1.9-m telescope of SAAO. Star A is of mid-to-late K spectral type. This spectral classification is corroborated by CCD colour photometry obtained at the SAAO

Table 1. Observing log of the 17th run of the Delta Scuti Network

Telescope	Instrument	Observer(s)	Hours of measurement
McDonald 0.9-m	PMT2	G. Handler, J. A. Guzik, T. E. Beach	104.7
McDonald 2.1-m	PMT2	G. Handler	54.0
ESO 0.9-m Dutch	CCD	T. Arentoft, C. Sterken	102.2
SAAO 0.75-m	PMT1	P. Martinez, F. Podmore, A. Habanyama, P. Meintjes, J. Brink	70.5
Siding Spring 0.6-m	PMT1	R. R. Shobbrook	40.9
Siding Spring 1.0-m	PMT1	R. R. Shobbrook	20.1
Perth 0.6-m	PMT1	P. V. Birch, P. Crake, G. Lowe, T. Smith	57.2
SARA 0.9-m	CCD	M. A. Wood, T. Oswalt, C. F. Claver	54.9
SAAO 1.0-m	CCD	L. A. Crause, D. W. Kurtz	22.1
Wise 1.0-m	CCD	E. M. Leibowitz, P. A. Ibbetson	10.4
SAAO 1.0-m	PMT1	R. Medupe	9.6
Kavalur 1.0-m	PMT3	B. N. Ashoka, N. E. Raj	3.2
Itajuba 0.6-m	CCD	J. E. S. Costa	0
Total			549.8

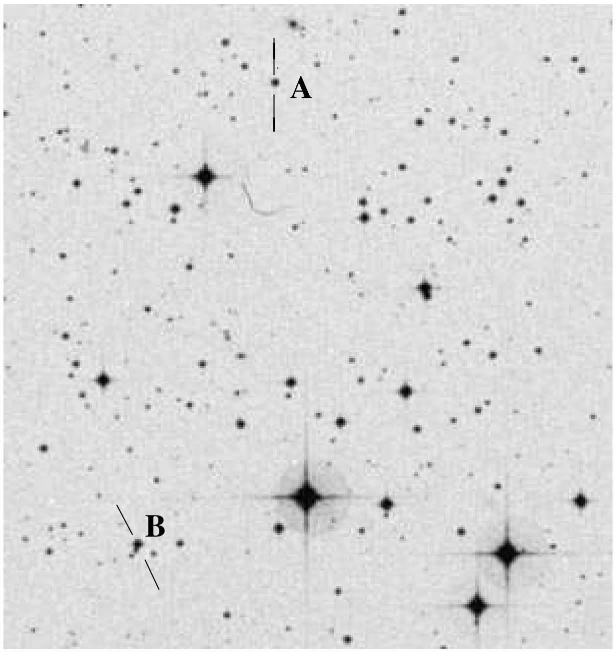

Figure 1. Finding chart for the new variables in the field of XX Pyx. Coordinates (Epoch 2000.0) are: Star A: α: $08^{\mathrm{h}}58^{\mathrm{m}}34\overset{\mathrm{s}}{.}2$, δ: $-24^{\mathrm{h}}33^{\mathrm{m}}52^{\mathrm{s}}$; Star B: α: $08^{\mathrm{h}}58^{\mathrm{m}}43\overset{\mathrm{s}}{.}7$, δ: $-24^{\mathrm{h}}40^{\mathrm{m}}28^{\mathrm{s}}$. The coordinates for star B are from the Guide Star Catalogue and should therefore be accurate, whereas the coordinates of star A were only roughly determined by us. North is on top and east to the left, the field of view is approximately $8 \times 8\,\mathrm{arcmin}^2$.

1.0-m telescope, which yielded $V = 15.12 \pm 0.02$, $(B - V) = 1.31 \pm 0.02$, $(V - R_{\mathrm{c}}) = 0.72 \pm 0.04$, and $(V - I_{\mathrm{c}}) = 1.40 \pm 0.05$. In accordance with the observed variability we think this is most likely a spotted star. Star B has a spectral type of late A/early F. It is therefore probably a variable star of the γ Doradus type. Needless to say, neither object was used as a comparison for XX Pyx.

3.2 Initial PMT reductions; constancy of the comparison star

The photoelectric measurements were reduced in a very similar way to that described by HPO (differences will be stated in what follows), i.e. we made use of the time-series of SAO 176755 to compensate for transparency variations or thin clouds (the latter naturally only in the case of multichannel observations) whenever necessary. This, of course, requires that this star be constant within the detection limit of oscillations of XX Pyx.

Non-variability of SAO 176755 had already been demonstrated for the new WET observations presented by HPO. However, the present study is based on a considerably larger amount of data. Therefore the expected noise level is much lower than previously, and the constancy of SAO 176755 has to be evaluated again. Another reason for doing so is that some variable stars can change their amplitude of variability with time; as a result some stars may appear constant at certain times, but variable at others.

We first considered the CCD photometry. Usable measurements of SAO 176755 were obtained during the first 11 nights (50.4 h) of SARA observation. On all the other frames the fields were either too small to acquire the star or its images were partly saturated (for obvious reasons the integration times were optimized for XX Pyx and not for one of its potential comparison stars). We computed an amplitude spectrum of these reduced data and found

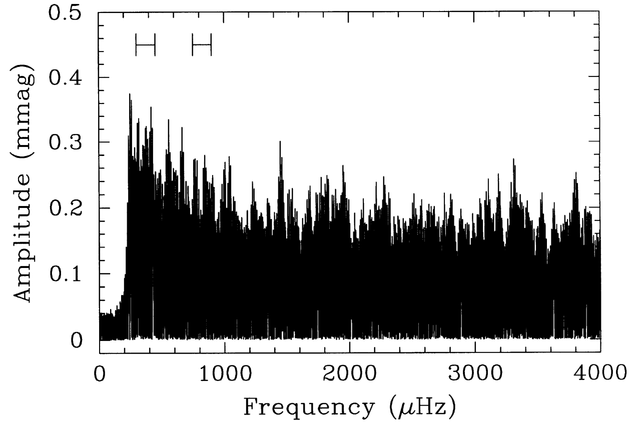

Figure 2. Amplitude spectrum of the time series of the comparison star SAO 176755 out to the Nyquist frequency. No variability with an amplitude larger than 0.4 mmag can be discerned; the distribution of the peaks is compatible with noise. The sharp decrease in amplitude at frequencies below $\approx 200\,\mu$Hz is due to low-frequency filtering. The frequency ranges of interest for XX Pyx are indicated.

no variations with an amplitude larger than 1 mmag. Despite our attempts to suppress image motion on the frames, we found a clear $1/f$ component in the amplitude spectrum. As this is also true for the other comparison stars, we do not consider it to be intrinsic to SAO 176755.

Our next step was to select the photoelectric multichannel data which were taken under photometric conditions (25 nights from McDonald Observatory) and to reduce the comparison star data. We subtracted a polynomial or spline fit to the sky background, removed bad points and corrected for extinction. We also performed some low-frequency filtering of the data (as we will do later for the programme star observations as well; we will discuss this procedure further below) as we wanted to eliminate possible PMT drifts and because we were only interested in variability occurring on the same time-scale as the target star's pulsations. We then filtered out the slow variations in the CCD time-series, multiplied the resulting magnitudes by 1.32 (the average theoretical B/V amplitude ratio for δ Scuti-type pulsations following Watson 1988), and merged it with the photoelectric light curves after converting the times of measurement into Heliocentric Julian Date (HJD). Then we calculated the amplitude spectrum of the combined time-series comprising 143.1 h of measurement, which is shown in Fig. 2.

There is no evidence for variability of SAO 176755 in Fig. 2 within the accuracy of our observations. We therefore conclude that it can be used safely to correct the programme star time-series if taken under non-perfect photometric conditions. Thus we were able to proceed to the reduction of the variable star time series obtained with PMTs. As before, we first corrected for sky background, bad points and extinction. Whenever necessary, a differential time series relative to SAO 176755 was constructed. For multichannel photometers, this was done on a point-by-point basis. However, boxcar smoothing of the Channel 2 data was applied whenever possible so that as little additional noise as possible was introduced in the light curves of XX Pyx; the width of the smoothing function was chosen depending on the time-scale on which transparency variations occurred. In the case of single-channel photoelectric observations, low-order polynomials or splines were fitted through the comparison star measurements and the fits were subtracted from the target star observations.

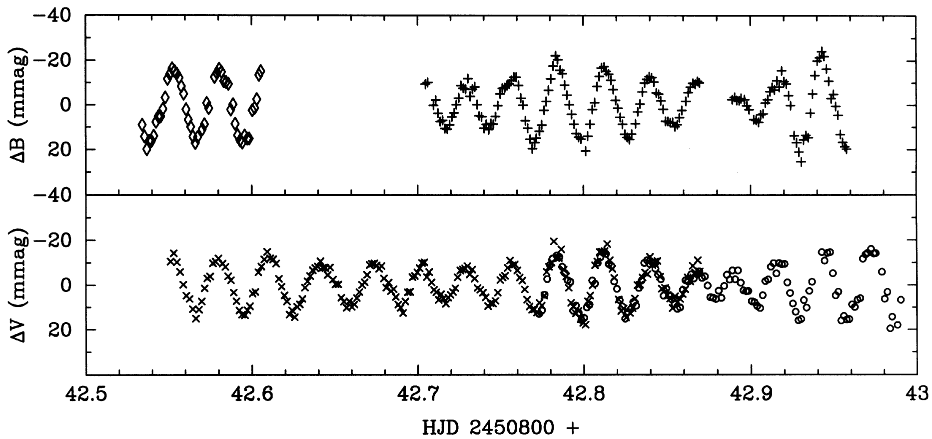

Figure 3. Some light curves obtained during the campaign. Diamonds: photoelectric SAAO data, plus signs: photoelectric McDonald observations, crosses: CCD measurements from ESO, open circles: SARA CCD light curve

3.3 Final reductions; low-frequency filtering

Because our primary goal is to detect as many pulsation frequencies of XX Pyx as possible, we are interested in obtaining the lowest possible noise level in the frequency range of interest. However, low-frequency noise generated for example by residual sky transparency variations, tube drift or image motion on the CCD detector can increase the noise at higher frequencies due to spectral leakage. Therefore, we decided to subject our time series to low-frequency filtering. We are aware that this destroys possible long-period stellar signals, but our combined data set is so inhomogeneous that such signals are hardly to be trusted. This had actually been a severe problem in the analysis of the first multisite data on the star (Handler 1994). We must further note that low-frequency filtering can be a dangerous procedure and has therefore to be applied with great care. By no means do we want to compromise the information supplied by the intrinsic variability of the star.

We proceeded as follows: we calculated the HJD for the preliminarily reduced light curves and combined the data for the different filters. Then we performed a frequency analysis of these data sets and removed a synthetic light curve consisting of all the detected signals due to pulsation from the time-series. This gave us a good indication of the frequency range excited in the star; we found that pulsational variability of XX Pyx only occurs at frequencies larger than 300 μHz. Based on this result we decided to filter out variations with frequencies less than 230 μHz ($20\,\mathrm{d}^{-1}$).

To accomplish this, we split the original and residual light curves into those of the individual runs. We visually inspected them and we calculated amplitude spectra of all these different residual time series. Then we calculated synthetic light curve fits to the residual data, by fitting straight lines and/or sinusoids with all detected frequencies below 230 μHz to these residuals and we subtracted these synthesized low-frequency signals from the corresponding original light curves.

As the last step, we summed the final PMT and CCD light curves into 120-s bins to give all the observations equal weight and to decrease the number of data points to a reasonable amount. This time-series will be frequency-analysed in the next section.

We show some examples of our reduced light curves in Fig. 3. These were obtained during the part of the campaign with the highest duty cycle of the observations, but they are typical concerning data quality; they are not our best light curves. We refrain from showing all our data, as this would fill five journal pages at a reasonable scale. We will do that, however, in a publication to be submitted to the Journal of Astronomical Data, where we will also make our reduced data (9139 *B* and 5415 *V* measurements after binning) publicly available.

4 FREQUENCY ANALYSIS

4.1 Linear frequency analysis

Our frequency analysis was performed with an updated version of the program PERIOD (Breger 1990). This package applies single-frequency Fourier analysis and simultaneous multifrequency sine-wave fitting. We extended it to be able to handle large data sets with a rich frequency content.

We calculated the spectral window and amplitude spectra of our data as well as amplitude spectra of residual light curves where the previously identified periodicities were removed by means of a fit consisting of simultaneously optimized frequencies, amplitudes and phases. The frequencies were derived from the *B* filter data (which have a better spectral window and span a larger time base) and were kept fixed for the *V* filter observations to minimize effects on the amplitudes and phases due to mutual influence of the different signals.

All the parameters of our multifrequency fits are here assumed to be constant over the duration of the data set. Therefore we call this part of our frequency analysis *linear*. Results for the different filters are plotted in Fig. 4.

After the detection of 13 frequencies we decided to combine the residual *B* and *V* light curves; aliasing in the *V* filter data does not allow a convincing representation of the results in this filter after that point. We made use of these 13 frequencies to determine a scale factor required to merge the *B* and *V* residuals. It must be pointed out that different pulsation modes ought to have different amplitude ratios in the two filters; this is a known tool for mode discrimination. Therefore one should only merge such data as late as possible during a frequency analysis, i.e. the error of the determination of the amplitude ratio must considerably exceed its intrinsic scatter to avoid the introduction of artefacts.

Consequently, we determined the amplitude ratios for all the 13 modes and we adopted the median of these ratios (which amounted to 1.29) as the multiplication factor for the *V* filter

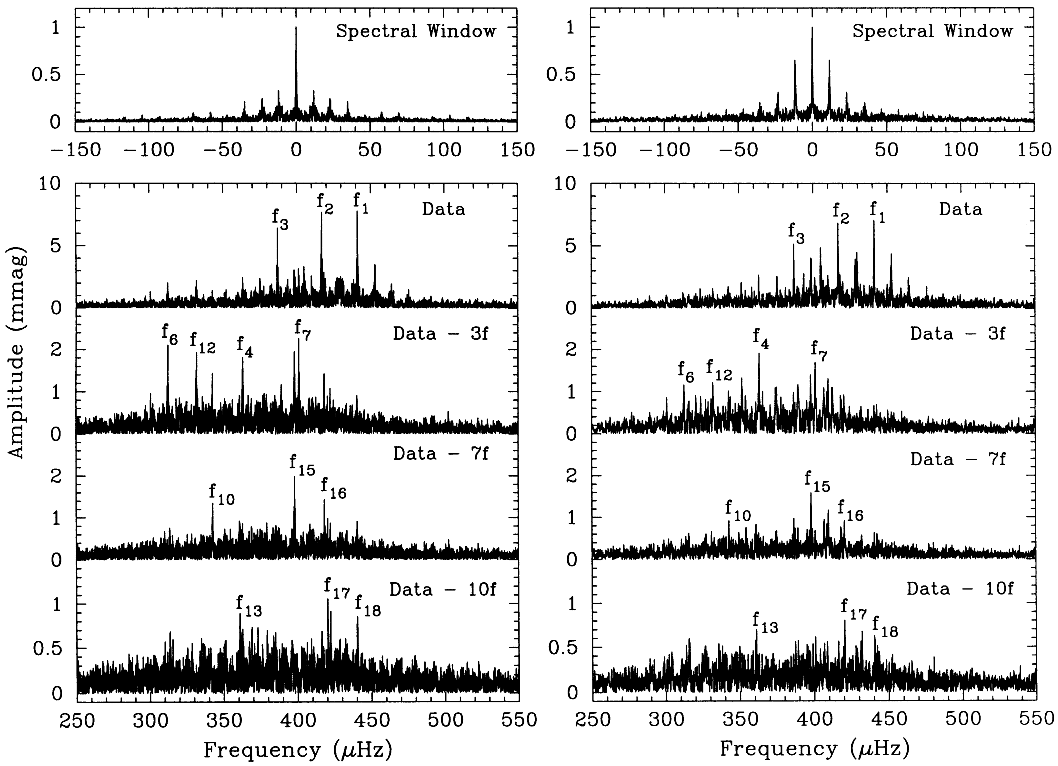

Figure 4. Spectral window and amplitude spectra of our *B* (left-hand side) and *V* (right-hand side) light curves and the results of removing three, seven and ten simultaneously optimized frequencies. The signals taken out from one panel to the next are labeled; the numbering is consistent with that used by HPO. Frequencies already known are f_1–f_{14}, all peaks with higher indices correspond to new modes which are now at higher amplitude due to the star's well-known amplitude variations. For reasons of presentation we stop this analysis after the detection of 13 frequencies.

residual light curves. We prefer the median over the mean to minimize the effects of 'outliers'. We then searched the combined data for further periodicities and display the result in Fig. 5. The frequencies derived at this step were determined from optimizing the fit for the combined residual data set, but they were kept fixed for the following determination of the amplitudes in the different filters for the same reason as explained before.

We need to clarify the steps of the frequency analysis presented in Fig. 5. In the combined residual data set (after removal of the contribution of 13 periodicities) we first tried to identify frequencies which were already detected by HPO, but not yet found in the present data set. These frequencies are labeled with arrows together with their identification in the upper half of the second panel of Fig. 5. All of them are present, however with small amplitude.

In the lower half of the second panel of Fig. 5 we show the residual amplitude spectrum after removing 17 periodicities. We can detect two more pulsation frequencies (again denoted with arrows and their identifications), and we indicate two further peaks with arrows close to them.

These two peaks and the peak labelled f_{18} in Fig. 4 have something in common: they are very close (within 0.5 μHz) to the pulsation frequencies f_1, f_2 and f_4. They are, however, fully resolved. The two unlabelled arrows in Fig. 5 actually denote the exact frequencies of f_2 and f_4. These close peaks are reason for concern as will be explained below; we stop the search for pulsation frequencies by means of linear frequency analysis at this point. We just add that the highest peaks believed to be noise in this frequency range have an amplitude of about 0.5 mmag.

However, we can still search for the presence of combination frequencies in our data.[1] Some have already been detected by Handler et al. (1996), but only one $2f$-harmonic was significant. Because of our large new data set we can hope to increase the number of confirmed combination frequencies. Of course, the data reduction techniques applied only allow us to look for frequency sums; the frequency differences lie in the low-frequency range where we have previously filtered the data.

The lowest panel of Fig. 5 presents the frequency spectrum of XX Pyx in the range where combination frequencies are to be expected. In the upper half of this panel three peaks stand out; they all correspond to combination frequencies. After including the signals due to these frequencies in the light curve solution, the three next highest peaks can also be identified with combination frequencies (lower half of the lowest panel of Fig. 5). We note that a residual amplitude spectrum after adopting these three further signals exhibits more peaks whose frequencies coincide with combinations of pulsation frequencies but their amplitudes are comparable to those of the highest noise peaks (≈0.18 mmag) in the corresponding frequency domain. We therefore refrain from taking them into account.

At this point we find it useful to summarize our preliminary results from the linear frequency analysis and we do so in Table 2. To give an impression of the accuracy of these values, we also quote formal linear least-squares error sizes on our frequencies and amplitudes using the formulae of Montgomery & O'Donoghue (1999). These error bars should only be taken as a rough guide and are certainly underestimates, as will become clear in Section 4.3.

[1] This will provide us with an important clue used in the following analysis and in the interpretation of our results.

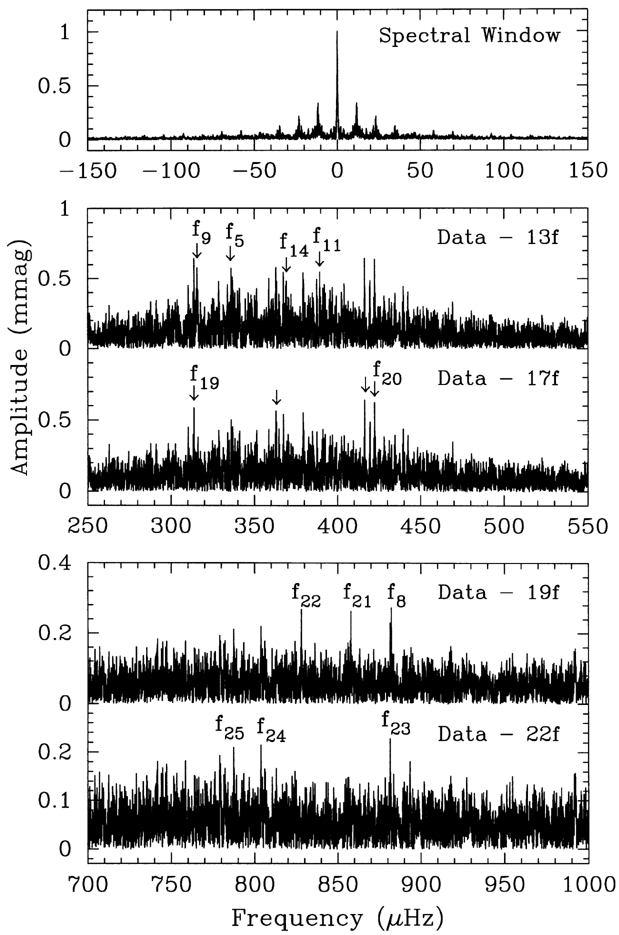

Figure 5. Spectral window and amplitude spectra of our combined B and V data for both pulsation as well as combination frequencies. The train of thought in this part of the analysis and the meaning of the indicated peaks are explained in the text.

4.2 Why go non-linear?

The main goal of our frequency analysis is to detect as many intrinsic pulsation frequencies of XX Pyx as possible. However, based on a simple numerical simulation we suspect that we have not yet exploited the full frequency content of our data: we calculated amplitude spectra of data consisting of white noise only, with the same standard deviation, number of data points and time distribution as the real data and 'reduced' them in the same way as the original measurements; the resulting noise level was about a third of that of the observations, suggesting that further signals could be present in the data.

As has been pointed out in the Introduction, XX Pyx is known to exhibit detectable amplitude variations on time-scales as short as a month (HPZ). Our data set spans almost three months. Therefore it can be suspected that these peaks close to several of the stronger modes could be caused by intrinsic amplitude (and possibly frequency) variations during the observations.[2] Preliminary tests showed that this is indeed the case and we must conclude that classical frequency analysis methods such as applied in Section 4.1 are not adequate for the present data set. To reach our goal of detecting the maximum number of intrinsic pulsation frequencies and to examine the suspected amplitude and/or frequency variations during the observations, the latter have to be quantified; we need to perform a *non-linear frequency analysis*.

[2] Another reason for the appearance of such close peaks would be mismatches in the filter passbands between the different observatories, generating apparent amplitude modulations. Estimates of the size of such effects (Handler 1998) showed however that they would not be noticeable in the amplitude spectra.

Table 2. Results of the linear multifrequency solution for XX Pyx derived from the Delta Scuti Network measurements acquired in 1998. Formal frequency error estimates range from ±0.0004 μHz for the strongest modes to ±0.02 μHz for the weakest combination frequencies; the formal errors in amplitude are ±0.055 mmag for B and ±0.054 mmag for V.

ID	Freq. (μHz)	Freq. (d^{-1})	B ampl. (mmag)	V ampl. (mmag)
f_1	441.085	38.1098	7.80	6.53
f_2	416.813	36.0126	7.69	6.49
f_3	387.009	33.4376	5.88	4.56
f_4	363.424	31.3998	1.94	1.99
f_5	335.621	28.9977	0.27	0.45
f_6	312.624	27.0107	2.08	1.22
f_7	401.188	34.6626	2.43	1.99
$f_8 = 2f_1$	882.171	76.2196	0.30	0.20
f_9	315.494	27.2587	0.55	0.35
f_{10}	342.779	29.6161	1.53	1.00
f_{11}	389.271	33.6330	0.44	0.49
f_{12}	332.178	28.7002	2.06	1.32
f_{13}	361.143	31.2028	0.91	0.72
f_{14}	369.207	31.8995	0.64	0.17
f_{15}	398.166	34.4016	2.15	1.83
f_{16}	418.248	36.1366	1.54	0.75
f_{17}	420.446	36.3265	1.15	0.77
f_{18}	440.571	38.0653	1.01	0.72
f_{19}	313.678	27.1018	0.58	0.51
f_{20}	422.322	36.4887	0.77	0.35
$f_{21} = f_1 + f_2$	857.898	74.1224	0.26	0.22
$f_{22} = f_1 + f_3$	828.095	71.5474	0.26	0.20
$f_{23} = f_1 + f_{18}$	881.656	76.1751	0.21	0.23
$f_{24} = f_2 + f_3$	803.822	69.4502	0.20	0.18
$f_{25} = f_{11} + f_{15}$ or $f_{14} + f_{16}$	787.437	68.0345	0.22	0.18

Before starting with this procedure, we turn to the discussion of those close peaks appearing in the vicinity of the pulsation frequencies f_1, f_2 and f_4. We have labelled one of them as f_{18} and included it in our linear frequency solution, but we have not yet explained why.

We have reason to believe that this is an independent pulsation mode. f_{18} is very close to the mode f_1; the latter is the only independent pulsation mode for which a $2f$ harmonic is reliably detected (we called it f_8). This harmonic is just the mathematical result of the non-sinusoidal pulse shape of f_1. Yet we also found a peak very close to this harmonic – f_{23} – which is the sum frequency of f_1 and f_{18} (see Table 2). If f_{18} were an artefact which describes an amplitude and/or frequency variation of f_1, the harmonic of f_1 would be modulated in exactly the same way; therefore the presence of f_{23} would be expected. However, in this case the amplitude *ratio* of f_1/f_{18} and f_8/f_{23} must then be the same. These amplitude ratios and their error sizes amount to 7.72 ± 0.39 for f_1/f_{18} and 1.36 ± 0.38 for f_8/f_{23} and are therefore significantly different from each other. We note, however, that this argument is only valid under the assumption that the pulse shape of f_1 does not vary when this mode changes its amplitude. HPZ have shown that this assumption is justified.

Regrettably, we cannot use similar arguments for all the other peaks appearing close to those corresponding to the dominating pulsation modes, because f_1 is the only mode with a detectable

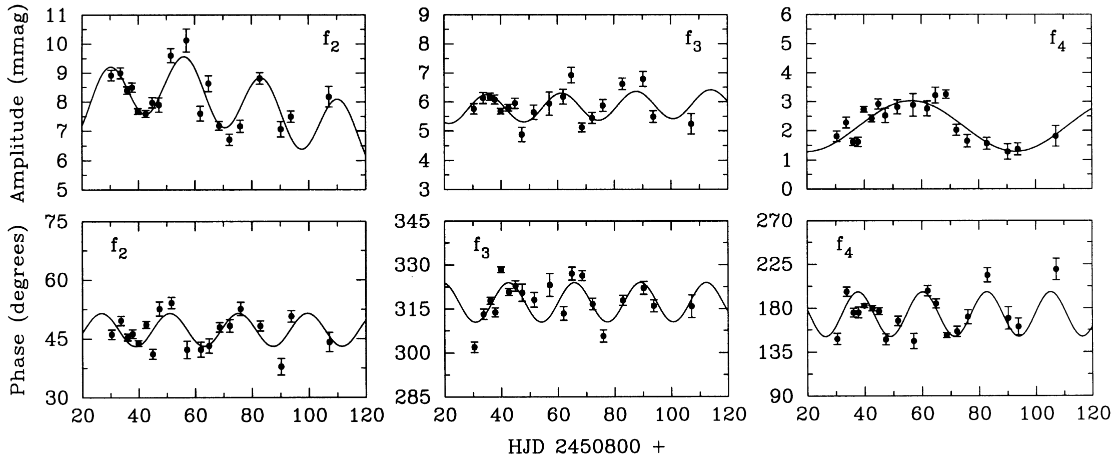

Figure 6. Amplitude and frequency variations of the three most unsteady modes. The adopted fit to compensate for them is superposed.

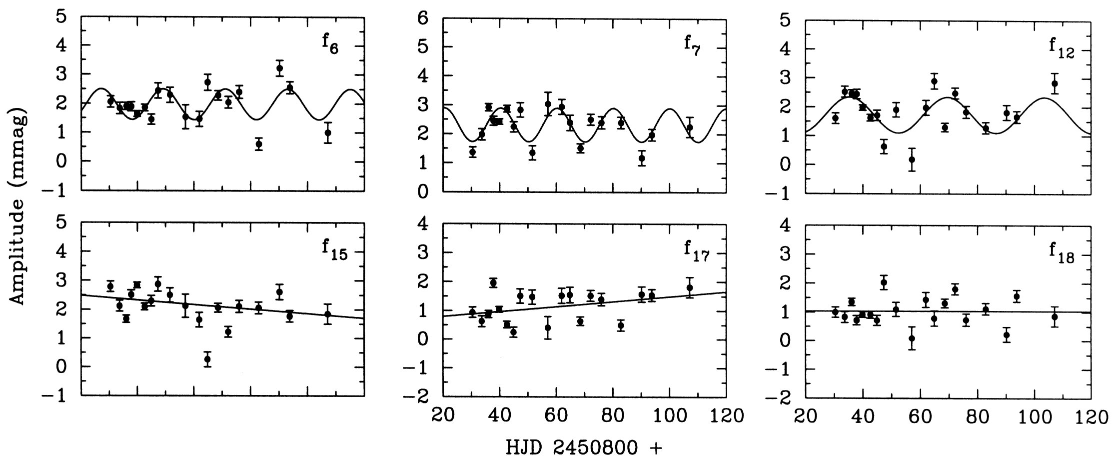

Figure 7. Temporal behaviour of all the other modes which were classified as having variable amplitudes. For comparison, the result for one mode with constant amplitude (f_{18}) is also displayed; the correspondingly adopted fits are shown as well.

harmonic. To be conservative, we will therefore not consider these close peaks to be caused by possible pulsation modes.

Having set the stage this way, we can now start with our non-linear frequency analysis. This is of course a very delicate procedure and has, to our knowledge, never been attempted before in a similar way. Consequently, we will proceed as carefully as possible, describing our analysis as comprehensively as possible. We will also provide discussions or justifications of our decisions whenever deemed necessary.

4.3 Non-linear frequency analysis

To start our analysis, we first needed to isolate the light variations of the mode whose amplitude and/or phase variations were to be characterized. Therefore, we fitted the complete linear frequency solution to all the data, determined all the frequencies, amplitudes and phases and stored them. For each frequency under consideration, we then calculated a synthetic light curve from this solution, leaving out the parameters of the signal in question. This serves to minimize the effects of mutual influence of the frequencies as opposed to calculating an optimized $(n-1)$-frequency fit to the data. Our fit was subtracted from the data, leaving them with only the light variation due to this single mode plus noise (plus possible further periodic signals). This was done for all the 19 pulsation modes detected so far and we will call the resulting data sets 'single-mode data sets' in what follows.

We note that this fit was calculated for the combined *B* plus scaled *V* data set (again a median amplitude ratio of 1.29 was adopted). In this way we gained a better time-distribution of the data at the expense of increasing the uncertainty in amplitude determination; the latter is easier to take into account and we will attempt to do so later.

We then had to split the data sets into suitable subsets for examining amplitude and phase stability. The optimal solution would be to have as many subsets as possible, and all of these should have good spectral window functions in order to suppress the influence of other modes on the one under scrutiny. With real data this cannot always be achieved. Consequently, we attempted to partition the data as optimally as possible; for sections of data where we could not obtain a very clean spectral window we increased the time-base. We ended up with 19 non-overlapping subsets of data containing between 367 and 1152 points and spanning between 1.28 and 4.85 d. In other words, we had at least 13 cycles of any mode in each subset of data available.

Continuing the analysis, we took all the single-mode data sets, fitted the corresponding frequencies again and optimized them. Then we fixed the frequency and determined the corresponding amplitude and phase, as well as the error estimates for those quantities (following Montgomery & O'Donoghue 1999; actual values will be shown in Figs. 6 and 7), in all the 19 subsets. The temporal behaviour of the amplitudes and phases of the different modes was investigated for variability.

We noticed that several modes seemed to show amplitude and phase variations, which prompted us to seek criteria to distinguish modes which were variable in time. However, this could not be done in a generally applicable way. First of all, we noticed that our errors were not random. Comparing the rms scatter of the amplitudes and phases determined for all the modes in all the subsets with the mean of the standard errors we derived before, we found that the real scatter was a factor of 2 or more higher than the mean of the formal error estimates.[3] The latter has also been recognized by Koen (1999) in his analysis of high-speed photometry.

Furthermore, the behaviour of the amplitudes in time was quite different from mode to mode: some seemed to be linearly increasing or decreasing, some exhibited apparent cyclical variations, and some showed combinations of the features described above. Finally, the error in phase does, of course, depend on the amplitude itself. Because of all this, distinguishing between variability and constancy is not straightforward; we decided to rely upon common sense and experience. In other words: our results will reflect personal bias.

After having classified the amplitude or phase behaviour of the modes initially as:

(i) variable in amplitude and phase;
(ii) variable in amplitude only;
(iii) constant;

we modified the fitting procedure. We first note that we did not find a mode which was variable in phase only, but this could be serendipity. Another result of this first examination was that allowing for phase variability of low-amplitude (<1.5 mmag) modes is not useful; the phases of such modes are too weakly constrained. Therefore any apparent variability is doubtful.

The modification of the fitting procedure consisted of leaving phase as a free parameter only for those modes where definite phase variations were detected. For all the other modes we fixed the phase and, if the mode was found to be constant in amplitude as well, also the amplitude. This decreases the number of free parameters in the fitting procedure and was intended to avoid generating artefacts. For example, the calculated amplitudes of weak modes tend to become systematically too large when allowing their phases to be free parameters, exposing the analysis to the danger of overcompensating for their contributions.

The resulting diagrams of amplitude and phase versus time were then fitted according to which kind of variability these parameters exhibited. Besides the diverse behaviour of the amplitudes described above, cyclical phase variations were also detected for some of the stronger modes. Consequently, we constructed synthetic light curves for all the different modes according to their behaviour, i.e. we generated sinusoids whose amplitudes and phases varied in time correspondingly.

[3]This is probably partly due to mutual influence of the different modes; we performed simulations by generating multiperiodic synthetic light curves sampled the same way as the observations, using the frequencies from the linear solution, constant amplitudes and phases of the component signals, convolved with Gaussian noise and analysing them just as the real data. We found some small systematic trends in the reconstructed amplitude and phase behaviour over time. Another source of systematic error would be the presence of further pulsation modes or of residual transparency variations in our data. To examine the contribution of the latter, we compared the rms scatter of amplitude determinations of subsets of our comparison star data with the mean of the formal errors thereof. We found that the 'real' errors were about 50 per cent larger than the formal values. All these effects together can therefore explain at least a large fraction of the discrepancy between the observed and formal errors.

Table 3. Amplitude and phase variations of some pulsation modes of XX Pyx during the 1998 observations; in case of cyclical variability an approximate time scale is given. Only variable modes are listed.

ID	Amplitude variability	Phase variability
f_2	Linear and cyclical (25 d)	Cyclical (25 d)
f_3	Cyclical (25 d)	Cyclical (25 d)
f_4	Cyclical (70 d)	Cyclical (25 d)
f_6	Cyclical (22 d)	–
f_7	Cyclical (20 d)	–
f_{12}	Cyclical (35 d)	–
f_{15}	Linear	–
f_{17}	Linear	–

This is, of course, not yet the best solution. We already mentioned the potential danger of mutual influence of the pulsation modes. Hence we decided to apply our non-linear frequency analysis iteratively. Therefore, we again calculated synthetic light curves, including the preliminary results from the nonlinear frequency analysis for the construction of the single-mode data sets. We then repeated the procedure of searching for and classifying the temporal variability, fitting these data with as few free parameters as possible and finally constructing synthetic light curves for the individual modes. After this iteration, the scatter in the amplitudes and phases for the different subsets of data decreased, indicating convergence and thereby justifying the iteration.

At this point we can finally display the results of our analysis. Our final classifications of the amplitude and phase variability of the modes are summarized in Table 3; the determined amplitude and phase variations are displayed in Figs 6 and 7. We point out that the terms we use to describe the amplitude and frequency variations correspond to the functions we fitted to compensate for them; their intrinsic shape might well be different. We stress again that our main aim in constructing the fits was to suppress spurious peaks in the amplitude spectrum due to the temporal variability of some modes. We seek no physical justification for the types of the fits; some might be more suggestive, some less.

Still, we found it useful to derive some formal assessment for our choices of the fits. We evaluated our solutions by means of the Bayes Information Criterion (BIC)

$$\mathrm{BIC} = \frac{p \log N}{N} + \log s^2,$$

where p is the number of free parameters of a model fitted to data, N the number of data points and s the standard deviation of the residuals. The BIC means that for every free parameter introduced into the fitted model the standard deviation of the residuals should be decreased by a certain amount; the goal of testing models with the BIC is to minimize the latter. In the present case ($N = 19$) the rms residuals must decrease by 8 per cent for each new free parameter to be accepted.

We tested several models with the BIC for each mode: constant amplitude/phase ($p = 1$), linearly changing amplitude ($p = 2$; a

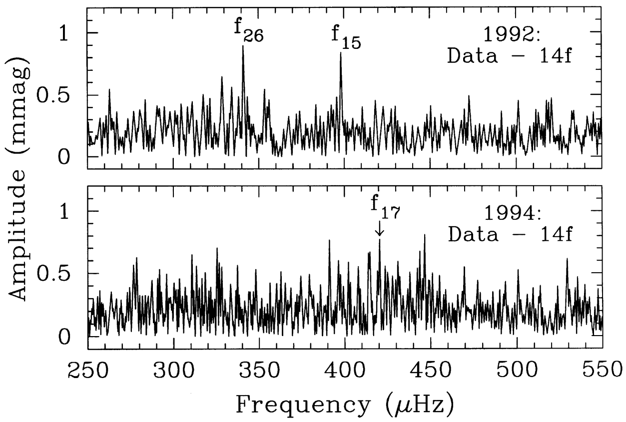

Figure 8. Amplitude spectra of the residuals of the 1992 and 1994 WET observations after prewhitening the frequency solution determined by HPO. In the 1992 data, the new mode f_{15} found in this study is present, and a completely new mode (f_{26}) is also revealed. In the 1994 data, our new mode f_{17} can be detected. No other new modes could be found in these smaller data sets.

linearly changing phase would of course mean the chosen frequency is incorrect) and sinusoidal amplitude/phase modulation ($p = 4$). The results of these tests supported our selections of the employed fits in every case; we were actually more conservative than the BIC would be. We note that the amplitude variations of f_2 were fitted with a higher-order model (sinusoid plus two straight lines, $p = 6$). The BIC also confirmed this choice.

Having quantified the amplitude and phase variations of the modes this way, we can now apply our non-linear multifrequency fit to the data. However, this again requires caution. The scale factor we applied to the *V* filter data is, as mentioned previously, not expected to be the same for all the modes. In addition to the dependence of the amplitude ratio on the type of the pulsation mode, the amplitude variations also have an effect, as our *B* and *V* filter data are mostly not simultaneous and therefore sample different phases of the amplitude variations of different modes. Before our nonlinear frequency analysis this was an unknown factor and could not possibly have been taken into account; at this point it can (at least to first order). On the other hand, deviations of the originally adopted scale factor from its 'real' value would only generate noticeable results for the three strongest modes: our previous detection level was around 0.5 mmag. Therefore, even a large difference (say, 10 per cent) from the real amplitude ratio would only generate noise peaks much smaller than this detection level for the weaker modes.

Consequently, we split the full non-linear synthetic light curve into two subsets corresponding to the original *B* and *V* data. Then we performed a linear frequency analysis on these data as described in Section 4.1, adopting the exact frequencies determined there. We stopped at the point where the *B* and *V* residuals were originally merged. Then we compared the amplitude ratios between the results in Table 2 and those for the non-linear solution in each filter for each mode and determined scale factors for each of the three strongest modes separately. These were applied to the fits for the corresponding mode, and the resulting synthetic light curves were added together and adopted as our final non-linear multifrequency fits. These were subtracted from the observed light curves in each filter. The residuals were again combined with a scale factor of 1.29 for the *V* filter data and subjected to additional linear frequency analysis. Before presenting these results, we will however reconsider the published observations of XX Pyx.

4.4 Reanalysis of the 1992 and 1994 data

As already mentioned in the Introduction, amplitude variations of pulsating stars can serve to detect more modes over time than would be possible with one data set obtained in a short period of time only. XX Pyx was initially observed during two WET runs. The analysis of these observations (HPO) resulted in 13 pulsation frequencies, but also suggested that more modes are likely to be excited in the star. Obviously, some of these suspected further modes might already have been detected in the present data set, and one can hope that by including the corresponding frequencies in a reanalysis of the older data, some more modes which have amplitudes too low to be detected in the new data can be revealed in the WET observations because of the consequently decreased noise level.

Therefore we re-reduced the WET observations in accordance with the procedure outlined in Section 3.3, subtracted the multifrequency solution by HPO from these data and searched the residual amplitude spectra for new modes. We display the result in Fig. 8.

Indeed, in the 1992 data, the new mode f_{15} clearly detected in this study is obviously present. After removing this signal from the data, a completely new mode f_{26} dominates the residual amplitude spectrum. This peak has already been discussed by HPO and it barely escaped detection then. Now we have no doubt it is intrinsic to XX Pyx as it is also present (but not detected) in the 1998 data. We note that the combination frequencies f_{21} and f_{22} are also present in this data set (see Handler et al. 1996 for a graphical representation) and can now be included as well.

The lower panel of Fig. 8 shows the residual amplitude spectrum of the WET measurements in 1994. Here we can only detect f_{17} in addition, but no further peaks can seriously be claimed as being due to pulsation modes in this data set alone. It should be noted that the 1994 WET data do not have a very good spectral window. Therefore some modes may have artificially decreased amplitudes there because of spectral leakage of prominent neighbours which were prewhitened. Finally, we would like to comment that the time bases of individual WET runs on XX Pyx are smaller than any time scale of amplitude or frequency variations we discovered in the new DSN data. Hence they should hardly affect the frequency analysis of the 1992 and 1994 measurements.

4.5 Frequency analysis of the combined residuals

As the last step of our frequency search, we put all the residual data together and we looked for possible further frequencies in the combined data set. Of course, it would perhaps be more correct to merge all the original data, then perform a frequency analysis on this data set with fixed-frequency solutions allowing for variable amplitudes and phases and to examine the resulting residuals. However, because of the nature of the amplitude and frequency variations already discovered and because of the large gaps in the combined data set, this would lead to severe complications in the analysis. In addition, we would need to combine the *B* and scaled *V* data beforehand, which have different amplitude ratios and which could also show phase shifts relative to each other. We are therefore afraid that such an approach would generate more

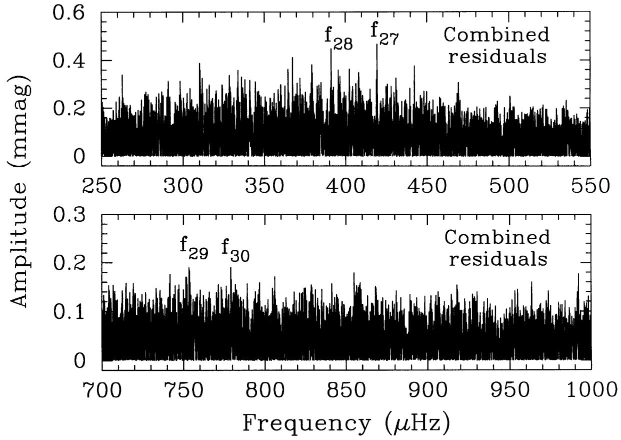

Figure 9. Upper panel: amplitude spectra of the residuals of all three multisite campaigns. Two further pulsation modes can be detected. Lower panel: two more combination frequencies manifest themselves.

artefacts than everything else and refrain from it. Instead, we just examine the combined residuals consisting of the data from each campaign pre-whitened separately. This could suppress possible intrinsic peaks, which can then not be detected, but it is definitely the safer modus operandi.

Fig. 9 shows the results of the analysis of the combined residuals. In its upper panel, the detection of two more frequencies of pulsation is presented. We note that peaks at these frequencies are present (often prominently) in the residuals of each of the 1992, 1994 and 1998 data sets. In the lower panel of Fig. 9, the two highest peaks in the domain of combination frequencies occur at sums of known mode frequencies; the frequency of peak f_{29} can be identified with f_1+f_6, whereas f_{30} is consistent with three frequency combinations: f_3+f_{28} or $f_{13}+f_{16}$ or $2f_{11}$. We cannot judge which of the identifications is correct.

4.6 Frequency content of the light curves of XX Pyx and significance of mode detection

Until now, we did not attempt to prove that the frequencies claimed by us represent significant detections. This was intentional, because different modes were found in different data sets, for which different circumstances apply and separate discussions might hence have generated confusion. We now consider this altogether.

The most widespread (and in our view most useful) criterion to assess the significance of detections in frequency analyses was proposed by Breger et al. (1993), which adopts an amplitude signal-to-noise ratio of 4 as the limit for a reliable detection. We refer to the aforementioned paper and to Handler et al. (1996) for discussions of this criterion and for prescriptions for its use. Later, Breger et al. (1999) suggested that a somewhat lower signal-to-noise ratio of 3.5 would serve as a good gauge for the reality of combination peaks as these must occur at predictable frequencies. So far, these criteria have never led to spurious answers and we will therefore adopt them for our analysis as well.

We calculated the amplitudes of all the modes and combination signals for the data sets in which the detections were reported in this paper. Then we determined the noise level following Handler et al. (1996) and calculated the resulting signal-to-noise ratios for all the peaks. The outcome is summarized in Table 4.

As one can see from this table, all the new frequencies correspond to certain detections according to the criterion used, although we caution that the combination peak with $S/N=3.5$ only reached this value after rounding.

Table 4. The frequency content of XX Pyx from the combined analysis of the 1992–1998 multisite observations. The quoted amplitudes and signal-to-noise ratios correspond to different data sets, namely those where the amplitudes of the modes were determined for the *S*/*N* calculation: 98B means the *B* amplitude of the 1998 data, 98C denotes amplitudes in the combined 1998 *B* and *V* data set, 92 labels the 1992 WET data (mode detection in hindsight) and 929498 is the data set consisting of the combined residuals of all the multisite observations. Entries in the columns for amplitude and *S*/*N* labelled with colons correspond to modes which are variable in amplitude. The modes f_5 and f_{14} are not significant here, but they were clear detections by HPO.

ID	Freq. (μHz)	Freq. (d^{-1})	Ampl. (mmag)	*S*/*N*	Data set
f_1	441.09	38.110	7.80	65.3	98B
f_2	416.81	36.013	7.7:	61:	98B
f_3	387.01	33.438	5.9:	46:	98B
f_4	363.42	31.400	1.9:	15:	98B
f_5	335.63	28.998	0.35	2.9	98C
f_6	312.63	27.011	2.1:	18:	98B
f_7	401.18	34.662	2.4:	19:	98B
f_8	882.16	76.219	0.27	4.9	98C
f_9	315.50	27.259	0.51	4.3	98C
f_{10}	342.78	29.616	1.53	12.2	98B
f_{11}	389.28	33.634	0.52	4.0	98C
f_{12}	332.18	28.700	2.1:	17:	98B
f_{13}	361.14	31.203	0.91	7.1	98B
f_{14}	369.21	31.900	0.45	3.3	98C
f_{15}	398.17	34.402	2.2:	17:	98B
f_{16}	418.25	36.137	1.54	12.4	98B
f_{17}	420.45	36.327	1.2:	10:	98B
f_{18}	440.57	38.065	1.01	8.7	98B
f_{19}	313.67	27.101	0.59	4.7	98C
f_{20}	422.32	36.489	0.63	5.1	98C
f_{21}	857.91	74.123	0.27	4.7	98C
f_{22}	828.12	71.549	0.26	4.4	98C
f_{23}	881.52	76.163	0.24	4.3	98C
f_{24}	803.83	69.451	0.21	3.6	98C
f_{25}	787.37	68.029	0.21	3.5	98C
f_{26}	341.07	29.468	0.87	4.1	92
f_{27}	419.50	36.245	0.47	4.5	929498
f_{28}	391.20	33.799	0.44	4.2	929498
f_{29}	753.32	65.087	0.19	3.7	929498
f_{30}	779.03	67.308	0.19	3.6	929498

We find it useful to comment on the problem of mode detection a little further. Because we are investigating a very large data set, one could suspect that noise peaks can rather easily exceed our adopted *S*/*N* threshold. Scargle (1982) inferred a so-called false alarm probability criterion on which the reliability of frequency detection can be judged. It has however been pointed out by various authors (e.g. Martinez 1989) that this criterion gives overoptimistic results. The results are also quite dependent on the time-distribution of the data (Horne & Baliunas 1986). Because of all this, a comparison using the formal methods developed in the original papers does not seem useful.

We decided to do the following: we considered a hypothetical signal which is present in the 1998 data set with a *S*/*N* of exactly 4.0. To derive the false alarm probability of such a detection, we generated 300 data sets consisting of our residual data, but shuffled in time (investigating the combined data set of all campaigns would require an impracticably large amount of computing time), and performed frequency searches on them. About 1.5 million peaks in the amplitude spectra were considered and their *S/N* was calculated in exactly the same way as for our observations. We found 12 peaks that exceeded the empirical criterion of $S/N = 4.0$, corresponding to a false alarm probability of 8.0×10^{-6} for a peak with this *S/N*. A similar experiment by generating data sets of random noise with the same temporal distribution as our real data gave a similar result (false alarm probability 7.1×10^{-6} for $S/N = 4.0$). The residuals of the observations are of course not random, but we use a determination of the *local* noise in our calculations. We therefore take the effects of non-random noise into account in first order. In any case, we add that we do not use such formal criteria alone to judge the reliability of peaks in the amplitude spectra. Other tests, such as investigating subsets of data are always performed in addition.

Finally, we carried out some experiments to find other possible frequencies, for example by dividing the data into carefully chosen subsets, e.g. the data of highest quality. We also invoked some frequency analysis techniques which employ weighting (Arentoft et al. 1998) but in no case could we discover further credible pulsation frequencies. We note however that the residual light curves often show features which clearly indicate periodic variability with the time scale of the detected pulsations, but these do not seem to be coherent. Amplitude spectra of subsets of such residual data often show strong peaks, but they never quite reach $S/N = 4.0$, which can be taken as further support for the use of this criterion. This apparent incoherence could be intrinsic (short mode life-times, amplitude variations of yet undetected modes) or be a result of multiperiodicity.

5 MODE TYPING

5.1 Frequency spacing

HPO reported the discovery of a preferred separation within the frequencies of pulsation modes they revealed in the light curves of XX Pyx. These authors suggested this was due to the presence of modes with alternating even and odd values of the pulsational quantum number ℓ for the following reasons:

(i) The number and frequency distribution of the detected modes required that more than a one ℓ-family be present.

(ii) Pulsational models show such sets of modes should occur alternatively in the excited range of radial overtones.

(iii) The evolutionary state of XX Pyx is consistent with this hypothesis only.

(iv) The characteristic frequency spacing is too large to be interpreted in terms of rotational splitting.

Making use of this result, HPO could infer the frequency spacing due to consecutive radial overtones and hence derive the mean density of XX Pyx; the latter is possible because this characteristic spacing is simply a measure of the sound crossing time through the star. Because this preferred separation is not the asymptotic one, HPO had to invoke model calculations to determine the mean density of XX Pyx.

For obvious reasons it is very interesting to check whether this mean frequency spacing is still present as we have now almost twice as many modes available. Therefore, we repeated the analysis described by HPO and we display the result in Fig. 10, which contains the Fourier power spectrum of the frequency values with amplitudes normalized to unity.

Comparing our result to that of HPO, we find practically no difference. In fact, the characteristic frequency spacing became even more significant. We follow the method described by HPO to refine the mean frequency spacing of consecutive radial overtones of XX Pyx to $53.6 \pm 0.5\,\mu$Hz. With this value we can also refine the star's mean density to $\bar{\rho} = 0.241 \pm 0.008\bar{\rho}_{\odot}$.

As mentioned in the Introduction, the discovery of more pulsation modes of XX Pyx should lead to obvious patterns within the frequency values of the modes. To examine this idea, we show a schematic frequency spectrum with all the pulsation modes in Fig. 11.

Our prediction turned out to be correct. The modes of XX Pyx are grouped within narrow frequency intervals with some gaps in between. This is a clear indication of the expected essentially pure p-mode spectrum split by rotation.

As a matter of fact, the appearance of this schematic frequency spectrum can be used to estimate the stellar rotational velocity. If one considers a series of model frequency spectra of δ Scuti stars in the evolutionary state of XX Pyx and studies the development of their patterns depending on rotational velocity, the following features become apparent: for a slowly rotating model, the multiplet patterns form non-overlapping close groups. The faster the model rotates, the more the multiplets begin to overlap in frequency; gaps between the groups disappear. In a certain range of rotational rates, the modes seem to form regular groupings again, but the different subgroups are mixed in ℓ. The reason for

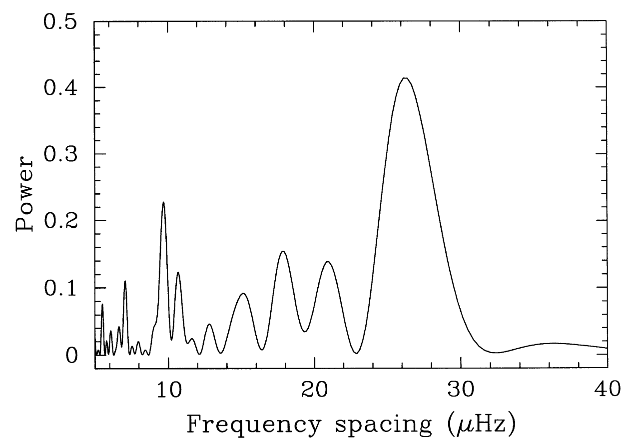

Figure 10. Search for a preferred frequency separation within the 22 detected pulsation modes of XX Pyx. This diagram is very similar to fig. 7 of HPO and therefore dramatically confirms their result for 13 frequencies.

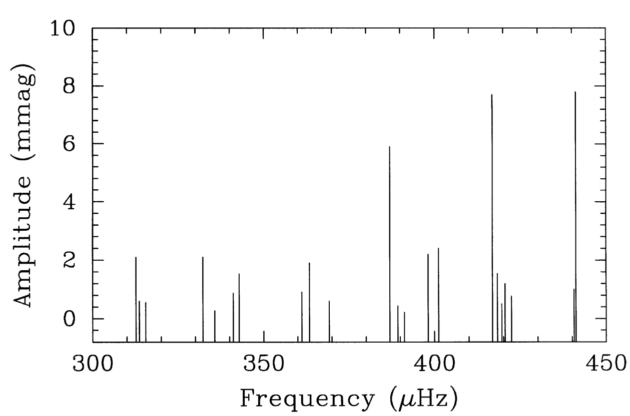

Figure 11. Schematic frequency spectrum of XX Pyx. Clear groupings of modes can be seen.

this 'clumping' of modes is that the second-order effects of rotation are of similar size as the first-order effects, causing the modes with $m \leq 0$ of the same k and ℓ to be very closely spaced in frequency, whereas the modes with $m > 0$ are mixed into the next groups of closely spaced modes at lower frequency. Increasing rotation even more, these groups again disappear, because the second-order effects begin to dominate. As we know that XX Pyx has a projected rotational velocity $v \sin i = 52 \pm 2\,\mathrm{km\,s^{-1}}$ (HPO), we can immediately rule out that the groupings seen in Fig. 11 consist of members of the same ℓ; rotational splitting would be too large even if $i \approx 90°$. Consequently, the rotational velocity of the star must be in the correct range for modes closely spaced in frequency, separated by gaps, to appear again. Hence we can predict that the rotation frequency of XX Pyx must be around $1.1\,\mathrm{d^{-1}}$ or its $v_{\mathrm{rot}} \approx 110 \pm 30\,\mathrm{km\,s^{-1}}$.

As pointed out by the referee, one would expect to see evidence for rotational splitting within the pulsation frequencies of XX Pyx. Considering the large number of theoretically expected modes we detected, the presence of several pairs of modes of $m = +1$ and $m = -1$ of the same k and ℓ is very likely. Such mode pairs should have very similar frequency differences ($\approx 2\nu_{\mathrm{rot}}$), as first-order rotational effects are small, second-order effects cancel for frequency differences of modes of the same $|m|$ and third- and higher-order effects are negligible. We actually performed a search for such frequency differences, but our results were inconclusive. The reason for this could either be unfavourable mode excitation or differential rotation.

Adopting the ranges of mean density and rotational frequency inferred above and assuming that most observed modes must be p-modes of radial order 4–6 (HPO) with $\ell \leq 2$, we attempted to perform an identification of all the modes by examining the mode patterns. Regrettably, our initial attempts failed, although parts of some solutions appeared quite promising. For example, the mode groups (f_9, f_{12}, f_5), (f_{14}, f_3, f_{11}) and (f_{17}, f_{18}, f_1) would be consistent with $\ell = 1$ triplets of $k = 4$, 5, 6 for a rotational frequency $\Omega = 0.9\,\mathrm{d^{-1}}$, but several of the remaining modes can then not be fitted reasonably with the remaining possibilities of $\ell = 0$ and 2. A definite mode identification therefore probably has to await detailed model calculations.

5.2 Phase shifts and amplitude ratios

To aid in identifying the excited modes with their pulsational quantum number ℓ, time-series colour photometry can be employed. Pulsation modes with different ℓ behave slightly differently when observed at different wavelengths, which can in principle be used as a mode discrimination tool (Balona & Stobie 1979; Watson 1988; Garrido, Garcia-Lobo & Rodriguez 1990; Balona & Evers 1999). The most widespread method utilizes amplitude ratios and phase shifts of the pulsations in two different filters for determining ℓ.

These values are in principle easy to determine from the observed light curves. However, as we have shown in Section 4.3, the amplitudes and frequencies of several modes are variable, which complicates the analysis. As a matter of fact, for these modes it only appears safe to use those parts of the data where simultaneous B and V filter photometry has been obtained to determine amplitude ratios and phase shifts: the intrinsic shape of the star's amplitude and frequency variations is not known. Thus, correcting for these to allow use of the whole data set is not justified. There are, however, only about 60 h of overlapping B and V measurements available.

Still, we calculated the amplitude ratios and phase shifts for each of the 11 strongest modes; the results are listed in Table 5. For modes which appear to be constant in amplitude and phase, the values in Table 5 were calculated from a linear multifrequency fit with fixed frequencies for the B and V data. For all the other modes, we examined the overlapping data pre-whitened by the other frequencies. These overlapping data were subdivided into parts which were significantly smaller than the time scales of the amplitude and frequency variations, and amplitude ratios and phase differences were calculated for each subset by fixing the frequencies. We adopted the mean value of the individual determinations as our result and the mean error of this mean for our error estimate. The error sizes for the modes constant in amplitude and phase in Table 5 are based on the formulae by Montgomery & O'Donoghue (1999), but the results were multiplied by a factor of two because of the correlated noise (see Section 4.3) to yield approximately realistic estimates.

As one can see from Table 5, the error estimates for the amplitude ratios and phase shifts for the modes f_1–f_3 are the lowest, which makes these modes the best candidates for a determination of ℓ. However, a comparison between the observed amplitude ratios and phase shifts for these modes and the theoretical 'areas of interest' (kindly calculated and provided by M.H. Montgomery) in an amplitude ratio/phase shift diagram for a

Table 5. Amplitude ratios and phase shifts for 11 modes of XX Pyx. See text for information on the determination of the quantities listed.

ID	Freq. (μHz)	A_B/A_V	$\phi_B - \phi_V$ (degrees)
f_1	441.09	1.194 ± 0.027	$+1.0 \pm 1.3$
f_2	416.81	1.245 ± 0.056	$+2.3 \pm 1.1$
f_3	387.01	1.272 ± 0.056	-2.3 ± 1.9
f_4	363.42	1.125 ± 0.016	-12.1 ± 7.7
f_6	312.63	1.449 ± 0.183	$+21.2 \pm 16.5$
f_7	401.18	1.204 ± 0.070	-3.6 ± 3.9
f_{10}	342.78	1.530 ± 0.207	-1.3 ± 7.8
f_{12}	332.18	1.758 ± 0.319	-1.0 ± 2.5
f_{15}	398.17	1.175 ± 0.196	$+8.5 \pm 6.2$
f_{17}	420.45	1.063 ± 0.306	$+31.2 \pm 16.4$
f_{18}	440.57	1.402 ± 0.272	$+1.0 \pm 11.1$

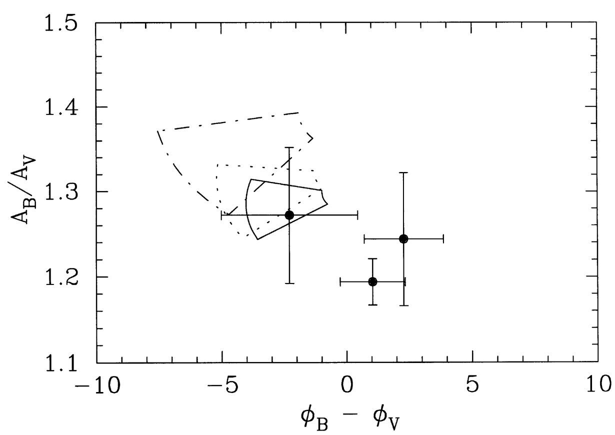

Figure 12. Amplitude ratios and phase shifts for the three strongest modes of XX Pyx compared with theoretically predicted values. Boundaries for the $\ell = 0$ area of interest are shown with full lines, those for the $\ell = 1$ area with dotted lines and those for $\ell = 2$ with dash-dotted lines. No meaningful result can be obtained from this diagram.

$T_{\rm eff} = 8414\,{\rm K}$, $\log g = 4.20$, model for a pulsation constant $Q = 0.016\,{\rm d}$ (Fig. 12) shows obvious disagreement between the theoretically predicted values and the observations.[4] We therefore advise against the use of the information in Table 5 for mode identification at face value. We cannot say whether the disagreement is due to systematic errors in the determination of the amplitude ratios and phase shifts or due to a problem of the method itself.

Assuming the latter to be true, we can gain some understanding when recalling the principles of this mode identification technique. As mentioned above, it relies on the fact that the amplitude and phase at a given passband depends on the spherical harmonic degree, ℓ (see, for example, Balona & Evers 1999). The dependence is due to the geometric variation and the integral of the limb darkening. The limb darkening term is, however, of little importance in determining the amplitude and phases. The gravity and temperature variations do not depend on ℓ (Balona & Dziembowski, private communication). Furthermore, the temperature term is always larger than the geometric term and rapidly dominates as the period decreases, since it is proportional to the square of the pulsational frequency. This means that the dependence of the amplitudes and phases on ℓ diminishes very rapidly for higher-order p modes. For XX Pyx which is on the main sequence and has such p modes excited, the amplitudes and phases are practically independent of ℓ. The photometric method of mode identification therefore fails in this case.

6 DISCUSSION OF THE AMPLITUDE AND FREQUENCY VARIATIONS

One of the results of Section 4.3 was that three modes were variable in amplitude and phase during the observations; five more modes appeared to show amplitude variations only. In the following, we would like to comment on this result and its implications.

First of all, it must be pointed out that some of the five modes for which only amplitude variations were reported may be variable in frequency as well, but our data set is not sufficient to prove this. Some of these modes have low amplitude; phase determinations are therefore not well constrained. Second, it is now clear that the analysis of the amplitude and frequency variations of XX Pyx by HPZ can only be taken as a guide towards the long-term behaviour of this star's modes. The variability we found in the present paper is generally smaller in amplitude, but the time scales are shorter; the data set of HPZ is insufficient to sample these variations adequately. In any case, it appears pointless to attempt assigning one certain time scale to the observed variations, although approximate time-scales should be discussed.

Starting with the three modes that are variable both in amplitude and phase, we need to say that the time scales of both variations are the same (within the errors of determination) for two modes (f_2 and f_3), but they are vastly different for f_4. The latter mode also shows the largest relative amount of variability, both in amplitude and phase. On the other hand, the amplitude variability of f_2 seems to be the most complicated of all modes.

Concerning the modes examined in Fig. 7, it is also evident that not all amplitude variations necessarily contain a short-term cyclic component with a time scale shorter than the length of our data set. Some amplitudes just seem to change slowly in time. For some modes with cyclically variable amplitudes it appears that the amplitude of these variations is not necessarily constant (e.g. f_6).

Finishing our description of the observed behaviour, we consider the variability time-scales of all modes with cyclic amplitude variations. It seems that they are all about the same (except for f_4 and maybe f_{12}). How does all that relate to the results of HPZ?

The diverse behaviour of the different modes rules out any presently known explanations for the cause of the amplitude and frequency variability, except resonances between the modes (see HPZ for more detailed arguments). In this case one would expect amplitude modulations with a time-scale of the order of the inverse growth rates of the modes. HPZ examined that possibility and suggested it is consistent with the observations, within the uncertainties of the observations and of the growth rates (there is no unique model for XX Pyx yet). One quantitative statement can, however, be added now: the growth rates of the pulsation modes of the models depend on frequency (e.g. see fig. 5 of HPZ). For models of XX Pyx, this means that the growth rates for modes near 320 μHz are much smaller than those for modes around 420 μHz (0.3 versus 8 $\rm yr^{-1}$ for the specific model used by HPZ). However, the time scales of the amplitude variations of the star are not consistent with this picture; they do not show a frequency dependence. The hypothesis of resonances being responsible for the amplitude and frequency variations is however not invalidated: a suitable choice of parameters for model calculations might be able to reproduce the observed behaviour. The major drawback of this hypothesis therefore manifests itself: it is extremely difficult to verify observationally. Finally, we should add that theoretical growth rates for mixed modes are quite different from those of pure p-modes, which could also at least partly be responsible for the apparent disagreement between observations and theory.

XX Pyx is not the only δ Scuti star with well-documented temporal variability of its pulsation spectrum: the star 4 CVn has been observed for more than 30 yr. The amplitude variations of 4 CVn have most recently been described by Breger (2000). Regrettably, possible frequency variability could not be examined reliably because of large gaps in the data. We can therefore only compare the amplitude variations of the two stars. Those of 4 CVn seem to occur on much longer time scales (we caution again that the data set for this star contains large gaps, as did that of HPZ; therefore some variations could be undersampled) than those of XX Pyx. Therefore, no repeated cycles can yet be seen in the amplitude variations of 4 CVn. Still, some features are similar in principle: there is no obvious correspondence between the behaviour of the different modes, and it is also hard to define a single characteristic time scale on which the variations of the individual modes occur.

In addition, 4 CVn also shows one mode whose variations are more dramatic than all the others, similar to our f_4. This mode of 4 CVn also showed an apparent phase jump by 180°. We note for completeness that we also observed this for some weak modes of XX Pyx, but because these phase jumps occurred at very low amplitude, the corresponding errors in phase determination are large and this led us to doubt the reality of such features.

We finally mention that Breger (2000) noticed that the most unstable mode of 4 CVn also generates the largest number of combination frequencies, which he took as support for the idea that the amplitude variations are caused by transfer of energy between the modes. This is not the case for XX Pyx, where the presence of combination terms rather seems to be dependent on the amplitude of the parent modes. As a matter of fact, no

[4]It could be suspected that the signs of the observed phase shifts are wrong. This is not the case.

(possible) identification of the combination frequencies of XX Pyx involves the most variable mode, f_4. We do not wish to comment further on this topic as the exact physical nature of the combination frequencies is far from being understood, which will make any statement relying on these features highly speculative.

7 SUMMARY AND CONCLUSIONS

The 17th run of the Delta Scuti Network, devoted to the unevolved pulsator XX Pyx, resulted in the largest single data set ever reported for a pulsating star other than the Sun: 550 h of multisite measurements obtained in 125 clear observing nights at eight different sites. Both photomultiplier and CCD detectors were employed; filters were selected to take advantage of their different wavelength sensitivities.

As a first result, our data analysis revealed two new variable stars in the fields of some of the CCDs used. Turning to the programme star, we found the frequency analysis of its time-series photometric measurements disturbed by amplitude and frequency variations occurring during our observations. We developed a *non-linear frequency analysis* method which was employed to take the temporal variability of the pulsation spectrum into account. We also found that noise correlation leads to error estimates in frequency, amplitude and phase that are approximately a factor of two higher than their formal values. Finally, we were able to detect 22 independent mode frequencies for XX Pyx, which is the most ever found for a δ Scuti star. In addition, eight combination frequencies were revealed. Compared to previous work on the star, we therefore increased the number of pulsation frequencies by nine and the number of combination frequencies by eight.

We found a preferred frequency separation within the pulsation modes, confirming the result originally published by HPO. Having now almost twice as many mode frequencies available, we find that their values show clear patterns as well: they consist of distinct groups of closely spaced modes. These results lead to a refinement of the mean density ($\bar{\rho} = 0.241 \pm 0.008\,\bar{\rho}_{\odot}$) and to a new constraint on the rotation rate of XX Pyx ($\nu_{\rm rot} = 1.1 \pm 0.3\,{\rm d}^{-1}$). Attempts to identify the modes by pattern recognition failed. In addition, potential mode diagnostics obtained by the analysis of our colour photometry failed as well. Consequently, asteroseismology of the star requires detailed model calculations.

The diverse behaviour of the amplitude and frequency variations of some of the modes leaves resonances as the only plausible possibility for their explanation. We attempted to point out possible inconsistencies of the observations with the predictions of this theory, although we are aware that it is difficult to conflict with observations as it has little predictive power.

ACKNOWLEDGMENTS

This work was partially supported by the Austrian Fonds zur Förderung der wissenschaftlichen Forschung under grant S–7304. TA and CS acknowledge financial support from the Belgian Fund for Scientific Research (FWO). This project was supported by the Flemish Ministry for Foreign Policy, European Affairs, Science and Technology. Perth observations were made possible by the technical expertise of Arie Verveer, technical manager at Perth Observatory, and by the continued support of the Government of Western Australia. Observations at the Wise Observatory are supported in part by the Foundation for Basic Research of the Israeli Academy of Sciences. We are grateful to Mike Montgomery for the calculation of theoretical values of amplitude ratios and phase shifts applicable to our target star. Scot Kleinman is thanked for supplying his code for automatic identification of combination frequencies. The referee, Wojtek Dziembowski, provided constructive criticism on mode identification.

This paper is based on observations obtained at McDonald Observatory, the European Southern Observatory (ESO, application 60D0148), the South African Astronomical Observatory (SAAO), Siding Spring Observatory, Perth Observatory, the Southeastern Association for Research in Astronomy (SARA) Observatory, Wise Observatory and Vainu Bappu Observatory.

REFERENCES

Arentoft T., Kjeldsen H., Nuspl J., Bedding T. R., Fronto A., Viskum M., Frandsen S., Belmonte J. A., 1998, A&A, 338, 909
Balona L. A., Evers E. A., 1999, MNRAS, 302, 349
Balona L. A., Stobie R. S., 1979, MNRAS, 189, 649
Bond H. E. et al., 1996, AJ, 112, 2699
Breger M., 1990, Commun. Asteroseismol., 20, 1 (University of Vienna)
Breger M., 2000, MNRAS, 313, 129
Breger M. et al., 1993, A&A, 271, 482
Breger M. et al., 1999, A&A, 349, 225
Dziembowski W. A., Pamyatnykh A. A., 1991, A&A, 248, L11
Dziembowski W. A., Krolikowska M., 1990, Acta Astron., 40, 19
Garrido R., Garcia-Lobo E., Rodriguez E., 1990, A&A, 234, 262
Handler G., 1994, Master's thesis, University of Vienna
Handler G., 1995, Baltic Astron., 4, 434
Handler G., 1998, Baltic Astron., 7, 227
Handler G., Kanaan A., Montgomery M. H., 1997, A&A, 324, 566
Handler G. et al., 1996, A&A, 307, 529
Handler G. et al., 1997, MNRAS, 286, 303 (HPO)
Handler G., Pamyatnykh A. A., Zima W., Sullivan D. J., Audard N., Nitta A., 1998, MNRAS, 295, 377 (HPZ)
Horne J. H., Baliunas S. L., 1986, ApJ, 302, 757
Kjeldsen H., Frandsen S., 1992, PASP, 104, 413
Kleinman S. J. et al., 1998, ApJ, 495, 424
Koen C., 1999, MNRAS, 309, 769
Martinez P., 1989, MNRAS, 238, 439
Montgomery M. H., O'Donoghue D., 1999, Delta Scuti Star Newslett., 13, 28 (University of Vienna)
Nather R. E., Winget D. E., Clemens J. C., Hansen C. J., Hine B. P., 1990, ApJ, 361, 309
Pamyatnykh A. A., Dziembowski W. A., Handler G., Pikall H., 1998, A&A, 333, 141
Renzini A., 1987, A&A, 188, 49
Scargle J. D., 1982, ApJ, 263, 835
Templeton M. R., Bradley P. A., Guzik J. A., 2000, ApJ, 528, 979
Watson R. D., 1988, Ap&SS, 140, 255
Zima W., 1997, Delta Scuti Star Newslett., 11, 37 (University of Vienna)

This paper has been typeset from a TEX/LATEX file prepared by the author.

2.2.6 Low-frequency variations and binarity of the δ Scuti star XX Pyx

Original paper:

T. Arentoft, C. Sterken, **G. Handler,** MNRAS 326, 192

Mon. Not. R. Astron. Soc. **326,** 192–202 (2001)

Low-frequency variability and binarity of the δ Scuti star XX Pyx

T. Arentoft,[1★] C. Sterken[1] and G. Handler[2]
[1]*University of Brussels (VUB/OBSS), Pleinlaan 2, B-1050 Brussels, Belgium*
[2]*South African Astronomical Observatory, PO Box 9, Observatory 7935, South Africa*

Accepted 2001 April 9. Received 2001 April 6; in original form 2001 January 26

ABSTRACT

We analyse 147 h of single-site CCD time series photometry of the multiperiodic low-amplitude δ Scuti star XX Pyx with the aim of investigating variability at low frequencies. Part of the data were obtained in the context of the 1998 multisite campaign on XX Pyx, the results of which were described by Handler et al. We find that periodic low-frequency variations are present in the XX Pyx light curves, and we detect two frequencies at $f_{\mathrm{A}} = 0.8695\,\mathrm{cycle\,d^{-1}}$ and $f_{\mathrm{B}} = 1.7352\,\mathrm{cycle\,d^{-1}}$, respectively, with amplitudes of 4.5 and 5.4 mmag. The low-frequency variability is intrinsic to XX Pyx, and cannot be attributed to instrumental or atmospheric effects. The near 2:1 ratio of the frequencies leads us to suggest that XX Pyx is a δ Scuti star in a binary system, with a possible binary period of 27.6 h. This is strongly supported by the detection of radial velocity variations from the re-analysis of echelle spectra obtained by Handler et al. However, in the absence of a spectroscopic period, alternative explanations of the photometric variability involving pulsation are also possible; the variations occur close to possible combination frequencies of the short-period (δ Scuti) variations, but high Q values of 0.57 and 0.28 d suggest that the variations are not a result of normal (p-)modes. They could possibly be due to g-modes excited to observable amplitudes as a result of resonance effects. Surface features (spots) are unlikely to be the cause of the variations.

We searched for combination frequencies $(f_i - f_j)$, f being the normal δ Scuti frequencies detected by Handler et al., but failed to detect any.

Key words: methods: data analysis – techniques: photometric – stars: individual: XX Pyx – stars: individual: CD−24 7599 – δ Scuti.

1 INTRODUCTION

XX Pyx is one of the best studied low-amplitude multiperiodic δ Scuti stars, with close to 1000 h of photometric data collected since its discovery as a variable star in 1992. In 1998 it was the target of a large multisite campaign, organized in the framework of The Delta Scuti Network (DSN). From this and earlier efforts, 22 independent pulsation frequencies and eight combination frequencies (one harmonic and seven at frequency sums of $f_i + f_j$) were detected in the light curves of the star (Handler et al. 2000a, hereafter HAS). Apart from detecting a number of previously unknown frequencies and linear combinations, HAS also detected frequency and amplitude variations on time-scales as short as 20 d. They did not, however, consider light variations with frequencies below $20\,\mathrm{cycle\,d^{-1}}$, since their data set was not sufficiently homogeneous to trust low-frequency peaks in the amplitude spectrum. The history of the study of XX Pyx is briefly reviewed by HAS, and an overview is also given by Arentoft & Handler (2000).

In this paper we investigate the low-frequency part of the amplitude spectrum of XX Pyx, below $7\,\mathrm{cycle\,d^{-1}}$, the lower frequency limit in the paper of Handler et al. (1996). No study has so far looked at this extreme low-frequency part of the amplitude spectrum, because the major part of the existing data had been obtained using non-differential high-speed photoelectric photometry, which is not suitable for investigating low-frequency variability.

We are here exploring a region of the frequency spectrum often not considered in multisite campaigns on δ Scuti stars, mainly arising from problems with instrumental instability and with merging of data sets from different observatories, as discussed by Breger (1994). However, recent campaigns have investigated the low-frequency region of the amplitude spectrum also; examples are the δ Scuti stars 4 CVn (Breger et al. 1999), where combination frequencies were found at values of $f_i - f_j$, and Θ Tuc (Paparó et al. 1996; Sterken 1997), where two peaks at low frequencies in a 2:1 resonance were explained with the variable being a component of an ellipsoidal binary system. This explanation was later confirmed spectroscopically by De Mey, Daems & Sterken (1998).

★E-mail: tarentof@vub.ac.be

Among possible explanations for low-frequency variations are: binarity, frequency differences as a result of mode coupling, actual modes excited at frequencies favoured by resonant pulsation energy transfer (Dziembowski 1982) or surface features, like spots. Other possibilities include g-modes as in the γ Dor stars.

As discussed by Breger (1994), and also by Sterken (2000), it is indeed necessary in a multisite campaign to investigate light variations at all time-scales, and not just those where pulsation frequencies are expected to be found a priori. This is necessary for obtaining a full asteroseismological picture of the star and for searching for variability caused by effects other than pulsation. Breger (1994) discusses the extension of multisite campaigns to frequency ranges outside the ones normally considered (below 5 and above 50 cycle d^{-1}). He suggests that slow variations can be searched for by obtaining a large amount of data from one site, using the same instrumental set up, therefore avoiding merging problems, e.g. as was mentioned above for XX Pyx. The data presented in this paper meet this requirement; we have collected a large amount (147 h) of homogeneous photometric time series CCD data on XX Pyx using the Dutch 91-cm telescope at European Southern Observatory (ESO), La Silla, Chile. The major part of the data was obtained during the 1998 multisite campaign, but additional data have been obtained before and up to one year after the campaign. The part of the data set obtained during the 1998 campaign is discussed and published by Arentoft & Sterken (2000).

In the present paper we search for low-frequency variations in these data. In Section 2 we briefly discuss the observations and reductions; in Section 3 we analyse the data and discuss the results in Section 4. Finally, conclusions are drawn in Section 5.

2 THE DATA

The CCD observations were carried out in 1997–1999 using the Dutch 91-cm telescope at ESO, La Silla, Chile. Details of the observations can be seen in Table 1.

The photometric reduction procedure was described by HAS and in detail by Arentoft & Sterken (2000). The only difference from the procedures described there is that the reduction parameters have now been optimized and applied to all data together, thus not on a night-to-night basis.

We have furthermore obtained *BV* magnitudes of the stars in the observed field from CCD observations taken during a photometric night on 1998 May at SAAO, South Africa. The frames were taken in a sequence (within 10 min); no correction for extinction was therefore applied. The colours have been roughly transformed to the standard system, using the known colours of XX Pyx and GSC 6589–0348, another catalogued star in the (larger) SAAO field. The resulting colour–magnitude diagram is shown in Fig. 1 and the colours of XX Pyx and the brightest of the comparison stars are listed in Table 2. XX Pyx is not only the brightest, but also the bluest star in the field. We will return to this point later in the discussion.

Table 1. Log of CCD observations of XX Pyx with the Dutch 91-cm telescope at ESO, La Silla.

Run	Number of nights	Number of frames	Length (h)	Observer
1997 October	4	221	5.5	CS
1998 January(a)	9	1025	16.2	CS
1998 January(b)	17	4688	89.4	TA
1998 February	5	336	6.1	CS
1998 March	4	386	7.0	CS
1998 April	2	157	4.7	TA
1999 January(a)	7	124	2.4	TA
1999 January(b)	9	477	8.9	CS
1999 March	4	356	6.9	CS
Total	61	7770	147.1	

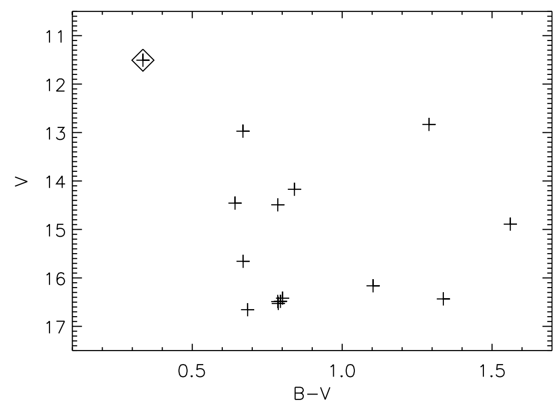

Figure 1. Colour–magnitude diagram of the stars in the field observed at ESO. The colours have been obtained from CCD frames at SAAO by Handler. The position of XX Pyx is marked with a diamond.

Table 2. Colours of the brightest comparison stars, based on observations obtained at SAAO. The identification of the comparison stars is given as the extension to GSC 6589. GSC 6589–0504 was not in the field of view of the SAAO images.

Star:	XX Pyx	0504	0180	1726	0441	0756	0654
V	11.50	13.88	14.46	12.83	12.97	14.49	14.17
$B-V$	0.34	–	0.64	1.29	0.67	0.79	0.84

3 LOW-FREQUENCY VARIATIONS

In this section we search the photometric data for long-term changes and variability. The data obtained at ESO during the 1998 DSN campaign suggested the presence of slow variations, as can be seen from the light curves in Fig. 2 and from the amplitude spectrum shown in Fig. 3. The light curves indicate low-amplitude variations on a longer time-scale superimposed on the main δ Scuti pulsations, which have periods of about 35–60 min. The amplitude spectra in Fig. 3, which were produced with the computer program PERIOD98 (Sperl 1998), show that some $1/f$ noise is present in the data (in both the comparison stars and XX Pyx), but they also clearly indicate that variability on a 5–6 mmag level is present in XX Pyx at frequencies below 5 cycle d^{-1}.

Owing to these slow variations, we decided to continue the monitoring of XX Pyx during the observing runs in early 1999. These observations were conducted in a manner different from the campaign observations; instead of continuous time series observations we typically obtained groups of 4–5 CCD frames taken 1–2 h apart, mostly complemented with a long continuous stretch of 1–2 h. Such observations sample low-frequency variations and night-to-night changes but are, of course, also affected by the multiperiodic behaviour of XX Pyx.

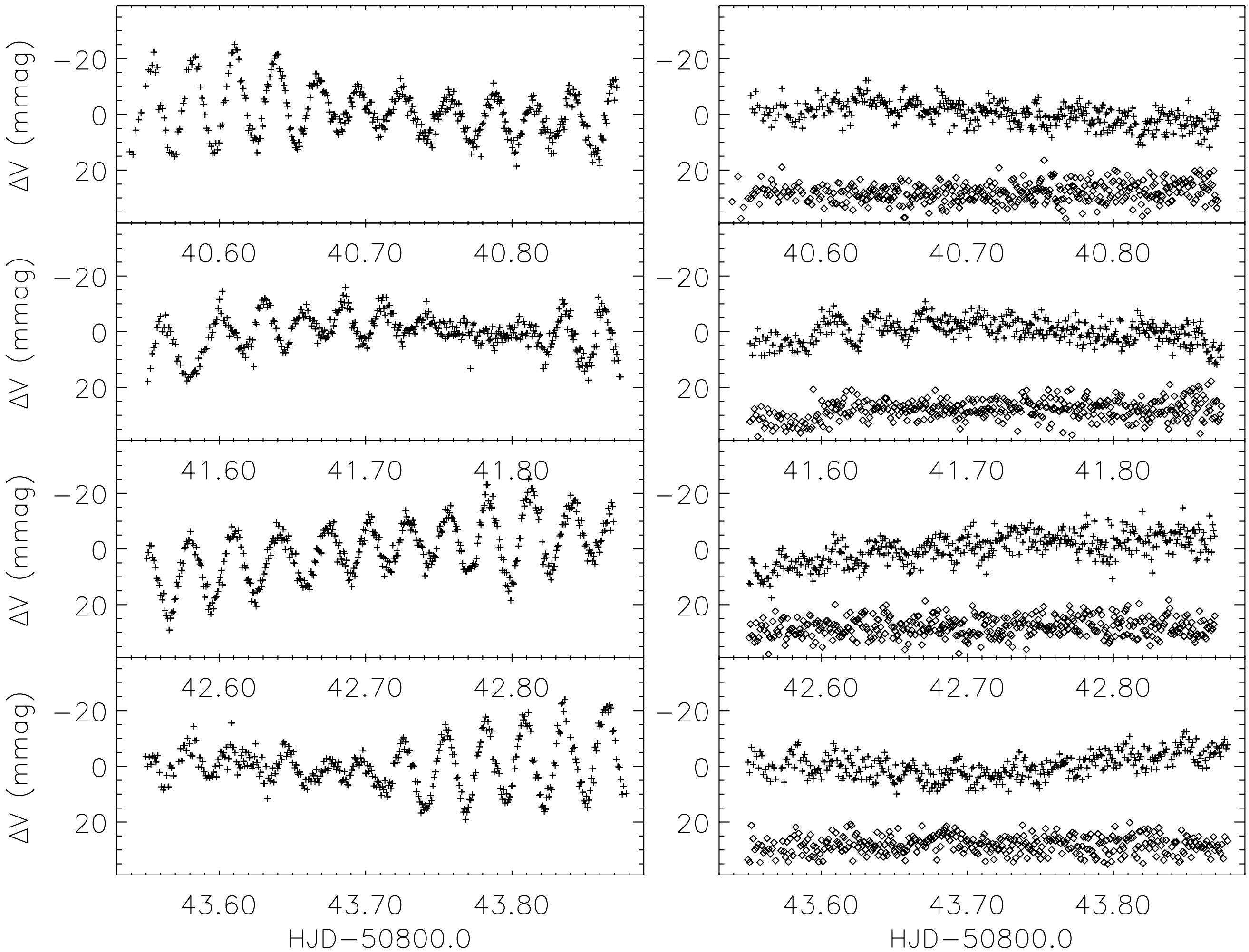

Figure 2. Differential light curves of XX Pyx, obtained at ESO, from several nights during the multisite campaign in 1998 January, before (left) and after (right) pre-whitening with the frequencies detected in the campaign by HAS. Parts of the residuals still show signs of short-period variability, because of the fact that the frequency solution found by HAS does not describe the observed light curves completely, as is also discussed by Handler et al. (2000b). Furthermore, the subtracted solution does not take into account frequency and amplitude variability detected by HAS. The right panel also plots the light curves of one of the constant stars (diamonds).

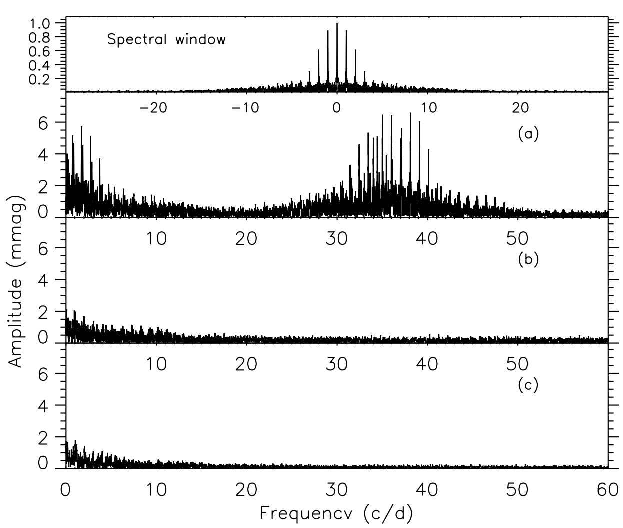

Figure 3. Spectral window (top) and amplitude spectra up to 60 cycle d^{-1} for XX Pyx (a) and two constant stars (b, c) from the data obtained during the DSN campaign in 1998.

3.1 Long-term behaviour

To investigate the behaviour of XX Pyx on time-scales from days to months, we proceeded as follows: for each night we determined the mean differential magnitude of XX Pyx and subtracted this from the light curve of that night, which leads to a data set corrected for night-to-night variations. This was done to remove the 28 frequencies (20–80 cycle d^{-1}) – found to be present in the complete 1998 campaign data obtained by HAS – in the most optimal way. The purpose was to obtain precise values of the nightly averages, not affected by the pulsations (which might especially affect the smaller 1999 data set), and to check whether the *normal* δ Scuti variations have any effect on the signal at low frequencies. In this procedure we also checked for bad data points. As the reductions were done semi-automatically we did not inspect each CCD frame visually. We therefore searched the light curves for data points that deviate by 3σ (rms) or more from the nightly averages, and for these points we checked the corresponding CCD frames. If a frame was found to be bad (because of clouds, overexposure, bad centring etc.), the data point was removed. In this way we discarded a total of only 25 points out of 7770. From

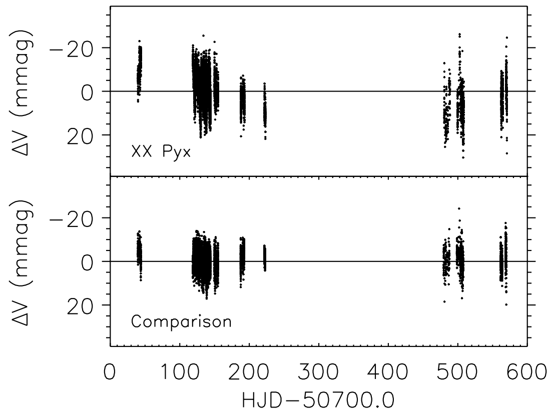

Figure 4. The XX Pyx light curve pre-whitened with 28 frequencies (top) and that of a comparison star (bottom), showing the data from the whole period, i.e. 1997 October–1999 March.

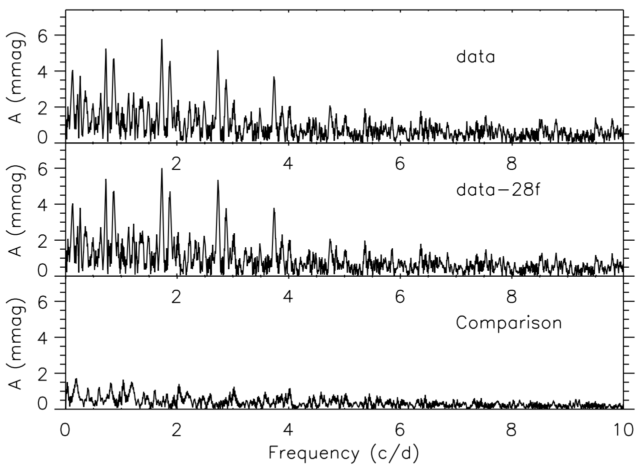

Figure 5. The XX Pyx amplitude spectrum before (top) and after (middle) pre-whitening the data with the 28 frequencies detected by HAS, based on data obtained just before and during the 1998 multisite campaign. The lowest panel shows the amplitude spectrum of one of the comparison stars.

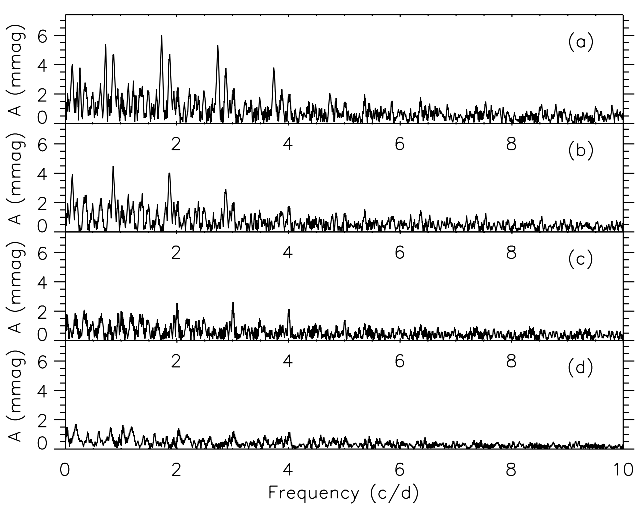

Figure 6. The amplitude spectrum of XX Pyx before pre-whitening (a), after pre-whitening with the 1.733 cycle d^{-1} frequency (b), and after simultaneous pre-whitening with both the 1.733 and the 0.869 cycle d^{-1} frequencies (c). The lower panel (d) plots the spectrum of one of the constant stars for comparison.

the resulting cleaned data set we subtracted the frequency solution found by HAS, using simultaneous fitting. We then added the previous estimates of the nightly averages to the residuals, and re-determined the averages.

In Fig. 4 we show in the upper panel the long-term behaviour of the XX Pyx residuals, and in the lower panel the same for a comparison star. Although the scatter seems higher for XX Pyx, it is fairly constant on long time-scales (months). Below we will discuss variability on time-scales of days.

3.2 Fourier analysis at low frequencies

For analysing the low-frequency part of the periodogram we use the residual data with the 28 frequencies subtracted, and the initially removed nightly averages added. The data obtained in 1999 are too sparse (950 points over 3 months) to allow simultaneous fitting of 28 frequencies, and amplitude and frequency variations detected by HAS may imply that the frequency solution found in 1998 was not valid in 1999. Thus the analysis presented below will focus on the data obtained in 1998. The 1999 data will be used mainly for confirmation and will be discussed separately.

We adopt the criterion that a peak should have a signal-to-noise (S/N) ratio in amplitude of at least four to be significant, as discussed by Breger et al. (1993). For peaks at combination frequencies, the criterion can be lowered to 3.5 (Breger et al. 1999). In Fig. 5 we show the 1998 amplitude spectrum at low frequencies before and after fitting the 28 frequencies significant in the complete HAS data set. This figure shows that subtracting the pulsations at higher frequencies has only marginal influence on the low-frequency part of the spectrum. This is expected because the data set is extensive and the frequency regions are well separated. It is thus not important whether we analyse the original data, or the data pre-whitened with the 28 frequencies. Fig. 5 also shows clear peaks present at low frequencies in the XX Pyx data, and that the same peaks are not present in the amplitude spectra of the comparison stars. This proves that the variation is not an instrumental effect; the other stars in the field (two shown in Fig. 3) have some low-level $1/f$ noise in their amplitude spectra, but no significant peaks.

Furthermore, Fig. 5 shows that the window function is poor, i.e. peaks arising from periodic variations have prominent 1 cycle d^{-1} aliases.

Two peaks (with sidelobes) stand out in the XX Pyx amplitude spectrum (Fig. 5). The highest peak has an amplitude of about 5.7 mmag, and is positioned around 1.7 cycle d^{-1}. The second highest peak, disregarding the sidelobes of the first, is at 0.87 cycle d^{-1} with an amplitude of about 4.7 mmag. The highest peak in the comparison star amplitude spectrum reaches 1.6 mmag and appears to be a result of the $1/f$ noise.

Determining the frequencies and amplitudes of these two peaks using simultaneous fitting gives the frequency values of 0.869 and 1.733 cycle d^{-1}, with amplitudes of 4.5 and 5.9 mmag, respectively. In Fig. 6 we show how the spectrum looks after pre-whitening with one (Fig. 6b) and two (Fig. 6c) frequencies. The pre-whitened spectrum shows a group of peaks centred around 3 cycle d^{-1}, with an amplitude of 2.4 mmag. The noise level in the pre-whitened spectrum is 0.7 mmag; this peak is thus not significant on a 4σ level (even pre-whitening with this frequency as well does not lower the noise level sufficiently for it to become significant). Furthermore, 3 cycle d^{-1} roughly corresponds to the length of the night. This peak remains present when nights with many data points only are used, but in this case it is no longer the highest low-frequency peak (no peaks are in this case outstanding),

Table 3. Signal-to-noise (S/N) ratios of the detected low-frequency variations in different sections of the data. The noise is calculated as the mean value between 0 and 5 cycle d^{-1} in the residual spectrum after pre-whitening with 30 frequencies. The error in the frequency, following Montgomery & O'Donoghue (1999), is, on the frequencies found from the complete data set, about 0.000 05 cycle d^{-1}. This may however be an underestimate, as was discussed by HAS and Arentoft & Sterken (2000).

Data set	Label	Frequency (cycle d^{-1})	Amplitude (mmag)	Noise (mmag)	S/N
All data	f_A	0.8695	4.50	0.77	5.82
	f_B	1.7352	5.39	0.77	6.97
1998 data	f_A	0.869	4.50	0.71	6.32
	f_B	1.733	5.86	0.71	8.23
1999 data	f_A	0.868	4.20	0.76	5.55
	f_B	1.734	6.35	0.76	8.39

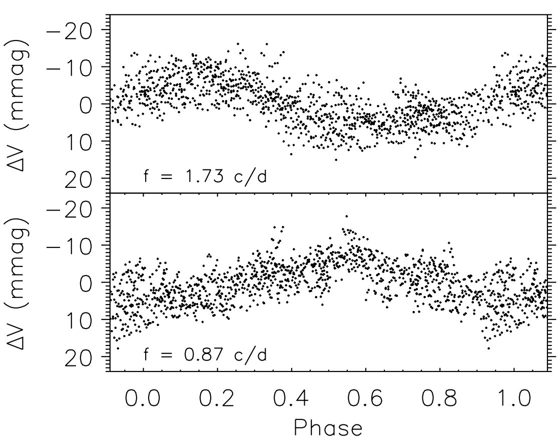

Figure 7. The XX Pyx light curves folded with the low-frequency at 1.73 (top) and 0.87 cycle d^{-1} (bottom). The other frequency has in both cases been subtracted before the phase diagram was calculated. This plot is based on data from 1998 January–February binned in 4-min bins, and pre-whitened for the 28 δ Scuti frequencies.

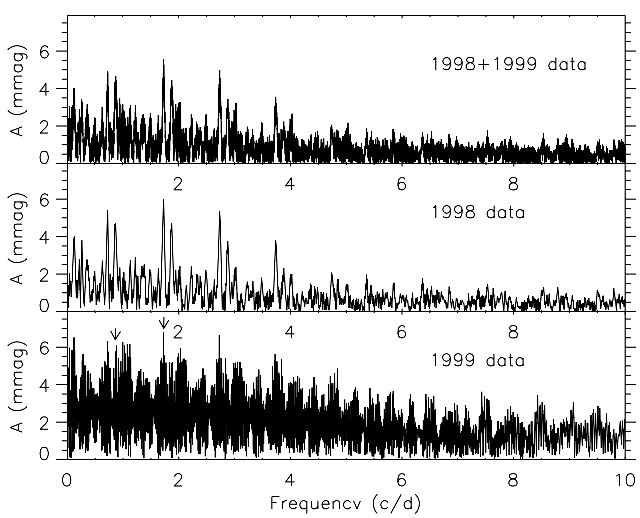

Figure 8. Amplitude spectra of XX Pyx, based on all data (top), the 1998 data alone (middle), and the 1999 data alone (bottom). In the lower panel are the positions of the two detected frequencies indicated with arrows.

and its amplitude is lower (about 2 mmag). The two frequencies at 0.869 and 1.733 cycle d^{-1} are, with the above-mentioned amplitudes and noise level, clearly significant (S/N $>$ 4), and are thus detected. We label them as f_A and f_B to distinguish these *slow* variations from the frequencies detected by HAS ($f_{1\text{–}30}$). The motivation for doing so is that, as will become clear below, the cause of the variations is not unambiguously determined. The phased light curves are shown in Fig. 7 where the variations are visible, but with amplitudes only slightly higher than the scatter in the individual light curves. The results are tabulated in the 1998 entry of Table 3. The two other entries in this table will be discussed below.

3.2.1 *Including the 1997 and 1999 data*

As a result of the limitations of the 1999 data set, we decided to treat it separately. In Fig. 8 we show the amplitude spectrum at low frequencies based on the 1999 data alone (lowest panel). The central panel shows the spectrum of the 1998 data (discussed above, for comparison), and the upper panel shows the amplitude spectrum based on all obtained data. The latter displays the same peaks as are present in the 1998 amplitude spectrum, with similar amplitudes. The complete data set is used for determining the frequencies, since it has the longest time-base (about 1.5 yr) and therefore the highest frequency resolution. The 1997 data set only consists of a few hundred data points and cannot be analysed separately.

The amplitude spectrum of the 1999 data indicates that this data set is not extensive enough to allow a detailed analysis. However, as the highest peak at low frequencies occurs at 1.73 cycle d^{-1}, and a peak is present at frequency 0.87 cycle d^{-1}, the data support the results found from the 1998 data set. Furthermore, fitting a synthetic curve using the nine frequencies of highest amplitude detected by HAS to the 1999 light curves works better if the two low frequencies detected here are included. Residuals without the latter have a scatter of 7.6 mmag, while including them brings the scatter down to 5.7 mmag. We will also show below that the two-frequency solution fits the light curves well.

We have collected the frequencies and amplitudes determined from the complete data set and from the 1998, 1999 data sets alone in Table 3. In all cases, fitting the two frequencies and calculating the noise from the pre-whitened spectrum leads to significant detections. However, in the 1999 data set, f_A is not the strongest signal after pre-whitening with f_B, and would not be found from this data set alone. After pre-whitening the 1999 data with f_A and f_B, the noise level in the amplitude spectrum decreases quite drastically, as compared with the lower panel of Fig. 8. The two frequencies have maintained constant phase during the observing period, i.e. the 1999 data are in phase with the 1998 data. This will be discussed further below.

3.2.2 *Fit to the light curves*

In Figs 9 and 10 we show the fit of the two-frequency solution to the XX Pyx residuals, where the data have been summed into 3-h bins. This fit follows the residual data well, except for a couple of points, e.g. from the night 50824, 32 and 34 (HJD, Fig. 9). In the first case, the zero-point of the original light curve is shifted by several mmag upwards as compared with the synthetic 30-frequency fit, which otherwise agrees well with the shape of the light curve from that night. This is also the case on HJD 50834, whereas the light curve from HJD 50832 is of rather poor quality

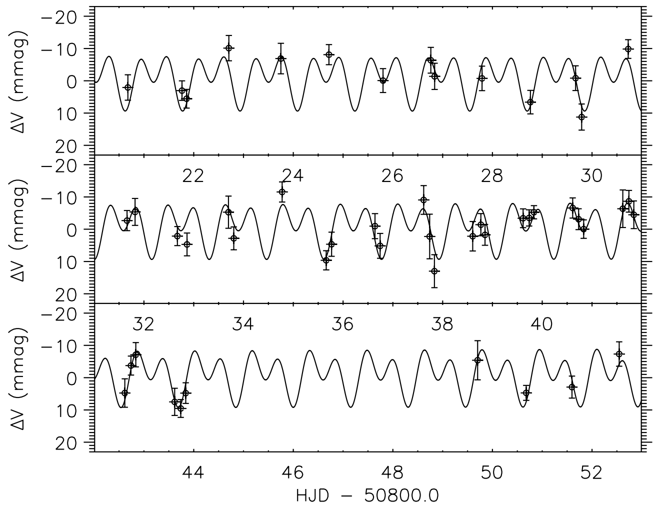

Figure 9. Fit of the two-frequency solution to the XX Pyx residuals (1998, only where long uninterrupted observations were obtained). The data have been summed into bins of 3 h (or shorter for nights with shorter coverage) for clarity. The synthetic curve fits the residuals well, but there are some deviating points. The error bars correspond to the rms scatter in the bins. See text for further discussion.

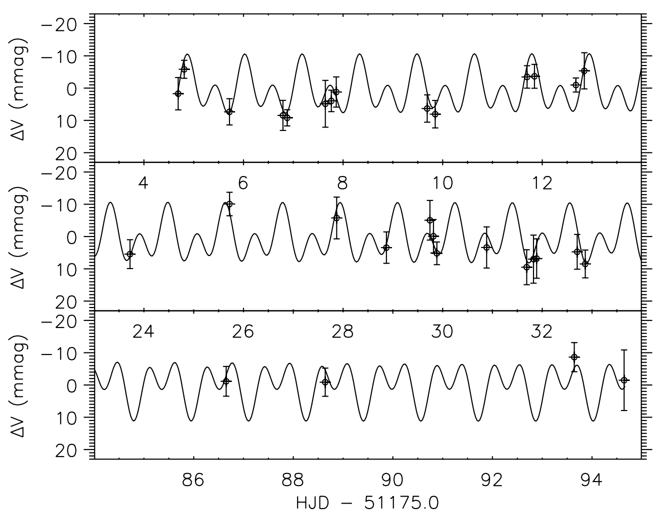

Figure 10. As Fig. 9, but for part of the data obtained in 1999.

(as a result of the Moon being very close to the field). Except for the latter night, we have no explanations for these deviations. Fig. 10 shows that the same low-frequency variations as in 1998 are present in the 1999 light curves. Data from a couple of nights were of very low quality, and have been omitted.

3.3 Variability and amplitudes of the main δ Scuti frequencies

HAS found eight frequencies to be variable in amplitude, three of them also variable in phase. The time-scale of the variability is 20–70 d for the amplitudes, and 25 d for the phases. Such variations are not expected to influence the amplitude spectrum at low frequencies, as we have already shown the modes themselves have no effect. We did, however, perform tests which confirm this expectation.

As the low-frequency variation is directly visible in the light curves, we can immediately rule out the possibility of a spurious signal from the Fourier analysis. We constructed synthetic data from the fits used by HAS, which include the frequency and amplitude variations, using the times of observations of our data obtained during the 1998 multisite campaign. Calculating the amplitude spectrum from these data did not result in any signal at low frequencies. Also, subtracting the fit with the amplitude and frequency variations included instead of simultaneously fitting the 28 frequencies alone proved to have no effect on the shape of the amplitude spectrum at low frequencies; the same low-frequency variations are present in the residual data, with the same amplitudes.

Table 4. Amplitudes (in mmag) of the three main frequencies of XX Pyx in the 1998 and 1999 data sets. The formal errors on the amplitudes are, calculated following Montgomery & O'Donoghue (1999), 0.06 mmag for the 1998 data, and 0.16 mmag for the 1999 data. The actual errors are certainly larger than the formal ones because of the high number of frequencies and the poor window function.

ID	Frequency (cycle d^{-1})	Amplitude 1998	Amplitude 1999
f_1	38.110	6.6	12.8
f_2	36.013	6.4	2.8
f_3	33.438	4.8	5.3

Although the amplitudes from the fit to the 1999 data are uncertain as a result of an extremely poor spectral window function – especially in the region of 25–40 cycle d^{-1} where a large number of frequencies is present – it seems that f_1 (at 38.110 cycle d^{-1}, labelling as in HAS) had a much higher amplitude in 1999 than in 1998, more than 12 mmag as compared with the 6.53 mmag (V) found by HAS. f_2 seems to have only half the amplitude it had in 1998, whereas the amplitudes of f_3 and f_4 seem to have remained constant. f_6 has seemingly more than doubled its amplitude, whereas f_7 and f_{10} have a slightly higher amplitude. f_{15} also seems to have increased its amplitude. Fitting only the three frequencies of highest amplitude (f_1, f_2, f_3) to the 1998 and 1999 data separately (thus minimizing the risk of overfitting the 1999 data) results in the amplitude values collected in Table 4. Such rather large variations in amplitude have been observed before for XX Pyx (Handler et al. 1998).

3.4 Correlation with observational parameters

It is well known that instrumental and atmospheric effects can cause higher noise levels at low frequencies and also produce spurious peaks. However, as the low-frequency variations are not present in the differential light curves of the constant stars, we believe that they are not a result of instrumental effects. Still the fact that XX Pyx is the bluest star in the field may lead to the suspicion that the variations are due to a high-order extinction effect. This is not the case as the maxima of the slow variations do not coincide with meridian passage, although in many cases we observed during the full night starting and ending at large airmass. The slow variability, by nature, causes the light curve to coincide with the trend in airmass only for some nights.

A way to test the influence of parameters like airmass, seeing, sky-background and position on the CCD (x, y offset) is to investigate the correlation between the light curves and those

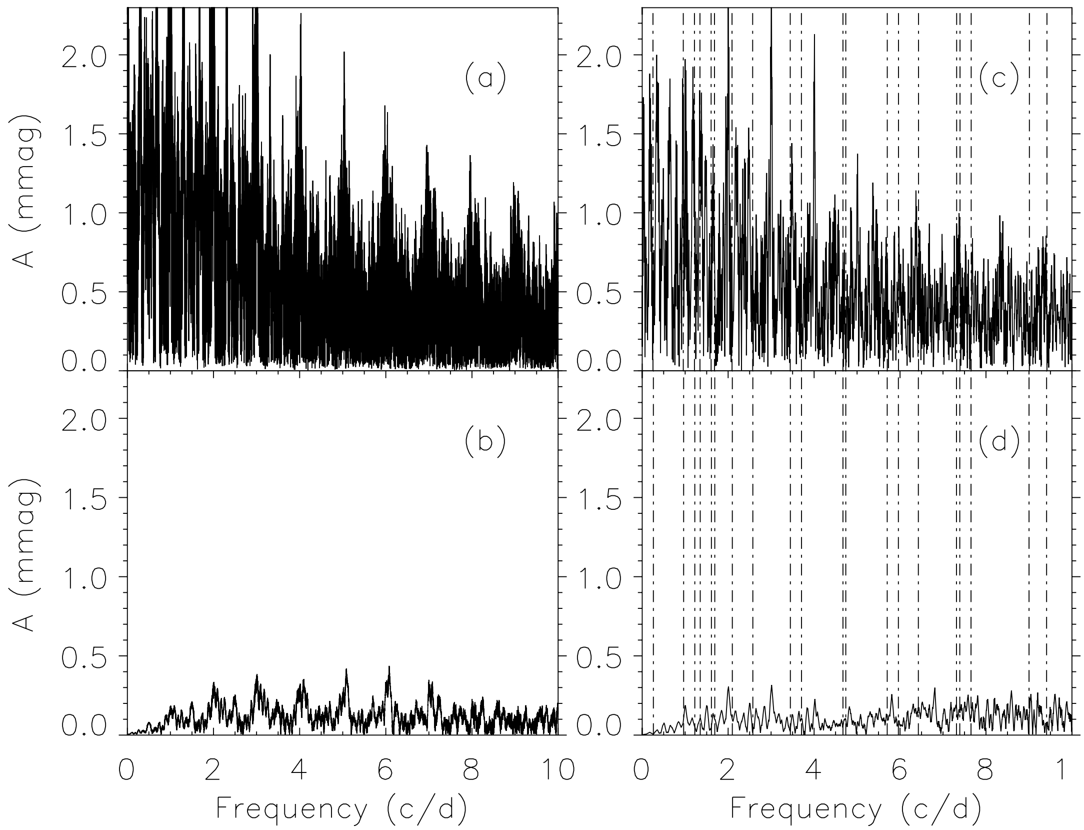

Figure 11. The effect of decorrelating on a night-to-night basis with observational parameters like seeing, sky-background, x, y offset and airmass. The left panel plots the results for one of the constant stars, (a) before decorrelation and (b) after; the right panel plots the results for XX Pyx, (c) before decorrelation and (d) after. In panels (c) and (d) we also show the expected positions of the combination frequencies as a result of differences between the δ Scuti frequencies.

parameters. However, correlating the XX Pyx light curves with these quantities is difficult, as the time-scale of the variations in the light curves is of the same order as e.g. the changes in sky-background in the case of a rising or setting Moon, or the changes in airmass. Thus for some nights one would expect large correlations with certain parameters, while not so for others. This is exactly what we find when we calculate correlation coefficients within each night; for some nights the correlation with e.g. the airmass is high, for other nights it is not, and blind decorrelation with the mentioned parameters will surely lead to an erroneous result. For several nights, however, there is no correlation with any of the parameters, whereas the slow variation is directly visible in the light curve. This is, e.g., the case for the nights of HJD = 50835, 50836, 50840 and 50843 (see Figs 2 and 9).

After pre-whitening the XX Pyx light curves with the detected frequencies, there appears to be nothing but noise left in the amplitude spectrum (Fig. 6). We can then try to decorrelate the residuals with the observational parameters to search for very low-amplitude peaks (e.g. combination frequencies). As described above, we risk destroying the signal at low frequencies, but although it is difficult to estimate the amplitudes of the combination frequencies (see e.g. Breger et al. 1998) we expect them to be very low. The sum frequencies detected by HAS all have amplitudes below 0.3 mmag, and if the frequency differences had similar amplitudes, they would, without decorrelation, be completely hidden in the noise (see Fig. 11c). We therefore tried decorrelation by fitting one overall multiple linear regression fit of the five parameters to all the data, and by fitting the same function on a night-to-night basis, i.e.

$$V = a_0 + a_1F + a_2s + a_3X + a_4x + a_5y, \tag{1}$$

where, on a given CCD frame, F is the full width at half-maximum (FWHM) of the stellar profile (seeing), s is the sky-background, X is the airmass, and x,y the x,y offsets relative to a fiducial frame. These methods were also applied by Frandsen et al. (1996) in a search for δ Scuti stars in NGC 6134. The overall fit to all data did not show any correlation with the observational parameters, and decorrelation did not improve the noise level. Fitting within the individual nights, however, there is occasionally some correlation with one or two of the parameters. As shown in Fig. 11, the decorrelation on a night-to-night basis has a dramatic effect on the $1/f$ noise, which is almost completely removed. The left panels show the effects of the decorrelation on one of the constant stars suffering from $1/f$ noise which is very efficiently removed. The same is the case for XX Pyx, which is shown in the right-hand panels of Fig. 11. However, one of the effects of this decorrelation is to remove differences in nightly zero-points, and applying only this simple correction to the data leads to improvements almost as significant as the ones seen in Fig. 11 – although the general noise levels are somewhat higher, and the peak at 3 cycle d^{-1} is not as suppressed as in the decorrelated case. An effect of the zero-point correction is that the amplitudes of possible signals decrease (Breger 1994), making the combination frequencies even harder to detect.

The fact that applying zero-point corrections, e.g. with the purpose of removing $1/f$ noise, does alter the amplitude spectrum at low frequencies is clearly demonstrated if the correction is applied to XX Pyx before searching for low-frequency signals. The resulting amplitude spectrum exhibits only one signal at low frequencies, and not two as detected in the present paper, and the highest peak occurs at a 1 cycle d^{-1} alias to 1.73 cycle d^{-1}, with an amplitude of only about 60 per cent of the real amplitude. As Breger (1994) puts it, *the temptation to shift the zero-points of individual nights of data should be resisted*.

In Figs 11(c) and (d) we show the expected position of frequency differences, involving the strongest modes detected by HAS, in the amplitude spectrum before and after decorrelation. The highest peaks do not correspond to these values, and we do not detect any combination frequencies in this part of the spectrum.

4 DISCUSSION

We find no instrumental or atmospheric explanation for the slow variations in XX Pyx; the low-frequency variations reported in the present paper are intrinsic to the star. Below we discuss possible explanations for these variations.

4.1 Binarity

The two detected frequencies are close to a 2:1 ratio, the difference of $2f_\mathrm{A}$ from f_B is only 0.0038 cycle d^{-1}. This is still considerably larger than the formal error quoted in Table 3, but there may be other effects present which affect the frequency determination, as discussed by Arentoft & Sterken (2000), and the formal errors are certainly underestimates. In fact, the noise level in the amplitude spectrum at high frequencies (90 cycle d^{-1}) is about 0.1 mmag, which is what is expected for the number of data points and the noise per point. However, the noise at low frequencies is about seven times higher, and if we scale the error estimate with the noise ratio we get an error of 0.00035 cycle d^{-1}, still one order of magnitude smaller than the deviation quoted above.

Still the near 2:1 ratio of the frequencies and the shape of the light curves suggest that XX Pyx may be an ellipsoidal variable. If binarity is indeed the cause of the low-frequency variations, the 2:1 ratio should be exact. Subtracting a forced $f_\mathrm{A} + 2f_\mathrm{A}$ fit from the data removes the low-frequency variation, but leaves, as one would expect, higher residual noise when compared with subtracting a fit where both frequencies are left as free parameters. To assess formally if the deviation from the 2:1 ratio is real, we apply the Bayes Information Criterion (BIC)

$$\mathrm{BIC} = \frac{p \log N}{N} + \log s^2, \qquad (2)$$

where p is the number of free parameters included in the fit, N is the number of data points, and s is the standard deviation of the residuals. Since equation (2) should be minimized, introducing an additional free parameter should reduce the standard deviation of the residuals sufficiently for the extra free parameter to be accepted. We have compared the fitting of two frequencies as free parameters ($p = 7$; two frequencies, amplitudes and phases and one zero-point) with a forced $f_\mathrm{A} + 2f_\mathrm{A}$ fit ($p = 6$) to the 1998 and 1999 data sets, and we find that the BIC is smaller using seven free parameters (with $s = 5.274$ mmag for $p = 7$ and $s = 5.939$ mmag for $p = 6$). 7527 data points were used in the fits. The BIC thus argues against a binary explanation for the low-frequency variations. Calculating forced fits with varying frequency ratios (between 1.9 and 2.1) indicates by how much the optimal solution differs from the 2:1 ratio. This is illustrated in Fig. 12, lower panel, where the optimal choice of the frequency ratio appears to be closer to 1.99 – with even a local maximum at a ratio of 2. This plot is based on the extensive 1998 data set.

The question is if this deviation from 2 is significant or not. It should be noted that in the very similar case of θ Tuc (Paparó et al. 1996), the two low-frequency peaks below 1 cycle d^{-1} were found to deviate from a 2:1 ratio by a comparable amount as we find for XX Pyx, but were later shown to be caused by binarity (De Mey et al. 1998). However, Paparó et al. (1996) do not discuss a forced $f + 2f$ fit to their data. We therefore re-analysed their ESO data set along the same lines as above, to check whether our approach would point towards the correct solution, i.e. binarity. Data were obtained in *uvby*, with residual scatter ranging from about 4 mmag in y to 5.5 mmag in u. Although the sampling rate was lower, the data set is very similar to our data set on XX Pyx from 1998 January and February, in both quality and extent. Calculating the BIC for a free fit of two frequencies and for a forced $f + 2f$ fit showed that the y, b and v data support a forced fit, and thus the binary solution, but the u data set supports a free fit. For the y data, the BIC as a function of frequency ratio is shown in Fig. 12, upper panel. The optimal frequency ratio is very close to 2. For the u data, curiously, the optimal ratio is closer to 1.95. Binning our 1998 January–February XX Pyx data to a similar sampling rate as the θ Tuc data, and calculating the BIC from these data actually supports the forced fit. This is not the case when we consider the equivalent unbinned data. We conclude that in this case, the BIC cannot be used to distinguish between different solutions.

We then re-considered the spectroscopic data acquired by Handler et al. (1997, see this paper for a more complete description of the observations). We re-reduced the spectra, but did not co-add them all as did Handler et al. (1997), whose main aim was to determine the rotational velocity of the star. Instead, we only combined the spectra of the two individual nights. Because of varying observing conditions (cloud and bad seeing in the first night, clear and good seeing in the second night), the combined spectrum from 1996 March 28 had an average continuum S/N ≈ 12 whereas the spectrum from 1996 March 30 had S/N ≈ 33.

The radial velocities from these two spectra were then calculated by L. A. Balona by cross-correlating a synthetic spectrum with the observed one. Individual measurements from eight echelle orders where suitable spectral lines could be detected were averaged, which also provides a good error estimate. We find average heliocentric radial velocities of $+48 \pm 7\,\mathrm{km\,s^{-1}}$ from the combined spectrum of the first night, and $+88 \pm 5\,\mathrm{km\,s^{-1}}$ for the second

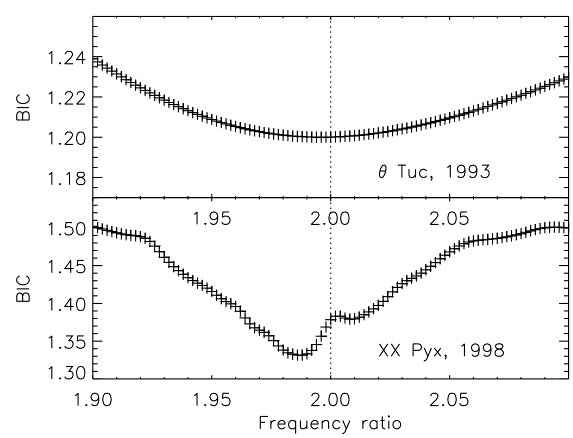

Figure 12. BIC, calculated from (2), as a function of the ratio of the fitted frequencies. See text for details.

night. This radial velocity variation is significant, showing that XX Pyx is in fact a binary star. It remained undetected by Handler et al. (1997), as their available methods let them doubt any result from the poor-quality spectrum of the first night.

We note for completeness that the rotational velocity of $52\,\mathrm{km\,s^{-1}}$, as quoted by Handler et al. (1997) is still the best estimate available; this result does not change when we analyse the spectrum of the second night alone. The mean radial velocity ($+72\,\mathrm{km\,s^{-1}}$) quoted in that paper is however obsolete, as it basically represents a weighted average of our two nightly measurements.

The radial velocity shift of about $40\,\mathrm{km\,s^{-1}}$ gives us a lower limit of the radial velocity amplitude of $20 \pm 8.6\,\mathrm{km\,s^{-1}}$. If the period is 1.15 d (27.6 h), i.e. the photometric period (indicating a close system), we can obtain an estimate of the mass function of the possible binary system assuming circular orbits:

$$\frac{(m_2 \sin i)^3}{(m_1 + m_2)^2} = 0.001 \pm 0.001\,\mathrm{M}_\odot; \tag{3}$$

and of the projected orbital radius:

$$a \sin i = 0.45 \pm 0.2\,\mathrm{R}_\odot. \tag{4}$$

The companion must be a low-mass or compact object, as the spectrum is not double-lined, and the inclination must be low given that the system is not eclipsing. For the sum of the two masses to exceed the mass of XX Pyx, we obtain from Kepler's laws of motion that the separation must be at least $5.6\,\mathrm{R}_\odot$, given a mass of XX Pyx equal to $1.85\,\mathrm{M}_\odot$ as found by Pamyatnykh et al. (1998), who also found a radius for XX Pyx of $1.95\,\mathrm{R}_\odot$. This indicates a low value of i, but, of course, the radial velocity amplitude is likely to be higher than $20\,\mathrm{km\,s^{-1}}$.

We can estimate the radial velocity amplitude for different values of i as a function of the companion mass, as illustrated in Fig. 13. This figure shows that it is possible to find a configuration of a low-mass companion in an orbit with low inclination giving rise to the lower limit of the radial velocity amplitude of $20 \pm 8.6\,\mathrm{km\,s^{-1}}$. Also, if we assume the companion is a normal star, i is probably higher than 10°, otherwise the companion would be massive enough to be seen in the spectra.

If the mass ratio is around 2 we obtain, following e.g. the approximation by Eggleton (1983), an effective Roche lobe radius of $r_{\mathrm{Roche}} \sim 0.44$. With a radius of XX Pyx equal to $1.95\,\mathrm{R}_\odot$, the required separation between the components is at least $4.4\,\mathrm{R}_\odot$ for XX Pyx to be within the Roche lobe, compatible with the required distance following Kepler. With this required distance ($5.6\,\mathrm{R}_\odot$), XX Pyx would still be within its Roche limit even for a mass ratio of 1.

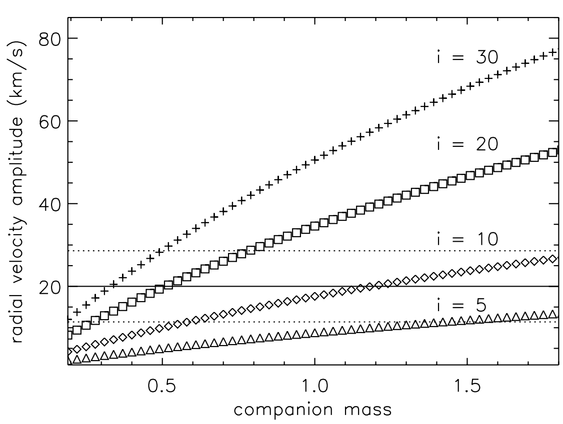

Figure 13. Predicted radial velocity amplitude as a function of the companion mass (in $\mathrm{M}_\odot$) for different values of i. The solid horizontal line shows the lower limit on the radial velocity amplitude as found from spectroscopy, the dotted lines delineate the 1σ uncertainty (see text).

We note that the frequency and amplitude variations found by HAS occur at a longer time-scale than the binary period, should the latter be the photometric period of 27.6 h; the two phenomena do not appear to be directly related.

The referee suggested that orbital motion of XX Pyx could cause observable frequency variations as a result of the light-time effect. This effect would be most easily detectable by the appearance of peaks in the amplitude spectrum that are symmetrically separated by the orbital frequency and its harmonics from the dominating pulsation frequencies.

We have therefore determined the amplitudes of such peaks which are a function of the size of the light-time effect and of the amplitude of the stellar pulsation frequencies. The detection level for signals in the highest S/N ratio data available, the 1998 data set, is 0.466 mmag, whereas the amplitude of the strongest mode of XX Pyx in that data set is 8.1 mmag. For sidelobes caused by orbital motion to exceed this detection level, a light-time effect larger than 40 s would be required. This corresponds to a projected orbital radius of XX Pyx equal to $17.5\,\mathrm{R}_\odot$. With an orbital period of 1.15 d, the projected radial velocity amplitude of XX Pyx would be approximately $800\,\mathrm{km\,s^{-1}}$, which is highly unlikely. Hence we conclude that the pulsational frequency variations induced by a hypothetical companion in a 1.15-d orbit can by no means be detected in the available photometric data. If XX Pyx was a binary with an orbital period longer than 10 d, orbital variations could manifest themselves more easily, but we have no evidence for the pairs of sidelobes predicted in such a case.

We have, however, used BINARY MAKER 2.0 (Bradstreet 1993) to estimate the effect of low-mass or compact binary companions on the photometric light curves of XX Pyx. We found that binarity could account for the low-frequency variations reported in the present paper: variations as those seen in Figs 9 and 10 can be generated by different combinations of companion mass and inclination.

We also investigated the stability of the phases of the low-frequency variations over the observing period. If we determine the frequencies from the complete data set, and fit those frequencies to the 1998 and 1999 data sets individually, we obtain stable phases for the combined and individual data sets if we leave both frequencies free. If we use a forced $f_{\mathrm{A}} + 2f_{\mathrm{A}}$ fit instead, there seem to be inconsistencies in the phases from the two different years for f_{A}, but this is highly sensitive to the exact choice of frequency, and may not be real – the overall solution is dominated by the 1998 data, and the phases and frequencies may not be determined to a sufficiently high precision. The actual errors may, as discussed above, be severely underestimated in a formal assessment, and the differences could be because of the uncertainties in the treatment of the observational errors in this low-frequency part of the amplitude spectrum.

With the detected radial velocity variations, it would be advantageous to obtain high-resolution high S/N ratio spectra of XX Pyx. Owing to the faintness of the star this will require a large telescope with a sensitive spectrograph, and should be carried out to search for the faint companion and to obtain a spectroscopic binary period.

4.2 Other possibilities

Since we do not know the spectroscopic period of XX Pyx, there is a possibility that the low-frequency variations detected in the present paper are not a result of binarity – and could be because of pulsation instead. One g-mode is expected to be excited in XX Pyx, but at higher frequency (around 30 cycle d^{-1}, Handler et al. 1997). The low-frequency variations could be due to g-modes, as is seen in the γ Dor stars. However, g-modes are normally not expected to reach observable amplitudes at the surface of δ Scuti stars, but the 2:1 ratio may give rise to resonance effects.

The γ Dor instability strip does overlap the δ Scuti instability strip, near the cool border of the latter, and pulsations connected with both the δ Scuti and the γ Dor phenomenon may be excited in some stars (Handler 1999). However, XX Pyx is situated near the hot border of the δ Scuti instability strip, and γ Dor variations are thus not expected. Of course, this does not rule out that g-modes could be present, but the detection of radial velocity variations in the spectra, and thus binarity, makes g modes less likely to be the cause of the variations. However, g-modes cannot be ruled out even if a spectroscopic investigation finds a binary period that agrees with the photometric frequency (f_A) found in the present paper, as they may become tidally excited. Extensive and homogenous single-site two-colour photometry will be useful for examining the possibility of the presence of g-modes.

f_A and f_B fall in the region of the frequency spectrum where combination frequencies, arising from differences between the main δ Scuti pulsations (at 25–40 cycle d^{-1}), are expected to be found. However, the amplitudes of the slow variations are of the same order as the highest of the rapid pulsations, making simple combination frequencies an unlikely explanation. This is especially the case for the frequency at 0.8695 cycle d^{-1}, as the only possible close-by combination is between frequencies with B amplitudes of 2.4 and 0.44 mmag, respectively. Furthermore, the difference between these two modes (f_7 and f_{30} in HAS) is 0.863 cycle d^{-1}, and the match is thus not exact. Three possible difference values fall near the frequency at 1.7352 cycle d^{-1}, but here also the match is not perfect. A possible explanation could be normal modes excited near the combination frequencies by resonant mode coupling (Dziembowski 1982). However, this was found not to be the case for the sum frequencies: Handler et al. (1996) found that the amplitudes of those peaks were larger in a subset of data with larger light modulation than in the one with smaller light modulations. If the peaks at sum frequencies were normal modes excited by the resonant mode coupling, then the amplitudes were expected to remain constant. In the present data the amplitudes of f_A and f_B do remain roughly constant from 1998 to 1999, although the overall amplitude of the δ Scuti variations appears to have increased. However, with a mean stellar density of XX Pyx, $\rho = 0.241\rho_\odot$, the Q values are too high (0.565 and 0.283 d for the two frequencies) for acoustic modes to be a likely explanation, as the Q values expected for δ Scuti p-modes are much lower.

The low-frequency variations could be connected with the rotation of the star, as was suggested for FG Vir (surface feature, Viskum et al. 1998). The rotation rate of XX Pyx is 1.1 ± 0.3 cycle d^{-1} (HAS), consistent within the uncertainty with f_A. The variations could be caused by spots, possibly in connection with differential rotation. At least one spot should remain visible on the surface most of the time, as seen from the Earth, otherwise part of the light curve would be flat, which does not seem to be the case. The surface features should have remained on the surface over a period of more than one year, which is very well possible (e.g. FK Com, Korhonen et al. 1999, who found the same group of spots to be present on the surface over 11 months, but drifting in phase by 0.2 because of the differential rotation). However, the high temperature of XX Pyx (over 8000 K) argues against a starspot model, unless the starspots are caused by magnetic effects, i.e. if XX Pyx is an oblique rotator. Photometric and spectroscopic data (e.g. Handler et al. 1997) do not suggest that XX Pyx is a chemically peculiar star, which makes starspots less likely to be the cause of the low-frequency variations.

5 CONCLUSION

We have detected two low-frequency signals in the photometric light curves of XX Pyx. The two frequencies, f_A at 0.8695 and f_B at 1.7352 cycle d^{-1}, are close to having a 2:1 ratio. We also report the detection of a significant radial velocity variation from a re-analysis of the spectra obtained by Handler et al. (1997), showing that XX Pyx is a member of a binary system. The companion must be a low-mass or compact object. We find it most likely that the photometric variations are caused by the binarity, but the possibility of the presence of g-modes is intriguing. Further spectroscopic investigation is needed to search for the companion of this relatively faint star, and to determine the spectroscopic binary period.

ACKNOWLEDGMENTS

TA and CS acknowledge financial support from the Belgian Fund for Scientific Research (FWO). This project was supported by the Flemish Ministry for Foreign Policy, European Affairs, Science and Technology. We thank Luis Balona for kindly determining the radial velocities of XX Pyx upon our request. We thank our referee, Dr W. Dziembowski, for his useful comments. This research has made use of the SIMBAD data base operated at CDS, Strasbourg, France, and the NASA Astrophysics Data System. This study was based on observations obtained at the European Southern Observatory at La Silla, Chile (applications ESO 60H–0110, 60D–0148 and 64L–0182) and at the South African Astronomical Observatory (SAAO).

REFERENCES

Arentoft T., Handler G., 2000, in Breger M., Montgomery M., eds, ASP Conf. Ser. Vol. 210, Delta Scuti and Related Stars. Astron. Soc. Pac., San Francisco, p. 396
Arentoft T., Sterken C., 2000, J. Astron. Data, 6, 4C
Bradstreet D. H., 1993, in Milone E. F., ed., Light Curve Modeling of Eclipsing Binary Stars. Springer-Verlag, p. 151
Breger M., 1994, in Sterken C., de Groot M., eds, NATO ASI Ser. C, Vol. 436, The Impact of Long–Term Monitoring on Variable Star Research: Astrophysics, Instrumentation, Data Handling, Archiving. Kluwer, Dordrecht, p. 393
Breger M. et al., 1993, A&A, 271, 482
Breger M. et al., 1998, A&A, 331, 271
Breger M. et al., 1999, A&A, 349, 225
De Mey K., Daems K., Sterken C., 1998, A&A, 336, 527
Dziembowski W., 1982, Acta Astron., 32, 147
Eggleton P., 1983, ApJ, 268, 368
Frandsen S. et al., 1996, A&A, 308, 132
Handler G., 1999, MNRAS, 309, L19
Handler G. et al., 1996, A&A, 307, 529
Handler G. et al., 1997, MNRAS, 286, 303
Handler G., Pamyatnykh A. A., Zima W., Sullivan D. J., Audard N., Nitta A., 1998, MNRAS, 295, 377
Handler G. et al., 2000a, MNRAS 318, 511, (HAS)
Handler G. et al., 2000b, J. Astron. Data, 6, 4A
Korhonen H., Berdyugina S. V., Hackman T., Duemmler R., Ilyin I. V., Tuominen I., 1999, A&A, 346, 101
Montgomery M. H., O'Donoghue D., 1999, Delta Scuti Star Newsletter, 13, 28
Pamyatnykh A. A., Dziembowski W. A., Handler G., Pikall H., 1998, A&A, 333, 141

Paparó M., Sterken C., Spoon H. W. W., Birch P. V., 1996, A&A, 315, 400
Sperl M., 1998, Master's Thesis, Univ. Vienna
Sterken C., 1997, A&A, 325, 563
Sterken C., 2000, in Breger M., Montgomery M., eds, ASP Conf. Ser. Vol. 210, Delta Scuti and Related Stars. Astron. Soc. Pac., San Francisco, p. 99
Viskum M., Kjeldsen H., Bedding T. R., Dall T. H., Baldry I. K., Brunt H., Frandsen S., 1998, A&A, 335, 549

This paper has been typeset from a TEX/LATEX file prepared by the author.

2.2.7 The δ Scuti star XX Pyx is an ellipsoidal variable

Original paper:

C. Aerts, **G. Handler,** T. Arentoft, B. Vandenbussche, R. Medupe, C. Sterken, 2002, MNRAS 333, L35

Mon. Not. R. Astron. Soc. **333,** L35–L39 (2002)

The δ Scuti star XX Pyx is an ellipsoidal variable

C. Aerts,[1★] G. Handler,[2] T. Arentoft,[3,4] B. Vandenbussche,[1] R. Medupe[2] and C. Sterken[4]†

[1]*Instituut voor Sterrenkunde, Katholieke Universiteit Leuven, Celestijnenlaan 200 B, B-3001 Leuven, Belgium*
[2]*South African Astronomical Observatory, PO Box 9, Observatory 7935, South Africa*
[3]*Koninklijke Sterrenwacht van België, Ringlaan 3, 1180 Brussels, Belgium*
[4]*Astronomy Group, Vrije Universiteit Brussel, Pleinlaan 2, 1050 Brussels, Belgium*

Accepted 2002 April 29. Received 2002 April 29; in original form 2002 April 17

ABSTRACT

We present spectroscopic and multicolour photometric evidence supporting the binary nature of the δ Scuti star XX Pyx (CD−24 7599). Applying a cross-correlation technique to the spectra, we find clear radial-velocity variations with a large amplitude. We derive the orbital parameters and confirm an orbital period of 1.15 d, as suggested previously on the basis of photometric variations. The amplitude of the slow variations present in our new multicolour data is wavelength independent, pointing also to a geometric effect as origin of the variability. They are thus fully consistent with the spectral variations and are interpreted as ellipsoidal variations. XX Pyx has a circular orbit of which the radial-velocity variations have a semi-amplitude of $17.8 \pm 0.4\,\mathrm{km\,s^{-1}}$.

The single-lined binary nature of the star, together with the mass function, lead us to conclude that the orbital inclination must be larger than 10°. The orbital solution is compatible with a synchronized M3V companion. The deformation of the primary due to tidal forces is very probably the reason for the failure of detailed seismic modelling efforts done recently.

Key words: binaries: spectroscopic – stars: individual: XX Pyx – stars: oscillations.

1 INTRODUCTION

Observations of δ Scuti stars gathered with networks of small telescopes around the globe have given a new and strong impetus to the study of their variability. Such multisite campaigns have indeed revealed a wealth of frequencies for some selected targets, the best-known being FG Vir (A5V) with 19 modes (Breger et al. 1998), 4 CVn (F3III-IV) with 18 modes (Breger et al. 1999) and XX Pyx (A4V) with 22 pulsational frequencies (Handler et al. 2000). With such a large number of detected modes, one can hope to recognize patterns in the periodograms to eliminate the difficult problem of mode identification for all the excited modes individually (Handler 1998). Indeed, by producing pulsation models for appropriate stellar parameters, and by confronting the theoretically excited frequencies with the observed ones, one can iteratively build the most appropriate model for the target star.

The most in-depth attempt for such a seismic analysis came from Pamyatnykh et al. (1998), who considered the frequencies of the 13 oscillation modes detected for XX Pyx by Handler et al. (1997). The goal of Pamyatnykh et al. (1998) was to construct a seismic model whose low-ℓ mode frequencies reproduce the observed ones. Unfortunately, this goal was not reached for several reasons. First, several distinct mode identifications and stellar models which lead to frequency fits of similar quality were found. Secondly, and more importantly, none of the fits could be regarded as acceptable according to the observational standard errors of the frequencies. This is very unsatisfactory, as it prevents an in-depth seismic analysis of the internal structure of the star.

Handler et al. (2000) were able to disentangle 22 independent and six combination frequencies in the light variability of XX Pyx from an analysis of a combination of multisite data gathered between 1992–1998. The independent frequencies range between 27.0107 and $38.0653\,\mathrm{c\,d^{-1}}$. The discovery of additional modes in XX Pyx did not resolve the difficulties in modelling the star, however. In the present paper we provide at least one explanation for the problem by showing that XX Pyx is an ellipsoidal variable, and hence is a deformed star.

Arentoft, Sterken & Handler (2001) shed new light on the nature of XX Pyx by suggesting the presence of a close companion. This hypothesis was based on two facts:

(i) the detection of two low frequencies, $f_B = 1.7352 \pm 0.0001\,\mathrm{c\,d^{-1}}$ and its probable subharmonic $f_A \approx f_B/2$, in the extensive photometric data set they gathered for the star,

(ii) a shift of some $40\,\mathrm{km\,s^{-1}}$ in the radial velocity of the star, derived from two spectra taken by Handler et al. (1997).

Arentoft et al. (2001) concluded that XX Pyx may have a low-mass

★E-mail: conny@ster.kuleuven.ac.be
†Research Director, Belgian Fund for Scientific Research (FWO).

companion and gave some preliminary constraints on its mass and the orbital inclination based on the velocity shift in the spectra published by Handler et al. (1997).

The goal of the present paper is to investigate the validity of the binary scenario for XX Pyx by means of a new spectroscopic and multicolour photometric study. The paper is organized as follows. The data are described in Section 2 and clearly point out the binary nature. The orbital parameters and photometric variations are derived in Section 3 and we end the paper with a short discussion in Section 4.

2 THE NEW DATA

2.1 Spectroscopic data

We have observed XX Pyx with the CORALIE spectrograph attached to the 1.2-m Swiss Euler telescope from La Silla in Chile from 2001 December 28 until 2002 January 10. CORALIE is a high-resolution echelle spectrograph with a resolution of 50 000. The total wavelength range covered by the 68 orders is 3900–6800 Å. The reduction of the spectra involved standard reduction techniques, including flat-fielding, blaze correction and wavelength calibration by means of Th-Ar spectra.

We have gathered 22 spectra with a total time-base of 2 weeks. Typically, two spectra per night were taken, one at the beginning and one at the end of the night, with the goal to cover as well as possible the probable orbital period of 1.15 d suggested by Arentoft et al. (2001). The exposure time for each spectrum was 45 min. This integration time was chosen as it is slightly longer than the periods of the three main modes of XX Pyx, so one hopes to have averaged the largest pulsational velocity in a fairly efficient way. At the same time, it results in a good temporal resolution of less than 3 per cent of the suggested period of 1.15 d. The total length of the run was chosen to resolve the beating between the possible 1.15-d period and the 1-d sampling caused by daytime gaps. The integration time resulted in a signal-to-noise ratio of about 25 for each spectrum.

2.2 Photometric data

These measurements mostly consist of differential CCD photometry through the Johnson–Cousins BVI_c filters, and are to be separated into four subsets. The first was acquired with the 1.0-m telescope at the Sutherland station of the South African Astronomical Observatory (SAAO), and the University of Cape Town CCD camera (O'Donoghue 1995) operated in frame-transfer mode. XX Pyx was observed in 11 clear nights between 2001 December 11–23 for about 0.8–2.0 h each, resulting in an average spacing of 76 s between consecutive data points in the different filters.

The second subset also came from the 1.0-m telescope at the South African Astronomical Observatory (SAAO), but a normal CCD was used, yielding a mean sampling interval of 5.7 min in each filter. Runs with lengths of 1.2–3.3 h in seven clear nights between 2001 December 25 and 2002 January 7 were acquired. Both the first and second subset are sufficient to resolve the individual ellipsoidal and multiperiodic pulsational variations of the star and their alias structures.

Thirdly, photometric data were acquired at the European Southern Observatory (ESO), La Silla, using the Danish 1.54-m telescope and the Danish Faint Object Spectrograph and Camera (DFOSC) detector. The data were obtained on the nights of 2002 January 10 and 12 as well as February 1 and 3. Instead of the I_c filter, a Gunn *i*-filter was used, which did not affect our results. A mean sampling rate of 2.6 min per data point in each filter was reached during the individual 1–3 h runs.

The last data set again originated from the 1.0-m telescope at SAAO with the standard CCD. Observations were carried out on the seven consecutive, mostly clear, nights of 2002 April 2–8; runs between 1.8 and 7.4 h duration with a mean sampling interval of 5.1 min in each filter could be acquired. The individual pulsations of XX Pyx are not resolved in this last data set, but an orbital phase coverage of 95 per cent was achieved. The total amount of useful photometric data from all four observing runs is 72 h.

We started data reduction with the corrections for bias and flatfield. No correction for dark counts was found to be necessary and mean flatfields were used for each data subset. Photometric measurements on the reduced frames were made with the programme MOMF (Kjeldsen & Frandsen 1992), which applies a combination of point spread function (PSF) and aperture photometry relative to a user-specified ensemble of comparison stars. No variability of any star other than the target in the different CCD fields was found, and the comparison star ensemble and photometric aperture resulting in the lowest scatter in the target star light-curves were chosen for each data subset.

The photometric zero-points for the subsets were determined by means of the brightest comparison star contained in all fields, but they were not quite consistent, probably due to the different wavelength responses of the individual detector/filter combinations. Therefore, some small additional zero-point shifts between the three subsets were applied and it was checked that they did not affect our results. Our measurements will be made publicly available in a forthcoming publication (Arentoft et al., in preparation).

3 ANALYSIS

3.1 Determination of the spectroscopic orbit

As the spectra are of low signal-to-noise ratios, and because individual spectral lines are difficult to treat, we have used a cross-correlation technique to derive the radial velocities of the star. We constructed a mask with the spectral lines expected for an A4V star with $T_{\rm eff} = 8300$ K and $\log g = 4.25$, which are the stellar parameters of XX Pyx derived from photometry (Handler et al. 1997). We have derived all the predicted spectral lines for such a star between 3900 and 6800 Å from the Vienna Atomic Line Database (VALD; Piskunov et al. 1995). We have subsequently used this line list to construct a mask, taking into account that the average line broadening amounts to some 50 km s^{-1} (Handler et al. 1997). In general, we excluded from the mask all lines for which Stark broadening is important. We used this procedure for the creation of a number of masks, taking into account a range of 1000 K for $T_{\rm eff}$.

The cross-correlation function $C(v)$ is then calculated according to the formulation by Baranne et al. (1996):

$$C(v) = \sum_l \sum_{x,o} p_{l,x,o} f_{x,o} \qquad (1)$$

for each velocity point v. In this expression, $f_{x,o}$ is the value of the 2-dimensional spectrum for order o at pixel position x and $p_{l,x,o}$ is the fraction of the lth line of the mask which falls into the pixel (x, o) at velocity v. Subsequently, the cross-correlation function is normalized and shifted to the heliocentric reference frame.

For each of the masks and for each spectrum, we determined the cross-correlation profile. The latter contains complex patterns which can be ascribed to the multiperiodic pulsation of the star. As an example, we show two cross-correlation profiles in Fig. 1, from which it is clear that the radial velocity is variable with a large amplitude. Such a large velocity change cannot be due to pulsation of an A star exhibiting a total light amplitude of typically 0.05 mag (see Section 4.2). It is also evident from Fig. 1 that the star exhibits line-profile variations induced by its pulsation, as the profiles are clearly asymmetric and show sub-features. This indicates that some modes probably have $\ell > 2$. As a result of the substructures we decided not to fit the correlation profile with a Gaussian (as is usually done) but to determine its centroid for all points with a value below 0.996. The integration limits for the calculation of the centroid are also marked on Fig. 1. This approach is similar to the calculation of the first moment of a line profile (see e.g. Aerts, De Pauw & Waelkens 1992). The uncertainty of the radial velocity was derived from the centroid values computed from the different masks and by taking into account different integration limits. This results in standard errors between 0.1 and 4.6 km s^{-1} for each individual radial velocity measurement and an average standard error of 1.1 km s^{-1}. We continued the analysis with the radial-velocity values derived from the mask for $T_{\mathrm{eff}} = 8300$ K and $\log g = 4.25$, which are best estimates for XX Pyx.

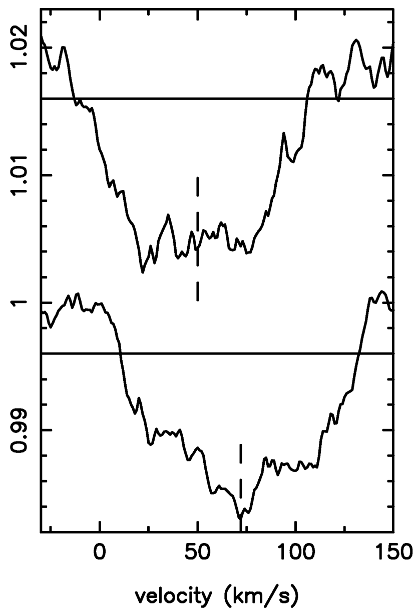

Figure 1. Two cross-correlation profiles derived from spectra taken on two different nights. The integration limits for the determination of the value of the centroid are indicated as full line. The centroid values of the lower and upper profiles are 71 and 50 km s^{-1}, respectively; they are indicated by the dashed lines.

A frequency analysis immediately leads to a frequency of 0.87 c d^{-1} dominating the radial velocities. This is precisely the subharmonic frequency f_A found by Arentoft et al. (2001) in the photometry of the star, as expected for an ellipsoidal variable. As our time-base is limited, we imposed $f_{\mathrm{orb}} = f_A$ as now adoptable from Arentoft et al. (2001).

We subsequently determined the orbital parameters of XX Pyx with the method of Lehmann-Filhés (see e.g. Green 1985), both by keeping the orbital frequency fixed to f_{orb} and by taking it as a free

Table 1. Orbital parameters of XX Pyx.

Parameter	Value
Period	1.1500 d (fixed)
eccentricity	0.0
Amplitude	17.8 ± 0.4 km s^{-1}
γ-velocity	59.2 ± 0.3 km s^{-1}
$a_1 \sin i$	0.404 ± 0.009 R$_\odot$
$f(M)$	0.00067 ± 0.00004 M$_\odot$

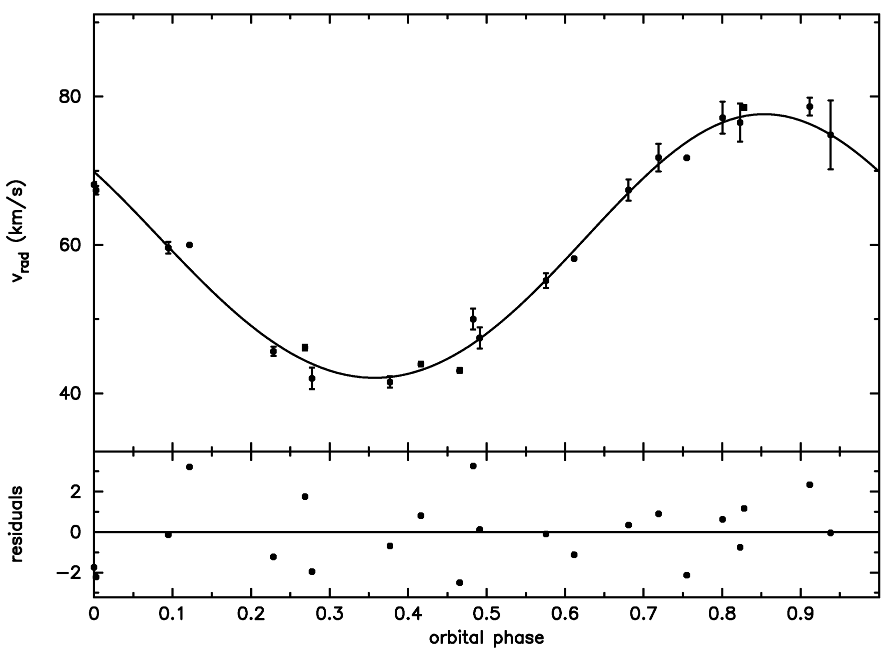

Figure 2. A phase diagram of the orbital velocity of XX Pyx (upper panel) and of the residuals after prewhitening with the fit constructed using the orbital parameters listed in Table 1 (lower panel).

parameter. This leads to the same overall result. The orbital elements are listed in Table 1 and the orbital solution is compared with the data in Fig. 2. The orbit is circular. The radial-velocity variations have an amplitude of $17.8 \pm 0.4\,\mathrm{km\,s^{-1}}$, which is somewhat smaller than – but not significantly different from – the $20 \pm 9\,\mathrm{km\,s^{-1}}$ estimated by Arentoft et al. (2001). The fit is very satisfactory, particularly if one takes into account the fact that the pulsational broadening is not completely cancelled out in a time span of 45 min.

From the mass function and the mass estimate $M_1 = 1.85 \pm 0.05\,\mathrm{M_\odot}$ (Pamyatnykh et al. 1998) for XX Pyx we have determined all possible combinations (i, M_2). For $i < 10°$ we would have found a double-lined binary, a solution already excluded by Handler et al. (1997). All other solutions lead to a low-mass companion and a separation of some $6\,\mathrm{R_\odot}$. We note that the orbital inclination cannot be large, as no eclipses are seen in the photometry.

3.2 Multicolour photometry

Before performing a frequency analysis of our data, we re-binned all measurements to the lowest sampling rate obtained at the four telescope/instrument combinations to avoid artifacts due to implicit weighting. We then applied the program PERIOD98 (Sperl 1998), which uses both Fourier and sinusoidal light-curve fitting algorithms. We calculated amplitude spectra of our data (Fig. 3) and concentrated on the pulsational variations first.

As XX Pyx is well known to exhibit short-term amplitude variations, we checked their possible occurrence in our four data subsets, and found (somewhat surprisingly) that none were present at a significant level. Consequently, we analysed all the measurements together. We detected seven of the known pulsation modes of XX Pyx in our data. We determined their frequencies, amplitudes and phases simultaneously, and prewhitened these signals.

We then searched for the low-frequency variations in the residuals; $2f_{\mathrm{orb}}$ was immediately obvious in the data of all the three bands. The orbital frequency itself was detectable in the V and I_c filter data, but not in B. We determined the amplitudes and phases of these variations as well, starting with the frequencies given by Arentoft et al. (2001) and fixing their relative values to exactly 2:1 within PERIOD98. We list the final results of the frequency analysis of our photometric data in Table 2, using the same identifications of the detected frequencies as in previous works.

We note that the relative amplitudes of the orbital modulation and its harmonic are different in our V data compared to those determined by Arentoft et al. (2001). In addition, the orbital light curves become more asymmetric towards longer wavelengths. It is beyond the scope of the present paper to discuss these findings in detail, so we refer the reader to Arentoft et al. (in preparation).

4 DISCUSSION

Handler et al. (1997) derived a rotational frequency of $1.1 \pm 0.3\,\mathrm{c\,d^{-1}}$ for XX Pyx, by arguing that the observed p-mode frequency groupings are only consistent with values in this range. As XX Pyx is moving in a short-period circular orbit and as the synchronization time-scale for the surface layers is two orders of magnitude shorter than the circularization time-scale (Zahn 1992), we propose here that the outer layers of the star are synchronized with the orbit: $f_{\mathrm{rot}} \approx f_{\mathrm{orb}}$, which is fully consistent with the asteroseismological value derived by Handler et al. (1997). Hence

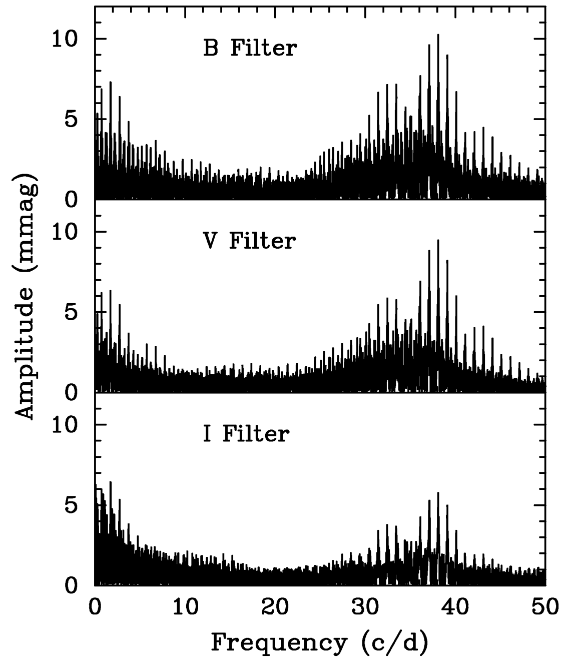

Figure 3. Amplitude spectra of our *BVI* photometric data of XX Pyx. The pulsational variations around $35\,\mathrm{c\,d^{-1}}$ decline in amplitude towards longer wavelengths, whereas the low-frequency variability has roughly the same amplitude in each filter.

Table 2. Photometric multifrequency solution for XX Pyx from our new measurements. Formal error estimates (lower limits to the real errors) of the amplitudes are ± 0.3 mmag in all filters.

ID	Frequency ($\mathrm{c\,d^{-1}}$)	B Ampl. (mmag)	V Ampl. (mmag)	I Ampl. (mmag)
f_1	38.110	10.1	9.2	6.2
f_2	36.013	6.7	5.4	2.6
f_3	33.438	7.7	6.2	3.3
f_4	31.401	3.7	2.9	2.2
f_7	34.672	1.8	1.7	1.1
f_{12}	28.700	1.6	1.8	1.1
f_{14}	31.902	1.7	1.4	0.8
$f_A = f_{\mathrm{orb}}$	0.8687	<1.5	2.6	5.7
$f_B = 2f_{\mathrm{orb}}$	1.7374	6.2	6.1	5.6

the assumption $i_{\mathrm{orb}} \approx i_{\mathrm{rot}}$ seems justified. Moreover, i_{orb} cannot reach high values, as no eclipses are seen in the light curve of XX Pyx.

From the radius estimate of $1.95 \pm 0.05\,\mathrm{R_\odot}$ we hence find an equatorial rotation velocity of $86\,\mathrm{km\,s^{-1}}$. An estimate of $v \sin i$ of $52 \pm 2\,\mathrm{km\,s^{-1}}$ was already provided by Handler et al. (1997, unaware of the orbital motion) on the basis of the addition of several lines in some high-resolution spectra taken during two nights. We estimated $v \sin i$ from our 22 correlation profiles by determining their full width at half maximum (FWHM). The average broadening we find in this way is $42 \pm 4\,\mathrm{km\,s^{-1}}$. However, the FWHM leads to only an upper limit of $v \sin i$ as the profiles are also broadened intrinsically and by the pulsation of the star. From the bottom panel of Fig. 2 we estimate the pulsational broadening to be about $2-3\,\mathrm{km\,s^{-1}}$, which is also the range we find from the photometric amplitude. The intrinsic broadening for an A4V star is typically also a few $\mathrm{km\,s^{-1}}$. Taking this into account leads to

$i \simeq 25° - 30°$ and subsequently $M_2 \approx 0.3\,M_\odot$, which corresponds to an M3V star. Note that this result is not sensitive to moderate deviations from $i_{orb} \approx i_{rot}$.

It is clear that the ellipsoidal variations found for XX Pyx point out that the star deviates significantly from spherical symmetry. This deformation was not taken into account in the modelling efforts done by Pamyatnykh et al. (1998). Both the tides and the rotation of the star can cause departure from spherical symmetry. The tidal deformation of a star is determined by the tide-generating potential, which is proportional to the small dimensionless parameter $\varepsilon_T = (R_1/a)^3(M_2/M_1)$ (see e.g. Willems & Aerts 2002). For XX Pyx we find $\varepsilon_T \simeq 6 \times 10^{-3}$. On the other hand, the effect of rotational deformation on the pulsations due to the centrifugal forces is dependent on the square of the ratio of the rotation and pulsation frequencies, which equals 5×10^{-4} for the main mode of XX Pyx. Hence, the effect of the deformation due to the tide-generating potential is clearly more important for the pulsational behaviour than the one due to rotation in XX Pyx. This tidal deformation may well cause the discrepancy between the frequencies of the theoretical models calculated by Pamyatnykh et al. (1998) and the observed frequencies.

Assessment studies of the power of seismic modelling with the goal to derive the internal structure parameters of stars are, although still scarce, very important. As far as main-sequence stars with κ-driven modes are concerned, such studies have at present mainly concentrated on a few selected δ Scuti stars, as the number of detected frequencies in these objects is by far superior to any other type of pulsating star near the main sequence. For a recent modelling effort with regards to FG Vir, for example, we refer to Templeton, Basu & Demarque (2001), who stress that unambiguous mode identification of only a few of the excited modes allows one to choose among the competing seismic models. Our study clearly points out that XX Pyx is not the optimum target to evaluate the method of detailed seismic modelling and that spectral validation of photometric results is extremely important. This should be taken into account for the target selection of the future asteroseismic space missions *MOST*, *MONS* and *COROT*.

ACKNOWLEDGMENTS

This paper is based on observations obtained with the 1.2-m Swiss Euler and 1.5-m Danish telescopes, situated at La Silla, Chile and with the 1.0-m telescope at SAAO Sutherland, South Africa. The authors thank the staff of the Geneva observatory for the allocated time on the 1.2-m Euler telescope and for the use of the reduction software package for the CORALIE spectra. This research has made use of the Vienna Atomic Line Database provided by the University of Vienna. GH thanks the technical support staff at SAAO for unbureaucratically attaching the CCD photometer to a telescope otherwise vacant. TA acknowledges financial support from the Belgian State, Office of the Prime Minister – Federal Office for Scientific, Technical and Cultural Affairs, under contract number MO/33/007. CS acknowledges financial support from the Belgian Fund for Scientific Research (FWO). This project was supported by the Flemish Ministry for Foreign Policy, European Affairs, Science and Technology, under contracts BIL 98/11/52 and BIL 99/2, and by the National Research Foundation of South Africa.

REFERENCES

Aerts C., De Pauw M., Waelkens C., 1992, A&A, 266, 294
Arentoft T., Sterken C., Handler G., 2001, MNRAS, 326, 192
Baranne A. et al., 1996, A&AS, 119, 373
Breger M. et al., 1998, A&A, 331, 271
Breger M. et al., 1999, A&A, 349, 225
Green R. M., 1985, Spherical Astronomy. Cambridge Univ. Press, Cambridge
Handler G., 1998, Baltic Astron., 7, 227
Handler G. et al., 1997, MNRAS, 286, 303
Handler G. et al., 2000, MNRAS, 318, 511
Kjeldsen H., Frandsen S., 1992, PASP, 104, 413
O'Donoghue D., 1995, Baltic Astron., 4, 519
Pamyatnykh A. A., Dziembowski W. A., Handler G., Pikall H., 1998, A&A, 333, 141
Piskunov N. E., Kupka F., Ryabchikova T. A. et al., 1995, A&AS, 112, 525
Sperl M., 1998, MSc thesis, Univ. Vienna
Templeton M., Basu S., Demarque P., 2001, ApJ, 563, 999
Willems B., Aerts C., 2002, A&A, 384, 441
Zahn J.-P., 1992, in Duquennoy A., Mayor M., eds, Binaries as Tracers of Stellar Formation. Cambridge Univ. Press, Cambridge, p. 253

This paper has been typeset from a TEX/LATEX file prepared by the author.

2.3 HD 106384 = FG Virginis

2.3.1 The δ Scuti star FG Virginis: I. Multiple pulsation frequencies determined with a combined DSN/WET campaign

Original paper:

M. Breger, **G. Handler,** R. E. Nather, D. E. Winget, S. J. Kleinman, D. J. Sullivan, Z.-P. Li, J.-E. Solheim, S.-Y. Jiang, Z.-L. Li, M. A. Wood, T. K. Watson, W. A. Dziembowski, E. Serkowitsch, H. Mendelson, J. C. Clemens, J. Krzesinski, G. Pajdosz, 1995, A&A 297, 473

Astron. Astrophys. 297, 473–482 (1995)

ASTRONOMY
AND
ASTROPHYSICS

The δ Scuti star FG Virginis

I. Multiple pulsation frequencies determined with a combined DSN/WET campaign

M. Breger[1], G. Handler[1], R. E. Nather[2], D. E. Winget[2], S. J. Kleinman[2], D. J. Sullivan[3], Li Zhi-ping[4], J. E. Solheim[5], Jiang Shi-yang[4], Liu Zong-li[4], M. A. Wood[6], T. K. Watson[2], W. A. Dziembowski[7], E. Serkowitsch[1], H. Mendelson[8], J. C. Clemens[9], J. Krzesinski[10], and G. Pajdosz[10]

[1] Astronomisches Institut der Universität Wien, Türkenschanzstr. 17, A-1180 Wien, Austria
INTERNET: breger@astro.ast.univie.ac.at
[2] Astronomy Department, University of Texas at Austin, Austin, TX 78712, USA
[3] Physics Department, Victoria University of Wellington, P. O. Box 600 Wellington, New Zealand
[4] Beijing Observatory, Academy of Sciences, Beijing, China
[5] Institute of Mathematical and Physical Sciences, University of Tromso, N-9037 Tromso, Norway
[6] Dept. of Physics and Space Sciences, Florida Institute of Technology, 150 W. University Blvd., Melbourne, FL 32901-6988, USA
[7] Copernicus Astronomical Center, Bartycka 18, PL-00-716 Warsaw, Poland
[8] Wise Observatory, Sackler Faculty of Exact Sciences, Tel Aviv University, Tel Aviv 69978, Israel
[9] Dept. of Physics and Astronomy, Iowa State University, Ames, IA 50211, USA
[10] Mt. Suhora Observatory, Cracow Pedagogical University, PL-30-083 Cracow, Poland

Received 14 September 1994 / Accepted 16 October 1994

Abstract. A coordinated photometric campaign of FG Vir at nine observatories covering 170 hours was undertaken by DSN (Delta Scuti Network) and WET (Whole Earth Telescope). Two different observing techniques were adopted for the two telescope networks in order to optimize different frequency ranges.

Ten pulsation frequencies between 9.19 and 34.12 c/d (112 and 395 μHz) were detected with amplitudes ranging from 0.8 to 22 mmag. Pulsational instability is observed only in specific frequency regions. Additional frequencies of pulsation within these regions probably exist, but do not reach the significance criterion of amplitude signal/noise adopted by us. Comparisons with previously obtained data show that the amplitudes of the main frequencies are stable over a year or longer.

A preliminary identification of the ten dominant frequencies is proposed in a stellar model with $1.8M_{\odot}$ in advanced main-sequence phase of evolution. The frequencies correspond to low order p and g modes with $\ell \leq 2$ and radial order 1 to 6. According to the linear nonadiabatic calculations, the identified modes are driven by the opacity mechanism along with many other modes. For asteroseismology of δ Scuti stars, FG Vir is an extremely important candidate, especially because of the probable presence of g modes.

Key words: δ Scu – stars: oscillations – stars: individual: HD 106384=FG Vir – techniques: photometric

Send offprint requests to: M. Breger

1. Introduction

The δ Scuti stars are pulsating variables situated inside the classical Instability Strip on and above the main sequence. A number of extensive observing campaigns covering individual δ Scuti stars have shown that the majority pulsates with a large number of simultaneously excited modes. While the variables with small rotational velocities tend to be radial pulsators with large amplitudes, the vast majority of the δ Scuti stars pulsate nonradially with a multitude of small-amplitude p modes. Photometrically, low-degree ($\ell \leq 3$) and low-order (n = 0 to 4) modes are commonly seen. A good example is the star θ^2 Tau (Breger et al. 1989). On the other hand, studies of line-profile variations favor the detection of high-degree sectorial modes with $\ell = |m|$. For κ^2 Bootis, the available spectroscopic data have been matched by a low-degree mode (ℓ = 0 to 2) and a high-degree $\ell = |m| \sim 12$ mode (Kennelly et al. 1991).

The observed short-period limit of the δ Scuti stars is consistent with the low-order p mode identification. For the star V624 Tau (Breger 1972; Seeds & Stephens 1977) a period around 34 minutes has been found. Even this period is much longer than those found for the roAp stars (Kurtz 1990), for which periods between about 6 and 15 minutes are detected. As a group, the roAp stars have similar temperatures and luminosities as the δ Scuti stars. Because of the different range of periods, for each of the two groups of variable stars two different observing techniques (viz. the three-star and high-speed techniques, see below), have been adopted, each designed for maximum precision in the respective period domain. It is not surprising that outside these domains the precision of each technique is lower, so that small-amplitude pulsations with unfavorable frequencies could have been missed in previous investigations. It is, therefore, important to examine the question whether δ Scuti stars have photometrically detectable high-order pulsation modes with periods shorter than 30 minutes. A promising approach appears to be to concentrate on a single δ Scuti star for the presence of both long and short periods of pulsation by multisite campaigns using both techniques.

With the three-star technique adopted by the Delta Scuti Network, the required high photometric accuracy is achieved by alternating measurements of the variable star with those of two carefully chosen comparison stars. The same photometric channel is used for all three measurements. The procedure can produce the required long-term stability of 2 mmag or better (also within different observatories), but yields a variable-star measurement only every five minutes. The technique is working well for periods between 30 minutes and several days and has been described by Breger (1993).

The high-speed measurements adopted by WET (Whole Earth Telescope) are obtained with two-channel and three-channel photometers. Measurements of the intensities of the target and a nearby comparison star are made simultaneously, and in the case of three-channel photometers, the sky brightness is also measured continuously. The technique works well for periods under about 30 minutes. At longer time-scales, instrumental drifts (and residual transparency variations) rapidly dominate. The operation of WET has been described by Nather et al. (1990).

The two multisite networks and their techniques complement each other in allowing the investigation of periods between a few minutes up to several days. The δ Scuti star FG Vir was selected for the present study for two reasons: the presence of a large number of pulsation modes with photometrically visible amplitudes is suspected, and the position of the star in the Herzsprung-Russell Diagram is similar to those of the the known roAp pulsators (Kurtz & Martinez 1993).

The variability of FG Vir = HD 106384 was discovered by Eggen (1971), who deduced a period of 0.07 d and a semi-amplitude of 0.025 mag from one night of observation. In 1982, Lopez de Coca et al. (1984) observed the star for three nights through specially chosen narrowband filters, while one night of V data was collected in 1986 (Gonzalez-Bedolla & Rodriguez 1990). More extensive photometric data covering 26 nights were obtained by Dawson (1990) during 1985 and 1986. These data, however, are of somewhat lower photometric precision. They show a dominant variation with a period of about 0.08 d and will be the subject of a later paper in this series. Colomba et al. (1991) reported a presently unpublished observational program of FG Vir. During 1992, Mantegazza et al. (1994, hereafter referred to as MPB) measured FG Vir photometrically for 8 nights and spectroscopically for one night. MPB were confident about the correct identification of six frequencies, while a seventh mode of pulsation was also suggested.

The present paper reports a multisite campaign of FG Vir using both the three-star and high-speed techniques and the pulsational properties of the star at the frequencies typical for a δ Scuti star. An investigation at higher frequencies will be reported in Paper II.

2. New photoelectric measurements

In order to eliminate the serious aliasing caused by regular observing gaps, a multisite campaign was organized utilizing the WET (Whole Earth Telescope) Network for high-speed measurements and the Delta Scuti Network for low frequencies. During 1993 March and April, 170.4 h of usable data were obtained at nine different observatories. The V filter was used. On six nights, additional measurements with the B filter were obtained in order to estimate the phase shifts and amplitude ratios between the different wavelength regions for the primary pulsation mode. These nights are indicated with "BV" under the "Technique" column of Table 1, which presents a journal of all observations. Since two different techniques were used, we will discuss the acquisition and reductions of the two data groups separately.

2.1. Measurements made with the three-star technique

During 17 nights between 1993 March 12 through April 5, photoelectric measurements of FG Vir were obtained at two observatories with the three-star technique.

For the measurements at McDonald Observatory the following two comparison stars were used: HD 106952 (F8V) and HD 105912 (F5V). No variability of the comparison stars could be detected and the two comparison stars indicated a precision of between $\pm$ 3 and 4 mmag per single measurement. This can also be taken as an estimate of the accuracy of the FG Vir measurements. No serious problems were experienced during either the observations or data reductions. The resulting measurements of the variability of FG Vir is denoted in this paper as data set A.

During four nights of observations at McDonald Observatory, the standard three-star technique was modified in order to examine the accuracy of a hybrid technique in which the telescope was moved to the two comparison stars only once every hour. In principle, this hybrid technique could combine the advantage of the photometric stability of the three-star technique with the high duty cycle of the high-speed technique. The resulting measurements were indeed of very high quality and the comparison of the different techniques will be discussed elsewhere. We only note here that the application of the hybrid technique requires very high atmospheric and instrumental stability and cannot be recommended for general use. The 30.1 hours of data (data set B) obtained with the hybrid technique can be used for both high and low-frequency analyses.

Additional data (data set C) with the three-star technique were also obtained at the Xing-Long observatory located in China. These data are important since the longitude of these observatories complements the longitude of the major other observing site, McDonald Observatory. These data contain sev-

Table 1. Journal of the observations of FG Vir

Observatory	Observer(s)	Date (UT)	Length (hrs)	Technique	Data set
Xing Long 0.6m	Jiang shi-yang	12 Mar 93	4.2	Three star	C
Xing Long 0.6m	Jiang shi-yang	14 Mar 93	4.9	Three star	C
McDonald 2.1m	T.K. Watson & R.E. Nather	16 Mar 93	3.9	High speed	D
Siding Spring 0.6m	S.J. Kleinman	16 Mar 93	1.8	High speed	D
SAAO 0.75m	J.E. Solheim	16 Mar 93	3.9	High speed	D
McDonald 0.8m	E. Serkowitsch & G. Handler	17 Mar 93	7.5	Three star, BV	A
McDonald 2.1m	T.K. Watson & R.E. Nather	17 Mar 93	6.8	High speed	D
Siding Spring 0.6m	S.J. Kleinman	17 Mar 93	3.2	High speed	D
Xing Long 0.6m	Liu zong-li	17 Mar 93	3.7	Three star	C
SAAO 0.75m	J.E. Solheim	17 Mar 93	6.8	High speed	D
Siding Spring 0.6m	S.J. Kleinman	18 Mar 93	9.8	High speed	D
Xing Long 0.6m	Liu zong-li	18 Mar 93	4.1	Three star	C
Siding Spring 0.6m	S.J. Kleinman	19 Mar 93	2.2	High speed	D
Mauna Kea 0.6m	M.A. Wood	20 Mar 93	2.9	High speed	D
Mt. John 1.0m	D.J. Sullivan	22 Mar 93	6.9	High speed	D
Wise 1.0m	H. Mendelson	25 Mar 93	3.7	High speed	D
McDonald 0.9m	J.C. Clemens	26 Mar 93	3.6	High speed	D
Mauna Kea 0.6m	M.A. Wood	26 Mar 93	4.1	High speed	D
McDonald 0.8m	G. Handler	27 Mar 93	6.1	Three star, BV	A
Xing Long 0.6m	Li zhi-ping	27 Mar 93	5.1	Three star	C
Xing Long 0.6m	Li zhi-ping	28 Mar 93	5.0	Three star	C
McDonald 0.8m	G. Handler	29 Mar 93	4.2	Three star, BV	A
McDonald 0.8m	G. Handler	30 Mar 93	6.6	Three star, BV	A
McDonald 0.8m	G. Handler	31 Mar 93	7.5	Hybrid	B
Xing Long 0.6m	Li zhi-ping	31 Mar 93	3.7	Three star	C
Mt. Suhora 0.6m	J. Krzesinskski & G. Pajdosz	1 Apr 93	1.2	High speed	D
McDonald 0.8m	G. Handler	1 Apr 93	7.8	Hybrid	B
Mt. John 0.6m	D.J. Sullivan	1 Apr 93	7.0	High speed	D
Mt. Suhora 0.6m	J. Krzesinskski & G. Pajdosz	2 Apr 93	4.0	High speed	D
McDonald 0.8m	G. Handler	2 Apr 93	7.2	Hybrid	B
McDonald 0.8m	G. Handler	3 Apr 93	7.6	Hybrid	B
McDonald 0.8m	G. Handler	4 Apr 93	6.0	Three star, BV	A
McDonald 0.8m	G. Handler	5 Apr 93	7.4	Three star, BV	A

eral individual data points which deviate by large amounts from both their neighboring data points as well as the overall solution. Since the problem is present in this data set only, it should be interpreted as observational errors. Consequently, we have applied a conservative 3.5 σ criterion and eliminated those data points which deviated from the overall solution by more than 3.5 standard deviations.

2.2. *Measurements made with the high-speed technique*

In order to adapt the WET data for searching at low frequencies, the standard procedure to reduce WET photometry needed to be extended. For data obtained with multichannel photometers, sky subtraction was performed on a point-by-point basis after an adjustment of the sensitivity ratios of the different photometer channels. For two-channel photometers the background measurements were interpolated. After the background corrections were applied, the data were edited and incorrect data points eliminated. With the high-speed technique such editing is necessary, since the measurements are made continuously and include even those times when the telescope is moving away from the star.

Since FG Vir varies with a relatively high amplitude and the possibility of tube sensitivity drift could not always be ruled out, extinction corrections are not straightforward. A synthetic light curve predicted from the three-star data was subtracted from the variable star data substantially decreasing the variance of the data. Bouguer diagrams of these residuals and the comparison star data were examined for variable extinction or tube drift, and an appropriate extinction coefficient was determined for each night. In cases where trends in the residuals due to atmospheric or equipment problems remained, an additional polynomial fit was subtracted from the data. The two data sets from Poland showed substantial transparency variations and scintillation noise (caused by the high air masses at which the measurements were obtained), so that the polynomial fit was replaced by a spline fit determined from the channel 2 data. We

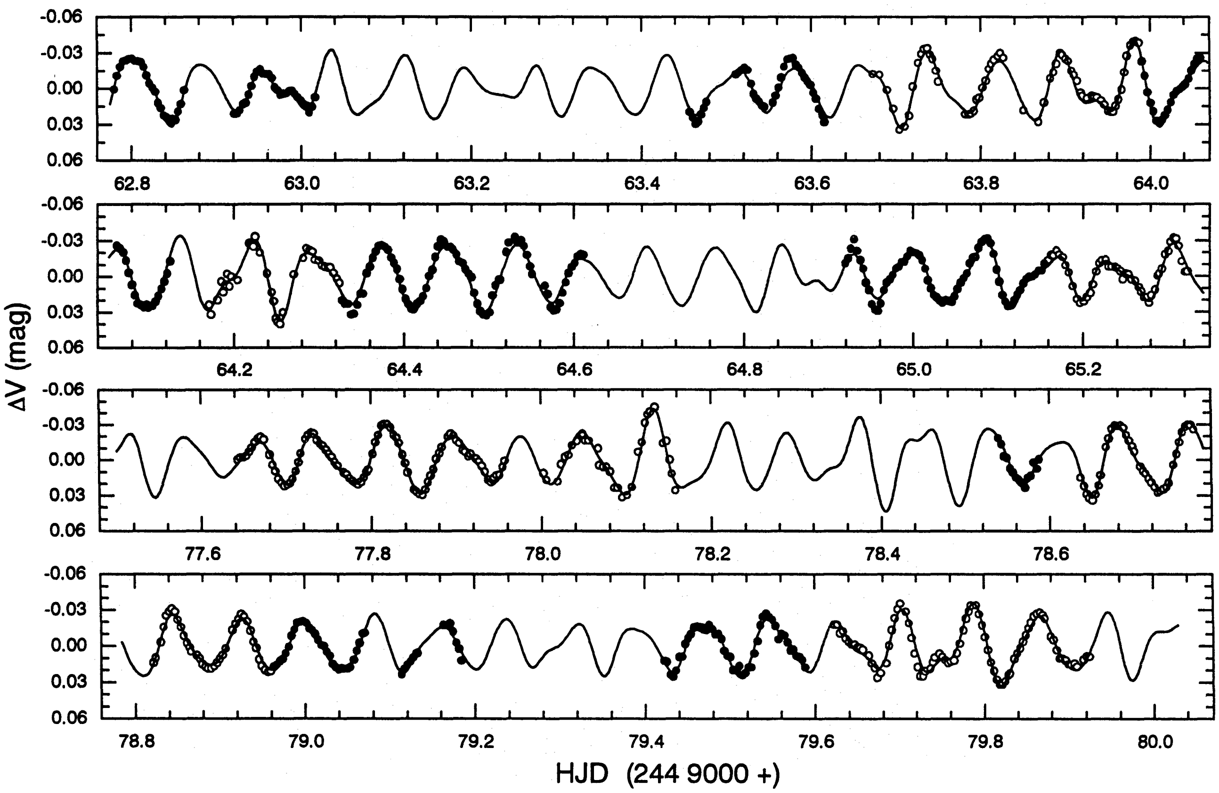

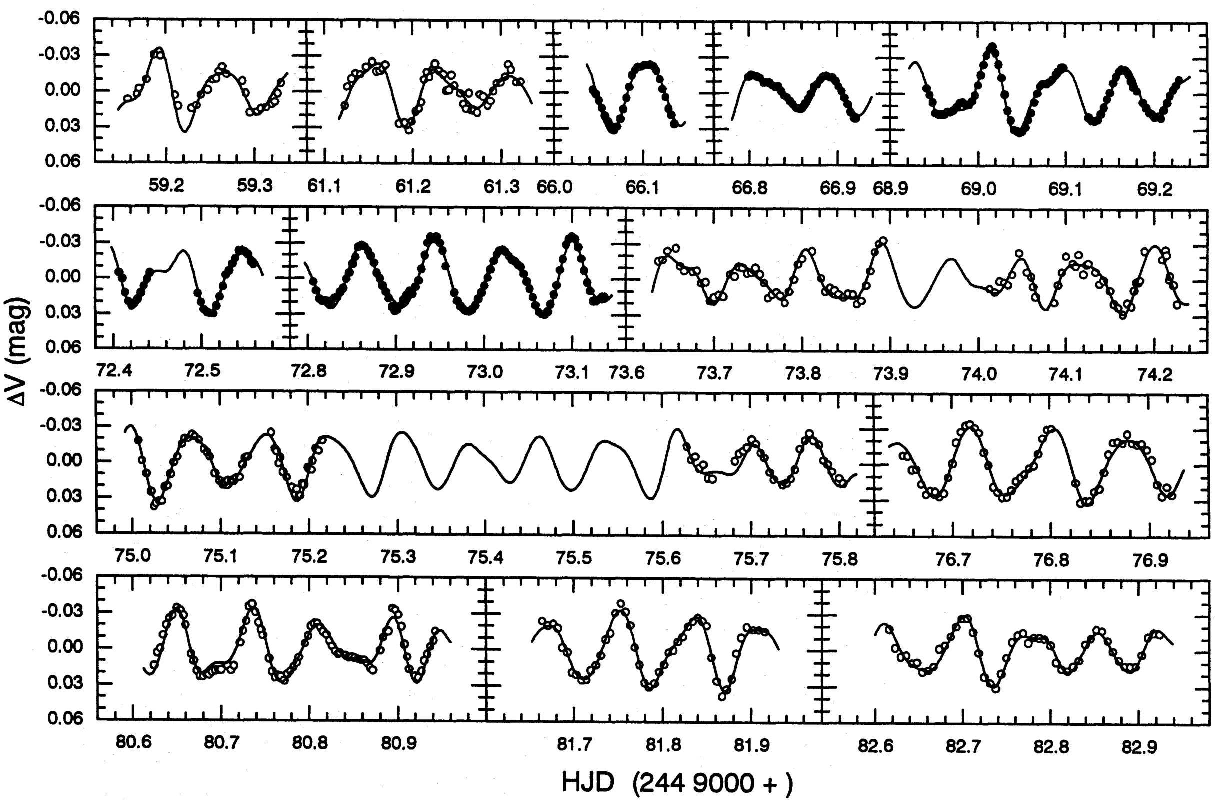

Fig. 1a and b. Multisite photometry of FG Vir obtained during the 1993 campaign. ΔV is defined to be the magnitude difference (variable - comparison stars) normalized to zero. The open circles refer to measurements obtained with the three-star technique, while the filled circles are averages of continuous (high-speed) measurements. The fit of the ten-frequency solution derived in this paper is shown as a solid curve. Note the excellent agreement between the measurements and the fit

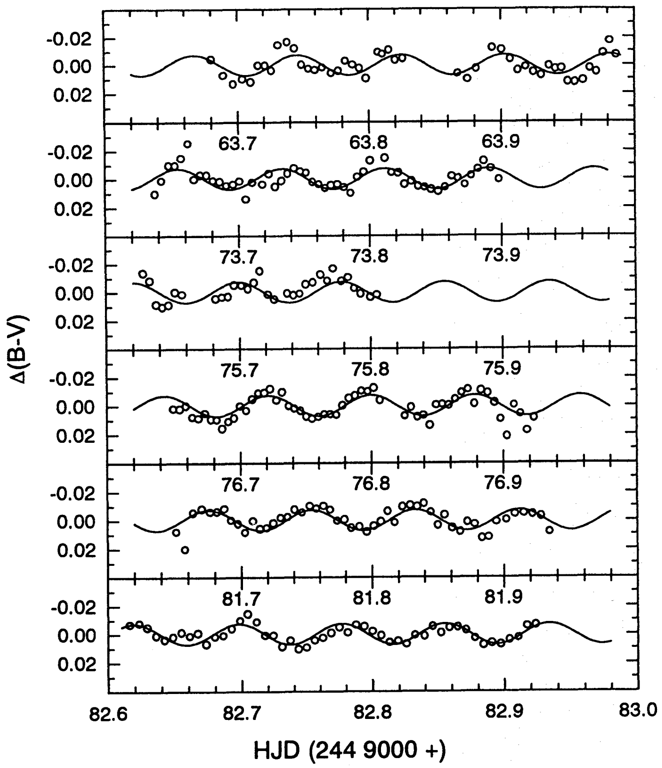

Fig. 2. $B - V$ variations of FG Vir obtained during six nights. The solid curve represents the fit obtained with the dominant frequency of 12.72 c/d

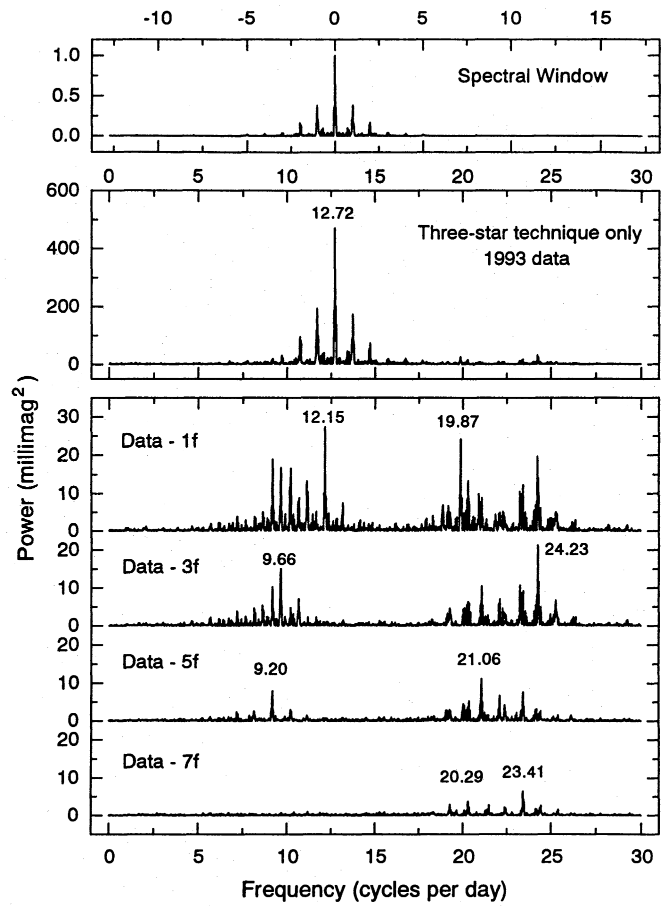

Fig. 3. Power spectrum of FG Vir in the 0 to 30 c/d range using the new multisite measurements obtained with the three-star technique (data sets ABC). This technique alternates measurements of FG Vir with those of two comparison stars. The spectra are shown before and after applying multiple frequency solutions

found that the Polish data reduced in this manner could be used for low-frequency analyses (but not for high frequencies).

The final data were converted to Heliocentric Julian date (HJD) and summed into 5 minute bins for the low-frequency analysis.

The observed variability of FG Vir obtained during the 1993 campaign with both the three-star (open circles) and high-speed techniques (filled circles) is shown in Fig. 1 together with the predicted ten-frequency fit derived below. The color variations are presented in Fig. 2.

3. Pulsation frequencies up to 30 c/d

The pulsation frequency analyses were performed with a package of computer programs with single-frequency and multiple-frequency techniques (program PERIOD, Breger 1990a), which utilize Fourier as well as multiple-least-squares algorithms. The latter technique fits a number of simultaneous sinusoidal variations in the magnitude domain and does not rely on prewhitening. For the purposes of presentation, however, prewhitening is required if the low-amplitude modes are to be seen. Therefore, the various power spectra are shown as a series of panels, each with one or two additional frequencies removed relative to the panel above. The analyses were performed using the traditional units of magnitude. We note that for the small amplitudes present in FG Vir any differences between using intensity and magnitude variations are negligible.

One of the most important questions in the examination of multiperiodicity concerns the decision of which of the detected peaks in the power spectrum can be regarded as variability intrinsic to the star. Due to the presence of nonrandom errors in photometric observations and because of observing gaps the predictions of standard statistical false-alarm tests give answers which are considered by us to be overly optimistic. In a previous paper (Breger et al. 1993) we have argued that a ratio of amplitude signal/noise = 4.0 provides a useful criterion for judging the reality of a peak. Subsequent comparisons have confirmed that this restrictive limit of 4.0 cannot be lowered significantly for typical photometric data. This means that peaks below signal/noise values of 3.5 should be regarded with suspicion, although some of them may be intrinsic to the star.

In the present study the noise was calculated by averaging the amplitudes (oversampled by a factor of 20) over 10 c/d regions centered around the frequency under consideration. The rather large range of 10 c/d was chosen in order to deemphasize the effects of a single additional pulsation mode on the computed noise level. The curves shown in the diagrams of the

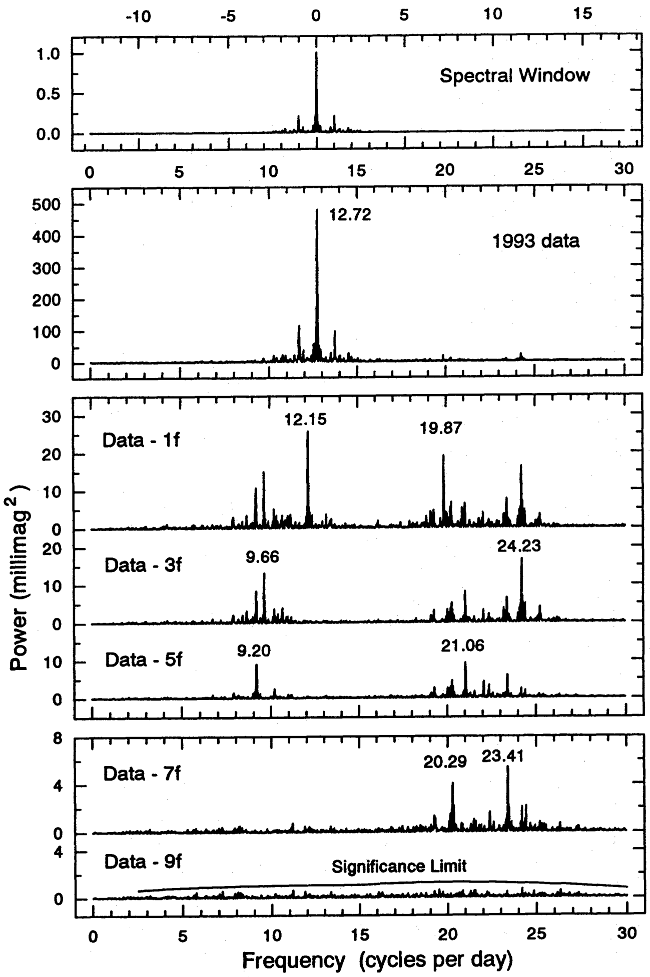

Fig. 4. Power spectrum of FG Vir in the 0 to 30 c/d range using all the new multisite measurements (data sets ABCD). The spectra are shown before and after applying multiple frequency solutions

power spectra entitled "significance limits" are smoothed fits of the power values corresponding to amplitude signal/noise ratios of 4.

As a first step we should restrict the analysis to the data obtained with the three-star technique because of the relative accuracy in the low-frequency domain given by the regular observing of comparison stars. This corresponds to data sets ABC. Of course, the spectral window of the partial data is not as clean as that for the three-star and high-speed data together. Nevertheless, the uncertainties caused by 1 c/d aliasing are quite small for the main frequencies of pulsation. This is demonstrated at the top of Fig. 3, which shows the spectral window pattern based on the times of available measurements. The next panels show the power spectra of the data before and after subtraction of one, three, five and seven frequencies. We note that the star pulsates with a dominant frequency at 12.72 c/d (147 μHz) and at least eight additional frequencies. Seven frequencies can already be regarded as certain.

However, an additional important result of the frequency analyses of the data obtained with the three-star technique is the absence of variability below 9 c/d. This means that the high-speed data, for which measurements of comparison stars had not been obtained with the same photometer channel, can now be included. Addition of the high-speed data lowers the noise level in the power spectrum and also improves the spectral window.

Figure 4 shows the power spectra of all the 1993 campaign data before and after subtracting the best one, three, five, seven and nine-frequency solutions. These nine frequencies can be regarded as well-established and should be free of 1 c/d aliasing. The best multi-frequency solution obtained with PERIOD is listed in Table 2. We have also repeated the analysis with the inclusion of the 53 hours of MPB data obtained during 1992 (called data set E). The resulting power spectrum looks essentially identical to the power spectrum of the 1993 data alone shown in Fig. 4 and is consequently not presented as a separate diagram. Nevertheless, the existence of a data set obtained a year earlier significantly improved the frequency resolution. The last two decimal places listed in Table 2 were determined from comparing the 1992 and 1993 data sets. In spite of the improved resolution, the large gap between the observations causes annual aliasing (Δf = 1/365 c/d = 0.0027 c/d = 0.032 μHz). While we have selected the values which gave the lowest residuals between the measurements and the prediction, the values of the frequencies with smaller amplitudes may be affected by annual aliasing.

4. Pulsation frequencies larger than 30 c/d

In this frequency range the long-term stability of the photometric equipment and the atmospheric conditions over several hours become less important, so that the regular observations of two comparison stars with the same photometer channel are not essential. Consequently, the high duty cycle of the high-speed observations with their essentially continuous coverage of FG Vir, makes these observations very important. On the other hand, those three-star measurements with relatively lower accuracy (data set C) can be omitted, since they do not improve the signal/noise ratio in the high frequency range. The analyses of our new data were then repeated while including data set E.

Figure 5 shows the power spectrum in the 30 to 100 c/d range. In order to avoid power leakage from the lower frequencies found in the previous section, we have prewhitened the best low-frequency solution for each data set. The power spectrum shows significant power only in the 30 - 40 c/d region. Of these peaks, (only) the frequency at 34.12 c/d is significant according our adopted signal/noise criteria. The amplitude of f_{10} derived from the ABD data alone is 0.80 mmag, in agreement with the 0.84 mmag derived from the larger ABDE set. The associated amplitude signal/noise ratio of 4.7 makes the identification as a frequency intrinsic to the star quite easy. In order to exclude the possibility that the peak is caused by systematic errors in a particular data set, solutions with locked phase were made for each individual data set A to E. The restriction of fixed phase reduced the number of free parameters for these solutions to only one, viz. the amplitude. We find that the frequency is dominant in four of the five data sets (A, B, D and E), and absent in the

Table 2. Multiple-frequency V-filter solution for FG Vir

	Frequency c/d	μHz	Q value days	Amplitude (1993)[1] mmag	S/N	Epoch (HJD) 244 9000+	Amplitude[2] mmag	S/N
f_1,	12.7162	147.2	0.027	22.4	85.6	72.2369	22.0	91.6
f_2,	19.8679	230.0	0.017	4.4	15.2	72.2882	4.4	16.4
f_3,	12.1542	140.7	0.028	4.4	16.9	72.2808	4.1	17.0
f_4,	24.2312	280.5	0.014	4.0	14.2	72.2752	4.2	15.4
f_5,	9.6562	111.8	0.036	3.7	14.4	72.2301	3.8	15.6
f_6,	9.1962	106.4	0.037	3.0	11.6	72.2604	2.8	11.4
f_7,	21.0576	243.7	0.016	3.0	10.2	72.2980	2.7	9.7
f_8,	23.4063	270.9	0.015	2.6	9.0	72.2700	2.4	8.5
f_9,	20.2878	234.8	0.017	2.3	7.9	72.2617	2.0	7.4
f_{10},	34.1159	394.9	0.010	(0.6)	(3.2)	72.3036	0.8	4.7
Residuals				$\pm$ 3.7			$\pm$ 3.8	

[1] Data sets ABCD
[2] Data sets ABDE (see text)

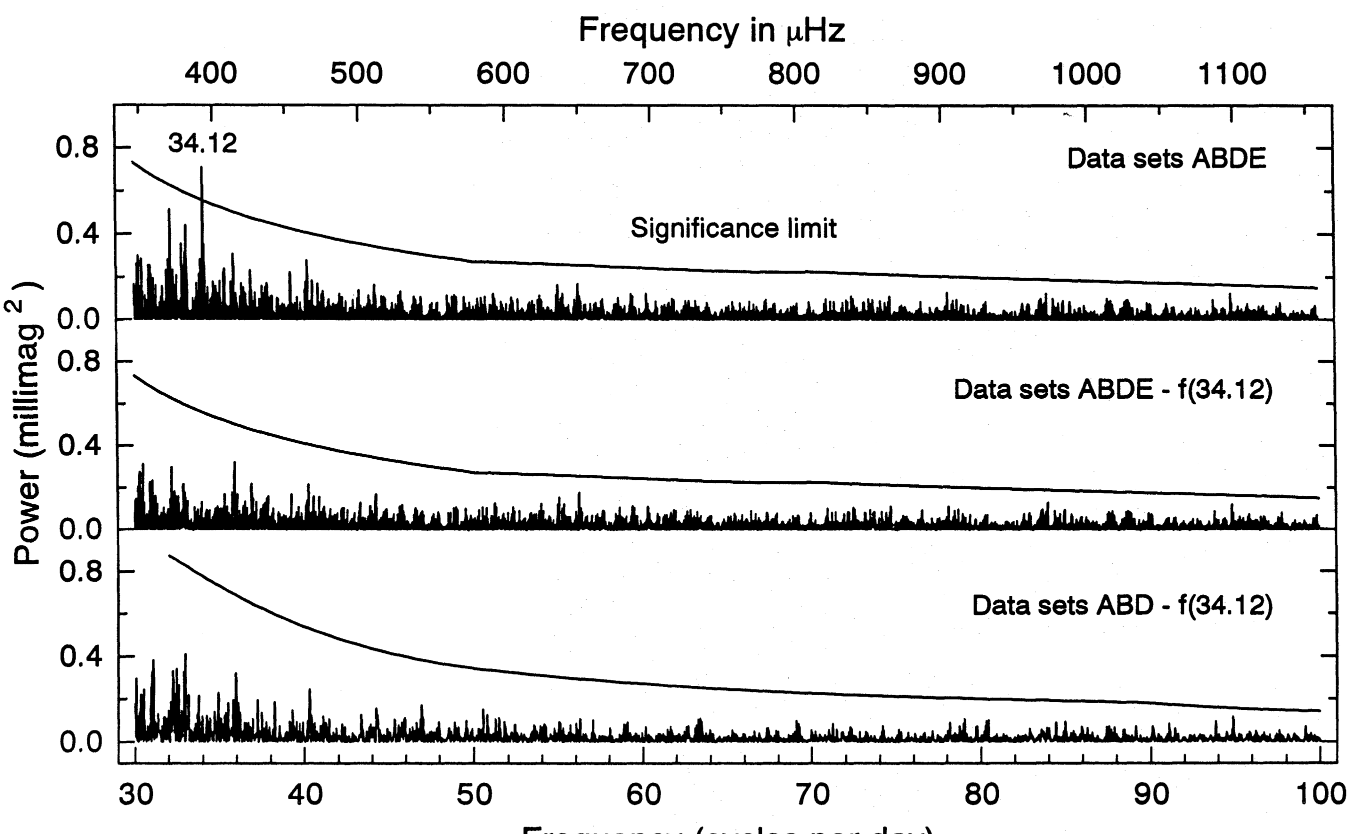

Fig. 5. Power spectrum of FG Vir in the 30 to 100 c/d range, after prewhitening the nine frequencies in the low-frequency 9 to 24 c/d region. The power spectra before and after prewhitening the frequency at 34.12 c/d are shown. See the text for the definition of the different combined data sets. The lower panel corresponds to data restricted to our 1993 multisite campaign and confirms that no further significant peaks are present

relatively noisy data set C. This also affects the value derived for the combined data set ABCD and we have bracketed the value of the amplitude (0.64 mmag) listed in Table 2.

No other peaks in the 0 to 100 c/d (0 to 1160 μHz) range exceed the significance limit adopted for our studies. Some of the peaks evident in the data below of the significance level are probably real and intrinsic to the star, but we cannot make definite decisions concerning individual peaks. Table 3 lists the most promising of the additional peaks. Most of the additional peaks are in 19 - 27 c/d (220 - 313 μHz) range. We note that the frequency of the peak at 11.19 c/d corresponds to $(f_1 + f_5)/2$, but the astrophysical interpretation of this numerical agreement should wait until the existence of this peak has been confirmed with a higher level of significance. Additional photometric studies of sufficient length to lower the noise level should be able to examine the richness of the pulsation modes of this δ Scuti star.

The large number of additional peaks in the 19 - 27 c/d region increases the computed noise figure for this frequency region. If some of these peaks are real, the noise will have been overestimated for this region. Since it is uncertain which of the peaks are intrinsic to the star, the computed noise figure cannot be lowered. This explains in part why in this frequency range peaks with amplitudes of 0.9 mmag are not statistically significant, while at higher frequencies pulsation modes with smaller amplitudes can already be detected reliably.

Table 3. Additional promising peaks for FG Vir

Frequency		Amplitude (1993)[1]		Amplitude[2]	
c/d	μHz	mmag	S/N	mmag	S/N
11.19	129.5	0.8	3.1	0.8	3.3
19.23	222.5	0.8	3.0	0.9	3.4
21.48	248.6	0.7	2.5	0.8	3.5
24.19	280.0	0.8	3.0	0.9	3.4
26.33	304.8	0.7	2.9	0.9	3.6
40.29	466.3	0.5	3.0	0.5	3.0

[1] Data sets ABCD
[2] Data sets ABDE (see text)

5. Steps towards identifying the pulsation modes

The identification of the observed frequencies of pulsation with particular pulsation modes requires the knowledge of the basic parameters of the star. The values of narrowband photometry adopted here take into account the misprint of the definition of $[c_1]$ in Eggen (1971), see the notes below Table I in Breger (1979). The new c_1 average, therefore, differs slightly from those listed in the $uvby\beta$ catalogs, e. g. Hauck & Mermilliod (1990). The measurements by Eggen (1971), Olsen (1983) and Olsen & Perry (1984) give the following average values for FG Vir: $b - y = 0.160$, $m_1 = 0.180$, $c_1 = 0.840$ and $\beta = 2.766$.

The calibrations given by Crawford (1979) indicate no interstellar reddening and $M_V = 1.71$. The $uvby\beta$ photometry can also be used to derive the $T_{\rm eff}$ and log g values. We adopt the values derived by MPB with a slight adjustment to account for the increased c_1 value. The relative shift was calculated by using the Kurucz (1991) models. We find $T_{\rm eff}$ = 7500 $\pm$ 150K, log g = 3.89 $\pm$ 0.15.

The values of the pulsation constants Q can be estimated from the following equation:

$$\log Q_i = -6.456 + \log P_i + 0.5 \log g + 0.1\, M_{\rm bol} + \log T_{\rm eff}.$$

The observed Q values, listed in Table 2, range from 0.010 ($\pm$ 0.002) to 0.037 ($\pm$ 0.007) d (for details on the error estimate for this method see Breger 1990b). This generally unavoidable uncertainty in the Q values is caused by the uncertainty of the photometry and its calibrations. It is this uncertainty which makes an identification of the observed frequencies with specific pulsation modes based on the values of the frequencies *alone* impossible. Additional information for this identification is provided by (i) an examination of amplitude ratios and phase differences between measurements at different wavelengths (see Garrido et al. 1990; Watson 1988; Balona & Stobie 1980), (ii) spectroscopic analyses, (iii) recognition of measured frequency patterns with those from computed models. Here we can apply all three techniques.

The color variations were measured during six nights of this campaign. These data are sufficient to derive reliable phase shift and amplitude ratio values for (only) the primary frequency. The uncertainty can be estimated by calculating the effect on the phase and amplitude of using only the primary frequency (instead of all ten frequencies) and by calculating the effects of using only six nights of V data as opposed to the whole V data set. For the primary frequency, f_1, we find

Color phase shift, $\phi_{\rm B-V} - \phi_{\rm V} = -10.4 \pm 2°$.

Amplitude ratio, $A_{\rm B-V}/A_{\rm V} = 0.33 \pm 0.03$, where the listed errors are estimates of internal errors.

A comparison of the observed negative color phase shift with the models of Watson (1988) and Garrido et al. (1990), scaled to $B - V$, excludes the possibility of radial pulsation ($\ell = 0$) for f_1 (12.7 c/d). Both $\ell = 1$ and 2 are possible. However, from spectroscopy, MPB identified f_1 with radial pulsation. These contradictory results cannot be resolved at this stage. MPB also suggested that two other observed modes (9.7, 19.9 c/d) are non-axisymmetric and a fourth mode (24.2 c/d) is axisymmetric. They determined $v \sin i$ = 21 km s^{-1} and estimated $i \sim 30°$ from their spectroscopic data. This leads to a rotational period of 2.8 d, or $\Omega \sim 0.36$, which can be included for calculations of rotationally split m modes.

6. Pulsation models

A powerful tool to assist with mode identifications is given by the calculation of stellar models, especially when the uncertainty in the Q, ℓ and m values are considered. Such models should include the effects of convective overshooting and allow for a nonuniform rotation rate. We have calculated a series of equilibrium stellar models and their oscillation frequencies. The range of models takes into account the uncertainties of the observationally determined input parameters in $\log T_{\rm eff}$, $\log g$ as well as the chemical composition parameters, X and Z, and

Table 4. Preliminary mode identifications (Model A)

Observed frequency c/d	μHz	Mode type	n	ℓ	m	Predicted frequency c/d	μHz
9.20	106	g	5	2	1	9.27	107
9.66	112	g	4	2	-2	9.84	114
12.15	141	g	3	2	1	12.15	141
12.72	147	p	1	0	0	12.67	146
19.87	230	p	2	2	-1	19.90	230
20.29	235	p	3	0	0	20.33	235
21.06	244	p	3	1	1	21.19	245
23.41	271	p	3	2	0	23.54	272
24.23	281	p	4	0	0	24.26	281
34.12	395	p	6	1	1	34.24	396

the rotation rate, Ω. Some additional information on the physics of the models can be found in Dziembowski & Goode (1992) and Dziembowski & Pamyatnykh (1991).

A good tactic for stars such as FG Vir is to look first for possible identifications of the observed periodicities with radial modes. For these modes, effects of rotation and convective overshooting are relatively unimportant and may be ignored initially. Furthermore, the period ratios of radial modes are relatively insensitive to variations of the parameters adopted for the models. The preliminary model of FG Vir was selected from a family of stellar main-sequence models with $T_{\rm eff}$ = 7500K, X = 0.7, Z = 0.02, without convective overshooting. The stellar mass was considered as an adjustable parameter within the observed uncertainty range of $\log g = 3.89 \pm 0.15$. In the model selected, three radial modes have frequencies within $\pm$ 0.05 c/d of the observed frequencies. The model (Model A) has the following mean parameters: $M = 1.80 M_\odot, \log L = 1.13, \log g = 4.01$.

In Table 4, the identifications of all ten observed periodicities are given. The rotational splitting was calculated assuming v_{rot} = 46.3 km/s and a uniform rotation rate. All nonradial modes, except for f_{10}, are of a dual nature. Their identification as a p or g mode follows the rule adopted by Dziembowski & Pamyatnykh (1991), which is based on the nature of the modes on the ZAMS, where the two types of modes are well separated in frequency. With such a definition, p modes are modes that are partially trapped the acoustic propagation zone i.e, in the outer envelope. Their frequencies decrease during the main-sequence evolution approximately $\propto R^{-1.5}$. On the other hand, the g modes penetrate the deep interior and their frequencies increase during the evolution. In the present model, which is in an advanced phase of core hydrogen burning (X_c = 0.22), the g_1 mode occurs between p_3 and p_4 at $\ell = 1$ and between p_6 and p_7 at $\ell = 2$.

All identified modes were found to be unstable in the model. Their frequencies span almost the whole frequency range in which the model shows instability. However, the observed modes represent only 10 % of all the unstable modes with $\ell \leq$ 2. There are two wide frequency ranges (13 to 19, 25 to 33 c/d) in which no mode is observed to be excited to a detectable level. This selection of which modes are excited by the star presents a challenge to the nonlinear theory of stellar oscillations.

The mode identification based on model A is in agreement with the constraints provided by the spectroscopic determinations (radial overtone, one axisymmetric and two nonradial non-axisymmetric modes) given by MPB. In spite of this consistency it must be pointed out that both the model adopted for FG Vir as well as the mode identification given in Table 4 must still be regarded as preliminary and that alternative identifications of the peaks should be considered as well. In the previous section, the color phase shift indicated that f_1 could be a dipole or quadrupole (rather than a radial) mode. This could be modelled with $M = 1.98 M_\odot$, $\log g$ = 3.86. In that model, f_1 would be identified with p_2, $\ell = 1$ and f_4 with p_6, $\ell = 0$. The different model and mode identification would not substantially change the conclusions of the present paper, but demonstrate the need towards observationally identifying additional pulsation modes in order to make the model selection more unique.

Efforts towards achieving an accurate fit of the calculated and measured frequencies should yield constraints on the internal structure and rotation of the star. FG Vir is one of the most promising of the known δ Scuti stars for seismic probing of the stellar interior due to the relatively slow rotation and the large number of detectable modes. Of particular interest are data on g modes, which probe the deep interior.

Acknowledgements. Part of the investigation has been supported by the Austrian Fonds zur Förderung der wissenschaftlichen Forschung, project number P8543-GEO. Observations at the Wise Observatory are partially supported by The Basic Research Foundation of the Israeli Academy of Sciences, while observations at Mt. Suhora were supported in part by the Polish National Committee for Scientific Research Grant 2-2109-91-02.

References

Balona, L. A., Stobie, R. S., 1980, MN 190, 931
Breger, M., 1972, ApJ 176, 367
Breger, M., 1979, PASP 91, 5
Breger, M., 1990a, Comm. Asteroseismology (Vienna) 20, 1
Breger, M., 1990b, Delta Scuti Star Newsletter (Vienna) 2, 13

Breger, M., 1993, Proc. IAU Coll. 136, Cambridge University Press, New York, p. 106
Breger, M., Garrido, R., Huang, L., et al., 1989, A&A 214, 209
Breger, M., Stich, J., Garrido, R., et al., 1993, A&A 271, 482
Colomba, A., De Benedetto, G., Ielo, A., 1991, IBVS 3597
Crawford, D. L., 1979, AJ 84, 1858
Dawson, D. W., 1990, BAAS 22, 831
Dziembowski, W. A., Goode, P. R., 1992, ApJ 394, 670
Dziembowski, W. A., Pamyatnykh, A. A., 1991, A&A 248, L11
Eggen, O. J., 1971, PASP 83, 762
Garrido, R., Garcia-Lobo, E., Rodriguez, E., 1990, A&A 234, 262
Gonzalez-Bedolla, S. F., Rodriguez, E., 1990, IBVS 3426
Hauck, B., Mermilliod, M., 1990, A&AS 86, 107
Kennelly, E. J., Walker, G. A. H., Hubeny, I., 1991, PASP 103, 1250
Kurucz, R. L., 1991, Van Vleck Obs. Contr. 11, 27
Kurtz, D. W., 1990, ARA&A 28, 607
Kurtz, D. W., Martinez, P., 1993, ASP. Conf. Ser. 44, 561
Lopez de Coca, P., Garrido, R., Costa, V., Rolland, A., 1984, IBVS 2465
Mantegazza, L., Poretti, E., Bossi, M., 1994, A&A 287, 95
Nather, R. E., Winget, D. E., Clemens, J. C., Hansen, C. J., Hine, B. P., 1990, ApJ 361, 309
Olsen, E. H., 1983, A&AS 54, 55
Olsen, E. H., Perry, C. L., 1984, A&AS 56, 229
Seeds, M. A., Stephens, C. J., 1977, IBVS 1273
Watson, R. D., 1988, Ap&SS 140, 255

This article was processed by the author using Springer-Verlag LaTeX A&A style file version 3.

2.3.2 The δ Scuti star FG Virginis: II. A search for high pulsation frequencies

Original paper:

M. Breger, **G. Handler,** E. Serkowitsch, P. Reegen, J. Provencal, M. A. Wood, J. C. Clemens, M. S. O'Brien, D. E. Winget, R. E. Nather, S. J. Kleinman, A. Kanaan, T. K. Watson, M. H. Montgomery, P. A. Bradley, D. J. Sullivan, E. Leibowitz, H. Mendelson, J. Krzesinski, G. Pajdosz, P. Moskalik, J.-E. Solheim 1996, A&A 309, 197

Astron. Astrophys. 309, 197–202 (1996)

ASTRONOMY
AND
ASTROPHYSICS

The δ Scuti star FG Virginis

II. A search for high pulsation frequencies

M. Breger[1], G. Handler[1], E. Serkowitsch[1], P. Reegen[1], J. Provencal[2], M.A. Wood[3], J.C. Clemens[4], M.S. O'Brien[4], D.E. Winget[5], R.E. Nather[5], S.J. Kleinman[5], A. Kanaan[5], T.K. Watson[5], M.H. Montgomery[5], P.A. Bradley[6], D.J. Sullivan[7], E. Leibowitz[8], H. Mendelson[8], J. Krzesinski[9], G. Pajdosz[9], P. Moskalik[10], and J.-E. Solheim[11]

[1] Astronomisches Institut der Universität Wien, Türkenschanzstr. 17, A-1180 Wien, Austria
Internet: BREGER@astro.ast.univie.ac.at
[2] Department of Physics and Astronomy, University of Delaware, Newark, DE 19716, USA
[3] Department of Physics and Space Sciences, Florida Institute of Technology, 150 W. University Blvd., Melbourne, FL 32901, USA
[4] Department of Physics and Astronomy, Iowa State University, Ames, IA 50211, USA
[5] Astronomy Department, University of Texas at Austin, Austin, TX 78712, USA
[6] Los Alamos National Laboratory, X-2, MS B220, Los Alamos, NM 87545, USA
[7] Department of Physics, Victoria University of Wellington, P.O. Box 600 Wellington, New Zealand
[8] Wise Observatory, Sackler Faculty of Exact Sciences, Tel Aviv University, Tel Aviv 69978, Israel
[9] Mt. Suhora Observatory, Cracow Pedagogical University, PL-30083 Cracow, Poland
[10] Copernicus Astronomical Center, Bartycka 18, PL-00-716 Warsaw, Poland
[11] Institute of Mathematical and Physical Sciences, Auroral Observatory, University of Tromsø, N-9037 Tromsø, Norway

Received 10 June 1995 / Accepted 23 September 1995

Abstract. Although the δ Scuti and roAp variables occupy similar positions on and near the main sequence, δ Scuti variables pulsate with lower radial and nonradial overtones and lower frequencies. To test whether high frequencies (as found in the roAp stars) are also present in δ Scuti stars, a multisite campaign with the Whole Earth Telescope (WET) was carried out for the star FG Vir. The 96.7 hours of WET photometry were supplemented by measurements made with the Delta Scuti Network (DSN), because the DSN technique includes regular measurements of comparison stars and is better suited to monitoring the low frequencies (≤ 500 μHz). This made possible the correction for low-frequency variability (10 pulsation frequencies from 106 to 395 μHz and amplitudes from 0.001 to 0.02) in order to prevent spectral leakage into the high-frequency domain. It is shown that such a correction is essential.

In the 1 - 10 mHz region of interest (corresponding to periods between 17 and 1.7 minutes) no significant stellar variability could be detected. The highest peaks in the amplitude spectra ranged from 0.00023 (near 1 mHz) to 0.00012 near 10 mHz, where the amplitudes are expressed in units of fractional intensity. Statistical tests show that these peaks are caused by noise.

These results indicate that for FG Vir the multimode pulsations in the low-frequency region (with individual amplitudes up to 0.02) are not accompanied by photometrically detectable high overtone pulsation at high frequencies. This result is consistent with the hypothesis that high-order p-mode pulsations in the millimag range require a large magnetic field, as detected in the roAp stars.

Key words: stars: delta Scuti – stars: oscillations – stars: individual: HD 106384 = FG Vir

1. Introduction

Two types of pulsating variables are found on the main sequence part of the classical instability strip: the δ Scuti variables include the stars with normal abundances, while the rapidly oscillating Ap (roAp) stars are cool Ap stars which approximately share the luminosity, temperature and evolutionary status of the δ Scuti stars. While the δ Scuti stars pulsate with periods of about 30 minutes to six hours (frequencies of about 50 to 500 μHz), the roAp stars pulsate much more rapidly with periods in the range of 6 to 15 minutes (frequencies of 1 to 3 mHz). For further information on the roAp stars, we refer to an excellent review by Kurtz (1990). The Cape Rapidly Oscillating Ap Star Survey by Martinez (1993) demonstrated that in the Hertzsprung–Russell Diagram the roAp stars are generally situated inside the δ Scuti star instability strip.

While the photometrically detectable oscillations of both the δ Scuti and the roAp stars are identified with nonradial p modes of low degree ($\ell \leq 3$), the two groups differ to a remarkable extent in the value of the radial quantum number: δ Scuti

Send offprint requests to: M. Breger

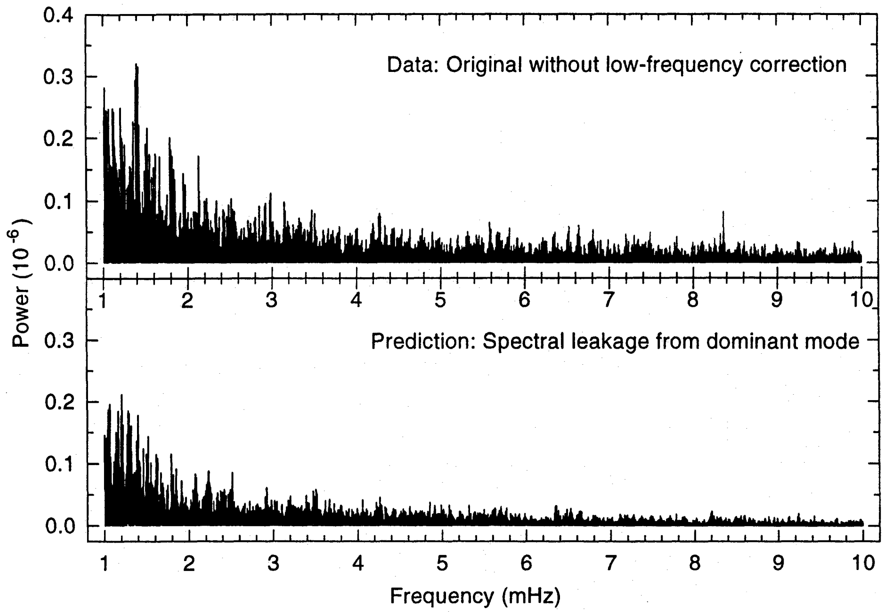

Fig. 1. Top: Power spectrum of the FG Vir high-speed data in the high-frequency domain. This power spectrum is affected by spectral leakage from the pulsation of FG Vir at low frequencies. Bottom: Predicted spectral leakage into the high-frequency domain of the dominant low-frequency pulsation mode at 147.2 μHz (amplitude = 0.021). This figure shows that in spite of good multisite coverage, reliable high-frequency analyses require knowledge and correction of low-frequency variability

stars pulsate with low overtones (k $\sim$ 0 to 6) and the roAp stars with very high overtones (k $\sim$ 10 to 80). It is also interesting to note that the roAp stars do not show low-order pulsation, at least not with photometrically detectable amplitudes. It is the purpose of this investigation to test this picture of 'mutually exclusive' pulsation orders by examining a normal δ Scuti star in the high-frequency domain by applying the appropriate observing techniques.

The search for pulsation modes at high frequencies ($\geq$ 1 mHz) in δ Scuti stars is made more difficult by the stellar variability at lower frequencies. Due to the possibility of spectral leakage between the different frequency ranges, the survey of high-frequency variability should be accompanied by a simultaneous determination of the pulsation at low frequencies at less than 500 μHz. This requirement holds especially for the data subsets covering a single night, where the large dynamic range of the sizes of the amplitudes at low frequencies and the low noise at high frequencies makes aliasing noticeable. It will be shown later that spectral leakage from low frequencies could also seriously affect the analysis of the combined multisite data in the 1 - 10 mHz range.

Consequently, the measurements need to be corrected for the variability at lower frequencies. This motivated us to carry out a multisite photometric campaign designed to examine both low and high frequencies. The observing techniques differ substantially for these two ranges: for low frequencies, observations are alternated with those of two comparison stars (the Three-Star Technique, see Breger 1993), and for high frequencies, essentially continuous coverage for several hours is required (which is referred to as the High-Speed Technique). We need multisite campaigns utilizing both observing techniques to eliminate aliases due to regular daylight observing gaps and spectral leakage of low frequency power into the high frequency domain of interest to us.

The δ Scuti star FG Vir was chosen for the study since the presence of a large number of pulsation modes with photometrically visible amplitudes was suspected. This was confirmed by Breger et al. 1995 (Paper I, which also lists the observational history of the star) for the low-frequency region. The present paper examines the 1 - 10 mHz region.

2. New photoelectric measurements

In order to eliminate the serious aliasing caused by regular observing gaps, a multisite campaign was organized utilizing the WET (Whole Earth Telescope) Network for high-speed measurements and the Delta Scuti Star Network for the detection of low frequencies. During 1993 March and April, 170.4 h of usable data were obtained at nine different observatories. Paper I of this series presented the results and analysis of the multisite campaign in the low frequency domain. Ten frequencies of pulsation were identified, ranging from 106 to 395 μHz (9.20 to 34.12 c/d).

Since the observational campaign was motivated by the simultaneous search for both low and high frequencies, different observational techniques were used: the three-star technique (Breger 1993) to detect the frequencies below $\sim$ 400 μHz, and the high-speed observing technique to examine the higher frequency range. The high-speed data are used in the present analysis and are listed in Table 1, while a journal of all the observations obtained for FG Vir has already been given in Paper I.

The data were obtained through Johnson V filters using continuous 5-s integrations with occasional interruptions for sky brightness measurements and, for some of the McDonald Observatory data, hourly checks of comparison stars. The April 1 measurements at Mt. John were sampled in ten-second bins. Two data sets were given half weight in the final analysis, which combined all the data: the March 26 data of McDonald Observatory were slightly affected by Fabry-lens problems, while the

Table 1. High-speed measurements of FG Vir used in the analysis

Observatory	Observer(s)	Date (UT)	Length (hrs)	Notes
McDonald 2.1m	T.K. Watson & R.E. Nather	16 Mar 93	3.9	
Siding Spring 0.6m	S.J. Kleinman	16 Mar 93	1.8	1
SAAO 0.75m	J.E. Solheim	16 Mar 93	3.9	
McDonald 2.1m	T.K. Watson & R.E. Nather	17 Mar 93	6.8	1
Siding Spring 0.6m	S.J. Kleinman	17 Mar 93	3.2	1
SAAO 0.75m	J.E. Solheim	17 Mar 93	6.8	1
Siding Spring 0.6m	S.J. Kleinman	18 Mar 93	9.8	1
Siding Spring 0.6m	S.J. Kleinman	19 Mar 93	2.2	1
Mauna Kea 0.6m	M.A. Wood	20 Mar 93	2.9	
Mt. John 1.0m	D.J. Sullivan	22 Mar 93	6.9	
Wise 1.0m	H. Mendelson	25 Mar 93	3.7	
McDonald 0.9m	J.C. Clemens	26 Mar 93	3.6	3
Mauna Kea 0.6m	M.A. Wood	26 Mar 93	4.1	
McDonald 0.8m	G. Handler	31 Mar 93	7.5	
McDonald 0.8m	G. Handler	1 Apr 93	7.8	
Mt. John 0.6m	D.J. Sullivan	1 Apr 93	7.0	2
McDonald 0.8m	G. Handler	2 Apr 93	7.2	
McDonald 0.8m	G. Handler	3 Apr 93	7.6	3

[1] Data show presence of periodic telescope tracking errors
[2] Data sampled in ten second bins
[3] Data given half weight

April 3 data had to be sampled with a small aperture (leading to slightly lower precision) because of the high sky brightness caused by moonlight. Measurements obtained at Mt. Suhora (Poland) covering 5.2 hours were not included in the present analysis due to lower accuracy, caused by the high air mass during the times of measurement.

All data were corrected for coincidence losses and barycentric corrections added to the Heliocentric Julian Dates. For data obtained with three-channel photometers, sky subtraction was performed on a point-by-point basis after an adjustment of the sensitivities of the different photometer channels. The single channel or two-channel sky measurements were also cross-calibrated and connected by a spline fit. This fit was subtracted from the measurements of both the variable and the comparison star. As is customary for the essentially continuous WET data, some filtering using low-order polynomials was applied. This becomes necessary when comparison stars are not regularly observed with the same channel to correct for detector sensitivity drifts as well as extinction uncertainties in the case of single-channel data.

3. Spectral leakage from low-frequency variations

The power spectrum in the 1 to 10 mHz domain (86.4 to 864 c/d) was computed for the data set combining all the available high-speed data of FG Vir. The results are shown in the top panel of Fig. 1. The power spectrum may be affected by spectral leakage from the low-frequency variability of the star. Ten low-frequency pulsation modes (at 106 to 395 μHz) have been detected and reported in Paper I. The star has a dominant mode at 147.2 μHz with an amplitude of 0.021, while the amplitudes of the other nine detected modes are much smaller and range from 0.001 to 0.004. Following WET convention, in this paper we express amplitudes and power in intensity units, rather than in magnitude units.

To evaluate the effects of spectral leakage, we have computed the predicted power spectrum of the dominant pulsation mode. This is shown in the bottom panel of Fig. 1. The computation demonstrates that consideration of spectral leakage is essential, especially in the frequency range below 3 mHz.

To correct for spectral leakage, we have applied the best ten-frequency solution (Paper I), which was subtracted from the data by using the nonlinear least-squares algorithm (program PERIOD, Breger 1990). The data set corrected in this manner will be used for the high-frequency analyses in the next section of this paper.

Finally, we need to estimate the spectral-leakage effect caused by additional low-frequency variations of FG Vir beyond the known ten frequencies. The extensive data set used in Paper 1 indicated the existence of such additional frequencies with small amplitudes, although their detection could at this stage not be regarded as statistically significant. One of the best examples is a peak at 222.5 μHz (19.23 c/d) with an amplitude of 0.0008. Furthermore, it is known from large-amplitude δ Scuti stars that 2f terms exist and that nonlinear effects lead to interactions between different pulsation modes. Such frequency combinations in the power spectrum have now also been detected in

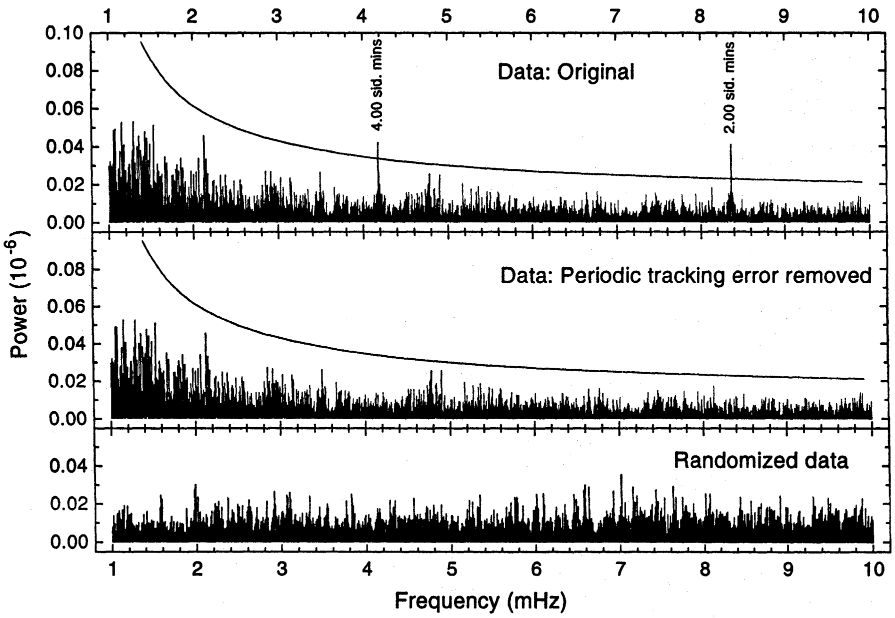

Fig. 2. Power spectrum of the FG Vir data in the high-frequency domain. The spectral window (not shown) would essentially be a δ function. The curves drawn represent the limits of significance for the data (see text). The top two panels demonstrate the low noise level and the lack of periodic signals intrinsic to the star. The randomized data in the lower panel show slightly higher peaks at high frequencies due to the distribution of low-frequency noise towards higher frequencies

a low-amplitude δ Scuti star, CD-24 7599 (Handler et al. 1995). Consequently, the leakage caused by these frequencies needs to be estimated. A search for such peaks in the available data indicates that the highest amplitude is found for a frequency at twice the frequency value of the dominant 147.2 μHz pulsation mode. We have calculated the predicted leakage for the 2f peak as well as each of the promising additional frequencies listed in Paper I. We find that the highest peaks in the power spectrum are between $10\,10^{-10}$ and $10\,10^{-9}$ and can be neglected. Consequently, any additional single frequency should not affect our analysis. However, the combined effect of a large number of undetected low frequencies with small amplitudes could cause an unknown amount of spectral leakage into the high-frequency domain.

Table 2. Results of the high-frequency search

Frequency range mHz	Noise x 10^{-3}	Highest peak in amplitude spectrum: Frequency mHz	Amplitude x 10^{-3}	Amplitude S/N
1 - 2.5	0.070	1.155	0.23	3.3
2.5 - 4	0.050	2.849	0.17	3.3
4.5 - 6	0.044	4.782	0.16	3.7
6 - 8	0.040	6.770	0.13	3.2
8.5 - 10	0.036	9.865	0.12	3.3

4. Search for high frequencies

The power spectrum in the 1 to 10 mHz domain (86 to 864 c/d) after correction for the low-frequency pulsation is shown at the top of of Fig. 2. The most noticeable result is the absence of high peaks: the highest peaks have a power below $6\,10^{-8}$.

In order to judge which peaks are significant (rather than noise), we adopt two independent methods of investigation. The first method compares the height of the peaks in amplitude or power spectra with a computed noise level. In a previous paper (Breger et al. 1993) it was argued that below 1 mHz a ratio of amplitude signal/noise = 4.0 provides a useful criterion for judging the reality of peaks. Subsequent analyses of new, independent data sets have confirmed that significantly lowering the signal/noise limit adopted by us leads to unreproducible results for typical photometric data. We therefore retain the criterion and extend it to higher frequencies. Although power is numerically equal to the square of the amplitude, an amplitude signal/noise value of 4 does not correspond to a power signal/noise ratio of 16, but to a value around 12. The reason for this lies in the fact that the average noise is defined as the average amplitude in a frequency region and that $< A >^2 \neq < A^2 >$. The precise value of the power signal/noise limit depends on the actual distribution of peaks. For the present data, the noise level as a function of frequency was calculated using the conservative initial assumption that all the peaks in the power spectrum (except for the 4.00 and 2.00 sidereal minute peaks, see below) are due to noise. The average amplitude was then calculated for successive 500 μHz regions. The corresponding curve of significance in the power spectrum was smoothed and is shown in Fig. 2.

The second method relies on re-ordering the measured brightness values at random without changing the times of observation, as proposed by Kepler (1993). The peaks of the scrambled data are, of course, not real and provide a guide to the effects of the noise inherent in the data. As a numerical experiment, we have scrambled the present data 100 times and computed the corresponding power spectra for each set of shuffled data. This is part of a larger program to investigate false alarm probabilities in real data sets. A preliminary result involving the present data set is the excellent agreement between the two different

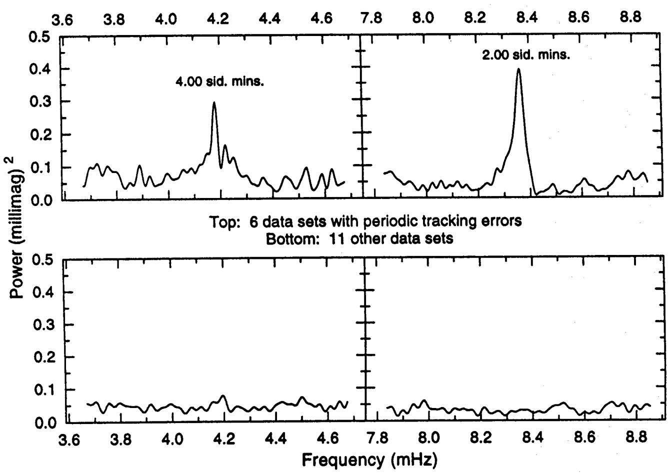

Fig. 3. Average nightly power spectra for the data sets with and without periodic tracking errors. Note that for the averages shown, periodic signals do not have to be in phase for the different nights. The diagrams show that the variations at 4 and 2 siderial minutes are present only in six specific data sets. This separation, and the fact that during the six nights the variations are not in phase, support the interpretation of an instrumental origin of the two peaks

methods adopted here for estimating the significance of peaks. A typical power spectrum produced by the scrambling is shown in the bottom panel of Fig. 2.

4.1. The 2.00 and 4.00 sidereal minute periods

Two peaks with a power of 4 10^{-8} at 4.18 and 8.36 mHz, corresponding to periods of exactly 4.00 and 2.00 sideral minutes, respectively, stand out in the power spectrum. The detection of both periods is statistically significant (amplitude S/N = 4.5 and 5.5, respectively), but the values of these periods suggests an instrumental origin, viz. a periodic tracking error coupled with slightly imperfect Fabry action in the photometer. The present detection is made possible by the high precision and low noise of the present data.

Because nine different telescopes were used to obtain the present measurements, it is possible to distinguish instrumental effects from variations intrinsic to the star, even if these were short-lived: for instrumental artifacts, the variation should depend on which of the nine telescopes were used. Furthermore, the variations in the different data sets should not be in phase.

To test these predictions, power spectra were computed for each individual night and telescope. This showed clearly that the 4.00 and 2.00 sidereal minute peaks are present in only 6 out of 17 data sets. These 6 data sets originate on three different telescopes: The Siding Spring 0.6 m (present on all four nights), the McDonald Observatory 2.1 m (one out of two nights) and the SAAO 0.75 m telescope (one out of two nights). The fact that the peaks are seen only in one of the two SAAO nights is easily explained: in order to avoid a possible systematic periodic tracking error, during the (second) night of 17 Mar 93, particular attention was paid to careful tracking and guiding. It is this precaution which made the spurious signal so regular that it could be detected! We strongly suspect that poorer guiding and tracking rates during the night would have smeared out the otherwise periodic signal.

It is possible to examine transient and other unphased variations with a different type of power spectrum: the *average* of the nightly power spectra. This differs from the *total* power spectrum of a combined data set in a fundamental way: in the average power spectrum the periodic variations do not have to be in phase in the different data sets; only the presence of periodic behavior lasting a few hours is required. Mathematically, the phase information present in the nightly Fourier transforms is disregarded. There is a price to be paid for this convenience: adding more data improves the signal of the peaks, but the noise level cannot be lowered substantially.

The average power spectra for those nights with and without the 2 and 4 sidereal minute peaks were computed. The different nights were weighted according to the number of measurements available. Fig. 3 shows the results for 1 mHz wide regions centered on the two peaks. We note that, as expected, the average noise is much higher than that shown in Fig. 2. The differences between the two data sets of 6 and 11 nights, respectively, are striking. The 2 and 4 sidereal minute periodicities are essentially absent during the 11 nights and very pronounced during the six nights. Further examination of the data (using specific options in the PERIOD package, see Breger 1990) from those six nights shows that these variations are not in phase from night to night. This is the expected behavior of an instrumental effect.

We conclude that the two peaks are instrumental in origin. It is therefore legitimate to prewhiten the two peaks and this was done for each of the the six nights. This corrects for most, but not all, effects of periodic tracking errors on the power spectra. If 4.00 and 2.00 sidereal minute periods were present, one could also suspect the existence of other multiples, e. g. at 1.00 sidereal minutes. These and other undetected periodicities could increase the noise level. The results are shown in the middle panel of Fig. 2, where the removal changed very little outside the 2 and 4 sidereal minute peaks.

The existence of systematic drive errors at some telescopes and their effects on the search for high frequencies of pulsation has been noticed before. The photometric study of HR 3831 by Kurtz et al. (1993) clearly shows a peak at 8.4 mHz caused by (only) one of the telescopes used in their study, the SAAO 0.75 m telescope. For the same telescope a periodic tracking error was also found in the present study.

4.2. Limits to high-frequency stellar variability

The measured high-frequency variability of FG Vir is plotted as a power spectrum in the middle panel of Fig. 2. The observed dependence of the noise on frequency has a standard shape: almost flat at high frequencies and a 1/f component dominating at frequencies lower than ~ 2 mHz due to atmospheric effects and residual instrumental drift (Kurtz 1984, Kjeldsen & Frandsen 1992).

We have divided the 1 to 10 mHz range into three subregions in order to avoid the frequencies of the periodic tracking errors. Table 2 lists the highest peak in each of these three regions. None of these peaks exceeds an amplitude signal/noise ratio of 4.0, which was adopted by us as one of the two criteria to judge significance. We therefore interpret the peaks as noise.

This interpretation is supported by the second test of significance provided by randomizing the data. The power spectra of the shuffled data show similar signal/noise ratios as the data set with the measurements. The average noise levels as well as the peaks of the scrambled data at frequencies higher than 2 mHz are actually slightly *higher* than the corresponding values of the unscrambled data. This can be explained as an artifact of shuffling the data and distributing the low-frequency (0 to 2 mHz) noise over all frequencies. This higher noise at low frequencies is caused by the observational 1/f component (see above) as well as suspected additional undetected low-frequency pulsation modes present in FG Vir.

Is the noise level realistic considering the 96.7 h of high-speed data available? Let us compare the present results with the measurements of the roAp star HR 3831 (Kurtz et al. 1993) which represent some of the best similar data available. For 167 h of data, Kurtz et al. find a noise level of $2\,10^{-5}$ at 5.7 mHz, while for 96.7 h of data we find $4\,10^{-5}$. At a lower frequency of 2.8 mHz, the corresponding numbers are $2\,10^{-5}$ and $5\,10^{-5}$, respectively. The two studies have different time coverage. To a first approximation, the noise should be proportional to $1/\sqrt{t}$, where t is the length of observation. For our data we have confirmed that this relationship is valid. If we correct for the different time coverage of the two studies, then in the high-frequency domain the Kurtz et al. study of HR 3831 shows about 60% of the noise of the present study. Similar ratios betwen the two studies are found when one considers the amplitudes of the highest noise peaks.

We conclude that no high-frequency variations have been detected. These results indicate that for FG Vir the pulsation in the low-frequency region (with amplitudes up to 0.02 in intensity) is not accompanied by detectable pulsation in high overtones at high frequencies, at least within the detection limit of amplitudes of 0.0002 in intensity.

These new results for FG Vir are consistent with the theory that the p-mode pulsation in stars of spectral type A or early F occurs either in low order (the δ Scuti stars) or high order. Such high-order p-mode pulsation in the millimag range would require fairly large magnetic fields as can be found in the roAp stars.

Acknowledgements. Part of the investigation has been supported by the Austrian Fonds zur Förderung der wissenschaftlichen Forschung, project number S7304. Observations at the Wise Observatory are partially supported by The Basic Research Foundation of the Israeli Academy of Sciences. The observations at Mt. Suhora Observatory were supported in part by National Committee for Scientific Research Grant 2-2109-91-02 (Poland). MAW was partially supported by the AAS Small Grant Program. DJS thanks the VUW IRG Committee for financial support.

References

Breger, M., 1990, Comm. Asteroseismology (Vienna) 20, 1
Breger, M., 1993, Accuracy in Variable-Star Work: The Three-Star Single Channel Technique. In: Butler, C. J., Elliott, I. (eds.) Proc. IAU Coll. 136, Stellar Photometry - Current Techniques and Future Developments. Cambridge University Press, New York, p. 106
Breger, M., Stich, J., Garrido, R., et al. 1993, A&A 271, 482
Breger, M., Handler, G., Nather, R. E., et al. 1995, A&A 297, 473
Handler, G., Breger, M., Sullivan, D. J., et al 1995, A&A, in press
Kepler, S. O., 1993, Baltic Astron. 2, 515
Kjeldsen, H., Frandsen, S., 1992, PASP 104, 413
Kurtz, D. W., 1984, NASA Conf. Publ. 2350, 56
Kurtz, D. W., 1990, ARA&A 28, 607
Kurtz, D. W., Kanaan, A., Martinez, P., 1993, MNRAS 260, 343
Martinez, P., 1993, unpublished dissertation, University of Cape Town

This article was processed by the author using Springer-Verlag LaTeX A&A style file version 3.

2.3.3 Detection of 75+ pulsation frequencies in the δ Scuti star FG Virginis

Original paper:

M. Breger, P. Lenz, V. Antoci, E. Guggenberger, R. R. Shobbrook, **G. Handler,** B. Ngwato, F. Rodler, E. Rodriguez, P. Lopez de Coca, A. Rolland, V. Costa, 2005, A&A 435, 955

A&A 435, 955–965 (2005)
DOI: 10.1051/0004-6361:20042480

Astronomy & Astrophysics

Detection of 75+ pulsation frequencies in the δ Scuti star FG Virginis

M. Breger[1], P. Lenz[1], V. Antoci[1], E. Guggenberger[1], R. R. Shobbrook[2], G. Handler[1], B. Ngwato[3], F. Rodler[1], E. Rodriguez[4], P. López de Coca[4], A. Rolland[4], and V. Costa[4]

[1] Institut für Astronomie der Universität Wien, Türkenschanzstr. 17, 1180 Wien, Austria
e-mail: michel.breger@univie.ac.at
[2] Research School of Astronomy and Astrophysics, Australian National University, Canberra, ACT, Australia
[3] Theoretical Astrophysics Programme, University of the North-West, Private Bag X2046, Mmabatho 2735, South Africa
[4] Instituto de Astrofisica de Andalucia, CSIC, Apdo 3004, 18080 Granada, Spain

Received 3 December 2004 / Accepted 31 January 2005

Abstract. Extensive photometric multisite campaigns of the δ Scuti variable FG Vir are presented. For the years 2003 and 2004, 926 h of photometry at the millimag precision level were obtained. The combinations with earlier campaigns lead to excellent frequency resolution and high signal/noise. A multifrequency analysis yields 79 frequencies. This represents a new record for this type of star. The modes discovered earlier were confirmed.
Pulsation occurs over a wide frequency band from 5.7 to 44.3 c/d with amplitudes of 0.2 mmag or larger. Within this wide band the frequencies are not distributed at random, but tend to cluster in groups. A similar feature is seen in the power spectrum of the residuals after 79 frequencies are prewhitened. This indicates that many additional modes are excited. The interpretation is supported by a histogram of the photometric amplitudes, which shows an increase of modes with small amplitudes. The old question of the "missing modes" may be answered now: the large number of detected frequencies as well as the large number of additional frequencies suggested by the power spectrum of the residuals confirms the theoretical prediction of a large number of excited modes.
FG Vir shows a number of frequency combinations of the dominant mode at 12.7162 c/d ($m = 0$) with other modes of relatively high photometric amplitudes. The amplitudes of the frequency sums are higher than those of the differences. A second mode (20.2878 c/d) also shows combinations. This mode of azimuthal order $m = -1$ is coupled with two other modes of $m = +1$.

Key words. stars: variables: δ Sct – stars: oscillations – stars: individual: FG Vir – techniques: photometric

1. Introduction

The δ Scuti variables are stars of spectral type A and F in the main-sequence or immediate post-main-sequence stage of evolution. They generally pulsate with a large number of simultaneously excited radial and nonradial modes, which makes them well-suited for asteroseismological studies. The photometric amplitudes of the dominant modes in the typical δ Scuti star are a few millimag. It is now possible for ground-based telescopes to detect a large number of simultaneously excited modes with submillimag amplitudes in stars other than the Sun (e.g., Breger et al. 2002; Frandsen et al. 2001). Because photometric studies measure the integrated light across the stellar surface, they can detect low-degree modes only. This is a simplification for the interpretation because of fewer possibilities in mode identification.

A typical multisite photometric campaign allows the discovery of about five to ten frequencies of pulsation from about 200 to 300 h of high-precision photometry (e.g., V351 Ori, Ripepi et al. 2003; V534 Tau, Li et al. 2004). These excellent observational studies are then compared to theoretical pulsation models, but the fit is hardly unique (e.g., θ^2 Tau, Breger et al. 2002b). The uniqueness problem can be lessened by studies with even lower noise in the power spectrum. This can be achieved by very accurate measurements from space and by larger ground-based studies with more data, which concentrate on a single selected star. These more extensive ground-based studies also lead to to higher frequency resolution. The latter is important, because δ Scuti stars can show a large number of very close frequency pairs (or groups), which can only be resolved through long-term studies lasting many months or years. The question of frequency resolution is an important aspect in planning asteroseismological space missions (e.g., see Handler 2004; Garrido & Poretti 2004).

The Delta Scuti Network (DSN) is a network of telescopes situated on different continents. The collaboration reduces the effects of regular daytime observing gaps. The network is engaged in a long-term program (1000 + hours of observation, 10 + years, photometry and spectroscopy) to determine the structure and nature of the multiple frequencies of selected

δ Scuti stars situated in different parts of the classical instability strip. The star FG Vir is the present main long-term target of the network. This 7500 K star (Mantegazza et al. 1994) is at the end of its main-sequence evolution. The projected rotational velocity is very small (21.3 ± 1.0 km s^{-1}, Mittermayer & Weiss 2003, see also Mantegazza & Poretti 2002).

A number of photometric studies of the variability of FG Vir are available: a lower-accuracy study by Dawson from the years 1985 and 1986 (Dawson et al. 1995, data not used here), high-accuracy studies from 1992 (Mantegazza et al. 1994), as well as previous campaigns by the Delta Scuti Network in 1993, 1995 and 2002 (Breger et al. 1995, 1998, 2004). Furthermore, for the year 1996, additional *uvby* photometry is available (Viskum et al. 1998). 12 nights of data were of high accuracy and could be included.

Because of the large scope of the long-term project on the pulsation of FG Vir, the photometric, spectroscopic and pulsation-model results cannot be presented in one paper. Here we present the extensive new photometric data from 2003 and 2004 as well as multifrequency analyses to extract the multiple frequencies excited in FG Vir. The analyses concentrate on the available three years of extensive coverage (2002–2004) and also consider the previous data (1992–1996).

Separate studies, presently in progress, will (i) present mode identifications based mainly on high-dispersion line-profile analyses and the data presented in this paper; (ii) examine the nature of close frequencies; (iii) compute asteroseismological models of stellar structure to fit the observed frequency spectrum.

2. New photometric measurements

During 2003 and 2004, photometric measurements of the star FG Vir were scheduled for ~350 nights at four observatories. Of these, 218 nights were of high photometric quality at the millimag level with no instrumental problems. These are listed in Table 1 together with the additional details:

1. The APT measurements were obtained with the T6 0.75 m Vienna Automatic Photoelectric Telescope (APT), situated at Washington Camp in Arizona (Strassmeier et al. 1997; Breger & Hiesberger 1999). The telescope has been used before for several lengthy campaigns of the Delta Scuti Network, which confirmed the long-term stability and millimag precision of the APT photometry.
2. The OSN measurements were obtained with the 0.90 m telescope located at 2900 m above sea level in the South-East of Spain at the Observatorio de Sierra Nevada in Granada, Spain. The telescope is equipped with a simultaneous four-channel photometer (*uvby* Strömgren photoelectric photometer). The observers for 2003 were: E. Rodriguez, P. López de Coca, A. Rolland, and V. Costa.
3. The SAAO measurements were made with the Modular Photometer attached to the 0.5 m and the UCT photometer attached to the 0.75 m telescopes of the South African Astronomical Observatory. The observers were V. Antoci, E. Guggenberger, G. Handler and B. Ngwato.
4. The 0.6-m reflector at Siding Spring Observatory, Australia, was used with a PMT detector. The observers were P. Lenz and R. R. Shobbrook.

The measurements were made with Strömgren v and y filters. Since telescopes and photometers at different observatories have different zero-points, the measurements need to be adjusted. This was done by zeroing the average magnitude of FG Vir from each site and later readjusting the zero-points by using the final multifrequency solution. The shifts were in the submillimag range. We also checked for potential differences in the effective wavelength at different observatories by computing and comparing the amplitudes of the dominant mode. No problems were found.

The measurements of FG Vir were alternated with those of two comparison stars. Details on the three-star technique can be found in Breger (1993). We used the same comparison stars as during the previous DSN campaigns of FG Vir, viz., C1 = HD 106952 (F8V) and C2 = HD 105912 (F5V). No variability of these comparison stars was found. The two comparison stars also make it possible to check the precision of the different observing sites. The residuals from the assumed constancy were quite similar, i.e., for the (C1–C2) difference we find a standard deviation of ±3 mmag for all observatories and passbands except for ±2 mmag (2004 SAAO75 v as well as y passbands) and ±4 mmag (2004 APT75 v and 2003 OSN90 y measurements. The power spectrum of the C1–C2 differences does not reveal any statistically significant peaks.

The resulting light curves of FG Vir are shown in Figs. 1 and 2, where the observations are also compared with the fit to be derived in the next section.

3. Multiple frequency analysis

The pulsation frequency analyses were performed with a package of computer programs with single-frequency and multiple-frequency techniques (PERIOD04, Lenz & Breger 2005; `http://www.astro.univie.ac.at/~dsn/dsn/Period04/`), which utilize Fourier as well as multiple-least-squares algorithms. The latter technique fits up to several hundreds of simultaneous sinusoidal variations in the magnitude domain and does not rely on sequential prewhitening. The amplitudes and phases of all modes/frequencies are determined by minimizing the residuals between the measurements and the fit. The frequencies can also be improved at the same time.

Our analysis consists of two parts: We first examine the extensive 2002−2004 data and then add the available 1992−1996 data.

3.1. Frequencies detected in the 2002–2004 data

The following approach was used in an iterative way:

(i) The data were divided into two data sets to separate the y and v filters, each covering the total time period from 2002−2004. This is necessary because the amplitudes and phasing of the pulsation are strongly wavelength dependent. In principle, the different amplitudes could be

Article published by EDP Sciences and available at http://www.edpsciences.org/aa or http://dx.doi.org/10.1051/0004-6361:20042480

Table 1. Journal of the PMT observations of FG Vir for 2003 and 2004.

Start HJD	Length hours	Obs./ Tel.	Start HJD	Length hours	Obs./ Tel.	Start HJD	Length hours	Obs./ Tel.	Start HJD	Length hours	Obs./ Tel.
245 000+		Year 2003	2748.29	4.6	SAAO50	2788.89	4.5	SSO60	3108.63	4.8	APT75
2656.99	1.7	APT75	2748.64	6.5	APT75	2792.66	2.9	APT75	3109.62	6.9	APT75
2667.81	5.7	APT75	2748.89	4.9	SSO60	2796.66	2.7	APT75	3110.26	2.0	SAAO50
2668.91	3.6	APT75	2749.25	5.9	SAAO50	2798.67	2.3	APT75	3110.63	6.9	APT75
2670.81	5.8	APT75	2749.64	6.5	APT75	2802.66	2.4	APT75	3111.63	6.8	APT75
2671.64	0.7	OSN90	2749.89	6.7	SSO60	2803.66	2.3	APT75	3113.23	6.5	SAAO50
2673.79	6.1	APT75	2750.26	5.5	SAAO50	2805.66	2.2	APT75	3114.64	5.3	APT75
2674.61	3.4	OSN90	2750.70	5.0	APT75	2806.66	2.0	APT75	3115.63	6.5	APT75
2675.62	3.1	OSN90	2750.93	5.8	SSO60	2809.88	2.8	SSO60	3117.63	5.9	APT75
2676.63	3.0	OSN90	2751.36	2.9	OSN90	2812.66	1.6	APT75	3118.63	6.3	APT75
2677.78	4.4	APT75	2751.37	2.3	SAAO50	2813.66	1.8	APT75	3119.63	6.1	APT75
2686.81	0.7	APT75	2751.91	2.8	SSO60	2813.87	1.8	SSO60	3120.63	6.0	APT75
2692.75	6.0	APT75	2752.90	3.4	SSO60	2814.65	0.8	APT75	3123.74	3.2	APT75
2693.82	4.2	APT75	2753.24	6.0	SAAO50	2816.66	1.4	APT75	3125.63	5.8	APT75
2699.96	1.9	APT75	2753.64	6.2	APT75		Year 2004		3130.64	5.1	APT75
2703.77	1.8	APT75	2754.25	5.7	SAAO50	3022.83	5.3	APT75	3131.65	4.8	APT75
2706.71	7.3	APT75	2754.64	6.0	APT75	3023.83	5.0	APT75	3132.66	4.6	APT75
2707.72	1.5	APT75	2754.90	4.4	SSO60	3031.81	1.3	APT75	3136.64	4.8	APT75
2709.71	7.4	APT75	2755.25	5.4	SAAO50	3032.81	5.8	APT75	3137.25	3.1	SAAO50
2710.71	7.3	APT75	2755.66	5.5	APT75	3033.93	2.8	APT75	3137.64	4.7	APT75
2711.71	6.1	APT75	2756.25	5.5	SAAO50	3034.85	4.9	APT75	3138.23	2.7	SAAO50
2712.67	1.2	OSN90	2757.65	5.6	APT75	3035.82	5.1	APT75	3138.64	4.4	APT75
2713.70	4.0	APT75	2758.64	3.9	APT75	3049.98	1.6	APT75	3139.24	3.1	SAAO50
2714.44	3.1	OSN90	2758.95	4.6	SSO60	3051.00	1.0	APT75	3139.64	4.4	APT75
2719.77	5.3	APT75	2759.65	5.6	APT75	3051.80	5.9	APT75	3140.22	3.2	SAAO50
2720.02	2.4	SSO60	2759.88	4.8	SSO60	3052.76	5.9	APT75	3141.64	1.9	APT75
2720.81	4.2	APT75	2760.37	3.6	OSN90	3053.90	0.8	APT75	3142.22	3.1	SAAO50
2720.98	6.1	SSO60	2760.64	5.6	APT75	3057.74	7.2	APT75	3144.23	3.9	SAAO75
2721.68	7.4	APT75	2760.93	5.4	SSO60	3060.76	6.6	APT75	3145.74	1.6	APT75
2722.67	7.4	APT75	2761.72	3.7	APT75	3061.73	7.4	APT75	3146.20	1.7	SAAO75
2722.98	5.7	SSO60	2761.88	4.6	SSO60	3062.90	0.9	APT75	3146.65	3.3	APT75
2723.75	4.3	APT75	2762.36	4.1	OSN90	3064.73	6.8	APT75	3147.21	4.4	SAAO75
2724.69	6.8	APT75	2762.64	5.5	APT75	3075.69	1.9	APT75	3147.64	3.8	APT75
2725.76	5.0	APT75	2762.88	5.6	SSO60	3079.71	6.8	APT75	3148.64	3.7	APT75
2726.75	5.3	APT75	2763.36	3.6	OSN90	3080.72	6.5	APT75	3149.65	3.7	APT75
2727.66	6.7	APT75	2764.65	4.8	APT75	3081.68	7.6	APT75	3152.20	4.1	SAAO75
2729.64	7.6	APT75	2765.65	4.0	APT75	3082.67	7.7	APT75	3153.65	3.3	APT75
2729.95	1.5	SSO60	2766.75	2.5	APT75	3086.74	4.8	APT75	3155.20	3.1	SAAO75
2730.64	7.6	APT75	2768.03	0.6	SSO60	3087.66	7.6	APT75	3156.19	4.0	SAAO75
2733.64	7.4	APT75	2768.65	4.9	APT75	3088.79	4.6	APT75	3157.30	1.5	SAAO75
2734.63	7.6	APT75	2769.36	3.6	OSN90	3090.84	0.8	APT75	3160.65	1.7	APT75
2735.63	7.5	APT75	2769.89	1.7	SSO60	3091.65	3.9	APT75	3161.65	2.7	APT75
2735.99	1.2	SSO60	2770.36	2.3	OSN90	3092.66	7.3	APT75	3162.65	2.7	APT75
2736.63	7.4	APT75	2771.08	1.2	SSO60	3093.64	7.5	APT75	3163.65	2.1	APT75
2736.94	1.0	SSO60	2775.65	4.1	APT75	3094.66	7.1	APT75	3165.65	2.4	APT75
2737.63	7.3	APT75	2776.65	4.5	APT75	3095.37	2.4	SAAO50	3166.65	2.3	APT75
2738.64	4.1	APT75	2777.75	1.9	APT75	3101.24	6.8	SAAO50	3167.65	2.5	APT75
2740.65	6.7	APT75	2778.65	4.0	APT75	3102.24	6.8	SAAO50	3168.65	2.5	APT75
2743.99	4.4	SSO60	2779.66	4.0	APT75	3102.73	4.9	APT75	3171.65	2.2	APT75
2744.28	5.1	SAAO50	2781.65	4.1	APT75	3103.63	7.3	APT75	3172.65	2.2	APT75
2745.26	1.8	SAAO50	2784.67	3.3	APT75	3104.62	0.7	APT75	3173.65	2.1	APT75
2745.90	4.6	SSO60	2785.65	3.8	APT75	3106.26	6.1	SAAO50	3174.65	1.8	APT75
2747.10	1.7	SSO60	2785.90	3.2	SSO60	3107.28	5.8	SAAO50	3175.65	1.9	APT75
2747.66	6.1	APT75	2786.67	2.5	APT75	3107.65	6.6	APT75	3177.65	1.8	APT75
2747.94	5.3	SSO60	2787.66	1.9	APT75	3108.24	6.7	SAAO50	3187.65	1.0	APT75

Article published by EDP Sciences and available at http://www.edpsciences.org/aa or http://dx.doi.org/10.1051/0004-6361:20042480

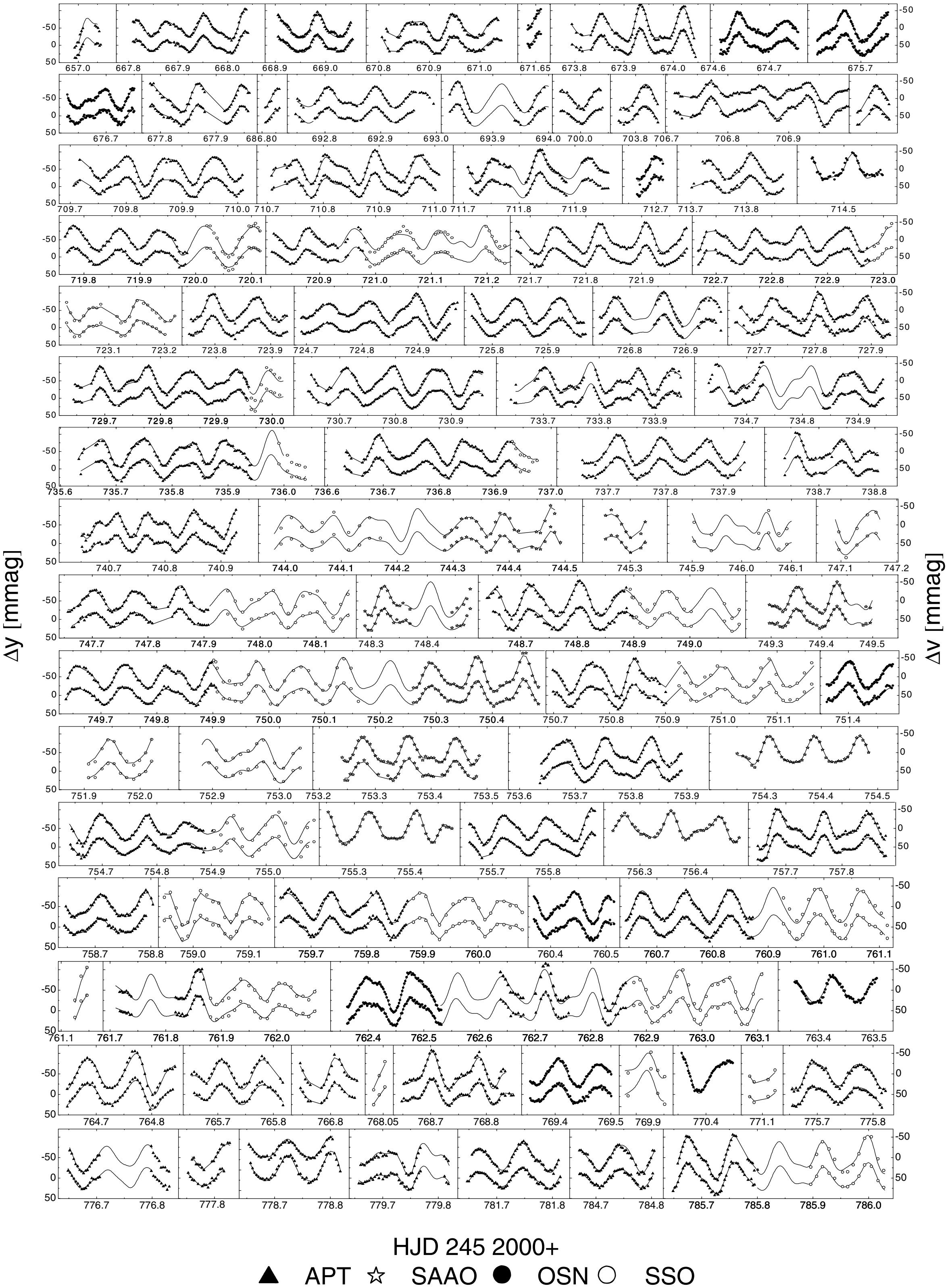

Fig. 1. Multisite photoelectric three-star-photometry of FG Vir obtained during the 2003 and 2004 DSN campaigns. Δy and Δv are the observed magnitude differences (variable – comparison stars) normalized to zero in the narrowband *uvby* system. The fit of the 79-frequency solution derived in this paper is shown as a solid curve. Note the excellent agreement between the measurements and the fit.

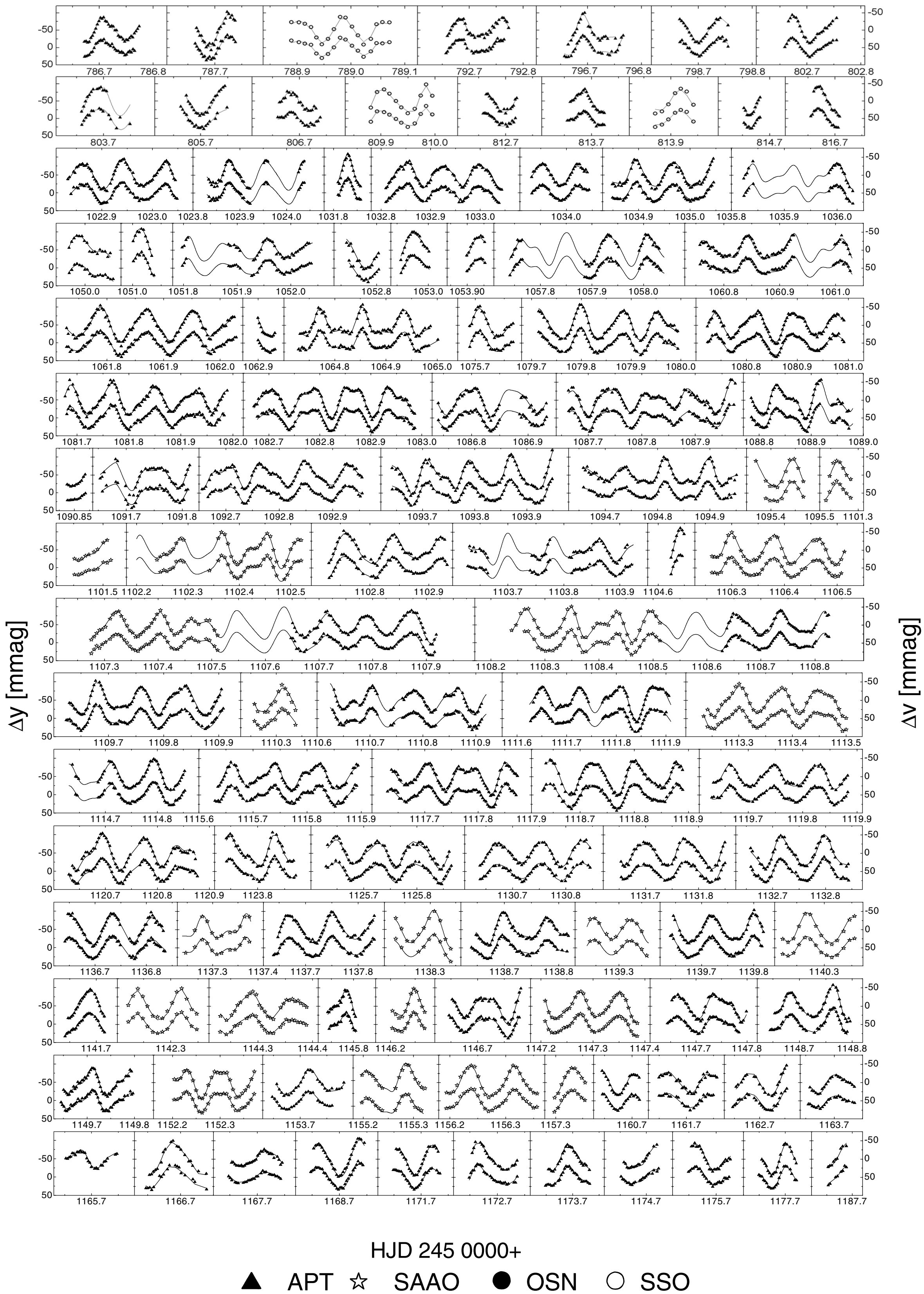

Fig. 2. Multisite photoelectric three-star-photometry of FG Vir obtained during the 2003 and 2004 DSN campaigns, continued.

Article published by EDP Sciences and available at http://www.edpsciences.org/aa or http://dx.doi.org/10.1051/0004-6361:20042480

Table 2. Frequencies of FG Vir from 2002 to 2004.

Frequency cd^{-1}	Frequency name	Type	Detection[1] amplitude S/N ratio	Amplitude v filter millimag	Amplitude y filter millimag	Frequency cd^{-1}	Name	Type	Detection amplitude S/N ratio	Amplitude v filter millimag	Amplitude y filter millimag
				±0.04	±0.05					±0.04	±0.05
5.7491	f_{47}		5.7	0.48	0.28	23.3974	f_{12}	[2]	22	1.73	1.25
7.9942	f_{44}		5.9	0.42	0.34	23.4034	f_4	[2]	71	5.65	4.02
8.3353	f_{78}	$f_6 - f_1$	*3.8*	0.33	0.17	23.4258	f_{53}		4.9	0.37	0.28
9.1991	f_7		53	3.82	2.78	23.4389	f_{24}		9.0	0.68	0.52
9.6563	f_5		71	5.20	3.61	23.8074	f_{48}		5.5	0.45	0.32
10.1687	f_{25}		8.6	0.64	0.42	24.0040	f_{58}		4.6	0.35	0.31
10.6872	f_{79}	$f_4 - f_1$	3.5	0.26	0.15	24.1940	f_{10}		29	2.26	1.58
11.1034	f_{20}		11	0.67	0.65	24.2280	f_3		74	5.79	4.20
11.2098	f_{38}		6.4	0.35	0.43	24.3485	f_{18}		12	0.99	0.63
11.5117	f_{70}	$f_3 - f_1$	4.0	0.30	0.18	24.8703	f_{36}	$f_1 + f_2$	6.4	0.48	0.38
11.6114	f_{50}		5.3	0.35	0.27	25.1788	f_{30}		7.3	0.59	0.39
11.7016	f_{33}		6.9	0.42	0.44	25.3793	f_{45}		5.7	0.37	0.31
11.8755	f_{63}		4.4	0.27	0.25	25.4324	f_{15}	$2f_1$	16	1.23	0.89
11.9421	f_{29}		7.6	0.55	0.38	25.6387	f_{68}		4.0	0.30	0.26
12.1541	f_2	[2]	85	6.09	4.21	26.5266	f_{71}		*4.7*	0.30	0.20
12.1619	f_{14}	[2]	16	1.13	0.83	26.8929	f_{61}		4.5	0.34	0.27
12.2158	f_{52}		5.1	0.38	0.24	26.9094	f_{75}		*4.2*	0.34	0.19
12.7162	f_1		442	31.74	21.92	28.1359	f_{19}		11	0.87	0.55
12.7944	f_{17}		13	0.88	0.66	29.4869	f_{51}	$f_7 + f_{11}$	5.2	0.39	0.28
13.2365	f_{27}		8.3	0.45	0.56	30.9146	f_{60}		4.5	0.31	0.27
14.7354	f_{49}		5.3	0.29	0.38	31.1955	f_{57}		4.6	0.35	0.27
16.0711	f_{13}		20	1.56	1.07	31.9307	f_{34}		6.6	0.49	0.40
16.0909	f_{31}		7.3	0.55	0.39	32.1895	f_{32}		7.0	0.56	0.38
19.1642	f_{26}		8.6	0.55	0.59	33.0437	f_{74}	[4]	*4.3*	0.29	0.19
19.2278	f_9		30	2.51	1.69	33.7677	f_{43}	$f_1 + f_6$	5.9	0.44	0.31
19.3259	f_{41}		6.3	0.53	0.34	34.1151	f_{22}		9.8	0.75	0.49
19.6439	f_{65}		4.3	0.40	0.22	34.1192	f_{72}		*4.7*	0.21	0.25
19.8679	f_8	[3]	55	4.44	3.19	34.1864	f_{54}		4.9	0.37	0.25
19.8680		[3]	30	2.40	1.78	34.3946	f_{55}		4.6	0.31	0.28
20.2878	f_{11}		26	2.13	1.45	34.5737	f_{23}		9.3	0.69	0.45
20.2925	f_{56}		4.6	0.31	0.39	35.8858	f_{76}		*4.1*	0.22	0.21
20.5112	f_{35}		6.6	0.41	0.52	36.1196	f_{40}	$f_1 + f_4$	6.3	0.40	0.31
20.8348	f_{39}		6.3	0.53	0.38	36.9442	f_{37}	$f_1 + f_3$	6.4	0.43	0.27
21.0515	f_6		55	4.43	3.08	39.2165	f_{69}		4.0	0.27	0.16
21.2323	f_{16}		14	1.06	0.80	39.5156	f_{59}	$f_9 + f_{11}$	4.5	0.24	0.25
21.4004	f_{46}		5.7	0.52	0.33	42.1030	f_{64}	$2f_6$	4.3	0.22	0.28
21.5507	f_{28}		7.9	0.61	0.42	42.1094	f_{62}		4.5	0.24	0.25
22.3725	f_{42}	$f_1 + f_5$	6.2	0.52	0.35	43.0134	f_{73}		*4.4*	0.21	0.15
23.0253	f_{66}		4.1	0.30	0.23	43.9651	f_{67}		4.0	0.26	0.17
23.3943	f_{21}		11	0.85	0.60	44.2591	f_{77}		*4.0*	0.20	0.18

[1] The noise for the amplitude signal/noise ratios were calculated over a 4 cd^{-1} range. Limits for a significant detection are 4.0 for independent frequencies and 3.5 for combination modes with known values. Numbers in italics indicate 1992−2004 data (see text).
[2] The close frequencies, 12.1541 and 12.1619 as well as 23.3974 and 23.4034 c/d, are all separate modes. In short data sets this could lead to an erroneous identification as single modes with variable amplitude.
[3] For the possible frequency pair near 19.868 c/d the existence of two separate modes cannot be proved at this point. A single frequency with a slowly variable amplitude (beat period ~21.5 years) is also possible.
[4] The 2002–2004 data clearly show a mode at 33.044 c/d, though with considerably reduced amplitudes from 1992–1995 data. Breger et al. (1998) listed the value of the frequency as 33.056 c/d, which was the highest peak from a broad selection of peaks separated by annual aliases 0.0027 c/d apart. We note that in the new data, a value separated by 1 annual alias, viz., 33.0461 c/d, is also possible.

compensated for by multiplying the v data by an experimentally determined factor of 0.70 and increasing the weights of the scaled v data accordingly. (Anticipating the results presented later in Table 2, we note that this ratio is confirmed by the average amplitude ratio of the eight modes with highest amplitudes.) However, the small phase shifts of a few degrees cannot be neglected for the larger-amplitude modes. Consequently, the data were

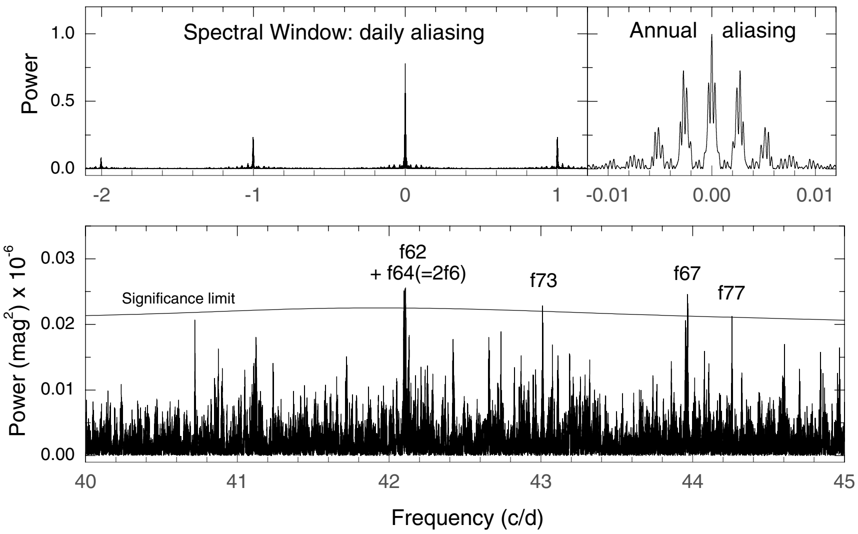

Fig. 3. Example of power spectra of the 1992–2004 data. *Top*: spectral windows showing effects of the daily and annual aliasing. *Bottom*: new frequencies detected in the most difficult frequency region with the lowest amplitudes. The diagram shows that in the 40–45 c/d region pulsation modes are present and have been detected. The choice of which peaks are statistically significant depends somewhat on the details of the analysis.

analyzed together for exploratory analysis, but not for the final analyses.

(ii) We started with the single-frequency solution for the two data sets using the program PERIOD04. For the Fourier analyses the two data sets were combined to decrease the noise, while for the actual fits to the data, separate solutions were made.

(iii) A Fourier analysis was performed to look for additional frequencies/modes from the combined residuals of the previous solutions. Additional frequencies were then identified and their signal/noise ratio calculated. Following Breger et al. (1993), a significance criterion of amplitude signal/noise = 4.0 (which corresponds to power signal/noise of ~12.6) was adopted for non-combination frequencies. The most clearly detected additional frequencies were included in a new multifrequency solution. In order for a new frequency to be accepted as real, the signal/noise criterion also had to be fulfilled in the multifrequency solution. This avoids false detections due to spill-over effects because the Fourier technique is a single-frequency technique. Furthermore, since there exist regular annual gaps, trial annual alias values (separated by 0.0027 c/d) were also examined. We note that the choice of an incorrect annual alias value usually has little or no effect on the subsequent search for other frequencies. The choice of an incorrect daily alias (separated by 1 c/d) would be more serious and we carefully examined different frequency values.

(iv) The previous step was repeated adding further frequencies until no significant frequencies were found. Note that only the Fourier analyses assume prewhitening; the multiple-frequency solutions do not.

In this paper we omit the presentation of very lengthy diagrams showing the sequential detection of new frequencies, except for the example shown in the next subsection. A detailed presentation of our approach and its results can be found in our analysis of the 2002 data (Breger et al. 2004).

FG Vir contains one dominant frequency: 12.7162 c/d with a photometric amplitude five times higher than that of the next strongest mode. To avoid potential problems caused by even small amplitude variability, for this frequency we calculated amplitudes on an annual basis. The results of the multifrequency analysis are shown in Table 2. The numbering scheme of the frequencies corresponds to the order of detection, i.e., the amplitude signal/noise ratio, and therefore differs from that used in previous papers on FG Vir.

3.2. Further frequencies detected in the 1992–2004 data

An extensive photometric data set covering 13 years is essentially unique in the study of δ Scuti stars, promising new limits in frequency resolution and noise reduction in Fourier space. The noise reduction is especially visible at high frequencies, where the effects of systematic observational errors are small. The analysis of the combined data had to work around two problems: the earlier data is not as extensive as the 2002−2004 data and there exists a large time gap between 1996 and 2002.

The time gap did lead to occasional uniqueness problems for the frequencies with amplitudes in the 0.2 mmag range: next to the annual aliasing of 0.0027 c/d we find peaks spaced 0.00026 c/d, corresponding to a ~10 year spacing (see Fig. 3, top right). Fortunately, the excellent coverage from 2002−2004 minimized these ambiguities.

The relatively short coverage of the data from 1992 and 1996 excluded the computation of 79-frequency solutions for individual years (to avoid overinterpretation). We have

Article published by EDP Sciences and available at http://www.edpsciences.org/aa or http://dx.doi.org/10.1051/0004-6361:20042480

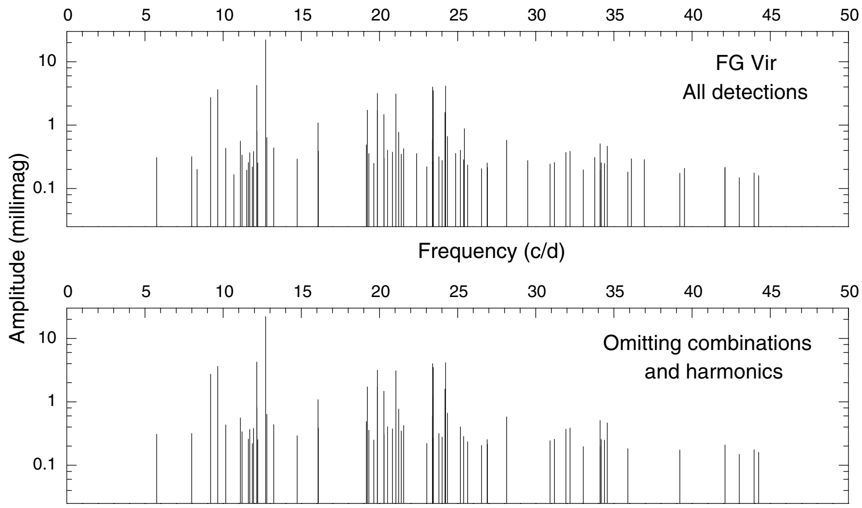

Fig. 4. Distribution of the frequencies of the detected modes. The diagram suggests that the excited pulsation modes are not equally distributed in frequency.

consequently combined all the y measurements from 1992 to 1996 as well as the available 1995 and 1996 v data. Together with the y and v data sets from 2002−2004, we had four data sets.

Figure 3 illustrates some examples of the resulting power spectra. Due to the large amount of APT data from 2002−2004, which therefore dominates, the 1 c/d aliases are not zero (top left). Nevertheless, due to the excellent frequency resolution, these aliases are very narrow so that the aliasing problem is not severe. The figure also shows the power spectrum of the measurements in the 40−45 c/d region, which was the most difficult region for us to analyze due to the small amplitudes of all the detected frequencies.

The new detections are included in Table 2.

A comparison with the frequencies published in earlier papers shows that all the previously detected frequencies were confirmed. This also includes those previously detected modes not found to be statistically significant in the 2002 data alone. In a few cases, different *annual* aliases were selected. However, the main result is the increase in the number of detected frequencies to 79, which more than doubles the previous results.

Figure 4 shows the distribution of frequencies in frequency space. We note the wide range of excited frequencies, which is unusual for δ Scuti stars, as well as the clustering of the excited frequencies. This clustering persists even after the suspected combination frequencies and $2f$ harmonics are removed.

A new feature is the detection of frequencies with values between 40 and 45 c/d. They all have small amplitudes of $\Delta y \sim 0.2$ mmag. The lower noise of the new data now made their detection possible.

3.3. Color effects

The light curves of pulsating stars are not identical at different wavelengths. In fact, amplitude ratios and phase shifts provide a tool for the identification of nonradial modes (e.g., see Garrido et al. 1990; Moya et al. 2004). For δ Scuti stars, the amplitude ratios between different colors are primarily dependent on the surface temperature. For the individual pulsation modes, the phase differences and deviations from the *average* amplitude ratio are small. This means that observational errors need to be small and any systematic errors between the different colors should be avoided.

For most nights there exist both v and y passband data, so that amplitude ratios as well as phase differences can be derived. However, our 79-frequency solution is not perfect. In order not to introduce systematic errors in the phase differences and amplitude ratios, for the calculation of amplitude ratios and phase differences, we have omitted those nights for which two-color data are not available. Consequently, no data from 1992 and 1993 were used and all 1995 (single-color) CCD measurements were omitted.

Table 3 lists the derived phase differences and amplitude ratios for the modes with relatively high amplitudes. The uncertainties listed were derived from error-propagation calculations based on the standard formulae given by Breger et al. (1999). The results can now be used together with spectroscopic line-profile analyses to identify the pulsation modes.

4. Combination frequencies

We have written a simple program to test which of the 79 frequencies found can be expressed as the sum or differences of other frequencies. Due to the excellent frequency resolution of the 2002−2004 data, we could be very restrictive in the identification of these combinations. A generous limit of ±0.001 c/d was adopted. The probability of incorrect identifications is correspondingly small. A number of combinations was found and these are marked in Table 2. They generally agreed to ±0.0002 c/d.

How many accidental agreements do we expect? We have calculated this number through a large number of numerical simulations, assuming a reasonable agreement of the observed frequency to within 0.0002 c/d of the predicted frequency. We obtain an average of 0.93 accidental matchings of peaks with

Table 3. Phase differences and amplitude ratios.

	Frequency c/d	Phase differences in degrees $\phi_v - \phi_y$ 2002–2004	1995–2004[1]	Amplitude ratios v/y 2002–2004	1995–2004
f_1	12.716	–1.7 ± 0.1	–1.5	1.45 ± 0.00	1.45
f_2	12.154	+3.1 ± 0.7	+2.8	1.44 ± 0.02	1.44
f_3	24.227	–3.0 ± 0.7	–3.0	1.38 ± 0.02	1.40
f_4	23.403	–3.5 ± 0.7	–3.3	1.40 ± 0.02	1.42
f_5	9.656	–5.1 ± 0.8	–4.5	1.44 ± 0.02	1.43
f_6	21.051	–3.7 ± 1.0	–4.2	1.44 ± 0.02	1.45
f_7	9.199	–6.7 ± 1.1	–6.6	1.38 ± 0.03	1.40
f_8	19.868[2]	–4.3 ± 1.9	–2.9	1.45 ± 0.05	1.44
f_9	19.228	–4.6 ± 1.7	–3.9	1.48 ± 0.05	1.46
f_{10}	24.194	–1.2 ± 1.9	–0.6	1.43 ± 0.07	1.38

[1] Error estimates omitted: usually lower than for 2002–2004, but some instability is possible due to large time gap.
[2] Using single frequency with annual amplitude variations.

combination frequencies. We conclude that most or all detected combination frequencies are not accidental. The argument is strengthened by the fact that the combinations detected by us all contain one of two specific modes, which reduces the chance of accidental agreements to essentially zero.

We also note that the lowest frequency detected, f_{47} at 5.749 c/d, can be expressed as a *triple* combination of f_1, f_3 and f_{57}. This may be accidental.

4.1. Combinations of the dominant mode at 12.7163 c/d

Due to the presence of a dominant mode at 12.7163 c/d (f_1), it is not surprising that some combination frequencies, $f_1 \pm f_i$, exist and are detected (see Table 2). In order to examine this further, we have performed additional calculations with the 2002−2004 data. We have repeated our multifrequency solutions described earlier while omitting all frequency combinations of f_1. The residuals of the y and v data were combined to form the sum (y + 0.70v) to account for the different amplitudes at the two passbands. A new multifrequency solution containing the possible combinations of the dominant mode with f_2 through f_8 was made. The results are shown in Table 4, in which small differences compared to Table 2 are caused by the different procedures of our analyses. The amplitudes of the sums ($f_1 + f_i$) are higher than those of the differences ($f_1 - f_i$). We believe the result to be real and intrinsic to the star. The differences are generally found at low frequencies, where the observational noise is higher. Increased noise should lead to higher amplitudes, which are not found.

Table 4. Combination frequencies involving the dominant mode.

$f_1 \pm$	Amplitude in y (2002–2004) Sum of frequencies mmag	Difference of frequencies mmag
f_2	0.35	(0.06)
f_3	0.28	0.19
f_4	0.31	0.17
f_5	0.33	(0.16)
f_6	0.39	0.21
f_7	(0.10)	(0.07)
f_8	(0.07)	(0.13)

The amplitudes in brackets are too low for fulfilling the adopted criterion of statistical significance.

4.2. Combinations of the 20.2878 c/d mode

Apart from the mode combinations involving the dominant mode, f_1, two other two-mode combinations are found, both involving f_{11} at 20.2878 c/d. While the mode identifications are still in progress, this mode can to a high probability be identified as a $\ell = 1$, $m = -1$ mode (Zima et al. 2003). At first sight, this appears surprising, since the photometric amplitude is only 1.5 mmag. However, for the known inclination and mode identification, we calculate a geometric cancellation factor of ∼3.6, so that the real amplitude of this mode is 5 mmag or larger.

The fact that the m value is not equal to zero has some interesting consequences for the observations of combination frequencies. The reason is that there are two frames of reference: the stellar frame corotating with the star, and that of the observer. For nonradial modes of m values ≠ 0 (i.e., waves traveling around the star), the frequencies between the two frames of reference differ by $m\Omega$, where Ω is the rotation frequency of the star (see Cox 1984, for an excellent discussion). The frequency combinations occur in the corotating (stellar) frame, and not the observer's frame of reference. Consequently, many possible combinations involving non-axisymmetric modes should not be observed as simple sums or differences of observed frequency values.

It follows that for the non-axisymmetric ($m = -1$) mode at 20.2878 c/d, our simple method to search for combination frequencies from the observed frequency values may only detect combinations, $f_i + f_j$, with $m = +1$ modes.

Article published by EDP Sciences and available at http://www.edpsciences.org/aa or http://dx.doi.org/10.1051/0004-6361:20042480

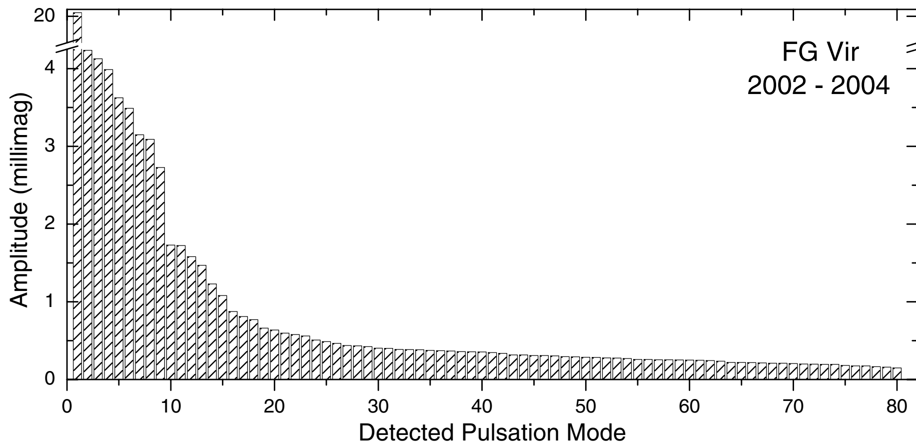

Fig. 5. Distribution of the amplitudes of the frequencies with significant detections. To increase the accuracy, we have computed amplitudes from 0.5*(y amplitude + 0.70 v amplitude) to simulate the amplitude in the y passband. Note the large number of detected modes with amplitudes near the detection limit of 0.2 mmag. This suggests that even moderate increases in the amount of data lead to considerably higher number of detections.

This strict requirement is met by the two identified combinations of 20.2878 c/d! Both coupled modes, f_9 = 19.2278 c/d as well as f_{11} = 20.2878 c/d have been identified as m = +1 modes. Such a combination of m values of opposite sign can be detected because the combination is invariant to the transformation between the two frames of reference: $-m\Omega + m\Omega = 0$.

5. The problem of missing frequencies solved?

δ Scuti star models predict pulsational instability in many radial and nonradial modes. The observed number of low-degree modes is much lower than the predicted number. The problem of mode selection is most severe for post-main-sequence δ Scuti stars, which comprise about 40 percent of the observed δ Scuti stars. The theoretical frequency spectrum of unstable modes is very dense. Most modes are of mixed character: they behave like p-modes in the envelope and like g-modes in the interior. For example, for a model of the relatively evolved star 4 CVn, the models predict 554 unstable modes of ℓ = 0 to 2, i.e., 6 for ℓ = 0, 168 for ℓ = 1, and 380 for ℓ = 2 (see Breger & Pamyatnykh 2002). However, only 18 (and additional 16 combination frequencies) were observed (Breger et al. 1999). The problem also exists for other δ Scuti stars. A complication occurs since the models so far cannot predict the amplitudes of the excited modes.

Two explanations offer themselves: the missing modes exist, but have amplitudes too small to have been observed, or there exists a mode selection mechanism, which needs to be examined in more detail. Promising scenarios involve the selective excitation of modes trapped in the envelope (Dziembowski & Królikowska 1990) or random mode selection.

Let us turn to the star FG Vir. Unpublished models computed by A. A. Pamyatnykh predict 80 unstable modes with ℓ = 0, 1 and 2 in the 8−40 c/d range. This number is smaller than that mentioned previously for the more evolved star 4 CVn, but until now this large number was not observed either. The present study addresses the question by lowering the observational amplitude threshold to 0.2 mmag. We have detected 79 frequencies, of which 12 could be identified as harmonics or combination frequencies. This leaves 67 independent frequencies. There also exists considerable evidence that many more modes are excited:

(i) consider the amplitude distribution of the detected modes shown in Fig. 5. There is a rapid increase in the number of modes as one goes towards low amplitudes. The present limit near 0.2 mmag is purely observational. Consequently, the number of excited modes must be much larger.
(ii) consider the power spectrum of the residuals after subtraction of the *multifrequency* solution (Fig. 6). We see excess power in the 10−50 c/d range. This is exactly the region in which the previously detected modes were found. This indicates that many additional modes similar to the ones detected previously are excited at small amplitude.

We can exclude the possibility that the large number of observed frequencies is erroneous because of imperfect prewhitening due to amplitude variability. We have examined this possibility in great detail, with literally thousands of different multifrequency solutions allowing for amplitude variability. In no case was it possible to significantly reduce the structure in the power spectrum of the residuals. In fact, the "best" multifrequency solution adopted treated the two colors as well as the 1992−1996 and 2002−2004 data separately and allowed annual amplitude variability of the dominant mode at 12.7162 c/d. Amplitude variability, therefore, cannot explain the excess power.

Consequently, the problem that the number of detected modes is much smaller than the number of predicted low-ℓ modes no longer exists, at least for FG Vir. Of course, we cannot conclude that each theoretically predicted mode is really excited and has been detected. This would require much more extensive mode identifications than are available at this stage.

In the previous discussion, we have concentrated on the low-ℓ modes which are easily observed photometrically. One also has to consider that at low amplitudes, variability from modes of higher ℓ values might also be seen photometrically.

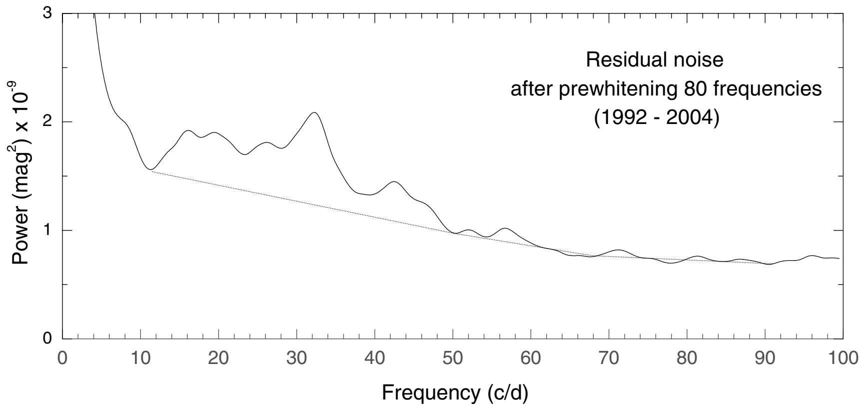

Fig. 6. Power of the residual noise of the 1992–2004 data after subtracting 80 (79) frequencies. (The additional frequency is the close doublet at 19.868 c/d adopted for the long time span.) The average amplitude in the amplitude spectrum was calculated for 2 c/d regions and squared to give power. The strong increase towards lower frequencies is caused by observational noise and standard in terrestrial photometry. Note the excess power in 10−50 c/d region, shown above the dotted curve. This shows that many additional pulsation modes exist in the same frequency region in which the already detected frequencies occur.

The geometric cancellation effects caused by the integration over the whole surface only become important for $\ell \geq 3$. This is shown by Daszyńska-Daszkiewicz et al. (2002), who calculated the amplitude reduction factors caused by temperature variations across the disk. From this paper we can roughly estimate a cancellation factor of ~50 in the y passband for $\ell = 3$ modes, implying that only the largest-amplitude modes could be photometrically detected. Such modes would have amplitudes similar to, or larger, than that of the observed dominant ($\ell = 1$) mode at 12.7162 c/d and might therefore be expected to be few. Regrettably, the situation is somewhat more complicated. The results presented in Fig. 2 of the Daszyńska-Daszkiewicz et al. paper are actually based on models with higher surface temperatures and could fit the β Cep variables. A. Pamyatnykh has kindly calculated specific models fitting the star FG Vir. Here the geometric cancellation factor becomes smaller by a factor of two or three. Consequently, some of the low-amplitude modes observed by us could also be $\ell = 3$ modes.

We conclude that the large number of detected frequencies as well as the large number of additional frequencies suggested by the power spectrum of the residuals confirms the theoretical prediction of a large number of excited modes. A mode-by-mode check for each predicted mode is not possible at this stage.

Acknowledgements. This investigation has been supported by the Austrian Fonds zur Förderung der wissenschaftlichen Forschung. The Spanish observations were supported by the Junta de Andalucía and the DGI under project AYA2000-1580. We are grateful to P. Reegen for help with the APT measurements, M. Viskum for providing a table of the individual measurements of the 1996 photometry not listed in his paper, A. A. Pamyatnykh and J. Daszyńska-Daszkiewicz for preliminary pulsation models, as well as W. Dziembowski and W. Zima for important discussions.

References

Breger, M., 1993, in Stellar Photometry – Current Techniques and Future Developments, ed. C. J. Butler, I. Elliott, IAU Coll., 136, 106
Breger, M., & Hiesberger, F. 1999, A&AS, 135, 547
Breger, M., & Pamyatnykh, A. A. 2002, ASP Conf Ser., 259, 388
Breger, M., Stich, J., Garrido, R., et al. 1993, A&A, 271, 482
Breger, M., Handler, G., Nather, R. E., et al. 1995, A&A, 297, 473
Breger, M., Zima, W., Handler, G., et al. 1998, A&A, 331, 271
Breger, M., Handler, G., Garrido, R., et al. 1999, A&A, 349, 225
Breger, M., Garrido, R., Handler, G., et al. 2002a, MNRAS, 329, 531
Breger, M., Pamyatnykh, A. A., Zima, W., et al. 2002b, MNRAS, 336, 249
Breger, M., Rodler, F., Pretorius, M. L., et al. 2004, A&A, 419, 695
Cox, J. P. 1984, PASP, 96, 577
Daszyńska-Daszkiewicz, J., Dziembowski, W. A., Pamyatnykh, A. A., et al. 2002, A&A, 392, 151
Dawson, D. W., Breger., M., & López de Coca, P. 1995, PASP, 107, 517
Dziembowski, W., Królikowska, M., 1990, Acta Astron., 40, 19
Frandsen, S., Pigulski, A., Nuspl, J., et al. 2001, A&A,376, 175
Garrido, R., & Poretti, E. 2004, ASP Conf. Ser., 310, 560
Garrido, R., Garcia-Lobo, E., & Rodriguez, E. 1990, A&A, 234, 262
Handler, G. 2004, ESA SP-538, 127
Lenz, P., & Breger, M. 2005, CoAst, in press
Li, Z.-P., Michel, E., Fox Machado, L., et al. 2004, A&A, 420, 283
Mantegazza, L., & Poretti, E. 2002, A&A, 396, 911
Mantegazza, L., Poretti, E., & Bossi, M. 1994, A&A, 287, 95
Mittermayer, P., & Weiss, W. W. 2003, A&A, 407, 1097
Moya, A., Garrido, R., & Dupret, M. A. 2004, A&A, 414, 1081
Ripepi, V., Marconi, M., Bernabei, S., et al. 2003, A&A, 1047, 2003
Strassmeier, K. G., Boyd, L. J., Epand, D. H.,& Granzer, T. H. 1997, PASP, 109, 697
Viskum, M., Kjeldsen, H., Bedding, T. R., et al. 1998, A&A 335, 549
Zima, W., Heiter, U., Cottrell, P. L., et al. 2003, in Asteroseismology across the HR Diagram, ed. M. J. Thompson, M. S. Cunha, M. J. P. F. G. Monteiro (Kluwer Academic Publishers), 489

2.4 Other seismically interesting δ Scuti stars

2.4.1 30+ frequencies of the δ Scuti star 4 Canum Venaticorum. Results of the 1996 multisite campaign

Original paper:

M. Breger, **G. Handler,** R. Garrido, N. Audard, W. Zima, M. Paparó, F. Beichbuchner, Z.-P. Li, S.-Y. Jiang, Z.-L. Li, A.-Y. Zhou, H. Pikall, A. Stankov, J. A. Guzik, M. Sperl, J. Krzesinski, W. Ogloza, G. Pajdosz, S. Zola, T. Thomassen, J.-E. Solheim, E. Serkowitsch, P. Reegen, T. Rumpf, A. Schmalwieser, M. H. Montogmery, 1999, A&A 349, 225

Astron. Astrophys. 349, 225–235 (1999)

ASTRONOMY AND ASTROPHYSICS

30+ frequencies for the δ Scuti variable 4 Canum Venaticorum: results of the 1996 multisite campaign

M. Breger[1], G. Handler[1], R. Garrido[2], N. Audard[1], W. Zima[1], M. Paparó[3], F. Beichbuchner[1], Li Zhi-ping[4], Jiang Shi-yang[4], Liu Zong-li[4], Zhou Ai-ying[4], H. Pikall[1], A. Stankov[1], J.A. Guzik[5], M. Sperl[1], J. Krzesinski[6], W. Ogloza[6], G. Pajdosz[6], S. Zola[6,7], T. Thomassen[8], J.-E. Solheim[8], E. Serkowitsch[1], P. Reegen[1], T. Rumpf[1], A. Schmalwieser[1], and M.H. Montgomery[1]

[1] Astronomisches Institut der Universität Wien, Türkenschanzstrasse 17, A-1180 Wien, Austria (breger@astro.univie.ac.at)
[2] Instituto de Astrofisica de Andalucia, CSIC, Apdo. 3004, E-18080 Granada, Spain
[3] Konkoly Observatory, Box 67, H-1525 Budapest XII, Hungary
[4] Beijing Observatory, Academy of Sciences, Beijing, P.R. China
[5] Los Alamos National Laboratory, XTA, MS B220, Los Alamos, NM 87545, USA
[6] Mt. Suhora Observatory, Cracow Pedagogical University, PL-30-083 Cracow, Poland
[7] Jagiellonian University, U1. Orla 171 PL-30-244 Cracow, Poland
[8] Department of Physics, University of Tromsø, N-9037 Tromsø, Norway

Received 8 April 1999 / Accepted 9 July 1999

Abstract. The evolved δ Scuti variable 4 CVn was observed photometrically for 53 nights on three continents. We found a total of 34 significant and 1 probable simultaneously excited frequencies. Of these, 16 can be identified as linear combinations of other frequencies. All significant frequencies outside the 4.5 to 10 cd^{-1} (52 to 116 μHz) range can be identified with frequency combinations, $f_i \pm f_j$, of other modes with generally high amplitudes. There exists a number of closely spaced frequencies with separations of $\sim$ 0.06 cd^{-1}. This cannot be explained in terms of amplitude variability.

The results show that even for stars on and above the main sequence other than the Sun, a very large number of simultaneously excited nonradial oscillations can be detected by conventional means.

Since all pulsation modes with photometric amplitudes of 1 mmag or larger have now been detected for this star, a presently unknown mode selection mechanism must exist to select between the 1000+ of low-degree modes predicted to be excited for this (and many other) stars.

Phase differences and amplitude ratios between the y and v colors are determined for the ten main modes. The phase differences indicate p_1 to p_4 modes of ℓ = 1 for four of these modes.

The formulae to determine the uncertainties in the amplitudes and phases of sinusoidal fits to observational data are derived in the Appendix.

Key words: stars: variables: δ Sct – stars: oscillations – stars: individual: AI CVn – stars: individual: 4 CVn

1. Introduction

The δ Scuti variables pulsate with a large number of simultaneously excited radial and nonradial modes, which makes them well-suited for asteroseismological studies. The amplitudes of the more dominant modes in the typical δ Scuti star are a few millimag, which is much higher than found in the Sun. It is now possible for ground-based telescopes to detect a large number of simultaneously excited modes with millimag amplitudes in stars other than the Sun. Because photometric studies measure the integrated light across the stellar surface, they can detect low-degree modes only. These studies require hundreds of telescope hours at observatories spread around the world in order to reduce aliasing caused by observing gaps and to lower the noise level in the power spectra.

The Delta Scuti Network (DSN) is engaged in a long-term program to determine the multifrequency structure of selected δ Scuti stars situated in different parts of the classical instability strip. These stars include 4 CVn (cool, evolved), BI CMi (cool, less evolved), FG Vir (center), XX Pyx (hot, unevolved) and θ^2 Tau (hot, evolved).

The star 4 CVn is of particular interest for a number of reasons: (i) The star is highly evolved ($\log\ g$ = 3.5 $\pm$ 0.1 at $T_{\rm eff}$ = 6900 ± 100K) for a δ Scuti variable and is on its way to the giant branch. For these stars, a very dense forest of excited modes is predicted (Dziembowski & Krolikowska 1990). (ii) The star exhibits amplitude variability with a typical time scale of years, but some rapid changes are also known. An example is the rapid change of the amplitude of the 7.38 cd^{-1} mode between 1974 and 1976. (iii) The amplitude variability may be connected with transferring power between different modes through resonances. In this respect, a study of combination frequencies, $f_i \pm f_j$, is important.

Send offprint requests to: M. Breger

Table 1. Journal of photoelectric measurements of 4CVn

Start HJD	Length hours	Obs.	Start HJD	Length hours	Obs.
116.71	6.39	McD	153.09	6.43	XL
117.88	3.97	McD	154.39	1.91	SNO
118.73	7.68	McD	154.65	8.97	McD
119.70	8.31	McD	155.65	8.86	McD
120.48	1.46	Suh	157.64	9.16	McD
121.71	8.08	McD	158.64	9.10	McD
122.73	7.62	McD	159.11	5.19	XL
123.48	2.49	Suh	159.36	4.29	Skib
123.81	5.47	McD	159.64	9.34	McD
127.72	7.62	McD	160.17	4.60	McD
128.68	6.60	McD	160.34	9.21	SNO
139.47	4.83	Pisz	161.01	8.18	XL
140.32	8.12	Pisz	161.35	5.93	Suh
141.35	6.01	Pisz	161.57	1.55	SNO
142.32	8.24	Pisz	162.48	5.76	SNO
143.21	3.73	XL	162.69	7.76	McD
144.14	5.77	XL	163.64	8.91	McD
145.12	6.54	XL	164.34	5.46	SNO
146.21	4.07	XL	164.80	2.81	McD
147.66	5.11	McD	165.93	2.00	McD
151.09	6.93	XL	168.69	6.22	McD
151.40	5.89	Pisz	170.33	7.34	SNO
151.68	8.26	McD	170.66	6.24	McD
152.09	7.40	XL	171.35	5.82	SNO
152.33	7.34	Skib	171.38	3.29	Suh
152.33	5.28	Pisz	171.88	2.60	McD
152.63	8.78	McD			

McD: McDonald, Suh: Suhora, Pisz: Piszkéstető
XL: Xing Long, Ski: Skibotn, SNO: Sierra Nevada

The variability of 4 CVn (HR 4715 = HD 107904 = AI CVn, F3III–IV) was discovered by Jones & Haslam (1966). Subsequent period determinations based on observations of only a few nights each led to a large number of reported periods and solutions, usually in disagreement with each other. Extensive unpublished single-site photometry by Fitch and coworkers (Fitch 1980) showed the multiperiodicity, but did not present a consistent picture of this complex variability. The multisite campaign of the Delta Scuti Network carried out in 1983 and 1984 (Breger et al. 1990, hereafter called Paper I) revealed five frequencies of pulsation. A subsequent analysis of the previous published and unpublished data extended the number of frequencies to 7 and showed that the complex behavior of 4 CVn was caused by amplitude variability of pulsation modes with essentially constant frequencies (Breger 1990a, Paper II). A photometric study undertaken with the Vienna Automatic Photoelectric Telescope (APT) in Arizona covering 204 hours increased the number of detected frequencies to 19 (Breger & Hiesberger 1999, Paper III). 6 of the 19 were combination frequencies.

The present paper reports the results of a multisite photometric campaign carried out by the Delta Scuti Network on three continents and the considerable increase in the number of pulsation modes detected in 4 CVn.

2. New measurements

During 1996 February and March, 4 CVn was observed photometrically together with two comparison stars for 53 nights (325 hours) at six observatories. The following telescopes were used: McDonald Observatory 0.9m (observers Handler, Audard); Xing Long, China, 0.85m (observer Li Zhiping); Sierra Nevada Observatory, Spain, 0.9m (observers Garrido, Beichbuchner); Piszkéstető, Hungary, 0.5m (observers Paparó, Pikall, Stankov, Zima); Mt. Suhora, Poland, 0.6m (observers Ogloza, Pajdosz, Zola); and Skibotn, Norway, 0.5m (observer Thomassen). The dates of observation can be found in Table 1.

The three-star technique, in which measurements of the variable star are alternated with those of two comparison stars, was adopted. With the three-star technique adopted by the Delta Scuti Network, the required high photometric accuracy is achieved by alternating measurements of the variable star with those of two carefully chosen comparison stars. The same photometric channel is used for all three measurements. The procedure can produce the required long-term stability of 2 mmag or better (also within different observatories), but yields a variable-star measurement only every five minutes. The technique works well for periods between 30 minutes and several days and has been described by Breger (1993).

The two comparison stars, HR 4843 (F6IV) and HR 4728 (G9III), have been used before as comparison stars. No evidence for any variability has been found. At McDonald and Sierra Nevada Observatories the measurements were made through the Stromgren v and y filters to provide a relatively large baseline in wavelength. The large baseline is needed to determine reliable phase differences (see Sect. 4) and cannot achieved with the b filter. The u filter was also not chosen because of the very large potential for systematic observational errors. At the other observatories, only the Johnson V filters was used, which has the same effective wavelength as the Stromgren y filter.

The resulting light curves are shown in Fig. 1, where the observations can also be compared with the fit to be derived in the next section.

3. Detection of the pulsation frequencies

The pulsation frequency analyses were performed with a package of computer programs with single-frequency and multiple-frequency techniques (programs PERIOD, Breger 1990b; PERIOD98, Sperl 1998), which utilize Fourier as well as multiple-least-squares algorithms. The latter technique fits a number of simultaneous sinusoidal variations in the magnitude domain and does not rely on prewhitening. For the purposes of presentation, however, prewhitening is required if the low-amplitude modes are to be seen. Therefore, the various power spectra are presented as a series of panels, each with additional frequencies removed relative to the panel above.

One of the most important questions in the examination of multiperiodicity concerns the decision as to which of the detected peaks in the power spectrum can be regarded as variability intrinsic to the star. Due to the presence of nonrandom errors in photometric observations and because of observing gaps, the

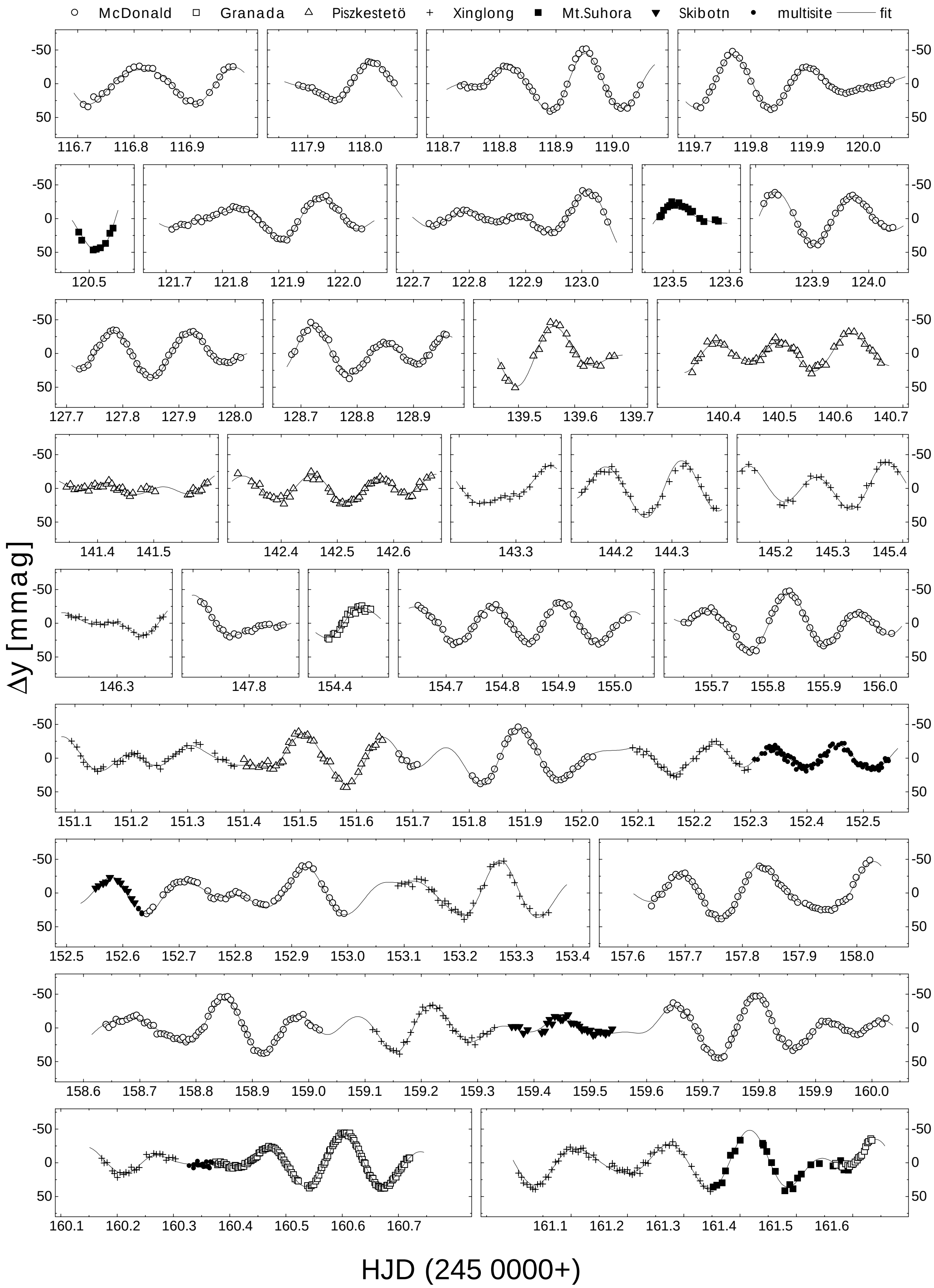

Fig. 1. Multisite photoelectric three-star-photometry of 4 CVn obtained during the 1996 DSN campaign. Δy and Δv are the observed magnitude differences (variable – comparison stars) normalized to zero in the narrowband $uvby$ system. The fit of the 34-frequency solution derived in this paper is shown as a solid curve. Note the excellent agreement between the measurements and the fit

predictions of standard statistical false-alarm tests give answers which we consider to be overly optimistic. In a previous paper (Breger et al. 1993) we argued that a ratio of amplitude signal/noise = 4.0 provides a useful criterion for judging the re-

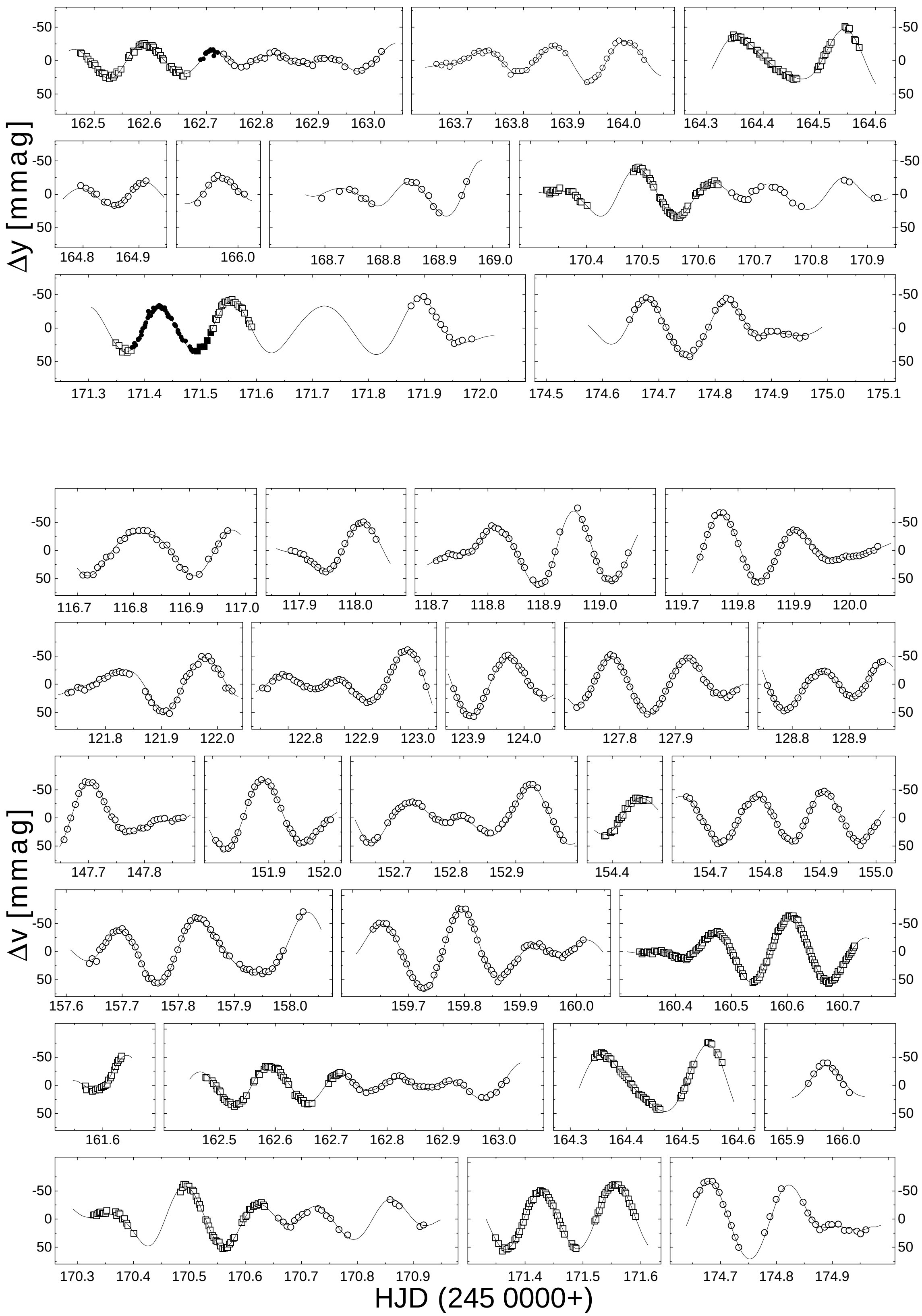

Fig. 1. (continued)

ality of a peak. This empirically determined limit now has some theoretical underpinning (Kuschnig et al. 1997).

For peaks at harmonics or combination frequencies, we must relax the criterion. The reason is the statistically different ques-

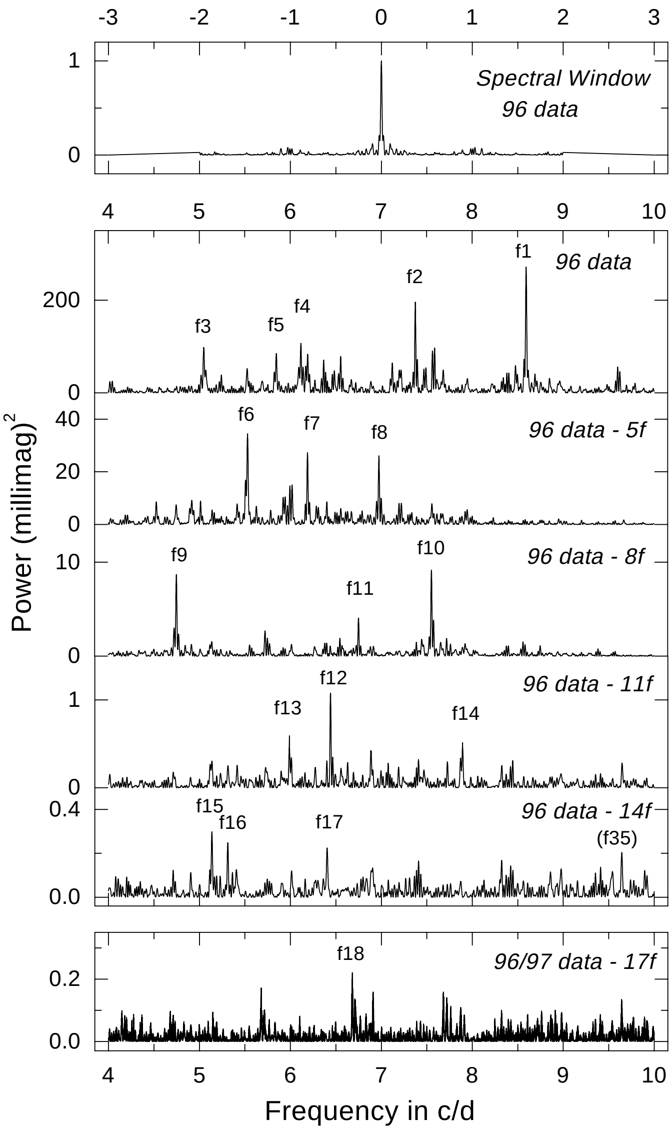

Fig. 2. Power spectrum of 4 CVn in the 4 to 10 cd^{-1} range, where the main pulsation frequencies are situated. The spectra based on the 1996 v and y data are shown before and after applying multiple frequency solutions. See text for the numbering scheme and a discussion of significance levels

tion asked. In a general search we must consider the occurrence of even a single accidental peak among a large number of possible frequencies from 0 to the Nyquist frequency, f_n. For known frequency values (such as combination frequencies), we only have to consider the possibility of an accidental peak occurring in a narrow frequency range near the expected combination frequency. In the following paragraph, we provide a rough estimate of the significance criterion for combination frequencies which should have the same false alarm probability as the 4.0 criterion does for the identification of general frequencies.

For the present case, using the first 18 frequencies we have $18^2 = 324$ potential combination peaks, and in the neighborhood of each expected peak we examine a frequency range of length $2\sqrt{2}\sigma = 0.0028$ cd^{-1} ($\sigma = 0.001$ cd^{-1} is taken to be a representative error bar for frequencies determined in the 1996 campaign). We are thus examining a total frequency range of $324 \cdot 0.0028$ cd$^{-1} = 0.907$ cd^{-1}. According to Scargle (1982), the significance level z_0 (signal to noise ratio in *power*) for detection scales like

$$z_0 = \text{const.} + \ln(N),$$

where N is the number of independent frequencies searched. Clearly, N is proportional to the frequency range considered, so for a subset Δf of the total frequency range we can write

$$z_0 = 12.57 + \ln(\Delta f / f_n),$$

where $f_n \approx 120$ cd^{-1} is the Nyquist frequency; for $\Delta f = f_n$, we have $z_0 = 12.57$, where the value of this constant has been chosen so as to yield our empirically chosen cutoff of 4.0 when translated back into amplitude ($2\sqrt{z_0/\pi} = 4.0$). If we instead set $\Delta f = 0.907$ cd^{-1}, in order to search for combination frequencies, we find $z_0 \approx 7.7$, which implies a signal to noise in amplitude of ≈ 3.1. For the present analysis, we have chosen to use the more conservative value of 3.5 for our significance criterion; various tests with the present data set involving randomly selected frequency combinations suggest that this value provides a very strict detection criterion.

The amplitude signal/noise values listed in Table 2 refer to formally computed values from the combined y and v data set. Because of slight phase shifts between different colors, the true detection significance is probably higher, e.g. a phase shift of 6.5 degrees between y and v leads to an underestimate of the shifted amplitude of 7.2% of its value. For the modes with possible amplitude variability, the S/N values of the detection were computed from the combined 1996/7 data sets and are shown in italics. The noise was calculated by averaging the amplitudes (oversampled by a factor of 20) over 3 cd^{-1} regions centered around the frequency under consideration. In the low-frequency 0–4 cd^{-1} range, the value from 0.5 to 4 cd^{-1} was computed. These fairly large frequency regions make the detection criterion relatively insensitive to isolated peaks in the power spectrum.

For the frequency detection, we combined the y (2164 measurements) and v data (1185 measurements). The dependence of the pulsation amplitude on wavelength was compensated by multiplying the v data set by an experimentally determined factor of 0.66. This scaling also offsets the higher noise level of the v data in the frequency region under consideration. After the 1996 data were analyzed up to the noise level, the analysis was repeated by adding the measurements from 1997 (Paper III) and weighting according to the length of coverage (1996: 335 hours, 1997: 204 hours). This allowed the detection and confirmation of the pulsation modes with variable amplitudes between the two years. Furthermore, the increased time base made it possible to determine more accurate frequency values, which may, however be afflicted by annual aliasing of ± 0.0026 cd^{-1}.

Note that different colors and data sets were only combined to detect the frequencies and to determine the significance of the detection. The amplitudes listed in Table 2 were calculated with separate solutions for each color. If we assume completely random photometric errors, the expected uncertainties in the

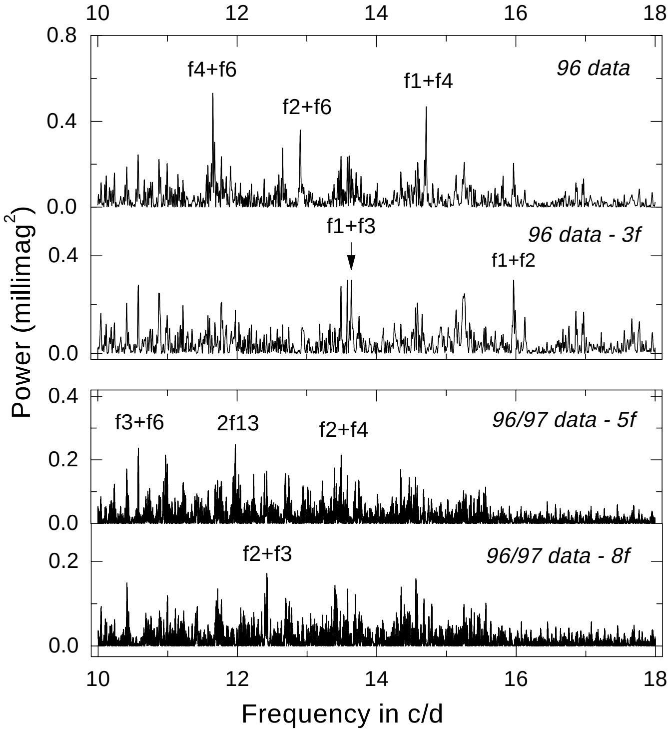

Fig. 3. Power spectrum of 4 CVn in the high-frequency range. The highest nine peaks can be matched exactly by expected combination frequencies, f_i+f_j

values of the derived amplitudes can be calculated from the residuals of the two photometric data sets. The equation used and the derivation is shown in the Appendix. The uncertainties $\sim$ 0.1 mmag are shown in Table 2.

Anticipating the results, we divide the frequency spectrum into three separate regions based on the nature of the peaks in the power spectrum.

3.1. The main pulsation frequencies

The main pulsation frequencies of 4 CVn are found in the region of 4 to 10 cd^{-1}. Fig. 2 and Table 2 show the results of the multiperiod analysis: 18 statistically significant and one additional promising peak are found. All modes with photometric amplitudes $\sim$ 1 mmag or larger have been detected. A formal limit of 0.5 mmag, corresponding to an amplitude signal/noise limit of 4.0, is derived. The power spectrum of the residuals suggests that additional modes with small amplitudes are excited as well.

An interesting feature of the results concerns a number of closely spaced frequencies: 6.190 and 6.117 cd^{-1}, 6.750 and 6.680 cd^{-1} (see below), and 6.440 and 6.404 cd^{-1}. Before one accepts these detected frequencies as separate pulsation modes, one needs to eliminate the possibility of a single frequency with amplitude variability. Such numerical tests are included in the reduction packages, PERDET and PERIOD98, used in the present investigation. These tests show that such a single-frequency fit with a variable amplitude cannot reproduce the observed behavior.

3.2. The high-frequency region: Combination frequencies

We now turn to the frequency range above 10 cd^{-1}. Fig. 3 shows the existence of a number of peaks in the 1996 data, which was analyzed in the same manner as for the 4–10 cd^{-1} range. The five main peaks can be immediately identified with combination frequencies, f_i+f_j. The agreement cannot be accidental since the values of these expected frequencies are quite accurate to $\pm$0.001 cd^{-1}. Four of these five peaks were already known from the analysis of the 1997 APT data (Paper III).

The 1996 data also show additional promising peaks. Some of these peaks become statistically significant once the 1997 data are included in the analysis. Altogether we find eight combination frequencies.

The peak at 11.9729 cd^{-1}, which has higher amplitude in the 1997 than in the 1996 data, may be related to f_{13} at 5.98647 cd^{-1}. The formal multifrequency solution indicates a frequency ratio of 1.99999. This indicates exact doubling if the uncertainties in the frequency determinations are considered. The probability of an accidental agreement is small. In principle, a frequency match with f_4+ f_5, which occurs at 11.9674 cd^{-1}, is also possible, although the frequency resolution of the combined 1996/7 data may exclude this. Since f_4+f_5 only has about half the power of the 2. f_{13} identification, we regard the 2. f_{13} identification as the more probable one.

The existence of a 2f term is not unusual in variable stars of large amplitude and indicates a light curve which is not strictly sinusoidal. While this usually occurs for modes of high amplitude, the observed photometric amplitude of f_{13} is very small ($\sim$ 1 mmag). It is possible to argue that f_{13} is an ℓ = 3 or 4 mode with a large physical amplitude, which only appears small due to a large geometric reduction factor. Using formulae given in Dziembowski (1977), we find, for models appropriate to 4 CVn, that an ℓ = 3 mode would have in general only about 10% the observed amplitude of an ℓ = 1 mode, if both modes are assumed to have the same physical amplitude. In principle, f_{13} could therefore be a high-amplitude, intermediate-ℓ mode, for which nonlinear distortion effects could produce a 2f term. In this case, the surface flux perturbations associated with the harmonic would not (for $\ell \neq 0$) have the same spherical harmonic structure as the original mode, and thus might well experience less geometrical cancellation (Brassard et al. 1995). However, this explanation is somewhat contrived. Another perhaps more plausible explanation is simply a resonance: due to a resonance, f_{13} excites another p-mode at exactly twice its frequency value.

3.3. The low-frequency region: Combination frequencies

In the frequency region of 0 to 4 cd^{-1} we expect to find g modes as well as combinations of the pulsation modes, f_i–f_j. This is also the region in which the observational uncertainties may become larger, both due to the 1/f dependence of atmospheric effects as well as residual extinction and zero-point difficulties.

The results at low frequencies are similar to those at high frequencies: the dominant peaks are combination frequencies. Fig. 4 shows that the six dominant peaks can be identified with

Table 2. The frequency spectrum of 4 CVn in 1996

Frequency cd^{-1}	μHz/ID	Amplitude 1996 y filter mmag	v Filter mmag	Significance Ampl. S/N
Significant frequencies		$\pm$ 0.09	$\pm$ 0.11	
f_1, 8.595	99.48	15.3	22.9	118
f_2, 7.375	85.36	11.6	17.4	96
f_3, 5.048	58.42	10.7	16.4	95
f_4, 6.117	70.80	9.2	14.3	83
f_5, 5.851	67.72	10.1	15.0	90
f_6, 5.532	64.03	6.4	10.1	57
f_7, 6.190	71.64	5.7	8.1	51
f_8, 6.976	80.75	5.0	7.4	45
f_9, 4.749	54.96	3.2	4.9	27
f_{10}, 7.552	87.41	3.3	4.9	26
f_{11}, 6.750	78.13	0.9	1.6	9
f_{12}, 6.440	74.54	1.6	2.4	14
f_{13}, 5.986	69.29	0.8	1.4	7.7
f_{14}, 7.896	91.39	0.8	0.9	6.6
f_{15}, 5.134	59.42	0.8	1.1	6.8
f_{16}, 5.314	61.51	0.8	1.0	5.8
f_{17}, 6.404	74.12	0.4	1.3	5.1
f_{18}, 6.680	77.32	0.2	0.5	*5.1*
f_{19}, 11.649	$= f_4 + f_6$	0.7	1.4	6.2
f_{20}, 14.712	$= f_1 + f_4$	0.7	1.0	5.4
f_{21}, 12.907	$= f_2 + f_6$	0.4	0.5	4.1
f_{22}, 15.970	$= f_1 + f_2$	0.6	0.7	4.2
f_{23}, 13.643	$= f_1 + f_3$	0.5	0.6	3.6
f_{24}, 10.580	$= f_3 + f_6$	0.6	0.8	4.4
f_{25}, 11.973	$= 2f_{13}$	0.4	0.5	*4.1*
f_{26}, 13.492	$= f_2 + f_4$	0.5	0.6	3.6
f_{27}, 12.423	$= f_2 + f_3$	0.3	0.3	*3.7*
f_{28}, 3.063	$= f_1 - f_6$	0.6	0.9	4.6
f_{29}, 1.069	$= f_4 - f_3$	0.5	1.0	4.4
f_{30}, 2.327	$= f_2 - f_3$	0.2	0.4	*4.2*
f_{31}, 1.258	$= f_2 - f_4$	0.6	0.5	4.0
f_{32}, 1.929	$= f_8 - f_3$	0.5	0.5	3.9
f_{33}, 1.185	$= f_2 - f_7$	0.3	0.5	3.8
f_{34}, 1.220	$= f_1 - f_2$	0.5	0.5	3.5
Probable frequencies				
f_{35}, 9.645	111.63	0.6	0.6	3.8
Residuals, single msmt.		3.0	2.7	

known values from combination frequencies. The matches are exact. A seventh frequency at 2.327 cd^{-1} = f_2–f_3, previously found in the 1997 data (Paper III), had very small amplitudes during 1996. More details can be found in Table 2.

Near 1.2 cd^{-1} a triple peak is found and three closely spaced combination modes can be identified. The detection of the three modes is significant and should be correct. However, due to the frequency separation of only $\sim$ 0.04 cd^{-1}, the amplitudes of those three modes listed in Table 2 may be uncertain. Such an uncertainty in the v amplitude also exists for the f_{29} at 1.069 cd^{-1} due to the closeness of the frequency to 1 cd^{-1} and the relatively small data set.

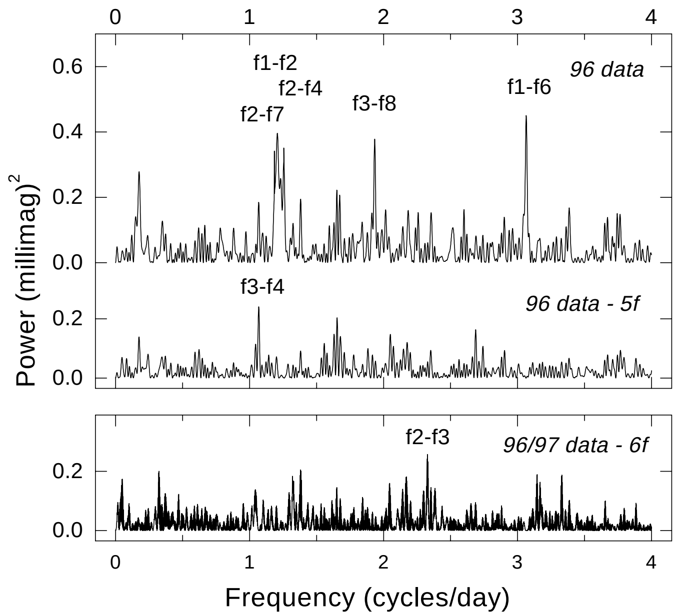

Fig. 4. Power spectrum of 4 CVn for the low-frequency range. The seven highest and significant peaks can be identified with mode combinations, f_i–f_j

Table 3. Phase differences of 4 CVn

	Frequency cd^{-1}	Amplitude ratio v/y	Phase differences in degrees $\phi_v - \phi_y$
f_1	8.595	1.492 $\pm$ 0.007	–2.0 $\pm$ 0.3
f_2	7.375	1.508 $\pm$ 0.010	–2.3 $\pm$ 0.4
f_3	5.048	1.530 $\pm$ 0.011	–1.9 $\pm$ 0.4
f_4	6.117	1.534 $\pm$ 0.012	–4.5 $\pm$ 0.5
f_5	5.851	1.484 $\pm$ 0.012	–6.8 $\pm$ 0.4
f_6	5.532	1.61 $\pm$ 0.02	–4.8 $\pm$ 0.8
f_7	6.190	1.49 $\pm$ 0.02	–2.0 $\pm$ 0.8
f_8	6.976	1.50 $\pm$ 0.02	+1.2 $\pm$ 0.9
f_9	4.749	1.61 $\pm$ 0.04	–1.3 $\pm$ 1.6
f_{10}	7.552	1.43 $\pm$ 0.03	–5.1 $\pm$ 1.1

We note that the pulsation frequencies involved in the detectable combinations, f_i–f_j, are those with high amplitudes. We will return to a more detailed analysis of which modes form interactions and the possible time variability of these components in a later section.

We note that all pulsation modes with photometric amplitudes of 1 mmag or larger excited during the years 1996 and 1997, should have been detected for this star. However, theoretical modelling has predicted the presence of 1000+ of unstable low-degree modes predicted to be excited in 4 CVn (Dziembowski 1997). Since the number of detected modes is relatively small, a presently unknown mode selection mechanism must exist to select between these modes.

3.4. Comparison between the 1996 and 1997 results

The multisite campaign reported in this paper was more extensive than the single-site set observations carried out during 1997

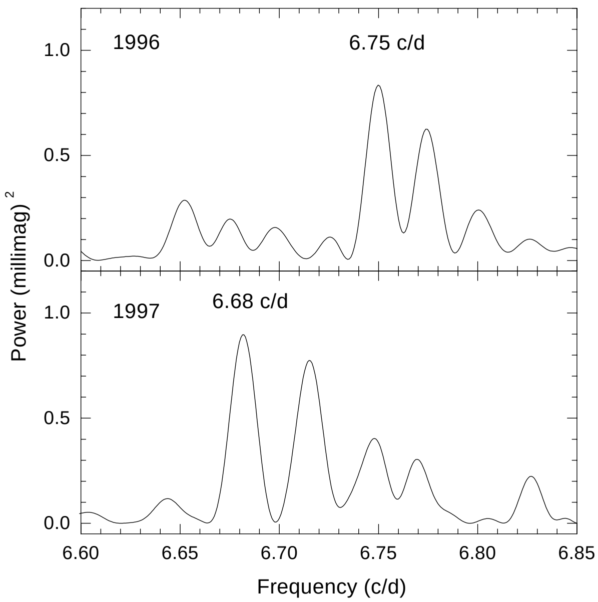

Fig. 5. The change of the modes around 6.7 cd^{-1} between 1996 and 1997. The power spectrum of the residuals after multifrequency solutions without the two modes near 6.7 cd^{-1} are shown. The width of the individual peaks also indicates that the 6.68 and 6.75 cd^{-1} peaks cannot be the same peak affected by insufficient frequency resolution

using the APT. Consequently, the number of frequencies discovered could be extended considerably: from 19 to 34. For most detected modes, the results for the two years are in excellent agreement with each other. This verifies that the significance criterion leads to reliable results.

The amplitudes of the different modes found for 1996 and 1997 also are very similar and generally within the precision limits of determining these amplitudes. This is not surprising, since the amplitude variability of 4 CVn generally occurs with time scales of 10 years or more (Paper II).

We will now discuss a few interesting modes for which the results differed for the two years:

(i) For 1996 a frequency at 6.75 cd^{-1} was found, free of 1 cd^{-1} aliasing. The 1997 data showed a value of 6.68 cd^{-1} (or 5.68, 7.68 cd^{-1}). Could these two peaks correspond to the same mode? The frequency resolution for the two years is considerably higher than the separation of the two peaks. In order to examine the separation in more detail, we computed full multifrequency solutions without these two modes for both years. This method discriminates against these two modes since aliasing causes some power to be picked up by other pulsation modes. Nevertheless, both modes were still present. This is demonstrated in Fig. 5, which shows the power spectra in this region for the two years. We have also tested the hypothesis that an unknown phenomenon causes the frequency to drift by 0.07 cd^{-1} in one year. The data sets cover 58 and 69 days, respectively. Such a frequency drift should be visible within the two data sets. No frequency drift was found. Note that the precision of the measurements is insufficient to detect amplitude drifts of a few tenths of a millimag within the annual data. We conclude that the two modes are real and show amplitude variability between 1996 and 1997.

(ii) The amplitude of the dominant mode of pulsation, f_1, increased by 12% from 1996 to 1997 (12.3% in y, 12.6% in v: the difference between the two colors is not significant). This small change is not unusual and was also observed in the time period 1974–1978 (Paper II).

(iii) The amplitudes of the combination frequencies can also be variable. The best example is provided by the pair, f_2+f_3 and f_2-f_3. Both combinations increased from the level of detectability in 1996 to about 1 mmag in 1997. The fact that both varied similarly argues in favor of an astrophysical, rather than observational, origin. It is a fascinating speculation that the behavior may be related to the fact that f_2 is one of the modes with the most rapid amplitude variability.

4. Phase differences and amplitude ratios between v and y

The study of asteroseismology requires detailed pulsation mode identifications: the pulsational quantum numbers (n, ℓ, m) need to be determined. One of several promising methods uses the sizes of the observed phase differences between the light curves at different wavelength (e. g. Watson 1988, Garrido et al. 1990), since the sizes of the phase differences are a function of ℓ. The method has been applied successfully before (e. g. the star FG Vir, Breger et al. 1999). The application to 4 CVn requires accurate observational determinations as well as detailed model calculations. While the theoretical modelling is the subject of a later paper, here we can derive the measured values. We note that high photometric precision is needed to determine these reliably.

Due to a number of potential sources of error, the determination of the phase differences from the observational data is not straightforward. In order to avoid systematic errors caused by the (small) amplitude variability between 1996 and 1997, separate multifrequency solutions need to be made for the two years. This leads to a large number of degrees of freedom associated with 34 frequencies and 4 data sets (two colors each for 1996 and 1997). While the mode detections are statistically significant, for most modes with small amplitudes, the derived phase differences between v and y are not meaningful. In fact, only for the ten modes with the highest amplitudes do we regard the differences as significant.

A preliminary analysis indicated an average amplitude ratio of v/y = 1.51 and phase differences, $\phi_v - \phi_y$, near zero. This suggests how the number of degrees of freedom can be reduced: for the many modes with small amplitudes, f_{11} to f_{34}, an amplitude ratio of 1.51 and zero phase difference were assumed. For the ten modes with relatively large amplitudes, the phase differences and amplitude ratios were computed and shown in Table 3. Numerical simulations with different noise levels confirmed that this conservative approach is reasonable.

The expected uncertainties in the values of the derived phase differences and amplitude ratios can now be calculated from the residuals of the four photometric data sets. For the 1996 data, the observational details have been discussed in the previous section. For the 1997 APT data we find formal values of amplitude uncertainties, σ(a), of 0.074 mmag in y and 0.079 in v (see the Appendix for the equations). Finally, the statistical uncertainties of the amplitude ratios and phase differences were computed with standard error propagation relations and are listed in Table 3. We note again that these values are the formal uncertainties based on the assumption of random observational noise with no correlation between the four different data sets. Two deviations from the assumption likely to be present are the similar noise behavior of the two colors obtained almost simultaneously and the effect of unresolved additional frequencies. Both effects would cause us to $overestimate$ the size of the true errors.

The application of the derived phase differences for mode identifications is beyond the scope of this paper and requires the computation of specific pulsation models, which has only been started at this time. However, some important, tantalizing observation can already be made: Four frequencies (f_3, f_7, f_2 and f_1) show essentially identical phase differences near –2.1 degrees. The spacings of these frequencies are 1.14, 1.18 and 1.22 cd^{-1}, respectively, which correspond to adjacent radial orders for 4 CVn. Preliminary calculations indicate p_1, p_2, p_3 and p_4 modes of ℓ = 1.

5. Combination frequencies

The present study has detected a large number of combination frequencies in both the low- and high-frequency domains. The modes involved in the combinations are those with high amplitudes. A scaling of the amplitudes involved indicates that the low-amplitude modes could also be coupled, but would lead to combination amplitudes too small to be detected. There does not exist a one-to-one relationship between the amplitudes of the combination and the main frequencies involved in the combinations. This is not surprising because the measured photometric amplitudes refer to the integrated brightness change across the stellar disk and not the true pulsational amplitude. Since the combination frequencies may have a different angular dependence than the parent modes (e.g. see Dziembowski 1982), they will experience a different amount of geometric cancellation.

As shown in Garrido & Rodriguez (1996), it is possible to estimate phases and amplitudes of the combination terms in a high-amplitude radially pulsating star. The method takes into account the information contained in the harmonic series to predict the combinations terms. The analysis for 4 CVn shows no harmonic high enough to be significant, except for the exceptional case of f13. It could be interesting to apply the results found for the radial modes of SX Phe by Garrido & Rodriguez to this star in order to confirm the nonradial nature of the modes exhibited by 4 CVn. A detailed comparison will be the subject of the next paper on this star.

The following modes were most often involved in forming combinations with detectable amplitudes: f_2 and f_3 (each 7 times), f_1 and f_4 (each 5 times) and f_6 (4 times). Note that no combination frequencies were detected for f_5, which also shows a high amplitude in integrated light. Other interesting properties are:

(i) The amplitudes of the combination frequencies can vary strongly from year to year. This is not accompanied by large amplitude variations of the main pulsation modes involved in the combination frequencies. An example is the combinations of f_2 and f_3, which changed their amplitudes by more than a factor of 3 between 1996 and 1997. The fact that both f_2+f_3 and f_2–f_3 changed similarly argues against a possible explanation in terms of observational errors.

(ii) The amplitudes of f_i+f_j and f_i–f_j are often, but not always, similar in size. An example is provided by the peak at 11.649 cd^{-1}=f_4+f_6, which is the most dominant combination frequency found in this study. The corresponding peak in the power spectrum of f_4–f_6 is not seen, although it should have been easily detected.

(iii) The present study has detected about twice as many sums of frequencies as differences. This result is probably an observational artifact because of the lower observational noise at high frequencies.

Acknowledgements. It is a pleasure to thank Alosha Pamyatnykh and Paul Bradley for stimulating discussions. This investigation has been supported by the Austrian Fonds zur Förderung der wissenschaftlichen Forschung, project number S7304. The observers were partially supported by the following grants: Polish National Committee for Scientific Research Grant 2-2109-91-02, the Chinese National Natural Science Foundation, Hungarian research grant OTKA No. T02528, and NASA Astrophysics Theory grant S-398340-F.

Appendix A: derivation of the uncertainties in the amplitude and phase in photometric data

Suppose we have N measurements of the magnitudes, m_i, at times t_i. We assume that the times of the observations are error free, but that the brightness measurements m_i are subject to random errors, Δm_i, which have an average of zero, a constant root-mean-square amplitude, and are not correlated in time. Mathematically, we write these conditions as

$$\begin{aligned} \langle \Delta m_i \rangle &= 0, \\ \langle \Delta m_i \Delta m_j \rangle &= \langle (\Delta m_i)^2 \rangle \delta_{ij} \\ &= \sigma^2(m) \delta_{ij}, \end{aligned} \tag{A1}$$

where the brackets $\langle\rangle$ denote a statistical average, and δ_{ij} is the Kronecker δ, which is equal to 1 if $i = j$ and is 0 otherwise.

In order to analyze our time series data, we wish to fit a sinusoid to it. Specifically, we fit the function

$$f(t) = a_0 + a \sin(\omega t_i + \phi), \tag{A2}$$

where for the purposes of this derivation the frequency ω is assumed to be known, but where the amplitude a and phase ϕ are yet to be determined; this situation is encountered, for example, if one has data from previous observations which tightly constrain a known frequency, and one wishes to solve for the amplitude and phase of the signal in the current data set. The parameter a_0 represents a constant offset, and can be related to the mean value of the signal, as we show below. We define

$$\begin{aligned}\chi^2 &\equiv \sum_{i=1}^{N}[m_i - f(t_i)]^2 \\ &= \sum_{i=1}^{N}[m_i - a_0 - a\sin(\omega t_i + \phi)]^2 \,, \end{aligned} \qquad \text{(A3)}$$

where the minimum in χ^2 corresponds to the best fit solution of the model parameters.

Minimizing χ^2 with respect to a_0, a, and ϕ, we obtain the following three relations:

$$\frac{\partial\chi^2}{\partial a_0} = 0 \;\Rightarrow a_0 = \frac{1}{N}\sum_{i=1}^{N} m_i \qquad \text{(A4)}$$

$$\frac{\partial\chi^2}{\partial a} = 0 \;\Rightarrow a = \frac{2}{N}\sum_{i=1}^{N} m_i\sin(\omega t_i + \phi) \qquad \text{(A5)}$$

$$\frac{\partial\chi^2}{\partial \phi} = 0 \;\Rightarrow 0 = \sum_{i=1}^{N} m_i\cos(\omega t_i + \phi), \qquad \text{(A6)}$$

where we have assumed that the time series is of such a length that the relations $\sum_{i=1}^{N}\sin^2(\omega t_i + \phi) = N/2$ and $\sum_{i=1}^{N}\sin(\omega t_i + \phi)\cos(\omega t_i + \phi) = 0$ are valid.

In general, the random errors in magnitude, Δm_i, produce small variations in the fit parameters $(\Delta a, \Delta\phi)$ from their "true" values. If we take a total differential of Eq. A5 with respect to (m_i, a, ϕ), then we obtain

$$\begin{aligned}\Delta a &= \frac{2}{N}\sum_{i=1}^{N}[\Delta m_i\sin(\omega t_i+\phi) + m_i\cos(\omega t_i+\phi)\Delta\phi] \\ &= \frac{2}{N}\sum_{i=1}^{N}\Delta m_i\sin(\omega t_i+\phi), \end{aligned} \qquad \text{(A7)}$$

where the second term has vanished through the application of Eq. A6. If we square this expression and then take a statistical average, we find

$$\begin{aligned}\langle(\Delta a)^2\rangle &= \frac{4}{N^2}\sum_{i=1}^{N}\sum_{j=1}^{N}\langle\Delta m_i\Delta m_j\rangle\sin(\omega t_i+\phi) \\ &\quad \sin(\omega t_j+\phi) \\ &= \frac{4}{N^2}\sum_{i=1}^{N}\langle(\Delta m_i)^2\rangle\sin^2(\omega t_i+\phi) \\ &= \frac{4}{N^2}\sigma^2(m)\sum_{i=1}^{N}\sin^2(\omega t_i+\phi) \\ &= \frac{2}{N}\sigma^2(m), \end{aligned} \qquad \text{(A8)}$$

where we have made use of the relations in A1. Writing $\sigma^2(a) = \langle(\Delta a)^2\rangle$, we have

$$\sigma(a) = \sqrt{\frac{2}{N}}\cdot\sigma(m), \qquad \text{(A9)}$$

which is the desired relation between photometric and amplitude uncertainties.

We now repeat this analysis for the phase ϕ. From Eq. A6, we have

$$0 = \sum_{i=1}^{N}[\Delta m_i\cos(\omega t_i+\phi) - m_i\Delta\phi\sin(\omega t_i+\phi)]\,, \qquad \text{(A10)}$$

which can be rewritten as

$$\Delta\phi\sum_{i=1}^{N} m_i\sin(\omega t_i+\phi) = \sum_{i=1}^{N}\Delta m_i\cos(\omega t_i+\phi). \qquad \text{(A11)}$$

Substituting the expression for a in Eq. A5, we have

$$\frac{N}{2}a\Delta\phi = \sum_{i=1}^{N}\Delta m_i\cos(\omega t_i+\phi). \qquad \text{(A12)}$$

Squaring both sides and taking averages, we find that

$$\begin{aligned}\langle(\Delta\phi)^2\rangle &= \frac{4}{N^2a^2}\sum_{i=1}^{N}\sum_{j=1}^{N}\langle\Delta m_i\Delta m_j\rangle\cos(\omega t_i+\phi) \\ &\quad \cos(\omega t_j+\phi) \\ &= \frac{4}{N^2a^2}\sigma^2(m)\sum_{i=1}^{N}\cos^2(\omega t_i+\phi) \\ &= \frac{2}{N}\frac{\sigma^2(m)}{a^2}. \end{aligned} \qquad \text{(A13)}$$

Setting $\sigma^2(\phi) = \langle(\Delta\phi)^2\rangle$, we finally arrive at

$$\sigma(\phi) = \sqrt{\frac{2}{N}}\frac{\sigma(m)}{a}, \qquad \text{(A14)}$$

which is the desired relation between the photometric error, the amplitude of the signal, and the error in the phase determination.

It is common among observers to express ϕ in degrees and to relate the uncertainties in amplitude and phase. The equation then becomes

$$\sigma(\phi) = 57.3\;\sigma(a)/a \qquad \text{(A15)}$$

If the star is multiperiodic, Eq. (A2) should be expanded for the different frequencies. If there are no (or only small) cross terms between the frequencies in the data, the uncertainties can be calculated by applying Eqs. (A9) and (A14) to each pulsation frequency separately.

The expressions derived in this appendix have been thoroughly tested by using the computer program codes of Bevington (1969) for a least-squares fit of an arbitrary function. These programs were applied to a multiperiodic solution of the present data set of 4 CVn. Full agreement with the numbers calculated from the formulae derived above was obtained.

References

Bevington P.R., 1969, In: Data Reduction and Error Analysis for the Physical Sciences. McGraw-Hill, 204

Brassard P., Fontaine G., Wesemael F., 1995, ApJS 96, 545

Breger M., 1990a, A&A 240, 308 (Paper II)

Breger M., 1990b, Comm. Asteroseismology (Vienna) 20, 1
Breger M., 1993, In: Butler C.J., Elliott I. (eds.) Stellar Photometry - Current Techniques and Future Developments. Cambridge University Press, 106
Breger M., Hiesberger F., 1999, A&AS 135, 54 (Paper III)
Breger M., McNamara B.J., Kerschbaum F., et al., 1990, A&A 231, 56 (Paper I)
Breger M., Stich J., Garrido R., et al., 1993, A&A 271, 482
Breger M., Pamyatnykh A.A., Pikall H., Garrido R., 1999, A&A 341, 151
Dziembowski W., 1977, Acta Astronomica 27, 203
Dziembowski W., 1982, Acta Astronomica 32, 147
Dziembowski W., 1997, In: Provost J., Schmieder F.-X. (eds.) Sounding solar and stellar interiors. Proc. IAU Symp. 181, Kluwer, Dordrecht, p. 317
Dziembowski W., Krolikowska M., 1990, Acta Astronomica 40, 19
Fitch W.S., 1980, Lecture Notes in Physics 125, 7
Garrido R., Garcia-Lobo E., Rodriguez E., 1990, A&A 234, 262
Garrido R., Rodriguez E., 1996, MNRAS 281, 696
Jones D.H.P., Haslam C.M., 1966, The Observatory 86, 34
Kuschnig R., Weiss W.W., Gruber R., et al. 1997, A&A 328, 544
Scargle J.D., 1982, ApJ 263, 835
Sperl M., 1998, Comm. in Asteroseismology (Vienna) 111, 1
Watson R.D., 1988, Ap&SS 140, 225

2.4.2 29 frequencies for the δ Scuti variable BI CMi: the 1997–2000 multisite campaigns

Original paper:

M. Breger, R. Garrido, **G. Handler,** M. A. Wood, R. R. Shobbrook, K. M. Bischof, F. Rodler, R. O. Gray, A. Stankov, P. Martinez, D. O'Donoghue, R. Szabó, W. Zima, A. B. Kaye, C. Barban, U. Heiter, 2002, MNRAS 329, 531

Mon. Not. R. Astron. Soc. **329,** 531–542 (2002)

29 frequencies for the δ Scuti variable BI CMi: the 1997–2000 multisite campaigns

M. Breger,[1★] R. Garrido,[2] G. Handler,[1,3] M. A. Wood,[4] R. R. Shobbrook,[5] K. M. Bischof,[1] F. Rodler,[1] R. O. Gray,[6] A. Stankov,[1] P. Martinez,[3] D. O'Donoghue,[3] R. Szabó,[7] W. Zima,[1] A. B. Kaye,[8] C. Barban[9,10] and U. Heiter[1]

[1]*Astronomisches Institut der Universität Wien, Türkenschanzstr. 17, A–1180 Wien, Austria*
[2]*Instituto de Astrofisica de Andalucia, CSIC, Apdo. 3004, E-18080 Granada, Spain*
[3]*SAAO, PO Box 9, Observatory 7935, Cape Town, South Africa*
[4]*Department of Physics and Space Sciences & SARA Observatory, Florida Institute of Technology, Melbourne, FL 32901, USA*
[5]*Department of Physics, University of Sydney, Australia*
[6]*Department of Physics and Astronomy, Appalachian State University, Boone, NC 28608, USA*
[7]*Konkoly Observatory, PO Box 67, H-1525 Budapest XII, Hungary*
[8]*Applied Physics Division, X-5, Los Alamos National Laboratory, Mail Stop F-663, Los Alamos, NM 87545, USA*
[9]*Observatoire de Paris, DASGAL, UMR 8633, 92105 Meudon, France*
[10]*National Solar Observatory, 950 N. Cherry, Tucson, AZ 85719, USA*

Accepted 2001 September 6. Received 2001 July 24

ABSTRACT

A multisite campaign of BI CMi was carried out with excellent frequency resolution and high photometric accuracy from 1997 to 2000, including two long observing seasons. 29 pulsation frequencies could be extracted from the 1024 h (177 nights) of photometry used. The detected frequencies include 20 pulsation modes in the main pulsation frequency range from 4.8 to 13.0 cycle d^{-1} (55 to 150 μHz), eight linear combinations of these frequencies, and a very low frequency at 1.66 cycle d^{-1}. Since the value of the low frequency at 1.66 cycle d^{-1} cannot be identified with a linear combination of other frequencies, g-mode pulsation is suspected, but rotational modulation of abundance spots cannot be ruled out. BI CMi, which is situated near the cool edge of the classical instability strip, may be both a δ Scuti and a γ Doradus star. Another outstanding property of BI CMi is the presence of a number of close frequency pairs in the power spectrum with separations as small as 0.01 cycle d^{-1}.

A rotational velocity of $v \sin i = 76 \pm 1\,\mathrm{km\,s^{-1}}$ was determined from a high-dispersion spectrum. From phase differences, the dominant modes can be identified with ℓ values from 0 to 2. The spectral type and evolutionary status of BI CMi are examined.

Key words: techniques: photometric – stars: individual: BI CMi – stars: oscillations – stars: rotation – δ Scuti.

1 INTRODUCTION

The Delta Scuti Network is engaged in ground-based asteroseismology of non-radially pulsating stars. The adopted method recognizes the fact that the successes of helioseismology are a consequence of the large amount of data available. Consequently, for carefully chosen single stars, a maximum of information is obtained with different techniques optimized for specific deductions. At the present time, high-precision photometry between 500 and 1000+ hours is used to derive 30 or more frequencies of pulsation per star. Because of cancellation effects across the stellar surface, the modes detected by photometry have low values of the spherical degree, ℓ. We obtain photometry in at least two wavelength regions, so that the phase differences can be used to identify the ℓ values. Since millimagnitude-accuracy photometry for most δ Scuti stars can be obtained on a telescope of 1 m or smaller, a multisite campaign covering many months of observation can be organized.

BI CMi (HD 66853, F2) is situated near the cool border of the classical instability strip in the Hertzsprung–Russell diagram. The star was chosen for an extensive multisite campaign by the Delta Scuti Network because there exists the possibility that this star might be both a δ Scuti (p modes) and a γ Doradus (g modes) star. The latter group represents a type of pulsation with low frequencies

★E-mail: breger@astro.univie.ac.at

found (mainly) outside the cool border of the classical instability strip. The light variability of BI CMi was discovered by Kurpinska-Winiarska, Winiarska & Zola (1988), when it was used as a comparison star for the eclipsing binary YY CMi.

Mantegazza & Poretti (1994) deduced from the analysis of 16 nights of observation that in addition to the δ Scuti-type frequencies, BI CMi showed two frequencies with very low values, namely, 0.149 and 0.659 cycle d^{-1}. The star might, therefore, present a transition between both types of pulsators (Breger & Beichbuchner 1996). More extensive measurements and analyses are needed to confirm the frequencies, examine possible 1 cycle d^{-1} aliasing and exclude the possibility of other explanations such as the peaks in the power spectrum being caused by combination frequencies, f_i–f_j.

2 NEW PHOTOMETRY

During the time periods 1997 January, 1998 November to 1999 March, as well as 1999 December to 2000 March, the star BI CMi was observed photometrically at six observatories. Both photomutiplier (PMT) and charge-coupled device (CCD) detectors were used. It is customary for DSN campaigns to disregard all data from sites with poor instrumentation, poor weather or other sources of *systematic* errors in excess of 10 mmag. In the present campaign a total of 1024 hours of observations on 177 nights were found to be of high quality, as judged by the constancy of the chosen comparison stars. These observations were retained.

The majority of observations were obtained with standard photoelectric photometers, using photomultiplier tubes as detectors. All

Table 1. Journal of photoelectric measurements of BI CMi.

Start HJD	Length (h)	Obs.	Start HJD	Length (h)	Obs.	Start HJD	Length (h)	Obs.	Start HJD	Length (h)	Obs.
245 0000+			245 0000+			245 0000+			245 0000+		
465.70	6.83	APT	1185.68	8.38	APT	1231.34	6.05	SNO	1553.68	8.19	APT
466.70	4.33	APT	1186.68	8.38	APT	1232.83	1.61	APT	1554.68	8.18	APT
468.69	5.13	APT	1187.67	8.30	APT	1235.61	6.81	APT	1555.67	8.25	APT
476.66	2.71	APT	1188.67	5.32	APT	1236.60	7.03	APT	1556.67	8.18	APT
478.66	2.84	APT	1189.85	3.97	APT	1237.60	6.81	APT	1558.67	3.28	APT
479.63	7.65	APT	1191.39	4.21	SAAO	1238.62	5.11	APT	1559.75	6.13	APT
480.61	8.14	APT	1191.67	8.13	APT	1239.67	4.26	APT	1560.66	3.71	APT
1138.81	5.72	APT	1192.35	5.79	SAAO	1240.61	6.27	APT	1569.63	5.78	APT
1139.80	5.79	APT	1192.76	2.53	APT	1241.60	3.32	APT	1570.66	7.33	APT
1140.80	5.88	APT	1193.75	6.02	APT	1246.62	1.24	APT	1571.63	8.27	APT
1141.84	4.86	APT	1193.99	6.23	SSO	1248.61	5.53	APT	1573.93	0.78	APT
1142.81	5.64	APT	1194.30	4.31	SAAO	1250.61	5.24	APT	1574.62	0.96	APT
1143.80	3.10	APT	1194.85	3.68	APT	1251.62	5.43	APT	1576.62	3.05	APT
1147.93	2.79	APT	1195.68	7.31	SARA	1252.67	2.64	APT	1577.62	7.86	APT
1148.89	3.63	APT	1196.47	1.90	SAAO	1253.62	5.07	APT	1578.75	4.79	APT
1151.77	4.97	APT	1196.65	8.37	APT	1256.62	5.07	APT	1579.60	8.18	APT
1152.77	6.92	APT	1196.70	8.21	SARA	1263.91	3.67	SSO	1580.82	2.97	APT
1153.94	2.67	APT	1196.97	6.65	SSO	1514.79	6.28	APT	1581.61	6.70	APT
1155.76	7.07	APT	1197.65	8.38	APT	1515.78	6.36	APT	1582.60	4.17	APT
1156.76	7.06	APT	1197.64	9.61	SARA	1516.78	6.53	APT	1584.72	5.05	APT
1157.76	0.42	APT	1197.15	0.99	SSO	1517.78	6.54	APT	1585.77	3.91	APT
1159.75	7.30	APT	1198.62	9.79	SARA	1519.77	6.88	APT	1586.61	7.53	APT
1160.75	7.33	APT	1198.65	8.07	APT	1520.81	3.52	APT	1588.60	7.64	APT
1161.74	7.57	APT	1199.69	5.66	SARA	1521.80	1.34	APT	1590.60	7.42	APT
1163.80	5.56	APT	1200.31	6.01	SAAO	1523.76	1.01	APT	1595.60	7.34	APT
1166.17	1.55	SSO	1201.63	9.48	SARA	1524.79	3.34	APT	1601.24	5.12	PIZ
1166.73	1.60	APT	1201.64	8.38	APT	1525.77	6.43	APT	1601.61	6.61	APT
1167.73	5.71	APT	1202.33	5.67	SAAO	1526.75	2.10	APT	1602.23	6.06	PIZ
1169.08	3.57	SSO	1203.36	4.94	SAAO	1529.74	7.10	APT	1602.61	4.69	APT
1169.72	8.08	APT	1204.32	5.12	SAAO	1530.74	7.16	APT	1603.23	6.35	PIZ
1170.03	4.55	SSO	1213.63	2.12	APT	1531.74	3.25	APT	1605.61	6.19	APT
1170.75	5.46	APT	1218.30	8.22	SNO	1532.73	7.41	APT	1606.61	6.18	APT
1171.05	4.11	SSO	1220.30	8.03	SNO	1533.73	7.61	APT	1607.62	6.19	APT
1171.86	4.79	APT	1221.30	7.86	SNO	1535.72	7.72	APT	1612.62	5.73	APT
1172.72	8.25	APT	1222.45	2.27	SNO	1537.72	8.13	APT	1613.65	5.04	APT
1173.71	3.94	APT	1223.56	1.23	SNO	1538.72	4.43	APT	1614.62	5.66	APT
1175.71	8.26	APT	1224.31	7.00	SNO	1539.72	1.85	APT	1615.62	4.12	APT
1176.71	8.24	APT	1225.36	6.23	SNO	1545.70	8.19	APT	1617.72	2.88	APT
1177.70	8.28	APT	1225.59	2.99	APT	1546.70	8.22	APT	1618.64	4.84	APT
1179.70	8.40	APT	1226.30	7.26	SNO	1547.69	8.22	APT	1619.74	2.26	APT
1180.69	8.40	APT	1228.47	3.45	SNO	1548.69	8.19	APT	1620.61	5.36	APT
1181.69	8.38	APT	1229.36	5.43	SNO	1549.69	8.19	APT	1621.61	5.16	APT
1182.69	8.51	APT	1230.31	7.23	SNO	1550.69	7.95	APT	1622.67	3.83	APT
1183.69	8.50	APT	1230.73	4.19	APT	1551.68	8.19	APT	1623.62	4.93	APT
1184.97	1.58	APT									

APT: Arizona; SSO: Siding Spring Observatory, Australia, Shobbrook; SNO: Sierra Nevada, Garrido; SARA: at KPNO, Wood; SAAO: South African Astronomical Observatory; PIZ: Piszkéstető, Szabo, Bischof.

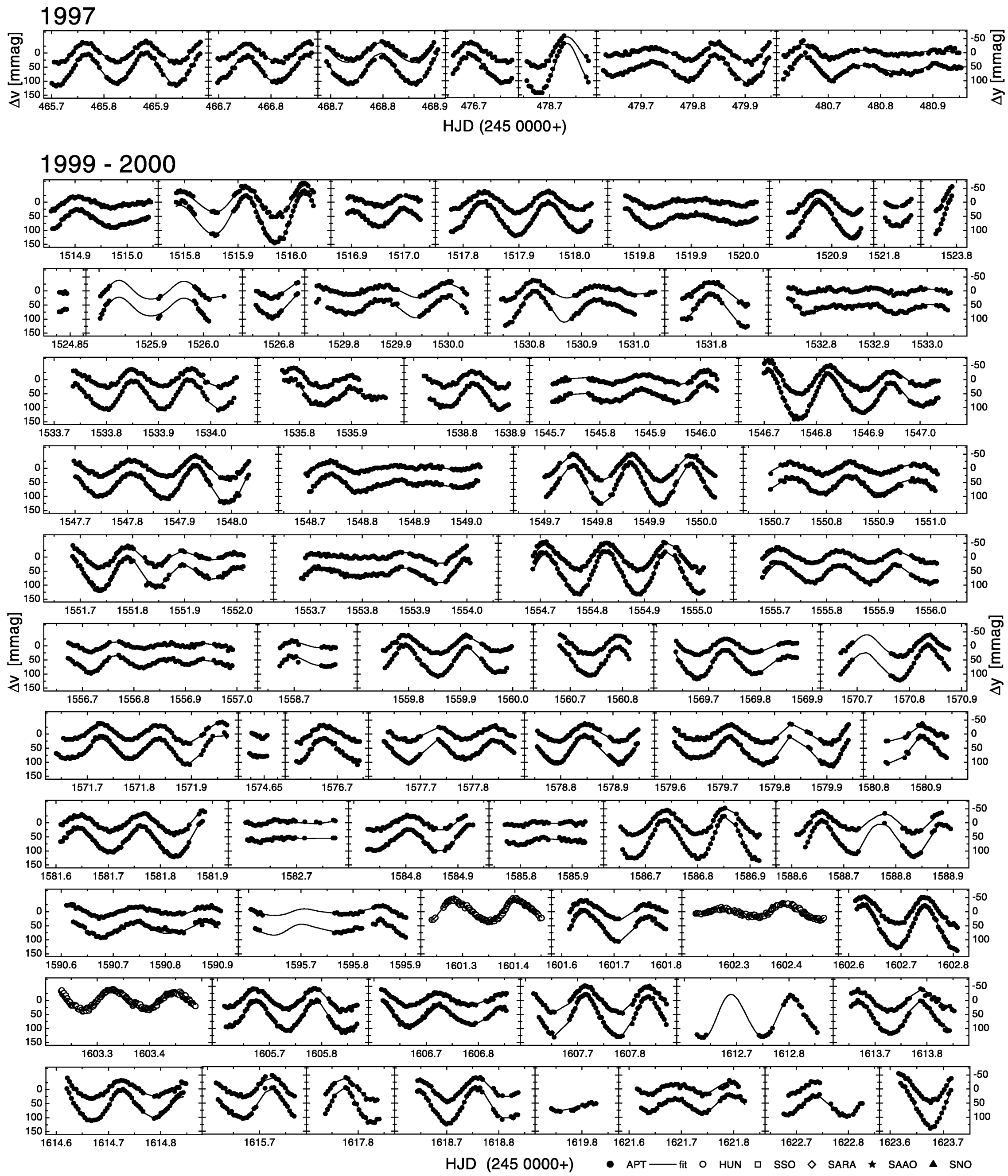

Figure 1. Multisite photometry of BI CMi obtained during the 1997 and 1999–2000 DSN campaigns. Δy and Δv are the observed magnitude differences (variable − comparison stars) normalized to zero in the narrowband *uvby* system. The fit of the 29-frequency solution derived in this paper is shown as a solid curve. Filled circles: APT; open circles: Piszkéstető; open rectangles: SSO; filled stars: SAAO; open diamonds: SARA; filled triangles: SNO.

measurements were made through the Strömgren v and y filters to provide a relatively large baseline in wavelength. The three-star technique (Breger 1993), in which measurements of the variable star are alternated with those of two comparison stars, was adopted. Since the same photometric channel is used for all three measurements, the procedure can produce the required long-term stability of 2 mmag or better. For the PMT measurements, two comparison stars, HD 66925 and HD 66829, were used. HD 66925 has been used as a comparison star before by Mantegazza & Poretti (1994), who found no variability. HD 66829 was used by them as a second comparison star for only two nights, after a previously used comparison star was found by them to be a microvariable. In a later section we will show that the early F star, HD 66829, also exhibits microvariability of about 2 mmag. The time-scale of this variability is consistent with a γ-Doradus type of variability, known to occur at this spectral type (e.g. see Kaye et al. 1999). Consequently, the star was only used for short-term smoothing of the unavoidable scatter of the measurements of the comparison star, HD 66925.

The following telescopes were used:

(i) The 0.75-cm Vienna Automatic Photoelectric Telescope (APT), situated at Washington Camp in Arizona, USA, was used

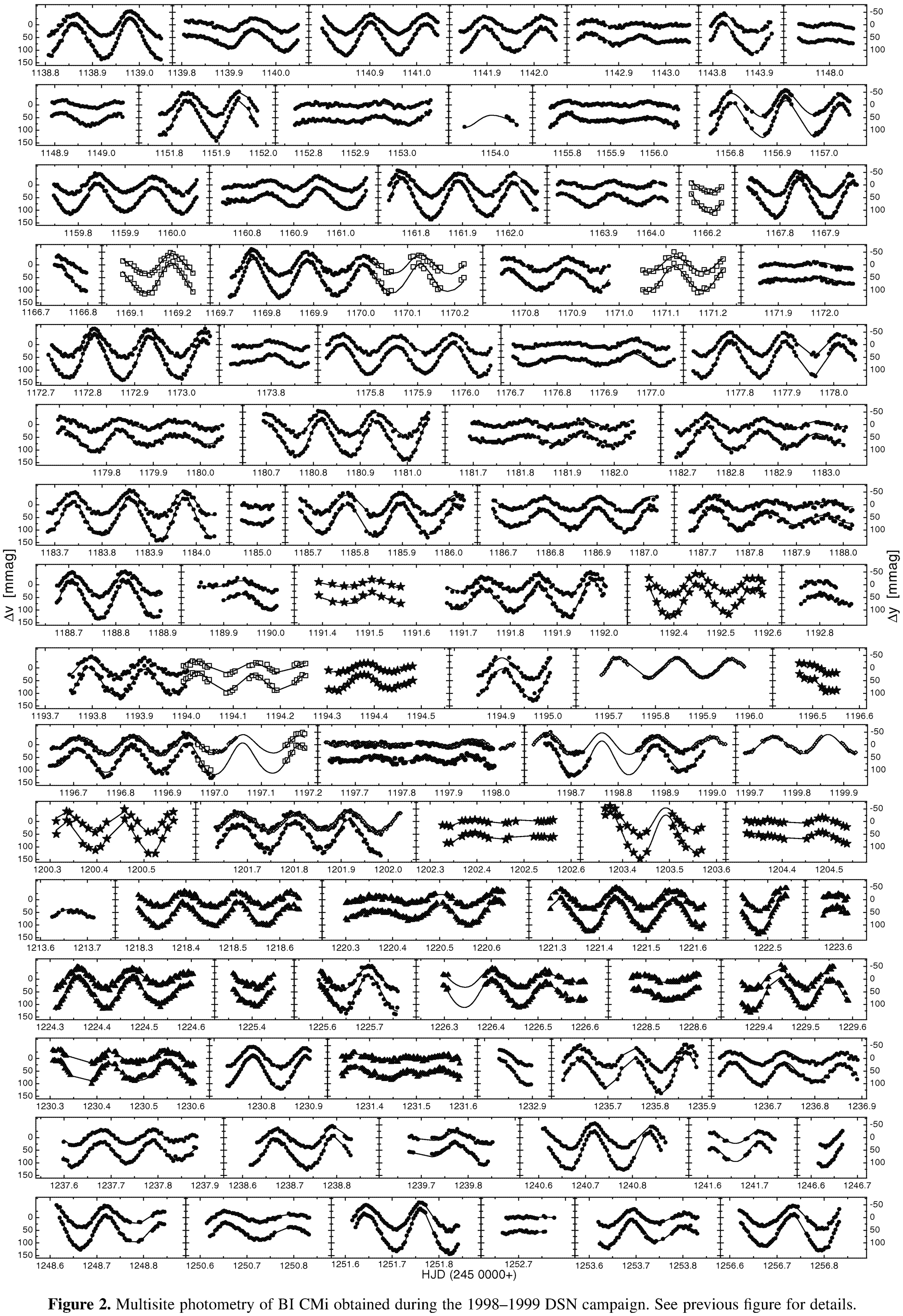

Figure 2. Multisite photometry of BI CMi obtained during the 1998–1999 DSN campaign. See previous figure for details.

(see Breger & Hiesberger 1999). Details on the observations, reductions and results for the present campaign can be found in Rodler & Handler (2001).

(ii) Observations from the Observatorio de Sierra Nevada (OSN), located at 2900 m above sea level in the south-east of Spain, were made using the simultaneous four-channel *uvby* Strömgren photoelectric photometer attached to a 0.9-m telescope. The telescope and photometer are automatically controlled by software developed at the Institito de Astrofisica de Andalucia. A PMT detector was used. The measurements consisted of 30-s integrations using a 30-arcsec diaphragm. Reductions were made using software installed at OSN giving standard magnitude differences.

(iii) Differential single-channel v and y photometric observations were acquired on eight nights in 1999 January using the modular photometer attached to the 0.5-m telescope of the SAAO (South African Astronomical Observatory). The detector used in these observations was a Hamamatsu AE733 GaAs photomultiplier with a system dead time of 30 ns. Photometric diaphrams of 30–40 arcsec were used, depending on the telescope's tracking performance and on the seeing.

(iv) The 60-cm reflector at Siding Spring Observatory was used with a PMT detector and the Johnson V and the Strömgren v filters.

(v) The 0.9-m Southeastern Association for Research in Astronomy (SARA) telescope, located at Kitt Peak National Observatory in Arizona, USA, was equipped with a CCD camera, consisting of an Apogee AP4 and a Kodak KAF–4200 grade 0 2048 × 2048 chip, binned 2 × 2. The image scale was 0.5 arcsec per binned pixel. Read noise was approximately $30\,e^-$ rms, and the gain $6.7\,e^-\,ADU^{-1}$. The CCD measurements made by M. Wood, were reduced by K. Bischof in the standard fashion with the APPHOT routines of the IRAF[1] package. This included bias subtraction, flat-field division, sky subtraction, and choosing the optimum aperture size (diameter ~12 pixels). All the stars brighter than the twelfth magnitude present on the CCD frames were examined: four relatively bright objects were found to be non-variable and were selected as comparison stars.

The SARA CCD measurements had an excellent coverage with a data point every 40 s. This seeming advantage of a large number of measurements is offset by the fact that the observational errors of successive measurements are not independent of each other: the deviations are systematic. Consequently, we feel justified in grouping together a number (~7) of successive measurements to simulate the coverage from the other observatories. A positive side effect is the reduction in the average residuals of these CCD measurements, so that they could be given full weight in the multifrequency solutions.

(vi) The 1-m telescope at the Piszkéstető Observatory in Hungary was used together with a CCD photometer. The high-accuracy data were reduced in the same way as the SARA measurements (above).

Table 1 provides the journal of observations. The light curves are shown in Figs 1 and 2, which also include a comparison with the fit derived in the next section.

[1] IRAF is distributed by the National Optical Astronomy Observatories, which is operated by the Association of Universities for Research in Astronomy, Inc., under contract to the National Science Foundation.

3 DETECTION OF THE PULSATION FREQUENCIES

The pulsation frequency analyses were performed with a package of computer programs with single-frequency and multiple-frequency techniques (programs PERIOD, Breger 1990; PERIOD98, Sperl 1998), which utilize Fourier as well as multiple least-squares algorithms. The latter technique fits a number of simultaneous sinusoidal variations in the magnitude domain and does not rely on pre-whitening. In a previous paper (Breger et al. 1993) we argued that a ratio of amplitude signal/noise = 4.0 provides a useful criterion for judging the reality of a peak. For the detection of frequency combinations, such as the $2f$ term, the criterion was relaxed to 3.5, since the frequency values during the search are already known (for more details see Breger et al. 1999).

For the frequency detection, we combined the y (9011 new measurements) and v data (8220 new measurements). The dependence of the pulsation amplitude on wavelength was compensated by multiplying the v data set by an experimentally determined factor of 0.632 and increasing the weight of the data points by 1/0.632. This scaling creates similar amplitudes but does not falsify the power spectra. Note that different colours and data sets were only combined to detect new frequency peaks in the Fourier power spectrum and to determine the significance of the detection. The effects of imperfect amplitude scaling and small phase shifts between colours can be shown to be very small.

A difficulty with detecting and fitting low-amplitude modes concerns the relatively small number of very divergent data points. An example would be a data point with a deviation of, say, 15 mmag. This residual cannot be caused by undetected modes if these have amplitudes of 1 mmag. For the first time, we have included a weighting scheme to de-emphasize the effect of very divergent points. In this very conservative scheme, a full weight of 1.0 is assigned to the vast majority of data points, while the very deviant points are assigned a lower weight. This is done without knowing or being able to justify why a particular point was of poor quality. The following weighting scheme is used when $\sigma(i)$ is the deviation of the ith point from the solution.

For $\sigma(i) \leq$ Limit : Weight$(i) = 1$.

For $\sigma(i) >$ Limit : Weight$(i) = (\text{Limit}/\sigma(i))**2$.

If the weighting limit is chosen correctly and conservatively, such a scheme does not suppress the discovery of additional frequencies. It is important to note that a limit of the same order as the amplitudes to be detected should not be used, e.g. adopting such a weighting scheme is not advantageous for the dominant modes of the star. Furthermore, if the distribution of residuals is Gaussian, then such a weighting scheme is not suitable. For the present data set of BI CMi, there are a number of divergent points beyond the statistically expected number. Consequently, for f_{20} and beyond, the weighting scheme improves the detection efficiency. Experimentation with different limits led us to an admittedly nearly arbitrary limit allowing 80 per cent of the points to have full weight. For our final solutions we have adopted the limits of 7.3 mmag in v and 6.2 mmag in y. This resulted in 81 per cent of the data points having full weight and 7 per cent having a weight of less than 0.5. The deviant points are not completely distributed at random.

To detect the frequencies of pulsation, we have performed Fourier analyses of the combined data. A number of statistically significant peaks were selected in order to compute a

Table 2. The frequency spectrum of BI CMi from 1997 to 2000.

Frequency cycle d^{-1}	μHz/ID	Detection Significance Ampl. signal/noise	Amplitude v filter 1999–2000 mmag	1998–1999 mmag	1997 mmag	Amplitude y filter 1999–2000 mmag	1998–1999 mmag	1997 mmag
			±0.1	±0.1	±0.3	±0.1	±0.1	±0.3
f_1, 8.2455	95.43	192	36.5	35.7	34.6	22.6	22.5	22.0
f_2, 8.8663	102.62	169	31.5	31.4	31.6	20.0	19.8	20.6
f_3, 8.5134	98.53	53.3	10.0	9.4	10.4	6.5	5.9	6.6
f_4, 7.4244	85.93	46.2	8.9	8.0	6.7	5.4	5.0	4.3
f_5, 10.4289	120.71	33.4	5.8	5.1	5.3	3.8	3.7	2.9
f_6, 10.4365	120.79	21.6	4.3	4.3	4.8	2.4	2.8	2.9
f_7, 7.8839	91.25	15.2	3.0	2.9		1.5	1.9	
f_8, 17.1119	f_1+f_2	18.4	2.6	2.9		1.6	1.9	
f_9, 9.5244	110.23	16.2	2.9	2.8		2.1	1.9	
f_{10}, 4.7826	55.35	11.5	2.4	1.7		1.3	1.3	
f_{11}, 1.6619	19.23	7.5	1.8	1.6		1.4	0.7	
f_{12}, 13.0227	150.73	11.4	1.7	2.2		1.2	1.5	
f_{13}, 8.6577	100.21	12.4	1.5	2.3		1.5	1.6	
f_{14}, 11.2608[a]	130.33	15.0	2.7	1.5	4.4	1.6	0.7	3.3
f_{15}, 17.0266	$=2f_3$	14.2	2.1	1.5		1.4	1.2	
f_{16}, 8.6405	100.01	11.4	1.6	1.7		1.1	1.6	
f_{17}, 4.8178	55.76	8.4	1.6	1.7		0.9	0.9	
f_{18}, 16.4911	$=2f_1$	13.1	1.7	1.7		1.1	1.0	
f_{19}, 10.2413	118.53	8.5	1.7	1.8		0.9	1.3	
f_{20}, 15.6699	f_1+f_4	8.2	1.0	1.3		0.8	0.7	
f_{21}, 12.3500	142.94	8.4	1.2	0.9		0.7	0.8	
f_{22}, 17.7327	$=2f_2$	9.0	0.7	0.9		0.8	0.8	
f_{23}, 6.1776	71.50	5.7	1.2	0.7		0.6	0.6	
f_{24}, 12.8321	148.52	4.4	0.8	1.2		0.5	0.6	
f_{25}, 16.7588	f_1+f_3	5.2	0.8	0.6		0.4	0.6	
f_{26}, 16.2907	f_2+f_4	4.3	0.8	0.7		0.4	0.6	
f_{27}, 9.0988	105.31	5.1	0.6	0.8		0.7	0.7	
f_{28}, 12.3268	142.67	4.1	1.1	0.8		0.4	0.5	
f_{29}, 17.3796	f_2+f_3	3.8	0.5	0.7		0.3	0.5	
Residuals, single measurement			4.5	5.0	4.6	3.8	4.3	4.2

[a] f_{14} has a time-variable amplitude, see text.

multifrequency solution to the observed light curve. For computing multifrequency solutions, the amplitudes and phases were computed separately for each colour, so that even these small errors associated with combining different colours are avoided. Because of the daytime and observing-season (annual) gaps, different alias possibilities were tried out and the fit with the lowest residuals selected.

The resulting optimum multifrequency solution was then prewhitened and Fourier analyses computed from the residuals. This led a number of new peaks, which were tested for statistical significance. The previous procedure was then repeated. Note that the new multifrequency solutions always were computed from the observed (not the pre-whitened) data.

The analysis was repeated while adding more and more frequencies, until the new peaks were no longer statistically significant. We have also repeated the complete frequency-finding analysis for each observing season and each colour separately, in order to confirm that the detected frequencies are indeed present in all the data. This also made it possible to check for amplitude variability: only one frequency, namely, f_{14}, showed strong amplitude variability. This was taken into consideration for the multifrequency solutions.

29 statistically significant peaks are found with the following properties.

(i) 20 peaks are independent pulsation frequencies in a limited frequency range, which defines a frequency region of pulsational excitation. The region is found to range from 4.8 to 13.0 cycle d^{-1} (55 to 150 μHz).

(ii) A very low frequency of 1.66 cycle d^{-1} is found, which is not a combination frequency.

(iii) Three peaks can be identified with the $2f$ terms of the three dominant pulsation modes.

(iv) Five further frequencies are linear combinations of other frequencies with large amplitudes with a mathematical form, $f_i + f_j$. Our inability to find the corresponding f_i–f_j values is, in large part, connected with the larger observational uncertainties (zero points) in the frequency range below 0.5 cycle d^{-1}.

(v) The value of f_{12} (see Table 2) is related to two other modes by the relation $f_{12} = f_{10} + f_1 - 0.005438$ cycle d^{-1}. The constant is approximately equal to twice the reciprocal of the number of days in a year. It corresponds to approximately twice the separation caused by annual aliasing. We have tested the combination frequency, $f_{10} + f_1 = 13.0281$, and find a much poorer fit of only 1-mmag amplitude (instead of 2 mmag) in v. We can, at this stage, neither confirm nor reject the possibility that f_{12} might be a combination frequency.

Fig. 3 and Table 2 show the results of the multiperiod analysis. In the figure, the various power spectra are presented as a series of panels, each with additional frequencies removed relative to the panel above.

4 IS THE DETECTED LOW FREQUENCY REALLY PRESENT IN BI CMI?

In the previous section, we have detected a low frequency peak at 1.662 cycle d^{-1}. The reliable detection of such low frequencies is

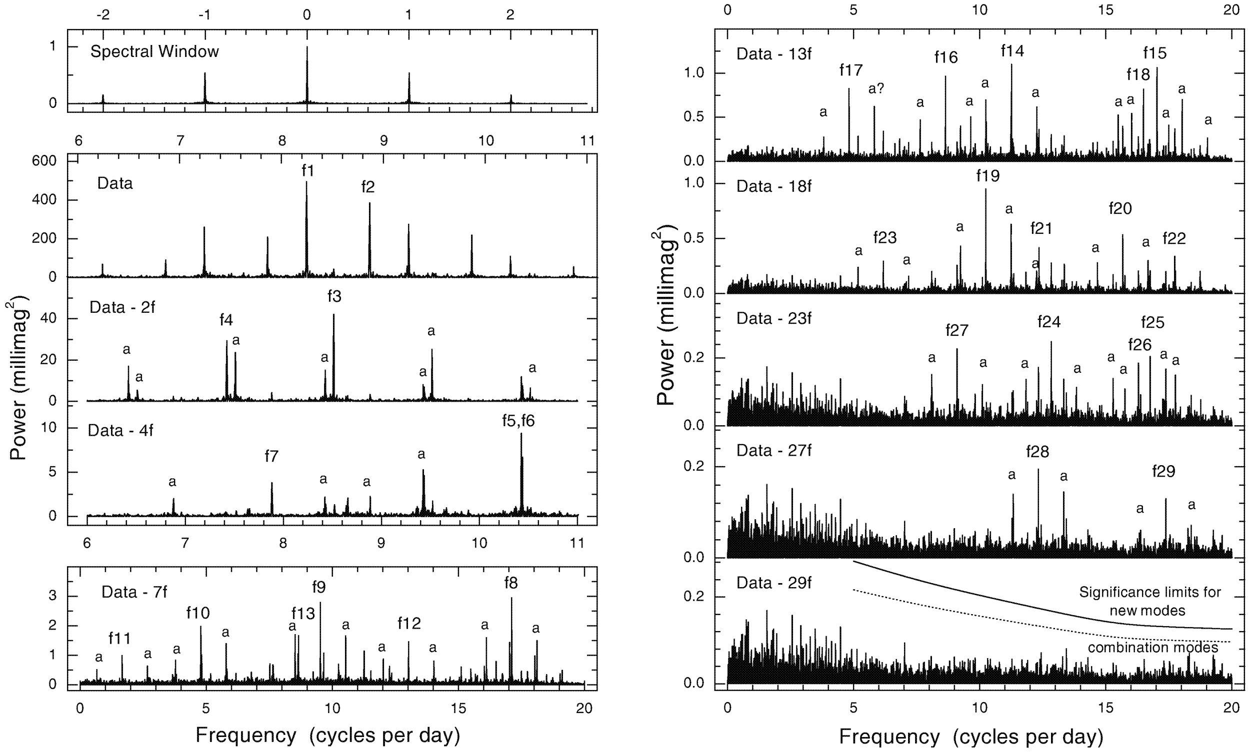

Figure 3. Power spectrum of BI CMi. The spectra are based on the combined 1997–2000 data in both the y and v colours and are shown before and after applying multifrequency solutions. Some 1 cycle d^{-1} aliases are marked with 'a' for clarity. See text for the numbering scheme and a discussion of significance levels.

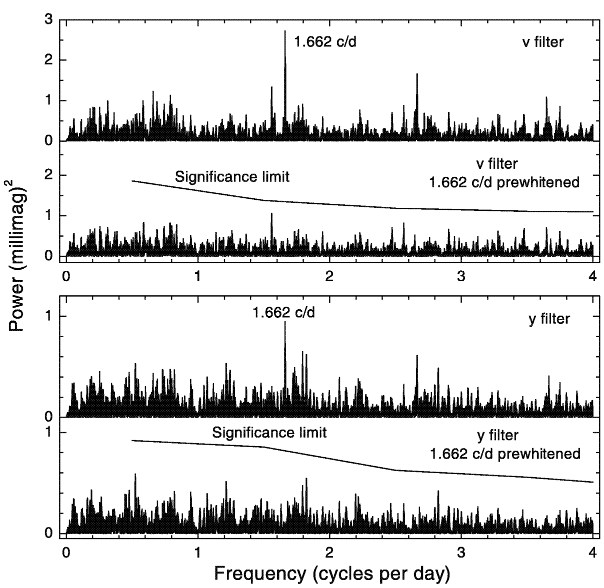

Figure 4. Power spectrum of BI CMi in the low-frequency domain using only data with secure zero-point stability. Results are shown for the two filters, v and y, separately before and after pre-whitening the 1.662 cycle d^{-1} peak. This shows that the 1.662 cycle d^{-1} peak is present in both filters. Furthermore, only this peak is statistically significant.

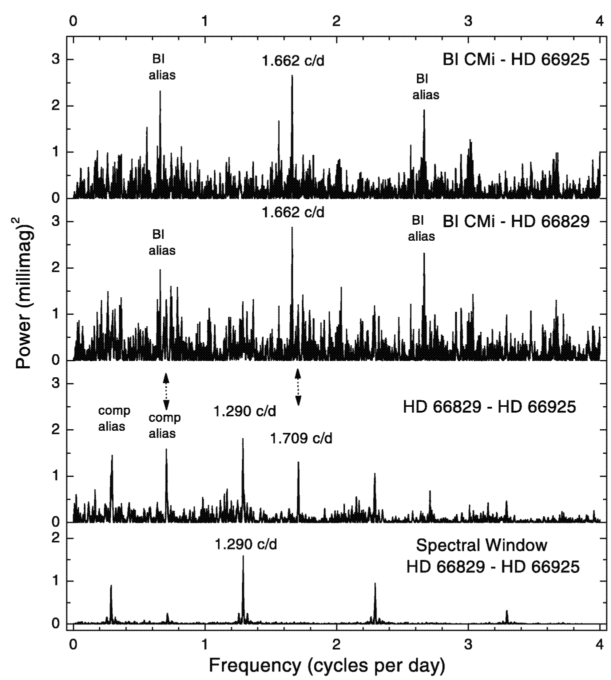

Figure 5. A comparison of the power spectra of the measured magnitude differences in the v filter between BI CMi and the two comparison stars used. The origin of a peak can be inferred if it occurs in two (and only two) of these panels. The diagram shows that the 1.662 cycle d^{-1} peak originates in BI CMi, while the 1.29/1.71 cycle d^{-1} combination comes from the early F star, HD 66829.

relatively difficult owing to the higher observational errors in the low frequency domain. In particular, extinction errors, slow zero-point drifts and slowly varying comparison stars can cause spurious frequency detections. In order to examine the reality of this detection, we have re-analysed the 1998–1999 and 1999–2000 data by using only the parts with the most reliable instrument stability, i.e. the available data with zero-point stability of 1 mmag or better. This excludes the block of 29 nights of 1998–1999 APT measurements from JD 245 1169 to 245 1226, the JD 245 1147 night and the three nights of Hungarian CCD data from the 1999–2000 season. For the analysis we have pre-whitened all the known frequencies in the higher-frequency domain in order to avoid spectral leakage.

Fig. 4 shows the Fourier spectrum in the low-frequency domain for the two filters. The 1.662 cycle d^{-1} peak can be seen to be dominant in both filters. We also find that the next highest peaks in BI CMi are not found in both filters and also lie below the formal level of significance.

The possibility that the 1.662 cycle d^{-1} peak originates in one of the two comparison stars still needs to be tested. We have repeated the complete data reduction for the v and y filters. Both filters give similar conclusions, but we will concentrate here on the v filter, which has a higher signal/noise ratio. The photometric differences, (BI CMi − HD 66925), (BI CMi − HD 66829), as well as (HD 66829 − HD 66925) were calculated. The power spectra are shown in Fig. 5. This figure shows the following.

(i) The 1.662 cycle d^{-1} peak is present in both power spectra involving BI CMi, but absent in the difference between the two comparison stars. This confirms that the 1.662 cycle d^{-1} originates in BI CMi.

(ii) HD 66829 shows some microvariability with peaks at 1.290 and 1.709 cycle d^{-1} and its 1 cycle d^{-1} aliases. These peaks are only present in the power spectra involving HD 66829. The time-scales are consistent with a γ Doradus type of variability common in early F stars. Note that, owing to the excellent frequency resolution of the campaign, the peaks at 1.662 (BI CMi) and 1.709 cycle d^{-1} (HD 66829) are clearly separated. We also note that the 1 cycle d^{-1} aliases of these two frequencies are themselves related through an alias, namely, $0.29 + 0.71 = 1.00$. Nevertheless, a spectral window centred on 1.290 cycle d^{-1} cannot explain all the peaks of HD 66829. Consequently, we are not able to pinpoint the exact frequency(ies) of HD 66829. However, a best solution is obtained with a combination of 0.706 *and* 1.287 cycle d^{-1}.

(iii) The difference between HD 66925 and HD 66829 shows considerably lower noise at low frequencies than the differences between BI CMi and each of these stars. Since BI CMi and HD 66829 have similar apparent magnitudes of $V = 9.2$, brightness differences are not the cause. We strongly suspect that the higher noise level of BI CMi is caused by the presence of undetected low-frequency modes in BI CMi. We note here that various frequency combinations, $f_i + f_j$, were detected but that the existence of their expected counterparts, f_i–f_j, could not be shown. We have examined the data for the expected modes: only the peak at f_1–$f_4 = 0.821$ cycle d^{-1} is seen, while the others are hidden in the noise. This peak is not statistically significant owing to the high noise (i.e. the presence of other peaks). It appears prudent to stop at this point in order to avoid potential overinterpretation of the data.

4.1 Physical cause of the 1.662 cycle d^{-1} variation

We have already noted that the 1.662 cycle d^{-1} frequency of BI CMi could be the result of γ Doradus type variation. This would make the star one of the most evolved γ Doradus candidates known to date (see Handler 1999). However, our data are insufficient for BI CMi being considered a good candidate adopting the criteria of Kaye et al. (1999): there is only one period in the γ Doradus range and no time-resolved spectroscopy is available. Consequently, we cannot prove that γ Doradus pulsations are excited in BI CMi; alternative explanations need to be considered.

Those other possibilities include ellipsoidal variations and abundance spots on the stellar surface. Concerning the latter possibility, it is important to note that our spectral classification from Section 8.2 (F2 IIIp SrEuCr:) suggests that the star is chemically peculiar, which makes a spot hypothesis non-negligible. Assuming a stellar radius of 3.7 $R_\odot$ (see Section 8.2) and a rotation frequency of 1.662 cycle d^{-1}, we obtain a rotational velocity of 310 km s^{-1} and an orbital inclination of $i = 14°$. This leaves little horizon behind which possible spots can disappear, but this would also provide a natural explanation of the small amplitude of the signal. We add that the rotational light curves of Ap stars often show a double-wave variation, which would then yield $i = 29°$, again consistent with the observed variation and basic stellar parameters. Abundance spots on the stellar surface thus remain a viable explanation for the 1.662 cycle d^{-1} frequency of BI CMi.

Turning to ellipsoidal variations, we note that the observed long period (both for single- and double-wave light curves) is also consistent with this hypothesis; it actually fits the observed period–temperature relation for ellipsoidal variables (see Morris 1985) well. The low photometric amplitude can easily be explained with high orbital inclination. However, the amplitude ratios between the v and y filters we find for this frequency (1.28 ± 0.12 for the 1999–2000 season and 2.3 ± 0.3 for 1998–1999) are inconsistent with the equal v and y amplitudes an ellipsoidal variation is expected to produce.

We suggest that the 1.662 cycle d^{-1} variation of BI CMi originates from either pulsation or abundance spots, but more data, in particular time-resolved spectroscopy, are required to settle this issue.

5 ANNUAL PULSATION SOLUTIONS

Now that 29 frequencies have been determined, we can derive the amplitudes and examine the data for amplitude variability. For the extensive 1998–1999 and 1999–2000 observing seasons, we have computed separate 29-frequency solutions for each year and each of the two colours. This approach could not be adopted for the 1997 single-filter (y) data, since only seven nights of observation are available. Even with the frequency values known, a 29-frequency solution contains 58+1 (zero-point) degrees of freedom. In order to avoid an overinterpretation of the data, we have only computed the amplitudes and phases for the dominant modes, f_1 to f_6, and the one mode, f_{14}, with variable amplitudes. For all the other modes, the average amplitude and phase computed from the available y data for all years was assumed in the 1997 solution.

An examination of annual amplitude variability requires a knowledge of the uncertainties associated with the derived values. The expected uncertainties in the values of the derived amplitudes, $\sigma(a)$, can be calculated from the average residuals, $\sigma(m)$, of the fit to the data of N measurements with random errors (for a derivation of the formulae see the appendix in Breger et al. 1999):

$$\sigma(a) = \sqrt{\frac{2}{N}}\sigma(m). \quad (1)$$

The uncertainties computed in this manner are shown with the amplitudes in Table 2. In order to avoid circular arguments, the listed residuals refer to solutions using data in which extremely deviant points were assigned full weight.

For one pulsation mode, f_{14}, strong annual amplitude variability was detected. For the two extensive data sets (1998–1999 and 1999–2000) the significance of amplitude variability exceeds four standard deviations; the even larger amplitude found for 1997 is less significant because of the relatively small data set for 1997.

We also note the presence of several close frequency pairs, e.g. 10.4289 and 10.4365 cycle d^{-1}. The data are of sufficient resolution to detect such a small separation of 0.008 d, namely, 125 d in 1998–1999 and 109 d in 1999–2000. The double structure was detected through our standard procedure involving pre-whitening detected frequencies and then looking for additional peaks. Nevertheless, we checked the reality of the detections with multifrequency solutions involving the pairs: the pairs gave the lowest residuals. Additional tests to examine the reality of the frequency pairs (as opposed to artefacts caused by insufficient resolution, incorrect analyses and amplitude variability) will be applied in a separate paper, in which the problem of close frequencies in δ Scuti stars will be examined in detail.

6 COMPARISON WITH PREVIOUS RESULTS

Mantegazza & Poretti (1994) presented a multifrequency solution of their BI CMi data with 10 frequencies. It is important to note that some of the frequencies with small amplitudes were not regarded by them as reliable.

If one takes into account the lower frequency resolution and possible 1 cycle d^{-1} aliasing of the previous results, the agreement is good. The 0.149 cycle d^{-1} peak is not seen by us and two other frequencies are 1 cycle d^{-1} aliases: the 9.44 cycle d^{-1} peak probably corresponds to our 10.43 cycle d^{-1} doublet and the 0.66 cycle d^{-1} peak becomes 1.66 cycle d^{-1}. Since our multisite campaign is much more extensive than the previous data, the new values are probably applicable.

As was previously the case for our 1997 data, a 29-frequency solution leads to an overinterpretation of the 1991 data (16 nights) with an unstable solution in which modes articificially increase each other's amplitudes to unrealistic values. Consequently, we have adopted the approach used previously for the 1997 data: (i) we determined the 29 best frequency, amplitude and phasing values for the 1991 to 2000 time period (allowing for annual amplitude variations of f_{14}), and (ii) for 1991, we determined the amplitudes and phasing of f_1 through f_6 as well as f_{14}, while assuming the average values for the many other modes with small amplitudes.

For the dominant six frequencies, the amplitudes found for the other years were confirmed within the observational uncertainties. We conclude that the earlier results are in agreement with our new solutions and that the star BI CMi shows very little amplitude variability.

7 THE ROTATIONAL VELOCITY OF BI CMI

In 1999 December, a high-dispersion spectrum of BI CMi was obtained at Kitt Peak National Observatory with the 0.9-m coudé feed telescope and spectrograph. This spectrum covers a wavelength range slightly larger than 300 Å centred on λ6566, and was obtained using grating A, camera 5, and the long collimator. Filter RG610 was used to block both higher and lower orders. Data were recorded on the F3KB CCD (3k × 1k pixels, 15 × 15μm pixel size, 75 per cent DQE at 6560 Å). The exposure time was 1200 s, resulting in a signal/noise ratio of about 50. Th–Ar exposures used for wavelength calibration were taken immediately before and after the stellar exposure.

The spectrum was reduced at the National Optical Astronomy Observatories offices in Tucson, Arizona in the standard fashion using IRAF and included optimal aperture extraction, bias subtraction and flat-field division. The spectrum was then continuum-normalized by means of a polynomial fit to known continuum points.

The projected rotational velocity $v \sin i$ of BI CMi was estimated with the program ROTATE (Piskunov 1992). To this end, we calculated a model atmosphere with the semi-automatic tool AAP (Gelbmann et al. 1997), with $T_{\rm eff} = 6800$ K, $\log g = 4.0$ and $[M/H] = 0.5$. The particular choice of parameters does not affect the $v \sin i$ value to be determined. We then matched rotationally broadened theoretical spectra with the observed ones by determining individual $v \sin i$ values for each suitable spectral line, i.e. the strongest, unblended metal lines. We obtained an average $v \sin i = 76 \pm 1$ km s^{-1} from 14 such lines and adopted this result as our final projected rotational velocity of BI CMi.

8 THE EVOLUTIONARY STATUS AND MODE IDENTIFICATIONS OF BI CMI

8.1 The photometric approach

Knowledge of the effective temperature and luminosity are important for the matching of the observed frequency spectrum with pulsation models. It is unfortunate that for BI CMi a unique value of luminosity (or surface gravity) cannot be determined at this time.

The standard method of deriving the important parameters for δ Scuti stars relies on the calibrations of the photometric $uvby\beta$ system. For BI CMi, Mantegazza & Poretti (1994) have measured the following values: $b - y = 0.226$, $m_1 = 0.203$, $c_1 = 0.707$, $\beta = 2.734$. Using the standard calibrations for absolute magnitude, we find $E(b - y) = 0.013$, $\delta m_1 = -0.028$, and $M_v = 2.4$. Note that the standard uncertainties in M_v are usually in the vicinity of ± 0.3 mag. If the metals were normal, BI CMi could be identified with a main-sequence dwarf.

However, the luminosity of BI CMi is underestimated by these calibrations, possibly extremely so. The metallicity index, δm_1, indicates that the star is not normal and may belong to a class with unusual surface abundances, denoted in different classification schemes as the δ Del or ρ Pup class (for a review see Kurtz 2000). A property of these stars is that the photometric calibrations do not represent the true luminosity. In extreme cases, the error may even be several magnitudes (e.g. see table 8 in Rodriguez & Breger 2000).

It is possible to improve the photometrically determined absolute magnitude and to estimate a rough correction for δm_1 and the relatively slow rotation of BI CMi. This can be done by using the known Hipparcos parallaxes for other δ Scuti stars. Fig. 7 of Rodriguez & Breger (2000) indicates a correction of ~0.6 mag based on both the rotational velocity and metallicity measured for BI CMi. We must emphasize again that for chemically peculiar stars these values are very uncertain. We now find a corrected estimate of $M_v \sim 1.8$. This value is similar to that obtained by Mantegazza & Poretti (1994), who corrected for the metallicity effect using earlier estimates for such corrections in the literature.

The model-atmosphere calibrations of Moon & Dworetsky (1985) give $T_{\rm eff} = 7100$ K. Since the measured Balmer jump is not a correct indicator of luminosity and surface gravity, which led to the correction term to the luminosity, $\log g$ needs to be derived from the corrected absolute magnitude. The evolutionary tracks of Pamyatnykh (2000) indicate a mass of 1.8 solar masses for a star with such a temperature and absolute magnitude, which leads to a $\log g$ value of 3.87. These values indicate a radius of 2.6 solar radii and a rotational frequency, $\Omega \geq 0.58\,\mathrm{rev\,d^{-1}}$. This compares to $0.35\,\mathrm{cycle\,d^{-1}}$ for the frequency difference of two identified $\ell = 1$ modes, f_2 and f_3. An explanation for this contradiction is, again, that the luminosity of the star has been underestimated and that the radius of the star is considerably larger. An alternative explanation would require extremely asymmetric rotational splitting.

A further difficulty with the photometrically determined luminosity comes from the relatively low frequencies. If we adopt the values shown above, the pulsational constant, Q, ranges from 0.025 to 0.068 d, with the dominant modes possessing Q values from 0.037 to 0.039 d. Since the radial fundamental mode has $Q = 0.033$ d, in BI CMi even the dominant modes would have to be gravity modes! Inspection of the frequency spectra of well-studied δ Scuti stars shows this to be improbable.

We conclude that the photometric calibrations are not applicable, even with the estimated corrections for metallicity.

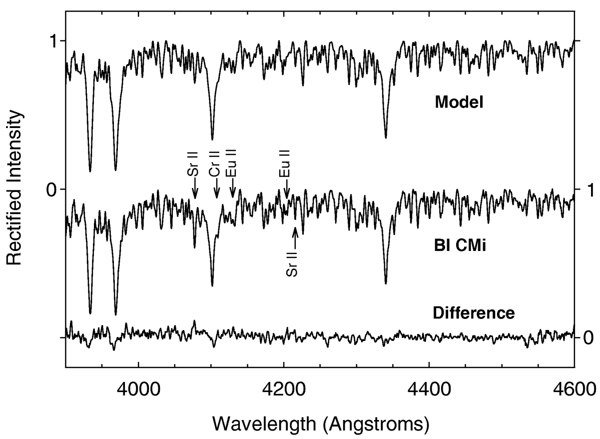

Figure 6. The model fit to BI CMi using the simplex method of Gray et al. (2001), including a difference spectrum between the model and observed spectra. Enhanced lines, owing to Sr II, Eu II and Cr II, are indicated in the spectrum of BI CMi. The scale on the left-hand ordinate indicates the continuum and zero-point levels for the model spectrum, the right-hand scale for the observed spectrum.

8.2 The spectroscopic approach

Spectroscopic analyses confirm that BI CMi is actually an evolved star. In order to investigate the chemical peculiarity and luminosity of BI CMi in more detail, we have obtained a classification-resolution spectrum of BI CMi on the Dark Sky Observatory 0.8-m telescope of Appalachian State University. This spectrum has a spectral range from 3800–4600 Å, a two-pixel resolution of 1.8 Å and signal/noise > 300. We have classified this star on the MK system using standard stars obtained with the same instrumental set-up. The spectrum of BI CMi is a close match to that of β Cas (F2 III), including the K line and the hydrogen lines, except for some chemical peculiarities. The most outstanding peculiarities are an enhanced Sr II λ4077, Eu II (both λ4129 and λ4205 are visibly enhanced), and a possible enhancement of Cr II (there is a line at $\lambda\lambda$4109–4110 which might be Cr II, but this identification is not certain, as it should be closer to λ4111). We give this star a F2 IIIp SrEuCr: classification.

We can obtain an estimate of the basic physical parameters of BI CMi using the multidimensional downhill simplex method developed by Gray, Graham & Hoyt (2001). This method finds the best simultaneous fit to the observed line spectrum and fluxes (from *uvby* photometry) using synthetic spectra and fluxes calculated from Kurucz (1993) models. The resulting fit, illustrated in Fig. 6, gives $T_{\mathrm{eff}} = 6925 \pm 75$ K, $\log g = 3.69 \pm 0.10$, $[M/H] = 0.04 \pm 0.10$ and $\xi_t = 3.6 \pm 0.5\,\mathrm{km\,s^{-1}}$. These parameters are very similar to those found by Gray et al. (2001) for β Cas ($T_{\mathrm{eff}} = 6940$ K, $\log g = 3.65$). We note that the photometric calibrations by Moon & Dworetsky (1985) give similar values for β Cas, namely, $T_{\mathrm{eff}} = 6975$ K, $\log g = 3.55$.

If we assign the values of $T_{\mathrm{eff}} = 6950$ K, $\log g = 3.6$ to BI CMi, then the Q values of the pulsation modes range from 0.015 to 0.041 d for the non-combination modes, with the dominant mode at 0.022 d, respectively. This corresponds to the value that is expected to the second (± 1) radial overtone and is normal for a δ Scuti star. The temperature and gravity values lead to a radius of 3.7 solar radii for BI CMi together with a rotational frequency, $\Omega \geq 0.40\,\mathrm{rev\,d^{-1}}$. The observed frequency difference ($0.35\,\mathrm{cycle\,d^{-1}}$) of two identified $\ell = 1$ modes, (namely, f_2 and f_3, identified in the next section), is also in agreement.

8.3 Phase difference and amplitude ratios

The campaign was carried out using the v and y filter of the $uvby\beta$ system. This allows us to compare the different pulsation modes in the two colours. In particular, the amplitude ratios and phase differences can be used for mode identifications.

Table 3. Phase differences and amplitude ratios for BI CMi.

Frequency cycle $\mathrm{d^{-1}}$	Phase differences in degrees $\phi_v - \phi_y$	Amplitude ratio vy	Probable mode identification
f_1, 8.246	3.48 ± 0.21	1.62 ± 0.01	$\ell = 0$
f_2, 8.866	-0.36 ± 0.24	1.60 ± 0.01	$\ell = 1$
f_3, 8.513	-0.95 ± 0.77	1.58 ± 0.04	$\ell = 1$
f_4, 7.424	-1.13 ± 0.93	1.67 ± 0.05	$\ell = 1$
f_5, 10.429	-6.60 ± 1.36	1.48 ± 0.05	$\ell = 2$
f_6, 10.437	0.91 ± 1.75	1.62 ± 0.08	$\ell = 0$, (1)
f_9, 9.524	-8.04 ± 2.49	1.44 ± 0.09	$\ell = 2$
Uncertain values			
f_7, 7.884	-4.15 ± 2.67	1.72 ± 0.14	$\ell = 2$, 1
f_{10}, 4.783	5.30 ± 4.00	1.59 ± 0.18	$\ell = (0)$

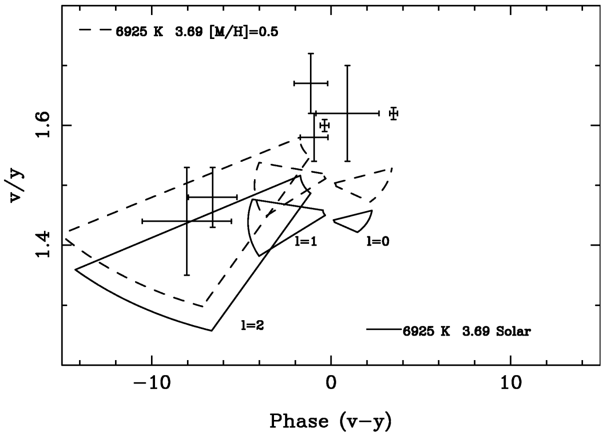

Figure 7. Diagnostic diagram to determine ℓ values from Strömgren v and y colours. Measurements are shown with their error bars, while the loops represent the models for different ℓ values. Note that the phase differences, but not the amplitude ratios, are used for mode identifications.

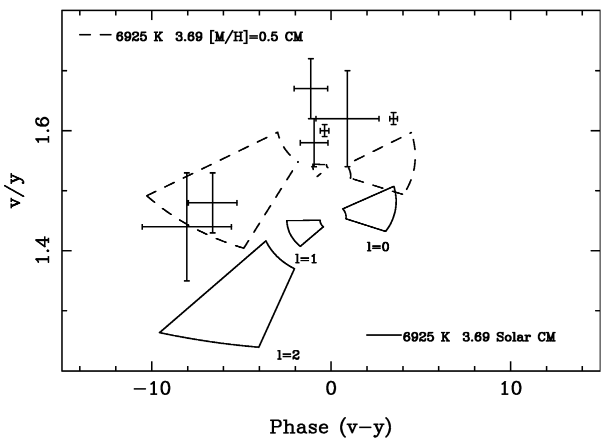

Figure 8. Same as Fig. 7, but with a non-standard treatment of convection from Canuto & Mazzitelli (1992).

Table 3 presents the observed results for the dominant modes of BI CMi. The unavoidable photometric uncertainties do not permit the derivation of reliable values of phase differences and amplitude ratios for the modes with very small amplitudes. The listed uncertainties were calculated from the residuals of the individual data points and assume random errors. To test the validity of the calculated uncertainties, we have subdivided the data into two parts: the 1998–1999 observing season versus the 1999–2000 season with the 1997 data added to this smaller data set. We compared the amplitude ratios and phase differences for both data sets and determined an experimental multiplication factor to the theoretical uncertainties. To our surprise, we obtained a factor of 1.0, i.e. the theoretically computed uncertainties in the amplitude ratios and phase differences are applicable.

Theoretical models to calculate amplitude ratios and phase differences were computed using different assumptions. Fig. 7 shows a comparison of the observed and computed values for two Kurucz stellar atmospheres (6925 K and $\log g = 3.69$, solar composition as well as for enhanced metals of $[M/H] = 0.5$). A phase lag between 90° and 135° and a parameter $R = 1$ to 0.1 have been assumed to calculate the regions where the different ℓ values are more probably located. These values of phase lag and R describe δ Scuti stars very well (Garrido 2000). Note that the higher metal content only increases the amplitude ratios, but does not affect the phase differences in a significant way. The reason is that for models containing more metals, the derivatives with respect to temperature, used for the computation of amplitude ratios, increase differentially more when one goes to shorter wavelengths.

We have also computed models with a non-standard treatment of convection from Canuto & Mazzitelli (1992). This is shown in Fig. 8. The net effect of this change is the increase of the vy ratio, but not the phase differences. The phase depends only on the phase lag, which is usually between 90° and 150° for δ Scuti stars, as well as on the size of the frequency.

The uncertainties based on different assumptions in the models, as well as the luminosity of BI CMi, mostly affect the size of the amplitude ratios, but have little effect on the phase differences. Consequently, the phase differences are the main diagnostic tool to identify the ℓ values. We note a good match with observations for the phase differences, but the computed amplitude ratios are too small.

8.4 Mode identifications

Table 3 lists the results of the mode identifications based on the observed phase differences. The photometrically identified modes range from $\ell = 0$ to 2. This result is typical for δ Scuti stars. The two dominant modes have $\ell = 0$ and 1.

At this stage we would like to defer a detailed discussion of the excited modes to later investigations, for which a variety of specific pulsation models will be computed to compare with the observations.

9 CONCLUSION

The results of this paper can be summarized as follows.

(i) The multisite campaign of BI CMi from 1997 to 2000 was characterized by excellent frequency resolution and high photometric accuracy. 1024 h obtained during 177 nights were used. This campaign utilized both photomultiplier and CCD photometry. The results from the two detectors could be combined at millimagnitude precision.

(ii) The early F star, HD 66829, which had been intended to be used as a second comparison star, was found to be a γ Doradus star with a millimagnitude amplitude.

(iii) For BI CMi, 29 pulsation frequencies could be extracted. These include 20 pulsation modes in the main pulsation frequency range from 4.8 to 13.0 cycle d^{-1} (55 to 150 μHz), eight linear combinations of other frequencies, and a very low frequency at 1.66 cycle d^{-1}.

(iv) The value of the low frequency at 1.66 cycle d^{-1} cannot be identified with a linear combination of other frequencies. Elliposidal variations can be excluded. The most likely explanations are pulsation or abundance spots. If pulsation is the origin, then BI CMi would be both a δ Scuti and a γ Doradus star, which is interesting considering its location in the Hertzsprung–Russell diagram: it is the range where both types of pulsators are found (near the cool edge of the classical instability strip). However, alternative explanations for this long-period variability need to be considered as well.

(v) Another outstanding property of BI CMi is the presence of a number of close frequency pairs in the power spectrum with separations as small as 0.01 cycle d^{-1}.

(vi) A rotational velocity of $v \sin i = 76 \pm 1\,\mathrm{km\,s^{-1}}$ was determined from a high-dispersion spectrum. We classify the star to have the spectral type of F2 IIIp SrEuCr:.

(vii) From phase differences, the dominant modes can be identified with ℓ values from 0 to 2. Arguments in favour of BI CMi being an evolved δ Scuti star such as 4 CVn and β Cas have been presented.

Further work presently under way involves the examination of the extremely close frequency pairs as well as modelling the detected frequencies with pulsation models.

ACKNOWLEDGMENTS

It is a pleasure to thank Dr Margit Paparó for helping to organize the Hungarian observations and Dr Mike Montgomery for helpful discussions. This investigation has been supported by the Austrian Fonds zur Förderung der wissenschaftlichen Forschung.

REFERENCES

Breger M., 1990, Comm. Asteroseismol., 20, 1
Breger M., 1993, in Butler C. J., Elliott I., eds, Stellar Photometry – Current Techniques and Future Developments. Cambridge Univ. Press, Cambridge, p. 106
Breger M., Beichbuchner F., 1996, A&A, 313, 858
Breger M., Hiesberger F., 1999, A&AS, 135, 547
Breger M., Stich J., Garrido R. et al., 1993, A&A, 271, 482
Breger M., Handler G., Garrido R. et al., 1999, A&A, 349, 225
Canuto V. M., Mazzitelli I., 1992, ApJ, 389, 724
Garrido R., 2000, in Breger M., Montgomery M. H., eds, ASP Conf. Ser. Vol. 210, Delta Scuti and Related Stars. Astron. Soc. Pac., San Francisco, p. 67
Gelbmann M., Kupka F., Weiss W. W., Mathys G., 1997, A&A, 319, 630
Gray R. O., Graham P. W., Hoyt S. R., 2001, AJ, 121, 2159
Handler G., 1999, MNRAS, 309, L19
Kaye A. B., Handler G., Krisciunas K., Poretti E., Zerbi F. M., 1999, PASP, 111, 840
Kurpinska-Winiarska M., Winiarska M., Zola S. T., 1988, IBVS, 3275
Kurtz D. W., 2000, in Breger M., Montgomery M. H., eds, ASP Conf. Ser. Vol. 210, Delta Scuti and Related Stars. Astron. Soc. Pac., San Francisco, p. 287
Kurucz R. L., 1993, CD-ROM 13, ATLAS9 Stellar Atmosphere Programs and 2 $\mathrm{km\,s^{-1}}$ Grid. Smithsonian Astrophys. Obs., Cambridge
Mantegazza L., Poretti E., 1994, A&A, 281, 66
Moon T. T., Dworetsky M. M., 1985, MNRAS, 217, 305
Morris S. L., 1985, ApJ, 295, 143
Pamyatnykh A. A., 2000, in Breger M., Montgomery M. H., eds, ASP Conf. Ser. Vol. 210, Delta Scuti and Related Stars. Astron. Soc. Pac., San Francisco, p. 215
Piskunov N. E., 1992, in Glagolevskij Y. V., Romanyuk I. I., eds, Stellar Magnetism. Nauka, St Petersburg, p. 92
Rodler F., Handler G., 2001, Comm. Asteroseismol., 140, 27
Rodriguez E., Breger M., 2000, A&A, 366, 178
Sperl M., 1998, Comm. Asteroseismol., 111, 1

This paper has been typeset from a TEX/LATEX file prepared by the author.

2.4.3 The rapidly rotating δ Scuti star AV Ceti[1]

Original paper:

T. H. Dall, **G. Handler,** M. B. Moalusi, S. Frandsen, 2003, A&A 410, 983

[1]There is a misprint in the title of the original paper due to an error of the publisher

A&A 410, 983–991 (2003)
DOI: 10.1051/0004-6361:20031327

Astronomy & Astrophysics

The rapidly rotating δ Scuti star AV Cetei*

T. H. Dall[1], G. Handler[2,3], M. B. Moalusi[4], and S. Frandsen[5]

[1] European Southern Observatory, Alonso de Cordova 3107, Casilla 19001, Santiago 19, Chile
[2] Institut für Astronomie, Universität Wien, Türkenschanzstrasse 17, 1180 Vienna, Austria
[3] South African Astronomical Observatory, PO Box 9, Observatory 7935, South Africa
[4] Department of Physics, University of the North-West, Private Bag X2046, Mmabatho 2735, South Africa
[5] Department of Physics and Astronomy, Aarhus University, 8000 Aarhus C, Denmark

Received 18 June 2003 / Accepted 22 August 2003

Abstract. We present results from an international spectroscopic and photometric campaign on the δ Scuti star AV Cet. The star has a rich and complex pulsation spectrum, and we find 7 individual frequencies, with evidence for many more present below our detection limit. We investigate the prospects for mode identification in fast rotators, using several different techniques. We compare the methods and conclude that although no single technique can give unambiguous mode identification, the collective evidence does allow some conclusions to be drawn, suggesting the presence of one radial mode at 14.598 d^{-1}. During the campaign we found the star HD 9139 to be a variable. From our photometry we find evidence for a variability time scale around 1 day, but we cannot find an unambiguous interpretation for its light variations.

Key words. stars: oscillations – stars: variable: δ Scuti – stars: individual: AV Cet – stars: individual: HD 9139

1. Introduction

Among the most promising targets for successful application of asteroseismology are the δ Scuti stars. They have rich sets of oscillation modes which in many cases are readily observable. Unfortunately, each δ Scuti star is only found to oscillate in a seemingly random subset of possible modes, making it difficult to identify exactly which modes are observed. To further complicate matters, many of these stars are rapid rotators, which causes displacement of the frequencies. In fact, the proper treatment of rotation seems to be one of the major obstacles for real progress in our understanding of the δ Scuti stars.

In the last years, considerable effort has been expended to establish reliable mode identifications for a number of δ Scuti stars, but in most cases we are left with some ambiguity. Purely photometric techniques have the advantage of greater efficiency, and ultimately the ability to observe fainter stars than is possible with spectroscopy. A secure mode identification seems only possible if several techniques agree. Especially for rapidly rotating stars, there are too many free parameters and the understanding of rotation is too poor for one method alone to give a unique answer.

In this paper we present results on the fast rotating δ Scuti star AV Cet (HD 8511, F0V, $V = 6.21$, $v \sin i = 212\ \mathrm{km\,s}^{-1}$), discussing mode identification using both purely photometric techniques and a technique that combines simultaneous photometry and low dispersion spectroscopy.

The star AV Cet is a relatively poorly studied star, although it was recognised as a variable more than 30 years ago by Jørgensen et al. (1971). Gonzalez-Bedolla (1990) and Gonzalez-Bedolla et al. (1990) found one frequency interpreted as the fundamental mode, and also some evidence of another mode. From their short photoelectric light curves it is evident that the star is multiperiodic. The multiperiodicity was also evident from the line index variations of Hβ and Hγ, found by Dall & Frandsen (2002), from only four hours of spectroscopy. Despite the poor time coverage, the modes found by Gonzalez-Bedolla could be confirmed and moreover, evidence for more modes at higher frequencies was found. It was thus clear that the pulsational content of AV Cet was not secured and that more observations were needed.

In this paper we report a multi-observatory campaign conducted in October and November of 2001, aimed at establishing the main pulsational modes of AV Cet and, via spectroscopy and multicolour photometry, attempting a mode identification. This strategy is the same as was used by e.g. Viskum et al. (1998) and by Dall et al. (2002): by knowing the frequencies found from a photometric campaign, we can measure the amplitudes of the spectroscopic line indices of the Balmer lines Λ^{H}, without having to solve for the frequencies simultaneously. Moreover, we can compare the results from using different mode identification techniques.

Send offprint requests to: T. H. Dall, e-mail: `tdall@eso.org`

* Based partly on observations made with the Danish 1.5 m telescope at ESO, La Silla, Chile.

Table 1. Details on the telescopes and observations.

Observatory	Telescope diam. [cm]	Nights assigned/observed	Hours obtained	Remarks
ESO, La Silla	50	9/6	41.5	*uvby* photometry
SAAO, Sutherland	50	14/9	42.2	*vby* photometry
ESO, La Silla	154	9^a/6	35.4	spectroscopy

[a] Granted 8 nights, but received half a non-photometric night from previous observer who needed photometric conditions.

2. Observations

In order to determine the frequency content of AV Cet and to be able to resolve modes with close frequencies, we needed long continuous photometric coverage. We observed in the Strömgren photometric filters in order to determine the pulsation periods, and the amplitudes in the *vby* bands, to be used for pulsation modelling and mode identification.

On the Danish 50 cm Strömgren Automatic Telescope (SAT) on La Silla we collected simultaneous *uvby* data with the four-channel photometer. On the 50 cm telescope at the South African Astronomical Observatory (SAAO), we acquired sequential *vby* data, excluding *u* because of its restricted use for mode identification of δ Scuti stars and to achieve denser data sampling.

With the Danish 1.54 m and DFOSC on La Silla, we had 8 nights of low resolution long slit spectroscopy. Resolution was around 6 Å with a 1.5″ slit, covering the Balmer lines from Hα to Hϵ. The CCD was windowed to improve the duty cycle, which with exposure times around 25–30 s was around 40%. These observations were carried out simultaneously with the photometric campaign.

Table 1 summarises the observations, which were all conducted between 24 Oct. and 4 Nov. 2001.

3. Data reduction

3.1. Strömgren photometry

The data from SAT and SAAO were reduced independently and later combined. For both data sets, we used HD 8070 (F2, $V = 6.6$) and HD 9139 (F5, $V = 6.7$) as comparison stars. It later turned out that HD 9139 is variable, and thus only HD 8070 was used as comparison. We will discuss the case of HD 9139 in Sect. 4.

The SAT data were reduced using the standard software developed at Copenhagen University Observatory. The reduction included airmass correction using standard extinction coefficients, and transformation to the standard photometric system.

The SAAO photometry was also reduced in a standard way. The correction for coincidence losses was followed by sky background subtraction. Nightly extinction coefficients were determined by means of the measurements of the constant comparison star HD 8070, and relative light curves of AV Cet and HD 9139 were computed with respect to HD 8070.

The timings were converted to Heliocentric Julian Date before combining the data sets from the two observatories.

3.2. Spectroscopy

The spectra were reduced using standard methods with IRAF[1].

After extraction of a spectrum, it was normalised to unity by dividing it by a fit to the sum of all the spectra. The spectra were neither wavelength calibrated nor flux calibrated, since the equivalent width (EW) and the line indices are relative quantities that are internally normalised by the continuum level. Consequently, they are not dependent on the precise intensity unit. Also, since we are looking for relative changes to this relative quantity, the amplitudes will be dimensionless, hence there is no need to convert pixel coordinates into true wavelength coordinates.

The line indices Λ^{H} were calculated for the Balmer lines Hα, Hβ, Hγ, and Hδ following the procedures described by Dall (2000) and applied by Dall et al. (2002) and Dall & Frandsen (2002). In short, a line index can be considered an analogue to a colour index, using software "filters" centered on the lines. The filters we have used are so-called super-Gaussians;

$$W = \exp\left(-\left(\frac{x - x_0}{b}\right)^8\right), \tag{1}$$

where x_0 is the position of the line centre, and b is the HWHM. Note the exponent of 8.

4. HD 9139: An unclassified variable star

It was clear from the light curves that HD 9139 was not suited as a comparison star, and it is also clear that some seemingly periodic variations are the cause. A period analysis gives two dominant signals at $0.34\,\mathrm{d}^{-1}$ and $0.91\,\mathrm{d}^{-1}$, but shows no signs of periods shorter than 1 day. However, there is a considerable amount of scatter at higher frequencies, which was why we were led to reject it as a comparison. We will discuss the cause of these variations in terms of damped pulsation, magnetic/rotational activity and nearby stellar companions.

The star is listed as F5 in SIMBAD with no indication of luminosity class. Also, no measurements of $v \sin i$ have been made so far.

HD 9139 was a target of the HIPPARCOS mission (ESA 1997), and Strömgren photometric indices are available from

[1] IRAF is distributed by the National Optical Astronomy Observatories, which are operated by the Association of Universities for Research in Astronomy, Inc., under cooperative agreement with the National Science Foundation.

the Lausanne-Geneva data base[2]. The calibrations of Crawford (1975) suggest the star is unreddened and has $M_v = 1.25 \pm 0.30$. It also seems metal-rich, as Nissen's (1988) calibration of the metallicity indicator δm_0 results in $[M/H] = 0.26$ for HD 9139. The HIPPARCOS parallax of the star implies $M_v = 1.68 \pm 0.23$, roughly in agreement with the absolute magnitude from the Strömgren colours. The model atmosphere calibrations of Kurucz (1991) then yield $T_{\rm eff} = 6850 \pm 100$ K and $\log g = 3.3 \pm 0.1$, which is near the red edge of the δ Scuti instability strip.

We have obtained high-resolution spectra of HD 9139 using the FEROS spectrograph on the ESO 1.52-m at La Silla Observatory. From the Fe I line at 4405 Å we estimate $v \sin i \sim 75$ km s^{-1}, hence a moderate rotation rate for a star at this position in the HR diagram. Comparison with spectra compiled by R. O. Gray[3] leads to a spectral type F5III-IV, based on the Ca II K line, the G-band, the strength of the Balmer lines, and the Ca I, Fe I and Mn I lines in the 4000–4400 Å range. The luminosity class was derived from the λ4077 Sr II and $\lambda\lambda$4172-8 Ti II, Fe II lines. This again places HD 9139 near the red edge of the instability strip, making it a δ Scuti or γ Doradus candidate. We plan to analyse the spectrum in detail and describe the characteristics in terms of basic parameters, abundances and $v \sin i$. With the knowledge of the abundance pattern we can try to sort out, whether the variability is due to a pulsational instability of some sort, due to magnetic effects (spots) coupled with rotation or due to some other phenomenon. This will be the subject of a later paper.

Using the abovementioned M_v and $T_{\rm eff}$ we can estimate a radius $R = 3.75\ R_\odot$ for HD 9139. The star then should have a fundamental radial mode period of ∼1 day (corresponding to a pulsation constant $Q = 0.033$ d), which agrees with one of the two time scales found. This argues immediately against an interpretation of HD 9139 as a γ Doradus star, as those objects have high-order g-modes excited ($Q > 0.23$ d, Handler & Shobbrook 2002). We also note that, within the errors, the amplitudes of these two variations do not change significantly between the *vby* bands, which is inconsistent with pulsational variability.

Another possibility is magnetic activity on the star, implying an Ap (or Fp) spectral type, which would produce a rotationally modulated variation. We find from the derived value of $v \sin i$ an upper limit on the rotational period around 2.5 days, which within the errors agree with the $0.34\,{\rm d}^{-1}$ found. This would imply a near equator-on view of the star. However, we would still expect to see colour variation if the variation is due to surface abundance inhomogeneities. More importantly however, the spectrum of HD 9139 indicates that it is a normal F-star with no peculiar abundances.

The apparent variability might be explained by contamination from a nearby star, letting varying amounts of light into the diaphragm of the photometer, although this is expected to lead to shorter time scales. We do not find any likely contaminating source in the vicinity of HD 9139. The nature of HD 9139 and its variability thus is still not clear.

5. Time series analysis

As stated earlier, the spectroscopic analysis was never expected to deliver the mode frequencies, but only to provide amplitudes and phases in the line indices $\Lambda^{\rm H}$ to be used for mode identification.

The photometry on the other hand is crucial in establishing the frequency content of AV Cet, and also for providing amplitudes and phases for the mode identification. Below, we will describe first the analysis of the photometric data, and present the results. Next, with the resulting mode frequencies, we will derive amplitudes and phases for the line indices.

5.1. Strömgren photometry: Finding the mode frequencies

Before commencing the frequency analysis, both series were individually cleaned of deviant points, using a 4σ criterion, and then merged. Since there is no overlap between the two series, we avoid problems with distortion of the window function, caused by having higher weight in the overlap regions. The differences between the mean values of the two data sets in any filter are of the order of 0.3%. The correction of this offset was found to have no effect on the time series analysis.

The observing procedure at the SAT yielded one *uvby* data point every few minutes, largely oversampling the time series. Hence, we combined points in the SAT data, bringing the sampling of the two data sets closer, in order not to artificially weight one set more than the other. The combination was done using a weight based on the point to point scatter, multiplied by a time-difference sensitive Gaussian weight. Our optimisation lead to a re-sampling close to 11 min for the SAT data. This re-sampling was also found to be optimal with respect to S/N in the amplitude spectrum.

The weighting scheme applied here is the one recommended by Handler (2003), which is an improvement of a scheme used by e.g. Viskum et al. (1998) and Frandsen et al. (1995), using a weight proportional to σ^{-x}, where σ is an estimate of the internal scatter, and x in general is close to 1. The best value was in our case found to be $x = 0.9$, by optimising the final S/N in the amplitude spectrum. The internal scatter was calculated from a high-pass filtered series, and the weights were Fourier analysed to check for any periodicities; none were found.

The frequency analysis was done using Period98 (Sperl 1998) finding and prewhitening one frequency at a time, until no more peaks above 4σ were present in the amplitude spectrum. At each step care was taken to avoid errors due to aliasing, by checking also the $\pm 1\,{\rm d}^{-1}$ solutions. Finally, frequencies, amplitudes and phases were determined by a simultaneous fit around the final frequency table. The formal uncertainty on the frequencies is $0.05\,{\rm d}^{-1}$ from the total time span of the observations of 10.04 days. We estimated the additional errors introduced by underlying modes and aliases by applying several schemes of weighting and extraction of the frequencies

[2] http://obswww.unige.ch/gcpd/gcpd.html

[3] http://nedwww.ipac.caltech.edu/level5/Gray/frames.html

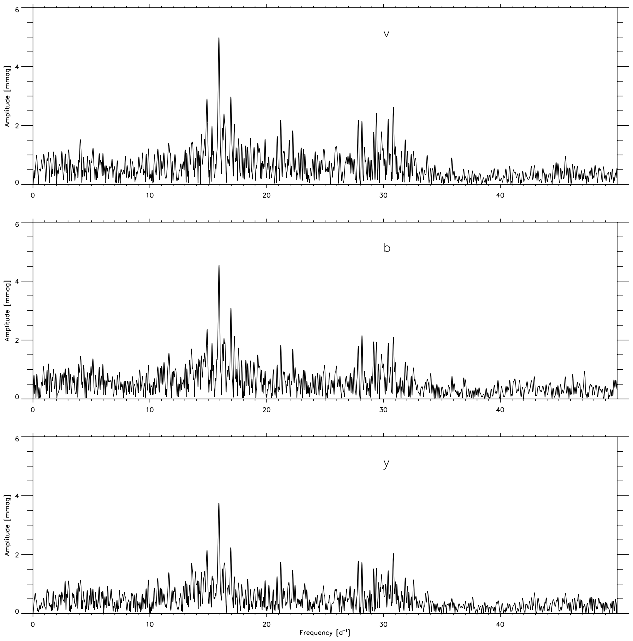

Fig. 1. The *vby* amplitude spectra of AV Cet.

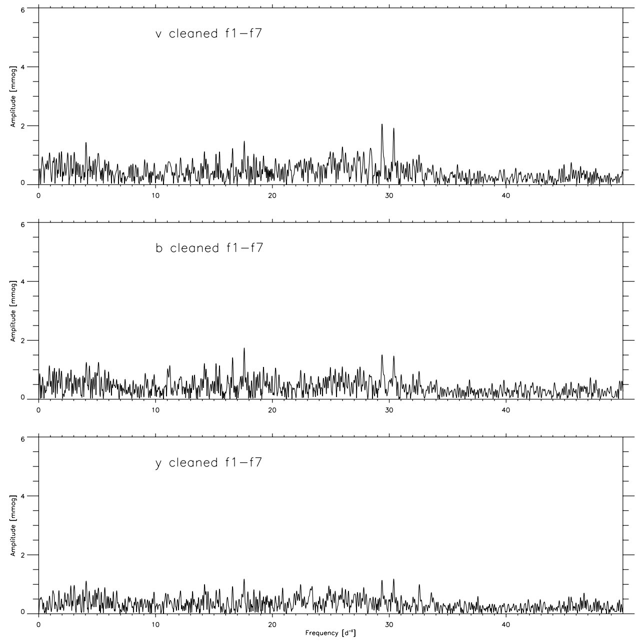

Fig. 2. The *vby* amplitude spectra of AV Cet after prewhitening with the frequencies f1–f7. There are quite evidently more modes present, most noticeable around 17 d^{-1} and 30 d^{-1} but these all have severe aliasing problems. See Table 2 and text for discussion.

Table 2. Modes detected in AV Cet. f1–f7 we regard as "safe", while the remaining modes all have some problems. See text for discussion.

ID	Frequency $[d^{-1}]$	Amplitude [mmag] v	b	y	S/N_v
f1	15.915	6.00 ± 0.44	5.46 ± 0.50	4.39 ± 0.36	13.6
f2	14.598	3.09 ± 0.43	2.96 ± 0.46	2.54 ± 0.34	7.2
f3	21.200	2.14 ± 0.48	1.76 ± 0.44	1.71 ± 0.40	4.5
f4	30.833	2.58 ± 0.54	2.01 ± 0.47	2.03 ± 0.37	4.8
f5	28.158	2.17 ± 0.64	2.12 ± 0.57	1.70 ± 0.46	3.4
f6	16.356	2.00 ± 0.47	1.69 ± 0.52	1.31 ± 0.37	4.3
f7	10.681	1.64 ± 0.39	1.38 ± 0.40	1.28 ± 0.33	4.2
The following modes are uncertain. See text for discussion.					
n8	17.59	1.49	1.75	1.19	
n9	14.19	1.03	1.14	1.00	
n10	30.38	1.91	1.39	1.17	

to the individual filters. The rms on the extracted frequencies was for all modes less than 0.01 d^{-1}, hence we adopt an error of 0.05 d^{-1} for the frequencies f1–f7 to be conservative. The results are summarised in Table 2. The amplitude spectra in the filters *vby* are shown in Fig. 1, while Fig. 2 show the corresponding spectra after removal of the frequencies f1–f7.

The errors on f1–f7 were calculated from the local residuals in the amplitude spectra after prewhitening with f1–f7. These errors do also include the contributions from n8–n10 and from any other undetected modes present. The noise level at frequencies above 40 d^{-1}, where the spectrum is essentially flat, was about a factor 2–2.5 better than the ones listed here, suggesting the presence of many unresolved low amplitude modes. Note that f5 is not detected above 4σ in any individual band ($S/N = 3.7$ in b and y). However, based on the collective evidence and on the fact that we find this mode above 4σ in all the line indices (Sect. 5.2), we have confidence in its reality.

The interpretation of the "modes" n8–n10 listed at the bottom of Table 2 is very problematic in such densely populated amplitude spectra. We do not feel confident about claiming accuracy or even reality for these modes, although they all stand out better than 4σ above the noise in at least one of the bands. Still, we find it worthwhile to list them for later reference. The inclusion of these modes in the solution for the amplitudes and phases, does not alter the solutions for f1–f7 noticeably.

For n8, we note that it is close to f2 + 3d^{-1}. On the other hand, it has significant amplitude, suggesting an independent mode interfering with the aliases of f2. The frequency of this mode however, must remain very uncertain given the large amount of unresolved modes evident in this region. The variations at frequency n9 may very well be an alias peak, and is merely included to show the level of unresolved power around this frequency. From Fig. 2 one may see two peaks around 30 d^{-1} separated by 1 d^{-1}. Whether this represents two modes interfering with each others aliases, or just a single mode (n10) is not clear.

5.2. Spectroscopic time series analysis

The calculation of the line indices involves choosing an integration filter for each line. This was done in the same way for all lines, finding the super-Gaussian filter that would optimise the S/N on the amplitude of f1.

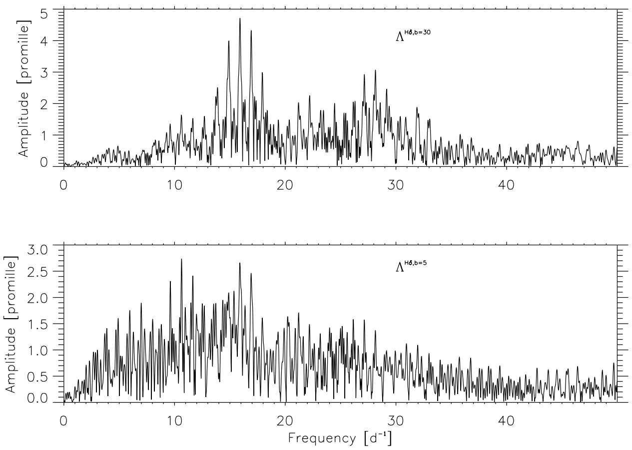

Fig. 3. Amplitude spectra of $\Lambda^{H\delta}$. The upper panel shows the amplitude spectrum for an integration filter including most of the line, while the lower one shows the result for a filter integrating only the core of the line.

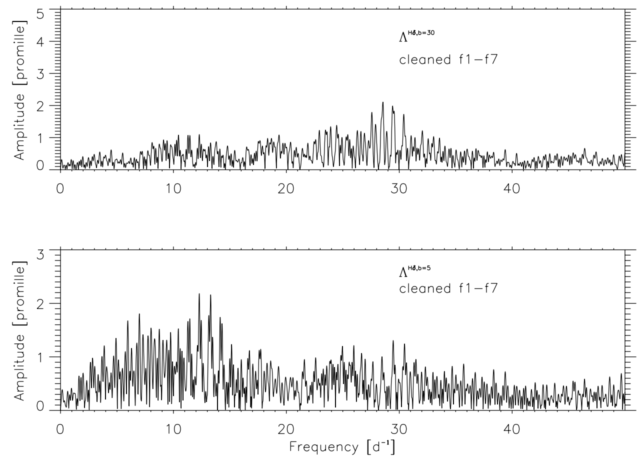

Fig. 4. Amplitude spectra of $\Lambda^{H\delta}$ after prewhitening with the frequencies f1–f7. The upper panel is for an integration filter including most of the line, while the lower panel shows the result for a filter integrating only the core of the line. As is evident, there are unresolved modes hidden in the noise.

Table 3. Results from prewhitening the line indices with f1–f7. All amplitudes are for the filter labelled $b = 30$ (Eq. (1)), except for $\Lambda^{H\delta,5}$ which lists the amplitudes in a filter that integrates only the core of the Hδ line. See text for discussion.

	Amplitude [promille][a]				
ID	$\Lambda^{H\beta}$	$\Lambda^{H\gamma}$	$\Lambda^{H\delta}$	$\Lambda^{H\delta,5}$	$S/N_{H\delta}$
f1	4.64 ± 0.50	5.27 ± 0.72	4.65 ± 0.40	3.09 ± 0.48	11.6
f2	1.78 ± 0.50	1.26 ± 0.72	1.78 ± 0.40	2.79 ± 0.42	3.0
f4	2.03 ± 0.73	2.14 ± 0.78	1.82 ± 0.75	1.11 ± 0.47	2.4
f5	3.08 ± 0.73	3.21 ± 0.79	3.13 ± 0.72	1.37 ± 0.49	4.1
f6	0.99 ± 0.50	2.00 ± 0.72	1.38 ± 0.40	1.71 ± 0.47	3.5
f7	0.99 ± 0.55	0.83 ± 0.71	0.99 ± 0.52	1.95 ± 0.66	1.9

[a] *Promille* is parts-per-thousand. One promille equals 1.086 mmag.

The line indices of the Balmer lines were analysed using the frequencies f1–f7 found in the Strömgren photometry as input. Before analysis the raw series was sigma-clipped to remove very deviant points. There were some obvious drifts in the series, which can often be removed by decorrelation with independent parameters that do not contain the pulsation signal. However, an investigation of external parameters like position of the spectrum on the CCD, seeing, continuum curvature etc. did not reveal any correlations or did not contain traces of the pulsational signal. Hence, we decided not to apply decorrelation to the series. Instead, the series was high-pass filtered to remove the drifts, while retaining the information in the (known) region of interest from ~8 d^{-1} and higher. Proper weights were constructed as outlined in the previous section.

The results from prewhitening with f1–f7 are summarised in Table 3. The amplitude spectrum, and the residuals after prewhitening are shown in Fig. 3.

As evident from Fig. 4 there are more modes excited in this star than the seven removed, which means that the accuracy of the amplitude determinations will suffer, as was the case for the photometry. The noise varies from ~0.6 promille around 10 d^{-1}, rising to ~0.8 promille at 30 d^{-1}, and levels out to around ~ 0.3 promille above 40 d^{-1}, which is the white noise level. Thus, the major contribution to the uncertainties comes from the unresolved modes, without which we would have gained up to a factor of 2.5 on the S/N.

Although the formal errors on the weaker modes are large, we can still have confidence in them since AV Cet is known to pulsate with these frequencies, found from the photometry.

In Table 3 we have listed the amplitudes of a Hδ line index $\Lambda^{H\delta,5}$ which is a very narrow integration filter that measures the amplitude in the core of the line. Note that f7 is significantly stronger here than in the line as a whole, meaning either that the variation is taking place only in the line core, or that the phase of the mode is changing between the core and the wings. Unfortunately, we do not have sufficient S/N to separate these two hypotheses, but an analysis of the line wings indicates that the mode is present but with a changing phase through the line. The other modes have a constant phase regardless of the position in the line.

We do not have a good model of the cause for this behaviour, but we might suggest that the nature of the mode is different from the other modes. The apparent presence of nodal lines in the phase suggests high m i.e. it could be a mode of $m \geq 2$. The low frequency of this signal lets us speculate that it could also be a g-mode or a mixed mode. Another explanation offered by Dall & Frandsen (2002) is that we see the effect of two very close unresolved modes, whose eigenfunctions are sampled differently at different depths of the atmosphere. As we have strong indications of many unresolved modes, this seems likely, although we do not have a precise model of such a scenario.

Table 4. Comparison between this work and earlier data. The formal errors on the GB amplitudes are 0.50 mmag.

	2001	1984
ID	y	V
f1	4.39	2.61
f2	2.54	4.45
f3	1.71	2.41
f4	2.03	0.98
f5	1.70	1.21
f6	1.31	0.79
f7	1.28	0.78

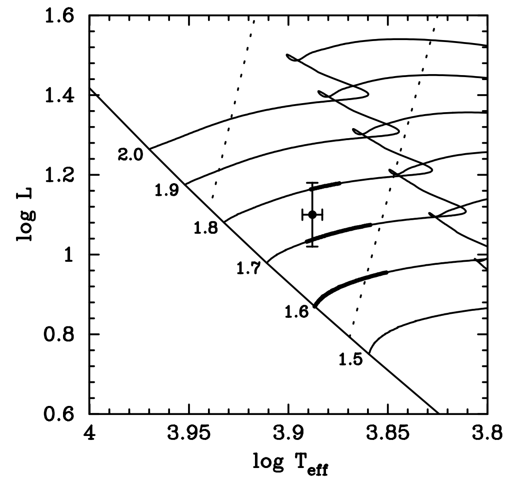

Fig. 5. AV Cet in the theoretical HR diagram. The filled circle shows the temperature and luminosity constraints we derived; error bars on these determinations are indicated. Stellar evolutionary tracks for models with $[Z] = 0.015$ and $v_{\rm rot,ZAMS} = 250$ km s^{-1} are indicated and labelled with their masses. The slanted solid line depicts the ZAMS for these models, and the slanted dotted lines are the edges of the δ Scuti instability strip. The thick sections of the evolutionary tracks correspond to models whose range of unstable pulsational frequencies matches that of AV Cet.

5.3. Consistency with previous results?

The findings by Dall & Frandsen (2002) of three modes in AV Cet from four hours of line index measurements in Oct. 2000, can now be reassessed. Given the low frequency resolution many of the determinations are ambiguous, hence f1, f2 and f6 can not be disentangled. Fitting these three as a single mode, and keeping f3, f4, f5 and f7, we are able to fit the short data set very well. Notably, we find that the high frequency modes have amplitudes comparable to the main mode.

We have investigated the photoelectric data of Gonzalez-Bedolla (1990), to check if the modes we have found in our data from Oct. 2001 were also present in Sep. 1984. Gonzalez-Bedolla reported the dominant mode at 14.593 d^{-1} (our f2 mode) with another mode around 19.186 d^{-1} (likely to be our f3 mode). In Table 4 we present the results of a reanalysis of the data using our f1–f7. As Gonzalez-Bedolla, we find f2 to be dominant with f1 and f3 also present. The modes f4–f7 are not present above the 4σ level. Hence, no measurable high frequency modes were present in 1984, and thus there was significant redistribution of the pulsational energy in the course of 16 years, possibly including amplitude variations and excitation of new modes.

6. Discussion

6.1. Temperature and luminosity of AV Cet

The discussion of the pulsational behaviour of AV Cet requires some knowledge of the star's position in the HR diagram. As AV Cet was both a target of the HIPPARCOS mission (ESA 1997) and as standard photometric colours in both the Strömgren and Geneva systems are also available[4], its effective temperature and luminosity can be determined.

The calibrations of the Strömgren system by Crawford (1979) applied to AV Cet suggest that the star is unreddened, slightly metal deficient ($\delta m_0 = 0.016$) and that it has an absolute magnitude $M_v = 2.1 \pm 0.3$. This is in excellent agreement with the HIPPARCOS result: $\pi = 14.83 \pm 0.77$ mas combined with $V = 6.21$ gives $M_v = 2.07 \pm 0.12$. Smalley's (1993) calibration in terms of metallicity suggests $[M/H] = -0.09$ for AV Cet and the model atmosphere grids by Kurucz (1991) imply $T_{\rm eff} = 7820$ K as well as $\log g = 4.1$.

Applying the calibration of Geneva photometry by Künzli et al. (1997) to AV Cet, we find $T_{\rm eff} = 7650$ K, $\log g = 4.0$ as well as $[M/H] = -0.2$, which is in good agreement with the outcome from the application of the Strömgren colour calibrations. Consequently, we adopt $T_{\rm eff} = 7730 \pm 90$ K as our temperature estimate, and with the bolometric corrections by Flower (1996) and Drilling & Landolt (2000) we find $M_{\rm bol} = 2.0 \pm 0.2$.

To place AV Cet in a theoretical HR diagram, its projected rotational velocity is also required. Two determinations are available from the literature: Abt & Morrell (1995) determined $v \sin i = 195$ km s^{-1}, and Royer et al. (2002) measured $v \sin i = 212$ km s^{-1}. As this is close to the break-up rotational velocity of a main-sequence A star, we must see AV Cet close to equator-on.

We computed evolutionary sequences of stellar models with the Warsaw-New Jersey code (see e.g. Pamyatnykh et al. 1998 for a description). Owing to the observational constraints determined above, we chose models with a heavy-element abundance $[Z] = 0.015$ and a rotational velocity of $v_{\rm rot} = 250$ km s^{-1} on the ZAMS. No convective core overshooting was used. We compare these tracks with the temperature and luminosity of AV Cet in Fig. 5.

It is suggested that AV Cet is a star of $1.75 \pm 0.06\ M_\odot$ about halfway in its main sequence evolutionary phase. We can check this finding with the application of a pulsational stability analysis (as explained by Pamyatnykh 2003). In brief, the range of unstable pulsation frequencies of a given pulsational model changes as it evolves. This frequency range can be matched

[4] `http://obswww.unige.ch/gcpd/gcpd.html`

with the one actually observed in the star. We have applied this method to AV Cet (taking into account rotational splitting due to fast rotation as well) along the evolutionary tracks plotted in Fig. 5, where models that reproduce the observed frequency range with their $\ell = 0{-}2$ modes are located along the thick parts of the tracks. We find very good agreement between the parameter space occupied by those models and the observationally determined position of AV Cet in the HR diagram. The modes excited in the models that match our constraint on the temperature from the colour photometry range from (almost) pure g modes that start as g_3 on the ZAMS through mixed modes up to pure p modes of radial order 5.

However, since such a fast rotating star will be highly flattened with many complicated phenomena going on like mixing, meridional circulations etc., we do not expect any current state-of-the-art models to fully describe AV Cet.

6.2. On mode identifications

As is evident from Figs. 2 and 4, we have not succeeded to extract all the pulsation modes that our formal accuracy would have allowed us to, mostly because of severe aliasing problems in regions very densely populated with unresolved modes. This is true both for the Strömgren photometry and for the line index spectroscopy, and it may even be different modes that dominate the residuals. As there is still substantial power left we can not expect to be able to make very accurate mode identifications based on amplitude ratios and phase differences.

Nevertheless, we present in Fig. 6 some mode identification plots suggested in the literature. Without attempting any definite mode identification, we will in the following compare the methods and discuss whether they collectively can point to any conclusions.

In the Viskum-diagram (e.g. Viskum et al. 1998, upper left-hand side panel of Fig. 6) the modes are grouped according to their spatial structure, i.e. to their ℓ or m values, with low-ℓ, m in the lower left and high-ℓ, m towards the upper right. This plot does indeed seem to indicate groupings, leading to f2 and f7 being radial modes. Alternatively, given the large errors on f7, its special phase values in Fig. 6 and its low frequency, a better interpretation is that f7 is a low degree ($\ell = 1$) g-mode. As discussed by Dall & Frandsen (2002), radial modes in δ Scuti stars seem to fall near amplitude ratios of 0.5, in support of the interpretation of f2 being radial. However, error bars are large. Certainly, the Viskum diagram has been used with success for a number of pulsating stars of various classes in recent years; (apart from FG Vir, the most notable are the roAp star α Cir, Baldry et al. 1998, 1999 and the EC 14026 star PG 1605+072, O'Toole et al. 2003). However, it is very likely that in the regime of very fast rotation, the geometrical properties on which the method relies are so heavily distorted that the interpretation is no longer correct. For the moderately fast rotator BN Cnc, Dall et al. (2002) discussed the interpretation of the amplitude ratios, noting that for such fast rotation the ratios would depend largely on m in combination with the inclination angle because of the large amount of gravity darkening in addition to the limb darkening. Thus, we would need to know the rotation period and $v \sin i$ independently. The modes with low amplitude ratios would nevertheless still have the smallest amount of spatial structure, so if we were to look for any radial modes, we would have to look among these modes. In the case of AV Cet, this means that if the star has radial modes, they would likely be found among the modes f2 and f7.

The multi-colour photometric method has been very successful in the past, using the Garrido-diagram (Garrido et al. 1990). One of the most serious shortcomings in this case is the lack of understanding of the effects of fast rotation, and of models able to take those into account. Such models would be necessary to assign "regions of interest" for specific values of ℓ within the diagram. But even if such models were at hand, the effort would be unfruitful because of the high rotation rate of AV Cet, which would cause the "regions of interest" to be not only inaccurate, but also to a great extent overlapping, hence making any identifications ambiguous. It is worth noting the large range in phase difference for AV Cet: for most other stars $\phi_{b-y} - \phi_y$ spans no more than 50°, while here we have a range of at least 200°, and even if we disregard the most uncertain point (f7), the range is more than 100°.

In the case of FG Vir, Breger et al. (1999) pointed out the very good agreement between the Garrido-diagram and the Viskum diagram in determining the ℓ values for the strongest modes of FG Vir. In the diagram presented by Breger et al., the modes are clearly grouped along a line of negative slope. One grouping corresponding to the radial modes was located at low $A(\mathrm{H})/A(v)$ and $\phi_v - \phi_y \sim 2°$, while high-ℓ modes were grouped at high $A(\mathrm{H})/A(v)$ and $\phi_v - \phi_y \sim -7°$. Only if we take the errors into consideration in the Breger-diagram of AV Cet do we find some resemblance, which would then indicate high spherical degree for the f3 mode, while the rest would have considerable ambiguity.

Without making any physical assumptions, Paparo & Sterken (2000) tested all possible combinations of photometric amplitude ratios and phase differences for the groupings of modes, that might be useful for mode identification in the star θ Tuc. They found that the combination $A(b)/A(y)$ versus $\phi_{b-y} - \phi_b$ was particularly useful for separating modes of different degree and radial order without giving any exact assignments to particular groups. The corresponding Paparo/Sterken-diagram for AV Cet may indeed show some separations. Following the interpretation of the phase difference reflecting the degree, we may here see at least three different groupings, with f7 belonging to the lowest one. If we exclude f7, the mode with the highest positive phase difference is f2, which we already suspected as the radial mode. The errors on the amplitude ratios are quite high, and do not allow us to suggest any groupings. As with the Garrido-diagram the phase differences span a large range: here the modes cover at least 100°, while for θ Tuc the range was ~35°.

7. Conclusions

We have found a previously unknown variable star, HD 9139, the nature of which is still unclear. Under a pulsational hypothesis, the Q-value disagrees with an interpretation of HD 9139

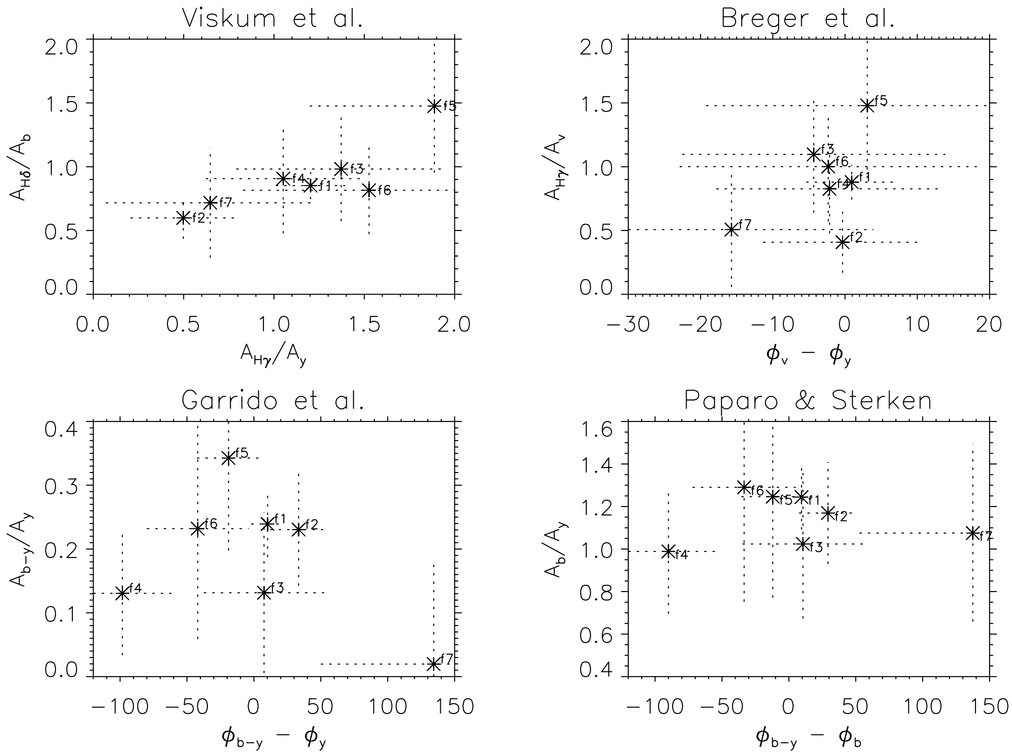

Fig. 6. The different mode identification plots suggested in the literature. The top left plot is the one used by Viskum et al. (1998) and Dall et al. (2002), while the top right one is the plot used by Breger et al. (1999) to demonstrate the good agreement in the case of FG Vir between the method of Viskum et al. and the photometric method – which is the plot on the lower left (Garrido et al. 1990). The lower right plot is similar to that empirically suggested by Paparo & Sterken (2000) for θ Tuc.

as a star of the γ Doradus type, but the star could be a δ Scuti star just leaving the instability strip.

Another explanation may be abundance inhomogeneities, possibly induced by magnetic activity, which coupled with rotation produces the variation. The spectrum seems however to indicate a normal F star. Both scenarios are somewhat limited by the absence of amplitude variations with colour.

The rapidly rotating δ Scuti star AV Cet has turned out to be an extremely interesting object. From this observing campaign we find seven individual pulsation modes with good evidence for more, and from comparison with old data, we see significant redistribution of pulsational energy, suggesting that the star has undergone amplitude variations and excitation of new modes during the course of 16 years.

The fast rotation is the main cause of the difficulties involved in establishing secure mode identifications for this star. We have compared several methods previously used for other δ Scuti stars, but find that none of them provides any clear interpretation of the mode nature. Based on the collective evidence, we do however propose the mode f2 $= 14.598\,\mathrm{d}^{-1}$ as our best candidate to be radial based on the tendency for low degree modes to give small amplitude ratios in the Viskum diagram. This is supported by the positive phase difference $\phi_{b-y} - \phi_y$. Likewise, we suggest that f5 $= 28.158\,\mathrm{d}^{-1}$ may be a high-degree ($\ell = 2$–3) mode, based on the high amplitude ratios demonstrated by the Viskum-, Breger-, and Garrido-diagrams. We also suggest that the mode f7 $= 10.68\,\mathrm{d}^{-1}$ may be a mode of $m \geq 2$ and/or a low order g-mode, based on the peculiar behaviour in the line profile of the Balmer lines, and on its very large phase differences, which point to a different mode nature.

We have shown that the various diagrams used for mode identification show significant differences between the seven detected modes. The interpretation is difficult due to the fast rotation of AV Cet, although one gets an idea about the division of the modes in low and high spatial structure modes. A better theoretical understanding of the effects of rotation on observable parameters is needed. AV Cet is a highly interesting target for further studies in this direction because of its unevolved nature and its large number of observable pulsation modes.

Acknowledgements. We wish to thank L. F. Olesen for giving us half a night of her assigned observing time at the Danish 1.54 m. This research was supported by the Danish Natural Science Research Council through its centre for Ground-Based Observational Astronomy, IJAF. This research has made use of the SIMBAD database, operated at CDS, Strasbourg, France.

References

Abt, H., & Morrell, N. I. 1995, ApJS, 99, 135
Baldry, I. K., Bedding, T. R., Viskum, M., et al. 1998, MNRAS, 295, 33
Baldry, I. K., Viskum, M., Bedding, T. R., et al. 1999, MNRAS, 302, 381

Breger, M., Pamyatnykh, A. A., Pikall, H., & Garrido, R. 1999, A&A, 341, 151
Crawford, D. L. 1975, AJ, 80, 955
Crawford, D. L. 1979, AJ, 84, 1858
Drilling, J. S., & Landolt, A. U. 2000, in Allen's Astrophysical Quantities, 4th ed., ed. A. N. Cox (Springer Verlag), 392
Dall, T. H. 2000, in NOT in the 2000's, ed. N. Bergvall, L. O. Takalo, & V. Piirola (Univ. of Turku), 54
Dall, T. H., & Frandsen, S. 2002, A&A, 386, 964
Dall, T. H., Frandsen, S., Lehmann, H., et al. 2002, A&A, 385, 921
ESA 1997, The Hipparcos and Tycho catalogues, ESA SP-1200
Flower, P. J. 1996, ApJ, 469, 355
Frandsen, S., Jones, A., Kjeldsen, H., et al. 1995, A&A, 301, 123
Garrido, R., Garcia-Lobo, E., & Rodriguez, E. 1990, A&A, 234, 262
Gonzalez-Bedolla, S. 1990, Rev. Mex. A&A, 21, 401
Gonzalez-Bedolla, S., Rolland, A., Rodríguez, E., & Lopez de Coca, P. 1990, IBVS, 3533
Handler, G., & Shobbrook, R. R. 2002, MNRAS, 333, 251
Handler, G. 2003, Balt. Astron., 12, 253
Jørgensen, H. E., Johansen, K. T., & Olsen, E. H. 1971, A&A, 12, 223
Künzli, M., North, P., Kurucz, R. L., & Nicolet, B. 1997, A&AS, 122, 51
Kurucz, R. L. 1991, Van Vleck Obs. Contr., 11, 27
Nissen, P. E. 1988, A&A, 199, 146
O'Toole, S. J., Jørgensen, M. S., Kjeldsen, H., et al. 2003, MNRAS, 340, 856
Pamyatnykh, A. A. 2003, in Asteroseismology Across the HR Diagram, ed. M. J. Thompson, M. S. Cunha, & M. J. P. F. G. Monteiro (Kluwer), in press
Pamyatnykh, A. A., Dziembowski, W. A., Handler, G., & Pikall, H. 1998, A&A, 333, 141
Paparó, M., & Sterken, C. 2000, A&A, 362, 245
Royer, F., Grenier, S., Baylac, M.-O., Gomez, A. E., & Zorec, J. 2002, A&A, 393, 897
Smalley, B. 1993, A&A, 274, 391
Sperl, M. 1998, Comm. Asteroseismol., 111, 1
Viskum, M., Kjeldsen, H., Bedding, T. R., et al. 1998, A&A, 335, 549

2.5 Metallicism and pulsation

2.5.1 UBVRIJH photometry of two new luminous δ Scuti Stars and discovery of δ Scuti pulsation in the most evolved Ap star known

Original paper:

C. Koen, D. W. Kurtz, R. O. Gray, D. Kilkenny, **G. Handler,** F. Van Wyk, F. Marang, H. Winkler, 2001, MNRAS 326, 387

Mon. Not. R. Astron. Soc. **326,** 387–396 (2001)

UBVRIJH photometry of two new luminous δ Scuti stars and the discovery of δ Scuti pulsation in the most evolved Ap star known

C. Koen,[1★] D. W. Kurtz,[2,3,4] R. O. Gray,[5] D. Kilkenny,[1] G. Handler,[1] F. Van Wyk,[1] F. Marang[1] and H. Winkler[6]

[1]*South African Astronomical Observatory, PO Box 9, Observatory, 7935 Cape, South Africa*
[2]*Laboratoire d'Astrophysique de l'OMP, CNRS UMR 5572, Observatoire Midi-Pyrénées, 14 avenue Edouard Belin, F-31400 Toulouse, France*
[3]*Centre for Astrophysics, University of Central Lancashire, Preston PR1 2HE*
[4]*Department of Astronomy, University of Cape Town, 7701 Rondebosch, South Africa*
[5]*Department of Physics and Astronomy, Appalachian State University, Boone, NC 28608, USA*
[6]*Department of Physics, Soweto Campus, Vista University, Private Bag X09, 2013 Bertsham, South Africa*

Accepted 2001 April 24. Received 2001 April 18; in original form 2000 December 29

ABSTRACT

Time-series photometry of the *Hipparcos* variable stars HD 199434 and 21190 is reported. Both stars are pulsators of the δ Scuti type. Reclassifications of the MK types of the stars, based on new spectrograms, are given. HD 21190 is found to be F2III SrEuSi:, making it the most evolved Ap star known. Its Strömgren photometric indices support the peculiar spectral type. It is also one of the most evolved δ Scuti stars known. Its combined Ap–δ Scuti nature makes it an important test of models of pulsation in peculiar stars recently developed by Turcotte et al., although it is more extreme than any model they examined. Physical parameters of both stars are estimated from Strömgren and Hβ photometry, and *Hipparcos* absolute magnitudes. We attempt mode identifications based on amplitude ratios and phase differences from our photometry. The dominant pulsation of HD 21190 may be an overtone radial mode. The model fits for HD 199434 are even less satisfactory, but favour an $\ell = 2$ mode. Given the good quality and wavelength coverage of our data, the poor results from the application of the photometric theory of mode identification may call into question the use of that technique.

Key words: techniques: photometric – stars: individual: HD 199434 – stars: individual: HD 21190 – stars: oscillations – δ Scuti.

1 INTRODUCTION

The *Hipparcos* catalogue contains many new periodic variables. This paper is concerned with multiwavelength observations of two of these, HD 199434 (V388 Pav) and HD 21190 (CP Oct). Neither star is assigned to a specific variable class in the *Hipparcos Variability Annex* (European Space Agency 1997). Both stars have light curves that appear sinusoidal with peak-to-peak V amplitudes of about 0.05 mag and periods below 4 h. The spectral classifications of these stars are: F2/3Ib/II (Houk & Cowley 1975) and F2III SrEuSi: (this paper) for HD 21190; and F5II (Houk & Cowley 1975) and F5II–III with slightly narrow Ca II H and K lines (this paper) for HD 199434. *Hipparcos* parallaxes, which we discuss in Section 4 along with Strömgren photometry, support our luminosity types and suggest that the spectra are peculiar.

The spectral types place both stars in the δ Scuti instability strip. This, along with their observed amplitudes and periods, leaves no doubt that they are δ Scuti stars. Their luminosity classifications and *Hipparcos* luminosities place them amongst the most evolved δ Scuti stars. For example, the δ Scuti catalogue of Rodríguez et al. (1994) contains only four stars with luminosity classes II–III, and only one star that is classified as being of luminosity class II, out of about 300 stars.

It was the fact that the *Hipparcos* parallaxes indicated that these two stars are not as bright as their published luminosity classes that led us to obtain new spectra and spectral classifications for them. Those classifications, the *Hipparcos* luminosities and the Strömgren photometry indicate that HD 21190 is an evolved Ap star – probably the most evolved such star yet found – and HD 199434 may be an evolved Am (ρ Puppis star). While there are examples known, δ Scuti pulsation in Ap stars and Am stars is very uncommon. This problem of metallicity and pulsation has been extensively discussed recently from an observational point of view by Kurtz (2000) and from a theoretical point of view by Turcotte

★E-mail: ck@da.saao.ac.za

et al. (2000). We discuss this and the implications of our observations of HD 21190 further in Section 4.

We undertook *UBVRIJH* photometry of the two stars with the two aims of confirming them as δ Scuti stars, and comparing the light variations in different wavebands so as to test theoretical predictions. In the case of the δ Scuti star 1 Mon, Balona et al. (2001) pointed out that the long wavelength base of their observations (Strömgren *u* to Cousins *I*) stood them in good stead when attempting photometric mode identification. The present observations enable us to evaluate the usefulness of extending observations to the infrared.

Observations of the two stars are described in the next two sections. Derivations of the physical parameters of the stars follow in Section 4. Mode identification on the basis of the relations between the variations in different colours is dealt with in Section 5. Conclusions are drawn in Section 6.

2 TIME-SERIES PHOTOMETRY OF HD 199434

2.1 *Hipparcos* photometry

An amplitude spectrum of the 154 useful *Hipparcos* photometric measurements of HD 199434 appears in the top panel of Fig. 1. The effect of the 0.16-d periodicity identified in the *Hipparcos* catalogue is obvious near $f = 6.3\,\mathrm{d}^{-1}$, as is a second feature near $17\,\mathrm{d}^{-1}$. The window function plotted in Fig. 2 explains the origin of the secondary peak: it is the most prominent alias of the main feature. This is confirmed by the featureless spectrum obtained when pre-whitening the observations by a linear least-squares-fitted sinusoid (bottom panel of Fig. 1).

Fig. 3 shows an expanded view of the central part of the window function: it confirms that the frequency identification process is, for practical purposes, alias-free. A non-linear least-squares fit to the data of a sinusoid gave a best frequency of $6.31869 \pm 0.00003\,\mathrm{d}^{-1}$. The corresponding amplitude is 38 ± 3 mmag.

The *Hipparcos* photometric passband is very wide, the response being above 20 per cent of the peak value over the interval 3800–7000 Å; it essentially includes Johnson's *B* and *V*, and part of the R_C band.

2.2 *UBVRIJH* photometry

Optical measurements were made with the (photoelectric) Modular Photometer mounted on the SAAO 0.5-m telescope; see Kilkenny et al. (1988) for a description of the instrument. The *UBV* filters used had standard Johnson passbands; the *R* and *I* filters were from the Cousins system. The infrared observations were made utilizing the SAAO Mk II Infrared Photometer attached to the SAAO 0.75-m telescope. The instrument is a slightly upgraded version of the Mk I instrument described by Glass (1973). Logs of the 36 h of *UBVRI* and 24 h of *JH* differential photometry are given in Table 1. Comparison stars used were HD 201477 (F6V) and HD 196480

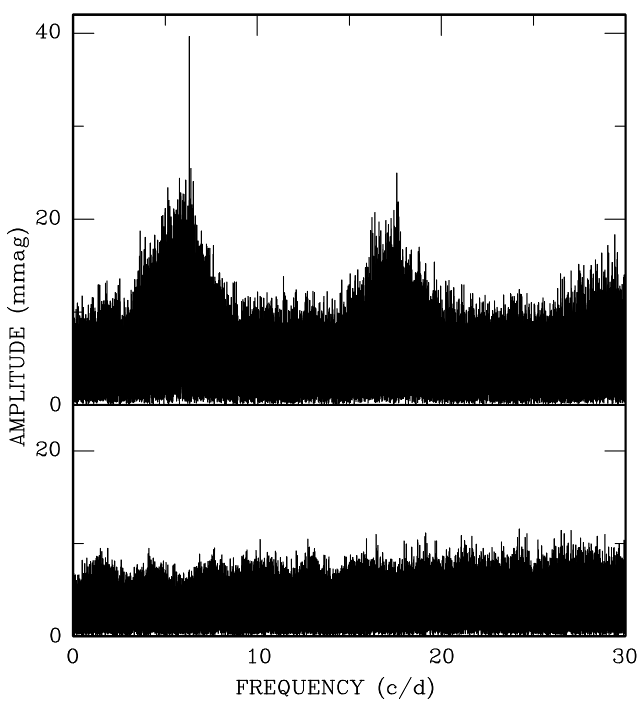

Figure 1. An amplitude spectrum of the *Hipparcos* observations of HD 199434, over the frequency range of interest (top panel). The bottom panel shows the spectrum of the residuals after removal of the best-fitting sinusoid with frequency equal to the peak frequency in the top panel.

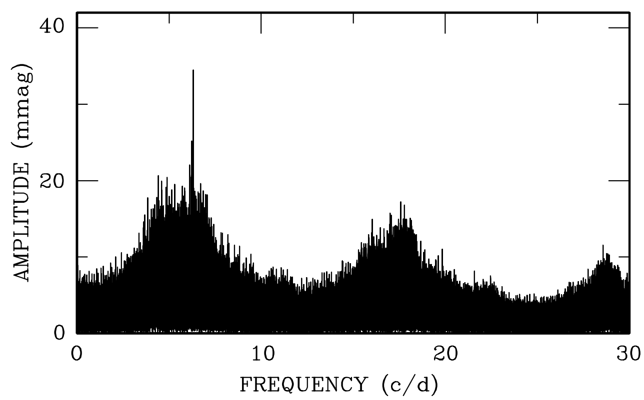

Figure 2. The window function of the *Hipparcos* photometry of HD 199434. This spectral window has been generated from a noise-free artificial sinusoid sampled at exactly the times of observation and with the same frequency and amplitude as the highest peak in Fig. 1. The asymmetry is a result of the reflection of the window pattern at zero frequency or, alternatively, from spillover of the negative-frequency window function.

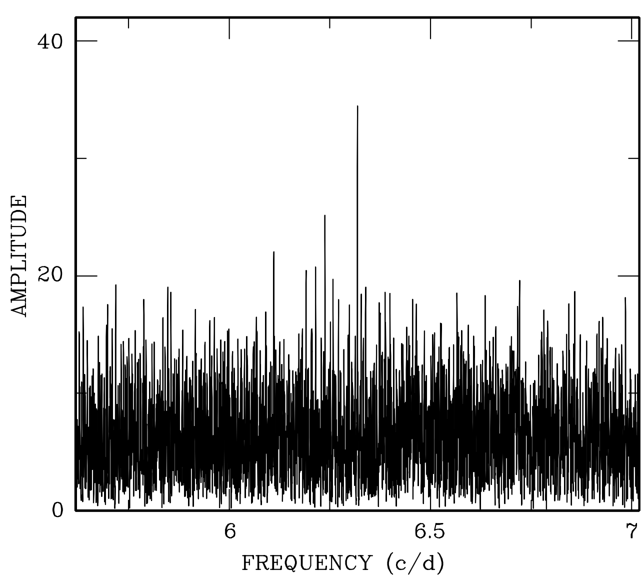

Figure 3. A detailed view of the central portion of Fig. 2.

Table 1. Log of the *UBVRI* and *JH* differential observations of HD 199434. Measurements were made in the visual with the photoelectric Modular Photometer attached to the 0.5-m telescope, and in the infrared with the Mk II Infrared Photometer attached to the 0.75-m telescope, of the South African Astronomical Observatory. In the last column the number of differential observations, *N*, is given.

Starting time JD 245 0000+	Run length (h)	N
	UBVRI	
1006.385	6.13	54
1017.295	8.25	76
1086.261	4.47	33
1087.366	1.74	15
1088.256	4.49	30
1089.259	4.47	35
1091.305	3.36	29
1111.293	1.14	8
1112.300	2.26	18
Total:	36.3	298
	JH	
1086.312	2.99	54
1088.231	4.90	81
1089.271	3.92	58
1091.303	3.15	53
1107.259	2.73	52
1109.261	2.65	39
1112.250	3.38	52
Total:	23.7	389

Table 2. Linear least-squares solutions for a fit of a sinusoid with $f = 6.31869\,\mathrm{d}^{-1}$ to the observations of HD 199434 in the various wavebands. The formal standard errors are known to underestimate the true errors. Phases are with respect to $T_0 =$ JD 245 1006.3846.

Filter	Amplitude (mmag)	Phase (rad)
U	37.1 ± 0.4	0.67 ± 0.01
B	36.3 ± 0.4	0.59 ± 0.01
V	25.5 ± 0.3	0.61 ± 0.01
R	19.8 ± 0.3	0.62 ± 0.02
I	16.2 ± 0.4	0.68 ± 0.02
J	9.3 ± 0.6	0.70 ± 0.06
H	6.9 ± 0.5	0.58 ± 0.07

(F2IV) in the optical, and HD 203608 (HR 8181, γ Pav; F6V) in the infrared. The comparison stars were chosen to be within 7° of the programme star to minimize differential extinction; at the far southerly declination of these stars ($-65°$ to $-72°$) this problem is minimal. For the optical photometry the measurement sequence (comparison star 1 – programme star – comparison star 2 – programme star) was repeated throughout the run; in the infrared, the comparison star was observed every 20–30 min. The measurements of the comparison stars were time-interpolated and used to correct the programme star observations for the effects of atmospheric transparency changes.

The means of the photometric indices were calculated for each night, and the mean values from the longest runs were used to estimate mean indices and their standard errors. The results are $V = 8.728 \pm 0.009$, $B - V = 0.467 \pm 0.007$, $U - B = 0.166 \pm 0.005$, $V - R = 0.259 \pm 0.007$, $V - I = 0.506 \pm 0.006$, $J = 7.920 \pm 0.002$ and $H = 7.701 \pm 0.002$; the standard errors were calculated from the nightly means.

Fitting a sinusoid to the *B*-band data by a non-linear least-squares technique leads to a frequency of $6.31868 \pm 0.00004\,\mathrm{d}^{-1}$. The agreement with the *Hipparcos* result is remarkable. We adopt the *Hipparcos* frequency as definitive, and fit sinusoids with this frequency to the observations in the various wavebands. The solutions for the amplitudes and phases are given in Table 2. As expected, the amplitude declines with increasing wavelength.

For illustrative purposes, some of the data for the *B* and *J* bands are plotted in Figs 4 and 5.

The two optical comparison stars show no variability in the amplitude spectrum of their differential magnitudes with respect to each other. Since HD 196480 (F2IV) lies on the red edge of the observed δ Scuti instability strip and within the γ Dor instability strip (see Handler 1999a), and HD 201477 (F6V) lies at the red edge of the γ Dor instability strip (Handler 1999a), it is significant that we can put upper limits to their potential variability of 2 mmag at frequencies of 4–$50\,\mathrm{d}^{-1}$ appropriate for δ Scuti stars, and 3 mmag for frequencies of 0.3–$3\,\mathrm{d}^{-1}$ appropriate for γ Dor stars. We also note that, although the SIMBAD data base has HD 203608, our infrared comparison star, flagged as a variable star, there is no evidence of variability in the *Hipparcos* data for this star at the level of 2 mmag between 0 and $50\,\mathrm{d}^{-1}$, nor is there evidence of variability in SAAO infrared observations, for which it is a standard star.

3 TIME-SERIES PHOTOMETRY OF HD 21190

3.1 *Hipparcos* photometry

There are 121 useful *Hipparcos* epoch photometric measurements of HD 21190. An amplitude spectrum of the data appears in Fig. 6; the highest peak in the top diagram corresponds to a frequency of $6.67775\,\mathrm{d}^{-1}$. Pre-whitening by this frequency leaves the spectrum shown in the bottom panel; this has no evidence of remaining periodicities. As we showed in Figs 2 and 3 with HD 199434, there is no confusion with aliases from the window pattern, so we do not show the spectral window in this case. Fitting a sinusoid to the data by a non-linear least-squares technique gives a best frequency of $6.67773 \pm 0.00004\,\mathrm{d}^{-1}$. The corresponding amplitude is 26 ± 2 mmag.

3.2 *UBVRIJH* photometry

Logs of the 25 h of *UBVRI* and 23 h of *JH* differential photometry are given in Table 3. Comparison stars used were HD 25254 (F3II/III) and HD 22237 (F5V) in the optical, and HD 29116 (F1III) in the infrared. As with HD 199434, the comparison stars were chosen to be close (within 3°) to the programme star to minimize differential extinction; at the far southerly declination of these stars ($-81°$ to $-84°$) this problem is minimal. The observations were obtained and reduced as for HD 199434. Results based on the nightly means from the longer runs are $V = 7.603 \pm 0.024$, $B - V = 0.396 \pm 0.005$, $U - B = 0.151 \pm 0.005$, $V - R = 0.210 \pm 0.002$, $V - I = 0.417 \pm 0.007$, $J = 6.976 \pm 0.006$ and $H = 6.772 \pm 0.006$. The *UBVRI* photometry agrees very well with that of Moreno & Carrasco (1986).

Results for the night of JD 245 1112 were not included in the

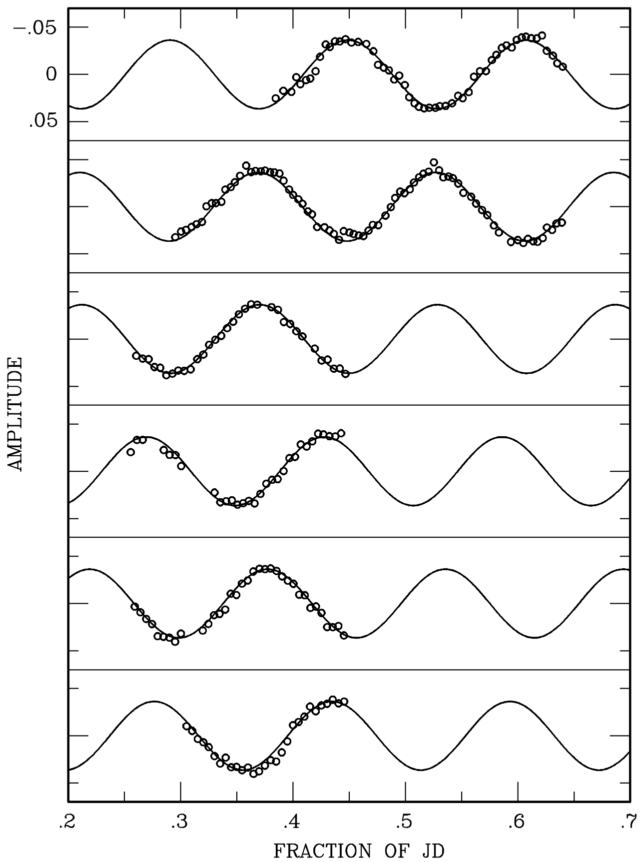

Figure 4. The best-fitting sinusoid with a frequency of 6.31869 d^{-1} superimposed on the *B*-band observations of HD 199434. The zero-point has been set to the mean of the data ($B = 9.195$). Only the six longest runs from Table 1 are shown.

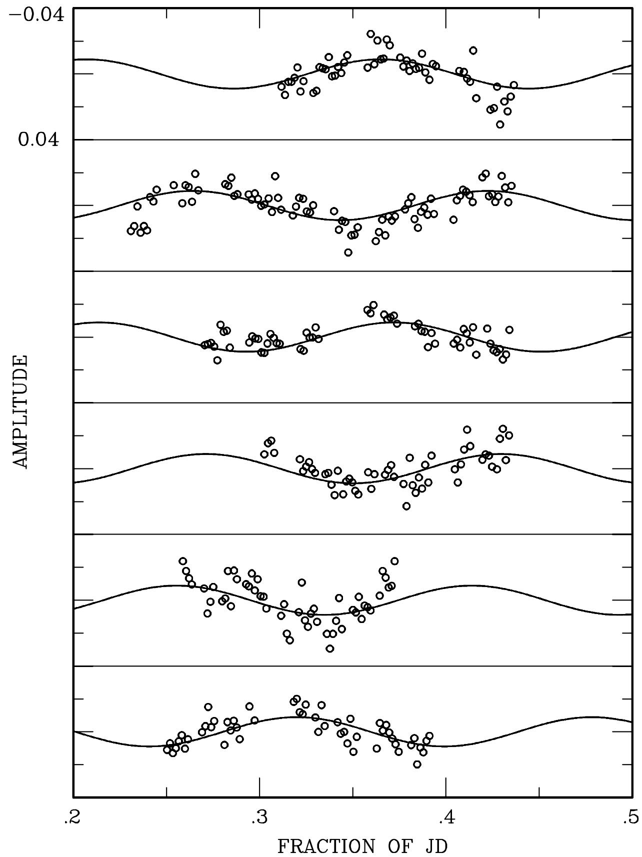

Figure 5. The best-fitting sinusoid with a frequency of 6.31869 d^{-1} superimposed on the *J*-band observations of HD 199434. The zero-point has been set to the mean of the data ($J = 7.92$). Only the six longest runs from Table 2 are shown.

mean calculations reported above: the seeing during the second part of the night was very poor, necessitating the use of very large apertures. A close companion star of HD 21190, CPD-83 64B, with $V \approx 10.8$, was within the aperture on this night. Mean brightnesses of HD 21190 in the different wavebands for this night were adjusted to bring them into line with the other nights.

The best-fitting frequency to the *B*-band data is $6.6792 \pm 0.0009\,d^{-1}$. This is acceptably close to the *Hipparcos* frequency, so we adopt the latter, 6.67773 d^{-1}, as definitive. After pre-whitening by that frequency, an examination of the amplitude spectrum shows that there is considerable power left in the residuals. Successive pre-whitening of the data by sinusoids with frequencies corresponding to the highest periodogram peaks led to the results shown in Fig. 7. Consideration of the *UBVR* data sets led to the conclusion that there are at least three modes in addition to that observed by *Hipparcos*, with frequencies near 6.1, 8.6 and 11.9 d^{-1} (or aliases of these). However, a glance at Fig. 7 shows very clearly that an unambiguous solution is out of the question. Fortunately – as might have been anticipated from the *Hipparcos* results, and as is confirmed by Fig. 7 – the light variations are dominated by the 6.67773-d^{-1} cycle, so that the solution for this mode (Table 4) is reasonable. It is noteworthy that the errors on the amplitudes in Table 4 are largest for the *U* and *B* bands. The reason lies in the different constitutions of the photometric noise, which consists of both a random and a systematic component. The former is due to measurement error, while the latter can be ascribed to the presence of further pulsation modes. The systematic noise becomes more and more dominant towards the blue, as the amplitudes of the

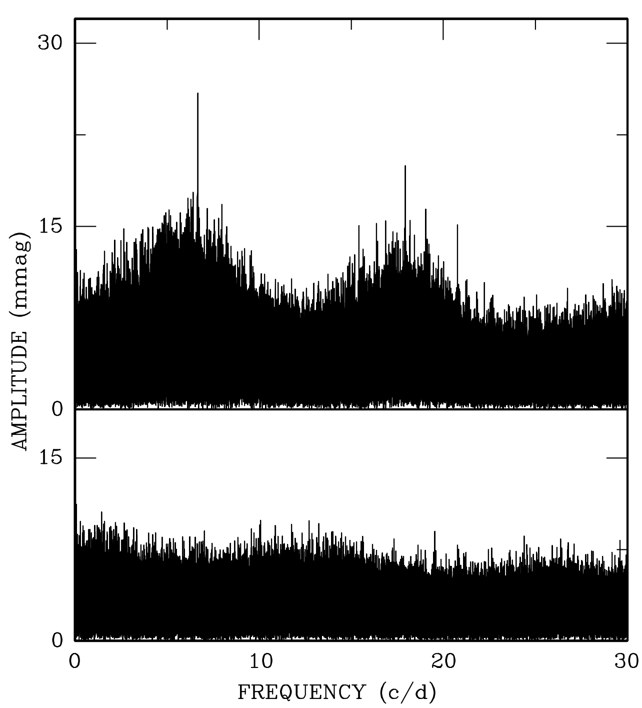

Figure 6. An amplitude spectrum of the *Hipparcos* observations of HD 21190, over the frequency range of interest (top panel). The bottom panel shows the spectrum of the residuals after removal of the best-fitting sinusoid with frequency equal to the peak frequency in the top panel.

Table 3. Log of the *UBVRI* and *JH* observations of HD 21190. The experimental setups were as for the observations of HD 199434. In the last column the number of differential observations, *N*, is given.

Starting time JD 245 0000+	Run length (h)	*N*
	UBVRI	
1088.460	4.00	30
1089.460	3.75	30
1091.457	3.96	32
1101.406	1.93	16
1104.463	3.57	25
1109.435	4.08	33
1112.443	3.78	29
Total:	25.1	195
	JH	
1088.462	4.23	74
1089.462	3.90	52
1091.457	4.37	76
1109.412	4.39	71
1111.345	1.96	28
1112.430	3.71	45
Total:	22.6	346

Table 4. Linear least-squares solutions for a fit of a sinusoid with $f = 6.67773\,\mathrm{d}^{-1}$ to the observations of HD 21190 in the various wavebands. The formal standard errors given are known to underestimate the true errors. Phases are with respect to $T_0 =$ JD 245 1088.4603.

Filter	Amplitude (mmag)	Phase (rad)
U	34.6 ± 1.0	2.61 ± 0.03
B	34.4 ± 1.1	2.53 ± 0.03
V	24.1 ± 0.7	2.58 ± 0.03
R	19.2 ± 0.7	2.51 ± 0.04
I	14.7 ± 0.5	2.62 ± 0.04
J	9.6 ± 0.6	2.37 ± 0.06
H	7.2 ± 0.6	2.26 ± 0.09

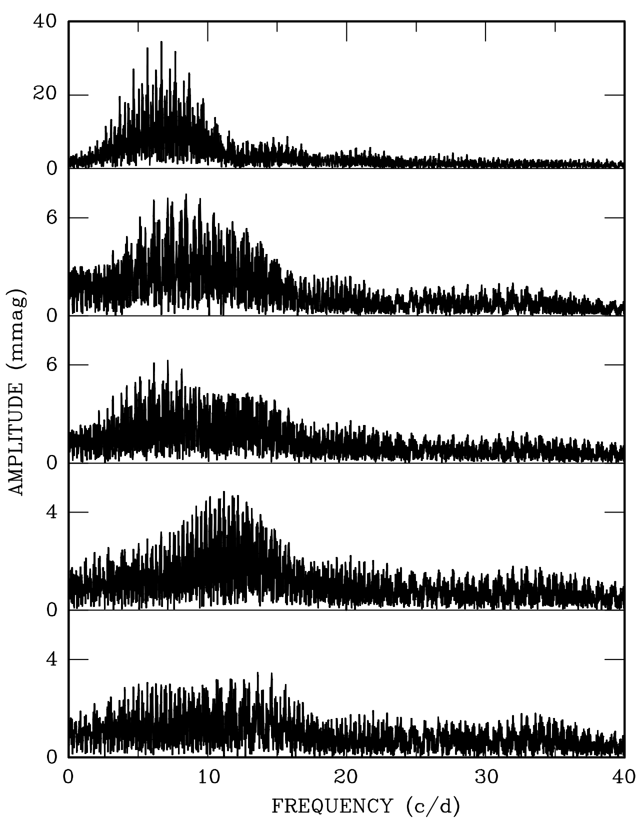

Figure 7. The top panel contains an amplitude spectrum of the *B*-band observations of HD 21190. The second panel shows the spectrum of the residuals after pre-whitening the data by the *Hipparcos*-determined frequency. Further panels show the effects of pre-whitening by the frequency corresponding to the highest peak in the preceding panel. Note the different vertical scales used.

unresolved pulsation modes increase towards shorter wavelengths by a larger relative amount than the measurement error does.

4 PHYSICAL CHARACTERISTICS OF HD 199434 AND 21190

The *Hipparcos* parallax of HD 199434 is 3.65 ± 1.09 mas. Using the mean photometric measurement quoted above then yields $M_V = 1.54 \pm 0.65$ where the contribution from the uncertainty in V is negligible. This value of M_V is consistent with $M_V = 1.6$ given by Schmidt-Kaler (1982) for an F5III star, but is too faint for the luminosity class II assigned by Houk & Cowley (1975). The parallax of HD 21190 is 4.16 ± 0.63 mas, which implies that $M_V = 0.70 \pm 0.33$. The value of the absolute visual brightness is about one magnitude brighter than that of an F2III star, according to Schmidt-Kaler (1982), but again probably too faint for the Houk & Cowley (1975) classification F2/3Ib/II.

The discrepancies between the absolute magnitudes derived from the parallaxes and those inferred from the MK types prompted us to obtain new spectra. Spectroscopic observations of HD 21190 and 199434 were made with the unit spectrograph and charge-coupled device (CCD) detector on the 1.9-m telescope at the Sutherland site of the SAAO during 1998 October and December. To assist in classifying these HD stars, observations were also made of bright (HR) stars with similar spectral types but having a range of luminosity classes. These were: HR 856 (F5III), 1173 (F3III), 1746 (F5II), 6615 (F2Ia) and 7264 (F2II–III).

All data were obtained with grating 6, giving a reciprocal dispersion of approximately 100 Å mm^{-1} and a resolution of about 3.5 Å. The spectrograms were centred on about 4400 Å and have a useful range of ~3600–5200 Å. Arc spectrograms were obtained before and after every stellar spectrogram for wavelength calibration, and the usual sky and dome flats were taken at the start of each night for calibration of the CCD detector. All reductions were carried out with standard IRAF procedures to produce normalized, wavelength-calibrated results. These spectra are very similar in resolution and spectral range to those obtained by one of us (ROG) on the Gray/Miller spectrograph of the Dark Sky Observatory (Appalachian State University). MK standards from this spectrograph were used to supplement the above HR stars for classification purposes.

Comparison of the spectra with those of the above well-classified stars and MK standards led to the following conclusions:

The spectrum of HD 21190 is best classified as F2III SrEuSi:. This star is very similar to β Cas (F2III), except for the enhancements of Sr II 4077 Å and Eu II 4205 Å. The Si II doublet at 4128–31 Å is also enhanced, but a silicon peculiarity in such a late spectral type is unusual – hence the colon after Si. The spectrum of HD 199434 is very similar to that of HR 7495 (F5II–III), except that HD 199434 has slightly narrower Ca II K and H lines. This may indicate that this star shows mild Am/ρ Pup characteristics. However, as these discrepancies are not particularly remarkable, the appropriate classification is F5II–III.

4.1 Strömgren indices and evidence for spectral peculiarities

It is of interest to compare the above results with those obtainable from Strömgren $uvby\beta$ photometry. A number of Strömgren system measurements of HD 21190 are available, and these are reproduced in Table 5. Because there is a large scatter in these measurements, particularly for the c_1 index, we also include Hauck & Mermilliod's (1998) weighted values. Only one measurement of HD 199434 could be found in the literature (Handler 1999b), prompting us to obtain more intermediate-band absolute photometry, which is summarized in Table 6, along with the measurements of Handler (1999b). The Strömgren photometry was supplemented by 18 β-index measurements (mean 2.701 ± 0.007), which were obtained during a 3.1-h period on JD 245 1109.

Application of Crawford's (1975) F-star calibration to the weighted indices for HD 21190 leads to a value of $\delta m_1 = -0.059$ for the metallicity index and $\delta c_1 = 0.175$ for the luminosity index. The reddening correction in this case is zero. The absolute magnitude calibration of the δc_1 index (Crawford 1975, 1979) can be compared with the *Hipparcos* absolute magnitude for HD 21190 ($M_V = 0.70 \pm 0.33$, which implies that the c_1 index should be 0.833, using (Crawford 1975)

$$\Delta M_V = -[9 + 20(2.720 - \beta)]\delta c_1.$$

Thus the observed c_1 index is ≈0.1 smaller than would be expected for a normal star. This, plus the result for the δm_1 index, is typical for Ap stars and is indicative of a depression in the flux in the Strömgren v band. Since $c_1 = u - 2v + b$ and $m_1 = v - 2b + y$, we should expect the effect, if it is due to a flux depression in the v band, to be twice as large in c_1 as in m_1 and in the opposite direction, which is exactly what we see (note that because of the way the δm_1 index is defined, a negative δm_1 index corresponds to an *increase* in m_1). The depression in the v-band flux can be partially explained by the presence of the enhanced Sr II 4077 Å and Eu II 4129 Å lines, which lie in the Strömgren v band, but we have carried out numerical experiments that indicate that the extra blanketing produced by those two lines can only produce 10 per cent of the observed results. A high general metallicity [M/H] = 0.50 would produce the desired δm_1, but would actually result in a slight *increase* in δc_1 [see Lester, Gray & Kurucz (1986), although we have redone the calculations with the latest Kurucz models (Kurucz 1993)]. Thus a high metallicity is not consistent with the above discussion, nor is it consistent with our spectral type, which indicates that the star is very similar to the F2III standard β Cas, except for the enhancements of the Sr II and Eu II lines. A more probable explanation is the presence in this Ap star of the broad λ4100 flux depression common in CP2 stars (cf. Masana et al. 1998), which coincides with the Strömgren v band. This explanation obviously needs to be verified by more detailed spectrophotometry. The presence of the λ4100 flux depression is often accompanied by a flux depression centred on λ5200, which is the basis of Δa photometry used to detect Ap stars (Maitzen 1976). This flux depression is in the wing of the Strömgren y band, but has only a small effect on the flux in that band. Thus, we anticipate that the fluxes in the u, b and y bands for this star will be nearly normal.

Masana et al. (1998) have derived a peculiarity index for Ap stars based on Strömgren $uvby\beta$ photometry. Their peculiarity index for HD 21190 is $\Delta p = 1.8$, which is also supportive of our Ap classification, especially for such a cool Ap star.

With the *Hipparcos*-derived luminosity placing HD 21190 2.5 mag above the zero-age main sequence (ZAMS), the evidence is strong that it is the most evolved Ap star yet known. This is a

Table 5. Strömgren and Hβ photometry of HD 21190 from the literature.

y	$b-y$	m_1	c_1	β	Reference[a]
7.607 ± 0.005	0.226 ± 0.004	0.222 ± 0.006	0.753 ± 0.007		1, 2
7.62 ± 0.005	0.230 ± 0.003	0.210 ± 0.006	0.791 ± 0.005	2.710 ± 0.007	3
7.638 ± 0.005	0.240 ± 0.003	0.212 ± 0.004	0.716 ± 0.006		4
	0.233 ± 0.007	0.217 ± 0.005	0.735 ± 0.019	2.710	5

[a]Key: 1, Olsen (1983); 2, Perry (1991); 3, Eggen (1992); 4, Olsen (1994); 5, Hauck & Mermilliod (1998).

Table 6. Log of the Strömgren system observations of HD 199434. Measurements were made with the Modular Photometer attached to the 0.5-m telescope of the South African Astronomical Observatory. The standard errors of the nightly means are given.

Starting time JD 245 0000+	Run length (h)	N	y	$b-y$	m_1	c_1	β
1103	1.9	10	8.735 ± 0.022	0.271 ± 0.007	0.225 ± 0.007	0.663 ± 0.013	
1104	2.9	17	8.747 ± 0.017	0.283 ± 0.004	0.213 ± 0.005	0.661 ± 0.016	
1107	2.5	15	8.740 ± 0.015	0.289 ± 0.005	0.212 ± 0.007	0.656 ± 0.015	
1109	3.1	18					2.701 ± 0.007
All	7.3	42	8.741 ± 0.018	0.282 ± 0.008	0.215 ± 0.008	0.660 ± 0.015	
Handler (1999b)			8.71	0.271	0.205	0.690	

most interesting result. It has long been known that few δ Scuti stars are peculiar and that few peculiar stars in the δ Scuti instability strip pulsate. There is a good observational case for pulsation in some Am stars, but the case for δ Scuti pulsation in magnetic Ap stars has been contentious – see the papers by Kurtz (2000) and Turcotte et al. (2000). While Turcotte et al. (2000) do not deal with differences between Am and Ap stars, they find that peculiarities can coexist with pulsation for evolved stars towards the red edge of the δ Scuti instability strip.

Since our discussion above indicates that, apart from enhancements in strontium and europium, and the probable presence of a broad flux depression at λ4100, HD 21190 is fairly normal, we have estimated the basic parameters ($T_{\rm eff}$, $\log g$, [M/H] and $\xi_{\rm t}$, the microturbulent velocity) using a multidimensional downhill simplex technique recently developed by Gray, Graham & Hoyt (2001). This technique simultaneously finds the best fit to the observed spectrum and fluxes (from Strömgren *uby* photometry) from an interpolated four-dimensional grid of synthetic spectra and fluxes computed using model atmospheres from the stellar atmosphere program ATLAS9 (Kurucz 1993). Coincidentally, this method does not use the flux in the v band (because of the presence of Hδ in that band, which makes it useless for estimating continuum fluxes), and thus avoids the complications that we have mentioned above. While the v-band region is contained in our classification spectrum of HD 21190, utilized in the simplex method, the resulting basic parameters are hardly changed even if that region is given a weight of zero in the calculation.

For HD 21190, we derive the following parameters: $T_{\rm eff} = 6780 \pm 100\,{\rm K}$ $(\log T_{\rm eff} = 3.83)$, $\log g = 3.34 \pm 0.15$, $[{\rm M/H}] = -0.05 \pm 0.15$, $\xi_{\rm t} = 3.5 \pm 0.5\,{\rm km\,s^{-1}}$. This fit is illustrated in Fig. 8. We note that our fit is consistent with the monochromatic flux in the *R* filter.

The $T_{\rm eff}$ and $\log g$ derived from the simplex method are very close to what we expect for an F2III star (cf. Gray et al. 2001). It is of interest to note that the simplex results yield an overall metallicity that is nearly solar. This result is consistent with our spectral type, as well as with our above discussion of the Strömgren photometry, and strengthens our assertion that the effects in δm_1 and δc_1 are due, not to an enhanced overall metallicity, but to the presence of the λ4100 flux depression.

The *Hipparcos* luminosity (combined with a bolometric correction of 0.022 – Flower 1996) yields $\log(L/{\rm L}_\odot) = 1.6$. In Fig. 9 we reproduce the theoretical Hertzsprung–Russell (HR) diagram of Turcotte et al. (2000, their fig. 1, with kind permission of the authors) with the positions of HD 21190 and 199434 shown using the parameters derived above. This places HD 21190 near the red edge of the δ Scuti instability strip and shows it to be more evolved than any of the other stars discussed by them – supporting our suggestion that it is the most evolved Ap star known. From their evolutionary tracks it can be seen that HD 21190 has evolved from an early-A or even late-B main-sequence star. Since Turcotte et al. argue that the onset of pulsation does not erase diffusion-generated peculiarities that are already present, it would seem that

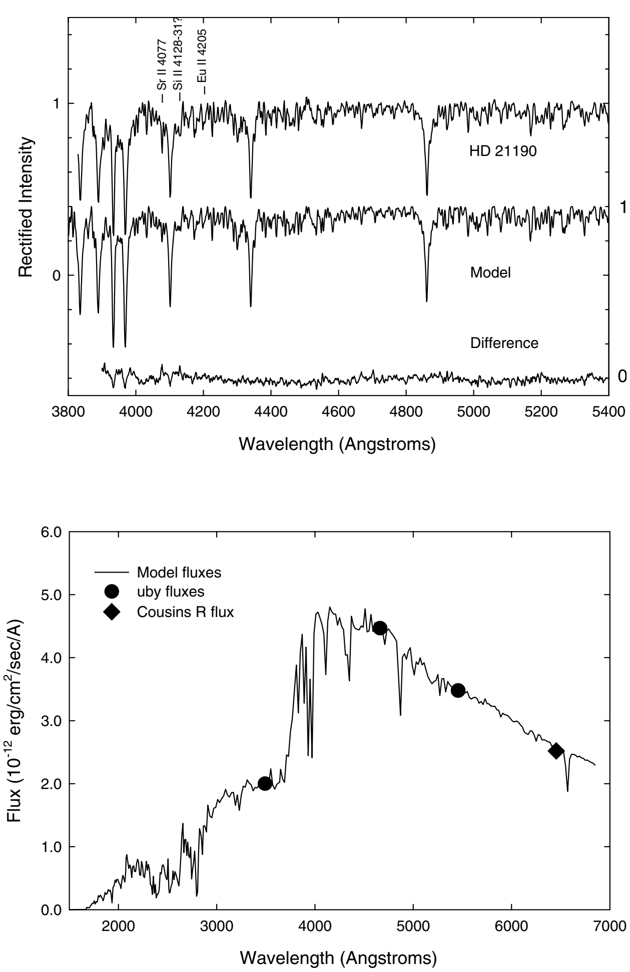

Figure 8. The multidimensional simplex method fit to the spectrum and fluxes for HD 21190. The top panel shows the model fit to the rectified intensity spectrum, with the difference spectrum below. Enhanced lines due to Sr II, Eu II and Si II are indicated in the observed spectrum. The low-frequency structure in the difference spectrum is due to errors in the rectification, and the high-frequency structure is due to line-to-line differences between the model and observed spectrum, slight wavelength differences between the two, and noise. The bottom panel shows the model fit to the Strömgren fluxes. Also shown is the monochromatic flux derived from the Cousins *R* filter, using the calibration of Bessell (1979).

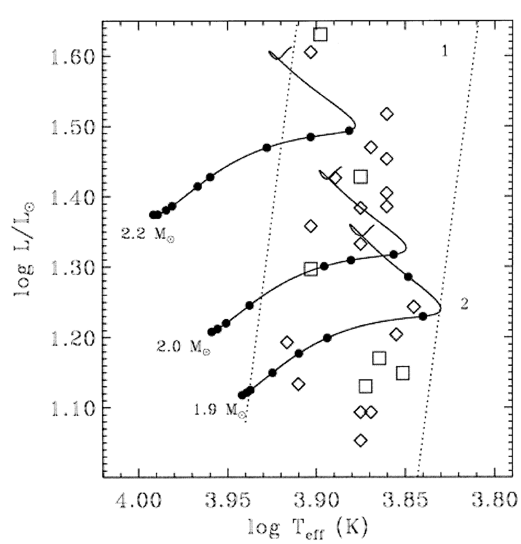

Figure 9. A theoretical HR diagram from Turcotte et al. (2000, with permission of the authors) showing the positions of HD 21190 (marked as 1) and HD 199434 (marked as 2). The evolutionary tracks are from models discussed by Turcotte et al. (2000); the squares are positions of δ Del stars (now preferably called ρ Pup stars – see Gray & Garrison 1989) from Kurtz (1976); the diamonds are δ Scuti stars from Russell (1995). See Turcotte et al. (2000) for a full discussion of this diagram.

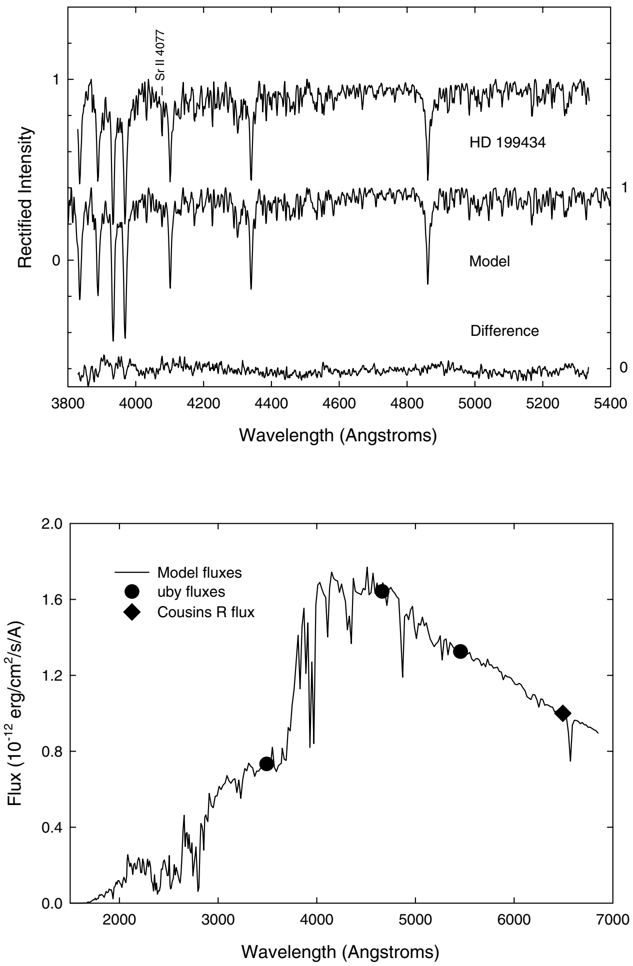

Figure 10. The same as Fig. 8, except for HD 199434.

HD 21190 has evolved from a (magnetic) Si star, and hence still shows the Si anomaly. A detailed study of this star's spectrum would be very rewarding, as would a test for a magnetic field.

HD 199434 is less extreme in every way than HD 21190, but still of some interest. Although we classified it as a normal star, we did note a slightly narrow Ca II K line, indicating a mild Am/ρ Pup nature. The Strömgren indices give some indication as well that it is peculiar. The intrinsic relations of Crawford (1975) indicate, for $E(b-y) = 0.035$, $\delta m_1 = -0.054$. This δm_1 suggests an Am or Ap star, although its interpretation is somewhat problematical for such an evolved star (luminosity type II–III), as it is near the limit in luminosity of Crawford's calibration. Applying the multidimensional downhill simplex technique yields the following basic parameters: $T_{\rm eff} = 6590 \pm 100\,{\rm K}$ $(\log T_{\rm eff} = 3.82)$, $\log g = 3.17 \pm 0.15$, $[{\rm M/H}] = -0.03 \pm 0.15$ and $\xi_{\rm t} = 3.2 \pm 0.5\,{\rm km\,s^{-1}}$ (see Fig. 10 for a comparison of the model with the observations). Again, these parameters are very much in line with what we would expect for an F5II–III star. It is interesting to note that the metallicity from the simplex result again appears to be nearly solar, a result that should be verified with high-resolution spectroscopy given our suspicion that this star shows a mild Am/ρ Pup nature. The *Hipparcos* luminosity combined with a bolometric correction of 0.012 yields $\log(L/{\rm L}_\odot) = 1.24$. That falls slightly to the red of several known Am–δ Scuti stars and the H-exhaustion bend of the evolutionary track for a 1.9-M$_\odot$ model of Turcotte et al. (2000) (see Fig. 9), making this star one of the coolest known ρ Pup stars, if the peculiarity that we suggest is correct.

The simplex technique was devised to work only with stars that have a solar abundance pattern, and not stars that have markedly peculiar abundances (Gray et al. 2001). Despite this, we decided to use the simplex technique on HD 21190 and 199434 because, apart from enhancements in Sr II and Eu II for HD 21190 and a suspicion of an Am/ρ Pup nature for HD 199434, these stars look fairly normal and are quite close matches with the respective MK standards. Thus we felt justified in going ahead and using this powerful technique to derive the basic parameters of these stars. One of us (ROG) intends to investigate the effectiveness of this technique on more extreme chemically peculiar stars.

5 CONSTRAINTS ON PULSATION MODE IDENTIFICATION

The well-known relation

$$P\sqrt{\rho/\rho_\odot} = Q$$

can also be written in the form

$$\log Q = -6.454 - \log f + \tfrac{1}{2}\log g + 0.1 M_{\rm bol} + \log T_{\rm eff}, \qquad (1)$$

where f is in d^{-1}, Q is in d, and g is in cgs units. Using the values of $T_{\rm eff}$ and $\log g$ determined above, and applying bolometric corrections of -0.1 mag to the absolute visual magnitudes, we find $Q = 0.019$ for HD 21190 and $Q = 0.020$ for HD 199434. These values are indicative of pulsation in the second or third overtone for both stars if the pulsations are radial (using the models of Stellingwerf 1979).

The predictions of Turcotte et al. (2000) for Am stars with diffusion included in the model calculations are that the stars should be stable on the main sequence and that low-overtone modes become unstable as the stars evolve. Models without diffusion show higher overtones $n \approx 8$ excited when they are younger, and lower overtones becoming excited as they age. The above results for HD 21190 and 199434 are consistent with Turcotte et al.'s models. However, it should be kept in mind that HD 21190 is more evolved than any model tested by Turcotte et al. (2000), so it is a stimulus to explore this new territory theoretically.

We now attempt identification of the spherical harmonic degree ℓ of the pulsations, by comparing the theoretical amplitude ratios and phase differences of the variations in different wavebands with the values observed (Watson 1988; Garrido 2000). Theoretical quantities are calculated from the pulsation constant Q, and from $T_{\rm eff}$ and $\log g$; the required observed quantities follow from Tables 2 and 4. Details of the procedure can be found in Koen et al. (1999); here we just mention that theoretical fluxes were taken from Kurucz (1992); limb darkening coefficients from Claret, Díaz-Cordovés & Giménez (1995) and Díaz-Cordovés, Claret & Giménez (1995); and filter response functions from Bessell (1990) and Glass (private communication). The identification procedure is reduced to the minimization of a weighted sum of squares (WSS), with respect to the three variables ℓ, R and Ψ. The parameters $0 \le R \le 1$ and $\Psi - \pi$ describe the deviations in amplitude and phase of the fractional temperature at the stellar surface from the adiabatic values $R = 1$ and $\Psi = \pi$ (Watson 1988). Results are given in Table 7. The solutions for HD 199434 are based on the parameter values ($Q = 0.020$, $\log g = 3.25$, $T_{\rm eff} = 6625$), and those for HD 21190 on the parameters ($Q = 0.019$, $\log g = 3.25$, $T_{\rm eff} = 6750$). The radial mode is indicated for HD 21190, $\ell = 2$ for HD 199434.

A little statistical theory is useful for the interpretation of the

Table 7. The results of fitting theoretical amplitude ratios and phase differences to the observed values extracted from Tables 2 and 4. The merit of a solution is determined by the weighted sum of squares (WSS) – therefore the solutions with $\ell = 2$ (HD 199434) and $\ell = 0$ (HD 21190) are the best. The values of the non-adiabaticity parameters R and Ψ are also shown.

ℓ	WSS	R	Ψ
	HD 199434		
0	68.1	0.41	2.74
1	54.9	0.34	1.95
2	46.0	0.89	2.21
3	5923.1	1.00	7.20
4	334.2	1.00	6.28
	HD 21190		
0	23.9	0.26	2.41
1	35.4	0.21	2.95
2	42.7	0.50	3.78
3	41.2	0.08	3.32
4	200.6	1.00	5.54

numerical values of WSS in Table 7. The weighted sum of squares is defined as

$$\mathrm{WSS} = (z - z_\mathrm{p})\boldsymbol{\Sigma}^{-1}(z - z_\mathrm{p})^\mathrm{t},$$

where z is a twelve vector with components equal to observed amplitude ratios and phase differences, while z_p contains the theoretically predicted quantities (Koen et al. 1999; Koen 2000). The matrix $\boldsymbol{\Sigma}$ is the covariance matrix of z. Koen (2000) has pointed out that roughly

$$\mathrm{WSS} - \mathrm{WSS}_\mathrm{min} \sim \chi^2(3),$$

i.e. the difference between any other value of WSS and its minimum, has a chi-squared distribution with three degrees of freedom. This allows a crude comparison between different WSS to be made: for example, differences of 6.25, 7.82 and 11.35 are significant at the 10 per cent, 5 per cent and 1 per cent levels respectively.

Unfortunately, further probing reveals that all is probably not well with the covariance matrix $\boldsymbol{\Sigma}$: if it is assumed that z is approximately Gaussian, with mean value z_p and covariance matrix $\boldsymbol{\Sigma}$, then WSS itself ought to have a $\chi^2(12)$ distribution. The mean of a $\chi^2(k)$ distribution is equal to k, so the expected value of our 'best' WSS is roughly 12. Clearly something is wrong – either the theoretical predictions we have used are wrong or inappropriate, or the covariance matrix is suspect. Strong evidence in favour of the latter hypothesis is presented below.

The parameter space around the point (Q, $\log g$, T_eff) was explored in order to find out whether small changes in these quantities would lead to better fits. In the case of HD 21190, no improvement was found, but for HD 199434 better fits were obtainable by changing Q, $\log g$ and/or T_eff: for example, the minimum WSS decreases to 30.7 if $Q = 0.014$, $\log g = 3.0$ and $T_\mathrm{eff} = 6750$ are assumed ($\ell = 0$); and WSS(min) = 18.0 if $Q = 0.010$, $\log g = 3.0$ and $T_\mathrm{eff} = 6625$ ($\ell = 2$). It may be concluded that the solution for HD 199434 is less well determined, but that probably $\ell = 0$ or $\ell = 2$.

The impact of the data for each individual filter was investigated by running the program for all data excluding each filter in turn. Because of the uncertainty about the solutions for HD 199434

Table 8. The effects on the weighted sum of squares of excluding one waveband at a time from the analysis of HD 21190 reported in Table 7.

Filter excluded	ℓ 0	1	2	3	4
none	23.9	35.4	42.7	41.2	200.6
U	18.3	25.2	22.8	35.0	190.7
B	22.8	31.5	36.4	26.2	150.9
V	20.3	32.9	36.9	29.8	193.0
R	22.9	33.7	40.8	39.7	200.1
I	12.7	31.3	32.7	31.7	149.6
J	21.8	23.6	34.3	33.4	174.5
H	17.1	20.5	36.5	30.1	47.9

mentioned in the previous paragraph, this exercise was only carried out for HD 21190. Inspection of the results in Table 8 shows that the fits are improved substantially if the I and/or H bands are ignored. The implication is that the agreement between theory and observations is poorest for these two wavebands.

The disagreements between theory and observations can be traced to the relatively high H amplitude (reducing it from 7.2 mmag to 5.2 mmag lowers WSS by 6.9 units) and the high value of the I-band phase (reducing it from 2.62 to 2.50 lowers WSS by 11 units). Given the quoted measurement errors on these quantities – which are probably underestimates – the fault may lie with the observations, rather than the theory.

6 CONCLUSIONS

We have reported two unusual δ Scuti stars, HD 199434 and 21190, selected for study on the basis of their *Hipparcos* photometry. The spectral classifications of both stars prompted a more extensive study, and we suggest both to be chemically peculiar.

HD 199434 is probably an evolved mild Am, therefore ρ Pup star, which is then one of the coolest members of its class; it is also slightly, but not significantly, outside the red edge of the δ Scuti instability strip. Pulsation among ρ Pup stars has long been known as unexceptional (e.g. Kurtz 1976), and recent pulsation/diffusion models (Turcotte et al. 2000) can account for it. The more interesting case is HD 21190. Our spectral classification (F2III SrEuSi:) makes it the most evolved Ap star known to date, and we have also proven it to be a δ Scuti star. Pulsations of the δ Scuti type are unusual among Ap stars, with very few cases known (Kurtz 2000).

For several reasons, HD 21190 definitely deserves further study. It probably has evolved from an early-A/late-B main-sequence star, which could explain its Si anomaly. We also suggest that it has fairly strong anomalies of the rare-earth elements and lanthanides, but not the iron-peak elements. This warrants a high-resolution spectroscopic study. In addition, we demonstrated that the star's pulsations are multiperiodic. This, together with its presumably slow rotation, makes it an interesting target for asteroseismology. As Turcotte et al. (2000) have not studied such extreme cases as HD 21190, observations as suggested above may also stimulate further theoretical studies.

We attempted mode identification of the stars by comparing theoretical and observed amplitude ratios and phase differences. The results were inconclusive, and suggested that, despite the incorporation of the error estimates of the observed quantities, the procedure was not entirely self-consistent. Given that the quality of our photometry is on a par with other studies of this type, and that our wavelength coverage is much greater, a critical evaluation of published photometric mode identifications is clearly called for. The reader should therefore also interpret our identifications of the modes in HD 21190 (second or third overtone of the radial mode) and HD 199434 (radial or dipole mode) with caution.

ACKNOWLEDGMENTS

We thank Sylvain Turcotte for kindly providing fig. 9 for reproduction in this paper. We also thank the referee, Jaymie Matthews, for many useful suggestions that have improved this paper. This research has made use of the SIMBAD data base, operated at CDS, Strasbourg, France.

REFERENCES

Balona L. A. et al., 2001, MNRAS, 321, 239
Bessell M. S., 1979, PASP, 91, 589
Bessell M. S., 1990, PASP, 102, 1181
Claret A., Díaz-Cordovés J., Giménez A., 1995, A&AS, 114, 247
Crawford D. L., 1975, AJ, 80, 955
Crawford D. L., 1979, AJ, 84, 1858
Díaz-Cordovés J., Claret A., Giménez A., 1995, A&AS, 110, 329
Eggen O. J., 1992, AJ, 103, 1381
European Space Agency, 1997, The Hipparcos and Tycho Catalogues, Vol. 12. ESA Publications Division, Noordwijk
Flower P. J., 1996, ApJ, 469, 355
Garrido R., 2000, in Breger M., Montgomery M. H., eds, ASP Conf. Ser. Vol. 210, Delta Scuti and Related Stars. Astron. Soc. Pac., San Francisco, p. 67
Glass I., 1973, MNRAS, 164, 155
Gray R. O., Garrison R. F., 1989, ApJS, 69, 301
Gray R. O., Graham P. W., Hoyt S. R., 2001, AJ, 121, 2159
Handler G., 1999a, MNRAS, 309, L19
Handler G., 1999b, Inf. Bull. Variable Stars, 4817
Hauck B., Mermilliod M., 1998, A&AS, 129, 431
Houk N., Cowley A. P., 1975, Michigan Catalogue of Two-Dimensional Spectral Types for the HD Stars, Vol. 1. Dept Astronomy, Univ. Michigan
Kilkenny D., Balona L. A., Carter D. B., Ellis D. T., Woodhouse G. F. W., 1988, Mon. Notes Astron. Soc. S. Afr., 47, 69
Koen C., 2000, MNRAS, 316, 613
Koen C., Van Rooyen R., Van Wyk F., Marang F., 1999, MNRAS, 309, 1051
Kurtz D. W., 1976, ApJS, 32, 651
Kurtz D. W., 2000, in Breger M., Montgomery M. H., eds, ASP Conf. Ser. Vol. 210, Delta Scuti and Related Stars. Astron. Soc. Pac., San Francisco, p. 287
Kurucz R. L., 1992, in Barbuy B., Renzini A., eds, Proc. IAU Symp. 149, The Stellar Populations of Galaxies. Kluwer, Dordrecht
Kurucz R. L., 1993, CD-ROM 13, ATLAS9 Stellar Atmosphere Programs and 2 km/s Grid. Smithsonian Astrophys. Obs., Cambridge, MA
Lester J. B., Gray R. O., Kurucz R. L., 1986, ApJS, 61, 509
Maitzen H. M., 1976, A&A, 51, 223
Masana E., Jordi C., Maitzen H. M., Torra J., 1998, A&AS, 128, 265
Moreno H., Carrasco G., 1986, A&AS, 65, 33
Olsen E. H., 1983, A&AS, 54, 55
Olsen E. H., 1994, A&AS, 106, 257
Perry C. L., 1991, PASP, 103, 494
Rodríguez E., López de Coca P., Rolland A., Garrido R., Costa V., 1994, A&AS, 106, 21
Russell S. C., 1995, ApJ, 451, 747
Schmidt-Kaler T., 1982, in Schaifers K., Voigt H. H., eds, Landolt-Börnstein Series, Vol. 2b. Springer-Verlag, Berlin
Stellingwerf R. F., 1979, ApJ, 227, 935
Turcotte S., Richer J., Michaud G., Christensen-Dalsgaard J., 2000, A&A, 360, 603
Watson R. D., 1988, Ap&SS, 140, 255

This paper has been typeset from a TEX/LATEX file prepared by the author.

2.5.2 On the period-luminosity-colour-metallicity relation and the pulsation characteristics of λ Bootis-type stars

Original paper:

E. Paunzen, **G. Handler,** W. W. Weiss, N. Nesvacil, A. Hempel, E. Romero-Colmenero, F. F. Vuthela, P. Reegen, R. R. Shobbrook, D. Kilkenny, 2002, A&A 392, 515

A&A 392, 515–528 (2002)
DOI: 10.1051/0004-6361:20020854

Astronomy & Astrophysics

On the Period-Luminosity-Colour-Metallicity relation and the pulsational characteristics of λ Bootis type stars*

E. Paunzen[1,2], G. Handler[3], W. W. Weiss[1], N. Nesvacil[1], A. Hempel[4,5], E. Romero-Colmenero[3], F. F. Vuthela[3,6], P. Reegen[1], R. R. Shobbrook[7], and D. Kilkenny[3]

[1] Institut für Astronomie der Universität Wien, Türkenschanzstr. 17, 1180 Wien, Austria
[2] Zentraler Informatikdienst der Universität Wien, Universitätsstr. 7, 1010 Wien, Austria
[3] South African Astronomical Observatory, PO Box 9, Observatory 7935, South Africa
[4] Department of Physics, University of Cape Town, Private Bag, Rondebosch 7701, South Africa
[5] Max-Planck-Institut für Astronomie, Königsstuhl 17, 69117 Heidelberg, Germany
[6] Department of Physics, University of the North-West, Private Bag X2046, Mmabatho 2735, South Africa
[7] Research School of Astronomy and Astrophysics, Australian National University, Canberra, ACT 0200, Australia

Received 12 April 2002 / Accepted 6 June 2002

Abstract. Generally, chemical peculiarity found for stars on the upper main sequence excludes δ Scuti type pulsation (e.g. Ap and Am stars), but for the group of λ Bootis stars it is just the opposite. This makes them very interesting for asteroseismological investigations. The group of λ Bootis type stars comprises late B- to early F-type, Population I objects which are basically metal weak, in particular the Fe group elements, but with the clear exception of C, N, O and S. The present work is a continuation of the studies by Paunzen et al. (1997, 1998), who presented first results on the pulsational characteristics of the λ Bootis stars. Since then, we have observed 22 additional objects; we found eight new pulsators and confirmed another one. Furthermore, new spectroscopic data (Paunzen 2001) allowed us to sort out misidentified candidates and to add true members to the group. From 67 members of this group, only two are not photometrically investigated yet which makes our analysis highly representative. We have compared our results on the pulsational behaviour of the λ Bootis stars with those of a sample of δ Scuti type objects. We find that at least 70% of all λ Bootis type stars inside the classical instability strip pulsate, and they do so with high overtone modes ($Q < 0.020$ d). Only a few stars, if any, pulsate in the fundamental mode. Our photometric results are in excellent agreement with the spectroscopic work on high-degree nonradial pulsations by Bohlender et al. (1999). Compared to the δ Scuti stars, the cool and hot borders of the instability strip of the λ Bootis stars are shifted by about 25 mmag, towards smaller $(b-y)_0$. Using published abundances and the metallicity sensitive indices of the Geneva 7-colour and Strömgren *uvbyβ* systems, we have derived $[Z]$ values which describe the surface abundance of the heavier elements for the group members. We find that the Period-Luminosity-Colour relation for the group of λ Bootis stars is within the errors identical with that of the normal δ Scuti stars. No clear evidence for a statistically significant metallicity term was detected.

Key words. stars – λ Bootis ; stars – chemically peculiar; stars – early type

1. Introduction

In this paper we present an extensive survey to analyse the pulsational characteristics of the λ Bootis stars. This small group comprises late B- to early F-type, Population I stars which are metal weak (particularly the Fe group elements), but with the clear exception of C, N, O and S. Only a maximum of about 2% of all objects in the relevant spectral domain are believed to be λ Bootis type stars.

Several theories were developed to explain the peculiar abundance pattern for members of this group. The most acknowledged models include diffusion as main mechanism together either with mass-loss (Michaud & Charland 1986; Charbonneau 1993) or with accretion of circumstellar material (Venn & Lambert 1990; Turcotte & Charbonneau 1993). Another two theories deal with the influence of binarity on this phenomenon (Andrievsky 1997; Faraggiana & Bonifacio 1999). Heiter (2002) and Heiter et al. (2002) also tried to explain the abundance pattern in the context of the proposed theories.

In general, chemical peculiarity inhibits δ Scuti type pulsation (e.g. for Ap and Am stars, see Kurtz 2000 for a recent discussion) but for the group of λ Bootis stars it is just the

Send offprint requests to: E. Paunzen,
e-mail: `ernst.paunzen@univie.ac.at`

* Based on observations from the Austrian Automatic Photoelectric Telescope (Fairborn Observatory), SAAO and Siding Spring Observatory.

opposite. In two previous studies (Paunzen et al. 1997, 1998), we presented non-variable as well as pulsating λ Bootis stars. Since then, we have observed 22 additional objects and found eight new pulsators and confirmed another. Furthermore, new spectroscopic data (Paunzen 2001) has allowed us to sort out misidentified candidates and to add true members of the group.

Turcotte et al. (2000) investigated the effect of diffusion (probably the main cause of the λ Bootis phenomenon) on the pulsation of stars at the upper main sequence. Although these authors mainly investigated the theoretical behaviour of apparently metal-rich objects, their conclusions also have an impact for the λ Bootis group: little direct pulsational excitation from Fe-peak elements was found, but effects due to settling of helium along with the enhancement of hydrogen are important. Turcotte et al. (2000) find that, as their models of peculiar stars evolve, they become generally pulsationally unstable near the red edge of the instability strip, whereas the behaviour at the blue edge is mainly sensitive to the surface metal abundance. Although the proposed models are still simplified (e.g. treatment of convection) these preliminary results already point towards the most important effects on the theoretical pulsational instability and behaviour of chemically peculiar stars.

The aim of the present paper is to analyse the pulsational characteristics of the group of λ Bootis stars and to test for the presence of a possible Period-Luminosity-Colour-Metallicity relation. The latter is especially interesting in the light of the models by Turcotte et al. (2000). The pulsational characteristics of the λ Bootis group (e.g. ratio of variable to non-variable objects and distribution of pulsational constants) may help to put tighter constraints on these models.

2. Program stars, observations and reductions

Since our previous works (Paunzen et al. 1997, 1998) several then-selected group members were investigated with classification resolution spectroscopy and found to be misclassified. These are: HD 66920, HD 79025, HD 82573, HD 141851, HD 143148, HD 145782, HD 149303, HD 179791, HD 188164 and HD 192424 (Paunzen 2001). In total, 65 members were selected from the lists of Gray & Corbally (1993) and Paunzen (2001) which contain well established as well as good candidate λ Bootis type objects. Together with the two newly discovered objects (HD 42503 and HD 213669; Sect. 2.3.1), we have a sample of 67 λ Bootis type stars.

The photometric observations were performed as described by Paunzen et al. (1998) using photoelectric detectors (except for Ref. "4", Table 1, for which a CCD was used) and (if possible) two comparison stars. A standard reduction method for dealing with dead-time, dark counts and tube drifts was applied. The sky measurements (typically one per half hour) were subtracted and differential light curves were generated. For the reduction of the CCD frames for HD 290492 the standard SAAO reduction package as well as the program MOMF (Kjeldsen & Frandsen 1992) were used. Figure 1 shows light curves of some of our variable program stars.

Frequencies and amplitudes for the variable program stars (listed in Table 2) were derived using a standard Fourier algorithm (Deeming 1975). An analysis with the Phase-Dispersion-Minimization (Stellingwerf 1978) gave essentially the same results. A star is considered to be constant, if the Fourier spectrum of the differential light curve does not contain a statistically significant peak (Paunzen et al. 1997). These objects are listed in Table 3.

Table 1. Sites, dates and telescopes used for our survey.

Site	Date	Telescope	Stars	Ref.
APT (Fairborn)	05.2001	0.75	3	1
SAAO	04.2001	0.50	8	2
	07.2001			
	08.2001			
	09.2001			
	10.2001			
SAAO	12.2000	0.75	9	3
	01.2001			
SAAO	08.2001	1.00	1	4
Siding Spring	01.2002	0.60	1	5

2.1. Previously known pulsating λ Bootis stars

The following nine stars were already known as variable. With the only exception of HD 75654 (see below), they have not been re-observed by us:

- **HD 6870**: Breger (1979) lists a period of 94 min and an amplitude of 15 mmag for Johnson [V].
- **HD 11413**: This star is multiperiodic (Waelkens & Rufener 1983) with a dominant frequency of 54 min and an amplitude of 18 mmag. New measurements (Koen, private communication) confirm the multiperiodic pulsations of this object.
- **HD 15165**: The multiperiodicity of VW Arietis motivated the fifth STEPHI campaign (Liu et al. 1996). Seven significant periods between 1.8 and 3.9 hr were found in a data set of about 150 hr.
- **HD 75654**: This object was discovered as a δ Scuti type pulsator by Balona (1977), who reported a period of 0.087 d (11.49 d^{-1}). Since no other photometric measurements were published, we decided to re-observe this object. We find two frequencies (14.80 and 15.99 d^{-1}) based on observations during six nights.
- **HD 87271**: The suspected variability of this star (Handler 2002) was confirmed by Handler et al. (2000). Although the measured light curve spans only several hours, multiperiodicity with a time scale of about 80 min is evident.
- **HD 105759**: Martinez et al. (1998) performed a multisite campaign, detecting five pulsation periods between 1.0 and 2.8 hr, as well as a detailed abundance analysis for this star.
- **HD 110377**: Radial velocity variations as well as multiperiodicity with periods between 0.5 and 2.0 hr were reported by Bartolini et al. (1980b). Evidence for amplitude and frequency variations makes this object very interesting for detailed follow-up investigations. Such observations are however beyond the scope of this paper.

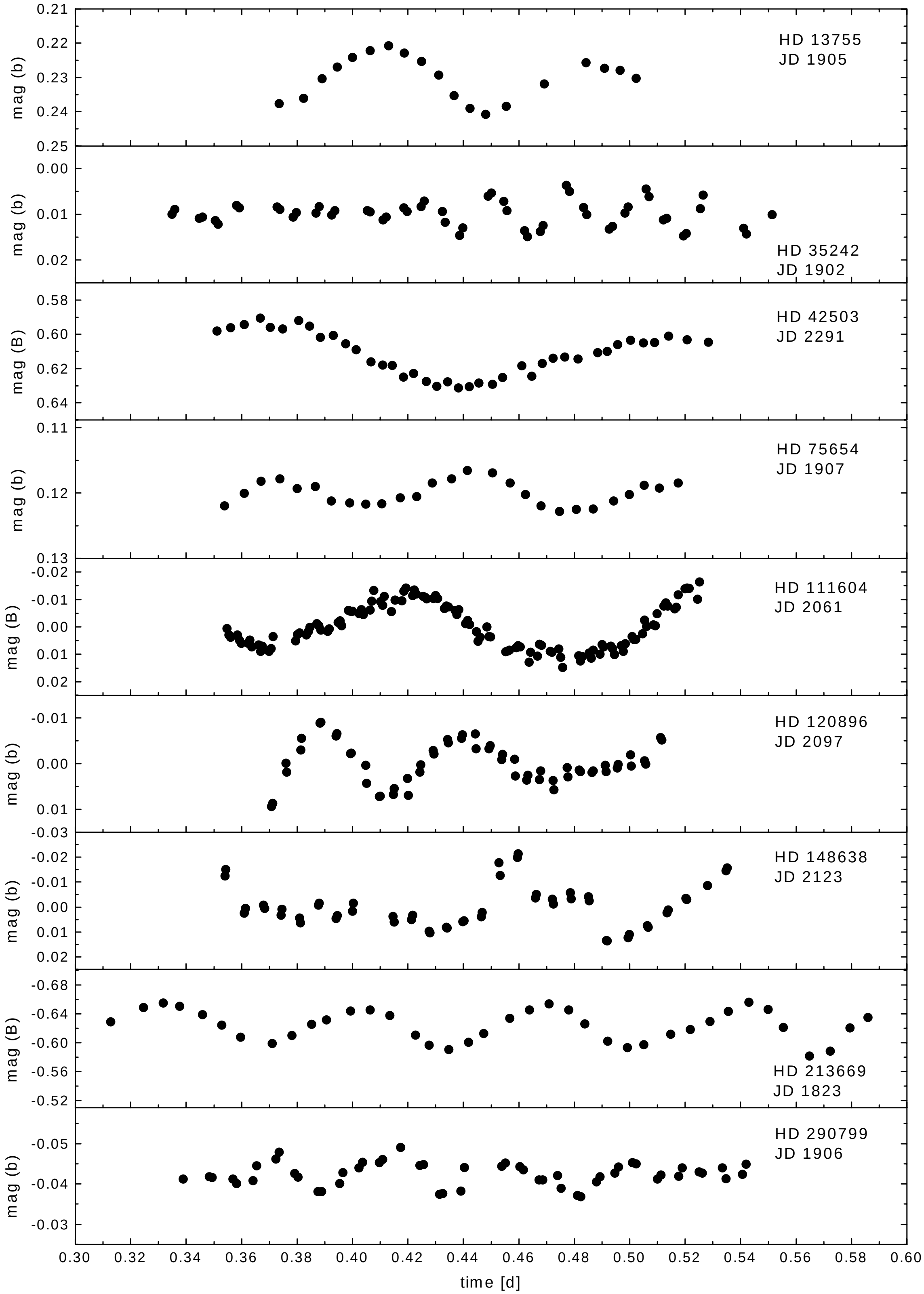

Fig. 1. Differential light curves of eight newly discovered and one confirmed (HD 75654) pulsating λ Bootis stars in Strömgren b and Johnson B; the dates of the corresponding nights are given as JD 2 450 000+ (Table 2).

Table 2. Observing log of eight newly discovered and one confirmed (HD 75654) pulsating λ Bootis stars. Some information on the comparison stars is also given. The differential light curves are shown in Fig. 1.

HD	JD	hrs	m_V [mag]	Spec.	Freq. [d^{-1}]	Amp. [mag]	Ref.
13755	2 451 899	3.2	7.84	λ Boo	12.50	0.015	3
	2 451 903	2.5			16.85	0.007	
	2 451 905	3.1					
	2 451 909	3.1					
13602			8.52	F6			
13710			8.32	K5			
35242	2 451 900	2.1	6.35	λ Boo	38.61	0.005	3
	2 451 902	5.4			34.16	0.003	
	2 451 908	3.3			41.33	0.003	
35134			6.74	A0			
34888			6.78	A5			
42503	2 452 291	4.2	7.45	λ Boo	7.00	0.015	5
	2 452 292	1.9					
42058			6.99	A0			
43452			7.71	F5			
75654	2 451 898	3.0	6.38	λ Boo	14.80	0.005	3
	2 451 902	1.8			15.99	0.002	
	2 451 905	3.1					
	2 451 906	1.2					
	2 451 907	3.8					
	2 451 909	3.6					
74978			6.87	A1			
75272			6.98	B9.5			
111604	2 452 061	4.1	5.89	λ Boo	8.77	0.020	1
112412			5.61	F1			
110375			8.33	F5			
120896	2 452 097	3.9	8.50	λ Boo	17.79	0.010	2
121372			8.67	G5			
148638	2 452 097	4.6	7.90	λ Boo	16.32	0.016	2
	2 452 123	5.0					
148596			8.60	F2			
148573			8.63	B9			
213669	2 451 823	6.5	7.42	λ Boo	15.01	0.023	2
	2 451 826	1.6					
	2 451 827	1.1					
211878			7.70	F5			
214390			7.90	F3			
290799	2 451 904	3.0	10.63	λ Boo	23.53	0.006	3
	2 451 906	4.8					
37652			7.35	F5			
290798			10.40	A2			

- **HD 153747**: Desikachary & McInally (1979) reported multiperiodicity (periods between 0.96 and 1.2 hr) as well as a variable frequency spectrum of this object. Unfortunately no further references on the pulsational behaviour of this star were found.
- **HD 192640**: This star's variability was discovered by Gies & Percy (1977). Since 1995 permanent multisite observations have been performed. No detailed overall analysis has been published to date. Data subsets (Kusakin & Mkrtichian 1996; Paunzen & Handler 1996; Mkrtichian et al. 2000) suggest multiperiodicity with a main period of 38 min and an amplitude of 20 mmag in Johnson V.

We have used the published frequencies and amplitudes of these objects from the above-mentioned references in our analysis. If more than one frequency has been published, we have weighted the individual periods with the squared amplitude to obtain a mean period.

2.2. Group members not observed by us

Five well established members of the λ Bootis group were not photometrically investigated: HD 110411, HD 125889, HD 170680, HD 184779 and HD 198160. For three of them

Table 3. Observing log of thirteen λ Bootis stars not found to pulsate as well as some comparison star information.

HD/BD	JD	hrs	m_V [mag]	Spec.	Limit [mmag]	Ref
7908	2 451 898	2.0	7.29	λ Boo	0.3	3
	2 451 907	2.3				
7629			7.13	A9		
7896			7.95	G6		
24472	2 451 900	2.9	7.09	λ Boo	0.8	3
24616			6.70	G8		
25385			7.40	F0		
54272	2 451 908	2.6	8.80	λ Boo	1.4	3
54692			8.51	A0		
+19 622			8.90	A2		
74873	2 451 904	3.5	5.89	λ Boo	1.6	3
74228			5.65	A3		
75108			8.38	G5		
83277	2 451 901	3.5	8.30	λ Boo	1.4	3
83547			8.62	A0		
82709			8.04	A9		
90821	2 452 039	2.0	9.47	λ Boo	2.2	1
90878			7.82	F8		
90748			8.67	F8		
107223	2 452 003	5.2	7.35	λ Boo	1.9	2
107143			7.87	A1		
107265			8.76	A0		
111005	2 452 004	1.9	7.96	λ Boo	2.1	2
110705			8.36	F0		
110989			8.41	F8		
130767	2 452 039	5.5	6.91	λ Boo	1.2	1
130556			7.84	F1		
130396			7.41	F8		
149130	2 452 127	5.6	8.50	λ Boo	2.4	2
148597			8.25	B9		
149471			8.94	F6		
216847	2 452 190	2.9	7.06	λ Boo	1.7	2
	2 452 191	3.2				
216349			7.84	K1		
217686			7.56	F7		
290492	2 451 901	3.0	9.27	λ Boo	1.8	2
	2 452 190	2.2				
	2 452 192	4.0				
290575			9.85	F5		
−00 984			8.37	HgMn		
261904	2 452 190	2.1	10.20	λ Boo	3.5	4
	2 452 191	2.2				
261941			10.94	A2		

(HD 110411, HD 170680 and HD 198160) photometric measurements in the HIPPARCOS and TYCHO catalogues (ESA 1997) were found. Since these observations are not optimal to find δ Scuti type pulsation, only a rough estimate for variability can be made. We find a level of non-variability based on the HIPPARCOS photometry of 3 mmag for HD 110411 and HD 170680, and 4 mmag for HD 198160. In fact, HD 110411 was suspected as variable by Bartolini et al. (1980a), but Antonello & Mantegazza (1982) concluded that there is no evidence for periodic terms in the light curve: different oscillation modes may be excited occasionally and then be damped again. We therefore treat this star as being constant within a limit of 3 mmag. Consequently, the other two objects (HD 125889 and HD 184779) were not considered in the following analysis.

2.3. Notes on individual stars

In the following sections we describe special properties of some individual stars in more detail.

2.3.1. HD 42503 and HD 213669

These two objects were suspected δ Scuti type pulsators based on HIPPARCOS photometry (Handler 2002). Handler (1999) presented Strömgren $uvby\beta$ photometry which puts these stars well within the typical area of the λ Bootis objects in a m_1 versus $(b-y)$ diagram (Paunzen et al. 1998). Our photometric measurements confirmed the pulsation.

We have performed additional spectroscopic observations to establish the nature of these stars. These observations were done on the 1.9 m telescope at SAAO in the night of 03./04.10.2000. The Grating Spectrograph with the SITe CCD together with the 600 lines mm^{-1} grating resulted in a useful wavelength range of 1600 Å, a resolution of 2 Å and a signal-to-noise ratio of about 200. The wavelength calibration was done with the help of a CuAr lamp within standard IRAF routines. The classification was done within the system described by Paunzen (2001). Both objects are very good λ Bootis candidates, with derived spectral types of A2 V (λ Boo) and kA1hF0mA1 V λ Boo for HD 42503 and HD 213669, respectively. The notation of the spectral classification is according to Gray (1988) where *k* stands for the classification of the Ca II K line, *h* for the hydrogen lines and *m* for the appearance of the metallic-line spectrum compared to MK standards. We therefore included them in our sample. Figure 2 shows their spectra together with those of two well established λ Bootis stars (HD 107233 and HD 198160; taken from Paunzen 2001) which exhibit similar spectral characteristics. However, we note that a final decision on their group membership has to be made after a detailed determination of their chemical abundances (especially of C, N, O and S) which was not done so far.

2.3.2. HD 64491 and HD 111786

Both stars are δ Scuti type pulsators and were reported as well established members of the group by Gray (1988) and Paunzen & Gray (1997). However, both objects are spectroscopic binary systems (Faraggiana & Bonifacio 1999; Iliev et al. 2001). The published information on these stars does not allow us to decide whether they are true λ Bootis type objects, thus we have not included either of them in our sample.

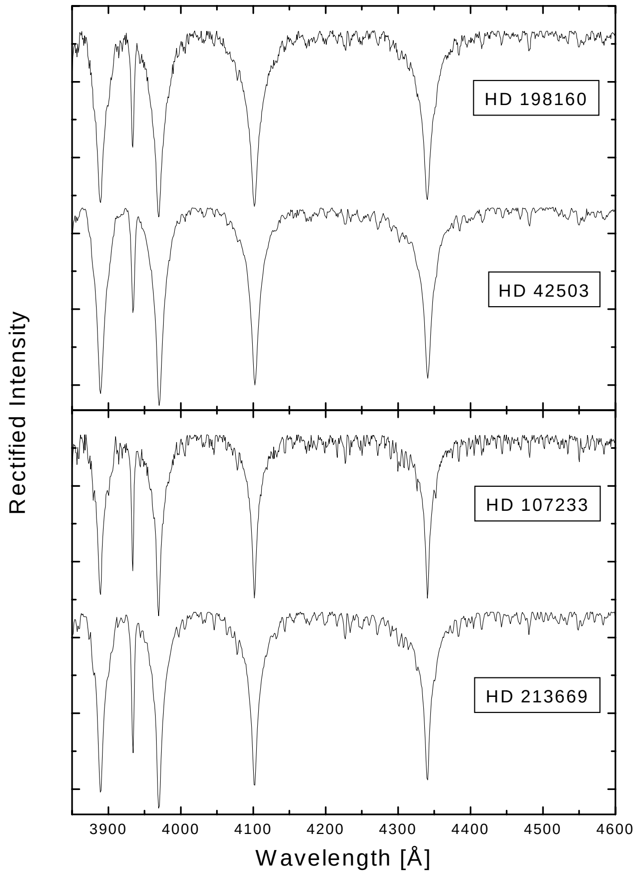

Fig. 2. Classification resolution spectra of the two newly discovered λ Bootis candidates HD 42503 (A2 V λ Boo; upper panel) and HD 213669 (kA1hF0mA1 V λ Boo; lower panel) together with the two well established objects HD 107233 (kA1hF0mA1 V λ Boo) and HD 198160 (A2 Vann λ Boo) for comparison.

2.3.3. HD 74873

We have re-observed this object because the upper limit for non-variability given by Paunzen et al. (1997) was very high (9.4 mmag). Our new observations showed no variability within a limit of 1.6 mmag.

2.3.4. HD 175445

This object exhibits a peculiar behaviour which we have, so far, been unable to understand. During our first short observing run (on 06/07 July 2001), its magnitude and colour were consistent with their standard values from the literature ($b = 7.85$, $v - b = 0.222$), and marginal evidence for pulsational variability was found. However, when we attempted to re-observe the star on 05/06 August 2001, it appeared much fainter and redder than in the previous month.

Consequently, we double-checked its correct identification and re-examined the literature. We found no evidence for a misidentification or previous peculiar behaviour. We obtained a 3 hr light curve on the night of 06/07 August 2001, where the object appeared as a star of $b = 10.67$ and $v - b = 1.17$. These observations are consistent with an eclipse by a late K subgiant companion. However, the evolutionary history of such a system would require the binary to be close, and no other possible eclipses have yet been reported.

2.3.5. HD 290799

Paunzen et al. (1998) reported this star as constant with an upper limit of 10 mmag in Geneva V_1. Our new observations show the star to be pulsating with a frequency of 23.53 d^{-1} and an amplitude of 6 mmag in Strömgren b.

3. Basic stellar parameters

In this section we describe the calibration procedures within various photometric systems and derivation of the basic stellar parameters required to analyse the pulsational characteristics of these stars, such as the effective temperature, surface gravity and the luminosity.

The required standard photometric colours were taken from the General Catalogue of Photometric Data (GCPD; `http://obswww.unige.ch/gcpd/`) as well as the HIPPARCOS and TYCHO databases (ESA 1997). If available, averaged and weighted mean values were used.

The following calibrations for the individual photometric systems were used to derive effective temperatures and surface gravities:

- Johnson UBV: Napiwotzki et al. (1993);
- Strömgren $uvby\beta$: Moon & Dworetsky (1985) and Napiwotzki et al. (1993);
- Geneva 7-colour: Kobi & North (1990) and Künzli et al. (1997).

The calibrations for the Johnson UBV and Geneva 7-colour system need an a-priori knowledge of the reddening, which is, in general, not easy to estimate.

Normally, the reddening for objects within the solar neighborhood is estimated using photometric calibrations in the Strömgren $uvby\beta$ system (Strömgren 1966; Crawford 1979; Hilditch et al. 1983). These calibrations are not very reliable for stars with spectral types from A0 to A3 (Gerbaldi et al. 1999), mainly because for these stars, the reddening free parameter β is no longer a temperature indicator alone but is also sensitive to the luminosity. From the photometry we find that two of our pulsating (HD 125162 and HD 183324) and nine constant (HD 23392, HD 31295, HD 36726, HD 74873, HD 110411, HD 130767, HD 170680, HD 261904 and HD 294253) program stars fall into A0 to A3 spectral region.

An independent way to derive the interstellar reddening is to use galactic reddening maps, which are derived from open clusters as well as from galactic field stars. Several different models have been published in the literature (Arenou et al. 1992; Hakkila et al. 1997). Chen et al. (1998) compared the results from Arenou et al. (1992) and those derived from the HIPPARCOS measurements and found an overestimation of previously published results from Arenou et al. (1992) for distances less than 500 pc. They consequently proposed a new

Table 4. Pulsating λ Bootis stars; an asterisk denotes stars without an accurate HIPPARCOS parallax; $\sigma(b-y) = \pm 0.005$ mag. In parenthesis are the errors in the final digits of the corresponding quantity.

HD	$(b-y)_0$ [mag]	$\log T_{\rm eff}$ [dex]	$\log g$ [dex]	$v \sin i$ [km s^{-1}]	[Z] [dex]	M_V [mag]	M_B [mag]	$\log L_*/L_\odot$ [dex]	$\log P$	Q [d]
6870	0.164	3.865(6)	3.84(11)	165	−1.03(20)	+2.29(42)	+2.20	1.02(17)	−1.19	0.023
11413	0.104	3.899(7)	3.91(21)	125	−1.17(10)	+1.49(10)	+1.36	1.35(4)	−1.38	0.014
13755	0.181	3.850(10)	3.26(10)	–	−0.75(30)	+0.93(10)	+0.83	1.57(4)	−1.12	0.010
15165	0.189	3.846(12)	3.23(10)	90	−1.15(17)	+1.12(16)	+1.01	1.50(6)	−0.87	0.017
30422	0.098	3.896(6)	4.00(20)	135	−1.50(20)	+2.35(2)	+2.23	1.01(1)	−1.68	0.010
35242	0.058	3.916(5)	3.90(14)	90	−1.40(20)	+1.75(22)	+1.60	1.26(9)	−1.58	0.010
42503	0.110	3.885(16)	3.10(10)	–	−0.83(20)	−0.03(4)	−0.14	1.96(2)	−0.85	0.013
75654	0.158	3.866(6)	3.77(11)	45	−0.91(11)	+1.83(12)	+1.74	1.20(5)	−1.18	0.019
83041	0.185	3.852(13)	3.76(20)	95	−1.03(8)	+1.70(30)	+1.60	1.26(12)	−1.18	0.018
84948B*	0.196	3.833(13)	3.70(15)	55	−0.82(19)	+1.63(30)	+1.75	1.20(12)	−1.11	0.020
87271	0.149	3.876(13)	3.43(10)	–	−1.11(30)	+1.02(8)	+0.92	1.53(3)	−1.27	0.009
102541	0.141	3.885(10)	4.22(16)	–	−0.95(20)	+2.34(21)	+2.23	1.01(9)	−1.30	0.029
105058	0.127	3.889(10)	3.77(30)	140	−0.82(7)	+0.86(30)	+0.75	1.60(12)	−1.40	0.010
105759	0.142	3.874(6)	3.65(10)	120	−0.92(30)	+1.35(21)	+1.25	1.40(8)	−1.20	0.015
109738*	0.144	3.881(8)	3.90(13)	–	−1.02(20)	+1.85(30)	+1.75	1.20(12)	−1.49	0.012
110377	0.120	3.888(5)	3.97(14)	170	−0.83(20)	+1.96(11)	+1.85	1.16(5)	−1.45	0.014
111604	0.112	3.890(8)	3.61(25)	180	−1.04(3)	+0.48(7)	+0.37	1.75(3)	−0.94	0.022
120500	0.064	3.915(4)	3.86(10)	125	−0.73(14)	+0.85(34)	+0.70	1.62(13)	−1.32	0.014
120896*	0.166	3.861(5)	3.76(10)	–	−0.82(30)	+1.90(30)	+1.81	1.18(12)	−1.25	0.016
125162	0.042	3.941(8)	4.07(9)	115	−1.61(24)	+1.71(23)	+1.54	1.28(9)	−1.64	0.011
142703	0.177	3.861(9)	3.93(12)	100	−1.32(5)	+2.41(12)	+2.32	0.97(5)	−1.43	0.015
142944*	0.198	3.845(8)	3.19(4)	180	−0.91(38)	+0.80(30)	+0.69	1.62(12)	−0.85	0.016
148638*	0.106	3.882(13)	3.39(10)	–	−0.80(30)	+0.33(30)	+0.23	1.81(12)	−1.21	0.009
153747	0.068	3.914(5)	3.70(24)	–	−0.86(20)	+1.24(30)	+1.09	1.46(12)	−1.31	0.013
168740	0.128	3.883(5)	3.88(14)	145	−0.91(8)	+1.82(2)	+1.72	1.21(1)	−1.44	0.013
168947*	0.145	3.878(11)	3.67(10)	–	−0.74(20)	+1.28(30)	+1.18	1.43(12)	−1.23	0.014
183324	0.032	3.952(10)	4.13(4)	90	−1.47(6)	+1.64(42)	+1.44	1.32(17)	−1.68	0.011
191850*	0.163	3.869(9)	3.61(10)	–	−0.96(30)	+1.50(30)	+1.41	1.34(12)	−1.13	0.017
192640	0.095	3.900(5)	3.95(18)	80	−1.46(8)	+1.84(2)	+1.71	1.22(1)	−1.55	0.011
210111	0.136	3.878(7)	3.84(15)	55	−1.04(20)	+1.76(15)	+1.66	1.23(6)	−1.36	0.014
213669	0.155	3.872(8)	3.82(17)	–	−0.93(20)	+1.79(21)	+1.69	1.22(8)	−1.18	0.021
221756	0.046	3.930(10)	3.90(3)	105	−0.71(3)	+1.16(16)	+1.00	1.50(6)	−1.36	0.015
290799*	0.114	3.889(5)	4.18(10)	70	−0.82(26)	+2.62(30)	+2.51	0.90(12)	−1.37	0.025

model for galactic latitudes of ±10°, but otherwise find excellent agreement with the model by Sandage (1972). We have used the proposed model by Chen et al. (1998) to derive the interstellar reddening for all program stars. The values from the calibration of the Strömgren *uvbyβ* and the model by Chen et al. (1998) are in very good agreement. To minimize possible inconsistencies we have averaged the values from both approaches.

In Table 7, we compare our photometrically derived effective temperatures and surface gravities of 29 program stars from this work (TW) with those of Table 1 from Heiter et al. (2002), which contains averaged values from the literature based on spectroscopic analyses. The average difference for the effective temperature is $\Delta T_{\rm eff} = T_{\rm eff}({\rm Lit.}) - T_{\rm eff}({\rm TW}) = +72(210)$ K, and for the average surface gravity $\Delta \log g = \log g({\rm Lit.}) - \log g({\rm TW}) = +0.07(24)$ dex. We note that there are some stars for which the spectroscopically derived values are significantly different from the photometrically derived ones (e.g. HD 106223 and HD 107233). These cases were already extensively discussed by Heiter et al. (2002). Although such deviating cases obviously exist, we believe that our calibration method is consistent and therefore suitable for a statistical analysis.

For all program stars photometrically calibrated absolute magnitudes (assuming that all objects are single) were estimated with an error of ±0.3 mag. As an independent source we have taken the HIPPARCOS parallaxes (if available) to derive absolute magnitudes using the visual magnitude and reddening. Since we also corrected for the Lutz-Kelker effect (Koen 1992) which is only possible for parallax measurements with an absolute error of $[\sigma(\pi)/\pi] < 0.175$ it seriously limits the useful data. Oudmaijer et al. (1998) showed that this effect has to be taken into account if individual absolute magnitudes are calculated using HIPPARCOS parallaxes. Stars without measurements satisfying $[\sigma(\pi)/\pi] < 0.175$ are marked with an asterisk in Tables 4 and 6 (20 stars in total). For the other 45 objects we are able to derive weighted means (taking the errors as weights, i.e. a larger error is a lower weight) for the absolute magnitude using the values from the photometric calibration procedure and the conversion of the HIPPARCOS parallax measurements.

Table 5. δ Scuti stars selected from the list by Rodriguez et al. (2000); $\sigma(b-y) = \pm 0.005$ mag; $\sigma[Z] = \pm 0.15$ dex. In parenthesis are the errors in the final digits of the corresponding quantity.

HD	$(b-y)_0$ [mag]	$\log T_{\rm eff}$ [dex]	$\log g$ [dex]	$v \sin i$ [km s^{-1}]	$[Z]$ [dex]	M_V [mag]	M_B [mag]	$\log L_*/L_\odot$ [dex]	$\log P$	Q [d]
432	0.211	3.841(4)	3.44(7)	70	+0.45	1.19(29)	1.08	1.47(11)	−1.00	0.017
3112	0.127	3.883(5)	3.59(9)	80	+0.28	0.54(84)	0.44	1.73(34)	−1.31	0.009
4490	0.156	3.867(3)	3.55(9)	180	+0.22	0.92(15)	0.83	1.57(6)	−0.98	0.019
4849	0.168	3.862(2)	3.78(8)	–	+0.52	1.65(30)	1.56	1.27(12)	−1.26	0.016
7312	0.169	3.861(3)	3.79(6)	–	+0.24	1.71(28)	1.62	1.25(11)	−1.38	0.012
8511	0.134	3.880(4)	3.96(6)	190	−0.06	2.04(1)	1.94	1.12(1)	−1.16	0.027
8781	0.213	3.838(6)	3.46(6)	–	−0.03	1.57(18)	1.46	1.32(7)	−0.95	0.020
9065	0.200	3.844(6)	3.46(6)	–	−0.14	1.72(21)	1.61	1.26(8)	−1.02	0.018
9100	0.087	3.899(8)	3.53(22)	120	−0.34	0.43(28)	0.30	1.78(11)	−0.87	0.024
11522	0.162	3.861(5)	3.41(6)	120	−0.04	0.76(13)	0.67	1.63(5)	−1.04	0.014
15550	0.152	3.871(3)	3.84(6)	170	+0.13	1.89(1)	1.80	1.18(1)	−1.17	0.022
15634	0.179	3.858(2)	3.81(7)	140	+0.28	1.57(50)	1.48	1.31(20)	−1.01	0.028
17093	0.133	3.883(8)	4.04(11)	75	−0.10	2.22(4)	2.12	1.05(2)	−1.45	0.016
19279	0.063	3.913(8)	3.76(17)	285	−0.16	1.69(61)	1.54	1.28(25)	−1.16	0.022
23728	0.178	3.859(5)	3.70(16)	105	−0.21	1.62(15)	1.53	1.29(6)	−1.00	0.025
24809	0.119	3.890(10)	4.26(20)	130	−0.36	2.51(7)	2.40	0.94(3)	−1.26	0.035
24832	0.158	3.865(4)	3.69(13)	140	+0.12	1.12(30)	1.03	1.49(12)	−0.81	0.035
26574	0.196	3.847(4)	3.49(12)	100	+0.62	1.22(38)	1.11	1.46(15)	−1.13	0.013
27397	0.166	3.864(3)	3.96(5)	100	+0.22	2.30(5)	2.21	1.02(2)	−1.26	0.022
27459	0.123	3.884(5)	3.96(13)	75	+0.25	1.92(21)	1.82	1.17(9)	−1.44	0.014
28024	0.159	3.865(7)	3.40(18)	210	+0.22	0.77(24)	0.68	1.63(9)	−0.83	0.022
28319	0.093	3.901(9)	3.70(12)	80	+0.16	0.32(78)	0.19	1.82(31)	−1.12	0.016
28910	0.139	3.877(4)	3.97(5)	125	+0.19	1.58(75)	1.48	1.31(30)	−1.17	0.024
30780	0.114	3.887(3)	3.87(11)	150	+0.23	1.41(50)	1.30	1.38(20)	−1.38	0.013
32846	0.189	3.845(9)	3.37(10)	–	−0.19	1.16(5)	1.05	1.48(2)	−0.87	0.021
50018	0.217	3.836(6)	3.35(10)	135	+0.78	0.49(1.03)	0.37	1.75(41)	−0.81	0.019
57167	0.214	3.844(2)	3.97(3)	100	+0.18	2.49(15)	2.38	0.95(6)	−1.33	0.019
71496	0.133	3.878(4)	3.61(8)	130	+0.41	1.18(10)	1.08	1.47(4)	−1.02	0.021
71935	0.140	3.872(4)	3.67(9)	160	+0.32	1.14(20)	1.04	1.49(8)	−1.15	0.016
73575	0.137	3.874(5)	3.41(12)	150	+0.32	0.38(21)	0.28	1.79(8)	−0.99	0.015
74050	0.106	3.892(7)	3.85(16)	145	+0.25	1.71(44)	1.59	1.26(18)	−1.24	0.019
84999	0.192	3.851(4)	3.41(8)	110	+0.13	1.09(27)	0.99	1.50(11)	−0.88	0.021
88824	0.153	3.870(2)	3.83(10)	235	+0.08	1.76(2)	1.67	1.23(1)	−0.90	0.039
94985	0.088	3.903(9)	3.62(5)	–	−0.11	0.82(16)	0.69	1.62(6)	−0.82	0.032
103313	0.110	3.889(4)	3.67(8)	70	+0.24	0.79(36)	0.68	1.63(14)	−1.10	0.017
104036	0.086	3.899(7)	4.09(14)	–	+0.01	1.67(40)	1.54	1.28(16)	−1.52	0.013
107131	0.097	3.897(5)	4.03(20)	185	−0.08	1.91(25)	1.78	1.19(10)	−1.18	0.029
107904	0.224	3.837(6)	3.20(12)	115	+0.68	0.83(15)	0.72	1.61(6)	−0.93	0.013
109585	0.208	3.841(4)	3.59(10)	80	+0.16	1.80(18)	1.69	1.22(7)	−1.09	0.018
115308	0.199	3.846(6)	3.36(8)	75	+0.06	1.16(2)	1.05	1.48(1)	−0.93	0.017
117661	0.095	3.900(4)	3.95(11)	55	+0.14	1.70(12)	1.57	1.27(5)	−1.37	0.016
124675	0.111	3.884(6)	3.67(17)	120	−0.11	1.02(29)	0.91	1.54(12)	−1.19	0.015
125161	0.128	3.885(8)	4.10(19)	135	+0.08	2.40(14)	2.29	0.98(5)	−1.58	0.013
127762	0.112	3.890(3)	3.69(12)	130	+0.02	0.94(2)	0.83	1.57(1)	−1.14	0.017
127929	0.143	3.876(3)	3.65(11)	70	+0.00	0.80(29)	0.70	1.62(12)	−1.06	0.018
138918	0.146	3.870(5)	3.77(23)	85	+0.16	0.19(1.13)	0.10	1.86(45)	−0.81	0.032
143466	0.177	3.863(5)	3.92(15)	145	+0.24	2.29(8)	2.20	1.02(3)	−1.12	0.029
152569	0.160	3.864(3)	3.81(13)	195	+0.16	1.83(4)	1.74	1.21(2)	−1.12	0.023
155514	0.119	3.886(6)	3.90(16)	175	+0.08	1.49(17)	1.38	1.35(7)	−1.05	0.029
171369	0.159	3.863(3)	3.79(8)	80	+0.05	1.64(20)	1.55	1.28(8)	−1.04	0.026
176723	0.200	3.848(3)	3.62(9)	265	+0.10	1.66(19)	1.56	1.27(8)	−0.87	0.031
177392	0.168	3.861(6)	3.54(16)	140	+0.15	0.96(10)	0.87	1.55(4)	−0.96	0.020
177482	0.161	3.862(5)	3.45(8)	145	+0.26	0.86(14)	0.77	1.59(6)	−1.01	0.016
181333	0.138	3.877(4)	3.53(6)	55	+0.38	0.47(47)	0.37	1.75(19)	−0.82	0.025
182475	0.194	3.850(3)	3.63(14)	130	+0.32	1.61(47)	1.51	1.30(19)	−1.11	0.018

Table 5. continued.

HD	$(b-y)_0$ [mag]	$\log T_{\rm eff}$ [dex]	$\log g$ [dex]	$v \sin i$ [km s^{-1}]	[Z] [dex]	M_V [mag]	M_B [mag]	$\log L_*/L_\odot$ [dex]	$\log P$	Q [d]
185139	0.157	3.869(2)	3.80(7)	–	+0.29	1.38(51)	1.29	1.39(20)	−1.19	0.018
186786	0.181	3.856(2)	3.86(8)	–	+0.19	2.09(3)	2.00	1.10(1)	−1.10	0.027
188520	0.123	3.885(7)	4.05(15)	–	+0.03	2.19(19)	2.08	1.07(8)	−1.26	0.025
199124	0.167	3.859(3)	3.74(8)	150	−0.12	1.89(13)	1.80	1.18(5)	−1.00	0.028
199908	0.192	3.848(4)	3.42(7)	60	+0.27	1.23(21)	1.13	1.45(8)	−1.10	0.013
206553	0.171	3.859(4)	3.70(15)	–	+0.20	1.46(2)	1.37	1.35(1)	−1.20	0.016
208435	0.198	3.844(5)	3.26(8)	–	+0.36	0.67(43)	0.56	1.68(17)	−0.83	0.017
211336	0.170	3.862(3)	3.90(7)	90	+0.17	2.12(2)	2.03	1.09(1)	−1.39	0.015
214441	0.205	3.847(4)	3.55(11)	–	+0.45	1.28(59)	1.18	1.43(23)	−0.90	0.024
215874	0.163	3.863(4)	3.48(5)	100	+0.23	0.88(20)	0.79	1.58(8)	−1.06	0.015
217236	0.152	3.868(4)	3.52(8)	100	+0.22	0.51(59)	0.42	1.73(24)	−0.90	0.020
219891	0.076	3.902(8)	3.77(15)	165	−0.02	0.80(6)	0.67	1.63(3)	−1.00	0.025
220061	0.100	3.882(17)	3.51(2)	140	+0.04	0.95(14)	0.85	1.56(6)	−1.27	0.010
223781	0.098	3.897(4)	3.92(12)	165	−0.20	1.47(8)	1.34	1.37(3)	−1.22	0.021

For the remaining 20 stars only photometrically calibrated absolute magnitudes are available. We then calculated luminosities ($\log L_*/L_\odot$) using the absolute bolometric magnitude of the Sun $M_{\rm Bol}(\odot) = 4.75$ mag (Cayrel de Strobel 1996) and bolometric corrections taken from Drilling & Landolt (2000).

For HD 84948B we have used the astrophysical parameters listed by Iliev et al. (2002; Table 1). This is an evolved spectroscopic binary system which contains two similar λ Bootis components; Iliev et al. (2002) have taken the binary nature into account.

Individual abundances and projected rotational velocities for members of the λ Bootis group were published by Uesugi & Fukuda (1982), Venn & Lambert (1990), Stürenburg (1993), Abt & Morrell (1995), Holweger & Rentzsch-Holm (1995), Chernyshova et al. (1998), Heiter et al. (1998), Paunzen et al. (1999a,b), Kamp et al. (2001), Solano et al. (2001), Heiter (2002) and Andrievsky et al. (2002). The individual values were weighted (if possible) with the errors listed in the references and averaged.

The published abundances do not allow an investigation of the correlation of individual abundances of different elements (which have different diffusion properties) with the pulsational period. It is well known that the typical abundance pattern of λ Bootis stars is characterized by moderate to strong underabundances of elements heavier than C, N, O and S. To get an overall estimate of the (surface) abundance we have applied the following method:

- A weighted mean for Mg, Ca, Sc, Ti, Cr and Fe was calculated and taken as a measurement of [Z]. This should minimize measurement errors for individual elements;
- We determined Δm_2 from the Geneva 7-colour as well as Δm_1 from the Strömgren $uvby\beta$ photometric system (for the definition of these parameters see Golay 1974);
- Then we correlated Δm_2 or Δm_1 with [Z] for stars without published individual element abundances.

The third step is only valid for effective temperatures cooler than 8500 K; otherwise the metallicity indices are no longer sensitive. This method was applied to nine pulsating λ Bootis type objects: HD 6870, HD 30422, HD 42503, HD 102541, HD 109738, HD 110377, HD 153747, HD 168947 and HD 213669.

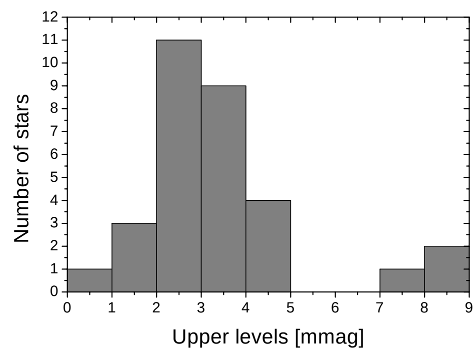

Fig. 3. The histogram of our upper levels for non-variability. See text for details.

4. Results

Besides two objects (HD 125889 and HD 184779), all members of the λ Bootis group were photometrically investigated. All previously published results were taken from Paunzen et al. (1997, 1998) as well as from the references quoted in Sect. 3. Of these 65 stars, 32 are presumed to be constant whereas 33 are pulsating. The upper limits for non-variability, which are below 5 mmag for all but three stars (HD 31925, HD 91130 and HD 294253), are shown in Fig. 3.

In order to investigate the pulsational characteristics of the λ Bootis stars as a group, we compare them with those of "normal" δ Scuti variables. The next subsection describes the compilation of the latter sample.

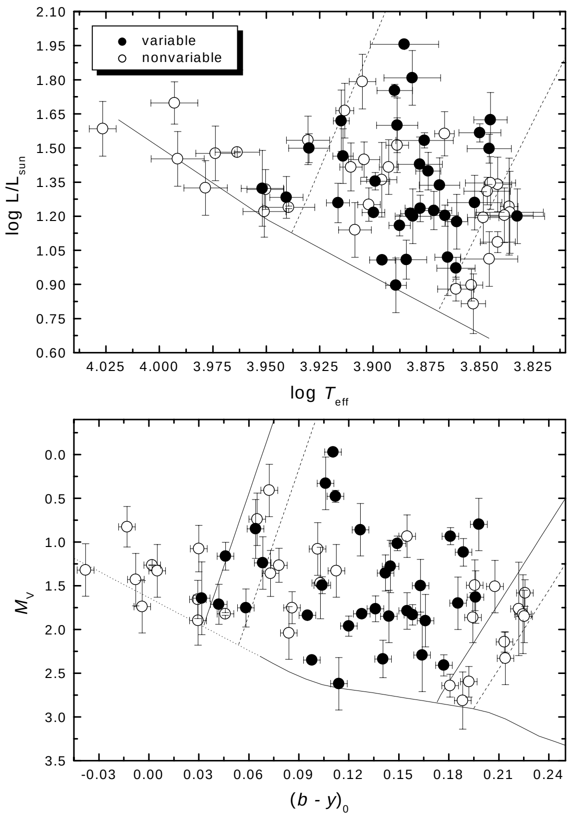

Fig. 4. The $\log L_*/L_\odot$ versus $\log T_{\rm eff}$ (upper panel) and M_V versus $(b-y)_0$ (lower panel) diagrams for the non-variable (open circles) and pulsating (filled circles) λ Bootis stars. The Zero Age Main Sequences are taken from Crawford (1979) and Claret (1995). The borders of the classical instability strip (dotted lines) are taken from Breger (1995). The observed borders from our sample are indicated as filled lines in the lower panel.

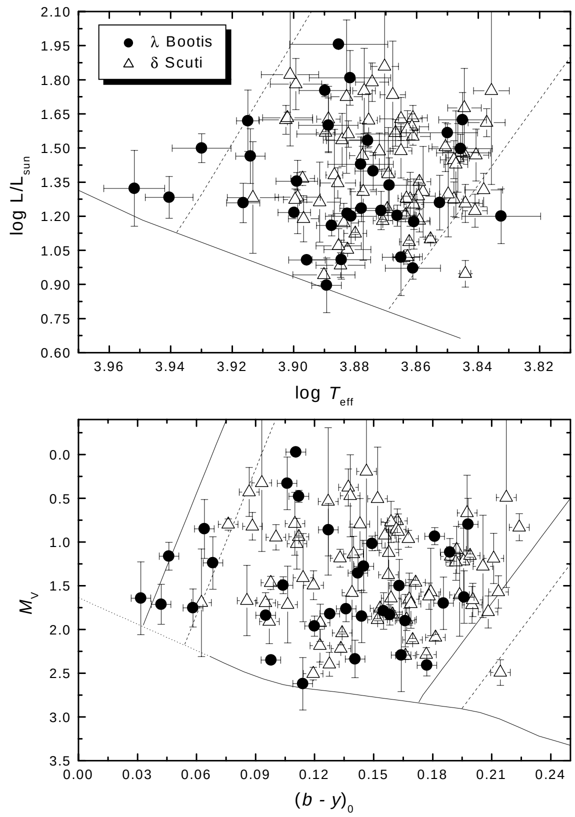

Fig. 5. The $\log L_*/L_\odot$ versus $\log T_{\rm eff}$ (upper panel) and M_V versus $(b-y)_0$ (lower panel) diagrams for pulsating λ Bootis (filled circles) and selected δ Scuti (open triangles) stars. The location of both samples are comparable justifying our selection criteria of the δ Scuti type stars. The lines are the same as in Fig. 4.

4.1. A sample of δ Scuti stars

As a basis we have used the catalogue of Rodriguez et al. (2000). From this sample, stars have been rejected following these criteria:

- Classification as Am, Ap, δ Delphini and SX Phoenicis objects;
- $v \sin i < 45\,{\rm km\,s^{-1}}$ (if available);
- $\sigma(\pi)/\pi > 0.175$;
- $\log P < -1.7$ and $\log P > -0.8$;
- Amplitude > 0.08 mag (if no $v \sin i$ available);
- without Johnson and Geneva photometry;
- $E(b-y) > 0.05$ mag.

Such a choice is based on the characteristics of our λ Bootis type sample and is hoped to guarantee a comparable sample of δ Scuti type stars. In total, 69 objects remain in the sample. The basic parameters, etc. were derived in exactly the same way as for the λ Bootis type objects, as described in Sect. 3. Table 5 lists all calibrated parameters together with the periods given by Rodriguez et al. (2000).

4.2. Hertzsprung-Russell-diagram and the pulsational characteristics

First of all, we have investigated the location of all λ Bootis stars within the $\log L_*/L_\odot$ versus $\log T_{\rm eff}$ and M_V versus $(b-y)_0$ diagrams (Fig. 4). The borders of the classical instability strip are taken from Breger (1995). There are several conclusions from this figure:

- The published hot and cool borders of the δ Scuti instability strip within the M_V versus $(b-y)_0$ diagram do not coincide with the observed ones for the λ Bootis stars. The latter are bluer at the Zero Age Main Sequence (ZAMS hereafter) by about 25 mmag. However, the borders are in accordance with the observations within the $\log L_*/L_\odot$ versus $\log T_{\rm eff}$ diagram;
- Taking the average of variable to non-variable objects within the classical instability strip for both diagrams then we derive a value of at least 70% pulsating objects.

Figure 5 shows the same diagrams for this sample (filled circles) together with those of the selected δ Scuti stars (open triangles). Besides one object (HD 57167), the cool borders are in excellent agreement with the observations. However, there are four hot λ Bootis type pulsators: HD 120500, HD 125162,

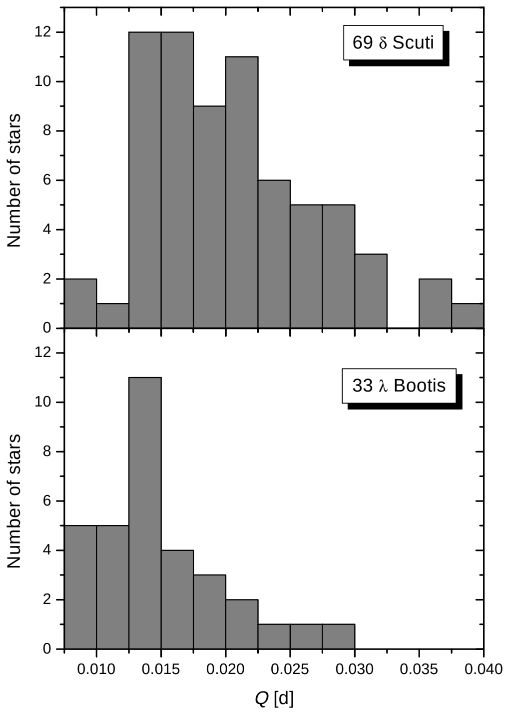

Fig. 6. The histograms of the pulsational constant Q for the selected δ Scuti (upper panel) and λ Bootis (lower panel) stars.

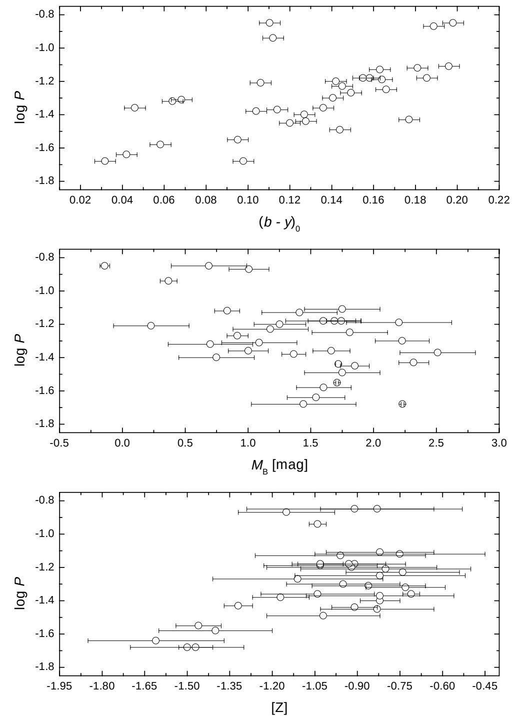

Fig. 7. Correlation of $(b-y)_0$, the absolute magnitude and metallicity with $\log P$ for all λ Bootis type stars.

HD 183324 and HD 221756. The reason for these shifts is not yet clear. We are able to exclude measurements errors (mean values from several references were used) and the effects of rotation (all stars have moderate $v \sin i$ values). In addition, taking the unreddened colours, all four stars are still outside the hot border. Therefore it is somewhat surprising that only one object (HD 183324) lies significantly outside the borders within the $\log L_*/L_\odot$ versus $\log T_{\rm eff}$ diagram.

As a next step towards analyzing the pulsational characteristics we have calculated the pulsation constants given by

$$\log Q = -6.456 + 0.5 \log g + 0.1 M_B + \log T_{\rm eff} + \log P.$$

The resulting Q-values are listed in Table 4 and in Table 5 for our program λ Bootis stars and for the comparison sample of δ Scuti stars, respectively. For the λ Bootis group, the Q-values range from 0.038 to 0.033 for the fundamental radial modes and decrease to about 0.012 for the fifth radial overtone (Stellingwerf 1979; Fitch 1981). Figure 6 (lower panel) shows a histogram of the Q-values for the pulsating program stars. It seems that only a few stars, if any, pulsate in the fundamental mode, but there is a high percentage with $Q < 0.020$ d (high overtone modes).

The distribution of the Q-values for the λ Bootis type stars is different from that of the δ Scuti type sample (Fig. 6, upper panel) at a 99.9% level (derived from a t-test).

We also noticed four pulsators (HD 15165, HD 42503, HD 111604 and HD 142994) that have considerably longer periods ($\log P > -0.94$ corresponding to $P < 8.7\,{\rm d}^{-1}$) than the rest of our sample. They do, however, show a similar behaviour to the remaining group members.

4.3. The Period-Luminosity-Colour-Metallicity (PLCZ) relation

A Period-Luminosity-Metallicity relation was found for Population II type variables such as RR Lyrae and SX Phoenicis stars as well as Cepheids (Nemec et al. 1994). These objects pulsate in the radial fundamental, first and second overtone modes. The dependence of the pulsational period on the metallicity is purely evolutionary, i.e. older objects exhibit a lower overall abundance and a different pulsational period. The Period-Luminosity-Metallicity relation serves as a distance indicator widely used for extragalactic objects.

The situation for λ Bootis stars is very different. All evidence indicates that we find only peculiar surface abundances whereas the overall abundance of the stars is solar, i.e. these stars are true Population I objects. The conclusion that λ Bootis stars are true Population I objects is based on their galactic space motions (Faraggiana & Bonifacio 1999) combined with their location in the Hertzsprung-Russell-diagram (Fig. 4). With the exception of the SX Phe stars, Population II type objects are located at much higher absolute magnitudes and thus luminosities than found for the λ Bootis group. However, the space motions of SX Phe stars are inconsistent with Population I, which facilitates an easy separation from λ Bootis stars.

To examine the presence of a PLCZ relation, the following basic approach was chosen:

$$\log P = a + b(b-y)_0 + c(M_B) + d[Z].$$

The $[Z]$-values range from -0.71 dex to -1.61 dex for the λ Bootis type sample whereas the δ Scuti type stars have

Table 6. Nonvariable λ Bootis stars, an asterisk denotes stars without an accurate HIPPARCOS parallax; $\sigma(b-y) = \pm 0.005$ mag. In parenthesis are the errors in the final digits of the corresponding quantity.

HD	$(b-y)_0$ [mag]	$\log T_{\rm eff}$	M_V [mag]	$\log L_*/L_\odot$
319	+0.078	3.904(7)	1.27(19)	1.45(8)
7908	+0.192	3.854(5)	2.60(18)	0.90(7)
23392*	−0.008	3.991(12)	1.43(30)	1.45(12)
24472	+0.213	3.842(8)	2.14(11)	1.09(5)
31295	+0.029	3.950(9)	1.66(22)	1.32(9)
36726*	−0.004	3.978(10)	1.74(30)	1.32(12)
54272*	+0.214	3.846(13)	2.33(30)	1.01(12)
74873	+0.046	3.940(12)	1.82(1)	1.24(1)
81290*	+0.225	3.839(13)	1.85(30)	1.20(12)
83277	+0.196	3.845(12)	1.49(29)	1.35(12)
84123	+0.226	3.847(11)	1.58(15)	1.31(6)
90821*	+0.065	3.913(4)	0.74(30)	1.66(12)
91130	+0.073	3.910(5)	1.36(26)	1.42(11)
101108*	+0.113	3.893(4)	1.33(30)	1.42(12)
106223	+0.225	3.836(16)	1.83(45)	1.22(18)
107233	+0.181	3.861(9)	2.64(13)	0.88(5)
110411	+0.029	3.951(10)	1.90(28)	1.22(11)
111005	+0.222	3.836(4)	1.76(53)	1.24(21)
130767	+0.002	3.964(10)	1.27(2)	1.48(1)
149130*	+0.208	3.842(6)	1.51(30)	1.34(12)
154153	+0.194	3.848(7)	1.86(29)	1.19(11)
156954	+0.188	3.853(6)	2.81(33)	0.82(13)
170680	−0.013	3.993(11)	0.83(23)	1.70(9)
175445	+0.030	3.930(10)	1.08(27)	1.53(11)
193256*	+0.101	3.889(5)	1.08(30)	1.51(12)
193281*	+0.072	3.905(6)	0.41(30)	1.79(12)
198160	+0.103	3.896(7)	1.47(41)	1.36(16)
204041	+0.086	3.902(5)	1.75(18)	1.25(7)
216847	+0.155	3.867(5)	0.93(24)	1.56(10)
261904*	+0.005	3.974(9)	1.33(30)	1.48(12)
290492*	+0.084	3.908(8)	2.04(30)	1.14(12)
294253*	−0.038	4.027(6)	1.32(30)	1.58(12)

values from −0.36 dex to +0.78 dex compared to the Sun. The coefficients for the PLCZ relation were determined simultaneously, applying a multiregression analysis (Christensen 1996). This takes into account the individual errors of the bolometric absolute magnitude and metallicity as weights, whereas the errors for the period and colour were assumed to be constant for all stars. The solution was determined using a least-squares fit and a maximum-likelihood method. Both give consistent results, as summarized in Table 8. Figure 7 shows the individual correlations. The correlations of the bolometric magnitude and color with the pulsational period are compatible with those found for the δ Scuti stars.

To investigate whether the [Z] term is indeed significant, a plot [$\log P - 2.86(b-y)_0 + 0.195(M_B)$] versus [$Z$] was drawn (Fig. 8). The coefficients for $(b-y)_0$ and M_B are the mean values from Table 8 and are consistent within the errors for both the δ Scuti and λ Bootis samples. Figure 8 shows that both samples exhibit a trend with [Z] (with an offset of about 1 dex). Whereas

Table 7. Comparison of effective temperatures and surface gravities for λ Bootis stars from Heiter et al. (2002; Table 1; columns "Literature") and this work; $\Delta T_{\rm eff} = T_{\rm eff}({\rm Lit.}) - T_{\rm eff}({\rm TW})$ = +72(210) K; $\Delta \log g = \log g({\rm Lit.}) - \log g({\rm TW})$ = +0.07(24) dex.

	Literature		This work	
HD	$T_{\rm eff}$ ±200 K	$\log g$ ±0.3 dex	$T_{\rm eff}$	$\log g$
319	8100	3.8	8020(135)	3.74(8)
11413	7900	3.8	7925(124)	3.91(21)
15165	7200	3.7	7010(167)	3.23(10)
31295	8800	4.2	8920(177)	4.20(1)
74873	8900	4.6	8700(245)	4.21(11)
75654	7250	3.8	7350(104)	3.77(11)
81290	6780	3.5	6895(214)	3.82(28)
84123	6800	3.5	7025(145)	3.73(17)
101108	7900	4.1	7810(90)	3.90(18)
105759	8000	4.0	7485(102)	3.65(10)
106223	7000	4.3	6855(247)	3.49(18)
107233	7000	3.8	7265(143)	4.03(10)
109738	7575	3.9	7610(145)	3.90(13)
110411	9100	4.5	8930(206)	4.14(14)
111005	7410	3.8	6860(66)	3.72(10)
125162	8650	4.0	8720(156)	4.07(9)
142703	7100	3.9	7265(150)	3.93(12)
156954	6990	4.1	7130(93)	4.04(13)
168740	7700	3.7	7630(81)	3.88(14)
170680	10000	4.1	9840(248)	4.15(6)
183324	9300	4.3	8950(204)	4.13(4)
192640	7960	4.0	7940(96)	3.95(18)
193256	7800	3.7	7740(94)	3.69(17)
193281	8070	3.6	8035(115)	3.54(4)
198160	7900	4.0	7870(129)	3.99(9)
204041	8100	4.1	7980(97)	3.97(8)
210111	7530	3.8	7550(123)	3.84(15)
221756	9010	4.0	8510(188)	3.90(3)

Table 8. Estimates for $\log P = a + b(b-y)_0 + c(M_B) + d[Z]$ for all pulsating program stars (left upper column), for stars with $[Z] > -1.3$ excluding HD 30422, HD 35242, HD 125162, HD 142703, HD 183324 and HD 192640 (right upper column) as well as for the selected δ Scuti stars (lower column); F denotes the significance level of the test for a zero hypothesis; in brackets are the standard errors of the estimates.

coeff.	value	F [%]	value	F [%]
λ Bootis				
a	−1.25(9)	<0.01	−1.41(9)	<0.01
$b(b-y)_0$	+3.01(41)	<0.01	+2.71(46)	<0.01
$c(M_B)$	−0.20(3)	<0.01	−0.19(3)	<0.01
$d[Z]$	+0.14(6)	13.20	−0.06(17)	74.49
δ Scuti				
a	−1.17(6)	<0.01		
$b(b-y)_0$	+2.71(43)	<0.01		
$c(M_B)$	−0.23(3)	<0.01		
$d[Z]$	−0.28(7)	<0.01		

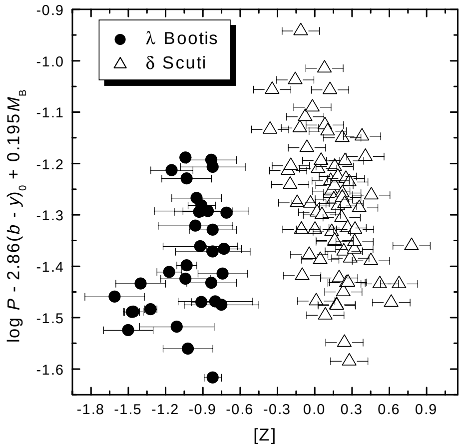

Fig. 8. Correlation of $[Z]$ for the λ Bootis (filled circles) and selected δ Scuti type (open triangles) stars.

the $[Z]$ term is statistically significant for the selected sample of δ Scuti stars, it is caused by only six λ Bootis stars with strong underabundances (HD 30422, HD 35242, HD 125162, HD 142703, HD 183324 and HD 192640) and vanishes after excluding them. We have also tested the sample for possible correlations of the $[Z]$ term by excluding other data points. We find no other selection criteria of objects by means of a physical explanation, only "suitable" discarding would yield a clear correlation. This implies that the peculiar abundances do not affect the pulsational period for the group of λ Bootis type stars. However, we find within the errors no difference of the PLC relation for the λ Bootis and δ Scuti type stars.

5. Conclusions

We have investigated the pulsational characteristics of a group of λ Bootis stars and compared it to a sample of δ Scuti pulsators. The latter was chosen such that it matches our program stars within the global astrophysical parameters. The following properties of the λ Bootis stars are different from those of the δ Scuti pulsators:

- At least 70% of all λ Bootis types stars inside the classical instability strip pulsate.
- Only a maximum of two stars pulsate in the fundamental mode but there is a high percentage with $Q < 0.020$ d (high overtone modes).
- The instability strip of the λ Bootis stars at the ZAMS is 25 mmag bluer in $(b-y)_0$ than that of the δ Scuti stars.

We find no clear evidence for a significant term for a $[Z]$ correlation with the period, luminosity and colour but the PLC relation is within the errors identical with that of the δ Scuti type stars. We note that for all but one of the investigated pulsators, high-degree nonradial modes were detected spectroscopically (Bohlender et al. 1999), which represents excellent agreement with our work. The spectral variability of the λ Bootis stars is very similar to that seen in rapidly rotating δ Scuti stars (Kennelly et al. 1992).

Acknowledgements. This work benefitted from the Fonds zur Förderung der wissenschaftlichen Forschung, project *P14984*. ERC would like to thank D. Romero, E. Colmenero and S. Potter for their support. Use was made of the SIMBAD database, operated at CDS, Strasbourg, France and the GCPD database, operated at the Institute of Astronomy of the University of Lausanne. We are also indebted to the committees of the SAAO, Siding Spring and Fairborn Observatory who granted observing time.

References

Abt, H. A. 1984, in The MK Process and Stellar Classification, ed. R. F. Garrison (David Dunlap Observatory, Toronto), 340
Abt, H. A., & Morrell, N. I. 1995, ApJS, 99, 135
Andrievsky, S. M. 1997, A&A, 321, 838
Andrievsky, S. M., Chernyshova, I. V., Korotin, S. A., et al. 2002, A&A, in preparation
Antonello, E., & Mantegazza, L. 1982, A&AS, 49, 709
Arenou, F., Grenon, M., & Gómez, A. 1992, A&A, 258, 104
Balona, L. A. 1977, Mem. R. Astr. Soc., 84, 101
Bartolini, C., Dapergolas, A., Piccioni, A., & Voli, M. 1980a, IBVS, 1753
Bartolini, C., Dapergolas, A., Piccioni, A., & Voli, M. 1980b, IBVS, 1757
Bohlender, D. A., Gonzalez, J. F., & Matthews, J. M. 1999, A&A, 350, 553
Breger, M. 1979, PASP, 91, 5
Breger, M. 1995, PASPC, 76, 596
Cayrel de Strobel, G. 1996, A&AR, 7, 243
Charbonneau, P. 1993, ApJ, 405, 720
Chen, B., Vergely, J. L., Valette, B., & Carraro, G. 1998, A&A, 336, 137
Chernyshova, I. V., Andrievsky, S. M., Kovtyukh, V. V., & Mkrtichian, D. E. 1998, Contrib. Astron. Obs. Skalnaté Pleso, 27(3), 332
Christensen, R. 1996, Analysis of Variance, Design and Regression, Applied statistical methods (Chapman & Hall, London), 391
Claret, A. 1995, A&AS, 109, 441
Crawford, D. L. 1979, AJ, 84, 1858
Deeming, T. J. 1975, Ap&SS, 36, 137
Desikachary, K., & McInally, C. J. 1979, MNRAS, 188, 67
Drilling, J. S., & Landolt, A. U. 2000, in Allen's Astrophysical Quantities, 4th edition, ed. A. N. Cox (Springer Verlag), 388
ESA (European Space Agency) 1997, The Hipparcos and Tycho Catalogues (ESA Publications, Noordwijk)
Faraggiana, R., & Bonifacio, P. 1999, A&A, 349, 521
Fitch, W. S. 1981, ApJ, 249, 218
Gerbaldi, M., Faraggiana, R., Burnage, R., et al. 1999, A&AS, 137, 273
Gies, D. R., & Percy, J. R. 1977, AJ, 82, 166
Golay, M. 1974, Introduction to astronomical photometry (D. Reidel Publishing Co., Dordrecht)
Gray, R. O. 1988, AJ, 95, 220
Gray, R. O., & Corbally, C. J. 1993, AJ, 106, 632
Hakkila, J., Myers, J. M., Stidham, B. J., & Hartmann, D. H. 1997, AJ, 114, 2043
Handler, G. 1999, IBVS, 4817
Handler, G. 2002, in Observational Aspects of Pulsating B- and A Stars, ed. C. Sterken, & D. W. Kurtz (San Francisco: Astronomical Society of the Pacific), ASP Conf. Proc., 256, 113
Handler, G., Gray, R. O., & Shobbrook, R. R. 2000, IBVS, 4876
Heiter, U. 2002, A&A, 381, 959
Heiter, U., Kupka, F., Paunzen, E., Weiss, W. W., & Gelbmann, M. 1998, A&A, 335, 1009

Heiter, U., Weiss, W. W., & Paunzen, E. 2002, A&A, 381, 971
Hilditch, R. W., Hill, G., & Barnes, J. V. 1983, MNRAS, 204, 241
Holweger, H., & Rentzsch-Holm, I. 1995, A&A, 303, 819
Iliev, I. Kh., Paunzen, E., Barzova, I. S., et al. 2001, IBVS, 5199
Iliev, I. Kh., Paunzen, E., Barzova, I. S., et al. 2002, A&A, 381, 914
Kamp, I., Iliev, I. Kh., Paunzen, E., et al. 2001, A&A, 375, 899
Kennelly, E. J., Walker, G. A. H., & Merryfield, W. J. 1992, ApJ, 400, L71
Kjeldsen, H., & Frandsen, S. 1992, PASP, 104, 413
Kobi, D., & North, P. 1990, A&AS, 85, 999
Koen, C. 1992, MNRAS, 256, 65
Künzli, M., North, P., Kurucz, R. L., & Nicolet, B. 1997, A&AS, 122, 51
Kupka, F., Piskunov, N. E., Ryabchikova, T. A., Stempels, H. C., & Weiss, W. W. 1999, A&AS, 138, 1
Kurtz, D. W. 2000, in Delta Scuti and Related Stars, ed. M. Breger, & M. H. Montgomery, ASP Conf. Ser., 210, 287
Kusakin, A. V., & Mkrtichian, D. E. 1996, IBVS, 4314
Liu, Y. Y., Jiang, S. Y., Michel, E., et al. 1996, A&AS, 120, 179
Martinez, P., Koen, C., Handler, G., & Paunzen, E. 1998, MNRAS, 301, 1099
Michaud, G., & Charland, Y. 1986, ApJ, 311, 326
Mkrtichian, D. E., Kusakin, A. V., Koval, V. A., et al. 2000, in The Impact of Large-Scale Surveys on Pulsating Star Research, ed. I. Szabados, & D. Kurtz, ASP Conf. Ser., 203, 494
Moon, T. T., & Dworetsky, M. M. 1985, MNRAS, 217, 305
Napiwotzki, R., Schönberner, D., & Wenske V. 1993, A&A, 268, 653
Nemec, J. M., Nemec, A. F. L., & Lutz, T. E. 1994, AJ, 108, 222
Oudmaijer, R. D., Groenewegen, M. A. T., & Schrijver, H. 1998, MNRAS, 294, L41
Paunzen, E. 2001, A&A, 373, 633
Paunzen, E., & Handler, G. 1996, IBVS, 4318
Paunzen, E., & Gray, R. O. 1997, A&AS, 126, 407
Paunzen, E., Kuschnig, R., Handler, G., Gelbmann, M., & Weiss, W. W. 1997, A&AS, 124, 23
Paunzen, E., Weiss, W. W., Kuschnig, R., et al. 1998, A&A, 335, 533
Paunzen, E., Kamp, I., & Iliev, I. Kh. 1999a, A&A, 351, 981
Paunzen, E., Andrievsky, S. M., Chernyshova, I. V., et al. 1999b, A&A, 351, 981
Rodriguez, E., Lopez-Gonzalez, M. J., & Lopez de Coca, P. 2000, A&AS, 144, 469
Sandage, A. 1972, ApJ, 178, 1
Solano, E., Paunzen, E., Pintado, O. I., & Varela, J. 2001, A&A, 374, 957
Stellingwerf, R. F. 1978, ApJ, 224, 953
Stellingwerf, R. F. 1979, ApJ, 227, 935
Strömgren, B. 1966, ARA&A, 4, 433
Stürenburg, S. 1993, A&A, 277, 139
Turcotte, S., & Charbonneau, P. 1993, ApJ, 413, 376
Turcotte, S., Richer, J., Michaud, G., & Christensen-Dalsgaard, J. 2000, A&A, 360, 603
Uesugi, A., & Fukuda, I. 1982, Revised Catalogue of Stellar Rotational Velocities, Department of Astronomy, Kyoto Univ., Kyoto
Venn, K. A., & Lambert, D. L. 1990, ApJ, 363, 234
Waelkens, C., & Rufener, F. 1983, Hvar Obs. Bull., 7, 301

Chapter 3

Gamma Doradus stars

3.1 Introduction

The group of γ Doradus stars is only known for about a decade. For several years, they were regarded as "variables without a cause", until it became clear that they were indeed pulsating variables. Section 3.2 gives the definition of the γ Doradus pulsators which is still valid today. Soon after this definition, a careful analysis of the time-resolved photometric data from the Hipparcos satellite allowed the first outline of their instability region in the HR diagram (Sect. 3.3). We note that two thirds of the "prime candidates" for γ Doradus stars, that needed to be invoked to find the borders of their instability region in Sect. 3.3, were later observed from the ground and all but one of them were shown to be indeed members of this group of variables (Henry et al. 2001, 2005, 2007, Henry & Fekel 2003). This demonstrates the value of careful manual frequency analyses carried out by experienced scientists.

Section 3.3 also showed that the domains of the γ Doradus and δ Scuti stars in the HR Diagram overlap. Since there is no a priori reason that mutually excludes pulsation of either type in any given star, it was suspected that objects showing both types of pulsation can exist. Section 3.4 examines this question by searching for δ Scuti-type pulsations in γ Doradus stars. It also gives improved boundaries for the γ Doradus domain in the HR diagram (still valid to date), a criterion on how to distinguish γ Doradus and δ Scuti stars, and reports the discovery of the first "hybrid" pulsator that has modes of both types of variables excited. This star, HD 209295, is extensively studied in Sect. 3.5, with the result that some of the γ Doradus pulsation modes are likely to be tidally excited by a close companion that has been looked for, but not found. HD 209295 is still the best case for tidally excited pulsations known so far.

3.2 γ Doradus stars: defining a new class of pulsating variables

Original paper:

A. B. Kaye, **G. Handler,** K. Krisciunas, E. Poretti, F. Zerbi, 1999, PASP 111, 840

Publications of the Astronomical Society of the Pacific, 111:840–844, 1999 July

γ Doradus Stars: Defining a New Class of Pulsating Variables

Anthony B. Kaye
Applied Theoretical and Computational Physics Division, Los Alamos National Laboratory; kaye@lanl.gov
Gerald Handler
Institut für Astronomie, Universität Wien
Kevin Krisciunas
Department of Astronomy, University of Washington
and
Ennio Poretti and Filippo M. Zerbi
Osservatorio Astronomico di Brera/Merate
Received 1999 March 18; accepted 1999 April 16

ABSTRACT. In this paper we describe a new class of pulsating stars, the prototype of which is the bright, early, F-type dwarf γ Doradus. These stars typically have between 1 and 5 periods ranging from 0.4 to 3 days with photometric amplitudes up to 0.1 mag in Johnson V. The mechanism for these observed variations is high-order, low-degree, nonradial, gravity-mode pulsation.

1. INTRODUCTION

Cousins & Warren (1963) discovered that the bright F0 V star γ Doradus was variable over a range of several hundredths of a magnitude with two principal periods ($0^{\mathrm{d}}.733$ and $0^{\mathrm{d}}.757$). The star γ Doradus has an absolute magnitude similar to that of a δ Scuti star but is somewhat cooler, and thus for many years it was deemed a "variable without a cause." Cousins (1992) stated: "The suggested W-UMa type no longer seems a possibility, but rotation with starspots and/or tidal distortion might account for the variability. The light-curve and dual periodicity would favor some form of pulsation, but the period is much longer than expected for a δ Scuti star." Balona, Krisciunas, & Cousins (1994) tried to model the star using two starspots and differential rotation. They found that the large size of the required spots and the high stability of their periods did not bode well for the starspot hypothesis. Furthermore, they found evidence of a third period, later confirmed by Balona et al. (1996), which further diminishes the likelihood of the starspot hypothesis.

9 Aurigae (=HD 32537), a star very similar to γ Doradus, was first noted to be variable by Krisciunas & Guinan (1990). Krisciunas et al. (1993) found evidence for two photometric periods between 1.2 and 3 days. Using infrared and *International Ultraviolet Explorer* data, Krisciunas et al. (1993) found no evidence for a close companion nor for a lumpy ring of dust surrounding the star, but they could not rule out the idea of starspots.

Over the past decade, more than 40 variable stars with spectral types and luminosity classes similar to γ Doradus have been discovered that exhibit variability on a timescale that is an order of magnitude slower than that of δ Scuti stars. Mantegazza, Poretti, & Zerbi (1994), Krisciunas (1994), and Hall (1995) suggested that these objects may constitute a new class of variable stars. Breger & Beichbuchner (1996) investigated whether any known δ Scuti stars also showed γ Doradus–type behavior and found no clear-cut examples of stars that show both "fast" and "slow" variability; Figure 1 of their paper nicely illustrates the locations of the two kinds of variables on the color-magnitude diagram. However, not all of their γ Doradus stars are regarded as bona fide members of the group.

Krisciunas (1998) provides a good summary of our knowledge of γ Doradus stars as a new class, but to date there is no publication in the refereed journal literature which summarizes and "defines" the characteristics of the class itself. It was quite evident early on that significant advancement in the understanding of the physical nature of γ Doradus stars could be made only on the basis of a large observational effort. Hence, activities were concentrated on international multilongitude photometric and spectroscopic campaigns.

On the basis of extensive photometry, radial velocities, and line-profile variations, it has been proven that 9 Aurigae (Krisciunas et al. 1995b; Zerbi et al. 1997a; Kaye 1998a), γ Doradus (Balona et al. 1996), HD 164615 (Zerbi et al. 1997b; Hatzes 1998), HR 8330 (Kaye et al. 1999b), HD 62454 and HD 68192 (Kaye 1998a), and HR 8799 (Zerbi et al. 1999) are indeed pulsating variable stars. Given the nature of the observed variability in these stars, the cause must be high-order (n), low-degree (l), nonradial g-modes. We assert this on the basis of evidence *for* nonradial g-modes and the lack of convincing evidence for other explanations, including starspots. Furthermore, we argue that since this small (but growing) group of objects all have similar physical characteristics and show broadband light— and line-profile variations resulting from the same physical mechanism—they form a new class of variable stars. In this paper, we indicate the cohesiveness of this group and its differences from other variable star classes. Finally, we provide a set of criteria by which new candidates may be judged.

2. GENERAL CHARACTERISTICS OF THE CLASS

Our list of bona fide γ Doradus stars is complete to 1999 April, and all objects of this class have extensive enough photometric and/or spectroscopic data sets to rule out other variability mechanisms. A complete, commented, up-to-date list of all proposed candidates for this group, as well as their observational history, is maintained by G. Handler and K. Krisciunas.[1]

[1] The list of γ Doradus stars is available at http://www.astro.univie.ac.at/~gerald/gdor.html.

Table 1 lists the observed quantities of each of the 13 objects used to define this new class of variable stars. Column (1) gives the most common name of each object. Column (2) provides the best available value of $b-y$; columns (3) and (4) list the average apparent visual magnitude of each object ($\langle V \rangle$) and the best determined spectral type. Column (5) lists the best available value of the projected equatorial velocity, $v \sin i$, in km s^{-1}. Column (6) reports the *Hipparcos* trigonometric parallax in milliarcseconds (ESA 1997).

Table 2 presents derived properties of the 13 objects. Estimates for the total metallicity ([Me/H]) are derived from the relations of Nissen (1988) and Smalley (1993), which are precise to within 0.1 dex in [Me/H] and are listed in column (2). The absolute visual magnitudes (col. [3]) are calculated from the *Hipparcos* parallaxes. Luminosities, using bolometric corrections listed in Lang (1992, p. 138) and $M_{\mathrm{bol},\odot} = 4.75$ (Allen 1973, p. 161), are presented in column (4). The effective temperatures are determined from the new calibration of Strömgren photometry by Villa (1998), for which we estimate errors of ± 100 K (col. [5]); stellar radii precise to $\pm 0.05\ R_\odot$ are then calculated (col. [6]). Finally, masses which are precise to $\pm 0.03\ M_\odot$ (internal model error) are inferred by comparison with solar-metallicity evolutionary tracks by Pamyatnykh et al. (1998) (col. [7]). The final row in Table 2 represents the unweighted average of each of the columns; presumably, these are the physical parameters of a "typical" γ Doradus variable.

We present a color-magnitude diagram of all 13 stars, using the *Hipparcos* parallaxes to calculate accurate values

TABLE 1

OBSERVATIONAL PARAMETERS OF THE CONFIRMED γ DORADUS VARIABLES

Star (1)	$b-y$ (mag) (2)	$\langle V \rangle$ (mag) (3)	Spectral Type (4)	$v \sin i$ (km s^{-1}) (5)	π (mas) (6)	Principal Reference (7)
HD 224945......	0.192	6.93	F0+ V[a]	55	16.92	1
γ Doradus.......	0.201	4.25	F0 V	62	49.26	2
9 Aurigae........	0.217	5.00	F0 V	18	38.14	3
BS 2740	0.219	4.49	F0 V	40	47.22	4
HD 62454.......	0.214	7.15	F1 V[b]	53	11.18	5
HD 68192.......	0.227	7.16	F2 V[a]	85	10.67	5
HD 108100......	0.234	7.14	F2 V	68	12.10	6
BS 6277	0.167	6.20	F0 V	185	13.70	7
HD 164615......	0.226	7.06	F2 IV[a]	66	14.36	8
BS 6767	0.183	6.40	F0 Vn[a]	135	17.44	5
BS 8330	0.225	6.20	F2 IV[a]	38	19.90	8
BS 8799	0.181	5.99	kA5 hF0 mA5 V; λ Boo[c]	45	25.04	9
HD 224638......	0.198	7.49	F1 Vs[a]	24	12.56	10

REFERENCES.—(1) Poretti et al. 1996; (2) Balona, Krisciunas, & Cousins 1994; (3) Zerbi et al. 1997a; (4) Poretti et al. 1997; (5) Kaye 1998a; (6) Breger et al. 1997; (7) Zerbi et al. 1997b; (8) Kaye et al. 1999b; (9) Zerbi et al. 1999; (10) Mantegazza, Poretti, & Zerbi 1994.

[a] See Gray & Kaye 1999b.

[b] HD 62454 is the primary star of a double-lined spectroscopic binary. See Kaye 1998b.

[c] See Gray & Kaye 1999a.

TABLE 2

Calculated and Inferred Basic Properties of the Confirmed γ Doradus Variables

Star (1)	[Me/H] (2)	M_V (mag) (3)	$L/L_\odot$ (4)	$T_{\rm eff}$ (K) (5)	$R/R_\odot$ (6)	$M/M_\odot$ (7)
HD 224945......	−0.30	3.07	5.1	7250	1.43	1.51
γ Doradus.......	−0.02	2.72	7.0	7200	1.70	1.57
9 Aurigae........	−0.19	2.89	6.0	7100	1.62	1.52
BS 2740	−0.15	2.86	6.2	7100	1.64	1.53
HD 62454	0.16	2.39	9.5	7125	2.02	1.66
HD 68192	0.05	2.30	10.5	7000	2.20	1.71
HD 108100......	−0.03	2.53	8.5	6950	2.01	1.62
BS 6277	0.09	1.93	14.7	7350	2.36	1.84
HD 164615......	0.20	2.82	6.5	7000	1.73	1.53
BS 6767	−0.10	2.59	7.9	7300	1.76	1.61
BS 8330	−0.01	2.67	7.4	7000	1.85	1.57
BS 8799	−0.36	2.96	5.7	7375	1.46	1.54
HD 224638......	−0.15	2.98	5.5	7200	1.51	1.52
Average	−0.06	2.69	7.6	7160	1.77	1.59

of M_V in Figure 1. The observed zero-age main sequence (Crawford 1975) and the observed edges of the δ Scuti instability strip (Breger 1979) are shown as a solid line and dashed lines, respectively.

The truly intriguing characteristic of γ Doradus stars is that they are variable; considering the part of the Hertzsprung-Russell (HR) diagram in which they lie, previous pulsational models say they should not be. The outer

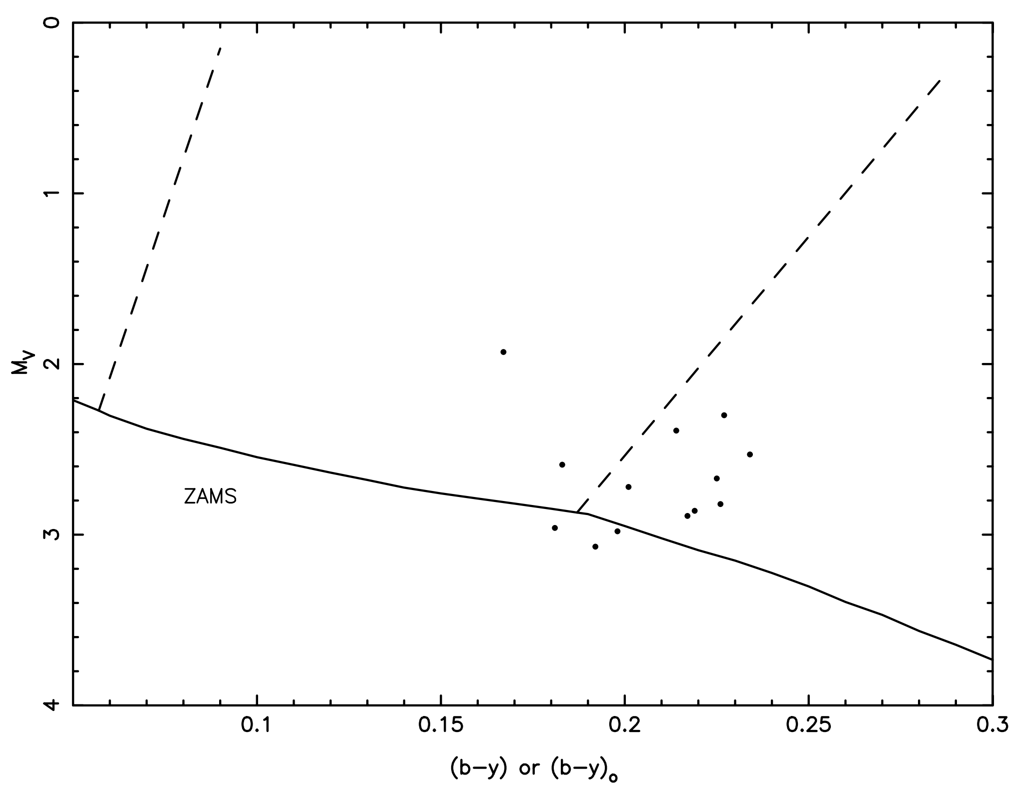

Fig. 1.—Color-magnitude diagram showing the positions of the confirmed γ Doradus stars. Solid points indicate the position of each object, the solid line represents the observed zero-age main sequence, and the boundaries of the observed δ Scuti instability strip are indicated by dashed lines.

convection zones of these stars are too shallow to generate and sustain a large magnetic dynamo, thus making starspots improbable. Most of the γ Doradus stars are multiperiodic; the average period is close to 0.8 days. The observed variations are not necessarily stable and may be highly dynamic (Kaye & Zerbi 1997). Typical amplitudes cluster around 4% ($= 0^{\mathrm{m}}.04$) in Johnson V and may vary during the course of an observing season by as much as a factor of 4. For the best-studied stars (e.g., γ Doradus itself, 9 Aurigae, and HR 8330), line-profile variations with periods equal to the photometric periods have been confirmed (Balona et al. 1996; Kaye 1998a; Kaye et al. 1999b). No high-frequency signals have been detected in either the photometry or the spectroscopy, indicating a lack of the p-mode pulsation common in δ Scuti stars.

Despite their commonality, a small subset of γ Doradus stars shows remarkably peculiar pulsation characteristics. In several objects (e.g., HD 224945: Poretti et al. 1996; HD 224638: Mantegazza et al. 1994; and 9 Aurigae: Krisciunas et al. 1995b; Zerbi et al. 1997a; Kaye 1998a), amplitude variability of order 50% over a few years is observed. Other objects (e.g., γ Doradus: Cousins 1992; HD 164615: Zerbi et al. 1997b; and HR 8799: Zerbi et al. 1999) show amplitude modulation selectively located at the moment of *maximum* brightness, a characteristic of variability that is new to the field of stellar pulsation. Still other objects (e.g., HD 68192) show remarkably constant periods and amplitudes over long timescales. Clearly, these peculiarities within the γ Doradus class need many more long-term observations to be explained.

3. DEFINING A NEW CLASS

We argue that the qualities and characteristics of the 13 above named and described stars form a homogeneous set based on their physical characteristics and their mechanism for variability and, thus, form the basis for a new class of variable stars.

In following with the informal discussions at the "Astrophysical Applications of Stellar Pulsation" conference (Stobie & Whitelock 1995) held in 1995 at Cape Town, South Africa, and in recent papers in the literature (see, e.g., Krisciunas et al. 1993; Balona et al. 1996; Zerbi et al. 1997a; Poretti et al. 1997; Kaye 1998a; Kaye et al. 1999b), we propose that this type of variable star henceforth be known and recognized by the name *γ Doradus variable stars*. The extent of the γ Doradus phenomenon, as it is currently known, consists of variable stars with an implied range in spectral type A7–F5 and in luminosity class IV, IV-V, or V; their variations are consistent with the model of high-order (n), low-degree (l), nonradial, gravity-mode oscillations. Although it is conceivable that variations such as those of the stars in this class may occur outside of this region, it is likely that other mechanisms of variability would then dominate, and thus this combination of spectral type, luminosity class, and (most importantly) variability mechanism forms a suitable definition.

From an observational point of view, the g-mode oscillations seen in γ Doradus variable stars are characterized by periods between 0.4 and 3 days and peak-to-peak amplitudes $\lesssim 0^{\mathrm{m}}.1$ in Johnson V. The presence of multiple periods and/or amplitude modulation is common among these stars, but this is not included in the formal definition presented here. Spectroscopic variations are also observed, and these manifest themselves both as low-amplitude radial-velocity variations (that cannot be attributed to duplicity effects) and as photospheric line-profile variations.

In addition to these features, we stress that any object put forth for consideration as a confirmed γ Doradus variable star must not vary *exclusively* by other mechanisms, including p-mode pulsations (e.g., δ Scuti stars), rotational modulation of dark, cool, magnetically generated starspots; rotational modulation of bright, hot, abundance-anomaly regions; duplicity-induced variations; or other rotational effects. Obviously, dual-nature objects (e.g., pulsating stars showing both γ Doradus– and δ Scuti–type behavior) must not be rejected. Prime candidates for γ Doradus stars should therefore *not* be primarily variable as a result of the rotational modulation occuring in Am, Ap, Fm, RS CVn, or BY Dra stars. However, candidates *may* be members of a spectroscopically defined class (e.g., λ Boötis stars; see, e.g., Gray & Kaye 1999a).

4. CONCLUDING PERSPECTIVE

The γ Doradus stars constitute a new class of variable stars because they all have about the same mass, temperature, and luminosity and the same mechanism of variability. They are clearly not a subclass of any of the other A/F-type variable or peculiar stars in this part of the HR diagram, and they may offer additional insight into stellar physics when they are better understood (e.g., they may represent the cool portion of an "iron opacity instability strip" currently formed by the β Cephei stars, the slowly pulsating B stars, and the subdwarf B stars; they may also offer insight into the presence of g-modes in solar-like stars). Modeling by Kaye et al. (1999a) is beginning to shed light on the theoretically required interior structure and on the specific physics driving the observed variability, but much theoretical work lies ahead.

To understand the behavior of γ Doradus stars and to investigate how they differ from the δ Scuti variables and spotted stars, we need to investigate a number of star clusters of differing ages, perhaps up to as old as 1 Gyr. The fact that the Hyades have no γ Doradus variables (Krisciunas et al. 1995a) may be a quirk of the Hyades rather than proof that stars $\approx$600 Myr old are too old to exhibit γ Doradus–type behavior. Clearly, the " outliers " of the γ Doradus candidates that would extend the limits of the region of the HR diagram in which these new variables are found should be checked carefully for both photometric and spectroscopic evidence indicative of pulsations versus starspots, duplicity effects, and other causes of variability not consistent with the definition presented above (see, e.g., Aerts, Eyer, & Kestens 1998). Finally, additional observations of individual γ Doradus stars are clearly warranted in order to understand better the nature of these objects. After all, 13 objects does not an instability strip make. In the meantime, we must keep an open and critical mind about these variables.

This work was performed under the auspices of the US Department of Energy by the Los Alamos National Laboratory under contract W-7405-Eng-36. We gratefully acknowledge the unpublished spectral types of some of the stars in this paper from R. O. Gray, and we thank Holger Pikall for computing evolutionary models upon request. A. B. K. also gratefully acknowledges Drs. Guzik and Bradley for reading various drafts of this paper. G. H. was partially supported by the Austrian Fonds zur Förderung der wissenschaftlichen Forschung under grant S7304-AST.

REFERENCES

Aerts, C., Eyer, L., & Kestens, E. 1998, A&A, 337, 790
Allen, C. W. 1973, Astrophysical Quantities (3d ed.; London: Athlone)
Balona, L. A., Krisciunas, K., & Cousins, A. W. J. 1994, MNRAS, 270, 905
Balona, L. A., et al. 1996, MNRAS, 281, 1315
Breger, M. 1979, PASP, 91, 5
Breger, M., & Beichbuchner, F. 1996, A&A, 313, 851
Breger, M., et al. 1997, A&A, 324, 566
Cousins, A. W. J. 1992, Observatory, 112, 53
Cousins, A. W. J., & Warren, P. R. 1963, Mon. Notes Astron. Soc. South Africa, 22, 65
Crawford, D. L. 1975, AJ, 80, 955
ESA. 1997, The Hipparcos Catalogue (ESA SP-1200) (Noordwijk: ESA)
Gray, R. O., & Kaye, A. B. 1999a, AJ, submitted
———. 1999b, PASP, in preparation
Hall, D. S. 1995, in ASP Conf. Ser. 79, Robotic Telescopes: Current Capabilities, Present Developments, and Future Prospects for Automated Astronomy, ed. G. W. Henry & J. A. Eaton (San Francisco: ASP), 65
Hatzes, A. P. 1998, MNRAS, 299, 403
Kaye, A. B. 1998a, Ph.D. thesis, Georgia State Univ.
———. 1998b, Inf. Bull. Variable Stars, 4596
Kaye, A. B., Guzik, J. A., & Bradley, P. A. 1999a, in Variable Stars as Essential Astrophysical Tools, ed. C. Ibanoglu (Dordrecht: Kluwer), in press
Kaye, A. B., Henry, G. W., Fekel, F. C., & Hall, D. S. 1999b, MNRAS, in press
Kaye, A. B., & Zerbi, F. M. 1997, Delta Scuti Star Newsl., 11, 32
Krisciunas, K. 1994, Comments Astrophys., 17, 213
———. 1998, in IAU Symp. 185, New Eyes to See Inside the Stars, ed. F. L. Deubner (Dordrecht: Kluwer), 339
Krisciunas, K., Crowe, R. A., Luedeke, K. D., & Roberts, M. 1995a, MNRAS, 277, 1404
Krisciunas, K., Griffin, R. F., Guinan, E. F., Luedeke, K. D., & McCook, G. P. 1995b, MNRAS, 273, 662
Krisciunas, K., & Guinan, E. F. 1990, Inf. Bull. Variable Stars, 3511
Krisciunas, K., et al. 1993, MNRAS, 263, 781
Lang, K. 1992, Astrophysical Data: Planets and Stars (New York: Springer)
Mantegazza, L., Poretti, E., & Zerbi, F. M. 1994, MNRAS, 270, 439
Nissen, P. E. 1988, A&A, 199, 146
Pamyatnykh, A. A., Dziembowski, W. A., Handler, G., & Pikall, H. 1998, A&A, 333, 141
Poretti, E., Koen, C., Martinez, P., Breuer, F., Haupt, H., & de Alwis, D. 1997, MNRAS, 292, 621
Poretti, E., et al. 1996, in Proc. IAU Symp. 181, Sounding Solar and Stellar Interiors, Poster Volume, ed. J. Provost & F.-X. Schmider (Dordrecht: Kluwer), 279
Smalley, B. 1993, A&A, 274, 391
Stobie, R. S., & Whitelock, P. A., eds. 1995, ASP Conf. Ser. 83, Astrophysical Applications of Stellar Pulsation (San Francisco: ASP)
Villa, P. 1998, M.Sc. thesis, Univ. Vienna
Zerbi, F. M., et al. 1997a, MNRAS, 290, 401
———. 1997b, MNRAS, 292, 43
———. 1999, MNRAS, 303, 275

3.3 The domain of γ Doradus variables in the HR diagram

Original paper:

G. Handler, 1999, MNRAS 309, L19

Mon. Not. R. Astron. Soc. **309**, L19–L23 (1999)

The domain of γ Doradus variables in the Hertzsprung–Russell diagram

G. Handler

South African Astronomical Observatory, PO Box 9, Observatory 7935, South Africa

Accepted 1999 July 30. Received 1999 July 30; in original form 1999 July 7

ABSTRACT

70 new γ Doradus candidates were identified from *Hipparcos* photometry, which represents more than a doubling of the presently known number. Selecting the objects with good evidence for multiperiodicity, it is found that these stars, together with bona fide members of the class, occupy a well-defined region in a colour–magnitude diagram. This domain corresponds to a range of 7200–7700 K on the zero-age main sequence (ZAMS) and 6900–7500 K one magnitude above it, which partly overlaps with the instability strip of δ Scuti stars.

For the first time, γ Doradus stars can be discussed as a group. They can be found over a significant fraction of the main sequence lifetimes for objects in the relevant temperature range. An upper limit on the surface metallicity of γ Doradus stars is apparent, which may guide the search for their pulsation driving mechanism. The importance of possible objects exhibiting both γ Doradus and δ Scuti-type pulsations is discussed.

Key words: Hertzsprung–Russell (HR) diagram – stars: oscillations – δ Scuti – stars: variables: other.

1 INTRODUCTION

The γ Doradus stars are a new class of pulsating variables. They are non-radial *g*-mode pulsators of high radial overtone with typical periods between 8 and 80 hours. In the HR diagram, they appear to cluster around the intersection of the red edge of the classical instability strip with the main sequence.

On the basis of the 13 bona fide members of the class, Kaye et al. (1999a) gave an accurate description of the γ Doradus variables. In particular, they pointed out that these pulsators can easily be confused with other variables, the light modulations of which are induced by *p*-mode pulsations, rotation or binarity. Consequently, Kaye et al. (1999a) provided guidelines which help to distinguish γ Doradus stars from different groups of variable stars.

Because of this potential confusion and, more importantly, since the pulsational driving mechanism of γ Doradus variables is presently not understood, knowledge of the circumstances under which the observed pulsations can occur is highly desirable. In other words, the domain in the HR diagram occupied by γ Doradus stars needs to be determined. Kaye et al. (1999a) noted that 13 stars are not sufficient to define an instability region. Aerts, Eyer & Kestens (1998) suggested that the γ Doradus phenomenon extends to temperatures slightly higher than that of the Sun.

A continuously updated so-called Master List of bona fide γ Doradus stars, plus further candidates proposed in the literature, is made available to the community at the WWW site www.astro.univie.ac.at/~gerald/gdor.html; major revisions are announced whenever deemed necessary (Krisciunas & Handler 1995; Handler & Krisciunas 1997). While working on the latest update of this master list (Handler, Kaye & Krisciunas, in preparation), it was found useful to subdivide the proposed γ Doradus variables. On the basis of the available time-series photometric data only (see Section 2 for details), the proposed objects were separated into 'prime' and 'other' candidates; no assumptions about 'expected' temperatures, luminosities, etc. were made. When comparing the locations of the prime candidates with those of the bona fide γ Doradus stars in a colour–magnitude diagram, excellent agreement was found: a clear indication for the existence of a well-defined instability domain.

Encouraged by this result, it was decided to perform an extensive search for further γ Doradus stars in the *Hipparcos* database (ESA 1997). Contrary to previous studies (Aerts et al. 1998; Eyer 1998), the 'unsolved' *Hipparcos* variables were also included in the initial sample, following the idea that lack of a clear periodicity could be because of unrecognized multiperiodic light variations. The results of this effort are reported below.

2 CANDIDATE SELECTION AND CLASSIFICATION

As a first step, all *Hipparcos* variables with spectral types of A–G, periods between 0.3 and 10 d (for the 'periodic' variables), amplitudes less than 0.2 mag and brighter than $H_p = 8.5$ mag at minimum, which were not classified as supergiants were selected. This resulted in more than 1000 candidates. Then the individual light curves were examined and obvious non-γ Doradus stars (e.g.

Table 1. Prime γ Doradus candidates.

Star	Periods (d)	References
HD 277	0.925 0.900 0.744	H99
HD 2842	0.562 0.5:	H99
HD 7169	0.549 1.25:	H99
HD 9365	0.626 0.7:	H99
HD 17310	2.030 2.917?	H99
HD 23874	0.443 0.75:	H99
HD 27377	2.848 1.824?	H99
HD 40745	0.824 1.492	AEK
HD 41448	0.420 0.37:	E98
HD 48271	1.907 1.151	E98
HD 65526	0.644 0.598	H99, K99
HD 69715	0.423 0.5:	H99
HD 70645	0.825 1.25:	H99
HD 80731	1.116 1.4:	H99, K99
HD 86358	0.775 0.844	H99
HD 86371	2.459 1.1:	H99
HD 100215	0.757 0.434?	H99
HD 103257	0.817 0.873	H99
HD 105458	1.398 0.757 0.687	H99
HD 110606	0.977 1.461	H99
HD 112429	0.425 0.446	AEK
HD 113867	1.073 0.762	H99
HD 115466	0.927 0.703	H99
HD 124248	0.671 0.617	H99
HD 137785	0.573 0.950	H99
HD 144451	0.442 0.553	H99
HD 147787	1.456 3:	AEK
HD 149989	0.427 0.5:	AEK
HD 152896	0.746 0.844	H99
HD 155154	0.345 0.323 0.294	H99
HD 160295	0.755 0.7:	H99
HD 167858	1.307 0.85:	AEK, PM
HD 171244	1.004 0.817	H99
HD 173977	0.900 1.327	H99
HD 175337	0.787 1.057	H99
HD 187028	0.695 1.25:	AEK
HD 195068/9	0.800 3.7?	E98
HD 197541	1.400 1.093	H99
HD 206043	0.416 0.407 0.458	E98
HD 206481	0.623 0.7:	H99
HD 209295	0.885 0.434 0.388 0.853	H99
HD 211699	1.072 1.693?	H99, K99
HD 216910	0.694 0.614	AEK
HD 221866	1.140 0.589	H99
HD 224288	1.130 1.016	H99
M34 UVa 144	0.659 0.781	KP

References: H99: this paper, AEK: Aerts et al. 1998, E98: Eyer 1998, PM: Paunzen & Maitzen 1998, K99: Koen, private communication, KP: Krisciunas & Patten 1999.Notes: Entries labelled with colons denote average values of several possible further periods; question marks label uncertain periods.

δ Scuti stars, eclipsing binaries, low-amplitude Cepheids, rotationally modulated Ap stars, etc.) were rejected. For the remainder of the stars (≈ 450 objects), a period search was performed (utilizing the programs of Breger 1990 and Martinez & Koen 1994) and γ Doradus candidates were selected. These stars were required to exhibit variations on a time-scale longer than the fundamental radial mode period.

The remaining 70 stars and candidates proposed in the literature (see Handler et al., in preparation, and references therein) were subdivided into two groups on the basis of the appearance of their amplitude spectra. The prime candidates had to fulfill a number of criteria as follows.

(i) Good evidence for multiperiodicity had to exist. After prewhitening with the frequency leaving the smallest residuals in the data, the resulting amplitude spectrum had to show at least a second peak or significant residuals in the same frequency range as that of the first frequency. In this way, possibly singly-periodic γ Doradus stars are not considered,[1] but this effectively discriminates against all other causes of variability besides pulsation.

(ii) Stars for which two frequencies were found which were harmonically related were rejected, as this could be because of rotational modulation or ellipsoidal variations.

(iii) If two close frequencies (within a few per cent) were determined, the corresponding stars were not judged to be prime candidates, as this could be an artifact owing to starspot evolution or differential rotation of a spotted star (e.g. see Strassmeier & Bopp 1992).

(iv) Stars for which the actual time-scale of light variation could not be unambiguously determined were not considered as prime candidates. As a result of the sampling of the *Hipparcos* photometry (cf. Eyer & Grenon 1998), strong aliasing is present in amplitude spectra. This can mimic spurious signals in the frequency range of interest for γ Doradus stars, especially for

Table 2. Further new γ Doradus candidates.

Star	Period (d)	Comment
HD 12901	2.18:	δ Sct star?
HD 21788	~ 5	period uncertain
HD 23005	0.61:	δ Sct star?
HD 27093	0.558	δ Sct star?
HD 35187	3.75?	period uncertain
HD 63436	0.7:	weak signal
HD 85693	0.835	δ Sct star?
HD 91201	0.605	singly periodic?
HD 104860	1.6:	weak signal
HD 109032	0.7:	weak signal
HD 109838	14? 2.9?	period uncertain
HD 109799	1.058	singly periodic?
HD 112934	0.8:	weak, complicated signal
HD 113357	1.216	δ Sct star?
HD 122300	0.629	weak signal
HD 126516	0.493	weak signal
HD 133803	0.445	singly periodic?
HD 139095	0.634	δ Sct star?
HD 155854	2:	singly periodic?
HD 166114	0.469	singly periodic?
HD 172416	0.827	singly periodic?
HD 173794	1.624	δ Sct star?
HD 181998	1.334?	complicated signal
HD 187353	0.6:	weak signal
HD 187615	0.498 0.508	spotted star?
HD 188032	0.630	δ Sct star?
HD 189631	0.6:	weak, complicated signal
HD 197187	0.828	singly periodic?
HD 197451	1.803	Am or Ap star?
HD 198528	0.526	δ Sct star?
HD 199143	1.6:	complicated signal
HD 201985	1.332	δ Sct star?
HD 207651	0.735	δ Sct star?
HD 213617	0.569	weak signal
HD 216108	0.762	singly periodic?
HD 219843	1.790	δ Sct star?

Notes: same as those for Table 1.

[1] Kaye et al. (1999b) pointed out that about 30 per cent of the bona fide γ Doradus stars are singly periodic. Since these objects do not have any remarkable features in any other respect, no systematic bias is expected for the present study owing to the possible exclusion of such stars.

objects which actually vary with periods around two hours, i.e. some δ Scuti stars.

The most reliable γ Doradus candidates from our study and from the investigation of stars proposed in the literature are summarized in Table 1 together with the results of our period search. New objects considered in this work, which may be γ Doradus stars, but whose nature remained uncertain, can be found in Table 2 with a comment explaining possible doubts. Eyer & Grenon (1998) pointed out that a search for multiple periods in *Hipparcos* photometry is difficult and can lead to spurious results. However, it was found useful to quote the time-scales present in the variations of the different stars. To allow the reader to judge the classification, plots with amplitude spectra for the individual stars have been placed at www.astro.univie.ac.at/~gerald/gdoratlas.html. The new γ Doradus candidates listed in Tables 1 and 2 more than double the number of related objects presently known. We note that *Hipparcos* data are available for all 'bona fide' γ Doradus stars. We recovered some of them in our search, but for most objects the accuracy of the *Hipparcos* photometry was insufficient to claim variability.

3 RESULT

A colour–magnitude diagram including all γ Doradus candidates is shown in Fig. 1. The Strömgren $(b-y)$ colour index was used as a temperature indicator (dereddened whenever necessary), since it is available for most of the stars. For the remainder, $(b-y)$ was estimated from the *Hipparcos* $(B-V)$ using the relations of Caldwell et al. (1993). Absolute magnitudes were determined from the *Hipparcos* parallaxes whenever available or were calculated from Strömgren photometric indices.

In Fig. 1, the location of all the 'prime' candidates identified by us (again, selected by the appearance of their frequency spectra only) is strikingly similar to that of the bona fide γ Doradus variables. This strongly suggests that most of these stars are indeed γ Doradus stars and it is clear evidence that these objects occupy a well-defined small region in the HR diagram.

The cool boundary of this region is defined more clearly than its hotter counterpart, simply because there are more stars available. One object (HD 209295) lies outside the blue edge. There is no doubt that it is a γ Doradus star, since it is the only object for which four frequencies from the *Hipparcos* photometry could be determined (three are independent, one is a linear combination), but when comparing its published $(b-y)$ with the corresponding H_β index and with its $(B-V)$ it appears that $(b-y)$ is too small by 0.015–0.020 mag. Hence, this object was not considered for defining the blue edge. Clearly, new Strömgren photometry of HD 209295 needs to be obtained.

Consequently, the instability region for γ Doradus stars can be outlined for the first time. Its extent is indicated in Fig. 1. Using the model atmosphere results of Kurucz (1991), it can be translated into an effective temperature range of 7200–7700 K on the ZAMS ($\log g \approx 4.33$), while the luminous end occurs about 1 magnitude above it ($\log g \approx 4.0$) between effective temperatures of 6900 and 7500 K.

4 DISCUSSION

One of the most widespread ideas about the γ Doradus phenomenon is that it is related to stellar age. For instance, Krisciunas (1998) gave arguments that γ Doradus stars are younger than 300 Myr. In Fig. 1, several objects well above the ZAMS (up to 1.3 mag) can be discerned, suggesting that γ Doradus-type pulsations can exist in somewhat evolved main-sequence stars, unless these γ Doradus stars are binaries or pre-main sequence objects. The binary hypothesis can be checked by comparing the absolute magnitudes derived from parallaxes with those calculated from Strömgren photometry (see Crawford 1975, 1979). Fig. 2 shows the results of such a comparison.

For most of the stars the absolute magnitudes determined using

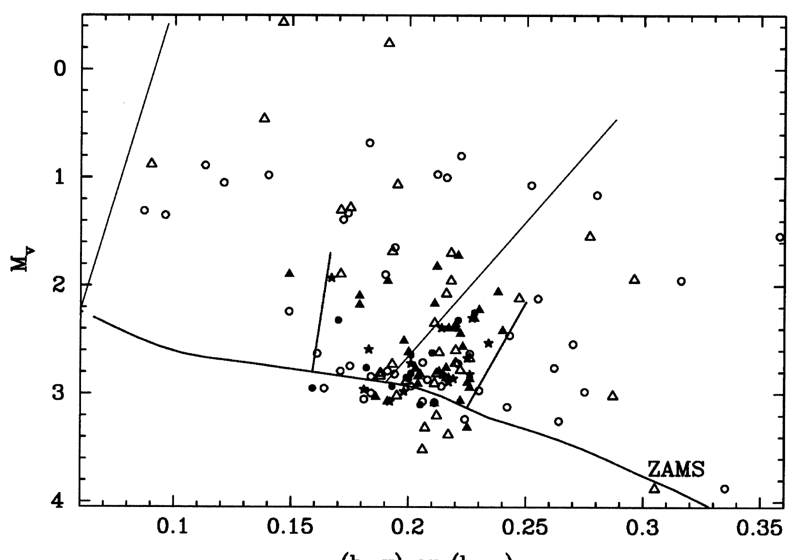

Figure 1. The colour–magnitude diagram of the presently known or suspected γ Doradus variables. Star symbols: bona fide γ Doradus stars, dots: prime candidates from the literature, open circles: other candidates from the literature (see Handler et al., in preparation), filled triangles: prime candidates from this paper, open triangles: further candidates from this work. The observed zero-age main sequence (ZAMS: Crawford 1975, 1979) is shown together with the boundaries of the δ Scuti star instability strip (thin lines almost normal to the ZAMS, Breger 1979). The domain of γ Doradus stars is indicated with thick lines approximately normal to the ZAMS; the single filled-triangle outlier is likely to have an erroneous $(b-y)$ colour index (see text).

both methods agree well within the errors (rms of about ± 0.3 mag for the photometric absolute magnitudes, mean rms approximately ± 0.25 for the *Hipparcos* absolute magnitudes). A few objects may indeed be binaries, but not all of the more luminous objects in Fig. 1 can be explained by this hypothesis. It is therefore suggested that the γ Doradus phenomenon can occur over a significant fraction of the main sequence lifetime of stars in the relevant temperature range.

One of the arguments in favour of the idea that γ Doradus stars are very young objects came from the apparent absence of such pulsators in the Hyades (Krisciunas et al. 1995). The Hyades are also relatively metal-rich. It is therefore logical to ask whether metallicity could play a role for γ Doradus-type pulsation. This is examined in Fig. 3.

On the average, γ Doradus stars have metallicites comparable to that of the Sun (using Smalley's (1993) calibration, $[M/H]$ is found to be between -0.37[2] and $+0.12$). Objects enriched in metals are absent; this is different from the situation for δ Scuti stars.[3] In fact, there may be a strict upper limit on the metallicity of γ Doradus stars. In Fig. 3 it can also be seen that hotter objects seem to have a larger range in metal abundance than cooler stars.

This can shed some light on the driving mechanism for the pulsations of γ Doradus stars. Kaye, Guzik & Bradley (1999) outline a possible κ-mechanism located in a zone of iron enhancement due to diffusion and radiative levitation as found in models by Turcotte, Richer & Michaud (1998). The observation that γ Doradus stars are only found in a certain range of surface metallicity can then be taken as a clue that diffusion processes (settling of metals) may indeed play an important role for the excitation of their pulsations. It would be interesting to perform detailed abundance analyses of γ Doradus stars in order to check whether they show any peculiarities in their chemical composition.

Kaye et al. (1999) also discuss a conjectured mode selection mechanism operating in the surface convection zone. This requires a weak, but non-negligible stellar dynamo, i.e. a Rossby number (ratio of stellar rotation period to convective turnover time) of order unity. Consequently, Kaye (1998) suggested that under this hypothesis, the instability region for γ Doradus stars in the HR diagram should be tilted from hot to cool and more luminous to less, i.e. tilt upward and to the left. The reader is referred to the two references above for more details. Based on the available data, the color-magnitude diagram shown in Fig. 1 is not consistent with this theoretical prediction.

The instability region for γ Doradus stars partly overlaps with that of δ Scuti stars. For the latter objects, the blue edge is generated by the driving region being too close to the stellar surface, while the red edge is believed to be caused by surface convection becoming effective. The physical mechanisms responsible for the hot and cool borders of the γ Doradus instability region are not obvious.

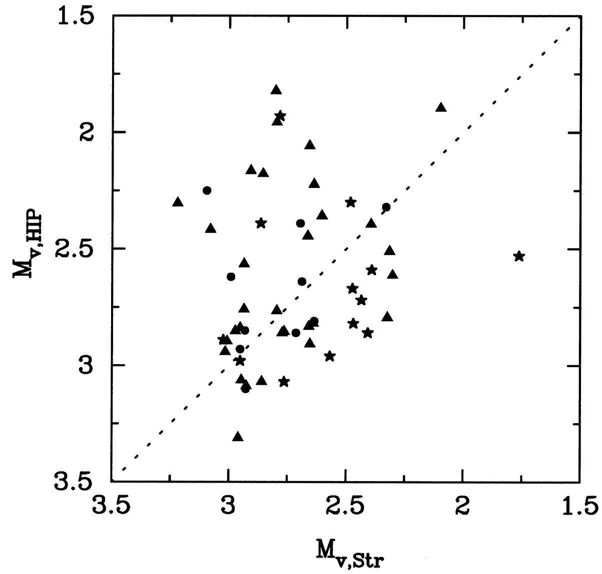

Figure 2. The *Hipparcos* absolute visual magnitude versus the same quantity derived from Strömgren photometry. Plot symbols are the same as in Fig. 1, but only bona fide γ Doradus stars and prime candidates are considered.

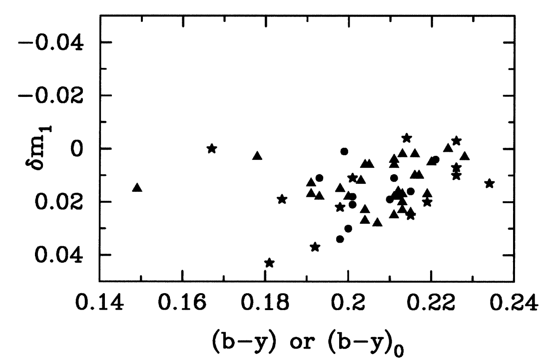

Figure 3. The Strömgren metallicity parameter δm_1 versus colour index $(b-y)$ for the bona fide γ Doradus stars and prime candidates. No metal-rich object is found. A correlation between metallicity and temperature can be discerned.

The possible connection between the γ Doradus and δ Scuti variables has been discussed by Breger & Beichbuchner (1996), based on a much smaller sample of γ Doradus variables than available to date. The question then arises, is there is an exclusion between the two groups (and if so, what causes it) or do 'hybrid' objects exist?

If stars exhibiting simultaenous γ Doradus and δ Scuti-type pulsations could be found, this would greatly increase the possibilities for asteroseismology of both classes of variable star. The pulsation modes in the higher-frequency region may easily be identified, since main-sequence δ Scuti stars should mainly show the signatures of pure p-mode pulsation. Hence, their position in the HR diagram can be tightly constrained (e.g. see Handler et al. 1997). Then the γ Doradus-type g-modes (whose radial order is practically impossible to be derived without further constraints because the high-order g-mode spectrum is very dense) can be used to probe the deep interior of the stars.

[2] For the λ Bootis star HR 8799, the object with the largest positive δm_1 in Fig. 3, Gray & Kaye (1999) determined $[M/H] = -0.47$ by spectral synthesis.

[3] A t-test shows that the metallicity distribution of the stars in Fig. 3 is different from that of δ Scuti stars (taken from the latest catalogue by Zechner, private communication) in the same temperature range to the 99.9 per cent confidence level. We caution, however, that our candidate selection process discriminated against Ap/Fp stars (but not Am/Fm stars) and therefore this value may be too high.

ACKNOWLEDGMENTS

This work would not have been undertaken without the input of a number of colleagues, especially Tony Kaye and Chris Koen. The author is grateful for constructive comments on draft versions of this paper by Don Kurtz, Michel Breger, Luis Balona and, again, Tony Kaye. He also thanks Stephen Potter for improving the English style of the manuscript and Renate Zechner for permission to use her catalogue of δ Scuti stars prior to publication.

REFERENCES

Aerts C., Eyer L., Kestens E., 1998, A&A, 337, 790 (AEK)
Breger M., 1979, PASP, 91, 5
Breger M., 1990, Comm. Asteroseism, 20, 1 (Univ. Vienna)
Breger M., Beichbuchner F., 1996, A&A, 313, 851
Caldwell J. A. R., Cousins A. W. J., Ahlers C. C., van Wamelen P., Maritz E. J., 1993, SAAO Circ., 15, 1
Crawford D. L., 1975, AJ, 80, 955
Crawford D. L., 1979, AJ, 84, 1858
ESA, 1997, The Hipparcos and Tycho catalogues, ESA SP-1200
Eyer L., 1998, PhD thesis, Univ. Geneva (E98)
Eyer L.,Grenon M., 1998, in Deubner F. et al., eds, New Eyes to See Inside the Sun and Stars. p. 291
Gray R. O., Kaye A. B., 1999, AJ, submitted
Handler G., Krisciunas K., 1997, Delta Scuti Star Newsletter, 11, 3 (Univ. Vienna)
Handler G. et al., 1997, MNRAS, 286, 303
Kaye A. B., 1998, PhD thesis, Georgia State Univ.
Kaye A. B., Guzik J. A., Bradley P. A., 1999, in Ibanoglu C., ed., Variable Stars as Important Astrophysical Tools. NATO-ASI, in press
Kaye A. B., Handler G., Krisciunas K., Poretti E., Zerbi F., 1999a, PASP, 111, 840
Kaye A. B. et al., 1999b, AJ, submitted
Krisciunas K., 1998, in Deubner F. L. et al., eds, New Eyes to See Inside the Sun and Stars. p. 339
Krisciunas K., Handler G., 1995, Inf. Bull. Variable Stars, 4195
Krisciunas K., Patten B. M., 1998, Inf. Bull. Variable Stars, 4705 (KP)
Krisciunas K., Crowe R. A., Luedeke K. D., Roberts M., 1995, MNRAS, 277, 1404
Kurucz R. L., 1991, Van Vleck Obs. Contr., 11, 27
Martinez P., Koen C., 1994, MNRAS, 267, 1039
Paunzen E., Maitzen H. M., 1998, A&AS, 133, 1 (PM)
Smalley B., 1993, A&A, 274, 391
Strassmeier K. G., Bopp B. W., 1992, A&A, 259, 183
Turcotte S., Richer J., Michaud G., 1998, ApJ, 504, 559

This paper has been typeset from a TEX/LATEX file prepared by the author.

3.4 On the relationship between the δ Scuti and γ Doradus pulsators

Original paper:

G. Handler, R. R. Shobbrook, 2002, MNRAS 333, 251

Mon. Not. R. Astron. Soc. **333,** 251–261 (2002)

On the relationship between the δ Scuti and γ Doradus pulsators

G. Handler[1]★ and R. R. Shobbrook[2,3]

[1]*South African Astronomical Observatory, PO Box 9, Observatory 7935, South Africa*
[2]*PO Box 518, Coonabarabran, NSW 2357, Australia*
[3]*Research School of Astronomy and Astrophysics, Australian National University, Weston Creek PO, ACT 2611, Australia*

Accepted 2002 February 6. Received 2002 February 6; in original form 2001 December 19

ABSTRACT

We searched for δ Scuti-type pulsations amongst known and candidate γ Doradus stars. The motivations for such a project come from the need to understand the relationship of these two classes of pulsator better, from the present poor knowledge of the hot border of the γ Doradus phenomenon, and from the exciting prospects for asteroseismology should stars be found which have both types of pulsation excited. We acquired 270 h of observations and monitored a total of 26 stars. One target, HD 209295, turned out to be a member of both classes of pulsating star, but this object is peculiar in the sense that it is a close binary. We classify six of our targets as new bona fide γ Doradus stars, whereas nine more are good γ Doradus candidates, and three turned out to be ellipsoidal variables. One of our programme stars was found to be a δ Scuti star, with no additional γ Doradus variations. Furthermore, one star was already known to be a bona fide γ Doradus star, and we could not find an unambiguous explanation for the variability of five more stars. The analysis of our data together with improved knowledge of stars from the literature enabled us to revise the blue border of the γ Doradus phenomenon towards cooler temperatures. This new blue edge is much better defined than the previous one and extends from a temperature of about 7550 K on the ZAMS to 7400 K one magnitude above it. Five bona fide γ Doradus stars we observed are located inside the δ Scuti instability strip, but none of them exhibited observable δ Scuti pulsations. We therefore suggest that γ Doradus stars are less likely to be δ Scuti pulsators compared with other normal stars in the same region of the lower instability strip. In addition, we show that there is a clear separation between the pulsation constants Q of δ Scuti and γ Doradus stars. The γ Doradus stars known to date all have $Q > 0.23$ d.

Key words: techniques: photometric – stars: oscillations – δ Scuti – stars: variables: other.

1 INTRODUCTION

The relationship between the γ Doradus and δ Scuti stars is not yet clear. Although the two classes of pulsator share a similar parameter space in the HR diagram and even partly overlap (Handler 1999), the γ Doradus stars are high-radial-order gravity (g)-mode pulsators (Kaye et al. 1999a), whereas the δ Scuti stars are believed to be mostly low-radial-order pressure (p)-mode pulsators (e.g. Breger 2000). The driving mechanism of the two classes should be different because of the different types of modes excited. Hence, there should be different thermal time-scales in the driving regions. Indeed, δ Scuti pulsations are known to be driven by the κ-mechanism (Chevalier 1971), whereas the only presently feasible driving mechanism for the γ Doradus stars is similar to convective blocking (Guzik et al. 2000, 2002). The latter mechanism is also expected to weaken or even exclude the driving of δ Scuti-type pulsations.

Several open questions still remain. Is the presence of δ Scuti- and γ Doradus-type pulsations mutually exclusive? Is there an overlap or a separation between these pulsators? Are there stars that show both types of oscillation? What determines the type of mode that a particular star pulsates in? To tackle those questions, we decided to observe a large number of γ Doradus candidates located within the δ Scuti instability strip to search for short-period pulsations.

In addition, this allows us to check whether these γ Doradus candidates are indeed pulsators. This is important as most of these candidates were identified from *Hipparcos* photometry (ESA 1997), the quality of which is poor compared with ground-based work and which contains no time-series colour information. Furthermore, there is usually strong aliasing in amplitude spectra of *Hipparcos* photometry caused by a pseudo-sampling frequency near 12 cycle day^{-1} (see Eyer & Grenon 1998), which often leads

★E-mail: gerald@saao.ac.za

to difficulties in period determinations. For instance it is often not possible to distinguish a δ Scuti star with a 2-hour period from a γ Doradus candidate from *Hipparcos* photometry only. We conclude that these technical facts make a good assessment of the presence of γ Doradus pulsations from *Hipparcos* data alone difficult: γ Doradus stars can easily be confused with spotted stars, ellipsoidal variables and δ Scuti stars (see Kaye et al. 1999a and Handler 1999 for more extensive discussions).

Our ground-based observations introduced above are probably the most effective way to assess the relationship between the γ Doradus and δ Scuti stars: about one third of all non-Am and non-Ap stars in the lower instability strip are indeed δ Scuti stars (Breger 2000 and references therein) and Am and Ap stars are rare (or even absent) amongst the γ Doradus stars (Handler 1999). Consequently, a statistical assessment of the incidence of δ Scuti pulsations in γ Doradus stars becomes possible. We note that Breger & Beichbuchner (1996) already looked for possible γ Doradus pulsators among δ Scuti stars in the literature, but their results were largely inconclusive because of observational selection effects, the small number of γ Doradus stars then known and because the incidence of observable γ Doradus pulsations among stars with basic parameters in the γ Doradus star domain is as yet unknown.

The results to be expected from our search are manifold.

(i) The number of known bona fide γ Doradus stars is still small (<20). Discovering more of these stars will aid the understanding of the class as a whole.

(ii) If both types of pulsation could be identified in the same star, this would be exciting news for asteroseismology: the δ Scuti pulsations in such hypothesized stars could be used to determine (at least) accurate basic parameters, which can then aid in identifying the γ Doradus modes and in probing the deep stellar interior. It would also mean that in stellar models in which γ Doradus-type modes are driven, δ Scuti oscillations must not be damped.

(iii) If no such 'hybrid' stars are found, the reason for their absence can be examined, and some observational discriminants may be found. Of course, the driving mechanism for the γ Doradus stars will also need to explain such a result.

(iv) An improved assessment of the hotter candidate γ Doradus stars may also enable us to locate the currently poorly-defined blue edge of the γ Doradus region better in the HR diagram (Handler 1999); pulsational models must explain it. The location of the red edge of the δ Scuti instability strip can also be better examined.

Hence, whatever the implications of the present survey, the driving mechanism for the γ Doradus pulsations will be observationally much better constrained.

2 OBSERVATIONS

As mentioned in the Introduction, we selected known candidate γ Doradus stars located within the overlap region of the lower instability strip (adopted from Breger 1979) and the domain of the γ Doradus stars in the HR diagram (Handler 1999). All stars observable from intermediate Southern geographical latitudes were included in our survey, and we chose two comparison stars for each. In addition, we included further γ Doradus candidates (regardless of their position in the HR diagram) which were located within eight degrees of the main targets into the observing sequence whenever practical to examine the physical nature of these stars as well. Finally, we also decided to monitor a few more candidates that seemed to be of special astrophysical interest.

Our measurements were acquired as differential photoelectric photometry at the 0.5-m and 0.75-m telescopes at the Sutherland station of the South African Astronomical Observatory (SAAO) and at the 0.6-m telescope (see Shobbrook 2000 for a description) at Siding Spring Observatory (SSO) from 1999 October to 2001 October. We used the Johnson B and V filters with a total integration time of about one minute in each filter as a compromise between good time resolution and optimum colour information, but we sometimes added the Cousins I_c if deemed necessary (possible reasons will be listed below). A few runs obtained on the SAAO 0.5-m telescope were taken as high-speed photometric observations through the BVI_c filters, with comparison star observations every 30–45 min, which also results in some long-term photometric stability (Breger & Handler 1993). For all runs, apertures of 30–45 arcsec on the sky were chosen. Sky measurements were taken depending on the brightness and proximity of the Moon.

Observing sequences were chosen for both good coverage of possible short-period δ Scuti pulsations and for best long-term stability. We adopted the sequences C1-C2-V-C1-C2-V... (the Cs denote the comparison stars and the Vs the variables) for SAAO observations and C1-V-C2-V-C1... for SSO measurements (where it was more difficult to move the telescope from one star to the next) in case one programme star was in the group. This resulted in one programme star measurement about every 7 min. If we had two variables in a group, the sequence C1-V1-C2-V2-C1-V1... was chosen, yielding a variable star measurement about every 15 min. These duty cycles apply to BV observations.

We attempted to observe each target star for at least two half nights to check them for δ Scuti-type variability and in order not to be susceptible to beating phenomena (negative interference from multiple pulsation modes). With this strategy, long-term variability is often detected in one night, and the second run will fulfil the same aim whilst making it possible to check for light variations from night to night as well. The data were reduced as soon as possible after they had been obtained in order to judge their quality and to be able to make decisions about future observing strategies and the scientific content of our data. This would for instance result in a change of the observing sequence or in the inclusion of the I_c filter or in a decision of whether to follow the star up or not.

Data reduction was performed in a standard way: correction for coincidence losses, sky background and extinction was followed by calculating differential magnitudes between the comparison stars, and if these were judged to be constant, construction of the differential target star light curve. Finally, the time base of our observations was converted to Heliocentric Julian Date (HJD). We summarize our observations in Table 1; the data are available at http://www.saao.ac.za/~gerald/delgamscudor in electronic form.

3 ANALYSIS

3.1 Results on the individual stars

Before proceeding to the astrophysical implications of our survey as a whole, the individual stars also need to be discussed, as a wide variety of behaviour was detected. We also need to make clear which criteria we use to distinguish between the different types of variable to be found in the region of the HR diagram under consideration.

We classify a star as a δ Scuti variable if it shows a variability time-scale that leads to pulsation constants Q of 0.04 d or less. The

Table 1. Journal of the differential photometric observations. We normally used the Johnson BV filters, but runs marked with one asterisk also utilized the I_c filter; those with two asterisks were high-speed photometry BVI_c with occasional comparison star measurements.

Target star(s)	Site	Run start JD − 245 0000	Run length, h
HD 10167	SAAO	1457.40	4.1
	SSO	2111.19	3.1
	SSO	2112.16	1.6
	SSO	2131.16	2.6
HD 12901	SAAO	1460.38	4.1
	SAAO	2154.48	2.0**
	SAAO	2155.47	4.5**
HD 14147	SAAO	1463.39	3.0
HD 27093	SAAO	1461.25	3.7
	SAAO	1466.48	2.2
HD 40745 and	SSO	1549.96	5.4
HD 41448	SSO	1554.96	1.9
	SSO	1555.95	5.1
HD 65526	SAAO	1576.30	3.5
	SAAO	1581.30	3.7
HD 81421	SAAO	1577.32	2.3
	SAAO	1578.31	6.2
	SSO	1578.95	7.0
	SAAO	1579.30	7.3
	SAAO	1581.57	1.0
	SAAO	1582.54	1.7
	SSO	1588.93	4.0
	SSO	1589.96	5.6
	SSO	1590.97	4.7
HD 85693 and	SAAO	1580.30	3.8
HD 86371	SAAO	1582.33	5.0
HD 110606 and	SAAO	1576.46	2.9
HD 113357	SAAO	1580.45	0.4
	SAAO	1581.46	2.7
	SSO	1621.12	4.1
	SSO	1630.00	2.6
	SSO	1631.96	2.9
HD 139095	SAAO	2045.29	1.6
	SSO	2102.85	6.1
	SSO	2110.86	6.2
	SSO	2111.86	5.1
HD 167858	SAAO	2045.44	5.4
	SAAO	2051.54	3.1
BD+8 3658	SSO	2105.01	1.6
	SSO	2130.90	4.3
	SSO	2134.94	3.2
	SSO	2140.88	2.6*
HD 173794	SSO	2131.87	8.3
	SSO	2133.12	1.0
	SSO	2135.09	2.6
	SSO	2135.87	7.7*
	SSO	2140.99	3.0*
	SSO	2144.88	7.1*
HD 181998	SSO	2146.87	1.4
	SAAO	2154.33	3.4**
	SAAO	2155.24	5.6**
HD 188032 and	SAAO	1458.26	2.5
HD 189631	SSO	2107.10	1.9
	SSO	2113.03	5.2
	SAAO	2192.23	2.9*
	SAAO	2193.30	0.6*
HD 198528 and	SAAO	1461.25	1.1
HD 201985	SAAO	1462.25	3.6
	SAAO	1466.26	3.6
	SSO	2119.10	4.1
	SSO	2119.95	6.3
HD 207223	SAAO	1463.25	3.2
HD 207651	SAAO	1463.25	3.2
	SAAO	2191.26	3.0**
HD 209295	SAAO	1464.33	4.2
	SAAO	1465.25	6.5
	SSO	1467.03	2.3
	SSO	1468.91	6.4
HD 211699	SAAO	1468.25	1.1
	SAAO	1469.26	4.5
	SAAO	2176.26	2.1*
	SAAO	2190.26	4.2**
HD 221866	SAAO	1466.41	1.6
	SAAO	1467.28	4.6
Total			269.5

pulsation constant Q is calculated as

$$\log Q_{\mathrm{i}} = C + 0.5 \log g + 0.1 M_{\mathrm{bol}} + \log T_{\mathrm{eff}} + \log P_{\mathrm{i}}, \qquad (1)$$

adopting $T_{\mathrm{eff},\odot} = 5780\,\mathrm{K}$, $\log g_{\odot} = 4.44$, $M_{\mathrm{bol},\odot} = 4.75$ (Allen 1976) and thus $C = -6.456$. The units of the quantities in the right-hand side of this equation are dex, magnitudes, kelvins and days, respectively. Our limit on Q follows from the fundamental radial mode of a δ Scuti star having $Q = 0.033$ d, and we allow for some 18 per cent error in its determination from the uncertainties of the physical parameters derived for the star (see Breger 1989 for a discussion). These parameters can be determined from calibrations of Strömgren photometry (Crawford 1975, 1979) and model atmosphere predictions (Kurucz 1991). Bolometric corrections were taken from Drilling & Landolt (2000).

There are also possibilities for separating γ Doradus stars, ellipsoidal variables and rotationally-modulated chemically peculiar objects. The latter two types of variable will only have one or two dominant periods in a frequency analysis based on Fourier spectra and sine-wave fitting (which are our main tools for the analysis), and if there are two periods, they will be harmonically related. In that respect, residualgram analysis (Martinez & Koen 1994) can become powerful. This method performs a least-squares fit of a sine wave with M harmonics to the measured time series and evaluates the residuals at each trial frequency, where M can be chosen. For rotationally-modulated light curves or those of ellipsoidal variables, $M = 2$ is usually the best choice, and is used throughout this paper.

Returning to the discrimination between the different types of slow variables, we note that multiperiodic γ Doradus stars can be easily identified if the different periods of variability are not harmonically related. However, if only a single period can be determined from the measurements, unravelling the cause of the variability of the star under consideration becomes more difficult.

A further diagnostic can be obtained from relative amplitudes and phases of the measured signals in different photometric filters. Ellipsoidal variables or eclipsing binaries of the W UMa-type show little colour modulation (B/V amplitude ratios less than 1.05) as their light variations are dominated by geometrical effects. The latter two types of variable can be distinguished by their light-curve shape; those of the W UMa-type have typical flat maxima and sharp minima. The light curves of rotationally-modulated Ap stars, on the other hand, often show quite large colour variations and in case of double-wave light modulations, phase shifts between the different filters can become quite large (e.g. see Kurtz et al. 1996). Colour amplitude ratios for γ Doradus pulsations will be quite similar to those of δ Scuti stars. For instance, typical B/V amplitude ratios for γ Doradus stars pulsating with photometrically detectable modes (spherical degree $\ell = 1$ or 2) would, according to model calculations (e.g. Garrido 2000), be between 1.2 and 1.35. The latter range is also expected for radial δ Scuti pulsation. Phase shifts between different filters are not a good indicator of pulsations in the present case, as our data sets are generally too small to obtain significant phase shifts.

We caution, however, that amplitude ratios could be misleading, in particular in cases of insufficient phase coverage of the orbital period of an ellipsoidal variable or of the rotation period of an Ap star. Both types of variable can then show colour-amplitude ratios similar to those of pulsating stars. Consequently, this diagnostic alone is not sufficient for a clear distinction; all the information available on the stars needs to be combined carefully to arrive at a safe classification.

3.1.1 HD 10167

The variability of this star was discovered by Eyer & Aerts (2000) in Geneva photometry. These authors could however not pinpoint the physical nature of the star. Our measurements show very little variation during the individual nights and night-to-night variations of a few hundredths of a magnitude. The B/V colour-amplitude ratio (1.24 ± 0.12) suggests pulsation as the cause for these variations. No δ Scuti-type variability is detected within a limit of 0.9 mmag in the V-filter amplitude spectrum. We classify HD 10167 as a γ Doradus candidate.

3.1.2 HD 12901

Handler (1999) suggested that this star could be a γ Doradus variable, but aliasing in the *Hipparcos* photometry also left the possibility that it could be a δ Scuti star. Eyer & Aerts (2000) clarified the situation by means of Geneva photometry and suggested that HD 12901 is a γ Doradus star. Our observations confirm their conclusion; no δ Scuti pulsations are detected (within 1.2 mmag) and the B/V and V/I_c colour-amplitude ratios (1.29 ± 0.02 and 1.9 ± 0.1, respectively) for the dominant period of the slow variations (0.8227 d, Eyer & Aerts 2000) in our data confirm that they are caused by pulsation of the star. Supported by the results of Eyer & Aerts (2000), we classify HD 12901 as a bona fide γ Doradus star.

3.1.3 HD 14147

This star was classified as a δ Scuti star with a period of 6.48 h by the *Hipparcos* group (ESA 1997). However, a re-analysis of these data reveals that HD 14147 is in fact an ellipsoidal variable with an orbital period of 12.95 h (Fig. 1). One can suspect low-amplitude δ Scuti variations with a period of about 1.5 h ($Q = 0.04$ d) being superposed on our single night of observation and the *Hipparcos* light curve.

3.1.4 HD 27093

From the time-resolved *Hipparcos* photometry alone it was not clear whether this star is a δ Scuti or a γ Doradus star (Handler 1999). However, the more rapid time sampling of our ground-based observations clearly shows that HD 27093 is a δ Scuti star; a combined analysis of both data sets results in a dominant frequency of 14.51837 ± 0.00006 cycle day^{-1}, corresponding to $Q = 0.018$ d. Semi-amplitudes of 18 ± 2 mmag in the *Hipparcos* H_p-band, 15 ± 1 mmag in the B filter and with 11.8 ± 0.6 mmag in

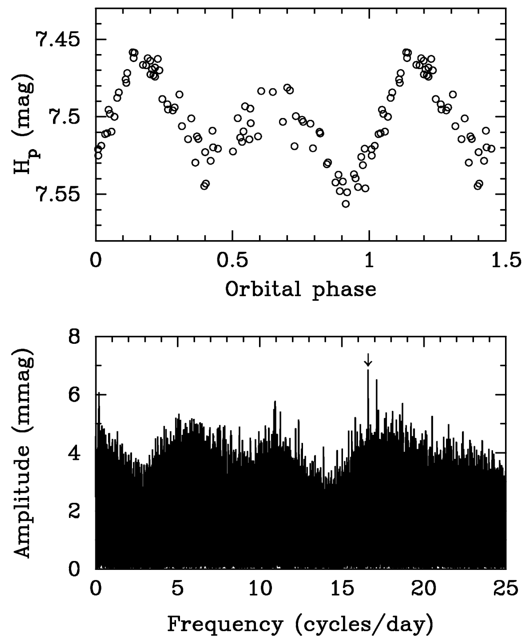

Figure 1. Upper panel: phase diagram of the *Hipparcos* photometry of HD 14147 folded with a frequency of 1.8528 cycle day^{-1}. Ellipsoidal variability of this star is strongly implied. Lower panel: residual amplitude spectrum of this star's *Hipparcos* photometry after removing the orbital modulation. A possible signal near 16.6 cycle day^{-1} can be suspected.

V could be determined (error estimates were derived from the formulae of Montgomery & O'Donoghue 1999). Some evidence for more δ Scuti periods is seen, but no long-term variations are detected within a limit of 2 mmag.

3.1.5 HD 40745 and HD 41448

These two stars could be observed in one group due to their proximity in the sky. Both are slow variables, with B/V colour-amplitude ratios (1.25 ± 0.21 for HD 40745 and 1.31 ± 0.12 for HD 41448) indicative of pulsation. These amplitude ratios were derived by fitting their dominant *Hipparcos* frequency to our data, in which these frequencies are also detected. In accordance with published frequency analyses of the *Hipparcos* data of the stars, we also find evidence for multiperiodicity for the slow variations of both. On the other hand, no δ Scuti-type variability is detected within a limit of 3.0 mmag (HD 40745) and 2.7 mmag (HD 41448), respectively. Because of the rather large errors on the colour-amplitude ratios, we can only confirm both stars as prime γ Doradus candidates.

3.1.6 HD 65526

For this prime γ Doradus candidate (Handler 1999), we obtained two nights of observation which were of excellent quality. The B/V colour-amplitude ratio in our data (1.19 ± 0.04) implies pulsation as the cause of the slow multiperiodic light variations of HD 65526. No δ Scuti variations are detected at a limit of 0.5 mmag in the amplitude spectrum. Thus HD 65526 is reclassified as a bona fide γ Doradus star.

3.1.7 HD 81421

This is one of the most difficult cases we encountered in our

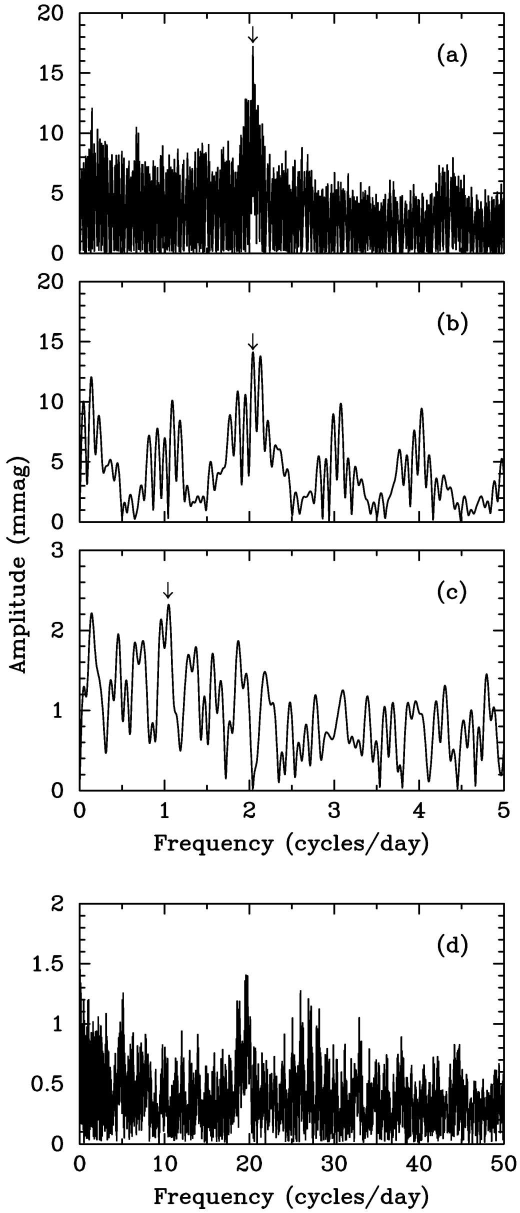

Figure 2. (a) Amplitude spectrum of the *Hipparcos* photometry of HD 81421; the frequency in these data is indicated with an arrow. (b) Amplitude spectrum of our ground-based *V*-filter observations; the *Hipparcos* period is confirmed. (c) Amplitude spectrum of our measurements after prewhitening of the *Hipparcos* frequency. Residual variation near 1 cycle day^{-1} is suspected. (d) Amplitude spectrum of our measurements after prewhitening of the *Hipparcos* frequency and its subharmonic. A wider range is chosen to show the suspected presence of δ Scuti pulsations.

survey; we must comment on this star in more detail. The star is classified as a periodic *Hipparcos* variable (ESA 1997), and its period is 11.75 h (see also Fig. 2(a)). This means that for consecutive nights of ground-based measurements practically the same phase of its light curve is always observed. For this reason, we coordinated the observations of this star from both sites to overlap and we attempted to cover a time baseline longer than usual.

Regrettably, these attempts were somewhat unlucky as our combined observations always covered the same branch of the light curve with the exception of one night where we could observe it from both sites, albeit with a 1.6-h gap in between. As we had no overlap between SSO and SAAO, we transformed the instrumental magnitude differences to the standard system to homogenize the data as much as possible. This procedure pointed us to a zero-point problem just in the single SSO night taken in between two nights of SAAO data, which has to be kept in mind as well.

The frequency analysis of our data corroborated the *Hipparcos* period (cf. Fig. 2(b)), and the amplitudes in our $B - (19.0 \pm 0.4)-$ and $V - (14.9 \pm 0.3) -$ filter data suggest that this variability is due to pulsation. However, after prewhitening this variation from the data, some residual amplitude near 1.0 cycle day^{-1}, half the dominant frequency, remains. Such a variation can of course also be caused by a problem with the nightly zero-points or by imperfect extinction corrections etc. However, an examination of the SAAO data only (which show excellent long-term stability as judged from the measurement of the constant comparison stars) suggests that this 1.0 cycle day^{-1} variation could be intrinsic to HD 81421. It could therefore be a subharmonic of the 11.75-h period, indicative of ellipsoidal variation, but our data are insufficient to confirm or reject this idea.

A search for δ Scuti pulsations of this star proved to be difficult as well. Although a short-period variation with a time-scale of about one hour seemed to be superposed on the slow variability of the star, and although the rms scatter of the nightly light curves of HD 81421 after removing the long-term trends is higher than that of the difference of the comparison stars, we cannot prove its presence. An amplitude spectrum of all our data after prewhitening the *Hipparcos* frequency and its suspected subharmonic (Fig. 2(d)) shows evidence for low-amplitude δ Scuti variability, but the signal-to-noise ratio is too small for a definite detection.

On the basis of our data and those by the *Hipparcos* satellite we can therefore still not pinpoint the physical nature of HD 81421. It could be a γ Doradus pulsator or an ellipsoidal variable, and it could additionally be a δ Scuti star. More observations of the star are needed. Photometric measurements with a suitable time distribution and/or time series spectroscopy are required to understand this object.

3.1.8 HD 85693

Although the *Hipparcos* photometry suggests variability with a light range in excess of 0.1 mag, this star showed only very-small-amplitude slow variability during our observations. Therefore, the error in the *B*/*V* colour-amplitude ratio is too large to allow us to pinpoint the cause of the light variations. We retain the star as a γ Doradus candidate and place an upper limit of 0.8 mmag on the presence of δ Scuti pulsations in our light curves.

3.1.9 HD 86371

We are unable to recover the *Hipparcos* period suggested by Handler (1999) in our photometry, but the complicated light curves and our measured *B*/*V* colour-amplitude ratio (1.20 ± 0.03) suggest pulsation as the reason for this star's variability. Our upper limit for δ Scuti variability of this star is 0.8 mmag. The multiperiodicity from the *Hipparcos* photometry, which is confirmed with a residualgram analysis, and the colour-amplitude ratio derived above lead us to classify HD 86371 as a bona fide γ Doradus star.

3.1.10 HD 110606 and HD 113357

The light curves of both stars appear quite complicated. Neither the *Hipparcos* data nor our observations allowed the detection of a dominant period, which suggests the presence of multiperiodic γ Doradus pulsations. The *B*/*V* colour-amplitude ratios in our data are 1.26 ± 0.06 for HD 110606 and 1.34 ± 0.07 for HD 113357, further supporting this idea. No δ Scuti variability is present within a limit of 1.0 mmag in either of the stars. We cautiously classify HD 110606 and HD 113357 as prime γ Doradus candidates, but we think that further observations can easily prove they are bona fide members of the group.

3.1.11 HD 139095

We suggest that this is a bona fide γ Doradus star. The *Hipparcos* and the ground-based light curves are multiperiodic, and the *B*/*V* colour-amplitude ratio is 1.23 ± 0.02, typical for pulsational variability of a late A/early F star. There is no evidence for δ Scuti-type variability within a limit of 1.1 mmag in the amplitude spectrum.

3.1.12 HD 167858

The *Hipparcos* data of the star imply it is a multiperiodic γ Doradus pulsator of quite high amplitude. This is confirmed with our ground-based data, and the *B*/*V* colour-amplitude ratio (1.29 ± 0.06) implies pulsation as the cause for these light variations. The search for δ Scuti pulsations of HD 167858 in two nights yielded a null result, with no variation detected within 1.0 mmag in the second night of our measurements, which was of much better quality than the first one. We classify HD 167858 as a bona fide γ Doradus star.

3.1.13 BD+8 3658

In his search for multiperiodic variability among *Hipparcos* variables, Koen (2001) found one frequency typical for γ Doradus variations (1.00064 cycle day^{-1}) and a second one suggesting δ Scuti variability of BD+8 3658. This star was therefore of considerable interest for us. Weak δ Scuti modulations with a peak-to-peak amplitude of about 0.01 mag at a time-scale of 2.5 h (Q = 0.035 d) and evidence for multiperiodicity are indeed present in our data. However, we cannot identify the cause of the slow variability with certainty. Our ground-based measurements show almost no slow variability, a combined result of the *Hipparcos* period being very close to 1 d and of insufficient phase sampling. Therefore we cannot calculate meaningful colour-amplitude ratios. However, the phase diagram of the *Hipparcos* photometry relative to the long period (Fig. 3) is not typical for pulsational variability. More observations of this star are needed, including standard Strömgren photometry and spectroscopy.

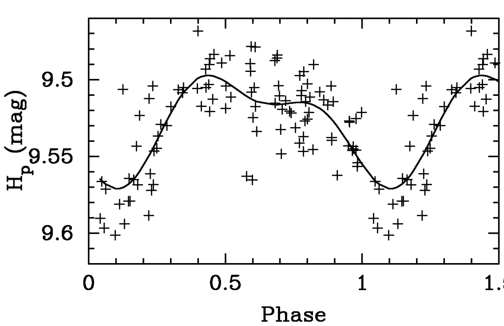

Figure 3. The phase diagram of the *Hipparcos* photometry of BD+8 3658 relative to a frequency of 1.00064 cycle day^{-1}. The solid curve is the result of a two-harmonic fit to these data. The light curve shape is not indicative of pulsational variability.

3.1.14 HD 173794

Handler (1999) could not decide whether this star shows variations close to 1.5 d or of one or two hours because of the aliasing problem in the *Hipparcos* data mentioned in the Introduction. In fact, both types of variation are present, as already seen from our first ground-based light curve (Fig. 4a). There are clear

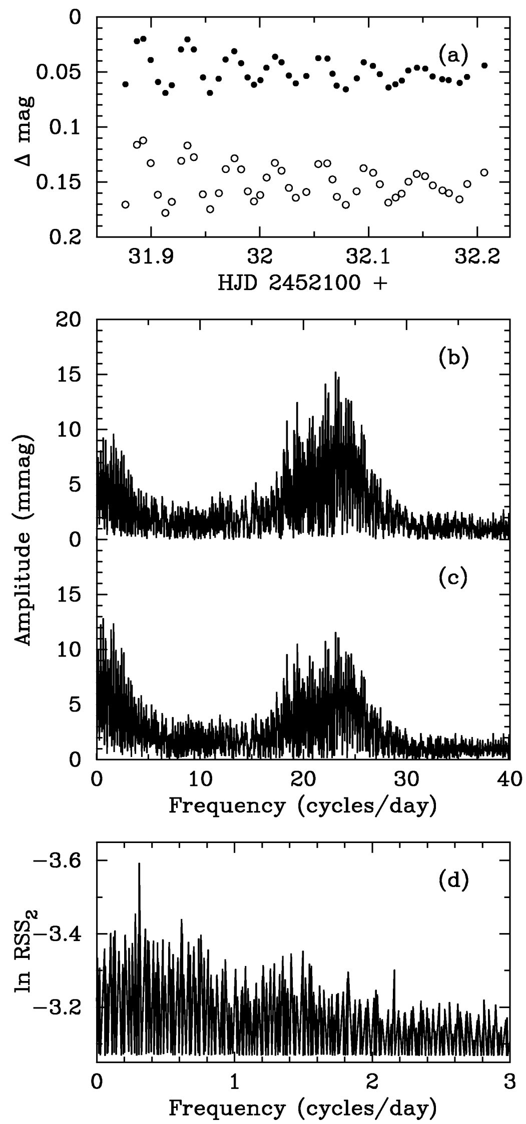

Figure 4. (a) Our first photometric measurements of HD 173794, showing both multiperiodic δ Scuti pulsation and a slow drop in mean magnitude (about 0.02 mag during this run). Filled circles are *V*-filter data, open circles the *B*-filter measurements. (b) Amplitude spectrum of all our ground-based *B*-filter observations. (c) Amplitude spectrum of all our *V*-filter measurements. Note that the δ Scuti pulsations have higher amplitude in the *B* filter, whereas the slow variability has slightly higher amplitude in *V*. (d) Residual sum of squares spectrum of a 2-harmonic fit (RSS_2) to the *Hipparcos* photometry of HD 173794.

multiperiodic δ Scuti pulsations superposed on slow variations which have very similar amplitude in the *B*- and *V*-bands (cf. Figs 4b and c). This raises the suspicion that HD 173794 is an ellipsoidal variable with a δ Scuti component. We therefore re-analysed the *Hipparcos* photometry of that star with the residualgram method; the result is shown in Fig. 4(d). The dominant peak in this plot is at 0.3078 cycle day^{-1}, exactly 1/2 the frequency found by Fourier analysis (Handler 1999). The phase diagram of the *Hipparcos* photometry relative to this frequency is typical for an ellipsoidal variable, and the corresponding frequency solution explains all the slow variability in these data.

These two frequencies also explain the slow variability in our data. We have therefore fitted them to our measurements, adopting the *Hipparcos* frequencies as definite and performed a frequency analysis of the residuals to examine the δ Scuti variability in more detail. The short-period pulsations turned out to be quite complicated, at least five frequencies in the range 19–26 cycle day^{-1} appear to be excited. We refrain from quoting exact values because of the aliasing problem. In any case, the short-period pulsations are quite interesting. All evidence, the *Hipparcos* parallax of the star, its spectral classification (A3 III-IV, Houk 1978) and the long period of the ellipsoidal variation, suggests it is rather evolved and thus pulsates in quite high radial overtones ($Q \approx 0.006, k \approx 10$).

3.1.15 HD 181998

We suggest that this star is a bona fide γ Doradus star. Our two longer nights of observations show slow variability that is not singly-periodic, consistent with the complicated amplitude spectrum of its *Hipparcos* photometry. These results combined with the colour-amplitude ratios ($B/V = 1.22 \pm 0.03$, $V/I_c = 1.68 \pm 0.03$) in our data show that the slow variations of HD 181998 are due to pulsation. An upper limit of 1.1 mmag is placed on the presence of δ Scuti pulsations.

3.1.16 HD 188032

The analysis of the *Hipparcos* data of this star (Handler 1999) left some doubt about its being a good γ Doradus candidate or a more rapid variable. In our ground-based observations, only slow variations with an amplitude below 0.02 mag are detected. From these we infer a B/V colour-amplitude ratio of 1.25 ± 0.1, suggestive of pulsation. Short-period variability in the δ Scuti domain remains undetected within 0.9 mmag. We classify this star as a γ Doradus candidate.

3.1.17 HD 189631

This star was found to be slowly variable within individual nights, but we are unable to determine the time-scale of the light variations. The colour-amplitude ratios ($B/V = 1.36 \pm 0.04$, $V/I_c = 1.82 \pm 0.12$) imply pulsation as the cause of this variability, which reached a peak-to-peak amplitude in excess of 0.05 mag from night to night. We conservatively classify HD 189631 as a γ Doradus candidate and note the absence of δ Scuti pulsation within an upper limit of 0.9 mmag.

3.1.18 HD 198528

We found slow variations with amplitudes of several hundredths of a magnitude in our four longest observing runs. However, only very small colour variability (B/V amplitude ratio < 1.04) was noted as well, raising the suspicion that the star is an ellipsoidal variable. A combined analysis of the *Hipparcos* photometry (with the decisive clue coming from residualgram analysis, see Fig. 5) and our new observations confirmed this interpretation. We found that a double-wave light curve (inconsistent with W UMa-type variability) corresponding to an orbital period of 0.807 d satisfactorily explains all the data. The period given by Handler (1999) based on Fourier analysis of *Hipparcos* photometry only is therefore incorrect, probably owing to the small number of observations (49 measurements distributed over 3 yr). No δ Scuti variation is detected within a limit of 1.5 mmag in the amplitude spectrum, although we note that a very weak 45-minute variation seemed to be present in both filters in our best data.

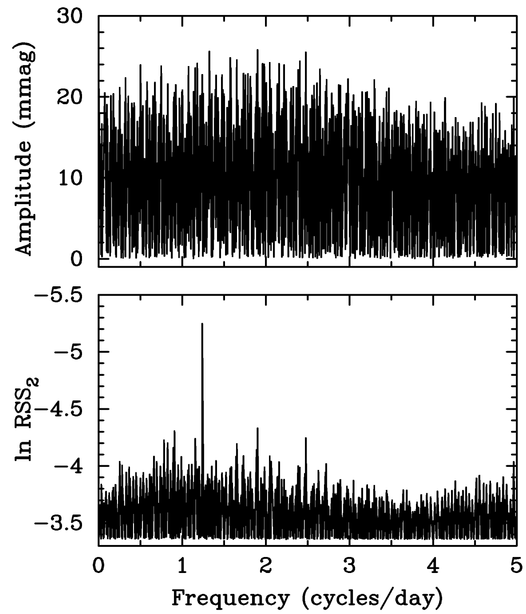

Figure 5. Upper panel: amplitude spectrum of the *Hipparcos* photometry of HD 198528. No periodicity can be found. Lower panel: residual sum of squares spectrum of a 2-harmonic fit (RSS_2) of the same data. The correct frequency of light variation is now quite clear.

3.1.19 HD 201985

This star remains unsolved. Although the *Hipparcos* photometry implies a range of variability of a few hundredths of a magnitude, little variation was seen during our observations (a few millimagnitudes at best), with one exception: during the first run from SAAO, the star was 0.15 mag fainter than on the other nights. An instrumental problem or misidentification on the sky is ruled out, as the star's mean $(B-V)$ colour on that night was the same as on the other four within fractions of a millimagnitude, and as the relative zero-points of the other three stars in the ensemble were consistent with the other nights. We note that little colour variability seems to accompany the magnitude changes, and we can place an upper limit of 2.0 mmag to the presence of δ Scuti pulsations. HD 201985 could be an eclipsing binary.

3.1.20 HD 207223

This is a singly-periodic bona fide γ Doradus star (Aerts & Kaye 2001) located close to HD 207651 in the sky. We tested HD 207223 for δ Scuti variability in a single night. None was detected within a limit of 1.5 mmag in the amplitude spectrum (cf. Kaye et al. 1999b).

3.1.21 HD 207651

The *Hipparcos* photometry seemed to indicate two frequencies of 1.4 and 6 cycle day^{-1} (Handler 1999), whereas our runs show a dominant δ Scuti variation with a time-scale of 1.5–2 h with superposed long-term modulations. The associated colour amplitudes corroborate the δ Scuti interpretation, but are inconclusive with respect to the slower variability. Estimating the absolute magnitude of the star from its *Hipparcos* parallax results in $M_v = -0.4 \pm 0.5$, but Strömgren photometric calibrations (Crawford 1979) yield $M_v = +0.8 \pm 0.3$. This may be an indication of binarity. In any case, we are unable to pinpoint the nature of the star on the basis of our data alone; more observations are needed. The Q values of the δ Scuti pulsations are 0.007 and 0.015 d for the two absolute-magnitude values, respectively.

3.1.22 HD 209295

This is our only detection of both δ Scuti and γ Doradus pulsations in the same star. It was already clear from the analysis of the *Hipparcos* photometry (Handler 1999) that multiperiodic γ Doradus variability is present in the star's light curves, and multiperiodic δ Scuti pulsations were clearly detected in our first nights of observation as well (Fig. 6). HD 209295 was studied in great detail by Handler et al. (2002), and we refer to this paper for more information. For the present purposes, we only note that these authors present evidence that the γ Doradus pulsations of HD 209295 are tidally excited. The star should therefore not be considered a normal γ Doradus star.

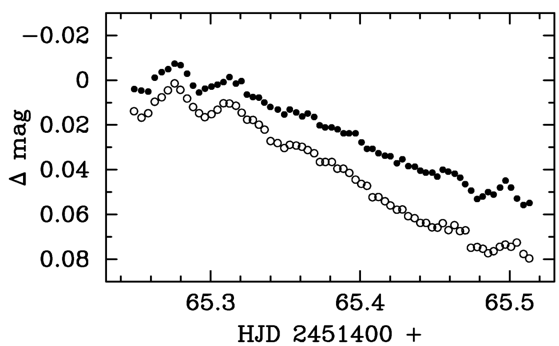

Figure 6. An example light curve of HD 209295. Filled circles are *V*-filter data, open circles the *B*-filter measurements. Multiperiodic δ Scuti pulsations are superposed on a gradual decline in brightness. Note the higher amplitude of the slow variations in the *B*-filter data, confirming their pulsational origin.

3.1.23 HD 211699

This prime γ Doradus candidate (Handler 1999) showed very little variability during our individual nights of observation, which may be due to the dominant period of light variation being close to one day. However, we were able to detect changes in the mean magnitude from night to night, whose B/V colour-amplitude ratio (1.29 ± 0.09) suggests that pulsations are causing them. We therefore retain this star as a γ Doradus candidate and we also note the absence of δ Scuti pulsations within an upper limit of 0.8 mmag.

3.1.24 HD 221866

Classified as a prime γ Doradus candidate by Handler (1999), this star showed clear evidence of slow variability. The *Hipparcos* period fits our data and results in a B/V colour-amplitude ratio of 1.18 ± 0.02, consistent with pulsation. δ Scuti-type variability remains undetected within a limit of 0.9 mmag in the amplitude spectrum. We conservatively retain this star as a γ Doradus candidate because of the rather low colour-amplitude ratio.

3.1.25 Variable comparison stars

Out of the 40 comparison stars used in this study, two turned out to be variable as well. The first, HD 86301, was a comparison star in the HD 85693/HD 86371 group. It is located near the hot luminous border of the δ Scuti instability strip and was found to be a very-low-amplitude variable. The light curve appears multiperiodic with a time-scale of 3.8–6 h and a total amplitude of about 0.01 mag. Our period estimate yields a range of $0.035\,\mathrm{d} < Q < 0.054\,\mathrm{d}$. We tentatively classify HD 86301 as a new δ Scuti star.

The second variable comparison star was HD 183452, chosen for the HD 181998 group. During our first short run on this group, it already showed conspicuous magnitude changes. After realizing the star was classified as variable from measurements with the *Tycho* satellite (ESA 1997), we added another comparison star into the sequence, but continued to monitor HD 183452 as well. The total amplitude of its light variations is in excess of 0.1 mag, but there is very little colour variation. We thus suspect that HD 183452 is an ellipsoidal variable. A double-wave light curve assuming a preliminary orbital period of 0.692 d fits our data very well.

Table 2. Programme star classifications. Objects indicated with an asterisk are δ Scuti stars in addition to their main type of variability, whereas stars indicated with two asterisks have suspected additional δ Scuti variations.

γ Doradus/δ Scuti 'hybrid'	*Bona fide* γ Doradus stars	γ Doradus candidates	Ellipsoidal variables	δ Scuti stars	Unsolved variables
HD 209295	HD 12901	HD 10167	HD 14147**	HD 27093	HD 81421**
	HD 65526	HD 40745	HD 173794*		HD 86593
	HD 86371	HD 41448	HD 198528**		BD+8 3658*
	HD 139095	HD 110606			HD 201985
	HD 167858	HD 113357			HD 207651*
	HD 181998	HD 188032			
	HD 207223	HD 189631			
		HD 211699			
		HD 221866			

3.2 Summary of survey results

We performed photometric monitoring of a total of 26 stars that seemed to be related to the γ Doradus phenomenon. One of them, HD 209295, turned out to be both a γ Doradus and a δ Scuti pulsator, but this object is peculiar, as its g-mode pulsations appear strongly coupled to its binary orbit (Handler et al. 2002).

We believe that six of our targets are new γ Doradus pulsators, and nine more stars are probable γ Doradus stars. We discovered three ellipsoidal variables and one δ Scuti star. The classifications of our target stars are summarized in Table 2. The detection limits we achieved for δ Scuti pulsations compare well with those of other ground-based variability surveys (starting with Breger 1969), to which our results are to be compared. Of course, the presence of very-low-amplitude δ Scuti pulsations in some of our targets cannot be ruled out. Such variability has been detected down to limits of 0.4 mmag with the help of extensive multisite campaigns (Handler et al. 2000), and space missions are expected to decrease these limits considerably.

4 THE HOT BORDER OF THE γ DORADUS PHENOMENON

As already mentioned in the Introduction, it is not quite clear up to what effective temperatures γ Doradus pulsations can be excited. With our new results added to those available in the literature, we can take a closer look at this problem. We show all the presently known γ Doradus stars and suspects (taken from the on-line catalogue by Handler & Kaye 2001) in a colour–magnitude diagram in Fig. 7.

Even a brief glance at Fig. 7 suggests that the blue edge of the γ Doradus instability region as outlined by Handler (1999) requires revision. (We again exclude HD 209295, the hottest bona fide γ Doradus star from the discussion because of its close-binary nature.) The three hottest stars referred to by Handler (1999) were HD 152569 (Kaye 1998), 57 Tau (Paparó et al. 2000) and M34 UVa 144 (Krisciunas & Patten 1999). HD 152569 was reclassified as a δ Scuti star (Kaye et al. 2000); thus it is not plotted in Fig. 7.

57 Tau is also a δ Scuti star, but it exhibits slow, apparent multiperiodic, variability with an amplitude of a few mmag (Paparó et al. 2000) in addition; the period of the highest-amplitude slow variation is 1.246 d. However, Kaye (1999) showed that 57 Tau is a spectroscopic binary with an orbital period of 2.486 d, almost exactly twice the value from the photometry. As there seems to be very little colour variation in the slow variations noted by Paparó et al. (2000), we think that 57 Tau is in fact an ellipsoidal variable. Therefore we do not any longer consider the star a good γ Doradus candidate.

The star UVa 144 in the open cluster M34 is a multiperiodic slow variable. However, the two periods found by Krisciunas & Patten (1999), 1.52 and 1.28 cycle day^{-1}, could be harmonics of each other allowing for some aliasing ambiguities. In any case, the $(b-y)$ colour of this star adopted by Handler (1999) is erroneous, as he was unaware of the measurements by Canterna, Perry & Crawford (1979) showing the star to be redder than previously thought.

Consequently, a revision of the blue boundary of the γ Doradus region in the colour–magnitude diagram is in order. The new blue edge is already included in Fig. 7. Compared to the original one by Handler (1999), it is about 150 K cooler on the ZAMS and about 75 K cooler one magnitude above it. There are now four stars that define it, the bona fide variable HD 218396 (Zerbi et al. 1999), as well as HD 41448 (Eyer 1998; Handler 1999; and this work), HD 211699 and HD 221866 (Handler 1999; and this work). As the evidence for the γ Doradus nature of all these stars is quite good, we think that another shift of this blue edge towards redder colours is no longer possible.

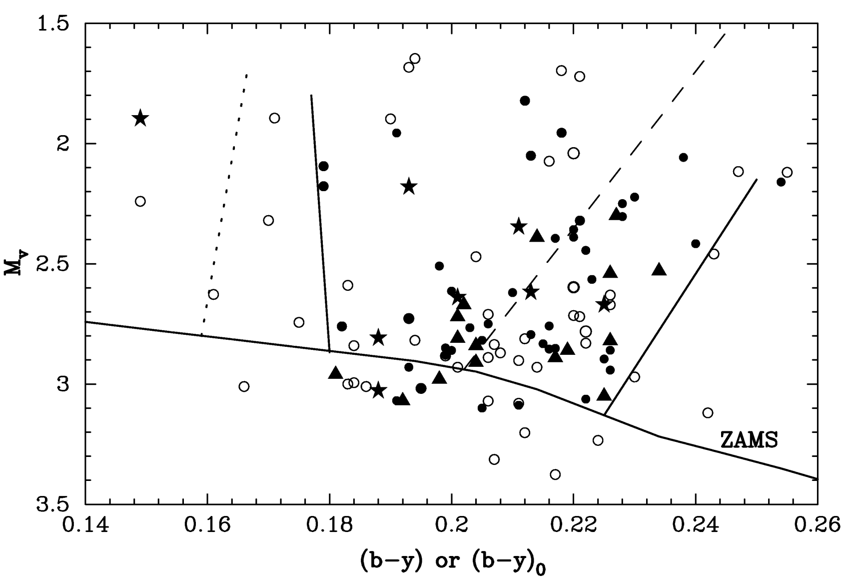

Figure 7. The domain of the γ Doradus pulsators in the colour–magnitude diagram. Star symbols denote bona fide γ Doradus stars observed by us and filled triangles are bona fide γ Doradus stars from the literature. The filled circles are prime γ Doradus candidates and the open circles are other γ Doradus candidates (including our unsolved variables). Ellipsoidal variables have been omitted. The approximately horizontal line is the Zero-Age Main Sequence (ZAMS)(Crawford 1975, 1979), and the dotted line is the blue boundary of the γ Doradus region derived by Handler (1999), which is superseded by this work. The lines almost normal to the ZAMS are the presently known boundaries of the γ Doradus region. The dashed line almost normal to the ZAMS represents the red edge of the δ Scuti instability strip (Rodriguez & Breger 2001). The γ Doradus star outlying far to the blue is HD 209295.

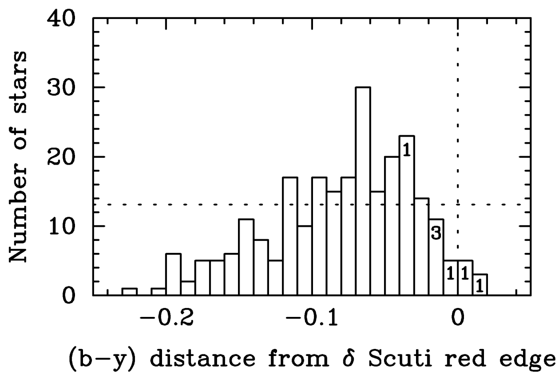

Figure 8. The number of δ Scuti stars as a function of $(b-y)$ distance from the red edge of the lower instability strip (vertical dotted line). In this diagram, the blue edge is located at $\Delta(b-y) = -0.19$ on the ZAMS and at $\Delta(b-y) = -0.23$ at the luminous end of the δ Scuti strip. The horizontal dotted line is the average number of stars per bin for $-0.19 < \Delta(b-y) < 0$. The numbers inside some of the bins are the number of bona fide γ Doradus stars tested for δ Scuti variability corresponding to their $\Delta(b-y)$.

5 THE INCIDENCE OF δ SCUTI PULSATIONS AMONGST γ DORADUS STARS

With the exception of the unusual variable HD 209295, we have observed five bona fide γ Doradus stars located inside the δ Scuti instability strip (HD 12901, HD 65526, HD 86371, HD 167858 and HD 181998) adopting the red edge for δ Scuti pulsations by Rodriguez & Breger (2001)[1]. Another star, HD 139095, falls on this red edge.

We did not find δ Scuti pulsations in any of these stars. Does this mean that, except under special circumstances such as the close binarity of HD 209295, γ Doradus stars cannot be δ Scuti pulsators at the same time?

As mentioned in the Introduction, the average incidence of photometrically detectable δ Scuti pulsations of chemically normal stars located inside the lower instability strip is 1/3. However, the γ Doradus star domain only overlaps with a region close to the cool edge of the δ Scuti instability strip. Hence it is quite possible that the incidence of δ Scuti pulsations in that overlap region is generally smaller than, for instance, in the middle of the δ Scuti strip.

To examine this idea, we assume that all stars tested for δ Scuti pulsations so far are uniformly distributed over $(b-y)$. We selected all 249 δ Scuti stars from the recent catalogue of Rodriguez, López-González & López de Coca (2000), for which uvbyβ photometry is available and determined their distance from the red edge of the δ Scuti instability strip, as defined by Rodriguez & Breger (2001). We then determined the number of stars in strips 0.01 mag wide in $(b-y)$, which are parallel to the red edge, and we show the number of bona fide γ Doradus stars we observed in those bins (Fig. 8).

As suspected, the number of δ Scuti stars decreases towards the red edge; stars near this red edge have an incidence of δ Scuti pulsation that is lower than average. We need to take this into account if we want to examine the significance of the absence of δ Scuti pulsation in the bona fide γ Doradus stars we observed.

Thus, the probability that we do not find δ Scuti pulsations in any of our observed bona fide γ Doradus stars inside the δ Scuti strip, results in 18 per cent. This suggests that γ Doradus stars are less likely to be δ Scuti pulsators than non-γ Doradus stars in the same domain of the colour–magnitude diagram. Obviously, more stars need to be observed to strengthen this conclusion.

[1] This revised red edge only became available near the end of this work and could therefore not be adopted for target selection (Section 2).

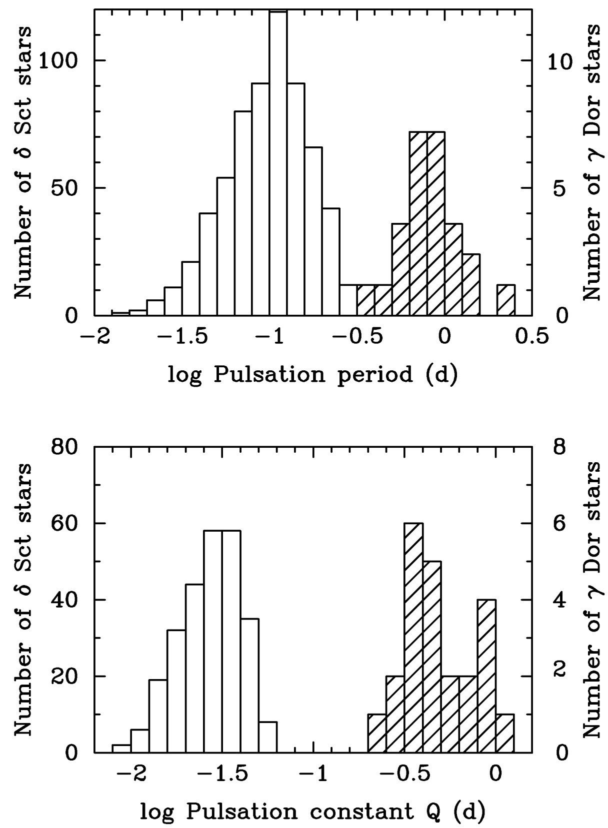

Figure 9. Upper panel: the number of δ Scuti (open histogram bars) and γ Doradus (hatched histogram bars) stars within certain ranges of pulsation period. The two groups of pulsator almost overlap in this diagram. Lower panel: the distribution of the pulsation constants of δ Scuti (open bars) and γ Doradus (hatched bars) stars. There is a clear separation between the two.

6 PULSATION PERIODS AND PULSATION CONSTANTS

The longest pulsation periods of δ Scuti stars listed in the catalogue of Rodriguez et al. (2000) are around 6.5 h; the possible δ Scuti stars AC And (Fernie 1994) and V823 Cas (Antipin 1997) even have periods of 17 and 16 h, respectively. The shortest pulsation periods of γ Doradus stars found so far were around 7.5 h (Handler 1999; Henry et al. 2001). This may lead to the suspicion that there might be an overlap in the pulsational behaviour of those two classes of pulsator, making a distinction hard for certain stars.

However, as the γ Doradus stars are so far only found on the main sequence, and as the long-period δ Scuti stars all seem to be evolved, this overlap is not a physical one. To support this suggestion, we compared the distribution of the pulsation periods of 636 δ Scuti stars in the catalogue of Rodriguez et al. (2000) to that of the bona fide stars (except HD 209295) listed by Handler & Kaye (2001). We show it in the upper panel of Fig. 9. As implied by the previous discussion, there is almost an overlap between the two groups.

On the other hand, if one uses the pulsation constant Q (calculated with equation 1 and the method described in Section 3.1) to discriminate between δ Scuti and γ Doradus stars, the ambiguity is removed (lower panel of Fig. 9, 262 δ Scuti stars from Rodriguez et al. 2000 for which pulsation constants could be calculated). There is a clear gap between the two groups. Thus we confirm that δ Scuti and γ Doradus stars can be separated via their pulsation constants; all bona fide γ Doradus stars known to date have $Q > 0.23$ d.

7 CONCLUSIONS

We performed a photometric search for δ Scuti pulsations among candidate γ Doradus stars to examine the interrelations between these two groups of pulsators. We observed altogether 26 stars, of which 65 per cent turned out to be bona fide γ Doradus stars or excellent candidates. However, none of these objects exhibited δ Scuti pulsations with the exception of the close binary HD 209295 (Handler et al. 2002), which is therefore anomalous.

Our results indicate that γ Doradus stars are less likely to be δ Scuti pulsators than non-γ Doradus stars in the same temperature range. This conclusion is not yet definite because of the small number of bona fide γ Doradus stars inside the δ Scuti domain investigated so far. This situation can be improved by performing a similar project in the Northern Hemisphere and by more extensive observations of the γ Doradus candidates we already examined, in order to prove their γ Doradus nature.

We were also able to locate the blue edge of the γ Doradus domain in the colour–magnitude diagram more accurately. Finally, we showed that the δ Scuti stars and the γ Doradus pulsators are clearly separated by the values of their pulsation constants Q; the known γ Doradus stars all have $Q > 0.23$ d.

Although we are still at the beginning of understanding the whole extent of the γ Doradus phenomenon, we think we now have the basic data for quantitative comparisons between observations and model calculations. Acceptable models for γ Doradus pulsators must be able to reproduce the observed constraints on pulsational instability in temperature, luminosity, metallicity and period.

ACKNOWLEDGMENTS

GH thanks Eloy Rodriguez for making an ASCII version of his δ Scuti star catalogue available and Chris Koen for his support of this project and for carefully proofreading a draft version of this paper. Michel Breger, Laurent Eyer and Tony Kaye also commented on a draft version of this work. We appreciate the constructive comments of the referee, Joyce Guzik.

NOTE ADDED IN PRESS

As pointed out to the authors by G. W. Henry, the star HD 221866 is located incorrectly in our Fig 7. Its measured $(b-y)_0$ is 0.151, which would place it near HD 209295. However, we doubt the correctness of the published $(b-y)_0$ as it is inconsistent with measurements of its $B-Y$ and $V-I$ colours. We suggest that new standard Strömgren photometry of HD 221866 be obtained.

REFERENCES

Aerts C., Kaye A. B., 2001, ApJ, 553, 814
Allen C. W., 1976, Astrophysical Quantities. Athlone Press, London, p. 161ff
Antipin S., 1997, A&A, 326, L1
Breger M., 1969, ApJS, 19, 79
Breger M., 1979, PASP, 91, 5
Breger M., 1989, Communications in Asteroseismology. Univ. Vienna, 7, 1
Breger M., 2000, in Breger M., Montgomery M. H., eds, ASP Conf. Ser. 210, Delta Scuti and Related Stars. Astron. Soc. Pac., San Francisco, p. 3
Breger M., Beichbuchner F., 1996, A&A, 313, 851
Breger M., Handler G., 1993, Baltic Astron., 2, 468
Canterna R., Perry C. L., Crawford D. L., 1979, PASP, 91, 263
Chevalier C., 1971, A&A, 14, 24
Crawford D. L., 1975, AJ, 80, 955
Crawford D. L., 1979, AJ, 84, 1858
Drilling J. S., Landolt A. U., , Cox A. N. 2000, Allen's Astrophysical Quantities, 4th edn. Springer Verlag, p. 388
ESA, 1997, The *Hipparcos* and *Tycho* catalogues, ESA SP-1200
Eyer L., 1998, PhD thesis, Univ. Geneva
Eyer L., Aerts C., 2000, A&A, 361, 201
Eyer L., Grenon M., 1998, in Deubner F. L. et al., eds, New Eyes to See Inside the Sun and Stars, p. 291
Fernie J. D., 1994, MNRAS, 274, L19
Garrido R., 2000, in Breger M., Montgomery M., eds, ASP Conf. Ser. 210, Delta Scuti and Related Stars, p. 67
Guzik J. A., Kaye A. B., Bradley P. A., Cox A. N., Neuforge C., 2000, ApJ, 542, L57
Guzik J. A., Kaye A. B., Bradley P. A., Cox A. N., Neuforge-Verheecke C., Warner P. B., 2002, in Aerts C.et al., ed., ASP Conf. Ser., Radial and Nonradial Oscillations as Probes of Stellar Physics, p. 502
Handler G., 1999, MNRAS, 309, L19
Handler G., Kaye A. B., 2001, http://www.saao.ac.za/~gerald/gdorlist.html
Handler G. et al., 2000, MNRAS, 318, 511
Handler G. et al., 2002, MNRAS, 333, 262 (Paper II, this issue)
Henry G. W., Fekel F. C., Kaye A. B., Kaul A., 2001, AJ, in press
Houk N., 1978, Michigan Spectral Catalogue, Vol. 2. University of Michigan, Ann Arbor
Kaye A. B., 1998, PhD thesis, Georgia State Univ.
Kaye A. B., 1999, IBVS, 4697
Kaye A. B., Handler G., Krisciunas K., Poretti E., Zerbi E., 1999a, PASP, 111, 840
Kaye A. B., Henry G. W., Fekel F. C., Hall D. S., 1999b, MNRAS, 308, 1081
Kaye A. B., Henry G. W., Rodriguez E., 2000, IBVS, 4850
Koen C., 2001, MNRAS, 321, 44
Krisciunas K., Patten B. M., 1999, IBVS, 4705
Kurtz D. W., Marang F., van Wyk F., Roberts G., 1996, MNRAS, 280, 1
Kurucz R. L., 1991, Van Vleck Obs. Contrib., 11, 27
Martinez P., Koen C., 1994, MNRAS, 267, 1039
Montgomery M. H., O'Donoghue D., 1999, Delta Scuti Star Newsletter, 13. Univ. Vienna, p. 28
Paparó M. et al., 2000, A&AS, 142, 1
Rodriguez E., Breger M., 2001, A&A, 366, 178
Rodriguez E., López-González M. J., López de Coca P., 2000, A&AS, 144, 369
Shobbrook R. R., 2000, JAD, 6, 4E
Zerbi F. M. et al., 1999, MNRAS, 303, 275

This paper has been typeset from a TEX/LATEX file prepared by the author.

Mon. Not. R. Astron. Soc. **333,** 262–278 (2002)

Discovery and analysis of p-mode and g-mode oscillations in the A-type primary of the eccentric binary HD 209295★

G. Handler,[1]† L. A. Balona,[1] R. R. Shobbrook,[2,3] C. Koen,[1] A. Bruch,[4] E. Romero-Colmenero,[1] A. A. Pamyatnykh,[5,6] B. Willems,[7] L. Eyer,[8,9] D. J. James[10,11,12,13] and T. Maas[8]

[1]*South African Astronomical Observatory, PO Box 9, Observatory 7935, South Africa*
[2]*PO Box 518, Coonabarabran, NSW 2357, Australia*
[3]*Research School of Astronomy and Astrophysics, Australian National University, Weston Creek PO, ACT 2611, Australia*
[4]*Labóratorio Nacional de Astrofísica, Itajubá, Brazil*
[5]*Copernicus Astronomical Center, ul. Bartycka 18, 00-716 Warsaw, Poland*
[6]*Institute of Astronomy, Russian Academy of Sciences, Pyatnitskaya 48, 109017 Moscow, Russia*
[7]*Department of Physics and Astronomy, The Open University, Walton Hall, Milton Keynes MK7 6AA*
[8]*Instituut voor Sterrenkunde, Katholieke Universiteit Leuven, B-3001 Leuven (Heverlee), Belgium*
[9]*Astrophysical Sciences Department, Princeton University, Princeton, NJ 08544, USA*
[10]*Observatoire de Genève, Chemin des Maillettes 51, CH-1290 Sauverny, Switzerland*
[11]*Laboratoire d'Astrophysique, Observatoire de Grenoble, Université Joseph Fourier, BP 53, F-38041, Grenoble Cedex 9, France*
[12]*School of Physics & Astronomy, University of St Andrews, North Haugh, St Andrews, Fife KY16 9SS*
[13]*475 N. Charter Street, 5534 Sterling Hall, Madison, WI 53706-1582, USA*

Accepted 2001 December 18. Received 2001 December 17; in original form 2001 October 18

ABSTRACT

We have discovered both intermediate-order gravity mode and low-order pressure mode pulsation in the same star, HD 209295. It is therefore both a γ Doradus and a δ Scuti star, which makes it the first pulsating star to be a member of two classes.

The analysis of our 128 h of multisite spectroscopic observations carried out over two seasons reveals that the star is a single-lined spectroscopic binary with an orbital period of 3.10575 ± 0.00010 d and an eccentricity of 0.352 ± 0.011. Only weak pulsational signals are found in both the radial velocity and line-profile variations, but we have succeeded in showing that the two highest-amplitude γ Doradus pulsation modes are consistent with $\ell = 1$ and $|m| = 1$.

These two modes dominated our 280 h of BVI_C multisite photometry, also obtained over two seasons. We detected altogether ten frequencies in the light variations, one in the δ Scuti regime and nine in the γ Doradus domain. Five of the γ Doradus frequencies are exact integer multiples of the orbital frequency. This observation leads us to suspect they are tidally excited. Attempts to identify modes from the multicolour photometry failed.

We performed model calculations and a stability analysis of the pulsations. The frequency range in which δ Scuti modes are excited agrees well with observations. However, our models do not show excitation of γ Doradus pulsations, although the damping is smaller in the observed range. We also investigated tidal excitation of γ Doradus modes. Some of the observed harmonics of the orbital period were found to be unstable. The observed orbital harmonics which are stable in the models can be understood as linear combinations of the unstable modes.

We could not detect the secondary component of the system in infrared photometry, suggesting that it may not be a main-sequence star. Archival data of this star show that it has a strong ultraviolet (UV) excess, the origin of which is not known. The orbit of the primary is consistent with a secondary mass of $M > 1.04\,M_\odot$, which is indicative of a neutron star, although a white dwarf companion is not ruled out.

★ Dedicated to the memory of A. W. J. Cousins, discoverer of the variability of γ Doradus.
†E-mail: gerald@saao.ac.za

3.5 Discovery and analysis of p-mode and g-mode oscillations in the A-type primary of the eccentric binary HD 209295

Original paper:

G. Handler, L. A. Balona, R. R. Shobbrook, C. Koen, A. Bruch, E. Romero-Colmenero, A. A. Pamyatnykh, B. Willems, L. Eyer, D. J. James, T. Maas 2002, MNRAS 333, 262

Mon. Not. R. Astron. Soc. **333,** 262–278 (2002)

Discovery and analysis of p-mode and g-mode oscillations in the A-type primary of the eccentric binary HD 209295★

G. Handler,[1]† L. A. Balona,[1] R. R. Shobbrook,[2,3] C. Koen,[1] A. Bruch,[4] E. Romero-Colmenero,[1] A. A. Pamyatnykh,[5,6] B. Willems,[7] L. Eyer,[8,9] D. J. James[10,11,12,13] and T. Maas[8]

[1]*South African Astronomical Observatory, PO Box 9, Observatory 7935, South Africa*
[2]*PO Box 518, Coonabarabran, NSW 2357, Australia*
[3]*Research School of Astronomy and Astrophysics, Australian National University, Weston Creek PO, ACT 2611, Australia*
[4]*Labóratorio Nacional de Astrofísica, Itajubá, Brazil*
[5]*Copernicus Astronomical Center, ul. Bartycka 18, 00-716 Warsaw, Poland*
[6]*Institute of Astronomy, Russian Academy of Sciences, Pyatnitskaya 48, 109017 Moscow, Russia*
[7]*Department of Physics and Astronomy, The Open University, Walton Hall, Milton Keynes MK7 6AA*
[8]*Instituut voor Sterrenkunde, Katholieke Universiteit Leuven, B-3001 Leuven (Heverlee), Belgium*
[9]*Astrophysical Sciences Department, Princeton University, Princeton, NJ 08544, USA*
[10]*Observatoire de Genève, Chemin des Maillettes 51, CH-1290 Sauverny, Switzerland*
[11]*Laboratoire d'Astrophysique, Observatoire de Grenoble, Université Joseph Fourier, BP 53, F-38041, Grenoble Cedex 9, France*
[12]*School of Physics & Astronomy, University of St Andrews, North Haugh, St Andrews, Fife KY16 9SS*
[13]*475 N. Charter Street, 5534 Sterling Hall, Madison, WI 53706-1582, USA*

Accepted 2001 December 18. Received 2001 December 17; in original form 2001 October 18

ABSTRACT

We have discovered both intermediate-order gravity mode and low-order pressure mode pulsation in the same star, HD 209295. It is therefore both a γ Doradus and a δ Scuti star, which makes it the first pulsating star to be a member of two classes.

The analysis of our 128 h of multisite spectroscopic observations carried out over two seasons reveals that the star is a single-lined spectroscopic binary with an orbital period of 3.10575 ± 0.00010 d and an eccentricity of 0.352 ± 0.011. Only weak pulsational signals are found in both the radial velocity and line-profile variations, but we have succeeded in showing that the two highest-amplitude γ Doradus pulsation modes are consistent with $\ell = 1$ and $|m| = 1$.

These two modes dominated our 280 h of BVI_C multisite photometry, also obtained over two seasons. We detected altogether ten frequencies in the light variations, one in the δ Scuti regime and nine in the γ Doradus domain. Five of the γ Doradus frequencies are exact integer multiples of the orbital frequency. This observation leads us to suspect they are tidally excited. Attempts to identify modes from the multicolour photometry failed.

We performed model calculations and a stability analysis of the pulsations. The frequency range in which δ Scuti modes are excited agrees well with observations. However, our models do not show excitation of γ Doradus pulsations, although the damping is smaller in the observed range. We also investigated tidal excitation of γ Doradus modes. Some of the observed harmonics of the orbital period were found to be unstable. The observed orbital harmonics which are stable in the models can be understood as linear combinations of the unstable modes.

We could not detect the secondary component of the system in infrared photometry, suggesting that it may not be a main-sequence star. Archival data of this star show that it has a strong ultraviolet (UV) excess, the origin of which is not known. The orbit of the primary is consistent with a secondary mass of $M > 1.04\,M_\odot$, which is indicative of a neutron star, although a white dwarf companion is not ruled out.

★ Dedicated to the memory of A. W. J. Cousins, discoverer of the variability of γ Doradus.

†E-mail: gerald@saao.ac.za

Key words: binaries: close – binaries: spectroscopic – stars: individual: HD 209295 – stars: neutron – stars: oscillations – δ Scuti.

1 INTRODUCTION

Four different classes of multimode pulsating variables are found near the intersection of the classical instability strip and the main sequence. However, asteroseismology (probing the stellar interior through such pulsations) of these stars has proven to be more difficult than expected. None the less, the example of helioseismology and its enormous reward in terms of the physical understanding of the Sun's interior (e.g. see Gough 2000) has been a great motivation for continuing efforts in probing the structure of these stars by means of their pulsational properties.

Many attempts to detect solar-type oscillations in stars have resulted in inconclusive results, although success has been claimed in some instances (e.g. Kjeldsen et al. 1995). Because of their extremely low amplitude, it is only recently (e.g. Bedding et al. 2002) that we are beginning to see detections which may be considered significant. Successful asteroseismology based on the analysis of solar-type oscillations now appears immanent.

The rapidly oscillating Ap stars (see Kurtz & Martinez 2000 for a recent comprehensive review) are high-radial order p-mode pulsators. Their pulsation spectra resemble that of the Sun. In these stars, only a few independent modes are observed. Moreover, the presence of a strong magnetic field is expected to modify the frequencies and eigenfunctions of the modes. Successful modelling of these pulsations does not seem possible at this time. Nevertheless, some progress is currently being made (e.g. Cunha & Gough 2000).

The third group of pulsators in this region of the Hertzsprung–Russell (HR) diagram are the δ Scuti (δ Sct) stars, which are low-radial order p- and probably mixed-mode pulsators (see Breger & Montgomery 2000). For some of these stars, tens of pulsations modes have been detected and their frequencies determined with high precision (see e.g. Handler et al. 2000). Although mean densities, and even asteroseismological distances (Handler et al. 1997) have been estimated, the problem of mode identification and shortcomings in the stellar models are major difficulties (see e.g. Pamyatnykh et al. 1998 for a discussion).

The γ Doradus (γ Dor) stars are high-overtone gravity (g) mode pulsators (Kaye et al. 1999a). In these stars only a few modes are excited to observable amplitude amongst a dense forest of possible modes. As a result, accurate starting values of the basic stellar parameters are required to enable observed and calculated frequencies to be matched.

In principle, it is possible for δ Sct and γ Dor pulsations to co-exist in a star as they occupy overlapping regions in the HR diagram. This offers new opportunities for successful astero-seismology, as noted by Handler (1999a). In such stars it may be possible to use the δ Sct pulsations to place strong constraints on the stellar parameters, easing the mode identification problem of the γ Dor pulsations. In this way it may be possible to obtain information about the deep interior which is unobtainable for pure δ Sct stars.

Consequently, Handler & Shobbrook (2002) searched for δ Sct pulsations in all known candidate γ Dor stars located within the δ Sct instability strip and accessible from intermediate southern geographical latitudes. About one third of all non-Am and non-Ap stars in the lower instability strip are indeed δ Sct stars (Breger 1975). Because Am and Ap stars are rare (if not absent) amongst the γ Dor stars (Handler 1999a), detection of some 'hybrid' stars may be expected if δ Sct and γ Dor pulsations are not mutually exclusive. In this paper we report the discovery and analysis of such a star, HD 209295 (Sangam Mani).

This is a $V = 7.3$ mag southern ($\delta = -64°$) star of spectral type A9/F0 V (Houk & Cowley 1975). It was discovered as variable by the *Hipparcos* mission (ESA 1997). Handler (1999a) performed a frequency analysis of these data and detected four periods; we show the results in Fig. 1 and Table 1. We are aware that a search for multiple periods in *Hipparcos* photometry is difficult and can lead to spurious results (Eyer & Grenon 1998). However, the case of HD 209295 is so simple and convincing that an error in the analysis is considered improbable. The multiperiodicity leaves no doubt that HD 209295 is a bona fide γ Dor star.

HD 209295 is considerably hotter than all other γ Dor stars. Handler (1999a) suggested that the published Strömgren $(b - y)$ of this star (Twarog 1980) is too blue compared to $(B - V)$. Handler (1999b) obtained new Strömgren photometry and confirmed the

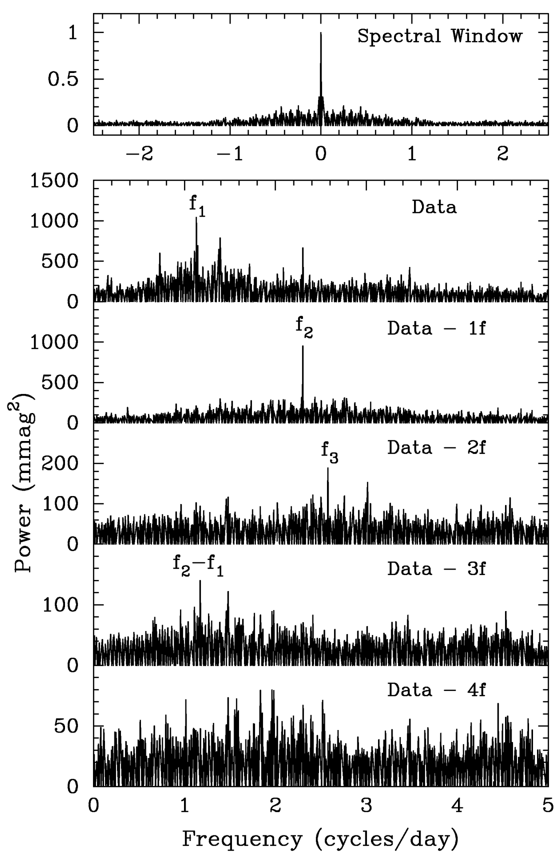

Figure 1. Spectral window and amplitude spectra of *Hipparcos* photometry of HD 209295 with consecutive pre-whitening of detected frequencies. The combination peak $f_2 - f_1$ is only considered significant because it occurs at a 'predicted' frequency.

Table 1. Multifrequency solution for the γ Dor variability of HD 209295 from *Hipparcos* observations. Formal error estimates were derived from Montgomery & O'Donoghue (1999). The signal-to-noise ratio (S/N) was calculated following Breger et al. (1993); a S/N $\geq$ 4 corresponds to a significant detection.

ID	Frequency (cycle d^{-1})	H_p Amplitude (mmag)	S/N
f_1	1.12957 ± 0.00002	37 ± 2	12
f_2	2.30222 ± 0.00003	31 ± 2	10
f_3	2.57579 ± 0.00005	16 ± 2	5
$f_4 = f_2 - f_1$	1.1726 ± 0.0001	12 ± 2	4

Table 2. Published $uvby\beta$ photometry of HD 209295. The differences in the magnitudes and photometric indices are consistent with stellar pulsation. When brighter the star it is bluer and the c_1 and H_β indices are larger.

V	$b-y$	m_1	c_1	β	Reference
7.32	0.149	0.182	0.819	2.781	Twarog (1980)
7.29	0.139	0.185	0.840	2.821	Handler (1999b)

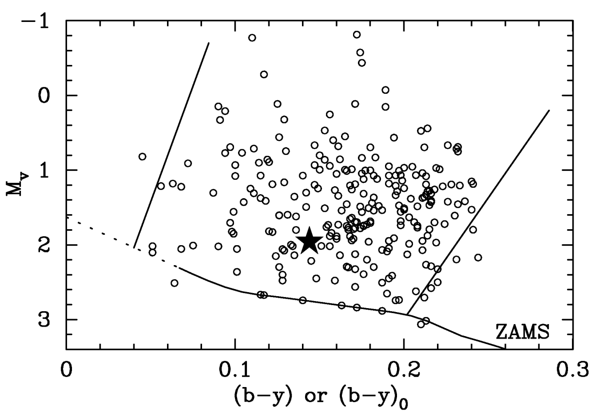

Figure 2. The location of HD 209295 (star symbol) in the colour–magnitude diagram compared to 252 known δ Sct stars (open circles) with available Strömgren photometry from the catalogue of Rodriguez, López-González & López de Coca (2000). The blue and red edges of the δ Sct instability strip (Rodriguez & Breger 2001) are indicated.

discrepancy (cf. Table 2). Grenier et al. (1999) made two measurements of the radial velocity of the star using an echelle spectrograph and the cross-correlation technique. They did not comment on binarity or any other peculiarity.

Using the mean of the Strömgren indices from Table 2 (which indicate zero reddening), the effective temperature and gravity of HD 209295 can be estimated. Kurucz's (1991) calibration yields $T_{\mathrm{eff}} = 7750 \pm 100$ K, $\log g = 4.10 \pm 0.05$.

The *Hipparcos* parallax of HD 209295 is 8.19 ± 0.72 mas. Using $V_0 = 7.32 \pm 0.01$, $BC = -0.01 \pm 0.01$, the parallax gives $\log L/\mathrm{L}_\odot = 1.15 \pm 0.08$. With $\log T_{\mathrm{eff}} = 3.889$ as determined above, $R/\mathrm{R}_\odot = 2.08 \pm 0.09$ and, by means of evolutionary tracks calculated using the Warsaw–New Jersey code (see e.g. Pamyatnykh et al. 1998), a mass of $1.84 \pm 0.07\,\mathrm{M}_\odot$ is determined. We can then also calculate a semi-independent second value for $\log g$, namely 4.07 ± 0.05, consistent with the previous value. HD 209295 is therefore the hottest γ Dor star known to date; it lies in the middle of the δ Sct instability strip on the main sequence (Fig. 2).

Because of its location in the colour-magnitude diagram, HD 209295 is a good candidate δ Sct star. Indeed, multiperiodic δ Sct pulsations were found by Handler & Shobbrook (2002), thus placing HD 209295 as a member of two classes of pulsating star. Spectroscopic and photometric follow-up observations were organized immediately after this discovery, and a multisite campaign was conducted in 2000 August. We report the results of these campaigns.

2 OBSERVATIONS

2.1 Optical photometry

As comparison stars, we used HD 207802 (B9/B9.5V, $V = 8.0$) and HD 209829 (F3V, $V = 7.7$) in our photoelectric photometry. Measurements were obtained at the 1.0-, 0.75- and 0.5-m telescopes of the Sutherland station of the South African Astronomical Observatory (SAAO), the 0.6-m telescope at Siding Spring Observatory (SSO) in Australia (Shobbrook 2000), and the 0.6-m Zeiss telescope at the Osservatório do Pico dos Dias (LNA, Brazil). Observations were conducted from 1999 October to 2000 October. Most measurements were obtained in 2000 August and September in a coordinated multisite effort. A journal of the observations is given in Table 3.

We used the Johnson B and V filters as well as the Cousins I_C filter (the latter only in the year 2000) with a total integration time of ~1 min in each filter as a compromise between good time resolution and maximum colour information. Apertures of 30–45 arcsec on the sky were used. Sky measurements were taken at suitable intervals depending on the brightness and proximity of the Moon.

The observing sequence was chosen to result in both good coverage for the short-period δ Sct pulsations and best long-term stability. We adopted the sequence C1-V-C2-V-C1... (C1 and C2 are the comparison stars and the V is the variable), which resulted in one variable star measurement every ~6 min. Supplementary observations of $UBV(RI)_C$ standard stars were also acquired.

Data reduction was performed in the standard way, i.e. corrections for coincidence losses, sky background and extinction were followed by calculating differential magnitudes between the comparison stars. The latter were examined for variability. It seems that one of the two stars is slightly variable on a time scale of about 1.1 or 10 d with a V amplitude of 2 mmag. We investigated whether this could be due to differential colour extinction and found no support for such an interpretation. As our programme star exhibits long-term variability with much higher amplitude, we cannot determine unambiguously which of the two stars is the potential variable, but we suspect HD 209829.

In any case, we proceeded by constructing a differential target star light curve relative to the measurements of both comparison stars. We standardized these magnitude differences by using the transformation equation slopes calculated from the standard star observations mentioned above. We note that the photometric zero-points of the different telescope/instrument combinations agreed to better than 2 mmag for each filter or colour used during the multisite campaign, but we experienced some difficulties with homogenizing the data from the discovery season. Finally, the time-base of our observations was converted to Heliocentric Julian Date (HJD). Most of the light curves obtained during the central part of the multisite campaign are shown in Fig. 3.

Table 3. Journal of the photometric observations. The measurements before HJD 2451600 were made in the Johnson *BV* system, whereas later observations utilized Johnson–Cousins BVI_C except for one night of *BV* observations, marked with an asterisk.

Telescope	Run start HJD −245 0000	Run length (h)	Observer
SAAO 0.75-m	1464.335	3.31	GH
SAAO 0.75-m	1465.249	6.34	GH
SSO 0.6-m	1467.033	2.78	RRS
SSO 0.6-m	1468.916	6.05	RRS
SSO 0.6-m	1491.937	2.35	RRS
SSO 0.6-m	1498.918	2.35	RRS
SAAO 0.5-m	1502.282	1.85	GH
SAAO 0.5-m	1503.268	2.62	GH
SAAO 0.5-m	1505.267	2.57	GH
SAAO 0.5-m	1507.310	1.08	GH
SAAO 0.5-m	1509.295	1.63	GH
SSO 0.6-m	1510.924	1.85	RRS
SAAO 0.5-m	1511.264	2.40	GH
SSO 0.6-m	1512.933	2.18	RRS
SSO 0.6-m	1513.926	0.94	RRS
SSO 0.6-m	1516.930	2.04	RRS
SSO 0.6-m	1517.921	1.20	RRS
SAAO 0.5-m	1518.266	0.86	LE
SAAO 0.5-m	1519.283	0.48	LE
SSO 0.6-m	1524.930	1.63	RRS
SSO 0.6-m	1754.110	3.41	RRS
SSO 0.6-m	1754.962	5.45	RRS
SAAO 0.75-m	1758.343	3.46	ERC
SSO 0.6-m	1759.947	8.11	RRS
SAAO 0.75-m	1761.343	7.87	ERC
SAAO 0.75-m	1762.364	7.25	ERC
SSO 0.6-m	1762.944	7.75	RRS
SAAO 0.75-m	1763.337	8.11	ERC
SAAO 0.75-m	1764.278	6.53	ERC
SSO 0.6-m	1767.227	2.28	RRS
SAAO 0.75-m	1768.241	10.25	GH
SAAO 0.75-m	1769.239	10.27	GH
LNA 0.6-m	1769.819	0.24	AB
SAAO 0.75-m	1770.234	10.37	GH
LNA 0.6-m	1770.514	6.84	AB
SAAO 0.75-m	1771.237	10.27	GH
LNA 0.6-m	1771.498	3.19	AB
SAAO 0.75-m	1772.238	10.27	GH
SAAO 0.75-m	1773.226	10.49	GH
SAAO 0.75-m	1775.223	4.99	GH
LNA 0.6-m	1775.575	5.59	AB
LNA 0.6-m	1776.651	3.91	AB
LNA 0.6-m	1777.486	7.56	AB
SSO 0.6-m	1777.904	6.14	RRS
SAAO 0.75-m	1778.493	3.67	GH
SAAO 1.0-m*	1785.256	9.94	GH
SSO 0.6-m	1785.918	8.45	RRS
SSO 0.6-m	1786.991	0.67	RRS
SSO 0.6-m	1787.898	9.58	RRS
SAAO 0.5-m	1789.242	8.74	GH
SSO 0.6-m	1789.935	8.52	RRS
SAAO 0.5-m	1791.337	1.27	GH
SAAO 0.5-m	1792.253	8.42	GH
SAAO 0.5-m	1850.284	1.51	DJJ
SAAO 0.5-m	1852.277	1.78	DJJ
SAAO 0.5-m	1853.332	0.41	DJJ
SAAO 0.5-m	1857.270	2.45	DJJ
SAAO 0.5-m	1858.276	1.82	DJJ
SAAO 0.5-m	1859.274	1.92	DJJ
SAAO 0.5-m	1862.278	2.04	DJJ
Total		280.35	

2.2 Infrared photometry

In addition to the optical data, L. A. Crause obtained infrared *JHKL* measurements on the night of 2000 September 1 using the 0.75-m telescope of the SAAO with the MkII infrared photometer (an upgraded version of the instrument described by Glass 1973). The data were reduced to the SAAO system by using standard stars defined by Carter (1990). As the infrared observations were obtained simultaneously with optical photometry, standard BVI_C-*JHKL* magnitudes could be calculated (Table 4). The star was approaching a local minimum in its light curve when these measurements were taken.

These optical and infrared colours are consistent with the spectral type of the star as inferred from standard relations (Drilling & Landolt 2000; Tokunaga 2000), but agree less well with the effective temperature determined from $uvby\beta$ photometry. However, this may be due to the high amplitude of the light variations. The total colour amplitude implies temperature variations of ≈ 500 K between light extrema, sufficiently large to explain the apparent discrepancy.

2.3 Spectroscopic observations

Spectroscopic observations of HD 209295 were obtained with three different telescopes. We used the 1.9-m telescope at SAAO, the 1.9-m telescope at Mt. Stromlo (MS) in Australia, and the 1.2-m Euler telescope at the European Southern Observatory (ESO) in Chile. A summary of these measurements can be found in Table 5.

The bulk of the data originated from SAAO using the GIRAFFE echelle fibre-fed spectrograph attached to the Cassegrain focus of the 1.9-m telescope. The GIRAFFE spectrograph has a resolving power of about 32 000. The 1024×1024 TEK CCD chip gives a resolution of 0.06–0.09 Å per pixel. A ThAr arc lamp was used for wavelength calibration with arc spectra taken at regular intervals to calibrate possible drifts. The wavelength range was 4400–6680 Å, spread over 45 orders. Exposure times were normally 10 min for a signal-to-noise (S/N) ratio of about 30–60. A total of 422 spectra of HD 209295 was obtained during three observing runs.

The spectroscopic observations at MS were obtained with the coude echelle spectrograph on the Mount Stromlo 1.9-m telescope. Spectra with a resolution of ~ 0.15 Å at Hα were recorded on a 2048×4096 pixel TEK CCD. The wavelength range obtained with this set-up was 4500–6900 Å, spread over 42 orders. Exposure times were between 17.5–20 min for a S/N ratio of about 25–60. A ThAr arc lamp was used for wavelength calibration. As a result of poor weather, a total of only 15 spectra of HD 209295 was obtained.

The spectroscopic observations in Chile were performed with the Swiss 1.2-m Ritchey-Chretien Euler telescope at ESO, La Silla. Euler is equipped with a high-resolution echelle spectrograph, CORALIE, and a 2k × 2k CCD camera with 15-μm pixels. The resolving power amounts to 50 000 and the total wavelength range is 3900–6800 Å in 68 orders, without any gaps in the coverage. The CORALIE spectra are extracted on-line following a standard echelle reduction procedure. In the case of our measurements, wavelength calibration utilized the most recently obtained ThAr spectrum. Each order of the stellar spectrum was then divided by the blaze function. For a full description of the reduction scheme we refer the reader to Baranne et al. (1996). The integration times were adapted to the atmospheric conditions (seeing, presence of clouds) and ranged from about 15 to 18 min. The typical S/N ratio was ≈ 30. In total, 38 spectra were obtained during one week.

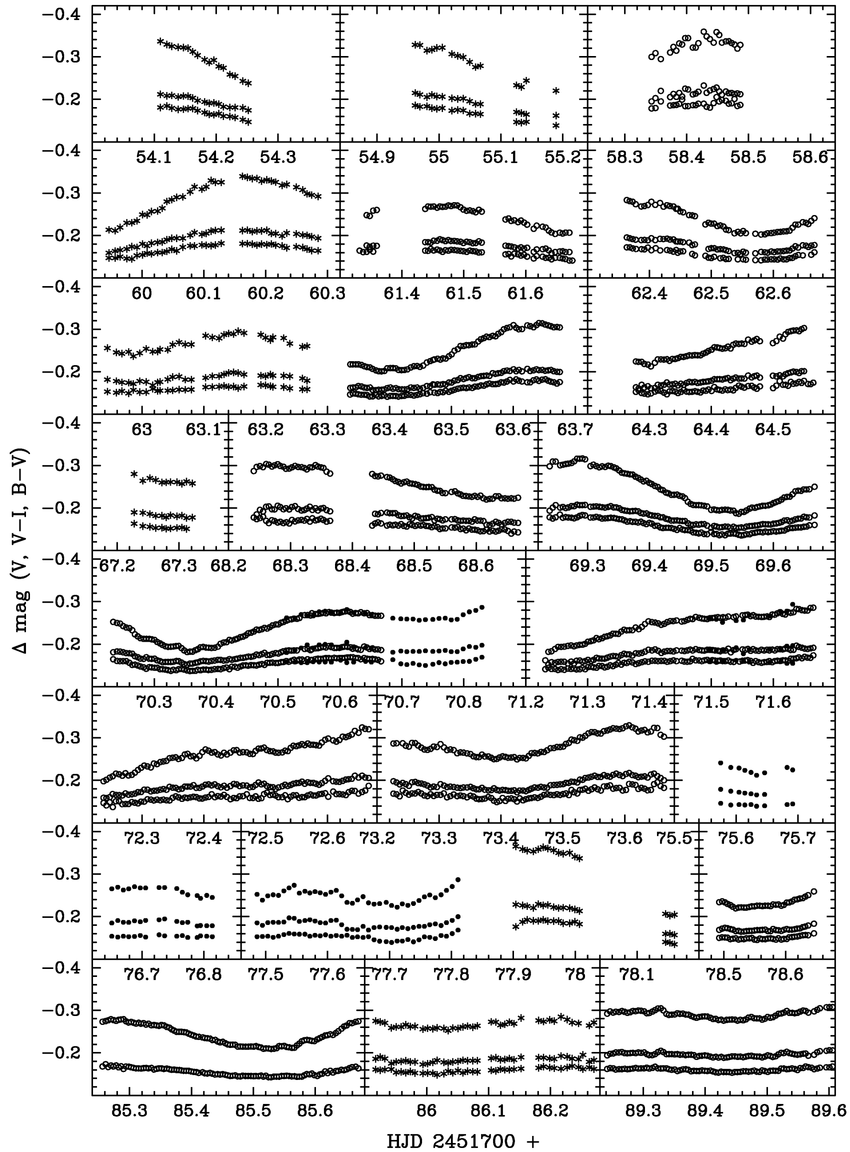

Figure 3. Light curves of HD 209295 obtained during the multisite campaign in 2000 August. The asterisks are measurements from SSO, the open circles those from SAAO and the filled circles are LNA data. The upper light curves in each panel are the V data, the $(V - I_C)$ variations are shown in the middle and the lowest are the $(B - V)$ light curves. Zero-points are relative to HD 209829; the V zero-point is shifted by $+0.11$ mag for a better display. Note the multiperiodic slow and rapid light variability and the corresponding colour changes.

Table 4. Standard optical and infrared magnitudes of HD 209295 as measured on HJD 245 1792.462.

Filter	Magnitude
B	7.623 ± 0.005
V	7.370 ± 0.005
I_C	7.070 ± 0.005
J	6.872 ± 0.009
H	6.727 ± 0.007
K	6.746 ± 0.008
L	6.721 ± 0.081

In contrast to the photometric observations, the spectroscopic measurements were not reduced centrally. For the SAAO data, we used the local reduction software (see http://www.saao.ac.za/facilities/) for corrections for bias and flat-field, order extraction and wavelength calibration. The same reduction steps for the MS data were performed in IRAF.

3 ANALYSIS

3.1 The photometry

Our frequency analysis was performed with the programme PERIOD 98 (Sperl 1998). This package applies single-frequency power spectrum analysis and simultaneous multifrequency sine-wave fitting, but also has some advanced options which will be described

Table 5. Log of the spectroscopic observations of HD 209295. The date with respect to HJD 245 0000, the run lengths, the mean integration times *t* and the number of spectra, *N*, are given.

Site	Run start HJD − 245 0000	Length (h)	*t* (s)	*N*	Observer
SAAO	1501.250	3.02	600	16	LAB
SAAO	1502.268	2.39	600	13	LAB
SAAO	1503.262	2.39	600	13	LAB
SAAO	1504.249	2.99	600	16	LAB
MS	1505.029	0.33	1200	1	DJJ
SAAO	1505.255	2.42	600	13	LAB
SAAO	1506.250	0.35	600	2	LAB
SAAO	1507.297	1.29	600	7	LAB
SAAO	1508.249	2.81	600	15	LAB
SAAO	1509.251	2.54	600	12	LAB
MS	1509.960	0.68	1200	3	DJJ
MS	1510.924	2.22	1050	6	DJJ
SAAO	1511.256	2.42	600	13	LAB
MS	1511.942	1.62	1050	5	DJJ
SAAO	1512.254	2.44	600	13	LAB
ESO	1762.741	2.70	975	8	TM
ESO	1763.700	3.69	1100	10	TM
SAAO	1765.347	0.17	600	1	CK
ESO	1765.744	3.69	1100	8	TM
ESO	1766.703	2.92	1100	7	TM
SAAO	1768.347	8.08	1095	21	CK
ESO	1768.802	1.91	1100	5	TM
SAAO	1769.336	8.21	1016	24	CK
SAAO	1770.325	6.95	1000	21	CK
SAAO	1771.345	8.12	975	24	CK
SAAO	1772.345	7.70	1200	20	CK
SAAO	1773.354	7.70	1000	23	CK
SAAO	1774.406	1.34	1400	3	CK
SAAO	1776.328	0.90	1500	2	CK
SAAO	1777.388	1.23	1600	3	CK
SAAO	1778.348	5.55	1557	7	CK
SAAO	1849.267	2.42	600	12	LAB
SAAO	1850.271	2.56	600	14	LAB
SAAO	1851.274	2.50	600	10	LAB
SAAO	1852.262	2.81	600	15	LAB
SAAO	1853.258	2.68	600	14	LAB
SAAO	1855.354	0.55	700	2	LAB
SAAO	1856.258	2.44	600	13	LAB
SAAO	1857.265	2.47	600	13	LAB
SAAO	1858.264	2.25	600	12	LAB
SAAO	1859.263	2.21	600	12	LAB
SAAO	1860.265	2.23	600	12	LAB
SAAO	1862.262	2.30	600	12	LAB
Total		128.19		476	

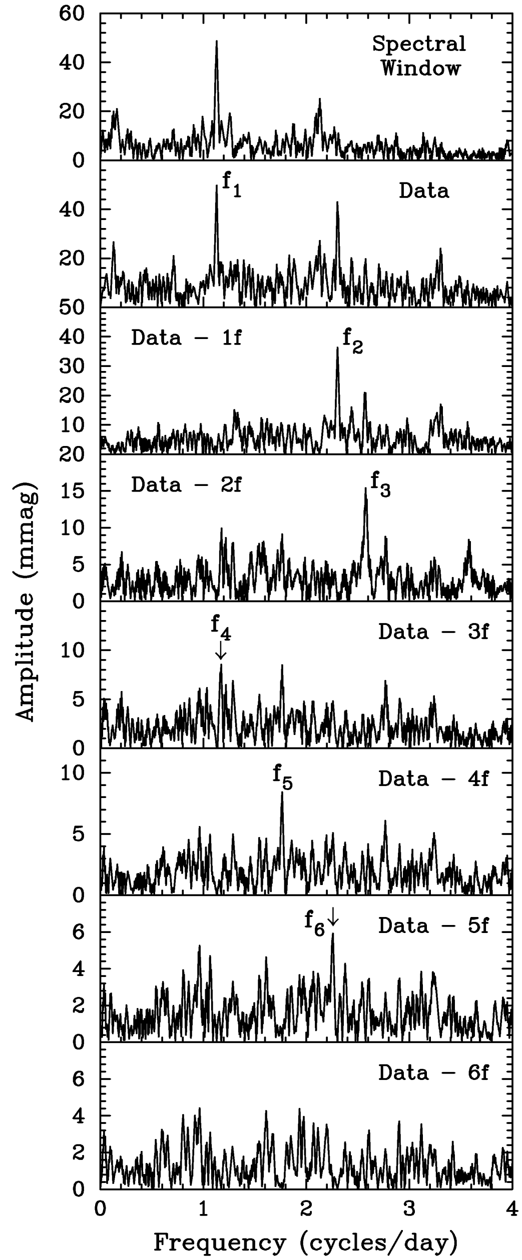

Figure 4. Top panel: Spectral window of the *B*-filter time-series photometry of HD 209295 obtained in the year 2000. The other panels show the amplitude spectra of the data with consecutive pre-whitening. Six significant periodicities are present.

later as necessary. We calculated the spectral window and amplitude spectra of our data as well as the amplitude spectra of residual light curves after the previously identified periodicities had been removed using a multiperiodic fitting algorithm. Similar analyses were performed for all the three filters used. We adopted the mean frequencies for our final solution.

Our analysis was concentrated on multisite data from the year 2000. As a result of the different telescopes and detectors used, the 1999 data analysis is complicated by zero-point calibration problems. Also, the data runs were rather short in 1999 and the possibility exists that the star may have had a different amplitude at this time. We used the 1999 data only when the zero-point problems were relatively minor.

3.1.1 The γ Dor pulsations

In Fig. 4 we show amplitude spectra of the *B*-filter data with consecutive pre-whitening by the low frequencies. For the 2000 data we calculated the window function as the Fourier transform of a single sinusoid with frequency 1.129 cycle d^{-1} and amplitude of 50 mmag. Because of the multisite coverage, aliasing is not a problem. We detected six significant frequencies in the light variations. The first four frequencies were already shown in Table 1.

The significance of a detection was estimated using the S/N ratio criterion of Breger et al. (1993). The residuals after pre-whitening this frequency solution suggest that more periodicities are present. The highest peaks in the residual spectra are located at the same frequencies in each of the *B*, *V*, and I_C data sets, and the 'noise

Table 6. Results of a multifrequency solution for HD 209295 derived from the photometric data. Frequency error estimates range from ± 0.0001 cycle d^{-1} to ± 0.002 cycle d^{-1}, for the strongest and weakest γ Dor mode, respectively, and ± 0.005 cycle d^{-1} for the δ Sct mode. Signal-to-noise ratios following Breger et al. (1993), calculated from the *B* filter data from the year 2000, are also given. A *S/N* > 4 is taken to be a significant detection of a signal.

			Measurements from the year 2000			Measurements from the year 1999	
ID	Frequency (d^{-1})	*S/N*	*B* amplitude (mmag) ± 0.4	*V* amplitude (mmag) ± 0.3	*I* amplitude (mmag) ± 0.2	*B* amplitude (mmag) ± 0.6	*V* amplitude (mmag) ± 0.5
γ Dor frequencies							
f_1	1.1296	35.9	49.6	38.5	23.0	35.9	26.9
f_2	2.3024	28.3	39.1	28.3	15.5	24.5	17.3
f_3	2.5758	11.6	16.0	11.4	6.2	21.7	15.8
f_4	1.1739	9.0	12.4	7.9	4.6	5.4	4.9
f_5	1.7671	7.0	9.7	7.4	4.1	11.0	8.5
f_6	2.2572	5.4	7.4	5.3	3.1	n/a	n/a
δ Sct frequency							
f_A	25.9577	5.3	1.8	1.4	0.8	1.5	1.3

level' decreases from *B* to I_C. This suggests that most of the 'noise' in the blue may well be due to additional periodicities. The derived frequencies and amplitudes are listed in Table 6.

3.1.2 The δ Sct pulsations

The zero-point uncertainties in the data set from 1999 have little effect in the frequency range in which the δ Sct pulsations are present. Consequently, we can incorporate these observations into the frequency analysis. We therefore pre-whitened the data by the six-frequency solution discussed above from the 2000 data. For the 1999 data we pre-whitened by the first five of these frequencies which were found in common with the analysis of the 2000 data. This pre-whitening is important because low-frequency variations can artificially increase the noise level in the high-frequency domain through spectral leakage. The amplitude spectrum of the combined *B*-filter data and subsequent pre-whitening are shown in Fig. 5.

Although several peaks in the amplitude spectra in Fig. 5 are prominent, only one signal is a significant detection. This is surprising, as typical multiperiodic beating is seen in the light curves of Fig. 3, e.g. HJD 245 1770.35 versus HJD 245 1770.55. We therefore checked whether these signals could be non-coherent by analysing several subsets of data. No evidence for short-lived δ Sct type variations or variations with changing amplitude was found. In fact, several of the more conspicuous signals were present in all data subsets (e.g. in different subsets of the multisite data or in individual filters). Thus we suspect that several such periodicities may be real. A multifrequency solution with f_A and the three next strongest variations in the δ Sct regime fits the short-term variations reasonably. The corresponding peaks are marked with arrows in the lowest panel of Fig. 5. The frequency range of possibly excited δ Sct pulsations can be constrained to 10–32 cycle d^{-1}. We list the results of our frequency analysis of the photometric data in Table 6.

We need to make two remarks here. First, the results for the data from 1999 are only listed for completeness in Table 6. We suspect that the amplitudes of the γ Dor pulsations in this data set are artificially decreased not only because of zero-point problems, but also because of poor data sampling. Secondly, we stress that these

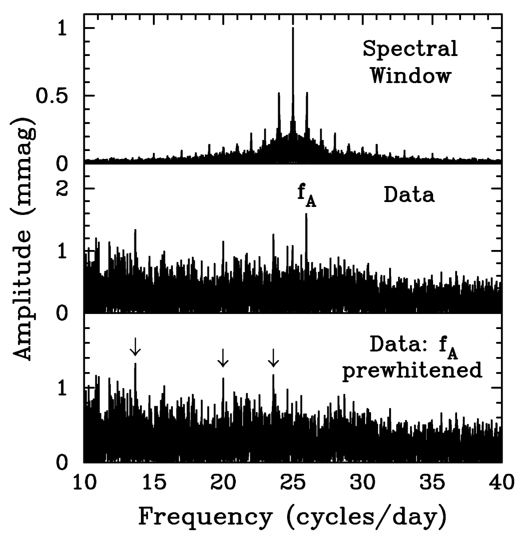

Figure 5. The spectral window of the combined residual *B*-filter data and amplitude spectra in the frequency domain of the δ Sct pulsations. Only one frequency is convincingly detected, but the presence of several low-amplitude modes in a range of 12–25 cycle d^{-1} is suspected; some possible further frequencies are indicated.

are only preliminary results. We will revisit the frequency analysis in Section 3.4.

3.2 Spectroscopic analyses

The first step in the analysis is to rectify the spectra, i.e. to place the continuum. This was done by using an unbroadened synthetic spectrum with $T_{\rm eff} = 7500$ K, $\log g = 4.00$ as a template, using the SPECTRUM code (Gray & Corbally 1994). A running median of each echelle order was divided by the corresponding section of the synthetic spectrum and taken to represent the response function of the instrument. A polynomial of degree 5 was fitted to the response function and used to correct the observed spectrum. The result is the rectified spectrum of the star used for cross-correlation.

3.2.1 *Radial velocities*

For each order, the observed rectified spectrum was correlated with the corresponding section of the synthetic spectrum after removing the unit continuum. The resulting correlation function is, in effect, the mean line profile with the continuum removed. The 'radial velocity' for each order is obtained by fitting a quadratic to the correlation function and finding the position of the maximum. The mean radial velocity from all the orders is also obtained. A standard error of typically $1-3\,\mathrm{km\,s^{-1}}$ was found for the SAAO spectra.

A few of the spectroscopic observations listed in Table 5 turned out to be of a quality too poor for further use. Four spectra were discarded, and 472 were retained. Some slight deviations ($<0.5\,\mathrm{km\,s^{-1}}$) in the seasonal radial velocity zero-points in the SAAO spectra were rectified by means of telluric lines.

An immediate finding from our time-resolved spectroscopy is that the radial velocities of HD 209295 are strongly variable. The total radial velocity amplitude is in excess of $100\,\mathrm{km\,s^{-1}}$, which cannot be due to the pulsations of the star. HD 209295 must be a member of a binary system.

We therefore attempted to determine the orbital period. Visual inspection of the radial velocity curve suggests $P_{\mathrm{orb}} \sim 3\,\mathrm{d}$, and Fourier analysis (upper panel of Fig. 6) indeed implies an orbital frequency near $0.32\,\mathrm{cycle\,d^{-1}}$, but our data set is affected by aliasing. Pre-whitening trial frequencies suggested that the shape of the orbital radial velocity curve is not sinusoidal.

This is a situation in which use of the residualgram method (Martinez & Koen 1994) is indicated, which is based on a least-squares fit of a sine wave with M harmonics. The residual sum of squares at each trial frequency is evaluated; M can be chosen freely. In that way, alias ambiguities can be circumvented by taking advantage of the information in the Fourier harmonics. Preliminary trials with Fourier analysis suggested that $M = 3$ is a good choice for a residualgram, as shown in the lower panel of Fig. 6.

The residualgram method eliminated the aliasing problem for the determination of the orbital frequency. We use its result for a refinement of the orbital frequency by using PERIOD 98 (Sperl 1998). This leads to an improved orbital frequency of $f_{\mathrm{orb}} = 0.32198\,\mathrm{cycle\,d^{-1}}$ ($P_{\mathrm{orb}} = 3.10575\,\mathrm{d}$).

To determine the orbital solution from our radial velocities, we first used the SAAO data only, which are the most extensive (almost 90 per cent of all spectra) and are homogeneous. We weighted the individual measurements based on their standard errors. Measurements with standard errors smaller than $2\,\mathrm{km\,s^{-1}}$ were given a weight of 1; the weights decreased down to 0.2 for a few measurements with standard errors between $8-9\,\mathrm{km\,s^{-1}}$. We determined an initial orbital solution from these data with an updated version (Strassmeier, private communication) of the differential-correction method (Barker, Evans & Laing 1967).

Using the initial parameters from these methods, we examined the relative zero-points of the three blocks of SAAO measurements; no third body in the system was detected. We then fitted all the campaign data with these orbital parameters and examined the zero-points of the measurements from the other sites. The ESO radial velocities needed to be shifted by $+7\,\mathrm{km\,s^{-1}}$. We then

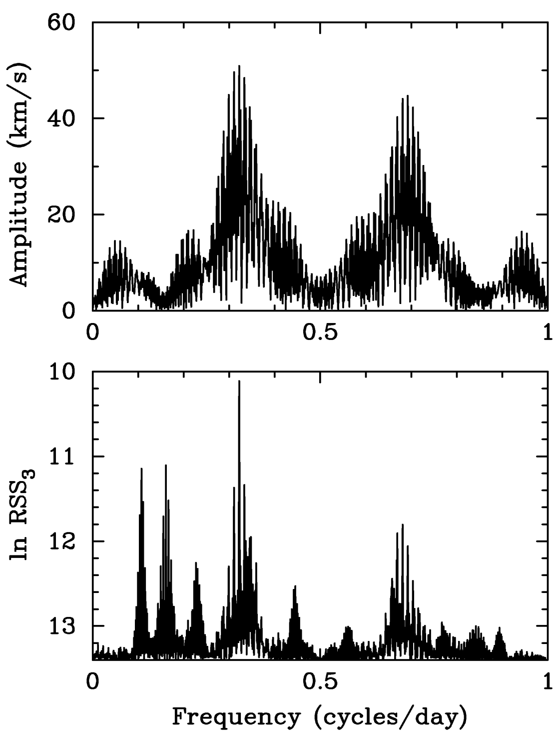

Figure 6. Upper panel: Fourier amplitude spectrum of the radial velocities of HD 209295. An orbital period near 3 d is implied, but severe aliasing is present. Lower panel: residual sum of squares spectrum of a three-harmonic fit (RSS_3) to the radial velocities. Although some power leaks into subharmonics, the correct orbital frequency is now unambiguously detected.

Table 7. The orbital solution from radial velocities of HD 209295. The symbols have their usual meanings; ω is the argument of periastron.

Parameter	Unit	Value
P_{orb}	(d)	3.10575 ± 0.00010
γ	($\mathrm{km\,s^{-1}}$)	-23.7 ± 0.4
K	($\mathrm{km\,s^{-1}}$)	54.2 ± 0.7
e		0.352 ± 0.011
ω	(°)	31.1 ± 2.0
T_0	(HJD)	$245\,1771.864 \pm 0.014$
$a_1 \sin i$	($R_\odot$)	3.11 ± 0.04
$f(m)$	($M_\odot$)	0.042 ± 0.002

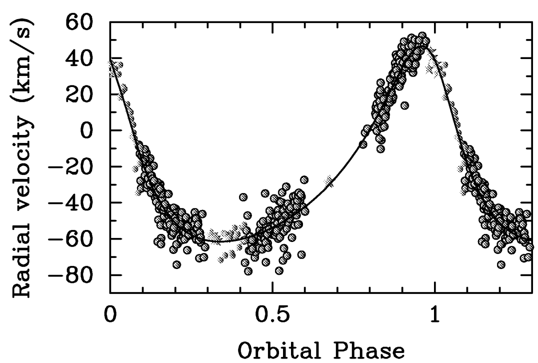

Figure 7. Radial velocities of HD 209295 phased with the orbital solution (solid line). Open circles are SAAO radial velocities, filled circles are ESO radial velocities and star symbols denote the MS measurements. We note that although the number of spectra from ESO and MS is small, they cover important phases of the orbit and are therefore quite valuable. The formal radial velocity errors quoted in Section 3.2.1 underestimate the true errors.

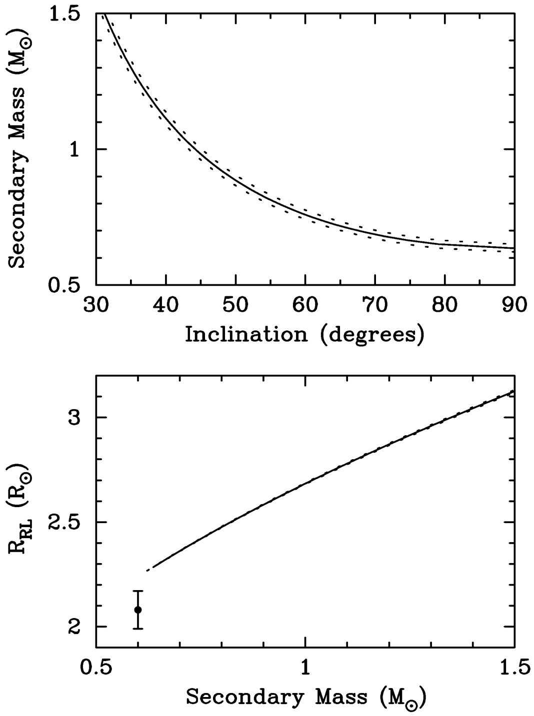

Figure 8. Upper panel: the mass of the companion of HD 209295 versus orbital inclination. The solid line is for a primary mass of $1.84\,M_\odot$ as inferred in Section 1.1, the dotted lines represent the 1σ limits of this determination. Lower panel: the Roche Lobe radius of the HD 209295 primary at periastron depending on secondary mass, again for $M = 1.84 \pm 0.07\,M_\odot$. The filled circle with the error bar shows our radius determination for HD 209295 from Section 1.1.

calculated our final solution from all the data, with the mean radial velocity fixed. This orbital solution is shown in Table 7 and Fig. 7.

We note that an extrapolation of our orbital solution to the measurements of Grenier et al. (1999) quoted in the introduction results in a good fit. The two measurements by these authors were taken at similar orbital phases, which explains the comparably small radial velocity difference.

Having solved for the orbital parameters, we can now discuss two issues: the nature of the companion and the possibility of mass transfer in the system. In the upper panel of Fig. 8, we show the dependence of the secondary mass on orbital inclination for various values of the primary mass. From this, we see that $M_2 > 0.62\,M_\odot$. The lower panel of Fig. 8 shows that HD 209295 may come close to filling its Roche Lobe (calculated with the approximation by Eggleton 1983) at periastron if the companion has a small mass. However, we will show in Section 4.1 that the companion is probably too massive for the primary to fill its Roche Lobe.

Assuming that the companion of HD 209295 is a main-sequence star, its absolute magnitude $M_v > 4.4$; otherwise its spectral lines would be detected. A spectral type of G0 and later is therefore suggested with a mass $< 1.05\,M_\odot$ (Drilling & Landolt 2000). Our photometry also shows no eclipses (within a conservative limit of 4 mmag), allowing us to infer the constraint $i < 80°$. A main-sequence companion of $0.62 < M_2 < 1.05\,M_\odot$ should be detected by means of its infrared excess. We will examine this in Section 3.5.

After removal of the orbital variation, the residual radial velocities can be searched for pulsational signals. The amplitude spectrum of these residuals can be found in Fig. 9. Although there are signals in the same frequency range as in the photometry, none give a reliable detection according to the signal-to-noise ratio criterion of Breger et al. (1993). Consequently, we need to continue the examination of the spectroscopic evidence of the pulsations of HD 209295 by looking at the line-profile variations.

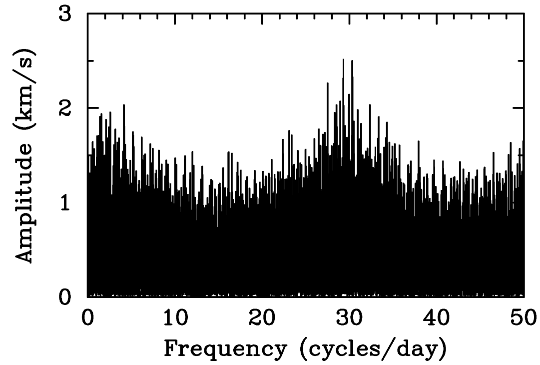

Figure 9. The amplitude spectrum of the residual radial velocities of HD 209295 after removing the orbital solution.

3.2.2 *Projected rotational velocity*

The correlation profiles for each season can be co-added (after correcting with our orbital solution) to form what is essentially a mean line profile. The projected rotational velocity, $v \sin i$, can be determined by fitting a model profile of a rotating star. The model is spherical with a linear limb darkening coefficient $u = 0.3$ and the visible hemisphere is divided into a large number of surface elements. The intrinsic line profile for each element summed over the hemisphere, weighted according to limb darkening, is computed. The projected rotational velocity and mean radial velocity are adjusted until a best fit to the observed profile is obtained. We obtain $v \sin i = 108 \pm 10\,\mathrm{km\,s^{-1}}$ for the SAAO measurements from 1999 and the second set from 2000, and $v \sin i = 98 \pm 10\,\mathrm{km\,s^{-1}}$ for the first data set of the year 2000. Because of the uncertainty in the wings of the correlation profile, the fit was performed using the part of the profile within $90\,\mathrm{km\,s^{-1}}$ of the line centre.

3.2.3 *The high-order profile variations*

In a recent paper on the δ Sct star 38 o^1 Eri, Balona (2000) was able to show that pulsation modes of high spherical degree ℓ are easy to resolve in stars with moderate to high rotational velocities. Bearing in mind the result from the previous paragraph, HD 209295 falls within this category. We will only use the SAAO spectra for the following analysis, as these are the most homogeneous and best sampled.

Line profile variations due to modes of high degree are seen as moving subfeatures in the correlation profiles of the spectra used to determine the radial velocities. As a particular subfeature crosses the centre of the profile, it determines the radial velocity. A short while later another travelling subfeature will appear and the radial velocity will suddenly change. These discontinuous jumps are partly responsible for the rather high errors of the radial velocities.

From the spacing of the travelling subfeatures, we estimate that the spherical degree is $\ell \approx 5$. To enhance the profile variations, we

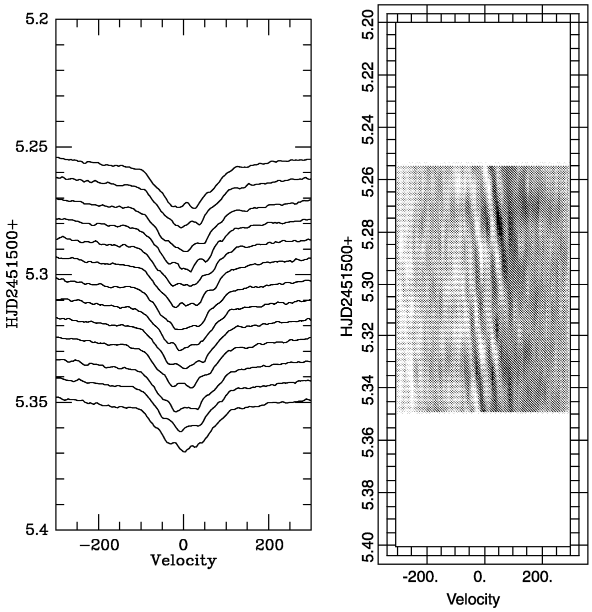

Figure 10. Left-hand panel – correlation function; right-hand panel – grey-scale difference after removing the correlation function. The data are from the 1999 season. The abscissa is in km s^{-1} and the ordinate is the HJD measured from HJD 245 1500.000.

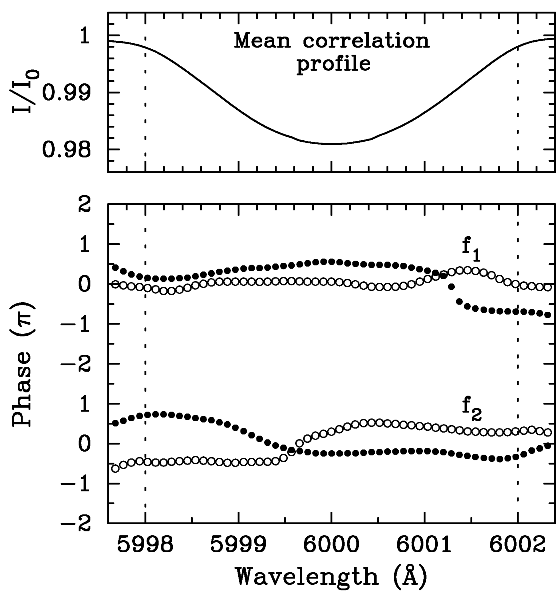

Figure 11. Phase diagram for two modes of HD 209295 (lower panel) through the correlation profile (upper panel), which is arbitrarily centred at 6000 Å. The full circles denote the phases of the mode frequency, and the open circles that of its first harmonic. The zero-points in the phases are arbitrary. The dotted vertical lines indicate $v \sin i$, as determined in Section 3.2.2, translated into units of wavelength. This is also the position in the correlation profile where we determine the total phase change.

removed the orbital motion and constructed the mean correlation profile from the SAAO data. Each correlation profile was divided by the mean profile to construct 'difference' profiles at the given times. The moving features are most clearly seen when these difference profiles are arranged in a time sequence and converted to a grey-scale image. An example is shown in Fig. 10.

Table 8. The total phase variation of the mode frequencies $\Delta\phi$, their first harmonics $\Delta\phi_1$, and the implied mode identifications following Telting & Schrijvers (1997).

ID	$\Delta\phi_0$ (π rad)	$\Delta\phi_1$ (π rad)	ℓ	$\lvert m\rvert$
f_1	0.85	−0.05	1	1
f_2	1.06	−0.77	1	1

While it is clear from Fig. 10 that periodic high-order line profile variations are present, it is not possible to determine the frequencies from the radial velocities alone, as shown before. Clearly, the radial velocity is a poor indicator for modes of high degree.

A common method to determine periodicities in line profile variations is to calculate the periodogram along wavelength bins throughout the line profile, or across the correlation profile. Most of the signal in this analysis is located at frequencies very close to the orbital period and its aliases, suggesting that the removal of the orbital variation did not work satisfactorily. However, we found the signatures of two previously detected modes in the line profiles, although they cannot be detected without prior knowledge. These are the photometric γ Doradus modes f_1 and f_2.

This finding gives us the possibility to attempt a mode identification with the method proposed by Telting & Schrijvers (1997). This technique utilizes the phase change of a mode as it progresses through the line profile, and provides some simple mode identification diagnostics depending on the total phase change of the mode frequency and its first harmonic (e.g. $\Delta\phi_0 \approx \pi\ell$). We calculated these phase changes for the two modes which we think are present and we show their behaviour through the correlation profile in Fig. 11. The mode identification implied by this analysis is summarized in Table 8.

We note that Telting & Schrijvers (1997) have given error estimates for the mode identifications with this method with ± 1 for ℓ and ± 2 for m. The identifications are plausible: f_1 and f_2 have high photometric amplitude.

3.3 Combining the spectroscopic and photometric information

Comparing the frequencies of the γ Dor pulsations in Table 6 to the orbital frequency we see that the photometric mode f_3 corresponds exactly to $8f_{\mathrm{orb}}$, and f_6 is, within the errors, consistent with $7f_{\mathrm{orb}}$. As noted in Section 1.1, the relation $f_4 = f_2 - f_1$ is also present within the mode frequencies.

Consequently, we revisited the frequency analysis of the photometric data. We again restricted ourselves to the data from 2000. This time, however, we used PERIOD 98's capability to fix signal frequencies to certain values, in our case integer multiples of the orbital frequency, and to perform non-linear least-squares fits with frequencies thus fixed.

We started by using the six γ Dor frequencies in Table 6, and proceeded by the usual pre-whitening procedure. The corresponding amplitude spectra can be found in Fig. 12; they are generated by combining the B-filter residuals with the V-filter residuals multiplied by a factor of 1.29.

The highest-amplitude peak in the upper panel of Fig. 12 does, indeed, correspond to $3f_{\mathrm{orb}}$. In addition $5f_{\mathrm{orb}}$ (second panel of

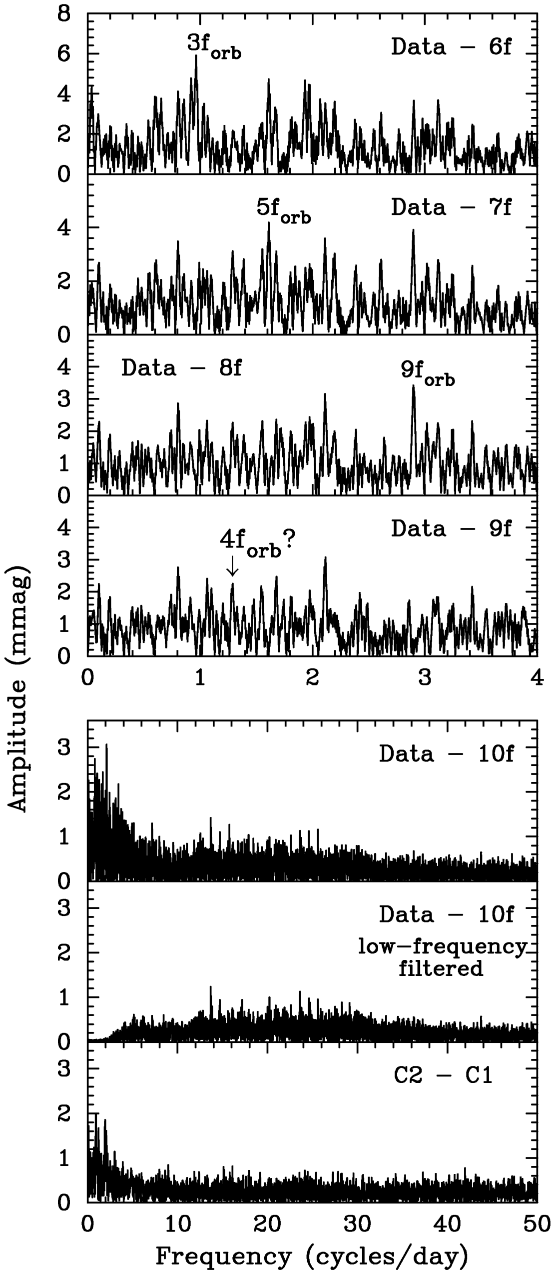

Figure 12. Top panel: the amplitude spectrum of the combined *B* and scaled *V*-filter residuals of HD 209295 after subtraction of the frequency solution of Table 6. Another harmonic of the orbital frequency is detected. In the following three panels we show the effects of further pre-whitening. All new detections are again harmonics of f_{orb}. Third panel from bottom: the residual amplitude spectrum in a wider frequency range. Second panel from bottom: the residual amplitude spectrum after filtering the residual low-frequency variations. Bottom panel: amplitude spectrum of the differential magnitudes of the comparison stars.

Fig. 12) and $9f_{\mathrm{orb}}$ (third panel of Fig. 12) are also found. This latter frequency corresponds to exactly $f_1 + f_5$. We therefore fixed this frequency combination to its exact value before proceeding. After pre-whitening these frequencies, some peaks, including one at $4f_{\mathrm{orb}}$, are still visible in each filter, but not at a level considered significant.

The third panel from the bottom of Fig. 12 shows the residual amplitude spectra in a wider frequency range after pre-whitening by the δ Sct mode, f_A. Again, there is evidence of additional γ Dor and weak δ Sct periodicities. The referee suggested to filter out the slow variability to examine the claimed δ Sct variability further. This is done in the second panel from the bottom of Fig. 12; albeit somewhat affected by the filtering, the additional δ Sct variations remain with similar amplitudes. They are therefore not artefacts from spectral leakage of the low frequencies. In the lowest panel of Fig. 12 we show the amplitude spectrum of the comparison star data. Although the number of observations of each comparison star is half that of the program star, the noise level in this periodogram is lower still, again suggestive of further periodicities below the detection level.

In Table 9 we show the final multifrequency solution for the 2000 data set. The corresponding results for 1999 are of little value, as the data sampling is too poor to attempt such a fit. Error estimates are formal values following Montgomery & O'Donoghue (1999). While they should be quite realistic for the δ Sct modes, they probably underestimate the errors for the γ Dor modes by a factor of 3–4.

The rms residual errors per single data point for this solution are 7.0 mmag in the *B* filter, 5.7 mmag in the *V* filter and 4.5 mmag in the *I* filter. These values again suggest undetected periodicities, because the rms scatter of a single comparison star measurement is 5.1 mmag in *B*, 4.0 mmag in *V* and 4.2 mmag in *I*.

Another estimate of the orbital period can be made from the frequency analysis. We find $P_{\mathrm{orb}} = 3.1057 \pm 0.0010$, consistent with the determination in Section 3.2.1. We have examined the residual light curve for possible ellipsoidal variations, but found none exceeding 2 mmag. Finally, one might suspect that $f_6 = 2f_1$, but a fit assuming this relation gives a significantly poorer solution than the one listed in Table 9.

3.4 Attempts at mode identification from colour photometry

The main reason for observing HD 209295 in more than one filter was to attempt a mode identification. This method relies on comparing theoretical amplitude ratios and phase differences of the variations in different wavebands with the observed values. The high amplitude of the light variations of HD 209295 makes the star very well suited for this method. Because of the very low amplitude of the δ Sct pulsations, only the γ Dor modes are considered. However, our calculations indicate that the amplitude ratios and phase differences for the δ Sct mode are consistent with pulsation.

We first attempted to apply the method developed by Koen et al. (1999) to the γ Dor modes. This technique uses the observed amplitude ratios and phase differences in all filters simultaneously. Unfortunately, no meaningful results were obtained. We then constructed two-colour diagnostic diagrams showing amplitude ratio as a function of phase difference (Watson 1988). In such diagrams, the theoretically determined areas of interest are specified and compared with the observations. We used the Warsaw–New Jersey stellar evolution and W. A. Dziembowski's NADROT pulsation code for models of 1.8 and 1.9 $M_{\odot}$ with effective temperatures between 7250 and 7800 K. These models span the possible range of parameters for HD 209295. We then computed theoretical amplitude ratios and phase shifts for the eigenmodes of those models following Balona & Evers (1999) and examined their location in the corresponding diagrams. We noticed that (except for a few combinations of Q and ℓ) the results clustered in well-defined regions depending on ℓ. Hence, we defined those regions

Table 9. The final multifrequency solution for HD 209295 from all the year 2000 photometry. Pulsational phases for mean light level are given with respect to a time of periastron passage, HJD 245 1771.864. Amplitude signal-to-noise ratios are calculated from Fig. 12.

ID	Combination	Frequency (d^{-1})	*S/N*	*B* Ampl. (mmag) ± 0.3	*B* phase (°)	*V* Ampl. (mmag) ± 0.2	*V* phase (°)	*I* Ampl. (mmag) ± 0.2	*I* phase (°)
γ Dor frequencies									
f_1		1.12934 ± 0.00005	63.7	50.3	−39.4 ± 0.3	38.9	−40.3 ± 0.3	23.5	−42.6 ± 0.4
f_2		2.30217 ± 0.00006	49.9	39.4	−115.4 ± 0.4	28.7	−116.4 ± 0.4	15.4	−117.0 ± 0.6
f_3	$8f_{\rm orb}$	2.57593 ± 0.00011	23.2	18.3	66.5 ± 0.8	13.2	67.2 ± 0.9	7.3	64.3 ± 1.3
f_4	$f_2 - f_1$	1.17283 ± 0.00004	14.4	11.4	−80.4 ± 1.3	7.6	−73.3 ± 1.5	4.0	−68.5 ± 2.4
f_5	$9f_{\rm orb} - f_1$	1.76859 ± 0.00005	13.6	10.8	96.5 ± 1.3	8.2	95.4 ± 1.4	4.8	86.2 ± 2.0
f_6	$7f_{\rm orb}$	2.25394 ± 0.00011	10.6	8.4	2.0 ± 1.7	6.6	−1.0 ± 1.8	3.5	2.0 ± 2.8
f_7	$3f_{\rm orb}$	0.96597 ± 0.00011	8.9	7.0	−39.2 ± 2.0	6.2	−35.9 ± 1.9	4.9	−33.3 ± 1.9
f_8	$5f_{\rm orb}$	1.60996 ± 0.00011	5.8	4.6	−162.1 ± 3.1	3.9	−158.6 ± 3.0	1.9	−173.9 ± 5.2
f_9	$9f_{\rm orb}$	2.89792 ± 0.00011	5.7	4.5	47.0 ± 3.2	3.5	48.9 ± 3.3	2.2	53.5 ± 4.3
δ Sct frequency									
f_A		25.9577 ± 0.0015	5.2	1.8	158.9 ± 8.3	1.4	162.8 ± 8.3	0.8	179.1 ± 12.2
	$f_{\rm orb}$	0.32199 ± 0.00011							

as our regions of interest and compared the observations to them. An example is shown in Fig. 13.

Before evaluating the potential for mode identifications from Fig. 13, two comments need to be made. First, we only show the results for the B and I_C filter pair, as the diagrams are similar in appearance for the other two possible filter combinations, but the observational errors are larger.

Secondly, the locations of the areas of interest depend quite strongly on the pulsation constant Q. This is a well-known result (e.g. discussed by Garrido 2000), and is the reason why we have separated the results into three subsets which depend on Q. We chose a suitable subdivision based on the observed γ Dor frequencies.

The implications from Fig. 13 can be summarized as follows. For modes with $Q > 0.2$ d, the mode identification method gives meaningless results. For the modes with $Q < 0.2$ d there is some agreement, but this might be coincidence. In any case, the amplitude ratios of the photometric modes are consistent with $\ell = 1$ or 2, but not with $\ell = 3$.

3.5 The infrared colours and the companion of HD 209295

In Section 3.2.1 we have shown that the binary companion of HD 209295 must have a mass of at least $0.6\,M_\odot$. If it were a main-sequence star, this would correspond to a spectral type of K5. The most luminous possible main-sequence companion to HD 209295 is a G0 star. A star more luminous than this would be detected in the spectrum. We decided to search for a companion in the infrared. For this purpose we show of the system optical and infrared colours in Table 4. We note that interstellar reddening is insignificant because of the proximity of the star ($d = 122$ pc) and its high galactic latitude ($b = -44°$); there is also no evidence for reddening in the observed Strömgren colours (Table 2).

We adopted standard relations for absolute magnitude as well as optical and infrared colours of main-sequence stars from the tables of Tokunaga (2000) and Drilling & Landolt (2000). Given the observed V magnitude and $(V - I_C)$ colour of the system, we added the fluxes of hypothetical G0, K0 and K5 main-sequence companions. For the flux of the primary we used a suitable interpolation between A7 and F0 to reproduce the observed V and $(V - I_C)$. The infrared colours of those models were then compared to observations. The result, displayed in Fig. 14, shows the relative infrared excess of the observations and of some of the binary models compared to the expected infrared magnitudes.

Whereas the infrared J and H magnitude seem to indicate the presence of a companion, the K magnitude argues against this idea; the L magnitude is too uncertain to be useful. The infrared excess we calculated also depends on the uncertainties of the standard relations and the accuracy of our measurements. We conclude that we cannot pinpoint the nature of the companion of HD 209295 from the infrared data alone.

4 FURTHER DISCUSSION OF THE OBSERVATIONS

4.1 The secondary component and evolutionary history of the HD 209295 system

We were unable to detect the secondary component of the HD 209295 system in the infrared. However, we can still obtain further constraints on its nature. The first constraint is the absence of ellipsoidal variability.

Morris (1985) derived theoretical expressions for system parameters of ellipsoidal variables from the observed light curves. Using his equation (6), a limb darkening coefficient of 0.59 from Claret (2000), a gravity darkening exponent of 0.84 (Claret 1999), and a conservative upper limit of 5 mmag on the peak-to-peak amplitude of possible ellipsoidal variations of HD 209295, we can determine the minimum orbital inclination of the system as a function of secondary mass. The result is shown in Fig. 15.

Combining this information with the dependence of secondary mass on inclination from the mass function of the binary (upper panel of Fig. 8), we can derive a refined lower limit of the secondary mass. The result is $M_2 > 1.04\,M_\odot$. This lower limit on the secondary mass has two implications. First, it means that the primary is quite well within the Roche limit. Secondly, the secondary mass is very close to the upper limit $1.05\,M_\odot$ derived in

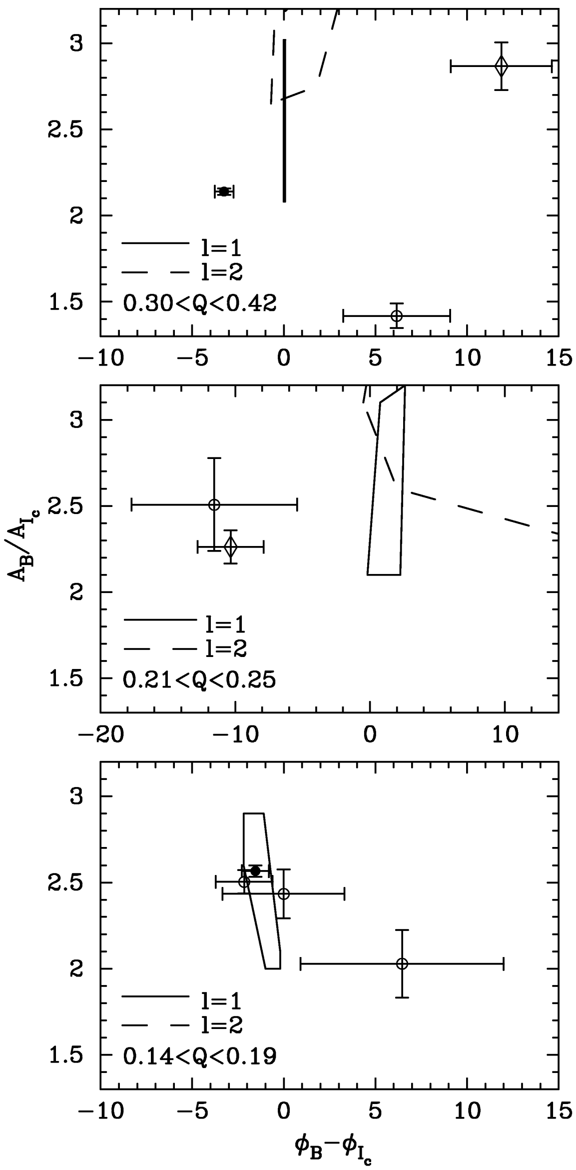

Figure 13. Comparison of theoretical and observed B/I_C colour amplitude ratios and phase differences with observations. Upper panel: variations with frequencies less than 1.2 cycle d^{-1}. Middle panel: variations with frequencies between 1.6 to 1.8 cycle d^{-1}. Lower panel: variations with frequencies greater than 2.2 cycle d^{-1}. The areas outlined by the full lines are theoretical predictions for $\ell = 1$, and areas represented by dashed lines correspond to $\ell = 2$. Symbols with error bars are the observed values. Filled circles correspond to independent modes, open circles to harmonics of the orbital period and diamonds to combination frequencies. Note the different abscissa scale in the middle panel. Regions of interest were also calculated for $\ell = 3$, but they are off scale towards higher amplitude ratios. The $\ell = 2$ area for $0.14 < Q < 0.19$ is off scale towards larger positive phase shifts.

Section 3.2.1, assuming a main-sequence secondary. In addition, the orbit of the system is also quite eccentric, which is surprising as one would have expected circularization to have taken place.

Claret, Giménez & Cunha (1995) and Claret & Cunha (1997) compared theoretical orbital circularization and synchronization times for main-sequence binaries with observations. From their results, and using the surface gravity of HD 209295 as an age

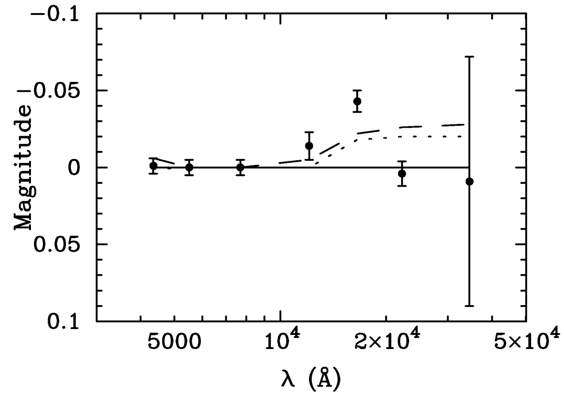

Figure 14. A search for infrared excess in the energy distribution of HD 209295. The solid horizontal line represents an interpolation of standard relations for A-type stars to the observed $(V - I_C)$ colour of HD 209295. The dotted line is the same with a G0 main-sequence companion added, and the dashed line shows the expected colours if a K5 main-sequence companion were present. A K0 companion would be practically indistinguishable from a G0 star in this diagram. The filled circles with the error bars are the actual observations.

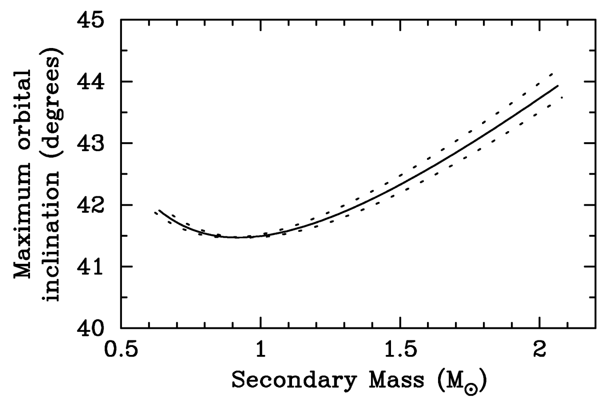

Figure 15. The maximum inclination of the binary orbit of HD 209295, consistent with the absence of ellipsoidal variability, as a function of secondary mass. The full line corresponds to a primary mass of $1.84\,M_\odot$, whereas the dotted lines delineate our 1σ error estimate of $\pm 0.07\,M_\odot$.

indicator, we conclude that the orbital eccentricity of HD 209295 is inconsistent with normal main-sequence binary evolution. For a star similar in age to HD 209295 ($\log t \approx 8.86$ as inferred from comparison with pulsational and evolutionary models), one would expect $e < 0.1$. There is reason to believe, therefore, that the secondary star may be a degenerate object. A white dwarf may have a mass in excess of $1.04\,M_\odot$. However, in such a scenario orbital circularization would again have taken place, because such a system must have undergone a previous mass transfer phase.

We investigated the ultraviolet (UV) fluxes of the object as measured by the *TD-1* satellite (Thompson et al. 1978) and compared it to the optical *uby* fluxes. For this purpose, we converted the measured *uby* magnitude of HD 209295 to fluxes using the formulae of Gray (1998). We omitted the v band because it is dominated by the H_δ line. A Kurucz model atmosphere with $T_{\rm eff} = 7750$ K (cf. Section 1.1) and $\log g = 4.3$ gave the best match. We then compared the predicted UV fluxes from this fit with the *TD-1* measurements (Fig. 16). There is quite a strong UV excess in the *TD-1* measurements at 1965 and 2365 Å compared to

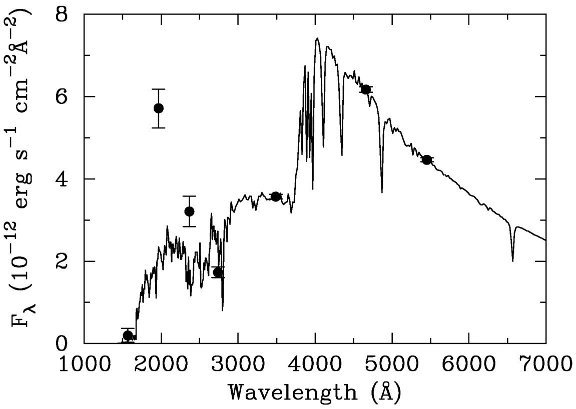

Figure 16. Comparison of optical *uby* and UV fluxes of HD 209295 to a $T_{\rm eff} = 7750$ K, $\log g = 4.3$ Kurucz model atmosphere. A clear UV excess is notable.

the model atmosphere, but little flux at 1565 Å. The shape of this excess resembles an energy distribution of an object of $T_{\rm eff} \approx 15\,000$ K. This is a suggestion that a white dwarf companion could be responsible.

Consequently, we attempted to fit some white dwarf star model atmospheres (Koester, private communication) for $\log g = 8$ and $10\,000 < T_{\rm eff} < 16\,000$ K to this excess. The *V* flux was normalized to the value predicted for a star at the distance of HD 209295. While we could reproduce the approximate shape of the UV excess, the resulting white dwarf luminosity is far too small. A white dwarf star would only be able to generate 0.1–0.2 per cent of the observed UV excess. Hotter white dwarf models would be able to explain a larger fraction of the excess, but they would be inconsistent with the low *TD-1* flux at 1565 Å.

It is hard to imagine an astronomical object or a physical process which could be made responsible for this UV excess and still be consistent with other observations. A less-massive white dwarf is inconsistent with our mass constraints. A subdwarf would be seen in the optical and is inconsistent with the primary being a Population I star. A late-type active companion would be detected in X-rays. We need to leave the reason for the UV excess unanswered; it may be possible that the *TD-1* measurements are in error. Unfortunately, the star was not observed by *IUE* (NASA–ESA 1999).

We also need to consider that the secondary may be a neutron star. In this case, the high orbital eccentricity would be a result of the supernova outburst, and the orbit would not be expected to circularize during the main sequence life span of the present primary (see Zahn 1977, whose work also suggests that the rotation of the primary should not be synchronized with the orbital motion of the compact secondary).

Comparing the orbital eccentricity and separation of the HD 209295 system with the X-ray binary population simulations of Terman, Taam & Savage (1996) shows that the observed orbital parameters can be comfortably explained in this scenario. The undetected companion of HD 209295 could therefore be a neutron star, and the system will evolve into an intermediate-mass X-ray binary after the present primary has left the main sequence. The neutron star hypothesis is testable. The previous evolutionary phases should have left their marks in the chemical composition of HD 209295. However, the Strömgren metallicity index $\delta m_1 = 0.016$ and our spectra appear normal.

If the unknown companion of HD 209295 were a neutron star, one would also expect that it would be detectable in X-rays. However, the star has not been detected by *ROSAT* (Voges et al. 1999, 2000) or *Einstein* (Moran et al. 1996). Finally, the neutron star should have suffered an impulse from the supernova explosion, which might modify the space motion of the binary system. We therefore calculated the galactic *U*, *V*, and *W* velocities of HD 209295 from its γ velocity from Table 7, its *Hipparcos* parallax (see Section 1.1) and proper motion [$\mu_\alpha \cos\delta = 26.84 \pm 0.59$ mas, $\mu_\delta = -58.82 \pm 0.41$ mas as measured by the *Hipparcos* satellite (ESA 1997)]. We find $U = -21\,{\rm km\,s^{-1}}$, $V = -12\,{\rm km\,s^{-1}}$ and $W = +28\,{\rm km\,s^{-1}}$ (already corrected for the solar motion) which is not unusual for an early-F main-sequence star (cf. Gilmore & Zeilik 2000). The neutron star interpretation for the secondary in the HD 209295 system therefore also has its weaknesses; we cannot at present identify the nature of this star with certainty.

4.2 Evidence for forced oscillations

In Section 3.4 we reported the discovery that many of the photometric frequencies are exact integer multiples of the orbital frequency. This raises the suspicion that they might not be free oscillation modes of the star, but are rather triggered by tidal interactions. Tidally induced non-radial oscillations have been searched for observationally, but the results have not been very convincing, with the possible exception of the slowly pulsating B star HD 177863 (De Cat 2001, Willems & Aerts 2001). As there are quite a number of frequencies which are exact integer multiples of the orbital frequency, there is reason to believe that HD 209295 is the best case for forced oscillations. Further support for this interpretation needs to be sought. Some general information about tidal excitation is therefore useful.

This effect has been studied by several authors theoretically, most often in connection with neutron star/main-sequence binaries. For instance, Kumar, Ao & Quatert (1995) showed that stellar p, f and low-order g-modes are not easily excitable through tidal effects, but that intermediate-order g-modes may be excited. These are, of course, exactly the modes in which γ Dor stars (and SPB stars) pulsate.

Furthermore, tidally excited modes will have a shape adjusted to the gravitational potential of the exciting star. The tidal deformation can be decomposed into a linear superposition of the g- and p-mode oscillations of the star (Press & Teukolsky 1977). Their dominating components are the $\ell = 2$, $|m| = 2$ modes (e.g. see Kosovichev & Severnyj 1983). Unfortunately, we did not succeed in providing mode identifications for one or more of the variations suspected to be forced oscillations. However, if we are really dealing with forced oscillations, they should be approximately in phase at periastron, where the tidal force is at maximum.

We have already listed pulsational phases of the different modes at a periastron passage in Table 9. The phase values are similar and seem to show some alignment of the suspected tides. This is also the case for $f_8 = 5f_{\rm orb}$, assuming it is an $\ell = 2$, $|m| = 2$ mode, as there is a 180° phase ambiguity. The variations are, however, not perfectly in phase, possibly as a result of non-adiabatic effects.

4.3 The photometric and radial velocity amplitudes

It is somewhat puzzling that there is little correspondence in amplitude between the photometric and radial velocity data. The two highest-amplitude γ Dor modes in the photometry are undetected in the radial velocities. While the range in frequency of δ Sct instability is in approximate agreement in the photometry and

Table 10. A comparison of simultaneous V-filter light and radial velocity amplitudes for γ Dor stars from the literature.

Star	$2K$ ($\mathrm{km\,s^{-1}}$)	ΔV (mmag)	$2K/\Delta V$ ($\mathrm{km\,s^{-1}\,mag^{-1}}$)	ℓ	Ref.
γ Dor	0.6 ± 0.2	23 ± 1	26 ± 9	3	1
	2.6 ± 0.2	27 ± 1	96 ± 8	1	
	1.2 ± 0.2	13 ± 1	92 ± 8	1	
9 Aur	1.7 ± 1.2	35 ± 1	48 ± 34	3	2,3
	3.0 ± 0.8	20 ± 1	148 ± 39	3	2,3
	3.1 ± 1.1	18 ± 1	172 ± 61		2,3
HR 8330	5.2 ± 0.1	15 ± 1	350 ± 20	2	4,5
HD 68192	2.2 ± 0.2	21.7 ± 0.2	101 ± 10		6
HD 209295	<1	38.9 ± 0.2	<26	1	7
	<1	28.7 ± 0.2	<35	1	7

References: 1: Balona et al. (1996); 2: Zerbi et al. (1997); 3: Aerts & Krisciunas (1996); 4: Kaye et al. (1999b); 5: Aerts & Kaye (2001); 6: Kaye et al. (1999c); 7: this paper.

radial velocities, there is no clear match to individual frequencies between the two data sets.

Breger, Hutchins & Kuhi (1976) determined the ratios of velocity to light amplitudes in several δ Sct stars and found values between $2K/\Delta V$ of $50\text{–}125\,\mathrm{km\,s^{-1}\,mag^{-1}}$. Using this value for the δ Sct pulsations in HD 209295, we would expect the photometrically detected modes to have radial velocity amplitudes smaller than $0.2\,\mathrm{km\,s^{-1}}$, and hence they would not be detected. However, we detected radial velocity variations with amplitudes of around $2\,\mathrm{km\,s^{-1}}$ in the δ Sct range, which should then generate photometric V amplitudes of at least 15 mmag, but there is no trace of them. The only plausible explanation is that the short-period variations in the spectroscopy are not due to pulsation.

We can get limits to the radial velocity amplitude of the two independent γ Dor modes of HD 209295 by fitting the radial velocities with the photometric periods. This results in an upper limit of $1\,\mathrm{km\,s^{-1}}$ for the amplitude of both modes. We then obtain $2K/\Delta V < 26\,\mathrm{km\,s^{-1}\,mag^{-1}}$ for f_1 and $2K/\Delta V < 35\,\mathrm{km\,s^{-1}\,mag^{-1}}$ for f_2.

In Table 10 we show all available amplitude determinations from photometric and radial velocity measurements of γ Dor stars from the literature. We only considered data sets in which simultaneous radial velocity and photometry was obtained to avoid being sensitive to amplitude variations. Only those cases where individual mode periods could be resolved are listed.

It appears that not only is there an order of magnitude spread in the $2K/\Delta V$ values for the different stars, but also for different modes of the same star. The limits we obtained for HD 209295 are at the lower end of the range to be found in Table 1. However, the lowest $2K/\Delta V$ values were obtained for modes of $\ell = 3$, not for $\ell = 1$ as suggested for the two independent modes of HD 209295.

Aerts & Krisciunas (1996) offered an explanation for such diverse behaviour: the photometric variations are mostly due to temperature variations, which hardly affect the radial velocities. In addition Aerts & Krisciunas (1996) suggest that, due to stellar rotation, toroidal corrections become important. These may be the cause for the large scatter in $2K/\Delta V$ in Table 10. High-resolution, high signal-to-noise ratio spectra of the more rapidly rotating γ Dor stars with simultaneous photometry are necessary to test this hypothesis.

5 THEORY

We have carried out a stability analysis of the pulsations to check whether the inferred evolutionary state of HD 209295 is consistent with its pulsational behaviour, and whether tidally induced oscillations are reasonable.

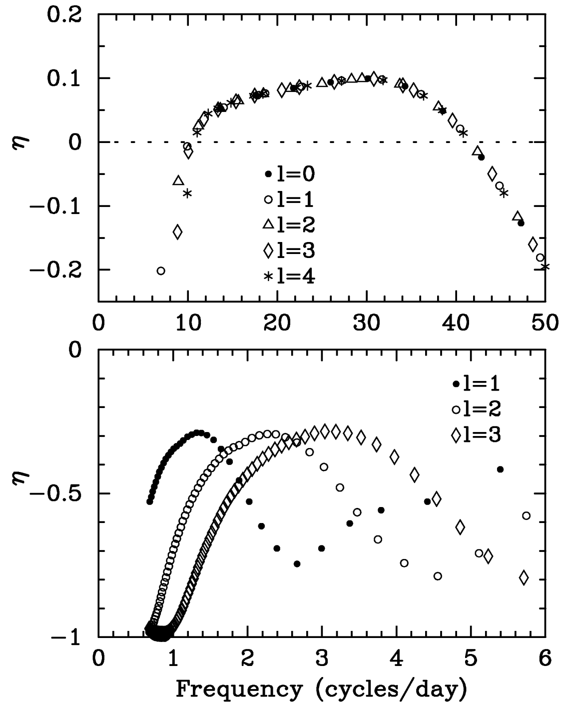

Figure 17. Normalized linear growth rates, η, for a model matching the effective temperature and surface gravity HD 209295. $\eta = 1$ means that a mode is driven throughout the whole model, whereas $\eta = -1$ means that a mode is damped throughout the whole model; modes with $\eta > 0$ are pulsationally unstable. Upper panel: the whole computed frequency range. Lower panel: the γ Dor pulsation frequency domain. In certain frequency regions (depending on ℓ), less damping is present.

5.1 Stability analysis

We used the Warsaw–New Jersey stellar evolution and the NADROT pulsation codes to generate a series of models for HD 209295. We then investigated the pulsation modes for stability. The results for the model which best matches the parameters of HD 209295 ($M = 1.8\,\mathrm{M_\odot}$, $\log T_{\mathrm{eff}} = 3.88$, $\log L = 1.10$, $\log g = 4.03$) are shown in Fig. 17.

The observed frequency domain of the δ Sct pulsations of HD 209295 is very well reproduced. The unstable frequency range does not depend on ℓ, which is also consistent with the observations. γ Doradus modes are not driven in our models, as this currently requires a special treatment of convection (Guzik et al. 2000). In our computations we used the standard mixing-length convection theory and we ignored the Lagrangian perturbation of the convective energy flux when computing oscillations. Our attempts to reproduce the results by Guzik et al. (2000) concerning pulsational instability were unsuccessful, and we plan to study this matter in the future.

It is interesting to note that there are frequency regions in which damping is not as strong, and that they depend on ℓ. We performed these computations up to $\ell = 8$, and found that the trend is maintained. The $\ell = 1$ and $\ell = 2$ frequency regions coincide with the ones actually observed.

5.2 Tidal excitation

We investigated the possibility of tidally excited oscillations in HD 209295 by determining the amplitude of tidally induced radial-velocity variations using the expressions derived by Willems & Aerts (2001). We calculated both the free and the forced oscillations of a $1.8\,M_{\odot}$ stellar model in the linear, adiabatic approximation. Because the amplitude may become quite large in the adiabatic approximation, we restricted ourselves to calculating the radial-velocity variations at orbital periods for which the relative differences between the forcing frequencies of the dynamic tides and the eigenfrequencies of the free oscillation modes are not too small (for details see Willems & Aerts 2001).

The resulting amplitudes of the tidally induced radial-velocity variations seen by an observer are displayed in Fig. 18 as a function of the orbital period. The companion mass is assumed to be $1.5\,M_{\odot}$, which corresponds to an orbital inclination of 31.2° and to a rotational frequency between $f_{\rm rot} = 1.635\,{\rm d}^{-1}$ and $f_{\rm rot} = 1.998\,{\rm d}^{-1}$.

A high peak in the amplitudes is seen to occur near the observed orbital period of HD 209295. The peak results from the resonant excitation of the modes g^{+}_{14} and g^{+}_{16} by the dynamic tides associated with the forcing frequencies $3f_{\rm orb}$ and $4f_{\rm orb}$, respectively. Both tides are of spherical degree $\ell = 2$ and azimuthal order $m = -2$. This result is quite encouraging, as a signal at $3f_{\rm orb}$ was detected in the photometry, and one at $4f_{\rm orb}$ was suspected. On the other hand, not all of the detected orbital harmonics are excited in the model, but they can be reconciled with linear combinations of these two signals.

We need to make several remarks here. First, the above 'solution' is probably not unique. In addition, the calculations have been performed using an adiabatic code, so they show the presence of the resonances, but not the real amplitudes. Secondly, attempts with lower companion masses (and thus lower rotational frequencies) were not very successful. This is interesting, as it may help to constrain the nature of the orbital companion of HD 209295.

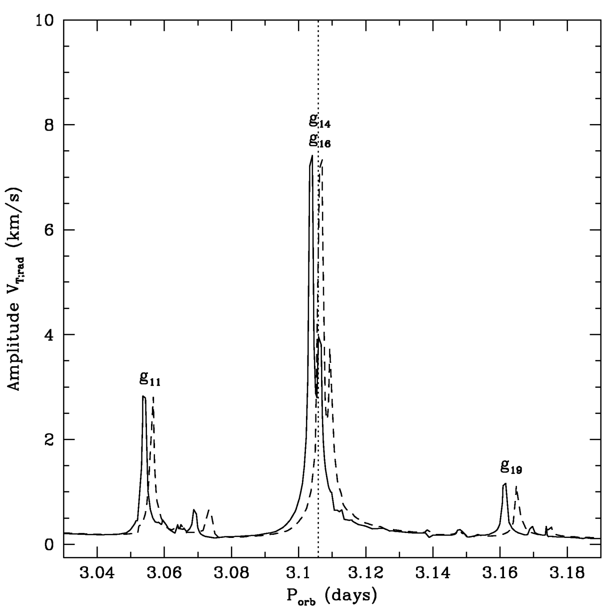

Figure 18. Observed amplitude of the tidally induced radial velocity variations in a model for HD 209295. The full line corresponds to a rotational frequency $f_{\rm rot} = 1.852\,{\rm d}^{-1}$ and the dashed line to a rotational frequency $f_{\rm rot} = 1.854\,{\rm d}^{-1}$. The orbital period of HD 209295 is indicated by the dotted vertical line.

We conclude that resonant excitation is possible, but for precise results there are still too many degrees of freedom. The prospect of developing tides as a probing tool is a promise for future studies.

6 CONCLUSIONS AND OUTLOOK

By means of 128 h of time-resolved high-resolution spectroscopic and 280 h of time-series photometric observations, we have shown that HD 209295 is not only the first pulsating star to be a member of two classes (a γ Dor as well as a δ Sct star), but we have also discovered good evidence for the presence of tidally excited pulsation modes. The binary companion is probably a neutron star or a white dwarf.

These findings make HD 209295 a rather interesting astrophysical laboratory. We were able to confront photometric and spectroscopic mode identification methods. Whereas the method by Telting & Schrijvers (1997) yielded reasonable assignments for the two independent modes dominating the photometry (both are $\ell = 1$, $|m| = 1$), analysing the photometric colour amplitude ratios and phase differences did not yield any meaningful results. The necessity of using as many mode identification methods as possible to secure reliable results is stressed.

We showed that the presence of tidally induced modes can be explained by theoretical models, but not all the observations can be understood. It would be important to calculate more realistic models of tidal interaction.

We do not fully understand the wealth of information provided by the variations in HD 209295. Large coordinated efforts will be required for further progress as our data are already fairly extensive. Another multisite photometric and spectroscopic campaign on an even larger scale would be desirable. This should be carried over a long time-base in order to resolve the γ Dor pulsations, and a large data set is needed to detect more δ Sct modes. Large telescopes are required for the spectroscopy to obtain high time-resolution and a high signal-to-noise ratio. This is necessary for identifying further modes and for detailed line-profile analysis. Photometric observations in more filters than previously obtained are necessary, perhaps extending the wavelength range into the near infrared. UV and infrared spectroscopy would be useful in a search for the companion star, and an abundance analysis may reveal an unusual chemical composition caused by the possible previous evolution of the system through mass transfer, common envelope and/or supernova stages.

ACKNOWLEDGMENTS

We are indebted to Lisa Crause for obtaining and reducing the infrared photometry of HD 209295 at our request and for commenting on a draft version of this paper. DJJ and BW thank the British Particle Physics and Astronomy Research Council (PPARC) for post-doctoral research fellowships. DJJ would also like to acknowledge the continued positive influences of Mrs J Pryer, for much love and support during this work, and the Royal Society for a European research grant. ERC thanks S. Potter, D. Romero and E. Colmenero for their support. AAP would like to thank L. A. Balona and the staff of the SAAO (Cape Town) for their hospitality during his visit to the institute. BW is grateful to

Antonio Claret for providing a 1.8-$M_\odot$ stellar model. GH thanks Darragh O'Donoghue for giving him one night of his observing time for this project and Detlev Koester for providing white dwarf model atmospheres. GH also wishes to express his gratitude to several colleagues for helpful comments: Brian Warner, Marten van Kerkwijk, Matt Burleigh and Stephen Potter. Ennio Poretti and Kevin Krisciunas are thanked for commenting on a draft version of this paper.

REFERENCES

Aerts C., Kaye A. B., 2001, ApJ, 553, 814
Aerts C., Krisciunas K., 1996, MNRAS, 278, 877
Balona L. A., 2000, MNRAS, 318, 289
Balona L. A., Evers E. A., 1999, MNRAS, 302, 349
Balona L. A. et al., 1996, MNRAS, 281, 1315
Baranne A. et al., 1996, A&AS, 119, 373
Barker E. S., Evans D. S., Laing J. D., 1967, Bull. Roy. Obs., No. 130
Bedding T. R. et al., 2002, in Aerts C., Bedding T. R., Christensen-Dalsgaard J., eds, ASP Conf. Ser. Vol. 259, Radial and Nonradial Oscillations as Probes of Stellar Physics. Astron. Soc. Pac., San Fransisco, in press
Breger M., 1975, in Sherwood V., Plaut L., eds, Proc. IAU Symp. 67, Variable Stars and Stellar Evolution. Reidel, Dordrecht, p. 231
Breger M., Montgomery M. H., 2000, in Breger M., Montgomery M. H., eds, ASP Conf. Ser. Vol. 210, Delta Scuti and Related Stars. Astron. Soc. Pac, San Francisco
Breger M., Hutchins J., Kuhi L. V., 1976, ApJ, 210, 163
Breger M. et al., 1993, A&A, 271, 482
Carter B. S., 1990, MNRAS, 242, 1
Claret A., 1999, A&AS, 131, 395
Claret A., 2000, A&A, 363, 1081
Claret A., Cunha N. C. S., 1997, A&A, 318, 187
Claret A., Giménez A., Cunha N. C. S., 1995, A&A, 299, 724
Crawford D. L., 1979, AJ, 84, 1858
Cunha M. S., Gough D. O., 2000, MNRAS, 319, 1020
De Cat P., 2001, PhD thesis, Katholieke Universiteit Leuven
Drilling J. S., Landolt A. U., 2000, in Cox A. N., ed., Allen's Astrophysical Quantities, 4th edn. Springer Verlag, Berlin, p. 392
Eggleton P., 1983, ApJ, 268, 368
ESA, 1997, The *Hipparcos* and *Tycho* catalogues, ESA SP-1200. ESA Publications Division, Noordwijk
Eyer L., Grenon M., 1998, in Deubner F. L., Christensen-Dalsgaard J., Kurtz D. W., eds, New Eyes to See Inside the Sun and Stars, p. 291
Garrido R., 2000, in Breger M., Montgomery M., eds, ASP Conf. Ser. Vol. 210, Delta Scuti and Related Stars. Astron. Soc. Pac., San Francisco, p. 67
Gilmore G. F., Zeilik M., 2000, in Cox A. N., ed., Allen's Astrophysical Quantities, 4th edn. Springer Verlag, Berlin, p. 493
Glass I. S., 1973, MNRAS, 164, 155
Gough D. O., 2000, in Brekke P., Fleck B., Gurman J. B., eds, Proc. IAU Symp. 203, Recent Insights into the Physics of the Sun and Heliosphere. Astron. Soc. Pac., San Fransisco, p. 1
Gray R. O., 1998, AJ, 116, 482
Gray R. O., Corbally C. J., 1994, AJ, 107, 742
Grenier S., Burnage R., Faraggiana M., Gerbaldi M., Delmas F., Gómez A. E., Sabas V., Sharif L., 1999, A&AS, 135, 503
Guzik J. A., Kaye A. B., Bradley P. A., Cox A. N., Neuforge C., 2000, ApJ, 542, L57
Handler G., 1999a, MNRAS, 309, L19
Handler G., 1999b, IBVS, 4817
Handler G., Shobbrook R. R., 2002, MNRAS, 333, 251 (Paper I, this issue)
Handler G. et al., 1997, MNRAS, 286, 303
Handler G. et al., 2000, MNRAS, 318, 511
Houk N., Cowley A. P., 1975, Michigan Spectral Catalogue, Vol. 1. Kluwer, Dordrecht
Kaye A. B., Handler G., Krisciunas K., Poretti E., Zerbi F. M., 1999a, PASP, 111, 840
Kaye A. B., Henry G. W., Fekel F. C., Hall D. S., 1999b, MNRAS, 308, 1081
Kaye A. B. et al., 1999c, AJ, 118, 2997
Kjeldsen H., Bedding T. R., Viskum M., Frandsen S., 1995, AJ, 109, 1313
Koen C., Van Rooyen R., Van Wyk F., Marang F., 1999, MNRAS, 309, 1051
Kosovichev A. G., Severnyj A. B., 1983, Pis'ma Astron. Zh., 9, 424
Kumar P., Ao C. O., Quataert E. J., 1995, ApJ, 449, 294
Kurtz D. W., Martinez P., 2000, Baltic Astron., 9, 253
Kurucz R. L., 1991, Van Vleck Obs. Contr., 11, 27
Martinez P., Koen C., 1994, MNRAS, 267, 1039
Montgomery M. H., O'Donoghue D., 1999, Delta Scuti Star Newsletter 13. Univ. Vienna, Vienna, p. 28
Moran E. C., Helfand D. J., Becker R. H., White R. L., 1996, ApJ, 461, 127
Morris S. L., 1985, ApJ, 295, 143
NASA–ESA, 1999, Merged Log of *IUE* observations. Available online from http://vizier.u-strasbg.fr/cgi-bin/VizieR, catalogue No. VI/99
Pamyatnykh A. A., Dziembowski W. A., Handler G., Pikall H., 1998, A&A, 333, 141
Press W. H., Teukolsky S. A., 1977, ApJ, 213, 183
Rodriguez E., Breger M., 2001, A&A, 366, 178
Rodriguez E., López-González M. J., López de Coca P., 2000, A&AS, 144, 369
Shobbrook R. R., 2000, J. Astron. Data, 6, 4E
Sperl M., 1998, MSc thesis, Univ. Vienna
Telting J. H., Schrijvers C., 1997, A&A, 317, 723
Terman J. L., Taam R. E., Savage C. O., 1996, MNRAS, 281, 552
Thompson G. I., Nandy K., Jamar C., Monfils A., Houziaux L., Carnochan D. J., Wilson R., 1978, Catalogue of stellar ultraviolet fluxes (TD1). The Science Research Council, UK
Tokunaga A. T., 2000, Cox A. N., ed., Allen's Astrophysical Quantities, 4th edn. Springer Verlag, Berlin, p. 151
Twarog B. A., 1980, ApJS, 44, 1
Voges W. et al., 1999, A&A, 349, 389
Voges W. et al., 2000, IAU Circ., 7432
Watson R. D., 1988, Ap&SS, 140, 255
Willems B., Aerts C., 2002, A&A, 384, 441
Zahn J.-P., 1977, A&A, 57, 383
Zerbi F. M. et al., 1997, MNRAS, 290, 401

This paper has been typeset from a TEX/LATEX file prepared by the author.

Chapter 4

Rapidly oscillating Ap stars

4.1 Introduction

The first representatives of these elusive rapid (periods between about 5 to 20 minutes) magnetic pulsators were found by accident (Kurtz 1982), and later during focused searches guided by their (suspected) group properties. Section 4.2 reports the results of such a biased search for roAp stars, mostly aimed to discover Northern Hemisphere pulsators. Indeed, one new roAp star was discovered and one suspect was confirmed.

Both of these objects were studied with multisite observing campaigns (Sect. 4.3 and 4.4). While HD 122970 (nowadays also known as PP Vir, Kazarovets et al. 2003) first seemed promising for some asteroseismic inferences, it later changed its behaviour to a less interesting state. HD 99563 (= XY Crt) has only a single pulsation mode, which is however distorted by its magnetic field. This fact could be used to constrain the geometry of this pulsator and to infer its rotation period.

The state of the art in asteroseismology of roAp stars is reported in Sect. 4.5 and 4.6. An extended Whole Earth Telescope campaign allowed the discovery of a pulsation mode predicted by theory, but not observed before, and resulted in a data set of a quantity and quality that can hardly be surpassed by any ground-based observational effort.

4.2 A search for rapid oscillations in chemically peculiar A-type stars

Original paper:

G. Handler, E. Paunzen, 1999, A&AS 135, 57

Astron. Astrophys. Suppl. Ser. **135**, 57–63 (1999)

A search for rapid oscillations in chemically peculiar A-type stars

G. Handler and E. Paunzen

Institut für Astronomie, Universität Wien, Türkenschanzstraße 17, A-1180 Wien, Austria

Received August 27; accepted September 25, 1998

Abstract. In 1995 we initiated a Northern Hemisphere survey for rapidly oscillating Ap stars. This paper presents the results including one new roAp star (HD 122970), the confirmation of rapid oscillations of HD 99563 and apparent null results for other stars.

Using Hipparcos data a statistical analysis of the absolute magnitudes and galactic distributions of all known roAp and noAp stars (also taken from the literature) was made.

A systematic trend for most of the program stars in a M_V vs. β (index of the Strömgren $uvby\beta$ system) diagram was detected leading to the conclusion that β is systematically influenced by the chemical peculiarity and/or magnetic field.

Three roAp stars are outside the δ Scuti instability strip which implies that the driving mechanism of the two classes of pulsating star is different. This is also suggested by new pulsation models. No statistical difference between the galactic distribution of roAp and noAp stars was found.

Key words: stars: chemically peculiar — stars: oscillations

1. Introduction

Among the magnetic chemically peculiar A-type stars, the rapidly oscillating Ap (roAp) stars are quite outstanding. This group exhibits rapid photometric and spectroscopic variations with periods of minutes and very small amplitudes ($A_B \leq 10\,$mmag). These oscillations are probably low spherical degree, high overtone p-modes. Using the (in general) rich oscillation spectra, several important astrophysical parameters such as the (asteroseismological) luminosity, the rotational period, the magnetic field strength and the atmospheric structure can be inferred.

Since the early eighties, the South African working group has spent a lot of time in detecting new roAp stars. They discovered more than twenty new roAps (e.g. see Martinez & Kurtz 1995) and published also an extensive list of null results (Martinez & Kurtz 1994). Several surveys in the Northern Hemisphere were also devoted to find new members of this group (e.g. Heller & Kramer 1988; Nelson & Kreidl 1993). Unfortunately, only one new roAp star (HD 176232, 10 Aql) was detected. Recently, Dorokhova & Dorokhov (1998) announced the discovery of a second roAp star (HD 99563) discovered at a Northern Hemisphere observatory.

This situation leads to a dilemma when trying to make a statistically sound analysis for this group. Two main problems arise:

- A bias is naturally introduced having only (beside two) southern roAp stars.
- Follow-up observations (e.g. high resolution spectroscopy) need to be performed in the Southern Hemisphere where telescope time is rare.

Since only one observatory (Mt. Dushak-Erekdag, Central Asia; Dorokhova & Dorokhov 1998) regularly searches for new roAp stars, we decided to initiate a Northern Hemisphere survey for roAp stars in 1995. Observations are carried out with one of the twin 0.75 m Austrian Automatic Photoelectric Telescopes at Fairborn Observatory and at McDonald Observatory.

In this paper we report the discovery of one new equatorial roAp star (HD 122970), the confirmation that HD 99563 shows rapid oscillations and the apparent null results of our survey. With the help of Hipparcos data we examine the absolute magnitudes and galactic distribution of all investigated stars.

2. Target selection and observations

Since the main aim of our program was a statistical exploration of the roAp phenomenon, we attempted to bias our target selection towards the detection of new roAp stars. Most of these objects are cool SrCrEu stars. Regrettably, systematic spectral classifications for

Send offprint requests to: G. Handler

Northern Hemisphere objects are still missing in the literature. Therefore we chose a different approach.

Nelson & Kreidl (1993) explored the positions of pulsating and nonpulsating Ap stars in several color-color diagrams for the Strömgren and Geneva photometric systems. While they did not find a clear separation of the two groups, the Strömgren $[m_1]$, $[c_1]$ and Geneva Δ, $[g]$ diagrams appear useful to select promising roAp candidates. Consequently, we searched existing Strömgren (Hauck & Mermilliod 1998) and Geneva catalogues (Rufener 1989) for potential target objects.

Since this procedure does not allow one to distinguish between Am and Ap stars, we attempted to find spectral classifications for the objects of interest in the literature. Consequently, priorities were assigned to the different stars and observations were performed according to them.

Three telescopes at two observatories were employed for our survey: the 0.9 m and 2.1 m telescopes at McDonald Observatory, Ft. Davis, Texas together with a standard two-channel photometer (Grauer & Bond 1981) and one of the twin 0.75 m Austrian Automatic Photoelectric Telescopes (APT, Strassmeier et al. 1997) at Fairborn Observatory, Washington Camp, Arizona with a single-channel photometer.

The observations (see Table 1 for an overview) were carried out as continuous 10-second integrations through a Johnson B filter. Large apertures ($> 35''$) were employed to minimize the contributions of seeing and guiding[1].

The reductions were performed using the standard technique for roAp star observations (e.g. Martinez 1993), including some low-frequency filtering in the presence of sky transparency variations by low-order polynomial fits or involving the Channel 2 comparison star, if found appropriate. The final reduced light curves were searched for rapid oscillations by means of a standard Fourier technique (Breger 1990). Amplitude spectra of our runs are displayed in Figs. 1–3 (see below for more details).

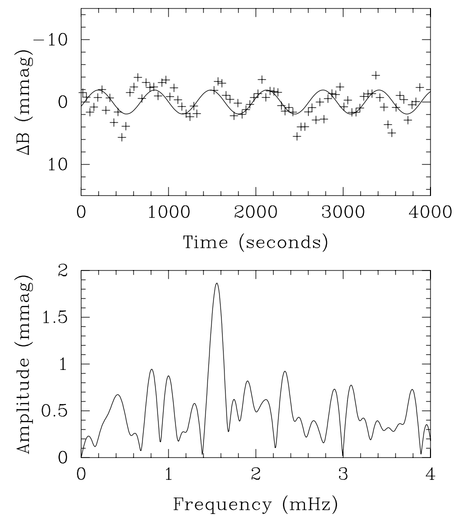

Fig. 1. Upper panel: a portion of our light curve of HD 99563. Lower panel: The amplitude spectrum of the whole run

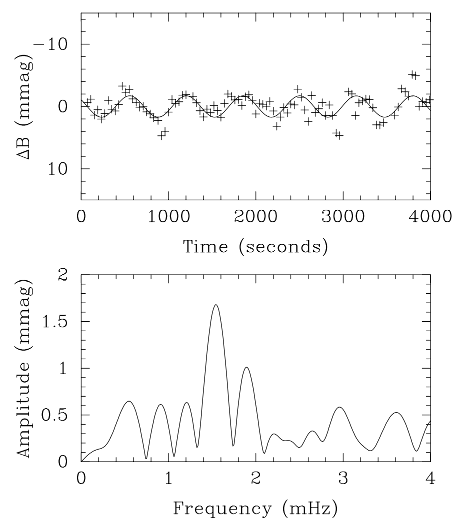

Fig. 2. Upper panel: the discovery light curve of HD 122970. Lower panel: The amplitude spectrum of this run

2.1. Comments on individual stars

BD+39 654A: This star was our most promising roAp candidate. It has been classified at SrCrEu by Bidelman (1983). Schneider's (1986) Strömgren photometry yields $(b-y)_0 = 0.136$, $\delta m_1 = -0.095$ and $\delta c_1 = -0.267$, while Geneva photometry (Burki et al. 1998) results in $[\Delta] = 0.163$ and $[g] = 0.162$. All these features are typical for roAp stars. However, BD+39 654A did not show any rapid variability, but ironically, its Channel 2 comparison star, HD 17892, turned out to be a new δ Scuti variable (Handler 1998). In any case, we consider it worthwhile to continue testing BD+39 654A for rapid oscillations.

BD+40 175A: This is the only object for which we have no color photometry available. However, its spectral classification (SrCrEu, Bidelman 1985) and its effective temperature estimate (7100 $\pm$ 400 K, Babel & North 1997) make it a good roAp candidate.

We took a short run under non-ideal photometric conditions, where this target seemed to show rapid oscillations with an amplitude of 6 mmag and a period of 9.1 minutes. Two further runs, one with the McDonald 2.1 m telescope considerably decreasing scintillation noise, did not confirm this possible variability. We suggest further observations of BD+40 175A as well.

[1] For HD 83965B, which has a close bright companion, a $18''$ aperture was used to exclude the companion; continuous guiding on the Channel 2 star was performed to check telescope tracking.

Table 1. Journal of the observations

Date (UT)	Start (UT)	Length (hrs)	Target	V	Observatory	Comment
19 Jan. 1998	1:32:00	0.68	BD+40 175A	8.9	McD	roAp?
23 Jan. 1998	1:52:30	0.58	BD+40 175A		McD	
26 Jan. 1998	1:43:20	1.04	BD+40 175A		McD (2.1 m)	
17 Jan. 1998	1:27:00	3.08	BD+39 654A	9.48	McD	
03 Feb. 1996	1:32:30	1.79	HD 31437	6.88	McD	
06 Feb. 1996	1:39:00	3.16	HD 33505	9.21	McD	
05 Feb. 1996	1:30:10	2.94	HD 35353	7.68	McD	
28 Mar. 1998	2:07:29	2.99	HD 51596	7.52	Fairborn	
10 Feb. 1996	1:40:20	1.28	HD 57955	7.68	McD	
22 Jan. 1998	11:19:40	1.03	HD 83965B	11.87	McD	
22 Mar. 1998	4:02:45	2.07	HD 99563	8.32	Fairborn	roAp
23 Feb. 1998	10:46:50	1.39	HD 108449	8.31	McD	
29 Jan. 1998	11:08:00	1.07	HD 108873	9.56	McD (2.1 m)	
25 Feb. 1998	10:36:00	1.53	HD 112515A	8.51	McD	
28 Mar. 1998	5:12:23	1.81	HD 113894	8.55	Fairborn	
15 Jan. 1998	11:48:20	1.00	HD 122970	8.31	McD	roAp
17 Jan. 1998	11:40:20	1.24	HD 122970		McD	
18 Jan. 1998	11:03:40	1.00	HD 122970		McD	
19 Jan. 1998	11:32:10	1.34	HD 139478	6.74	McD	
09 Aug. 1995	2:42:50	0.81	HD 151839	9.28	McD	
12 Aug. 1995	10:28:55	0.59	HD 223839	7.28	McD	

HD 99563: Dorokhova & Dorokhov (1998) announced the variability of this object with a period of about 11.2 minutes. We reobserved this star with the APT. The amplitude spectrum of our data shows a dominant peak with an amplitude of 2.0 mmag with a period of 10.7 minutes (Fig. 1). Therefore we consider the roAp nature of this star to be confirmed.

HD 122970: This is a new roAp star. We discovered rapid oscillations with an amplitude of 2.0 mmag and a period of 11.1 minutes in the first night we observed it (Fig. 2). This behaviour was confirmed during two subsequent runs. This star was followed up with multisite photometric and single-site spectroscopic observations; the results of this effort will be reported in a subsequent paper.

3. Analysis

For our explorations of possible group properties of roAp stars, we only considered stars which have been tested for rapid light variations. The list of known roAp stars was taken from Kurtz & Martinez (1993), five additional roAp stars were added, namely: HD 9289, HD 99563, HD 122970, HD 185256, HD 213637 resulting in 31 roAp stars known at the writing of this paper. The null results (noAp) were taken from Martinez & Kurtz (1994), including results from other surveys (see Tables 1 and 2 in Martinez & Kurtz 1994) as well. No further references on null results were found in the literature. We have to emphasize that the temperature range for the noAp stars (15000 − 6000 K) is wider than that of the roAp stars (8500 − 6500 K), i.e. some objects desgined as noAp may in fact be Bp stars.

We have used the Hipparcos and Tycho catalogues (Perryman et al. 1997) to retrieve parallaxes and apparent places for all stars. For the given sample (31 roAp and 229 noAp stars) only stars with $\frac{\sigma(\pi)}{\pi} < 0.18$ ($\sigma(M_V) <$ 0.3 mag) were considered. A Lutz-Kelker correction according to Koen (1992) was applied. Because of the chosen error limit for the parallax, the Lutz-Kelker correction is very small for all program stars. We have *not* applied any correction for interstellar extinction because of two reasons:

- Most of our program stars are within 100 pc resulting in negligible reddening.
- Values for $(B-V)_0$, $(b-y)_0$ and $(B2-V1)_0$ are derived for "normal" type stars only. It has been proven that these calibrations are, in general, not valid for magnetic chemically peculiar stars ("blueing effect").

Taking all considerations into account we are left with 12 roAp and 54 noAp stars. Figure 4 shows the $M_V(Hip)$ vs. β diagram. There are several points evident from the figure:

- All roAp stars behave "normal", in the sense that the fall in the region of other main sequence stars.
- Most of the noAp stars are above the normality line. This could mean that either the β-values are systematically too large or that the absolute magnitude is systematically too bright. Latter cannot be explained by reddening since it would even more brighten the stars.

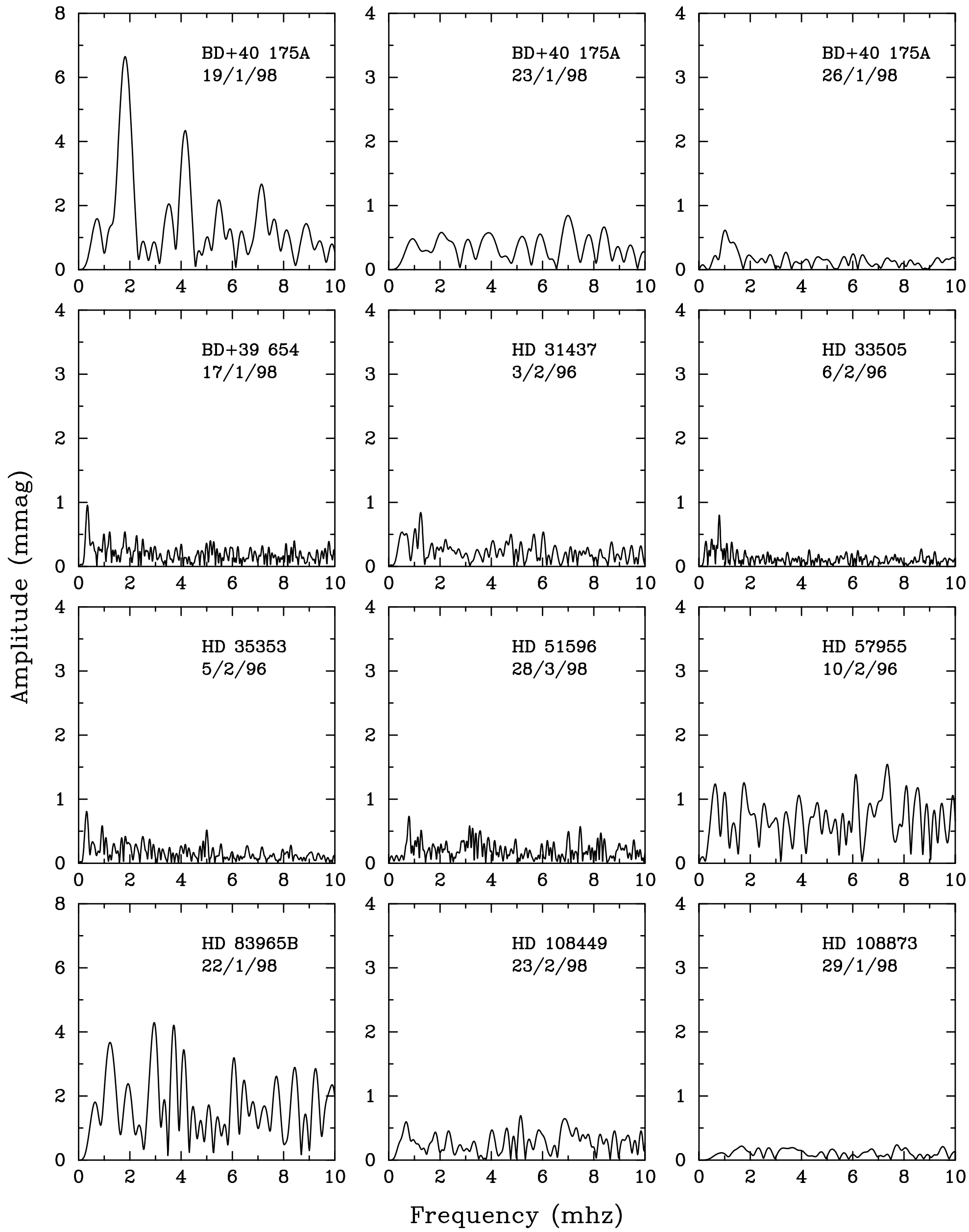

Fig. 3. Amplitude spectra of our null results. Note the larger ordinate scales for the first run on BD+40 175A and for the run on HD 83965B

It is worthwhile to note that the roAp stars are separated from the noAp's in Fig. 4: they are all rather cool main-sequence objects. Only a few stars, for which no rapid oscillations have been detected, are located close to the pulsators (HD 15233, HD 25354, HD 35353, HD 62140, HD 115708, HD 154708, HD 170397 and HD 188854). HD 25354 and HD 170397 are probably Bp stars (as judged from their Stromgren indices), while HD 35353 is poorly observed and there is no spectral classification available (hence it could be an Am star). The remaining three stars are well observed and from Fig. 4 there is no reason why they should not be roAp stars, except that HD 15233 and HD 188854 may be too evolved. We note

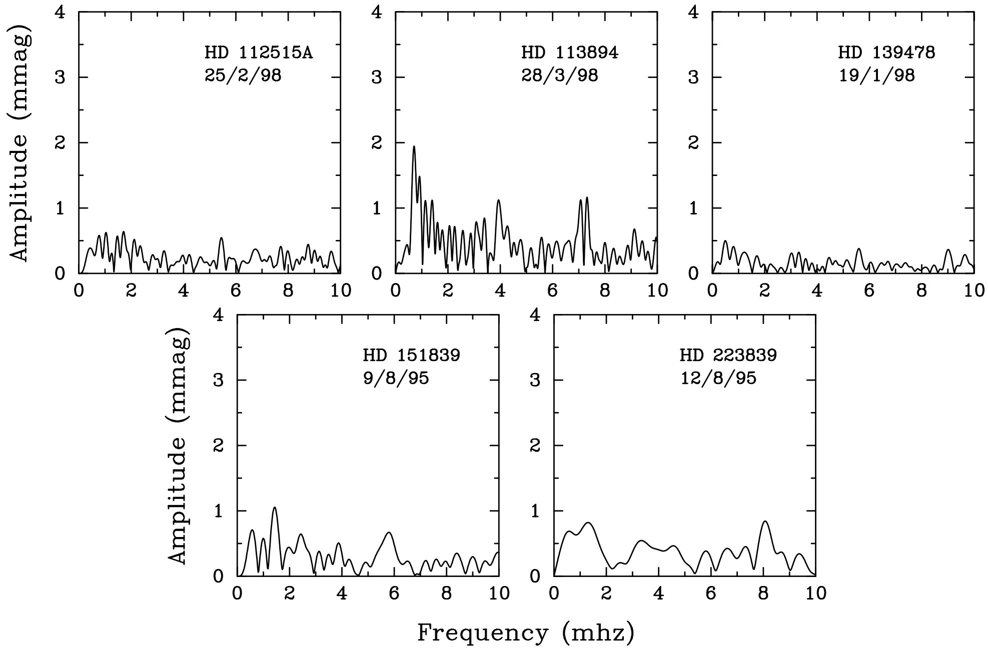

Fig. 3. continued

that the most famous noAp star, HD 137909 (β CrB), appears to be hotter and more evolved than all roAp stars.

There is more evidence that effective temperatures for Ap stars determined from β are systematically too high. Alonso et al. (1996) compared $T_{\rm eff}$ values from the Infrared Flux method with β measurements for a large range of metallicities. They found a clear trend of increasing β with increasing metallicity for fixed $T_{\rm eff}$.

Matthews et al. (1998) compared asteroseismological parallaxes with those measured by Hipparcos. They noted that the Hipparcos parallaxes are generally larger than the asteroseismic ones[2], and suggested this may be due to systematically incorrect effective temperatures estimated from β.

Some more support for this idea comes from a comparison of β-temperatures and those determined by model atmosphere analysis for a number of roAp stars (Gelbmann 1998 and references therein). This is summarized in Fig. 5. We find that the best fitting model atmospheres generally point towards lower effective temperatures. The mean temperature difference is -80 ± 90 K, which is not significant. However, this analysis can be improved when higher resolution spectra of (ro)Ap stars become available (allowing to determine more accurate temperatures) and a larger sample is investigated.

The Hipparcos parallaxes strongly suggest that the roAp stars are main-sequence objects. This is supported by the study of Gómez et al. (1998), who examined the positions of Bp–Ap stars in the HR diagram. They show that these stars are on the main sequence, and this also holds for the SrCrEu stars, i.e. the spectral subgroup containing the roAp stars. When examining the effective temperatures of roAp stars one obtains from β by using the calibrations of Moon & Dworetsky (1985), it can be noted that three[3] out of the 31 roAp stars (HD 122970, HD 213637, HD 217522) are clearly outside the cool border of the δ Scuti instability strip, especially since these temperatures are presumably overestimates.

For some years, it has been believed that the δ Scuti and roAp instability strips coincide, which has been taken as an argument that the driving mechanism for these two classes of pulsating star could be the same (partial He^+ ionisation). Very recently, Gautschy et al. (1998) presented model calculations, which led them to suggest that the actual driving of roAp pulsations might be due to

[2] There is a caveat: the seismological parallaxes are inferred by applying asymptotic theory. Although roAp stars pulsate in high radial overtones, the frequency spacing for these consecutive overtones is still smaller than the asymptotic one, resulting in (by several percent) systematically smaller seismological parallaxes. Furthermore, model calculations by Gautschy et al. (1998) show that significant deviations of observed frequency spacings from the asymptotic values can occur due to nonadiabatic effects.

[3] We deliberately do not consider HD 101065 here, since this object is so peculiar that its effective temperature cannot even be estimated with some confidence.

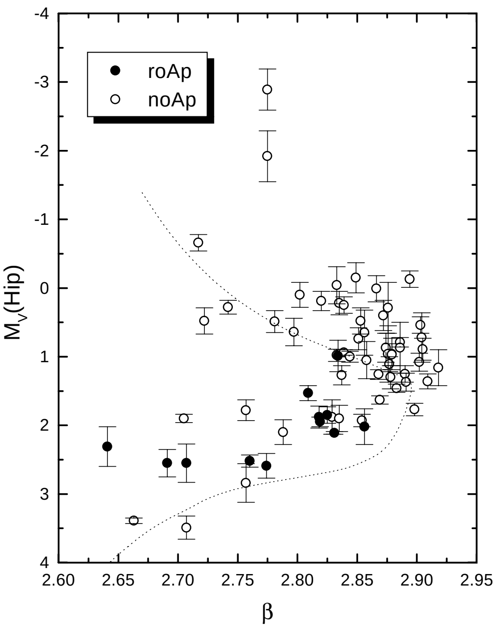

Fig. 4. M_V (*Hip*) vs. β diagram for 12 roAp (filled cricles) and 54 noAp (open circles) stars, the normality line is from Crawford (1979)

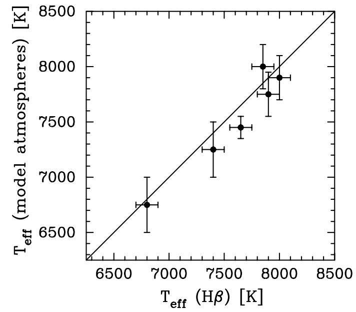

Fig. 5. Effective temperatures for six roAp stars from Hβ photometry compared with those from model atmosphere analysis. The solid line corresponds to exact agreement. Except for one star (HD 166473), the Hβ temperatures are always higher

partial H/He ionisation. They obtained overstable high-order modes by assuming that these stars have chromospheres and therefore a temperature inversion in their atmospheres. Under these assumptions their models showed roAp pulsations outside the cool edge of the δ Scuti instability strip, and hence they can explain why the three stars mentioned above do pulsate.

In Fig. 6 we present a l vs. b diagram for all program stars. Beside the "southern hemisphere effect" no systematic differences of the galactic distribution for roAp and noAp stars are evident.

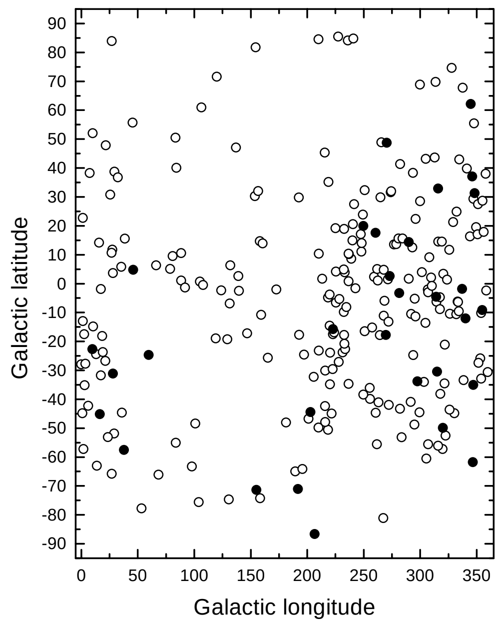

Fig. 6. l vs. b diagram for all program stars

4. Summary

We have presented first results of our Northern Hemisphere survey for roAp stars including photometric observations for 17 stars. One star (HD 122970) turned out to be a new roAp star, furthermore rapid oscillations for HD 99563 were confirmed.

Including all program stars from other surveys, a statistical analysis of absolute magnitudes (using Hipparcos data) and galactic coordinates has been made. The galactic distribution of roAp and noAp stars show no significant differences whereas the absolute magnitudes and/or the effective temperatures show systematic trends. Evidence is given that the effective temperatures for roAp stars are systematically too high when "standard" calibrations for Hβ photometry are applied.

Absolute magnitudes from Hipparcos data for roAp stars establish them as main sequence objects. Three objects are outside the δ Scuti instability strip which points towards a different excitation mechanism of the two classes of pulsating star. This is also suggested by new pulsation models.

Acknowledgements. The Austrian Fonds zur Förderung der wissenschaftlichen Forschung partially supported this work under grants *S7303-AST* and *S7304-AST*. APT observations were supported under grant *S7301-AST* to K. G. Strassmeier.

References

Alonso A., Arribas S., Martinez-Roger C., 1996, A&A 313, 873
Babel J., North P., 1997, A&A 325, 195
Bidelman W.P., 1983, AJ 88, 1182
Bidelman W.P., 1985, AJ 90, 341
Breger M., 1990, Communications in Asteroseismology 20, 1 (University of Vienna)
Burki G., et al., 1998 (in preparation)
Crawford D.L., 1979, AJ 84, 1858
Dorokhova T.N., Dorokhov N.I., 1998, in Proceedings of the 26th meeting of the European Working Group on CP stars, North P., Schnell A., Žižňovský J. (eds.), Contributions of the Astronomical Observatory Skalnaté Pleso. Slovak Academy of Sciences, p. 338
Gautschy A., Saio H., Harzenmoser H., 1998, MNRAS (in press)
Gelbmann M.J., 1998, PhD thesis, University of Vienna
Gómez A.E., Luri X., Grenier S., et al., 1998, A&A 336, 953
Grauer A.D., Bond H.E., 1981, PASP 93, 388
Handler G., 1998, IBVS 4550
Hauck B., Mermilliod M., 1998, A&AS 129, 431
Heller C.H., Kramer K.S., 1988, PASP 100, 583
Koen C., 1992, MNRAS 256, 65
Kurtz D.W., Martinez P., 1993, IBVS 3966
Martinez P., 1993, in Precision Photometry, Kilkenny D. et al. (eds.). South African Astronomical Observatory, p. 134
Martinez P., Kurtz D.W., 1994, MNRAS 271, 129
Martinez P., Kurtz D.W., 1995, Ap&SS 230, 29
Matthews J.M., Kurtz D.W., Martinez P., 1998, ApJ (in press)
Moon T.T., Dworetsky M.M., 1985, MNRAS 217, 305
Nelson M.J., Kreidl T.J., 1993, AJ 105, 1903
Perryman M.A.C., Høg E., Kovalevsky J., Lindegren L., Turon C., 1997, The Hipparcos and Tycho Catalogues, ESA SP-1200
Rufener F., 1989, A&AS 78, 469
Schneider H., 1986, A&A 161, 203
Strassmeier K.G., Boyd L.J., Epand D.H., Granzer T., 1997, PASP 109, 697

4.3 The pulsational behaviour of the rapidly oscillating Ap star HD 122970 during two photometric multi-site campaigns

Original paper:

G. Handler, W. W. Weiss, E. Paunzen, R. R. Shobbrook, R. Garrido, J. A. Guzik, A. Hempel, M. B. Moalusi, T. E. Beach, R. Medupe, F. Chagnon, J. M. Matthews, P. Reegen, T. Granzer, 2002, MNRAS 330, 153

Mon. Not. R. Astron. Soc. **330**, 153–159 (2002)

The pulsational behaviour of the rapidly oscillating Ap star HD 122970 during two photometric multisite campaigns

G. Handler,[1,2★†] W. W. Weiss,[2] E. Paunzen,[2] R. R. Shobbrook,[3] R. Garrido,[4] J. A. Guzik,[5†] A. Hempel,[6‡] M. B. Moalusi,[1,7] T. E. Beach,[8†] R. Medupe,[1,9] F. Chagnon,[10] J. M. Matthews,[10] P. Reegen[2] and T. Granzer[2,11]

[1]*South African Astronomical Observatory, PO Box 9, Observatory 7935, South Africa*
[2]*Institut für Astronomie, Universität Wien, Türkenschanzstraße 17, A-1180 Wien, Austria*
[3]*Visiting Fellow, Australian National University, Canberra, ACT, Australia*
[4]*Instituto de Astrofisica de Andalucia, Apt. 3044, E-18080 Granada, Spain*
[5]*Los Alamos National Laboratory, X-2, MS B220, Los Alamos, NM 87545-2345, USA*
[6]*Department of Physics, University of Cape Town, Private Bag, Rondebosch 7701, South Africa*
[7]*Department of Physics, University of the North-West, Private Bag X2046, Mmabatho 2735, South Africa*
[8]*University of New Mexico, Los Alamos, 4000 University Drive, Los Alamos, NM 87544, USA*
[9]*Department of Astronomy, University of Cape Town, Rondebosch 7700, South Africa*
[10]*Department of Physics and Astronomy, University of British Columbia, Vancouver, B.C. V6T 1Z4, Canada*
[11]*Astrophysikalisches Institut Potsdam, An der Sternwarte 16, D-14482 Potsdam, Germany*

Accepted 2001 October 15. Received 2001 October 15; in original form 2001 June 19

ABSTRACT

We undertook two time-series photometric multisite campaigns for the rapidly oscillating Ap star HD 122970. The first one, conducted in 1998, resulted in 119 h of data and in the detection of three pulsation frequencies. The presence of possible further modes which held the promise of deriving a mode identification motivated a second worldwide campaign in the year 2001. This second campaign resulted in 203 h of measurement, but did not reveal further modes. Rather, one of the previously detected signals disappeared. The two modes common to both data sets have different spherical degree. They also showed slight frequency modulation, and one of them varied in amplitude as well. Possible causes of the latter behaviour include intrinsic instability of the pulsation spectrum or precession of the pulsational axis and orbital motion in a binary system. Frequency analysis of the *Hipparcos* observations of the star did not allow us to determine the stellar rotation period. The amplitude and phase behaviour of the two modes of HD 122970 in the Strömgren *uvby* bands is quite similar to that observed for other roAp stars.

Key words: techniques: photometric – stars: individual: HD 122970 – stars: oscillations – stars: variables: other.

1 INTRODUCTION

1.1 Rapidly oscillating Ap (roAp) stars and the oblique pulsator model

The roAp stars are pulsating representatives of the cool magnetic Ap stars of the SrCrEu subtype. Their pulsation periods are between about 5 and 16 min, suggesting that high radial overtone modes are excited. The photometric semi-amplitudes associated with these pulsations are less than 0.02 mag, in most cases only a few mmag, which makes them difficult to detect.

Kurtz (1978) was the first to discover (accidentally) such light variations, in Przybylski's star HD 101065. He then started a search for related objects, initially discovering four further rapid pulsators (Kurtz 1982). In the same paper, he proposed the oblique pulsator model to explain the basic behaviour of the pulsations.

This model, whose validity has been confirmed by many studies, and whose correctness we will assume throughout the rest of this paper, states that the star's pulsational axis is not aligned with its rotational axis (inclined to the line of sight by the angle i), but with its magnetical axis, which itself is tilted with respect to the rotational axis by an angle β_0,[1] the magnetic obliquity. Therefore the pulsation modes excited in the roAp stars are seen at different aspects through the pulsation cycle, which, for non-radial modes,

★E-mail: gerald@saao.ac.za
†Guest Observer, McDonald Observatory, University of Texas at Austin.
‡Present address: Max-Planck-Institut für Astronomie, Königsstuhl 17, D-69117 Heidelberg, Germany.

[1] This angle is usually designated by β, but we refer to it as β_0 throughout this paper to avoid confusion with the index β derived from Hβ photometry.

causes amplitude modulation over the rotation period (which can then be inferred), and allows us to obtain constraints on the geometry of the pulsator.

The oblique pulsator model, in its simplest form, then predicts that (except for special geometric orientations of the axes) dipole ($\ell = 1$) pulsation modes will be split into equally spaced triplets. Quadrupole ($\ell = 2$) modes will give rise to equally spaced frequency quintuplets, where the spacing of consecutive multiplet components is exactly the stellar rotational frequency. However, observations (see, e.g., Kurtz 1992) showed that the situation is more complicated than that; pulsation modes of some stars are distorted by the presence of the magnetic field. Consequently, Kurtz (1992) developed an empirical spherical harmonic decomposition method, which allows a formal description of the distortion with spherical harmonics. This approach was later physically justified by Shibahashi & Takata (1993).

In the present paper we report multisite time-series photometric observations of one of the most recently discovered roAp stars and the application of the oblique pulsator model to it. For more general information on roAp stars we refer to the excellent extensive review by Kurtz & Martinez (2000).

1.2 HD 122970

HD 122970 (BD+06° 2827, HIP 68790) is an equatorial $V = 8.31$ mag star. Strömgren–Crawford photometry (Perry & Johnston 1982) yields $\beta = 2.707$, $\delta m_1 = -0.005$ and $\delta c_1 = -0.011$, indicating enhanced metallicity and line blocking. Furthermore, the reddening-free 'bracket-quantities' $[m_1] = 0.261$ and $[c_1] = 0.488$ put the star well within the regime occupied by roAp stars (cf. fig. 4 of Nelson & Kreidl 1993) in a $[m_1]$, $[c_1]$ diagram.

Although no spectral classification of the star was available at that time, the photometric indices rendered it promising enough to be tested for rapid light variations. It was discovered to be variable with a period of about 11 min and an amplitude of 1.7 mmag (see Handler & Paunzen 1999), which made it clear that HD 122970 was a new roAp star.

To determine the position of the star in the HR diagram, we cannot simply apply Crawford's (1975) calibrations for normal stars, as the Strömgren colours could be affected by the chemical peculiarity of HD 122970; line-blanketing may let the star appear less luminous than it actually is. Instead, we start with the star's *Hipparcos* parallax, 7.74 ± 1.01 mas. This yields a distance of 129^{+19}_{-15} pc. Because of the peculiar flux distribution of Ap stars, which generally makes them appear to be reddened, we also refrain from determining the reddening of the star from Strömgren photometry. Instead, we follow Matthews, Kurtz & Martinez (1999) and estimate the maximum reddening of the star from the maps of Burstein & Heiles (1982) and Perry & Johnston (1982). We find no reddening from this method, but this is not surprising because of the star's high galactic latitude (+62°). The bolometric correction for HD 122970 was interpolated from the values derived by Matthews et al. (1999) for 12 roAp stars: $BC = 0.06$ mag. Consequently, $M_{\mathrm{bol}} = 2.69 \pm 0.28$ mag.

We can now infer the effective temperature of the star from β by assuming that this index is not affected by the spectral peculiarity. We first apply the calibration of Crawford (1975) in combination with the M_v determined in the preceding paragraph. This yields a 'corrected' $c_{1,\mathrm{corr}}$ of 0.609 ± 0.030, which is 0.074 mag higher than the measured value. The model atmosphere calibration of Villa (1998) then gives $T_{\mathrm{eff}} = 6900 \pm 150$ K and $\log g = 4.1 \pm 0.15$, which yield a 'photometric radius' of $1.8 \pm 0.1\,\mathrm{R}_\odot$ and a 'photometric mass' of $1.5 \pm 0.5\,\mathrm{M}_\odot$.

With the T_{eff} and M_{bol} values derived above, one can also make use of evolutionary tracks to determine the mass and radius of HD 122970; this procedure yields smaller errors than the simple calculation of 'photometric masses'. Using the Warsaw–New Jersey stellar evolution and pulsation code (see Pamyatnykh et al. 1998), we infer $M = 1.57 \pm 0.09\,\mathrm{M}_\odot$ and $R = 1.83 \pm 0.06\,\mathrm{R}_\odot$. We caution that this assumes the chemical peculiarity to be only a surface effect, as we used models with solar metallicity. In any case, the physical parameters of HD 122970 derived by us put it about 400 K *outside* the cool edge of the δ Scuti instability strip, as defined by Breger (1995), and make it one of the coolest roAp stars known.

The spectrum of HD 122970 has been analysed in detail by Ryabchikova et al. (2000), using T_{eff} and $\log g$ values consistent with the ones derived above. These authors estimated a mean magnetic field modulus of $B = 2.0$–2.3 kG for HD 122970, and obtained a projected rotational velocity $v \sin i$ of $5.5 \pm 0.5\,\mathrm{km\,s^{-1}}$ from the lines of the iron-peak elements and $4.5 \pm 0.5\,\mathrm{km\,s^{-1}}$ from the rare-earth elements, which points towards a latitudinally dependent surface distribution of the different elements. Such inhomogeneous distributions of elements in atmospheres of magnetic stars is not unusual, and they are investigated with the Doppler imaging technique (e.g. Kuschnig et al. 1999, and references therein). In extreme cases, abundance differences between spots and mean abundance of several orders of magnitude are reported. However, these numbers have to be taken with caution, because up to now only atmospheres with abundances scaled to solar values have been used for Doppler imaging.

The discovery of the light variations of HD 122970 happened at the beginning of a large multisite campaign devoted to the δ Scuti star XX Pyx (Handler et al. 2000a), undertaken in 1998. Because the latter target was not available all night at the end of the campaign, it was decided to include HD 122970 as a second target in that campaign because of its suitable position in the sky and as the observing method used for XX Pyx was also optimal for HD 122970. In Section 2 we report the results of this effort, and describe our motivations to undertake a second campaign in 2001, which we will detail in Section 3. Section 4 reports our analysis of the *Hipparcos* measurements of the star and, finally, Section 5 contains the discussion of the combined results of both campaigns and our conclusions based thereupon.

2 THE FIRST MULTISITE CAMPAIGN

2.1 Observations and reductions

Our multisite observations in the year 1998 were carried out with seven different telescopes at six observatories: the 0.9- and 2.1-m telescopes at McDonald Observatory (McD), Ft. Davis, Texas together with a standard two-channel photometer (Grauer & Bond 1981), one of the twin 0.75-m Austrian Automatic Photoelectric Telescopes (APT) (Strassmeier et al. 1997) at Fairborn Observatory, Washington Camp, Arizona, the 1.0-m telescope at the Sutherland station of the South African Astronomical Observatory (SAAO), the 1.0-m telescope at Australia's Siding Spring Observatory (SSO), and the 1.5-m telescope at San Pedro Mártir Observatorio Astronómico Nacional (OAN), Mexico, all with single-channel photometers and the Johnson B filter. Furthermore, the simultaneous six-channel $uvby\beta$ photometer (Nielsen 1983) attached to the Sierra Nevada Observatory (OSN)

Table 1. Journal of the observations of HD 122970 in 1998. σ is the rms scatter of the residual light curves after pre-whitening and low-frequency filtering; the remaining columns are self-explanatory.

Telescope	Date (UT)	Start (UT)	Length (hrs)	σ (mmag)
McD 0.9m	15 Jan	11:48:20	1.00	1.88
McD 0.9m	17 Jan	11:40:20	1.24	1.49
McD 0.9m	18 Jan	11:03:40	1.00	1.14
OSN 0.9m	25 Feb	23:54:58	5.15	4.2/2.6/1.9/2.4
OSN 0.9m	26 Feb	23:31:23	5.99	4.0/2.4/2.1/2.5
OSN 0.9m	1 Mar	23:40:53	5.68	3.9/2.3/1.8/2.4
OSN 0.9m	2 Mar	23:33:21	4.86	4.3/2.7/2.0/2.5
McD 0.9m	3 Mar	9:27:10	2.86	0.82
McD 0.9m	4 Mar	9:13:10	2.07	1.93
McD 0.9m	5 Mar	9:08:30	2.06	1.63
McD 0.9m	7 Mar	11:24:40	1.11	2.25
McD 2.1m	9 Mar	8:43:00	3.68	0.85
McD 2.1m	10 Mar	8:21:50	4.15	0.94
McD 2.1m	11 Mar	8:25:20	4.05	0.90
SAAO 1.0m	18 Mar	23:54:40	2.69	1.26
SSO 1.0m	19 Mar	16:23:07	1.10	2.69
SAAO 1.0m	19 Mar	23:54:20	2.75	1.12
APT 0.75m	20 Mar	8:00:41	4.32	1.48
SAAO 1.0m	21 Mar	0:28:50	2.57	1.27
SSO 1.0m	21 Mar	16:02:31	2.95	2.05
APT 0.75m	22 Mar	6:15:21	5.14	1.37
SSO 1.0m	22 Mar	16:44:21	2.18	2.61
SAAO 1.0m	23 Mar	23:30:50	1.13	1.69
APT 0.75m	24 Mar	5:29:18	6.46	1.08
APT 0.75m	28 Mar	7:26:34	4.68	1.65
APT 0.75m	31 Mar	7:40:03	4.37	1.53
McD 0.9m	1 Apr	7:57:55	3.76	1.30
McD 0.9m	2 Apr	7:34:13	4.21	1.76
McD 0.9m	3 Apr	7:20:30	4.24	2.17
McD 0.9m	4 Apr	7:27:46	4.24	1.77
McD 0.9m	5 Apr	7:08:32	4.54	1.75
McD 0.9m	7 Apr	4:49:12	6.76	1.59
OAN 1.5m	12 Jun	4:00:56	2.46	1.55
OAN 1.5m	13 Jun	4:09:44	1.99	1.63
OAN 1.5m	15 Jun	3:57:40	1.84	1.30
Total		*B*	97.60	1.56
		uvby	21.68	4.1/2.5/2.0/2.5

0.9-m telescope was used to acquire *uvby* time-series photometry as well. An overview of these observations is given in Table 1.

The measurements were generally acquired as continuous 10-s integrations. Large apertures (>35 arcsec) were employed to minimize the contributions of seeing and guiding. The observations of the target star were interrupted at irregular intervals (depending on the brightness and position of the Moon) to obtain measurements of sky background.

Reductions were performed by first correcting for coincidence losses (dead-time correction), then for sky background and extinction. Some low-frequency filtering to remove residual transparency variations or tube sensitivity drifts with time-scales longer than 30 min was applied. Finally, the measurements were binned into 40-s integrations, the times of the observation were converted to Heliocentric Julian Date (HJD), and all the data were joined into a combined single light curve.

2.2 Frequency analysis

The reduced *B* filter light curves were analysed with a computer program using single-frequency Fourier and multiple-frequency least-squares techniques (Sperl 1998). This program calculates the best fit to the data with all given frequencies simultaneously by minimizing the residuals between light curve and fit.

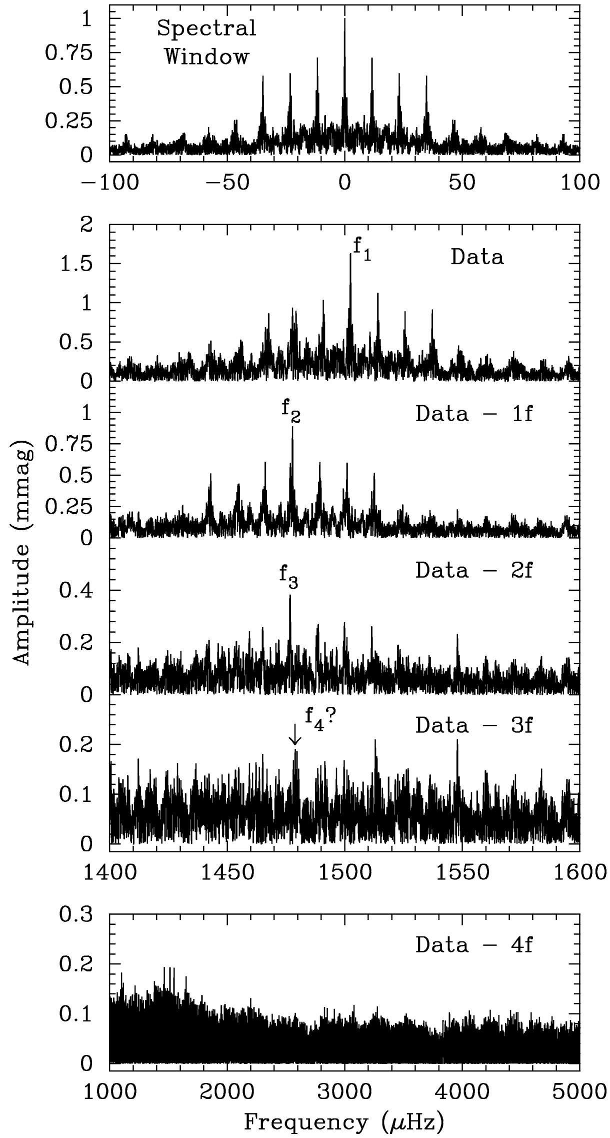

Figure 1. Amplitude spectra of HD 122970 from the multisite observations in the year 1998 with successive pre-whitening of the detected frequencies. The peak indicated with f_4 in the second lowest panel would complete an equally spaced triplet with f_2 and f_3 (see text for a discussion).

We calculated amplitude spectra of the combined light curve, searched it for its component frequencies (Fig. 1) and pre-whitened the detected signals consecutively. The presence of three frequencies is obvious, but we have also indicated a fourth signal in Fig. 1. This frequency is an exact match to a prediction of the oblique pulsator model: together with f_2 and f_3 it forms an exactly equally spaced triplet. We therefore derived the amplitude and phase of this possible further signal formally by fixing its frequency to the predicted value, and we include it in Table 2, where we summarize our multifrequency solution for HD 122970.

We have calculated formal error estimates using the formulae of Montgomery & O'Donoghue (1999) to give an approximate indication of the accuracy of our determinations. However, as has been shown by other studies (e.g. Handler et al. 2000a), such errors

Table 2. Multifrequency solution for our B filter data of the roAp star HD 122970 from 1998. Phases are relative to HJD 245 0907.007 767 (pulsation amplitude maximum). Amplitude signal-to-noise ratios (S/N) are calculated with Breger et al.'s (1993) method. Error sizes corresponding to 1σ values are determined following Montgomery & O'Donoghue (1999). As formal error sizes on the frequencies ($<10^{-4}\,\mu$Hz) are implausibly small using the full data set, which has a large time base due to a few runs outside the central campaign, we rather adopted the time base given by the March and April observations only.

ID	Frequency (μHz)	B Amplitude (mmag)	Phase (radians)	S/N
f_1	1502.480 ± 0.003	1.66 ± 0.03	−0.576 ± 0.015	28.9
f_2	1477.827 ± 0.006	0.85 ± 0.03	0.40 ± 0.03	14.4
f_3	1476.801 ± 0.011	0.45 ± 0.03	−0.36 ± 0.06	7.8
(f_4)	1478.853 ± 0.026	0.19 ± 0.03	−0.99 ± 0.13	3.2

are often underestimates due to non-random observational errors. As a test, we compared the noise level in the frequency region of interest with the noise level of a data set of the same time distribution and rms scatter as the observations themselves; we generated that by simply shuffling the residual magnitudes randomly. We found that the noise level in the amplitude spectrum of the data between 1400 and 1600 μHz is 80 per cent higher, as would be expected from white noise only.

This result is supported by the lowest panel of Fig. 1, where we show the amplitude spectrum of our data in a wider frequency range. It demonstrates that the remaining noise level between 1400 and 1600 μHz is conspicuously higher than in the neighbouring frequency regions. This is an indication that further low-amplitude frequencies may be present.

We therefore had strong motivations to carry out new observations of the star: the hypothesized third triplet component would allow a detailed application of the oblique pulsator model to HD 122970, and it could provide a mode identification. Intriguingly, this would leave radial pulsation as the only possibility for f_1, as the suspected multiplet around f_2 must then be due to a non-radial mode and the frequency difference between f_1 and f_2 is too small for them to be consecutive radial overtones of the same spherical degree (Handler et al. 2000b). Data with a higher duty cycle may also reveal a number of further intrinsic frequencies in the light curves of HD 122970. As we knew from our initial results what data quantity and quality would be required to achieve our scientific goals, we organized a second multisite campaign in the year 2001.

2.3 *uvby* colour photometry

The simultaneous *uvby* measurements from SNO give us the possibility to investigate the wavelength dependence of the pulsation amplitudes and phases of HD 122970. The time span of this data set is 5.2 d, which is too small to resolve the close peaks around 1477 μHz, but it is sufficient to resolve f_1 from this structure. We determined the pulsation amplitudes as a function of wavelength for both modes separately. This was done by adopting f_1 and f_2 from Table 2, keeping them fixed, thus leaving only the amplitudes, phases and the zero-point as free parameters. In this way, little room should be left for the occurrence of spurious results. The results of this analysis are summarized in Table 3. We note that we attempted to combine the *uvby* light curves or sensitive subsets thereof with the B-filter data to have a larger combined data set, but we concluded that this cannot be done in a sensible and reliable way.

Table 3. Pulsation amplitudes and phases of the roAp star HD 122970 in the different Strömgren filters from the 1998 observations. Phases are relative to HJD 245 0907.007 767.

	A_u (mmag)	A_v (mmag)	A_b (mmag)	A_y (mmag)
f_1	2.10 ± 0.15	2.43 ± 0.09	1.34 ± 0.07	0.82 ± 0.09
f_2	1.18 ± 0.15	1.24 ± 0.09	0.66 ± 0.07	0.33 ± 0.09
	ϕ_u (radians)	ϕ_v (radians)	ϕ_b (radians)	ϕ_y (radians)
f_1	−0.76 ± 0.07	−0.54 ± 0.04	−0.33 ± 0.05	−0.36 ± 0.11
f_2	0.52 ± 0.13	0.61 ± 0.07	0.91 ± 0.11	1.20 ± 0.28

3 THE SECOND MULTISITE CAMPAIGN

3.1 Observations and reductions

The new multisite observations in the year 2001 were obtained at five different telescopes at four observatories, all of which had already participated in the first campaign: the 0.75-m APT, the 1.0- and 0.5-m telescopes at SAAO, the 0.6-m reflector at SSO, and the 0.9-m telescope at OSN. The last observations again consisted of *uvby* photometry, whereas all the other telescopes used the B filter only. The new measurements are summarized in Table 4.

We collected almost twice as much B-filter photometry of similar quality as in the first campaign, which should allow a detection of f_4, if present and if the star did not change its pulsational behaviour. Data reduction was performed in the same way as described in Section 2.1, but we also kept a data set not filtered for low-frequency variations for comparison.

3.2 Frequency analysis

We used the same methods as outlined in Section 2.2; the spectral window, amplitude spectrum, and pre-whitened amplitude spectra are displayed in Fig. 2. The multifrequency solution for the 2001 data is presented in Table 5.

Comparing the results of the second campaign to those of the first one, several differences are noteworthy:

(i) f_3 seems to have disappeared;
(ii) none of the suspected further frequencies is detected;
(iii) both f_1 and f_2 have slightly lower frequencies than during the first campaign;
(iv) f_2 dropped somewhat in amplitude;
(v) the residual noise level is 71 per cent of the corresponding value of the 1998 campaign, and
(vi) again, some further low-amplitude modes can be suspected, but are not detected.

A comparison of the results in Table 5 and of a frequency analysis of the unfiltered measurements results in frequencies, amplitudes and phases which are the same within the quoted errors. No evidence for long-period signals is detected. However, the residual noise level of the unfiltered data in the frequency domain of the detected signals is 40 per cent higher than that in the filtered time series, demonstrating the value of low-frequency filtering.

Table 4. Journal of the observations of HD 122970 in 2001; σ is the rms scatter of the residual light curves after pre-whitening and low-frequency filtering; the remaining columns are self-explanatory.

Telescope	Date (UT)	Start (UT)	Length (h)	σ (mmag)
APT 0.75m	13 Mar	08:02:51	4.39	1.49
APT 0.75m	18 Mar	06:04:56	4.48	1.79
APT 0.75m	19 Mar	06:08:44	6.22	1.36
APT 0.75m	20 Mar	05:56:25	6.41	1.41
APT 0.75m	21 Mar	07:05:49	3.63	1.34
APT 0.75m	22 Mar	07:29:41	2.82	1.42
APT 0.75m	23 Mar	06:05:30	5.60	1.58
APT 0.75m	24 Mar	05:56:16	6.36	1.49
APT 0.75m	25 Mar	05:54:26	5.93	1.31
APT 0.75m	26 Mar	05:49:07	6.08	1.61
SSO 0.6m	26 Mar	17:10:42	1.84	2.24
APT 0.75m	27 Mar	05:45:25	6.65	1.64
SSO 0.6m	27 Mar	12:42:48	6.28	2.30
SAAO 0.5m	27 Mar	21:50:31	5.22	1.68
APT 0.75m	28 Mar	06:58:14	5.08	1.69
SSO 0.6m	28 Mar	14:44:20	3.16	2.34
SAAO 0.5m	28 Mar	21:46:03	5.37	2.37
APT 0.75m	29 Mar	05:37:17	6.73	1.72
SSO 0.6m	29 Mar	16:46:02	2.11	2.21
SAAO 0.5m	29 Mar	21:29:44	2.43	1.79
APT 0.75m	31 Mar	05:56:36	3.91	1.64
SSO 0.6m	31 Mar	13:06:08	2.84	1.81
SSO 0.6m	01 Apr	13:00:02	5.72	1.73
SAAO 1.0m	03 Apr	22:54:03	1.23	1.22
SSO 0.6m	04 Apr	13:05:41	5.86	2.11
SSO 0.6m	05 Apr	12:34:40	6.02	1.82
SSO 0.6m	06 Apr	11:43:17	5.69	2.03
APT 0.75m	07 Apr	04:44:44	5.26	1.60
APT 0.75m	08 Apr	04:42:38	4.57	1.84
APT 0.75m	09 Apr	04:35:33	4.95	1.64
OSN 0.9m	09 Apr	23:31:29	4.31	9.4/3.9/3.9/5.2
SAAO 0.5m	10 Apr	20:36:20	5.49	2.08
OSN 0.9m	11 Apr	01:20:41	3.22	8.1/3.7/3.9/4.9
SAAO 0.5m	11 Apr	21:13:23	4.97	1.57
OSN 0.9m	12 Apr	00:50:27	3.61	8.0/4.0/4.1/4.7
APT 0.75m	12 Apr	04:35:39	4.71	1.56
SAAO 0.5m	13 Apr	00:34:40	1.59	1.82
APT 0.75m	13 Apr	04:38:23	5.87	1.41
APT 0.75m	14 Apr	04:33:41	7.26	1.79
SAAO 0.5m	14 Apr	22:11:51	2.69	1.97
APT 0.75m	15 Apr	04:18:09	7.51	1.73
APT 0.75m	16 Apr	04:18:56	7.09	1.77
APT 0.75m	21 Apr	04:20:58	5.56	2.21
SSO 0.6m	26 Apr	15:41:20	1.21	1.69
Total		*B*	191.46	1.78
		uvby	11.13	8.6/3.9/4.0/5.0

3.3 Analysis of the combined *B* filter data from both campaigns

As a final step, we combined the two data sets and analysed them together as a single data set. Because our measurements had already been transformed to a common time base (Heliocentric Julian Date) and the variability is expressed as deviations around a mean magnitude of zero, no further homogenization was necessary. In the light of our previous results it is not surprising that two dominating frequencies, the mean values of f_1 and f_2 from Tables 2 and 5, are obtained. Pre-whitening those, f_3 is detected, but of course it is affected by its amplitude variability.

Because f_1 and f_2 had significantly different values in the different years, we proceeded by pre-whitening them from the individual campaign data sets, and removing f_3 from the 1998 data as well. We then combined these residuals and calculated an amplitude spectrum of these; we display it in Fig. 3.

Again, no new frequency is detected. The single outstanding peak in this amplitude spectrum has an S/N of 3.7, which renders it insignificant. We also note that there is no evidence for the previously hypothesized signal f_4, or for any combination frequency of the detected modes.

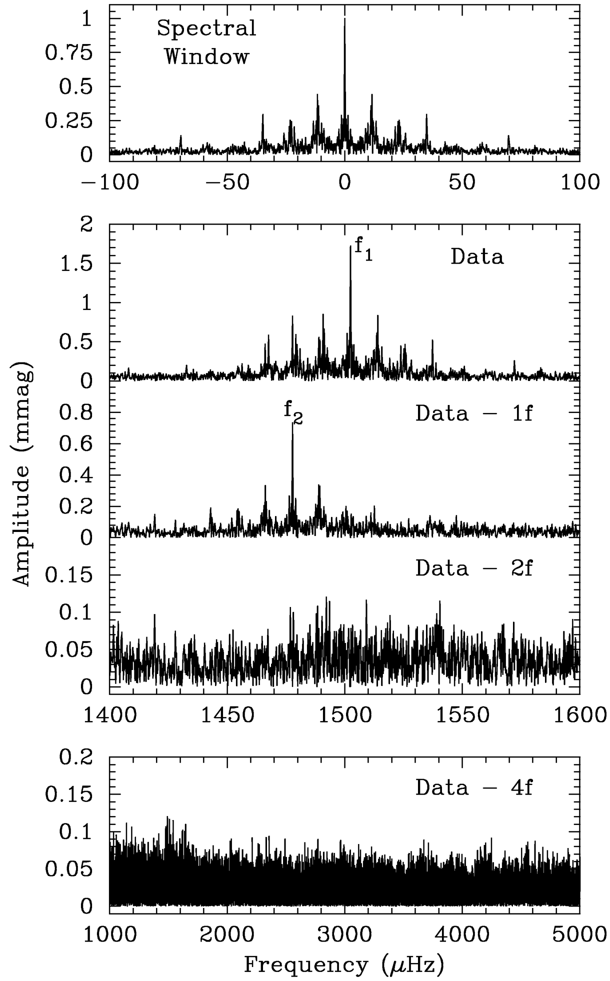

Figure 2. Amplitude spectra of HD 122970 with successive pre-whitening of the detected frequencies from the measurements in 2001. The previously detected frequencies f_1 and f_2 are again present, but f_3 is missing and no convincing evidence for further periodicities can be found.

Table 5. Multifrequency solution for the roAp star HD 122970. Phases are relative to HJD 245 2014.778 186 (pulsation amplitude maximum); amplitude signal-to-noise ratios are calculated with Breger et al.'s (1993) method, and error sizes correspond to 1σ values determined following Montgomery & O'Donoghue (1999).

	Frequency (μHz)	*B* Amplitude (mmag)	Phase (radians)	S/N
f_1	1502.439 ± 0.002	1.68 ± 0.02	+0.001 ± 0.012	44.7
f_2	1477.781 ± 0.004	0.74 ± 0.02	−0.002 ± 0.027	19.6

3.4 *uvby* colour photometry

Regrettably, the new *uvby* observations are less extensive, of

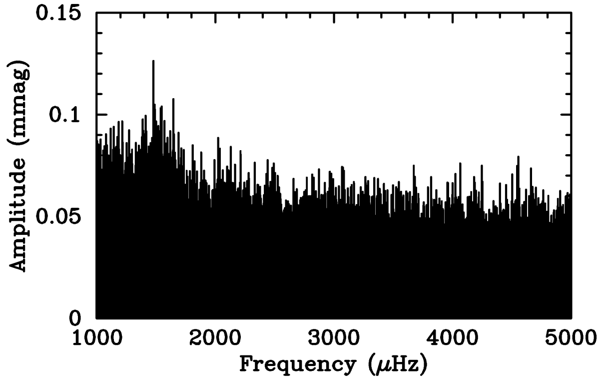

Figure 3. Amplitude spectrum of the combined residual time series of HD 122970 from both campaigns. No peak is significant.

Table 6. Pulsation amplitudes and phases of the roAp star HD 122970 in the different Strömgren filters from the 2001 observations. Phases are relative to HJD 245 2014 778 186.

	A_u (mmag)	A_v (mmag)	A_b (mmag)	A_y (mmag)
f_1	2.0 ± 0.4	2.4 ± 0.2	1.3 ± 0.2	0.5 ± 0.3
f_2	0.5 ± 0.4	1.3 ± 0.2	0.8 ± 0.2	0.9 ± 0.3
	ϕ_u (radians)	ϕ_v (radians)	ϕ_b (radians)	ϕ_y (radians)
f_1	−0.32 ± 0.22	−0.26 ± 0.09	−0.53 ± 0.16	−0.32 ± 0.58
f_2	0.87 ± 0.82	−0.46 ± 0.16	−0.22 ± 0.26	−0.52 ± 0.28

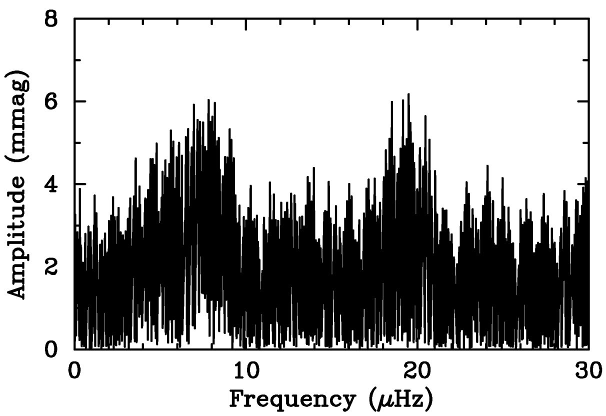

Figure 4. The amplitude spectrum of the *Hipparcos* photometric data of HD 122970.

poorer quality, and have a shorter time base than those from 1998. Nevertheless, we have listed the amplitudes and phases of f_1 and f_2 derived from those data in Table 6 for completeness. Note that the alias patterns of f_1 and f_2 are not quite resolved in those data, and that f_2 was not affected by another signal in the present data; the results must therefore be taken with some caution. In any case, they are roughly consistent with our findings from Section 2.3.

4 *HIPPARCOS* PHOTOMETRY

As mentioned in the introduction, HD 122970 was also a target of the *Hipparcos* mission (ESA 1997). The photometric data set acquired by the satellite comprises a total of 169 accepted transits, which we can use to check whether modulation in the mean magnitude of the star caused by inhomogenous distribution of different chemical elements on the stellar surface is present. This would allow us to determine the rotational period of HD 122970. The amplitude spectrum of the *Hipparcos* photometry is shown in Fig. 4.

Although there seems to be some low-frequency variability of HD 122970, no significant peak is present in this amplitude spectrum. This conclusion remains unchanged when performing period analyses with software allowing for non-sinusoidal variations.

5 DISCUSSION AND CONCLUSIONS

Although we did not reach the main goal of this study, a definite mode identification of the pulsations of HD 122970, several interesting results can be obtained. The physical parameters of the star derived in Section 1.2 yield a mean stellar density of $\bar{\rho} = 0.26 \pm 0.03\rho_{\odot}$. Hence the asymptotic frequency spacing of consecutive radial overtones of the star is 68 ± 4 μHz (following Ulrich 1986). The frequency difference between the modes f_1 and f_2 is 24.66 μHz, suggesting that these two modes have different spherical degree ℓ. f_1 and f_2 cannot be rotationally split components of modes of the same ℓ, as roAp stars are intrinsically slow rotators (see, e.g., Kurtz & Martinez 2000).

The disappearance of f_3 first prompted us to test whether this signal was an artefact from the frequency analysis of the 1998 data, but we found that it is definitely present throughout this year's data set. A physical interpretation for f_3's vanishing is not unambiguous because of our poor knowledge of the nature of the star's pulsation modes. If f_3 were an independent pulsation mode, intrinsic amplitude modulation would have occurred. Were it a rotational sidelobe of f_2, one could speculate that the magnetic obliquity β_0 has changed, possibly due to precession of the rotation axis in a binary system. However, this would require a drop in the intrinsic amplitude of the mode producing f_2 and f_3 (which was 1.21 mmag in 1998; cf. Table 2), because f_2, the only component visible in 2001, had dropped to smaller amplitude (0.74 mmag; Table 5). Regrettably, we cannot say whether f_2 and f_3 are produced by the same mode, as intrinsic amplitude variations are known to be present in roAp stars (see, e.g., Matthews, Kurtz & Wehlau 1987).

Frequency variability is also not a phenomenon newly discovered for roAp stars. For instance, the frequency variations of the singly periodic star HR 3831 are very well studied (Kurtz et al. 1997). Given our results for HD 122970, we can only state that the frequencies f_1 and f_2 remained constant throughout the individual years of observation within the errors. It is interesting to note that their values shifted, again within the errors, by the same small amount between the two different campaigns. A radial velocity change of about 8.5 km s^{-1} would already be sufficient to explain these frequency shifts in terms of a binary hypothesis. Spectroscopic or long-term photometric monitoring of HD 122970 would therefore be desirable to examine the cause for binarity of the star.

Turning to the *uvby* colour photometry, we find that the amplitude versus wavelength relation of HD 122970 as listed in Table 3 is quite similar to that of the other objects studied so far (Medupe & Kurtz 1998). The relative amplitudes and phases of the two modes, which are of different ℓ, are the same within the errors. This means either that *uvby* photometry is not suitable for mode discrimination in roAp stars, or that our data are not extensive enough for such an analysis.

The lack of detection of rotational light modulations in the *Hipparcos* photometry of HD 122970 may be due to the *Hipparcos* band being not very suitable for the search of rotational light modulation of Ap stars. More physically, it can also be the case that HD 122970 is not strongly spotted, or that it is viewed nearly pole-on.

ACKNOWLEDGMENTS

The Austrian Fonds zur Förderung der wissenschaftlichen Forschung partially supported this work under grants S7303-AST and S7304-AST. We are grateful to I. Iliev, A. Antov and P. Eenens for their unsuccessful attempts to obtain additional measurements. GH thanks Holger Pikall for supplying stellar evolution and pulsation models, and Don Kurtz for proofreading a draft version of this paper.

REFERENCES

Breger M., 1995, in Ulrich R. K. et al., eds, ASP Conf. Ser. Vol. 76, Helio- and Astero-Seismology from the Earth and Space. Astron. Soc. Pac., San Francisco, p. 596
Breger M. et al., 1993, A&A, 271, 482
Burstein D., Heiles C., 1982, AJ, 87, 1165
Crawford D. L., 1975, AJ, 80, 955
ESA, 1997, The *Hipparcos* and Tycho Catalogues, ESA SP-1200
Grauer A. D., Bond H. E., 1981, PASP, 93, 388
Handler G., Paunzen E., 1999, A&AS, 135, 57
Handler G. et al., 2000a, MNRAS, 318, 511
Handler G. et al., 2000b, in Szabados L., Kurtz D., eds, ASP Conf. Ser. Vol. 203, The Impact of Large-Scale Surveys on Pulsating Star Research. Astron. Soc. Pac., San Francisco, p. 490
Kurtz D. W., 1978, Inf. Bull. Variable Stars No. 1436
Kurtz D. W., 1982, MNRAS, 200, 807
Kurtz D. W., 1992, MNRAS, 259, 701
Kurtz D. W., Martinez P., 2000, Baltic Astronomy, 9, 253
Kurtz D. W., van Wyk F., Roberts G., Marang F., Handler G., Medupe R., Kilkenny D., 1997, MNRAS, 287, 69
Kuschnig R., Ryabchikova T. A., Piskunov N. E., Weiss W. W., Gelbmann M. J., 1999, A&A, 348, 924
Matthews J. M., Kurtz D. W., Wehlau W. H., 1987, ApJ, 313, 782
Matthews J. M., Kurtz D. W., Martinez P., 1999, ApJ, 511, 422
Medupe R., Kurtz D. W., 1998, MNRAS, 299, 371
Montgomery M. H., O'Donoghue D., 1999, Delta Scuti Star Newsletter, 13, 28 (Univ. Vienna)
Nelson M. J., Kreidl T. J., 1993, AJ, 105, 1903
Nielsen R. F., 1983, in Hauge O., ed., Inst. Theor. Astrophys. Oslo Report No. 59, p. 141
Pamyatnykh A. A., Dziembowski W. A., Handler G., Pikall H., 1998, A&A, 333, 141
Perry C. L., Johnston L., 1982, ApJS, 50, 451
Ryabchikova T. A., Savanov I. S., Hatzes A. P., Weiss W. W., Handler G., 2000, A&A, 357, 981
Shibahashi H., Takata M., 1993, PASJ, 45, 617
Sperl M., 1998, Master's thesis, Univ. Vienna
Strassmeier K. G., Boyd L. J., Epand D. H., Granzer T., 1997, PASP, 109, 697
Ulrich R. K., 1986, ApJ, 306, L37
Villa P., 1998, Master's thesis, Univ. Vienna

This paper has been typeset from a TEX/LATEX file prepared by the author.

4.4 The rapidly oscillating Ap star HD 99563 and its distorted dipole pulsation mode

Original paper:

G. Handler, W. W. Weiss, R. R. Shobbrook, E. Paunzen, A. Hempel, S. K. Anguma, P. C. Kalebwe, D. Kilkenny, P. Martinez, M. B. Moalusi, R. Garrido, R. Medupe, 2006, MNRAS 366, 257

Mon. Not. R. Astron. Soc. **366,** 257–266 (2006) doi:10.1111/j.1365-2966.2005.09849.x

The rapidly oscillating Ap star HD 99563 and its distorted dipole pulsation mode

G. Handler,[1,2★] W. W. Weiss,[1] R. R. Shobbrook,[3] E. Paunzen,[1] A. Hempel,[4] S. K. Anguma, [5]P. C. Kalebwe,[6] D. Kilkenny,[2] P. Martinez,[2] M. B. Moalusi,[7] R. Garrido[8] and R. Medupe[2]

[1]*Institut für Astronomie, Universität Wien, Türkenschanzstraße 17, A-1180 Wien, Austria*
[2]*South African Astronomical Observatory, PO Box 9, Observatory 7935, South Africa*
[3]*Research School of Astronomy and Astrophysics, Australian National University, Canberra, ACT, Australia*
[4]*Observatoire de Genève, Chemin des Maillettes 51, CH-1290 Sauverny, Switzerland*
[5] *Department of Physics, Mbarara University of Science and Technology, PO Box 1410, Mbarara, Uganda*
[6]*Physics Department, The University of Zambia, PO Box 32379, Lusaka, Zambia*
[7]*Department of Physics, University of the North-West, Private Bag X2046, Mmabatho 2735, South Africa*
[8]*Instituto de Astrofisica de Andalucia, Apt. 3044, E-18080 Granada, Spain*

Accepted 2005 November 8. Received 2005 November 3; in original form 2005 September 16

ABSTRACT

We undertook a time-series photometric multisite campaign for the rapidly oscillating Ap (roAp) star HD 99563 and also acquired mean light observations over four seasons. The pulsations of the star, which show flatter light maxima than minima, can be described with a frequency quintuplet centred on 1557.653 μHz and some first harmonics of it. The amplitude of the pulsation is modulated with the rotation period of the star that we determine with 2.91179 ± 0.00007 d from the analysis of the stellar pulsation spectrum and of the mean light data. We break up the distorted oscillation mode into its pure spherical harmonic components and find it is dominated by the $\ell = 1$ pulsation, and also has a notable $\ell = 3$ contribution, with weak $\ell =$ 0 and 2 components. The geometrical configuration of the star allows us to see both pulsation poles for about the same amount of time; HD 99563 is only the fourth roAp star for which both pulsation poles are seen and only the third where the distortion of the pulsation modes has been modelled. We point out that HD 99563 is very similar to the well-studied roAp star HR 3831. Finally, we note that the visual companion of HD 99563 is located in the δ Scuti instability strip and may thus show pulsation. We show that if the companion was physical, the roAp star would be a 2.03-$M_{\odot}$, object, seen at a rotational inclination of 44°, which then predicts a magnetic obliquity $\beta = 86\overset{\circ}{.}4$.

Key words: techniques: photometric – stars: individual: HD 99563 – stars: individual: XY Crt – stars: oscillations – stars: variables: other.

1 INTRODUCTION

Where the lower part of the classical instability strip intersects the main sequence, three distinct classes of multiperiodically pulsating variables can be found. The γ Doradus stars pulsate in gravity modes of high radial order and have periods of the order of 1 d (Kaye et al. 1999). The δ Scuti stars have periods of the order of a few hours (Breger 1979) and are thus pressure and gravity mode pulsators of low radial order.

The fastest pulsations in this domain in the Hertzsprung–Russell (HR) diagram are however excited in the rapidly oscillating Ap (roAp) stars (Kurtz 1982; Kurtz & Martinez 2000), with typical periods around 10 min, indicating pressure modes of high radial overtones. The photometric semi-amplitudes associated with these pulsations are in most cases only a few mmag, which makes them difficult to detect. The roAp stars are also remarkable because of their spectral peculiarities, because they are pulsating representatives of cool magnetic Ap stars of the SrCrEu subtype.

The magnetic fields of Ap stars cause elemental segregation on the stellar surface. In other words, the chemical elements are arranged in patches on the stellar surface (see, for example, Kochukhov et al. 2004 or Lueftinger et al. 2003 for well-documented examples). This causes modulation of the mean apparent brightness of the star with the rotation period. As the chemical elements show some alignment with the magnetic poles, the rotational light curves show a

★E-mail: handler@astro.univie.ac.at

single-wave structure if only one magnetic pole is seen and a double-wave variation if both magnetic poles come into view during a rotation cycle.

The strong magnetic fields present in the roAp stars are usually not aligned with the stellar rotation axis. Because the pulsation axis does however coincide with the magnetic axis, the roAp stars are oblique pulsators (Kurtz 1982). This means that the pulsation modes excited in the roAp stars are seen at different aspects during the rotation cycle, which, for non-radial modes, causes amplitude modulation over the rotation period (which can then be inferred) and allows us to put constraints on the geometry of the pulsator.

The oblique pulsator model (OPM), in its simplest form, then predicts that (except for special geometric orientations of the axes) dipole ($\ell = 1$) pulsation modes will be split into equally spaced triplets. Quadrupole ($\ell = 2$) modes will give rise to equally spaced frequency quintuplets, where the spacing of consecutive multiplet components is exactly the stellar rotational frequency.

The magnetic field of the roAp stars affects the pulsations in two additional ways. First, the pulsation frequencies are shifted with respect to their unperturbed value (Cunha & Gough 2000) and, secondly, the pulsation modes are distorted so that a single spherical harmonic can no longer describe them fully (e.g. Kurtz, Kanaan & Martinez 1993; Takata & Shibahashi 1995). This is observationally manifested by the presence of additional multiplet components surrounding the first-order singlets, triplets or quintuplets, which are spaced by integer multiples of the rotation frequency.

For a long time, the predominant observing method for studying the pulsations of roAp stars was time-resolved high-speed photometry, yielding interesting results on the pulsational behaviour, geometry and asteroseismology of these stars (see, for example, Matthews, Kurtz & Martinez 1999). The most recent observational advances however have come from time-resolved spectroscopy; because the vertical wavelengths of the pulsation modes are comparable to the size of the line-forming regions in the atmospheres of these stars, the vertical structure of the atmospheres can be resolved (Ryabchikova et al. 2002; Kurtz, Elkin & Mathys 2003).

Spectroscopy is also more sensitive to the detection of roAp star pulsations than photometry. Because of the vertical stratification of chemical elements in their atmospheres (e.g. Ryabchikova et al. 2002) the pulsational radial velocity amplitudes of some spectral lines (most notably rare-earth elements) can reach several kilometers per second.

The most extreme example of such high radial velocity amplitudes is HD 99563 (XY Crt). This star was photometrically discovered to pulsate by Dorokhova & Dorokhov (1998) and this was confirmed by Handler & Paunzen (1999). Elkin, Kurtz & Mathys (2005) discovered pulsational radial velocity variations with semi-amplitudes of up 5 km s^{-1} for some Eu II and Tm II lines in their time-resolved spectroscopy of this star. Such high amplitudes are capable of yielding information on the structure of the atmospheres of Ap stars with the best possible signal-to-noise (S/N).

However, one important piece of information that spectroscopy cannot supply at this point is detailed knowledge of the stellar pulsation spectrum. The reason is that the largest telescopes are necessary for obtaining spectra of the required time resolution and S/N. However, observing time on these telescopes is sparse. Therefore, lengthy photometric measurements of these stars on small telescopes are still required to decipher the pulsational spectra fully.

To this end, we included HD 99563 as a secondary target in a multisite campaign originally devoted to the roAp star HD 122970 (Handler et al. 2002) to be observed at times when the latter star was not yet accessible. However, HD 99563 turned out to be quite interesting, which is why we continued to observe it after the original campaign was finished. We also acquired mean light observations of HD 99563 in an attempt to determine its rotation period. In this paper, we report on the results of these measurements.

2 OBSERVATIONS AND REDUCTIONS

2.1 High-speed photometry

Our multisite time-series photometric observations were obtained with seven different telescopes at four observatories: the 0.75-m T6 Automatic Photometric Telescope at Fairborn Observatory (FAPT) in Arizona, the 0.5-, 0.75-, 1.0- and 1.9-m telescopes at the South African Astronomical Observatory (SAAO), the 0.6-m reflector at Siding Spring Observatory (SSO) in Australia and the 0.9-m telescope at Observatorio de Sierra Nevada (OSN) in Spain. Whereas the latter observations consisted of Strömgren *uvby* photometry, the other telescopes used the *B* filter only. The measurements are summarized in Table 1.

The time-series photometry was generally acquired as continuous 10-s integrations. Large apertures (>35 arcsec) were employed to minimize the contributions of seeing and guiding. The observations of the target star were interrupted at irregular intervals (depending on the brightness and position of the Moon) to obtain measurements of sky-background.

Reductions were performed by first correcting for coincidence losses (dead time correction), then for sky-background and extinction. Some low-frequency filtering to remove residual transparency variations or tube sensitivity drifts with time-scales longer than 30 min was applied by fitting low-order polynomials to the data and by subtracting these. Finally, the measurements were binned into 40-s integrations, the times of the observation were converted to Heliocentric Julian Date (HJD) and all the data were joined into a combined single light curve.

Some of our nightly measurements are shown in Fig. 1, clearly containing some interesting features. First, the pulsation amplitude can vary rather dramatically from almost zero to more than 10 mmag peak-to-peak, and it can also be seen to vary during a single night. Secondly, the shape of the light curves near maximum amplitude is peculiar, with the light maxima being flatter than the light minima.

2.2 Mean light observations

Differential multicolour photometry of HD 99563 was obtained with the 0.75-m Automatic Photometric Telescope at SAAO (Martinez et al. 2002) from 2001 March until 2004 June. Single-channel differential measurements were acquired with respect to the single comparison star HD 99506, which is not known to be variable, in the Johnson–Cousins *UBVRI* filters. Again, large apertures (>35 arcsec) were used to eliminate effects of scintillation and seeing.

Two nightly *UBVRI* measurements of HD 99563 were usually taken in between two measurements of HD 99506, ensuring that variations in sky transparency can be readily compensated for, but also aiming at averaging out the effects of the rapid oscillations on the mean magnitude. As the two integrations on the target were separated by about 380 s, about half the oscillation period, the pulsational signal was strongly suppressed.

The data of both stars were reduced by correction for coincidence losses, sky-background and extinction, and the timings were heliocentrically corrected. Differential magnitudes between the variable and the comparison star were computed by simple linear interpolation. After rejection of outliers and merging of the two nightly

Table 1. Journal of the observations of HD 99563. N_{40} is the number of 40-s data bins obtained on the respective night and σ is the rms scatter of the residual light curves after pre-whitening and low-frequency filtering; the remaining columns are self-explanatory.

Telescope	Date (UT)	Start (UT)	Length (h)	N_{40}	σ (mmag)
FAPT 0.75-m	18/03	04:54:24	0.64	55	1.98
FAPT 0.75-m	19/03	03:43:40	1.75	140	1.71
FAPT 0.75-m	20/03	03:39:41	2.15	180	1.40
FAPT 0.75-m	23/03	03:23:03	2.54	208	1.74
FAPT 0.75-m	24/03	03:16:41	2.53	210	2.21
FAPT 0.75-m	25/03	04:20:58	1.43	119	1.51
FAPT 0.75-m	26/03	03:10:24	2.52	209	1.73
FAPT 0.75-m	27/03	03:04:34	2.52	200	1.88
SAAO 0.5-m	27/03	18:47:49	2.68	188	1.75
SSO 0.6-m	28/03	09:49:16	2.01	166	2.04
SAAO 0.5-m	28/03	17:59:55	3.36	252	2.14
FAPT 0.75-m	29/03	02:58:32	2.52	174	2.14
SSO 0.6-m	29/03	09:20:27	3.59	271	2.21
SAAO 0.5-m	29/03	17:56:30	3.35	255	1.87
SAAO 0.5-m	30/03	20:31:12	0.72	59	1.85
FAPT 0.75-m	31/03	02:47:47	2.52	210	2.24
SSO 0.6-m	31/03	09:43:39	2.82	235	1.62
SSO 0.6-m	01/04	10:41:08	2.18	177	1.48
SAAO 0.5-m	02/04	18:03:43	2.96	192	2.19
SAAO 1.0-m	03/04	19:34:44	1.29	104	0.59
SSO 0.6-m	04/04	09:18:16	2.01	146	1.80
SAAO 1.0-m	04/04	19:15:49	1.62	137	0.65
SSO 0.6-m	05/04	11:01:34	1.37	101	1.61
FAPT 0.75-m	09/04	02:50:41	1.61	131	2.15
SAAO 0.5-m	09/04	17:43:48	1.08	64	2.11
SAAO 1.0-m	09/04	18:00:40	1.14	98	1.23
OSN 0.9-m	09/04	19:54:16	1.61	135	8.2/2.8/3.0/3.7
SAAO 0.5-m	10/04	17:50:42	2.59	191	1.47
SAAO 0.5-m	11/04	17:27:29	3.64	264	1.62
OSN 0.9-m	11/04	20:19:34	4.44	309	7.5/4.4/4.0/4.5
FAPT 0.75-m	12/04	02:55:06	1.57	127	1.71
SAAO 0.5-m	12/04	17:28:47	6.85	465	1.79
FAPT 0.75-m	13/04	02:53:47	1.61	135	1.56
FAPT 0.75-m	14/04	03:44:02	0.69	57	2.90
SAAO 0.5-m	14/04	17:09:07	4.13	305	1.87
FAPT 0.75-m	15/04	02:44:55	1.42	120	1.65
FAPT 0.75-m	16/04	02:57:02	1.23	102	1.60
FAPT 0.75-m	18/04	02:52:32	0.90	76	1.62
SSO 0.6-m	23/04	13:42:01	0.72	54	2.11
SSO 0.6-m	27/04	09:01:18	5.04	398	1.71
SAAO 1.9-m	30/04	17:14:35	0.69	60	0.95
SAAO 0.75-m	15/05	17:11:06	1.61	137	1.57
SSO 0.6-m	16/05	11:59:23	0.24	23	2.03
SAAO 0.75-m	16/05	20:50:28	0.68	58	1.24
SAAO 0.75-m	17/05	18:28:06	1.80	155	1.50
SAAO 0.75-m	18/05	16:59:33	3.40	257	1.43
SAAO 0.75-m	21/05	19:09:55	2.34	206	1.50

Table 1 – *continued*

Telescope	Date (UT)	Start (UT)	Length (h)	N_{40}	σ (mmag)
SSO 0.6-m	22/05	12:09:16	1.10	94	1.90
SSO 0.6-m	24/05	08:38:42	3.72	298	1.41
SSO 0.6-m	30/05	08:20:08	1.68	139	1.12
SAAO 0.5-m	01/06	18:09:26	2.76	222	1.20
SAAO 0.5-m	02/06	18:37:05	1.76	143	1.26
SAAO 0.5-m	04/06	17:14:49	3.18	253	1.60
SAAO 0.5-m	06/06	19:58:06	0.79	59	2.34
SAAO 0.5-m	07/06	16:38:51	2.54	183	1.73
SAAO 0.5-m	08/06	16:41:45	3.97	286	2.78
SAAO 0.5-m	09/06	16:36:15	4.00	296	1.59
SAAO 0.5-m	10/06	18:23:46	1.18	82	1.32
SAAO 0.5-m	11/06	17:40:49	2.75	202	1.56
Total		*B*	125.49	9728	1.82
		uvby	6.05	444	7.7/3.9/3.7/4.3

measurements, a total of 150 differential *UBVRI* magnitudes of HD 99563 were available.

3 FREQUENCY ANALYSIS (I)

3.1 High-speed photometry

The reduced *B* filter light curves were analysed with the computer program PERIOD98 using single-frequency Fourier and multiple-frequency least-squares techniques (Sperl 1998). This program has, amongst others, the capabilities of calculating Fourier periodograms, calculating the best fit to the data with all given frequencies simultaneously by minimizing the residuals between light curve and fit. Within the multifrequency fitting, combination frequencies (which in our case are expected because of the shape of the light curves) can be fixed to their expected values and their amplitudes and phases can be optimized together with the other independent parameters.

We show the amplitude spectrum of the combined light curve in the uppermost panel of Fig. 2. Two main regions of power are visible, one centred around 1500 μHz and a weaker one around 3100 μHz. The first of the sequence of panels on the left-hand side of Fig. 2 shows the spectral window of the data at an extended scale, computed as the Fourier transform of a single noise-free sinusoid with a frequency of 1553.67 μHz and an amplitude of 2.7 mmag. We see some alias patterns about 34.7 μHz away from the central peak. This is the 3 cd^{-1} alias, which is most prominent in our data because of the longitude distribution of the observatories used, combined with the short duration of most of the runs. Fortunately, neither this alias, nor any other, will have any influence on our results.

The second panel on the left-hand side contains the amplitude spectrum of the data. It is clearly more complicated than the spectral window. Pre-whitening the strongest signal from the data, we end up with the residual amplitude spectrum in the third (middle) panel of Fig. 2, left-hand side. Further pre-whitening of the strongest signal there reveals another, and continuing this procedure results in the detection of a fourth frequency in this domain, where no more signals can now be detected.

We continue the frequency analysis in the region around 3100 μHz, showing it in the sequence of panels on the right-hand side of Fig. 2. Following the same strategy as before, we detect five signals in this frequency domain. After pre-whitening these, we arrive at the residual amplitude spectrum in the lowest panel of Fig. 2. The noise level at frequencies below ∼ 800 μHz is artificially decreased as a result of our low-frequency filtering.

Consequently, we have separately analysed our longest ($\Delta T >$ 2 h) light curves from the best nights, leaving them unfiltered for low frequencies, and searched them for periodicities. We found no such variations, with detection thresholds of 1.8 mmag for frequencies

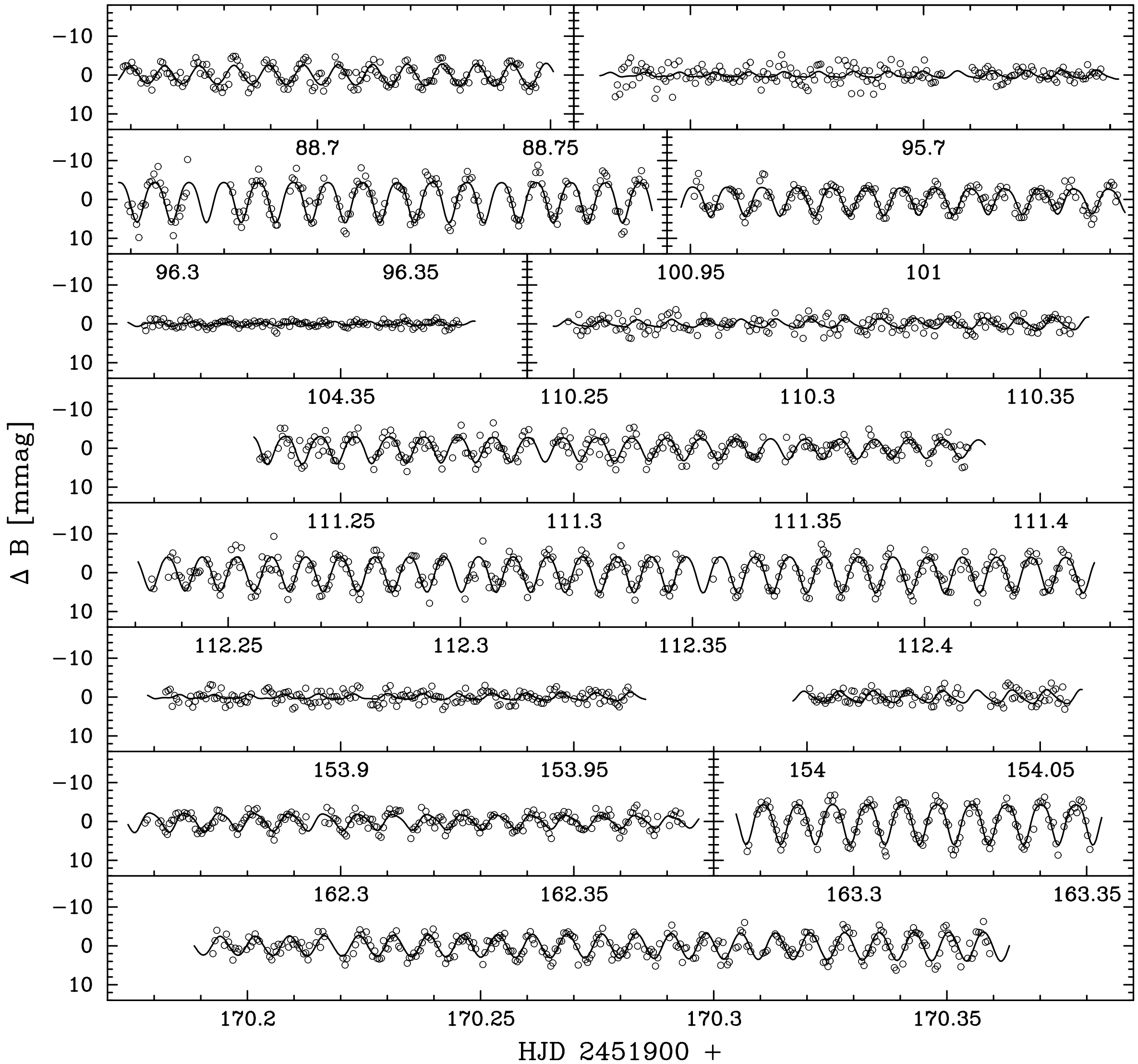

Figure 1. Some light curves of HD 99563 from our multisite observations showing its diverse nightly behaviour. The solid lines represent the multifrequency fit listed in Table 2, to guide the eye.

below 200 μHz, 0.8 mmag for frequencies between 200 and 450 μHz, and 0.5 mmag for frequencies between 450 and 1000 μHz.

More interesting is the excess mound of amplitude at frequencies around 1500 μHz on top of the essentially monotonically decreasing noise that can be discerned in the lowest panel of Fig. 2. This is the region where four signals have already been detected. The excess mound of amplitude may indicate the presence of further signals or of amplitude/frequency variability of some of the periodicities detected previously. In any case, a preliminary frequency solution derived in this way is listed in Table 2.

We have only accepted signals that satisfy the statistical criterion of S/N >4 for independent oscillations and S/N >3.5 for combination frequencies. These variations are regarded as statistically significantly detected. We refer to Breger et al. (1999) for a more in-depth discussion of this criterion, which has turned out to be extremely reliable in the past.

The independent frequencies in Table 2 can, at first sight, not be unambiguously be interpreted within the OPM. Although f_3, f_1 and f_2 form a triplet with a spacing of about 7.95 μHz, f_1, f_4 and f_2 can also be reconciled with a triplet with a spacing of approximately 3.98 μHz, allowing for a $\sim 3\sigma$ shift in frequency f_4. In this context it is important to note that the formal error estimates we use here are believed to underestimate the real errors by about a factor of 2 (Handler et al. 2000; Jerzykiewicz et al. 2005), and therefore we cannot simply reject the latter interpretation. Consequently, all four frequencies could even be part of an equally spaced quintuplet with a component missing near 1549.7 μHz.

3.2 Mean light observations

We again used PERIOD98 for the frequency analysis. Amplitude spectra of the measurements in the five *UBVRI* filters were computed. Although the nominal Nyquist frequency of our observations is 0.5 cd^{-1} ($\sim$6 μHz), we carefully examined a frequency range up to 25 μHz. We found variability in all the five passbands, with those in *U* having the highest amplitude, as shown in Fig. 3.

The upper panel of this figure contains the spectral window function of the data, calculated as the amplitude spectrum of a single

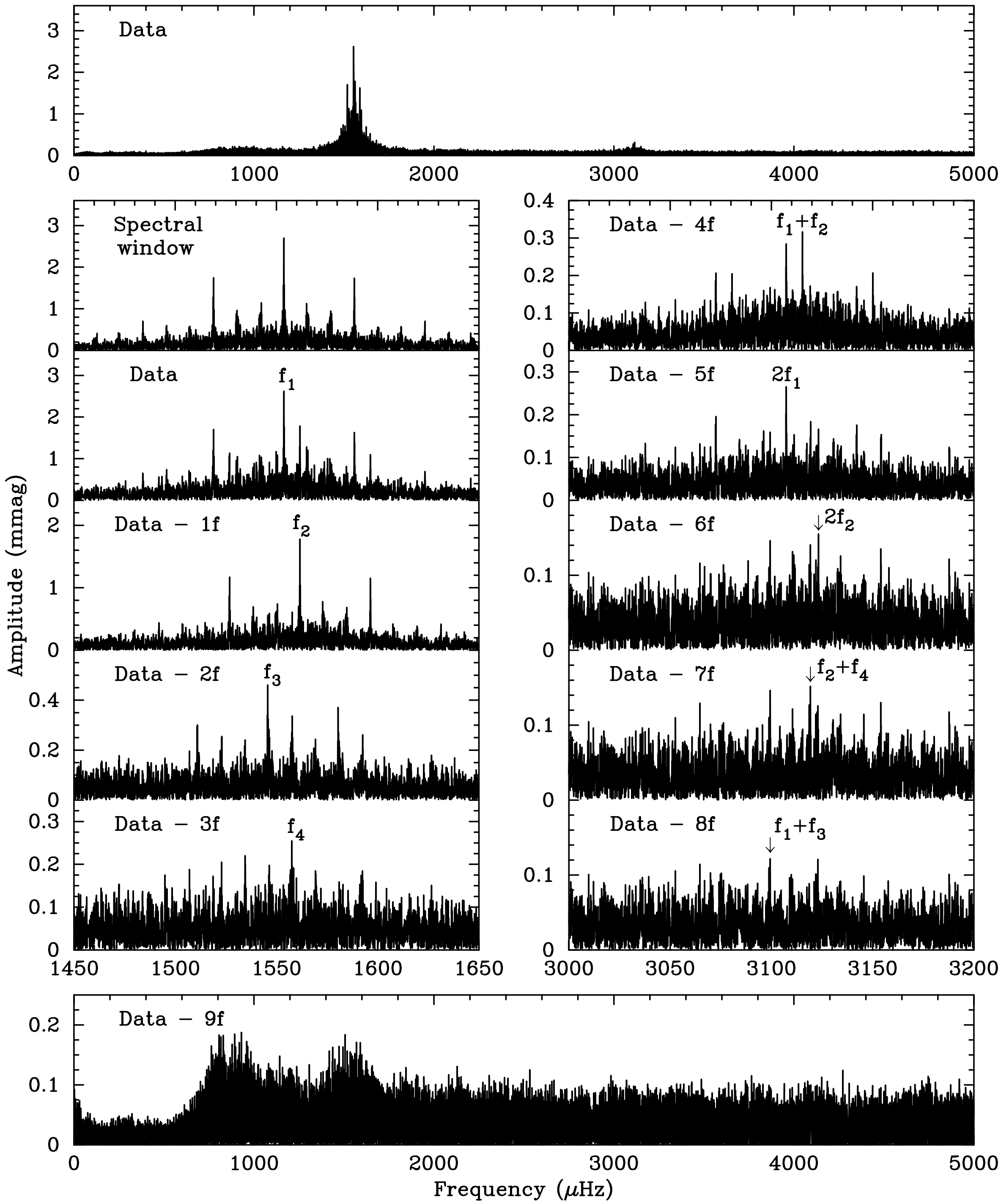

Figure 2. Amplitude spectra of HD 99563 from our multisite observations with successive pre-whitening of the detected frequencies.

noise-free sinusoid with a frequency of 7.95 μHz and an amplitude of 31 mmag. There is strong 1 cd^{-1} aliasing (the peak near 20 μHz), and also reflection of the aliasing pattern at frequency zero (peaks near 4 and 15 μHz). Nevertheless, the input signal produces the tallest peak in the window function. This is why we can be sure that the peak labelled in the amplitude spectrum of the data (middle panel of Fig. 3) is also the correct frequency present in the measurements, which is confirmed by the pre-whitened amplitude spectrum in the lower panel of this figure that contains noise only.

We encountered the same situation in the *B* filter data, where the mean light variations also have considerable amplitude. In *VRI* the situation is more complex, as the S/N of the variability is lower. Significant peaks at the same frequencies are however still present, but because of the effects of noise the tallest maxima are found at alias frequencies in *V* and *R*. After pre-whitening the signal near 7.95 μHz, the residual amplitude spectra in all filters contain noise only; in particular, no evidence for harmonics or subharmonics of this frequency can be detected.

Table 2. Preliminary multifrequency solution for our B filter data of the roAp star HD 99563, with the frequencies around 1500 μHz left as free parameters. Error estimates correspond to 1σ values are determined following Montgomery & O'Donoghue (1999).

ID	Frequency (μHz)	B amplitude (mmag)	S/N
f_1	1553.6780 ± 0.0007	2.69 ± 0.03	49.1
f_2	1561.6286 ± 0.0011	1.80 ± 0.03	32.9
f_3	1545.736 ± 0.004	0.46 ± 0.03	8.4
f_4	1557.639 ± 0.007	0.28 ± 0.03	5.1
$f_1 + f_2$ or $2f_4$	3115.3065	0.32 ± 0.03	9.1
$2f_1$	3107.3559	0.25 ± 0.03	7.2
$2f_2$	3123.2571	0.16 ± 0.03	4.7
$f_2 + f_4$	3119.268	0.14 ± 0.03	3.9
$f_1 + f_3$	3099.414	0.13 ± 0.03	3.6

Table 3. The amplitudes and phases of the mean light variations of HD 99563, once more with error estimates from Montgomery & O'Donoghue (1999). The phases are with respect to pulsation amplitude maximum at HJD 245 2031.29627.

Filter	Amplitude (mmag)	Phase (rad)
U	31.3 ± 1.0	−0.06 ± 0.03
B	20.4 ± 0.9	−0.00 ± 0.04
V	4.6 ± 0.8	+3.09 ± 0.17
R	9.2 ± 0.8	+3.09 ± 0.09
I	7.3 ± 0.7	+3.11 ± 0.10

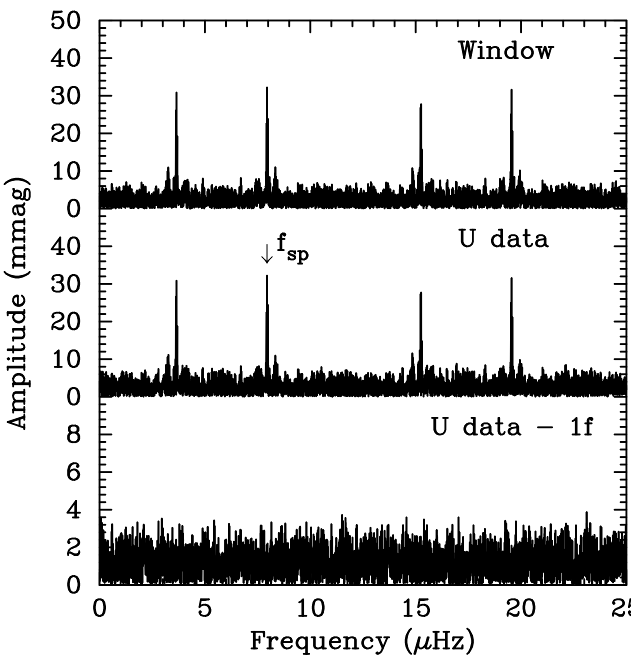

Figure 3. Amplitude spectra of the mean light observations of HD 99563 in the U filter. Upper panel: spectral window function of the time series. Middle panel: amplitude spectrum of the data themselves. Lower panel: residual amplitude spectrum after pre-whitening the strongest signal from the data. Note the five times larger ordinate scale of the lower panel.

Consequently, we can describe the variability present in the mean light variations of HD 99563 with a single frequency of 7.9498 ± 0.0002 μHz, as determined from a non-linear least-squares fit to the U data, which have the best S/N. This frequency is consistent with one of the possible multiplet spacings within the pulsational signals as determined in the previous section, but the ambiguity of whether this frequency or half of it corresponds to the rotation period of HD 99563 is not yet resolved. The amplitudes and phases of the mean light variations with respect to the frequency of 7.9498 μHz are listed in Table 3.

This table shows that the mean light maxima in the U and B filters occur at the same time as pulsation amplitude maximum in the light curves. In the V, R and I filters, mean light minimum coincides with pulsation amplitude maximum. We find no statistically significant phase lag of the mean light extrema relative to pulsation amplitude maximum.

4 ROTATION PERIOD OF HD 99563

To infer the pulsational and magnetic geometry of HD 99563, its rotation period has to be known with certainty. However, at this point it is not clear whether the 7.95-μHz signal in the mean light variations and the frequency splitting within the pulsational signals correspond to the rotation period or to half the rotation period.

Because the magnetic field of the star also varies with aspect, we can invoke published magnetic field measurements for HD 99563 to resolve this ambiguity. Hubrig et al. (2004) measured a longitudinal magnetic field strength of −688 ± 145 G on HJD 245 2494.479, whereas Kudryavtsev & Romanyuk (private communication to Elkin et al. 2005) measured +580 ± 100 G on HJD 245 3395.550.

Assuming a rotation frequency of 7.9498 ± 0.0002 μHz, the two measurements would have been taken 618.91 ± 0.02 rotational periods apart. Because these measurements would then have been taken at nearly the same rotation phase, but the magnetic field showed a reversal between these two measurements, such a rotation frequency can be ruled out. Using half this value (3.9749 ± 0.0001 μHz) implies that 309.455 ± 0.009 rotations have gone by, which is perfectly consistent with the magnetic field reversal between the two magnetic field observations and the absolute magnetic field strengths measured.

The correct value of the rotation period of HD 99563 is therefore close to 2.91 d. We show the corresponding phase diagram of the mean light variations of the star in Fig. 4.

5 FREQUENCY ANALYSIS (II)

Knowing that the rotation frequency of HD 99563 is near 3.975 μHz, we can now determine a final multifrequency solution for the pulsation data under the assumption of the OPM. We first examine the variations in the frequency domain near 1550 μHz. The spacings within all the frequencies already detected in this range are consistent with this rotation frequency and thus belong to the same multiplet. We therefore searched for possible further multiplet components in the residual amplitude spectra that have S/N > 3.5. We indeed detected a peak near f_5 = 1569.6 μHz that is consistent with this splitting and has S/N = 3.6. Adding this signal to the four previously detected, we find a symmetrical series of peaks centred on f_4 = 1557.6 μHz, for which we show a schematic graphical representation in Fig. 5.

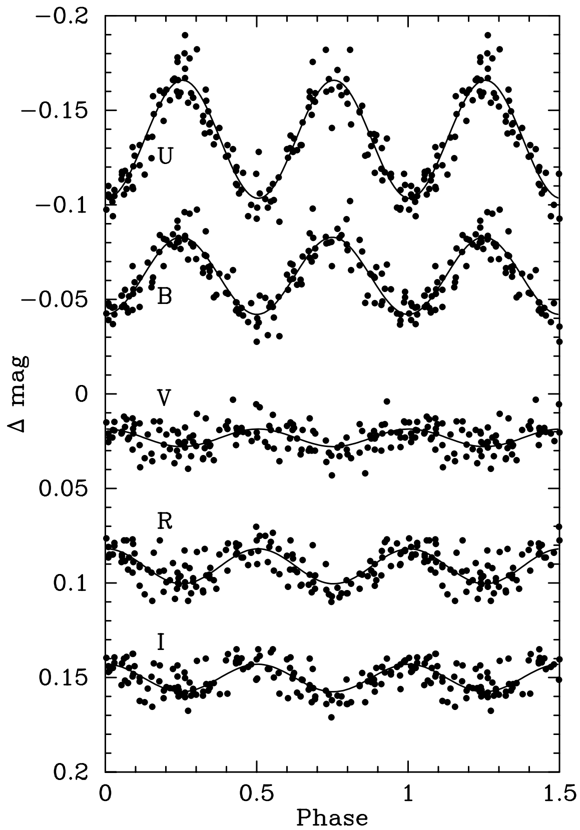

Figure 4. Mean *UBVRI* light variations of HD 99563 phased with a period of 2.91179 d. One and a half rotation cycles are shown. The solid line is the single-frequency fit from Table 3.

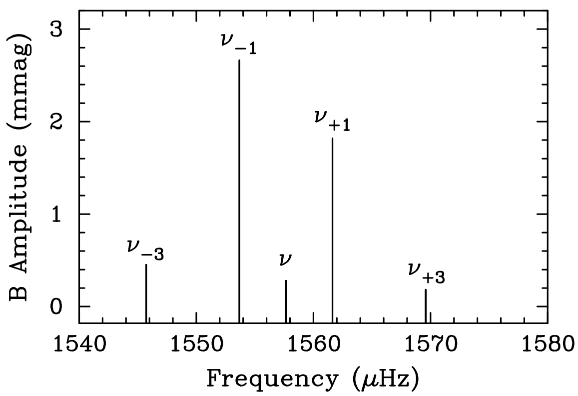

Figure 5. The frequency quintuplet detected in the light curves of HD 99563.

We can now derive a final frequency solution. To this end, we have started with the frequencies from the preliminary solution in Table 2, added f_5 and fitted these 10 signals to the data. During this process, we fixed the signal frequencies to equal splitting, using a starting value of 3.9749 μHz, and we also demanded that harmonics occurred at exactly twice the 'parent' frequency within PERIOD98. With this procedure, not only do we determine final frequency values, but also we reduce the number of free parameters in the fit to a minimum. This should guarantee the most reliable and most stable frequency solution, and the rotation frequency will also be determined most accurately this way. The final result of our frequency analysis can be found in Table 4.

Table 4. Final multifrequency solution for our *B* filter data of the roAp star HD 99563, again with error estimates from Montgomery & O'Donoghue (1999); errors on frequencies and amplitudes are given in Table 2. Pulsation phases are with respect to pulsation amplitude maximum at HJD 245 2031.29627.

ID	Frequency (μHz)	*B* amplitude (mmag)	Phase (rad)
$\nu = f_4$	1557.6530	0.29	$+2.63 \pm 0.09$
$\nu_{-1} = f_4 - f_{\rm rot}$	1553.6779	2.67	$+2.87 \pm 0.01$
$\nu_{+1} = f_4 + f_{\rm rot}$	1561.6281	1.82	$+2.83 \pm 0.01$
$\nu_{-3} = f_4 - 3f_{\rm rot}$	1545.7276	0.45	$+2.82 \pm 0.06$
$\nu_{+3} = f_4 + 3f_{\rm rot}$	1569.5784	0.18	$+3.00 \pm 0.15$
2ν	3115.3060	0.32	-1.03 ± 0.08
$2\nu_{-1}$	3107.3557	0.25	-0.27 ± 0.10
$2\nu_{+1}$	3123.2562	0.17	-0.76 ± 0.16
$2\nu + f_{\rm rot}$	3119.2811	0.15	-0.51 ± 0.18
$2\nu - 4f_{\rm rot}$	3099.4055	0.13	$+0.55 \pm 0.21$
$f_{\rm rot}$	3.9751		

The splitting between the rotationally split components of the pulsation mode of HD 99563 is 3.9751 ± 0.0003 μHz, which is the same as half the frequency of the mean light variations within the errors. Because we know that this splitting corresponds to the rotation frequency, we can fix the latter by averaging the two results into 3.9749 ± 0.0001 μHz, corresponding to a rotation period of 2.91179 ± 0.00007 d.

The referee has noted that relative phases of the first-order combination frequencies [$\phi(2\nu) - 2\phi(\nu) = 0.01 \pm 0.20$; $\phi(2\nu_{-1}) - 2\phi(\nu_{-1}) = -0.27 \pm 0.10$; $\phi(2\nu_{+1}) - 2\phi(\nu_{+1}) = 0.14 \pm 0.16$] are consistent with zero. This is an indication that the frequencies around 3115 μHz are indeed the first harmonics of the main pulsational signals near 1557 μHz.

6 DISCUSSION

The pulsational light variations of HD 99563 are the result of a single pulsation mode at a frequency of 1557.6530 μHz. Because of the rotation of the star with a period of 2.91179 d, we see it at different aspect during the rotation cycle, which gives rise to an equally spaced frequency triplet. Two more multiplet components separated by three times the rotation frequency were also detected. These are an indication that the pulsation mode of HD 99563 is not a pure dipole, but is distorted by the effect of its magnetic field.

To examine the nature of this pulsation mode, we first need to know the inclination of the stellar rotation axis to the line of sight, which in turn requires an estimate of the stellar radius. Consequently, we first infer the star's position in the HR diagram.

HD 99563 is a visual binary with a secondary component 1.2 mag fainter at a distance of 1.79 arcsec (Fabricius & Makarov 2000). Thus, photoelectric photometric observations of the system will include the secondary, which contributes 1/4 of the total light. (This also means that the amplitudes of the photometric variations we discuss here must be increased by one-third to give intrinsic values.) The *Tycho*-2 photometry of the two components (Fabricius & Makarov 2000) transformed to the standard Johnson system by using the relations by Bessell (2000) gives $V = 8.72$, $(B–V) = 0.20$ for HD 99563A and $V = 9.91$, $(B–V) = 0.285$ for HD 99563B.

These values suggest that the two components could be physically associated.

The *Hipparcos* parallax of the system (ESA 1997) is 4.27 ± 2.02 mas. The galactic reddening law by Chen et al. (1998) then results in $A_v = 0.010 \pm 0.002$. Therefore, we obtain $M_v = 1.9^{+0.8}_{-1.4}$ for HD 99563A and $M_v = 3.1^{+0.8}_{-1.4}$ for HD 99563B. Because of the large uncertainty of the *Hipparcos* parallax, we cannot therefore obtain a radius estimate of HD 99563A with sufficient accuracy, but we can, using also the $(B-V)$ estimated above, point out that HD 99563B is located inside the δ Scuti instability strip and may therefore also show pulsations. However, our check for low-frequency variability did not detect these.

To estimate the effective temperature of HD 99563 we can apply the calibration by Moon & Dworetsky (1985), who use the Strömgren H_β index as a temperature indicator. None of the other Strömgren indices is suitable for basic parameter determination of chemically peculiar A stars because of heavy line blanketing. The measured H_β value for HD 99563AB is 2.830 (Olsen & Perry 1984). With the V magnitude and $(B–V)$ colour differences given above, combined with the standard relation by Crawford (1979), we can determine $H_\beta = 2.844$ for HD 99563A and $H_\beta = 2.785$ for HD 99563B. The calibration by Moon & Dworetsky (1985) then gives $T_{\rm eff} \sim 8050$ K for HD 99563A and $T_{\rm eff} \sim 7400$ K for HD 99563B.

Elkin et al. (2005) performed a spectral analysis of HD 99563, which resulted in $T_{\rm eff} = 7700$ K, $\log g = 4.2$ and $[M/H] = 0.5$ for the roAp star. We assume a generous $T_{\rm eff} = 7900 \pm 300$ K and that HD 99563A is still on the main sequence, i.e. $\log g = 4.15 \pm 0.2$. Consequently, we estimate that $R = 1.9^{+0.6}_{-0.4}\ {\rm R}_\odot$. The projected rotational velocity of HD 99563A is 28.5 ± 1.1 km s^{-1} (Elkin et al. 2005). Combined with the rotation period determined before, we then derive $i = 60^{+30}_{-19}$ degrees, a poor constraint. However, this also implies $R \geqslant 1.58\ {\rm R}_\odot$.

As a final attempt to derive the basic parameters of HD 99563A, we assumed that HD 99563B is a physical companion. As a result of the wide separation of the two components, they would have evolved independently from each other. The goal now is to find two stellar models that have effective temperatures as determined above (for reasons of consistency, we take the photometric values for both stars), which have the same age, and the observed magnitude difference of HD 99563A and HD 99563B.

We used the Warsaw–New Jersey stellar evolution code (see, for example, Pamyatnykh et al. 1998, for a description) to find such a pair of models. We computed stellar evolutionary tracks in the range between 1.5 and 2.2 ${\rm M}_\odot$ for $Z = 0.02$. We indeed found two models that satisfy the observational constraints. They have masses of 2.03 ${\rm M}_\odot$ (HD 99563A) and 1.585 ${\rm M}_\odot$ (HD 99563B), luminosities of 21.6 and 7.1 ${\rm L}_\odot$, respectively, and ages of 620 Myr. The model for HD 99563A has a radius of 2.38 ${\rm R}_\odot$, which then implies $i = 43\overset{\circ}{.}6 \pm 2\overset{\circ}{.}1$. The internal accuracy of this method is high; changing the secondary mass by only $\pm 0.01\ {\rm M}_\odot$ already cannot reproduce the observations within the errors.

For the purpose of further discussion, we assume $i = 44^\circ$. We can now apply the OPM, which predicts

$$\frac{A_{+1} + A_{-1}}{A_0} = \tan i \tan \beta \tag{1}$$

(Shibahashi 1986), where A_r are the amplitudes of the rth rotational sidelobes, i is the inclination of the stellar rotational axis to the line of sight and β is the magnetic obliquity. From the amplitudes in Table 4, we obtain $\tan i \tan \beta = 15.5 \pm 1.5$, and hence $\beta = 86\overset{\circ}{.}4 \pm 0\overset{\circ}{.}3$. This is a perfectly reasonable result given the relative amplitudes in the central frequency triplet.

Within the framework of a regular perturbation treatment, Shibahashi & Takata (1993) derived an expected amplitude ratio

$$\frac{A_3 + A_{-3}}{A_2 + A_{-2}} = \frac{1}{6} \tan i \tan \beta, \tag{2}$$

which is consistent with our observational data that lead to a null result when searching for the ν_2 and ν_{-2} components of the stellar pulsation mode.

We further examine the distorted dipole mode of HD 99563 by applying the axisymmetric spherical harmonic decomposition method by Kurtz (1992), which is based on the theory by Shibahashi & Takata (1993), to our data. This technique breaks the magnetically distorted mode up into its pure $\ell = 0, 1, 2, \ldots$ spherical harmonic components and consequently allows us to infer the shape of the mode. We applied the method to our frequency solution (Table 4), assuming zero amplitude for the unobserved ν_{-2}, ν_{+2} components of the mode. The result is given in Tables 5 and 6.

From the values in Table 5 it can be seen that the mode of HD 99563 is dominated by the dipole component, which is reasonable as the magnetic fields in Ap stars are predominantly dipoles. The contribution of the $\ell = 0$ and $\ell = 2$ terms to the mode are fairly small, but the $\ell = 3$ component does have some influence. Table 6 shows that the observations are quite well reproduced by our fit. It would be interesting to see whether the theory by Saio & Gautschy (2004) is capable of reproducing our results.

We can now check how well our model reproduces the observed pulsational amplitudes and phases over the stellar rotation cycle. To this end, we subdivided the time series into pieces some four to five pulsation cycles long and determined the amplitudes and phases for the 1557.653-μHz variation within these subsets. The spherical harmonic decomposition method by Kurtz (1992) yields a fit to the amplitude/phase behaviour over the rotation cycle, and we show it together with the data in Fig. 6.

Table 5. Components of the spherical harmonic series description of the pulsation mode of HD 99563 for $i = 44^\circ$, $\beta = 86\overset{\circ}{.}4$.

ℓ	0	1	2	3
$A^{(\ell)}_{-3}$ (mmag)				0.450
$A^{(\ell)}_{-2}$ (mmag)			0.158	0.158
$A^{(\ell)}_{-1}$ (mmag)		3.405	0.037	−0.699
$A^{(\ell)}_{0}$ (mmag)	0.237	0.376	−0.093	0.042
$A^{(\ell)}_{+1}$ (mmag)		2.372	0.028	−0.524
$A^{(\ell)}_{+2}$ (mmag)			0.088	0.088
$A^{(\ell)}_{+3}$ (mmag)				0.180
$\phi^{(\ell)}$ (rad)	0.024	2.859	−0.322	2.820
$C_{n\ell}\ \Omega/K^{\rm mag}$		0.107	0.020	0.010

Table 6. Comparison of the observed amplitudes and phases of the distorted dipole pulsation mode of HD 99563 and our spherical harmonic fit.

ID	$A_{\rm obs}$	$A_{\rm calc}$	$\phi_{\rm obs}$	$\phi_{\rm calc}$
ν	0.29 ± 0.03	0.29	$+2.63 \pm 0.09$	+2.63
ν_{-1}	2.67 ± 0.03	2.67	$+2.87 \pm 0.01$	+2.87
ν_{+1}	1.82 ± 0.03	1.82	$+2.83 \pm 0.01$	+2.87
ν_{-2}	0.00 (assumed)	0.00	–	N/A
ν_{+2}	0.00 (assumed)	0.00	–	N/A
ν_{-3}	0.45 ± 0.03	0.45	$+2.82 \pm 0.06$	+2.82
ν_{+3}	0.18 ± 0.03	0.18	$+3.00 \pm 0.15$	+2.82

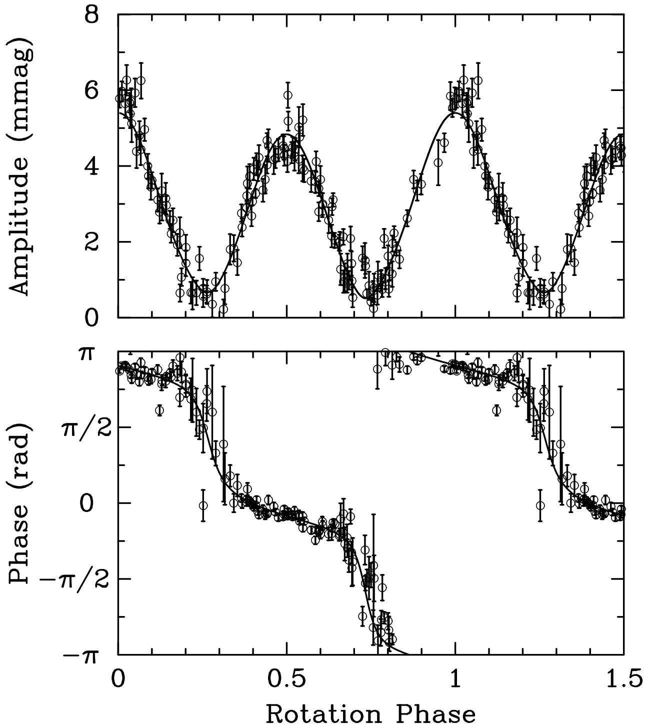

Figure 6. Pulsational amplitudes and phases relative to a rotation period of 2.91179 d. Phase zero corresponds to pulsation amplitude maximum, and one and a half rotation cycles are shown. The line is a fit computed with the Kurtz (1992) spherical harmonic decomposition method.

We can see that both magnetic (pulsation) poles are actually in view for approximately the same amount of time; the relative fractions are 53 and 47 per cent. This is also the reason why it was so difficult to determine the rotation period of the star; the pulsations as well as the mean light variations are almost symmetrical along the rotation period.

The fitted curves reproduce the observations fairly well, with one exception: the pulsation amplitude is overestimated for the pole that is for a shorter time in the line of sight, whereas the amplitude is underestimated for the other pole. The harmonic frequencies cannot be made responsible for this, because they do not affect the first-order amplitudes analysed here. Consequently, we believe that the poor fits near the pulsation amplitude maxima could be a result of presently undetected additional multiplet components of the pulsation mode; the amount of overfitting and underfitting can be fully explained with the noise level in our residual amplitude spectrum.

7 CONCLUSIONS

Our photometric multisite observations of the roAp star HD 99563 resulted in the detection of a frequency quintuplet which is due to a single distorted dipole pulsation mode. The splitting within this frequency quintuplet together with our mean light observations and published magnetic measurements allowed us to determine the stellar rotation period as 2.91179 ± 0.00007 d. Within the errors, the mean light extrema occur in phase with the pulsation amplitude maximum, suggesting that the abundance spots on HD 99563 should be fairly concentric around its magnetic poles.

To our knowledge, HD 99563 is only the fourth roAp star where both magnetic poles become visible throughout a rotation cycle – the others are HR 3831 (see, for example, Kurtz et al. 1993), HD 6532 (e.g. Kurtz et al. 1996) and HD 80316 (e.g. Kurtz et al. 1997) – and it is only the third whose pulsational mode distortion has been quantified. In this context it is interesting to note that the observational features of HD 99563 are in many aspects similar to another roAp star, the well-studied HR 3831 (e.g. Kurtz et al. 1993; Kochukhov 2004): their geometrical orientations, rotation period and effective temperatures are alike. Only the pulsation period of HD 99563 is some 10 per cent shorter, and the phases of its first-order combination frequencies are more consistent with them being harmonics. It would thus be very interesting to compare these two objects in detail.

This would however require more in-depth studies of HD 99563. Its basic parameters are still poorly known; the radius we have inferred is based on the assumption that the visual companion is physical, which needs to be checked. If HD 99563A and HD 99563B were a physical pair, then the separation of the components is too wide for motion around a common centre of mass to be determined in a reasonable period of time. However, common proper motion may be detectable within a few years.

The most efficient way to pin down the radius of the roAp star would perhaps come from a combination of magnetic and polarization measurements (Landolfi et al. 1997). With that, the inclination i and the magnetic obliquity β can be constrained, and given the accurate rotation period and $v \sin i$ already available, a fairly accurate radius could be obtained.

There are several other possibilities that make HD 99563 interesting for future observations. As already argued by Elkin et al. (2005), the star is a very attractive target for pulsational radial velocity measurements. Given the high amplitude of the mean light variations of the star and its favourable geometry, Doppler imaging of its surface should also be within reach. Finally, we have evidence that we have not yet deciphered the full pulsational content of the star's light curves. Another multisite campaign, aiming at obtaining >200 h of observations on 1-m class telescopes would therefore also be justifiable. As we have pointed out, HD 99563B is located within the δ Scuti instability strip and should therefore also be tested for pulsations, with more suitable means than ours.

ACKNOWLEDGMENTS

The Austrian Fonds zur Förderung der wissenschaftlichen Forschung partially supported this work under grants S7303-AST and S7304-AST. We are grateful to Don Kurtz for supplying results prior to publication, for helpful discussions and for comments on a draft version of this paper. We also thank Hiromoto Shibahashi for his accurate referee's report.

REFERENCES

Bessell M. S., 2000, PASP, 112, 961
Breger M., 1979, PASP, 91, 5
Breger M. et al., 1999, A&A, 349, 225
Chen B., Vergely J. L., Valette B., Carraro G., 1998, A&A, 336, 137
Crawford D. L., 1979, AJ, 84, 1858
Cunha M. S., Gough D. O., 2000, MNRAS, 319, 1020
Dorokhova T. N., Dorokhov N. I., 1998, in Proc. 26th Meeting of the European Working Group on CP stars. Contributions of the Astronomical Observatory Skalnaté Pleso, 27, 338
Elkin V. G., Kurtz D. W., Mathys G., 2005, MNRAS, 364, 864
ESA, 1997, The *Hipparcos* and *Tycho* catalogues, ESA SP-1200
Fabricius C., Makarov V. V., 2000, A&A, 356, 141
Handler G., Paunzen E., 1999, A&AS, 135, 57
Handler G. et al., 2000, MNRAS, 318, 511

Handler G. et al., 2002, MNRAS, 330, 153
Hubrig S., Szeifert T., Schöller M., Mathys G., Kurtz D. W., 2004, A&A, 415, 685
Jerzykiewicz M., Handler G., Shobbrook R. R., Pigulski A., Medupe R., Mokgwetsi T., Tlhagwane P., Rodríguez E., 2005, MNRAS, 360, 619
Kaye A. B., Handler G., Krisciunas K., Poretti E., Zerbi F. M., 1999, PASP, 111, 840
Kochukhov O., 2004, ApJ, 615, L149
Kochukhov O., Drake N. A., Piskunov N., de la Reza R., 2004, A&A, 424, 935
Kurtz D. W., 1982, MNRAS, 200, 807
Kurtz D. W., 1992, MNRAS, 259, 701
Kurtz D. W., Martinez P., 2000, Baltic Astron., 9, 253
Kurtz D. W., Kanaan A., Martinez P., 1993, MNRAS, 260, 343
Kurtz D. W., Martinez P., Koen C., Sullivan D. J., 1996, MNRAS, 281, 883
Kurtz D. W., Martinez P., Tripe P., Hanbury A. G., 1997, MNRAS, 289, 645
Kurtz D. W., Elkin V. G., Mathys G., 2003, MNRAS, 343, L5
Landolfi M., Bagnulo S., Landi degl'Innocenti M., Landi degl'Innocenti E., Leroy J. L., 1997, A&A, 322, 197
Lueftinger T., Kuschnig R., Piskunov N. E., Weiss W. W., 2003, A&A, 406, 1033
Martinez P. et al., 2002, Mon. Notes Astron. Soc. South Africa, 61, 102
Matthews J. M., Kurtz D. W., Martinez P., 1999, ApJ, 511, 422
Montgomery M. H., O'Donoghue D., 1999, Delta Scuti Star Newsletter, 13, 28 (University of Vienna)
Moon T. T., Dworetsky M. M., 1985, MNRAS, 217, 305
Olsen E. H., Perry C. L., 1984, ApJS, 56, 229
Pamyatnykh A. A., Dziembowski W. A., Handler G., Pikall H., 1998, A&A, 333, 141
Ryabchikova T., Piskunov N., Kochukhov O., Tsymbal V., Mittermayer P., Weiss W. W., 2002, A&A, 384, 545
Saio H., Gautschy A., 2004, MNRAS, 350, 485
Shibahashi H., 1986, in Osaki Y., ed., Hydrodynamic and Magnetohydrodynamic Problems in the Sun and Stars. University of Tokyo, Tokyo, p. 195
Shibahashi H., Takata M., 1993, PASJ, 45, 617
Sperl M., 1998, Master's thesis, Univ. Vienna
Takata M., Shibahashi H., 1995, PASJ, 47, 219

This paper has been typeset from a TEX/LATEX file prepared by the author.

4.5 Discovery of the "missing" mode in HR 1217 by the Whole Earth Telescope

Original paper:

D. W. Kurtz, S. D. Kawaler, R. L. Riddle, M. D. Reed, M. S. Cunha, M. Wood, N. Silvestri, T. K. Watson, N. Dolez, P. Moskalik, S. Zola, E. Pallier, J. A. Guzik, T. S. Metcalfe, A. S. Mukadam, R. E. Nather, D. E. Winget, D. J. Sullivan, T. Sullivan, K. Sekiguchi, X. Jiang, R. Shobbrook, B. N. Ashoka, S. Seetha, S. Joshi, D. O'Donoghue, **G. Handler,** M. Mueller, J. M. Gonzalez Perez, J.-E. Solheim, F. Johannessen, A. Ulla, S. O. Kepler, A. Kanaan, A. da Costa, L. Fraga, O. Giovannini, J. M. Matthews, 2002, MNRAS 330, L57

Mon. Not. R. Astron. Soc. **330,** L57–L61 (2002)

Discovery of the 'missing' mode in HR 1217 by the Whole Earth Telescope

D. W. Kurtz,[1,2,3★] S. D. Kawaler,[4] R. L. Riddle,[4] M. D. Reed,[4†] M. S. Cunha,[5,6] M. Wood,[7] N. Silvestri,[7] T. K. Watson,[8] N. Dolez,[3] P. Moskalik,[9] S. Zola,[10] E. Pallier,[3] J. A. Guzik,[11] T. S. Metcalfe,[12] A. S. Mukadam,[12] R. E. Nather,[12] D. E. Winget,[12] D. J. Sullivan,[13] T. Sullivan,[13] K. Sekiguchi,[14] X. Jiang,[15] R. Shobbrook,[16] B. N. Ashoka,[17] S. Seetha,[17] S. Joshi,[18] D. O'Donoghue,[19] G. Handler,[19] M. Mueller,[19] J. M. Gonzalez Perez,[20] J.-E. Solheim,[20] F. Johannessen,[20] A. Ulla,[21] S. O. Kepler,[22] A. Kanaan,[23] A. da Costa,[22] L. Fraga,[23] O. Giovannini[24] and J. M. Matthews[25] (the WET collaboration)

[1]*Centre for Astrophysics, University of Central Lancashire, Preston PR1 2HE*
[2]*Department of Astronomy, University of Cape Town, Rondebosch 7701, South Africa*
[3]*Observatoire Midi-Pyrénées, CNRS/UMR5572, 14 av. E. Belin, 31400 Toulouse, France*
[4]*Department of Physics and Astronomy, Iowa State University, Ames, IA 50011, USA*
[5]*Centro de Astrofísica da Universidade do Porto, Rua das Estrelas, 4150-762 Porto, Portugal*
[6]*Instituto Superior da Maia, Av. Carlos de Oliveira Campos, 4475-690, Avisoso S. Pedro, Castelo da Maia, Portugal*
[7]*Department of Physics & Space Sciences and SARA Observatory, Florida Institute of Technology, Melbourne, FL, USA*
[8]*Information Technology Services, Southwestern University, 1001 E. University Avenue, Georgetown, TX 78626, USA*
[9]*Nicolaus Copernicus Astronomical Centre, ul. Bartycka 18, 00-716 Warsawa, Poland*
[10]*Mt Suhora Observatory, Pedagogical University, ul. Podchorążych 2, 30-084 Krakow, Poland*
[11]*X-2, MS B220, Los Alamos National Laboratory, Los Alamos, NM 87545, USA*
[12]*McDonald Observatory, and Department of Astronomy, University of Texas, Austin, TX 78712, USA*
[13]*School of Chemical and Physical Sciences, Victoria University of Wellington, PO Box 600, Wellington 6001, New Zealand*
[14]*Subaru Telescope, National Astronomical Observatory of Japan, 650 North A'ohoku Place, Hilo, HI 96720, USA*
[15]*National Astronomical Observatories and Joint Laboratory of Optical Astronomy, Chinese Academy of Sciences, Beijing, 100012, China*
[16]*Research School of Astronomy & Astrophysics, Australian National University, Cotter Road, Weston, ACT 2611, Australia*
[17]*Indian Space Research Organization, Vimanapura PO, Bangalore 560 017, India*
[18]*State Observatory, Manora Peak, Naini Tal 263 129, India*
[19]*South African Astronomical Observatory, PO Box 9, Observatory 7935, South Africa*
[20]*Department of Physics, University of Tromso, N-9037 Tromso, Norway*
[21]*Depto. de Fisica Aplicada, Universidade de Vigo, 36200 Vigo, Spain*
[22]*Instituto de Fisica, UFRGS, Campus do Vale, CP 15051, Porto Alegre, RS, Brazil*
[23]*Universidade Federal de Santa Catarina, Florianópolis, SC, Brazil*
[24]*Departamento de Física e Química, Universidade de Caxias do Sul, 95001-970 Caxias do Sul, RS, Brazil*
[25]*Department of Physics and Astronomy, University of British Columbia, 6224 Agricultural Road, Vancouver V6T 1Z1, Canada*

Accepted 2001 December 21. Received 2001 December 21; in original form 2001 November 20

ABSTRACT

HR 1217 is a prototypical rapidly oscillating Ap star that has presented a test to the theory of non-radial stellar pulsation. Prior observations showed a clear pattern of five modes with alternating frequency spacings of 33.3 and 34.6 μHz, with a sixth mode at a problematic spacing of 50.0 μHz (which equals 1.5×33.3 μHz) to the high-frequency side. Asymptotic pulsation theory allowed for a frequency spacing of 34 μHz, but *Hipparcos* observations rule out such a spacing. Theoretical calculations of magnetoacoustic modes in Ap stars by Cunha predicted that there should be a previously undetected mode 34 μHz higher than the main group, with a smaller spacing between it and the highest one. In this Letter, we present preliminary results from a multisite photometric campaign on the rapidly oscillating Ap star HR 1217 using the 'Whole Earth Telescope'. While a complete analysis of the data will appear in a later paper, one outstanding result from this run is the discovery of a newly detected frequency in the pulsation spectrum of this star, at the frequency predicted by Cunha.

★E-mail: dwkurtz@uclan.ac.uk
†Visiting Astronomer: CTIO, National Optical Astronomy Observatories.

Key words: stars: individual: HR 1217 – stars: magnetic fields – stars: oscillations – stars: variables: other.

1 INTRODUCTION

After decades of trying, the search for solar-type oscillations in stars finally appears to have been successful; see, for example, Bouchy & Carrier (2001) – α Cen A; Bedding et al. (2001) and Carrier et al. (2001) – β Hyi. Although this led Gough (2001) to announce the 'birth of asteroseismology,' for the past two decades asteroseismology has successfully investigated the interiors of many types of stars other than the solar-type stars. Remarkable success stories of observational and theoretical investigations of white dwarf stars and rapidly oscillating Ap stars have amply demonstrated the power of asteroseismology as a tool to advance our knowledge of the physics of stellar interiors and the details of stellar evolution (see, for example, Kurtz et al. 1989; Winget et al. 1991; Kawaler & Bradley 1994; Matthews, Kurtz & Martinez 1999).

With these successes, some mysteries have remained. In this Letter, we address apparently contradictory interpretations of the pulsation spectrum of the rapidly oscillating Ap star HR 1217. This star, discovered to be a pulsator by Kurtz (1982), was investigated with an extensive global campaign in 1986 (Kurtz et al. 1989). A key result from that data set was a list of six principal pulsation frequencies, reproduced in Table 1. As expected from the asymptotic theory of non-radial pulsations, five of the modes are nearly equally spaced in frequency.

The asymptotic frequency spacing, ν_o, is a measure of the sound crossing time of the star, which in turn is determined by the star's mean density and radius. With a typical mass of Ap stars of about $2\,M_\odot$, ν_o reflects the radius of the star, with ν_o scaling as $R^{-3/2}$. In the asymptotic limit, the number of nodes in the radial direction, n, is larger than the spherical degree ℓ. Assuming adiabatic pulsations in spherically symmetric stars the pulsation frequencies are, to first order,

$$\nu_{n,\ell} = \nu_o(n + \ell/2 + \epsilon),$$

where ϵ is a (small) constant (Tassoul 1980, 1990). Without precise identification of the degree (ℓ) of the pulsation modes, asymptotic theory allows the frequency spacing to be uncertain by a factor of two, depending on whether modes of alternating even and odd ℓ are present (producing modes separated by $\nu_o/2$ in frequency), or only modes of consecutive n.

The results of the 1986 campaign were inconclusive as to whether ν_o was 68 or 34 μHz. The principal frequencies given in Table 1 correspond to those found by Kurtz et al. (1989) for the 15-day stretch of best coverage (for comparison with the new data presented in Table 3, later). The highest frequency of HR 1217 in those data was 50 μHz higher than the fifth mode, suggesting that ν_o was 34 μHz. But the fine structure of the spacings was suggestive of alternating ℓ values. Fortunately, the two possible values could be assessed if the luminosity of the star were precisely known. If ν_o were 34 μHz, then the radius of HR 1217 would be large enough that it would be far removed from the main sequence (i.e. more evolved) and therefore more luminous (Heller & Kawaler 1988). Matthews et al. (1999) used the *Hipparcos* parallax measurement to place HR 1217 unambiguously close to the main sequence – meaning that ν_o is indeed 68 μHz. This deepened the 'mystery of the sixth frequency,' now $\frac{3}{4}\nu_0$ higher. No clear theoretical construct could explain it.

The asymptotic frequency spacing given in the equation above is valid only for linear adiabatic pulsations in spherically symmetric stars. However, the magnetic field, the chemical inhomogeneities, and rotation all contribute to break the spherical symmetry in roAp stars. Therefore, it is important to know the effects that these deviations from spherical symmetry have on the theoretical amplitude spectra of roAp stars, before comparing the latter with the observed amplitude spectra. The effects of the chemical inhomogeneities have been discussed recently by Balmforth et al. (2001), but those will not concern us further here. The effects of the magnetic field on the oscillations of roAp stars (Dziembowski & Goode 1996; Bigot et al. 2000; Cunha & Gough 2000), as well as the conjoined effect of rotation and magnetic field (Bigot 2002), have been determined by means of a singular perturbation approach. While generally the magnetic field effect on the oscillations is expected to be small, Cunha & Gough (2000) found that, at the frequencies of maximal magnetoacoustic coupling, the latter is expected to become significantly large, resulting in an abrupt drop of the separation between mode frequencies.

The observational consequence of the results of Cunha & Gough (2000) suggests that we should see equally spaced modes in roAp stars, with an occasional mode much closer to its lower frequency counterparts. More recently, Cunha (2001) suggested that the explanation of the strange separation between the last two modes observed in HR 1217 could rest on the occasional abrupt decrease of the large separations predicted by Cunha & Gough (2000). For this prediction to hold, she argued that the observations of Kurtz et al. (1989) must have missed detecting a mode at a frequency 34 μHz higher than that of the fifth mode they observed. She predicted that new, more precise measurements would find this 'missing mode' if the Alfvénic losses were not large enough to stabilize it. Detailed re-examination of the data from 1986 shows no peak at the key position approximately 33 μHz above f5 at the 0.1 mmag level.

In 2000 November, we began an extensive, coordinated global photometry campaign on HR 1217 using the Whole Earth Telescope. A complete analysis of this extensive data set, which addresses many other aspects of roAp stars, is in preparation. In this Letter, we present a preliminary analysis of data from that run that clearly shows a previously unseen pulsation mode at a

Table 1. Principal frequencies in HR 1217 (data from Kurtz et al. 1989).

Number	frequency [μHz]	frequency spacing [μHz]	amplitude [mmag]
f1	2619.51 ± 0.05	–	0.28 ± 0.03
f2	2652.92 ± 0.02	33.41 ± 0.05	1.09 ± 0.03
f3	2687.58 ± 0.03	34.66 ± 0.04	0.94 ± 0.03
f4	2721.02 ± 0.02	33.44 ± 0.04	1.16 ± 0.03
f5	2755.49 ± 0.04	34.47 ± 0.04	0.49 ± 0.03
f6	–	–	<0.09
f7	2806.26 ± 0.06	50.77 ± 0.07	0.25 ± 0.03

Table 2. Observing log of selected high-speed photometry of HR 1217 from the Whole Earth Telescope Extended Coverage Campaign 20 (WET Xcov20).

Run Name	Date 2000	Start (UT)	Run (hr)	Observatory	Tel (m)
sa-od044	Nov 14	21:03:00	5.04	SAAO	1.9
mdr-142	Nov 15	01:28:10	5.06	CTIO	1.5
sa-od045	Nov 15	19:20:00	7.05	SAAO	1.9
teide01	Nov 16	00:42:10	3.56	Teide	0.8
mdr-143	Nov 16	01:23:00	7.23	CTIO	1.5
no1700q2	Nov 17	07:28:00	3.38	Mauna Kea	0.6
mdr-144	Nov 17	20:26:06	7.54	CTIO	1.5
teiden04	Nov 17	22:09:10	6.05	Teide	0.8
no1800q1	Nov 18	07:22:30	4.25	Mauna Kea	0.6
teiden05	Nov 18	22:53:20	5.40	Teide	0.8
sa-od047	Nov 18	23:29:00	1.45	SAAO	1.9
no1900q2	Nov 19	10:14:20	3.85	Mauna Kea	0.6
sa-od048	Nov 19	18:55:00	7.15	SAAO	1.9
teiden06	Nov 19	22:05:30	6.06	Teide	0.8
no2000q1	Nov 20	07:37:00	6.07	Mauna Kea	0.6
sa-od049	Nov 20	18:51:00	7.30	SAAO	1.9
sa-m0003	Nov 21	19:26:50	6.67	SAAO	0.75
sa-m0004	Nov 22	18:28:20	7.65	SAAO	0.75
no2300q1	Nov 23	07:15:50	4.59	Mauna Kea	0.6
teiden10	Nov 23	22:05:40	5.47	Teide	0.8
sa-m0006	Nov 24	18:18:00	7.76	SAAO	0.75
no2500q1	Nov 25	07:03:00	6.67	Mauna Kea	0.6
teiden12	Nov 25	22:09:20	5.61	Teide	0.8
joy-012	Nov 26	03:55:50	4.10	McDonald	2.1
no2600q2	Nov 26	06:59:30	6.47	Mauna Kea	0.6
sa-m0007	Nov 26	18:28:40	7.42	SAAO	0.75
no2700q1	Nov 27	06:38:00	5.55	Mauna Kea	0.6
jxj-0127	Nov 27	13:44:10	4.75	Beijing AO	0.85
sa-m0008	Nov 27	18:27:50	7.57	SAAO	0.75
teiden14	Nov 27	22:28:20	3.72	Teide	0.8
sa-h-046	Nov 28	18:54:30	6.41	SAAO	1.9
teiden15	Nov 28	22:01:50	5.52	Teide	0.8
no2900q1	Nov 29	06:41:00	6.77	Mauna Kea	0.6
sa-gh465	Nov 29	20:30:30	5.14	SAAO	1.9
teiden16	Nov 29	21:18:50	2.59	Teide	0.8
joy-028	Nov 30	03:54:20	5.24	McDonald	2.1
no3000q1	Nov 30	06:40:50	6.77	Mauna Kea	0.6
sa-gh466-9	Nov 30	19:30:20	6.26	SAAO	1.9
		Total	215.2		

frequency about 36 μHz above the fifth frequency, as predicted by Cunha (2001). In the next section, we describe the observational procedures and the data coverage and reduction. Section 3 presents the preliminary frequency analysis, and the results are discussed in Section 4, along with a brief discussion of the impact of this result on the theory of pulsations of roAp stars.

2 OBSERVATIONS

The WET run on HR 1217 began on 2000 November 6 at selected sites, and continued through early 2000 December. The bulk of the data, with the best global coverage, were obtained during 2000 November 14–30. A complete analysis of all of the available data is currently underway. For this Letter, we concentrate on the central portion of the WET run, with data from five sites. This subset of the full data set provides high signal-to-noise and a reasonable global coverage. It also extends over slightly more than one rotation cycle of HR 1217. Since the pulsation amplitude is modulated with the rotation period, this data subset is just long enough to begin to resolve rotational sidelobes of the main peaks.

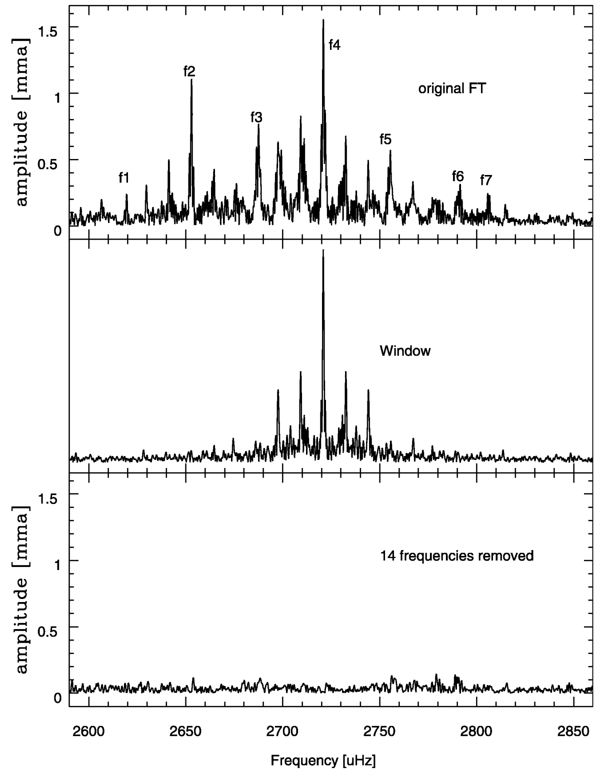

Figure 1. The Fourier transform of the subset of WET data used in our analysis. The top panel shows the FT of the data, the middle panel shows the spectral window, and the bottom panel shows the resulting FT after the data are pre-whitened by 14 frequencies. The unit mma means milli-modulation amplitude which is measured in parts per thousand in intensity units. For amplitudes as small as these here, it is very nearly equivalent to mmag.

Table 2 lists the individual observing runs in this data set. The telescopes used range in aperture from 0.6 to 2.1 m. Data from all sites were obtained using photoelectric photometers, with 10 s individual integrations. At Beijing Astronomical Observatory, McDonald Observatory, Mauna Kea Observatory, and Observatorio del Teide, the observers used three-channel photometers that are functionally similar to the equipment described in Kleinman, Nather & Phillips (1996). The South African Astronomical Observatory observations were made with a single-channel photometer, and the observations at CTIO with a two-channel photometer. At all sites, observations were made through a Johnson *B* filter, along with neutral density filters when needed to keep the count rates below $10^6\,s^{-1}$. Following the procedures described in

Table 3. Principal frequencies in HR 1217 in 2000.

Number	frequency [μHz]	frequency spacing [μHz]	amplitude [mma]
f1	2619.51 ± 0.03	–	0.24 ± 0.02
f2	2652.96 ± 0.01	33.45 ± 0.04	0.95 ± 0.02
f3	2687.58 ± 0.02	34.62 ± 0.02	0.68 ± 0.03
f4	2720.96 ± 0.02	33.38 ± 0.03	1.29 ± 0.02
f5	2755.35 ± 0.03	34.39 ± 0.04	0.34 ± 0.02
f6	2791.48 ± 0.03	36.13 ± 0.04	0.29 ± 0.02
f7	2806.43 ± 0.14	14.95 ± 0.14	0.22 ± 0.07

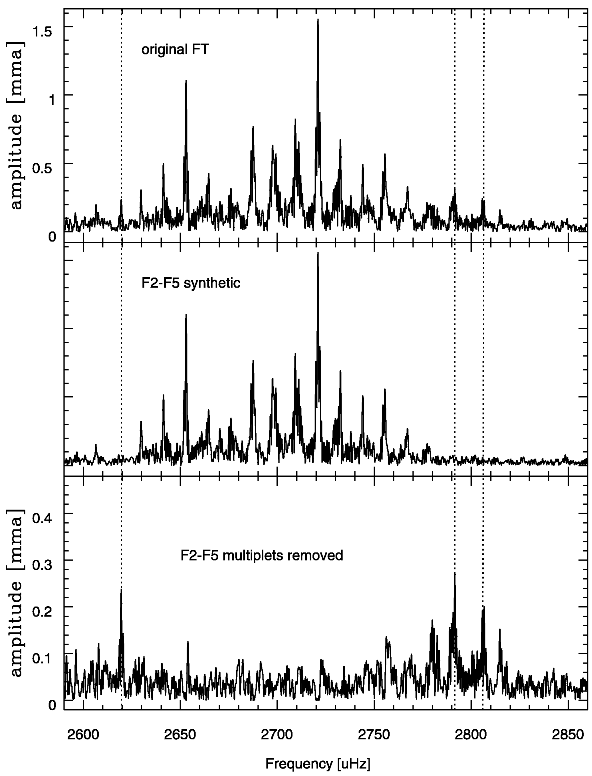

Figure 2. The Fourier transform of the subset of WET data used in our analysis. The top panel shows the FT of the data. The middle panel is a simulation of the FT that includes 10 frequencies – f2 through f5 along with their rotational sidelobes. The bottom panel shows the FT of the data pre-whitened by those 10 frequencies. Vertical dotted lines show the position of f1, f6 and f7.

Kleinman et al. (1996), the sky background was continuously monitored with the three-channel instruments. At sites using two-channel and single channel photometers, the sky was obtained several times during the night at irregular intervals, and then interpolated during reduction.

As can be seen in Table 2, we obtained 215.2 h of observations during the interval 2000 November 14–30, resulting in a duty cycle of 53 per cent. Longitude coverage was adequate, though the longitudes around central Asia were not as well covered as the others.

3 FREQUENCY ANALYSIS

The amplitude spectrum (produced using a Fourier transform – hereafter FT – for unequally spaced data) of the reduced data, in the frequency range where the pulsations are significant, is shown in the top panel of Fig. 1. The spectral window, shown in the middle panel of the figure, shows the response of the Fourier transform to a single, noise-free sinusoid sampled at the same times as the light curve of HR 1217. The side peaks correspond to aliases of 1 and $2\,\mathrm{d}^{-1}$. They are approximately 40 per cent of the amplitude of the principal peak, and are caused by the (small) daily gaps present in the data because of incomplete global coverage.

The principal periodicities that we found in HR 1217 are listed in Table 3. Following initial identification of the main peaks in the FT, we did a successive least-squares fit to the light curve including all of the main peaks. We then included the rotational sidelobes in the fit, sequentially. Throughout this process we pre-whitened the data by removing noise-free sinusoids at the fitted frequencies, amplitudes, and phases. We stopped when none of the remaining peaks was above the noise level. In all, we found 14 significant periodicities in this data set. In addition to the seven principal frequencies, both rotational sidelobes of f3 and f4 were found. We also found the low-frequency rotational sidelobe of f2, f5, and f7. The frequencies listed in Table 3 are from the fit that included all 14 frequencies.

The bottom panel of Fig. 1 shows the FT of the residual light curve following the removal of 14 frequencies, on the same scale as the top panel. There are some residual peaks in this plot at interesting frequencies. Analysis of the full data set, including runs outside of the subset that we used, shows that some of these are real. They will be described in further detail in the full analysis of the data which is in preparation.

4 RESULTS

4.1 Comparison with the 1989 data

Early in the run, it became clear that HR 1217 was pulsating with the same frequencies that were present in the 1986 data analysed by Kurtz et al. (1989). Tables 1 and 3 show that the principal frequencies from the 1986 study (f1 through f5 and f7) are highly consistent over a time span of 15 yr. Some of the amplitudes of these modes are higher in 2000 and some lower by small amounts than they were in 1986, but it is the frequencies (and presence or absence) of the modes that are of interest here.

The chief difference between the 2000 data and 1986 data is the presence of a frequency at 2791 μHz listed as f6 in Table 3. That mode was not detected in the data of Kurtz et al. (1989 – their table 1) but was a clear signal in the WET Xcov20 2000 data. To ensure that this frequency is not an artefact of the data reduction algorithm, we repeated the frequency analysis of our data fitting just the large-amplitude peaks f2, f3, f4 and f5, and their rotational sidelobes (if present). We then removed those 10 frequencies. The results are illustrated in Fig. 2. This figure shows the original FT, and the FT of the data simulated by including f2–f5 and their rotational sidelobes. Clearly, there is excess signal at the positions of f1 and f7, but also at 2791 μHz as well.

Thus we conclude that the 'new' frequency, f6, is real. Table 3 shows that it lies at nearly $\nu_o/2$ above f5, as expected if it is a normal p-mode and $\nu_o \approx 68$ μHz. It is much closer to f7 than $\nu_o/2$, as predicted by Cunha (2001).

Why is the new frequency, f6, present in the 2001 WET data and not in the 1986 data? There are two possibilities: (i) the mode was not excited in 1986, or (ii) its amplitude was smaller in 1986 than in 2001. Concerning the first possibility, the condition of maximal energy loss depends on the exact magnetic field structure and strength, and on the exact value of the mode frequency. If any of these change slightly, the resonance becomes better (or worse). What was a good enough resonance to stabilize the mode is no longer, or vice versa. In the second case we do not know exactly how the amplitudes of the modes are saturated (this is true for all pulsating stars), and whether the final amplitude depends on the growth rates. This emphasizes the importance of further observations of HR 1217 to see whether the mode 'disappears' again, as this has strong implications concerning possible changes in the star's magnetic field structure and/or strength.

4.2 Implications for roAp stars

Cunha (2001) speculated that the position of the f7 peak in the Kurtz et al. (1989) data is consistent with her model of the normal mode structure in Ap stars when magnetic fields are important to the pulsation dynamics. Since that peak was $\frac{3}{4}\nu_0$ above f5 (which is inexplicable in asymptotic theory), she suggested that there should be a peak at $\nu_o/2$ above f5. That is precisely what we see in the data from the WET run in November 2000 with the discovery of f6.

As discussed earlier, *other* explanations for the frequency spacing pattern from f5 to f7 are in direct conflict with the now well-determined *Hipparcos* luminosity of HR 1217, hence are ruled out. We therefore conclude that the frequency pattern in HR 1217 suggests that the pulsations we see in this star are consistent with normal p-mode pulsations whose frequencies are, in some cases, strongly affected by the magnetic field of the star.

Cunha (2001) suggested that large Alfvénic losses could help explain the missing f6 in the 1986 data, as these losses are maximal at the frequencies where the large separations experience the abrupt decrease. This energy loss could either stabilize the mode or contribute to decrease its amplitude (although it is not clear how the growth rates relate to the amplitude of the modes in roAp stars).

Since f6 is observed in the present data, the possibility that the Alfvénic losses are large enough to stabilize this mode can be ruled out, at least at the time of these observations. Whether at the time of the previous observations the efficacy of the magnetoacoustic coupling (which depends, among other things, on the exact frequency of the mode and on the characteristics of the magnetic field) was different, is something to which we do not have an answer. An attempt to monitor the amplitude of f6, as well as that of the other modes, in the future might, therefore, be worthwhile. However, the magnetic field does produce an important observable effect on the frequency of f7.

With the detection of f6, we move closer to a detailed understanding of the pulsation mechanism in roAp stars. Most intriguingly, this result for HR 1217 suggests that, with appropriately detailed models, we may soon be able to probe the magnetic field structure below the surfaces of these stars through their pulsation frequencies – another application of asteroseismology to probing stellar interiors.

ACKNOWLEDGMENTS

We gratefully acknowledge support from the US National Science Foundation through grant AST-9876655 to Iowa State University, and funding by UNESCO through the International Institute of Theoretical and Applied Physics at Iowa State. MC is supported by FCT-Portugal through the grant PD/18893/98 and the grant POCTI/1999/FIS/34549 approved by FCT and POCTI, with funds from the European Community programme FEDER. PM is supported by KBN (Poland) through grant 5-P03D-012-20.

REFERENCES

Balmforth N. J., Cunha M. S., Dolez N., Gough D. O., Vauclair S., 2001, MNRAS, 323, 362
Bedding T. R., Butler R. P., Kjeldsen H., Baldry I. K., O'Toole S. J., Tinney C. G., Marcy G. W., Kienzle F., Carrier F., 2001, ApJ, 549, L105
Bigot L., 2002, in Aerts C., Christensen-Dalsgaard J., Bedding T., eds, Proc. IAU Colloq. 185, ASP Conf. Ser. Vol. 259, Radial and Nonradial Pulsations as probes of Stellar Physics. Astron. Soc. Pac., San Francisco, in press
Bigot L., Provost J., Berthomieu G., Dziembowski W. A., Goode P. R., 2000, A&A, 356, 218
Bouchy F., Carrier F., 2001, A&A, 374, 5
Carrier F. et al., 2001, A&A, 378, 142
Cunha M. S., 2001, MNRAS, 325, 373
Cunha M. S., Gough D., 2000, MNRAS, 319, 1020
Dziembowski W., Goode P. R., 1996, ApJ, 458, 338
Gough D. O., 2001, Sci, 291, (5512), 2325
Heller C. H., Kawaler S. D., 1988, ApJ, 329, L43
Kawaler S. D., Bradley P. A., 1994, ApJ, 427, 415
Kleinman S. J., Nather R. E., Phillips T., 1996, PASP, 108, 356
Kurtz D. W., 1982, MNRAS, 200, 807
Kurtz D. W. et al., 1989, MNRAS, 240, 881
Matthews J. M., Kurtz D. W., Martinez P., 1999, ApJ, 511, 422
Tassoul M., 1980, ApJS, 43, 469
Tassoul M., 1990, ApJ, 358, 313
Winget D. E. et al., 1991, ApJ, 378, 326

This paper has been typeset from a TeX/LaTeX file prepared by the author.

4.6 Pushing the ground-based limit: 14-μmag photometric precision with the definitive Whole Earth Telescope asteroseismic data set for the rapidly oscillating Ap star HR 1217

Original paper:

D. W. Kurtz, C. Cameron, M. S. Cunha, N. Dolez, G. Vauclair, E. Pallier, A. Ulla, S. O. Kepler, A. da Costa, A. Kanaan, L. Fraga, O. Giovannini, M. A. Wood, N. Silvestri, S. D. Kawaler, R. L. Riddle, M. D. Reed, T. K. Watson, T. S. Metcalfe, A. S. Mukadam, R. E. Nather, D. E. Winget, A. Nitta, S. J. Kleinman, J. A. Guzik, P. A. Bradley, J. M. Matthews, K. Sekiguchi, D. J. Sullivan, T. Sullivan, R. Shobbrook, X. Jiang, P. V. Birch, B. N. Ashoka, S. Seetha, V. Girish, S. Joshi, P. Moskalik, S. Zola, D. O'Donoghue, **G. Handler,** M. Mueller, J. M. Gonzalez Perez, J.-E. Solheim, F. Johannessen, L. Bigot, 2005, MNRAS 358, 651

Mon. Not. R. Astron. Soc. **358,** 651–664 (2005) doi:10.1111/j.1365-2966.2005.08807.x

Pushing the ground-based limit: 14-μmag photometric precision with the definitive Whole Earth Telescope asteroseismic data set for the rapidly oscillating Ap star HR 1217

D. W. Kurtz,[1,2★] C. Cameron,[3] M. S. Cunha,[4] N. Dolez,[2] G. Vauclair,[2] E. Pallier,[2] A. Ulla,[5] S. O. Kepler,[6] A. da Costa,[6] A. Kanaan,[7] L. Fraga,[7] O. Giovannini,[8] M. A. Wood,[9] N. Silvestri,[9] S. D. Kawaler,[10] R. L. Riddle,[10] M. D. Reed,[10,11] T. K. Watson,[12] T. S. Metcalfe,[13] A. Mukadam,[13] R. E. Nather,[13] D. E. Winget,[13] A. Nitta,[14] S. J. Kleinman,[14] J. A. Guzik,[15] P. A. Bradley,[15] J. M. Matthews,[3] K. Sekiguchi,[16] D. J. Sullivan,[17] T. Sullivan,[17] R. Shobbrook,[18] X. Jiang,[19] P. V. Birch,[20] B. N. Ashoka,[21] S. Seetha,[21] V. Girish,[21] S. Joshi,[22] P. Moskalik,[23] S. Zola,[24,25] D. O'Donoghue,[26] G. Handler,[26] M. Mueller,[27] J. M. Gonzalez Perez,[28] J.-E. Solheim,[28] F. Johannessen[28] and L. Bigot[29]

[1]*Centre for Astrophysics, University of Central Lancashire, Preston PR1 2HE*
[2]*Observatoire Midi-Pyrénées, CNRS/UMR5572, 14 av. E. Belin, 31400 Toulouse, France*
[3]*Department of Physics and Astronomy, University of British Columbia, 6224 Agricultural Road, Vancouver, BC V6T 1Z1, Canada*
[4]*Centro de Astrofísica da Universidade do Porto, Rua das Estrelas, 4150-762 Porto, Portugal Instituto Superior da Maia, Lugar de Vilarinho, 4470 Castelo da Maia, Portugal*
[5]*Departamento de Fisica Aplicada, Universidade de Vigo, 36200 Vigo, Spain*
[6]*Instituto de Fisica, UFRGS, CP 15051, 91501-970 Porto Alegre, RS, Brazil*
[7]*Universidade Federal de Santa Catarina, Florianópolis, SC, Brazil*
[8]*Departamento de Física e Química, Universidade de Caxias do Sul, 95001-970 Caxias do Sul, RS, Brazil*
[9]*Department of Physics & Space Sciences and SARA Observatory, Florida Institute of Technology, Melbourne, FL 32901, USA*
[10]*Department of Physics and Astronomy, Iowa State University, Ames, IA 50011, USA*
[11]*Visiting Astronomer, CTIO, National Optical Astronomy Observatories, USA*
[12]*Southwestern University, 1001 E. University Avenue, Georgetown, TX 78626, USA*
[13]*McDonald Observatory, and Department of Astronomy, University of Texas, Austin, TX 78712, USA*
[14]*Apache Point Observatory, PO Box 59, Sunspot, NM 88349, USA*
[15]*X-2, MS T-085, Los Alamos National Laboratory, Los Alamos, NM 87545 USA*
[16]*Subaru Observatory, National Astronomical Observatory of Japan, 650 North A'ohoku Place, Hilo, HI 96720, USA*
[17]*School of Chemical and Physical Sciences, Victoria University of Wellington, PO Box 600, Wellington, New Zealand*
[18]*Research School of Astronomy & Astrophysics, Australian National University, Cotter Road, Weston, ACT 2611, Australia*
[19]*National Astronomical Observatories and Joint Laboratory of Optical Astronomy, Chinese Academy of Sciences, Beijing, 100012, China*
[20]*Perth Observatory, Walnut Rd, Bickley, Western Australia 6076, Australia*
[21]*Indian Space Research Organization, Vimanapura PO, Bangalore 560 017, India*
[22]*State Observatory, Manora Peak, Naini Tal 263 129, India*
[23]*Nicolaus Copernicus Astronomical Center, ul. Bartycka 18, 00-716 Warsaw, Poland*
[24]*Cracow Pedagogical University, ul. Podchorżych 2, Cracow, Poland*
[25]*Astronomical Observatory, Jagiellonian University, ul. Orla 171, 30-244 Cracow, Poland*
[26]*South African Astronomical Observatory, PO Box 9, Observatory 7935, South Africa*
[27]*Department of Astronomy, University of Cape Town, Rondebosch 7701, South Africa*
[28]*Department of Physics, University of Tromsø, N-9037 Tromsø, Norway*
[29]*Niels Bohr Institute, Juliane Maries Vej 30, 2100 Copenhagen, Denmark*

Accepted 2005 January 7. Received 2005 January 7; in original form 2004 September 13

ABSTRACT

HR 1217 is one of the best-studied rapidly oscillating Ap (roAp) stars, with a frequency spectrum of alternating even- and odd-ℓ modes that are distorted by the presence of a strong, global magnetic field. Several recent theoretical studies have found that within the observable

★E-mail: dwkurtz@uclan.ac.uk

atmospheres of roAp stars the pulsation modes are magneto-acoustic with significant frequency perturbations that are cyclic with increasing frequency. To test these theories a Whole Earth Telescope extended coverage campaign obtained 342 h of Johnson *B* data at 10-s time resolution for the roAp star HR 1217 over 35 d with a 36 per cent duty cycle in 2000 November–December. The precision of the derived amplitudes is 14 μmag, making this one of the highest precision ground-based photometric studies ever undertaken. Substantial support has been found for the new theories of the interaction of pulsation with the strong magnetic field. In particular, the frequency jump expected as the magnetic and acoustic components cycle through 2π rad in phase has been found. Additionally, comparison of the new 2000 data with an earlier 1986 multisite study shows clear amplitude modulation for some modes between 1986 and 2000. The unique geometry of the roAp stars allows their pulsation modes to be viewed from varying aspect with rotation, yielding mode identification information in the rotational sidelobes that is available for no other type of pulsating star. Those rotational sidelobes in HR 1217 confirm that two of the modes are dipolar, or close to dipolar; based on the frequency spacings and *Hipparcos* parallax, three other modes must be either $\ell = 0$ or 2 modes, either distorted by the magnetic field, or a mix of *m*-modes of given ℓ where the mixture is the result of magnetic and rotational effects. A study of all high-speed photometric Johnson *B* data from 1981 to 2000 gives a rotation period $P_{\rm rot} = 12.4572$ d, as found in previous pulsation and photometric studies, but inconsistent with a different rotation period found in magnetic studies. We suggest that this rotation period is correct and that zero-point shifts between magnetic data sets determined from different spectral lines are the probable cause of the controversy over the rotation period. This WET data set is likely to stand as the definitive ground-based study of HR 1217. It will be the baseline for comparison for future space studies of HR 1217, particularly the *MOST* satellite observations.

Key words: stars: individual: HR 1217 – stars: magnetic fields – stars: oscillations – stars: variables: other.

1 INTRODUCTION

The rapidly oscillating Ap (roAp) stars have been observed photometrically since their discovery by Kurtz (1982) over 20 years ago. Frequency analyses of their light curves have yielded rich asteroseismic information on the degrees of the pulsation modes, distortion of the modes from normal modes, magnetic geometries and luminosities. The latter, in particular, are derived asteroseismically and agree well with *Hipparcos* luminosities (Matthews, Kurtz & Martinez 1999).

New theoretical work on the interaction of pulsation with both rotation and the magnetic field by Bigot & Dziembowski (2002) has presented an entirely new look at the oblique pulsator model of these stars: they find that the pulsation axis is inclined to both the magnetic and rotation axes, and the pulsation modes are complex combinations of spherical harmonics that result in modes that, in many cases, can be travelling waves looking similar to (but are not exactly) sectoral *m*-modes. Bigot & Kurtz (2005) have shown that the improved oblique pulsator model of Bigot & Dziembowski obtains rotational inclination and magnetic obliqueness for the roAp star HR 3831 that are in agreement with those found from a magnetic studies by Bagnulo, Landolfi & degl'Innocenti (1999); however, Kochukhov (2004) finds a different magnetic and pulsation geometry for HR 3831 that is in good agreement with the old oblique pulsator model and is inconsistent with the Bagnulo et al. (1999) geometry. Further magnetic studies should differentiate between these two models.

In a similar study to that of Bigot & Dziembowski, Saio & Gautschy (2004) find modes that are aligned with the magnetic axis and are distorted by the magnetic field so that they cannot be described by single spherical harmonics; they note that horizontal motion can be comparable to vertical motion for these modes. It is the unique geometry of the pulsation modes in roAp stars that allows us to examine their non-radial pulsation modes from varying aspect as can be done with no other type of star.

1.1 High-resolution spectroscopy of roAp stars

The spectra of many roAp stars show a strong core–wing anomaly in the hydrogen lines, particularly the Hα line (Cowley et al. 2001; Kochukhov, Bagnulo & Barklem 2002). This indicates abnormal atmospheric structure, as does the fact that consistent abundances for the second and third ionization states of rare-earth elements, particularly Nd and Pr, cannot be found for these stars (Ryabchikova et al. 2002). Until atmospheric models can be found that solve these problems, caution is called for, but new high-resolution spectroscopic results for roAp stars suggest vertical stratification of some ions, particularly the rare earths, and they show the short vertical wavelength of the pulsation modes. It must also be cautioned that there are known horizontal abundance variations with concentration of rare-earth elements towards the magnetic poles. See, for example, studies of γ Equ (HD 201601) (Kochukhov & Ryabchikova 2001a), HD 166473 (Kurtz, Elkin & Mathys 2003), α Cir (Baldry et al. 1999; Kochukhov & Ryabchikova 2001b; Balona & Laney 2003), HR 3831 (Baldry & Bedding 2000; Kochukhov & Ryabchikova 2001b), HR 1217 (Balona & Zima 2002; Sachkov et al. 2004) and 33 Lib (HD 137949) (Mkrtichian, Hatzes & Kanaan 2003; Kurtz, Elkin & Mathys 2005). The results of these studies are plausibly interpreted in terms of vertical resolution of the pulsation mode structure in the atmospheres of these stars, possibly with stratification of some ions. In general, Fe lines originate near a radial node around an optical depth of $\tau_{5000} = 1$ with little or no radial velocity variations seen; the core of the Hα line forms higher in the atmosphere and shows radial velocity variations with amplitudes up to several km s^{-1}; lines from the first and second ionization states of the rare earths Pr and Nd arise from a thin layer around an optical depth of $\tau_{5000} = 10^{-3}$ and can also show amplitudes of several km s^{-1}.

The spectroscopic studies have thus allowed the beginning of a three-dimensional resolution of the pulsation modes, with the vertical stratification giving depth information, and the rotation of the oblique mode providing information on the surface geometry of the modes. While these spectroscopic tools are very powerful, they demand high spectroscopic resolution, high time resolution and high signal-to-noise ratio (S/N) – requirements that can only be met with large telescopes and optimized high-resolution spectrographs. It is thus not possible at present to study in detail the frequencies of many roAp stars spectroscopically because of the need for high duty cycle data sets over extended periods of time.

1.2 Photometry and asteroseismology of HR 1217

To obtain the frequencies that are the basic input data for asteroseismology it is thus necessary to observe roAp stars in multisite ground-based campaigns, as we report in this paper for the Whole Earth Telescope (WET) extended coverage campaign (Xcov20) on the roAp star HR 1217 (DO Eri; HD 24712), or to observe them from space with dedicated asteroseismic satellites. The first of these satellites, *MOST*, was launched on 2003 June 30 and observed HR 1217 for 30 d during 2004 November–December. Hence the discoveries in this work will provide a baseline to compare with the *MOST* results. The data set analysed in this paper from Xcov20 will be referred to throughout the rest of this paper as the '2000 data'.

Of the 34 known roAp stars, HR 1217 is one of the best-studied. This star, discovered to be a pulsator by Kurtz (1982), was investigated with an extensive global campaign in 1986 (Kurtz et al. 1989). A key result from that data set (which we will refer to in this paper as the '1986 data') was a list of six principal pulsation frequencies, five of which had alternating spacings of 33.4 and 34.5 μHz, the sixth of which was separated by a then inexplicable 50 μHz from the fifth frequency.

The asymptotic frequency spacing, ν_0 – known as the 'large spacing', is a measure of the sound crossing time of the star, which in turn is determined by the mean density and radius of the star. With a typical mass of Ap stars of approximately 2 M$_\odot$, ν_0 reflects the radius of the star, with ν_0 scaling as $R^{-3/2}$. In the asymptotic limit, the number of nodes in the radial direction, n, is much larger than the spherical degree ℓ. Assuming adiabatic pulsations in spherically symmetric stars the pulsation frequencies are

$$\nu_{n,\ell} = \nu_0(n + \ell/2 + \epsilon) + \delta\nu,$$

where ϵ is a (small) constant (Tassoul 1980, 1990) and $\delta\nu$, the 'small spacing', is a measure of the age of the star as it is sensitive to the central condensation, hence the core H mass fraction. Without precise identification of the degree (ℓ) of the pulsation modes, asymptotic theory allows the frequency spacing to be uncertain by a factor of 2, depending on whether modes of alternating even and odd ℓ are present (producing modes separated by $\nu_0/2$ in frequency), or only modes of the same ℓ with consecutive values of n.

The results of the 1986 campaign were inconclusive as to whether ν_0 was 68 or 34 μHz. Fortunately, the ambiguity could be resolved by a precise determination of the luminosity of the star. If ν_0 were 34 μHz, then the radius of HR 1217 would be large enough that it would be far removed from the main sequence (i.e. more evolved) and therefore more luminous (Heller & Kawaler 1988). Matthews et al. (1999) used the *Hipparcos* parallax measurement to place HR 1217 unambiguously close to the main sequence, thus determining that ν_0 is indeed 68 μHz. This deepened the 'mystery of the sixth frequency', lying $\frac{3}{4}\nu_0$ higher than the fifth frequency. It is easy to see from the above asymptotic frequency relation that there is no clear theoretical explanation for this spacing using the above asymptotic relation.

That asymptotic frequency spacing is valid only for linear adiabatic pulsations in spherically symmetric stars. However, the magnetic field, the chemical inhomogeneities and rotation all contribute to breaking the spherical symmetry in roAp stars. It is therefore important to know the effects that these deviations from spherical symmetry have on the theoretical frequency spectra of roAp stars, before comparing those with the observed frequency spectra. The effects of the chemical inhomogeneities have been discussed recently by Balmforth et al. (2001), but those will not concern us further here. The effects of the magnetic field on the oscillations of roAp stars (Dziembowski & Goode 1996; Bigot et al. 2000; Cunha & Gough 2000; Saio & Gautschy 2004), and the joint effect of rotation and magnetic field (Bigot & Dziembowski 2002), have been determined by means of a singular perturbation approach. While generally the magnetic field effect on the oscillations is expected to be small, Cunha & Gough (2000) found that at the frequencies of maximal magneto-acoustic coupling, the latter is expected to become significantly large, resulting in an abrupt drop of the separation between mode frequencies.

The observational consequence of the results of Cunha & Gough (2000) suggested that we should see equally spaced modes in roAp stars with an occasional mode much closer to its lower-frequency counterparts. More recently, Cunha (2001) suggested that the explanation of the strange separation between the last two modes observed in HR 1217 in the 1986 data could rest on the occasional abrupt decrease of the large separations predicted by Cunha & Gough (2000). For this prediction to hold, she argued that the observations of Kurtz et al. (1989) must have missed detecting a mode at a frequency 34 μHz higher than that of the fifth mode they observed. She predicted that new, more precise measurements would find this 'missing mode' if the Alfvénic losses were not large enough to stabilize it. Detailed re-examination of the 1986 data shows no peak at the key position approximately 33 μHz above ν_5 at the ∼0.1-mmag level.

In the preliminary analysis of the 2000 data we (Kurtz et al. 2002) found that missing mode, giving support to the theory of Cunha. In this paper we have analysed the data in far more detail and report in Section 4 that the new mode is in fact a pair of modes separated by 2.6 μHz, a value that is potentially the small spacing, $\delta\nu$. The small spacing has not been unambiguously determined for any roAp star. One of the pair of new modes fits the alternating 33.4, 34.5 μHz spacing of the first five modes, and is now separated by nearly precisely $\frac{1}{4}\nu_0$ from the highest detected frequency. The theoretical importance of this new result will be discussed in Section 4.

We also report in Section 4.1 significant amplitude modulation of some of the modes between the 1986 and 2000 data sets, particularly for the frequencies now identified in this paper as ν_3 and ν_4, but also for the newly discovered frequencies, ν_7 and ν_8. This explains why these frequencies were not seen in the 1986 data set – they were below the noise level for that data set, but grew to larger, detectable amplitudes in the Xcov20 2000 data set. Interestingly, we find that the total power for all observed modes is the same in the 1986 and 2000 data sets, even though there have been significant shifts of amplitude between modes, suggesting that the total pulsational energy may be conserved. This is the first time that an roAp star has been observed in enough detail with independent studies to determine this, and it is an important discovery to test against the upcoming *MOST* satellite data set, which will have far higher S/N ratio.

1.3 Astrophysical data for HR 1217

One of the strengths of studying HR 1217 is that there is a wealth of astrophysical information known about it. Its parallax was determined by *Hipparcos* giving a luminosity of $L = 7.8 \pm 0.7\,\mathrm{L}_\odot$ (Matthews et al. 1999). As mentioned earlier, the atmospheres of the most peculiar of the roAp stars show a strong core–wing anomaly (Cowley et al. 2001) in the H lines indicating an extremely abnormal temperature–depth structure to their atmospheres. HR 1217 has this core–wing anomaly. A first attempt at self-consistent atmospheric models that can account for the core–wing anomaly has been made (Kochukhov et al. 2002), but it is not yet even possible to model the Balmer lines fully. The effective temperatures of the roAp stars are thus notoriously difficult to determine. Nevertheless, various photometric and spectroscopic studies conservatively give $T_{\mathrm{eff}} \approx 7300 \pm 200$ K.

The magnetic field has been studied extensively over the years (Preston 1972; Mathys 1991; Bagnulo et al. 1995; Mathys & Hubrig 1997; Leone, Catanzaro & Catalano 2000; Wade et al. 2000). Bagnulo et al. found from broad-band linear polarimetry a polar field strength of approximately 3.9 kG, a rotational inclination of $i = 137^\circ$ and a magnetic obliquity of $\beta = 150^\circ$. The errors on these values are uncertain, but they give us a starting point to discuss the geometry of the pulsation modes.

The rotation period has been controversial, with some (but not all) studies of the magnetic field finding $P_{\mathrm{rot}} = 12.4610$ d and other studies of the magnetic field, the photometric variations and, particularly, the pulsation finding $P_{\mathrm{rot}} = 12.4572$ d. We discuss this problem in detail in Section 4.3 where we find that the pulsation data are definitely best-fitted with $P_{\mathrm{rot}} = 12.4572$ d.

The rotational sidelobes are the key to mode identification in the roAp stars, within the oblique pulsator model (Shibahashi & Takata 1993; Takata & Shibahashi 1995), the improved oblique pulsator model (Bigot & Dziembowski 2002) and the new theory of Saio & Gautschy (2004). We discuss these sidelobes in detail in Section 4.2 where we find they are unchanged between the 1986 and 2000 data sets, and that ν_2 and ν_4 seem to be dipole, or dipole-like modes. Arguments from standard A-star models and the frequency spacings suggests that the even-ℓ modes are probably distorted radial modes, but distorted quadrupole modes cannot be ruled out.

Pulsational radial velocity variations were discovered by Matthews et al. (1988) and have been studied in more detail recently by Balona & Zima (2002) who find rotationally modulated pulsational radial velocity variations that are consistent with the known photometric frequencies. As discussed above, there is a wealth of information in high-precision radial velocity studies of roAp stars. For HR 1217, with its multiple frequencies spaced by $\sim$3 d^{-1}, further progress in this field will need a multisite, 8-m-class telescope campaign. One continuous run of 24 h is all that is needed, so this is possible – especially as HR 1217 at $\delta = -12^\circ$ is accessible from both hemispheres.

1.4 The importance of the asteroseismic study of HR 1217

HR 1217 is important for both the study of roAp stars and for asteroseismology in general. Cunha, Fernandes & Monteiro (2003) have recently performed seismic tests of the structure of HR 1217. They find that the interior chemical composition has more effect on the theoretical oscillation spectrum than does convection and overshooting. Models with lower abundances of heavy elements in the interior and increased helium come closer to matching the observed frequencies, but they have difficulty finding a plausible model that can yet reproduce the seismic observations of HR 1217. Even though their theoretical predictions can be reconciled with the observations, when the uncertainty in the radius is accounted for, the fact that a systematic shift is found between predicted and observed large separations when different roAp stars are considered (Matthews et al. 1999) might indicate that something is still missing in the theoretical models.

Cunha et al. (2003) emphasize that one important aspect that is not yet well understood is the way in which waves are reflected near the surface of these stars. They argue that if the process of reflection of high-order modes in HR 1217 is frequency dependent, then the large separations could be different from those obtained in their work. Observationally, the complexity of the reflective boundary layer can now be seen for the roAp star 33 Lib (Kurtz et al. 2005). A theory that takes into account the magneto-acoustic nature of the waves near the surface of these stars should be used in order to improve the current models. Thus, the present observations can contribute to the follow-up of this work, not only because of the improvements that they bring to the power spectrum of HR 1217, but also because of their possible contribution to our understanding of the magnetic field of this star.

In this paper we report the frequency analysis of 342 h of high-speed photometry spanning 35 d with a duty cycle of 36 per cent. The resulting amplitude spectra have noise peaks no higher than 80 μma,[1] and least-squares errors in amplitude of only 14 μma, making this one of the highest precision photometric studies ever undertaken. As outlined in this introduction, we have learned much concerning HR 1217 from WET Xcov20. We have also learned again how complex the roAp stars are. WET Xcov20 is likely to stand as the definitive ground-based study of this star. This is the study that will provide the basis of comparison for higher precision space asteroseismic studies.

2 OBSERVATIONS

WET Xcov20 began on 2000 November 6 and continued for 35 d. Table 1 lists the individual observing runs used in this analysis. Many other runs on marginally photometric nights were rejected because of the demand for very high precision necessary for this study; some other runs were rejected because of equipment problems with particular telescopes in the network. In total

[1] μma denotes micromodulation amplitude and mma denotes millimodulation amplitude. These are in units of 10^{-6} and 10^{-3} of the intensity variation. For amplitudes as low as these they are equal to -1.087 μmag and -1.087 mmag, respectively. We use μma and mma throughout this study of the Whole Earth Telescope data newly presented here, but use μmag and mmag for older data where those were the units used in those studies.

Table 1. Observing log of high-speed photometry of HR 1217 from the Whole Earth Telescope Extended Coverage Campaign 20 (WET Xcov20). Columns 2 and 3 list the UT starting date and time of each run. Data were taken with 10-s integrations and then averaged to 40-s integrations; columns 4–6 list the number of 40-s integrations after bad points were removed, the duration of the run in hours and the standard deviation per point of the data in that run after low-frequency sky transparency variations were removed. The BJED start and finish times are for the 40-s integrations that were used in the analysis; in general the first few observations in a run were sky, so the BJED of the first point does not correspond precisely to the UT start time of the run – it begins a short time later. Where the number of points seems few for the duration of the run there are gaps in the data, usually because of cloud, but sometimes because of instrumental problems.

Run name	Date 2000	UT start	N	ΔT (h)	σ (mma)	BJED start	BJED end	Observatory	Tel (m)
mdr136	November 6	02:23:30	328	4.36	1.47	1854.609 565	1854.790 931	CTIO	1.5
mdr137	November 9	01:55:20	380	4.24	0.93	1857.695 708	1857.872 444	CTIO	1.5
mdr138	November 10	01:59:50	278	3.30	1.22	1858.590 508	1858.728 008	CTIO	1.5
mdr139	November 12	02:16:00	596	6.67	1.29	1860.601 051	1860.878 945	CTIO	1.5
mdr140	November 13	01:34:30	632	7.03	1.75	1861.573 740	1861.866 795	CTIO	1.5
mdr141	November 14	01:27:40	38	0.51	2.35	1862.567 839	1862.589 019	CTIO	1.5
sa-od044	November 14	21:03:00	419	4.82	2.44	1863.383 580	1863.584 274	SAAO	1.9
mdr142	November 15	01:28:10	655	7.27	1.95	1863.567 955	1863.870 964	CTIO	1.5
sa-od045	November 15	19:20:00	597	7.03	2.43	1864.311 936	1864.604 760	SAAO	1.9
teiden01	November 16	00:42:10	317	3.65	1.36	1864.535 778	1864.687 861	OTIAC	0.8
mdr143	November 16	01:23:00	674	7.52	2.21	1864.564 713	1864.878 139	CTIO	1.5
mdr144	November 17	01:18:20	678	7.53	2.11	1865.561 007	1865.874 549	CTIO	1.5
no1700q2	November 17	07:28:00	300	3.35	2.22	1865.817 025	1865.956 608	MKO	0.6
no1700q3	November 17	12:34:20	33	0.36	2.15	1866.030 797	1866..045 843	MKO	0.6
teiden04	November 17	22:09:10	541	6.03	2.11	1866.428 944	1866.680 029	OTIAC	0.8
no1800q1	November 18	07:22:30	401	6.26	1.78	1866.824 862	1867.085 655	MKO	0.6
teiden05	November 18	22:53:20	292	3.31	1.76	1867.459 609	1867.597 341	OTIAC	0.8
sa-od047	November 18	23:29:00	128	1.44	1.77	1867.484 841	1867.545 026	SAAO	1.9
no1900q2	November 19	10:14:20	343	3.84	1.62	1867.934 491	1868.094 444	MKO	0.6
sa-od048	November 19	18:55:00	579	6.76	1.28	1868.294 557	1868.576 270	SAAO	1.9
teiden06	November 19	22:05:30	547	6.13	1.32	1868.426 269	1868.681 478	OTIAC	0.8
asm-0079	November 20	03:58:40	473	5.78	1.86	1868.673 143	1868.913 999	McD	2.1
no2000q1	November 20	07:37:00	550	6.14	1.72	1868.825 340	1869.081 243	MKO	0.6
sa-od049	November 20	18:51:00	630	7.33	1.43	1869.291 656	1869.597 096	SAAO	1.9
asm0081	November 21	09:06:10	73	0.84	1.82	1869.887 947	1869.922 900	McD	2.1
sa-m0003	November 21	19:26:50	566	6.71	1.84	1870.316 357	1870.596 044	SAAO	0.75
sa-m0004	November 22	18:28:20	669	7.64	1.97	1871.275 902	1871.594 052	SAAO	0.75
teiden08	November 22	22:07:20	143	1.62	1.82	1871.427 513	1871.494 874	OTIAC	0.8
joy-002	November 23	03:59:50	455	5.22	1.58	1871.678 668	1871..896 029	McD	2.1
no2300q1	November 23	07:15:50	423	5.52	1.39	1871.810 495	1872.040 587	MKO	0.6
pvb1123	November 23	12:15:41	105	1.20	1.32	1872.057 263	1872..107 147	PO	0.6
sa-m0005	November 23	18:11:50	83	1.10	2.59	1872.265 350	1872..311 357	SAAO	0.75
teiden10	November 23	22:05:40	482	5.45	1.86	1872.426 459	1872.653 600	OTIAC	0.8
pvb1124	November 24	12:18:40	593	6.90	1.84	1873.018 928	1873..306 543	PO	0.6
sa-m0006	November 24	18:18:00	633	7.73	1.77	1873.271 528	1873.593 693	SAAO	0.75
teiden11	November 25	02:03:30	107	1.20	2.07	1873.586 220	1873.636 336	OTIAC	0.8
no2500q1	November 25	07:03:10	593	6.66	1.84	1873.801 439	1874.078 899	MKO	0.6
teiden12	November 25	22:09:20	492	5.59	2.52	1874.428 975	1874.662 019	OTIAC	0.8
joy-012	November 26	03:55:50	363	4.07	2.00	1874.669 481	1874..839 272	McD	2.1
no2600q2	November 26	06:59:30	583	6.47	2.31	1874.798 761	1875.068 205	MKO	0.6
jxj-0124	November 26	14:14:50	340	3.79	4.42	1875.101 533	1875.259 404	BAO	0.85
sa-m0007	November 26	18:28:40	652	7.47	2.90	1875.275 952	1875.587 352	SAAO	0.75
teiden13	November 26	21:50:30	34	0.40	1.67	1875.415 880	1875..432 546	OTIAC	0.8
joy-016	November 27	04:03:00	405	4.75	3.87	1875.674 440	1875..872 241	McD	2.1
no2700q1	November 27	06:38:00	562	6.72	2.66	1875.783 813	1876.063 790	MKO	0.6
jxj-0127	November 27	13:44:10	425	4.73	2.86	1876.079 525	1876.276 747	BAO	0.85
sa-m0008	November 27	18:27:50	668	7.56	3.57	1876.275 065	1876.589 880	SAAO	0.75
teiden14	November 27	22:28:20	330	3.70	2.94	1876.442 134	1876.596 185	OTIAC	0.8
joy-020	November 28	04:04:20	134	1.54	4.19	1876.675 347	1876..739 583	McD	2.1
no2800q1	November 28	06:45:00	44	1.84	2.97	1876.791 317	1876..868 053	MKO	0.6
sa-h-046	November 28	18:54:30	606	7.33	2.64	1877.295 357	1877.600 682	SAAO	1.9
teiden15	November 28	22:01:50	494	5.50	3.09	1877.423 711	1877.652 704	OTIAC	0.8
joy-025	November 29	04:00:40	436	5.21	2.80	1877.672 780	1877..889 678	McD	2.1
no2900q1	November 29	06:41:00	589	6.76	2.52	1877.785 972	1878.067 685	MKO	0.6
sa-gh465	November 29	20:30:30	427	5.19	2.34	1878.277 628	1878.493 948	SAAO	1.9
teiden16	November 29	21:18:50	239	2.64	2.38	1878.518 308	1878.628 494	OTIAC	0.8
joy-028	November 30	01:19:10	466	5.23	2.09	1878.668 360	1878..886 069	McD	2.1
no3000q1	November 30	06:40:50	592	6.76	2.11	1878.785 719	1879.067 200	MKO	0.6

Table 1 – *continued*

Run name	Date 2000	UT start	N	ΔT (h)	σ (mma)	BJED start	BJED end	Observatory	Tel (m)
sa-gh466	November 30	19:30:20	140	1.67	1.16	1879.318 577	1879.388 137	SAAO	1.9
teiden17	November 30	21:17:50	404	5.92	2.03	1879.393 112	1879.639 929	OTIAC	0.8
sa-gh467	November 30	21:19:50	67	0.75	2.00	1879.394 616	1879..425 982	SAAO	1.9
sa-gh468	November 30	22:15:20	204	2.33	1.48	1879.432 926	1879.530 032	SAAO	1.9
sa-gh469	December 1	00:39:00	131	1.52	2.31	1879.532 692	1879.596 118	SAAO	1.9
sa-gh470	December 1	18:57:20	294	3.45	1.46	1880.295 983	1880.439 849	SAAO	1.9
teiden18	December 1	22:04:00	338	3.85	1.46	1880.425 147	1880.585 390	OTIAC	0.8
sa-gh471	December 1	22:30:00	310	3.65	1.56	1880.443 549	1880.595 633	SAAO	1.9
sa-gh472	December 2	18:46:50	229	2.77	1.48	1881.289 014	1881.404 523	SAAO	1.9
sa-gh473	December 2	21:38:30	356	4.31	1.22	1881.407 992	1881.587 621	SAAO	1.9
teiden19	December 2	21:46:50	125	1.38	1.90	1881.413 316	1881.470 723	OTIAC	0.8
sa-gh474	December 3	18:35:20	616	7.47	1.59	1882.281 116	1882.592 459	SAAO	1.9
sa-gh475	December 4	21:51:00	329	4.20	1.22	1883.416 385	1883.591 500	SAAO	1.9
tsm-0087	December 5	05:50:40	249	2.99	1.46	1883.749 014	1883.873 782	McD	2.1
tsm-0089	December 6	03:47:00	321	4.00	2.02	1884.663 106	1884.829 657	McD	2.1
r00-022	December 6	18:55:00	201	2.22	1.82	1885.296 998	1885.389 591	ARIES	1.0
r00-025	December 7	16:53:20	202	2.24	1.96	1886.209 392	1886.302 563	ARIES	1.0
teiden22	December 8	21:37:40	121	1.40	2.42	1887.406 650	1887.465 099	OTIAC	0.8
teiden24	December 9	21:01:50	168	1.90	2.87	1888.381 731	1888.461 013	OTIAC	0.8
teiden27	December 11	00:20:40	201	2.22	2.49	1889.526 538	1889..619 189	OTIAC	0.8
	Total			341.94			35.01		

The observatories are: CTIO, Cerro Tololo Interamerican Observatory, La Silla, Chile; SAAO, South African Astronomical Observatory, Sutherland, South Africa; OTIAC, Observatorio del Teide de Instituto de Astrofisica de Canarias, Teide, Tenerife, Spain; MKO, Mauna Kea Observatory, Hawaii, USA; McD, McDonald Observatory, Mt Locke, Texas, USA; PO, Perth Observatory, Bickley, Western Australia, Australia; BAO, Beijing Astronomical Observatory, Beijing, China; ARIES, Aryabhatta Research Institute of Observational Sciences, Manora Peak, Naini Tal, India.

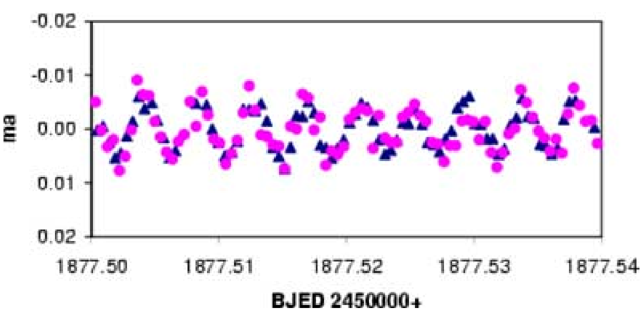

Figure 1. An example of a 1-h section of the light curve of HR 1217 with overlapping data from SAAO (triangles) and OTIAC (circles). The excellent agreement between the two observatories is apparent.

341.94 h of observations were analysed and are listed in Table 1. They span 35.01 d. There was overlap between observatories for 40.65 h of the 341.94 h total, so the duty cycle for the entire run was 36 per cent = (341.94–40.65)/(35.01 × 24). The overlapping light curves from pairs of observatories show good agreement, as can be seen in Fig. 1.

The telescopes used range in aperture from 0.6 to 2.1 m. Data from all sites were obtained using photoelectric photometers, with 10-s individual integrations. At Beijing Astronomical Observatory, McDonald Observatory, Mauna Kea Observatory, State Observatory at Naini Tal and Observatorio del Teide, the observers used three-channel photometers that are functionally similar to the equipment described in Kleinman, Nather & Phillips (1996). The South African Astronomical Observatory and Perth Observatory observations were made with single-channel photometers, and the observations at CTIO with a two-channel photometer. At all sites, observations were made through a Johnson B filter, along with neutral density filters when needed to keep the count rates below 10^6 s^{-1}. Following the procedures described in Kleinman et al. (1996), the sky background was continuously monitored with the three-channel instruments. At sites using two- and single-channel photometers, the sky was obtained several times during the night at irregular intervals, and then interpolated during reduction. Dead-time corrections were measured and applied for all photometers. After bad points were removed and the data reduced using standard procedures, low-frequency sky transparency noise was removed by successive prewhitening of low-frequency peaks until the low-frequency noise was of the same amplitude as that at higher frequencies; in general this procedure was applied to frequencies below 0.6 mHz (i.e. on time-scales longer than approximately 30 min), but for no run does the low-frequency filtering affect the pulsation frequencies near 2.7 mHz. The principal reason for removing low-frequency noise is to obtain white noise across the frequency spectrum for appropriate estimates of least-squares errors. The 10-s integrations were co-added to 40-s integrations to reduce the computing time and smooth high-frequency noise in the visual inspection of the light curves.

During a WET campaign data are reduced at headquarters by a variety of people to a high standard. Nevertheless, it is WET policy to re-reduce all data in a campaign uniformly. This is best performed by one person working diligently to the highest standard of precision. In the case of Xcov20 and the HR 1217 data analysed in this paper, all reductions were uniformly carried out by one of us (CC), and then double-checked by another of us (DWK).

3 FREQUENCY ANALYSIS

Fourier analysis of the data listed in Table 1 was performed using a discrete Fourier transform for unequally spaced data. Fig. 2 shows

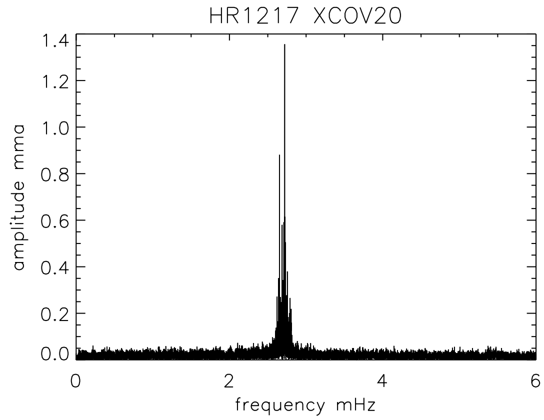

Figure 2. An amplitude spectrum of the entire data set showing that all of the signal is near 2.7 mHz. The first harmonic of the unresolved frequencies can be seen in some of the individual runs when the amplitude is highest, but not in the entire data set.

the amplitude spectrum over the range 0–6 mHz, where it can be seen that all of the signal is concentrated near 2.7 mHz.

In some of the individual data sets the first harmonic of the unresolved frequencies can be seen. Harmonics are commonly observed in roAp stars, so it is no surprise to find evidence of them for HR 1217, although they remain unexplained theoretically. Recently, Kurtz et al. (2005) have found that the 4.030-mHz harmonic in HD 137949 has a higher amplitude than the 2.015-mHz mode at some atmospheric depths; it is clear now that the harmonics of the modes in roAp stars can be studied in much more detail spectroscopically than photometrically. In any case, at the low S/N ratio available for the harmonics for HR 1217, there is nothing useful that we can do with them here.

In Fig. 3 we expand the region where there is signal to show the amplitude spectrum at higher resolution. The level of the highest noise peaks in the amplitude spectrum is approximately 80 μma making this one of the highest precision ground-based data sets ever obtained. The bottom panel of Fig. 3 shows the spectral window for our 36 per cent duty cycle data set. While there is still some cross-talk between the spectral windows of the real frequencies, it is possible with sequential pre-whitening to extract the component frequencies with considerable confidence.

We show some of this sequential pre-whitening in Fig. 4 for the three highest peaks. The techniques we used were: to identify the highest peak in the amplitude spectrum; fit the frequency of that peak and all previously determined peaks by linear least squares to the data with their rotational sidelobes fixed using the known rotation frequency (from $P_{\rm rot} = 12.4576$ d – Kurtz & Marang 1987 and Section 4.3 below); then use the non-linear least-squares method to optimize the frequencies, and the amplitudes and phases, and to determine formal errors on the frequencies; then to revert to the linear least-squares method using the mode frequencies from the non-linear least-squares fit, but again fixing the rotational sidelobes using the known rotational frequency spacing. The frequencies of the rotational sidelobes did not shift significantly in the non-linear least-squares fits, but it is important to keep them at exactly the rotational frequency spacing to examine their phases in the final interpretation of the data, as is seen in Section 4.2 below. (From our knowledge of roAp stars it seems a reasonable assumption that the rotational sidelobes are spaced at the rotational frequency. Tests of this assumption with the current data set are consistent with it.) The data were then pre-whitened by the solution and the next highest significant peak searched for. This was continued until no further significant peaks could be extracted.

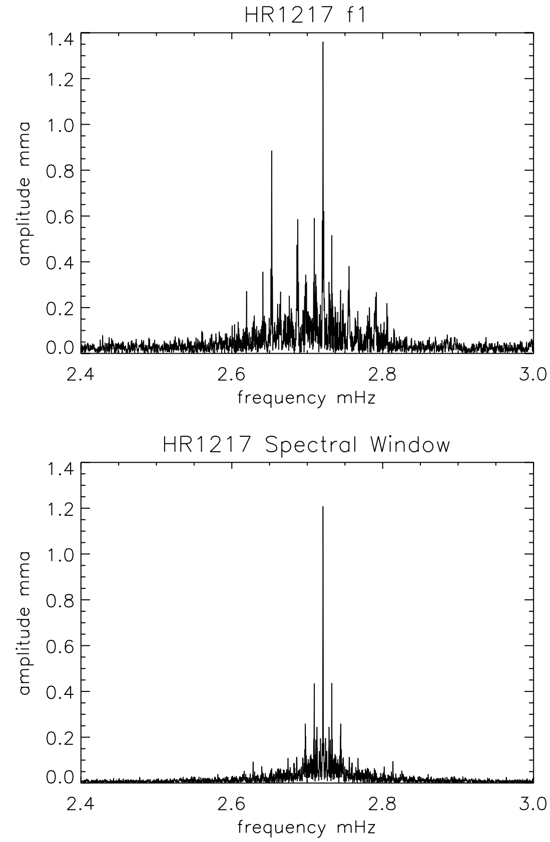

Figure 3. The top panel shows the amplitude spectrum for the entire data set over the frequency range where there is significant signal. The bottom panel shows the spectral window for the highest peak in the top panel. This has been generated by sampling a noise-free sinusoid with the same frequency and amplitude as the highest peak at the actual times of the observations. The amplitude used is taken from the final determination of the frequencies given in Table 2. The difference between the amplitudes of the highest peak in the top panel and in the spectral window in the bottom panel gives a good indication of the amount of cross-talk between the spectral windows of the real frequencies. In a careful examination of both panels the presence of the rotational sidelobes can be seen in the top panel, but not in the spectral window in the bottom panel.

From the panels in Fig. 4 it can be seen that the duty cycle is sufficient that crosstalk among the pulsation frequencies and their rotational sidelobes is not a major problem. Fig. 5 shows a schematic amplitude spectrum of the determined frequency solution and Table 2 gives the frequencies, amplitudes, phases and formal internal errors for that solution. Eight independent pulsation modes were found with significant first rotational sidelobes for most of them. The second rotational sidelobes did not have amplitudes higher than the highest noise peaks, so are not included in the solution, although for ν_4 they are formally significant. The lowest-amplitude rotational sidelobes fitted in Table 2 are only formally significant; as they have amplitudes lower than the highest noise peaks, they cannot be considered to be really detected, but the are included in the fit for completeness and to put a limit on their possible amplitudes.

Additional peaks were found near ν_2 and ν_3 and are listed in Table 2. Similar peaks were seen in the 1986 data (Kurtz et al. 1989) and are suspected to be caused by frequency and/or amplitude modulation over the time-span of the data set. As can be seen in Fig. 5

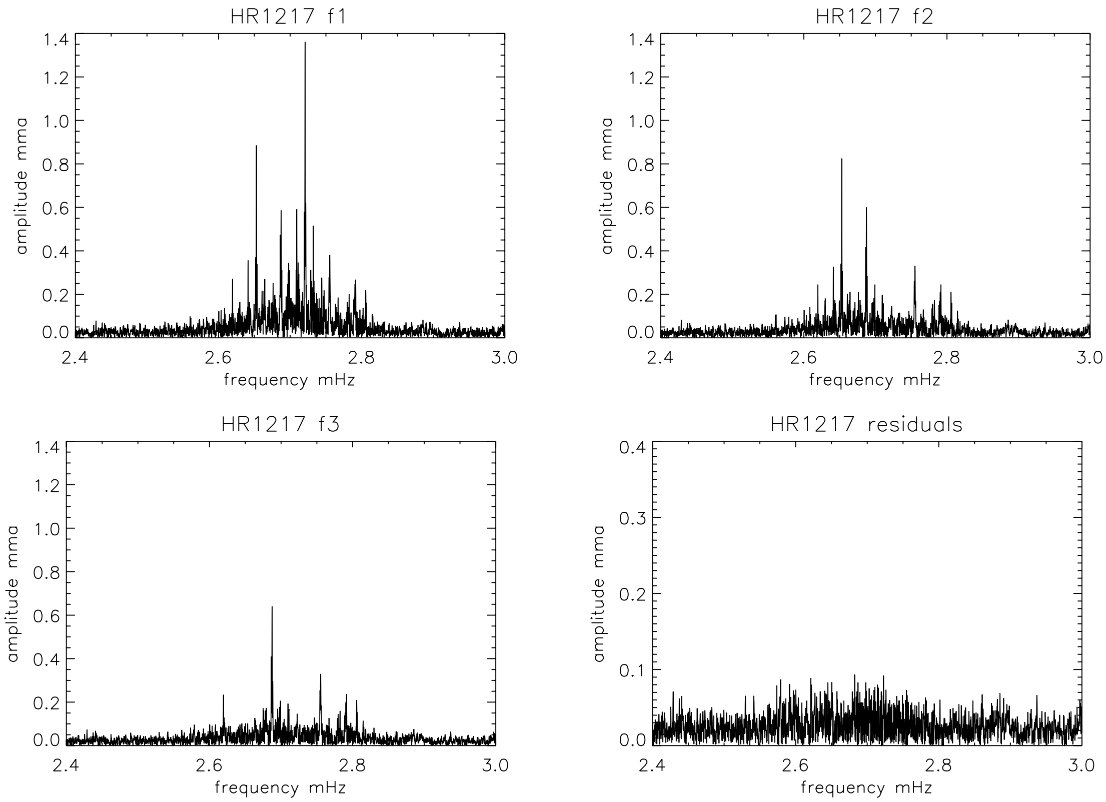

Figure 4. The upper left-hand panel shows the amplitude spectrum for the entire data set over the frequency range where there is significant signal. This is the same as the top panel in Fig. 3 and is reproduced here for easy comparison with the amplitude spectra in the other panels; the highest peak is ν_4 (where the frequencies are labelled in order of increasing frequency; see Table 2). The upper right-hand panel shows the amplitude spectrum after the highest peak, ν_4, and its rotational sidelobes have been pre-whitened; the highest peak here is ν_2. The lower left-hand panel shows the same after ν_4 and ν_2 and their rotational sidelobes have been pre-whitened; the highest peak is ν_3. The text explains the use of linear and non-linear least squares in the procedure. The lower right-hand panel skips many steps to show the residuals after ν_1 to ν_8, their rotational sidelobes and two other significant frequencies have been pre-whitened. Note the change of ordinate scale in the bottom right-hand panel. There is some amplitude left above the noise level. This could be caused by further, low-amplitude, undetected frequencies; by amplitude or frequency variation over the 35-d data set; or by imperfect pre-whitening because of some cross-talk among the spectral windows of the real frequencies.

and discussed in Section 4.1, there is clear amplitude modulation between the 1986 and 2000 data, making it believable that small amounts of such modulation may be detected over a 35-d time-span. These additional peaks, named ν_{2+} and ν_{3-} in Table 2 are not fully resolved from the peaks they are close to, so they are quoted to much lower precision in frequency. They should only be taken to be indicative of additional amplitude left in the amplitude spectrum after pre-whitening by the eight-frequency solution with rotational sidelobes.

4 RESULTS

In their preliminary analysis of the Xcov20 2000 data Kurtz et al. (2002) discovered the 'missing' mode in HR 1217 predicted by Cunha (2001). The most striking new result we find here in the analysis of the full data set is that the new frequency is actually two modes very closely spaced. In the determination of these frequencies we are working near the S/N ratio limit in even this outstandingly low-noise data set, so that confirmation of our results will have to await the analysis of the *MOST* data set. However, the frequencies determined have spacings with respect to the other frequencies that give us some confidence in their reality. We show the frequency spacings in Table 3 and compare them to those determined in the 1986 data set, where the errors on frequency for the 1986 data are from a new non-linear least-squares fit we have performed for those data.

Table 3 suggests that the frequency separations are variable by up to few tenths of a μHz. Given that it is known that there is frequency variability in roAp stars, with an amplitude of 0.12 μHz on a 1.6-yr time-scale in the case of HR 3831 (Kurtz et al. 1997), this variability in the frequency separations in HR 1217 seems to be real. The cause of this frequency variability in roAp stars is not known.

As can be seen from Table 3, and in Fig. 5, there is an alternating frequency spacing of approximately 33.4 and 34.5 μHz, consistent with an interpretation of alternating even and odd ℓ-modes, although, for HR 1217 the modes cannot be pure spherical harmonic modes. The spacing of $\nu_8-\nu_6$ is, within the errors, exactly half of the 33.4-μHz spacing, and the spacing of $\nu_7-\nu_6 = 2.6$ μHz is possibly the 'small spacing'.

Cunha (2001) suggested that in HR 1217 an optimal magneto-acoustic coupling, associated with large energy losses, takes place at a frequency – which we will call $\nu_{\rm jump}$ – lying between the last two modes observed in the 1986 data. If this suggestion is correct, then any mode in HR 1217 with an unperturbed frequency (i.e. the frequency that the mode would have if there were no magnetic field) above $\nu_{\rm jump}$ should have its frequency substantially reduced by the magnetic field. As two new modes were found with frequencies close to $\nu_{\rm jump}$, namely ν_6 and ν_7, we should ask whether these new

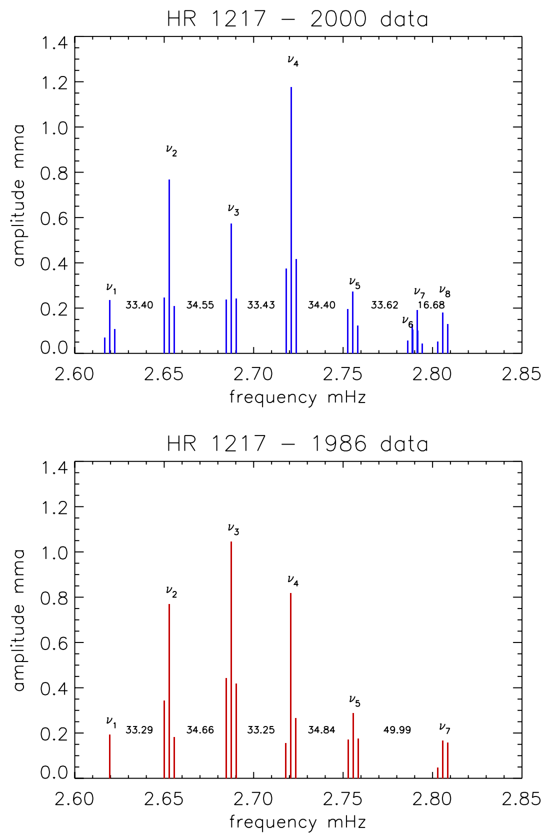

Figure 5. Top panel: a schematic amplitude spectrum of the adopted frequency solution given in Table 2. The spacing of the rotational sidelobes is exaggerated to make them easier to see. Bottom panel: the same for the 1986 data, again with exaggerated rotational sidelobe separations to make them easier to see.

Table 2. The frequency solution for HR 1217.

ID	ν (μHz)	A (mma)	ϕ (rad)
$\nu_1 - \nu_{rot}$	2618.617	0.069 ± 0.014	2.42 ± 0.20
ν_1	2619.546 ± 0.015	0.235 ± 0.014	2.24 ± 0.06
$\nu_1 + \nu_{rot}$	2620.475	0.106 ± 0.014	2.49 ± 0.13
$\nu_2 - \nu_{rot}$	2652.014	0.246 ± 0.014	1.09 ± 0.06
ν_2	2652.943 ± 0.005	0.767 ± 0.014	1.08 ± 0.02
$\nu_2 + \nu_{rot}$	2653.872	0.209 ± 0.014	1.02 ± 0.07
$\nu_3 - \nu_{rot}$	2686.566	0.238 ± 0.015	1.18 ± 0.06
ν_3	2687.495 ± 0.006	0.573 ± 0.014	0.53 ± 0.03
$\nu_3 + \nu_{rot}$	2688.424	0.241 ± 0.014	0.86 ± 0.06
$\nu_4 - \nu_{rot}$	2719.998	0.374 ± 0.014	-2.54 ± 0.04
ν_4	2720.927 ± 0.003	1.176 ± 0.014	-2.77 ± 0.01
$\nu_4 + \nu_{rot}$	2721.856	0.416 ± 0.014	-2.85 ± 0.03
$\nu_5 - \nu_{rot}$	2754.402	0.196 ± 0.014	-2.27 ± 0.07
ν_5	2755.331 ± 0.014	0.273 ± 0.014	-2.04 ± 0.05
$\nu_5 + \nu_{rot}$	2756.260	0.123 ± 0.014	-1.87 ± 0.11
$\nu_6 - \nu_{rot}$	2788.017	0.056 ± 0.014	1.12 ± 0.25
ν_6	2788.946 ± 0.037	0.105 ± 0.014	1.23 ± 0.14
$\nu_6 + \nu_{rot}$	2789.875	0.100 ± 0.014	0.37 ± 0.14
$\nu_7 - \nu_{rot}$	2790.624	0.130 ± 0.014	0.38 ± 0.11
ν_7	2791.553 ± 0.023	0.191 ± 0.014	0.26 ± 0.08
$\nu_7 + \nu_{rot}$	2792.483	0.042 ± 0.014	0.53 ± 0.34
$\nu_8 - \nu_{rot}$	2804.692	0.051 ± 0.014	1.23 ± 0.28
ν_8	2805.621 ± 0.021	0.180 ± 0.014	2.44 ± 0.08
$\nu_8 + \nu_{rot}$	2806.550	0.129 ± 0.014	1.51 ± 0.11
ν_{2+}	2653.4	0.114 ± 0.014	2.52 ± 0.13
ν_{3-}	2686.2	0.201 ± 0.015	0.66 ± 0.07

$\sigma_{\rm fit} = 1.65$ mma. $t_0 =$ BJED2451876.93.

modes have corresponding unperturbed frequencies below or above $\nu_{\rm jump}$. The simplest interpretation, in the light of Cunha's suggestion, is that ν_6 is the 'missing mode' already referred to in her work. In this case its unperturbed frequency is smaller than $\nu_{\rm jump}$ and is only slightly changed (enlarged) by the presence of the magnetic field. Assuming this interpretation holds, then ν_7 can either be a mode with an unperturbed frequency very close to that of ν_6, and also smaller than $\nu_{\rm jump}$, or it can be a mode where the frequency, in the absence of the magnetic field, would be above $\nu_{\rm jump}$, but has been greatly reduced due do the effect of the magnetic field.

In the first case, the simplest interpretation is that ν_6 and ν_7 are modes with consecutive orders and degrees differing by two, hence differing in frequency by the 'small spacing'. In that case only ν_8 would have its frequency greatly reduced by the magnetic field. Unfortunately, the theory developed by Cunha & Gough (2000) has to be improved before one can quantify with precision the amount by which the frequency of ν_8 is decreased. Preliminary results (Cunha, in preparation) indicate that modes with frequencies larger than that at which the maximum coupling takes place have their frequencies decreased by a fraction of the large separation, that fraction being determined by an integral that depends on the degree of the mode and the geometry of the magnetic field. However, in order to know whether that fraction is the 25 per cent implied by the observations, under this interpretation, it is necessary first to improve the theoretical model.

The second possibility considered here is more interesting, in the sense that it puts additional constraints on Cunha's interpretation. If the unperturbed frequency of ν_7 is above $\nu_{\rm jump}$, it is necessary to explain simultaneously the abrupt decrease in the frequencies of two modes, namely ν_7 and ν_8. In her preliminary calculations Cunha found that for a dipole field, the decrease in the frequency of $\ell = 0$ modes is considerably larger than the decrease in the frequencies of $\ell = 1$ and 2 modes. Thus, with the current models, the only combination that she found for which both ν_7 and ν_8 would have unperturbed frequencies above $\nu_{\rm jump}$ requires ν_7 to be an $\ell = 1$ mode and ν_8 to be an $\ell = 0$ mode. Moreover, this interpretation is possible only if ν_6 has even degree, which, due to the alternation between even and odd degrees in the power spectrum, would also imply even degrees for ν_2 and ν_4. As the latter two modes are more likely to be dipole modes, at the moment the interpretation that both new modes have unperturbed frequencies below $\nu_{\rm jump}$ and that their frequencies differ by an amount that is equal to the small spacing is favoured by Cunha's theory. We emphasize, however, that due to the strong dependence of Cunha's results on the geometry of the magnetic field, this conclusion might be modified if the magnetic field geometry of HR 1217 is not dipolar. We also note that in the work of Bagnulo et al. (1995) the authors state that their polarimetric study cannot distinguish between a dipolar magnetic field and one described by a dipole plus a co-linear quadrupole, i.e. a centred dipole field, or a displaced dipole field.

Recently, Saio & Gautschy (2004) have also studied the magnetic perturbations to the eigenfrequencies, and found results which are qualitatively in agreement with those of Cunha & Gough (2000). Rather than applying a variational principle, as Cunha & Gough did, Saio & Gautschy expanded the solutions in sums of spherical harmonics and determined, simultaneously, the perturbed

Table 3. Comparison of the HR 1217 frequency spacings between the 2000 WET data and the 1986 data.

ID	$\Delta\nu$ 2000	$\Delta\nu$ 1986	$\Delta_{\Delta\nu}$
$\nu_2 - \nu_1$	33.397 ± 0.016	33.268 ± 0.020	0.13 ± 0.03
$\nu_3 - \nu_2$	34.552 ± 0.008	34.712 ± 0.008	-0.16 ± 0.01
$\nu_4 - \nu_3$	33.432 ± 0.007	33.204 ± 0.007	0.23 ± 0.01
$\nu_5 - \nu_4$	34.404 ± 0.014	34.936 ± 0.018	-0.53 ± 0.02
$\nu_6 - \nu_5$	33.615 ± 0.039		
$\nu_7 - \nu_6$	2.607 ± 0.044		
$\nu_7 - \nu_5$	36.222 ± 0.027		
$\nu_8 - \nu_6$	16.675 ± 0.042		
$\nu_8 - \nu_7$	14.068 ± 0.031		
$2(\nu_8 - \nu_6)$	33.350 ± 0.085		
$\nu_8 - \nu_5$	50.290 ± 0.025	49.889 ± 0.029	0.40 ± 0.03
$(\nu_2 - \nu_1) - (\nu_4 - \nu_3)$	-0.035 ± 0.018	0.04 ± 0.11	
$(\nu_3 - \nu_2) - (\nu_5 - \nu_4)$	0.148 ± 0.016	-0.18 ± 0.11	

eigenfrequencies and eigenfunctions. This expansion in spherical harmonics had to be truncated in order to obtain the solutions, and generally no convergence was found for the frequencies at which the perturbation is most significant.

According to the suggestion of Cunha (2001), ν_6 lies precisely in the frequency region where the perturbation is greatest. Thus, just as in the case of Cunha & Gough (2000), caution should be applied when using Saio & Gautschy's frequency perturbations at the frequencies around ν_6. Despite the existence of quantitative differences in the absolute frequency perturbations found, the ratio between the 'frequency jumps' suffered by modes of different degrees is very similar in the two works. Thus, the above discussion regarding the interpretation of ν_6, ν_7 and ν_8 is maintained if the results of Saio & Gautschy (2004) are used, rather than those of Cunha & Gough (2000).

4.1 Amplitude variations between the 2000 and 1986 data sets

A question that arose in our preliminary study of the 2000 WET data (Kurtz et al. 2002), where the 'missing' frequency was discovered, was 'why was this frequency not seen in the 1986 data?' The amplitude found by Kurtz et al. was high enough that it should have been detected in the 1986 data, if it were there at the same amplitude. It is clear from the comparison of the amplitudes in the 2000 and 1986 data sets shown in Table 4 and in Fig. 5 that significant amplitude variability does occur for HR 1217. In particular, look at the amplitudes of the highest peak, ν_4, the mode next to it at ν_3 and their rotational sidelobes. Their amplitudes have changed by several tenths of an mma – much more than the amplitude of the newly discovered frequencies now called ν_6 and ν_7. We conclude that these newly discovered frequencies had amplitudes below the detection limit in the 1986 data; for the 2000 data the noise level was reduced and the amplitudes grew.

Interestingly, there is little difference in the sum of the power between the two data sets (given at the bottom of Table 4), indicating that the total pulsational energy has possibly been conserved, but that there has been transfer of some energy from one mode to another – particularly, from ν_3 to ν_4. It is not possible to be certain about this until we can characterize the modes completely, as distorted modes of differing ℓ have different projection factors, precluding relating pulsation power (amplitude squared) directly to pulsation energy. Some singly periodic roAp stars are known to have very stable amplitudes, such as HR 3831 (Kurtz et al. 1997) where there has been minimal amplitude change over 18 yr of observations. Other roAp stars, such as HD 60435 (Matthews, Wehlau & Kurtz 1987) have many more pulsation modes than HR 1217 and show significant amplitude modulation on a time-scale of only a few days. We conjecture that the multimode roAp stars transfer energy between modes, whereas the singly periodic stars cannot do that and have stable amplitudes. The results in Table 4 are the first data that can test whether total pulsation power is conserved in multimode stars where energy exchange occurs. Great caution is called for here, however, as so little is known concerning pulsation power stability. A counter-example to the above suggestion is the star HD 217522 (Kreidl et al. 1991) where an entirely new frequency appeared

Table 4. Amplitude variation between the 2000 and 1986 data. Only frequencies detected in both data sets are listed; i.e. only the frequencies found in the 1986 data, all of which are also found in the 2000 data, are listed. The values of the frequencies from the 2000 data set are given, and the identification labels are the same as those in Table 2.

ID	ν (μHz)	A 2000 (mma) ± 0.014	A 1986 (mma) ± 0.018	ΔA (mma) ± 0.023
ν_1	2619.546	0.235	0.193	0.042
$\nu_2 - \nu_{\mathrm{rot}}$	2652.014	0.246	0.343	−0.097
ν_2	2652.943	0.767	0.770	−0.003
$\nu_2 + \nu_{\mathrm{rot}}$	2653.872	0.209	0.183	0.026
$\nu_3 - \nu_{\mathrm{rot}}$	2686.566	0.238	0.442	−0.204
ν_3	2687.495	0.573	1.046	−0.473
$\nu_3 + \nu_{\mathrm{rot}}$	2688.424	0.241	0.418	−0.177
$\nu_4 - \nu_{\mathrm{rot}}$	2719.998	0.374	0.156	0.218
ν_4	2720.927	1.176	0.818	0.358
$\nu_4 + \nu_{\mathrm{rot}}$	2721.856	0.416	0.266	0.150
$\nu_5 - \nu_{\mathrm{rot}}$	2754.402	0.196	0.170	0.026
ν_5	2755.331	0.273	0.288	−0.015
$\nu_5 + \nu_{\mathrm{rot}}$	2756.260	0.123	0.176	−0.053
$\nu_8 - \nu_{\mathrm{rot}}$	2804.692	0.051	0.048	0.003
ν_8	2805.621	0.180	0.166	0.014
$\nu_8 + \nu_{\mathrm{rot}}$	2806.550	0.129	0.157	−0.028
Power = A^2 mma^2		3.1 ± 0.5	3.2 ± 0.7	0.1 ± 0.7

between data sets in 1982 and 1989 and power does not seem to have been conserved in a star with only two modes.

4.2 The rotational sidelobes

The oblique pulsator model (OPM) for the roAp stars (Kurtz 1982) has been the standard interpretation for the rotational amplitude and phase modulation for these stars since it was introduced. In this picture the pulsation modes are axisymmetric modes aligned with the magnetic axis which is itself inclined to the rotational axis by an angle β. The rotational axis is inclined to the line of sight by an angle i. The most developed theory of the standard OPM can be found in Takata & Shibahashi (1995) and Shibahashi & Takata (1993).

Recently, Bigot & Dziembowski (2002) have introduced the 'improved oblique pulsator model' (IOPM) which presents a very different picture. They find that the centrifugal distortion of the star has a greater effect on the pulsations than the Coriolis force, and that the combination of rotational and magnetic effects on the pulsation modes couples the $2\ell + 1$ magnetic levels for each given ℓ. In particular, for $\ell = 1$ they find three eigenmodes for which the axis of symmetry precesses in a plane that does not generally contain the magnetic axis.

Bigot & Kurtz (2005) find a geometry for the roAp star HR 3831 of $(i,\ \beta) = (84,\ 7)^\circ$ from the IOPM. This is in good agreement with $i = 90^\circ \pm 1^\circ$ and $\beta = 8^\circ \pm 1$ found by Bagnulo et al. (1999) from magnetic measurements. The old oblique pulsator model with a dipole-like pulsation aligned with the magnetic axis is not plausible with this geometry. The observed semi-amplitude for HR 3831 is approximately 5 mmag in B; with this geometry, if the mode could be seen from pole-on, then it would have a semi-amplitude of 36 mmag. This is vastly larger than the highest amplitude seen for any of the 34 known roAp stars of 8 mmag, in the case of HD 60435, and that is for multiple modes beating with each other. The highest-amplitude individual modes are for HD 101065 and HR 3831 and are approximately 5 mmag. However, Kochukhov (2004) finds a different magnetic and pulsation geometry for HR 3831 that is in good agreement with the old oblique pulsator model and is inconsistent with the Bagnulo et al. (1999) geometry. Further magnetic studies should differentiate between these two models.

Most recently, Saio & Gautschy (2004) have looked at the interaction of pulsation and the magnetic field in roAp stars and confirmed, as first found by Dziembowski & Goode (1996), that the pulsation modes cannot be characterized by a single spherical harmonic. They are distorted dipole and quadrupole modes that are aligned with the magnetic axis.

In all of these models the pulsation modes are inclined to the rotation axis so that they are viewed at varying aspect with the rotation of the star. This is a unique aspect of the roAp stars that allows their mode geometries to be studied in more detail than for any other kind of pulsating star. The information concerning the rotational modulation of the modes is contained in the amplitudes and phases of the rotational sidelobes to the mode frequencies. Those amplitudes and phases are listed in Table 2 and shown schematically in Fig. 5. Given that there is residual amplitude in the amplitude spectrum of the residuals to our frequency solution with highest peaks around 80 μma (see Fig. 4), we advise caution in interpreting the rotational sidelobes with amplitudes less than that, even though they are formally significant.

First, we will examine the phases of the rotational sidelobes in Table 2. We do not consider the rotational sidelobes for ν_6 and ν_7 to be significant enough to discuss further, and, as was found in the 1986 data by Kurtz et al. (1989), ν_8 seems to be a rotational doublet, rather than a triplet – or at least it has very different amplitudes for the rotational sidelobes. This has been found in two independent multisite data sets (1986 and 2000), so is significant, but we do not know the cause of it. So we will look at the rotational sidelobes for the first five modes, ν_1 to ν_5.

The zero point of the time-scale for the frequency solution in Table 2 is $t_0 =$ BJED2451876.93 and it was selected to set the phases of the rotational sidelobes of ν_1 to ν_5 equal to each other. It can be seen that the phases of the modes and their rotational sidelobes for each of the five modes under consideration here are nearly equal, in most cases they are not statistically significantly different within the formal errors, and those errors neglect the cross-talk problems that we know are still present in this 36 per cent duty cycle data set. This near equality of the phases of the frequency triplets means that the pulsation modes are being amplitude modulated with rotation, but not phase modulated. This significantly simplifies the interpretation of the rotational triplets; pure amplitude modulation is what we expect for axisymmetric normal modes seen from varying aspect.

All of the oblique pulsator models characterize the rotational triplets *for dipole modes* using two parameters. We will use the notation of Bigot & Dziembowski in the IOPM and call these two parameters γ^+ and γ^-. They are:

$$\gamma^+ = \frac{A_{+1} + A_{-1}}{A_0} \quad \text{and} \quad \gamma^- = \frac{A_{+1} - A_{-1}}{A_{+1} + A_{-1}},$$

where A_{+1} and A_{-1} refer to the amplitudes of the higher- and lower-frequency rotational sidelobes, respectively, and A_0 refers to the amplitude of the central frequency of the triplet. In Table 5 we list these parameters for the all eight modes in the 2000 data and compare them to the values found by Kurtz et al. (1989) for five of those modes in the 1986 data. The frequencies and frequency labels are those from the 2000 WET data set – this work. There is no difference in the values of γ^+ and γ^- greater than 3σ between the

Table 5. The values of γ^+ and γ^- that characterize the rotational amplitude modulation of the pulsation modes.

ID	Frequency	γ^+ (2000)	γ^- (2000)	γ^+ (1986)	γ^- (1986)
ν_1	2619.546	0.74 ± 0.10	0.21 ± 0.12		
ν_2	2652.943	0.59 ± 0.03	-0.08 ± 0.04	0.68 ± 0.04	-0.30 ± 0.05
ν_3	2687.495	0.84 ± 0.04	0.01 ± 0.04	0.82 ± 0.03	-0.03 ± 0.03
ν_4	2720.927	0.67 ± 0.02	0.05 ± 0.03	0.52 ± 0.03	0.26 ± 0.06
ν_5	2755.331	1.17 ± 0.09	-0.23 ± 0.06	1.20 ± 0.12	0.02 ± 0.07
ν_6	2788.946	1.49 ± 0.27	0.28 ± 0.13		
ν_7	2791.553	0.90 ± 0.12	-0.51 ± 0.13		
ν_8	2805.621	1.00 ± 0.13	0.43 ± 0.12	1.23 ± 0.20	0.53 ± 0.14

2000 and 1986 data sets, except for γ^+ for ν_4 which is technically at the 4σ level, but with some cross-talk between the frequencies in both data sets, we do not interpret that to be significant.

Kurtz et al. (1989) concluded that ν_2 and ν_4 are very nearly dipole modes within the standard OPM, but found that the other modes could not be purely spherical harmonic modes. Their argument came from the fact that within the OPM

$$\gamma^+ = \frac{A_{+1} + A_{-1}}{A_0} = \tan i \tan \beta.$$

In that model i and β are the same for a dipole pulsation mode and a dipole magnetic field. The most recent and best values for those parameters come from a broad-band linear polarization study by Bagnulo et al. (1995) who find $i = 137°$ and $\beta = 150°$. Those give $\gamma^+ = \tan\ i \tan\ \beta = 0.54$, close to the values of 0.59 and 0.67 found in Table 6 for ν_2 and ν_4, hence the suggestion that those modes are dipole pulsation modes, or at least something close to normal dipole modes. Matthews et al. (1999) showed from *Hipparcos* parallaxes and standard A-star models that the large spacing, $\Delta\nu_0$ equals 68 μHz for HR 1217, hence the modes are alternating even and odd ℓ-modes, or distorted alternating even and odd ℓ-modes. Shibahashi & Saio (1985) long ago argued from standard A-star models that the alternating spacing seen in HR 1217 (see Fig. 5) suggests that the even-ℓ modes should be radial modes, rather than quadrupole modes. Of course, those even-ℓ modes are amplitude modulated, so cannot be simple radial modes which would not vary with aspect, but neither can they be quadrupole modes – they do not modulate as expected for quadrupole modes, given the known i and β from magnetic measurements (see Kurtz et al. 1989). Hence the conclusion within the standard OPM is that the even-ℓ modes must be distorted by the magnetic field. The values of γ^+ for ν_1, ν_3 and ν_5 are close to each other in Table 5, so whatever the interpretation of them, they can be considered to have the same mode identification – i.e. they modulate in the same way with rotation.

The new theoretical work of Bigot & Dziembowski (2002) addresses the rotational and magnetic distortions directly; that of Saio & Gautschy (2004) addresses only the magnetic distortion. In the latter study the modes are truly distorted from simple spherical harmonic modes; in the former (IOMP) the modes are still described by spherical harmonics, but are combinations of azimuthal m-modes for a given ℓ. In the IOPM γ^+ depends on the rotational inclination, i, the inclination of the normal of the pulsation plane to the rotation axis, δ, and the ellipticity of the pulsation mode motion in the pulsation plane, ψ, all of which depend ultimately on the rotational and magnetic distortions and have to be modelled.

The values of γ^- are all less than unity. Within the standard OPM (Takata & Shibahashi 1995) this suggests that the rotational perturbation is small compared with the magnetic perturbations, as

$$\gamma^- = \frac{A_{+1} - A_{-1}}{A_{+1} + A_{-1}} = \frac{C_{n\ell}\Omega}{\omega_1^{(1)\mathrm{mag}} - \omega_0^{(1)\mathrm{mag}}},$$

where the numerator is a measure of the rotational perturbation and the denominator of the magnetic perturbation.

Within the IOPM of Bigot & Dziembowski (2002) the relative importance of the rotational and magnetic effects is described by the parameter

$$\mu = \frac{\omega_0^{\mathrm{mag}} - \omega_1^{\mathrm{mag}}}{D},$$

where ω_0^{mag} and ω_1^{mag} are the magnetic eigenfrequencies for modes with $m = 0$ and 1, respectively, and D is a measure of the centrifugal distortion. For HR 1217, with its relatively long 12.4572-d rotation period (see Section 4.3) and strong polar magnetic field strength of 3.9 kG (Bagnulo et al. 1995), we would expect a large value of μ. In that case, the IOPM predicts that one of modes should be nearly aligned with the magnetic field, independently of the magnetic obliquity, implying that for that mode $\psi \approx 0$ and $|\delta| \approx |\pi/2 - \beta|$.

Having fixed the inclination of the observer, $i = 137°$ (from Bagnulo et al. 1995), the observed values of $\gamma^\pm$ from Table 5 lead to the common value of $\delta \approx 56°$ for both eigenmodes, ν_2 and ν_4. This value of δ is relatively well determined with an error of approximately 2°–3°. The ellipticities of the modes ν_2 and ν_4 are small, $\psi \sim 1°$–3°. These two modes are then almost standing modes pulsating in the direction $\pi/2 + \delta \approx 146°$, which is the same as that found by Bagnulo for the inclination of the magnetic axis, within the observational error bars. We can conclude that, from the IOPM, the modes ν_2 and ν_4 are essentially $m = 0$ modes in the magnetic reference system. That these two frequencies are well represented by a single spherical harmonic could be in contrast with the expectations that the modes should be distorted (as found by Dziembowski & Goode 1996; Cunha & Gough 2000; Bigot & Dziembowski 2002; and Saio & Gautschy 2004). However, the degree of distortion depends on the entire geometry, on the strength of the coupling and on the averaging effect. For dipole modes, in particular, it is likely that the distortion seen is very small, as the averaging by cancellation of the higher ℓ components over the stellar disc would be greater than that of the $\ell = 1$ components. At present we can only say for ν_1, ν_3 and ν_5 that if they are radial modes, then they are distorted, as they are modulated with rotation; if they are quadrupole modes, then further study is needed to understand them within the OPM, the IOPM and the theory of Saio & Gautschy.

4.3 The rotation period

There is a controversy over the rotation period of HR 1217. Kurtz & Marang (1987) used a combination of measurements of magnetic field variability, mean light variability (i.e. rotational light variability) in Johnson and Strömgren colours and Eu II line strength variability – all from different authors and different studies – to derive a rotational ephemeris of

HJD (extremum) $= 2440578.23 \pm 0.09 + 12.4572 \pm 0.0003\,E$.

This derivation was made under the assumption that all of those parameters vary with exactly the same period, and that period is the rotation period. This is consistent with what is known of oblique rotation in many magnetic Ap stars.

Kurtz et al. (1989) found in their multisite study of the pulsation of HR 1217 that the times of magnetic and pulsation maximum are the same within 0.05 ± 0.03 rotation periods, but that the time of mean light extremum is slightly different by -0.031 ± 0.010 rotation periods to the pulsation maximum. These small differences over the many rotation periods studied in this star are not the source of the controversy over the rotation period. They are simply too small to matter at the precision that the rotation period is known. Kurtz et al. (1989) used the rotation period of Kurtz & Marang and gave an ephemeris for pulsation amplitude maximum of

HJD (amplitude maximum) $= 2446743.54 \pm 0.38 + 12.4572\,E$.

Mathys (1991) found this period to be incompatible with his and Preston's (1972) combined magnetic measurements. He derived a rotation period of 12.4610 ± 0.0025 d; although that value is formally compatible with the period of 12.4572 ± 0.0003 d found by Kurtz & Marang, Mathys found that the latter did not phase his and Preston's combined magnetic observations satisfactorily. He suggested that the assumed phase equality of the photometry in different colours and the Eu II line strengths may have caused Kurtz & Marang to derive a wrong period. For the problem to be in the magnetic measurements there must be a systematic shift between the observations of Mathys and those of Preston larger than is expected. Mathys & Hubrig (1997) obtained five new measurements of the magnetic field of HR 1217 to add to the two measurements of Mathys (1991) and compared with the measurements of Preston. They confirm the 12.4610-d rotation period and show that the 12.4572-d period cannot correctly phase their measurements with those of Preston.

Bagnulo et al. (1995) used broad-band linear polarimetry to derive measures of the longitudinal magnetic field of HR 1217 on 14 different dates between 1991 September and 1994 January. It is from their study that we quoted the best values of i and β in the last section. They obtained a rotation period of 12.4610 ± 0.0011 d, consistent with that of Mathys and inconsistent with that of Kurtz & Marang. They performed further error analysis, however, and concluded that the period of Kurtz & Marang cannot be ruled out by their study.

Wade et al. (2000) obtained four new measurements of the longitudinal field strength. They found that the 12.4572-d period phases all observations except those of Mathys & Hubrig (1997) well, whereas the 12.4610-d period does not. They suggest that a zero-point shift is needed to bring the measurements of Mathys & Hubrig and others into agreement.

Leone et al. (2000) obtained eight new measurements of the longitudinal magnetic field of HR 1217 over a time-span of 123 d. They concluded that the best rotation period is that of Kurtz & Marang, not that of Mathys. They found agreement between their measurements and those of Mathys, but suggested that those of Preston need to be shifted by -0.75 kG. They noted that 12.4572-d period phases the *Hipparcos* photometry and the single filter photometry of Wolff & Morrison (1973) well, while the 12.4610-d period is shifted by 0.15 periods.

We discussed in the introduction the clear spectroscopic observations of roAp stars that show horizontal and/or vertical abundance distributions in these stars that are obvious in the amplitudes and phases of the pulsational radial velocities. It is therefore possible from the conclusions of Leone et al. (2000) and Wade et al. (2000) above that the use of different sets of spectral lines to determine the magnetic field strengths in the different data sets has sampled the magnetic field differently, giving rise to a zero-point shift between data sets. A good test of this is to use one set of data to measure the magnetic field strengths using Preston's (1972) chosen lines and Mathy's (1991) chosen lines to see if there is a systematic shift in the measured magnetic field values.

We can calculate the rotation period from studies of the pulsation alone. We have collected all high-speed B photometric observations of HR 1217 dating back to 1981. We have fitted the highest amplitude frequency in our solution, $\nu_4 = 2.7209$ mHz to sections of the data five pulsation cycles long (30.63 min) and used a least-squares fit to derive the amplitude for that section. Of course, for sections that short the many modes beat against each other, but all the modes are rotationally modulated, so the highest-amplitude sections do vary with rotation clearly. This procedure gave us 1614 5-cycle amplitudes spanning 20 yr of observations. A Fourier analysis yielded a best value of the rotation period of 12.4572 d – the same as that derived by Kurtz & Marang, so we conclude that, a least for the pulsation data, that is the best value for the rotation period. Fig. 6 shows the relevant section of the amplitude spectrum.

We conclude that the photometric pulsation rotation period is probably correct, implying that some of the magnetic measurements need zero-point shifts larger than has heretofore been thought reasonable. It is not plausible that the magnetic period and photometric period may be different, as that would cause a drift in the relative times of maxima between the magnetic field and pulsation, making their present coincidence improbable.

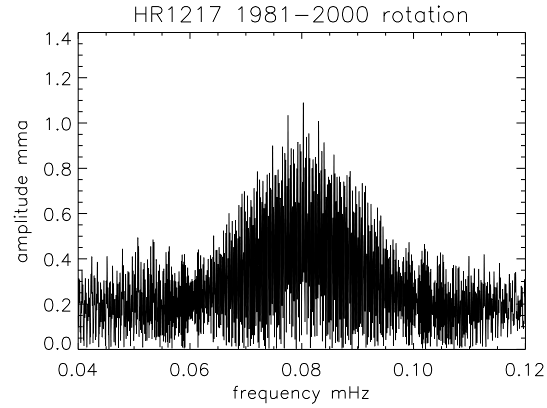

Figure 6. Amplitude spectrum of the pulsation amplitude determined by least squares for sections of the data 5 cycles, or 30.63-min long, for $\nu_4 = 2.7209$ mHz. The data span 20 yr from 1981. The highest peak is at $\nu_{\rm rot} = 0.080\,272$ d^{-1}, corresponding to a best period of 12.4572 d.

5 CONCLUSIONS

The alternating frequency spacing of HR 1217 makes its amplitude spectrum one of the most interesting known after that of the Sun for the study of non-degenerate stars asteroseismically. For this reason it is one of the best-studied roAp stars. The WET Xcov20 campaign on HR 1217 is likely to stand as the definitive ground-based study with a photometric precision of 14 μma. Future observations and studies will be from space; the first space data set has already been obtained with the *MOST* satellite. Observations with *MOST* have a precision many times better than in the WET data set; the data presented in this paper and those from the 1986 campaign have set the baseline to which the space data will be compared.

We have found the new frequency predicted by Cunha (2001), and also expected in the theory of Saio & Gautschy (2004), giving strong support to these studies. The results of our frequency analysis are so detailed, especially with the discovery of both ν_6 and ν_7 and the precise determination of their spacings from the previously known frequencies, that more theoretical development is needed to confront these results.

We have clearly shown that there is amplitude modulation for some of the modes in HR 1217 between the 1986 and 2000 multisite campaigns. This explains why the new frequencies were not detected in the 1986 data. It appears that the pulsational energy has been conserved between the 1986 and 2000 data sets, suggesting that energy is transferred between modes, although the case for this is not strong.

The rotational sidelobes confirm that the modes giving rise to ν_2 and ν_4 are close to dipolar, while the modes giving rise to ν_1, ν_3 and ν_5 are distorted even-ℓ modes, but whether $\ell = 0$ or 2 cannot be determined, for either the old oblique pulsator model or the new improved oblique pulsator model.

In the controversy over the rotation period we confirm that $P_{\rm rot} = 12.4572$ d fits *all* the photometric B pulsation data from 1981 to 2000. This suggests that some zero-point shifts between some of the magnetic measurements are needed.

ACKNOWLEDGMENTS

We thank Gautier Mathys for helpful discussion of the rotation period. We gratefully acknowledge support from the US National Science Foundation through grant AST-9876655 to Iowa State University, and funding by UNESCO through the International Institute of Theoretical and Applied Physics at Iowa State. MC is supported by FCT-Portugal through the grant PD/18893/98 and the grant POCTI/FNU/43658/2001 approved by FCT and POCTI, with funds from the European Community programme FEDER. PM is supported by KBN (Poland) through grant 5-P03D-030-20. J-ES and FJ thank the Norwegian Research Council for support.

REFERENCES

Bagnulo S., Landi degl'Innocenti E., Landolfi M., Leroy J. L., 1995, A&A, 295, 459
Bagnulo S., Landolfi M., degl'Innocenti M. L., 1999, A&A, 343, 865
Baldry I. K., Bedding T. R., 2000, MNRAS, 318, 341
Baldry I. K., Viskum M., Bedding T. R., Kjeldsen H., Frandsen S., 1999, MNRAS, 302, 381
Balmforth N. J., Cunha M. S., Dolez N., Gough D. O., Vauclair S., 2001, MNRAS, 323, 362
Balona L. A., Laney C. D., 2003, MNRAS, 344, 242
Balona L. A., Zima W., 2002, MNRAS, 336, 873
Bigot L., Dziembowski W. A., 2002, A&A, 391, 235
Bigot L., Kurtz D. W. 2005, A&A, in press
Bigot L., Provost J., Berthomieu G., Dziembowski W. A., Goode P. R., 2000, A&A, 356, 218
Cowley C. R., Hubrig S., Ryabchikova T. A., Mathys G., Piskunov N., Mittermayer P., 2001, A&A, 367, 939
Cunha M. S., 2001, MNRAS, 325, 373
Cunha M. S., Gough D., 2000, MNRAS, 319, 1020
Cunha M. S., Fernandes J. M. M. B., Monteiro M. J. P. F. G., 2003, MNRAS, 343, 831
Dziembowski W. A., Goode P. R., 1996, ApJ, 458, 338
Heller C. H., Kawaler S. D., 1988, ApJ, 329, L43
Kleinman S. J., Nather R. E., Phillips T., 1996, PASP, 108, 356
Kochukhov O., 2004, ApJ, 615, L149
Kochukhov O., Ryabchikova T., 2001a, A&A, 377, L22
Kochukhov O., Ryabchikova T., 2001b, A&A, 374, 615
Kochukhov O., Bagnulo S., Barklem P. S., 2002, ApJ, 578, L75
Kreidl T. J., Kurtz D. W., Bus S. J., Kuschnig R., Birch P. B., Candy M. P., Weiss W. W., 1991, MNRAS, 250, 477
Kurtz D. W., 1982, MNRAS, 200, 807
Kurtz D. W., Marang F., 1987, MNRAS, 229, 285
Kurtz D. W. et al., 1989, MNRAS, 240, 881
Kurtz D. W., van Wyk F., Roberts G., Marang F., Handler G., Medupe R., Kilkenny D., 1997, MNRAS, 287, 69
Kurtz D. W. et al., 2002, MNRAS, 330, L57
Kurtz D. W., Elkin V. G., Mathys G., 2003, MNRAS, 343, L5
Kurtz D. W., Elkin V. G., Mathys G., 2005, MNRAS, in press (doi: 10.1111/j.1745-3933.2005.00016.x)
Leone F., Catanzaro G., Catalano S., 2000, A&A, 355, 315
Mathys G., 1991, A&AS, 89, 121
Mathys G., Hubrig S., 1997, A&AS, 124, 475
Matthews J. M., Wehlau W. H., Kurtz D. W., 1987, ApJ, 313, 782
Matthews J. M., Wehlau W. H., Walker G. A. H., Yang S., 1988, ApJ, 324, 1099
Matthews J. M., Kurtz D. W., Martinez P., 1999, ApJ, 511, 422
Mkrtichian D. E., Hatzes A. P., Kanaan A., 2003, MNRAS, 345, 781
Preston G. W., 1972, ApJ, 175, 465
Ryabchikova T., Piskunov N., Kochukhov O., Tsymbal V., Mittermayer P., Weiss W. W., 2002, A&A, 384, 545
Sachkov M., Ryabchikova T., Kochukhov O., Weiss W. W., Reegen P., Landstreet J. D., 2004, in Kurtz D. W., Pollard K. R., eds, ASP Conf. Ser., Vol. 310, Variable Stars in the Local Group. Astron. Soc. Pac., San Francisco, p. 208
Saio H., Gautschy A., 2004, MNRAS, 350, 485
Shibahashi H., Saio H., 1985, PASJ, 37, 245
Shibahashi H., Takata M., 1993, PASJ, 45, 617
Takata M., Shibahashi H., 1995, PASJ, 47, 219
Tassoul M., 1980, ApJS, 43, 469
Tassoul M., 1990, ApJ, 358, 313
Wade G. A., Donati J.-F., Landstreet J. D., Shorlin S. L. S., 2000, MNRAS, 313, 851
Wolff S. C., Morrison N. D., 1973, PASP, 85, 141

This paper has been typeset from a TEX/LATEX file prepared by the author.

Chapter 5

Beta Cephei stars

5.1 Introduction

These early B main sequence stars have been made accessible to asteroseismology in recent years. We show some major steps that led to the exploration of the interior structure of some β Cephei stars.

The next two sections set the stage: a detailed list of all galactic β Cephei stars, i.e. the whole range of possible targets, and a detailed investigation of their group properties is presented in Sect. 5.2, and a first exploratory study of three pulsators to verify the validity of photometric mode identification for β Cephei stars comprises Sect. 5.3.

Section 5.4 is the central part of this chapter. It reports the observations, mode identification, and seismic study of the β Cephei star ν Eridani. For the first time, clear evidence for differential interior rotation of a massive main sequence star was found, and a limit on the convective core size was obtained. Some hints for a nonstandard interior chemical profile were reported as well.

Sections 5.5 and 5.6 describe the analysis of observational data of two further β Cephei stars that show pulsation spectra sufficiently rich for theoretical modelling. The results for θ Ophiuchi can be used to check the theory of rotation, and the richness of the oscillation spectrum of 12 Lac should allow detailed interior structure modelling of another β Cephei star. Finally, Sect. 5.7 reports some results on other massive B-type pulsators, where less constraints on their interior structure are to be expected, but some interesting questions on light curve shapes and pulsation geometry could be addressed.

5.2 Catalog of galactic β Cephei stars

Original paper:

A. Stankov, **G. Handler,** 2005, ApJS 158, 193

The Astrophysical Journal Supplement Series, 158:193–216, 2005 June

CATALOG OF GALACTIC β CEPHEI STARS

Anamarija Stankov
Research and Scientific Support Department, ESA-ESTEC, SCI-A, 2201 AZ Noordwijk, Netherlands; astankov@rssd.esa.int

and

Gerald Handler[1]
Institute for Astronomy, Türkenschanzstrasse 17, 1180 Vienna, Austria; handler@astro.univie.ac.at
Received 2004 November 19; accepted 2005 January 31

ABSTRACT

We present an extensive and up-to-date catalog of Galactic β Cephei stars. This catalog is intended to give a comprehensive overview of observational characteristics of all known β Cephei stars, covering information until 2004 June. Ninety-three stars could be confirmed to be β Cephei stars. We use data from more than 250 papers published over the last nearly 100 years, and we provide over 45 notes on individual stars. For some stars we reanalyzed published data or conducted our own analyses. Sixty-one stars were rejected from the final β Cephei list, and 77 stars are suspected to be β Cephei stars. A list of critically selected pulsation frequencies for confirmed β Cephei stars is also presented.

We analyze the β Cephei stars as a group, such as the distributions of their spectral types, projected rotational velocities, radial velocities, pulsation periods, and Galactic coordinates. We confirm that the majority of the β Cephei stars are multiperiodic pulsators. We show that, besides two exceptions, the β Cephei stars with high pulsation amplitudes are slow rotators. Those higher amplitude stars have angular rotational velocities in the same range as the high-amplitude δ Scuti stars ($P_{\rm rot} \gtrsim 3$ days).

We construct a theoretical HR diagram that suggests that almost all 93 β Cephei stars are main-sequence objects. We discuss the observational boundaries of β Cephei pulsation and the physical parameters of the stars. We corroborate that the excited pulsation modes are near to the radial fundamental mode in frequency and we show that the mass distribution of the stars peaks at 12 $M_\odot$. We point out that the theoretical instability strip of the β Cephei stars is filled neither at the cool nor at the hot end and attempt to explain this observation.

Subject headings: Hertzsprung-Russell diagram — stars: early-type — stars: fundamental parameters — stars: interiors — stars: oscillations — stars: variables: other

Online material: color figure, machine-readable tables

1. INTRODUCTION

The past decade has seen many profound advances in our understanding of β Cephei stars. The discovery of the κ-mechanism driving the pulsation of these stars (Moskalik & Dziembowski 1992; Dziembowski & Pamyatnykh 1993) and the organization of many high-profile observing campaigns can be seen as recent highlights, and research into the physical properties of the β Cephei stars has flourished in response. The number of known β Cephei pulsators increases constantly, and recent years have seen us make several improvements to the way in which we discriminate between the many types of variable B-type stars. The exact definition of β Cephei stars has itself been strongly debated over the years, and there is a good deal of ambiguity in most definitions. The recent advances in our understanding of β Cepheids demand that a new refined definition be developed and that a new β Cepheid catalog be constructed and refined in line with this, examining and reclassifying all stars that have been previously identified or proposed as β Cephei stars.

In recent years, two reviews on β Cephei stars were published, describing the known group members from photometric and spectroscopic viewpoints, respectively. Sterken & Jerzykiewicz (1993) published a review of all then-known β Cephei stars including an extensive observational review of their astrophysical properties, and providing constraints on many of their key parameters. At the time, 59 β Cephei stars had been identified. The following decade saw the identification of more than 40 new variables of this kind, bringing the total to almost 100, although the exact population has not been cataloged since the original 1993 review. In response to these new identifications, a complementary review paper was published investigating the spectral properties of bright β Cephei stars that had detectable line profile variations (Aerts & De Cat 2003). Twenty-six objects could be examined in this way, allowing a better description of their physical properties and summarizing their pulsational behavior.

An excellent overview over β Cephei and Slowly Pulsating B stars for which Geneva photometry is available is given by De Cat (2002) in the form of an online catalog.[2] It provides the values of the Geneva indices as well as an homogeneous determination of stellar parameters based on calibrations of the Geneva system. This extensive compilation was one of the starting points for the present catalog.

Recent work has even demonstrated the presence of β Cephei stars outside our own Galaxy (Pigulski & Kołaczkowski 2002; Kołaczkowski et al. 2004b) providing data for investigating this type of pulsation in objects of different metallicity (see § 4).

[1] Erwin Schrödinger Rückkehrer fellow, Fonds zur Förderung der Wissenschaftlichen Forschung, project R12-N02.

[2] See http://www.ster.kuleuven.ac.be/~peter/Bstars/.

All of these achievements originated from ground-based observations. Today, at the dawn of the 21st century, asteroseismologists are preparing to investigate variable stars from space, which will lead to the detection of many more excited pulsation modes in these stars. The first step in this direction was taken rather accidentally with the star camera of the *WIRE* satellite (Buzasi et al. 2000) after the failure of its primary science instrument. The first dedicated asteroseismology satellite, Canada's *MOST* (Matthews et al. 2000; Walker et al. 2003), was launched successfully in 2003 June and is returning valuable data on variable stars. Several other satellites investigating stellar pulsation will soon follow.

In this paper, we attempt to refine our understanding of β Cephei stars by cataloging the physical and pulsation properties of the entire confirmed population. This provides a comprehensive observational framework within which newly detected short-period pulsating stars can be classified. It will also be an aid for the classification of the vast amount of new pulsating stars that will be discovered in the near future. Using this observational framework, we reevaluate the membership of every object that was once classified as, or suspected to be, a β Cephei star.

Section 2 of this paper provides a brief description of the historical classification of β Cephei stars including information on asteroseismic space missions. In § 3 we describe different groups of variable stars of spectral type B, from which we derive our working definition of β Cephei stars. Section 4 lists the properties that have been examined for each of the stars in the catalog, explaining our reasoning behind their use. Section 5 provides detailed analyses of the entire data set from which we construct the observational framework, which in turn is later used to aid the identification of β Cephei stars.

In § 6 we discuss the observational boundaries of β Cephei pulsation. The conclusions and a definition of the β Cephei stars are presented in § 7. Tables of confirmed, candidate, and rejected β Cephei stars can be found in § 8 together with supplementary information on many of the objects. There we also give lists of pulsational frequencies for all confirmed β Cephei stars.

2. A BRIEF ASTROPHYSICAL HISTORY OF β CEPHEI STARS

The β Cephei pulsators have been known to the astronomy community for more than 100 years. The variability of the prototype of this class of variable stars, β Cephei, was discovered by Frost (1902). A spectral analysis led him to the conclusion that this star "is one of the Orion type . . . , of which group the typical star is β Canis Majoris." As a result, he named this group of stars the β Canis Majoris stars. At that time, the period of β Cephei could not be determined with certainty. Some years later, the first radial velocity curve for this star was published by Frost (1906). Guthnick (1913) discovered light variations of β Cephei with the same period as the radial velocity variations, and it was also noted that the amplitude of the latter was not constant (e.g., Henroteau 1918). The correct interpretation for this phenomenon was found by Ledoux (1951), who suggested that nonradial pulsations are present in some β Canis Majoris stars.

This group of stars comprised a rather wide range of variable B type stars and for many decades, at least up until the 1980s, these stars were known as β Canis Majoris or β Cephei stars. This redundant naming appears to have caused confusion among some authors. In, e.g., the *Hipparcos* catalog (ESA 1997), several stars are claimed to be classified as β Cephei stars for the first time, but were actually already classified as such under their previous name of β Canis Majoris stars.

Smith (1977) discovered that some of these β Canis Majoris stars were spectroscopic variables, and he called them the 53 Per stars. The term Slowly Pulsating B (SPB) stars was introduced by Waelkens (1991) for photometric B type variables pulsating in high radial order g-modes (gravity modes) with periods in the order of days. The 53 Per and SPB stars contain stars that are pulsating with periods longer than the fundamental radial mode and both groups have several members in common. The separation between β Cephei and SPB stars is a logical one based upon the physical fact that the first group pulsates mainly in p-modes (acoustic modes) of low radial order and the second in g-modes of high radial order. This implies that their pulsational driving mechanisms operate in zones of different thermal timescale. The β Cephei stars usually have one or more periods similar to that of the fundamental radial mode or the first nonradial p-mode (Lesh & Aizenman 1978).

In their extensive review paper, Lesh & Aizenman (1978) defined the class of β Cephei stars for the first time: "*These stars have the same short period for their light variation and radial velocity variation.*"

The pulsational driving mechanism for the β Cephei stars was unknown for a long time. After a revision of the metal opacities (Iglesias et al. 1987), Moskalik & Dziembowski (1992) were able to compute models for β Cephei stars in which the fundamental radial mode became pulsationally unstable for metallicities $Z > 0.03$. They found that the size of the theoretical instability strip for these stars depends on the abundance of heavy elements and that the pulsation mechanism prefers low-frequency oscillations. Only modes with a pulsation constant $Q > 0.032$ became unstable in these models. Furthermore, Moskalik & Dziembowski (1992) found that the theoretical instability region is larger than the β Cephei region in the HRD and that the same pulsation mechanism could be present in luminous blue variables (LBVs). Ninety years after the first discovery of the pulsation of β Cephei, models could be calculated where β Cephei type pulsation was driven.

Refined computations by Dziembowski & Pamyatnykh (1993) and Gautschy & Saio (1993) showed that pulsational instability could be reached for models with $Z > 0.02$. Instability was no longer restricted to the fundamental mode, but overtones were predicted to be pulsationally unstable as well. The current theoretical knowledge on the driving of β Cephei pulsations has been summarized by Pamyatnykh (1999).

Many β Cephei stars have been discovered to oscillate in several different pulsation modes (e.g., see Jerzykiewicz 1978). This opens the possibility to explore the interior structure of these stars by using asteroseismology, i.e., deciphering their pulsational mode spectra and modeling them theoretically. Examples can be found in, e.g., Dziembowski & Jerzykiewicz (1996, 1999). Indeed, Aerts et al. (2003) were able to understand the pulsational mode spectrum of the β Cephei V836 Cen and to perform a first seismic analysis of the star. A recent multisite, multitechnique campaign for another β Cephei star, ν Eridani (Handler et al. 2004; Aerts et al. 2004a) enabled seismic modeling as well (Pamyatnykh et al. 2004; Ausseloos et al. 2004).

The success of asteroseismic studies crucially depends on the detection and identification of as many modes of pulsation of the star under consideration as possible. Consequently, excellent measurement accuracy must be reached, which is best done from space.

MOST (*Microvariability and Oscillations of Stars*; Walker et al. 2003) is Canada's first space telescope and the very first dedicated asteroseismology satellite delivering data. It will be followed by *COROT* (Baglin 2003), a French-led European mission with the goal to perform asteroseismic observations as well as to detect exoplanets transiting a parent star.

All these developments in recent years led the authors of this work to the conclusion that it is time for an updated, homogeneous catalog of β Cephei stars. This is not only useful for the target selection process for the upcoming space missions, but also important for the understanding of this group of pulsating stars as a whole.

3. B-TYPE VARIABLES, DEFINITION AND SELECTION OF THE β CEPHEI STARS

As already mentioned, the β Cephei pulsators are generally considered to be early-type B stars (B0–B2.5) with light and radial velocity variations on timescales of several hours. As they are not the only variables of spectral type B, it is important to delineate what separates them from other variables. For instance, the SPB stars are later type B stars (B2–B9) with light, radial velocity, and line profile variability with periods of the order of a few days (De Cat & Aerts 2002).

The Be stars are defined as nonsupergiant B stars having shown Balmer line emission at least once (Collins 1987). They span the whole β Cephei and SPB instability regions and stretch from late O-type to early A-type stars. The hotter Be stars of spectral types B6e and earlier can show light, radial velocity, and line profile variations. Be stars that vary periodically (see Rivinius et al. 2003) are sometimes also called λ Eri stars. Some Be stars can also show additional β Cephei pulsations (see the discussion below).

ζ Ophiuchi stars are OB-type variables that show bumps moving through their line profiles, which may be caused by high-degree nonradial pulsation (Balona & Dziembowski 1999).

Some of the S Doradus stars or LBVs (see, e.g., van Genderen 2001), also have spectral types of or near B.

The chemically peculiar Bp stars can also show light and line profile variations (see, e.g., Briquet et al. 2004), and ellipsoidal variables may be present amongst variable B-type stars as well.

Two rather recently discovered classes of pulsating B stars are the short-period subdwarf B variables (sdBVs), also known as EC 14026 stars (Kilkenny et al. 1997), and the long-period sdBV stars (Green et al. 2003). The periods of the short-period sdBVs range between 2 and 9 minutes, and those of the long-period sdBVs are around 1 hr. Finally, the pulsating DB white dwarf stars also need to be mentioned.

Consequently, it is not easy to classify variable B-type stars correctly, in particular as some overlap between the different groups of variable stars occurs. For instance, β Cephei itself is also a Be and a Bp star (see Hadrava & Harmanec 1996 for a summary).

We therefore suggest the following definition of the β Cephei variables: *The β Cephei stars are massive nonsupergiant variable stars with spectral type O or B whose light, radial velocity and/or line profile variations are caused by low-order pressure and gravity mode pulsations.*

Our choice of this definition was motivated by several reasons. In our view, the main feature on which the classification of a pulsating star is based should be its pulsational behavior. For instance, any class of pulsating stars should be known to be driven by the same self-excitation mechanism, and their pulsational timescales should be different and separable from those of other types of pulsators. Of course, a particular locus in the HR diagram could also assist, and sometimes be incorporated, in the definition of a class of pulsating star.

Since the observational extent of the instability strip of the β Cephei stars may still not be accurately known (cf. § 6), we did not want to limit our definition to a narrow range of spectral types. In addition, we do not take the existence of radial pulsation to be a prerequisite for an object to be classified as a β Cephei star, because this would require a firm observational mode identification, which is in most cases not available. By dropping this criterion that has sometimes been used in the past, we make the pulsation constant our main criterion for classification. We also take into consideration that many β Cephei stars have been shown to pulsate both in radial and nonradial modes, or any subset of these.

To apply our definition to the stars under consideration, we must link it to observables. Consequently, we consider an object to be consistent with our definition of a β Cephei star in practice, if it shows convincing evidence for more than one variability period too short to be consistent with rotational or binarity effects, as checked by estimating the pulsation "constant" Q. Stars with only a single period were accepted if proof of the pulsational nature of the variations was found, such as color or radial velocity to light amplitude ratios typical of pulsation or variability (with, again, the period too short to be accounted for by other effects) present in more than one observable.

4. DESCRIPTION OF THE CATALOG

We list all objects that have to our knowledge ever been claimed to be β Cephei stars or candidates up to 2004 June. We selected them by an extensive search in the literature and in databases (such as SIMBAD), with the aim that we could collect all possible candidates. For all of them, thorough bibliographic studies were performed to investigate the latest findings on their nature. Where the data in the literature were insufficient or inconclusive, we reanalyzed some of the measurements or reevaluated the available information on these stars. We also performed frequency analyses of the *Hipparcos* photometry (ESA 1997) whenever possible to assist with the classification of the variables. We note that because of aliasing problems in the *Hipparcos* data we did not attempt to determine individual periods but mainly used them to check the timescales of the observed variability. Owing to the particular variability timescales involved, aliasing was therefore not a problem for our purposes.

The SIMBAD database initially prompted us with 128 β Cephei stars. Their classification often originated from the General Catalogue of Variable Stars (Kukarkin et al. 1971) and subsequent name lists. We could confirm 66 of these and placed the others either on a list of candidate or rejected β Cephei stars. The other objects in this catalog were selected from our literature searches.

We then scrutinized the literature on all these stars and checked whether they were consistent with our working definition of a β Cephei star. We designate objects that have been claimed as β Cephei stars, but where the observational evidence for their membership to the group is not fully conclusive owing to, e.g., poor or few data, as *candidate β Cephei stars*. Some of these objects will indeed be β Cephei pulsators, whereas others were added to this list because of the lack of evidence that they are not. In any case, all of these objects deserve more observational attention.

Stars that were claimed to be β Cephei variables, but where we found evidence that they are not, are called *rejected β Cephei candidates*. These are objects with variability timescales inconsistent with low-order p- or g-mode pulsation, objects whose claimed variability was disproved by subsequent or more extensive studies, or stars proven to vary because of effects other than β Cephei pulsation, etc. This list also includes stars that were rejected by other authors in order to give a complete overview over all stars that at some point had been considered to be β Cephei stars. We have also scrutinized the list of ζ Oph stars by Balona & Dziembowski (1999) as several of these variables have observed periods in the β Cephei range. We found that the periods *in the corotating frame* are consistent with β Cephei pulsation for only three stars, which we include in this catalog.

The importance of Tables 2 and 3 is, besides their relevance for the description of the β Cephei stars as a group, that they provide completeness of the catalog and that it can be traced how the less convincing candidates were judged by us.

We have not included β Cephei stars or candidates outside our Galaxy into this catalog because detailed lists of the objects reported by Kołaczkowski et al. (2004b) have not yet been published. For reasons of consistency we thus also exclude the LMC β Cephei candidates by Pigulski & Kołaczkowski (2002) and Sterken & Jerzykiewicz (1988).

In Table 1 we present the complete list of Galactic β Cephei stars. Table 2 contains the candidate β Cephei stars, and Table 3 lists the former candidates that are not considered β Cephei stars. In the following, we describe the contents of Table 1. Tables 2 and 3 only contain part of this information.

1. *Identifiers*.—The first five columns of the catalog contain the identifiers of the stars, HD number, HR number or cluster identification, *Hipparcos* numbers, and Durchmusterung (DM) numbers. As DM number for the Southern stars we used the Cordoba Durchmusterung (CD) numbers, not the Cape Photometric (CpD) numbers! Some objects do have CpD numbers, and no CD numbers, such as V1032 Sco.

The sixth column lists different names given to these stars, such as Bayer or Flamsteed numbers, or variable designations according to the General Catalogue of Variable Stars.

2. *Coordinates*.—Right ascension and declination (cols. [7] and [8]) are given with epoch 2000. If inaccurate coordinates were found in the databases, we used a finder chart and matched it to the Digital Sky Survey plates, thereby determining the coordinates to a precision of $\sim 2''$.

3. *Pulsation period*.—The period of pulsation is given in days in column (9). If a star is multiperiodic, the period of the pulsation mode with the highest amplitude is given and an asterisk (*) next to the period indicates the multiperiodicity. We apply the term "monoperiodic" to stars for which only one pulsation frequency was found *up to the current detection limit*. If pulsation was detected photometrically and spectroscopically, we give the photometrically determined period.

4. *Amplitude*.—It is difficult to specify a unique amplitude of a frequency for a variable star measured in different photometric passbands and/or in radial velocity. This applies in particular for the cases of multiperiodicity and amplitude variability. Therefore, we chose the following approach: for all stars with a resolved pulsation spectrum, we list photometric peak-to-peak amplitudes of the strongest pulsation mode. If a star shows amplitude variability caused by beating of unresolved frequencies, we adopt the average peak-to-peak amplitude, and in case of mild amplitude variability of individual modes we adopt the average peak-to-peak amplitude of the strongest mode. For the two stars with the strongest amplitude variations (Spica and 16 Lac) we list no amplitudes. Finally, no amplitude is given for the three stars where only spectroscopic variability was detected. This is denoted as "n/a" in the amplitude column.

We list Johnson V amplitudes whenever possible. If data from this filter were not available, we used Strömgren y, Geneva V (denoted $V_{\rm G}$ in Table 1), or Walraven V (denoted $V_{\rm W}$). In the latter case the logarithmic intensity amplitudes were multiplied by 2.5 to give magnitude units. All these filters have very similar effective wavelengths resulting in directly comparable amplitude values. Some stars have not been observed in these filters. In such cases we chose in order of decreasing preference Strömgren b, Johnson/Cousins R, Johnson B, and Cousins I. The use of data obtained in different filters was only applicable because the pulsation amplitudes of β Cephei stars are very similar in the wavelength range spanned by B to I.

5. *Apparent magnitude and spectral classification*.—The next two columns give the apparent magnitude in Johnson V and the spectral type according to the Morgan and Keenan system (MK). The V magnitudes are taken from The General Catalog of Photometric Data (GCPD)[3] by Mermilliod et al. (1997). The spectral types are taken from the SIMBAD database.

6. *Rotational and radial velocities*.—The projected rotational velocity ($v \sin i$) is given in the next column. If disagreements between different values in the literature were detected, either the more reliable source is quoted here or, if no distinction in quality of the data could be made, the lower value is given. Concerning the radial velocity (RV), the best or mean values are quoted, in an attempt to average out the RV variations over the pulsation cycle. The values for $v \sin i$ and RV are taken from various catalogs of radial velocities, or in some cases from original publications.

7. *Color indices from Strömgren photometry*.—Columns (13)–(16) the Strömgren color indices $(b-y)$, m_1, c_1, and β. These data were obtained from the GCPD. These indices are used in preference to the Geneva colors, which are available for roughly the same number of stars. The Strömgren filters are more widely available and according to our experience, the combination of measurement accuracy and its conversion to theoretical parameters such as effective temperature and surface gravity via calibrations of color photometry favors Strömgren photometry in terms of achieving better accuracy in the derived basic stellar parameters. In addition, only the c_1 index may show some variation over the pulsation cycle of a β Cephei star. We therefore find that the color indices we list are good representations of the mean colors of a star through its pulsation cycle.

For a detailed list of Geneva colors for many β Cephei stars we refer to De Cat (2002; see also footnote 2).

8. *References and notes*.—Numerical references are listed below each table. Short individual notes to several stars can be found in the table, whereas longer discussions of some objects are given in § 8. As references, we list selected papers that are directly related to the stellar pulsations or those which give useful additional information. These would typically be discovery papers, those that reported most about the pulsations, or did further analyses such as mode identifications. We give no more than six references per star.

4.1. *Table of Frequencies*

In Table 4 we present a list of frequencies for the stars from Table 1. We refrain from listing all the claimed frequencies for all stars because the data are qualitatively inhomogeneous and some sources may not be reliable. The choice of frequencies listed originates from critical evaluations of literature data.

[3] See http://obswww.unige.ch/gcpd/gcpd.html.

We consider a photometrically detected frequency as also spectroscopically detected if the variation is present and clearly recognizable in radial velocity analyses or line profile variations, but do not insist on detections in both of these spectroscopic observables.

For several stars, some frequencies reached detectable amplitudes only during some observations. We list all frequencies ever detected from analyses that convinced us.

5. ANALYSIS

5.1. *Basic Observational Quantities*

In this section we present analyses performed on the intrinsic 93 β Cephei variables. We analyze the distribution of spectral type (see Fig. 1), radial velocity (RV), projected rotational velocity ($v \sin i$), apparent brightness in Johnson V and pulsation period (P) (see Fig. 2). In addition, we examine the Galactic distribution (see Fig. 3) as well as the dependence of the pulsational amplitudes on the projected rotational velocities (see Fig. 4), and thereby describe the β Cephei stars as a group.

5.1.1. *Spectral Type and Luminosity Class*

The three-dimensional histogram in Figure 1, which is inspired by Figure 4 of Sterken & Jerzykiewicz (1993), shows the distribution of the confirmed 93 β Cephei stars according to their spectral type and luminosity class. It shows that ≈20% of the β Cephei stars appear to be B1 dwarfs. A total of 66% of the stars are of spectral type B1 and B2 and luminosity classes III–V. This distribution resembles very closely the spectral type range occupied by the confirmed β Cephei stars from Sterken & Jerzykiewicz (1993), where almost all stars lie within B0 and B2.5. Most of the class V variables are members of open clusters (80%). Two of the stars from Tab. 1 do not yet have a spectral type assigned (NGC 6910 27 and V2187 Cyg) and for 3 stars no luminosity class was associated to the spectral type (NGC 663 4, NGC 6910 16, and HN Aqr). As will be shown in § 5.2, the assignment of luminosity classes I–III to some of these stars must be erroneous.

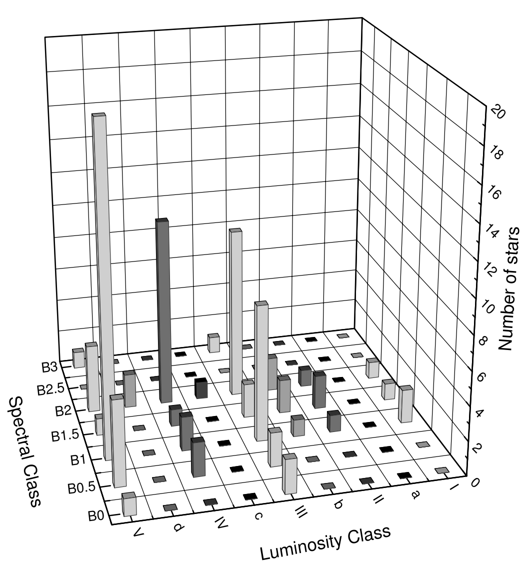

Fig. 1.—Distribution of stars according to spectral type and luminosity class. The letters a, b, c, and d correspond to the intermediate luminosity classes I–II, II–III, III–IV, and IV–V. [*See the electronic edition of the Supplement for a color version of this figure.*]

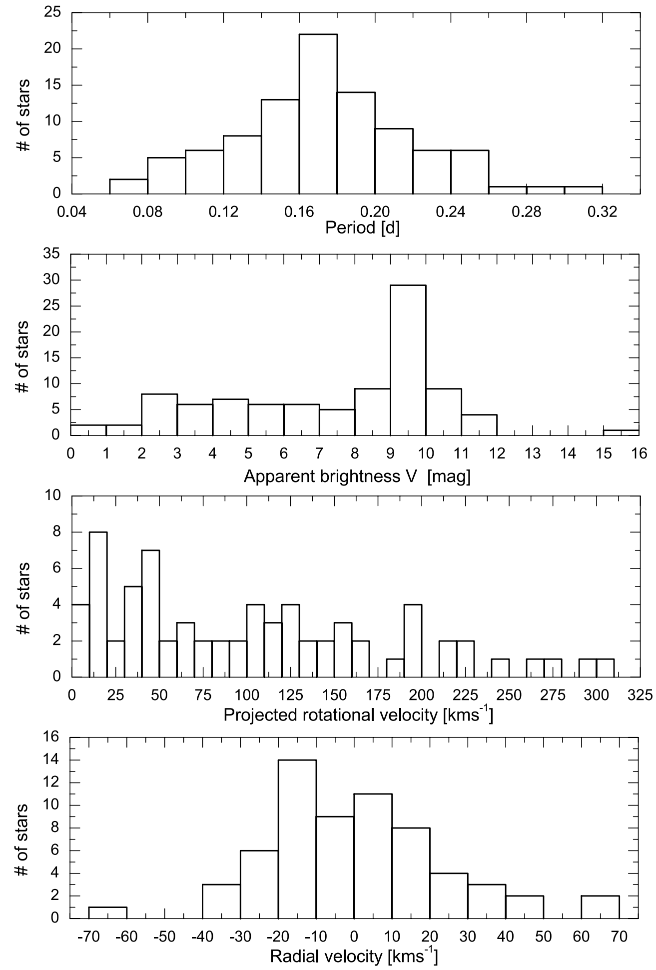

Fig. 2.—Histograms of radial velocity, projected rotational velocity, apparent magnitude, and pulsation period.

5.1.2. *Projected Rotational Velocity*

The range of projected rotational velocity, $v \sin i$, extends from 0 to 300 km s^{-1} with HD 165174 as the fastest rotator with 300 km s^{-1}, closely followed by NGC 4755 I with 296 km s^{-1}. HD 165174 is also a Be star, whereas NGC 4755 I went through

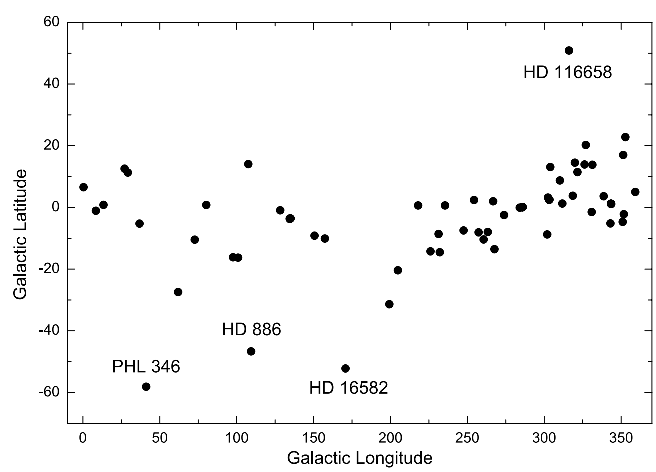

Fig. 3.—Distribution of stars according to Galactic longitude and latitude.

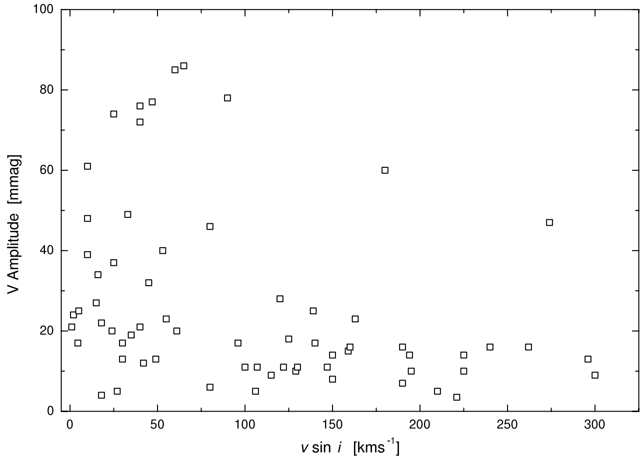

FIG. 4.—Photometric amplitudes of the β Cephei stars depending on their projected rotational velocity.

phases where its pulsations were clearly detectable, but at other times did not reach a detectable level. Most β Cephei stars seem to be rather slow rotators (average $v \sin i \sim 100$ km s^{-1}), although this could in part be due to a selection effect as the highest-amplitude pulsators are slowly rotating stars. Hence, their variability is more easily detectable and observable.

5.1.3. *Radial Velocity*

The radial velocities (RV) of the β Cephei stars, as seen in Figure 2 (*bottom*) appear to be centered around -10 km s^{-1} but stretch up to +65 km s^{-1}. This distribution is that of an average young galactic disk population, which is not surprising.

5.1.4. *Apparent Brightness*

The apparent brightness has a maximum at $V \sim 9.5$ mag with 31% of the stars; these are mostly cluster β Cephei stars. The range of apparent brightness is between 0.6 mag $< V <$ 15.4 mag, with β Cen, α Vir, β Cru, and λ Sco as brightest stars with V between 0.6 mag and 2.0 mag. The faintest stars with V of 11.9 mag and 15.4 mag are HN Aqr and V2187 Cyg, respectively. This information can be relevant for planning observational projects, and can be compared directly to Figure 3 of Rodríguez & Breger (2001).

5.1.5. *Pulsation Period*

The distribution of the pulsation periods has a peak at $\sim$0.17 day, corresponding to 4 hr. The shortest period is 0.0667 day for ω^1 Sco, the next shortest period is from Braes 929 with 0.0671 day. The two longest periods are 0.319 day for Oo 2299 and 0.2907 day for HD 165174.

Hence, we find that the observed range of periods for β Cephei stars is between 0.0667 and 0.319 day or 1.60 and 7.66 hr. The median of all periods is 0.171 day.

Three of the confirmed β Cephei stars show, so far, variability only in their line profiles. They are nevertheless included in the group of β Cephei stars because they exhibit the same basic behavior as the *classical* β Cephei stars. The lack of confirmation of their variability from photometric techniques is due to modes of high-degree ℓ in those stars, which are difficult to detect in photometric observations. We have only retained objects in Table 1 if their corotating variability period was consistent with β Cephei pulsation.

5.1.6. *Galactic Distribution*

The Galactic distribution of the confirmed β Cephei stars is shown in Figure 3. In agreement with the result from § 5.1.3, this again suggests a young disk population. The most interesting objects in this diagram are the "outliers," the only significant one being PHL 346, which may either have formed in the Galactic halo or could be a runaway star (Ramspeck et al. 2001).

5.1.7. *Pulsation Amplitude versus Rotation Rate and Pulsation Period versus Rotation Rate*

The dependence between pulsation amplitude and rotation rate is plotted in Figure 4. With the exception of HD 52918 and HD 203664, only stars with rotation velocities $v \sin i \leq 90$ km s^{-1} show pulsation amplitudes larger than $\sim$25 mmag. This is similar to the behavior of the δ Scuti stars (Breger 1982), and may also lend support to the hypothesis that rotation is an important factor in the amplitude limiting mechanism operating in these types of pulsators. In this context it is interesting to note that the range of the *angular* rotational velocities of high-amplitude δ Scuti stars is very similar to that of the β Cephei stars with the highest amplitudes. For a similar analysis based on the radial velocity pulsation amplitude we refer to Aerts & De Cat (2003).

We also examined the pulsation period versus rotation velocities $v \sin i$ and find that there is no dependence between these two quantities. This is also not a surprise as most of the known β Cephei stars are photometric variables and thus pulsate in modes of low spherical degree.

5.1.8. *Mono-versus Multiperiodicity*

As listed in Table 4, $\sim$40% of the confirmed β Cephei stars are monoperiodic. We suspect that several of these 37 stars may have additional pulsation periods that are undetected so far. On the other hand, our practical criteria to select β Cephei stars are likely to introduce a bias in favor of multiperiodic stars. In any case, it seems safe to say that most β Cephei stars are multiperiodic pulsators.

5.1.9. *Binarity*

Table 1 also contains information on binary β Cephei stars, which are indicated in the Notes column. Summarizing, we can say that there are eight spectroscopic binaries, four additional double-lined spectroscopic binaries, two suspected binaries, one eclipsing binary and one triple system. Thus, we find that $\approx$14% of all β Cephei stars are located in known multiple systems with physically associated companions.

A search for visual binaries in The Catalogue of Components of Double and Multiple Stars (Dommanget & Nys 2002) and the *Hipparcos* and Tycho Catalogs (ESA 1997) reveals that 16 stars of Table 1 are visual binaries. Five of these are already known to be spectroscopic binaries as well. Owing to these small numbers, we refrain from any statistical analysis. We also assume that several additional β Cephei stars will be proven to be spectroscopic binaries in the future.

5.2. *HR-Diagram, Masses, Pulsation Constants, and Period-Luminosity Relation*

To obtain more insight into the behavior of the β Cephei stars as a group, and for purposes of comparison with theoretical results, we have computed their temperatures and luminosities to place them in the HR diagram. To this end, we adopted the programs by Napiwotzki et al. (1993) (which can be used for B stars of all luminosity classes), using published Strömgren

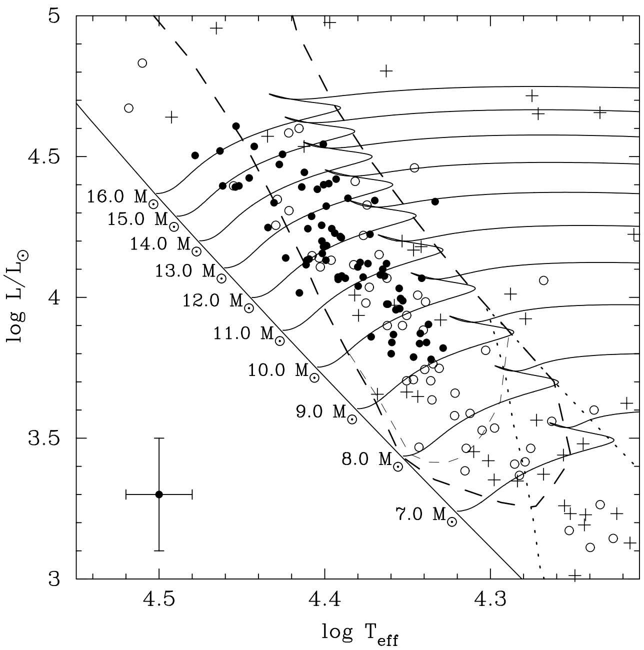

FIG. 5.—Theoretical HR diagram of the confirmed (*filled circles*) and candidate (*open circles*) β Cephei stars as well as the poor and rejected candidates (*plus signs*). The filled circles with the error bars in the lower left corner indicate the rms accuracy of each point in this diagram. The slanted solid line is the ZAMS, the thick dashed line describes the boundaries of the theoretical β Cephei instability strip for $Z = 0.02$, the thin dashed lines are the β Cephei boundaries for radial modes, and the dotted lines those of the SPB stars. Several stellar evolutionary tracks, labeled with their evolutionary masses, are also plotted. All the theoretical results were adopted from Pamyatnykh (1999).

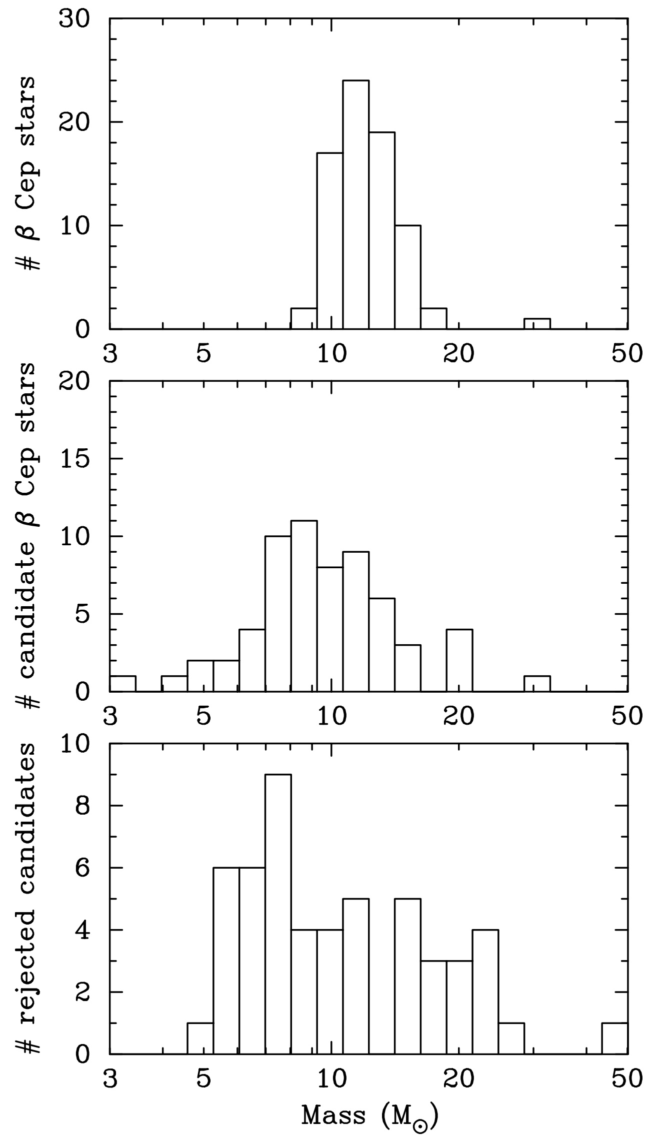

FIG. 6.—Distribution of the masses of the stars in Tables 1–3.

indices from the GCPD to derive $T_{\rm eff}$ via the calibration by Moon & Dworetsky (1985) and M_v from Balona & Shobbrook (1984). We did not use *Hipparcos* parallaxes, as accurate results are only available for a few stars and as we wanted to treat the whole sample homogeneously. We then determined bolometric corrections from the work by Flower (1996). The theoretical HR diagram constructed with these results is shown in Figure 5. The error estimates are ± 0.020 in $T_{\rm eff}$ and ± 0.20 in log L, which are hoped to include external uncertainties in the applied calibrations themselves.

We have also plotted the candidate β Cephei stars (Table 2) and the rejected candidates (Table 3) in this diagram for comparison. We compared the positions of the stars in Figure 5 with evolutionary tracks, which we computed with the Warsaw-New Jersey stellar evolution code (see, e.g., Pamyatnykh et al. 1998). This way we estimated the masses of these objects and we could consequently also compute the pulsation "constant" Q. The pulsation constant was derived from the period with the highest amplitude value. Given the uncertainties in our determinations of $T_{\rm eff}$ and L, we estimate an uncertainty of ± 30% in Q. The errors on $T_{\rm eff}$ and L should dominate the error introduced by not being able to use the frequencies in the corotating frame for most stars. This inability is due to missing mode identifications.

We adopted the theoretical boundaries of the β Cephei instability strip from the work by Pamyatnykh (1999). We prefer his results over those by Deng & Xiong (2001) because he applied newer versions of opacity tables and more reliable interpolation routines. The differences between these two approaches are discussed by Pamyatnykh (2002) in detail.

The confirmed β Cephei stars occupy a well-defined region in this plot with the exception of HD 165174, which appears to be so hot and luminous that it falls outside the boundaries of Figure 5. In contrast, the candidates and rejected stars are widely scattered. We note that the theoretically predicted instability strip is not completely filled with stars, a well-known problem that we will discuss in the next section.

In addition, a gap between the coolest β Cephei stars at a given mass and the theoretical TAMS may be suspected. It is unclear whether this is a real feature or whether the derived absolute magnitudes from the Strömgren indices could be biased. Heynderickx et al. (1994) discussed this problem in detail. In any case, it is reasonable to conclude that all known β Cephei stars are main-sequence objects. Consequently, the assignment of luminosity classes I–III to several confirmed β Cephei stars must be erroneous.

We can now also examine the mass distribution of the β Cephei stars and candidates (Fig. 6). The mass of the confirmed β Cephei stars peaks sharply at about 12 $M_\odot$. Whereas there is a slight indication for a similar maximum for the candidate β Cephei stars, the histogram of the masses of the rejected stars is featureless.

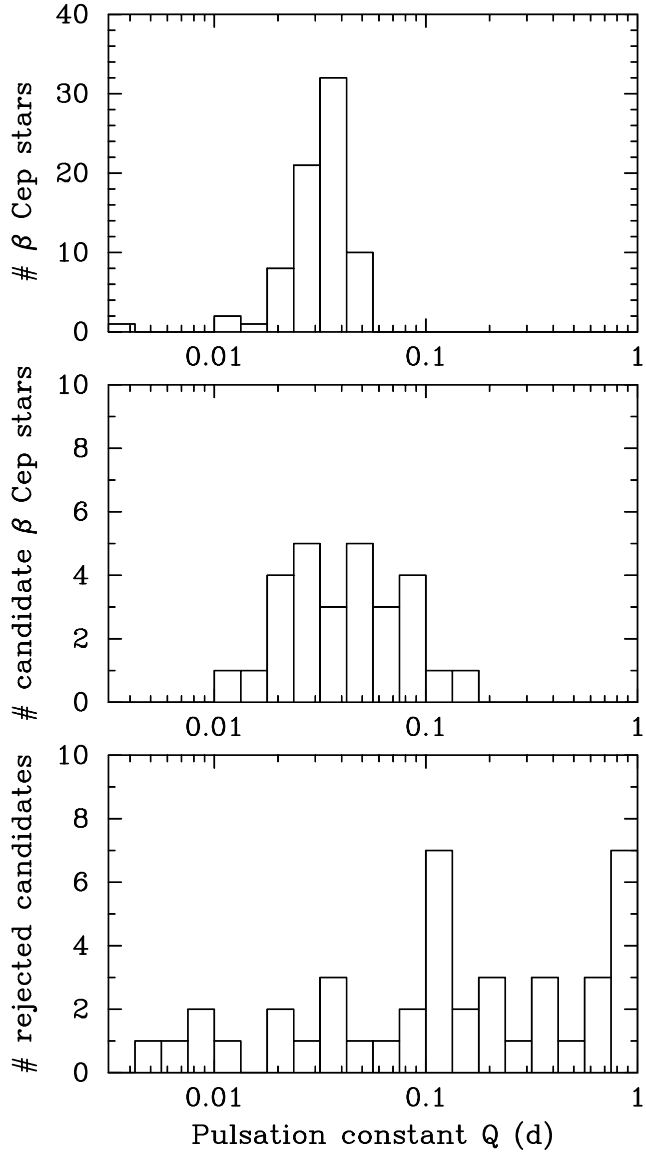

FIG. 7.—Distribution of the pulsation constant Q of the stars in Tables 1–3.

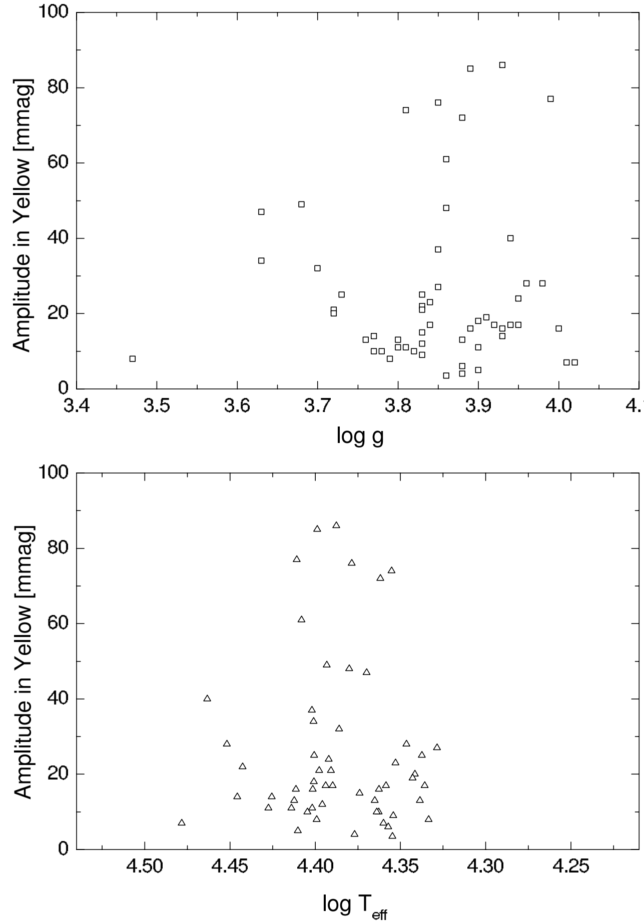

FIG. 8.—*Upper panel*: log g vs. amplitude. *Lower panel*: log $T_{\rm eff}$ vs. amplitude. The x-axis here shows the same scale as the x-axis in Fig. 5. The amplitudes in Johnson V and Strömgren y are shown for all stars where Strömgren indices were available. The amplitudes of the strongest modes are shown here as listed in Table 4.

Turning to the pulsation constant (Fig. 7), we again see a sharp peak for the confirmed β Cephei stars located at $Q = 0.033$ day, corresponding to the value for radial fundamental mode pulsation. More than half of the candidate β Cephei stars have Q-values in the same range, although there is a tail toward higher Q. We remind that several stars were classified as candidate β Cephei stars because of the lack of evidence that they are *not* pulsators. The histogram of Q of the rejected candidates shows no particular preferences. It is clear that Q-values for nonpulsating stars have no real relevance, but our aim here is to check whether our separation of the candidates in the three groups was successful. Comparing the different panels within Figure 6 and Figure 7, respectively, implies that the choice of our selection criteria is justified.

6. THE OBSERVATIONAL BOUNDARIES OF β CEPHEI PULSATION

As mentioned in §§ 2 and 5.2, several authors computed the instability region for β Cephei stars. Linear nonadiabatic analyses for low-degree ($\ell \leq 2$) modes predict that photometrically observable modes are also driven in slightly evolved O-type stars (e.g., Dziembowski & Pamyatnykh 1993), suggesting that there could be a population of late O-type β Cephei stars.

In 1998, the central region of the Cygnus OB2 association was investigated in search of short-period hot pulsators (Pigulski & Kołaczkowski 1998). No β Cephei type stars were found among the O-type variables. So far, only one O-type star, HD 34656 (O7e III) has been suggested to exhibit pulsations in the β Cephei domain (Fullerton et al. 1991). Pulsation was claimed from radial velocity measurements; the given period of 8.81 hr is a little above the typical range of pulsation periods for these stars. The authors were reluctant to identify this star as a β Cephei star. In addition, we are unsure whether the reported radial velocity variations of the star are statistically significant. Therefore, we cannot accept this O-star as a confirmed β Cephei star and place it therefore in Table 2.

There have been several similar attempts to discover O-type β Cephei pulsators observationally (e.g., Balona 1992). However, to date no convincing detections were made, and, with the exception of the Be star HD 165174, there is consequently an apparently well-defined high-mass edge to the population in the resulting HR-diagram (Fig. 5).

From Figure 5 we see that the blue edge is a cutoff for stars more luminous than log $L_{\odot} = 4.6$ and hotter than log $T_{\rm eff} = 4.48$. This result can be compared directly with Figure 8, where we show the pulsation amplitudes versus log g and log $T_{\rm eff}$ (*upper and lower panel*, respectively). In the lower panel we see that the highest pulsation amplitudes occur in the middle of the instability region, as is expected because of the strong dependence of the κ-mechanism on temperature and hence on the depth of the ionization layer in which it operates. This diagram also suggests that O-type β Cephei stars could exist, but that their pulsation amplitudes are small and therefore not yet detectable. Space missions could enable us to detect such pulsators.

There could be many reasons for the lack of observed O-type β Cephei stars, as mentioned above. The theoretical models may not necessarily predict the real behavior of the stars, as some physics may be missing from the models. For example, the linear approach taken in the calculation of pulsation instability may not realistically reflect the complex physical processes in real stars, such as the onset of strong stellar winds. As mentioned before, it is also possible that O-type β Cephei stars do exist, but with amplitudes below the current detection limits. In combination, these factors could prohibit the detection of O-type β Cephei stars (see also Pigulski & Kołaczkowski 1998).

In a recent publication, Tian et al. (2003) analyze a sample of 49 presumable β Cephei stars and show a HRD together with theoretical boundaries for the instability region computed by Deng & Xiong (2001). Their computations also include a boundary at the high-mass end of the instability region, which stands in contrast to the theoretical work of Pamyatnykh (1999) (see above). We compared their list of stars with our results and find that 27 of those stars are in our list of confirmed β Cephei stars, 6 are classified as candidates and the remaining 16 are in the list of rejected stars. When we compare their HRD with Figure 5, we see that the boundaries adopted by Tian et al. (2003) encompass all stars from Table 1. Therefore, from an empirical point of view, both instability regions by Pamyatnykh (1999) and Deng & Xiong (2001) fit our sample equally well.

The theoretical β Cephei instability strip is also not filled at the low-mass (red) end. As the theoretical results seem to be more reliable in this part of the HR diagram, the only explanation we have for this finding is again that the pulsational amplitudes are too small to be detected by current methods. We base this argument on analogy with the δ Scuti stars, whose pulsations are of the same nature (low-order p- and g-modes driven by the κ-mechanism) as those of the β Cephei stars, and whose number increases strongly with better detection levels (see, e.g., Breger 1979, Fig. 3). Support for this suggestion comes from intensive observations of individual β Cephei stars (see, e.g., Handler et al. 2003; Jerzykiewicz et al. 2005), for which more and more pulsation modes were detected with decreasing detection threshold.

We note that the low-mass boundary of the theoretical instability strip in Figure 5 for radial modes agrees better with the observations, but it is still too cool to be explained by errors in the temperature calibrations of the observed stars.

The empirical determination of the edges of the instability region is a very interesting challenge in the field of β Cephei stars. New surveys of the late O-type stars and early to mid B-type stars would therefore be of considerable astrophysical interest.

7. CONCLUSIONS

Of the 231 stars under consideration, 93 were confirmed as β Cephei type variable stars (Table 1). Their spectral types range from B0 to B3 with one exception, NGC 663 4, whose spectral type of B5 does not appear to be reliable. The periods of the strongest pulsation modes range from $P = 0.0667$ to 0.319 day or 1.6 to 7.7 hr with a median of 0.171 day. Projected rotational velocities $v \sin i$ range from 0 to 300 km s^{-1}, with a typical value of around 100 km s^{-1}. This suggests that β Cephei stars are rather slow rotators, although this result could be affected by a bias in detecting possible low-amplitude modes occurring in rapidly rotating stars. We expect more detections of β Cephei stars concerning lower amplitude, higher $v \sin i$ stars with space observations in the near future. The Galactic distribution of these stars does not yield evidence for a pulsator that has formed at high Galactic latitude.

There are 77 stars for which no clear classification could be made as a result of limited or conflicting data. These are listed in Table 2 as suspected β Cephei type variable stars; they deserve further attention. Additional notes are provided on interesting characteristics of 19 of these stars. Many of these stars seem good β Cephei candidates and it was often only the lack of recent data that forced us to put them in the list of candidate β Cephei stars.

Despite their previous classification as β Cephei type variables or candidates, 61 of the stars could not be considered as such (Table 3). In some cases authors were overconfident in classifying them as β Cephei stars. In other cases, later measurements have shown that they are either a different kind of variable, or that their variability is no longer detectable, casting doubt on the original observations. Some misclassifications are also due to historical reasons since, during the early days of work on β Cephei stars, the group was not as well known as it is today.

The pulsation constant Q calculated for all confirmed β Cephei stars lies below $Q = 0.06$ day with a peak at $Q = 0.033$ day. The Q-value encompasses many physical parameters, and its use as an observational constraint to classify this group of variable stars is therefore considered more accurate than previous classification techniques. These techniques often relied more heavily on limited information such as spectral type classification and pulsation period. This upper limit of $Q = 0.06$ day can provide an additional observational constraint for the classification of β Cephei stars, keeping the uncertainties in the determination of Q in mind.

The theoretical instability region for the β Cephei stars, as calculated by Pamyatnykh (1999), is not populated at both the low-mass/red end and the blue end. The lack of stars at the blue end, where one would expect late O-type stars, is expected (e.g., Balona 1992; Pigulski & Kołaczkowski 1998). We emphasize that this gap could be due to limitations in the theoretical modeling of the instability region, as well as to the difficulties inherent to observing hot stars exhibiting strong stellar winds and to possible pulsation amplitudes too low to be detected with past and present methods.

It is hoped that our new and refined catalog provides a useful framework within which to plan future observing campaigns, both ground-based and using the upcoming spaceborne observatories. The table of suspected β Cephei variables provides a list of 77 interesting candidates that require further investigation. In addition, the catalog provides improved constraints on the classification and physical nature of β Cephei variables, and these can in turn be used to correctly classify new early-type short-period variable stars.

8. TABLES

In Table 1 we present all confirmed β Cephei stars. In Table 2 we list candidate β Cephei stars and in Table 3 we give rejected β Cephei candidates. At the end of each table we give notes on individual stars as well as short explanations on interesting characteristics of some stars. Table 4 contains a list of pulsation frequencies for all stars from Table 1.

TABLE 1
Catalog of Galactic β Cephei Stars

HD (1)	*Hipparcos* (2)	Name (3)	HR/Cluster (4)	BD/CD (5)	Other Name (6)	R.A. (J2000) (7)	Decl. (J2000) (8)	Period (days) (9)	V (mag) (10)	Spectral Type (11)
886..............	1067	γ Peg	39	+14 14	Algenib	00 13 14	+15 11 00	0.1518	2.8	B2 IV
				+60 282	V909 Cas	01 36 39	+61 25 54	0.207	10.5	B1 III
			NGC 663 4			01 46 39	+61 14 06	0.194	11.0	B5
		Oo 692	NGC 869 692	+56 501	V611 Per	02 18 30	+57 09 03	0.1717	9.3	B0 V
			NGC 869 839	+56 508	V665 Per	02 18 48	+57 17 08	0.1949*	9.5	B2 V
		Oo 992	NGC 869 992	+56 520	V614 Per	02 19 00	+57 08 44	0.1326	9.9	B1 Vn
		Oo 2246	NGC 884 2246	+56 572		02 22 03	+57 08 26	0.1842*	9.9	B2 III
		Oo 2299	NGC 884 2299	+56 575	V595 Per	02 22 09	+57 08 28	0.319	9.1	B0.5 IV
16582...........	12387	δ Cet	779	−00 406	82 Cet	02 39 28	+00 19 42	0.1611	4.1	B2 IV
21803...........	16516	KP Per	1072	+44 734		03 32 38	+44 51 20	0.2018*	6.4	B2 IV
24760...........	18532	ϵ Per	1220	+39 895	45 Per	03 57 51	+40 00 36	0.1603*	2.9	B0.5 V
29248...........	21444	ν Eri	1463	−03 834	48 Eri	04 36 19	−03 21 08	0.1735*	3.9	B2 III
35411...........	25281	η Ori	1788	−02 1235	28 Ori	05 24 29	−02 23 50	0.13	3.2	B0.5 V
35715...........	25473	ψ^2 Ori	1811	+02 962	30 Ori	05 26 50	+03 05 44	0.0954*	4.6	B2 IV
44743...........	30324	β CMa	2294	−17 1467	Mirzam	06 22 41	−17 57 21	0.2513*	2.0	B1 II–III
46328...........	31125	ξ^1 CMa	2387	−23 3991	4 CMa	06 31 51	−23 25 06	0.2096	4.3	B1 III
50707...........	33092	EY CMa	2571	−20 1616	15 CMa	06 53 32	−20 13 27	0.1846*	4.8	B1 Ib
52918...........	33971	19 Mon	2648	−04 1788	V637 Mon	07 02 55	−04 14 21	0.1912*	4.9	B1 V
56014...........	34981	EW CMa	2745	−26 4057	27 CMa	07 14 15	−26 21 09	0.0919	4.7	B3 IIIe
59864...........	36500			−33 3879	V350 Pup	07 30 34	−34 05 26	0.238*	7.6	B1 III
61068...........	37036	PT Pup	2928	−19 1967		07 36 41	−19 42 08	0.1664*	5.7	B2 II
64365...........	38370	QU Pup	3078	−42 3610		07 51 40	−42 53 17	0.1678*	6.0	B2 IV
64722...........	38438		3088	−54 1966	V372 Car	07 52 29	−54 22 01	0.1034*	5.7	B1.5 IV
71913...........	41586	YZ Pyx		−34 4858		08 28 42	−34 43 53	0.2058	7.7	B1.5 II
78616...........	44790	KK Vel		−44 5150		09 07 42	−44 37 56	0.2157	6.8	B2 II–III
80383...........		IL Vel		−52 2955		09 17 31	−52 50 19	0.1832*	9.2	B2 III
90288...........				−56 3324	V433 Car	10 23 57	−57 27 52	0.1095*	8.2	B2 III–IV
303068.........			NGC 3293 11	−57 3329		10 34 48	−58 08 54	0.1458*	9.8	B1 V
303067.........			NGC 3293 10	−57 3340	V401 Car	10 35 30	−58 12 00	0.1684*	9.5	B1 V
			NGC 3293 16	−57 3344	V403 Car	10 35 41	−58 12 45	0.2506	8.7	B1 IV
			NGC 3293 65		V412 Car	10 35 45	−58 14 00	0.1135	9.9	B1 V
			NGC 3293 23		V404 Car	10 35 47	−58 14 30	0.1621	9.2	B1 III
			NGC 3293 14		V405 Car	10 35 48	−58 12 33	0.1524*	9.3	B0.5 V
			NGC 3293 24		V378 Car	10 35 54	−58 14 48	0.16*	9.2	B1 III
			NGC 3293 133		V440 Car	10 35 55	−58 13 00	0.179	9.1	B1 III
			NGC 3293 18		V406 Car	10 35 58	−58 12 30	0.1756*	9.3	B1 V
			NGC 3293 27	−57 3351	V380 Car	10 36 02	−58 15 10	0.227	8.9	B0.5 III
92024...........			NGC 3293 5	−57 3354	V381 Car	10 36 08	−58 13 05	0.1773*	9.0	B1 III
109885.........	61751	KZ Mus		−70 955		12 39 19	−71 37 18	0.1706*	9.0	B2 III
111123.........	62434	β Cru	4853		Mimosa	12 47 43	−59 41 19	0.1912*	1.3	B0.5 IV
		BS Cru	NGC 4755G (7)	−59 4454		12 53 21	−60 23 21	0.1508*	9.8	B0.5 V
			NGC 4755 113			12 53 26	−60 22 26	0.2332	10.2	B1 V
			NGC 4755 405			12 53 38	−60 22 39	0.1252*	10.2	B2 V
		CT Cru	NGC 4755 301			12 53 44	−60 22 29	0.1305	9.8	B1 V
		CV Cru	NGC 4755 I (9)			12 53 47	−60 18 47	0.1789*	9.9	B1 Vn
		CZ Cru	NGC 4755 202			12 53 52	−60 21 52	0.1589*	10.1	B1 V
		CX Cru	NGC 4755 201			12 53 52	−60 22 15	0.1825	9.4	B1 V
	62937	CY Cru	NGC 4755 307			12 53 52	−60 22 28	0.1592	9.7	B1 V
			NGC 4755 210			12 53 53	−60 21 46	0.0933	10.3	B2 Vn
	62949	BW Cru	NGC 4755 F (6)		ALS 2816	12 53 58	−60 24 58	0.2049*	9.1	B2 III
112481.........	63250			−49 7513	V856 Cen	12 57 36	−49 46 50	0.2596*	8.4	B2 Ib
116658.........	65474	α Vir	5056	−10 3672	Spica	13 25 11	−11 09 40	0.2717	0.9	B1 IV
118716.........	66657	ϵ Cen	5132	−52 5743		13 39 53	−53 27 59	0.1696*	2.3	B1 V
122451.........	68702	β Cen	5267	−59 5054	Agena	14 03 49	−60 22 22	0.1535*	0.6	B1 II
126341.........	70574	τ^1 Lup	5395	−44 9322	1 Lup	14 26 08	−45 13 17	0.1774	4.6	B2 IV
129056.........	71860	α Lup	5469	−46 9501		14 41 55	−47 23 17	0.2598*	2.3	B1.5 III
129557.........	72121	BU Cir	5488	−55 5809		14 45 10	−55 36 05	0.1276*	6.1	B2 IV
129929.........	72241			−36 9605	V836 Cen	14 46 25	−37 13 19	0.1431*	8.1	B3 V
136298.........	75141	δ Lup	5695	−40 9538		15 21 22	−40 38 51	0.1655	3.2	B2 IV
144470.........	78933	ω^1 Sco	5993	−20 4405	9 Sco	16 06 48	−20 40 09	0.0667	3.9	B1 V
145794.........				−52 7312	V349 Nor	16 15 26	−52 55 15	0.1599*	8.7	B2 II–III

TABLE 1—*Continued*

HD	$v \sin i$ (km s^{-1}) (12)	$(b-y)$ (mag) (13)	m_1 (14)	c_1 (15)	β (mag) (16)	RV (km s^{-1}) (17)	Ampl. (mmag) (18)	References (19)	Notes (20)
886..............	4.5	−0.107	0.093	0.116	2.627	3.5	17 (V)	1, 2, 3, 4	Visual binary
							50 (R)	5	
		0.486	−0.160	0.122	2.619		40 (V)	6, 7	Spectral type doubtful
							19 (V)	8	
							43 (V)	9	
							3 (V)	8	
							11 (V)	10	
	160						16 (V)	10, 11	
16582...........	5	−0.099	0.091	0.102	2.616	12.7	25 (V)	1, 2, 3, 12, 13	
21803...........	40	0.082	0.023	0.102	2.617	2.4	72 (V)	1, 2, 14, 15	
24760...........	130	−0.074	0.055	−0.047	2.594	0.8	11 (Hp)	3, 16, 17	Visual binary; amplitude from this paper
29248...........	25	−0.076	0.068	0.072	2.610	14.9	74 (y)	1, 2, 18, 19, 20, 21	Visual binary
35411...........	130	−0.058	0.071	−0.010	2.608	19.8	n/a	3, 22, 23	Eclipsing binary; multiple system
35715...........	141	−0.088	0.075	0.033	2.619	12	n/a	3, 18, 21, 24	Double-lined spectroscopic binary; visual binary
44743...........	1	−0.091	0.054	−0.003	2.593	33.7	21 (V)	2, 3, 18, 25, 26, 27	Visual binary
46328...........	16	−0.093	0.064	−0.022	2.585	26.9	34 (V)	1, 2, 14, 28	Visual binary
50707...........	49	−0.087	0.071	−0.014	2.594	28	13 (V)	1, 12, 14, 21, 26, 29	
52918...........	274	−0.073	0.065	0.023	2.591	32	47 (y)	1, 3, 30, 31, 32	
56014...........	150	−0.067	0.070	0.168	2.572	+16	8 (V)	32, 33, 34	Visual binary
59864...........		0.003	0.061	0.022	2.599	44	16 (B)	14, 28, 35, 36	
61068...........	10	−0.068	0.077	0.050	2.617	22	39 (b)	1, 8, 17, 37, 38	
64365...........	∼30	−0.075	0.076	0.112	2.622	32.2	13 (V_W)	1, 18, 21, 28	
64722...........	147	−0.046	0.075	0.023	2.610	18	11 (V_W)	1, 21, 28	
71913...........		−0.012	0.052	0.024	2.594		32 (V_G)	39	
78616...........	10	0.060	0.039	0.068	2.611	26	48 (V)	1, 3, 14, 35, 40	Visual binary
80383...........	65	0.097	0.013	0.072	2.617	19	86 (V)	1, 41	Visual binary
90288...........	240	−0.040	0.054	0.020	2.622	4	16 (V)	1, 28, 38, 41	Visual binary
303068.........	42	0.060	0.037	0.045	2.611	−7	12 (y)	1, 42, 43	
303067.........	125	0.082	0.034	0.047	2.604	−10	18 (y)	1, 14, 42, 44, 45	
	33	0.048	0.040	0.023	2.591	−23	49 (y)	1, 14, 42, 44, 45	
		0.074	0.037	0.073	2.585		8 (y)	42, 45, 46	
	10	0.083	0.025	0.036	2.604	3	61 (y)	28, 42, 45	
	129	0.020	0.048	0.016	2.596	−14	10 (y)	1, 42, 44, 45	
	194	0.089	0.025	0.006	2.593	−12	14 (y)	1, 14, 35, 42, 44, 45	
	225						14 (y)	42, 45	
	40	0.038	0.050	0.045	2.605	−16	21 (y)	1, 14, 35, 42, 44, 45	Visual binary
	61	0.122	−0.001	0.073	2.60	−15	20 (y)	1, 14, 35, 42, 45, 46	
92024...........	122	0.035	0.035	0.014	2.598	−16	11 (y)	1, 35, 42, 44, 45, 47	Eclipsing binary
109885.........	47	0.173	−0.010	0.060	2.620	−61.1	77 (V)	39, 41, 48, 49	
111123.........	18	−0.103	0.061	−0.041	2.596	15.6	22 (V)	2, 3, 12, 35, 50, 51	Visual binary
	27	0.175	−0.018	0.056	2.609	−23	5 (V)	42, 52, 53	
	106	0.172	0.019	0.116	2.632	−19	5 (B)	42, 52, 53, 54	
	18	0.146	0.023	0.090	2.613	−18	4 (V)	52, 53, 55	
	225	0.179	−0.021	0.103	2.605	−6	10 (V)	42, 52, 53, 54	
	296	0.227	−0.023	0.112	2.607	−32	13 (V)	42, 52, 53	
	262	0.148	0.020	0.113	2.617	−33	16 (V)	42, 52, 54	
	195	0.153	0.005	0.102	2.609	−16	10 (V)	42, 52, 53	
	107	0.174	−0.028	0.152	2.620	−27	11 (B)	42, 52, 53, 54	
		0.177	0.022	0.136	2.634		7 (V)	42, 52, 56	
	96	0.143	0.002	0.062	2.605	−22	17 (V)	42, 52, 53	
112481.........					2.604	−19	34 (V_G)	1, 35, 57, 58	
116658.........	160	−0.114	0.080	0.018	2.605	1	Var.	2, 3, 18, 28, 35, 50	Ellipsoidal variable
118716.........	159	−0.094	0.058	0.043	2.608	3	15 (V_W)	1, 3, 21, 35, 50, 59	Visual binary
122451.........	139	−0.092	0.045	−0.004	2.594	5.9	25 (V)	3, 21, 35, 43, 60, 61	Suspected binary (80)
126341.........	15	−0.047	0.064	0.132	2.621	−21.5	27 (V)	1, 2, 35, 50, 62	Visual binary
129056.........	24	−0.086	0.071	0.080	2.604	5.2	20 (V_W)	1, 2, 3, 21, 35, 62	Visual binary
129557.........	30	0.036	0.027	0.058	2.617	−6.4	17 (y)	1, 35, 62, 63	Visual binary
129929.........	2	−0.059	0.058	0.038	2.618	66	24 (V_G)	1, 28, 57, 64, 65	
136298.........	221	−0.101	0.075	0.076	2.616	0.2	3.5 (V)	12, 21, 35, 66, 67	
144470.........	89	0.037	0.043	0.010	2.618	−2.6	n/a	3, 21, 68, 69	Only spectroscopic variability detected so far
145794.........					2.615		28 (V_G)	1, 28, 38, 58	Spectroscopic binary

TABLE 1—*Continued*

HD (1)	*Hipparcos* (2)	Name (3)	HR/Cluster (4)	BD/CD (5)	Other Name (6)	R.A. (J2000) (7)	Decl. (J2000) (8)	Period (days) (9)	V (mag) (10)	Spectral Type (11)
147165..........	80112	σ Sco	6084	−25 11485	20 Sco	16 21 11	−25 35 34	0.2468*	2.9	B1 III
147985..........	80653			−43 10792	V348 Nor	16 26 57	−43 47 57	0.1323*	7.9	B1.5 II–III
		Braes 929	NGC 6231 253	−41 11018p	V945 Sco	16 53 55	−41 52 15	0.0671	9.6	B1 V
		Braes 930	NGC 6231 282		V1032 Sco	16 53 59	−41 48 42	0.1193*	9.8	B2 V
		Braes 932	NGC 6231 261	−41 11028	V946 Sco	16 54 02	−41 51 12	0.0988*	10.3	B2 IV–Vn
326330..........		Braes 672	NGC 6231 238		V964 Sco	16 54 18	−41 51 36	0.0878*	9.6	B1 Vn
		Braes 948	NGC 6231 110	−41 11056	V947 Sco	16 54 35	−41 53 39	0.1079*	9.8	B1 V
326333..........		Braes 675	NGC 6231 150	−41 11059	V920 Sco	16 54 43	−41 49 36	0.1012*	9.6	B1 Vn
156327B.......	84655			−34 11622	V1035 Sco	17 18 23	−34 24 31	0.146*	9.4	WC7 + B0 III
156662..........				−45 11411	V831 Ara	17 21 06	−45 58 56	0.1689*	7.8	B2 III
157056..........	84970	θ Oph	6453	−24 13292	42 Oph	17 22 01	−24 59 58	0.1405*	3.3	B2 IV
157485..........	85189			−26 12112	V2371 Oph	17 24 35	−26 55 29	0.2212*	9.1	B1.5 Ib
158926..........	85927	λ Sco	6527	−37 11673	Shaula	17 33 37	−37 06 14	0.2137*	1.6	B2 IV
160578..........	86670	κ Sco	6580	−38 12137		17 42 29	−39 01 48	0.1998	2.4	B1.5 III
163472..........	87812		6684	+00 3813	V2052 Oph	17 56 18	+00 40 13	0.1399*	5.8	B2 IV–V
164340..........	88352			−40 12092		18 02 33	−40 05 16	0.1529	9.3	B2 IV–V
165174..........	88522		6747	+01 3578	V986 Oph	18 04 37	+01 55 08	0.2907	6.2	B0 IIIn
165812..........	88884			−22 4581	V4382 Sgr	18 08 45	−22 09 38	0.1759*	7.9	B1.5 II
166540..........	89164			−16 4747	V4159 Sgr	18 11 48	−16 53 38	0.233*	8.1	B1 Ib
180642..........	94793			+00 4159	V1449 Aql	19 17 15	+01 03 34	0.1822	8.3	B1.5 II–III
			NGC 6910 18			20 22 59	+40 45 39	0.1565*	10.8	B1 V
			NGC 6910 16			20 23 07	+40 46 56	0.1922*	10.7	B3
			NGC 6910 14			20 23 08	+40 46 09	0.1904	10.4	B0.5 V
			NGC 6910 27			20 23 34	+40 45 20	0.143	11.8	
		V2187 Cyg				20 33 18	+41 17 39	0.2539	15.4	
199140..........	103191	BW Vul	8007	+27 3909		20 54 22	+28 31 19	0.201	6.5	B2 III
203664..........	105614	SY Equ		+09 4793		21 23 29	+09 55 55	0.1659*	8.6	B0.5 IIIn
205021..........	106032	β Cep	8238	+69 1173	Alfirk	21 28 40	+70 33 39	0.1905*	3.2	B2 IIIe
			NGC 7235 8			22 12 34	+57 15 29	0.2029*	11.9	B1.5 V
		HN Aqr			PHL 346	22 37 38	−18 39 51	0.1523	11.5	B2
214993..........	112031	DD Lac	8640	+39 4912	12 Lac	22 41 29	+40 13 21	0.1931*	5.3	B2 III
216916..........	113281	EN Lac	8725	+40 4949	16 Lac	22 56 24	+41 36 14	0.1692*	5.6	B2 IV

8.1. *Omitted Stars*

Several candidate β Cephei stars in Table 2 originate from the line profile variability surveys of Telting et al. (2002) and Schrijvers et al. (2002). They were not directly claimed as β Cephei candidates by these authors. Stars that show line profile variability but where we discovered that the variations are likely not to originate in nonradial pulsation do not appear in the following tables at all.

HD 11241 (1 Per).—No periodicities in the spectroscopic data of Janík et al. (2003).

HD 48977 (16 Mon).—Probably a rotationally variable star.

HD 64503 (QZ Pup).—Ellipsoidal variable with a residual variability of $P \sim 1$ day, see Haefner & Drechsel (1986).

HD 64740.—Rotational variable with a period of 1.33 days, see Lester (1979).

HD 154445.—*Hipparcos* data analysis results in a period of 4.5916 days with a peak-to-peak amplitude of 19 mmag.

HD 169467 (α Tel).—Microvariable in *Hipparcos* with a period of 0.909 day; it also is a He rich star and we suspect it to be a SPB star.

HD 172910.—*Hipparcos* data results in two periods: 1.1983 and 0.9812 days, and we suspect it to be a SPB star.

A similar comment applies to the ζ Ophiuchi stars listed in Table 1 of Balona & Dziembowski (1999). Objects from that work which can have corotating variability periods too long to be due to β Cephei-type pulsation as described by us were not included in this catalog.

8.2. *Notes on Individual β Cephei Stars*

V595 Per.—The period of its light variation is somewhat long and there seems to be only one. The position of this star in the HR diagram of Krzesiński & Pigulski (1997) leads to a pulsation constant of 0.039 day. In β Cephei models the value of Q for the radial fundamental mode is between 0.034 and 0.041 day (if one only looks at modes excited in solar-metallicity models, the upper

TABLE 1—*Continued*

HD	$v \sin i$ (km s^{-1}) (12)	$(b-y)$ (mag) (13)	m_1 (14)	c_1 (15)	β (mag) (16)	RV (km s^{-1}) (17)	Ampl. (mmag) (18)	References (19)	Notes (20)
147165...........	53	0.168	−0.032	0.003	2.604	−1	40 (V)	1, 3, 21, 70, 71, 72	Spectroscopic binary
147985...........	80						46 (V)	1, 3, 38, 73, 74	
	100	0.206	−0.020	0.031	2.596	Var.	11 (y)	75, 76, 77, 78	Double-lined spectroscopic binary
	80	0.201	−0.015	0.131	2.617		6 (y)	75, 76, 79	Double-lined spectroscopic binary
	140	0.228	−0.046	0.144	2.626	−32	17 (y)	75, 76, 77, 78, 80	Suspected binary (80)
326330...........	210	0.198	−0.004	0.015	2.615	−30, var	5 (y)	75, 76, 79	
	190	0.237	−0.011	0.006	2.612		7 (y)	75, 76, 77, 78	Double-lined spectroscopic binary
326333...........	150	0.215	−0.013	0.026	2.606	−47, var	14 (y)	51, 75, 76, 80	Suspected binary (80)
156327B.........							35 (V)	81	Eclipsing binary
156662...........	190	0.200	−0.044	0.074	2.614		16 (V_G)	1, 38, 73	
157056...........	35	−0.092	0.089	0.104	2.624	−5.6, var?	19 (y)	1, 21, 38, 82, 83, 84	Visual binary
157485...........					2.623		48 (V_G)	39	
158926...........	163	−0.105	0.072	0.074	2.613	18.6, var	23 (V)	1, 3, 21, 22, 85, 86	Spectroscopic triple system
160578...........	115	−0.100	0.073	0.073	2.613	0.2,var	9 (V)	2, 3, 85, 86, 87	Spectroscopic binary
163472...........	120	0.128	0.017	0.145	2.630	−17.6	28 (V)	1, 21, 38, 88, 89, 90, 91	Magnetic star
164340...........					2.584		25 (V)	92, 93	
165174...........	300	0.075	0.000	−0.119	2.567	+17, var	9 (b)	15, 94, 95, 96, 97, 98	Spectroscopic binary; mild Be star
165812...........		0.079	0.029	−0.001	2.611	−24	28 (V_G)	39, 99	Periods from *Hipparcos* photometry and Geneva data disagree
166540...........	55					−1.6	23 (V)	100	
180642...........	90	0.259	−0.035	0.031		−14	78 (V_G)	15, 39, 99	
		0.600	−0.110	0.140	2.636		15 (V)	101	
							17 (V)	101	
		0.670	−0.160	0.110	2.612		17 (V)	101	
		0.820	−0.180	0.170	2.625		9 (V)	101	
							34 (I)	102	
199140...........	60	−0.033	0.051	0.029	2.610	−8.5	85 (V)	1, 3, 63, 103, 104, 105	
203664...........	180					48	60 (V_G)	15, 39	
205021...........	25	−0.092	0.066	0.010	2.605	−3.1	37 (V)	2, 3, 106, 107, 108, 109	Spectroscopic binary; magnetic star; mild Be star; star is located in the overlap region of the BD and CD catalogs BD −22 4581=CD −22 12607
							29 (V)	110	
	45	−0.068	0.070	0.094		63	32 (V)	1, 38, 111, 112, 113	
214993...........	40	−0.034	0.052	0.050	2.609	−12.5	76 (y)	1, 3, 114, 115, 116, 117	Spectroscopic binary; star is located in the overlap region of the BD and CD catalogs BD −22 4581=CD −22 12607
216916...........	30	−0.047	0.066	0.092	2.629	−13	Var	1, 3, 118, 119, 120, 121	Spectroscopic binary; visual binary; eclipsing binary

Notes.—Units of right ascension are hours, minutes, and seconds, and units of declination are degrees, arcminutes, and arcseconds. Table 1 is also available in machine-readable form in the electronic edition of the *Astrophysical Journal Supplement*.

References.— (1) Cugier et al. 1994; (2) Lesh & Aizenman 1978; (3) Aerts & De Cat 2003; (4) Valtier et al. 1985; (5) Robb et al. 2000; (6) Pietrzynski 1997; (7) Pigulski et al. 2001; (8) Krzesiński et al. 1999; (9) Gomez-Forrellad 2000; (10) Krzesiński & Pigulski 1997; (11) Slettebak 1968; (12) Grady et al. 1987; (13) Jerzykiewicz et al. 1988; (14) Evans 1967; (15) De Cat et al. 2004; (16) De Cat et al. 2000; (17) Abt et al. 2002; (18) Wilson 1953; (19) Aerts et al. 2004a; (20) Handler et al. 2004; (21) Schrijvers et al. 2002; (22) De Mey et al. 1997; (23) Batten et al. 1989; (24) Telting et al. 2001; (25) Shobbrook 1973a; (26) Jakate 1979b; (27) Shobbrook 1985; (28) Heynderickx 1992; (29) Shobbrook 1973b; (30) Balona et al. 1992; (31) Irvine 1975; (32) Balona et al. 2002; (33) Balona 1995a; (34) Balona & Krisciunas 1994; (35) Duflot et al. 1995; (36) Sterken & Jerzykiewicz 1990; (37) Shobbrook 1981; (38) Heynderickx et al. 1994; (39) Aerts 2000; (40) Cousins 1982; (41) Handler et al. 2003; (42) Balona et al. 1997; (43) Balona 1977; (44) Feast 1958; (45) Balona 1994; (46) Engelbrecht 1986; (47) Freyhammer et al. 2004; (48) Kilkenny & Hill 1975; (49) Hill et al. 1974; (50) Gutierrez-Moreno & Moreno 1968; (51) Shobbrook 1979).; (52) Stankov et al. 2002; (53) Feast 1963; (54) Balona & Koen 1994; (55) Dachs & Kaiser 1984; (56) Schild 1970; (57) Hill 1970; (58) Waelkens & Heynderickx 1989; (59) Schrijvers et al. 2004; (60) Ausseloos et al. 2002; (61) Robertson et al. 1999; (62) Bernacca & Perinotto 1970; (63) Vander Linden & Sterken 1987; (64) Hill 1971; (65) Aerts et al. 2003; (66) Lloyd & Pike 1988; (67) Shobbrook 1972; (68) Telting & Schrijvers 1998; (69) Houk 1982; (70) Goosens et al. 1984; (71) Jerzykiewicz & Sterken 1984; (72) Chapellier & Valtier 1992; (73) Waelkens & Cuypers 1985; (74) Aerts et al. 1994; (75) Balona & Laney 1995; (76) Arentoft et al. 2001; (77) Balona 1983; (78) Balona & Shobbrook 1983; (79) Balona & Engelbrecht 1985a; (80) García & Mermilliod 2001; (81) Paardekooper et al. 2002; (82) Henroteau 1922; (83) Briers 1971; (84) Handler et al. 2005; (85) Shobbrook & Lomb 1972; (86) Lomb & Shobbrook 1975; (87) Uytterhoeven et al. 2001; (88) Jerzykiewicz 1993; (89) Jerzykiewicz 1972; (90) Kubiak & Seggewiss 1984; (91) Neiner et al. 2003; (92) J. Molenda-Żakowicz & G. Połubek 2005, in preparation; (93) Garrison et al. 1977; (94) Lynds 1959; (95) Jerzykiewicz 1975; (96) Cuypers et al. 1989; (97) Coté & van Kerkwijk 1993; (98) Balona 1995b; (99) Waelkens et al. 1998; (100)Waelkens et al. 1991) ; (101) Kołaczkowski et al. 2004a; (102) Pigulski & Kołaczkowski 1998; (103) Stankov et al. 2003; (104) Plaskett & Pearce 1931; (105) Aerts et al. 1995; (106) Frost 1906; (107) Pigulski & Boratyn 1992; (108) Telting et al. 1997; (109) Shibahashi & Aerts 2000; (110) Pigulski et al. 1997; (111) Waelkens & Rufener 1988; (112) Kilkenny & van Wyk 1990; (113) Dufton et al. 1998; (114) Young 1915; (115) Jerzykiewicz 1978; (116) Aerts 1996; (117) Dziembowski & Jerzykiewicz 1999; (118) Walker 1951; (119) Dziembowski & Jerzykiewicz 1996; (120) Thoul et al. 2003; (121) Jerzykiewicz & Pigulski 1999).

TABLE 2
CANDIDATE β CEPHEI STARS

HD (1)	*Hipparcos* (2)	Name (3)	HR/Cluster (4)	BD/CD (5)	Other Name (6)	R.A. (J2000) (7)	Decl. (J2000) (8)	Spectral Type (9)	V (mag) (10)	Reference (11)	Notes (12)
			NGC 663 114			01 46 40	+61 09 52	. . .	12.4	1	
13494..............		AG +56 243			V352 Per	02 13 37	+56 34 14	B1 III	9.3	2, 3	
14053..............			NGC 869 612	+56 498		02 18 23	+57 00 37	B1 II	8.5	2	
14250..............		AG +56 292		+56 545	V359 Per	02 20 16	+57 05 55	B1 IV	9.1	2	
		AG +57 301		+56 589	V360 Per	02 22 50	+57 30 42	B1 III	9.6	2	
21856..............	16518		1074	+34 674		03 32 40	+35 27 42	B1 V	5.9	4, 5	Not variable in 4; possible ζ Ophiuchi star
			NGC 1502 37			04 07 43	+62 19 39	B1.5 V	9.3	2, 6	
			NGC 150 26	+61 675		04 07 44	+62 10 04	B2 IV	9.6	6	
25638..............	19272		NGC 1502 1	+61 676A		04 07 51	+62 19 48	B0 III	6.9	6	
32990..............	23900		1659	+24 755	103 Tau	05 08 06	+24 15 55	B2 V	5.5	5	Spectroscopic binary
34656..............	24957			+37 1146		05 20 43	+37 26 19	O7e III	6.8	7, 8, 9, 10	
35149..............	25142	23 Ori	1770	+03 871		05 22 50	+03 32 40	B1 V	5.0	5, 11	Possible ζ Ophiuchi star
36166..............	25751		1833	+01 1032		05 29 55	+01 47 21	B2 V	5.7	5	Possible ζ Ophiuchi star
36512..............	25923	υ Ori	1855	−07 1106	36 Ori	05 31 56	−07 18 05	B0 V	4.6	12, 13, 14	
36695..............	26063	VV Ori	1868	−01 943		05 33 31	−01 09 22	B1 V	5.4	5, 11	Spectroscopic binary; possible ζ Ophiuchi star
36819..............	26248		1875	+23 954	121 Tau	05 35 27	+24 02 23	B2.5 IV	5.4	5, 11	Possible ζ Ophiuchi star
37756..............	26736		1952	−01 1004		05 40 51	−01 07 44	B2 IV–V	4.95	5	Spectroscopic binary
38622..............	27364		1993	+13 979	133 Tau	05 47 43	+13 53 59	B2 IV–V	5.27	5, 16	Double system with possible T Tauri component
39291..............	27658		2031	−07 1187	55 Ori	05 51 22	−07 31 05	B2 IV–V	5.3	5, 17, 18	Not variable in 18; possible ζ Ophiuchi star
40494..............	28199	γ Col	2106	−35 2612		05 57 32	−35 16 59	B2.5 IV	4.4	11, 16	Star in double system
252248............	29121	AG +13 539	NGC 2169 5		V917 Ori	06 08 27	+13 55 51	B2 V	8.8	2, 3, 19	Possible Be star
43078..............	29687	AG +22 667		+22 1243	LR Gem	06 15 15	22 18 04	B0 IV	8.8	2, 3	
44112..............	30073		2273	−07 1373	7 Mon	06 19 43	−07 49 23	B2.5 V	5.2	5, 11	Spectroscopic binary;; possible ζ Ophiuchi star
45546..............	30772		2344	−04 1526	10 Mon	06 27 57	−04 45 44	B2 V	5.04	5	Star in double system
51630..............	33447		2603	−22 1616		06 57 15	−22 12 10	B2 III/IV	6.6	20, 21	
53755..............	34234	ADS 5782 A	2670	−10 1862	V569 Mon	07 05 50	−10 39 36	B0.5 V	6.5	2, 22, 23, 24	
63949..............	38159	QS Pup	3058	−46 3460		07 49 12	−46 51 27	B1.5 IV	5.8	22, 25	
68324..............	39970	IS Vel	3213	−47 3653		08 09 43	−47 56 13	B2 IV	5.2	20, 22, 26	
69081..............	40321		3240	−35 4358	OS Pup	08 13 58	−36 19 20	B1.5 IV	5.1	11, 27	Possible ζ Ophiuchi star; in 27 slow variable
70839..............	40932		3293			08 21 12	−57 58 24	B1.5 III	5.9	11	Possible ζ Ophiuchi star
70930..............	41039	B Vel	3294	−48 3734		08 22 32	−48 29 25	B1 V	4.8	11	Double or multiple star; possible ζ Ophiuchi star
72108..............	41616		3358	−47 4004		08 29 05	−47 55 44	B2 IV	5.3	11	Double or multiple star
72127..............	41639		3359	−44 4462		08 29 28	−44 43 29	B2 IV	4.99	11	Double system; possible ζ Ophiuchi star
74071..............	42459	HW Vel	3440			08 39 24	−53 26 23	B5 V	5.4	21, 28	
74273..............	42614		3453	−48 4020		08 41 05	−48 55 22	B1.5 V	5.9	11	Double-lined spectroscopic binary; possible ζ Ophiuchi star
74455..............	42712	HX Vel	3462	−47 4251		08 42 16	−48 05 57	B1.5 Vn	5.5	11, 29	Susp. ell. var in 29; possible ζ Ophiuchi star
74575..............	42828	α Pyx	3468	−32 5651		08 43 36	−33 11 11	B1.5 III	3.7	21, 30, 31	IR standard star
74753..............	42834	D Vel	3476	−49 3761		08 43 40	−49 49 22	B0 IIIn	5.1	11	Possible ζ Ophiuchi star
86466..............	48799	IV Vel	3941	−52 3465		09 57 11	−52 38 20	B3 IV	6.1	27, 32	
89688..............	50684	RS Sex	4064	+03 2352	23 Sex	10 21 02	+02 17 23	B3.2 IV	6.6	3, 33, 34	$P_{Hipparcos} \sim 0.129$ day

TABLE 2—*Continued*

HD (1)	*Hipparcos* (2)	Name (3)	HR/Cluster (4)	BD/CD (5)	Other Name (6)	R.A. (J2000) (7)	Decl. (J2000) (8)	Spectral Type (9)	V (mag) (10)	Reference (11)	Notes (12)
96446........	54266	V430 Car		−59 3544		11 06 06	−59 56 59	B2 I He	6.7	35, 36	He strong
97533........	54753			−57 3772		11 12 36	−58 38 38	B1:Vn	8.4	37	
					V770 Cen	11 21 09	−60 32 13	B5 e	12.4	38	Be star
			NGC 3766 67		V847 Cen	11 36 14	−61 37 36	B2 Vp	9.9	39	
104337.......	58587	TY Crv	4590	−18 3295	31 Crt	12 00 51	−19 39 32	B1.5 V	5.3	5, 40	Spectroscopic binary; ell. var. in 40
108483.......	60823	σ Cen	4743	−49 7115		12 28 02	−50 13 50	B2 V	3.9	11, 18	Possible ζ Ophiuchi star
112092.......	63003	μ1 Cru	4898			12 54 36	−57 10 41	B2 IV–V	3.9	11, 41	Double syst., not var. in 27 and 41
120307.......	67464	ν Cen	5190			13 49 30	−41 41 15	B2 V	3.4	42, 43, 44, 45, 46, 47	
121743.......	68245	ϕ Cen	5248	−41 8329		13 58 16	−42 06 03	B2 IV	3.8	17, 27, 48, 11, 49	Var. in 17, not var. in 27 and 48
121790.......	68282	υ01 Cen	5249	−44 9010		13 58 41	−44 48 13	B2 IV–V	3.8	11, 48, 49	Possible ζ Ophiuchi star; not var. in 48
132058.......	73273	β Lup	5571	−42 9853		14 58 32	−43 08 02	B2 III	2.7	42, 43, 50	Possible ζ Ophiuchi star
132200.......	73334	κ Cen	5576	−41 9342		14 59 10	−42 06 15	B2 IV	3.1	11, 49	
136504.......	75264	ϵ Lup	5708	−44 10066		15 22 41	−44 41 23	B2 IV–V	3.4	11, 49	Spectroscopic binary; possible ζ Ophiuchi star
142669.......	78104	ρ Sco	5928	−28 11714	5 Sco	15 56 53	−29 12 51	B2 IV–V	3.9	11, 45	Spectroscopic binary; possible ζ Ophiuchi star
142883.......	78168		5934	−20 4364		15 57 40	−20 58 59	B3 V	5.9	4, 45, 51	
143018.......	78265	π Sco	5944	−25 11228	6 Sco	15 58 51	−26 06 51	B1 V	2.9	11, 40, 45	Spectroscopic binary; ecl. bin in 40
144218.......	78821	β Sco A	5985	−19 4308		16 05 27	−19 48 07	B2 V	4.9	24, 42, 52, 53	
145502.......	79374	ν Sco	6027	−19 4333	14 Sco A	16 11 59	−19 27 39	B2 IV	4.13	11, 45, 54	Spectroscopic binary
148703.......	80911		6143	−34 11044	N Sco	16 31 23	−34 42 16	B2 III–IV	4.22	11, 18, 49	
149881.......	81362			+14 3086	V600 Her	16 36 58	+14 28 31	B0.5 III	7.0	34, 55, 56, 57	
151985.......	82545	μ2 Sco	6252	−37 11037		16 52 20	−38 01 03	B2 IV	3.5	11, 49	
326327.......		Braes 669	NGC 6231 28	−41 11007	V962 Sco	16 53 39	−41 47 48	B1.5 Ve+sh	9.7	58, 59	Triple system?
			NGC 6231 289	−41 11027p		16 54 06	−41 51 13	B0.5 V	9.5	60, 61	
			NGC 6231 80		V963 Sco	16 54 14	−41 55 01	B0 Vn	10.3	60, 61	
			NGC 6231 104			16 54 16	−41 49 34	. . .	10.2	61	
			NGC 6231 SBL 515	−41 7736		16 54 21	−41 49 30	B1 Vn	11.2	61	
163868.......	88123			−33 12700		17 59 56	−33 24 29	B5 Ve	7.4	37	Be star
171034.......	91014		6960	−33 13338		18 33 58	−33 00 59	B2 IV–V	5.3	11, 18, 49	Possible ζ Ophiuchi star
176502.......	93177	ADS 11910 A	7179	+40 3544	V543 Lyr	18 58 47	+40 40 45	B3 V	6.2	51	
			NGC 6871 14		V1820 Cyg	20 05 39	+35 45 31	B2 III	10.8	62	
		IC 4996 Hoag 7			V1922 Cyg	20 16 45	+37 40 44	. . .	10.9	4, 63, 64	
					V2190 Cyg	20 33 25	+41 22 04	. . .	14.3	65	
201819.......	104579		8105	+35 4426		21 11 04	+36 17 58	B0.5 IVn	6.5	4	
210808.......	109505			+62 2045	V447 Cep	22 11 00	+63 23 58	B5	7.3	66	
			NGC 7419 BMD 451			22 54 17	60 48 23	. . .	15.9	67, 68	Be star
			NGC 7419 BMD 551			22 54 19	60 48 14	. . .	16.4	67, 68	Be star
217035.......		KZ Cep		+62 2136		22 56 31	+62 52 07	B0 V	7.7	2, 69	Maybe Be star

Notes.—Units of right ascension are hours, minutes, and seconds, and units of declination are degrees, arcminutes, and arcseconds. Table 2 is also available in machine-readable form in the electronic edition of the *Astrophysical Journal Supplement*.

References.—(1) Pigulski et al. 2001; (2) Hill 1967; (3) Kukarkin et al. 1971; (4) Jerzykiewicz 1993; (5) Telting et al. 2002; (6) Delgado et al. 1992; (7) Balona 1975; (8) Balona et al. 1992; (9) Fullerton et al. 1991; (10) Balona 1995b; (11) Schrijvers et al. 2002; (12) Waelkens 1991; (13) Balona & Engelbrecht 1985b; (14) Smith 1981; (15) Li & Hu 1998; (16) Gerbaldi et al. 2001; (17) Kukarkin et al. 1981; (18) Adelman 2001; (19) Jerzykiewicz et al. 2003; (20) Jerzykiewicz & Sterken 1977; (21) Balona 1977; (22) Wilson 1953; (23) Shobbrook 1983; (24) Abt et al. 2002; (25) Heynderickx et al. 1994; (26) Sterken & Jerzykiewicz 1993; (27) Jakate 1979b; (28) Renson & Sterken 1977; (29) Morris 1985; (30) Sterken & Vander Linden 1983; (31) Van Hoof 1973a; (32) Evans 1967; (33) Percy & Au-Yong 2000; (34) De Cat et al. 2004; (35) Matthews & Bohlender 1991; (36) Mathys 1994; (37) J. Molenda-Żakowicz & G. Połubek 2005, in preparation; (38) Vidal et al. 1974; (39) Balona & Engelbrecht 1986; (40) Kazarovets et al. 1999; (41) Pedersen & Thomsen 1977; (42) Duflot et al. 1995; (43) Aerts & De Cat 2003; (44) Gutierrez-Moreno & Moreno 1968; (45) Levato et al. 1987; (46) Cuypers et al. 1989; (47) Schrijvers & Telting 2002; (48) Balona 1982; (49) Sterken & Jerzykiewicz 1983; (50) Schrijvers 1999; (51) Koen & Eyer 2002; (52) Aerts et al. 1999; (53) Holmgren et al. 1997; (54) Van Hoof et al. 1963; (55) Morris 1985; (56) Antokhina & Barannikov 1996; (57) Hill et al. 1976; (58) Balona & Laney 1995; (59) García & Mermilliod 2001; (60) Balona & Engelbrecht 1985a; (61) Arentoft et al. 2001; (62) Delgado et al. 1984; (63) Delgado et al. 1985; (64) Hoag et al. 1961; (65) Pigulski & Kołaczkowski 1998; (66) Koen 2001; (67) Beauchamp et al. 1994; (68) Kołaczkowski et al. 2002; (69) Deupree 1970.

TABLE 3

Poor and Rejected β Cephei Candidates

HD (1)	*Hipparcos* (2)	Name (3)	HR/Cluster (4)	BD/CD (5)	Other Name (6)	R.A. (J2000) (7)	Decl. (J2000) (8)	Spectral Type (9)	V (mag) (10)	References (11)	Notes (12)
3379	2903	53 Psc	155	+14 76	AG Psc	00 36 47	15 13 54	B2.5 IV	5.9	1, 2	SPB star
				+61 285		01 32 37	+61 58 12	B0.5 III:	9.5	3	$P \sim 2$ days, aliasing mistake in reference
13051	10541	V351 Per		+55 554		02 09 26	+56 59 30	B1 IV:	8.6	4, 5	$P_{Hipparcos} \sim 2.5$ days
13544	10391	AG +53 218	+53 480		V353 Per	02 13 52	+53 54 53	B0.5 IV	8.9	6, 7, 8	
			NGC 869 49	+56 473	V356 Per	02 16 58	+57 07 49	B0.5 IIIn	9.2	4, 7, 9	Be star; claimed variability not confirmed
		NSV 776	NGC 869 963		Oo 963	02 18 58	+57 08 18	B2 IV	11.0	10	Claimed variability not confirmed
13745		AG +55 231			V354 Per	02 15 46	+55 59 47	O9.7 II	7.9	7, 11	No convincing variability in *Hipparcos* photometry
13831	10615			+56 469	V473 Per	02 16 39	+56 44 16	B0 IIIp	8.3	12	
13866	10641	V357 Per		+56 475		02 16 58	+56 43 08	B2 Ib	7.5	4, 7	Claimed variability not confirmed
15239	11604		St7−28	+60 487	V528 Cas	02 29 38	+60 39 26	B2.5 V+sh	8.5	13	$P_{Hipparcos} \sim 1$ day
15752	11953	AG +58 273		+57 589	V362 Per	02 34 12	+58 24 20	B0 III	8.8	7	No convincing variability in *Hipparcos* photometry
16429A	12495	STF 284A		+60 541	V482 Cas	02 40 45	+61 16 56	O9.5 III	7.9	7, 14	
19374	14514	53 Ari	938	+17 493	UW Ari	03 07 26	17 52 48	B1.5 V	6.1	15, 16, 17	Claimed variability not confirmed
23480	17608	Merope	1156	+23 522	V971 Tau	03 46 20	+23 56 54	B6 IVe	4.2	18, 19, 20	Periodic Be star, $P = 0.49$ day
24640	18434	NSV 1418	1215	+34 768		03 56 29	+35 04 51	B1.5 V	5.5	21, 22	
27396	20354	53 Per	1350	+46 872	V469 Per	04 21 33	+46 29 56	B4 IV	4.8	23, 24	SPB star
28114	20715		1397	+08 687	V1143 Tau	04 26 21	+08 35 25	B6 IV	6.1	25	SPB star
28446	21148	DL Cam	1417	+53 779	1 Cam	04 32 01	+53 54 39	B0 IIIn	5.8	26, 27	Probably SPB
33328	23972	λ Eri	1679	−08 1040	69 Eri	05 09 09	−08 45 15	B2 IVne	4.2	8, 20, 28, 29	Periodic Be star, $P = 0.702$ day
35468	25336	γ Ori	1790	+06 919	24 Ori	05 25 08	+06 20 59	B2 III	1.6	30, 31	
37776	26742			−01 1005	V901 Ori	05 40 56	−01 30 26	B2 IV	6.9	7, 32, 33	
38010	26998			+25 941	V1165 Tau	05 43 39	25 26 22	B1 Vpe	6.8	34	Be star, $P_{Hipparcos} \sim 0.67$ day
252214	29106	AG +13 535	NGC 2169 2	+13 1120	V916 Ori	06 08 18	13 58 18	B2.5 V	8.1	5, 7, 35	Claimed variability not confirmed
43837	30041	AG +20 661		+20 1369		06 19 17	+20 34 48	B2 Ibp…	8.5	6, 36	$P_{Hipparcos} \sim 2$ days
43818	30046	LU Gem		+23 1300	11 Gem	06 19 19	+23 28 10	B0 II	6.9	36, 37, 38	
47432	31766		2442	+01 1443	V689 Mon	06 38 38	+01 36 49	O 9.5 III	6.2	6, 39, 40	$P_{Hipparcos} \sim 2$ days
51309	33347	ι CMa	2596	−16 1661	20 CMa	06 56 08	−17 03 15	B3 Ib/II	4.4	2, 41, 42	
53974	34301	FN CMa	2678	−11 1790		07 06 41	−11 17 39	B0.5 IV	5.4	5, 7, 39	$P_{Hipparcos} \sim 1$ day
55857	34924	GY CMa	2734	−27 3789	ALS 255	+07 13 36	−27 21 23	B0.5 V	6.1	37, 43, 44	Claimed variability not confirmed
55958	34937	GG CMa	2741	−30 4143		07 13 47	−03 01 51	B2 IV	6.6	45, 46	Claimed variability not confirmed
57219	35406	υ02 Pup	2790	−36 3519	NW Pup	07 18 39	−36 44 34	B2 IVne	5.1	47, 48, 49	
65575	38827	χ Car	3117			07 56 47	−52 58 57	B3 IVp	3.4	8, 16, 41, 50	
67536	39530		3186	−62 330	V375 Car	08 04 43	−62 50 11	B2.5 Vn	6.2	8, 37, 51	Be star, $P_{Hipparcos} = 1.01646$ days
74195	42536	o Vel	3447			08 40 18	−52 55 19	B3 IV	3.6	52	SPB star

TABLE 3—*Continued*

HD (1)	*Hipparcos* (2)	Name (3)	HR/Cluster (4)	BD/CD (5)	Other Name (6)	R.A. (J2000) (7)	Decl. (J2000) (8)	Spectral Type (9)	V (mag) (10)	References (11)	Notes (12)
74375..........	42568	d Car	3457	−59 2020	V343 Car	08 40 37	−59 45 40	B1.5 III	4.3	6, 51, 53	$P_{Hipparcos} = 2.37952$ days
74280..........	42799	η Hya	3454	+03 2039	7 Hya	08 43 14	+03 23 55	B3 V	4.9	41, 54, 55	$P_{Hipparcos} \sim 2.2$ days
77002..........	43937	b01 Car	3582	−58 2347	V376 Car	08 56 58	−59 13 45	B2 IV−V	4.9	37, 56, 57	Claimed variability not confirmed
77320..........	44213	IU Vel	3593	−42 4875		09 00 22	−43 10 26	B2.5 Vne	6.1	19, 20, 47	Periodic Be star ($P = 0.612$ day)
85953..........	48527		3924	−50 4622	V335 Vel	09 53 50	−51 08 48	B2 III	5.9	52	SPB star
92007..........			NGC 3293 26	−57 3350	V379 Car	10 35 59	−58 14 15	B1 III	8.2	20, 58, 59, 60, 61	Periodic Be star ($P = 1.754$ days)
98410..........	55207	ALS 2299		−62 505	V536 Car	11 18 18	−62 58 28	B2/B3 Ib/II	8.8	26	$P_{Hipparcos} = 1.45325$ days
104841........	58867	θ^2 Cru	4603	−62 610		12 04 19	−63 09 57	B2 IV	4.7	37, 41	
106490........	59747	δ Cru	4656	−58 4466		12 15 09	−58 44 56	B2 IV	2.8	16, 39, 41, 62, 63, 64	
109668........	61585	α Mus	4798	−68 1104		12 37 11	−69 08 08	B2 IV−V	2.7	16, 37, 39, 41	
		BT Cru	NGC 4755 418	−59 4542		12 53 36	−60 23 46	B2 V	9.6	64, 65, 66, 67, 68	Claimed variability not confirmed
			NGC 4755 215			12 53 38	−60 22 49		11.6	58, 69, 70	$P = 0.355$ day, SPB star?
		BV Cru	NGC 4755 105			12 53 39	−60 21 12	B0.5 IIIn	8.7	65, 67, 68	$P \sim 1$ or 2 days, possible binary
112078........	63007	λ Cru	4897	−58 4794		12 54 39	−59 08 48	B4 Vne	4.6	5, 20, 47, 62, 71	$P_{Hipparcos} = 0.35168$ day, $Q = 0.11$ day
116072........			5034	−60 4639	V790 Cen	13 22 36	−60 58 19	B2.5 Vn	6.2	8, 72	β Lyr-type eclipsing binary
122980........	68862	χ Cen	5285	−40 8405		14 06 03	−41 10 47	B2 V	4.4	57	
130903........	72710	He 3−1034		−40 9037	V1018 Cen	14 51 58	−40 48 21	B2p	7.9	26, 73, 74	
160762........	86414	ι Her	6588	+46 2349	85 Her	17 39 28	+46 00 23	B3 IV	3.8	75, 76	
160124........	86432		NGC 6405 100	−32 13072	V994 Sco	17 39 38	−32 19 13	B3 IV	7.2	77, 78	SPB star
180125........	94588			+10 3839	V1447 Aql	19 14 58	+10 24 34	B8 V	7.4	26, 74	$P_{Hipparcos} = 2.1678$ days
180968........	94827	ES Vul	7318	+22 3648	2 Vul	19 17 44	+23 01 32	B0.5 IV	5.4	8, 20, 79	Periodic Be star ($P = 1.27$ days)
188439........	97845		7600	+47 2945	V819 Cyg	19 53 01	+47 48 28	B0.5 IIIn	6.3	6, 79	
189687........	98425	25 Cyg	7647	+36 3806	V1746 Cyg	19 59 55	+37 02 34	B3 IVe	5.1	80, 81	Be star
195556........	101138	ω^1 Cyg	7844	+48 3142	45 Cyg	20 30 04	+48 57 06	B2.5 IV	4.9	27	
204076........	105912	BR Mic		−32 16569		21 27 01	−31 56 20	B2 II	8.8	82	$P_{Hipparcos} \sim 3.6$ days
217811........	113802	LN And	8768	+43 4378		23 02 45	+44 03 32	B2 V	6.4	83	
224559........	118214	LQ And	9070	+45 4381	AG +46 2225	23 58 46	46 24 47	B4 Vne	6.5	20, 84, 85	Periodic Be star ($P = 0.619$ day)

Notes.—Units of right ascension are hours, minutes, and seconds, and units of declination are degrees, arcminutes, and arcseconds. Table 3 is also available in machine-readable form in the electronic edition of the *Astrophysical Journal Supplement*.

References.—(1) Le Contel et al. 2001; (2) Kukarkin et al. 1981; (3) Maciejewski et al. 2004; (4) Mahra & Mohan 1979; (5) Kukarkin et al. 1971; (6) Koen & Eyer 2002; (7) Hill 1967; (8) Grady et al. 1987; (9) Steele et al. 1999; (10) Krzesiński et al. 1999; (11) De Cat et al. 2004; (12) Garrido & Delgado 1982; (13) Percy & Madore 1972; (14) McSwain 2003; (15) Percy & Au-Yong 2000; (16) Adelman 2001; (17) Sterken 1988; (18) McNamara 1985; (19) Balona 1990; (20) Balona 1995a; (21) Jones 1960; (22) Telting et al. 2002; (23) De Ridder et al. 1999; (24) Chapellier et al. 1998; (25) Mathias et al. 2001; (26) Kazarovets et al. 1999; (27) Jerzykiewicz 1993; (28) Balona 1975; (29) Balona 1995b; (30) Krisciunas & Luedeke 1996; (31) Krisciunas 1994; (32) Catalano & Renson 1998; (33) Khokhlova et al. 2000; (34) Jaschek et al. 1980; (35) Jerzykiewicz et al. 2003; (36) Percy 1984; (37) Jakate 1979b; (38) Shobbrook 1978; (39) Balona 1977; (40) Balona & Engelbrecht 1981; (41) Elst 1979b; (42) Balona & Engelbrecht 1985b; (43) Breger et al. 1991; (44) Balona & Cuypers 1993; (45) Jerzykiewicz & Sterken 1977; (46) Morris 1985; (47) Balona et al. 1992; (48) Yudin 2001; (49) Dachs et al. 1981; (50) Leone & Catanzaro 1998; (51) Van Hoof 1973b; (52) Aerts et al. 1999; (53) Waelkens & Rufener 1983a; (54) Abt et al. 2002; (55) Saxena & Srivastava 1997; (56) Jakate 1979a; (57) Balona 1982; (58) Balona et al. 1997; (59) Cugier et al. 1994; (60) Duflot et al. 1995; (61) Feast 1958; (62) Shobbrook 1981; (63) Elst 1979a; (64) Schrijvers et al. 2002; (65) Balona & Koen 1994; (66) A. Stankov 2005, in preparation; (67) Jakate 1978; (68) Koen 1993; (69) Stankov et al. 2002; (70) Perry et al. 1976; (71) Evans 1967; (72) Waelkens & Rufener 1983b; (73) Dachs & Kaiser 1984; (74) ESA 1997; (75) Mathias & Waelkens 1995; (76) Chapellier et al. 2000; (77) Waelkens 1991; (78) Waelkens & Rufener 1985; (79) Lynds 1959; (80) Percy et al. 2002; (81) Pavlovski et al. 1997; (82) Hambly et al. 1994; (83) Shaw et al. 1983; (84) Matthews et al. 1991; (85) Percy & Lane 1977.

TABLE 4
PULSATION PERIODS FOR STARS FROM TABLE 1

Identifier (1)	Period (days) (2)	Reference, (Note) (3)
HD 886	0.1517502ps	1
V909 Cas	0.207p	2
NGC 663 4	0.194047p	3
V611 Per	0.1716946p	4
V665 Per	0.242342p	5
	0.199545p	This work
	+more	
V614 Per	0.1326359p	5
NGC 884 2246	0.184188p	6
	0.170765p	
V595 Per	0.31788p	6
HD 16582	0.1611ps	s: 7, p: 8
HD 21803	0.201779ps	9, 10
	0.198085ps	10, 11
	0.227099p	10, 11
	+more	10
HD 24760	0.1887s	12
	0.1698s	
	0.1600s	
	0.1455s	
	0.13976s	s: 13, not found in 12
	0.1911s	s: 13, not found in 12
HD 29248	0.1735126ps	14
	0.1768681ps	
	0.1779337ps	
	0.1773937ps	
	0.126619ps	
	0.16015ps	
	0.15969ps	
	0.16074s	
	0.1389p	
HD 35411	0.133s	15
HD 35715	0.0954s	16
	0.0932s	
HD 44743	0.2512988ps	p: 17, s: 18, rv: 19
	0.25003ps	17, 18, 20, rv: 19
	0.23904ps	17, rv: 19, 21
HD 46328	0.2095754p	22
HD 50707	0.18464ps	22
	0.1932ps	23
	0.1924p	
HD 52918	0.191207ps	24
	0.204517ps	
HD 56014	0.0919p	p: 25
HD 59864	0.238p:	26
	0.243p:	
HD 61068	0.166385p	22
	0.164921p	
HD 64365	0.201584p	This work
	+ more	
HD 64722	0.11541p	27
	0.1168 or 0.1323p	
HD 71913	0.20578p	28
HD 78616	0.21569ps	18, 22
HD 80383	0.18316p	29
	0.18647p	
	0.1847p	
HD 90288	0.10954p	29
	0.12024p	
	0.10344p	
	0.1295p	
HD 303068	0.1457p	30
	0.1487p	

TABLE 4—*Continued*

Identifier (1)	Period (days) (2)	Reference, (Note) (3)
HD 303067	0.1684p	30; similar situation as for HD 303068
	0.1751p	
	0.1643p	
V403 Car	0.251p	30; similar situation as for HD 303068
V412 Car	0.114p:	30
V404 Car	0.16p:	30
V405 Car	0.152p	30
	0.158p	
	0.1841p:	22
V378 Car	0.1600p	30
	0.2070p	
	0.177p:	
V440 Car	0.179p:	31
V406 Car	0.1756p	30; similar situation as for HD 303068
	0.1785p	
V380 Car	0.2274p	30
V381 Car	0.1773p	30
	0.1502p	32
	0.1397p	32
HD 109885	0.17054p	29
	0.16806p	
	0.1616p	
	0.1752p	
HD 111123	0.1911846ps	33
	0.1678228ps	34
	0.1827430ps	
BS Cru	0.151p	35
	0.156p	
	0.163p	
	0.137p	
	0.157978p	36
NGC 4755 113	0.233p	37
NGC 4755 405	0.125p	35
	0.128p	
CT Cru	0.131p	35
CV Cru	0.179p	35
	0.128p	
CZ Cru	0.159p	35
	0.108p	
	0.1386p	30
CX Cru	0.182p	35
CY Cru	0.159p	37
NGC 4755 210	0.093p	35
BW Cru	0.205p	35
	0.220p	
	0.190p	
	0.1623p	36
HD 112481	0.254537p	22
	0.259618p	
HD 116658	0.173787ps	38
HD 118716	0.169608ps	39, 40
	0.17696ps	40, 41
	0.1617s	
	0.1356s	
	0.1308s	
HD 122451	0.153496s	42
	0.155920s	(Balona's photometric period uncertain)
	0.153960s	
HD 126341	0.17736934ps	43
HD 129056	0.25984663ps	22
	0.2368ps	44

TABLE 4—*Continued*

Identifier (1)	Period (days) (2)	Reference, (Note) (3)
HD 129557	0.1275504ps	45
	0.142516p	46
	0.134769p	
HD 129929	0.1547581p	47
	0.1433013p	
	0.1550486p	
	0.1430527p	
	0.1517234p	
	0.1435509p	
HD 136298	0.198ps	39, 48
HD 144470	0.067s	49
HD 145794	0.15991p	50
	0.1918p	
HD 147165	0.246829ps	51
	0.239661ps	
HD 147985	0.132312ps	52
	0.144930ps	18
	0.156656ps	
V945 Sco	0.06706p	53
V1032 Sco	0.11928p	54
	0.07699p	
	0.12040p	
V946 Sco	0.09878p	53
	0.09544p	
	0.09071p	
	0.08550p	
	0.08302p	
V964 Sco	0.087846p	54
	0.067575p	
	0.055328p	
V947 Sco	0.10788p	53
	0.06096p	
V920 Sco	0.10119p	53
	0.10765p	
	0.10389p	
	0.12137p	
	0.09114p	
HD 156327B	0.146p	55
	0.136p	
HD 156662	0.16890p	52
	0.18861p	
	0.16978p	
HD 157056	0.1405280ps	56
	0.13722p	
	0.13569p	
	0.13391p	
	0.12877p	
	0.12699p	
	0.12542p	
HD 157485	0.2212p	28
	0.2240p	
HD 158926	0.2138272ps	57
	+ more	
HD 160578	0.19983ps	57
HD 163472	0.13989010ps	10, 58
	0.1466s	10, 59
HD 164340	0.1529341p	60
	0.1567948	60
HD 165174	0.303ps	10, 61
HD 165812	0.1759p	28
	0.2180p	
HD 166540	0.23299p	62
	0.22729p	
HD 180642	0.18225ps	10, 28

TABLE 4—*Continued*

Identifier (1)	Period (days) (2)	Reference, (Note) (3)
NGC 6910 18	0.156539p	63
	0.162486p	
	0.148877p	
NGC 6910 16	0.192198p	63
	0.171077p	
	0.239556p	
NGC 6910 14	0.190396p	63
NGC 6910 27	0.143010p	63
V2187 Cyg	0.25388p	64
HD 199140	0.20104444ps	65, 66
HD 203664	0.16587ps	10, 28
	+more	10
HD 205021	0.1904870ps	67
	0.2031s	68
	0.1967s	
	0.1859s	
	0.18460s	
NGC 7235 8	0.202890p	69
	0.177898p	
HN Aqr	0.15231ps	70, 71
HD 214993	0.23583ps	72
	0.19738ps	73
	0.19309ps	
	0.1917p	
	0.1884p	
	0.18747ps	
	0.18215ps	
	0.1711p	
	0.1350p	
HD 216916	0.1691670ps	74
	0.1708555ps	75
	0.1817325ps	
	0.1816843p	

Notes.—The letter “p” after a given period denotes a photometric detection and “s” denotes a spectroscopic one. Uncertainties of the periods are in the last digits. Table 4 is also available in machine-readable form in the electronic edition of the *Astrophysical Journal Supplement*.

References.—(1) Valtier et al. 1985; (2) Robb et al. 2000; (3) Pigulski et al. 2001; (4) Krzesiński et al. 1999; (5) Gomez-Forrellad 2000; (6) Krzesiński & Pigulski 1997; (7) Campos & Smith 1980; (8) Cugier & Nowak 1997; (9) Jarzebowski et al. 1981; (10) De Cat et al. 2004; (11) Struve & Zebergs 1959; (12) De Cat et al. 2000; (13) Gies et al. 1999; (14) De Ridder et al. 2004; (15) De Mey et al. 1996; (16) Telting et al. 2001; (17) Shobbrook 1973a; (18) Aerts et al. 1994; (19) Struve 1950; (20) Balona et al. 1996; (21) Kubiak 1980; (22) Heynderickx 1992; (23) Lynds et al. 1956; (24) Balona et al. 2002; (25) Balona & Krisciunas 1994; (26) Sterken & Jerzykiewicz 1990; (27) Sterken & Jerzykiewicz 1980; (28) Aerts 2000; (29) Handler et al. 2003; (30) Balona et al. 1997; (31) Balona 1994; (32) Freyhammer et al. 2004; (33) Cuypers et al. 2002; (34) Aerts et al. 1998; (35) Stankov et al. 2002; (36) Koen 1993; (37) Balona & Koen 1994; (38) Lomb 1978; (39) Shobbrook 1972; (40) Schrijvers et al. 2004; (41) Schrijvers 1999; (42) Ausseloos et al. 2002; (43) Cuypers 1987; (44) Mathias et al. 1994a; (45) Vander Linden & Sterken 1985; (46) Sterken & Jerzykiewicz 1983; (47) Aerts et al. 2004b; (48) Lloyd & Pike 1988; (49) Telting & Schrijvers 1998; (50) Waelkens & Heynderickx 1989; (51) Chapellier & Valtier 1992; (52) Waelkens & Cuypers 1985; (53) Balona & Shobbrook 1983; (54) Balona & Engelbrecht 1985a; (55) Paardekooper et al. 2002; (56) Handler et al. 2005; (57) Lomb & Shobbrook 1975; (58) Kubiak & Seggewiss 1984; (59) Neiner et al. 2003; (60) J. Molenda-Żakowicz & G. Połubek 2005, in preparation; (61) Cuypers et al. 1989; (62) Waelkens et al. 1991; (63) Kołaczkowski et al. 2004a; (64) Pigulski & Kołaczkowski 1998; (65) Aerts et al. 1995; (66) Sterken et al. 1993; (67) Telting et al. 1997; (68) Stebbins & Kron 1954; (69) Pigulski et al. 1997; (70) Kilkenny & van Wyk 1990; (71) Dufton et al. 1998; (72) G. Handler et al. 2005, in preparation; (73) Mathias et al. 1994b; (74) Lehmann et al. 2001; (75) Jerzykiewicz & Pigulski 1999.

boundary decreases to 0.036 day). Assuming twice the photometric period as the rotation period of a possible rotationally variable star, we derive a rotational velocity of $\sim$800 km s^{-1}. This value is higher than the break-up velocity and excludes the possibility of rotational variability. Therefore, V595 Per is confirmed to be a β Cephei star.

HD 24760 (ϵ Per).—Preliminary results by K. Uytterhoeven (2004, private communication) on this star show that several frequencies are probably excited in ϵ Per and that harmonics are also present. More research on this star is currently in progress. See also Harmanec (1999) and Gies et al. (1999).

HD 35715 (ψ^2 Ori).—Is also an ellipsoidal variable. Pulsation was not detected photometrically but in line profiles.

HD 52918 (19 Mon).—This is also a Be star (Hα emission discovered by Irvine (1975)) with a relatively high pulsation amplitude that may be connected to shock phenomena in the atmosphere. Balona et al. (2002) find three frequencies, two of them are due to β Cephei-type pulsation.

HD 56014 (27 (BW) CMa).—Balona (1995a) lists this star as a periodic Be star with a period of $P = 1.262$ days. Short-period pulsations were, however, detected by Balona & Krisciunas (1994), who report the redetection of a period of $P = 0.0918$ day. Next to HD 52918, this would be the second star to exhibit Be as well as β Cephei type variability. It is also a close optical double system, and therefore it is possible that the β Cephei variability does not originate in the Be star. More research on this star is needed.

HD 122451 (β Cen).—Very eccentric double-lined spectroscopic binary with two β Cephei components.

HD 158926 (λ Sco).—This is a triple system with a variable dominant period of around 4.679410 cycles day^{-1}. There are three additional significant frequencies that can, however, be attributed to either the primary or the tertiary component of this system (Uytterhoeven et al. 2004a, 2004b).

HD 160578 (κ Sco).—K. Uytterhoeven (2004, private communication) confirms one pulsation mode at 4.99922 cycles day^{-1}, together with its first harmonic. All other additional frequencies mentioned in the literature can be explained by means of a rotational modulation effect between a nonradial mode and the rotation of the star in presence of spots on the stellar surface, but a pure nonradial pulsation model cannot be excluded at the time being (Harmanec et al. 2004).

HD 165174 (V986 Oph).—This is by far the hottest, most massive and most luminous β Cephei star; it also has one of the longest periods. The nature of this mild Be star has been discussed in detail by Cuypers et al. (1989), and we agree with these authors that there is no compelling reason not to consider it a β Cephei star. It satisfies our definition of this group of pulsating stars.

8.3. *Notes on Individual Candidate β Cephei Stars*

NGC 1502 37.—According to Delgado et al. (1992), Hill (1967) confused this star with NGC 1502 A=NGC 1502 1. We give its correct identification here and note in addition that NGC 1502 37 is a visual binary.

HD 34656.—This O7e III star was investigated by Fullerton et al. (1991), who detected radial velocity variations with a period of 8.81 hr, of which we are however not convinced. Fullerton et al. (1991) inferred that HD 34656 is a pulsating star and excluded the possibilities of the variations originating in rotational modulation of a weak surface feature or motion in a binary system. They associated its variability with β Cephei type pulsation but were reluctant to identify it as such a variable at that time. This star is often cited to be the only O-type β Cephei star pulsator, despite the authors' caution.

HD 36512 (ν Ori).—Although the periods claimed for this star in the literature imply SPB-like variability, our amplitude spectrum of its *Hipparcos* data has the highest peak at a period of 0.146 day indicating a β Cephei nature of the pulsation.

HD 43078.—Hill (1967) suggests the presence of a fairly convincing 0.23887 day period for this star, which is, however, not present in the *Hipparcos* data. The Strömgren colors of this star are unusual, placing it considerably below the ZAMS, and are inconsistent with its spectral classification.

HD 53755 (V569 Mon).—Balona (1977) found a period of 0.18 day. In the *Hipparcos* data we could not detect any convincing periodicity. The highest peak in the amplitude spectrum of these data is at 0.66 day, which is too long for β Cephei type pulsation.

HD 63949 (QS Pup).—There are doubts about the presence of the 0.1182 day variation in the 1975 data set as well as about the 0.108 day variation (C. Sterken 2003, private communication). The *Hipparcos* amplitude spectrum for this star indicates no variability exceeding 4 mmag.

HD 74455.—Morris (1985) suspected it to be an ellipsoidal variable; confirmed in *Hipparcos* data (this work); see also Waelkens & Rufener (1983a).

HD 74575 (α Pyx).—Van Hoof (1973a) concluded from RV measurements that this star is a β Cephei variable; Balona (1977) found it not variable in RV, whereas Sterken & Vander Linden (1983) found a well-defined sinusoidal velocity curve with a probable period of 5 hr, but from one night only.

HD 86466 (IV Vel).—The available data are not conclusive. Jakate (1979b) places this star in his "suspected β Cephei stars" table. The highest peak in the amplitude spectrum of the *Hipparcos* data of the star is at a 0.105 day period, but a 0.55 day variation is almost equally probable.

HD 96446 (V430 Car).—This Bp star shows a 0.8514 day period resulting from rotation, but a possible secondary period near 0.26 day could be due to pulsation (Matthews & Bohlender 1991).

NGC 3766 67 (V847 Cen).—The frequency of the light variation of this candidate β Cephei star is close to 4 cycles per sidereal day, which could indicate an extinction problem, and low-frequency variability also seems to exist.

HD 104337.—Ellipsoidal variability is confirmed by *Hipparcos* data (this work).

HD 120307 (ν Cen).—This is a single-lined spectroscopic binary and a Be star; see Cuypers et al. (1989). The period of 0.4255 day results in $Q = 0.107$ day, which is too large for β Cephei pulsation. Most of the other periods found for this star are too long for β Cephei pulsation as well. Schrijvers & Telting (2002), however, detected seven frequencies spectroscopically that they attributed to high degree modes ($\ell > 5$), which could be connected to β Cephei type pulsation or be ζ Ophiuchi-like line profile variability.

HD 143018.—Ellipsoidal variable with $P = 1.570$ day, see Stickland et al. (1996).

HD 144218 (β Sco A).—Binary system; β Cep candidate with a tentative period of $P = 0.1733$ day (see Holmgren et al. 1997).

HD 149881 (V600 Her).—Possibly an ellipsoidal variable with a β Cephei component (De Cat et al. 2004). Pulsational variability not detectable in *Hipparcos* data within a limit of 4.5 mmag.

HD 176502 (V543 Lyr).—Visual double star. The *Hipparcos* data clearly indicate that the star is variable, but the timescale remains unknown because of aliasing; it could be either several days or 2.5 hr.

NGC 6871 14 (V1820 Cyg).—Few variability measurements of this candidate β Cephei star are available, and the star is underluminous for the rather longperiod claimed.

HD 210808 (V447 Cep).—The analysis of this star's *Hipparcos* photometry reveals a primary period of 0.314 day, and a possible secondary period of 0.460 day (Koen 2001). The late spectral type of the star is inconsistent with its Strömgren Hβ index (2.639), suggesting a possible Be nature. The star is also known as a visual binary and as an X-ray source.

8.4. *Notes on Individual Rejected β Cephei Stars*

HD 13544 (V353 Per).—Two periods of 0.6647 and 0.7724 day explain this star's *Hipparcos* photometry.

HD 13831 (V473 Per).—Be star. Published data indicate short-period variability, but *Hipparcos* photometry (this work) fails to confirm that.

HD 16429A (V482 Cas).—This star is a speckle binary in a triple system; also a radio emitter and an X-ray source. Timescales present in its *Hipparcos* light curves are of the order of $P = 1.7$–2.5 days.

HD 24640.—The published radial velocity curves are not convincing. Variability timescales in the star's *Hipparcos* photometry are longer than 1.5 days.

HD 28446 (1 (DL) Cam).—Our analysis of this star's *Hipparcos* photometry results in candidate periods considerably longer than those of β Cephei type pulsation; it is also possible that parts of eclipses were observed by the satellite.

HD 35468 (γ Ori).—Krisciunas (1994) and Krisciunas & Luedeke (1996) suspect this is a low-amplitude, possibly irregular variable. However, their measurements are too scarcely sampled to enable a search for periods in the range of β Cephei pulsations.

HD 37776 (V901 Ori).—This is a rapidly rotating magnetic CP star (Catalano & Renson 1998). We determine a period of 1.538 days from its *Hipparcos* photometry.

HD 43818 (11 (LU) Gem).—Most recent data (Percy 1984) show no evidence for variability on a timescale <0.2 day but on a timescale of >0.2 day or more likely >0.5 day. The period derived in that paper is $P = 1.25$ days. Period from *Hipparcos* $\sim$2.1 days (this work).

HD 51309 (ι CMa).—There are no new data since the work of Balona & Engelbrecht (1985b). In their work the star was defined as a 53 Per star with a tentative period of 1.3947 days.

HD 57219 (ν02 Pup).—Our analysis of this star's *Hipparcos* data shows little evidence for variability, contrary to the suggestion of low-signal variability by Balona et al. (1992). The spectral classification of the star is also a matter of debate (see Dachs et al. 1981). Renson et al. (1991) classify the star as B3 and He strong, which seems to be the classification most consistent with its Strömgren colors.

HD 65575 (χ Car).—The *Hipparcos* light curves show no evidence for variability within a limit of 3 mmag.

HD 104841 (θ^2 Cru).—Claimed to be an ultra–short-period pulsator (Jakate 1979b), but not confirmed. The *Hipparcos* photometry is consistent with a double-wave light variation with a period of 3.4 days.

HD 106490 (δ Cru).—Variability dubious, and if present, of long period (3.6 days). *Hipparcos* photometry shows no variability above 3 mmag.

HD 109668 (α Mus).—Variability dubious, and if present, of long period. *Hipparcos* photometry shows no variability above 2.5 mmag. Radial velocity variable.

HD 122980 (χ Cen).—No short-period light variations. The *Hipparcos* data indicate possible slower low-amplitude variability (this work). Radial velocity variable.

HD 130903 (V1018 Cen).—The *Hipparcos* data can be folded with a period of 1.65064 days to give a double-wave light curve. Although only few measurements are available, we suspect the star is a binary-induced variable.

HD 160762 (ι Her).—Slowly pulsating B star with suspected, but unconfirmed shorter period variations. Cannot be considered to be a β Cephei star for the time being.

HD 188439 (V819 Cyg).—The *Hipparcos* period of this OB runaway star is 0.71373 day, resulting in $Q = 0.10$ day.

HD 195556 (ω^1 Cyg).—The available data, including the *Hipparcos* photometry indicate several possible or unstable periods, all of which are, however, longer than 15 hr.

HD 217811 (LN And).—Claimed to be an ultra–short-period pulsator, but not confirmed. A three-day period explains the variations in the *Hipparcos* photometry.

8.5. *Notes on Individual Frequencies*

HD 24760 (ϵ Per).—A period at 0.0945 day was detected by Smith et al. (1987) as well as Gies et al. (1999). We assume that this is a harmonic of the main pulsation mode at $P = 0.1887$ day.

HD 35411 (η Ori).—A period at 0.43208 day was found by Waelkens & Lampens (1988) in their photometric data. It is doubtful if it originates from pulsation.

HD 52918 (19 Mon).—A period at 5.88 days was also detected (Balona et al. 2002), which is too long for β Cephei-type pulsation.

HD 59864 (V350 Pup).—Sterken & Jerzykiewicz (1990) demonstrated the multiperiodicity of this star, but could not give unambiguous period determinations because of aliasing. The choice of the primary frequency also affects all others. The periods we list are the most likely ones from the work by Sterken & Jerzykiewicz (1990).

HD 61068 (PT Pup).—Heynderickx (1992) reports two frequencies that we list in Table 4. This author, however, noted aliasing problems in his period determinations. Amplitude variability also seems present. In addition, the *Hipparcos* data for this star (Koen & Eyer 2002) do not confirm the periodicities listed by Heynderickx (1992). More observations of this star are clearly necessary to determine the periodic content of its variability properly.

HD 64365 (QU Pup).—Frequency analyses by Sterken & Jerzykiewicz (1980) and Heynderickx (1992) had periods of 0.1678 and 0.1927 day in common. However, our analysis of the *Hipparcos* photometry of that star resulted in a 0.2016 day period, which is the 1 cycle day^{-1} alias of the 0.1678 day period given by the previous authors. As we suspect that the prewhitening of this erroneous period from single-site data had generated spurious secondary signals, we only list the frequency found in the *Hipparcos* data. We do point out that the star is multiperiodic in any case.

HD 64722 (V372 Car).—Aliasing mistake by Heynderickx (1992), solved by reanalysis of *Hipparcos* data, this work.

HD 78616 (KK Vel).—There may be another independent pulsation mode at half the period we listed.

HD 303068.—Different authors list up to five different frequencies (see Engelbrecht 1986; Heynderickx 1992), of which only two are in common in the different studies.

V404 Car.—Additional periods of 0.1742 and 0.1506 day are listed by Engelbrecht (1986), but they were not confirmed by other work.

HD 111123 (β Cru).—More frequencies are possibly present, but we are unsure whether they originate from pulsation (Cuypers et al. 2002).

HD 116658 (α Vir).—The only periodicity that we regard convincing in the analyses of this star is 0.1738 day. Smith (1985) found a number of additional signals in his line-profile analysis. We support the suggestion by Aerts & De Cat (2003) that more spectroscopic data have to be analyzed before a definite conclusion about the presence of the additional periodicities can be made.

HD 136298 (δ Lup).—Photometric period likely an alias of the spectroscopic one quoted.

HD 145794 (V349 Nor).—The value of the second period of this star is uncertain because of aliasing (Waelkens & Heynderickx 1989).

HD 156327B (V1035 Sco).—The *V* amplitude is 35 mmag; spectroscopic variability was detected, but no period could be determined.

During most of this work, A. S. was a European Space Agency Postdoctoral Research Fellow. G. H. acknowledges support from the Austrian Fonds zur Förderung der wissenschaftlichen Forschung under grant R12-N02.

Several people have considerably helped the authors during the course of this work. First and foremost, we are indebted to Peter De Cat for his generous support of this work and for his valuable comments that improved this paper. One of the starting points for this work was his online catalog of β Cephei stars.

We are grateful to Alosha Pamyatnykh for sending us his compilation of β Cephei stars, for supplying theoretical instability strip boundaries and for permission to use the Warsaw-New Jersey code. We also thank Andrzej Pigulski and Katrien Uytterhoeven for making some results available to us before publication, as well as Chris Sterken and Lars Freyhammer for helpful comments on some stars. Finally, we wish to thank Mike Jerzykiewicz, Conny Aerts, and (again) Alosha Pamyatnykh, Andrzej Pigulski, and Peter De Cat for their valuable comments and suggestions on a draft version of this paper.

This research has made use of the SIMBAD database operated at CDS Strasbourg, France. In this work we made use of The General Catalog of Photometric Data (GCPD) II by Mermilliod et al. (1997).

REFERENCES

Abt, H. A., Levato, H., & Grosso, M. 2002, ApJ, 573, 359
Adelman, S. J. 2001, A&A, 367, 297
Aerts, C. 1996, A&A, 314, 115
———. 2000, A&A, 361, 245
Aerts, C., & De Cat, P. 2003, Space Sci. Rev., 105, 453
Aerts, C., Waelkens, C., & de Pauw, M. 1994, A&A, 286, 136
Aerts, C., et al. 1998, A&A, 329, 137
———. 1999, A&A, 343, 872
———. 1995, A&A, 301, 781
———. 2003, Science, 300, 1926
———. 2004a, MNRAS, 347, 463
———. 2004b, A&A, 415, 241
Antokhina, E. A., & Barannikov, A. A. 1996, Pis'ma Astron. Zh., 22, 819
Arentoft, T., et al. 2001, A&A, 380, 599
Ausseloos, M., Scuflaire, R., Thoul, A., & Aerts, C. 2004, MNRAS, 355, 352
Ausseloos, M., et al. 2002, A&A, 384, 209
Baglin, A. 2003, Adv. Space Res., 31, 345
Balona, L. A. 1975, MmRAS, 78, 51
———, L. A. 1977, MmRAS, 84, 101
———. 1982, Inf. Bull. Variable Stars, 2120, 1
———. 1983, MNRAS, 203, 1041
———. 1990, MNRAS, 245, 92
———. 1992, MNRAS, 254, 404
———. 1994, MNRAS, 267, 1060
———. 1995a, MNRAS, 277, 1547
———. 1995b, Ap&SS, 230, 17
Balona, L. A., Bregman, L., Letsapa, B. A., Magoro, B. T., & Walsh, S. E. 1996, Inf. Bull. Variable Stars, 4313, 1
Balona, L. A., & Cuypers, J. 1993, MNRAS, 261, 1
Balona, L. A., Cuypers, J., & Marang, F. 1992, A&AS, 92, 533
Balona, L. A., & Dziembowski, W. A. 1999, MNRAS, 309, 221
Balona, L. A., Dziembowski, W. A., & Pamyatnykh, A. 1997, MNRAS, 289, 25
Balona, L. A., & Engelbrecht, C. 1981, in Workshop: Pulsating B-Stars, 195
———. 1985a, MNRAS, 212, 889
———. 1985b, MNRAS, 214, 559
———. 1986, MNRAS, 219, 131
Balona, L. A., & Koen, C. 1994, MNRAS, 267, 1071
Balona, L. A., & Krisciunas, K. 1994, Inf. Bull. Variable Stars, 4022, 1
Balona, L. A., & Laney, C. D. 1995, MNRAS, 276, 627
Balona, L. A., & Shobbrook, R. R. 1983, MNRAS, 205, 309
———. 1984, MNRAS, 211, 375
Balona, L. A., et al. 2002, MNRAS, 333, 952
Batten, A. H., Fletcher, J. M., & MacCarthy, D. G. 1989, Publ. Dom. Astrophys. Obs. Victoria, 17, 1
Beauchamp, A., Moffat, A. F. J., & Drissen, L. 1994, ApJS, 93, 187
Bernacca, P. L., & Perinotto, M. 1970, Contrib. Obs. Astrophys. Univ. Padova, 239, 1
Breger, M. 1979, PASP, 91, 5
———. 1982, PASP, 94, 845
Breger, M., Balona, L. A., & Grothues, H.-G. 1991, A&A, 243, 160
Briers, R. C. 1971, Ph.D. thesis, KU Leuven, Belgium
Briquet, M., et al. 2004, A&A, 413, 273
Buzasi, D., et al. 2000, ApJ, 532, L133
Campos, A. J., & Smith, M. A. 1980, ApJ, 238, 250
Catalano, F. A., & Renson, P. 1998, A&AS, 127, 421
Chapellier, E., & Valtier, J. C. 1992, A&A, 257, 587
Chapellier, E., et al. 2000, A&A, 362, 189
———. 1998, A&A, 331, 1046
Collins, G. W. 1987, in IAU Colloq. 92, Physics of Be Stars (Cambridge: Cambridge Univ. Press), 3
Coté, J., & van Kerkwijk, M. H. 1993, A&A, 274, 870
Cousins, A. W. J. 1982, Inf. Bull. Variable Stars, 2158, 1
Cugier, H., Dziembowski, W. A., & Pamyatnykh, A. A. 1994, A&A, 291, 143
Cugier, H., & Nowak, D. 1997, A&A, 326, 620
Cuypers, J. 1987, A&AS, 69, 445
Cuypers, J., Balona, L. A., & Marang, F. 1989, A&AS, 81, 151
Cuypers, J., et al. 2002, A&A, 392, 599
Dachs, J., & Kaiser, D. 1984, A&AS, 58, 411
Dachs, J., et al. 1981, A&AS, 43, 427
De Cat, P. 2002, in ASP Conf. Ser. 259, Radial and Nonradial Pulsationsn as Probes of Stellar Physics, ed. C. Aerts, T. M. Bedding, & J. Christensen-Dalsgaard (San Francisco: ASP), 196
De Cat, P., & Aerts, C. 2002, A&A, 393, 965
De Cat, P., Telting, J., Aerts, C., & Mathias, P. 2000, A&A, 359, 539
De Cat, P., et al. 2004, in ASP Conf. Ser. 310, Variable Stars in the Local Group, ed. D. Kurtz & K. Pollard (San Francisco: ASP), 238
De Mey, K., Aerts, C., Waelkens, C., & Van Winckel, H. 1996, A&A, 310, 164
De Mey, K., et al. 1997, A&A, 324, 1096
De Ridder, J., Gordon, K. D., Mulliss, C. L., & Aerts, C. 1999, A&A, 341, 574
De Ridder, J., et al. 2004, MNRAS, 351, 324
Delgado, A. J., Alfaro, E. J., Garcia-Pelayo, J. M., & Garrido, R. 1992, AJ, 103, 891
Delgado, A. J., Alfaro, E. J., & Garrido, R. 1985, A&AS, 61, 89
Delgado, A. J., Garcia-Pelayo, J. M., Garrido, R., Vidal, S., & Alfaro, E. J. 1984, A&AS, 58, 447
Deng, L., & Xiong, D. R. 2001, MNRAS, 327, 881
Deupree, R. 1970, BAAS, 2, 308
Dommanget, J., & Nys, O. 2002, VizieR Online Catalog Data,1274
Duflot, M., Figon, P., & Meyssonnier, N. 1995, A&AS, 114, 269
Dufton, P. L., et al. 1998, MNRAS, 297, 565
Dziembowski, W. A., & Jerzykiewicz, M. 1996, A&A, 306, 436
———. 1999, A&A, 341, 480
Dziembowski, W., & Pamyatnykh, A. 1993, MNRAS, 262, 204
Elst, E. W. 1979a, Messenger, 17, 6
———. 1979b, Inf. Bull. Variable Stars, 1562, 1

Engelbrecht, C. A. 1986, MNRAS, 223, 189
ESA. 1997, VizieR Online Data Catalog, 239
Evans, D. S. 1967, in IAU Symp. 30, Determination of Radial Velocities and their Applications, 57
Feast, M. W. 1958, MNRAS, 118, 618
———. 1963, MNRAS, 126, 11
Flower, P. J. 1996, ApJ, 469, 355
Freyhammer, L. M., et al. 2004, in ASP Conf. Ser. 318, Spectroscopically and Spatially Resolving the Components of Close Binary Stars, ed. R. W. Hidlitch, H. Hensberge & K. Pavlovski (San Francisco: ASP), 334
Frost, E. B. 1902, ApJ, 15, 340
———. 1906, ApJ, 24, 259
Fullerton, A. W., Gies, D. R., & Bolton, C. T. 1991, ApJ, 368, L35
García, B., & Mermilliod, J. C. 2001, A&A, 368, 122
Garrido, R., & Delgado, A. J. 1982, Inf. Bull. Variable Stars, 2080, 1
Garrison, R. F., Hiltner, W. A., & Schild, R. E. 1977, ApJS, 35, 111
Gautschy, A., & Saio, H. 1993, MNRAS, 262, 213
Gerbaldi, M., Faraggiana, R., & Balin, N. 2001, A&A, 379, 162
Gies, D. R., et al. 1999, ApJ, 525, 420
Gomez-Forrellad, J. M. 2000, Inf. Bull. Variable Stars, 4924, 1
Goosens, M., Lampens, P., de Maerschalck, D., & Schrooten, M. 1984, A&A, 140, 223
Grady, C. A., Bjorkman, K. S., & Snow, T. P. 1987, ApJ, 320, 376
Green, E. M., et al. 2003, ApJ, 583, L31
Guthnick, P. 1913, Astron. Nachr., 195, 265
Gutierrez-Moreno, A., & Moreno, H. 1968, ApJS, 15, 459
Hadrava, P., & Harmanec, P. 1996, A&A, 315, L401
Haefner, R., & Drechsel, H. 1986, Ap&SS, 121, 205
Hambly, N. C., et al. 1994, MNRAS, 267, 1103
Handler, G., Shobbrook, R. R., & Mokgwetsi, T. 2005, MNRAS, submitted
Handler, G., et al. 2003, MNRAS, 341, 1005
———. 2004, MNRAS, 347, 454
Harmanec, P. 1999, A&A, 341, 867
Harmanec, P., Uytterhoeven, K., & Aerts, C. 2004, A&AS, 422, 1013
Henroteau, F. 1918, Lick Obs. Bull., 311, 155
———. 1922, Publ. Dom. Obs. Ottawa, 8, 1
Heynderickx, D. 1992, A&AS, 96, 207
Heynderickx, D., Waelkens, C., & Smeyers, P. 1994, A&AS, 105, 447
Hill, G. 1967, ApJS, 14, 263
Hill, G., Odgers, G. J., & Drolet, B. 1976, A&A, 51, 1
Hill, P. W. 1970, MNRAS, 150, 23
———. 1971, MmRAS, 75, 1
Hill, P. W., Kilkenny, D., & van Breda, I. G. 1974, MNRAS, 168, 451
Hoag, A. A., et al. 1961, Publ. US Naval Obs. Second Series, 17, 345
Holmgren, D., Hadrava, P., Harmanec, P., Koubsky, P., & Kubat, J. 1997, A&A, 322, 565
Houk, N. 1982, Michigan Spectral Survey, Vol. 3 (Ann Arbor: Univ. Michigan)
Iglesias, C. A., Rogers, F. J., & Wilson, B. G. 1987, ApJ, 322, L45
Irvine, N. J. 1975, ApJ, 196, 773
Jakate, S. M. 1978, AJ, 83, 1179
———. 1979a, AJ, 84, 1042
———. 1979b, AJ, 84, 552
Janík, J., et al. 2003, A&A, 408, 611
Jarzebowski, T., Jerzykiewics, M., Rios-Herrera, M., & Rios-Berumen, M. 1981, Rev. Mx. AA, 5, 61
Jaschek, M., Jaschek, C., Hubert-Delplace, A.-M., & Hubert, H. 1980, A&AS, 42, 103
Jerzykiewicz, M. 1972, PASP, 84, 718
———. 1975, Acta Astron., 25, 81
———. 1978, Acta Astron., 28, 465
———. 1993, A&AS, 97, 421
Jerzykiewicz, M., Handler, G., Shobbrook, R. R., Pigulski, A., Medupe, R., Mokgwetsi, T., Tlhaqwane, P., & Rodríguez, E. 2005, MNRAS, in press
Jerzykiewicz, M., Kopacki, G., Molenda-Zakowicz, J., & Kołaczkowski, Z. 2003, Acta Astron., 53, 151
Jerzykiewicz, M., & Pigulski, A. 1999, MNRAS, 310, 804
Jerzykiewicz, M., & Sterken, C. 1977, Acta Astron., 27, 365
———. 1984, MNRAS, 211, 297
Jerzykiewicz, M., Sterken, C., & Kubiak, M. 1988, A&AS, 72, 449
Jones, D. H. P. 1960, MNRAS, 120, 43
Kazarovets, A. V., et al. 1999, Inf. Bull. Variable Stars, 4659, 1
Khokhlova, V. L., Vasilchenko, D. V., Stepanov, V. V., & Romanyuk, I. I. 2000, Astron. Lett., 26, 177
Kilkenny, D., & Hill, P. W. 1975, MNRAS, 172, 649
Kilkenny, D., Koen, C., O'Donoghue, D., & Stobie, R. S. 1997, MNRAS, 285, 640
Kilkenny, D., & van Wyk, F. 1990, MNRAS, 244, 727
Koen, C. 1993, MNRAS, 264, 165
Koen, C. 2001, MNRAS, 321, 44
Koen, C., & Eyer, L. 2002, MNRAS, 331, 45
Kołaczkowski, Z., Kopacki, G., Pigulski, A., & Michalska, G. 2004a, Acta Astron., 54, 33
Kołaczkowski, Z., Pigulski, A., & Kopacki, G. 2002, in ASP Conf. Ser. 259, Radial and Nonradial Pulsationsn as Probes of Stellar Physics, ed. C. Aerts, T. R. Bedding, & J. Christensen-Dalsgaard (San Francisco: ASP), 150
Kołaczkowski, Z., et al. 2004b, in ASP Conf. Ser. 310, Variable Stars in the Local Group, ed. D. W. Kurtz & K. Pollard (San Francisco: ASP), 225
Krisciunas, K. 1994, Inf. Bull. Variable Stars, 4028, 1
Krisciunas, K., & Luedeke, K. D. 1996, Inf. Bull. Variable Stars, 4355, 1
Krzesiński, J., & Pigulski, A. 1997, A&A, 325, 987
Krzesiński, J., Pigulski, A., & Kołaczkowski, Z. 1999, A&A, 345, 505
Kubiak, M. 1980, Acta Astron., 30, 41
Kubiak, M., & Seggewiss, W. 1984, Acta Astron., 34, 41
Kukarkin, B. V., et al. 1971, in General Catalogue of Variable Stars (3rd ed.)
———. 1981, Nachr. Vereinigung der Sternfreunde, 1
Le Contel, J.-M., Mathias, P., Chapellier, E., & Valtier, J.-C. 2001, A&A, 380, 277
Ledoux, P. 1951, ApJ, 114, 373
Lehmann, H., et al. 2001, A&A, 367, 236
Leone, F., & Catanzaro, G. 1998, A&A, 331, 627
Lesh, J. R., & Aizenman, M. L. 1978, ARA&A, 16, 215
Lester, J. B. 1979, ApJ, 233, 644
Levato, H., Malaroda, S., Morrell, N., & Solivella, G. 1987, ApJS, 64, 487
Li, J. Z., & Hu, J. Y. 1998, A&AS, 132, 173
Lloyd, C., & Pike, C. D. 1988, A&AS, 76, 121
Lomb, N. R. 1978, MNRAS, 185, 325
Lomb, N. R., & Shobbrook, R. R. 1975, MNRAS, 173, 709
Lynds, C. R. 1959, ApJ, 130, 577
Lynds, C. R., Sahade, J., & Struve, O. 1956, ApJ, 124, 321
Maciejewski, G., Czart, K., & Niedzielski, A. 2004, Inf. Bull. Variable Stars, 5518, 1
Mahra, H. S., & Mohan, V. 1979, Inf. Bull. Variable Stars, 1698, 1
Mathias, P., Aerts, C., de Pauw, M., Gillet, D., & Waelkens, C. 1994a, A&A, 283, 813
Mathias, P., Aerts, C., Gillet, D., & Waelkens, C. 1994b, A&A, 289, 875
Mathias, P., & Waelkens, C. 1995, A&A, 300, 200
Mathias, P., et al. 2001, A&A, 379, 905
Mathys, G. 1994, in IAU Symp. 162, Pulsation, Rotation, and Mass Loss in Early-Type Stars, 169
Matthews, J. M., & Bohlender, D. A. 1991, A&A, 243, 148
Matthews, J. M., Walker, G. A. H., Harmanec, P., Yang, S., & Wehlau, W. H. 1991, MNRAS, 248, 787
Matthews, J. M., et al. 2000, in ASP Conf. Ser. 203, The Impact of Large-Scale Surveys on Pulsating Star Research, ed. L. Szabados & D. Kurtz (San Francisco: ASP), 74
McNamara, B. J. 1985, ApJ, 289, 213
McSwain, M. V. 2003, ApJ, 595, 1124
Mermilliod, J.-C., Mermilliod, M., & Hauck, B. 1997, A&AS, 124, 349
Moon, T. T., & Dworetsky, M. M. 1985, MNRAS, 217, 305
Morris, S. L. 1985, ApJ, 295, 143
Moskalik, P., & Dziembowski, W. A. 1992, A&A, 256, L5
Napiwotzki, R., Schönberner, D., & Wenske, V. 1993, A&A, 268, 653
Neiner, C., et al. 2003, A&A, 411, 565
Paardekooper, S. J., Veen, P. M., van Genderen, A. M., & van der Hucht, K. A. 2002, A&A, 384, 1012
Pamyatnykh, A. A. 1999, Acta Astron., 49, 119
———. 2002, Commun. Asteroseismology, 142, 10
Pamyatnykh, A. A., Dziembowski, W. A., Handler, G., & Pikall, H. 1998, A&A, 333, 141
Pamyatnykh, A. A., Handler, G., & Dziembowski, W. A. 2004, MNRAS, 350, 1022
Pavlovski, K., et al. 1997, A&AS, 125, 75
Pedersen, H., & Thomsen, B. 1977, A&AS, 30, 11
Percy, J. R. 1984, JRASC, 78, 241
Percy, J. R., & Au-Yong, K. 2000, Inf. Bull. Variable Stars, 4825, 1
Percy, J. R., Hosick, J., Kincaide, H., & Pang, C. 2002, PASP, 114, 551
Percy, J. R., & Lane, M. C. 1977, AJ, 82, 353
Percy, J. R., & Madore, K. 1972, AJ, 77, 381
Perry, C. L., Franklin, C. B., Landolt, A. U., & Crawford, D. L. 1976, AJ, 81, 632
Pietrzynski, G. 1997, Acta Astron., 47, 211
Pigulski, A., & Boratyn, D. A. 1992, A&A, 253, 178
Pigulski, A., Jerzykiewicz, M., & Kopacki, G. 1997, Acta Astron., 47, 365
Pigulski, A., & Kołaczkowski, Z. 1998, MNRAS, 298, 753
———. 2002, A&A, 388, 88
Pigulski, A., Kopacki, G., & Kolaczkowski, Z. 2001, Acta Astron., 51, 159

Plaskett, J. S., & Pearce, J. A. 1931, Publ. Dom. Astrophys. Obs. Victoria, 5, 1
Ramspeck, M., Heber, U., & Moehler, S. 2001, A&A, 378, 907
Renson, P., Gerbaldi, M., & Catalano, F. A. 1991, A&AS, 89, 429
Renson, P., & Sterken, C. 1977, Inf. Bull. Variable Stars, 1373, 1
Rivinius, T., Baade, D., & Štefl, S. 2003, A&A, 411, 229
Robb, R. M., Delaney, P. A., Cardinal, R. D., Chaytor, D., & Berndsen, A. 2000, Inf. Bull. Variable Stars, 4913, 1
Robertson, J. G., et al. 1999, MNRAS, 302, 245
Rodríguez, E., & Breger, M. 2001, A&A, 366, 178
Saxena, B. K., & Srivastava, R. K. 1997, Bull. Astron. Soc. India, 25, 103
Schild, R. E. 1970, ApJ, 161, 855
Schrijvers, C. 1999, Ph.D. thesis, Univ. Amsterdam
Schrijvers, C., & Telting, J. H. 2002, A&A, 394, 603
Schrijvers, C., Telting, J. H., & Aerts, C. 2004, A&A, 416, 1069
Schrijvers, C., Telting, J. H., & de Ridder, J. 2002, in ASP Conf. Ser. 259, Radial and Nonradial Pulsations as Probes of Stellar Physics, ed. C. Aerts, T. Bedding, & J. Christensen-Dalsgaard (San Francisco: ASP), 204
Shaw, J. S., Fraquelli, D. A., Martins, D. H., & Andrew, S. B. 1983, Inf. Bull. Variable Stars, 2288, 1
Shibahashi, H., & Aerts, C. 2000, ApJ, 531, L143
Shobbrook, R. R. 1972, MNRAS, 157, 5P
———. 1973a, MNRAS, 161, 257
———. 1973b, MNRAS, 162, 25
———. 1978, MNRAS, 184, 825
———. 1979, MNRAS, 189, 571
———. 1981, MNRAS, 196, 129
———. 1983, MNRAS, 204, 47P
———. 1985, MNRAS, 214, 33
Shobbrook, R. R., & Lomb, N. R. 1972, MNRAS, 156, 181
Slettebak, A. 1968, ApJ, 154, 933
Smith, M. A. 1977, ApJ, 215, 574
———. 1981, ApJ, 248, 214
———. 1985, ApJ, 297, 206
Smith, M. A., Fullerton, A. W., & Percy, J. R. 1987, ApJ, 320, 768
Stankov, A., Handler, G., Hempel, M., & Mittermayer, P. 2002, MNRAS, 336, 189
Stankov, A., Ilyin, I., & Fridlund, C. V. M. 2003, A&A, 408, 1077
Stebbins, J., & Kron, G. E. 1954, ApJ, 120, 189
Steele, I. A., Negueruela, I., & Clark, J. S. 1999, A&AS, 137, 147
Sterken, C. 1988, A&A, 189, 81
Sterken, C., & Jerzykiewicz, M. 1980, in Workshop: Nonradial and Nonlinear Stellar Pulsation (Berlin: Springer), 105
———. 1983, Acta Astron., 33, 89
———. 1988, MNRAS, 235, 565
———. 1990, Acta Astron., 40, 123
———. 1993, Space Sci. Rev., 62, 95
Sterken, C., Pigulski, A., & Liu, Z. 1993, A&AS, 98, 383
Sterken, C., & Vander Linden, D. 1983, Inf. Bull. Variable Stars, 2330, 1
Stickland, D. J., Lloyd, C., Koch, R. H., & Pachoulakis, I. 1996, Observatory, 116, 387
Struve, O. 1950, ApJ, 112, 520
Struve, O., & Zebergs, V. 1959, ApJ, 129, 668
Telting, J. H., Abbott, J. B., & Schrijvers, C. 2001, A&A, 377, 104
Telting, J. H., Aerts, C., & Mathias, P. 1997, A&A, 322, 493
Telting, J. H., & Schrijvers, C. 1998, A&A, 339, 150
Telting, J. H., Uytterhoeven, K., & Ilyin, I. 2002, in Asteroseismology across the HR Diagram, ed. M. J. Thompson, M. S. Cunha, & M. J. P. F. G. Monteiro (Dordrecht: Kluwer), 401
Thoul, A., et al. 2003, A&A, 406, 287
Tian, B., Men, H., Deng, L., Xiong, D., & Cao, H. 2003, Chinese J. Astron. Astrophys., 3, 125
Uytterhoeven, K., Telting, J. H., Aerts, C., & Willems, B. 2004a, A&A, 427, 593
Uytterhoeven, K., et al. 2001, A&A, 371, 1035
———. 2004b, A&A, 427, 581
Valtier, J. C., Chapellier, E., Morel, P. J., & Le Contel, J. M. 1985, Inf. Bull. Variable Stars, 2843, 1
van Genderen, A. M. 2001, A&A, 366, 508
Van Hoof, A. 1973a, Med. Kon. Vl. Ac., 35, 4
———. 1973b, Inf. Bull. Variable Stars, 807, 1
Van Hoof, A., Bertiau, F. C., & Deurinck, R. 1963, ApJ, 137, 824
Vander Linden, D., & Sterken, C. 1985, A&A, 150, 76
———. 1987, A&A, 186, 129
Vidal, N. V., Wickramasinghe, D. T., Peterson, B. A., & Bessell, M. S. 1974, ApJ, 188, 163
Waelkens, C. 1991, A&A, 246, 453
Waelkens, C., Aerts, C., Kestens, E., Grenon, M., & Eyer, L. 1998, A&A, 330, 215
Waelkens, C., & Cuypers, J. 1985, A&A, 152, 15
Waelkens, C., & Heynderickx, D. 1989, A&A, 208, 129
Waelkens, C., & Lampens, P. 1988, A&A, 194, 143
Waelkens, C., & Rufener, F. 1983a, A&A, 121, 45
———. 1983b, A&AS, 52, 13
———. 1985, A&A, 152, 6
———. 1988, A&A, 201, L5
Waelkens, C., van den Abeele, K., & Van Winckel, H. 1991, A&A, 251, 69
Walker, G., et al. 2003, PASP, 115, 1023
Walker, M. F. 1951, PASP, 63, 35
Wilson, R. E. 1953, General Catalog of Stellar Radial Velocities (Washington: Carnegie Inst. Washington)
Young, R. K. 1915, Publ. Dom. Obs. Ottawa, 3, 63
Yudin, R. V. 2001, A&A, 368, 912

5.3 Asteroseismological studies of three β Cephei stars: IL Vel, V433 Car and KZ Mus

Original paper:

G. Handler, R. R. Shobbrook, F. F. Vuthela, L. A. Balona, F. Rodler, T. Tshenye, 2003, MNRAS 341, 1005

Mon. Not. R. Astron. Soc. **341,** 1005–1019 (2003)

Asteroseismological studies of three β Cephei stars: IL Vel, V433 Car and KZ Mus

G. Handler,[1,2]⋆ R. R. Shobbrook,[3] F. F. Vuthela,[2,4] L. A. Balona,[2]
F. Rodler[1] and T. Tshenye[4]

[1] *Institut für Astronomie, Universität Wien, Türkenschanzstraße 17, A-1180 Wien, Austria*
[2] *South African Astronomical Observatory, PO Box 9, Observatory 7935, South Africa*
[3] *Visiting Fellow, Australian National University, Canberra, ACT, Australia*
[4] *Department of Physics, University of the North-West, Private Bag X2046, Mmabatho 2735, South Africa*

Accepted 2003 February 3. Received 2002 December 13

ABSTRACT

We have acquired between 127 and 150 h of time-resolved multicolour photometry for each of the three β Cephei stars IL Vel, V433 Car and KZ Mus over a time-span of 4 months from two observatories. All three objects are multiperiodic with at least three modes of pulsation.

Mode identification from the relative colour amplitudes is performed. We obtain unambiguous results for the two highest-amplitude modes of IL Vel (both are $\ell = 1$) and the three strongest modes of KZ Mus ($\ell = 2$, 0 and 1), but none for V433 Car. Spectroscopy shows the latter star to be a fast rotator ($v \sin i = 240$ km s^{-1}), whereas the other two have moderate $v \sin i$ (65 and 47 km s^{-1}, respectively).

We performed model calculations using the Warsaw–New Jersey stellar evolution and pulsation code. We find that IL Vel is an object of about 12 M$_\odot$ in the second half of its main-sequence evolutionary track. Its two dipole modes are most probably rotationally split components of the mode originating as p_1 on the zero-age main sequence; one of these modes is $m = 0$. V433 Car is suggested to be an unevolved 13-M$_\odot$ star just entering the β Cephei instability strip. KZ Mus seems less massive ($\approx$12.7 M$_\odot$) and somewhat more evolved, and its radial mode is probably the fundamental one. In this case its quadrupole mode would be the one originating as g_1, and its dipole mode would be p_1.

Two of our photometric comparison stars also turned out to be variable. HD 90434 is probably a new slowly pulsating B-type star, the dominant mode of which is a dipole, whereas the variability of HD 89768 seems to be a result of binarity.

It is suggested that mode identification of slowly rotating β Cephei stars based on photometric colour amplitudes is reliable; we estimate that a relative accuracy of 3 per cent in the amplitudes is sufficient for unambiguous identifications. Owing to the good agreement of our theoretical and observational results we conclude that the prospects for asteroseismology of multiperiodic slowly rotating β Cephei stars are good.

Key words: stars: early-type – stars: individual: IL Vel – stars: individual: V433 Car – stars: individual: KZ Mus – stars: oscillations – stars: variables: other.

1 INTRODUCTION

The β Cephei stars are a group of early B-type stars of luminosity classes III–V that pulsate in pressure (p) and gravity (g) modes of low radial overtone. Their pulsational behaviour is thus similar to that of the A-/F-type δ Scuti stars. Both classes of variable seem suitable for asteroseismological investigations: their pulsational frequencies may be used to sound their interiors as the associated modes penetrate deeply into the star.

As exciting as this possibility is in theory, practice has shown that several obstacles still need to be overcome before precise asteroseismology of β Cephei or δ Scuti stars can be performed. On the theoretical side an adequate description of higher-order rotational effects is being worked on (e.g. Soufi, Goupil & Dziembowski 1998), and mode coupling is expected to have major effects on the pulsational eigenspectra of fast rotators (see Daszyńska-Daszkiewicz et al. 2002). Observationally, the main problem is the detection and

⋆E-mail: handler@astro.univie.ac.at

identification of as many pulsation modes as possible because a complete set of mode spectra has not even nearly been detected for any of these pulsators.

It may be suspected that the δ Scuti stars offer better possibilities for asteroseismology than β Cephei stars do, as they generally have many more pulsation modes excited to observable amplitudes. This result is in agreement with theoretical investigations of mode excitation (e.g. Pamyatnykh 2003). However, the problem lies with mode identification, i.e. the match of the observed frequencies with the corresponding pulsation mode defined by the three parameters k, the radial overtone of the mode, the spherical degree ℓ and the azimuthal order m.

To accomplish such a match in the presence of incomplete observed pulsation spectra, it is necessary to use mode identification methods. However, the surface convection zones of δ Scuti stars are expected to affect some of these methods, such as the commonly used photometric method that utilizes amplitude ratios and/or phase shifts of the light curves in different filters, adversely (see Balona & Evers 1999), and it is not known whether they can be trusted. The β Cephei stars do not have surface convection zones and therefore the simple photometric method may be applicable with more confidence.

We have therefore chosen three β Cephei stars for which the literature data qualify them as interesting candidates for in-depth studies aiming at the detection of many pulsation frequencies and at their mode identification by photometric means. All of these objects have been reported as multiperiodic variables previously and photometric mode identifications have been attempted. However, in all cases the amount of data available was small enough to give us hope for a significant improvement over previous results if we can obtain $\gtrsim$ 100 h of observation.

The most comprehensive photometric study of IL Vel (HD 80383) was performed by Heynderickx & Haug (1994). They found four frequencies in their *UBV* light curves, three of which formed an equally spaced triplet, suggestive of rotational m-mode splitting. This frequency solution, however, did not fit additional data in the Walraven system within the precision of the measurements. Heynderickx, Waelkens & Smeyers (1994) used the Walraven data for mode identification and suggested that all modes are of degree $\ell =$ 0 and *1*.

The variability of V433 Car (HD 90288) was discovered by Lampens (1988) and followed up by Heynderickx (1992). The frequency analysis of all the Geneva and Walraven data available to Heynderickx (1992) allowed him to disentangle four frequencies in the light variations of V433 Car. The mode identification by Heynderickx et al. (1994) was somewhat ambiguous, but suggested a mixture of (possibly) radial and non-radial modes with spherical degrees ℓ up to four.

Our third target star, KZ Mus (HD 109885) was a discovery of the *Hipparcos* satellite (ESA 1997) reported by Waelkens et al. (1998). Aerts (2000) obtained new Geneva photometry for the star and performed both a frequency analysis of all the data and a mode identification. She suggested that the star pulsates with at least three frequencies, where the second strongest one appeared to be radial.

2 OBSERVATIONS

2.1 Photometry

We have studied IL Vel, V433 Car and KZ Mus from both the Siding Spring (SSO, Australia) and South African Astronomical (SAAO) Observatories. We used photoelectric photometers attached to the 0.6-m telescope at SSO and the 0.5- and 0.75-m telescopes at SAAO.

The most valuable part of the energy distribution of a β Cephei star for mode identification by means of photometry is in the blue (λ < 4200 Å). Therefore, the Geneva and (particularly) Walraven systems are well suited for such a purpose as they have several filters within this wavelength domain. Unfortunately, these are not widely available. Owing to the faintness of our variables ($V = 8.1$–9.1) we decided to utilize the standard Johnson *UBV* system, supplemented by Strømgren v whenever possible.

The periods of the known pulsations of our three targets are all longer than 150 min, and the stars are all located in an area covering some 30° on the sky. Consequently, we chose one local comparison star for each variable (the B5 IV star HD 79670 for IL Vel, the B9 IV/V star HD 90434, which was later replaced by the A1 IV/V star HD 89768 for V433 Car, and the B9 IV star HD 109082 for KZ Mus; all spectral types are from Houk & Cowley (1975), and our observing sequence included all six stars whenever reachable. The resulting cycle time of about 25 min (or less) per measurement of each variable sampled the light curves of all stars adequately.

Another aspect of the pulsations of β Cephei stars requires consideration when planning an observational effort such as ours. In many cases, closely spaced pulsation frequencies are present. Heynderickx & Haug (1994) reported just that for our target IL Vel. Consequently, a sufficient time baseline must be spanned by the observations (at least 2 months for IL Vel) for such frequencies to be resolved and the measurements should be distributed evenly over the observation period to avoid aliasing problems.

We have therefore also observed these objects during a multisite campaign for the δ Scuti star FG Vir (Breger et al., in preparation) when this star was not reachable. This only resulted in short runs up to 2 h that, however, covered important gaps in the total coverage, which made them quite valuable. The main body of our final data set spanned 95 d in 2002 February to May, during which data were obtained on 52 nights. A total of 146 h of measurement of IL Vel, 150 h of V433 Car and 127 h of KZ Mus was acquired.

Data reduction was performed in the standard way for differential photoelectric time-series photometry. First, we corrected the data for coincidence losses, followed by sky subtraction and by extinction determination using the time series of the constant stars in our ensemble. After the extinction correction, the differential light curves of the variables with respect to their local comparison stars and that of the three comparisons with respect to the others were calculated and the times of measurement were converted to a heliocentric Julian date (HJD). The light curves of the three β Cephei stars in the V filter are shown in Fig. 1.

As part of the reductions were already performed during the observational campaign, it was noticed that the comparison star HD 90434 was variable. Consequently, it was replaced by HD 89768. As it turned out during the final reductions after completion of the observations, this star is also variable. We will analyse these objects later, but for the time being let it suffice to say that we performed a frequency analysis of their differential light curves with respect to the constant comparison stars for the other targets. We then subtracted synthetic light curves constructed from the results of this frequency search from the differential measurements of V433 Car so the variability of its comparison stars will not affect the frequency analysis of this star. This procedure is valid as the time-scales of the variability of HD 90434 and 89768 are much longer than that of V433 Car.

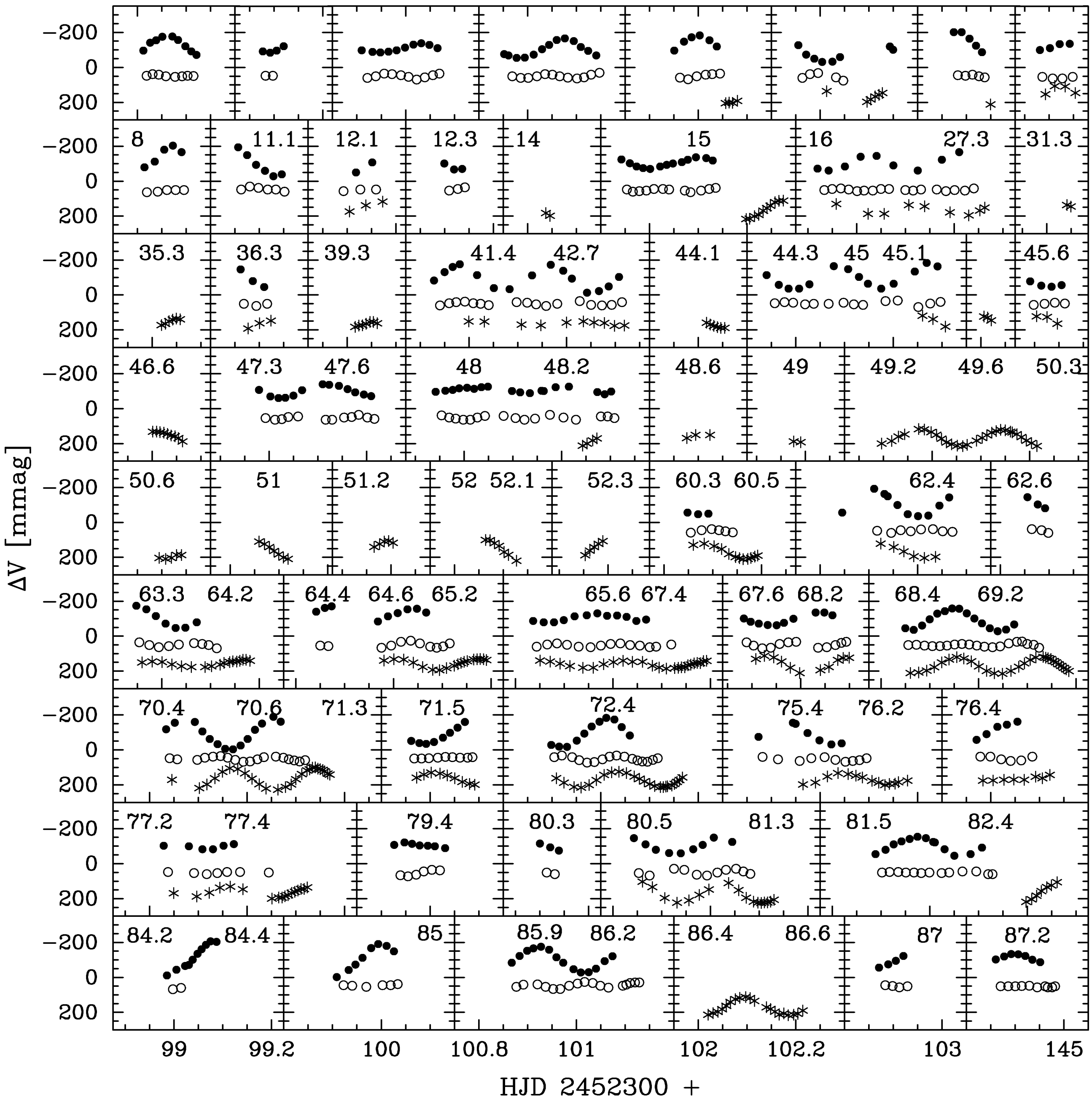

Figure 1. *V*-filter light curves from all our measurements of IL Vel (filled circles), V433 Car (open circles) and KZ Mus (asterisks). Note the shorter periods and much lower amplitude of V433 Car. Multiperiodicity of all three stars is evident.

2.2 Spectroscopy

With the main aim of determining the projected rotational velocities of IL Vel, V433 Car and KZ Mus, high-resolution spectra of the three β Cephei stars were obtained on the night of 2002 May 4 to 5 with the 1.9-m telescope at SAAO. We used the GIRAFFE echelle fibre-fed spectrograph attached to the Cassegrain focus of this telescope. The GIRAFFE spectrograph has a resolving power of about 32 000, giving a resolution of 0.06–0.09 Å pixel^{-1}. Exposure times were 1500 s for IL Vel and KZ Mus as well as 600 s for V433 Car for signal-to-noise (S/N) ratios of between 27 and 35. A Th–Ar arc lamp was used for wavelength calibration.

The spectra were normalized to the continuum using an unbroadened synthetic spectrum with $T_{\mathrm{eff}} = 23\,000$ K, log $g = 4.00$ as a template, using the SPECTRUM code (Gray & Corbally 1994). A running median of each echelle order was divided by the corresponding section of the synthetic spectrum and taken to represent the response function of the instrument. A polynomial of degree five was fitted to the response function and used to correct the observed spectrum.

For each order, the observed rectified spectrum was correlated with the corresponding section of the synthetic spectrum after removing the unit continuum, effectively resulting in the mean line profile with the continuum removed. A quadratic was then fitted to

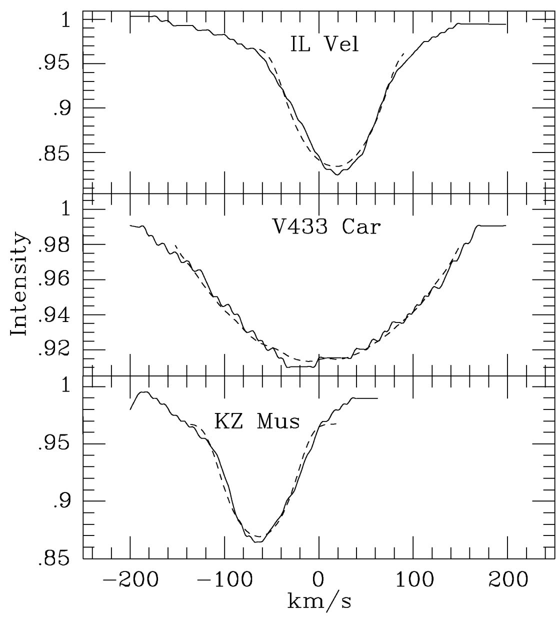

Figure 2. The average helium line profile for our three variables (full line) overlaid by a model atmosphere fit (dashed lines) to determine the projected rotational velocities. The line profile asymmetries are probably caused by non-radial stellar pulsation.

Table 1. Results of our determinations of the radial and projected rotational velocities.

Star	$v \sin i$ (km s^{-1})	$\langle Vr \rangle$ (km s^{-1})
IL Vel	65 ± 3	+19.0
V433 Car	240 ± 10	+4.0
KZ Mus	47 ± 3	−61.6

the correlation function, and its maximum adopted as the 'radial velocity' for each order. The mean radial velocity from all the orders is also obtained.

The correlation profiles can be co-added to form what is essentially a mean line profile. The projected rotational velocity, $v \sin i$, can be determined by fitting a model profile of a rotating star. The projected rotational velocity is adjusted until a best fit is obtained to the observed profile. We show these fits in Fig. 2 and the results from our spectroscopic analysis are summarized in Table 1.

3 FREQUENCY ANALYSIS OF THE PHOTOMETRIC TIME SERIES

Our frequency analysis was performed using the program PERIOD98 (Sperl 1998). This package applies single-frequency power spectrum analyses and simultaneous multifrequency sine-wave fits. One of its many advanced features is its capability of fixing dependent signal frequencies to certain values, e.g. to sum and difference terms, and to perform a simultaneous non-linear least-squares fits with such fixed frequencies.

Our strategy for the frequency analysis starts with the calculation of the spectral window of the data. It is computed as the Fourier amplitude spectrum of a single noise-free sine wave with the frequency of highest amplitude in our data. In this way, the reflection of the spectral window pattern at zero frequency, which may not be negligible as our observing nights often did not sample a full cycle of the light variations, can be evaluated.

We continue by computing amplitude spectra of our data as well as those of residual light curves after the previously identified periodicities had been removed using the multiperiodic fitting algorithm of PERIOD98. We continue this process until no significant peaks are left in the residual amplitude spectrum. We consider an independent peak significant if it exceeds four times the local noise level in the amplitude spectrum, following Breger et al. (1993). Combination signals only require S/N > 3.5 to be regarded as significant. Experience has shown that this criterion is both reliable and conservative.

Similar analyses were performed for all the four filters used. We note that, within the uncertainties of frequency determination, these detected frequencies were the same for all stars in every filter. This confirms that alias ambiguities do not affect our analysis. As our final values for the frequencies we adopted the mean values from the data in all four filters weighted by the associated signal-to-noise ratios. The deviations of the optimum frequencies in the individual filters from this mean are taken as our error estimate on the frequency determination.

3.1 KZ Mus

As the frequency analysis of this star was straightforward, it is the first that we chose to describe. The spectral window, amplitude spectra and pre-whitened versions thereof are shown in Fig. 3. We use the data obtained in the B filter for display as they have the best S/N ratio. Owing to our two-site coverage the spectral window is sufficiently clean that alias ambiguities do not represent a problem for the analysis.

The first three signals in the periodogram are easy to detect. After pre-whitening these, a more complicated residual amplitude spectrum (the fifth panel of Fig. 3), with several peaks standing out, remains. A closer look reveals that two of them are the combination sum and difference frequencies of the two strongest modes, whereas the remaining tall peak corresponds to an independent signal. With pre-whitening of all the six variations detected so far, the $2f$-harmonic of the second strongest mode also becomes notable.

After this signal is included in our multifrequency light-curve fit, no significant peaks remain in the residual amplitude spectrum of the B-filter data alone, and neither are there any present in the measurements in any other filter. However, we can attempt to increase the signal-to-noise ratio in our analysis by adding the data in all filters. Obviously, this must not be done for the original light curves, as different pulsation modes have different relative amplitudes in the different wavelength passbands (which are a diagnostic for mode identification!). However, it is safe to combine the residual light curves as we are working at low S/N ratio, i.e. the intrinsic differences in mode amplitude between the wavebands are small compared with the noise in the data.

To combine the different residual data sets we have therefore subtracted a multifrequency solution from all the individual filter observations, using exactly the same frequencies (determined as described in the previous section) for each waveband. We then roughly scaled the residuals to B amplitude by multiplying the U-filter residuals by 0.8 and the V-filter residuals by 1.1. We did not scale the v-filter data as the signals in it were found to have essentially the same amplitude as in B. The scalefactors are approximate average amplitude ratios of the modes previously detected.

All of these residual light curves were then added together, averaged and the periodogram was computed out to the Nyquist frequency (lowest panel of Fig. 3); we find no more significant signals. Interestingly, we do note two residual mounds of amplitude, one in the frequency region where the pulsational signals were found and

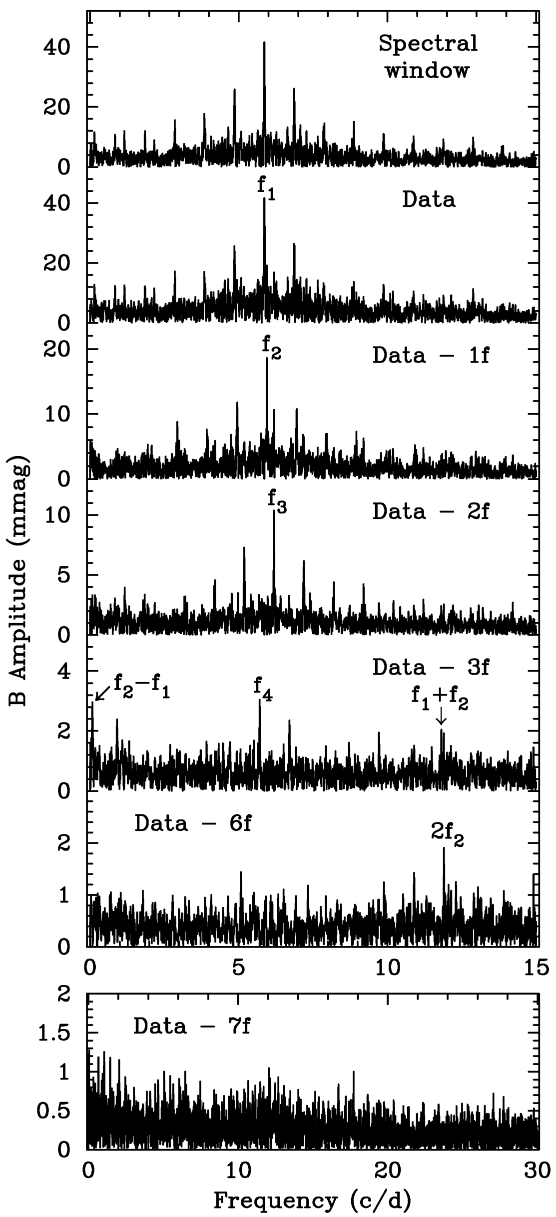

Figure 3. Spectral window and amplitude spectra of our *B*-filter data of KZ Mus. Some pre-whitening steps of the detected frequencies are shown in consecutive panels. The lowest panel shows the amplitude spectrum of the combined *UvBV* residuals after all significant signals have been removed from the measurements.

another one where combination frequencies would be expected. In fact, the two highest peaks in the latter region are located at exact sums of two known frequencies but they are not formally significant.

We can therefore claim the detection of seven signals in the light curves of KZ Mus; our final frequency solution is listed in Table 2. The rms scatter per single data point in the combined and averaged *UvBV* residuals is 3.0 mmag.

3.1.1 Re-analysis of published data

Our frequency solution in Table 2 differs somewhat from the results of Aerts (2000), who needed to base her frequency analysis on the *Hipparcos* data for the star. The first two signals detected by her agree with ours, but the third one is different; the remaining signals are below her detection level. Two possible reasons for the disagreement can be imagined, the more exciting one being intrinsic amplitude variability of the star and the other one being an alias problem in the poorly sampled *Hipparcos* photometry.

Consequently, we have re-analysed the time series of KZ Mus acquired by the *Hipparcos* satellite. The residual amplitude spectrum after pre-whitening the two consistent main frequencies contains the third signal claimed by Aerts (2000) as the tallest peak. However, our third signal is also visible and of similar strength. As our data are more extensive and of better quality than the *Hipparcos* photometry, we suggest that the third signal found by Aerts (2000) is an unfortunate artefact of the poor sampling of the *Hipparcos* measurements.

3.2 V433 Car

The upper panel of Fig. 4 shows that the spectral window function for our measurements of this star is also quite good. The amplitude spectrum is dominated by two peaks of similar strength that seem to imply an aliasing problem, but thanks to the long time base of our data they are well resolved and do not interfere with each other; they are simply two independent signals of similar amplitude.

Pre-whitening of these variations results in the detection of a third frequency and the next step reveals another significant peak. After these four periodicities have been removed, no obvious new candidate frequency can be discerned. We therefore combined the residual data as we did for KZ Mus, but used somewhat different scalefactors that seemed more appropriate for this star. We multiplied the *U* residuals by 0.83 and those in *V* by 1.05 to obtain approximate *B* amplitudes.

The amplitude spectrum of the residuals thus combined is shown in the lowest panel of Fig. 4, again out to the Nyquist frequency. The highest peak corresponds to a combination frequency difference and as it exceeds the noise level by more than 3.5 times, we adopt it as an additional term for our frequency solution. We would also like to point out the peak near 7 cycle d^{-1} in the lowest panel of Fig. 4. It is, in fact, a close doublet at 6.924 and 6.968 cycle d^{-1}, which is present in the residuals of all individual filters, but as it still does not exceed $S/N > 4$, we cannot be sure about its reality. We therefore adopt a five-frequency solution for our light curves that we list in Table 3.

The rms scatter of the combined residual light curves of V433 Car is 3.9 mmag per point. This is 30 per cent higher than for KZ Mus. Likely reasons for the increased noise are undetected further intrinsic signals and possible residual variations by the variable comparison stars that could not be taken out.

3.2.1 Comparison with literature data

Heynderickx (1992) reported the detection of four frequencies in his light curves of V433 Car. Two of them agree with the two strongest signals in our Table 3, and the other two are 1 cycle d^{-1} aliases of our values. We prefer the frequencies derived from our analysis because our data are more numerous, the results in the different filters were consistent and our two-site measurements have a much better spectral window function.

The order in which we detected the variation frequencies of V433 Car is different from that obtained by Heynderickx (1992). Although this author does not list the amplitudes of the signals he determined,

Table 2. Multifrequency solution for our KZ Mus data. Frequencies are mean values from results of all four filters weighted by the S/N ratio of the signal. Errors on the amplitudes were calculated with the formulae of Montgomery & O'Donoghue (1999). The S/N ratio quoted is the average of the values in the individual filters.

ID	Frequency (cycle d^{-1})	Amplitude U (mmag)	B (mmag)	V (mmag)	v (mmag)	Mean S/N ratio
f_1	5.863 84 ± 0.000 06	45.6 ± 0.3	40.9 ± 0.3	38.5 ± 0.3	41.2 ± 0.4	89.4
f_2	5.950 26 ± 0.000 11	28.8 ± 0.3	19.6 ± 0.3	16.4 ± 0.3	20.6 ± 0.4	45.6
f_3	6.1874 ± 0.0005	14.3 ± 0.3	11.0 ± 0.3	10.5 ± 0.3	11.8 ± 0.4	25.7
f_4	5.7090 ± 0.0024	3.4 ± 0.3	3.2 ± 0.3	2.4 ± 0.3	3.1 ± 0.4	6.6
$f_2 - f_1$	0.086 42	4.3 ± 0.3	2.8 ± 0.3	3.1 ± 0.3	3.1 ± 0.4	6.3
$f_1 + f_2$	11.814 10	2.5 ± 0.3	2.2 ± 0.3	2.5 ± 0.3	2.6 ± 0.4	5.7
$2f_2$	11.900 52	2.6 ± 0.3	1.9 ± 0.3	2.0 ± 0.3	2.6 ± 0.4	5.2

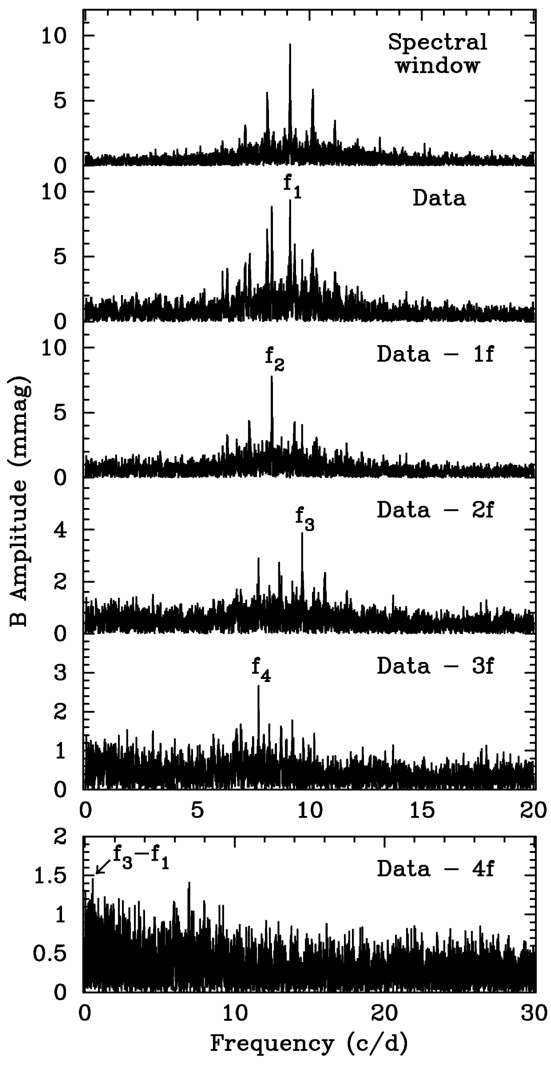

Figure 4. Spectral window and amplitude spectra of our B-filter data of V433 Car. Some pre-whitening steps of the detected frequencies are shown in consecutive panels. The lowest panel shows the amplitude spectrum of the combined $UvBV$ residuals after all previously significant signals have been removed from the measurements. One combination frequency is detected that way.

inspection of his published PDM periodograms suggests that the pulsations suffered amplitude variability in the 14 years that have elapsed between his and our observations.

3.3 IL Vel

The spectral window and amplitude spectra of our measurements of IL Vel are shown in Fig. 5. Two independent frequencies dominate the periodogram. After pre-whitening those, a third signal stands out, and including this in the multifrequency solution allows the detection of two combination frequencies. Combining the residuals in all filters, scaling the U data by a factor of 0.76 and the V data by 1.05, results in the uninformative periodogram in the lowest panel of Fig. 5. The frequency solution for IL Vel is given in Table 4.

This analysis may appear simple, but it is not. First, the third independent signal is located halfway in frequency between the first two, which are of much higher amplitude. Although it is well resolved from the two strong modes, some doubts remain as to its reality; it could be an artefact caused by amplitude/frequency variability of the two main signals.

We have therefore divided our data set into two halves (before and after JD 2452360) and analysed them separately. We adopted the frequencies of the two strongest modes and their detected combination signals as definite and fitted them to each half, but left their amplitudes and phases as free parameters. We then computed amplitude spectra of the residuals for each half in each filter. The signal f_3 was detected in each of the eight subsets of data; we conclude that it is real.

The second cause of concern is the rms residual of our five-frequency fit to the IL Vel light curves. After combination of the data in all four filters, it is an enormous 7.8 mmag per point, twice as large as for V433 Car and 2.6 times larger than for KZ Mus. The noise level in the lowest panel of Fig. 5 is also correspondingly higher.

We started our quest for the reason for the high residuals by investigating the constancy of the comparison star. We calculated differential light curves for all the other stars for which we had simultaneous data, but found no evidence for variability of HD 79670, at least at a level that could produce the high residuals observed. They must therefore be (mostly) caused by IL Vel.

When we checked the reality of f_3, we noted that its location in the amplitude spectra of the two halves of data was somewhat shifted and that there was more structure surrounding it than just the normal spectral window pattern plus noise. A plot of the residual

Table 3. Multifrequency solution for our V433 Car data. Frequencies are mean values from results of all four filters weighted by the S/N ratio of the signal. Errors on the amplitudes were calculated with the formulae of Montgomery & O'Donoghue (1999). The S/N ratio quoted is the average of the values in the individual filters.

ID	Frequency (cycle d^{-1})	Amplitude U (mmag)	B (mmag)	V (mmag)	v (mmag)	Mean S/N ratio
f_1	9.129 09 ± 0.000 14	9.9 ± 0.5	8.2 ± 0.3	8.2 ± 0.3	8.8 ± 0.5	17.9
f_2	8.316 49 ± 0.000 09	10.0 ± 0.5	8.2 ± 0.3	7.3 ± 0.3	8.0 ± 0.5	16.7
f_3	9.667 07 ± 0.000 24	4.3 ± 0.5	3.8 ± 0.3	4.0 ± 0.3	4.2 ± 0.5	8.5
f_4	7.7214 ± 0.0012	3.4 ± 0.5	2.8 ± 0.3	2.3 ± 0.3	2.6 ± 0.5	5.4
$f_3 - f_1$	0.537 98	1.8 ± 0.5	1.2 ± 0.3	1.5 ± 0.3	1.3 ± 0.5	3.7

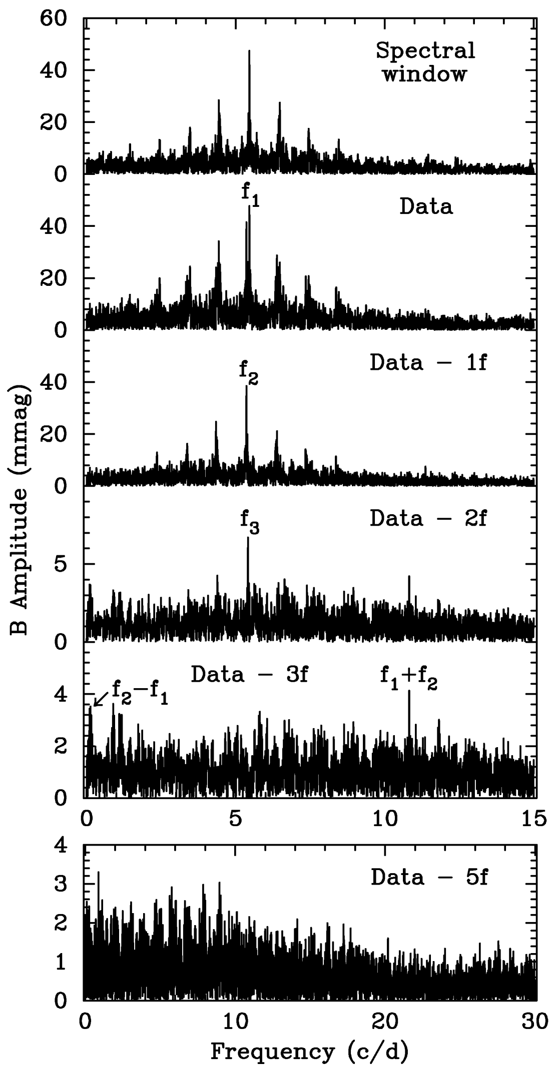

Figure 5. Spectral window and amplitude spectra of our *B*-filter data of IL Vel. Some pre-whitening steps of the detected frequencies are shown in consecutive panels. The lowest panel shows the amplitude spectrum of the combined *UvBV* residuals after all significant signals have been removed from the measurements.

light curves after subtraction of our five-frequency solution shows conspicuous variability on time-scales similar to those of the known pulsational signals. We are therefore inclined to think that further, presently unresolved, pulsation frequencies are present in the light curves of IL Vel and that a data set with an even longer time base than ours is required to detect them.

3.3.1 Re-analysis of published data

The results of our frequency analysis differ from those of Heynderickx & Haug (1994). Our first frequency is significantly different from theirs, but we agree on the second one. Heynderickx & Haug (1994) did not find our third frequency, whereas we did not detect their third and fourth signals.

To clarify the situation, we have retrieved the data of Heynderickx & Haug (1994) and re-analysed them. We show the periodogram analysis of their Johnson *B* data in Fig. 6, where we have assumed our frequencies to be correct, and used them as the initial values for light-curve-fitting and pre-whitening.

Our two frequencies f_1 and f_2 are sufficient to explain the dominant variations in these measurements. After they are pre-whitened, the residual amplitude spectrum (lowest panel of Fig. 6) shows no peak exceeding 5 mmag; the two additional frequencies claimed by Heynderickx & Haug (1994) had *B* amplitudes of 20 and 14 mmag, respectively. We conclude that these were artefacts originating from choosing an incorrect alias frequency.

The absence of our signal f_3 in their data may be due to a similar reason. Two out of their three yearly data sets spanned 2 weeks, and one consisted of two single-week runs spread by 25 d. The beating phenomenon of f_3 with either f_1 or f_2 is therefore never properly resolved. Owing to this particular unfortunate time distribution f_3 can be suppressed below detectability, as we have checked with numerical simulations. It is therefore certainly possible that our f_3 was present in their data but could not be detected. We note that the two combination frequencies detected in our data may also be present in the measurements by Heynderickx & Haug (1994), but if so, their amplitude was lower.

Finally, we would like to point out that the lowest panel of Fig. 6 also shows a residual mound of power, even more pronounced than in the residual periodogram of our data. The combined, scaled and average *UBV* residuals of the data of Heynderickx & Haug (1994) have an rms scatter of 9.8 mmag, also much higher than their measurement accuracy. As these authors used a comparison star different from ours, we strengthen the conclusion that there are unresolved frequencies in the light curves of IL Vel.

3.4 Variable comparison stars

3.4.1 HD 90434

This was the original local comparison star for V433 Car. When we examined amplitude spectra of the differential data reduced during

Table 4. Multifrequency solution for our IL Vel data. Frequencies are mean values from results of all four filters weighted by the S/N ratio of the signal. Errors on the amplitudes were calculated with the formulae of Montgomery & O'Donoghue (1999). The S/N ratio quoted is the average of the values in the individual filters.

ID	Frequency (cycle d^{-1})	Amplitude U (mmag)	B (mmag)	V (mmag)	v (mmag)	Mean S/N ratio
f_1	5.459 76 ± 0.000 12	59.9 ± 0.8	45.5 ± 0.6	43.2 ± 0.7	45.6 ± 0.7	43.2
f_2	5.362 93 ± 0.000 11	53.0 ± 0.8	40.7 ± 0.6	38.3 ± 0.7	40.6 ± 0.7	38.4
f_3	5.413 40 ± 0.0010	8.7 ± 0.8	7.1 ± 0.6	6.5 ± 0.7	7.3 ± 0.7	6.6
$f_1 + f_2$	10.822 69	5.2 ± 0.8	4.0 ± 0.6	4.1 ± 0.7	3.7 ± 0.7	4.2
$f_2 - f_1$	0.096 83	5.3 ± 0.8	3.3 ± 0.6	3.4 ± 0.7	4.4 ± 0.7	3.7

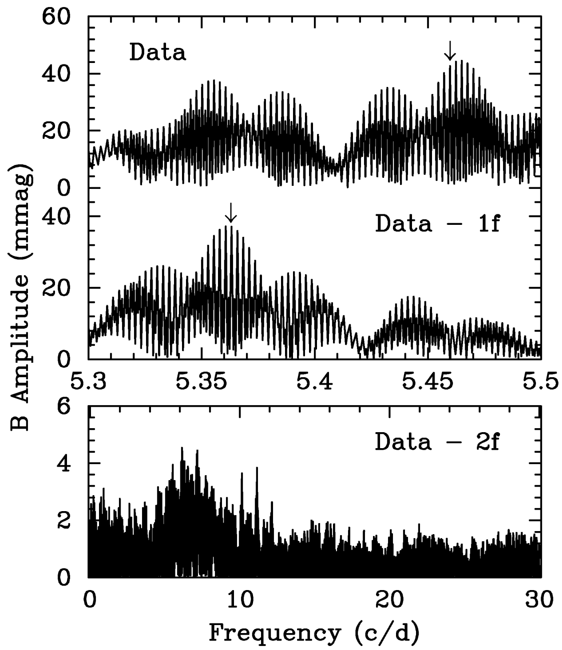

Figure 6. Amplitude spectra of Heynderickx & Haug's (1994) B-filter data of IL Vel; consecutive panels show some pre-whitening steps. The positions of our frequencies f_1 and f_2 are indicated with arrows and adopted as definite for the pre-whitening.

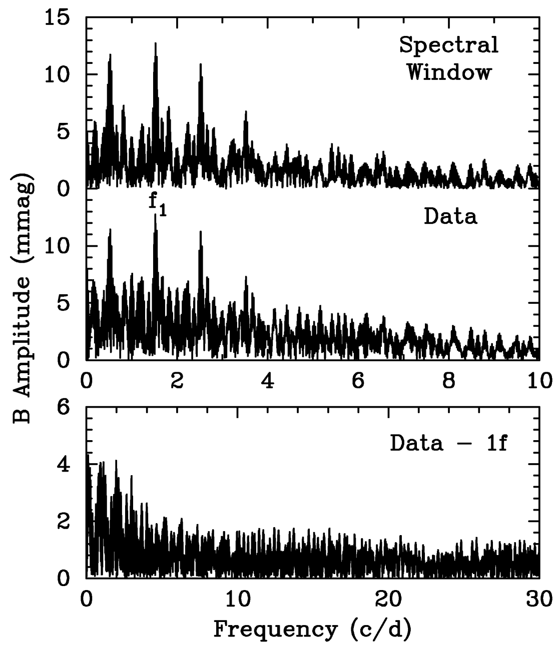

Figure 7. Upper two panels: spectral window and amplitude spectrum of our B-filter data of HD 90434 relative to HD 79670. Lower panel: pre-whitened amplitude spectrum of the combined residual light curves out to the Nyquist frequency.

the course of the observing campaign, we noted some additional low-frequency variability besides the pulsations of V433 Car. The differential light curves of HD 90434 relative to the comparison star for IL Vel, allowed us to identify HD 90434 unambiguously as a new variable. Fig. 7 contains the spectral window and amplitude spectra of these data.

We detect one variation frequency for this star. Pre-whitening it from the data, combining the residual light curves as for the β Cephei stars, and computing the amplitude spectrum of this data set results in some evidence for additional variability (lowest panel of Fig. 7), but produces no more detections. The increase in noise level at low frequencies may, however, also (partly) be owing to residual effects of extinction and sky transparency as the two stars are separated by about 10° in the sky. The frequency solution we derived for HD 90434 is given in Table 5. We note that the amplitude of the variability increases towards the blue, as confirmed by an examination for colour variations. No significant phase shifts between the light curves in the different filters were found.

Table 5. Results of the frequency analysis for the two comparison stars. Frequencies are mean values from results of all four filters weighted by the S/N ratio of the signal. Errors on the amplitudes were calculated with the formulae of Montgomery & O'Donoghue (1999). The S/N ratio quoted is the average of the values in the individual filters.

Star	HD 90434	HD 89768
Frequency (cycle d^{-1})	1.5229 ± 0.0012	0.6875 ± 0.0004
U amplitude (mmag)	15.9 ± 1.2	13.6 ± 1.2
B amplitude (mmag)	11.5 ± 0.8	14.8 ± 0.6
V amplitude (mmag)	9.2 ± 0.7	12.7 ± 0.5
v amplitude (mmag)	11.4 ± 1.0	15.5 ± 0.9
Mean S/N	5.9	9.0

3.4.2 HD 89768

After discovery of its variability, HD 90434 was replaced as a comparison star for V433 Car by HD 89768 for which the spectral type of A1 IV/V places it outside any known pulsational instability region, but we were no luckier with this star. In fact, we only noticed

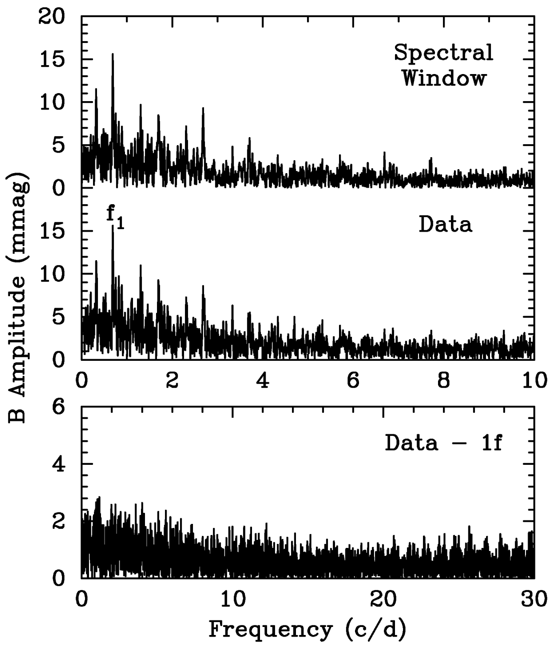

Figure 8. Upper two panels: spectral window and amplitude spectrum of our *B*-filter data of HD 89768 relative to HD 79670. Lower panel: prewhitened amplitude spectrum of the combined residual light curves out to the Nyquist frequency.

that this object was also variable when it was too late to replace it with yet another star.

We again constructed differential light curves with respect to HD 79670 and show its Fourier analysis in the same fashion as that in the previous section in Fig. 8. Again, a single frequency suffices to explain the observed light variations, and some residual low-frequency variability seems to be present that we attribute to atmospheric effects. Table 5 contains our results for HD 89768 as well.

From the amplitudes in the different filters listed in Table 5 it appears that this star also shows some colour variability. We have therefore analysed the colour light curves as well, but we could not confirm this suspicion. It seems that the different amplitudes in the four filters are generated by noise effects and our errors are underestimates for variations at these low frequencies.

4 BASIC STELLAR PARAMETERS

4.1 The β Cephei stars

The astrophysical analysis of our results is facilitated by first restricting the physical parameter space occupied by these stars. Consequently, we have estimated their masses and temperatures with calibrations of multicolour photometry, as meaningful trigonometric parallaxes are not available. Fortunately, all three stars have already been measured in the Strømgren, Geneva and Johnson systems. We have retrieved the corresponding standard values from the Lausanne–Geneva data base (http://obswww.unige.ch/gcpd/gcpd.html).

We have then applied different calibrations for the effective temperature, the surface gravity and the absolute magnitude to the three stars. It seems important to use more than one calibration as their results often deviate. We can then hope to obtain a good average result with a realistic determination of its uncertainty. Absolute visual magnitudes were calculated from the Strømgren β index using Crawford's (1978) results that also allow a determination of the interstellar reddening. We find $A_v = 0.90$ for IL Vel, $A_v = 0.38$ for V433 Car and $A_v = 1.24$ for KZ Mus.

Table 6. The adopted effective temperatures and luminosities for our target stars from standard photometry.

Parameter	IL Vel	V433 Car	KZ Mus
$T_{\rm eff}$ (kK)	23.6 ± 0.6	26.6 ± 0.7	26.0 ± 0.7
$\log L/L_\odot$	4.19 ± 0.22	4.20 ± 0.20	4.22 ± 0.20

We used the formulae by Napiwotzki, Schönberner & Wenske (1993) to calculate stellar temperatures from the Strømgren $[u - b]$ and $(b - y)_0$ indices as well as from Johnson's $(B - V)_0$. The tables by Flower (1996) allow another temperature estimate from $(B - V)_0$ and also provide bolometric corrections. The latter were also determined from Drilling & Landolt's (2000) tables. Estimates of the surface gravities of the three stars were obtained with the calibration by Smalley & Dworetsky (1995) from the Strømgren β index, including a correction proposed by Dziembowski & Jerzykiewicz (1999). Finally, we applied the work by Künzli et al. (1997) for the Geneva system that results in effective temperatures and surface gravities. Average values for the resulting effective temperatures and luminosities as well as error estimates are given in Table 6.

4.2 The variable comparison stars

The *Hipparcos* parallax of HD 90434 (ESA 1997) has a relative error that is too large to make it useful. The spectral classification and the Strømgren colours of the star imply it is a late B-type star. Johnson and Geneva colours of this object are also available in the Lausanne–Geneva data base. Consequently, we applied the same calibrations that we have already used for the β Cephei stars to determine its effective temperature and luminosity. We derive $T_{\rm eff} = 12.2 \pm 0.4$ kK and $\log L/L_\odot = 1.86 \pm 0.10$.

No standard photometry is available for HD 89768. However, from the mean magnitude differences of V433 Car from both of its comparison stars, we can estimate $(B - V) = 0.09$ and $(U - B) = 0.04$ for HD 89768. With the *Hipparcos* parallax of 2.09 ± 0.69 mas and the galactic reddening law of Chen et al. (1998), we can then estimate $(B - V)_0 = 0.01 \pm 0.03$ and $M_v = -0.7 \pm 0.9$. From the calibration by Napiwotzki et al. (1993) we then obtain $T_{\rm eff} = 9250 \pm 400$ K, and the luminosity results in $\log L/L_\odot = 2.3 \pm 0.4$.

4.2.1 *The nature of HD 90434 and 89768*

The effective temperature and luminosity of HD 90434 as derived above put it into the instability region of the slowly pulsating B (SPB) stars (Dziembowski, Moskalik & Pamyatnykh 1993). The colour variability we found combined with the variation being in phase in the different filters supports this hypothesis and argues against an interpretation in terms of rotational modulation of a chemically peculiar star; the Strømgren m_1 index for HD 90434 does not suggest it is an Ap star either.

On the other hand, HD 89768 is not located in any known pulsational instability region, and we could not detect colour variability in its light curves. We suspect that the variability may be binary-induced, but spectroscopic data would be required to confirm our hypothesis.

5 MODE IDENTIFICATION

The ranges in effective temperature and luminosity of the β Cephei stars listed in Table 6 are an essential ingredient for mode identification. We have followed the method proposed by Balona & Evers (1999, see their paper for a detailed description). It uses theoretically calculated non-adiabatic parameters to determine the amplitude ratios between different wavebands that are the discriminator between the different modes of pulsation.

We computed stellar evolutionary models by means of the Warsaw–New Jersey evolution and pulsation code (described, for instance, by Pamyatnykh et al. 1998) for solar chemical composition. The models spanned a mass range between 8 and 16 $M_\odot$ in steps of 1 $M_\odot$. Guided by the projected rotational velocities of the stars listed in Table 1, we chose a rotational velocity of 100 km s^{-1} on the zero-age main sequence (ZAMS) for models representing IL Vel and KZ Mus, but 260 km s^{-1} for V433 Car. By comparing the model evolutionary tracks with the stellar parameters in Table 6, we inferred that IL Vel is a star with a mass of between 10.5 and 13 $M_\odot$ in the second half of its main-sequence evolution, whereas KZ Mus and V433 Car are less evolved but somewhat more massive ($11.5 < M_* < 14$ $M_\odot$).

We then proceeded by calculating theoretical *UvBV* amplitudes for all pulsationally unstable modes along model sequences that spanned the physical parameter space of our targets, whereby we extended the error bars in Table 6 by up to a factor of 2 to be conservative. We did not consider the phase shifts between the different photometric bands because their measured relative error is much higher than that for amplitude ratios. We have not found phase shifts significant at the 3σ level and they have therefore no discriminative power.

The resulting theoretical amplitudes in the four passbands were normalized to that in the *U* filter, and the average amplitude ratio and its rms error were calculated. In this way we can also gain an idea of the uncertainties involved in the calculation of theoretical results that need to be considered when being matched with the observations.

The comparison between the theoretical and observed colour amplitude ratios of IL Vel is shown in Fig. 9. We also include the *UBV* colour amplitude ratios from the data of Heynderickx & Haug (1994) with the correct frequencies f_1 and f_2.

The identification for the two strongest modes of IL Vel is unambiguous: both have a spherical degree of $\ell = 1$. The third pulsation mode we found that has a frequency intermediate between the other two, is also non-radial and could be $\ell = 1$, 2 or 3. Our mode identification is therefore consistent with that of Heynderickx et al. (1994), although they have used an incorrect alias and spurious frequencies.

Observed and theoretical amplitude ratios for the four modes of V433 Car are plotted in Fig. 10. The identifications we derive from that figure are not as clear as those for IL Vel. Mode f_1 is most probably $\ell = 2$, and the amplitude ratios for f_2 agree best with $\ell = 1$. All we can say concerning mode f_3 is that it is non-radial ($\ell = 2$ or 4?), and mode f_4 may be $\ell = 0$, 1, 2 or 3.

Heynderickx et al. (1994) arrived at similar conclusions concerning the identification of the modes of V433 Car, and they also reported inconsistencies of their identifications in different photometric systems. We must therefore consider the attempts to derive mode identifications for V433 Car as being mostly inconclusive.

Turning now to KZ Mus, we show the comparison of its observed amplitude ratios with their theoretical predictions in Fig. 11. The identifications for the highest-amplitude modes of this star are very clear. The strongest mode of KZ Mus is quadrupole ($\ell = 2$), whereas mode f_2 is radial. This is in excellent agreement with the identification by Aerts (2000).

As we have a much larger data set available than Aerts (2000) did, we can also provide an identification for the third mode of KZ Mus, which is a dipole ($\ell = 1$). Only the identification for the weak fourth mode of this star does not point to an unambiguous spherical degree, but we can safely conclude that it is non-radial with $\ell \leqslant 3$; a radial identification is ruled out because the frequency of the mode is too close to that of the radial mode f_2.

Finally, we also look for a possible mode identification for our SPB candidate HD 90434. For this star, we adopted 3-$M_\odot$ models near the ZAMS guided by the results from Section 4.2 to determine the theoretical *UvBV* amplitude ratios. We then proceeded in the same manner as for the β Cephei stars, and present the comparison between theoretical and observed amplitude ratios in Fig. 12.

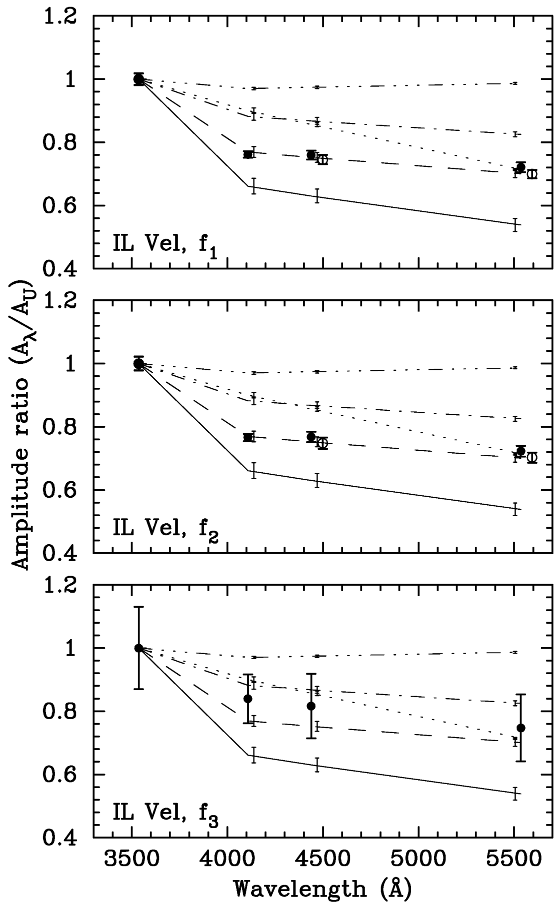

Figure 9. Observed and theoretical *UvBV* amplitude ratios (lines) for $0 \leqslant \ell \leqslant 4$ for IL Vel. Amplitudes are normalized at *U*. The filled circles with error bars are from our measurements, the open circles (somewhat shifted in wavelength for reasons of display) with error bars are for the data of Heynderickx & Haug (1984). The full lines are for radial modes, the dashed lines for dipole modes, the dashed-dotted lines for quadrupole modes, the dotted lines for modes of $\ell = 3$ and the dashed-dot-dot-dotted lines are for $\ell = 4$. The small error bars, also slightly shifted in wavelength, denote the uncertainty in the theoretical amplitude ratios. The upper panel is for mode f_1, the middle one for f_2 and the lower one for f_3.

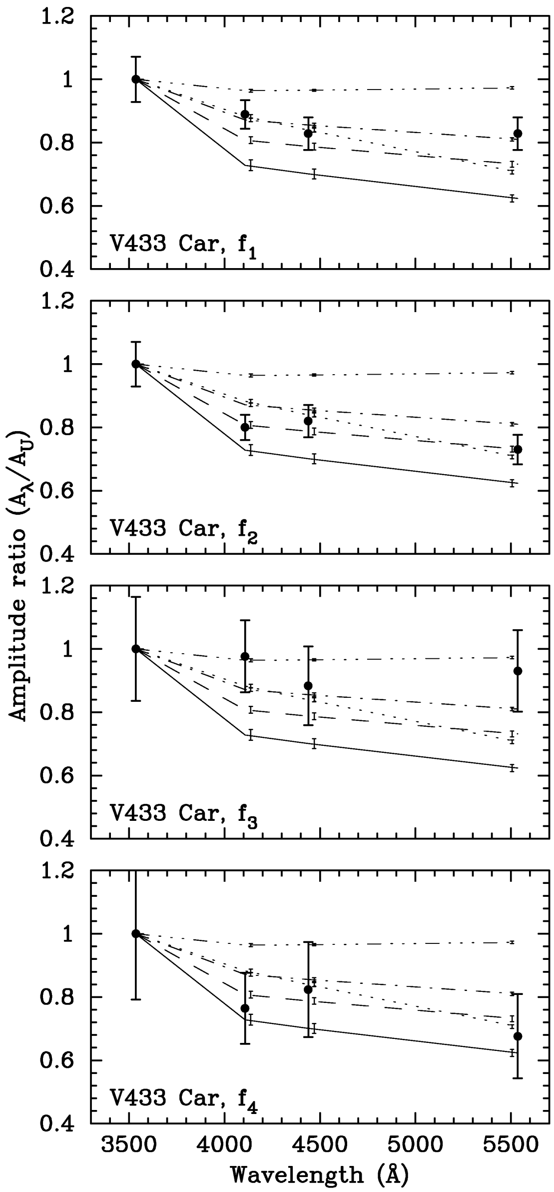

Figure 10. Observed (filled circles with error bars) and theoretical $UvBV$ amplitude ratios (lines) for $0 \leqslant \ell \leqslant 4$ for V433 Car. Amplitudes are normalized at U. The full lines are for radial modes, the dashed lines for dipole modes, the dashed-dotted lines for quadrupole modes, the dotted lines for modes of $\ell = 3$ and the dashed-dot-dot-dotted lines are for $\ell = 4$. The small error bars somewhat shifted in wavelength denote the uncertainty in the theoretical amplitude ratios. The upper panel is for mode f_1, the second for f_2, the third for f_3 and the lower one for f_4.

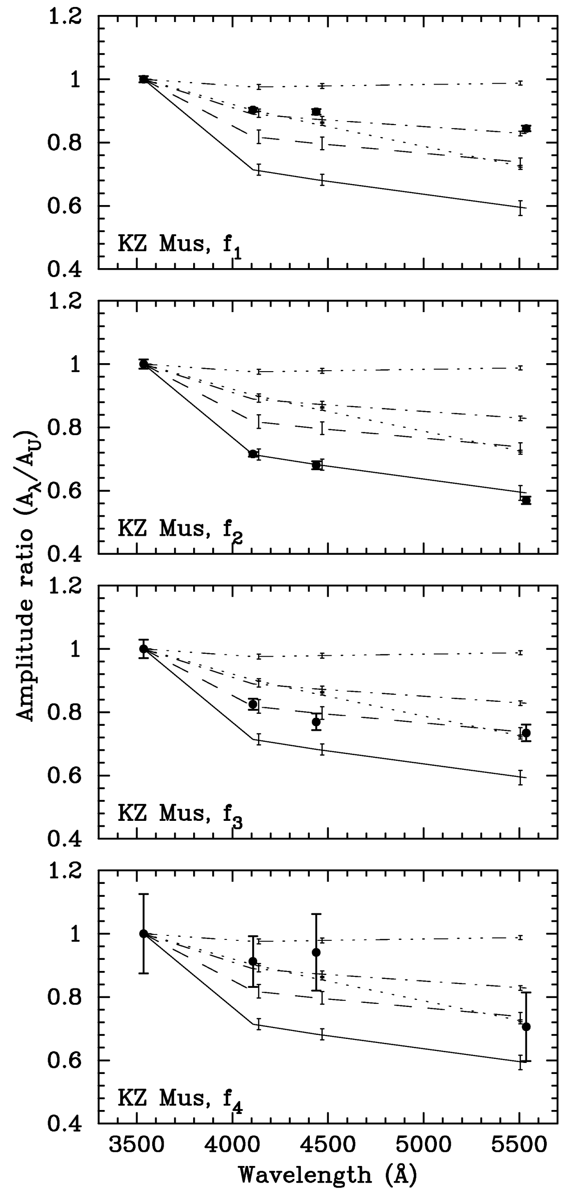

Figure 11. Observed (filled circles with error bars) and theoretical $UvBV$ amplitude ratios (lines) for $0 \leqslant \ell \leqslant 4$ for KZ Mus. Amplitudes are normalized at U. The full lines are for radial modes, the dashed lines for dipole modes, the dashed-dotted lines for quadrupole modes, the dotted lines for modes of $\ell = 3$ and the dashed-dot-dot-dotted lines are for $\ell = 4$. The small error bars somewhat shifted in wavelength denote the uncertainty in the theoretical amplitude ratios. The upper panel is for mode f_1, the second for f_2, the third for f_3 and the lower one for f_4.

Modes of spherical degrees $\ell = 1$ and 4 give the best agreement, but $\ell = 2$ also seems a viable identification. The long period of the star and the normalization of the amplitudes in the U band (where the absolute error on the amplitude is largest) are suspected to result in larger systematic contributions to the observational errors than the formal values we adopted would include. Taking the effects of geometrical cancellation (Dziembowski 1977) into account, the most likely reason for the variability of HD 90434 is pulsation in a dipole mode.

6 ASTEROSEISMOLOGY

6.1 IL Vel

We will now take advantage of the information gathered in the previous sections to understand the pulsational behaviour of our three target stars by means of a comparison with model calculations. We have again used the Warsaw–New Jersey stellar evolution and pulsation code for this part of the analysis. We note that we do not attempt an exhaustive seismic analysis of the stars because too few

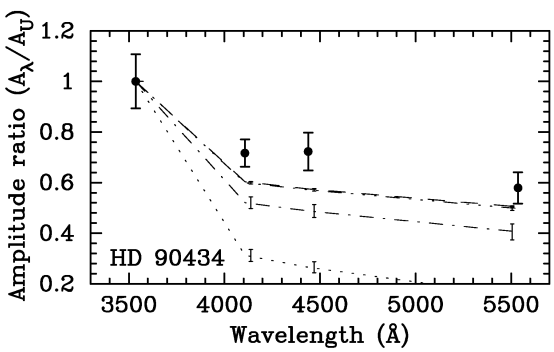

Figure 12. Observed (filled circles with error bars) and theoretical *UvBV* amplitude ratios (lines) for $1 \leqslant \ell \leqslant 4$ for HD 90434. Amplitudes are normalized at *U*. The dashed lines are for dipole modes, the dashed-dotted lines for quadrupole modes, the dotted lines for modes of $\ell = 3$ and the dashed-dot-dot-dotted lines are for $\ell = 4$. The small error bars somewhat shifted in wavelength denote the uncertainty in the theoretical amplitude ratios.

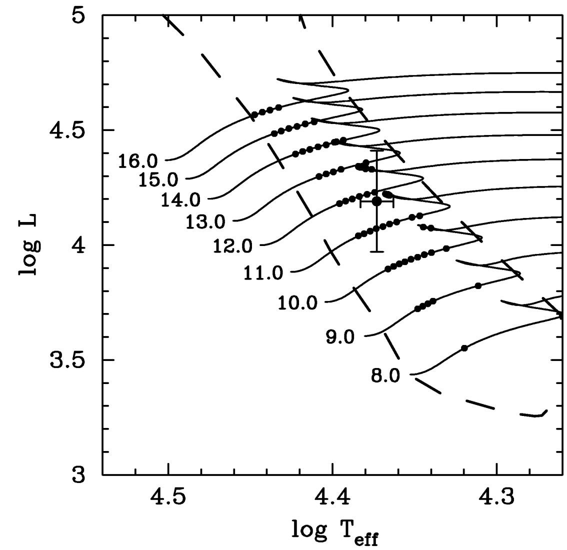

Figure 13. The position of IL Vel in the theoretical HR diagram. Some stellar model evolutionary tracks labelled with their masses (full lines) and the theoretical borders of the β Cephei star instability strip (Pamyatnykh 1999, dashed lines) are included for comparison. The sections of the evolutionary tracks that are marked with filled circles represent models in which the observed frequency range of the star is unstable.

identified pulsation modes are available for such purposes. Instead, we want to determine what we can learn concerning the stars by means of standard models and procedures and we want to assess the potential for asteroseismology of β Cephei stars.

One tool that has been established for constraining the range of physical parameters of the seismological model of a star is stability analysis (see Pamyatnykh 2003 for a review). As a model of a pulsating star evolves, its radius changes, and the range of pulsationally unstable radial overtones of the eigenfrequencies varies as well. In conclusion, the frequency range of the unstable eigenmodes depends on the location of the model in the instability strip. This frequency range can then be matched with that actually observed in the star.

Applying this method to IL Vel, we can take advantage of our mode identification. As all the modes for which we have a certain identification are $\ell = 1$, we can restrict the comparison to this single spherical degree only. Fig. 13 shows evolutionary tracks for models between 8 and 16 $M_\odot$ (we assumed a solar chemical composition and a rotational velocity of 100 km s^{-1} on the ZAMS) in the theoretical Hertzsprung–Russel (HR) diagram together with the parameters of the star from Table 6; models with a matching range of unstable frequencies are indicated.

Inspection of Fig. 13 shows very good agreement between the position of the star in the HR diagram and the range of models that are unstable over the same frequency domain. We note that the sequences of matching models sometimes have gaps as they evolve along the main sequence. This is the result of a change in the type of modes that produce the match and their frequency evolution, which is affected by avoided crossings. We caution that the strength of pulsational driving in β Cephei stars is strongly dependent on metal abundance (Moskalik & Dziembowski 1992; Pamyatnykh 1999). Therefore, the results in Fig. 13 are only an indication of the range of possible models for IL Vel.

The two $\ell = 1$ modes of IL Vel have similar frequencies; they are spaced by only 0.0986 cycle d^{-1}. The projected rotational velocity of the star ($v \sin i = 65$ km s^{-1}, cf. Table 1) implies a rotational period $P_{\rm rot} < 5.8$ d for the star assuming a mass of 12 $M_\odot$ as indicated by Fig. 13. At first glance, this suggests that those two modes cannot be caused by rotational splitting of a single mode. Three explanations for this close splitting may be possible. First, the pulsations of the star are just undergoing an avoided crossing phenomenon (e.g. see Aizenman, Smeyers & Weigert 1976), resulting in the close proximity of a p- and a g-mode. Secondly, the two $\ell = 1$ modes are the central and prograde components of a multiplet, and the second-order rotational splitting is large enough to produce such a small frequency difference. Thirdly, we may observe a gravity mode; the first-order rotational splitting of such a mode is approximately $\nu \approx \{1 - [\ell(\ell+1)]^{-1}\} P_{\rm rot}^{-1}$ (Winget et al. 1991).

We examine these hypotheses in Fig. 14, where we show the evolution of the rotational *m*-mode splitting and the frequencies of the $\ell = 1$ modes of a 12-$M_\odot$ model with $v_{\rm rot,ZAMS} = 70$ km s^{-1} along the main sequence. The first three pressure (p) and the first two gravity (g) modes are shown. From the upper panel of this figure it becomes clear that the observed frequency splitting of IL Vel can be easily reproduced by the model in the corresponding temperature range. In fact, this would be possible with models rotating as fast as 110 km s^{-1}. On the other hand, the rotational frequency splitting of any of these modes never becomes small enough that the observed frequency difference can be caused by $\ell = 1$ modes of the same type and radial overtone but with $m = 1$ and -1. This also implies that the third mode of IL Vel cannot be another member of this multiplet.

To determine the modes that are potentially responsible for the pulsations of IL Vel, we have traced the frequencies of the individual $\ell = 1$ modes of the same model as used before along the main sequence in the lower panel of Fig. 14. The mode originating as p_1 on the ZAMS has a frequency very similar to the two observed for IL Vel over the whole temperature range estimated for the star, and is unstable as well. This mode has already undergone an avoided crossing with the g_1 mode and should therefore also have gravity mode characteristics, i.e. it is a mixed mode. In higher-mass models, dipole modes at this frequency become stable against pulsations, and in models below 11 $M_\odot$ the g_1 mode reproduces the observed frequency in the temperature range appropriate for IL Vel.

Another observation from Fig. 14 is that the p_1 and g_1 modes never come closer together than about 0.5 cycle d^{-1}. It is therefore unlikely that the two modes observed in IL Vel originate from

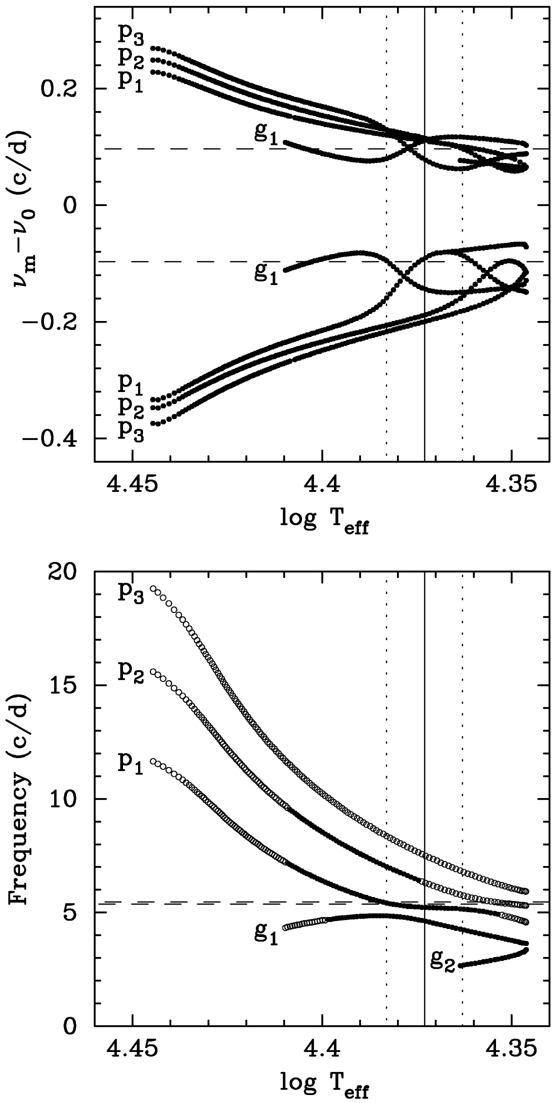

Figure 14. Upper panel: the size of rotational splitting for $\ell = 1$ modes of a 12-M$_{\odot}$ model with $v_{\mathrm{rot,ZAMS}} = 70$ km s^{-1} along its evolution along the main sequence. The first three p-modes and the first g-mode are indicated. The horizontal dashed lines denote the frequency difference between the two strongest modes of IL Vel, and the vertical solid line with parallel dotted lines is the effective temperature of the star and its error estimate from Table 6. Lower panel: stability and frequency evolution of $\ell = 1$, $m = 0$ mode frequencies in the same model. Modes that are pulsationally unstable are denoted with filled circles, the open circles are for stable modes. The two dashed lines represent the observed $\ell = 1$ frequencies and the vertical lines again label the effective temperature of the star and its error estimate. Note the avoided crossing of the p_1 and the g_1 mode starting at about log $T_{\mathrm{eff}} = 4.39$.

different modes that just happen to undergo an avoided crossing. If we consider the hypothesis that the proximity of the two observed $\ell = 1$ modes is caused by the effects of second-order rotational splitting, we find that $v_{\mathrm{rot}} \gtrsim 160$ km s^{-1}, and hence $i < 25°$, which is also unlikely. In addition, the high amplitude of the prograde mode and the absence of the retrograde component of the hypothesized triplet would also be difficult to explain.

We conclude that the two dipole pulsation modes of IL Vel are most likely to be caused by rotationally split components of the mode originating as p_1 on the ZAMS. One of these modes is $m = 0$, the other one is $|m| = 1$ and $65 < v_{\mathrm{rot}} < 110$ km s^{-1}.

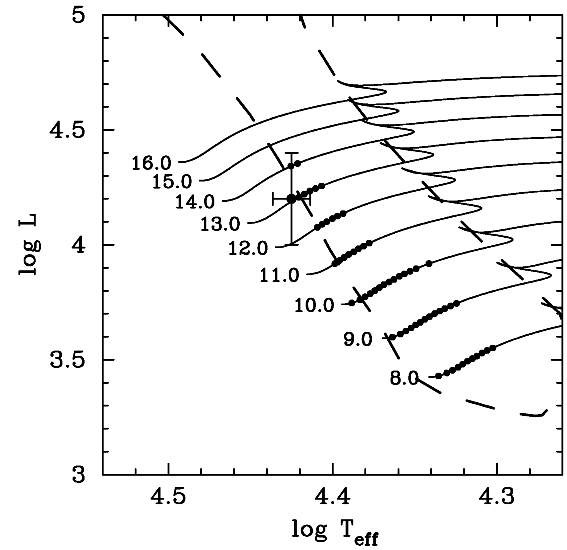

Figure 15. The position of V433 Car in the theoretical HR diagram. Some stellar model evolutionary tracks labelled with their masses (full lines) and the theoretical borders of the β Cephei star instability strip (Pamyatnykh 1999, dashed lines) are included for comparison. The sections of the evolutionary tracks that are marked with filled circles represent models in which the observed frequency range of the star is unstable. For some models, we obtain unstable pulsation modes somewhat outside the blue edge of the theoretical instability strip, which is caused by $\ell = 4$ modes; the borders indicated are only for $\ell \leqslant 2$.

6.2 V433 Car

We have performed a similar analysis for V433 Car. Regrettably, we could not obtain unambiguous ℓ identifications for any of its modes. On the other hand, the excited frequency range of the star is larger, which may, however, be related to it being a fast rotator. In any case, we show the match of unstable model frequencies to that of the observed ones in Fig. 15. The model evolutionary tracks are again for solar chemical composition, but for a rotational velocity of 260 km s^{-1} on the ZAMS, and we considered all modes with $0 \leqslant \ell \leqslant 4$.

Again, the agreement between theory and observation is fairly good, even when bearing in mind that our analysis does not take into account the frequency spread owing to fast rotation of the star. However, as the observational results only allow us a rough qualitative comparison between observations and theory for V433 Car, this is not regarded as being important. V433 Car appears to be an object of about 13 M$_{\odot}$ that has just entered the β Cephei star instability strip.

6.3 KZ Mus

The asteroseismological prospects of KZ Mus appear to be much better. In particular, we have unambiguously identified one of its modes as being radial, and two more modes also have unique ℓ assignments. In the same fashion as in the previous sections, we show model evolutionary tracks (for $v_{\mathrm{rot,ZAMS}} = 100$ km s^{-1}) in the theoretical HR diagram, the position of the star in it, and models with unstable modes in the observed frequency range in Fig. 16.

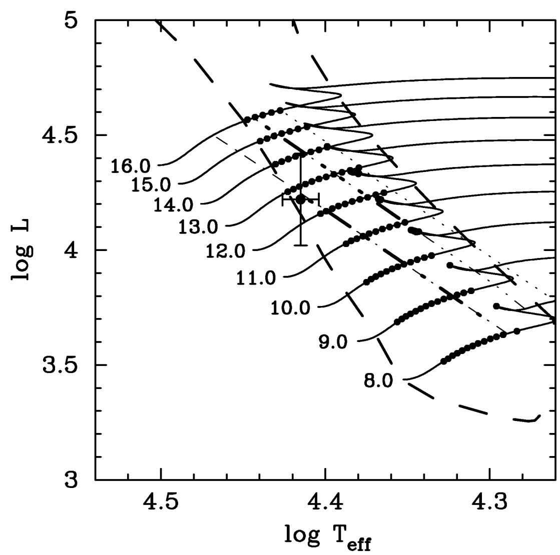

Figure 16. The position of KZ Mus in the theoretical HR diagram. Some stellar evolutionary tracks labelled with their masses (full lines) and the theoretical borders of the β Cephei star instability strip (Pamyatnykh 1999, dashed lines) are included for comparison. The sections of the evolutionary tracks that are marked with filled circles represent models in which the observed frequency range of the star is unstable. The lines going from the top left to the bottom right are locations of models that have a radial mode at 5.9506 cycle d^{-1}. For models on the dashed-dotted line this would be the fundamental radial mode, those connected by the dash-triple-dotted line show the first overtone at this frequency, and those connected by the dotted line have their second radial overtone at 5.9506 cycle d^{-1}. The thick parts of these lines connect the models, which are pulsationally unstable.

In addition, we have indicated the locations of models that have a radial mode at 5.9506 cycle d^{-1} as observed for KZ Mus.

As for the other two stars, we find no disagreement between models with unstable modes in the observed frequency range and the observationally determined position of the star in the HR diagram. Fig. 16 also allows us to reject the second overtone as the identification for the radial mode of KZ Mus, as it is inconsistent with the evolutionary state of the star, and it never becomes pulsationally unstable.

However, we cannot say at this point whether the radial mode is the fundamental or first overtone. Models with the fundamental radial mode at 5.9506 cycle d^{-1} are in better agreement with the stellar parameters from Table 6, but it may be stable in models with the mass inferred for the star. On the other hand, for this mode to be the first overtone, only models at the upper limits on mass and luminosity seem appropriate.

We attempted to find further constraints on the parameter space occupied by KZ Mus using the non-radial modes that we identified unambiguously; any model representing the star should have modes of the same ℓ in the correct frequency range. All models with the radial fundamental or first overtone mode at 5.9506 cycle d^{-1} that we investigated could be used to reproduce the observed non-radial modes given the unknown angular rotational velocity of the star. However, when imposing mode stability as an additional criterion, it is found that model sequences of 12 and 13 $M_{\odot}$ give the best agreement with the observations.

In this case, it is most likely that f_2 is the radial fundamental mode of KZ Mus. Then the $\ell = 1$ mode would be associated with the mode originating as p_1 at the ZAMS and the observed $\ell = 2$ most likely corresponds to the mode originating as g_1.

7 SUMMARY, DISCUSSION AND CONCLUSIONS

In an attempt to investigate the asteroseismological potential of the β Cephei stars, we have obtained 127–150 h of differential photoelectric photometry for each of the three pulsators IL Vel, V433 Car and KZ Mus. In line with the recent results of Stankov et al. (2002) and Cuypers et al. (2002), we have shown that low-amplitude pulsation modes are present in β Cephei stars, and that large observational efforts to determine their mode spectra in detail are justified. We therefore confirm the importance of β Cephei stars as asteroseismological targets for both ground- and space-based measurements.

Using the amplitude ratios of the different pulsation modes in the $UvBV$ filters of the Johnson and Strømgren systems, we performed mode identification. We obtained unambiguous results for all pulsation modes with photometric amplitudes larger than about 10 mmag in V, or with relative errors on their amplitude smaller than 3 per cent. The modes we could identify were the two dominant ones of IL Vel and the three strongest ones of KZ Mus, but none of V433 Car.

This may not only be a result of its photometric amplitudes that are small compared with those of the other two β Cephei stars. We have shown that V433 Car is a fast rotator, and therefore mode coupling (see Daszyńska-Daszkiewicz et al. 2002 and references therein) may occur. Mode coupling affects the predicted colour amplitude ratios and phase shifts. Since we have not taken this into account in our analysis, it may be at least partly responsible for the ambiguous mode identifications for this star.

On the other hand, our results for the more slowly rotating stars appear reliable, which represents a good motivation for studying a larger number of multiperiodic β Cephei stars in the future. Our limit of the relative error of 3 per cent of the photometric amplitudes for successful mode identification can then serve as a guideline for planning future campaigns.

We have performed model calculations for our three targets. The outcome was also quite encouraging. Although we only detected up to four modes per star (thus our obervational constraints on the models are not very strong), in no case are disagreements between the observational results and model predictions found. The observationally determined positions of the stars in the HR diagram could be reproduced by models that have the same range in unstable pulsation frequencies as are excited in the real stars.

In addition, we were able to place constraints on the types of mode observed in IL Vel and KZ Mus. We have shown that the most likely explanation for the two dipole modes of IL Vel are rotationally split components (one necessarily being $m = 0$) of the mode originating as p_1 on the ZAMS. The third mode of IL Vel cannot be another multiplet member, and the equatorial rotational velocity of the star must be smaller than 110 km s^{-1}. If the radial mode observed in KZ Mus is the fundamental, then the high-amplitude $\ell = 2$ mode is most likely that originating as g_1, and the $\ell = 1$ mode we identified is probably that originating as p_1.

We cannot push the asteroseismological analysis of the three stars further at this point because too few modes have been detected and identified for detailed modelling. However, we strongly suspect that more modes are present in IL Vel that just need better time resolution to be detected. KZ Mus may have more modes as well, and a unique mode identification for its fourth mode may place a constraint on the rotation frequency of the star. Further work on both stars should also include time-resolved spectroscopic observations to determine the azimuthal order m of the high-amplitude non-radial modes; although both objects are $V \approx 9.1$, the spectra we obtained suggests this is possible. Determinations of the metal abundances of the stars would also be a valuable ingredient for model calculations. With all of these observations in hand, precise asteroseismological studies of IL Vel and KZ Mus appear to be possible.

ACKNOWLEDGMENTS

This work has been supported by the Austrian Fonds zur Förderung der wissenschaftlichen Forschung under grant R12-N02 to GH and by travel support for FR and TT under grant P14546-PHY. We thank Wolfgang Zima for helping with some of the observations. GH is indebted to Alosha Pamyatnykh for helpful discussions, for providing theoretical instability domains for the β Cephei stars and to him and Anamarija Stankov for comments on a draft version of this paper. This research has made use of the SIMBAD and VizieR data bases, operated at CDS, Strasbourg, France and the GCPD data base, operated at the Institute of Astronomy of the University of Lausanne.

REFERENCES

Aerts C., 2000, A&A, 361, 245
Aizenman M., Smeyers P., Weigert A., 1976, A&A, 58, 41
Balona L.A., Evers E.A., 1999, MNRAS, 302, 349
Breger M. et al., 1993, A&A, 271, 482
Chen B., Vergely J.L., Valette B., Carraro G., 1998, A&A, 336, 137
Crawford D.L., 1978, AJ, 83, 48
Cuypers J., Aerts C., Buzasi D., Catanzarite J., Conrow T., Laher R., 2002, A&A, 392, 599
Daszyńska-Daszkiewicz J., Dziembowski W.A., Pamyatnykh A.A., Goupil M.-J., 2002, A&A, 392, 151
Drilling J.S., Landolt A.U., 2000, in Cox A.N., ed., Allen's Astrophysical Quantities, 4th edn. Springer-Verlag, Berlin, p. 392
Dziembowski W.A., 1977, Acta Astron., 27, 203
Dziembowski W.A., Jerzykiewicz M., 1999, A&A, 341, 480
Dziembowski W.A., Moskalik P., Pamyatnykh A.A., 1993, MNRAS, 265, 588
ESA, 1997, The *Hipparcos* and Tycho catalogues, ESA SP-1200
Flower P.J., 1996, ApJ, 469, 355
Gray R.O., Corbally C.J., 1994, AJ, 107, 742
Heynderickx D., 1992, A&AS, 96, 207
Heynderickx D., Haug U., 1994, A&AS, 106, 79
Heynderickx D., Waelkens C., Smeyers P., 1994, A&AS, 105, 447
Houk N., Cowley A.P., 1975, Michigan Spectral Catalogue, Vol. 1
Künzli M., North P., Kurucz R.L., Nicolet B., 1997, A&AS, 122, 51
Lampens P., 1988, PhD dissertation, Katholieke Universiteit Leuven, Belgium
Montgomery M.H., O'Donoghue D., 1999, Delta Scuti Star News., 13, 28 (Univ. Vienna)
Moskalik P., Dziembowski W.A., 1992, A&A, 256, L5
Napiwotzki R., Schönberner D., Wenske V., 1993, A&A, 268, 653
Pamyatnykh A.A., 1999, Acta Astron., 49, 119
Pamyatnykh A.A., 2003, in Thompson M.J., Cunha M.S., Monteiro M.J.P.F.G., eds, Asteroseismology Across the HR Diagram. Kluwer, Dordrecht, in press
Pamyatnykh A.A., Dziembowski W.A., Handler G., Pikall H., 1998, A&A, 333, 141
Smalley B., Dworetsky M.M., 1995, A&A, 293, 446
Soufi F., Goupil M.J., Dziembowski W.A., 1998, A&A, 334, 911
Sperl M., 1998, Master's thesis, Univ. Vienna
Stankov A., Handler G., Hempel M., Mittermayer P., 2002, MNRAS, 336, 189
Waelkens C., Aerts C., Kestens E., Grenon M., Eyer L., 1998, A&A, 330, 215
Winget D.E. et al., 1991, ApJ, 378, 326

This paper has been typeset from a TEX/LATEX file prepared by the author.

5.4 Asteroseismology of ν Eridani

5.4.1 Asteroseismology of the β Cephei star ν Eridani – I. photometric observations and pulsational frequency analysis

Original paper:

G. Handler, R. R. Shobbrook, M. Jerzykiewicz, K. Krisciunas, T. Tshenye, E. Rodriguez, V. Costa, A.-Y. Zhou, R. Medupe, W. M. Phorah, R. Garrido, P. J. Amado, M. Paparó, D. Zsuffa, L. Ramokgali, R. Crowe, N. Purves, R. Avila, R. Knight, E. Brassfield, P. M. Kilmartin, P. L. Cottrell, 2004, MNRAS 347, 454

Mon. Not. R. Astron. Soc. **347,** 454–462 (2004)

Asteroseismology of the β Cephei star ν Eridani – I. Photometric observations and pulsational frequency analysis

G. Handler,[1★] R. R. Shobbrook,[2†] M. Jerzykiewicz,[3] K. Krisciunas,[4,5] T. Tshenye,[6] E. Rodríguez,[7] V. Costa,[7] A.-Y. Zhou,[8] R. Medupe,[6,9] W. M. Phorah,[6] R. Garrido,[7] P. J. Amado,[7] M. Paparó,[10] D. Zsuffa,[10] L. Ramokgali,[6] R. Crowe,[11] N. Purves,[11] R. Avila,[11] R. Knight,[11] E. Brassfield,[11] P. M. Kilmartin[12] and P. L. Cottrell[12]

[1] *Institut für Astronomie, Universität Wien, Türkenschanzstrasse 17, A-1180 Wien, Austria*
[2] *Australian National University, Canberra, ACT, Australia*
[3] *Wroclaw University Observatory, ul. Kopernika 11, 51-622 Wroclaw, Poland*
[4] *Cerro Tololo Inter-American Observatory, National Optical Astronomy Observatory, Casilla 603, La Serena, Chile*
[5] *Las Campanas Observatory, Casilla 601, La Serena, Chile*
[6] *Theoretical Astrophysics Programme, University of the North-West, Private Bag X2046, Mmabatho 2735, South Africa*
[7] *Instituto de Astrofisica de Andalucia, C.S.I.C., Apdo. 3004, 18080 Granada, Spain*
[8] *National Astronomical Observatories, Chinese Academy of Sciences, Beijing 100012, China*
[9] *South African Astronomical Observatory, PO Box 9, Observatory 7935, South Africa*
[10] *Konkoly Observatory, Box 67, H-1525 Budapest XII, Hungary*
[11] *Department of Physics and Astronomy, University of Hawaii - Hilo, 200 West Kawili Street, Hilo, Hawaii, 96720-4091, USA*
[12] *Department of Physics and Astronomy, University of Canterbury, Christchurch, New Zealand*

Accepted 2003 September 12. Received 2003 September 12; in original form 2003 August 4

ABSTRACT

We undertook a multisite photometric campaign for the β Cephei star ν Eridani. More than 600 h of differential photoelectric *uvyV* photometry were obtained with 11 telescopes during 148 clear nights.

The frequency analysis of our measurements shows that the variability of ν Eri can be decomposed into 23 sinusoidal components, eight of which correspond to independent pulsation frequencies between 5 and 8 cd^{-1}. Some of these are arranged in multiplets, which suggests rotational *m*-mode splitting of non-radial pulsation modes as the cause. If so, the rotation period of the star must be between 30 and 60 d.

One of the signals in the light curves of ν Eri has a very low frequency of 0.432 cd^{-1}. It can be a high-order combination frequency or, more likely, an independent pulsation mode. In the latter case, ν Eri would be both a β Cephei star and a slowly pulsating B (SPB) star.

The photometric amplitudes of the individual pulsation modes of ν Eri appear to have increased by about 20 per cent over the last 40 years. So have the amplitudes of the dominant combination frequencies of the star. Among the latter, we could only identify sum frequencies with certainty, not difference frequencies, which suggests that neither light-curve distortion in its simplest form nor resonant mode coupling is their single cause.

One of our comparison stars, μ Eridani, turned out to be variable with a dominant time-scale of 1.62 d. We believe either that it is an SPB star just leaving its instability strip or that its variations are of rotational origin.

Key words: techniques: photometric – stars: early-type – stars: individual: μ Eridani – stars: individual: ν Eridani – stars: oscillations – stars: variables: other.

★E-mail: handler@astro.univie.ac.at
†Visiting Fellow.

1 INTRODUCTION

Lengthy multisite observations of multiperiodically pulsating stars have become a standard tool in variable star research. The benefits of such efforts are long, uninterrupted time series of the variations of the target stars, which are necessary to resolve complicated pulsational spectra. The more individual variations present in a given pulsator, the more we can learn about its interior by modelling the observed mode spectra. This technique is called asteroseismology.

The most extensive observational efforts for asteroseismology have been performed with dedicated telescope networks. For instance, the Whole Earth Telescope (Nather et al. 1990) has already observed 40 individual targets, more than half of which are pulsating white dwarf stars, the others being pulsating sdB stars, rapidly oscillating Ap stars, cataclysmic variables, etc. The Delta Scuti Network (e.g. Zima et al. 2002) has studied 10 different objects during 23 campaigns and acquired a total of more than 1000 h of measurement for some δ Scuti pulsators.

The very first coordinated multisite observations were obtained as early as 1956, on the β Cephei star 12 (DD) Lacertae (de Jager 1963). This effort even included both spectroscopic and multicolour photometric measurements. In more recent times, however, β Cephei stars were (aside from a large campaign for BW Vul; Sterken et al. 1986) rarely the targets of extended observing campaigns. The reason may be the sparse frequency spectra of β Cephei stars compared to pulsating white dwarfs or δ Scuti stars. For many years, the record holder was 12 (DD) Lac with five known independent modes of pulsation (Jerzykiewicz 1978), which was recently superseded by the six modes of V836 Cen (Aerts et al. 2003).

However, the apparent paucity of frequencies in the mode spectra of β Cephei stars may be questioned. Experience with δ Scuti stars has shown that the more the detection level for periodic light variations is pushed down, the more pulsation modes are detected (e.g. see the sequence of papers by Handler et al. 1996, 1997, 2000). In fact, most of the pulsation modes of these stars have light amplitudes around or below 1 mmag, an amplitude quite easily detected with the large data sets of 2–3 mmag precision differential photometry obtained during these campaigns. As the pulsational driving of the β Cephei stars (Moskalik & Dziembowski 1992) is based on essentially the same mechanism (the κ mechanism) as that of the δ Scuti stars, just operating on heavier chemical elements, it can be suspected that many low-amplitude modes are also excited in β Cephei stars but have not yet been detected simply because of a lack of suitable data. Indeed, this idea is supported by recent high-quality observations (Stankov et al. 2002; Cuypers et al. 2002; Handler et al. 2003).

Besides the detection of many pulsation modes, another necessary ingredient for asteroseismology is the correct identification of these modes with their pulsational quantum numbers, k, the radial overtone of the mode, the spherical degree ℓ and the azimuthal order m. For pulsating stars whose frequency spectra do not show any obvious regularities caused by rotationally split modes or consecutive radial overtones the use of mode identification methods is required. This may, for instance, be spectroscopic diagnostics from line profile variations or photometric colour amplitude ratios and phase shifts. Unfortunately, such methods may not always yield unambiguous results (see, for example, Balona 2000). However, Handler et al. (2003) recently showed that mode identification from photometric colour amplitudes works well for slowly rotating β Cephei stars and they estimated that a relative accuracy of 3 per cent in the amplitude determinations is sufficient to achieve an unambiguous determination of ℓ.

Consequently, β Cephei stars are indeed suitable for asteroseismic studies. If successful, many interesting astrophysical results can be expected. For instance, angular momentum transport in these stars can be studied. The frequencies of some pulsation modes of β Cephei stars are sensitive to the amount of convective core overshooting (Dziembowski & Pamyatnykh 1991). Deviations from the rotational frequency splitting of non-radial mode multiplets can be due to the interior magnetic field structure of those stars (Dziembowski & Jerzykiewicz 2003). Once the interior structures of several β Cephei stars in various phases of their evolution are determined, main-sequence stellar evolution calculations can be calibrated and more accurately extrapolated to the supernova stage, which can in turn constrain spectral and chemical evolution theories of galaxies.

Hence, it is justified to devote large observational efforts to β Cephei stars that seem suitable for asteroseismology. The selection of a good candidate is one of the most important prerequisites for such a study. For the present work, our choice was ν Eri (HD 29248, $V = 3.92$). Its mode spectrum reveals high asteroseismic interest; four pulsation frequencies were known, a singlet and an equally spaced triplet (Kubiak 1980; Cuypers & Goossens 1981). The singlet has been suggested to be a radial mode, and the triplet is consistent with a dipole (Aerts, Waelkens & de Pauw 1994; Heynderickx, Waelkens & Smeyers 1994).

If this triplet contained at least two rotationally split m-components of a mode, ν Eri would also be a slow rotator, a hypothesis supported by its measured $v \sin i$ (the most recent determination being 20 km s^{-1}; Abt, Levato & Grosso 2002). This is important because the adverse effects of rotational mode coupling (see Pamyatnykh 2003 or Daszyńska-Daszkiewicz et al. 2002) in a subsequent theoretical analysis would be diminished. Finally, ν Eri is a bright equatorial star, so it can be observed from both hemispheres with photometric and high-resolution spectroscopic instruments.

We therefore organized a multisite campaign for ν Eri, applying both observing methods mentioned above (Handler & Aerts 2002). In the following, we report on the results from the photometric measurements. The analysis of the spectroscopy, pulsational mode identification and seismic modelling of the identified oscillations will be the subject of future papers.

2 OBSERVATIONS AND REDUCTIONS

Our photometric observations were carried out with 11 different telescopes and photometers at 10 observatories on five different continents; these are summarized in Table 1. In most cases, single-channel differential photometry was acquired through the Strömgren *uvy* filters. However, at Sierra Nevada Observatory (OSN) a simultaneous *uvby* photometer was used, so we included the *b* filter as well, and at the four observatories where no Strömgren filters were available we used Johnson *V*. Some measurements through the H_β filters were also obtained at OSN. The total time base line spanned by our measurements is 157.9 d.

We chose two comparison stars for ν Eri: μ Eri (HD 30211, B5IV, $V = 4.00$) and ξ Eri (HD 27861, A2V, $V = 5.17$). Another check star, HD 29227 (B7 III, $V = 6.34$) was also monitored at OSN. We note that μ Eri was the single comparison star in all published extensive photometric studies of ν Eri (van Hoof 1961; Kubiak & Seggewiss 1991) and that its *Hipparcos* photometric data (ESA 1997) imply some slow variability (Koen & Eyer 2002). The star is also a spectroscopic binary ($P_{\rm orb} = 7.35890$ d, $e = 0.26$; Hill 1969). In the hope that we could also understand the variability of μ Eri with our multisite observations, and hoping to use that knowledge

Table 1. Log of the photometric measurements of ν Eri. Observatories are ordered according to geographical longitude. Sites that acquired V measurements only are marked with asterisks.

Observatory	Longitude	Latitude	Telescope	Amount of data		Observer(s)
				Nights	h	
Sierra Nevada Observatory	$-3^\circ\ 23'$	$+37^\circ\ 04'$	0.9-m	18	53.59	ER, VC, RG, PJA
Cerro Tololo Interamerican Observatory	$-70^\circ\ 49'$	$-30^\circ\ 09'$	0.6-m	8	43.19	KK
Fairborn Observatory	$-110^\circ\ 42'$	$+31^\circ\ 23'$	0.75-m APT	24	114.54	–
Lowell Observatory	$-111^\circ\ 40'$	$+35^\circ\ 12'$	0.5-m	10	46.01	MJ
Mauna Kea Observatory*	$-155^\circ\ 28'$	$+19^\circ\ 50'$	0.6-m	4	7.78	RC, NP, RA, RK, EB
Mount John University Observatory*	$+170^\circ\ 28'$	$-43^\circ\ 59'$	0.6-m	1	3.83	PMK
Siding Spring Observatory	$+149^\circ\ 04'$	$-31^\circ\ 16'$	0.6-m	31	117.70	RRS
Xing-Long Observatory*	$+117^\circ\ 35'$	$+40^\circ\ 24'$	0.85-m	3	15.72	AYZ
South African Astronomical Observatory	$+20^\circ\ 49'$	$-32^\circ\ 22'$	0.5-m	37	151.82	GH, TT, RM, WP, LR
South African Astronomical Observatory	$+20^\circ\ 49'$	$-32^\circ\ 22'$	0.75-m	7	39.31	GH
Piszkestetö Observatory*	$+19^\circ\ 54'$	$+47^\circ\ 55'$	0.5-m	5	11.86	MP, DZ
Total				148	605.35	

in re-analyses of the published data of ν Eri, we retained μ Eri as a comparison star. During data reduction, we took care that the variations of μ Eri would not influence the results on our primary target.

Data reduction was therefore started by correcting for coincidence losses, sky background and extinction. Nightly extinction coefficients were determined with the Bouguer method from the ξ Eri measurements only; second-order colour extinction coefficients were also determined. We then calculated differential magnitudes between the comparison stars (in the sense μ Eri–ξ Eri). Heliocentrically corrected versions of these time series were set aside for later analysis of the variability of μ Eri, to which we will return later.

The nightly (μ Eri–ξ Eri) differential magnitudes were fitted with low-order polynomials ($n < 4$). The residuals of the non-differential μ Eri magnitudes with respect to that fit were combined with the ξ Eri data and were assumed to reflect the effects of transparency and detector sensitivity changes only. Consequently, these combined time series were binned into intervals that would allow good compensation for the above-mentioned non-intrinsic variations in the target star time series and were subtracted from the measurements of ν Eri. The binning minimizes the introduction of noise in the differential light curve of the target.

The timings for this differential light curve were heliocentrically corrected as the next step. Finally, the photometric zero-points of the different instruments, which may be different because of the different colours of ν Eri and ξ Eri, were examined at times of overlap with a different site and adjusted if necessary. Measurements in the Strömgren y and Johnson V filters were treated as equivalent and analysed together due to the same effective wavelength of these filters. The resulting final combined time series was subjected to frequency analysis; we show some of our light curves of ν Eri in Fig. 1. In the end, we had more than 3000 measurements in each filter with accuracies of 3.7 (u filter), 3.0 (v filter) and 3.0 mmag (y/V filters) per data point available.

3 FREQUENCY ANALYSIS

3.1 The programme star

Our frequency analyses were mainly performed with the program PERIOD 98 (Sperl 1998). This package applies single-frequency power spectrum analysis and simultaneous multifrequency sine-wave fitting. It also includes advanced options, such as the calculation of optimal light-curve fits for multiperiodic signals including harmonic, combination, and equally spaced frequencies. As will be demonstrated later, our analysis requires some of these features.

We started by computing the Fourier spectral window of the final light curves in each of the filters. It was calculated as the Fourier transform of a single noise-free sinusoid with a frequency of 5.7633 cd^{-1} (the strongest pulsational signal of ν Eri) and an amplitude of 36 mmag sampled in the same way as were our measurements. The upper panel of Fig. 2 contains the result for the combined y and V data. Any alias structures that would potentially mislead us into incorrect frequency determinations are quite low in amplitude due to our multisite coverage.

We proceeded by computing the amplitude spectra of the data itself (second panel of Fig. 2). The signal designated f_1 dominates, but some additional structures not compatible with the spectral window side lobes are also present. Consequently, we pre-whitened this signal by subtracting a synthetic sinusoidal light curve with a frequency, amplitude and phase that yielded the smallest possible residual variance, and computed the amplitude spectrum of the residual light curve (third panel of Fig. 2).

This resulted in the detection of a second signal (f_2) and of another variation at the sum frequency of the two previously detected. We then pre-whitened a three-frequency fit from the data using the same optimization method as before and fixed the combination term to the exact sum of the two independent frequencies. We continued this procedure (further panels of Fig. 2) until no significant peaks were left in the residual amplitude spectrum.

We consider an independent peak statistically significant if it exceeds an amplitude signal-to-noise ratio (S/N) of 4 in the periodogram; combination signals must satisfy S/N $>$3.5 to be regarded as significant (see Breger et al. 1999, for a more in-depth discussion of this criterion). The noise level was calculated as the average amplitude in a 5-cd^{-1} interval centred on the frequency of interest.

We repeated the pre-whitening procedure with the u and v data independently and obtained the same frequencies within the observational errors. We then determined final values for the detected frequencies by averaging the values from the individual filters, weighted by their S/N. The pulsational amplitudes were then recomputed with those frequencies; the result is listed in Table 2.

The residuals from this solution were searched for additional candidate signals that may be intrinsic. We have first investigated the residuals in the individual filters, then analysed the averaged residuals in the three filters (whereby the u data were divided by 1.5 to scale them to amplitudes and rms scatter similar to that in the

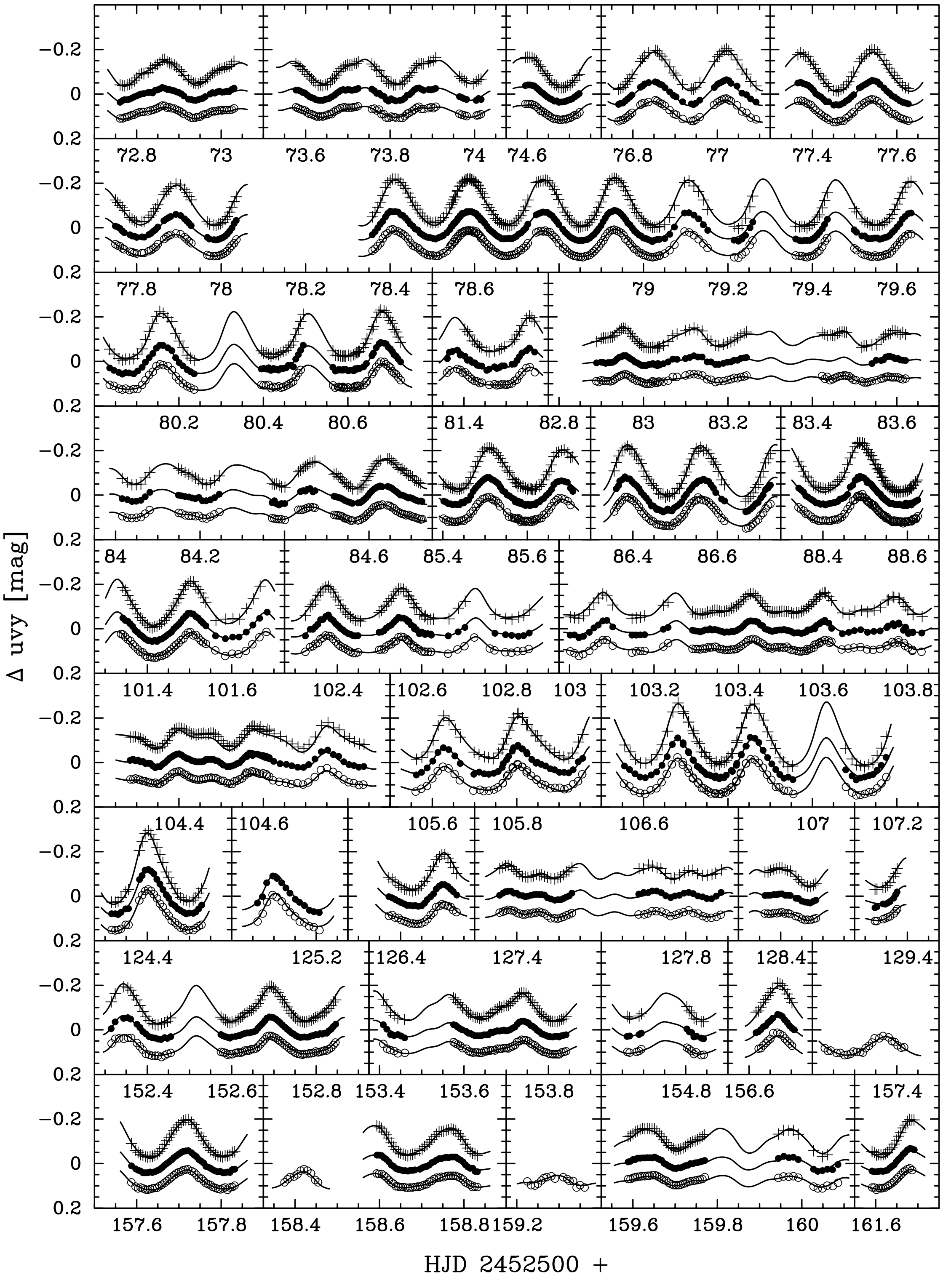

Figure 1. Some light curves of ν Eri. Plus signs are data in the Strömgren *u* filter, filled circles are our *v* measurements and open circles represent Strömgren *y* and Johnson *V* data. The full line is a fit composed of all the periodicities detected in the light curves (Table 2). The amount of data shown here is about half the total.

other two filters), and finally applied statistical weights according to the recommendation by Handler (2003). Some interesting features were found and are listed in Table 3.

In this table, the signal at 0.254 $\mathrm{c\,d^{-1}}$ is formally significant in the *v* filter data, and noticeable peaks are present at the same frequency in both the *u* and *y* filter data. However, we find the evidence from all the data sets taken together not sufficiently convincing to claim reality for this peak. Similar comments apply to the other signals listed in Table 3. We would, however, like to point out that the variations near 6–8 $\mathrm{c\,d^{-1}}$ may all be components of multiplets that

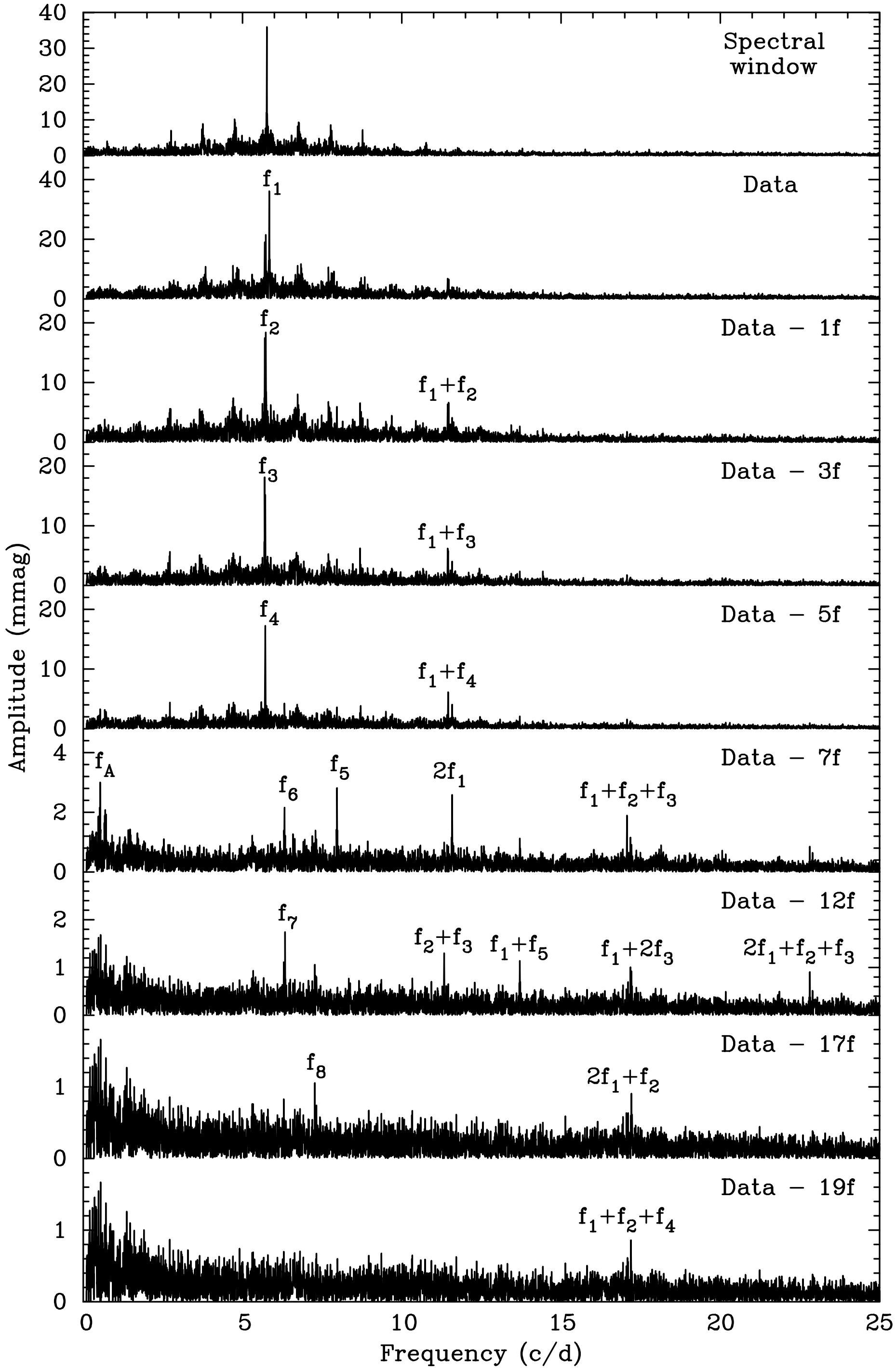

Figure 2. Amplitude spectra of ν Eri. The uppermost panel shows the spectral window of the data, followed by the periodogram of the data. Successive pre-whitening steps are shown in the following panels; note their different ordinate scales. See text for details.

include detected modes. The signals at frequencies higher than 17 cd^{-1} all coincide with combinations of detected modes.

3.2 The comparison stars

We still have to analyse the light curves of μ Eri–ξ Eri. To this end, we have computed the amplitude spectrum of these data and show it in the upper panel of Fig. 3. One peak stands out; pre-whitening it leaves strong evidence for further variability of this star (Fig. 3, second panel), but no more periodicities can be detected.

The single periodicity that may be present in the light curves of μ Eri has a frequency of 0.61638 ± 0.0005 cd^{-1} and *uvy* amplitudes of 10.2, 6.4 and 5.0 mmag, respectively. It is statistically significant with S/N ratios between 6.3 and 4.4 in the different filters, but it is not clear if its frequency and amplitude were constant throughout the observing window. The residual amplitude spectrum after pre-whitening this signal still shows a very strong 1/*f* component and indicates that the variability of μ Eri is complicated. However, further analyses of the differential μ Eri–ξ Eri light curves, such as searching for variations with non-sinusoidal pulse shapes using

Table 2. Multifrequency solution for our time-resolved photometry of ν Eri. Formal error estimates (following Montgomery & O'Donoghue 1999) for the independent frequencies range from ±0.00001 cd^{-1} for f_1 to ±0.00035 cd^{-1} for f_8. Formal errors on the amplitudes are ±0.2 mmag in u and ±0.1 mmag in v and y. The S/N ratio quoted is for the y filter data.

ID	Freq. (cd^{-1})	u ampl. (mmag)	v ampl. (mmag)	y ampl. (mmag)	S/N
f_1	5.76327	73.5	41.0	36.9	137.0
f_3	5.62006	34.6	23.9	22.7	83.6
f_4	5.63716	32.2	22.4	21.0	77.7
f_2	5.65393	37.9	26.4	25.1	92.6
f_6	6.24408	3.9	2.5	2.6	9.8
f_7	6.26205	2.9	1.9	1.8	6.8
f_8	7.19994	1.3	0.9	1.1	4.3
f_5	7.89780	4.3	3.1	3.0	11.7
f_A	0.43218	5.5	3.2	3.2	7.1
f_2+f_3	11.27399	2.8	1.7	1.4	6.4
f_1+f_3	11.38333	11.1	7.9	7.5	34.9
f_1+f_4	11.40043	10.9	7.7	7.1	33.2
f_1+f_2	11.41720	12.6	9.0	8.4	39.3
$2f_1$	11.52654	4.5	3.1	2.9	13.8
f_1+f_5	13.66107	1.6	1.2	1.1	6.4
$f_1+f_3+f_4$	17.02049	1.0	0.7	0.7	4.7
f_1+f_2+f3	17.03726	4.4	3.1	2.6	16.9
$f_1+f_2+f_4$	17.05435	1.0	0.8	0.9	6.1
f_1+2f_2	17.07113	0.8	0.7	0.5	3.5
$2f_1+f_3$	17.14660	1.8	1.4	1.2	8.0
$2f_1+f_4$	17.16370	1.7	1.2	1.0	6.6
$2f_1+f_2$	17.18047	1.9	1.4	1.3	8.2
$2f_1+f_2+f_3$	22.80053	1.5	1.0	0.9	6.9

Table 3. Possible further signals. The data set in which they attained highest S/N are indicated.

ID	Frequency (cd^{-1})	S/N
	0.2543	4.0 (v)
	6.221	3.6 (uvy, weighted)
	7.252	3.4 (uvy, weighted)
	7.914	3.1 (u)
f_1+2f_3	17.0034	3.2 (u)
$f_1+2f_2+f_3$	22.6912	3.5 (u)
$3f_1+f_2+f_3$	28.5638	3.1 (u)

the residualgram method (Martinez & Koen 1994) or by folding the data with the orbital period, all remained inconclusive.

On the other hand, we noticed that the amplitude spectrum of the de-trended comparison star magnitude differences (with a low-order polynomial fitted to each night of data to remove the slow variability of μ Eri) has the highest peak at 10.873 cd^{-1} in all the filters. It is even significant with a S/N =5.2 in the v filter data, where it reaches an amplitude of 0.6 mmag.

To examine whether this peak is real and, if so, from what star it originates, we computed the differential (ν Eri–μ Eri) and (ν Eri–ξ Eri) light curves. We then pre-whitened the frequency solution from Table 2 from these data and computed the residual amplitude spectra. We also examined the (ξ Eri–HD 29227) data from OSN for this purpose. Unfortunately, these tests were not fully conclusive because the noise level in these amplitude spectra is higher than in those of the de-trended differential comparison star magnitudes

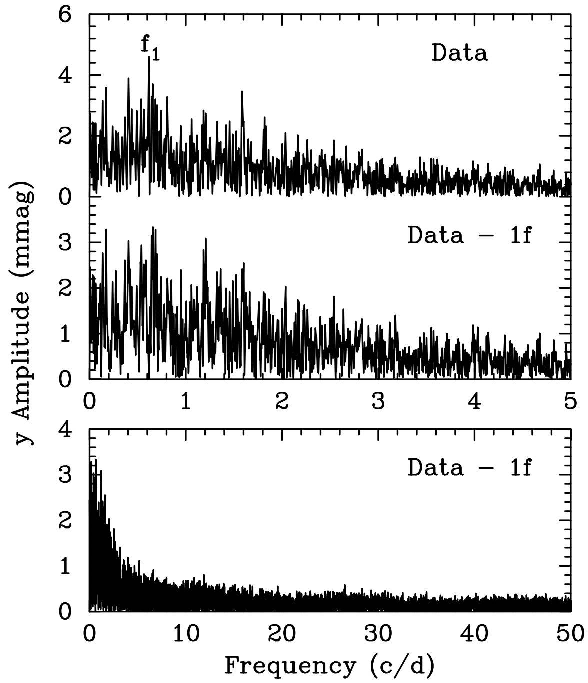

Figure 3. Upper panel: amplitude spectrum of (μ Eri–ξ Eri) in the y filter. Second panel: residual amplitude spectrum after pre-whitening f_1. Lower panel: residual amplitude spectrum of (μ Eri–ξ Eri) out to the Nyquist frequency; no further variations are detected.

only. All we can say is that, if real, the 10.873-cd^{-1} variation is more likely to originate from ξ Eri. In any case, our assumption that ξ Eri is photometrically constant does not affect our analysis of ν Eri.

3.3 Re-analysis of literature data

We have re-analysed the photometric measurements by van Hoof (1961) and Kubiak & Seggewiss (1991). The first data set was retrieved from the IAU archives (as deposited by Cuypers & Goossens 1981) and consists of two seasons of ultraviolet U and one season of yellow Y measurements (the Y bandpass is identical to Johnson V; see Lyngå 1959). The frequency analysis was performed on the U data as they are considerably more numerous, whereas we determined only the amplitudes in the Y data with frequencies fixed to the values derived from the U measurements.

We homogenized these data by averaging them into 7-min bins and by removing poor data, sometimes whole nights. The frequency analysis of the resulting U data set revealed the presence of frequencies f_1 to f_4 as well as the sum frequencies of f_1 with the f_2, f_3, f_4 triplet. The amplitude spectrum after pre-whitening the corresponding multifrequency fit shows a strong increase of noise that precludes the detection of further signals. We note that neither the low 0.432-cd^{-1} variation of ν Eri nor the suspected 0.616-cd^{-1} periodicity of μ Eri could be detected.

To enable a search for further signals known from our analysis in those data, we determined the zero-points of the residual light curves of the individual nights and subtracted them from the data. Fourier analysis of this modified data set allowed the detection of four more signals established in our measurements. Their frequencies and amplitudes recovered in van Hoof's U data are listed in Table 4 together with the corresponding Y amplitudes.

The photometric measurements by Kubiak & Seggewiss (1991) consist of two runs of 17.1-d and 5.1-d time base, respectively,

Table 4. Multifrequency solution for the U and Y data of van Hoof (1961). The identifications of the signals are the same as in Table 2. Formal error estimates (Montgomery & O'Donoghue 1999) for the independent frequencies range from ± 0.00001 cd^{-1} for f_1 to ± 0.00017 cd^{-1} for f_6. Formal errors on the U amplitudes are ± 0.3 mmag. However, the real errors are believed to be higher because of the zero-point adjustments we made. The formal uncertainty on the Y amplitudes is ± 0.8 mmag.

ID	Freq. (cd^{-1})	U ampl. (mmag)	Y ampl. (mmag)	S/N
f_1	5.76345	52.8	28.9	78.2
f_3	5.62018	25.5	20.1	37.7
f_4	5.63738	26.5	19.5	39.2
f_2	5.65385	27.9	20.8	41.3
f_6	6.24417	2.7	2.1	4.0
f_7	6.26227	3.7	4.0	5.6
f_5	7.89830	2.1	2.0	3.1
f_1+f_3	11.38363	8.1	6.2	13.0
f_1+f_4	11.40083	8.1	5.5	13.0
f_1+f_2	11.41730	9.2	7.0	14.7
$2f_1$	11.52690	2.8	3.8	4.4

separated by 4 yr. The f_2, f_3, f_4 triplet can, therefore, not be resolved in these data, but f_1 can be separated from it and its *uvby* amplitudes can be estimated. We obtain amplitudes of 55 ± 3 mmag in u, 30 ± 2 mmag in v, 28 ± 2 mmag in b and 27 ± 2 mmag in y for signal f_1. The 0.616-cd^{-1} variation of μ Eri may be present in these data.

4 DISCUSSION

4.1 The β Cephei type pulsation frequencies

We have detected eight independent signals in the light curves of ν Eri that are in the typical frequency domain for β Cephei star pulsation, i.e. they are pressure (p) and gravity (g) modes of low radial order. We show the schematic amplitude spectrum composed of these modes and of further suspected signals in Fig. 4.

This figure shows intriguing structures. Besides the known triplet of frequencies near 5.64 cd^{-1}, there is another doublet near 6.24 cd^{-1} with a suspected further component, and the two other signals near 7.2 and 7.9 cd^{-1} may also be parts of mode multiplets. We believe that these are signs of rotational splitting of non-radial pulsation modes. If so, the rotation period of ν Eri must be between 30 and 60 d, depending on the types of mode we see (p and/or g modes).

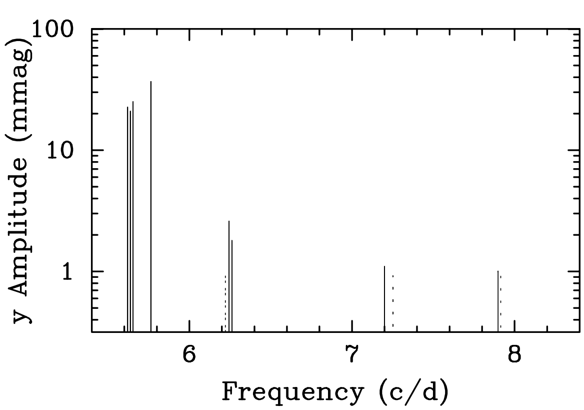

Figure 4. Schematic amplitude spectrum of ν Eri. The solid lines represent detected modes, whereas the dashed lines indicate the positions of possible further signals.

The low-frequency triplet is asymmetric. Dziembowski & Jerzykiewicz (2003) calculated the asymmetry as $A_{\mathrm{obs}} = f_2 + f_3 - 2f_4 = -7.1 \pm 0.3 \times 10^{-4}$ cd^{-1} (using the naming convention from Table 2) from archival data, whereas our measurements indicate $A_{\mathrm{obs}} = -3.3 \pm 0.4 \times 10^{-4}$ cd^{-1}. Comparing Tables 2 and 4, it appears that our value for the triplet centroid frequency f_4 is less accurate than the formal errors would suggest – which is plausible given that our observational time base is only about 2.6 times the inverse triplet splitting.

A comparison of Tables 2 and 4 allows another interesting conclusion; the pulsational amplitudes of all modes of ν Eri seem to have increased between the measurements of van Hoof and those of our studies. Allowing for the different wavelength passband of the archival U measurements that also included a silvered mirror (Lyngå 1959) and our Strömgren u data, an increase in the pulsational amplitudes of about 20 per cent can be estimated. It is possible that most of this increase has occurred in the last 15–20 yr as the u amplitude of f_1 in the data by Kubiak & Seggewiss (1991) is also considerably smaller than in our data.

4.2 The combination signals

The light curves of ν Eri are not perfectly sinusoidal (cf. Fig. 1); therefore, combination signals result from our method of frequency determination. It is not well known what the physical cause of combination frequencies is. Some of the most prominent hypotheses include simple light-curve distortions due to the pulsations propagating in a non-linearly responding medium or independent pulsation modes excited by resonances.

In case of the light-curve distortion hypothesis, the amplitudes and phases of the combination frequencies can be predicted. They also contain some information about the medium that distorts the light curves (see Wu 2001 and references therein). In the simplest case, the amplitudes of the combination signals scale directly with the product of the amplitudes of the parent modes (see, for example, Garrido & Rodríguez 1996).

As we do not have a pulsational mode identification available at this point, we cannot examine the two above-mentioned hypotheses quantitatively, but some statements can still be made. For instance, simple light-curve distortion should produce combination sum and difference frequencies of about the same amplitude. However, difference frequencies are completely absent in our multifrequency solution (Table 2) although the strongest of these signals should be easily detectable in our data.

The amplitude variations we reported before can also be examined. We note that the amplitude of the sum frequencies of f_1 with the f_2, f_3, f_4 triplet increased by about 20 per cent, which is the same as the increase of the individual amplitudes of the parent modes, but less than expected for the simple light-curve distortion hypothesis.

The absence of the difference frequencies also poses a problem for the resonant mode coupling hypothesis. As the stellar eigenmode spectrum is much denser at low frequencies than at high frequencies due to the presence of many gravity modes, we would expect to see many more difference frequencies in the case of mode coupling, which is not the case.

4.3 The low-frequency variation

We found a signal of 0.43218 cd^{-1} in the light curves of ν Eri and evidence for other periodic low-frequency signals. Such variability is an order of magnitude slower than β Cephei type pulsation. These variations are not due to the slowly variable comparison star μ Eri;

they occur at frequencies different from the dominant variation of the latter star and we have taken care that its variability does not affect our analysis of ν Eri in our reduction procedures. They are, therefore, present in our light curves of ν Eri.

Although this slow variability has been detected in the measurements in all three Strömgren filters used, we have taken special care in determining whether these variations are intrinsic to the star. Consequently, we computed amplitude spectra of the four largest homogeneous subsets of data (i.e. those that used the same filters and detectors throughout the whole campaign and that spanned a time base longer than 70 d) in all three filters. We have found a peak at 0.432 cd^{-1} present in all these amplitude spectra, and we are therefore sure it is not an artefact of the observing or reduction procedures; it is due to intrinsic variations of ν Eri.

Unfortunately, there is some doubt as to whether this is an independent frequency or not. A possible high-order combination frequency ($3f_1 - 3f_3$) would be located only 0.0026 cd^{-1} away from f_A, which is much larger than the formal error estimate of ± 0.0001 cd^{-1} for the frequency uncertainty of f_A, but smaller than the 0.0063-cd^{-1} frequency resolution of our data. It would be surprising if such a high-order difference frequency were present in our data when there is no evidence for lower-order ones. We thus suspect that f_A is an independent frequency, but only new measurements increasing the time base of our data set will allow us to answer this question unambiguously.

If f_A were an independent periodicity, what would be the physical reason for such a variability? As argued above, the rotation period of ν Eri must be between 30 and 60 d; the observed 2.3-d period can therefore not be connected to rotation. ν Eri is also not known to be a binary; extensive radial velocity studies are available and no variability except that due to the short-period pulsations has ever been reported. In addition, the wavelength dependence of the amplitude of the 0.432-cd^{-1} signal excludes a pure geometric origin of this variability.

Hence, the slow variations are probably due to high-order g-mode pulsations of the star, which is also consistent with the colour amplitudes. We note that Jerzykiewicz (1993) also detected a low-frequency variation in his light curves of the β Cephei star 16 (EN) Lac, which he interpreted to be either due to a pair of spots – or due to g-mode pulsation.

4.4 The variability of μ Eri

In Section 3.1 we reported that one of our comparison stars, μ Eri, shows rather complex light variations with a time-scale of about 1.6 d. To examine their origin, we first determined its position in the Hertzsprung–Russell (HR) diagram. As a start, we retrieved the standard Strömgren and Geneva colours of μ Eri from the Lausanne–Geneva data base (http://obswww.unige.ch/gcpd/gcpd.html).

The star's Geneva colours then imply $T_{\mathrm{eff}} = 15\,670 \pm 100$ K according to the calibrations by Künzli et al. (1997). The star's *Hipparcos* parallax (ESA 1997), combined with a reddening correction of $A_V = 0.06$ determined from its Strömgren colours and the calibration of Crawford (1978), the bolometric corrections by Flower (1996) and Drilling & Landolt (2000) result in $M_{\mathrm{bol}} = -3.6 \pm 0.4$. We can thus place μ Eri in the theoretical HR diagram (Fig. 5).

Interestingly, μ Eri seems to be an object just at or shortly after the end of its main-sequence life. It is located within the instability strip of the SPB stars, and the time-scale (cf. De Cat & Aerts 2002; Pamyatnykh 2002) and complexity of its variability as well as the colour dependence of its amplitudes on wavelength are consistent with it being an SPB star. μ Eri may have many pulsation modes

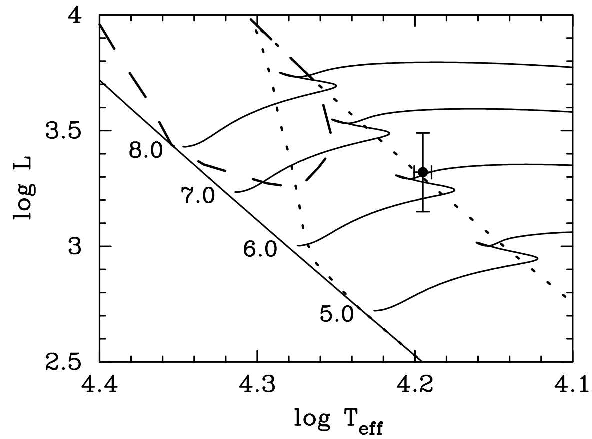

Figure 5. The position of μ Eri in the theoretical HR diagram. Some stellar model evolutionary tracks labelled with their masses (full lines) for $(v \sin i)_{\mathrm{ZAMS}} = 200$ km s^{-1} are included. The theoretical borders of the β Cephei and SPB star instability strips (Pamyatnykh 1999; thick dashed and dotted lines, respectively) are included for comparison. The evolutionary tracks are shifted to the zero-age main sequence (ZAMS; full diagonal line) and to the instability strip boundaries because the latter do not include rotational effects.

excited which are so closely spaced in frequency that we cannot resolve them with the time base of our measurements.

However, pulsation is not the only possible physical cause of the light variations of μ Eri. For the 1.622-d time-scale of the variability of the star to be due to rotational effects, an equatorial rotational velocity of 193 km s^{-1} is required. The published estimates of the projected rotational velocity $v \sin i$ of μ Eri range from 150 km s^{-1} (Abt et al. 2002) to 190 km s^{-1} (Bernacca & Perinotto 1970), which is consistent with that constraint. A double-wave light variation with twice that period would, however, be in conflict with the measured $v \sin i$. The complexity of the light variations of μ Eri argues against a rotational origin.

The same argument can be used against an interpretation of μ Eri's variability in terms of binarity. In addition (as argued above for the long period detected for ν Eri), the wavelength dependence of the colour amplitudes in our measurements suggests that a pure geometric origin of this variability is unlikely. Most importantly, however, the 7.3-d spectroscopic binary period of μ Eri is quite different from the observed time-scale of its light variability or from an integral multiple of it.

Hence, we cannot unambiguously determine the cause of the variability of μ Eri. A high-resolution, high S/N spectroscopic study will probably allow us to distinguish between the two viable hypotheses, pulsation or rotational modulation.

5 CONCLUSIONS

Our photometric multisite campaign of the β Cephei star ν Eri has resulted in the largest single data set ever obtained for such a pulsator. The frequency analysis of these measurements has revealed the presence of eight independent pulsation modes, which is the most ever detected for such a star. These are normal β Cephei type variations (p and g modes of low radial order), but one additional signal may be a high-order gravity-mode pulsation. ν Eri could therefore be not only a β Cephei star, but also an SPB star. It would thus be the second example of a star exhibiting two different types of pulsation. The high-order g-modes of the first such star, HD 209295, are however believed to be triggered by tidal effects (Handler et al.

2002). As we have no evidence for binarity of ν Eri, it may therefore be the first star in which two types of pulsation with time-scales more than an order of magnitude different are intrinsically excited.

The β Cephei type pulsation frequencies show some regular structures, i.e. some are contained in multiplets that may be due to non-radial m-mode splitting. If so, the rotation period of ν Eri is between 30–60 d, depending on the type of modes in these multiplets. These multiplets are a strong constraint for pulsational mode identification, which will be the subject of a future paper. In any case, the low-order p- and g-mode spectrum of ν Eri as reported here is suitable for detailed seismic modelling.

ACKNOWLEDGMENTS

This work has been supported by the Austrian Fonds zur Förderung der wissenschaftlichen Forschung under grant R12-N02. MJ's participation in the campaign was partly supported by KBN grant 5P03D01420. MJ would also like to acknowledge a generous allotment of telescope time and the hospitality of Lowell Observatory.

We thank the following students of the University of Hawaii for their assistance during some of the observations: Dan Bolton, Alexandre Bouquin, Josh Bryant, Thelma Burgos, Thomas Chun, Alexis Giannoulis, Marcus Lambert, Amanda Leonard, Alex MacIver, Danielle Palmese, Jennale Peacock, David Plant, Ben Pollard, Sunny Stewart, Dylan Terry and Brian Thomas.

GH wishes to express his thanks to Lou Boyd and Peter Reegen for their efforts in maintaining and controlling the Fairborn APTs, to Marcin Kubiak for supplying his archival measurements of ν Eri, to Jan Cuypers for helpful information on the passbands of the archival data, and to Conny Aerts and Anamarija Stankov for comments on a draft version of this paper.

REFERENCES

Abt H. A., Levato H., Grosso M., 2002, ApJ, 573, 359
Aerts C., Waelkens C., de Pauw M., 1994, A&A, 286, 136
Aerts C., Thoul A., Daszynska J., Scuflaire R., Waelkens C., Dupret M. A., Niemczura E., Noels A., 2003, Sci, 300, 1926
Balona L. A., 2000, in Breger M., Montgomery M. H., eds, ASP Conf. Ser. Vol. 210, Delta Scuti and Related Stars. Astron. Soc. Pac., San Francisco, p. 170
Bernacca P. L., Perinotto M., 1970, Contr. Oss. Astrof. Padova in Asiago, 239, 1B
Breger M. et al., 1999, A&A, 349, 225
Crawford D. L., 1978, AJ, 83, 48
Cuypers J., Goossens M., 1981, A&AS, 45, 487
Cuypers J., Aerts C., Buzasi D., Catanzarite J., Conrow T., Laher R., 2002, A&A, 392, 599
Daszyńska-Daszkiewicz J., Dziembowski W. A., Pamyatnykh A. A., Goupil M.-J., 2002, A&A, 392, 151
De Cat P., Aerts C., 2002, A&A, 393, 365
de Jager C., 1963, Bull. Astr. Inst., Netherlands, 17, 1
Drilling J. S., Landolt A. U., 2000, in Cox A. N., ed., Allen's Astrophysical Quantities, 4th edn. Springer Verlag, Berlin, p. 392
Dziembowski W. A., Jerzykiewicz M., 2003, in Balona L. A., Henrichs H. F., Medupe R., eds, ASP Conf. Ser. Vol. 305, Magnetic Fields in O, B and A Stars: Origin and Connection to Pulsation, Rotation and Mass Loss. Astron. Soc. Pac., San Francisco, in press
Dziembowski W. A., Pamyatnykh A. A., 1991, A&A, 248, L11
ESA, 1997, The *Hipparcos* and Tycho catalogues, ESA SP-1200
Flower P. J., 1996, ApJ, 469, 355
Garrido R., Rodríguez E., 1996, MNRAS, 281, 696
Handler G., 2003, Baltic Astron., 12, 253
Handler G., Aerts C., 2002, Comm. Asteroseismology, 142, 20
Handler G. et al., 1996, A&A, 307, 529
Handler G. et al., 1997, MNRAS, 286, 303
Handler G. et al., 2000, MNRAS, 318, 511
Handler G. et al., 2002, MNRAS, 333, 262
Handler G., Shobbrook R. R., Vuthela F. F., Balona L. A., Rodler F., Tshenye T., 2003, MNRAS, 341, 1005
Heynderickx D., Waelkens C., Smeyers P., 1994, A&AS, 105, 447
Hill G., 1969, Publ. DAO Victoria, 13, 323
Jerzykiewicz M., 1978, Acta Astron., 28, 465
Jerzykiewicz M., 1993, Acta Astron., 43, 13
Koen C., Eyer L., 2002, MNRAS, 331, 45
Kubiak M., 1980, Acta Astron., 30, 41
Kubiak M., Seggewiss W., 1991, Acta Astron., 41, 127
Künzli M., North P., Kurucz R. L., Nicolet B., 1997, A&AS, 122, 51
Lyngå G., 1959, Arkiv Astron., 2, 379
Martinez P., Koen C., 1994, MNRAS, 267, 1039
Montgomery M. H., O'Donoghue D., 1999, Delta Scuti Star Newsletter, 13, 28
Moskalik P., Dziembowski W. A., 1992, A&A, 256, L5
Nather R. E., Winget D. E., Clemens J. C., Hansen C. J., Hine B. P., 1990, ApJ, 361, 309
Pamyatnykh A. A., 1999, Acta Astron., 49, 119
Pamyatnykh A. A., 2002, Comm. Asteroseismology, 142, 10
Pamyatnykh A. A., 2003, Ap&SS, 284, 97
Sperl M., 1998, MSc thesis, Univ. Vienna
Stankov A., Handler G., Hempel M., Mittermayer P., 2002, MNRAS, 336, 189
Sterken C. et al., 1986, A&AS, 66, 11
Wu Y., 2001, MNRAS, 323, 248
van Hoof A., 1961, Z. Astrophys., 53, 106
Zima W. et al., 2002, in Aerts C., Bedding T. R., Christensen-Dalsgaard J., eds, ASP Conf. Proc., Vol. 259, Radial and Nonradial Pulsations as Probes of Stellar Physics. Astron. Soc. Pac., San Francisco, p. 598

This paper has been typeset from a TEX/LATEX file prepared by the author.

5.4.2 Asteroseismology of the β Cephei star ν Eridani – II. spectroscopic observations and pulsational frequency analysis

Original paper:

C. Aerts, P. De Cat, **G. Handler,** U. Heiter, L. A. Balona, J. Krzesinski, P. Mathias, H. Lehmann, I. Ilyin, J. De Ridder, S. Dreizler, A. Bruch, I. Traulsen, A. Hoffmann, D. James, E. Romero-Colmenero, T. Maas, M. A. T. Groenewegen, J. H. Telting, K. Uytterhoeven, C. Koen, P. L. Cottrell, J. Bentley, D. J. Wright, J. Cuypers, 2004, MNRAS 347, 463

Mon. Not. R. Astron. Soc. **347,** 463–470 (2004)

Asteroseismology of the β Cephei star ν Eridani – II. Spectroscopic observations and pulsational frequency analysis

C. Aerts,[1★] P. De Cat,[1] G. Handler,[2] U. Heiter,[3] L. A. Balona,[4] J. Krzesinski,[5,6] P. Mathias,[7] H. Lehmann,[8] I. Ilyin,[9] J. De Ridder,[1] S. Dreizler,[10] A. Bruch,[11] I. Traulsen,[10] A. Hoffmann,[10] D. James,[12] E. Romero-Colmenero,[4] T. Maas,[1] M. A. T. Groenewegen,[1] J. H. Telting,[13] K. Uytterhoeven,[1] C. Koen,[4] P. L. Cottrell,[14] J. Bentley,[14] D. J. Wright[14] and J. Cuypers[15]

[1]*Instituut voor Sterrenkunde, Katholieke Universiteit Leuven, Celestijnenlaan 200 B, B-3001 Leuven, Belgium*
[2]*Institut für Astronomie, Universität Wien, Türkenschanzstrasse 17, A-1180 Wien, Austria*
[3]*Department of Astronomy, Case Western Reserve University 10900 Euclid Ave Cleveland, OH 44106-7215, USA*
[4]*South African Astronomical Observatory, PO Box 9, Observatory 7935, South Africa*
[5]*Apache Point Observatory 2001 Apache Point Road PO Box 59, Sunspot, NM 88349-0059, USA*
[6]*Mt. Suhora Observatory, Cracow, Pedagogical University, ul. Podchorążych 2, 30-084, Poland*
[7]*Observatoire de la Côte d'Azur, BP 4229, F-06304 Nice Cedex 04, France*
[8]*Thüringer Landessternwarte, D-07778 Tautenburg, Germany*
[9]*Astronomy Division, PO Box 3000, 90014 University of Oulu, Finland*
[10]*Institut für Astronomie und Astrophysik, Abt. Astronomie, Sand 1, 72076 Tübingen, Germany*
[11]*Laboratório Nacional de Astrofísica, Rua Estados Unidos, 154 – Bairro das Nacões, 37504-364 Itajubá, Brazil*
[12]*Laboratoire d'Astrophysique, Observatoire de Grenoble, BP 53, F-38041 Grenoble Cedex 9, France*
[13]*Nordic Optical Telescope, Apartado 474, E-38700 Santa Cruz de La Palma, Spain*
[14]*Department of Physics and Astronomy, University of Canterbury, Christchurch, New Zealand*
[15]*Royal Observatory of Belgium, Ringlaan 3, B-1180 Brussels, Belgium*

Accepted 2003 September 12. Received 2003 September 11; in original form 2003 August 4

ABSTRACT

We undertook a multisite spectroscopic campaign for the β Cephei star ν Eridani. A total of 2294 high-resolution spectra were obtained from telescopes at 11 different observatories around the world. The time base of dedicated multisite observations is 88 d. To this data set we have added 148 older, previously unpublished spectra, such that the overall time-span of the 2442 spectra is 430 d. The analysis of the radial velocity variations derived from the Si III triplet centred on 4560 Å leads to 19 significant frequencies, of which seven correspond to independent pulsation frequencies. Five of these are members of multiplets with an average spacing of 0.018 ± 0.002 cd^{-1}. Our spectroscopic results agree well with those derived from a simultaneous multisite photometric campaign of the star, albeit that we do not recover their low frequency at 0.43218 cd^{-1}. We find three different candidate frequencies below 1 cd^{-1} instead. We also find that the radial velocity amplitude of the main mode has increased by some 30 per cent over the last 15 years, which is consistent with the photometry data. We derive a relative equivalent width variation of 6.5 per cent, which is completely dominated by the main radial mode. The phase difference between the radial velocity and light variations for the main frequency is $97\overset{\circ}{.}9 \pm 1\overset{\circ}{.}8$, which is clearly deviant from the adiabatic value and confirms the radial nature of the dominant mode. The spectral line broadening leads to an upper limit of 20 km s^{-1} for $v \sin i$, which is consistent with the long rotation period derived from the frequency splittings.

Key words: techniques: spectroscopic – stars: early-type – stars: individual: ν Eridani – stars: oscillations – stars: variables: other.

★E-mail: conny@ster.kuleuven.ac.be

1 INTRODUCTION

The research domain of asteroseismology has received a strong impetus since its successful application to the Sun (helioseismology), to several white dwarfs (for recent applications, see Vauclair et al. 2002; Handler, Metcalfe & Wood 2002) and also to solar-like stars (for a review, see Bedding & Kjeldsen 2003). So far, seismic studies have concentrated mainly on such stars because they have very rich frequency spectra consisting of short-period oscillations. However, stellar evolution codes are most uncertain for stars with large convective cores. A successful application of asteroseismology to these objects would lead to a large step towards our understanding of their evolution.

Most efforts to achieve high-precision seismology for stars more massive than the Sun with convective cores were concentrated on δ Scuti stars and relied on frequencies derived from photometric multisite campaigns (see Breger et al. 2002, for a recent example). The lack of unique mode identifications, however, hampered the detailed derivation of the internal structure of such stars.

Stars of spectral type B have even larger convective cores and longer oscillation periods than δ Scuti stars. However, their internal structure is relatively simple, as they do not possess an outer convective zone. Their oscillations are driven by the κ mechanism acting in the metal opacity bump situated around 200 000 K (Dziembowski & Pamyatnykh 1993; Gautschy & Saio 1993). Efforts to perform seismic studies of the B0–2 main-sequence β Cephei stars started in 1996 (Dziembowski & Jerzykiewicz 1996) for the star 16 (EN) Lac and, a few years later, for 12 (DD) Lac (Dziembowski & Jerzykiewicz 1999). Again, unknown mode identification of some of the non-radial modes limited the detailed modelling. New seismic analyses have been performed very recently by Handler et al. (2003) for the three stars IL Vel, V433 Car and KZ Mus and by Thoul et al. (2003) for 16 (EN) Lac. The most in-depth study so far was presented by Aerts et al. (2003b) for the star HD 129929, in which evidence for moderate overshooting with a parameter $\alpha_{\rm ov} =$ 0.1 and non-rigid rotation could be derived from six detected and well-identified oscillation modes, among which are components of frequency multiplets. The latter is the first study for which the standard structure models cannot explain the well-identified frequency values unless overshooting occurs.

A major drawback for additional seismic applications on β Cephei stars is the lack of agreement between photometric and spectroscopic mode identifications. The latter have been performed for many bright β Cephei stars (Aerts & De Cat 2003) but 16 (EN) Lac is one of the few multiperiodic objects for which both photometry and spectroscopy point towards the same mode identification for the detected non-radial modes (Aerts et al. 2003c). In an effort to improve this situation, and with the goal to perform the most in-depth seismic application on a β Cephei star, Handler & Aerts (2002) set up a large spectroscopic and photometric multisite campaign for the star ν Eridani (HD 29248, V mag 3.92, spectral type B2 III). This campaign took place between 2002 October and 2003 January. The first results, based only on the photometric data, together with the history of the target and our selection criteria are presented in Handler et al. (2004, hereafter Paper I). In the following, we report on results based on the radial velocities obtained from our spectroscopic data. The pulsational mode identification and seismic modelling of the identified oscillations will be the subject of future papers.

This paper is organized as follows. In Section 2 we begin with a description of our data and the reduction process. We then discuss our calculation of the time series of radial velocities of ν Eridani in Section 3. Section 4 is devoted to the detailed frequency analysis, and we end with discussions and future work in Section 5.

2 OBSERVATIONS AND DATA REDUCTION

The spectroscopic observations were carried out with 11 different telescopes at observatories on five continents; they are summarized in Table 1. In all but two of the cases, the instrument was an echelle spectrograph.

Table 1. Log of the spectroscopic measurements of ν Eridani. The Julian Dates are given in days, with respect to 245 2000. N denotes the number of spectra, ΔT is the time-span expressed in days, $\Delta\lambda$ is the wavelength step expressed in m Å resulting from the resolving power of the instrument at the position of the Si III triplet and S/N denotes the average signal-to-noise ratio measured at the continuum between 4550 and 4551 Å (see Fig. 1). A '⋆' denotes a linear array instead of an echelle spectrograph. The Mount John observations do not contain the Si III triplet, thus they were not included in the radial velocity analysis of the current paper; they will be used in future analyses.

Observatory	Longitude	Latitude	Telescope	Julian Date		Data amount and quality				Observer(s)
				Begin	End	ΔT	N	$\Delta\lambda$	S/N	
Mt. Stromlo Observatory, Australia	+149° 04′	−35° 19′	1.9-m	608	611	3.1	68			DJ
				623	628	5.0	79	51	210	DJ
South African Astronomical Observatory	+20° 49′	−32° 22′	1.9-m	598	604	6.3	132			ERC, GH
				626	632	6.2	168	69	120	LAB
Pico dos Dias Observatory, Brazil⋆	−45° 35′	−22° 32′	1.6-m	551	562	11.1	71	61	800	AB
Haute Provence Observatory, France⋆	+5° 43′	+43° 46′	1.52-m	590	616	26.1[a]	112	23	450	PM
Tautenburg Observatory, Germany	+11° 42′	+50° 59′	2.0-m	600	628	28.1[b]	73	28	370	HL
La Palma Observatory, Spain	−17° 53′	+28° 45′	2.6-m NOT	588	601	13.2	70	19	640	II, JHT, KU
Apache Point Observatory, USA	−105° 49′	+32° 47′	3.5-m	595	598	2.3	201	76	430	JK
Calar Alto Observatory, Spain	+2° 33′	+37° 13′	2.2-m	654	663	9.0	82	20	440	SD, IT, AH
McDonald Observatory, USA	−104° 01′	+30° 40′	2.1-m	599	606	7.3	318			UH
				654	663	9.2	488	43	480	PDC
La Silla Observatory, Chile	−70° 44′	−29° 15′	1.2-m Euler	227	240	13.1	148			TM, KU
				569	582	13.2	181			TM
				624	638	14.3	251	18	360	MATG
Mt. John Univ. Obs., New Zealand	+170° 28′	−43° 59′	1.0-m	627	629	2.1	19	–	–	PLC, JB, DJW
Total						429.9	2442			

[a]36 spectra taken on JD 245 2590 and the additional 76 spectra between JD 245 2612 and 245 2616.
[b]Six spectra taken on JD 245 2600, 30 on JD 245 2621 and 37 on JD 245 2628.

Table 2. Multifrequency solution for the radial velocities derived from our time-resolved spectroscopy of ν Eridani. Formal error estimates for the independent frequencies range from 8×10^{-6} cd^{-1} for f_1 to ± 0.00014 cd^{-1} for f_{10}.

Number	Identification	Freq. (cd^{-1})	Ampl. (km s^{-1})	S/N
1	f_1	5.763298	20.20 ± 0.07	152.9
2	f_2	5.654014	7.69 ± 0.10	57.8
3	f_3	5.620097	6.87 ± 0.10	51.7
4	f_4	5.637432	6.92 ± 0.09	52.0
5	$f_1 + f_2$	11.417312	2.36 ± 0.08	29.2
6	$f_1 + f_3$	11.383395	2.02 ± 0.09	25.0
7	$f_1 + f_4$	11.400730	1.87 ± 0.07	23.1
8	$f_1 + f_2 + f_3$	17.037409	1.26 ± 0.08	18.7
9	f_9	6.242458	0.78 ± 0.08	6.0
10	f_{10}	7.898225	0.78 ± 0.08	6.8
11	$2f_1 + f_2 + f_3$	22.800707	0.70 ± 0.07	11.7
12	$2f_1 + f_3$	17.146693	0.65 ± 0.09	9.7
13	f_{13}	6.221429	0.62 ± 0.09	4.8
14	$2f_1 + f_2$	17.180610	0.73 ± 0.10	10.9
15	$2f_1 + f_4$	17.163392	0.52 ± 0.07	7.8
16	$f_1 + f_{10}$	13.661523	0.39 ± 0.08	5.3
17	$3f_1$	17.289894	0.37 ± 0.08	5.5
18	$3f_4$	16.912296	0.32 ± 0.07	4.7
19	$1 + f_2 + f_3$	12.274111	0.30 ± 0.08	3.8

The integration times were typically ∼10 min, depending on the instrument and on the atmospheric conditions. This leads to a temporal resolution of <5 per cent for the main four intrinsic modes of ν Eridani (for their frequency values we refer to Table 2).

All raw data were subjected to the usual reduction process, which consists of de-biasing, flat-fielding, background subtraction and wavelength calibration by means of a Th/Ar and/or a quartz lamp. The spectra were shifted to the heliocentre, and the Heliocentric Julian Dates of mid-exposure were calculated.

Subsequently, the Si III triplet centred on 4552.622, 4567.840 and 4574.757 Å was considered. It is well known that these triplet lines in the spectrum of B0–2 main-sequence stars are the best for a study of the pulsational behaviour of such stars because they are not affected very much by blending, they are strong lines and they are so close to the top of the star's energy distribution that they are almost insensitive to temperature variations (De Ridder et al. 2002). (Re)Normalization of the continuum flux near this Si triplet was carried out in a homogeneous way by calculating the best-fitting cubic spline function through the continuum near these wavelengths and then dividing the local spectrum by this spline.

We superimpose in Fig. 1 the average profile of the Si III λ4553 Å line of ν Eridani from each observatory (note that the Mount John data are not included in this paper, as they do not contain the Si triplet). It is important to note that these averages are in good agreement with each other as far as the central position of the line is concerned, the small differences in depth being mainly due to the partial coverage of the beating of the numerous modes (for a list, see Paper I or Table 2 in this paper). The averages from two observatories appear to deviate from the others: the Pico dos Dias (upper curve) and Tautenburg (lower curve) averages. However, the data sets from both instruments contain profiles which are fully consistent with corresponding ones from the other instruments. This proves that different beating patterns and/or the limited time spread (as also indicated in the footnote of Table 1) are responsible for the deviant average profiles, and not the instrumental and/or signal-to-noise ratio (S/N) effects.

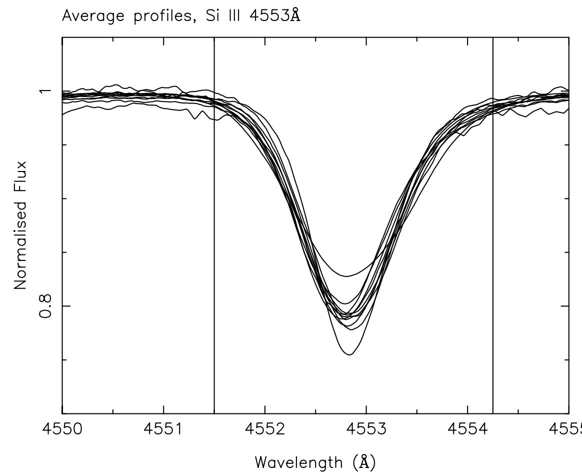

Figure 1. The average profile of the Si III λ4553 Å line of ν Eridani plotted for each of the observatories separately.

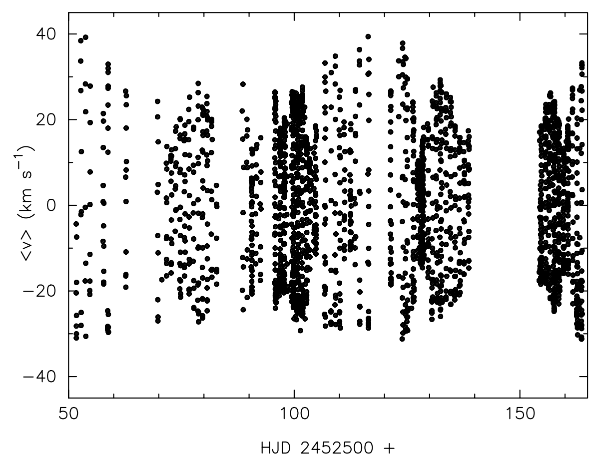

Figure 2. The time series of the average Si III radial velocities of ν Eridani derived from each spectrum taken during the dedicated multisite campaign.

The absence of large wavelength shifts in the central position of the average profiles allows us to exclude the possibility of ν Eridani being a spectroscopic binary with a period that would be relevant for the study of its intrinsic line-profile behaviour.

3 RADIAL VELOCITY AND EQUIVALENT WIDTH DETERMINATION

The radial velocities of ν Eridani we present in this paper correspond to the centroids of the Si III triplet lines. These centroids are calculated using the following equation

$$\mathrm{Vrad} = \frac{\sum_{i=1}^{N}(1 - I_i)(x_i - x_0)\triangle x_i}{\sum_{i=1}^{N}(1 - I_i)\triangle x_i}, \tag{1}$$

where I_i is the normalized flux value measured at wavelength pixel λ_i and $\triangle x_i \equiv x_i - x_{i-1}$ where x_i is the velocity corresponding to λ_i with respect to the laboratory wavelength λ_0. We made two different choices for the determination of the wavelength range $[x_1, x_N]$ in equation (1), which led to three different ways of determining Vrad:

(i) summation over a carefully chosen, constant region in wavelength (see, for example, the vertical lines indicated in Fig. 1);

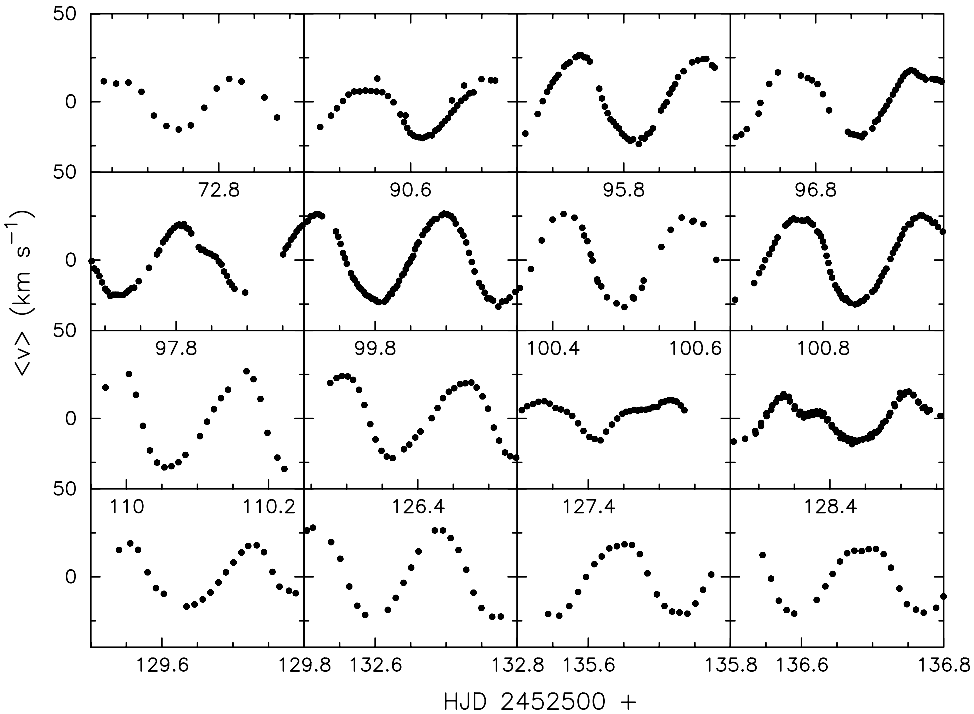

Figure 3. Radial velocities of ν Eridani during some selected nights of the dedicated multisite campaign.

(ii) summation over a dynamical region in wavelength, which typically extends over a few angstrom and which is adopted for each profile separately;

(iii) same as in (ii), but after a local renormalization of the continuum.

For each of these methods we then determined the average radial velocity per observatory for each of the three Si III lines. These averages range from 16.1 to 19.5 km s^{-1} for the bluest Si III line, with similar averages being found for the two redder lines. As was the case with the average line profiles, the difference in average radial velocities from the different observatories is again introduced by the different coverages of the overall beat pattern. We then duplicated our data sets and proceeded with our analysis by applying to one of the duplicates a correction for the small differences in radial velocity. This correction involved shifting the radial velocities to average zero per observatory, i.e. by determining the normalized first moment, $\langle v \rangle$ (for a definition, see Aerts, De Pauw & Waelkens 1992) for each of the Si III lines per spectrum per method.

For each spectrum we then calculated an average radial velocity from the three separate Si III lines, for each of the indicated methods. We show in Fig. 2 the time series of the first normalized moment variations computed with method (i) for the average of the three Si III lines, for the dedicated multisite campaign. The nightly variations for some selected nights are displayed in Fig. 3. A beating phenomenon resulting from multiperiodicity is clearly visible and the radial velocity amplitude is large, of the order of 20 km s^{-1}, in agreement with previous studies (e.g. Aerts, Waelkens & De Pauw 1994a). The error bars denoting the standard deviation resulting from this procedure are not indicated in Figs 2 and 3 for clarity, but they are plotted in Fig. 4, which we discuss further on. In what follows we present the results for this particular data set of normalized first moments, of which we have used only those radial velocity measurements with a standard error below 3 km s^{-1}. To this data set we have added the older, previously unpublished CORALIE data (see Table 1) using the same quality criterion. This new data set now contains 2367 data points[1] with an average standard deviation of 0.9 km s^{-1}. Our adopted quality criterion therefore implies a reduction of only 3 per cent of the data set size. We stress, however, that all the accepted frequencies (see Table 2) were also obtained with the complete data set of 2442 data points, regardless of the method used for the radial velocity calculation or whether we apply the correction to obtain $\langle v \rangle$.

We have also determined the equivalent width (EW), calculated as the denominator in equation (1), of each of the three lines of the Si III triplet, using the same three methods as outlined above as far as integration over the profile is concerned. It is well known that the EW variations of β Cephei stars are small, typically of the order of a few per cent (De Cat 2002). However, ν Eridani is one of the exceptions, because of its dominant radial large-amplitude mode (Aerts et al. 1994a; De Ridder et al. 2002). We display in Fig. 4 the phase diagrams for the main frequency of 5.763298 c d^{-1} of the EW for the bluest Si III line, as well as for the radial velocity and for the magnitude of the Strömgren y filter data presented in Paper I. The relative amplitude of the EW variation is 6.5 per cent. The EW variations are completely dominated by the radial mode (see the following section). It is therefore only useful to compare the phase behaviour of the EW, $\langle v \rangle$ and Strömgren y for this frequency. We find the following phase differences: $\phi_{\langle v \rangle} - \phi_y = 0.272 \pm 0.005$ and $\phi_{\rm EW} - \phi_y = 0.044 \pm 0.008$, expressed in radians. The $\phi_{\langle v \rangle} - \phi_y$ value implies a clear deviation from the adiabatic value of 0.25, while the antiphase behaviour between the EW and the photometric light curve agrees with the effective temperature of ν Eridani (De Ridder et al. 2002).

[1] This data set is available upon request from the first author.

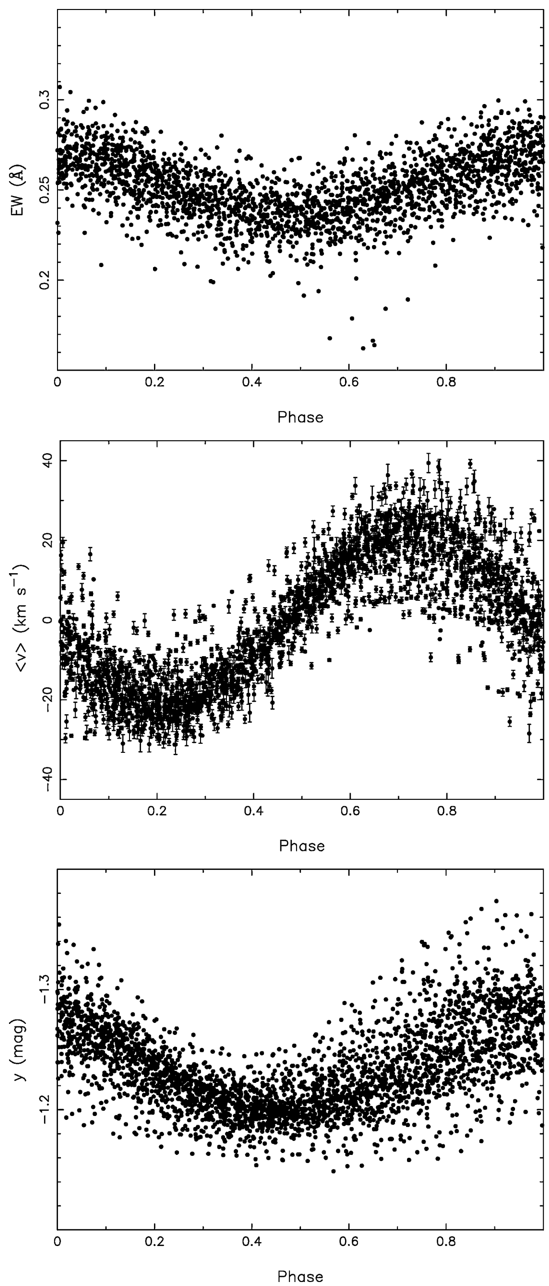

Figure 4. Phase diagram according to f_1 of the equivalent width of the Si III λ4553 Å line (top), of the radial velocity (including standard errors derived from averaging over the three Si lines of the triplet, middle) and of the Strömgren y data taken from Paper I (bottom). The reference epoch was each time taken to be HJD 245 2500.

4 FREQUENCY ANALYSIS

We have followed the same procedure outlined in Paper I in order to derive the intrinsic frequencies of ν Eridani from its radial velocity variations. We used PERIOD 98 (Sperl 1998) as well as unpublished software to do so. The results are graphically depicted in Fig. 5, while the frequency values and their amplitudes are listed in Table 2. The uppermost panel of Fig. 5 represents the spectral window, calculated in the same way as that presented in Paper I. A comparison with fig. 2 of Paper I shows that the spectroscopic data suffer slightly more from aliasing than the photometric data. However, the time base of the spectroscopy is longer, thus the accuracy for the frequency determination should, in principle, be higher.

The main frequency $f_1 = 5.6733$ cd^{-1} found in the photometry is even more dominant in the radial velocity variations. It has an amplitude of ∼20 km s^{-1}, corresponding to a S/N ratio of 153. The noise level was determined in the same way as in Paper I, i.e. it is the average amplitude (as determined by an integration over the periodogram) in a 5-cd^{-1} interval centred on the considered frequency, after pre-whitening by all significant peaks.

We pre-whitened the data with a synthetic sinusoidal curve with the frequency, amplitude and phase that led to the smallest residual variations. We then proceeded with a search for additional frequencies, in the same way as in Paper I, i.e. by optimizing each time the frequency values through a non-linear regression analysis with the frequencies as free parameters, using as a starting value the frequency found from the periodograms. We then found the same results as in photometry, i.e. three further independent frequencies f_2,f_3,f_4 and the combination frequencies f_1+f_2,f_1+f_3,f_1+f_4, $f_1+f_2+f_3$. We did not optimize the combination frequencies, but fixed them to the values resulting from the optimized intrinsic frequencies $f_1, \ldots, f_4$ (just as in Paper I). After pre-whitening with these eight mentioned frequencies, the amplitude at low frequencies becomes noticeable (see Fig. 5). We neglect this for the time being and concentrate on the higher frequencies. We clearly recover the two frequencies f_9 and f_{10} of the newly discovered modes we reported in Paper I. After further pre-whitening with these two modes and two more combination frequencies, we detect f_{13}, which is the lowest frequency component in the residuals of an apparent triplet around f_9. The photometric data (Paper I) clearly favour the right peak of this triplet because of less aliasing, but leave our f_{13} as an additional suspected frequency. As f_{13} has higher amplitude in our data, we then pre-whitened with that frequency. Besides f_{13}, we find six additional combination frequencies. All the 19 frequencies listed in Table 2 are significant with respect to the usual four S/N ratio criteria (3.5 for combination frequencies – see Breger et al. 1999).

After pre-whitening with the 19 frequencies given in Table 2, we turn to the study of the power at low frequency. This results in three candidate frequencies, f_{20}, f_{21}, f_{22}, with S/N above 3 (where the noise level is calculated from the same periodogram as for the accepted frequencies, i.e. after pre-whitening with the 19 frequencies listed in Table 2). They are listed in Table 3. None of these corresponds to the frequency $f_A = 0.432$ cd^{-1} found in Paper I.

The frequencies f_{20} and f_{21} do not reach the necessary amplitude to be accepted, given our adopted noise criterion. A natural question is whether any of the frequencies in the [0, 1] cd^{-1} range are due to the addition of the data sets from the different instruments. The frequencies f_{20} and f_{21} are also found independently in the CORALIE spectra (by far the most stable spectrograph among those used) after pre-whitening with $f_1, \ldots, f_{19}$, even if we consider only the ∼70-d time string. This suggests that f_{20} and f_{21} are probably real. However, the McDonald data, which have a time base of 64 d, do not reveal either f_{20} or f_{21} after pre-whitening with $f_1, \ldots, f_{19}$. Furthermore, these low frequencies are not found in the photometry (Paper I), thus we therefore caution against over-interpreting f_{20} and f_{21}. We do point out that the number 22 frequency of 0.01909 cd^{-1}, which is formally significant (see Fig. 6), corresponds to a period of 50.4 d, which might be the surface rotation period of the star. This frequency, however, is not present in any of the separate data sets after pre-whitening with $f_1, \ldots, f_{19}$. Future detailed seismic modelling should be able to shed light on this.

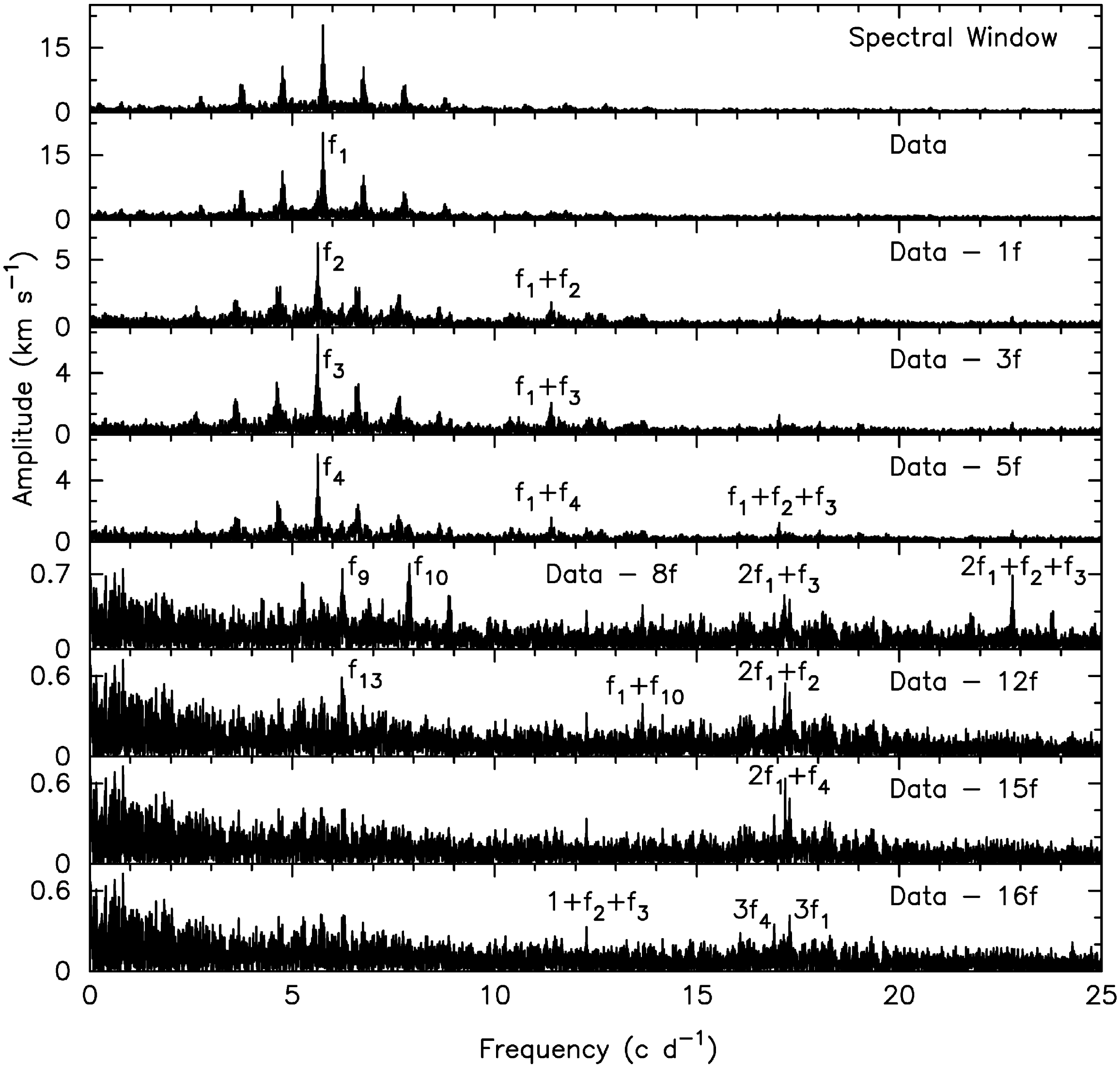

Figure 5. Amplitude spectra of ν Eridani computed from the radial velocities. The uppermost panel shows the spectral window of the data. All subsequent panels show the periodograms after different stages of pre-whitening (note the different scale). We refer to the text for details.

Table 3. Results from a multifrequency fit after subtraction of all frequencies listed in Table 2 for candidate additional frequencies. These are to be regarded as uncertain for the moment.

Number	Identification	Freq. (cd^{-1})	Ampl. (km s^{-1})	S/N
20	f_{20}	0.82443	0.74 ± 0.07	3.5
21	f_{21}	0.61384	0.73 ± 0.07	3.4
22	f_{22}	0.01909	0.90 ± 0.08	4.1

After pre-whitening with f_{20}, f_{21}, f_{22} we find a peak at 1.069 cd^{-1} with an amplitude corresponding to 2.7 S/N. From here on, all of the additional candidate frequencies have amplitudes below 3 S/N. We show in Fig. 6 the periodogram between 0 and 2 cd^{-1} after pre-whitening with all the frequencies listed in Table 2. The three frequencies listed in Table 3 are indicated in this figure, as is the noise level.

The final amplitude spectrum is shown in Fig. 7. This should be compared with that shown in fig. 4 of Paper I.

We next discuss the amplitude increase of 25 per cent of the modes in the photometric data over the past 40 years reported in Paper I. We have reconsidered the 74 spectra published in Aerts et al. (1994a), obtained between 1987 November 6–14 with the European Southern Observatory (ESO) Coudé Auxiliary Telescope (CAT). As already emphasized by Aerts et al. (1994a) this time base is insufficient to

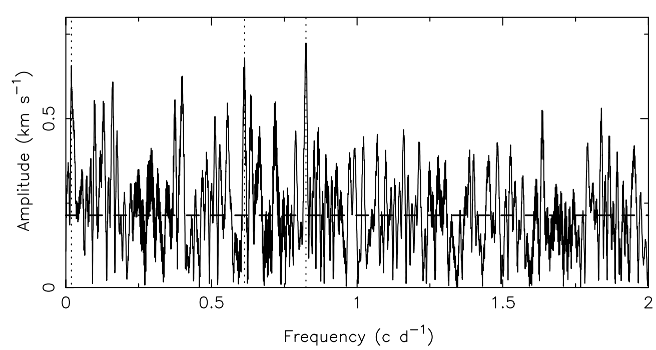

Figure 6. Amplitude spectrum of ν Eridani computed from residual radial velocities after pre-whitening with the 19 frequencies listed in Table 2. The dotted lines indicate the frequencies f_{19}, f_{20} and f_{21} given in Table 3. The dashed horizontal line indicates the noise level as defined in the text. We refer to the text for further details.

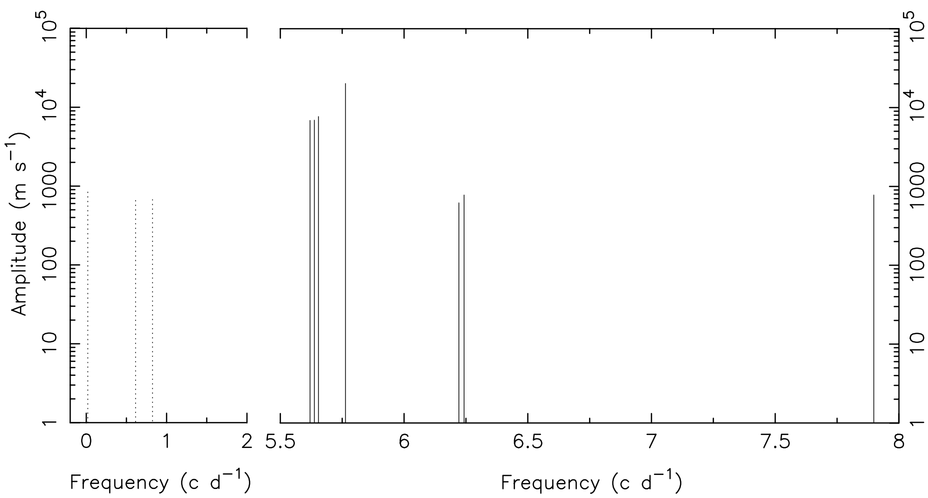

Figure 7. Final amplitude spectrum of the intrinsic frequencies derived from the radial velocities. The unambiguous intrinsic frequencies listed in Table 2 are indicated by a full line while the uncertain frequencies given in Table 3 are represented by the dotted lines. We stress that the *x*-axis is interrupted and has a different scale for both panels. Moreover, the *y*-axis is logarithmic and we have expressed the amplitudes in m s^{-1} in order to suppress the dominance of the main mode in the graph.

resolve the triplet f_2, f_3, f_4 and only f_1 and f_2 were found from a frequency analysis. We have fitted the first normalized moment of these older data by fixing f_1, f_2 as in Table 2 and we find the amplitudes $A_1 = (15.7 \pm 0.7)$ km s^{-1} and $A_2 = (9.1 \pm 0.8)$ km s^{-1}. Imposing f_1 an f_2 to the radial velocities from the CORALIE data taken in 2001 (see Table 1) leads to $A_1 = (19.6 \pm 0.5)$ km s^{-1} and $A_2 = (7.3 \pm 0.6)$ km s^{-1}, which agree with the current amplitudes listed in Table 2 within the errors. We therefore conclude that the main mode of ν Eridani has increased its radial velocity amplitude by 29 per cent between 1987 and 2001. This is consistent with the 25 per cent increase in the photometric amplitude of that mode found in Paper I. However, we find that the mode with f_2 has *decreased* its amplitude by 18 per cent, while an increase is reported in Paper I. Hence, the radial velocity data derived from modern high-resolution spectra suggest that the mode with frequency f_2 must have exchanged some of its energy with the main radial mode between 1987 and 2001, unless beating of the unresolved triplet components modified its measured amplitude.

Going further back in time, Kubiak (1980) performed frequency analyses on all radial velocity data available at that time, i.e. those gathered by Henroteau (1921, 1927), Struve et al. (1952) and Struve & Abhyankar (1955). He reported the amplitudes 19.3, 7.2, 8.0 and 6.3 km s^{-1} for f_1, f_2, f_3 and f_4 respectively, for the 455 data points with a time base of 457 d in 1923–1924 of Henroteau (1927). For the 345 data points gathered by Struve et al. (1952) and by Struve & Abhyankar (1955) in the years 1951–1954, Kubiak obtains 16.2, 11.3, 3.6 and 6.3 km s^{-1} for f_1, f_2, f_3 and f_4, respectively. Although Kubiak estimates the uncertainty of the amplitudes to be ~2 km s^{-1}, it seems that the amplitudes of the four strongest modes change on a time-scale of decades. Furthermore, it appears that the triplet mode with frequency f_2 has higher amplitude whenever the main radial mode's amplitude has decreased, and vice versa.

5 DISCUSSION AND FUTURE PLANS

We have provided the most extensive data set of high-resolution spectroscopic data of a β Cephei star so far. The previous record holders were 12 (DD) Lac (Mathias et al. 1994), β Cephei (Aerts et al. 1994b), β Crucis (Aerts et al. 1998), 16 (EN) Lac (Lehmann et al. 2001) and 19 Mon (Balona et al. 2002). Between 500 and 1400 spectra were obtained for each of these five stars, but all from single-site campaigns, thus only a limited number of mode frequencies were detected from these older data. Moreover, some of the detected modes in these stars have uncertain mode identifications, and this remains a problem for a seismic application to 19 Mon (Balona et al. 2002), β Crucis (Briquet & Aerts 2003), 12 (DD) Lac (Dziembowski & Jerzykiewicz 1999) and β Cephei (Telting, Aerts & Mathias 1997; Shibahashi & Aerts 2000). Seismic analyses of 16 (EN) Lac were carried out by means of photometric mode identification by Dziembowski & Jerzykiewicz (1996) and recently by means of the addition of spectroscopic mode identification by Thoul et al. (2003).

Our current spectra of ν Eridani were gathered during a three-month multisite campaign involving 11 spectrographs, which is the first of its kind for this type of pulsating star. A total of 2442 spectra were obtained. We disentangled 19 frequencies from the radial velocity data, while three frequencies are reported as additional candidates.

From the observed splittings, we infer a long rotation period of 56 d in the case of rigid rotation and a zero Ledoux splitting constant. An estimate of the rotation velocity of ν Eridani can be derived from the narrowest profiles we have at our disposal. Indeed, when the profiles are narrowest, the effect of the pulsational broadening to the overall line broadening is minimal. Overall, the profiles are broadened by pulsation, rotation and thermal motions. For ν Eridani's temperature, the thermal broadening amounts to ~8–10 km s^{-1}. The pulsational broadening is difficult to estimate without having solved the complete mode identification, including the derivation of the amplitude, of all the oscillation modes. However, it must be several km s^{-1} given that four high-amplitude modes are beating. The FWHM of the narrowest Si III profiles leads to a minimal overall broadening of ~ 23 ± 2 km s^{-1}. This implies that 20 km s^{-1} is a strict upper limit for $v \sin i$. Abt, Levato & Grosso (2002) also list a $v \sin i$ of 20 km s^{-1}. If we interpret the splittings as due to rigid rotation and pure acoustic modes, and if we assume a stellar radius of ~6 R$_\odot$, then we end up with an equatorial rotation velocity of ~5 km s^{-1}, which is compatible with our spectroscopically determined upper limit for $v \sin i$. Note that this upper limit for $v \sin i$ is a serious overestimate of the true equatorial rotation velocity resulting from the frequency splittings. This situation is completely analogous to the star HD 129929 (Aerts et al. 2003c) which is also a very slow rotator among the β Cephei stars. For ν Eridani we find a ratio between the intrinsic frequencies and the rotation frequency below 0.3 per cent assuming a zero Ledoux constant. This allows us to neglect rotational effects, such as the Coriolis force and the centrifugal forces, in future seismic modelling of the star.

The photometric frequency content of ν Eridani derived in Paper I consists of 23 accepted frequencies. Of those 23 frequencies, 17 are common to the 19 reported here from the radial velocities, given that our spectroscopic f_{13} may be either the left peak of the triplet, for which the right peak is found in Paper I, or the monthly alias of that right peak, and given that we find a 1-d alias of $f_2 + f_3$. The two other frequencies are harmonics of f_1 and f_4. A common set of 17 frequencies between multicolour photometry and high-resolution spectroscopy, among which are seven intrinsic frequencies, has never been obtained before for a β Cephei star. This constitutes a very promising starting point for mode identification and seismic modelling, the results of which will be presented in future papers. We point out that we will be searching for additional frequencies in several different line profile diagnostics, on which we will also report in the near future. This might reveal additional frequencies connected with higher-degree modes.

The biggest discrepant result from the photometric and radial velocity data sets is the absence of $f_A = 0.43218$ cd^{-1} (Paper I) in the latter. It is noteworthy that a similar situation occurs for the β Cephei star EN (16) Lac, for which Jerzykiewicz (1993) reported the frequency 0.165 cd^{-1} (which is twice the orbital frequency) from photometry, while this frequency was not found in the much more extensive spectroscopic data (Lehmann et al. 2001). The star 19 Mon is the only β Cephei star so far for which a low frequency is consistently found in both photometric and spectroscopic data (0.17019 cd^{-1}; Balona et al. 2002). It is not clear for any of these three β Cephei stars what the physical interpretation of the low frequency is.

ACKNOWLEDGMENTS

This study is partly based on observations obtained at the Observatorio do Pico dos Dias, Itajubá, Brazil, with the Apache Point Observatory 3.5-m telescope which is owned and operated by the Astrophysical Research Consortium and with the Nordic Optical Telescope operated on the island of La Palma jointly by Denmark, Finland, Iceland, Norway and Sweden, in the Spanish Observatorio del Roque de los Muchachos of the Instituto de Astrofisica de Canarias. CA is grateful to Prof. Michel Mayor for assigning us already in a very early stage the requested CORALIE runs, which helped us greatly to plan the additional spectroscopic campaigns. PDC and JDR are postdoctoral Fellows, Fund for Scientific Research of Flanders (FWO). This work has been supported by the Fund for Scientific Research of Flanders (FWO) under grant G.0178.02, by the Austrian Fonds zur Förderung der wissenschaftlichen Forschung under grant R12-N02 and by the Deutsche Forschungsgemeinschaft under grant DR 281/19-1. UH is supported by a grant from the National Science Foundation (NSF). The authors are much indebted to the technical staff at all the observatories for their help which contributed greatly to the success of this multisite campaign. We also thank Dietrich Baade, Thomas Rivinius and Stanislav Štefl of the HEROS team for having taken two additional ν Eridani spectra for us.

REFERENCES

Abt H. A., Levato H., Grosso M., 2002, ApJ, 573, 359
Aerts C., De Cat P., 2003, Space Sci. Rev., 105, 453
Aerts C., De Pauw M., Waelkens C., 1992, A&A, 266, 294
Aerts C., Waelkens C., De Pauw M., 1994a, A&A, 286, 136
Aerts C., Mathias P., Gillet D., Waelkens C., 1994b, A&A, 286, 109
Aerts C., De Cat P., Cuypers J., Becker S. R., Mathias P., De Mey K., Gillet D., Waelkens C., 1998, A&A, 329, 137
Aerts C., Lehmann H., Briquet M., Scuflaire R., Dupret M. A., De Ridder J., Thoul A., 2003, A&A, 399, 639
Aerts C. et al., 2003b, A&A, in press
Aerts C., Thoul A., Daszyńska J., Scuflaire R., Waelkens C., Dupret M. A., Niemczura E., Noels A., 2003, Sci, 300, 1926
Balona L. A., James D. J., Motsoasele P., Nombexeza B., Ramnath A., van Dyk J., 2002, MNRAS, 333, 952
Bedding T. R., Kjeldsen H., 2003, PASA, 20, 203
Breger M. et al., 1999, A&A, 349, 225
Breger M. et al., 2002, MNRAS, 329, 531
Briquet M., Aerts C., 2003, A&A, 398, 687
De Cat P., 2002, in Aerts C., Bedding T. R., Christensen-Dalsgaard J., eds, ASP Conf. Ser. Vol. 259, Radial and Nonradial Oscillations as Probes of Stellar Physics. Astron. Soc. Pac., San Francisco, p. 196
De Ridder J., Dupret M.-A., Neuforge C., Aerts C., 2002, A&A, 385, 572
Dziembowski W. A., Jerzykiewicz M., 1996, A&A, 306, 436
Dziembowski W. A., Jerzykiewicz M., 1999, A&A, 341, 480
Dziembowski W. A., Pamyatnykh A. A., 1993, MNRAS, 262, 204
Gautschy A., Saio H., 1993, MNRAS, 262, 213
Handler G., Aerts C., 2002, Comm. Asteroseismology, 142, 20
Handler G., Metcalfe T. S., Wood M. A., 2002, MNRAS, 335, 698
Handler G., Shobbrook R. R., Vuthela F. F., Balona L. A., Rodler F., Tshenye T., 2003, MNRAS, 341, 1005
Handler G. et al., 2004, MNRAS, 347, 452 (this issue) (Paper I)
Henroteau F., 1921, Publ. Dominion Obs., Ottawa, 5, 56
Henroteau F., 1927, Publ. Dominion Obs., Ottawa, 9, 117
Jerzykiewicz M., 1993, Acta Astron., 43, 13
Kubiak M., 1980, Acta Astron., 30, 41
Lehmann H. et al., 2001, A&A, 367, 236
Mathias P., Aerts C., Gillet D., Waelkens C., 1994, A&A, 289, 875
Shibahashi H., Aerts C., 2000, ApJ, 531, L143
Sperl M., 1998, Master's Thesis, University of Vienna
Struve O., Abhyankar H. D., 1955, ApJ, 122, 409
Struve O., McNamara D. H., Kung S. M., Kraft R. P., Williams A. D., 1952, ApJ, 116, 398
Telting J. H., Aerts C., Mathias P., 1997, A&A, 322, 493
Thoul A. et al., 2003, A&A, 406, 287
Vauclair G. et al., 2002, A&A, 381, 122

This paper has been typeset from a TEX/LATEX file prepared by the author.

5.4.3 Asteroseismology of the β Cephei star ν Eridani – III. extended frequency analysis and mode identification

Original paper:

J. De Ridder, J. H. Telting, L. A. Balona, **G. Handler,** M. Briquet, J. Daszyńska-Daszkiewicz, K. Lefever, A. J. Korn, U. Heiter, C. Aerts, 2004, MNRAS 351, 324

Mon. Not. R. Astron. Soc. **351,** 324–332 (2004) doi:10.1111/j.1365-2966.2004.07791.x

Asteroseismology of the β Cephei star ν Eridani – III. Extended frequency analysis and mode identification

J. De Ridder,[1★] J. H. Telting,[2] L. A. Balona,[3] G. Handler,[4] M. Briquet,[1] J. Daszyńska-Daszkiewicz,[1,5] K. Lefever,[1] A. J. Korn,[6] U. Heiter[6] and C. Aerts[1]

[1] *Instituut voor Sterrenkunde, K. U. Leuven, Celestijnenlaan 200B, B-3001 Leuven, Belgium*
[2] *Nordic Optical Telescope, Apartado 474, 38700 Santa Cruz de La Palma, Spain*
[3] *South African Astronomical Observatory, PO Box 9, Observatory 7935, Cape Town, South Africa*
[4] *Institut für Astronomie der Universität Wien, Türkenschanzstr. 17, 1180 Wien, Austria*
[5] *Astronomical Institute of Wrocław University, ul. Kopernika 11, 51-622 Wrocław, Poland*
[6] *Department of Astronomy and Space Physics, Uppsala Astronomical Observatory, Box 515, SE-75120 Uppsala, Sweden*

Accepted 2004 March 2. Received 2004 March 1; in original form 2004 February 6

ABSTRACT

Using the large photometric and spectroscopic data sets of the ν Eridani multisite campaign given in our two recent papers (Aerts et al. and Handler et al.), we present an extended frequency analysis and a photometric mode identification. For the extended frequency analysis, we used an improved radial velocity time series, the second-moment time series and the line profiles themselves. In the radial velocity time series, we can now detect an additional pulsation frequency that was previously only found in photometric time series. We also report several new candidate pulsation frequencies. For seven frequencies, the photometric mode identification indicates that they belong to a radial mode and six dipole modes, and for three frequencies the degree ℓ could not be unambiguously determined. We also placed ν Eri in the Hertzsprung–Russell diagram by determining T_{eff} using Geneva plus Strömgren photometric calibrations, spectral energy distribution fitting, by non-local thermodynamic equilibrium hydrogen, helium and silicon line profile fitting, and by determining $\log(L/\mathrm{L}_{\odot})$ using the *Hipparcos* parallax and an Hβ calibration.

Key words: techniques: photometric – techniques: spectroscopic – stars: early-type – stars: individual: ν Eridani – stars: oscillations – stars: variables: other.

1 INTRODUCTION

The massive B-type β Cephei stars are of particular asteroseismic interest. After all, they will be the next-generation supernovae, thereby chemically enriching our environment. Modelling their evolution, however, requires a thorough understanding of their convective core and of internal rotational mixing, two topics about which there is currently very limited knowledge. Using low-degree pulsation modes, which have very deep turning points, to probe this convective core currently seems the best way to resolve this problem.

The pulsation periods of β Cephei stars (3–8 h) are, however, significantly longer than those of δ Scuti stars or white dwarfs, making them more challenging targets to detect pulsational frequencies. This is why, from 2002 October until 2003 January, a large multisite and multitechnique campaign was set up for a β Cephei star. More than 2000 high-resolution spectra and 3000 photometric measurements in three passbands were obtained for ν Eridani (HD 29248, B2III). The data and a frequency analysis are presented in Handler et al. (2004, hereafter Paper Ia) and Aerts et al. (2004, hereafter Paper Ib). The present paper exploits these data sets further.

Successful seismic modelling involves not only detecting pulsation frequencies, but also mode identifications. Knowing the degree ℓ significantly reduces the number of possible mode matches, and can therefore help to narrow down the set of candidate models. In addition, it is essential to know whether we are dealing with an $m = 0$ mode, as the zonal modes are not affected by rotation in the first-order approximation.

In this paper we present the final frequency analysis results (Section 2) of both the spectroscopic and the photometric time series, as well as mode identification results (Section 4). In addition we determined the basic stellar parameters to put ν Eridani in the Hertzsprung–Russell (HR) diagram (see Section 3). These results serve as the starting point for stellar modelling papers (Pamyatnykh, Handler & Dziembowski 2004; Ausseloos et al., in preparation).

2 FREQUENCY ANALYSIS

The time series of ν Eri presented in Papers Ia and Ib are the largest ever collected for a β Cephei star, with the sole purpose of detecting

★E-mail: joris.deridder@ster.kuleuven.ac.be

as many pulsational frequencies as possible. In what follows we extend the frequency analysis done in the previous papers, by a reanalysis of the radial velocity time series, and for the first time a frequency analysis of the line profile time series.

2.1 The radial velocity

We carefully redetermined the moments (see Aerts, de Pauw & Waelkens 1992, for a definition) of each of the three Si lines of the Si III triplet around 456 nm. In the intervals [455.0, 455.6] nm, [456.4, 457.2] nm and [457.2, 457.75] nm around respectively the Si III 455.3 nm, the Si III 456.8 nm and the Si III 457.5 nm lines, we first locally renormalized the spectrum and then selected the part that should *not* be regarded as continuum. This part contains the spectral line as well as a bit of the continuum that is difficult to distinguish from the far wings of the line. The remaining part of the interval was used to compute the standard deviation σ of the normalized flux noise. The region of the spectrum with points at least 2σ in flux away from the continuum was then extracted as the line profile, of which the normalized moments were consequently computed. The integration boundaries of the moments are thus dynamically determined depending on the signal-to-noise (S/N) ratio ($\equiv \sigma^{-1}$) of the spectrum. The corresponding integration interval is much smaller than the wavelength intervals stated above. The advantage is a considerable noise reduction in the moments time series. As the main mode of ν Eri has a large amplitude ($\sim$22 km s^{-1}), the spectral lines show a rather large periodic Doppler shift. A fixed wavelength integration range would therefore have to be taken quite large to ensure that the entire line profile is always included. This would also mean the inclusion of noisy continuum on the red side when the line shows a blueshift and vice versa, which degrades the accuracy of the moments.

Note that, as in Paper Ib, we compute the radial velocity with the first moment of the line profile, and not by the central wavelength of a fitted Gaussian, as the Si line profiles are sometimes rather skewed. We also did not use the wavelength of the minimum flux point as this could lead to frequency harmonics in the $v_{\rm rad}$ data regardless of whether the star pulsates linearly or not.

After removing noisy data points (S/N < 150) and outliers, we retained 1740, 1874 and 1827 data points for respectively the Si III 455.3, 456.8 and 457.5 nm lines. We did a careful frequency analysis of these $v_{\rm rad}$ data and we tabulate the results later in this section. We find all the 'independent' frequencies mentioned in Paper Ib, and in addition we now find three (instead of only two) frequency peaks of the multiplet around 6.24 d^{-1}. We also find most of the 'combination' frequencies stated in Paper Ib, plus some additional ones. Just as in Papers Ia and Ib, we identify a combination frequency as a frequency outside the usual β Cephei frequency interval of [3, 8] d^{-1}, and which can be written as a linear combination of two or more independent frequencies within the estimated observational errors. During multifrequency solution determinations, these combination frequencies are fixed to their exact linear combination. We realize, however, that this approach is not without risk, as it might not be impossible that a linearly stable high-order eigenfrequency *close to* but not exactly equal to a linear combination frequency might be excited due to non-linear effects. In such a case, fixing the combination frequencies would lead to a biased estimate of the independent frequencies. We nevertheless choose to fix the combination frequencies as it seems unlikely that all or even most of them would be real eigenfrequencies. The alternative, i.e. introducing extra free parameters, would then lead to overfitting and thus to an excessive variance of the estimated independent frequencies.

We made an effort to determine the optimal multifrequency solution in an N-dimensional box with edges $2\Delta\nu$ around the initial estimate. One way of doing this is to make an N-dimensional grid in the box, with mesh size $\delta\nu$, and verify the performance of the frequency solution in each of the $(2\Delta\nu/\delta\nu + 1)^N$ grid points. This number of grid points is, however, computationally unfeasible for ν Eri, for which we have $N = 8$ and $\Delta\nu = 10^{-2}$ d^{-1} and for which we would like to have $\delta\nu = 10^{-4}$ d^{-1}. We therefore resorted to N-dimensional conjugate directions minimization (see e.g. Press et al. 1992), which we choose because there is no need for derivatives. The function to minimize was the χ^2 function with eight dependent and 12 combination frequencies in the case of a spectroscopic data set, and nine dependent frequencies and 14 combination frequencies in the case of a photometric data set. This method seemed to perform quite well in a reasonable amount of time. Unfortunately, the window function of the spectroscopic time series has local maxima at $\nu = 0.0023$ and 0.0046 d^{-1}, which may have led the algorithm to an alias frequency. We therefore also systematically checked whether the frequency combination

$$\{\nu_1 + n_1 \times 0.0023,\ \nu_2 + n_2 \times 0.0023, \ldots, \nu_8 + n_8 \times 0.0023\},$$

where $\{\nu_i\}$ is the solution after minimization and $n_i \in \{0, \pm 1, \pm 2\}$, has a better χ^2 value. The results of this optimization approach are given in Table 1, where we also give for each frequency the amplitude and phase together with their estimated uncertainties.

In fact, one reason for giving Table 1 in addition to table 2 of both Papers Ia and Ib is to provide a better feeling for the uncertainties involved. We underline that the error estimates on the frequencies given in Papers Ia and Ib are formal estimates (as clearly stated), derived under the assumption of an equidistant time series of a monoperiodic signal with uncorrelated noise. The different values of the derived frequencies for the different Si lines and for the different Strömgren passbands in Table 1 provides another way to assess the uncertainties on the frequencies. The uncertainties on the amplitudes and the phases were computed, as usual, with the local curvature of the χ^2 function where we assumed the frequencies to be known. The derived values of the amplitudes and phases (the latter are not given in Papers Ia and Ib) for the different Si lines provide another view on the uncertainties involved. Especially the phases seem to be rather inaccurately determined. We note that both the phase and its uncertainty depend on t_0 as well as on the exact value of the frequency.

Concerning the close frequencies around 6.24 d^{-1}, we easily find the frequencies ν_6 and ν_8 in the new radial velocity time series; these were also detected in the photometric time series. The frequency ν_8 is new for the spectroscopic data, as it was not found in the $v_{\rm rad}$ data of Paper Ib. A peak at the position of ν_7 (a frequency that was clearly detected in Paper Ib, and mentioned as a possible *photometric* signal in Paper Ia) is seen in the radial velocity time series of all three Si lines, but shows much less power than mentioned in Paper Ib, as can be read from Table 1. Much of the evidence for ν_7 therefore comes from both Papers Ia and Ib instead of from our new radial velocity time series.

At this point we would like to mention that we did a frequency analysis not only of the first moment, but also of the second moment $\langle v^2\rangle$. The motivation to do so is the β Cephei star β Crucis, for which some pulsation frequencies were found in the higher moments but not in $\langle v\rangle$ (Aerts et al. 1998), and which were later confirmed by satellite (*WIRE*) data (Cuypers et al. 2002). However, a frequency analysis of the second moment is notoriously difficult because of the many possible cross-term frequencies. If there are N frequencies ν_i detected in the first moment, there can be $N(N$

Table 1. Estimates of the frequencies, amplitudes and phases of the modes found in the radial velocity and photometric time series. Each frequency was assigned a unique identification. The signal is always written as $C + \sum_{i=1}^{N} A_i \sin[2\pi\nu_i(t - t_0) + \varphi_i]$, where t_0 = HJD 245 2000. Eight independent and 12 combination frequencies were found in the $v_{\rm rad}$ data, and nine independent and 14 combination frequencies were found in the photometric data. The combination frequencies were always fixed to their exact linear combination of independent frequencies. The uncertainties on the last given digit of the amplitudes and phases are given in parentheses.

	$v_{\rm rad}$ (Si III 455.3 nm)			$v_{\rm rad}$ (Si III 456.8 nm)			$v_{\rm rad}$ (Si III 457.5 nm)		
ID	Freq. (d^{-1})	A (km s^{-1})	φ (deg)	Freq. (d^{-1})	A (km s^{-1})	φ (deg)	Freq. (d^{-1})	A (km s^{-1})	φ (deg)
ν_1	5.76330	22.36(7)	318.0(2)	5.76330	22.50(6)	318.3(2)	5.76330	22.74(6)	318.7(2)
ν_2	5.65396	8.91(9)	69.5(6)	5.65394	9.04(8)	76.5(5)	5.65394	9.09(8)	77.1(5)
ν_3	5.62006	8.11(9)	27.8(6)	5.62006	8.18(8)	29.2(6)	5.62008	8.29(8)	23.6(5)
ν_4	5.63734	7.91(8)	182.8(6)	5.63731	8.00(7)	191.8(5)	5.63731	8.03(7)	191.4(5)
ν_5	7.89845	1.00(7)	307(4)	7.89847	1.00(6)	305(4)	7.89833	0.97(6)	340(4)
ν_6	6.24434	1.03(8)	152(4)	6.24500	1.03(7)	0(4)	6.24510	0.96(7)	335(4)
ν_7	6.22304	0.31(7)	272(15)	6.22099	0.36(6)	55(10)	6.22114	0.35(6)	17(11)
ν_8	6.26080	0.76(8)	86(7)	6.26231	0.76(7)	105(5)	6.26250	0.79(7)	64(5)
ν_{12}	$\nu_1 + \nu_3$	2.84(8)	184(2)	$\nu_1 + \nu_3$	2.82(8)	183(2)	$\nu_1 + \nu_3$	2.84(8)	184(2)
ν_{13}	$\nu_1 + \nu_4$	2.59(8)	345(2)	$\nu_1 + \nu_4$	2.59(7)	350(2)	$\nu_1 + \nu_4$	2.59(8)	345(2)
ν_{14}	$2\nu_4$	0.61(7)	153(7)	$2\nu_4$	0.59(6)	163(6)	$2\nu_4$	0.61(7)	153(7)
ν_{15}	$\nu_1 + \nu_2$	3.19(9)	229(2)	$\nu_1 + \nu_2$	3.20(8)	233(1)	$\nu_1 + \nu_2$	3.19(9)	229(2)
ν_{16}	$2\nu_1$	0.70(7)	96(6)	$2\nu_1$	0.75(6)	97(5)	$2\nu_1$	0.70(7)	96(6)
ν_{17}	$\nu_1 + \nu_5$	0.52(7)	93(8)	$\nu_1 + \nu_5$	0.48(6)	88(8)	$\nu_1 + \nu_5$	0.52(7)	93(8)
ν_{19}	$\nu_1 + \nu_2 + \nu_3$	1.45(7)	103(3)	$\nu_1 + \nu_2 + \nu_3$	1.50(6)	108(2)	$\nu_1 + \nu_2 + \nu_3$	1.45(7)	103(3)
ν_{22}	$2\nu_1 + \nu_3$	0.94(8)	351(5)	$2\nu_1 + \nu_3$	0.95(8)	347(5)	$2\nu_1 + \nu_3$	0.94(8)	351(5)
ν_{23}	$2\nu_1 + \nu_4$	0.88(8)	160(5)	$2\nu_1 + \nu_4$	0.76(7)	164(5)	$2\nu_1 + \nu_4$	0.88(8)	160(5)
ν_{24}	$2\nu_1 + \nu_2$	1.14(9)	37(5)	$2\nu_1 + \nu_2$	1.11(8)	40(4)	$2\nu_1 + \nu_2$	1.14(9)	37(5)
ν_{25}	$3\nu_1$	0.52(7)	178(8)	$3\nu_1$	0.50(6)	169(7)	$3\nu_1$	0.52(7)	178(8)
ν_{26}	$2\nu_1 + \nu_2 + \nu_3$	0.94(7)	261(4)	$2\nu_1 + \nu_2 + \nu_3$	0.92(6)	263(4)	$2\nu_1 + \nu_2 + \nu_3$	0.94(7)	261(4)

	Strömgren u			Strömgren v			Strömgren y		
ID	Freq. (d^{-1})	A (mmag)	φ (deg)	Freq. (d^{-1})	A (mmag)	φ (deg)	Freq. (d^{-1})	A (mmag)	φ (deg)
ν_1	5.76326	73.5(2)	63.4(2)	5.76327	41.0(1)	64.4(2)	5.76327	36.9(1)	63.0(2)
ν_2	5.65391	37.9(2)	172.7(3)	5.65396	26.5(1)	162.0(3)	5.65393	25.1(1)	168.1(3)
ν_3	5.62009	34.6(2)	111.7(3)	5.62007	23.9(1)	117.3(3)	5.62006	22.7(1)	118.4(3)
ν_4	5.63715	32.2(2)	319.8(4)	5.63720	22.4(2)	307.8(4)	5.63718	21.1(1)	313.6(4)
ν_5	7.89757	4.3(2)	246(3)	7.89769	3.1(1)	219(3)	7.89779	2.9(1)	195(2)
ν_6	6.24352	3.9(2)	61(3)	6.24406	2.6(1)	307(3)	6.24326	2.6(1)	114(3)
ν_8	6.26181	2.8(2)	317(4)	6.26178	1.9(1)	322(4)	6.26182	1.7(1)	309(4)
ν_9	7.20012	1.4(2)	109(8)	7.19984	1.0(1)	179(8)	7.19964	1.2(1)	223(6)
ν_{10}	0.43235	5.5(2)	187(2)	0.43190	3.2(1)	289(2)	0.43232	3.2(1)	192(2)
ν_{11}	$\nu_2 + \nu_3$	2.8(2)	11(4)	$\nu_2 + \nu_3$	1.7(1)	2(5)	$\nu_2 + \nu_3$	1.4(1)	2(5)
ν_{12}	$\nu_1 + \nu_3$	11.1(2)	297(1)	$\nu_1 + \nu_3$	7.9(1)	303(1)	$\nu_1 + \nu_3$	7.5(1)	300(1)
ν_{13}	$\nu_1 + \nu_4$	10.9(2)	150(1)	$\nu_1 + \nu_4$	7.7(2)	139(1)	$\nu_1 + \nu_4$	7.1(1)	143(1)
ν_{15}	$\nu_1 + \nu_2$	12.6(2)	5.6(9)	$\nu_1 + \nu_2$	9.0(1)	354.9(9)	$\nu_1 + \nu_2$	8.4(1)	358.8(9)
ν_{16}	$2\nu_1$	4.5(2)	183(3)	$2\nu_1$	3.1(1)	176(3)	$2\nu_1$	2.9(1)	175(3)
ν_{17}	$\nu_1 + \nu_5$	1.6(2)	44(7)	$\nu_1 + \nu_5$	1.2(1)	15(7)	$\nu_1 + \nu_5$	1.1(1)	349(6)
ν_{18}	$\nu_1 + \nu_3 + \nu_4$	1.0(2)	12(12)	$\nu_1 + \nu_3 + \nu_4$	0.7(1)	359(12)	$\nu_1 + \nu_3 + \nu_4$	0.7(1)	15(11)
ν_{19}	$\nu_1 + \nu_2 + \nu_3$	4.4(2)	256(3)	$\nu_1 + \nu_2 + \nu_3$	3.1(2)	257(3)	$\nu_1 + \nu_2 + \nu_3$	2.6(1)	263(3)
ν_{20}	$\nu_1 + \nu_2 + \nu_4$	1.0(2)	53(13)	$\nu_1 + \nu_2 + \nu_4$	0.9(1)	30(10)	$\nu_1 + \nu_2 + \nu_4$	0.9(1)	50(9)
ν_{21}	$\nu_1 + 2\nu_2$	0.9(2)	257(14)	$\nu_1 + 2\nu_2$	0.8(1)	236(11)	$\nu_1 + 2\nu_2$	0.6(1)	253(15)
ν_{22}	$2\nu_1 + \nu_3$	1.8(2)	113(7)	$2\nu_1 + \nu_3$	1.4(1)	106(6)	$2\nu_1 + \nu_3$	1.2(1)	106(6)
ν_{23}	$2\nu_1 + \nu_4$	1.8(2)	335(7)	$2\nu_1 + \nu_4$	1.2(1)	314(7)	$2\nu_1 + \nu_4$	1.1(1)	313(8)
ν_{24}	$2\nu_1 + \nu_2$	2.0(2)	181(6)	$2\nu_1 + \nu_2$	1.4(1)	162(6)	$2\nu_1 + \nu_2$	1.3(1)	166(6)
ν_{26}	$2\nu_1 + \nu_2 + \nu_3$	1.5(2)	65(7)	$2\nu_1 + \nu_2 + \nu_3$	1.0(1)	67(8)	$2\nu_1 + \nu_2 + \nu_3$	0.9(1)	69(8)

+ 1) frequencies present in the second moment: besides ν_i also $2\nu_i$, $\nu_i + \nu_j$ and $\nu_i - \nu_j$ (Aerts 1996). In the case of ν Eri this would imply that we can expect 420 frequencies, although not all of them need to have an amplitude above the noise level. The power spectrum of the second-moment time series of the Si III (456.8 nm) line indeed shows many peaks, and we do not list them here for the sake of brevity. The bottom line of our analysis is that, besides the many cross-term frequencies, we did not find any convincing new frequencies.

2.2 The line profiles

We continued our quest for frequencies by doing a frequency analysis on the line profiles of the Si III 455.3 and 456.8 nm lines. Indeed,

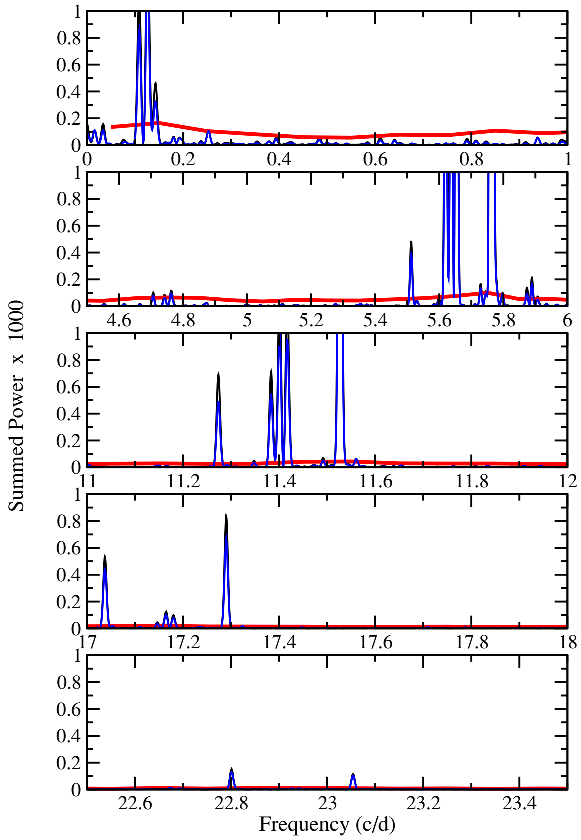

Figure 1. The power spectra of the Si III 455.3 and 456.8 nm line profiles, obtained by summing the power at each wavelength point in the intervals [455.16, 455.40] nm and [456.678, 456.922] nm, respectively. The power spectra are plotted on top of each other, and can hardly be distinguished. The CLEAN algorithm with gain parameter $g = 0.2$ was used. The thick almost horizontal line denotes the 1σ noise level of the non-CLEAN-ed Fourier power spectrum after prewhitening the time series with the 20 frequencies mentioned in Table 2, and was approximated at each frequency by the average power in a 0.1 d^{-1} interval around that frequency.

Table 2. All frequency peaks that are clearly present in both Si III 455.3 and 456.8 nm line profiles. We also list the suspected identification, where we have used the same notation as in Table 1.

Si III 455.3 nm Freq. (d^{-1})	Si III 456.8 nm Freq. (d^{-1})	Possible Identification
0.10880	0.10886	$\nu_1 - \nu_2$
0.12630	0.12622	$\nu_1 - \nu_4$
0.14270	0.14268	$\nu_1 - \nu_3$
5.51228	5.51224	$2\nu_4 - \nu_1$
5.61986	5.61986	ν_3
5.63760	5.63762	ν_4
5.65384	5.65390	ν_2
5.76334	5.76336	ν_1
5.88910	5.88910	$2\nu_1 - \nu_4$
11.27368	11.27364	ν_{11}
11.38330	11.38326	ν_{12}
11.40108	11.40104	ν_{13}
11.41688	11.41688	ν_{15}
11.52670	11.52672	ν_{16}
17.03752	17.03752	ν_{19}
17.16478	17.16480	ν_{23}
17.18004	17.18006	ν_{24}
17.28994	17.28996	ν_{25}
22.80086	22.80086	ν_{26}
23.05362	23.05360	$4\nu_1$

several examples of β Cephei stars exist for which some pulsation frequencies are clearly detected in the line profiles but not in the radial velocity data (e.g. ε Cen, Schrijvers, Telting & Aerts 2004).

We considered normalized flux time series at each wavelength point in the intervals [455.16, 455.40] nm and [456.678, 456.922] nm. We used the CLEAN algorithm (Roberts, Lehar & Dreher 1987) to search for frequencies but systematically verified with classical Fourier analysis that our results are not numerical artefacts. The frequency analysis was done in the interval [0, 30] d^{-1} with a frequency step of 2×10^{-6} d^{-1}. Consequently, we summed the power over all the wavelength bins to obtain an overall power spectrum. The result is shown in Fig. 1. In the corresponding Table 2 we list the 20 frequencies that are clearly present in both silicon line profiles. We also list each time the suspected identification, which is always either one of the independent frequencies also found in the radial velocity, or a linear combination of these independent frequencies. Besides these frequencies we also consider the low-amplitude frequencies 4.707 and 4.742 d^{-1}, worth comparing with theoretically predicted frequencies.

In Table 2 we list two frequency combinations as possible identifications for the frequencies 5.51 and 5.89 d^{-1}. We consequently asked ourselves the following question: As we have nine genuine eigenfrequencies $\nu_1, \ldots, \nu_9$, should we not expect that almost every newly found frequency peak in the β Cephei pulsational frequency range $[\nu_b, \nu_e] = [3, 8]$ d^{-1} can be written as *some* linear combination of these eigenfrequencies? Part of the answer is that it turns out that there are actually not many possible linear combinations that map frequencies from $[\nu_b, \nu_e]$ back into the same interval and that are at the same time not too far-fetched with respect to the linear combinations found in the Fourier spectrum of the radial velocity. Only the general combinations $2\nu_j - \nu_k$ and $\nu_j + \nu_k - \nu_i$ seem to be acceptable. We now compute the probability that a randomly chosen frequency coincides with a combination frequency ν_c. Given n independent frequencies, the number of possible combinations $2\nu_j - \nu_k$ is simply $n(n-1)$, and the number of different combinations $\nu_j + \nu_k - \nu_i$ is $n(n-1)(n-2)/2$. We consider a frequency to 'coincide' with a combination frequency ν_c if it is in the interval $[\nu_c - \delta\nu, \nu_c + \delta\nu]$ with $\delta\nu$ being the observational frequency precision. If n and/or $\delta\nu$ is (are) sufficiently small (as in our case) we can expect that none of these intervals will overlap with another interval. All of these intervals together occupy a fraction

$$\frac{\delta\nu}{\nu_e - \nu_b} n^2(n-1)$$

of the total β Cephei frequency range $[\nu_b, \nu_e]$, which is equal to the probability that a frequency randomly chosen in this interval falls into one of the intervals. Setting $n = 9$, $[\nu_b, \nu_e] = [3, 8]$ d^{-1} and $\delta\nu = 10^{-3}$ d^{-1} for the case of ν Eri, we can roughly estimate this probability to be 13 per cent, i.e. a non-negligible probability. We must note, however, that our assumption that the newly found frequency peak is independent of the confirmed eigenfrequencies might not be justified. If it is indeed a genuine eigenfrequency, the underlying pulsation physics may impose that it can or cannot be written as a linear combination of the other eigenfrequencies.

In fact, in Fig. 2 we find two indications that the frequencies 5.51 and 5.89 d^{-1} might indeed not be combination frequencies. This figure shows the morphology of the amplitude and the phase

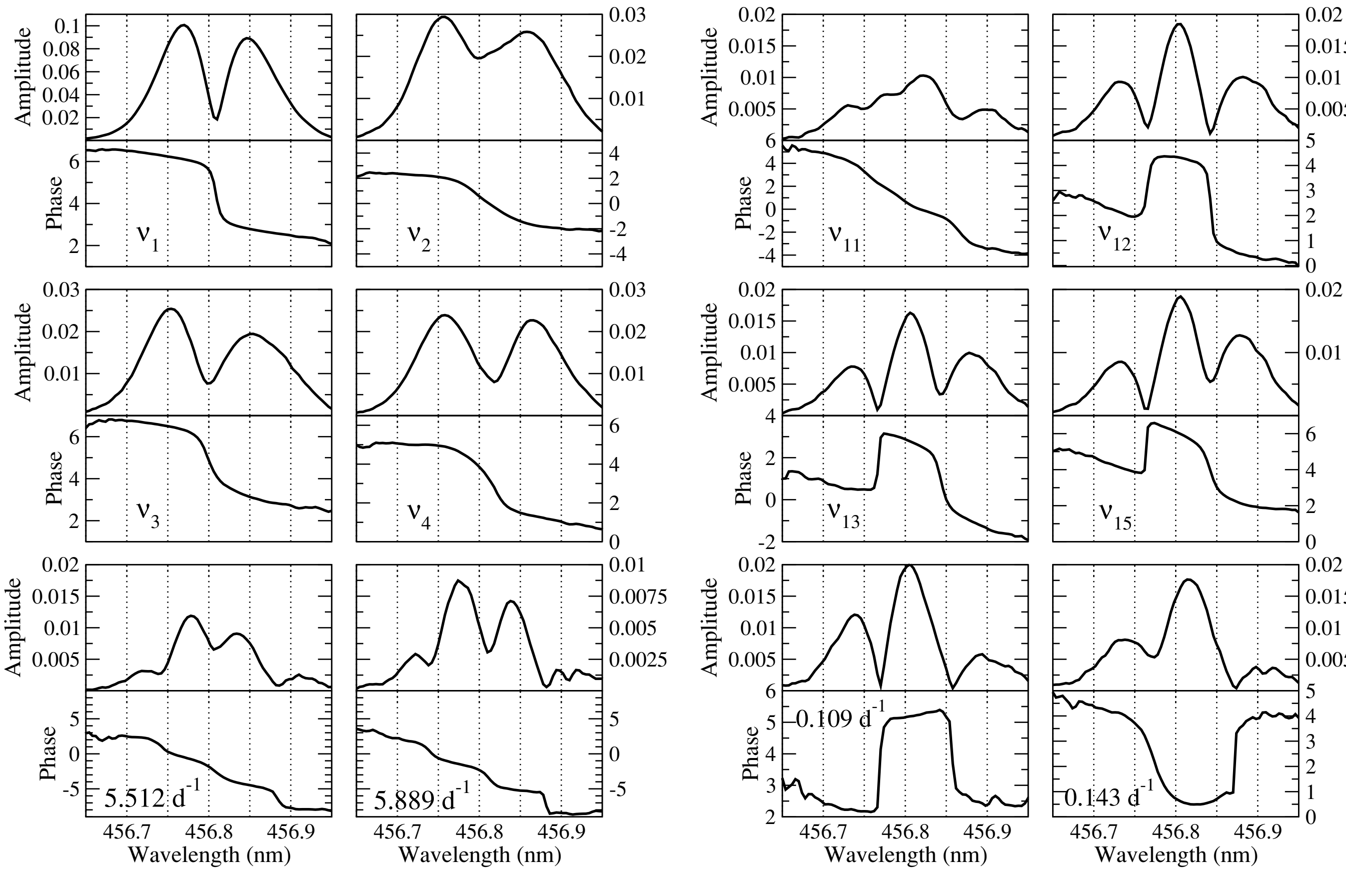

Figure 2. Amplitude and phase distributions for several frequencies, for the Si III 456.8 nm line. On the left-hand side the distributions of the genuine eigenfrequencies plus the frequencies 5.51 and 5.89 d^{-1} are shown. For comparison, on the right-hand side, we also show the distributions of some combination frequencies. The amplitudes are unitless as the line profiles are normalized. The phases are expressed in radians.

distribution of several frequencies found in the Si III 456.8 nm line profile time series. The amplitudes and phases were computed by fitting the flux time series at each wavelength point with a sum of 20 sines corresponding to the 20 frequencies listed in Table 2. The amplitude and phases of these sines then make up the distributions shown in Fig. 2. We show examples of both genuine eigenfrequencies and known combination frequencies. The phase diagrams of the 5.51 and 5.89 d^{-1} frequencies show a monotonic phase distribution across the line profile with a large phase range. Such behaviour is typical for higher-degree modes, which would explain why we do not see the frequencies in the photometry or the radial velocity data. However, this evidence is not conclusive, as the combination frequency ν_{11} shows the same phase behaviour in the line profile. Another indication is that for both 5.51 and 5.89 d^{-1} the line profile shows more variability in the line wings than in the line core, which is also systematically true for the eigenfrequencies, while it is vice versa for the combination frequencies. Again, this evidence is not conclusive, as we do not know what the velocity distribution of a combination frequency looks like at the surface of the star, so that we also do not know what kind of line profile variations we should expect.

3 BASIC STELLAR PARAMETERS

For a photometric mode identification it is useful to have the position of ν Eri in the HR diagram. This position and its error box can also be used as the initial guess and additional constraint for further asteroseismic investigations.

Geneva photometric colours of ν Eri were obtained from the General Catalogue of Photometric Data (Mermilliod, Mermilliod & Hauck 1997). From these colours, the Geneva indices X and Y can be deduced, which are independent of interstellar extinction for hot stars like ν Eri. We then used the calibration of Künzli et al. (1997) to obtain $T_{\rm eff} = 23084 \pm 234$ K and $\log\ g = 3.88 \pm 0.19$. We emphasize that the uncertainties quoted are lower limits, as the calibration for hot stars requires the metallicity to be known a priori, but we *assumed* it to be solar.

Besides Geneva photometry we also used Strömgren photometry to estimate the effective temperature. We used the large literature survey already done by Hauck & Mermilliod (1998) to obtain the following quantities for ν Eri: $V = 3.960$, $b - y = -0.076$, $m_1 = 0.068$, $c_1 = 0.072$ and $\beta = 2.610$. With these values we can compute the following reddening-free indices (Strömgren 1966):

$$[c_1] = c_1 - 0.2(b - y) = 0.087,$$

$$[m_1] = m_1 + 0.18(b - y) = 0.054,$$

$$[u - b] = [c_1] + 2[m_1] = 0.196.$$

Consequently, we used the $[u - b]$–$T_{\rm eff}$ calibration

$$\frac{5040\mathrm{K}}{T_{\rm eff}} = 0.1692 + 0.2828[u - b] - 0.0195[u - b]^2$$

of Napiwotzki, Schönberner & Wenske (1993) to estimate $T_{\rm eff} = 22\,500$ K.

We also estimated $T_{\rm eff}$ by fitting the spectral energy distribution (SED) of ν Eri. To do so, we collected optical and infrared fluxes

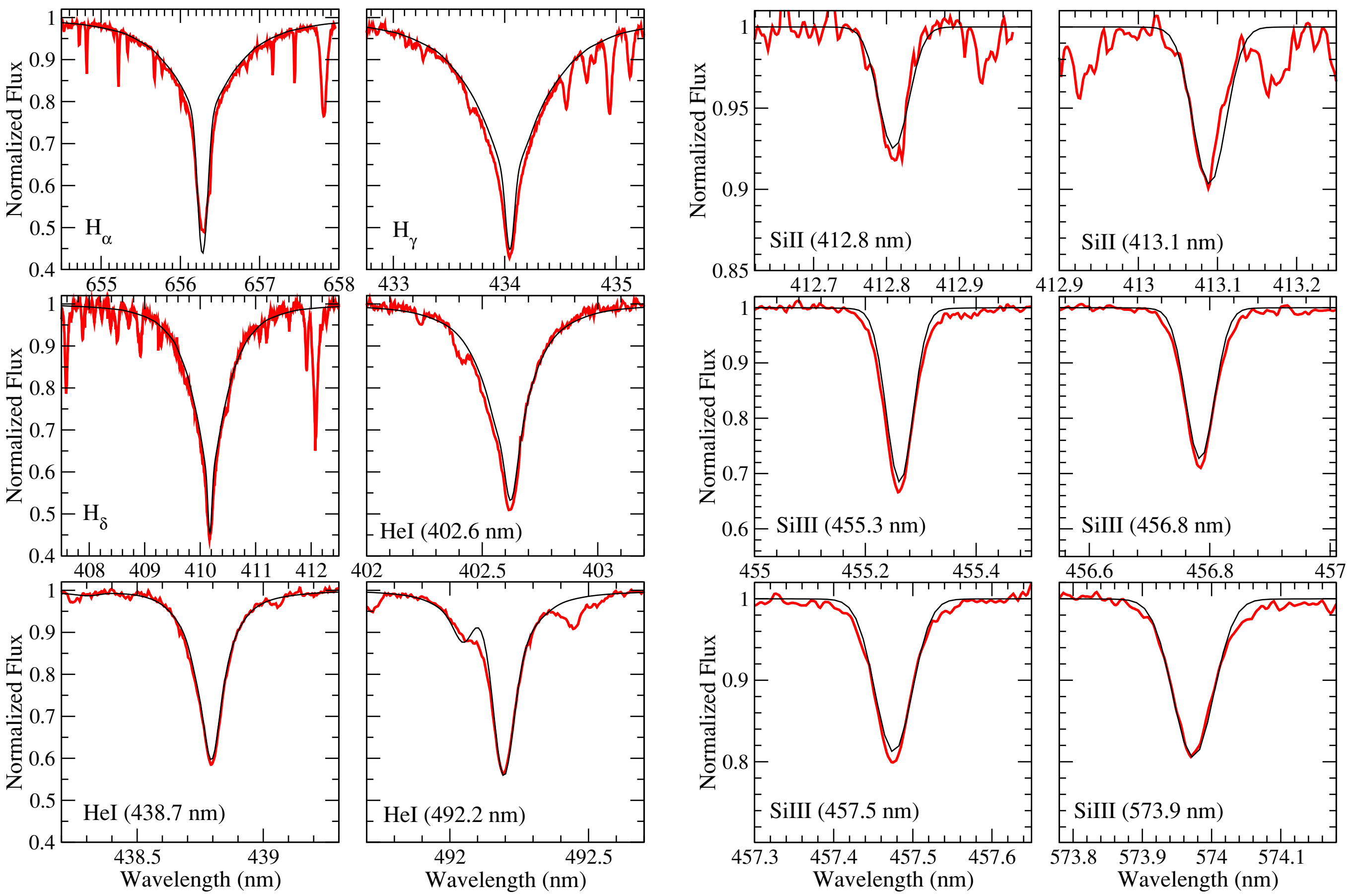

Figure 3. A selection of observational hydrogen, helium and silicon line profiles together with their best fits (smooth curves) obtained for $T_{\mathrm{eff}} = 24\,000$ K, log $g = 3.7$ and $n(\mathrm{He})/n(\mathrm{H}) = 0.12$.

of ν Eri from Glushneva et al. (1992) and ultraviolet fluxes from Jamar et al. (1976). It is difficult to estimate to what extent this SED is reddened, but we tried to correct for reddening by using Fitzpatrick's (1999) mean galactic interstellar extinction law. Next, we fitted the dereddened SED with theoretical SEDs computed from local thermodynamic equilibrium (LTE) Kurucz (1994) stellar atmosphere models. The best fit was obtained for a model with $T_{\mathrm{eff}} = 21\,900$ K. To have an idea about the uncertainty of this value, we examined the effects of small variations of the extinction or the observed ultraviolet fluxes (which are most important for our temperature determination) within their observational errors. From this, we roughly estimate the uncertainty to be about 1000 K.

We also used the echelle spectra obtained at the Calar Alto Observatory (see Paper Ib) to make a spectroscopic estimate for T_{eff}. To generate a grid of theoretical line profiles we ran the spherically symmetric non-local thermodynamic equilibrium (NLTE) atmosphere code FASTWIND, first introduced by Santolaya-Rey, Puls & Herrero (1997). The newest version of FASTWIND includes the effects of metal line blocking/blanketing (see Herrero, Puls & Najarro 2002) as well as a consistently calculated temperature structure based on the thermal balance of electrons, except for the innermost part of the atmosphere, where a flux-correction method is applied (see Kubat, Puls & Pauldrach 1999). We used five hydrogen lines (Hα up to Hϵ), six He I lines (402.6, 438.7, 447.1, 471.3, 492.2 and 667.8 nm), two Si II doublets (412.8–413.1 and 504.1–505.6 nm), two Si III triplets (455.3–456.8–457.5 and 481.3–481.9–482.9 nm) and two additional Si III lines (471.6 and 574.0 nm). These theoretical line profiles were then compared with the least pulsationally broadened observational line profiles to search for the T_{eff}, log g and particle number ratio $n(\mathrm{He})/n(\mathrm{H})$ for which the match is best. Especially the wings of the hydrogen lines and the ionization balance between Si II and Si III are useful to determine respectively the gravity and the temperature. Our best match turns out to be for the parameters $T_{\mathrm{eff}} = 24\,000$ K, log $g = 3.7$ and $n(\mathrm{He})/n(\mathrm{H}) = 0.12$. We estimate the uncertainties on these parameter values to be 1000 K, 0.1 dex and 0.02, respectively. In Fig. 3 we show fits of 12 of the 23 selected spectral lines as examples. The fact that we seem to find a slight He overabundance is not too surprising as the chemical analysis of Kilian (1992) shows that half of her sample of unevolved B stars are actually He overabundant. The very slow rotation of ν Eri (see Paper Ib) is in fact consistent with our findings in the sense that Zboril & North (1999) show that He-enhanced B stars are significantly slower rotators than normal B-type stars. We also refer to a recent abundance analysis of ν Eri of Korn & Heiter (in preparation), who, besides H, He and Si lines, also used oxygen lines to determine abundances. They find a slight He enhancement as well, although, as in our case, the uncertainties on the observed abundances cannot exclude a solar abundance. Also the derived abundances of Si and O are solar within the error bars.

Following the discussion above, we adopt conservatively $T_{\mathrm{eff}} = 22\,900 \pm 1100$ K, in the hope that the true value is indeed contained in this rather large interval.

In order to compute the luminosity from the visual magnitude V, we first need to compute the interstellar extinction A_V. Although

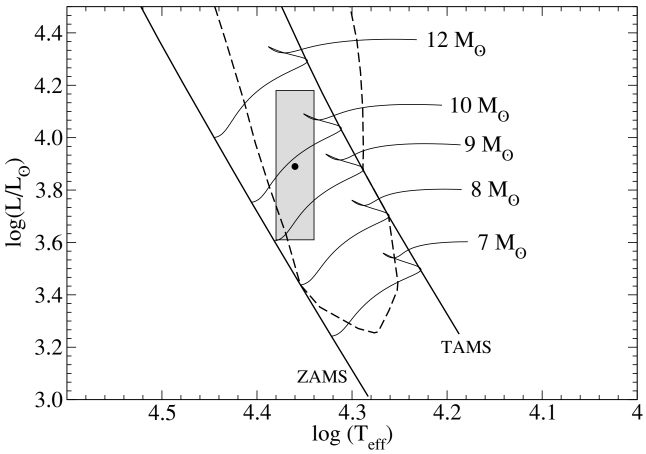

Figure 4. The estimated position and uncertainty box of ν Eri in the HR diagram, assuming that ν Eri has a solar chemical composition. Synthetic evolutionary tracks are drawn in thin full lines, the zero-age and terminal-age main sequences in thick full lines, and the theoretical β Cephei instability strip for ℓ up to 2 in a thick dashed line. Except for the evolutionary tracks, which we computed ourselves, the sequences and the strip were taken from Pamyatnykh (1999). They were computed with $X = 0.7$, $Z = 0.02$, a mixing length parameter $\alpha = 1.0$, and without taking into account the effects of convective core overshooting and rotation. We refer to Pamyatnykh for more details on this instability strip.

A_V is very difficult to estimate, we are somewhat fortunate that the Galactic latitude $b = -31^\circ$ of ν Eri implies that the star does not lie in the patchy Galactic plane, so that we can make a rough estimate of A_V with the work of Sandage (1972). This leads to $A_V \approx 0.2$, and thus to $V_0 \approx 3.76$. The *Hipparcos* parallax $\pi = 5.56 \pm 0.88$ mas implies a distance $d = 180 \pm 28$ pc. The absolute visual magnitude is therefore $M_{V_0} = -2.52 \pm 0.34$, where we assumed that most of the uncertainty on M_{V_0} comes from the uncertainty on the distance rather than from the uncertainty on the dereddened V_0 magnitude. From the work of Flower (1996) we derive a bolometric correction of BC $= -2.12 \pm 0.16$, where the uncertainty comes from the uncertainty on $T_{\rm eff}$. This leads to $M_{\rm bol} = -4.64 \pm 0.38$ and thus to $\log(L/{\rm L}_\odot) = 3.76 \pm 0.15$. Another way to estimate the luminosity is to use the strength of the Hβ Balmer line as measured by the Strömgren β index. We applied the Hβ luminosity calibration of Balona & Shobbrook (1984), and obtained $M_{V_0} = -3.16 \pm 0.40$ and therefore $M_{\rm bol} = -5.28 \pm 0.43$ and $\log(L/{\rm L}_\odot) = 4.01 \pm 0.17$, different from but not incompatible with our value obtained with the *Hipparcos* parallax.

Having two independent estimates for the luminosity, we adopt conservatively the mean value and the union of the error boxes: $\log(L/{\rm L}_\odot) = 3.89 \pm 0.29$. Deriving $\log(L/{\rm L}_\odot)$ from the radius $R = 5.1 \pm 0.8$ R$_\odot$ and the $T_{\rm eff} = 24\,000$ K of our best FASTWIND model mentioned above, leads to exactly the same value. This is not an independent estimate, however, since the radius for this model was computed with the method of Kudritzki (1980) using the *Hipparcos*-based M_{V_0} derived above. It is nevertheless reassuring that the values are at least consistent. The position of ν Eri in the HR diagram with the previously derived $T_{\rm eff}$ and $\log(L/{\rm L}_\odot)$ estimates, is shown in Fig. 4.

4 MODE IDENTIFICATION

We used the well-known method of photometric amplitude ratio fitting to determine the degree ℓ of each mode (see e.g. Cugier, Dziembowski & Pamyatnykh 1994; Balona & Evers 1999). The observational amplitude ratios (normalized with respect to the *u* filter) were computed from Table 1 for the nine independent frequencies. To compute the theoretical amplitude ratios, we used the Liège stellar evolution code CLES and the non-adiabatic pulsation code MAD (Dupret 2001) to compute the required non-adiabatic parameters, together with Kurucz (1994) atmosphere models. First we computed a series of models in the error box determined in Section 3. From each of these models we then extracted all modes with $0 \leqslant \ell \leqslant 4$ in the frequency range [5.5, 8] d^{-1}, except for the low-frequency mode ν_{10} for which we used the frequency range [0.3, 0.55] d^{-1}. For each of these modes, we computed the photometric amplitude ratios, and finally we took the average of these ratios and compared them with the observational ratios. To have an idea about the uncertainty of the theoretical amplitude ratios, we also computed the rms scatter, which allows us to define a minimal uncertainty region. The comparison between the theoretical and observational photometric amplitude ratios is shown in Fig. 5. We systematically omitted the theoretical $\ell = 3$ amplitude ratios as their peculiar wavelength dependence is easily recognized but not seen in the data. In addition, for $\ell = 3$ modes one expects very low light-curve amplitudes due to a considerable surface cancellation effect. From Fig. 5 we see that

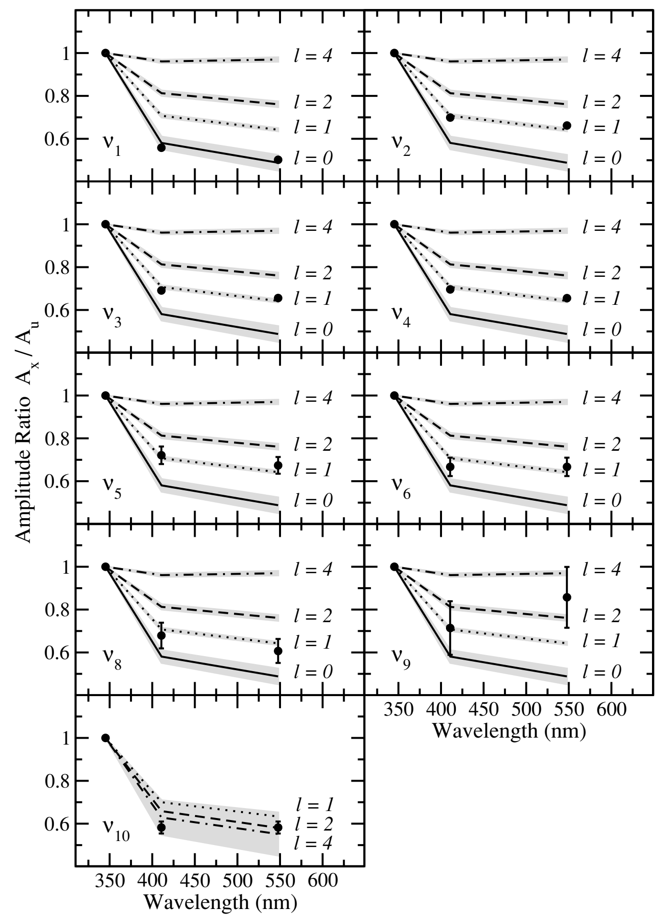

Figure 5. Observed (full circles with error bars) and theoretical *uvy* amplitude ratios (lines) for ν Eri. All amplitudes are normalized with respect to the *u* filter. Full lines are radial modes, dotted lines are $\ell = 1$ modes, dashed lines are $\ell = 2$ modes and dashed-dotted lines are $\ell = 4$ modes. The grey regions are the minimal uncertainty regions for the theoretical amplitude ratios, computed with the rms scatter of amplitude ratios of the different models in the error box in the HR diagram. The frequency identifications are the same as in Table 1.

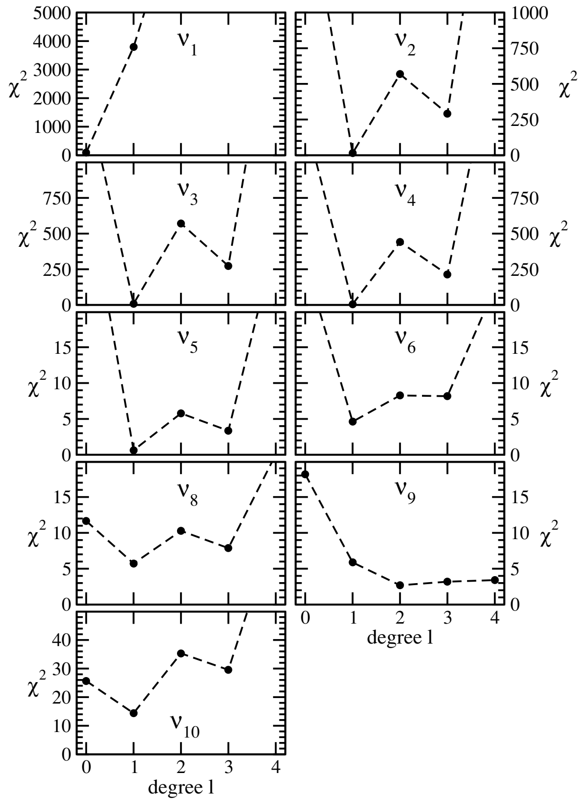

Figure 6. Plots of χ^2 as a function of the spherical degree ℓ for the model that best fits the observed photometric amplitude ratios and phase differences. This model has parameters $M = 9\ \mathrm{M}_\odot$, $Z = 0.016$ and $T_{\mathrm{eff}} = 22\,500$ K. For each mode observed in the photometric time series of Handler et al. (2004), the χ^2 value is shown as a function of the degree ℓ. The frequency identifications are the same as in Table 1.

ν_1 is clearly a radial mode and that ν_2, ν_3 and ν_4 are components of an $\ell = 1$ triplet. Also ν_5 is clearly an $\ell = 1$ mode. For ν_6 and ν_8 there might be some doubt between $\ell = 0$ and $\ell = 1$, but from theoretical frequency spectra we know that no radial mode can be as close to the radial mode ν_1 as ν_6 and ν_8 are. This implies that ν_6 and ν_8 are also $\ell = 1$ modes. No clear photometric mode identification is possible for ν_9, as its amplitude is too small. In the panel of the low-frequency mode ν_{10}, it can be seen that the rms scatter of the theoretical amplitude ratios is rather large. Moreover, this rms scatter is larger for higher degree ℓ. The uncertainty regions of $\ell = 1$ and $\ell = 2$ are still disjunct, but the uncertainty region of $\ell = 4$ overlaps both of them. The comparison with the observational amplitude ratios points towards an $\ell = 2$ or an $\ell = 4$ mode, although an $\ell = 1$ mode cannot be firmly excluded.

The photometric mode identification method outlined above features the characterization of an 'average' radial mode, an 'average' dipole mode, etc. This was done by computing the mean and the rms of theoretical amplitude ratios of all relevant modes of all stellar models in the error box in the HR diagram. We will now adopt a complementary approach where we search for the stellar model that fits best the photometric observations (in the χ^2 sense) but without trying to fit the observed frequency values themselves. Besides the photometric amplitude ratios A_v/A_u and A_y/A_u, we also fitted the photometric phase differences $\varphi_v - \varphi_u$ and $\varphi_y - \varphi_u$, and computed the χ^2 in the usual way. Given the errors on the photometric amplitudes and phases, the errors on the amplitude ratios and phase differences were computed assuming that measurements in different passbands are independent. This time the stellar models in the error box in the HR diagram were computed with the Warsaw–New Jersey stellar evolution code, and the non-adiabatic eigenfunctions with the pulsation code of Dziembowski (1977). We also allowed for variations in metallicity ($\in [0.015, 0.023]$) but we still neglected the effects of overshooting. The diagrams with χ^2 as a function of the degree ℓ for the best model are shown in Fig. 6. This model has a mass $M = 9\ \mathrm{M}_\odot$, a metallicity $Z = 0.016$ and an effective temperature $T_{\mathrm{eff}} = 22\,500$ K. It is reassuring to find essentially the same results as before. The main mode ν_1 is clearly a radial mode and modes ν_2 up to ν_8 and ν_{10} are best explained with dipole modes. The frequency ν_9 seems, however, to be best fitted with a degree ℓ higher than one.

One of the important differences between the two photometric mode identifications we presented is the selection of the modes. Fig. 5 is based on both stable and unstable modes, while Fig. 6 is based on unstable modes only (except for ν_{10}, for which we could only find stable modes). Stable modes are usually disregarded for a photometric mode identification, but for ν Eri we make an exception. As shown by Pamyatnykh et al. (2004) and by Ausseloos et al. (in preparation), the observed frequency values strangely cannot be explained with standard stellar models if one only considers unstable modes. We therefore included also stable modes for Fig. 5, but disregarded them for Fig. 6 to see to what extent the results would be altered. The important conclusion is that both approaches lead to the same mode identification.

For the modes $\nu_1, \ldots, \nu_4$ and the modes ν_6 and ν_8, we can be fairly confident about their degree ℓ as well as their azimuthal order m. Of the remaining frequencies for which we still need information, only ν_7 is also present in the spectroscopic data. To gain extra information about this frequency, and about the frequencies 5.51 and 5.89 d^{-1}, we attempted a spectroscopic mode identification by modelling the moments, the amplitude and phase distributions, and the line profiles. For all three techniques we encountered the problem of the enormous amount of computing power required to model reliably and usefully such a large spectroscopic time series containing so many frequencies. Modelling subsets of this time series did not allow the interesting frequencies to be resolved. One of the difficulties is that it is not possible to identify and 'remove' the modes one by one, as the effects of the different modes on the line profiles are coupled, much in contrast with the case of the photometric time series. We actually tried the one-by-one procedure with line profile fitting by binning the line profiles with the frequency with the highest amplitude, then identifying the mode by fitting a one-mode model, and consequently removing the mode by fitting a sinusoid to the line intensity variations at each wavelength and subtracting it from the data. We checked this procedure for the four main modes, for which we already know the wavenumbers, but the results were rather discouraging. To fit the amplitude and phase distributions, we worked initially with a model with four modes. We used both a simple but fast line profile model with a Gaussian intrinsic profile (Schrijvers & Telting 1999), as well as PULSTAR (De Ridder et al. 2002), which is slower to compute but uses more advanced Kurucz intensity spectra. We did not succeed, however, in finding a reliable fit to the observed amplitude and phase distributions. For ν_2, ν_3 and ν_4 this is mainly due to the fact that all three modes have a phase distribution with a negative slope (cf. Fig. 2), which would indicate that they are all prograde, which should not be the case for a dipole triplet. From a spectroscopic point of view, the frequencies around ν_4 are more likely explained by three peaks of an $\ell = 2$ quintuplet with azimuthal orders $m = 0$, $m = -1$ and $m = -2$. This suspicion was actually already raised by Smith

(1983), also from a spectroscopic investigation. In this sense there is a clear but unexplained discrepancy between the spectroscopic and the photometric mode identification for the frequencies ν_2, ν_3 and ν_4.

5 SUMMARY AND CONCLUSIONS

We can now summarize the observational results of the 2003 multisite and multitechnique campaign of the β Cephei star ν Eridani.

According to the photometric mode identification, we find in the radial velocity time series a high-amplitude radial mode ν_1, a dipole triplet ν_2, ν_3, ν_4, two close dipole modes ν_6 and ν_8 likely to be part of the same triplet, and yet another dipole mode ν_5 of which we are, however, uncertain whether it is a zonal or a sectoral mode. The degree ℓ of the frequency ν_7 could not be determined, and it is therefore uncertain whether it belongs to the same dipole triplet as ν_6 and ν_8. In addition to the frequencies just mentioned, two other significant frequency peaks (ν_9 and ν_{10}) are found in all three observed Strömgren passbands, although we were unable to determine uniquely their degrees ℓ. Concerning the low-frequency peak ν_{10}, we explicitly checked again if we could find it in the improved radial velocity time series, but with no positive result. This may cast some doubt upon whether this frequency is indeed a genuine eigenfrequency. The reasons why we included it nevertheless in Table 1 were given in Paper Ia and can be summarized as follows. First, this frequency appears in all three photometric filters. Secondly, its amplitude is far above the noise level. In fact, we find at least three eigenfrequencies with lower amplitudes in the photometry. Thirdly, in Paper Ia it is explicitly checked that the variability at this frequency is not due to the comparison stars μ Eri or ξ Eri. Fourthly, in the same paper it was also checked that this frequency is not a (reasonable) combination frequency. Finally, fifthly, the frequency is also detectable in the data sets of the individual observatories.

For the rotationally split multiplet around 5.63 d^{-1} we obtained the following frequency differences: $\nu_4 - \nu_3 = 0.017\,18(9)$ d^{-1}, $\nu_2 - \nu_4 = 0.016\,69(7)$ d^{-1}. For the frequencies around 6.24 d^{-1} we obtained the differences: $\nu_8 - \nu_6 = 0.017\,1(5)$ d^{-1} and $\nu_6 - \nu_7 = 0.021(3)$ d^{-1}. The uncertainty on the last-mentioned decimal place is given in parentheses, and was estimated from the scatter between the different values obtained from the different spectral lines and the different Strömgren passbands.

The list of combination frequencies found in the photometric time series is not the same list of combination frequencies found in the improved radial velocity time series, which is in turn not exactly the same as the list of combination frequencies found in the radial velocity time series of Paper Ib, although there is a great deal of overlap in all three lists. The common property of all combination frequencies is, however, that they never include a *difference* of two independent frequencies.

In the line profiles, a few other candidate frequencies were found in the β Cephei frequency range. They are not certain enough to be included in a seismic modelling of ν Eri but might be used to gain extra confidence in a model if this model turns out to be compatible with these candidate frequencies.

ACKNOWLEDGMENTS

KL and CA are much indebted to J. Puls for introducing them to the use of the latest version of FASTWIND and for hospitality during their visits to Munich. We thank R. Scuflaire for the use of the stellar evolution code CLES, and M.-A. Dupret for the use of the non-adiabatic pulsation code MAD. We thank W. Dziembowski and A. Pamyatnykh for the use of the Warsaw–New Jersey stellar evolution and pulsation codes. We thank M. Ausseloos for a careful reading of the manuscript. JDR and MB are Postdoctoral Fellows of the Fund for Scientific Research, Flanders. GH's work is supported by the Austrian Fonds zur Förderung der wissenschaftlichen Forschung under grant R12-N02. This study was made possible thanks to the support of the K. U. Leuven Research Fund under grant number GOA/2003/04.

REFERENCES

Aerts C., 1996, A&A, 314, 115
Aerts C., de Pauw M., Waelkens C., 1992, A&A, 266, 294
Aerts C., De Cat P., Cuypers J., Becker S. R., Mathias P., De Mey K., Gillet D., Waelkens C., 1998, A&A, 329, 137
Aerts C. et al., 2004, MNRAS, 347, 463 (Paper Ib)
Balona L. A., Evers E. A., 1999, MNRAS, 302, 349
Balona L. A., Shobbrook R. R., 1984, MNRAS, 211, 375
Cugier H., Dziembowski W. A., Pamyatnykh A. A., 1994, A&A, 291, 143
Cuypers J., Aerts C., Buzasi D., Catanzarite J., Conrow T., Laher R., 2002, A&A, 392, 599
De Ridder J., Dupret M.-A., Neuforge C., Aerts C., 2002, A&A, 385, 572
Dupret M.-A., 2001, A&A, 366, 166
Dziembowski W., 1977, Acta Astron., 27, 203
Fitzpatrick E. L., 1999, PASP, 111, 63
Flower P. J., 1996, ApJ, 469, 355
Glushneva I. N., Kharitonov A. V., Kniazeva L. N., Shenavrin V. I., 1992, A&AS, 92, 1
Handler G., Shobbrook R. R., Jerzykiewicz M. et al., 2004, MNRAS, 347, 454 (Paper Ia)
Hauck B., Mermilliod M., 1998, A&AS, 129, 431
Herrero A., Puls J., Najarro F., 2002, A&A, 396, 949
Jamar C., Macau-Hercot D., Monfils A., Thompson G. I., Houziaux L., Wilson R., 1976, Ultraviolet Bright-Star Spectrophotometric Catalogue. A Compilation of Absolute Spectrophotometric Data Obtained With the Sky Survey Telescope (S2/68) on the European Astronomical Satellite TD-1. ESA SR-27, Paris
Kilian J., 1992, A&A, 262, 171
Kubat J., Puls J., Pauldrach A. W. A., 1999, A&A, 341, 587
Kudritzki R.-P., 1980, A&A, 85, 174
Künzli M., North P., Kurucz R. L., Nicolet B., 1997, A&AS, 122, 51
Kurucz R. L., 1994, Solar Abundance Atmospheres, CD-ROM No 19. Smithsonian Astrophysical Observatory, Cambridge, MA
Leone F., Lanzafame A. C., 1998, A&A, 330, 306
Mermilliod J.-C., Mermilliod M., Hauck B., 1997, A&AS, 124, 349
Napiwotzki R., Schönberner D., Wenske V., 1993, A&A, 268, 653
Pamyatnykh A. A., 1999, Acta Astron., 49, 119
Pamyatnykh A. A., Handler G., Dziembowski W., 2004, MNRAS, in press
Press W. H., Teukolsky S. A., Vetterling W. T., Flannery B. P., 1992, Numerical Recipes in C: The Art of Scientific Computing, 2nd edn. Cambridge Univ. Press, Cambridge
Roberts D. H., Lehar J., Dreher J. W., 1987, AJ, 93, 968
Sandage A., 1972, ApJ, 178, 1
Santolaya-Rey A. E., Puls J., Herrero A., 1997, A&A, 323, 488
Schrijvers C., Telting J. H., 1999, A&A, 342, 453
Schrijvers C., Telting J. H., Aerts C., 2004, A&A, 416, 1069
Smith M. A., 1983, ApJ, 265, 338
Strömgren B., 1966, ARA&A, 4, 433
Vuille F., 2000, MNRAS, 313, 179
Zboril M., North P., 1999, A&A, 345, 244

This paper has been typeset from a TEX/LATEX file prepared by the author.

5.4.4 Asteroseismology of the β Cephei star ν Eridani – IV. The 2003–2004 multisite photometric campaign and the combined 2002–2004 data

Original paper:

M. Jerzykiewicz, **G. Handler,** R. R. Shobbrook, A. Pigulski, R. Medupe, T. Mokgwetsi, P. Tlhagwane, E. Rodriguez, 2005, MNRAS 360, 619

Mon. Not. R. Astron. Soc. **360,** 619–630 (2005) doi:10.1111/j.1365-2966.2005.09088.x

Asteroseismology of the β Cephei star ν Eridani – IV. The 2003–2004 multisite photometric campaign and the combined 2002–2004 data

M. Jerzykiewicz,[1⋆] G. Handler,[2] R. R. Shobbrook,[3]† A. Pigulski,[1] R. Medupe,[4,5] T. Mokgwetsi,[4] P. Tlhagwane[4] and E. Rodríguez[6]

[1] *Wroclaw University Observatory, ul. Kopernika 11, 51-622 Wroclaw, Poland*
[2] *Institut für Astronomie, Universität Wien, Türkenschanzstrasse 17, A-1180 Wien, Austria*
[3] *Research School of Astronomy and Astrophysics, Australian National University, Canberra, ACT, Australia*
[4] *Theoretical Astrophysics Programme, North West University, Private Bag X2046, Mmabatho 2735, South Africa*
[5] *South African Astronomical Observatory, PO Box 9, Observatory 7935, South Africa*
[6] *Instituto de Astrofísica de Andalucia, CSIC, Apdo. 3004, 18080 Granada, Spain*

Accepted 2005 April 6. Received 2005 April 6; in original form 2005 February 2

ABSTRACT

We report on the second multisite photometric campaign devoted to ν Eridani (ν Eri). The campaign, carried out from 2003 September 11 to 2004 February 16, was very nearly a replica of the first campaign, 2002–2003: the five telescopes and photometers we used were the same as those in the first campaign, the comparison stars and observing procedure were identical, and the numbers and time baselines of the data were comparable.

For ν Eri, analysis of the new data adds four independent frequencies to the nine derived previously from the 2002–2003 data: three in the range 7.20–7.93 d^{-1} and a low one, equal to 0.614 d^{-1}. Combining the new and the old data results in two further independent frequencies, equal to 6.7322 and 6.2236 d^{-1}. Altogether, the oscillation spectrum is shown to consist of 12 high and two low frequencies. The latter have u amplitudes about twice as large as the v and y amplitudes, a signature of high radial-order g modes. Thus, we confirm the suggestion, put forward on the basis of the data of the first campaign, that ν Eri is both a β Cephei and a slowly pulsating B (SPB) star.

Nine of the 12 high frequencies form three triplets, of which two are new. The triplets represent rotationally split $\ell = 1$ modes, although in case of the smallest-amplitude one this may be questioned. Mean separations and asymmetries of the triplets are derived with accuracy sufficient for meaningful comparison with models.

The first comparison star, μ Eri, is shown to be an SPB variable with an oscillation spectrum consisting of six frequencies, three of which are equidistant in period. The star is also found to be an eclipsing variable. The eclipse is a transit, probably total, the secondary is fainter than the primary by several magnitudes, and the system is widely detached.

The second comparison star, ξ Eri, is confirmed to be a δ Scuti variable. To the frequency of 10.8742 d^{-1} seen already in the data of the first campaign, another, equal to 17.2524 d^{-1}, is added.

Key words: stars: early-type – stars: individual: ν Eridani – stars: individual: μ Eridani – stars: individual: ξ Eridani – stars: oscillations – binaries: eclipsing.

1 INTRODUCTION

The first multisite photometric and spectrographic campaign devoted to the β Cephei star ν Eridani (ν Eri) was carried out between 2002 October and 2003 February. More than 600 h of differential $uvyV$ photometry on 148 nights and more than 2000 high-resolution spectra were obtained. A frequency analysis of the photometric data was reported by Handler et al. (2004, hereafter Paper I), while the spectrographic time series and their analysis were presented by Aerts et al. (2004, hereafter Paper II). An extended frequency analysis and mode identification was provided by De Ridder et al. (2004, hereafter Paper III).

⋆E-mail: mjerz@astro.uni.wroc.pl
†Visiting Fellow.

Seismic modelling of the oscillation spectrum of ν Eri has been undertaken by Pamyatnykh, Handler & Dziembowski (2004) and Ausseloos et al. (2004).

In Paper I, the light variation of ν Eri was shown to consist of 23 sinusoidal terms. These included eight independent terms with frequencies, $f_i, i = 1 \ldots 8$, spanning the range from 5.6 to 7.9 d^{-1}, 14 high-frequency combination terms, and a term with the low frequency $f_A = 0.432\ \mathrm{d}^{-1}$.

The four highest-amplitude terms, discovered long ago by Saito (1976), consist of a singlet with frequency $f_1 = 5.763\ \mathrm{d}^{-1}$, and a triplet very nearly equidistant in frequency ($f_3 = 5.620$, $f_4 = 5.637$ and $f_2 = 5.654\ \mathrm{d}^{-1}$). Before the campaign it was known that the singlet was a radial mode (Cugier, Dziembowski & Pamyatnykh 1994), and it was surmised that it was the fundamental (Dziembowski & Jerzykiewicz 2003), but the true nature of the triplet was unclear. From multicolour photometry, Heynderickx, Waelkens & Smeyers (1994) derived $\ell = 1$ for f_4, and suggested that the triplet was a rotationally split dipole mode. This was challenged by Aerts, Waelkens & de Pauw (1994), who – from an analysis of line-profile variations – identified the f_2 term with an axisymmetric mode. However, both results are questionable because in neither case the triplet had been resolved. The matter was settled in Paper III: the wavelength dependence of the *uvy* amplitudes of the triplet terms implies $\ell = 1$ for all of them. Pamyatnykh et al. (2004) showed then that the triplet was a g_1 mode.

A frequency triplet $f_- < f_0 < f_+$ can be characterized by its mean separation

$$S = 0.5(f_+ - f_-), \tag{1}$$

and asymmetry

$$A = f_- + f_+ - 2f_0. \tag{2}$$

In the case of a rotationally split triplet, S is determined by the angular rotation rate of the star, Ω, while A is sensitive to effects of higher order in Ω, as well as to the effects of a magnetic field. If these effects are negligible, $A = 0$.

For the $i = 3, 4, 2$ triplet, both parameters were derived before the campaign from archival data by Dziembowski & Jerzykiewicz (2003). The value of asymmetry they obtained, $A = (-7.1 \pm 0.3) \times 10^{-4}\ \mathrm{d}^{-1}$, was unexpectedly large for the small rotation rate implied by the triplet's $S = 0.0168\ \mathrm{d}^{-1}$. Dziembowski & Jerzykiewicz (2003) showed that this problem may be solved by postulating the existence of a 5–10 kG magnetic field in the outer envelope of the star. From the campaign data (see Paper III), we obtain $A = (-4.9 \pm 1.1) \times 10^{-4}\ \mathrm{d}^{-1}$, a value which is not in serious conflict with the observed S. Unfortunately, the large standard deviation of this result makes it useless. A longer time baseline than that of the 2002–2003 campaign would be needed to obtain a more reliable value of A and thus to decide whether invoking a magnetic field was necessary. This was one motivation for undertaking the sequel campaign.

In Paper III, the spherical harmonic degree of the $i = 5$, 6 and 7 terms was found to be $\ell = 1$, but an attempt to derive ℓ for the low-frequency $i = A$ term (referred to as the ν_{10} term in that paper) was unsuccessful because of its small *uvy* amplitudes and the poor resolution of diagnostic diagrams at low frequencies. Pamyatnykh et al. (2004) showed that the $i = 5$ term is a p_2 mode, while the $i = 6$ one is a p_1 mode. Moreover, they suggested that the low-frequency term is an $\ell = 1$, $m = -1$, g_{16} mode.

According to Pamyatnykh et al. (2004), only the $i = 1$, 2, 3 and 4 modes (i.e. the radial fundamental mode and the $\ell = 1$, g_1 triplet) are unstable in standard models. Modes with $f > 6\ \mathrm{d}^{-1}$ (i.e. the $i = 5$, 6 and 7 modes) and the low-frequency mode are stable. Pamyatnykh et al. (2004) demonstrate, however, that a fourfold overabundance of Fe in the driving zone would account for excitation of the high-frequency modes, and would make the low-frequency mode marginally unstable.

It has been noted in Paper I that if the low-frequency term were indeed a high-order g mode, ν Eri would be both a β Cephei variable and a slowly pulsating B (SPB) star. Unfortunately, f_A differs from the sixth-order combination frequency $3f_1 - 3f_3$ by less than 0.003 d^{-1}. This number is much larger than the formal error of f_A, but is smaller than half the frequency resolution of the campaign data. Thus, the possibility that f_A is the combination frequency – although rather unlikely – cannot be rejected. Again, a longer time baseline would help to settle the issue.

In addition to extending the time baseline, the sequel campaign was expected to double the number of data points, and thus lower the detection threshold, so that modes having amplitudes too low to be seen in the 2002–2003 frequency spectra could be discovered from the combined data.

Both comparison stars used in the 2002–2003 photometric observations turned out to be variable. For the first, μ Eri (HD 30211, B5 IV, $V = 4.00$), the analysis carried out in Paper I revealed a dominant frequency $f'_1 = 0.6164\ \mathrm{d}^{-1}$. (From now on, we use a prime to denote frequencies of μ Eri.) Pre-whitening with this frequency resulted in an amplitude spectrum with a very strong $1/f$ component, indicating a complex variation. Because the star is a spectroscopic binary with an orbital period $P_{\mathrm{orb}} = 7.35890$ d (Hill 1969), tests have been made to detect a non-sinusoidal signal with this period. Unfortunately, they were inconclusive.

Taking into account the star's position in the Hertzsprung–Russell diagram, the frequency f'_1 of the dominant variation, and the fact that the u amplitude was about a factor of 2 greater than the v and y amplitudes, it was concluded in Paper I that μ Eri is probably an SPB star. However, it was also noted that instead of pulsation, a rotational modulation could be the cause of the dominant variation.

In Paper I, the frequency analysis of detrended differential magnitudes of μ Eri revealed a small-amplitude variation with a frequency $f_x = 10.873\ \mathrm{d}^{-1}$. It was suggested that the second comparison star, ξ Eri (HD 27861, A2 V, $V = 5.17$), may be responsible.

The present paper reports the sequel photometric campaign, carried out from 2003 September 11 to 2004 February 16, and an analysis of the data of both campaigns. The 2003–2004 observations and reductions are described in Section 2. Section 3 contains an account of the frequency analysis of the new data and a comparison of the results with those of Paper I. Low frequencies in the variation of μ Eri and ν Eri from the *uvy* data of the first campaign are re-examined in Section 4. Section 5 is devoted to frequency analysis of the combined, 2002–2004 data. Finally, Section 6 provides a summary with an emphasis on clues for asteroseismology of the three stars, ν Eri, μ Eri and ξ Eri.

2 OBSERVATIONS AND REDUCTIONS

The observations were carried out with five telescopes on four continents. An observing log is presented in Table 1. Comparison of this table with table 1 of Paper I shows that the new data are almost as extensive as the old data. However, the 2003–2004 y data are less numerous than the v and u data (see below). The time baselines of the 2002–2003 and 2003–2004 sets are very nearly the same; they amount to 157.9 and 158.5 d for the old and new data, respectively.

The five telescopes and photometers were the same as those in the 2002–2003 campaign. Thus, single-channel photoelectric photometers were used at all sites but Sierra Nevada Observatory (OSN),

Table 1. Log of the photometric measurements of ν Eri in 2003–2004. Observatories are listed in the order of their geographic longitude.

Observatory	Longitude	Latitude	Telescope	Amount of data		Observer(s)
				Nights	h	
Sierra Nevada Observatory	−3° 23′	+37° 04′	0.9-m	4	10.64	ER
Fairborn Observatory	−110° 42′	+31° 23′	0.75-m APT	51	211.09	–
Lowell Observatory	−111° 40′	+35° 12′	0.5-m	25	87.10	MJ
Siding Spring Observatory	+149° 04′	−31° 16′	0.6-m	26	79.77	RRS
South African Astronomical Observatory	+20° 49′	−32° 22′	0.5-m	17	92.13	AP
South African Astronomical Observatory	+20° 49′	−32° 22′	0.5-m	19	48.52	RM, TM, PT
Total				142	529.25	

where a simultaneous *uvby* photometer was used. At OSN, the observations were obtained with all four Strömgren filters, at Fairborn, Lowell and Siding Spring, with u, v and y. At the South African Astronomical Observatory (SAAO), the y filter used in the 2002–2003 campaign had deteriorated to such a degree that it had to be discarded. Because no replacement was available, the data were taken with two filters, Strömgren u and v, except that on his first two nights AP used Johnson filters B and V.

The comparison stars and observing procedures were the same as in the first campaign.

The reductions, carried out separately for each of the three wavelength bands, u, v, and y or V, consisted of: (i) computing heliocentric JD numbers for the mean epochs of observations; (ii) computing the airmass for each observation; (iii) correcting instrumental magnitudes of ν Eri, μ Eri and ξ Eri for atmospheric extinction with first-order extinction coefficients derived from the instrumental magnitudes of ξ Eri by means of Bouguer plots; (iv) forming differential magnitudes 'ν Eri – ξ Eri' and 'μ Eri – ξ Eri'; (v) setting the mean light levels of the differential magnitudes from different telescope–filter combinations to the same values. In step (iii), second-order extinction corrections were not applied because no colour-dependent extinction effects could be detected in the uncorrected differential magnitudes (but see the last paragraph of Section 3.1). In step (iv), the magnitudes of ξ Eri were interpolated on the epoch of observation of ν Eri or μ Eri. In step (v), the mean light levels for each telescope–filter combination were derived using residuals from least-squares solutions with the four highest-amplitude terms (see Section 1).

3 FREQUENCY ANALYSIS OF THE NEW DATA

The analysis was carried out in essentially the same way as in Paper I; that is, frequencies were identified from periodograms, one at a time. Before each run, the data were pre-whitened with all frequencies found in previous runs. After several runs, the frequencies were refined by means of a non-linear least-squares fit using the values of independent frequencies read off the periodograms as starting values. The frequencies of the combination terms were computed from the independent frequencies. Thus, the unknowns in the normal equations were the corrections to the independent frequencies, to the mean magnitude, $\langle \Delta m \rangle$, and to the amplitudes, A_i, and phases, ϕ_i, appearing in the following expression:

$$\Delta m = \langle \Delta m \rangle + \sum_{i=1}^{N} A_i \sin[2\pi f_i (t - t_0) + \phi_i]. \quad (3)$$

Here, Δm is the differential magnitude in u, v or yV, N is the number of all frequencies, f_i, the combination terms included, and t_0 is an arbitrary initial epoch.

The difference with respect to the 2002–2003 analysis consisted of using different programs: the PERIOD98 package (see Paper I) was replaced with programs that have been in use by MJ since 1975 (see, for example, Jerzykiewicz 1978). Thus, by 'periodogram' we now mean a power spectrum, and not an amplitude spectrum as in Paper I; by 'power' we mean $1 - \sigma^2(f)/\sigma^2$, where $\sigma^2(f)$ is the variance of a least-squares fit of a sine curve of frequency f to the data, and σ^2 is the variance of the same data. However, for the purpose of estimating signal-to-noise (S/N) ratios (see below) we also computed amplitude spectra.

3.1 The programme star

The data used for analysis were the differential magnitudes 'ν Eri – ξ Eri'. Power spectra were computed independently from the u and v data. No power spectra were computed from the less numerous yV data, but non-linear least-squares solutions were carried out for all three bands, with the starting values of the independent frequencies for y (henceforth we use 'y' instead of 'yV') taken from v. The OSN b and SAAO B data were not used.

In the u and v power spectra, 14 independent and 15 combination frequencies could be clearly seen. They are identified in the first column of Table 2. The numbers in the table are from non-linear least-squares solutions. The values of the independent frequencies and their standard deviations, computed as straight means from the separate solutions for u, v and y, are given in column 2 in the upper half of the table. The combination frequencies, listed in the lower half of the table, were computed from the independent frequencies according to ID in the first column; their standard deviations were computed from the standard deviations of the independent frequencies assuming rms propagation of errors. The amplitudes, A_u, A_v and A_y, with the standard deviations, given in columns 3, 4 and 5, respectively, are from the independent solutions for u, v and y. The last column lists the v amplitude S/N ratio, defined as in Paper I, except that in Paper I the mean noise level was estimated in 5-d^{-1} intervals, while now we adopt 0.1-d^{-1} intervals for frequencies lower than 3 d^{-1}, and 1-d^{-1} intervals for higher frequencies. In all cases, the amplitude spectra of the data pre-whitened with the 29 frequencies of Table 2 were used for estimating the mean noise level.

In Paper I, a peak in the amplitude spectrum was considered to be significant if its S/N ratio exceeded 4 for an independent term or 3.5 for a combination term. As can be seen from Table 2, this condition is met by all terms identified from the 2003–2004 data, except the differential combination term $f_1 - f_4$ for which $S/N = 3.0$. This term may be spurious.

The standard deviations in Table 2 (and in the tables that follow), referred to as 'formal' in the remainder of this subsection and in the first three paragraphs of the next subsection, will be underestimated

Table 2. Frequencies and amplitudes in the differential magnitudes 'ν Eri – ξ Eri' from the 2003–2004 data. Independent frequencies are listed in the upper half of the table. The combination frequencies are listed in the lower half of the table. In both cases the frequencies are ordered according to decreasing v amplitude, A_v. The last column contains the v-amplitude S/N ratio. Frequencies f_x and f_y are due to ξ Eri.

ID	Frequency (d^{-1})	A_u (mmag)	A_v (mmag)	A_y (mmag)	S/N
f_1	5.763256 ± 0.000012	72.3 ± 0.19	40.6 ± 0.14	36.7 ± 0.15	165.0
f_2	5.653897 ± 0.000020	38.6 ± 0.19	27.2 ± 0.14	25.4 ± 0.15	110.6
f_3	5.619979 ± 0.000021	35.5 ± 0.19	25.0 ± 0.14	24.0 ± 0.15	101.6
f_4	5.637215 ± 0.000025	31.0 ± 0.18	21.8 ± 0.13	20.4 ± 0.16	88.6
f_5	7.89859 ± 0.00022	3.7 ± 0.19	2.7 ± 0.14	2.5 ± 0.16	11.0
f_7	6.26225 ± 0.00025	3.1 ± 0.19	2.2 ± 0.14	2.2 ± 0.16	8.8
f_A	0.43257 ± 0.00028	3.2 ± 0.19	2.0 ± 0.14	1.7 ± 0.16	5.0
f_6	6.24468 ± 0.00034	2.3 ± 0.18	1.6 ± 0.13	1.6 ± 0.15	6.4
f_B	0.61411 ± 0.00033	3.4 ± 0.18	1.5 ± 0.13	1.6 ± 0.15	4.3
f_x	10.8743 ± 0.0006	1.2 ± 0.18	1.4 ± 0.13	0.9 ± 0.15	5.7
f_{10}	7.9296 ± 0.0005	1.6 ± 0.19	1.2 ± 0.14	1.2 ± 0.16	5.3
f_9	7.9132 ± 0.0005	1.8 ± 0.18	1.1 ± 0.13	1.3 ± 0.16	4.9
f_8	7.2006 ± 0.0005	1.4 ± 0.18	1.0 ± 0.13	1.1 ± 0.15	4.4
f_y	17.2534 ± 0.0006	1.0 ± 0.19	0.9 ± 0.13	0.9 ± 0.15	4.6
$f_1 + f_2$	11.417153 ± 0.000023	12.3 ± 0.19	8.8 ± 0.14	8.4 ± 0.15	34.0
$f_1 + f_3$	11.383235 ± 0.000024	10.8 ± 0.19	7.6 ± 0.14	7.1 ± 0.15	29.3
$f_1 + f_4$	11.400471 ± 0.000028	9.9 ± 0.19	7.0 ± 0.14	6.6 ± 0.16	27.0
$2f_1$	11.526512 ± 0.000017	4.5 ± 0.18	3.1 ± 0.13	3.1 ± 0.15	12.0
$f_1 + f_2 + f_3$	17.037132 ± 0.000031	3.3 ± 0.18	2.2 ± 0.13	2.0 ± 0.15	11.3
$f_1 - f_2$	0.109359 ± 0.000023	2.7 ± 0.19	1.6 ± 0.14	1.6 ± 0.16	4.4
$2f_1 + f_4$	17.163727 ± 0.000030	1.9 ± 0.18	1.4 ± 0.13	1.3 ± 0.15	7.2
$2f_1 + f_2$	17.180409 ± 0.000026	1.9 ± 0.18	1.4 ± 0.13	1.3 ± 0.15	7.2
$f_2 + f_3$	11.273876 ± 0.000029	2.4 ± 0.19	1.3 ± 0.14	1.1 ± 0.15	5.0
$2f_1 + f_3$	17.146491 ± 0.000027	1.4 ± 0.18	1.2 ± 0.13	0.8 ± 0.15	6.2
$2f_2$	11.307794 ± 0.000028	1.1 ± 0.19	1.1 ± 0.14	0.6 ± 0.16	4.2
$f_1 - f_4$	0.126041 ± 0.000028	1.9 ± 0.18	1.1 ± 0.13	1.2 ± 0.15	3.0
$f_1 + f_3 + f_4$	17.020450 ± 0.000035	1.3 ± 0.18	1.1 ± 0.13	0.9 ± 0.15	5.6
$2f_1 + f_2 + f_3$	22.800388 ± 0.000034	1.3 ± 0.18	1.1 ± 0.13	0.8 ± 0.15	6.1
$f_1 + f_2 - f_3$	5.797174 ± 0.000031	1.5 ± 0.19	0.9 ± 0.14	1.3 ± 0.15	3.7

if the errors of differential magnitudes are correlated in time. For the case at hand (i.e. of fitting a sinusoid to time series data), the problem has been discussed by Schwarzenberg-Czerny (1991) and Montgomery & O'Donoghue (1999). These authors consider the factor, D, by which the formal standard deviations of a frequency, amplitude and phase should be multiplied in order to obtain correct values. (D is the same for frequencies, amplitudes and phases because the ratio of the formal standard deviations of any two of these quantities is determined by error-free numbers such as the epochs of observations and the starting values of the frequencies.) The factor depends on an estimate of the number of consecutive data points which are correlated. Unfortunately, this estimate is not easy to obtain, especially for time series such as ours, consisting of data from many nights and several observatories. We return to this point in Section 3.2.

Fig. 1 shows the power spectra of the u and v differential magnitudes 'ν Eri – ξ Eri' pre-whitened with the 29 frequencies of Table 2. In both panels of the figure, the highest peaks are seen at frequencies lower than about 5 d^{-1}. In the u spectrum (lower panel), the highest peak occurs at 0.314 d^{-1}, while in the v spectrum, the highest peak is at 1.498 d^{-1}. The u amplitude at 0.314 d^{-1} is equal to 2.2 mmag, while the v amplitude at 1.498 d^{-1} is equal to 1.1 mmag. The u- and v-amplitude S/N ratios amount to 2.7 in both cases. We conclude that these frequencies are probably spurious.

For frequencies higher than 5 d^{-1}, the highest peak in the u spectrum (lower panel) occurs at 5.015 d^{-1}. For this peak the u-amplitude S/N ratio is equal to 5.0, so that the significance condition mentioned earlier in this section is satisfied. However, there is no power at 5.015 d^{-1} in the v spectrum (upper panel); the peak closest to 5.015 d^{-1}, at 5.128 d^{-1}, is probably noise because it has S/N equal to 3.2. This, and the fact that 5.015 d^{-1} is very nearly equal to five cycles per sidereal day (sd^{-1}) suggest that the peak is due to colour extinction in the u band, which we neglected (see Section 2).

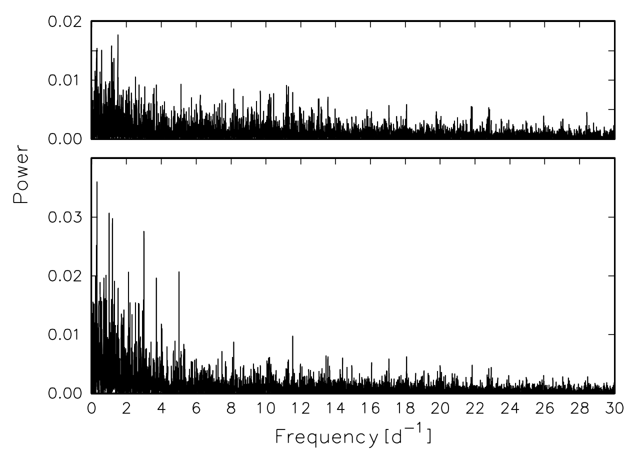

Figure 1. Power spectra of the u (lower panel) and v (upper) differential magnitudes 'ν Eri – ξ Eri' pre-whitened with the 29 frequencies of Table 2.

Indeed, the differential colour-extinction correction contains a term equal to $k'' X \Delta C$, where k'' is the second-order extinction coefficient, X is the airmass and ΔC is the differential colour index. Because of the second factor, X, the term causes a parabola-shaped variation symmetrical around the time of meridian passage. For a single observatory, this will produce a signal with frequency equal to n sd^{-1}, where n is a small whole number equal to the number of sine waves that best fit the variations on successive nights. In our case, this number is apparently equal to 5. For multisite data, phase smearing may occur, tending to wash out the signal. However, our time series is dominated by the data from Fairborn and Lowell, two observatories lying on nearly the same meridian and therefore introducing negligible phase shift. In addition, the greatest common divisor of the longitude differences between Fairborn and Lowell on one hand, and SAAO and Siding Spring on the other is close to 60°, making the 5-sd^{-1} signals from these observatories approximately agree in phase. We conclude that the 5.015-d^{-1} peak in the u spectrum in Fig. 1 is not due to an intrinsic variation of ν Eri.

3.2 Comparison of the 2003–2004 and 2002–2003 results for the programme star

Of the 14 independent terms in Table 2, nine appear in table 2 of Paper I. The differences between the 2003–2004 and 2002–2003 values of their frequencies and amplitudes are listed in Table 3. The standard deviations given in the table were computed from the standard deviations of the 2003–2004 and 2002–2003 least-squares solutions assuming rms propagation of errors. Thus, they are formal in the sense defined in the previous subsection.

We shall now return to the factor D by which the formal standard deviations are underestimated. Let us consider the nine independent frequencies common to 2002–2003 and 2003–2004. As can be seen from Table 3, the moduli of the frequency differences, $|\Delta f|$, are of the same order of magnitude as the formal standard deviations of Δf, $\sigma_{\Delta f}$. In four cases $|\Delta f| < \sigma_{\Delta f}$, in three cases $\sigma_{\Delta f} < |\Delta f| < 2\sigma_{\Delta f}$, and in two cases the differences exceed $2\sigma_{\Delta f}$. Taken at face value, these inequalities would indicate that four or five of the nine frequencies changed from 2002–2003 to 2003–2004 by $1\sigma_{\Delta f}$ or more, while f_3, f_5 and f_8 changed by $2\sigma_{\Delta f}$ or more. However, frequency changes in β Cephei stars have time-scales much longer than 1 yr. For the four first frequencies of ν Eri, this is shown to be the case by Handler et al. (in preparation). Although the existence of long-term variations does not exclude the possibility of year-to-year variations, let us assume that these four frequencies were strictly constant from 2002 to 2004. If the assumption were false, the value of D we derive in the next paragraph will be too large.

For f = const, where f is any of the four frequencies, the modulus of Δf can be thought of as the range of f in a two-element sample of f, the first element chosen from the parent population of f in 2002–2003 and the second element chosen from the same population in 2003–2004. For a normal distribution, an estimate of the standard deviation can be obtained by multiplying the range by a coefficient k, which is a function of the number of elements in the sample, n. For $n = 2$, table 12 of Crow, Davis & Maxfield (1960) reads $k = 0.886$. Multiplying $|\Delta f|$ by this value we obtain an estimate of the standard deviation of f. The latter number divided by the formal standard deviation of f from Table 2 yields the factor we are seeking. The mean value of the factor for the four frequencies turns out to be $D = 2.0$. If we applied the procedure to all nine frequencies, the result would be $D = 1.8$. If we used the formal standard deviations of the 2002–2003 solution, the results would be very nearly the same. Henceforth, we adopt $D = 2$. A standard deviation equal to the formal standard deviation times this factor we refer to as 'corrected', and from now on we drop the adjective 'formal', so that by 'standard deviation' we mean 'formal standard deviation'.

Multiplying the standard deviations of the 2003–2004 amplitudes by two, we find that the ratios of the amplitudes to the corrected standard deviations become approximately equal to the S/N ratios defined in the previous subsection. This is a pleasant surprise, lending support to our value of D. [Using the numbers from Table 2, the reader can verify the approximate equality of S/N and $A_v/(2\sigma_v)$, where σ_v is the standard deviation of A_v. Note that while for low frequencies $A_v/(2\sigma_v)$ is about 30 per cent larger than S/N, the approximate equality improves for high frequencies. This seems to be reasonable in view of the $1/f$ decrease of the noise level in the periodograms.] Additional support for $D = 2$ comes from the fact that a different line of reasoning applied to multisite data similar to ours has led Handler et al. (2000) to the same value.

Let us now return to Table 3. As can be seen from the table, $|\Delta A|$ are largest for f_A, f_6 and f_3 (in this order). Multiplying the standard deviations of ΔA by $D = 2$ we find the following. (i) The amplitude of the low-frequency term has decreased by $4.3\sigma_c$ in u, $3.0\sigma_c$ in v and $3.8\sigma_c$ in y, where by σ_c we denote the corrected standard deviation of ΔA. (ii) The amplitude of the $i = 6$ term has decreased by 3.0, 2.2 and $2.5\sigma_c$ in u, v and y, respectively. (iii) The amplitude of the $i = 3$ term has increased by 1.7, 2.5 and $3.2\sigma_c$ in u, v and y, respectively. For the remaining six terms, $|\Delta A| \leqslant 2.2\sigma_c$. We conclude that the decrease of the amplitude of the $i = A$ term is real, that of the $i = 6$ term may be real, while the amplitude increase of the $i = 3$ term is probably spurious. In the remaining cases, there is little or no evidence for amplitude variation.

Table 3. A comparison of the frequencies and amplitudes of the nine independent terms common to table 2 of Paper I and Table 2 of the present paper. The differences, Δ, are in the sense '2003–2004 minus 2002–2003.'

ID	Δf (d^{-1})	ΔA_u (mmag)	ΔA_v (mmag)	ΔA_y (mmag)
f_1	−0.000014 ± 0.000017	−1.2 ± 0.27	−0.4 ± 0.20	−0.2 ± 0.20
f_2	−0.000033 ± 0.000028	0.7 ± 0.27	0.8 ± 0.20	0.3 ± 0.20
f_3	−0.000081 ± 0.000030	0.9 ± 0.27	1.0 ± 0.20	1.3 ± 0.20
f_4	0.000055 ± 0.000035	−1.2 ± 0.27	−0.6 ± 0.20	−0.6 ± 0.20
f_5	0.00079 ± 0.00032	−0.6 ± 0.27	−0.4 ± 0.20	−0.5 ± 0.20
f_6	0.00060 ± 0.00048	−1.6 ± 0.27	−0.9 ± 0.20	−1.0 ± 0.20
f_7	0.00020 ± 0.00035	0.2 ± 0.27	0.3 ± 0.20	0.4 ± 0.20
f_8	0.00066 ± 0.00071	0.1 ± 0.27	0.1 ± 0.20	0.0 ± 0.20
f_A	0.00039 ± 0.00040	−2.3 ± 0.27	−1.2 ± 0.20	−1.5 ± 0.20

The five independent frequencies, which appear in the present Table 2 but not in table 2 of Paper I, are (in the order of decreasing v amplitude) f_B, f_x, f_{10}, f_9 and f_y. The low frequency f_B is very nearly equal to the frequency f_{21}, one of three low frequencies derived in Paper II from the radial velocities of ν Eri. However, in our 2003–2004 power spectra we did not see the other two low frequencies of Paper II. Frequency f_9 was listed in table 3 of Paper I as that of one of several 'possible further signals'. Frequencies f_{10} and f_y are new.

Frequency f_x was found in Paper I and tentatively ascribed to ξ Eri (see Section 1). We demonstrate in Section 3.3 that this frequency and f_y, the smallest-amplitude independent frequency in Table 2, are both due to ξ Eri.

In addition to nine independent terms, table 2 of Paper I lists 14 combination terms. In the 2003–2004 power spectra, we did not see three of them: $f_1 + f_5$, $f_1 + f_2 + f_4$ and $f_1 + 2f_2$. On the other hand, we detected differential combination terms, $f_1 - f_2$, $f_1 + f_2 - f_3$ and $f_1 - f_4$, which were not found in Paper I.

3.3 Comparison stars

The data used for analysis were the differential magnitudes 'μ Eri – ξ Eri'. Power spectra were computed independently from the u and v data. No power spectra were computed from the less numerous y data.

In the first-run u and v power spectra, the highest peaks occurred at the same frequency of 0.615 d^{-1}. This frequency is close to f'_1, the only one found for μ Eri in Paper I (see Section 1). The second and third runs yielded frequencies of 0.272 and 0.815 d^{-1}, again the same for u and v. The first of these numbers is close to twice the orbital frequency of μ Eri, $f'_{\rm orb} = 0.13589$ d^{-1}, while the second is close to six times this frequency. The low-frequency part of the power spectrum of the v differential magnitudes 'μ Eri – ξ Eri' pre-whitened with 0.615 d^{-1}, $2f'_{\rm orb}$ and $6f'_{\rm orb}$ is shown in Fig. 2. In this figure, the arrows indicate peaks at frequencies equal to $f'_{\rm orb}$, $3f'_{\rm orb}$, $4f'_{\rm orb}$, $5f'_{\rm orb}$ and $8f'_{\rm orb}$. Peaks at these frequencies are also present in the u power spectrum.

The occurrence of so many harmonics of the orbital frequency implies that the data contain a strongly non-sinusoidal signal of this frequency. The first possibility that comes to mind is an eclipse. Fig. 3, in which the differential magnitudes 'μ Eri – ξ Eri' pre-whitened with 0.615 d^{-1} are plotted as a function of orbital phase, shows that μ Eri is indeed an eclipsing variable.

Returning to frequency analysis of the comparison-star data, we rejected observations falling in the orbital phase range from 0.4 to 0.54 (i.e. the data affected by the eclipse) and recomputed the power spectra. In the first-run u and v power spectra, the highest peaks occurred at the same frequency of 0.615 d^{-1} as before. The highest peaks in the second and third u runs were at 0.701 and 0.813 d^{-1}, respectively, while the second and third v runs yielded 1.206 and 0.701 d^{-1}.

In the next step, we carried out non-linear least-squares solutions separately for the u, v and y data. As starting values, we used all four frequencies found above, i.e. 0.615, 0.701, 0.8132 and 1.206 d^{-1}. The results are presented in the first four lines of Table 4. The fifth frequency, f'_5, will be explained shortly. The frequencies and their standard deviations, listed in column 2, were computed as straight means from the separate solutions for the three bands. The amplitudes, A_u, A_v and A_y, and their standard deviations, are given in columns 4, 5 and 6. The v-amplitude S/N ratio, computed in the same way as in Section 3.1, is listed in the last column.

In the power spectra of the u and v differential magnitudes 'μ Eri – ξ Eri' pre-whitened with the first four frequencies of Table 4, the highest peaks occur at the same frequency of 0.659 d^{-1}. Because a term of very nearly the same frequency is prominent in the frequency spectra of the 2002–2003 comparison-star data (see Section 4.2), we conclude that the signals at 0.659 d^{-1} are intrinsic. A five-frequency non-linear least-squares solution yielded the value of the fifth frequency and the corresponding amplitudes given in the last line of Table 4.

The power spectra of the u and v differential magnitudes 'μ Eri – ξ Eri' pre-whitened with the five frequencies of Table 4 are shown in Fig. 4. In both spectra, the highest peak occurs at 1.182 d^{-1}. Although these peaks may represent another term in the variation of μ Eri, we terminate the analysis at this stage for fear of overinterpreting the data.

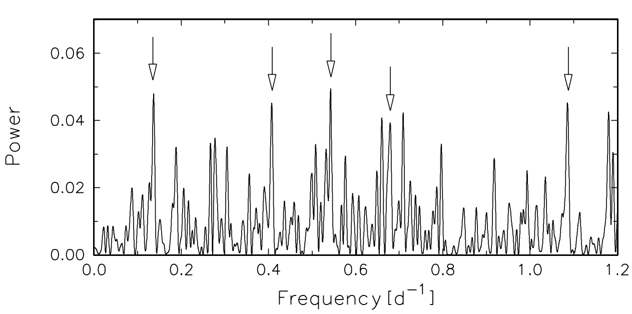

Figure 2. Low-frequency part of the power spectrum of the v differential magnitudes 'μ Eri – ξ Eri' pre-whitened with 0.615 d^{-1}, $2f'_{\rm orb}$ and $6f'_{\rm orb}$. Arrows indicate peaks at frequencies equal to $f'_{\rm orb}$, $3f'_{\rm orb}$, $4f'_{\rm orb}$, $5f'_{\rm orb}$ and $8f'_{\rm orb}$.

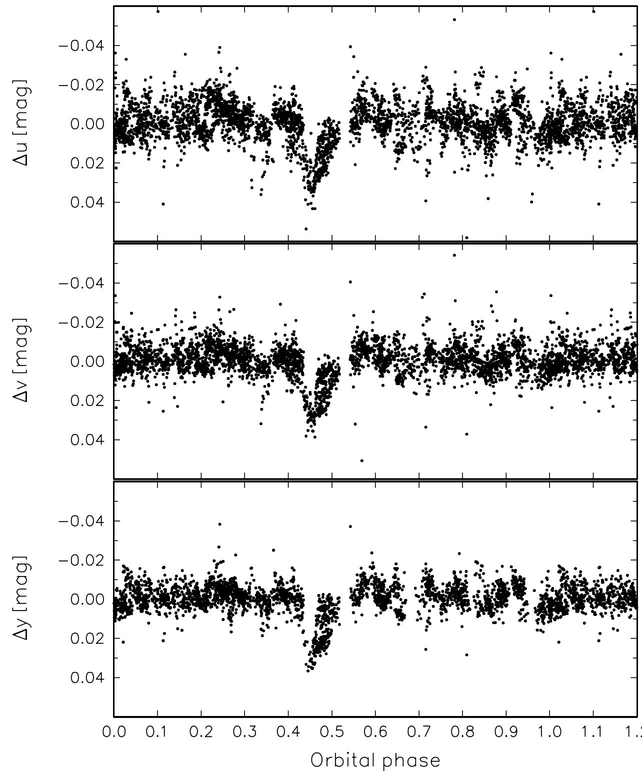

Figure 3. The u (top), v (middle) and y (bottom) differential magnitudes 'μ Eri – ξ Eri' pre-whitened with f'_1 are shown as a function of orbital phase of μ Eri. Phase zero corresponds to HJD 245 2800.

Table 4. Frequencies, periods and amplitudes in the out-of-eclipse differential magnitudes 'μ Eri – ξ Eri' from the 2003–2004 data. The last column contains the v-amplitude S/N ratio.

ID	Frequency (d^{-1})	Period (d)	A_u (mmag)	A_v (mmag)	A_y (mmag)	S/N
f'_1	0.61504 ± 0.00010	1.6259 ± 0.00026	9.4 ± 0.22	6.1 ± 0.17	5.7 ± 0.16	11.1
f'_2	0.70160 ± 0.00027	1.4253 ± 0.00055	4.0 ± 0.22	2.4 ± 0.16	2.2 ± 0.15	3.9
f'_3	0.81351 ± 0.00026	1.2292 ± 0.00039	3.3 ± 0.22	2.2 ± 0.17	2.5 ± 0.17	4.1
f'_4	1.20739 ± 0.00027	0.8282 ± 0.00019	3.1 ± 0.23	2.3 ± 0.17	2.3 ± 0.16	6.0
f'_5	0.65934 ± 0.00028	1.5167 ± 0.00064	3.4 ± 0.21	2.3 ± 0.16	2.4 ± 0.15	4.2

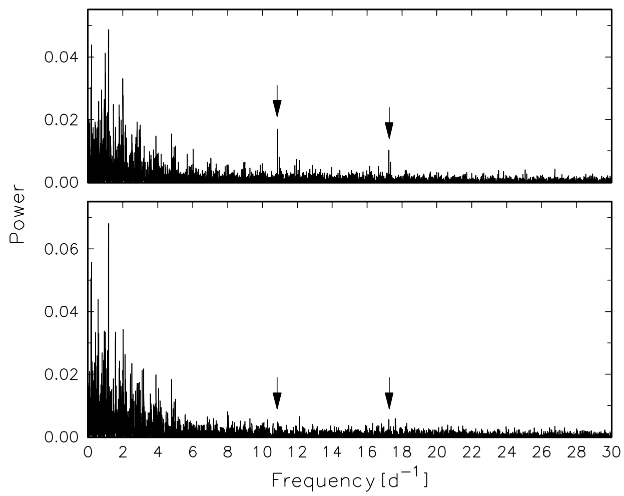

Figure 4. Power spectra of the u (lower panel) and v (upper) out-of-eclipse differential magnitudes 'μ Eri – ξ Eri' pre-whitened with the five frequencies of Table 4. Arrows indicate frequencies $f_x = 10.874$ and $f_y = 17.254$ d^{-1}.

At high frequencies, peaks at $f_x = 10.874$ and $f_y = 17.254$ d^{-1} can be clearly seen in the v spectrum (Fig. 4, upper panel). The v-amplitude S/N ratio is equal to 5.2 and 4.4 for f_x and f_y, respectively. Although in the u spectrum in the lower panel the peaks at these frequencies are masked by noise, a closer examination shows that they are present. For f_x, the u, v and y amplitudes computed from the differential magnitudes 'μ Eri – ξ Eri' amount to 0.9 ± 0.22, 1.2 ± 0.16 and 1.0 ± 0.16 mmag (formal σ), respectively. To within one formal σ, these numbers agree with the f_x amplitudes derived from the 'ν Eri – ξ Eri' differential magnitudes (see Table 2). For f_y, the u, v and y amplitudes computed from the differential magnitudes 'μ Eri – ξ Eri' are equal to 0.9 ± 0.22, 0.9 ± 0.16 and 0.7 ± 0.16 mmag, respectively. Again, there is a 1σ agreement with the amplitudes obtained from the 'ν Eri – ξ Eri' data (see Table 2). In addition, the phases agree to within 1σ in all cases. We conclude that both frequencies are due to an intrinsic variation of ξ Eri.

4 LOW FREQUENCIES FROM THE 2002–2003 DATA

4.1 The eclipse

We have to admit that in our original analysis of the 2002–2003 data we missed the eclipse of μ Eri (see Paper I and Section 1). Fig. 5 shows phase diagrams in which the 2002–2003 differential magnitudes 'μ Eri – ξ Eri' pre-whitened with f'_1 are plotted as a function of orbital phase. The eclipse can be seen clearly.

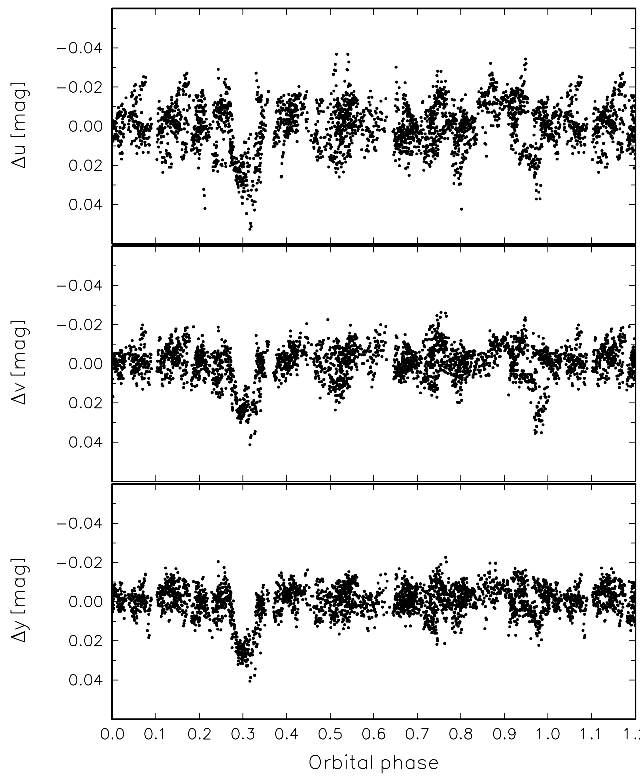

Figure 5. The u (top), v (middle) and y (bottom) 2002–2003 differential magnitudes 'μ Eri – ξ Eri' pre-whitened with f'_1 are shown as a function of orbital phase of μ Eri. As in Fig. 3, phase zero corresponds to HJD 245 2800.

A comparison of the phase diagrams in Figs 5 and 3 shows that while the middle of the eclipse in 2002–2003 falls at a phase of about 0.30, in 2003–2004 it does at about 0.47, indicating a problem with the Hill (1969) value of the orbital period. Assuming that Hill's value yields a correct cycle count between the first eclipse observed in 2002 and the last one in 2003, we arrive at the following ephemeris:

$$\text{Min. light} = \text{HJD } 245\,2574.04\,(4) + E/0.135490\,(18). \qquad (4)$$

Here, E is the number of cycles elapsed from the epoch given (which is that of the middle of the first eclipse we caught in 2002) and the numbers in parentheses are estimated standard deviations with the leading zeros suppressed. The question why our photometric period differs from Hill's spectrographic one will be addressed in a forthcoming paper.

4.2 Analysis of the out-of-eclipse μ Eri data

In 2002–2003 the numbers of differential magnitudes 'μ Eri – ξ Eri' in the three bands were nearly the same, amounting to 2823, 2830 and 2919 in u, v and y, respectively. After we rejected observations falling within the eclipse, these numbers were reduced to 2597, 2603 and 2688, still sufficient for analysis. Using these reduced data, we computed power spectra separately for u, v and y. The first two runs yielded the same frequencies of 0.616 and 0.701 d^{-1} in all three bands. These frequencies are very nearly equal to f'_1 and f'_2 of Table 4. In the third run, the highest peak in the u power spectrum was at 0.657 d^{-1}, while in the v and y power spectra the highest peaks were at the same frequency of 1.207 d^{-1}. The first of these numbers is close to f'_5, while the second is nearly identical with f'_4 (see Table 4).

The fourth run, however, was a disappointment. In the u power spectrum, the highest peak occurred at 1.000 d^{-1}, while in the v and y power spectra it occurred at 0.032 d^{-1}. Because neither of these frequencies is likely to be intrinsic, we did not attempt to compute fifth-run power spectra.

The four frequencies found above (i.e. 0.616, 0.701, 1.207 and 0.657 d^{-1}) were used as starting values in a four-frequency non-linear least-squares solution. Justification for including f'_4 in the u solution comes from the fact that a peak at this frequency is prominent in the fourth-run u power spectrum. Likewise, f'_5 was included in the v and y solutions because prominent peaks at this frequency can be seen in the fourth-run v and y power spectra.

The results of the four-frequency solutions are given in Table 5 in the upper part of the table. This table has the same format as Table 4. However, the S/N (last column) is now computed from the y data.

The four-frequency solutions did not include f'_3. Because peaks at this frequency were present in the fourth-run u and v power spectra, we carried out five-frequency non-linear least-squares solutions for all five frequencies of Table 4. The resulting values of f'_3, the amplitudes and S/N are given in Table 5 in the lower part of the table.

4.3 ν Eri

As explained in Paper I, the 2002–2003 differential magnitudes of ν Eri were computed as 'ν Eri minus the mean of comparison stars', but with the low-frequency variations of μ Eri filtered out. Thus, a peak at low frequency in the power spectrum of these differential magnitudes – if not caused by noise – would be due to an intrinsic variation of ν Eri or ξ Eri. In the latter case, however, the peaks would be suppressed by a factor of 4, while the corresponding amplitudes would be divided by 2.

In Paper I we found a prominent peak at 0.254 d^{-1} in the amplitude spectrum of the v differential magnitudes pre-whitened with all 23 frequencies identified from the 2002–2003 data. The power spectrum of the same data also shows a prominent peak at this frequency. However, there is little power at this frequency in the 2003–2004 spectra shown in Fig. 1. On the other hand, in the 2002–2003 u, v and y power spectra there are peaks at 0.615 d^{-1}, a frequency very nearly equal to f_B found in Section 3.1 from the 2003–2004 data. The 2002–2003 u, v and y amplitudes at this frequency amount to 2.5 ± 0.19, 1.2 ± 0.14 and 1.4 ± 0.12 mmag, respectively, in fair agreement with the 2003–2004 amplitudes listed in Table 2. Because multiplying the 2002–2003 amplitudes by 2 would make the agreement much worse, the possibility that f_B is due to ξ Eri can be rejected.

5 ANALYSIS OF THE COMBINED DATA

5.1 ν Eri

After slight mean light level adjustments, the 2002–2003 and 2003–2004 differential magnitudes of ν Eri were combined, separately for u, v and y. The combined 2002–2004 data have the time baseline of 525.8 d. The analysis of the 2002–2004 differential magnitudes was carried out in the same way as that of the 2003–2004 data (see Section 3). 16 independent and 20 combination frequencies could be identified from the power spectra. In all cases but two, the yearly aliases were significantly lower than the central peak, so that there was no ±1 yr^{-1} uncertainty. This was to be expected because the 2002–2003 and 2003–2004 observing windows span as much as 0.43 yr each (see Section 2). The two exceptions were f_6 and f_{12}. They are discussed later in this section.

The 36 frequencies derived from the combined data are listed in the first column of Table 6. As in Tables 2, 4 and 5, the values of the independent frequencies and their standard deviations, given in column 2, were computed as straight means from the separate solutions for u, v and y. The combination frequencies, listed in the lower half of the table, were computed from the independent frequencies according to ID in the first column; their standard deviations were computed from the standard deviations of the independent frequencies assuming rms propagation of errors. The amplitudes, A_u, A_v and A_y, given together with their standard deviations in columns 3, 4 and 5, respectively, are from the independent solutions for u, v and y. The v-amplitude S/N, computed in the same way as in Section 3.1, is given in the last column. It can be seen that all independent frequencies meet the significance condition of Paper I. Among combination frequencies, this condition is not satisfied in two cases: $f_3 + f_4$ and $f_1 - f_4$.

In addition to frequencies derived from the 2003–2004 data (see Table 2), Table 6 contains two further high frequencies due to ν Eri: f_{11} and f_{12}. The latter is close to that of one of several 'possible further signals' listed in table 3 of Paper I and to frequency ν_7 obtained in Paper III from radial velocities of the Si III triplet around 457 nm. Frequency f_{11} is new. In order to make sure that this frequency is not due to ξ Eri, we examined the 2002–2004 out-of-eclipse differential magnitudes 'μ Eri – ξ Eri' pre-whitened with the six frequencies of Table 7 (see Section 5.2). In the periodograms, there were no peaks at f_{11}; the highest peak in the vicinity, at 6.7168 d^{-1}, had

Table 5. Frequencies, periods and amplitudes in the out-of-eclipse differential magnitudes 'μ Eri – ξ Eri' from the 2002–2003 data. The last column contains the y-amplitude S/N ratio.

ID	Frequency (d^{-1})	Period (d)	A_u (mmag)	A_v (mmag)	A_y (mmag)	S/N
f'_1	0.61587 ± 0.00013	1.62372 ± 0.00034	9.9 ± 0.26	6.2 ± 0.19	4.9 ± 0.15	9.4
f'_2	0.70143 ± 0.00021	1.42566 ± 0.00043	6.9 ± 0.25	4.4 ± 0.19	3.3 ± 0.15	4.1
f'_4	1.20690 ± 0.00030	0.82857 ± 0.00021	3.2 ± 0.25	3.4 ± 0.19	2.7 ± 0.15	4.5
f'_5	0.65751 ± 0.00036	1.5209 ± 0.0008	4.2 ± 0.25	2.3 ± 0.19	2.2 ± 0.15	4.2
f'_3	0.8147 ± 0.0006	1.2275 ± 0.0009	3.1 ± 0.24	2.3 ± 0.19	0.8 ± 0.15	1.4

Table 6. Frequencies and amplitudes in the differential magnitudes of ν Eri from the combined 2002–2004 data. Independent frequencies are listed in the upper half of the table. The combination frequencies are listed in the lower half of the table. In both cases the frequencies are ordered according to decreasing v amplitude, A_v. Frequencies f_x and f_y are due to ξ Eri.

ID	Frequency (d^{-1})	A_u (mmag)	A_v (mmag)	A_y (mmag)	S/N
f_1	5.7632828 ± 0.0000019	72.8 ± 0.13	40.8 ± 0.10	36.7 ± 0.10	214.7
f_2	5.6538767 ± 0.0000030	38.5 ± 0.13	27.1 ± 0.10	25.4 ± 0.10	142.6
f_3	5.6200186 ± 0.0000031	35.0 ± 0.13	24.5 ± 0.10	23.2 ± 0.10	129.0
f_4	5.6372470 ± 0.0000038	31.8 ± 0.13	22.3 ± 0.10	21.0 ± 0.10	117.4
f_5	7.898200 ± 0.000032	3.6 ± 0.13	2.6 ± 0.10	2.5 ± 0.10	14.5
f_A	0.432786 ± 0.000032	4.1 ± 0.13	2.5 ± 0.10	2.5 ± 0.10	8.3
f_7	6.262917 ± 0.000044	2.8 ± 0.14	2.0 ± 0.10	1.8 ± 0.10	11.0
f_6	6.243847 ± 0.000042	3.0 ± 0.13	1.9 ± 0.10	2.1 ± 0.10	10.5
f_B	0.61440 ± 0.00005	3.0 ± 0.13	1.4 ± 0.10	1.6 ± 0.10	5.5
f_9	7.91383 ± 0.00008	1.7 ± 0.13	1.1 ± 0.10	1.2 ± 0.10	6.1
f_x	10.87424 ± 0.00012	0.8 ± 0.13	1.0 ± 0.10	0.7 ± 0.10	5.7
f_{10}	7.92992 ± 0.00010	1.2 ± 0.13	0.9 ± 0.10	0.9 ± 0.10	5.0
f_8	7.20090 ± 0.00009	1.4 ± 0.13	0.9 ± 0.10	0.9 ± 0.10	5.0
f_{11}	6.73223 ± 0.00012	1.0 ± 0.13	0.8 ± 0.10	0.6 ± 0.10	4.5
f_{12}	6.22360 ± 0.00012	0.9 ± 0.13	0.8 ± 0.10	0.8 ± 0.10	4.4
f_y	17.25241 ± 0.00016	0.6 ± 0.13	0.6 ± 0.10	0.5 ± 0.10	4.4
$f_1 + f_2$	11.4171595 ± 0.0000036	12.4 ± 0.13	8.8 ± 0.10	8.4 ± 0.10	50.9
$f_1 + f_3$	11.3833014 ± 0.0000036	10.8 ± 0.14	7.6 ± 0.10	7.3 ± 0.10	44.0
$f_1 + f_4$	11.4005298 ± 0.0000042	10.2 ± 0.14	7.2 ± 0.10	6.8 ± 0.10	41.7
$2f_1$	11.5265656 ± 0.0000027	4.4 ± 0.13	3.1 ± 0.10	2.9 ± 0.10	17.9
$f_1 + f_2 + f_3$	17.037178 ± 0.000005	3.6 ± 0.13	2.5 ± 0.10	2.3 ± 0.10	18.1
$f_2 + f_3$	11.2738953 ± 0.0000043	2.6 ± 0.13	1.5 ± 0.10	1.3 ± 0.10	8.7
$f_1 - f_2$	0.1094061 ± 0.0000036	2.6 ± 0.13	1.5 ± 0.10	1.6 ± 0.10	4.0
$2f_1 + f_2$	17.1804423 ± 0.0000040	1.9 ± 0.13	1.5 ± 0.10	1.3 ± 0.10	10.9
$2f_1 + f_4$	17.163813 ± 0.000005	1.7 ± 0.13	1.4 ± 0.10	1.2 ± 0.10	10.1
$2f_1 + f_3$	17.1465842 ± 0.0000041	1.6 ± 0.13	1.3 ± 0.10	1.1 ± 0.10	9.4
$2f_1 + f_2 + f_3$	22.800461 ± 0.000005	1.4 ± 0.13	1.0 ± 0.09	0.8 ± 0.10	8.3
$2f_2$	11.3077534 ± 0.0000042	0.8 ± 0.14	0.8 ± 0.10	0.5 ± 0.10	4.6
$f_1 + f_2 - f_3$	5.797141 ± 0.000005	1.0 ± 0.13	0.8 ± 0.10	0.8 ± 0.10	4.2
$f_1 + f_5$	13.661483 ± 0.000032	1.1 ± 0.13	0.7 ± 0.09	0.8 ± 0.10	4.5
$f_1 + f_3 + f_4$	17.020548 ± 0.000005	0.9 ± 0.14	0.7 ± 0.10	0.7 ± 0.10	5.1
$f_2 + f_4$	11.291124 ± 0.000005	0.8 ± 0.14	0.7 ± 0.10	0.6 ± 0.10	4.0
$f_1 + f_2 + f_4$	17.054406 ± 0.000005	0.8 ± 0.14	0.6 ± 0.10	0.8 ± 0.10	4.4
$f_1 - f_4$	0.1260358 ± 0.0000042	1.7 ± 0.13	0.6 ± 0.10	0.8 ± 0.10	1.6
$f_1 + 2f_2$	17.071036 ± 0.000005	0.6 ± 0.14	0.5 ± 0.10	0.4 ± 0.10	3.6
$f_3 + f_4$	11.257266 ± 0.000005	0.5 ± 0.14	0.5 ± 0.10	0.3 ± 0.10	2.9

Table 7. Frequencies, periods and amplitudes in the out-of-eclipse differential magnitudes 'μ Eri – ξ Eri' from the combined 2002–2004 data. The last column contains the v-amplitude S/N ratio.

ID	Frequency (d^{-1})	Period (d)	A_u (mmag)	A_v (mmag)	A_y (mmag)	S/N
f'_1	0.615739 ± 0.000016	1.624065 ± 0.000042	9.9 ± 0.16	6.3 ± 0.12	5.6 ± 0.11	12.2
f'_2	0.700842 ± 0.000034	1.42686 ± 0.00007	4.8 ± 0.16	3.0 ± 0.12	2.5 ± 0.10	6.5
f'_4	1.205580 ± 0.000043	0.829476 ± 0.000030	3.0 ± 0.16	2.6 ± 0.12	2.4 ± 0.10	7.2
f'_{4a} [a]	1.208346 ± 0.000042	0.827578 ± 0.000029	2.9 ± 0.16	2.5 ± 0.12	2.4 ± 0.10	6.9
f'_5	0.658876 ± 0.000039	1.51774 ± 0.00009	4.0 ± 0.16	2.5 ± 0.12	2.6 ± 0.11	4.8
f'_6	0.56797 ± 0.00005	1.76066 ± 0.00016	2.7 ± 0.16	2.0 ± 0.12	2.1 ± 0.11	3.1
f'_3	0.81272 ± 0.00006	1.23044 ± 0.00009	2.8 ± 0.16	1.9 ± 0.12	1.4 ± 0.10	4.0

[a] $f'_{4a} \approx f'_4 + 1\,y^{-1}$.

v amplitude equal to about 0.4 mmag and S/N <2.5. Analogous tests with the 2002–2003 data also proved negative.

We now discuss the two problematic frequencies, f_6 and f_{12}, mentioned in the first paragraph of this section. In the case of f_6, the central peak at 6.2438 d^{-1} was only slightly higher than the +1-yr^{-1} alias at 6.2465 d^{-1}. However, the 2002–2003 and 2003–2004 values of f_6 are both much closer to the frequency of the central peak than to that of the alias peak. Moreover, in each band, the non-linear least-squares fit converged to exactly the same solution regardless of whether the starting value of f_6 was the frequency of the central peak, the 2002–2003 value, or the 2003–2004 value. We conclude that f_6 given in Table 6 is unlikely to be in error by 1 yr^{-1}.

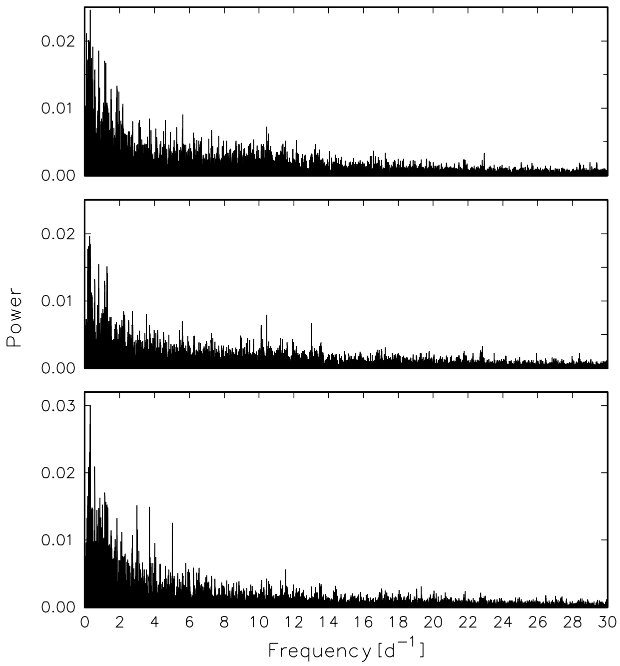

Figure 6. Power spectra of the combined 2002–2004 *u* (bottom), *v* (middle) and *y* (top) differential magnitudes of ν Eri pre-whitened with the 36 frequencies of Table 6.

The case of f_{12} is similar, but now the -1-yr^{-1} alias at 6.2210 d^{-1} is the problem. In *v* and *y* it is almost as high as the central peak at 6.2236 d^{-1}, while in *u* it is even slightly higher. Computing power spectra from the averaged *u*, *v* and *y* residuals, with proper weight given to each band, did not solve the problem. In Paper III, there is also the yr^{-1} uncertainty: the frequency is equal to 6.22304 d^{-1} for Si III 455.3 nm, but for Si III 456.8 and 457.5 nm it is close to 6.2210 d^{-1}. The frequency given in table 3 of Paper I is equal to the alias frequency. More data are needed to decide whether the value given in Table 6 is the correct value.

Fig. 6 shows the power spectra of the 2002–2004 data pre-whitened with the 36 frequencies of Table 6. In the *u* and *y* spectra (bottom and top panels, respectively) the highest peaks occur at 0.3142 d^{-1}, but in the *v* spectrum they occur at 0.2625 d^{-1}. The corresponding amplitudes amount to 1.9 and 1.2 mmag in *u* and *y*, and 1.1 mmag in *v*. In neither case does the S/N ratio exceed 3.4, so that these peaks are unlikely to be intrinsic. The reader may remember that in Section 3.1, a peak seen at 0.314 d^{-1} in the 2003–2004 *u* power spectrum was also dismissed as spurious.

The highest S/N peaks in Fig. 6 have frequencies equal to 5.0139 d^{-1} in *u* (S/N = 4.5), 13.0152 d^{-1} in *v* (S/N = 4.2) and 22.9440 d^{-1} in *y* (S/N = 4.1). The peak at 5.0139 d^{-1} can be explained in terms of colour extinction in the *u* band (see Section 3.1). At 13.0152 d^{-1}, there are low peaks in the *u* and *y* spectra with S/N equal to 2.9 and 2.4, respectively. No peaks at 13.0152 d^{-1} can be seen in the 'μ Eri – ξ Eri' power spectra, so that this frequency is not due to ξ Eri. Finally, the frequency of 22.9440 d^{-1} is very close to the combination frequency $3f_1 + f_2$. We conclude that while the latter frequency may be intrinsic, the former is probably spurious.

5.2 Out-of-eclipse variation of μ Eri

Combining the 2002–2003 and 2003–2004 out-of-eclipse differential magnitudes 'μ Eri – ξ Eri,' we obtained time series consisting of 5818, 5823 and 5189 data points in *u*, *v* and *y*, respectively.

The highest peaks in the successive power spectra of these data occurred at frequencies close to those found from the 2003–2004 and 2002–2003 time series separately (see Tables 5 and 4) and at the frequency $f'_6 = 0.568$ d^{-1}, which is new. In *u*, the frequencies appeared in the order f'_1, f'_2, f'_5, f'_3 and f'_{4a}, where the last frequency is the $+1$-yr^{-1} alias of $f'_4 = 1.2056$ d^{-1}. The two highest peaks in the sixth-run power spectrum occurred at 2.009 and 0.997 d^{-1}, neither of which is likely to be intrinsic. The third peak, only slightly lower than the second, was at f'_6. In *v*, the order was f'_1, f'_2, f'_4, f'_5, f'_6 and f'_3, but in the third run the peak at f'_4 was only slightly higher than that at f'_{4a}. In *y*, the order was the same as in *v*, except that in the last run the highest peak occurred at 0.997 d^{-1}, while the peak at f'_3 – although present – would be missed if it were not previously found in *u* and *v*.

The 1-yr^{-1} uncertainty which affects f'_4 did not plague other frequencies; in all other cases the yearly aliases were significantly lower than the central peak.

The results of the analysis are given in Table 7. The numbers for f'_{4a} are from non-linear least-squares fits in which the alias frequency read off the power spectrum was used as the starting value. In these fits, the other frequencies and the corresponding amplitudes were only slightly different from those given in the table.

The *u* to *y* amplitude ratio in Table 7 exceeds 1.2 for all frequencies. For four frequencies, the ratio is greater than 1.5, while for f'_4 and f'_6, it is equal to about 1.3. However, this dichotomy may be illusory because the (formal) standard deviation of the latter number amounts to about 0.10.

The reader may have noticed that $f'_1 \approx f_B$. Because neither frequency can be due to ξ Eri because the amplitudes and phases do not match (see also Section 4.3), this curious near-equality must be an accidental coincidence.

6 SUMMARY AND CLUES FOR ASTEROSEISMOLOGY

6.1 Independent high frequencies of ν Eri

Fig. 7 shows schematically the 11 independent high-frequency terms of ν Eri derived from the combined, 2002–2004 data. Comparing this figure with fig. 4 of Paper I we can see that two of the three high-frequency 'possible further signals' of Paper I are now upgraded to the status of certainty. This has already been mentioned in

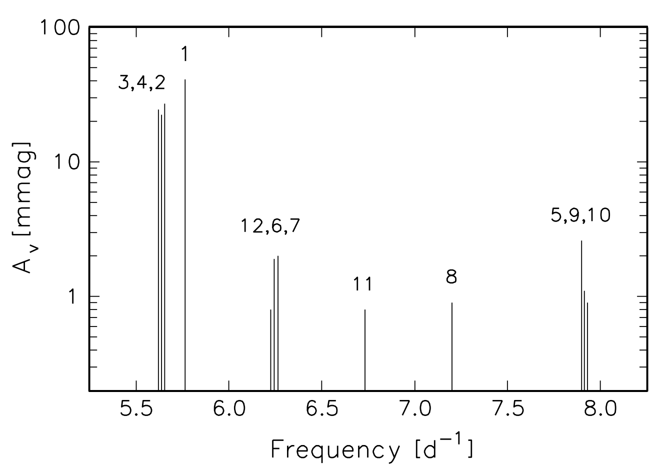

Figure 7. Schematic *v*-amplitude spectrum of ν Eri from the combined 2002–2004 data; the 11 independent high-frequency terms are numbered as in Table 6.

Table 8. The mean separation, *S*, and asymmetry, *A*, of the close frequency triplets in the oscillation spectrum of ν Eri.

Terms	S (d^{-1})	A (d^{-1})
3,4,2	0.0169290±0.0000022	−0.000600±0.0000087
12,6,7	0.019658 ±0.000064	−0.00118 ±0.00015
5,9,10	0.015860 ±0.00008	0.00046 ±0.00019

Sections 3.2 and 5.1. The terms in question are the $i = 9$ and 12 terms. Both are members of close frequency triplets.

The third high-frequency 'possible further signal' of Paper I, with frequency equal to 7.252 d^{-1}, must remain in limbo. Although in the power spectra pre-whitened with the 36 frequencies of Table 6 (see Fig. 6) there is a series of low peaks in the vicinity of 7.25 d^{-1}, the corresponding v amplitudes are smaller than 0.6 mmag and the S/N ratios do not exceed 3.6. In u, the amplitudes are smaller than 0.8 mmag and S/N <3.1. More data are needed to decide whether any of these peaks are intrinsic.

For the close frequency triplets seen in Fig. 7, the mean separation, *S*, and the asymmetry, *A*, are listed in Table 8.

In Section 5.1 we have warned that f_{12} may be in error by 1 yr^{-1}. If this were indeed the case, the values of *S* and *A* given in Table 8 for the 12, 6, 7 triplet should be replaced by 0.020964 and −0.00379 d^{-1}, respectively. Because of this uncertainty, and the suspicion of a long-term variation of the amplitude of the $i = 6$ term (Section 3.2), the triplet is not particularly suitable for asteroseismology at this stage. Fortunately, the other two triplets are well behaved. There are no yr^{-1} uncertainties, even for the lowest-amplitude term of the 5, 9, 10 triplet, and no signs of long-term amplitude variation. In addition, the $\ell = 1$ spherical harmonic identification for all members of the large-amplitude triplet and the $i = 5$ member of the 5, 9, 10 triplet are secure (see Paper III or Section 1). As can be seen from Fig. 8, the $i = 9$ and 10 members of the triplet have *uvy* amplitude ratios consistent with ℓ equal to 1 or 2. Unfortunately, the standard deviations of the amplitude ratios, especially those of the smallest-amplitude member, are too large to fix ℓ unambiguously.

6.2 Independent low frequencies of ν Eri

As we mentioned in Section 1, the frequency resolution of the 2002–2003 data was insufficient to reject the possibility that f_A is equal to

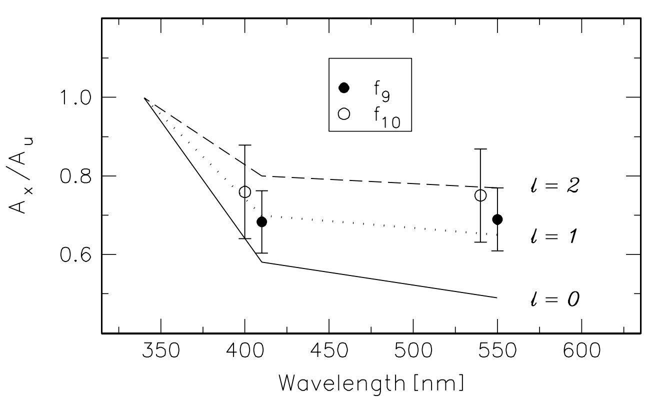

Figure 8. Observed *uvy* amplitude ratios for the small-amplitude members of the 7.91 d^{-1} triplet (circles with error bars) compared with theoretical amplitude ratios for $\ell \leqslant 2$. The observed ratios are from the 2002–2004 amplitudes (see Table 6), the theoretical ones from fig. 5 of Paper III. The open circles are shifted slightly in wavelength to avoid overlap.

the combination frequency $3f_1 - 3f_3$. As can be seen from Table 6, the difference between f_A and $3f_1 - 3f_3$ amounts to 0.0030 d^{-1}. This number is not only much larger than the standard deviation of f_A, but also larger than the frequency resolution of the 2002–2004 data by a factor of about 1.5. In fact, $3f_1 - 3f_3$ coincides with the −1-yr^{-1} alias of f_A. Because the alias has about the same height as the +1-yr^{-1} alias, the combination frequency amplitude must be below the detection threshold. Consequently, there is no longer any doubt that f_A is an independent low frequency in the variation of ν Eri. In addition, we have found another low frequency, f_B (see Tables 2 and 6). Because only high-order g modes have frequencies that low, the suggestion put forward in Paper I that ν Eri is both a β Cep variable and an SPB star is amply confirmed.

6.3 μ Eri

To the single frequency $f'_1 = 0.616$ d^{-1}, derived from the differential magnitudes 'μ Eri – ξ Eri' in Paper I, we add five further frequencies (see Table 7). The values of the frequencies and the decrease of the *uvy* amplitudes with increasing wavelength (for at least four frequencies) indicate that we are seeing high-radial-order g modes. Thus, as already suggested in Paper I, the star is an SPB variable. Note that rotational modulation, the second hypothesis put forward in Paper I for explaining the f'_1 term, is now untenable because it does not account for multiperiodicity.

As can be seen from Table 7, the periods P'_3, P'_2 and P'_1 are equally spaced, with the spacing equal to ∼0.20 d, while P'_4 precedes P'_3 by twice this value. The equal spacing in period may be a manifestation of the well-known asymptotic property of high-order g modes of the same ℓ. There are, however, the following two problems with this idea: (i) the term halfway between P'_3 and P'_4 is missing, and (ii) the period spacing is rather large. Better data may solve the first problem if the missing term is simply too weak to be detected in our data. The second problem requires a comparison with the theory. Unfortunately, the only SPB-star model available in the literature (Dziembowski, Moskalik & Pamyatnykh 1993) has $M = 4$ M$_\odot$, $\log L/\mathrm{L}_\odot = 2.51$ and $X_c = 0.37$, whereas μ Eri is more massive (by ∼2 M$_\odot$), more luminous (by ∼0.8 dex), and more evolved (see Paper I). In the model, the largest period spacing (for $\ell = 1$) is equal to ∼0.07 d, almost a factor of 3 smaller than observed in μ Eri. Whether this disagreement can be alleviated with a model which better matches the star remains to be verified. If this turns out to be unsuccessful, we can still invoke the unlikely idea that an unknown amplitude limitation mechanism is suppressing the modes halfway between those observed.

The possibility that instead of an equally spaced period triplet, P'_3, P'_2, P'_1, we have a rotationally split frequency triplet, f'_1, f'_2, f'_3, is much less likely. Indeed, for an $\ell = 1$ g mode with frequency equal to 0.7 d^{-1} in the SPB-star model of Dziembowski et al. (1993), the observed mean separation of the frequency triplet, equal to 0.09849 ± 0.00003 d^{-1}, leads to equatorial velocity of rotation, v_e, of about 30 km s^{-1} (see their fig. 13), whereas available estimates of $v_e \sin i$ of μ Eri range from 150 to 190 km s^{-1} (see Paper I). Increasing the model's radius in order to better match μ Eri may increase v_e to about 60 km s^{-1}, still much less than the observed values. An additional problem is posed by the large asymmetry of the frequency triplet. The asymmetry is equal to 0.0268 ± 0.0001 d^{-1}, while the rotational splitting seen in fig. 13 of Dziembowski et al. (1993) is nearly symmetric.

In addition to confirming the SPB classification of Paper I, we have found μ Eri to be an eclipsing variable. As can be seen from Figs 3 and 5, the eclipse is a transit, probably total, the secondary is fainter than the primary by several magnitudes, and the system is widely detached. As far as we are aware, the only other eclipsing variable with similar properties is 16 (EN) Lac (Jerzykiewicz 1979), except that in the latter case the eclipse is partial. (Interestingly, the discovery of an eclipse of this well-known β Cephei variable was a byproduct of a three-site campaign undertaken for observing the star's pulsations.) Solving the μ Eri system will yield the primary's mean density and its surface gravity. However, this is beyond the scope of the present paper.

6.4 ξ Eri

The frequencies $f_x = 10.8742$ and $f_y = 17.2524$ d^{-1} (see Tables 2 and 6) and the MK type of A2 V (see Section 1) leave no doubt that the star is a δ Scuti variable. The Strömgren indices, $c_1 = 1.076$ and $b - y = 0.038$ (Hauck & Mermilliod 1998), are not reddened. This is not inconsistent with the star's Hipparcos parallax of 15.66 ± 0.80 mas. Using the parallax and the V magnitude from Hauck & Mermilliod (1998), we obtain $M_V = 1.12 \pm 0.11$, a value which, together with the b–y index, places the star about 0.02 mag to the blue of the observational blue edge of the δ Scuti instability strip in the M_V versus b–y diagram (see, for example, Handler 2002). Apart from indicating the need for a slight revision of the blue edge, this position in the diagram suggests marginal pulsation driving as a possible explanation for the small uvy amplitudes. However, in view of the star's high $v \sin i$ of 165 km s^{-1} (Abt & Morrell 1995), another explanation may be provided by the hypothesis of Breger (1982) that fast rotation is a factor in limiting pulsation amplitudes.

Unfortunately, with only two small-amplitude modes the asteroseismic potential of ξ Eri is insignificant.

ACKNOWLEDGMENTS

The participation of MJ and AP in the campaign was supported by KBN grant 5P03D01420. MJ would also like to acknowledge a generous allotment of telescope time and the hospitality of Lowell Observatory. The work of GH was supported by the Austrian Fonds zur Förderung der wissenschaftlichen Forschung under grant R12-N02. ER is grateful for the support by the Junta de Andalucia and the Direccion General de Investigacion (DGI) under project AYA2003-04651. The referee, Dr C. Simon Jeffery, helped us to improve the paper.

REFERENCES

Abt H. A., Morrell N. I., 1995, ApJS, 99, 135
Aerts C., Waelkens C., de Pauw M., 1994, A&A, 286, 136
Aerts C. et al., 2004, MNRAS, 347, 463 (Paper II)
Ausseloos M., Scuflaire R., Thoul A., Aerts C., 2004, MNRAS, 355, 352
Breger M., 1982, PASP, 94, 845
Crow E. L., Davis F. A., Maxfield M. A., 1960, Statistics Manual. Dover, New York
Cugier H., Dziembowski W. A., Pamyatnykh A. A., 1994, A&A, 291, 143
De Ridder J. et al., 2004, MNRAS, 351, 324 (Paper III)
Dziembowski W. A., Jerzykiewicz M., 2003, in Balona L. A., Henrichs H. F., Medupe R., eds, ASP Conf. Ser. Vol. 305, Magnetic Fields in O, B and A Stars: Origin and Connection to Pulsation, Rotation and Mass Loss. Astron. Soc. Pac., San Francisco, p. 319
Dziembowski W. A., Moskalik P., Pamyatnykh A. A., 1993, MNRAS, 265, 588
Handler G., 2002, in Sterken C., Kurtz D. W., eds, ASP Conf. Ser. Vol. 256, Observational Aspects of Pulsating B and A Stars. Astron. Soc. Pac., San Francisco, p. 113
Handler G. et al., 2000, MNRAS, 318, 511
Handler G. et al., 2004, MNRAS, 347, 454 (Paper I)
Hauck B., Mermilliod M., 1998, A&AS, 129, 431
Heynderickx D., Waelkens C., Smeyers P., 1994, A&AS, 105, 447
Hill G., 1969, Publ. DAO Victoria, 13, 323
Jerzykiewicz M., 1978, Acta Astron., 28, 465
Jerzykiewicz M., 1979, IBVS No. 1552
Montgomery M. H., O'Donoghue D., 1999, Delta Scuti Star Newsletter, 13, 28
Pamyatnykh A. A., Handler G., Dziembowski W. A., 2004, MNRAS, 350, 1022
Saito K., 1976, in Fitch W. S., ed, Proc. IAU Coll. 29, Multiple Periodic Variable Stars. Akadémiai Kiadó, Budapest, Vol. 2, p. 47
Schwarzenberg-Czerny A., 1991, MNRAS, 253, 198

This paper has been typeset from a TEX/LATEX file prepared by the author.

5.4.5 Asteroseismology of the β Cephei star ν Eridani: interpretation and applications of the oscillation spectrum

Original paper:

A. A. Pamyatnykh, **G. Handler,** W. A. Dziembowski, 2004, MNRAS 350, 1022

Mon. Not. R. Astron. Soc. **350,** 1022–1028 (2004) doi:10.1111/j.1365-2966.2004.07721.x

Asteroseismology of the β Cephei star ν Eridani: interpretation and applications of the oscillation spectrum

A. A. Pamyatnykh,[1,2,3]★ G. Handler[3] and W. A. Dziembowski[1,4]

[1]*Copernicus Astronomical Centre, Bartycka 18, 00-716 Warsaw, Poland*
[2]*Institute of Astronomy, Russian Academy of Sciences, Pyatnitskaya Str. 48, 109017 Moscow, Russia*
[3]*Institut für Astronomie, Universität Wien, Türkenschanztrasse 17, A-1180 Wien, Austria*
[4]*Warsaw University Observatory, Al. Ujazdowskie 4, 00-478 Warsaw, Poland*

Accepted 2004 February 7. Received 2004 February 5; in original form 2004 January 5

ABSTRACT

The oscillation spectrum of ν Eri is the richest known for any variable of the β Cephei type. We interpret the spectrum in terms of normal mode excitation and construct seismic models of the star. The frequency data combined with data on mean colours set the upper limit on the extent of overshooting from the convective core. We use data on rotational splitting of two dipole ($\ell = 1$) modes (g_1 and p_1) to infer properties of the internal rotation rate. Adopting a plausible hypothesis of nearly uniform rotation in the envelope and increasing rotation rate in the μ-gradient zone, we find that the mean rotation rate in this zone is about three times faster than in the envelope. In our standard model only the modes in the middle part of the oscillation spectrum are unstable. To account for excitation of a possible high-order g mode at $\nu = 0.43$ cd^{-1} as well as p modes at $\nu > 6$ cd^{-1} we have to invoke an overabundance of Fe in the driving zone.

Key words: convection – stars: early-type – stars: individual: ν Eridani – stars: oscillations – stars: rotation – stars: variables: other.

1 INTRODUCTION

The rich oscillation spectrum of ν Eri obtained in a recent multisite campaign (Handler et al. 2004; Aerts et al. 2004) holds the best prospects for seismic sounding of the interior of a B star but also presents a considerable challenge to stellar pulsation theory. The sounding is facilitated by the fact that for several excited modes the spherical harmonic indices were determined (De Ridder et al. 2004). The challenge is to explain mode excitation in an unexpectedly broad frequency range.

The oscillation spectrum of ν Eri is shown in Fig. 1. Before the campaign only the $\ell = 0$ mode and the ($\ell = 1$, g_1) triplet were known. However, for the triplet, the identification of the spherical harmonic was uncertain. Now, thanks to the analysis of accurate multicolour photometry and high-resolution spectroscopy, the uncertainty was eliminated. Reliable information about ℓ is a crucial input for constructing seismic models of a star, that is the models constrained by the frequency data.

In this work, we attempt to make the best use of the frequency data to address unsolved problems in stellar evolution theory concerning element mixing in convectively stable layers and angular momentum evolution. The problems are related because rotation induces fluid flows that may cause mixing. It is important to disentangle effects of overshooting from the convective core and effects of rotationally induced element mixing. The first effect depends only on stellar mass. The second one depends on randomly distributed stellar angular momenta. In this context, ν Eridani, which is a very slowly rotating B star, yields a useful extreme case. However, it would be important to try to obtain similar quality data for more rapidly rotating objects.

We are very curious how the angular velocity of rotation behaves in stellar interiors. Let us remind that, while the results of helioseismic sounding of radial structure essentially confirmed the standard solar model, the results for the internal rotation rate came as a surprise. The outstanding question in the case of massive stars is whether a substantial radial gradient of the angular rotation rate may be present in their interiors. The question is related to another very interesting and important problem which is the origin of magnetic fields in B type stars.

A seismic model of a pulsating star should not only account for the measured frequencies but also for the instability of the detected modes. The latter requirement sets a different kind of constraint than the former as it concerns only properties of the outer layers, where most of contribution to mode driving and damping arises. Since the frequency spectrum of ν Eri seems unusually broad for an object of its type, constraints in this case are particularly interesting.

The structure of this paper is as follows. In Section 2 we construct models of the internal structure for ν Eri and calculate its oscillation frequencies. We find models for which the oscillation frequencies

★E-mail: alosza@camk.edu.pl

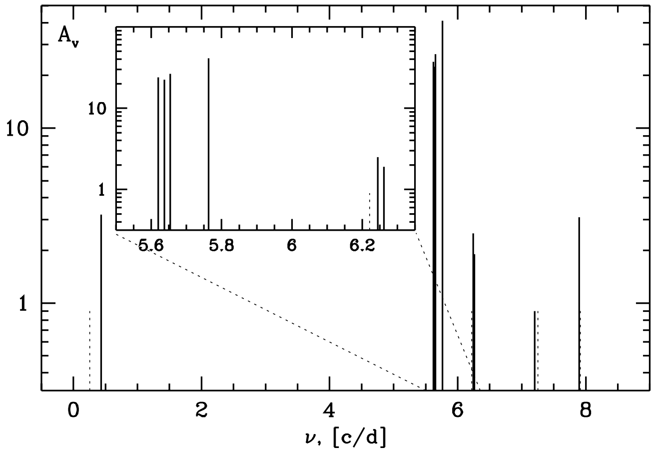

Figure 1. Oscillation spectrum of ν Eri. The peaks represented with the broken vertical lines are regarded uncertain. The four modes known before the campaign are between $\nu = 5.6$ and 5.8 cd^{-1}. De Ridder et al. (2004) identified them as an $\ell = 1$ triplet and an $\ell = 0$ singlet. The newly discovered triplet at $\nu \approx 6.25$ cd^{-1} is identified as $\ell = 1$ (De Ridder et al. 2004). In this paper we will show that the radial mode is the fundamental and the two dipole modes are g_1 and p_1, respectively. Only these mode frequencies are used in our seismic sounding.

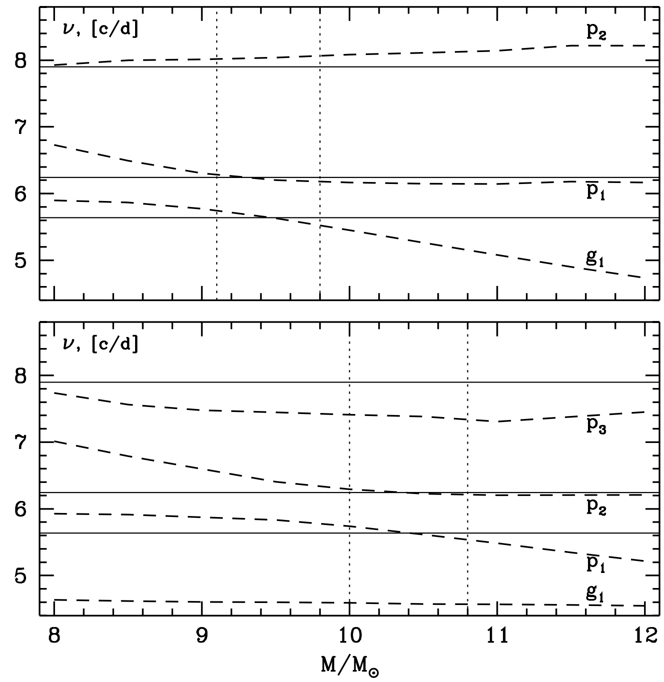

Figure 2. Identification of the radial overtone of the observed modes of ν Eri. We assume the radial mode to be the fundamental in the upper panel and to be the first overtone in the lower panel. The mass dependence of theoretical $\ell = 1$ mode frequencies (dashed lines) is compared to the observed $\ell = 1$ mode frequencies (horizontal lines). We find two ranges in mass (denoted by the vertical dotted lines) where the two $\ell = 1$ mode of lowest frequency match the observed frequencies well. However, the $\ell = 1$ mode near 7.9 cd^{-1} can only be reproduced in the case of the radial mode being the fundamental.

of three $m = 0$ modes – ($\ell = 0$, p_1), ($\ell = 1$, g_1) and ($\ell = 1$, p_1) – reproduce the observations as well as have effective temperatures and luminosities within the observational error box. In Section 3 we use these models and data on the triplet structure to infer the internal rotation of the star.

The problem of how to make the observed modes pulsationally unstable is discussed in Section 4. The tasks of constructing the model of ν Eri whose mode frequencies match the data and of the identification of the driving effect are not quite independent. The driving effect in B stars strongly depends on the iron content and its distribution in outer layers. In Section 5, we study how modification of the iron distribution affects the frequencies. We also propose plausible identifications of all modes detected in the ν Eri oscillation spectrum.

2 MODEL OF THE STELLAR INTERIOR

For the purpose of constructing models of ν Eri we ignored all effects of rotation which, as we have checked, was fully justified. Accordingly, we make use here only of the $m = 0$ mode frequencies despite, in general, rotation causes a shift of the centroid frequency. We consider models of massive main-sequence stars in the phase of radius expansion. A model is characterized by its mass, M, effective temperature, $T_{\rm eff}$, initial hydrogen, X, and heavy element, Z, abundance, as well as the overshooting parameter, $\alpha_{\rm ov}$. Here we assume the standard solar mixture of heavy elements (departures will be considered in Section 5) and fix X at 0.7. For opacity and the equation of state we use the OPAL tabular data (Iglesias & Rogers 1996; Rogers, Swenson & Iglesias 1996). The nuclear reaction rates are the same as used by Bahcall & Pinsonneault (1995).

2.1 ν Eridani's position in the theoretical Hertzsprung–Russell diagram

The position of the star in the $\log T_{\rm eff}$–$\log L$ diagram is not very accurately known. Our temperature determination is based on Strömgren photometry and on the tabular data by Kurucz (1998). For L we use the *Hipparcos* parallax, Lutz–Kelker correction to the absolute magnitude (Lutz & Kelker 1973), and the bolometric correction from Kurucz's data. In this way we obtained the following numbers:

$$\log T_{\rm eff} = 4.346 \pm 0.011 \quad \text{and} \quad \log L = 3.94 \pm 0.15.$$

For $\log T_{\rm eff}$ we include measurement errors and uncertainty of calibration. For $\log L$ we take into account errors of the parallax and uncertainty of the bolometric correction. Our numbers are similar to those quoted by Dziembowski & Jerzykiewicz (2003) and will be updated by De Ridder et al. (2004).

2.2 Identification of the radial overtone of the observed modes

Before starting seismic modelling of ν Eri, we must complete the mode identification. The work by De Ridder et al. (2004) provided unambiguous ℓ identifications for seven modes, and m determinations by inference, but the radial overtone of the modes has not been determined. Fortunately, one of the detected pulsation modes is radial, which eases this task considerably.

Consequently, we follow Dziembowski & Jerzykiewicz (1996) and only consider two one-dimensional families of models. The position of ν Eri in the HR diagram is only consistent with the radial mode at 5.7634 cd^{-1} being the fundamental or the first overtone (as indicated later in Fig. 3). For these two possibilities, we examine the mass dependence of theoretical $\ell = 1$ mode frequencies of standard models and match it to the observed $\ell = 1$ mode frequencies (Fig. 2).

Because of the mixed-type character of some of the modes we can only match the observed frequencies of the two lowest-order

Table 1. Parameters of fitted models. The symbols denote : X_c – hydrogen abundance in the core, M_{mix} – mass of the mixed core, which is the same as mass of the convective core at $\alpha_{ov} = 0$, r_c – radius of the convective core, r_{c0} – radius of the convective core at ZAMS, which corresponds to the top of the μ-gradient zone.

$M/M_\odot$	α_{ov}	Z	age [Myr]	$\log T_{eff}$	$\log L$	$R/R_\odot$	$\log g$	X_c	M_{mix}/M	r_c/R	r_{c0}/R
9.858	0.0	0.015	15.7	4.3553	3.969	6.279	3.836	0.2414	0.189	0.117	0.186
9.179	0.1	0.015	18.9	4.3399	3.891	6.165	3.821	0.2555	0.211	0.121	0.185

$\ell = 1$ modes within certain mass ranges. However, under the assumption of the radial mode being the first overtone, no acceptable fit can be found for the $\ell = 1$ mode of highest frequency. Hence we can eliminate this possible identification (which would also be less consistent with the star's position in the HR diagram) and identify the radial pulsation mode of ν Eri as the fundamental. Consequently, the $\ell = 1$ modes are the first g mode (g_1) and the first two p modes (p_1 and p_2). We note that the theoretical fit of the standard model to the observed p_2 mode is also not very satisfactory at first glance; we will return to this problem and its possible solution later.

2.3 Fitting frequencies of the $\ell = 0$ and two $\ell = 1$, $m = 0$ modes

We calculated frequencies of these three modes in evolutionary sequences of stellar models characterized by the parameters M, Z, α_{ov}. The first two of them and T_{eff} were regarded as adjustable parameters to fit the measured frequencies. The adopted precision of the fit was 10^{-3}. The precision of the data is much higher but matching to such a precision is neither interesting nor reasonable in view of the uncertainties of the model calculations, such as the limited accuracy of the opacity data. The upper limit of the α_{ov} parameter was derived from the bounds on the effective temperature.

We obtained models with $\alpha_{ov} = 0.0$ and $\alpha_{ov} = 0.1$ which satisfy all the observational constraints. The inferred value of the metallicity parameter is $Z = 0.0150 \pm 0.0001$, the same at $\alpha_{ov} = 0.0$ and 0.1. Parameters of the two selected models are given in Table 1.

Both models are well within the error box in the theoretical HR diagram shown in Fig. 3. Increasing α_{ov} above 0.12 would place the

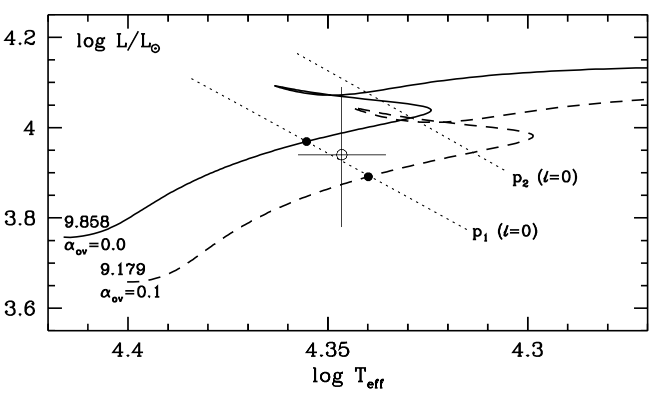

Figure 3. The evolutionary tracks for the models fitting frequencies of the ($\ell = 0$, p_1), ($\ell = 1$, g_1) and ($\ell = 1$, p_1) modes in ν Eri. Models were calculated with chemical composition parameters $Z = 0.015$ (adjusted) and $X = 0.7$ (fixed). The values of M and α_{ov} are indicated. The values of T_{eff} and $\log L$ inferred from photometry and the *Hipparcos* parallax are shown with the error bars. Two dotted lines connect models with 5.7633 c/d as the radial fundamental (p_1) and first overtone (p_2) mode.

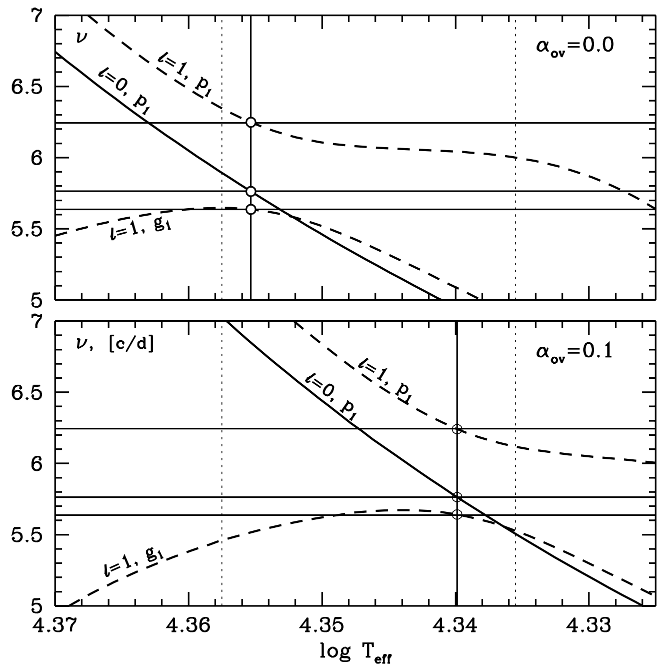

Figure 4. The evolution of the calculated frequencies of the selected modes in the model sequences shown in Fig. 2. Two dotted vertical lines mark the allowed T_{eff} range. Three horizontal lines correspond to the measured frequencies. Solid vertical lines correspond to T_{eff} for the fitted models. The fittings are marked by open circles. Note that the g_1 mode frequency comes close to the radial mode frequency in a very narrow range of T_{eff} and the location of this range is very sensitive to α_{ov}. Crossing of the two frequencies takes place at the point of the minimum frequency distance between the two $\ell = 1$ modes (avoided crossing). Before the avoided crossing, the ($\ell = 1$, p_1) mode is nearly a pure acoustic mode with its frequency evolution line being nearly parallel to the corresponding line for the radial mode. The ratio of the two frequencies depends on Z.

seismic model below the lower bound of T_{eff}. We, thus, conclude that the data on ν Eri are consistent with negligible overshooting distance and set an upper bound on it at $\alpha_{ov} = 0.12$. Further constraining the extent of overshooting may be possible when the effective temperature determination is improved. Our constraint is in agreement with $\alpha_{ov} = 0.10 \pm 0.05$ derived by Aerts et al. (2003) from frequency analysis for the β Cephei star HD 129929, which is also slowly rotating.

The frequency distance between the ($\ell = 1$, g_1) and ($\ell = 0$, p_1) modes is indeed a very sensitive probe of overshooting. This is illustrated in Fig. 4, where we show the evolution of the three mode frequencies as a function of T_{eff}. This is the main application of the ($\ell = 1$, g_1) mode. However, without the ($\ell = 1$, p_1) mode frequency the assessment of α_{ov} would not be possible unless we have an accurate observationally determined Z value, which we do not.

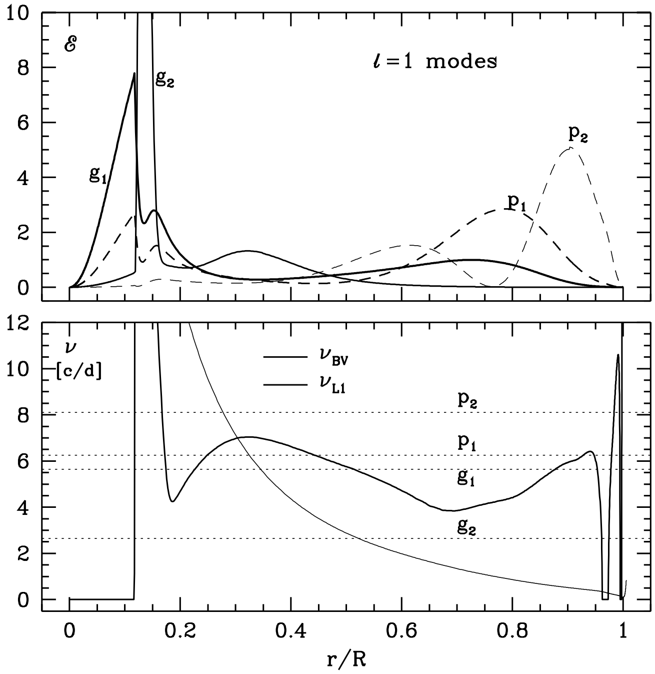

Figure 5. Upper panel: oscillation energy distribution, E, for low order $\ell = 1$ modes in the ν Eri model calculated with $\alpha_{\rm ov} = 0$. The plots are very similar in the models with $\alpha_{\rm ov} = 0.1$. Lower panel: the Brunt-Väisälä frequency, $\nu_{\rm BV}$, and the Lamb frequency at $\ell = 1$, $\nu_{\rm L1}$, in the same model.

2.4 Probing properties of low-order $\ell = 1$ modes

It is remarkable how much the three mode frequencies tell us about the internal structure of the star. Identification of a radial mode is important because its frequency yields an accurate constraint on the model parameters; however, much more interesting is the information contained in the $\ell = 1$ modes.

The probing property of a mode depends on the distribution of its oscillation energy, E, in the stellar interior. The plots in the upper panel of Fig. 5 show $\mathcal{E}$, the energy derivative with respect to the fractional radius, for the four consecutive $\ell = 1$ modes. In spite of rather close frequencies, modes g_1 and p_1 have a grossly different distribution of energy. This explains the differences in their evolution seen in Fig. 4 as well as the difference in the probing properties. One should also notice the peculiar $\mathcal{E}(r)$ dependence for the g_1 and p_1 modes in the deep interior. A maximum (absolute in the former and local in the latter case) is reached at the boundary of the convective core where the Brunt-Väisälä frequency has a derivative discontinuity. The g_2 and all higher order g modes have the maxima within the propagation zone. For our models it is the g_1 mode that has a frequency most sensitive to overshooting. In more evolved models this property will shift to p_1. Dziembowski & Pamyatnykh (1991) observed this property of certain low-order g modes, called by them g_c, in δ Scuti star models, and emphasized the importance of detecting such a mode in the context of the overshooting problem. ν Eri is the first object in which a g_c mode was definitely detected. More than that, its rotational splitting has been measured.

ν Eridani is not exceptional amongst β Cep stars, which are 9–12M$_\odot$ stars in the advanced main-sequence phase of evolution. In models of such stars we typically find that the ($\ell = 1$, g_1) and ($\ell = 1$, p_1) modes are both unstable. There are chances that they will be detected in a number of other stars of this type. The good luck in the case of ν Eri is that we capture it before the avoided crossing of the $\ell = 1$ modes. After it, the data on the modes yield much less orthogonal information.

3 INTERNAL ROTATION

3.1 The $\ell = 1$ triplets

The frequency structure of a rotationally split $\ell = 1$ mode may be characterized by the mean splitting $S = 0.5(\nu_{+1} - \nu_{-1})$ and the asymmetry $A = \nu_{-1} + \nu_{+1} - 2\nu_0$. If all effects of higher order in the angular rotation rate, Ω, as well as effects of a magnetic field are negligible, then $A = 0$. Both parameters, A and S, for the g_1 mode have been determined before the present campaign (Dziembowski & Jerzykiewicz 2003).

If we allow only an r dependence in Ω then

$$\nu_{\rm m} = \nu_0 + \frac{m}{2\pi}\int_0^R \frac{{\rm d}r}{R}\mathcal{K}\Omega + D_0 + m^2 D_1.$$

The rotational splitting kernel, $\mathcal{K}$, is given by

$$\mathcal{K} = \frac{(\xi_r^2 - 2\xi_r\xi_h + [\ell(\ell+1) - 1]\xi_h^2)r^2\rho}{\displaystyle\int_0^R \tfrac{{\rm d}r}{R}[\xi_r^2 + \ell(\ell+1)\xi_h^2]r^2\rho}, \qquad (1)$$

where ξ_r and ξ_h are defined by the following expression for the displacement eigenvector

$$\boldsymbol{\xi} = (\xi_r \boldsymbol{e}_r + \xi_h \nabla_h)Y_\ell^m.$$

The kernels for the two modes considered are shown in Fig. 6. The quantities D_0 and D_1 are quadratic in Ω. The asymmetry of the triplet arising from the quadratic effect of rotation is $2D_1$. The quantity D_0 represents the frequency shift of the $m = 0$ mode. As we have mentioned in Section 2.1, in principle, this shift should be subtracted from the measured frequencies of $m = 0$ modes when we fit frequencies calculated for a spherical model.

From the frequencies listed by Handler et al. (2004) for the g_1 mode we derive $S_{\rm g} = 1.69 \times 10^{-2}$ cd^{-1} (from here on we use subscript g to denote quantities referring to the g_1 mode, those referring to the p_1 mode will be subscribed with p), which is nearly the same as before (Dziembowski & Jerzykiewicz 2003). There is, however, a significant difference in the asymmetry for which the previous value was $A_{\rm g} = -7.1 \times 10^{-4}$ cd^{-1}, but from the most recent data we now determine a value which is by more than a factor of 2 smaller. The

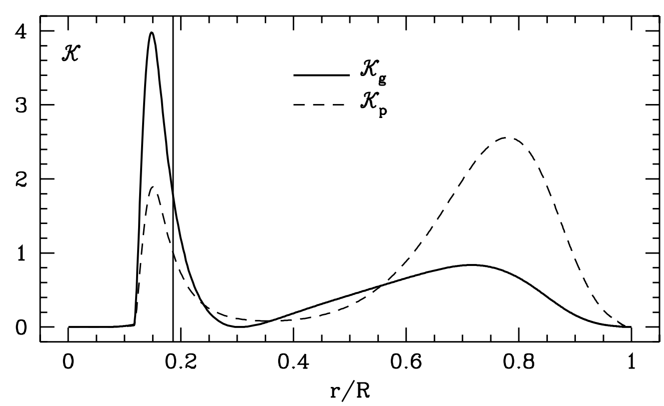

Figure 6. The rotational splitting kernel for the g_1 and p_1 modes in the model calculated with $\alpha_{\rm ov} = 0$. The vertical line at r_{c0}/R marks the top of the μ-gradient zone. Note the difference between K and E, shown in Fig. 5. Rotation within the convective core has hardly any effect on the $\ell = 1$ splitting.

former value was larger than calculated assuming uniform rotation with the rate inferred from S_g. Dziembowski & Jerzykiewicz (2003) considered two possible solutions. One was faster rotation in the envelope than in the interior, the second was a contribution to D_1 from a hypothetical magnetic field. The current data taken in a 158-d long campaign and their time distribution are insufficient for a precise determination of A_g. Thus we will not use this parameter here and we will not consider effects of a possible magnetic field. We will postpone interpretation of the A_g value until we have more precise determination from the future data analysis.

For the p_1 mode we have reliable frequencies only for the $m = 0$ and $+1$ components. The frequency of the $m = -1$ component may be estimated from the value of A_g, assuming that D_1 arises from the second order effect of rotation with the same rate for both modes. In this way we get (assuming A_g from earlier data that we regard as more reliable)

$$A_p = A_g \frac{D_{1,p}}{D_{1,g}} = -1.13 \times 10^{-3}\ \mathrm{cd}^{-1}$$

and

$$\nu_{-1,p} = 2\nu_{0,p} - \nu_{+1,p} + A_p = 6.2250\ \mathrm{cd}^{-1}.$$

We stress that choosing A_g from newer data or setting $A_g = 0$ will make very small difference. In a similar manner we find a frequency shift $D_{0,p} = 7 \times 10^{-4}$ for the $m = 0$ mode. The number is below the adopted precision of the frequency fit in our model construction. For the linear rotational frequency splitting we get

$$S_p = \nu_{+1,p} - \nu_{0,p} - 0.5A_p = 0.01797 + 0.00056 = 0.0185\ \mathrm{cd}^{-1}.$$

3.2 Rotation rate in the envelope and in the μ-gradient zone

Since we have data on rotational splitting only for two modes, our inference on the internal rotation must rely on simplifying assumptions. Results from seismic sounding of the solar internal rotation suggest that within chemically homogeneous radiative layers the rotation rate should be close to uniform. A possible steep gradient may occur only in the chemically inhomogeneous zone around the convective core, where the μ-gradient stabilizes differential rotation. With this in mind, we write

$$2\pi S_g = K_{c,g}\bar{\Omega}_c + K_{e,g}\bar{\Omega}_e$$

and

$$2\pi S_p = K_{c,p}\bar{\Omega}_c + K_{e,p}\bar{\Omega}_e,$$

where

$$K_{c,j} = \int_0^{r_{c0}} \frac{\mathrm{d}r}{R}\mathcal{K}_j, \qquad K_{e,j} = \int_{r_{c0}}^{R} \frac{\mathrm{d}r}{R}\mathcal{K}_j,$$

and $j \equiv p$ or g. In our fitted models we have

$$K_{c,g} = 0.187(0.168), \qquad K_{e,g} = 0.345(0.395),$$

$$K_{c,p} = 0.092(0.101), \qquad K_{e,p} = 0.718(0.682),$$

where numbers in brackets refer to the model calculated with $\alpha_{ov} = 0.1$. The results are nearly the same for both models. We find

$$\bar{\Omega}_c \approx 3\bar{\Omega}_e.$$

Fig. 6 shows the averaging kernels for Ω. The fact that the convective core virtually does not contribute to the splitting is an exclusive property of $\ell = 1$ modes which may be easily seen by considering the behaviour of eigenfunctions near the $r \to 0$ singularity. For finite $\boldsymbol{\xi}$ we have then $\xi_r \to \ell\xi_h$, implying (see equation 1) $\mathcal{K} \to 0$ if $\ell = 1$. Thus, the value $\bar{\Omega}_c$ refers only to the μ-gradient zone. It is clear that our result implies a very sharp decline of the rotation in the layer between the current core boundary and that at the zero-age main sequence (ZAMS) phase. How sharp the decline is depends on the form of the $\Omega(r)$ dependence. A factor $\sim$5 is derived if we assume a linear decrease of Ω between $r = r_c$ and r_{c0} and constant Ω for $r > r_{c0}$.

With this simple form of $\Omega(r)$ we find an equatorial velocity of rotation $v_e = 6.1$ km s^{-1}, which is 2/3 of the value inferred from S_g on the assumption of uniform rotation. Since the quadratic effect of rotation is still expected to arise mainly above $r = r_c$, we have a problem with accounting for the pre-campaign value of A_g. The values of the asymmetries calculated ignoring the contribution from below $r = r_{c0}$ are $A_g = -2.0 \times 10^{-4}$ and $A_p = -2.6 \times 10^{-4}$. The time for a new discussion of the triplet asymmetry will come when we have more precise frequencies of the modes in both triplets.

4 HOW THE MODES EXCITED IN ν ERI ARE DRIVEN

Oscillation driving in B-type stars seems rather well understood (see e.g. Pamyatnykh 1999). For low ℓ modes, theory predicts the occurrence of two instability domains within the main-sequence band. In models of stars with earlier spectral types (B1–B3) low order p and g modes are pulsationally unstable, as found in β Cep stars, and in stars with later spectral types (B4–B8) high-order g modes are predicted unstable, typically found in SPB stars. ν Eri is perhaps the first β Cep star where both kinds of modes are present (Handler et al. 2004). In the following, we assume that the 0.432 cd^{-1} signal in the light curves of ν Eri is an independent pulsation mode. There is a slight chance that it may be a combination signal, but its required order would be much higher than those of all the observed combination frequencies of similar amplitude. Thus we regard such an interpretation as highly unlikely.

In our fitted models we find unstable modes only in the 4.0–6.5 cd^{-1} frequency range. The instability measure, η, plotted in Fig. 7, is not a monotonic function of frequency. There is a noticeable maximum of the instability measure near $\nu = 0.5$ cd^{-1} for the $\ell = 1$ sequence and at somewhat higher frequency for $\ell = 2$. The existence of this maximum suggests that pulsational instability in this part of the eigenmode spectrum may be found upon some modification of our models.

Our proposal for extending the instability range is not original. We follow the idea of Charpinet et al. (1996, 1997) and Fontaine et al. (2003) that the combined effect of settling and radiative levitation may lead to significant overabundance of iron in the driving zone. Since we do not have a stellar evolution code treating these effects, we simply introduced an ad hoc factor 4 enhancement of the iron-group elements in the $\log T$ range 5.1–5.5 and matched it smoothly to the standard solar value outside. The result is shown in Fig. 7. We may see that, while an extension of the instability to higher order p modes is easy, obtaining instability in the high-order g-mode range is more difficult. We found unstable $\ell = 2$ g modes in the model calculated with $\alpha_{ov} = 0.1$, which is cooler, but only at $\nu \approx 0.8$ cd^{-1}. Because of the ad hoc nature of the proposed iron enhancement we regard these results merely as an indication of a direction where the solution of the driving problem of modes detected in ν Eri may be found. The proposal that the diffusion effects may play a role in this star seems not unreasonable in view of its very slow rotation which should not induce any appreciable mixing of elements and this is the first star where modes in such a broad

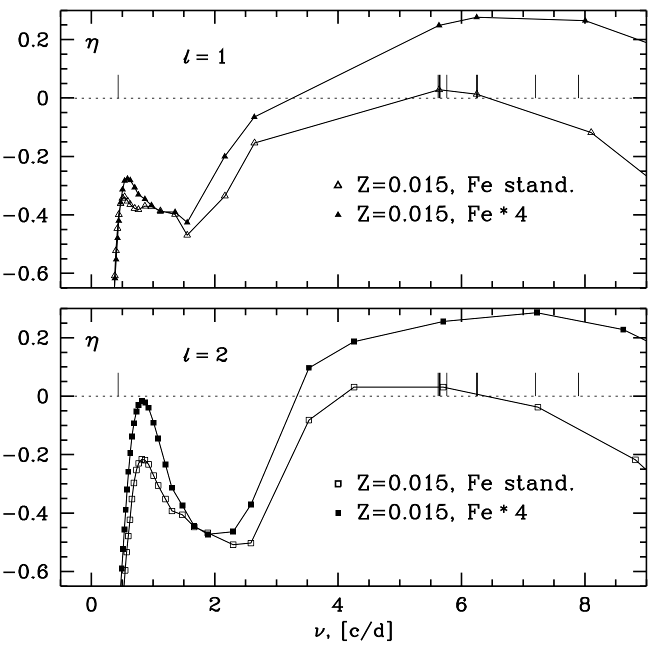

Figure 7. The instability measure, η, for $\ell = 1$ and $\ell = 2$ modes in a standard model calculated with $\alpha_{ov} = 0$ and in the corresponding model with the Fe enhancement in the driving zone. $\eta > 0$ for unstable modes. $\eta = -1$ if there is no active driving layer in the star for a particular mode and it is $+1$ if driving occurs in the whole interior. The position of the modes detected in ν Eri are marked with bars on the $\eta = 0$ axis.

frequency range were detected. However, slow rotation cannot be the sufficient condition for a broad-band excitation. In HD 129929, which is even a slower rotator, all modes detected so far are confined to the narrow frequency range of 6.45–7 cd^{-1}.

5 POSSIBLE IDENTIFICATION OF THE REMAINING MODES

Our manipulations on the Fe abundance in outer layers are not without consequences for mode frequencies and hence on the seismic model of ν Eri. It is not difficult to find a model with modified Fe that fits the three frequencies used in Section 2.1. The model cannot be very different; however, the frequencies of higher order p modes are more significantly changed.

Let us begin with the possible mode at $\nu = 0.432$ cd^{-1}. Though it is easier to find instability at higher degrees, the $\ell = 1$ identification seems more plausible because in this case the maximum of η occurs closer to the observed frequency. Assuming $\ell = 1$ and the rotational splitting the same as in the ($\ell = 1$, g_1) mode, we obtained 0.429 and 0.435 cd^{-1} for the frequency of the ($\ell = 1$, $m = -1$, g_{16}) mode in the models with $\alpha_{ov} = 0$ and 0.1, respectively. Thus, we regard such an identification for the $\nu = 0.432$ cd^{-1} peak as likely.

For the observed variation at $\nu = 7.20$ cd^{-1}, the only possible identification, regardless of the choice of α_{ov} and modification in the Fe abundance, is a mode of the ($\ell = 2$, p_0) quintuplet. In this case the effect of the Fe enhancement is more significant. The enhancement described in the previous section leads to a frequency decrease by 0.02, which is comparable with the rotational splitting. With this model the best fit is for $m = 1$, while with the standard models it is for $m = 2$.

The effect of the Fe enhancement increases with mode frequency. This is not surprising because the acoustic propagation zone expands to outer layers where the effect of the enhancement is largest. For the observed mode at $\nu = 7.90$ cd^{-1} we know the ℓ-value from photometry, and it is 1. In our standard seismic models the $\ell = 1$, p_2 modes have frequencies 8.10 and 8.03 cd^{-1} in models with $\alpha_{ov} = 0$ and 0.1, respectively. In this case, even with the freedom in choosing the m value we cannot reproduce the measured frequency. The frequency shift due to the Fe enhancement, which is about 0.1 cd^{-1}, brings the calculated frequencies close to the fit. We regard this fact as partial support for the proposed effect.

We note that fitting the frequencies of all the modes detected in the 5.6–7.9 cd^{-1} frequency range is possible in standard evolutionary models if one allows lower effective temperature and overshooting in the range $0.2 < \alpha_{ov} < 0.3$ (Ausseloos et al., in preparation).

6 CONCLUSIONS AND DISCUSSION

We believe that our seismic models of ν Eridani yield a good approximation to its internal structure and rotation but there is room for improvement and a need for a full explanation of mode driving. We did not fully succeed in the interpretation of the oscillation spectrum of ν Eridani with our standard evolutionary models and our linear non-adiabatic treatment of stellar oscillations. We fail to reproduce mode excitation in the broad frequency range, as observed, and to reproduce the frequency of the ($\ell = 1$, p_2) mode, associated with the highest frequency peak in the spectrum. We showed that both problems may be cured by allowing an enhancement of the iron abundance in the zone of the iron-opacity bump. The enhancement may result from effects of radiative levitation, as first proposed by Charpinet et al. (1996, 1997) to explain oscillations in sdB stars. Our proposal is based on models with an ad hoc iron enhancement in the bump zone and must be checked with use of stellar evolution codes that take into account effects of levitation and diffusion of chemical elements. We regard this as the most timely theoretical work aimed at the interpretation of ν Eridani.

The proposed modification concerns only the outer layers and has a small effect on models of the stellar interior and the frequencies of g and p_1 modes. Therefore we believe that our seismic models describe the deep internal structure of the star. These models reproduce frequencies of the fundamental radial modes and two $\ell = 1$ modes and have effective temperatures and luminosities within the measurement error box. Satisfactory models exist in a range of the overshooting parameter, α_{ov}= (0–0.12), which corresponds to the mass range (9.9–9.0) $M_\odot$, age range (16–20) Myr, and a fractional hydrogen depletion in the core range (0.34–0.38). Here the important finding is the upper limit for the extent of overshooting. There is a prospect for getting a more stringent constraint on α_{ov} with a more accurate determination of the star's effective temperature.

We believe that our most important finding concerns internal rotation. We presented evidence for a sharp decline of the rotation rate, Ω, through the μ-gradient zone, around the shrinking convective zone. With data on the splitting for only two $\ell = 1$ modes, our estimates had to rest on the assumed form of the $\Omega(r)$ dependence. Since a significant gradient of Ω is possible only in the μ-gradient zone, we adopted a constant Ω above it (rotation within the convective core has a negligible influence on the splitting). With this simplification we found that data require a decline by a factor $\sim$5 within the zone and an equatorial velocity of about 6 km s^{-1}. The second-order effect from this slow rotation in the envelope cannot account for the asymmetry of the ($\ell = 1$, g_1) triplet as determined from the pre-campaign data. Only with new observations we will be able to tell whether the problem is real. Our star is not the first

β Cephei star for which evidence for nonuniform rotation was put forward. However, we believe that in the ν Eri case the evidence is significantly stronger than in the case of HD 129929 (Aerts et al. 2003), because we relied on splitting data for modes having very different probing kernels.

ν Eridani proved to be a very important pulsating star. After the Sun, it so far is perhaps the most rewarding main-sequence object for asteroseismology. Many more modes were detected in several δ Scuti stars but in none of them have so many modes unambiguously been identified. This star deserves continued observational efforts. An extended data base is needed for precise determination of the frequencies of the modes in the $\ell = 1$ triplets. This is important for a more credible assessment of differential rotation. In this context it would be important to obtain a precise value of the projected equatorial velocity of rotation from spectroscopy. The best $v \sin i$ value currently available (Aerts et al. 2004) is higher than that of equatorial velocity inferred in this work which may however be in part due to the combined effects of pulsational and thermal line broadening.

ACKNOWLEDGMENTS

This work was supported by Polish KBN grants 5 P03D 012 20 and 5 P03D 030 20 and by the Austrian Fonds zur Förderung der wissenschaftlichen Forschung under grant R12-N02.

REFERENCES

Aerts C., Thoul A., Daszynska J., Scuflaire R., Waelkens C., Dupret M. A., Niemczura E., Noels A., 2003, Sci, 300, 1926
Aerts C. et al., 2004, MNRAS, 347, 463
Bahcall J. N., Pinsonneault M. H., 1995, Rev. Mod. Phys., 67, 781
Charpinet S., Fontaine G., Brassard P., Dorman B., 1996, ApJ, 471, L103
Charpinet S., Fontaine G., Brassard P., Chayer P., Rogers F. J., Iglesias C. A., Dorman B., 1997, ApJ, 483, L123
De Ridder J. et al., 2004, MNRAS, in press
Dziembowski W. A., Jerzykiewicz M., 1996, A&A, 306, 436
Dziembowski W. A., Jerzykiewicz M., 2003, in Balona L. A., Henrichs H. F., Medupe R., eds, ASP Conf. Ser. Vol. 305, Magnetic Fields in O, B and A stars: Origin and Connection to Pulsation, Rotation and Mass Loss. Astron. Soc. Pac., San Francisco, p. 319
Dziembowski W. A., Pamyatnykh A. A, 1991, A&A, 248, L11
Fontaine G., Brassard P., Charpinet S., Green E. M., Chayer P., Billeres M., Randall S. K., 2003, ApJ, 597, 518
Handler G. et al., 2004, MNRAS, 347, 454
Iglesias C. A., Rogers F. J., 1996, ApJ, 464, 943
Kurucz R. L., 1998, Grids of Model Atmospheres, http://kurucz.harvard.edu/grids.html
Lutz T. E., Kelker D. H., 1973, PASP, 85, 573
Pamyatnykh A. A, 1999, Acta Astron., 49, 119
Rogers F. J., Swenson F. J., Iglesias C. A., 1996, ApJ, 456, 902

This paper has been typeset from a TEX/LATEX file prepared by the author.

5.5 An asteroseismic study of the β Cephei star θ Ophiuchi: photometric results

Original paper:

G. Handler, R. R. Shobbrook, T. Mokgwetsi, 2005, MNRAS 362, 612

Mon. Not. R. Astron. Soc. **362,** 612–618 (2005) doi:10.1111/j.1365-2966.2005.09341.x

An asteroseismic study of the β Cephei star θ Ophiuchi: photometric results

G. Handler,[1★] R. R. Shobbrook[2] and T. Mokgwetsi[3]

[1]*Institut für Astronomie, Universität Wien, Türkenschanzstrasse 17, A-1180 Wien, Austria*
[2]*Research School of Astronomy and Astrophysics, Australian National University, Canberra, ACT, Australia*
[3]*Theoretical Astrophysics Programme, University of the North-West, Private Bag X2046, Mmabatho 2735, South Africa*

Accepted 2005 June 22. Received 2005 June 21; in original form 2005 March 25

ABSTRACT

We have carried out a three-site photometric campaign for the β Cephei star θ Oph from 2003 April to August. 245 h of differential photoelectric *uvy* photometry were obtained during 77 clear nights. The frequency analysis of our measurements has resulted in the detection of seven pulsation modes within a narrow frequency interval between 7.116 and 7.973 c d^{-1}. No combination or harmonic frequencies have been found. We have performed a mode identification of the individual pulsations from our colour photometry that shows the presence of one radial mode, one rotationally split $\ell = 1$ triplet and possibly three components of a rotationally split $\ell = 2$ quintuplet. We discuss the implications of our findings and point out the similarity of the pulsation spectrum of θ Oph to that of another β Cephei star, V836 Cen.

Key words: techniques: photometric – stars: early-type – stars: individual: θ Oph – stars: oscillations – stars: variables: other.

1 INTRODUCTION

Two recent ground-breaking studies have opened up the class of the β Cephei pulsators for asteroseismic investigations. For the star V836 Cen, Aerts et al. (2003, 2004a) acquired and analysed 21 yr of time-resolved Geneva photometry. They identified the six detected pulsation modes with their pulsational quantum numbers (the radial fundamental mode, an $\ell = 1$ triplet and two components of a rotationally split $\ell = 2$ mode). Consequent seismic modelling (Dupret et al. 2004) allowed the derivation of constraints on the position of the star in the Hertzsprung–Russell (HR) diagram and its convective core size, plus demonstrated that its interior rotation is not rigid.

A second β Cephei star, ν Eri, was studied with large photometric and spectroscopic multisite campaigns (Handler et al. 2004; Aerts et al. 2004b), yielding a total of almost 1200 h of measurement. The nine modes detected for this star were identified with the radial fundamental mode, two $\ell = 1$ triplets, one $\ell = 1$ singlet and one $\ell = 2$ mode (De Ridder et al. 2004). Seismic modelling (Pamyatnykh, Handler & Dziembowski 2004; Ausseloos et al. 2004) demonstrated that the pulsation spectrum of ν Eri cannot be reproduced with standard models, some convective core overshooting may be required and again non-rigid interior rotation must be present (with the edge of the convective core rotating about 3 times faster than the outer layers, consistent with the findings for V836 Cen). The seismic results indicate that it is possible that the interior chemical composition of the star is not homogeneous.

After some 15 years of frustration, asteroseismology of opacity-driven main-sequence pulsators has thus finally become reality. The reasons why some β Cephei stars are the first such objects to be studied may be summarized as follows: their pulsational mode spectra are sufficiently simple that few possibilities for erroneous or ambiguous mode identifications occur, yet the observed spectra are fairly complete; radial modes have been detected for the two above-mentioned stars (substantially reducing the number of possible seismic models); finally, the applied mode identification methods do work (e.g. see Handler et al. 2003).

The general astrophysical implications of seismic studies of the β Cephei stars are also highly interesting. Since these objects are main-sequence stars between 9 and 17 M$_\odot$ (Stankov & Handler 2005), they are progenitors of Type II supernovae, which in turn are largely responsible for the enrichment of the interstellar medium and thus for the chemical evolution of galaxies. Consequently, if we can trace the evolution of β Cephei stars by sounding their interiors in different evolutionary states, we not only are able to calibrate stellar structure and evolution calculations, but also could put constraints on the modelling of extragalactic stellar systems. Therefore it is highly desirable to determine the interior structure of several β Cephei stars.

One of the objects that seems well suited for an asteroseismic study is θ Oph. The variability of this bright ($V = 3.27$ mag) object has been known for a long time (Henroteau 1922), and the corresponding period determinations in the literature are partly controversial. Several authors (van Hoof & Blaauw 1958; van Hoof 1962; Briers 1971; Heynderickx 1992) noted variable shapes of their radial velocity and light curves, indicating multiperiodicity. However, no

★E-mail: handler@astro.univie.ac.at

consensus on the values of possible secondary and tertiary periods was reached.

Together with the presence of archival high-resolution spectroscopy (analysed in a companion paper by Briquet et al. 2005), the findings mentioned above made θ Oph an attractive target for a multisite study. Consequently, we carried out a photometric campaign on this star in mid-2003.

2 OBSERVATIONS AND REDUCTIONS

We acquired single-channel differential photoelectric photometry through the Strömgren *uvy* filters with three telescopes on three continents during the months of 2003 April to August. The measurements of θ Oph were obtained with respect to two comparison stars, 44 Oph (HD 157792, A3m, $V = 4.17$) and 51 Oph (HD 158643, A0 V, $V = 4.81$). Owing to the brightness of all three objects, some neutral density filters were applied to avoid damage of the photomultipliers. A short summary of the observations is given in Table 1. The total time base of our measurements is 124 d.

Data reduction was started by correcting for coincidence losses, sky background and extinction. Nightly extinction coefficients were determined with the Bouguer method or with the differential technique from the comparison stars (neither showed any variability during our measurements). As the comparison stars are considerably cooler than the variable, second-order colour extinction coefficients were also determined. We found colour extinction corrections to be necessary for the *u* data from Siding Spring Observatory (SSO) and the Automated Photometric Telescope (APT) and applied them correspondingly.

We then determined the mean u, v, y zero-points between the comparison star magnitudes and used them to combine the measurements of 44 and 51 Oph to a curve that was assumed to reflect the effects of transparency and detector sensitivity changes only. Consequently, these combined time series were binned into intervals that would allow good compensation for the above-mentioned non-intrinsic variations in the target star time series, and were subtracted from the measurements of θ Oph. The binning minimizes the introduction of noise in the differential light curve of the target.

The timings for this differential light curve were heliocentrically corrected as the next step. Finally, the photometric zero-points of the different sites, which may not be quite the same because of slightly different wavelength responses of the individual instrumental systems combined with the different colours of the variable and the comparison stars, were set to zero. The resulting final combined time series was subjected to frequency analysis; we show some of our light curves of θ Oph in Fig. 1. We note that the amplitude of the light variation is modulated, but its shape is not; it is always sinusoidal.

The accuracy of the differential light curves of the comparison stars was 4.8 mmag in the *u* filter, 4.3 mmag in *v* and 3.9 mmag in *y* per single data point. These rather high values are mostly caused by the high airmass of θ Oph and unstable weather conditions during the measurements at Fairborn Observatory.

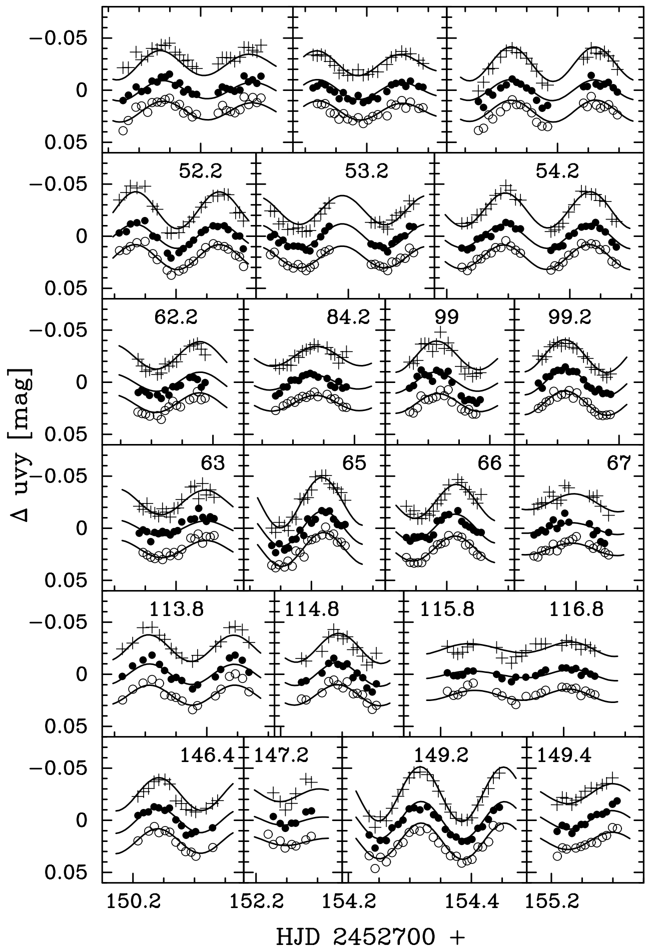

Figure 1. Some light curves of θ Oph. Plus signs are data in the Strömgren u filter, filled circles are our v measurements and open circles represent Strömgren y data. The full line is a fit composed of all the periodicities detected in the light curves (Table 2). The upper two panels are measurements from SSO, the middle two are from the APT and the lower two from the South African Astronomical Observatory (SAAO). The number of data shown here is about one-third of the total.

3 FREQUENCY ANALYSIS

Our frequency analyses were performed with the program PERIOD 98 (Sperl 1998). This package applies single-frequency power spectrum analysis and simultaneous multifrequency sine-wave fitting, and also includes advanced options.

Table 1. Log of the photometric measurements of θ Oph. Observatories are ordered according to geographical longitude.

Observatory	Longitude	Latitude	Telescope	Amount of data nights	h	points	Observer(s)
South African Astronomical Observatory (SAAO)	+20° 49′	−32° 22′	0.5-m	9	34.08	135	TM
Fairborn Observatory	−110° 42′	+31° 23′	0.75-m APT	44	106.68	662	–
Siding Spring Observatory (SSO)	+149° 04′	−31° 16′	0.6-m	24	104.35	506	RRS
Total				77	245.11	1303	

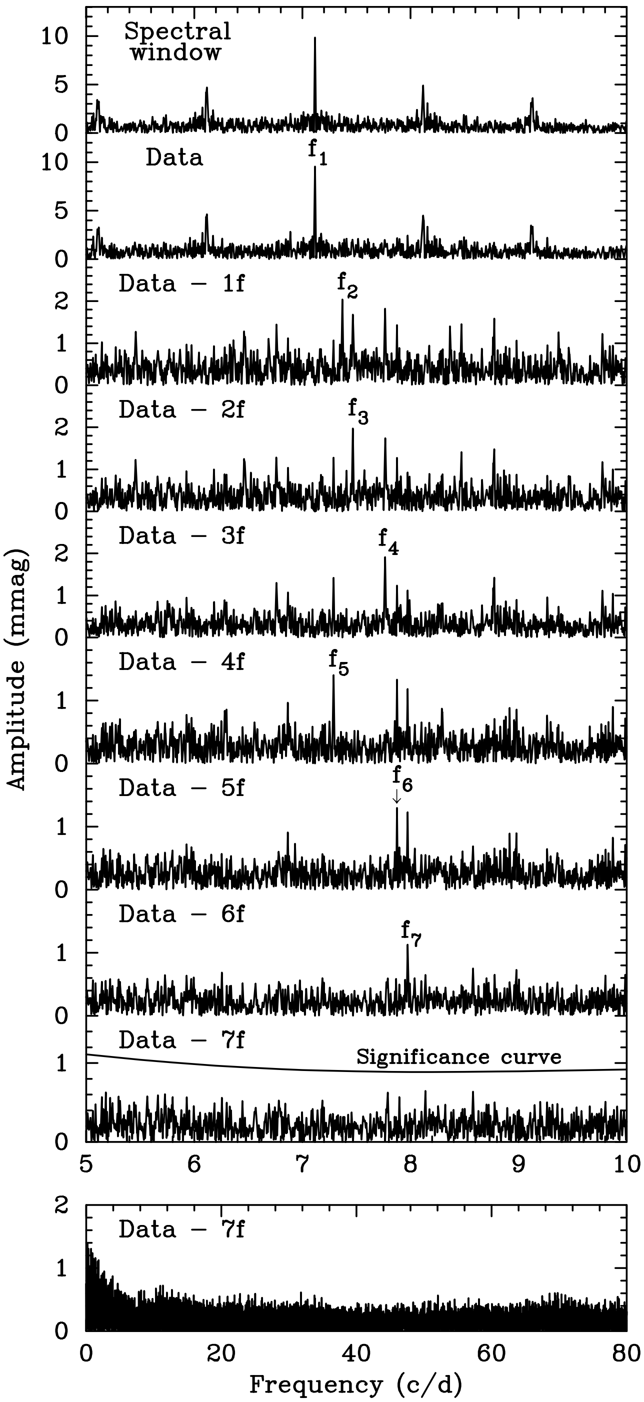

Figure 2. Amplitude spectra of θ Oph. The uppermost panel shows the spectral window of the data, followed by the periodogram of the data. Successive pre-whitening steps are shown in the following panels; note their different ordinate scales. The second lowest panel contains a significance curve; any peak to be regarded as real by us must exceed it. The lowest panel shows the residual amplitude spectrum in a wider frequency range, containing no evidence for further periodicities in our data.

We started by computing the Fourier spectral window of the final light curves in each of the filters. It was calculated as the Fourier transform of a single noise-free sinusoid with a frequency of 7.116 c d^{-1} (the strongest pulsational signal of θ Oph) and an amplitude of 10 mmag sampled in the same way as were our measurements. The upper panel of Fig. 2 contains the result for the y data. Any alias structures that would potentially mislead us into incorrect frequency determinations are reasonably low in amplitude because of our multisite coverage.

We proceeded by computing the amplitude spectra of the data itself (second panel of Fig. 2). The signal designated f_1 dominates. We pre-whitened it by subtracting a synthetic sinusoidal light curve with a frequency, amplitude and phase that yielded the smallest residual variance, and computed the amplitude spectrum of the residual light curve (third panel of Fig. 2).

This resulted in the detection of a second signal (f_2). We then pre-whitened a two-frequency fit from the data using the same optimization method as before, and continued this procedure (further panels of Fig. 2) until no significant peaks were left in the residual amplitude spectrum.

We consider an independent peak statistically significant if it exceeds an amplitude signal-to-noise ratio (S/N) of 4 in the periodogram (see Breger et al. 1993). The noise level was calculated as the average amplitude in a 5 c d^{-1} interval centred on the frequency of interest; the final detection limit corresponding to S/N = 4 is shown as a significance curve in the second lowest panel of Fig. 2.

We repeated the pre-whitening procedure with the u and v data independently and obtained the same frequencies within the observational errors. We then determined final values for the detected frequencies by averaging the values from the individual filters. The pulsational amplitudes were then recomputed with those frequencies. We regard this solution as representing our data set best; the result is listed in Table 2.

θ Oph has also been observed by the *Hipparcos* satellite (ESA 1997). We have reanalysed the corresponding photometry of the star and find a main frequency of 7.116 05 ± 0.000 02 c d^{-1} in these measurements, consistent with the result from our data within the errors. An analysis of our measurements combined with those by *Hipparcos* allows us to refine the value of the dominant frequency to 7.116 015 ± 0.000 002 c d^{-1}; aliases are outside the quoted errors for each individual determination. No amplitude variations of the strongest mode seem to have occurred between the *Hipparcos* measurements and ours; the other signals are not detected in the space-based photometry.

The residuals from the multifrequency solution in Table 2 were searched for additional candidate signals that may be intrinsic. We first investigated the residuals in the individual filters, then analysed the averaged residuals in the three filters (whereby the u data were divided by 1.5 to scale them to amplitudes and rms scatter similar to that in the other two filters), and found no evidence for additional significant periodicities in any case. The residuals between

Table 2. Multifrequency solution for our time-resolved photometry of θ Oph. The signals are ordered according to their frequencies, but labelled in the order of detection. Formal error estimates (following Montgomery & O'Donoghue 1999) are listed for the individual frequencies; formal errors on the amplitudes are ±0.20 mmag in u, ±0.18 mmag in v and ±0.16 mmag in y. The S/N quoted is for the y filter data.

ID	Freq. (c d^{-1})	u ampl. (mmag)	v ampl. (mmag)	y ampl. (mmag)	S/N
f_1	7.116 00 ± 0.000 08	12.7	9.2	9.4	41.4
f_5	7.2881 ± 0.0005	2.1	1.5	1.4	6.4
f_2	7.3697 ± 0.0003	3.6	2.9	2.4	10.8
f_3	7.4677 ± 0.0003	4.7	2.4	2.3	10.2
f_4	7.7659 ± 0.0003	3.4	2.3	2.1	9.7
f_6	7.8742 ± 0.0005	2.3	1.8	1.3	5.8
f_7	7.9734 ± 0.0005	2.4	1.6	1.2	5.6

light curve and fit are 5.2, 4.6 and 4.1 mmag per single *u*, *v* and *y* point, respectively, and are thus somewhat higher than the accuracy of the differential comparison star data, suggesting that additional, presently undetected, frequencies could be present.

We can now confront the results of our frequency analysis with those in the literature. The frequency of the dominant signal is consistent with all the earlier studies except Henroteau (1922), taking into account some slight (evolutionary?) frequency variability with respect to Brier's (1971) study. Concerning the remaining frequencies, we note that the resonance period of 0.137 255 d found by van Hoof (1962) is consistent with our signal f_5. On the other hand, none of the secondary or harmonic frequencies claimed by Heynderickx (1992) can be reconciled with our data. We suspect that this is due to the small number of data available to this author. Finally, we note that the *y* amplitude of our analysis is consistent with that in Heynderickx' (1992) Walraven *V* data, i.e. no amplitude variations seem to have occurred between the years 1987 and 2003.

4 MODE IDENTIFICATION

Our three-colour photometry gives us the possibility of deriving the spherical degree ℓ of the individual pulsation modes from an analysis of the colour amplitudes. This involves a comparison of the observed amplitudes with those predicted by models and first requires knowledge of the position of the star in the HR diagram.

However, θ Oph is not a single star. Besides its low-mass spectroscopic companion discovered by Briquet et al. (2005), it is also a speckle binary (McAlister et al. 1993). Shatsky & Tokovinin (2002) determined a *K* magnitude difference of 1.09 mag between the two components and argued that the companion to the β Cephei star (hereinafter called θ Oph A) is physical. From the standard relations by Koornneef (1983) we can infer that the speckle companion (hereinafter called θ Oph B) is 1.33 mag fainter in *V* and must thus be a B5 main-sequence star.

To determine the effective temperature and luminosity of θ Oph A, we must take the contribution of θ Oph B to the total light into account. We use the standard Strömgren photometry by Crawford, Barnes & Golson (1970), and adopt the mean *V* magnitude from the Lausanne Photometric data base (http://obswww.unige.ch/gcpd/gcpd.html, $V = 3.266$) for the system, and then reproduce it and the Strömgren c_1 index, which is a measure of the effective temperatures of the stars, with the help of the standard relations by Crawford (1978), and after dereddening. The results are shown in Table 3.

The observations are reasonably well matched, with the exception of the luminosity-sensitive β parameter. However, this is not a severe problem as we will derive the luminosity of the star from its parallax. We also note that β measurements by other authors are closer to our calculated results than to the results from Crawford et al. (1970).

The calibration by Napiwotzki, Schönberner & Wenske (1993) applied to the Strömgren indices listed in Table 3 then results in

Table 3. Johnson *V* magnitude and Strömgren colour indices of the θ Oph system.

	V	$b-y$	m_1	c_1	β
Observed	3.266	−0.092	0.089	0.104	2.617
Dereddened	3.223	−0.102	0.092	0.102	2.617
θ Oph A	3.546	−0.109	0.08	0.07	2.640
θ Oph B	4.876	−0.089	0.095	0.25	2.684
Combined	3.266	−0.104	0.083	0.105	2.650

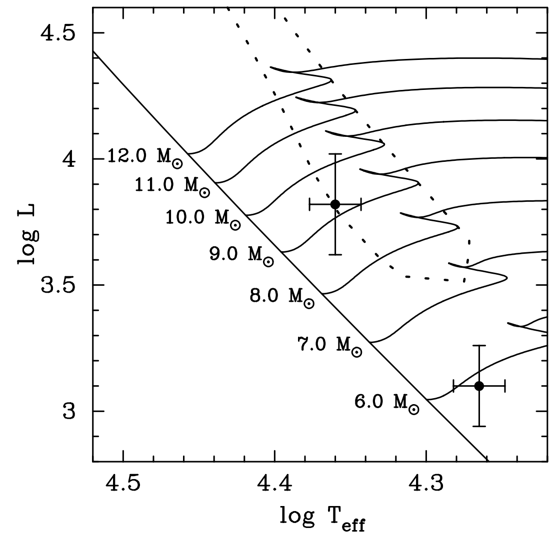

Figure 3. The positions of θ Oph A and θ Oph B in the theoretical HR diagram. Some stellar evolutionary tracks labelled with their masses (full lines) and the theoretical borders of the β Cephei star instability strip (Pamyatnykh 1999, dashed line) are included for comparison. All the theoretical results are for a metal abundance of $Z = 0.015$. θ Oph A is located within the instability strip, whereas θ Oph B is not.

$T_{\rm eff} = 22\,900 \pm 900$ K and $M_v = -2.5 \pm 0.5$ for θ Oph A, and $T_{\rm eff} = 18\,400 \pm 700$ K and $M_v = -1.3 \pm 0.5$ for θ Oph B. The analysis of *International Ultraviolet Explorer* spectra by Niemczura & Daszyńska-Daszkiewicz (2005) yielded $T_{\rm eff} = 22\,200 \pm 850$ K (consistent with the combined contribution of both system components), $\log g = 3.77$ and $[{\rm M/H}] = -0.15 \pm 0.12$. Finally, the *Hipparcos* parallax of the system (5.79 ± 0.69 mas) results in $M_v = -2.6 \pm 0.3$ for θ Oph A and $M_v = -1.3 \pm 0.3$ for θ Oph B, respectively, consistent with the result from Strömgren photometry. The tables by Flower (1996) then yield bolometric corrections of −2.2 and −1.7 mag, respectively, and thus $M_{\rm bol} = -4.8 \pm 0.5$ for θ Oph A as well as $M_{\rm bol} = -3.0 \pm 0.4$ for θ Oph B. We show the positions of the θ Oph components in the HR diagram derived in this way in Fig. 3. It becomes clear that the observed pulsations must originate from θ Oph A only.

To derive mode identifications for the pulsations of θ Oph A, we have computed theoretical colour amplitudes for modes of $0 \leqslant \ell \leqslant 4$ for models with masses between 8.5 and 10 $M_\odot$ (in steps of 0.5 $M_\odot$), effective temperatures in the range of $4.34 \leqslant \log T_{\rm eff} \leqslant 4.38$ and $Z = 0.015$. We first computed stellar evolutionary models by means of the Warsaw–New Jersey evolution and pulsation code (described, for instance, by Pamyatnykh et al. 1998). Then we derived the pulsational amplitudes of such models in the parameter space constrained above following Balona & Evers (1999). A range of theoretical frequencies of $6.5 \leqslant f \leqslant 8.5$ c d^{-1} was examined to allow for some non-radial mode splitting. Phase shifts between the light curves in the individual filters were not considered, as no such shifts were observationally found significant even at the 2σ level. We show a comparison of the observed and theoretical amplitude ratios of three modes in Fig. 4.

We note that we took the contribution of θ Oph B to the total light of the system into account when determining the observed amplitude ratios; we found that θ Oph B contributes some 23 per cent to the total flux in Strömgren *y*, 22 per cent in *v* and 19 per cent in *u*.

The reliability of the mode identifications in Fig. 4 is not easy to judge. Whereas the modes f_3 and f_4 can be identified with $\ell = 0$ and

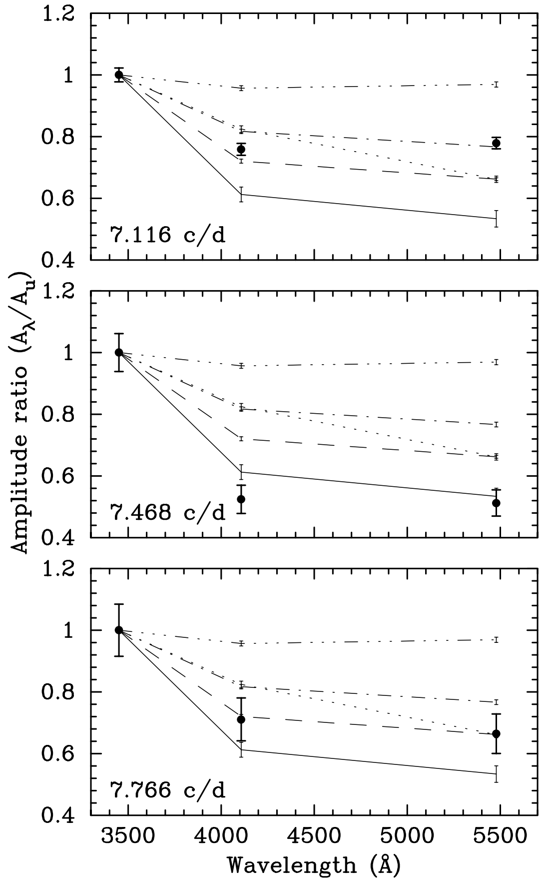

Figure 4. Observed and theoretical *uvy* amplitude ratios (lines) for three modes of θ Oph A and $0 \leqslant \ell \leqslant 4$. Amplitudes are normalized to unity at *u*. The filled circles with error bars are the observed amplitude ratios. The full lines are theoretical predictions for radial modes, the dashed lines are for dipole modes, the dot–dashed lines are for quadrupole modes, the dotted lines are for modes of $\ell = 3$ and the triple-dot–dashed lines are for $\ell = 4$. The small error bars denote the uncertainties in the theoretical amplitude ratios. The upper panel is for mode f_1, the middle one for f_3 and the lower one for f_4.

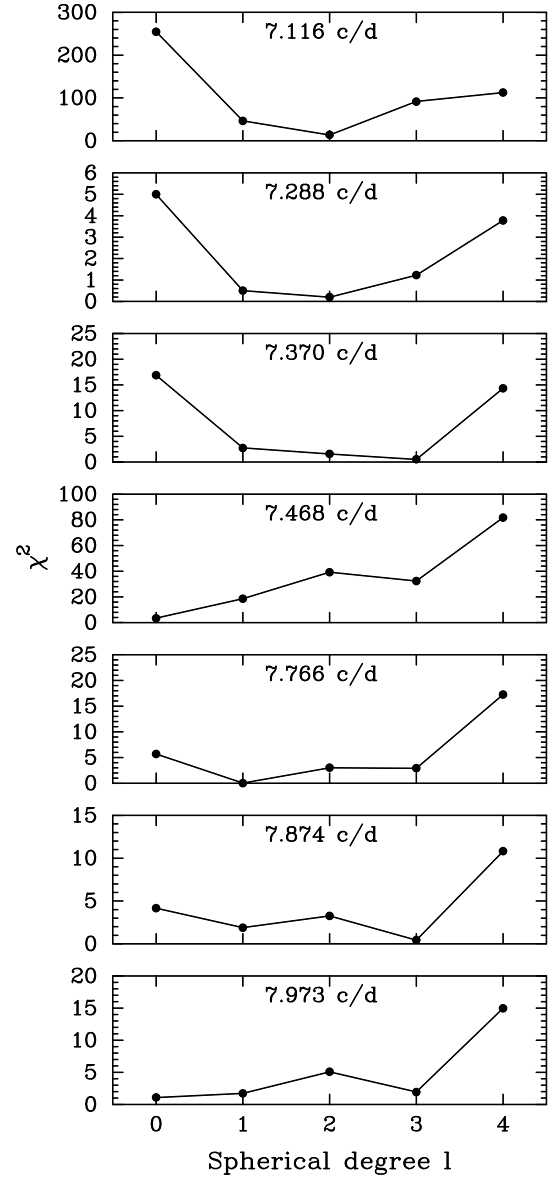

Figure 5. Mode typing for θ Oph A by means of the χ^2 method.

1, respectively, the situation is less clear for mode f_1 (upper panel of Fig. 4) where the u/v amplitude ratio points towards an $\ell = 1$ mode, but the u/y amplitude ratio suggests $\ell = 2$. Similar problems have been found for other modes that are not shown in this figure. We believe that the reason for these problems is a combination of several factors, for instance possible systematic errors in the determination of some of the pulsational amplitudes (which would be particularly severe in *u*), the uncertainties of the position of the star in the HR diagram, its poorly constrained surface metallicity [see Dupret et al. (2004) for a discussion of the latter], and the influence of the light of θ Oph B.

We have therefore chosen an alternative approach that appears more objective. We calculated the ratio of the individual *u*, *v*, *y* amplitudes with respect to their mean with the hope of compensating largely for systematic errors in the amplitude determinations. Then we compared these ratios to the theoretical ones treated in the same way by means of a χ^2 analysis, similar to Balona & Evers (1999) and Daszyńska-Daszkiewicz, Dziembowski & Pamyatnykh (2003), but disregarding the pulsational phases since they do, in our case, contain no information on the type of the modes as argued before. The behaviour of χ^2 depending on ℓ computed this way is shown in Fig. 5 for all modes.

Because of the systematic errors that may affect our mode identification, we believe that we cannot interpret the results in Fig. 5 in a strict statistical sense [i.e. by comparing the observational χ^2 values to the critical values of a $\chi^2(3)$ distribution and then assigning confidence levels to the derived mode identifications], but that we can use them to *eliminate* some ℓ values in the identification process. The ℓ assignments that we cannot rule out this way are listed in Table 4.

Our mode identifications are not very satisfactory at this point, but fortunately we can use other clues to constrain them further. First, since f_3 is clearly a radial mode, we can rule out that f_7 is also radial because the frequency ratio of these two modes ($f_3/f_7 = 0.9366$) is considerably larger than any period ratio of low-order radial modes in a β Cephei star can be.

Secondly, Heynderickx, Waelkens & Smeyers (1994) have identified f_1 as an $\ell = 2$ mode from their Walraven photometry. We have checked this identification with our method (again taking the contribution of θ Oph B to the total light into account) and also find

Table 4. Possible ℓ identifications of the individual modes of θ Oph A from our χ^2 analysis.

ID	Frequency (c d^{-1})	ℓ
f_1	7.116 00	2 or 1
f_5	7.2881	2, 1 or 3
f_2	7.3697	3, 2 or 1
f_3	7.4677	0
f_4	7.7659	1
f_6	7.8742	3 or 1
f_7	7.9734	0, 1 or 3

$\ell = 2$ to be clearly the best match between observed and theoretical colour amplitude ratios. Thirdly, Daszyńska-Daszkiewicz et al. (2002) demonstrated that modes of odd ℓ, starting with $\ell = 3$, suffer heavy geometric cancellation in photometric observations of β Cephei stars using filters. For instance, an $\ell = 3$ mode of the same intrinsic amplitude as an $\ell = 2$ mode will have only $\sim$1/10 of its photometric amplitude in the u, v, y filters. We therefore disregard all the possible $\ell = 3$ identifications in Table 4 as well.

Thus we have arrived at unique ℓ identifications for five of the seven modes that we detected: f_1 is $\ell = 2$, f_3 is radial, and f_4, f_6 and f_7 are all $\ell = 1$. f_2 and f_5 can be either $\ell = 1$ or 2. As the last step, we examine the frequency spectrum of θ Oph A (schematically plotted in Fig. 6) for the presence of structures that may be useful for further constraining the mode identifications.

Indeed, some interesting features can be discerned. The $\ell = 1$ modes f_4, f_6 and f_7 form a frequency triplet that is almost equally spaced. However, there is a slight asymmetry, and it is exactly in the sense expected for non-radial m-mode splitting due to the second-order effects of rotation. We therefore believe that f_4, f_6 and f_7 are indeed a rotationally split triplet of $\ell = 1$ modes.

The remaining four modes are also grouped together. Intriguingly, the spacing between f_2 and f_5 is approximately half the frequency difference of f_5 and the $\ell = 2$ mode f_1. Again, the asymmetry of this hypothesized f_1, f_5, f_2 multiplet is consistent with the second-order effects of rotation. f_3 does not fit this pattern, but this is not surprising as we have already identified it as a radial mode. The first-order rotational splitting obtained from the f_1, f_5, f_2 multiplet is similar to the splitting of the f_4, f_6 and f_7 triplet. Thus we suspect that f_1, f_5 and f_2 are part of a rotationally split $\ell = 2$ quintuplet with two components yet undetected.

Assuming that the mean splitting of the $\ell = 1$ triplet is a good approximation of the surface rotation frequency of θ Oph A (i.e. neglecting effects of the Coriolis force and possible differential internal rotation), we derive a rotation period of 9.6 d. The absolute magnitude and effective temperature of the star, as determined at the beginning of this section, result in a radius of 5.2 ± 1.3 R$_\odot$, and hence in a surface rotation velocity of 27 ± 7 km s^{-1}. As the measured projected rotational velocity of θ Oph A is about 30 km s^{-1} (e.g. Abt, Levato & Grosso 2002), there is a chance that we see the star close to equator-on.

5 AN ECLIPSING BINARY?

If we indeed saw θ Oph A equator-on, it can be suspected that the spectroscopic companion discovered by Briquet et al. (2005) may cause eclipses. The binary orbit derived by these authors leads to an ephemeris for the times of primary and secondary minimum, respectively. M. Briquet (private communication) predicts

$$t_{\mathrm{I}} = \mathrm{HJD}\ 245\,1811.002 + i \times 56.712,$$

$$t_{\mathrm{II}} = \mathrm{HJD}\ 245\,1834.599 + i \times 56.712,$$

where i is the number of orbital revolutions since epoch zero. Given the total mass of the spectroscopic binary system ($\sim$10 M$_\odot$), the orbital period and the radius of the primary determined above, we can also estimate the maximum duration of a possible eclipse, amounting to 17 ± 4 h.

Although we found no obvious evidence for eclipses in our photometric measurements, we folded our data according to this ephemeris and searched them again for possible eclipses. As it turns out, we have no measurements whatsoever during or even near the predicted times of primary minimum, which is not surprising given that our orbital coverage is only $\sim$17 per cent. We do have data around the expected times of secondary eclipse, but none is found, which is also not a surprise since the secondary of the spectroscopic binary would much less luminous than θ Oph A if we see the orbital plane (close to) edge-on, and consequently the depth of a secondary eclipse would be too small to be detected. We again conclude that there are no eclipses in our photometry of the θ Oph system.

6 DISCUSSION

Our photometric multisite campaign on the β Cephei star θ Oph resulted in the detection of seven independent pulsation modes. Our colour photometry that was intended for mode typing resulted in only two firm identifications, but we believe that this is mostly due to the small photometric amplitudes of all but one of the pulsation modes. However, also the strongest mode could not be unambiguously identified from our data; we had to invoke literature results.

Mode identification from colour photometry of β Cephei stars primarily rests on the amplitudes determined in the blue and ultraviolet ($\lambda < 4200$ Å). We have used a subset of the Strömgren filter system for our measurements as a compromise between wide availability and mode identification potential, with the drawback that the

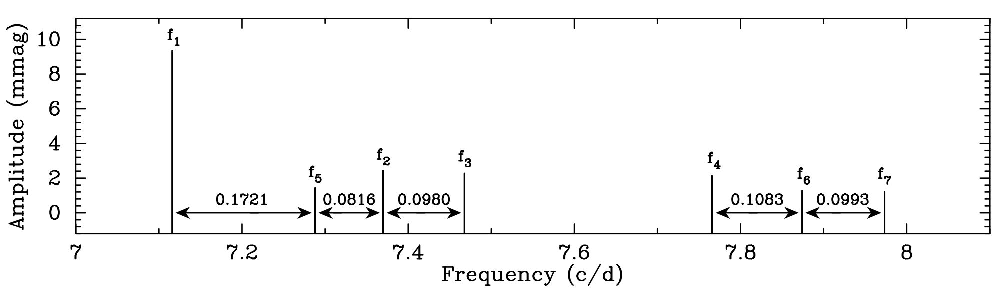

Figure 6. Schematic amplitude spectrum of θ Oph. The frequency differences between some of the modes are indicated.

identifications critically depend on the results in the u filter, which may be hard to verify. Consequently, any systematic error in the u measurements can heavily compromise the mode identifications.

The Walraven or the Geneva photometric systems would provide a solution to this dilemma, but they are unsuitable for multisite work since few observatories are equipped for their use. However, the pulsation spectrum of θ Oph A is reasonably simple and the range of excited frequencies is less than 1 c d^{-1}, so that an extensive single-site study of this star in one of these photometric systems should be sufficient to check the mode identifications at which we finally arrived by adding further constraints to the colour amplitude analysis.

We believe that our suggestion that f_1, f_5 and f_2 are part of a rotationally split $\ell = 2$ quintuplet can also be checked by theoretical model calculations. Since the asymmetry of the hypothesized multiplet due to the second-order effects of rotation has been measured to good relative accuracy, and since the rotation rate of the star is constrained by the f_4, f_6, f_7 triplet splitting, pulsational models should be able to reproduce the observed asymmetries if our identification of f_1, f_5 and f_2 is correct.

To perform a detailed asteroseismic study, one more ambiguity must then still be overcome: if f_1, f_5 and f_2 are $\ell = 2$ quintuplet members, their m values must be determined. From photometry alone, we cannot distinguish if they correspond to $m = (-2, 0, 1)$ or $m = (-1, 1, 2)$. However, the analysis of archival spectroscopy by Briquet et al. (2005) solves this ambiguity.

It is interesting to note that we found evidence that θ Oph A is seen close to equator-on (a result corroborated by Briquet et al. 2005). In such a configuration, the $m = 0$ component of $\ell = 1$ modes as well as the $|m| = 1$ components of $\ell = 2$ modes should suffer heavy geometric cancellation. However, such modes are apparently observed.

In any case, a seismic investigation of θ Oph A is possible. We note that we would not expect its outcome to be as fruitful as that for ν Eri (Pamyatnykh et al. 2004; Ausseloos et al. 2004) since fewer radial overtones of modes are excited, but the general applicability of earlier results could be tested. In addition, the detection of a possible eclipse of the primary would help to constrain the system parameters even more tightly, which can in turn assist the seismic modelling.

Finally, we would like to point out that the frequency structure of θ Oph A is remarkably similar to that of V836 Cen (Aerts et al. 2004a): a radial mode close to an incomplete $\ell = 2$ multiplet of somewhat lower frequency and a complete $\ell = 1$ triplet of higher frequency, and all modes are contained in a very narrow frequency interval (which is of extremely similar size in the co-rotating frame). The only differences are the somewhat higher pulsation frequencies of θ Oph A and its faster rotation. We thus speculate that once more pulsation spectra of β Cephei stars become known in detail, important clues on mode excitation can be gathered.

ACKNOWLEDGMENTS

This work has been supported by the Austrian Fonds zur Förderung der wissenschaftlichen Forschung under grant R12-N02. GH thanks Maryline Briquet for sharing her results prior to publication, Conny Aerts for sending a copy of R. Briers' dissertation, Jagoda Daszyńska-Daszkiewicz for supplying some unpublished information and for comments on a draft version of this paper, and Alosha Pamyatnykh for supplying theoretical instability strip borders for $Z = 0.015$, as well as Luis Balona and Wojtek Dziembowski and his group for permission to use their computer codes.

REFERENCES

Abt H. A., Levato H., Grosso M., 2002, ApJ, 573, 359
Aerts C., Thoul A., Daszyńska J., Scuflaire R., Waelkens C., Dupret M. A., Niemczura E., Noels A., 2003, Sci, 300, 1926
Aerts C. et al., 2004a, A&A, 415, 241
Aerts C. et al., 2004b, MNRAS, 347, 463
Ausseloos M., Scuflaire R., Thoul A., Aerts C., 2004, MNRAS, 355, 352
Balona L. A., Evers E. A., 1999, MNRAS, 302, 349
Breger M. et al., 1993, A&A, 271, 482
Briers R. C., 1971, PhD thesis, Katholieke Universiteit Leuven
Briquet M., Lefever K., Uytterhoeven K., Aerts C., 2005, MNRAS, in press (doi:10.1111/j.1365-2966.2005.09287.x) (this issue)
Crawford D. L., 1978, AJ, 83, 48
Crawford D. L., Barnes J. V., Golson J. C., 1970, AJ, 75, 624
Daszyńska-Daszkiewicz J., Dziembowski W. A., Pamyatnykh A. A., Goupil M.-J., 2002, A&A, 392, 151
Daszyńska-Daszkiewicz J., Dziembowski W. A., Pamyatnykh A. A., 2003, A&A, 407, 999
De Ridder J. et al., 2004, MNRAS, 351, 324
Dupret M.-A., Thoul A., Scuflaire R., Daszyńska-Daszkiewicz J., Aerts C., Bourge P.-O., Waelkens C., Noels A., 2004, A&A, 415, 251
ESA, 1997, ESA SP-1200, The *Hipparcos* and Tycho catalogues. ESA, Noordwijk
Flower P. J., 1996, ApJ, 469, 355
Handler G., Shobbrook R. R., Vuthela F. F., Balona L. A., Rodler F., Tshenye T., 2003, MNRAS, 341, 1005
Handler G. et al., 2004, MNRAS, 347, 454
Henroteau F., 1922, Publ. Dom. Obs. Ottawa, 8, 1
Heynderickx D., 1992, A&AS, 96, 207
Heynderickx D., Waelkens C., Smeyers P., 1994, A&AS, 105, 447
Koornneef J., 1983, A&A, 128, 84
Künzli M., North P., Kurucz R. L., Nicolet B., 1997, A&AS, 122, 51
McAlister H., Mason B. D., Hartkopf W. I., Shara M. M., 1993, AJ, 106, 1639
Montgomery M. H., O'Donoghue D., 1999, Delta Scuti Star Newsl. (Univ. Vienna), 13, 28
Napiwotzki R., Schönberner D., Wenske V., 1993, A&A, 268, 653
Niemczura E., Daszyńska-Daszkiewicz J., 2005, A&A, 433, 659
Pamyatnykh A. A., 1999, Acta Astron., 49, 119
Pamyatnykh A. A., Dziembowski W. A., Handler G., Pikall H., 1998, A&A, 333, 141
Pamyatnykh A. A., Handler G., Dziembowski W. A., 2004, MNRAS, 350, 1022
Shatsky N., Tokovinin A., 2002, A&A, 382, 92
Sperl M., 1998, Master's thesis, Univ. of Vienna
Stankov A., Handler G., 2005, ApJS, 158, 193
van Hoof A., 1962, Z. Astrophys., 54, 255
van Hoof A., Blaauw A., 1958, ApJ, 128, 273

This paper has been typeset from a TEX/LATEX file prepared by the author.

5.6 Asteroseismology of the β Cephei star 12 (DD) Lacertae: photometric observations, pulsational frequency analysis and mode identification

Original paper:

G. Handler, M. Jerzykiewicz, E. Rodriguez, K. Uytterhoeven, P. J. Amado, T. N. Dorokhova, N. I. Dorokhov, E. Poretti, J.-P. Sareyan, L. Parrao, D. Lorenz, D. Zsuffa, R. Drummond, J. Daszyńska-Daszkiewicz, T. Verhoelst, J. De Ridder, B. Acke, P.-O.Bourge, A. I. Movchan, R. Garrido, M. Paparó, T. Sahin, V. Antoci, S. N. Udovichenko, K. Csorba, R. Crowe, B. Berkey, S. Stewart, D. Terry, D. E. Mkrtichian, C. Aerts, 2006, MNRAS 365, 327

Mon. Not. R. Astron. Soc. **365,** 327–338 (2006) doi:10.1111/j.1365-2966.2005.09728.x

Asteroseismology of the β Cephei star 12 (DD) Lacertae: photometric observations, pulsational frequency analysis and mode identification

G. Handler,[1⋆] M. Jerzykiewicz,[2] E. Rodríguez,[3] K. Uytterhoeven,[4,5] P. J. Amado,[3] T. N. Dorokhova,[6] N. I. Dorokhov,[6] E. Poretti,[7] J.-P. Sareyan,[8] L. Parrao,[9] D. Lorenz,[1] D. Zsuffa,[10] R. Drummond,[4] J. Daszyńska-Daszkiewicz,[2,4] T. Verhoelst,[4] J. De Ridder,[4] B. Acke,[4] P.-O. Bourge,[11] A. I. Movchan,[6] R. Garrido,[3] M. Paparó,[10] T. Sahin,[12,13] V. Antoci,[1] S. N. Udovichenko,[6] K. Csorba,[10] R. Crowe,[14] B. Berkey,[14] S. Stewart,[14] D. Terry,[14] D. E. Mkrtichian[6,15] and C. Aerts[4]

[1]*Institut für Astronomie, Universität Wien, Türkenschanzstrasse 17, A-1180 Wien, Austria*
[2]*Wroclaw University Observatory, ul. Kopernika 11, 51-622 Wroclaw, Poland*
[3]*Instituto de Astrofisica de Andalucia, C.S.I.C., Apdo. 3004, 18080 Granada, Spain*
[4]*Instituut voor Sterrenkunde, K. U. Leuven, Celestijnenlaan 200B, B-3001 Leuven, Belgium*
[5]*Mercator Telescope, Calle Alvarez de Abreu 70, 38700 Santa Cruz de La Palma, Spain*
[6]*Astronomical Observatory of Odessa National University, Marazlievskaya, 1v, 65014 Odessa, Ukraine*
[7]*INAF-Osservatorio Astronomico di Brera, Via Bianchi 46, 23807 Merate, Italy*
[8]*Observatoire de la Côte d'Azur, Département GEMINI – UMR 6203, BP 4229, 06304 Nice Cedex 4, France*
[9]*Instituto de Astronomia UNAM, Apartado 70-264, C. U. 04510 Mexico D. F., Mexico*
[10]*Konkoly Observatory, Box 67, H-1525 Budapest XII, Hungary*
[11] *Institut d'Astrophysique et de Géophysique, Université de Liège, allée du Six Août 17, 4000 Liège, Belgium*
[12] *Physics Department, Akdeniz University, 07058 Antalya, Turkey*
[13] *Armagh Observatory, College Hill, Armagh BT61 9DG, Northern Ireland*
[14]*Department of Physics and Astronomy, University of Hawaii – Hilo, 200 West Kawili Street, Hilo, Hawaii 96720-4091, USA*
[15]*ARCSEC, Sejong University, Seoul 143-747, Korea*

Accepted 2005 October 10. Received 2005 October 5; in original form 2005 September 2

ABSTRACT

We report a multisite photometric campaign for the β Cephei star 12 Lacertae. 750 h of high-quality differential photoelectric Strömgren, Johnson and Geneva time-series photometry were obtained with nine telescopes during 190 nights. Our frequency analysis results in the detection of 23 sinusoidal signals in the light curves. Ten of those correspond to independent pulsation modes, and the remainder are combination frequencies. We find some slow aperiodic variability such as that seemingly present in several β Cephei stars. We perform mode identification from our colour photometry, derive the spherical degree ℓ for the five strongest modes unambiguously and provide constraints on ℓ for the weaker modes. We find a mixture of modes of $0 \leqslant \ell \leqslant 4$. In particular, we prove that the previously suspected rotationally split triplet within the modes of 12 Lac consists of modes of different ℓ; their equal frequency splitting must thus be accidental.

One of the periodic signals we detected in the light curves is argued to be a linearly stable mode excited to visible amplitude by non-linear mode coupling via a 2:1 resonance. We also find a low-frequency signal in the light variations whose physical nature is unclear; it could be a parent or daughter mode resonantly coupled. The remaining combination frequencies are consistent with simple light-curve distortions.

The range of excited pulsation frequencies of 12 Lac may be sufficiently large that it cannot be reproduced by standard models. We suspect that the star has a larger metal abundance in the pulsational driving zone, a hypothesis also capable of explaining the presence of β Cephei stars in the Large Magellanic Cloud.

⋆E-mail: handler@astro.univie.ac.at

Key words: techniques: photometric – stars: early-type – stars: individual: 12 (DD) Lacertae – stars: oscillations – stars: variables: other.

1 INTRODUCTION

12 (DD) Lacertae (hereafter briefly called 12 Lac) is one of the best-observed β Cephei stars, a class of variable early B-type stars whose light and radial velocity changes are due to gravity and pressure-mode pulsations of low radial order (Stankov & Handler 2005, and references therein). Radial velocity variations of 12 Lac were discovered nearly 100 years ago (Adams 1912) and light variations were detected soon thereafter (Stebbins 1917; Guthnick 1919).

After the recognition of the pulsational nature of the light variations of the β Cephei stars (Ledoux 1951) and because of the complicated nature of the variability of 12 Lac, the star became the target of one of the first worldwide observing campaigns (de Jager 1963), also called *The International Lacerta weeks*, during which a total of more than 700 h of time-resolved photometric and spectroscopic measurements were secured – back in 1956.

The photometric measurements obtained during this prototype multisite campaign were analysed by Barning (1963) who discovered four different variations in the light curves (one of them spurious). Jerzykiewicz (1978) provided an extensive re-analysis of these and some other data and proved the existence of five independent periodicities and one combination frequency in the data.

High-resolution spectroscopic observations of 12 Lac, confirming the six photometric frequencies, were carried out by Mathias et al. (1994). However, attempts to identify the underlying pulsation modes by spectroscopic means were unsuccessful due to the complicated behaviour of the star, and earlier mode identification results (e.g. the pioneering work by Smith 1980) could neither be confirmed nor rejected.

The most striking feature within the pulsation frequencies of 12 Lac is an equally spaced triplet at 5.179, 5.334 and 5.490 cd^{-1}. Owing to the narrowness of the interval these three frequencies span, it is clear that at least two of the underlying modes must be non-radial and it is straightforward to speculate that all are actually components of a rotationally split multiplet.

Because of this interesting possibility and because 12 Lac has been for a long time the β Cephei star with the largest number of known pulsation modes, it is an attractive target for asteroseismic investigations, i.e. deriving the interior structure of the star by modelling its pulsation frequencies. Dziembowski & Jerzykiewicz (1999) carried out such a study. They could only reproduce the equally spaced triplet with an $\ell = 2$ f-mode, and solely for models with specific values of temperature and surface gravity. The authors suggested that non-linear phase-lock could provide a way out of this dilemma.

Another intriguing possibility for interpreting the pulsation spectrum of 12 Lac that was not previously realized is that the ratio of the lowest pulsation frequency of the star (4.241 cd^{-1}) to that of another frequency at 5.490 cd^{-1} is perfectly consistent with the expected frequency ratio of the radial fundamental and first overtone modes. If such an interpretation were correct, it would be rather easy to perform seismic model computations, especially if more modes could be observationally detected. The problem with the equally spaced triplet would vanish as well because one of the suspected multiplet members would in fact be a radial mode.

Clearly, the interpretation of the pulsation spectrum of 12 Lac can potentially be extremely rewarding. Another observational effort similar to *The International Lacerta weeks*, with modern observing methods, seemed therefore quite worthwhile. In particular, new observations would be required to provide unique mode identifications for at least the five known pulsation modes for seismic modelling to commence. The discovery of additional low-amplitude pulsations would of course allow more insights into the interior structure of the star as well.

As recent observing campaigns have revealed many low-amplitude pulsation modes for some β Cephei stars [e.g. see Aerts et al. (2004) for V836 Cen; Jerzykiewicz et al. (2005) and references therein for ν Eridani; and Handler, Shobbrook & Mokgwetsi (2005) for θ Ophiuchi], it only seemed logical to organize a similar effort for 12 Lac. We have therefore carried out a multisite campaign for the star with both photometric and spectroscopic techniques. In addition, the closeby eclipsing binary β Cephei star 16 (EN) Lac was observed photometrically at the same time. Whereas we postpone the analysis of the latter star and that of the spectroscopy to forthcoming papers, we report here the results of the photometric measurements of 12 Lac.

2 OBSERVATIONS AND REDUCTIONS

Our photometric observations were carried out at nine different observatories with small- to medium-sized telescopes on three different continents (see Table 1). In most cases, single-channel differential photoelectric photometry was acquired; some additional CCD measurements turned out not to be useful. Wherever possible, the Strömgren *uvy* filters were used.

However, at the Sierra Nevada (OSN) and San Pedro Martir (SPM) Observatories simultaneous *uvby* photometers were available, including the *b* filter as well. On the other hand, the *u* data from SPM were unusable. At four other observatories where no Strömgren filters were available we used Johnson *V*. Finally, as the photometer at the Mercator telescope has Geneva filters installed permanently, we used this filter system.

We chose the two 'classical' comparison stars for 12 and 16 (EN) Lac: 10 Lac (O9V, $V = 4.88$) and 2 And (A3Vn, $V = 5.09$). Another check star, HR 8708 (A3Vm, $V = 5.81$), was additionally observed during one of the SPM runs.

Data reduction was begun by correcting for coincidence losses, sky background and extinction. Whenever possible, nightly extinction coefficients were determined with the differential Bouguer method (fitting a straight line to a plot of differential magnitude versus differential airmass) from the measurements of the two comparison stars. Second-order colour extinction coefficients were also determined and used to adjust the measurements of 2 And, which suffers lower extinction because it is redder than the other stars. On some nights, the coefficients were derived from 10 Lac with the usual Bouguer method.

It turned out that 2 And is a low-amplitude δ Scuti variable. Light variations of this star have already been strongly suspected by Sareyan et al. (1997). We will discuss these variations in the forthcoming paper devoted to 16 (EN) Lac because 2 And was mostly

Table 1. Log of the photometric measurements of 12 Lac. Observatories are ordered according to geographical longitude.

Observatory	Longitude	Latitude	Telescope	Amount of data		Filter(s)	Observer(s)
				Nights	h		
Sierra Nevada Observatory	−3°23′	+37°04′	0.9 m	18	81.2	*uvby*	ER, PJA, RG
Mercator Observatory	−17°53′	+28°46′	1.2 m	45	123.9	Geneva	KU, RD, JDD, TV JDR, BA, POB
Fairborn Observatory	−110°42′	+31°23′	0.75 m APT	55	201.5	*uvy*	–
Lowell Observatory	−111°40′	+35°12′	0.5 m	19	97.3	*uvy*	MJ
San Pedro Martir Observatory	−115°28′	+31°03′	1.5 m	20	102.7	*uvby*	EP, JPS, LP
Mt. Dushak-Erekdag Observatory	+57°53′	+37°55′	0.8 m	13	70.7	*V*	TND, NID
Tübitak National Observatory	+30°20′	+36°50′	0.5 m	1	2.5	*V*	TS
Mayaki Observatory	+30°17′	+46°24′	0.5 m	6	13.3	*V*	AIM
Piszkéstetõ Observatory	+19°54′	+47°55′	0.5 m	13	56.7	*V*	MP, DZ, DL, VA
Total				190	749.8		

used as the main-comparison star for the latter β Cephei star in the past. For the purpose of the present work, let it suffice to say that we only found evidence for a single periodicity in our light curves of 2 And. No evidence for photometric variability of 10 Lac was found.

We thus proceeded by pre-whitening the variability of 2 And with a fit determined from all its differential magnitudes relative to 10 Lac from the individual nights of measurement. The residual magnitudes of 2 And were then combined with the 10 Lac data into a curve that was assumed to reflect the effects of transparency and detector sensitivity changes only. Consequently, these combined time-series were binned into intervals that would allow good compensation for the above-mentioned non-intrinsic variations in the target star time-series and were subtracted from the measurements of 12 Lac. The binning minimizes the introduction of noise in the differential light curve of the targets.

The timings for the differential light curves were helio centrically corrected as the next step and the single-colour measurements were binned to sampling intervals similar to that of the multicolour measurements to avoid unwanted implicit weighting effects. Finally, the photometric zero-points of the different instruments were compared between the different sites and adjusted if necessary. Measurements in the Strömgren y and Johnson and Geneva V filters were treated as equivalent due to the same effective wavelength of these filters,

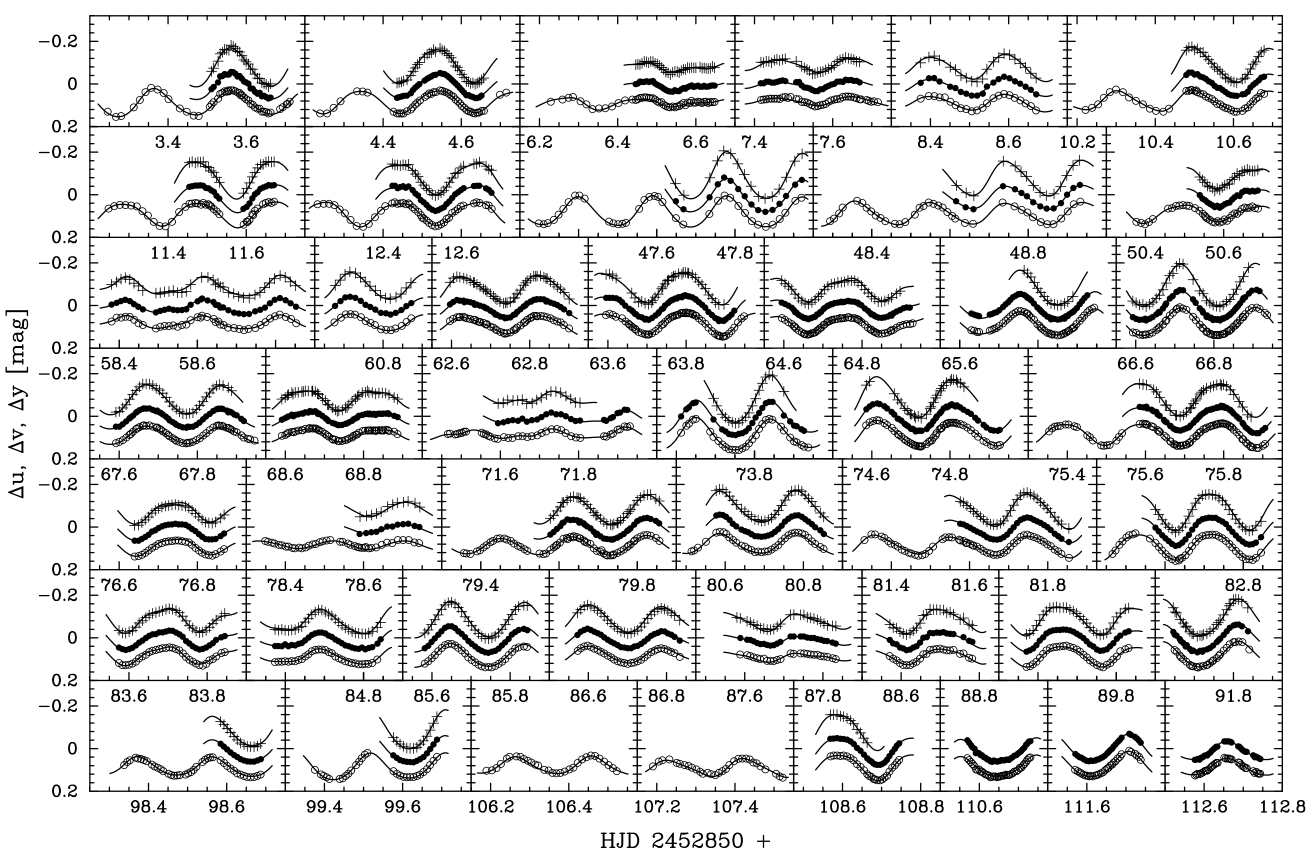

Figure 1. Some of our observed light curves of 12 Lac. Plus signs are data in the Strömgren u filter, filled circles are our v measurements and open circles represent the V data. The full line is a fit composed of the 23 periodicities detected in the light curves (Table 2). The amount of data displayed is about half the total.

and were analysed together. This combined light curve is henceforth referred to as 'the *V* filter data'.

The resulting final combined time-series was subjected to frequency analysis; we show some of our light curves of 12 Lac in Fig. 1. In the end, we had 3239 *V* filter measurements available (time-span 197.0 d), 2301 points in Strömgren *v* (time-span 179.2 d), 1739 points in Strömgren *u* (time-span 179.2 d) and 488 points in the Geneva filters (time-span 173.8 d)

3 FREQUENCY ANALYSIS

Our frequency analysis was mainly performed with the program PERIOD98 (Sperl 1998). This package applies single-frequency power spectrum analysis and simultaneous multi-frequency sine-wave fitting. It also includes advanced options such as the calculation of optimal light-curve fits for multiperiodic signals including harmonic, combination and equally spaced frequencies. As will be demonstrated later, our analysis requires some of these features.

We started by computing the Fourier spectral window of the *V* filter data. It was calculated as the Fourier transform of a single noise-free sinusoid with a frequency of 5.179 cd^{-1} (the strongest pulsational signal of 12 Lac) and an amplitude of 40 mmag, sampled in the same way as our measurements. The upper panel of Fig. 2 (left-hand side) contains the result. There are some alias structures in this window function due to our lack of measurements from Eastern Asian longitudes. We must therefore apply caution in identifying the correct frequencies in the light variations of the star.

We proceeded by computing the amplitude spectra of the data themselves (second panel of Fig. 2, left-hand side). The signal designated f_1 dominates. Pre-whitening it by subtracting a synthetic sinusoidal light curve with a frequency, amplitude and phase that yielded the smallest possible residual variance, and computing the

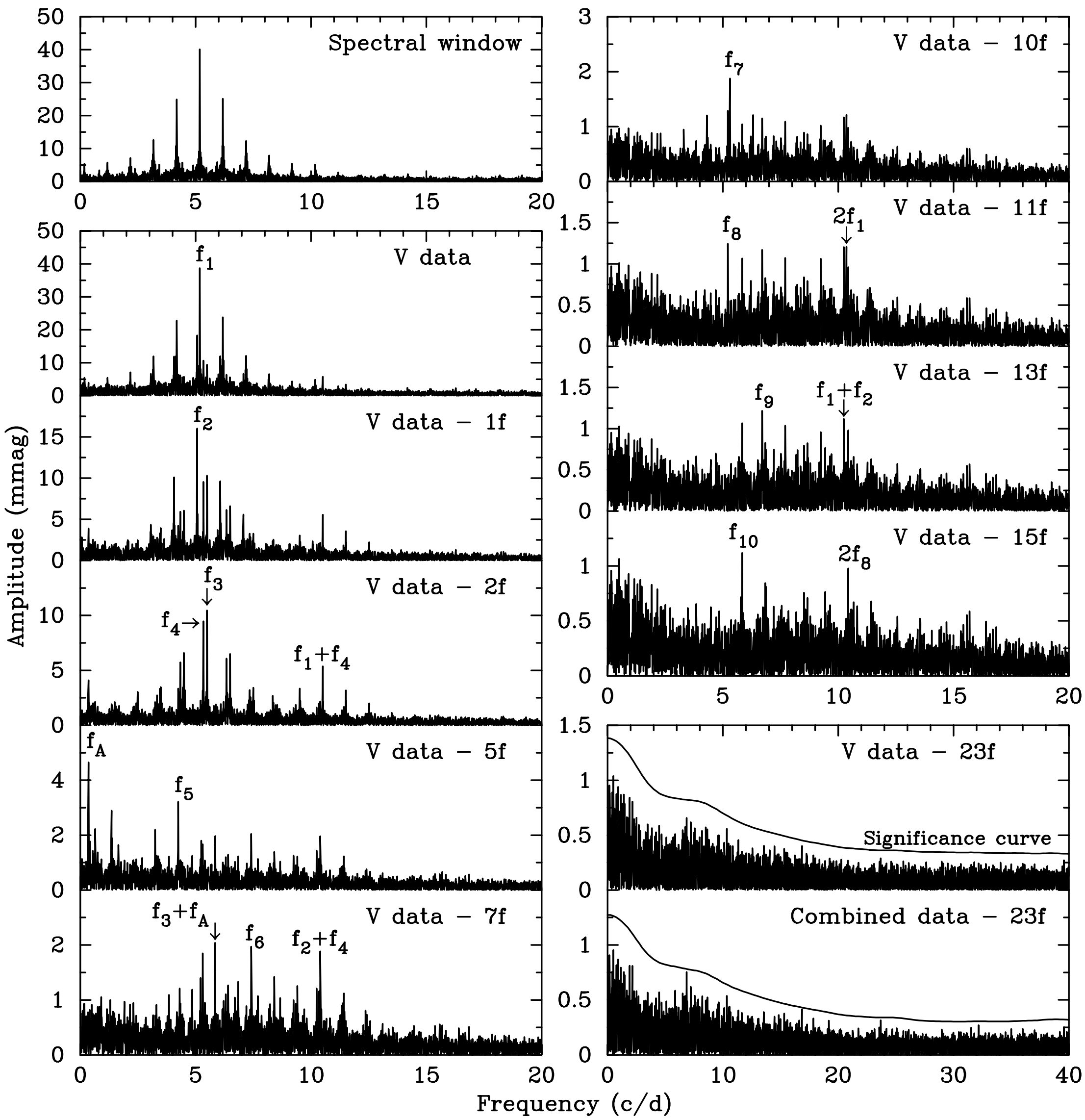

Figure 2. Amplitude spectra of 12 Lac. The uppermost panel on the left-hand side shows the spectral window of the data, followed by the periodogram of the data. Successive pre-whitening steps are shown in the following panels; note their different ordinate scales. After the detection of 17 periodicities (third panel from bottom, right-hand side), some low-amplitude combination frequencies were still found in the residuals. After their pre-whitening, the presence of some additional periodic signals in the light curves can still be suspected. Note the different abscissa scale in the last two panels.

amplitude spectrum of the residual light curve, results in the amplitude spectrum in the third panel of Fig. 2, left-hand side.

A second signal (f_2) can clearly be seen in this graph; other variations with similar frequencies also seem present, as proven by pre-whitening f_1 and f_2 simultaneously (fourth panel of Fig. 2, left-hand side). In this panel, we also note the presence of a combination frequency, the sum of f_1 and f_4, which was consequently also pre-whitened. We continued this procedure (further panels of Fig. 2) until no significant peaks were left in the residual amplitude spectrum.

We consider an independent peak statistically significant if it exceeds an amplitude signal-to-noise ratio of 4 in the periodogram; combination signals must satisfy $(S/N) > 3.5$ to be regarded as significant (see Breger et al. 1993, 1999, for a more in-depth discussion of this criterion). The noise level was calculated as the average amplitude in a 5 cd^{-1} interval centred on the frequency of interest. 23 statistically significant sinusoidal variations were found to be necessary to represent the observed light curves of 12 Lac. We note that the six lowest-amplitude variations have $S/N \sim 4$, whereas the other signals all have $S/N > 6$. We also point out that the low-frequency signal f_A is clearly present in the five largest single-site data sets (Fairborn, Mercator, OSN, SPM and Lowell) independently and is therefore certainly real.

Some of the signals we detected are labelled as sums of frequencies found earlier. All but one of these could be matched with a single pair of parent modes, and using PERIOD98 we first verified that the frequency of the combination would indeed correspond to the sum of the parent frequencies within the observational errors. Consequently, we fixed the combination frequencies to the exact predicted value.

We repeated the pre-whitening procedure with the u and v data independently and obtained the same frequencies within the observational errors. In particular, we note that we never encountered an alternative solution including an alias frequency that fitted the data better. We are therefore confident that our frequency determinations are not affected by alias ambiguities.

Since the V filter data are most numerous and have the largest time-span, we adopted the frequencies from this data set as our final values and recomputed the u and v amplitudes with them. Unsurprisingly, the amplitudes did not change significantly from the individually optimized frequency solution. The final result of our frequency analysis is listed in Table 2. All the signals were found to be in phase in all filters, keeping in mind the observational errors.

The residuals from this solution were searched for additional candidate signals that may be intrinsic. We have first investigated the residuals in the individual filters, then analysed the averaged residuals in the three main filters (whereby the u data were divided by 1.50 and the v data were divided by 1.07 to scale-possible signal amplitudes to the same level as in the V data; these scale factors were empirically derived from the amplitudes of the previously detected signals). The lowest panel on the right-hand side of Fig. 2 contains this final residual amplitude spectrum. The noise spectrum is not white: a marked increase in amplitude towards low frequency is clearly visible and additional pulsational signals may be present.

In particular, two peaks stand out in the combined *uvy* data prewhitened by 23 frequencies: a signal at 6.859 cd^{-1} and another one at 16.850 cd^{-1}, both with an amplitude signal-to-noise ratio of 3.9. The lower frequency is very close to the 1 cd^{-1} alias of the signal

Table 2. Multifrequency solution for our time-resolved photometry of 12 Lac. Formal error estimates (following Montgomery & O'Donoghue 1999) for the independent frequencies range from ± 0.000007 cd^{-1} for f_1 to ± 0.00023 cd^{-1} for f_{10}. Formal errors on the amplitudes are ± 0.2 mmag in u and ± 0.1 mmag in v and V. The S/N ratio, computed following Breger et al. (1993), is for the V filter data.

ID	Frequency (cd^{-1})	u Amplitude (mmag)	v Amplitude (mmag)	V Amplitude (mmag)	S/N
f_1	5.179034	56.4	40.7	38.1	178.6
f_2	5.066346	23.3	16.7	16.0	74.6
f_3	5.490167	14.2	11.7	11.1	52.4
f_4	5.334357	21.9	11.6	10.0	47.3
f_5	4.24062	4.4	3.7	3.6	15.8
f_A	0.35529	7.2	4.8	5.0	14.4
f_6	7.40705	2.8	2.1	2.0	9.7
f_7	5.30912	2.7	2.3	2.0	9.5
f_8	5.2162	1.3	1.3	1.3	6.2
f_9	6.7023	2.2	1.6	1.3	6.3
f_{10}	5.8341	1.8	1.2	1.3	6.1
$f_1 + f_4$	10.513392	8.3	5.9	5.5	32.9
$f_3 + f_A$	5.84546	2.3	1.6	1.8	8.7
$f_2 + f_4$	10.400704	2.3	1.7	1.7	10.3
$2f_1$	10.358069	1.9	1.2	1.2	6.9
$f_1 + f_2$	10.245381	1.7	1.3	1.2	6.9
$2f_8$	10.4324	1.5	1.4	1.0	6.1
$2f_4$	10.668715	1.0	0.8	0.7	4.3
$f_3 + f_4$	10.824524	0.8	0.7	0.6	3.9
$f_2 + f_3$	10.556514	1.1	0.8	0.7	4.0
$2f_1 + f_2$	15.424415	0.6	0.6	0.5	4.3
$f_1 + f_2 + f_4$	15.579738	1.0	0.6	0.5	4.5
$2f_1 + f_4$	15.692426	1.0	0.6	0.5	4.3

at $f_3 + f_{\rm A}$ and in fact its amplitude in a multifrequency fit strongly depends on whether $f_3 + f_{\rm A}$ is assumed to be a combination peak or whether its frequency was independently optimised. This suggests that $f_3 + f_{\rm A}$ and the signal at 6.859 cd^{-1} interact through aliasing. Therefore, the latter cannot be accepted at this point. As the signal at 16.850 cd^{-1} does not correspond to a combination of the previously identified periodicities (but could be an alias thereof), we cannot accept it either. These results corroborate the usefulness of the S/N > 4 criterion once more.

We note that including residual data in the remaining Geneva filters in addition did not turn out to be useful because those measurements are not sufficiently numerous and have a spectral window function too poor for pre-whitening a 23-frequency fit reliably.

3.1 Some comments on the frequency analysis results

The residuals between our observed light curves and the 23-frequency fit are considerably higher than the accuracy of our measurements would imply. For instance, the residual 12 Lac light curves from Lowell, Fairborn and SPM (our best data) have an rms scatter of 3.7 mmag per single measurement while the differential comparison-star magnitudes from the same sites, after removing the variability of 2 And, show a scatter of 2.1 mmag. The residual rms scatter for the full 12 Lac data set is 4.0 mmag.

This is not new as far as β Cephei stars and even 12 Lac are concerned. Jerzykiewicz (1978) already noted that the nightly zero-points of the data gathered during *The International Lacerta weeks* would vary by up to 0.02 mag.

In the present V data set, this effect is smaller but clearly present: the zero-points vary by up to ± 0.008 mag even for the sites with the most stable equipment. For comparison, the nightly zero-points of the V magnitude differences between the comparison stars were found to be constant within ± 0.002 mag. Thus, the increase of the noise level towards low frequencies seen in the last two panels of Fig. 2 does not originate from poor data reductions but is caused by variability of 12 Lac itself.

We believe that the smaller size of the zero-point variations in our data as compared with those in the 1956 data is partly due to the higher accuracy of our photometry and partly to pre-whitening our data with the low-frequency signal $f_{\rm A} = 0.3553$ cd^{-1} before computing the nightly zero-points.

It may be that long-term aperiodic variability of β Cephei stars is a common feature, as the same kind of low-frequency noise is present in the amplitude spectra of other pulsators as well (see Jerzykiewicz et al. 2005 for ν Eri or Handler et al. 2005 for θ Oph).

As mentioned in the previous section, we identified a sinusoidal term as a combination signal if its frequency coincided with the sum or difference of two or more previously detected oscillations within the observational errors. This has several implications. First, a combination frequency is always assumed to have a lower amplitude than the parent modes. Secondly, a data set with a better frequency resolution than ours may reveal that some of the combinations we assigned may be chance agreements. Thirdly, one of our assignments is not unambiguous: the signal identified with $2f_4$ can also be matched with $f_1 + f_3$ within the accuracy of our data. This combination may therefore be a mixture of the effect of both parents.

There are two pairs of close frequencies in Table 2, namely 5.309/5.334 cd^{-1} and 5.834/5.845 cd^{-1}. Their beat periods, 40 and 88 d, respectively, are well resolved in our data. After pre-whitening the two pairs of signals, no peaks in the vicinity of their frequencies can be found in the residual amplitude spectrum. Therefore we have no evidence that any of these variations are due to amplitude or frequency variability of the other partner in the doublet, and we will assume that all of them are variations intrinsic to 12 Lac.

4 MODE IDENTIFICATION

We now attempt to identify the spherical degree ℓ of the pulsation modes by means of the *uvy* and Geneva passband amplitudes of the pulsational signals detected in the light curves. These amplitudes are to be compared with theoretically predicted ones from model computations, requiring the model parameter space to be constrained first. In other words, we need to determine the position of 12 Lac in the HR diagram as a starting point.

The calibrations by Crawford (1978) applied to the mean Strömgren colour indices for 12 Lac listed in the Lausanne Photometric data base (http://obswww.unige.ch/gcpd/gcpd.html) result in $E(b - y) = 0.076$. The Strömgren system calibration by Napiwotzki, Schönberner & Wenske (1993) gives $T_{\rm eff} = 24\,000 \pm 1000$ K. With the Geneva colour indices (again obtained from the Lausanne Photometric data base) of 12 Lac, the calibrations by Künzli et al. (1997) provide $T_{\rm eff} = 23\,500 \pm 700$ K and $\log g = 3.4 \pm 0.4$. The analysis of International Ultraviolet Explorer (IUE) spectra of a number of β Cephei stars led Niemczura & Daszyńska-Daszkiewicz (2005) to derive that 12 Lac has $T_{\rm eff} = 23\,600 \pm 1100$ K and $\log g = 3.65$.

To determine the absolute magnitude of 12 Lac, we take advantage of the fact that it is part of the Lac OB1b association. The distance modulus of this association was determined with 8.3 ± 0.3 mag (Crawford & Warren 1976). With $V = 5.25$ and the reddening as determined before, we have $A_V = 0.33$ and thus $M_v = -3.4 \pm 0.3$, which we adopt for the remainder of this work.

According to de Zeeuw et al. (1999), the Hipparcos mean distance of Lac OB1b is 358 ± 22 pc, which yields $V - M_v = 7.77 \pm 0.13$ mag. These authors note that this value is smaller than most previous ones, for instance by -0.53 ± 0.33 mag from the one by Crawford & Warren (1976). One possible reason for this result could be a problem with systematic errors in Hipparcos parallaxes (Pinsonneault et al. 1998).

Summarizing the temperature determinations quoted before, we find $T_{\rm eff} = 23\,700 \pm 1000$ K for 12 Lac, quite similar to the results by Dziembowski & Jerzykiewicz (1999, $\log T_{\rm eff} = 4.374 \pm 0.020$). According to Flower (1996), this effective temperature corresponds to a bolometric correction of BC $= -2.28 \pm 0.10$ mag, and therefore $M_{\rm bol} = -5.7 \pm 0.4$ mag or $\log L = 4.18 \pm 0.16$.

The metal abundances derived for the star in the literature show considerable scatter and we are unable to identify a best value. Consequently, given the new solar abundances (Asplund et al. 2004), we assume a metallicity of $Z = 0.015$ for 12 Lac. We show the position of the star in a theoretical HR diagram in Fig. 3.

For the purpose of mode identification, we will therefore assume that 12 Lac is an object of about 11.5 $M_\odot$ approaching the end of its main-sequence life. We computed theoretical photometric amplitudes of the $0 \leqslant \ell \leqslant 4$ modes for models with masses between 10.5 and 12.5 $M_\odot$ in steps of 0.5 $M_\odot$, a temperature range of $4.355 \leqslant \log T_{\rm eff} \leqslant 4.395$ and a metallicity $Z = 0.015$. This approach is similar to that by Balona & Evers (1999). Theoretical mode frequencies between 4.0 and 7.6 cd^{-1} were considered, except for frequency f_A, for which a theoretical frequency range between 0.3 and 0.4 cd^{-1} was examined. We compare these theoretical photometric amplitude ratios to the observed ones in Fig. 4 for the Strömgren *uvy* filters. As we cannot be certain whether the signals $f_3 + f_{\rm A}$ and $2f_8$ are independent modes or not, we include them in our analysis.

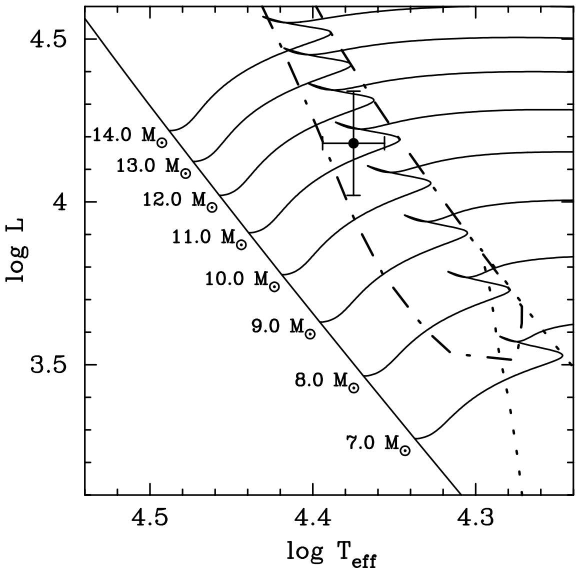

Figure 3. The position of 12 Lac in the theoretical HR diagram. Some stellar evolutionary tracks, for a metal abundance of $Z = 0.015$, labelled with their masses (full lines) are included for comparison. We also show the theoretical borders of the β Cephei instability strip (Pamyatnykh 1999, dashed–dotted line) for $Z = 0.015$, and the instability region for the Slowly Pulsating B (SPB) stars (dotted line).

The five pulsations of highest amplitude can be easily identified with their spherical degree; we see a mixture of $\ell = 0 - 2$ modes. For the lower-amplitudes modes, the identifications become less certain, but at least some possibilities can be eliminated. For instance, signal $f_9 = 6.702$ cd^{-1} cannot be $\ell = 2$ or 4, but it also cannot be $\ell = 0$ either because its frequency ratio with the radial mode $f_4 = 5.334$ cd^{-1} is inconsistent with those for low-order radial modes. Because of similar arguments with the frequency ratios, we can also reject $\ell = 0$ identifications for $f_3 + f_A$ and f_{10}. The mode identifications derived this way are listed in Table 3.

The observed amplitude ratios for the radial mode $f_4 = 5.334$ cd^{-1} are not well reproduced by theory. If we attempt to constrain Z from the observed amplitude ratios, we can only obtain a match if we require f_4 to be the fundamental radial mode. In that case, $Z > 0.02$. The observed amplitude ratios cannot be reproduced if f_4 was the first or second overtone (but it has to be a radial mode in any case). We hasten to add that changing the metal abundance will not significantly affect the theoretical amplitude ratios for the nonradial modes within the parameter space under consideration, hence it will not affect the ℓ identifications for any other mode.

Finally, we also show a comparison of theoretical and observed photometric amplitude ratios from our Geneva photometry, for the four strongest modes of 12 Lac (Fig. 5). The mode identifications derived from the *uvy* data are confirmed. For the lower-amplitude modes, such a consistency check is no longer useful as the observed Geneva amplitude ratios do not have sufficient accuracy because of the small number of data points available in these filters.

5 DISCUSSION

5.1 The independent pulsation modes

As mentioned in Section 1, two hypotheses to explain the pulsation spectrum of 12 Lac seemed promising before our multisite campaign took place: first, the presence of a rotationally split triplet consisting of the modes (f_1, f_3, f_4) and secondly, the presence of the fundamental and first radial overtones (modes f_5, f_3). Our mode identification allows us to judge these hypotheses: neither is correct.

The suspected rotationally split structure consists of modes of $\ell = 1, 0, 2$, and the suspected radial modes both turned out to be $\ell = 2$. Consequently, all previous attempts to understand the pulsation spectrum of 12 Lac were not correct.

Fortunately, our mode identifications also resulted in the detection of a radial mode (f_4). This will be particularly helpful for the asteroseismic interpretation of the pulsation spectrum of the star, since the parameter space in the HR diagram where its seismic model will be located is greatly reduced. On the other hand, none of the other signals we detected occurs at a frequency indicative of another radial mode, as estimated from their frequency ratios to f_4.

Two of the strongest modes of 12 Lac are $\ell = 1$. It is tempting to suspect that these would be components of a rotationally split multiplet. The location of the star in the HR diagram as inferred above implies a radius of $7.0 \pm 1.8\,R_\odot$. Depending on whether the two modes would be $|m| = (0, 1)$ or $m = (-1, 1)$, a rotational velocity of 40 ± 10 or 20 ± 5 km s^{-1} can be inferred, assuming that this splitting reflects that surface rotation period. The measured $v \sin i$ of 12 Lac is 30 km s^{-1} (Abt, Levato & Grosso 2002), suggesting that these $\ell = 1$ modes are more likely to be $|m| = (0, 1)$. Spectroscopic determination of the m values of at least the three strongest non-radial modes would be extremely helpful for understanding this pulsation spectrum of this star.

The frequency range spanned by the independent modes of 12 Lac (between 4.241 and 7.407 cd^{-1}) is fairly large, and corresponds to three or four radial overtones. A similarly large range of excited pulsation frequencies has been found for another β Cephei star, ν Eri (e.g. see Jerzykiewicz et al. 2005), and could not be reproduced by standard theoretical models (Ausseloos et al. 2004; Pamyatnykh, Handler & Dziembowski 2004). Consequently, one could suspect that there is a fundamental problem with our understanding of pulsational driving in the β Cephei stars.

More interesting (and more likely) is the idea that the interior chemical composition of the star is not homogeneous, a suggestion first brought forward by Pamyatnykh et al. (2004). To drive all the observed modes of ν Eri, these authors invoked an ad hoc increase of the abundance of the iron-group elements by a factor of 4 in the pulsational driving region. It may be possible to reconcile pulsational driving of 12 Lac in a similar way. Theoretical investigations of the question whether or not diffusion can lead to the required increase of heavy elements in the driving region while β Cephei stars are still on the main sequence are currently underway (Bourge et al., in preparation).

We also found a low-frequency signal in the light curves of 12 Lac. Its observed photometric amplitude ratios are consistent with non-radial pulsation in a $\ell = 1$, 2 or 4 mode. On the other hand, f_A is the only signal in this frequency range and the position of the star in the HR diagram is far away from the SPB star instability strip (Fig. 3). Therefore we cannot be sure about the astrophysical cause of this variation; it could, for instance, be due to rotational modulation. However, in such a case the star would rotate rather fast ($v_{rot} \sim 120$ km s^{-1}, or $v_{rot} \sim 60$ km s^{-1}, if the observed frequency was the first harmonic of the rotation period) which seems unlikely given its measured $v \sin i$ and the conjectured rotational splitting within the modes of 12 Lac.

5.2 The combination frequencies–resonant mode coupling

We detected several interesting features in the amplitude spectrum of 12 Lac concerning combination frequencies that prompted us to

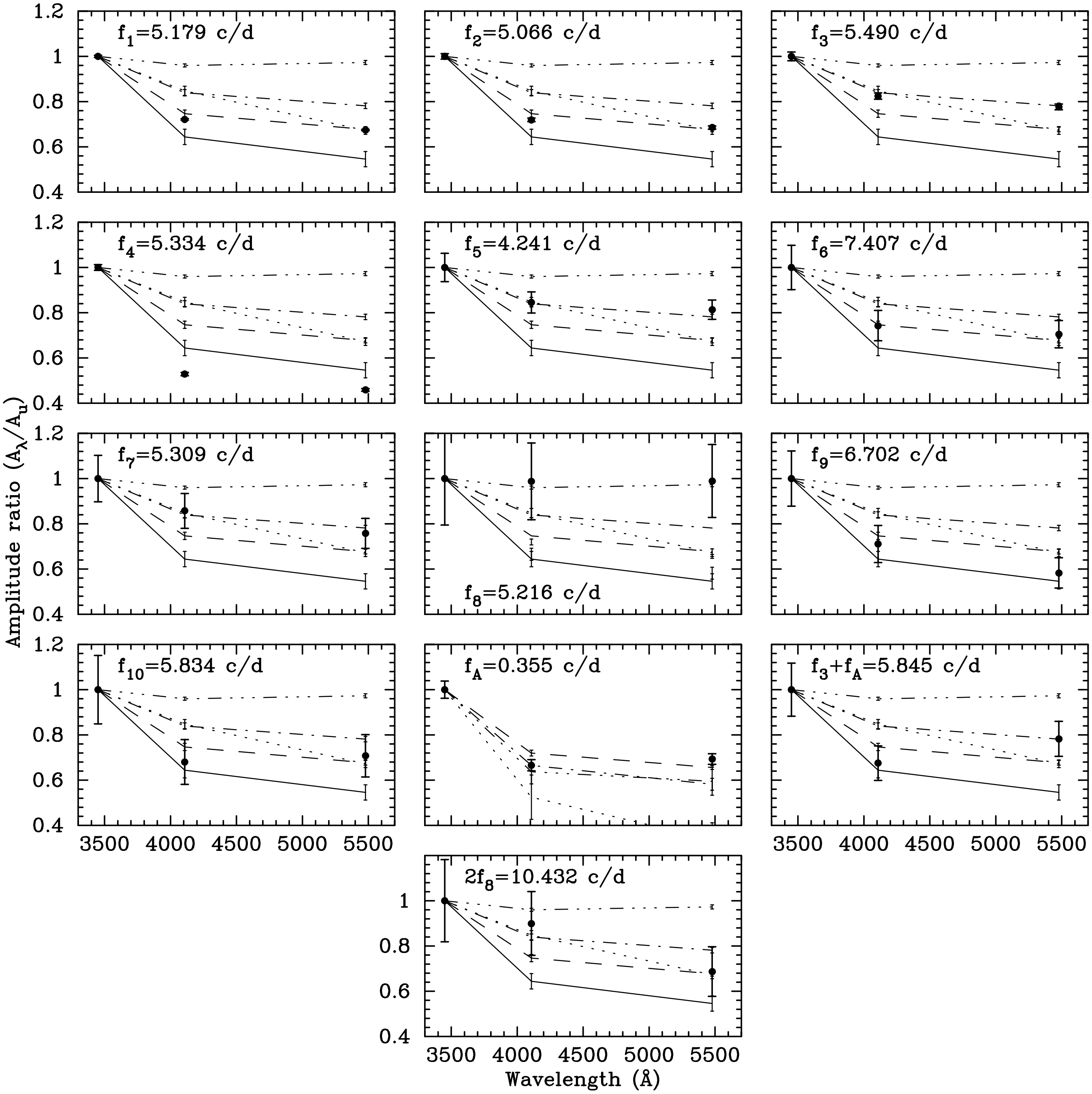

Figure 4. Mode identifications for 12 Lac from a comparison of observed and theoretical *uvy* amplitude ratios, normalized to unity at *u*. The filled circles with error bars are the observed amplitude ratios. The full lines are theoretical predictions for radial modes, the dashed lines for dipole modes, the dashed–dotted lines for quadrupole modes, the dotted lines for $\ell = 3$ modes, and the dashed–dot–dot–dotted lines are for $\ell = 4$. The thin error bars denote the uncertainties in the theoretical amplitude ratios.

have a closer look at these signals. For instance, only combination frequency sums were found; no frequency differences were detected. If frequency differences originating from the same parents as the observed frequency sums had the same amplitudes, three of them should have been detected in our data. This is similar to what we found for ν Eri (Handler et al. 2004).

The single low frequency f_A is also involved in a combination which resulted in a signal within the range where the intrinsic pulsation mode frequencies of 12 Lac are located. The amplitude of this combination signal is unusually high and it is rather unexpected that f_A chose to combine with f_3 only, and not with the highest amplitude mode f_1 or the radial mode f_4 which are involved in more combinations than f_3.

Quite interestingly as well, the low-amplitude signal f_8 was found to have a harmonic of comparable amplitude, $2f_8$, that could not be identified with any other combination of parent frequencies. On the other hand, $2f_8$ may be an independent signal that just happens to occur at the expected frequency of a harmonic. To shed more light

Table 3. Mode identifications for 12 Lac from our analysis of the photometric amplitude ratios.

ID	Frequency (cd^{-1})	l
f_1	5.179034	1
f_2	5.066346	1
f_3	5.490167	2
f_4	5.334357	0
f_5	4.24062	2
f_A	0.35529	1, 2 or 4
f_6	7.40705	1 or 2
f_7	5.30912	2 or 1 or 3
f_8	5.2162	4 or 2
f_9	6.7023	1
f_{10}	5.8341	1 or 2
$f_3 + f_A$	5.84546	2 or 1
$2f_8$	10.4324	1 or 2 or 3

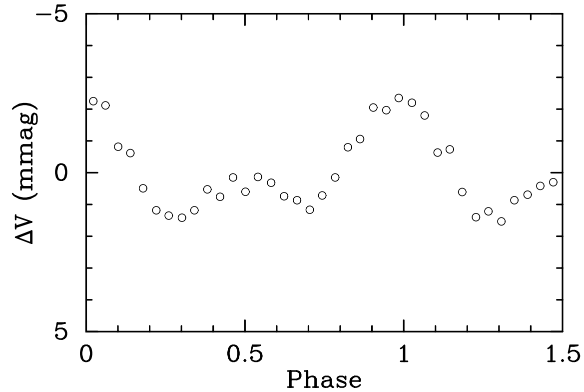

Figure 6. Phase diagram for the signal at $f_8 = 5.216$ cd^{-1}. The data are summed into 25 equally sized bins for clarity of representation.

on the nature of f_8 and its possible harmonic, we have constructed its pulse shape. We pre-whitened the V filter data with all signals but f_8 and $2f_8$, and then phased the residuals with the parent frequency. The resulting phase diagram is shown in Fig. 6. This graph shows a clear double-wave pulse shape, which is unlike the 'normal' phase diagrams of stellar pulsations, although it should be noted that some stars show similar (unphased) light curves (e.g. see Joshi et al. 2003).

There are two interpretations for the occurrence of combination frequencies: light-curve distortions and resonant-mode coupling. Under the first hypothesis, the combinations are caused by the stellar material being unable to respond totally elastically to the full acceleration due to pulsation. It should result in combination frequencies whose amplitudes scale with the product of their parent modes and with their geometrical cancellation factors. The phases of such combinations relative to those of their parents should also be similar.

However, such relationships should in general not be followed by modes excited by resonant-mode coupling (Dziembowski 1982). It is the distinction between the hypotheses of light-curve distortion and resonant mode coupling as the cause of combination frequencies in the amplitude spectra of 12 Lac that we are trying to achieve here.

Consequently, we examined the relative amplitudes $A_{ij}/(A_i/A_j)$, where A_{ij} is the amplitude of the combination frequency and A_i and A_j are the amplitudes of the parent modes, respectively, and phases $\phi_{ij} - (\phi_i + \phi_j)$, where ϕ_{ij} is the phase of the combination signal and ϕ_i and ϕ_j are the phases of the parent modes of the first-order combination frequency sums with respect to their parents. Such an analysis has been successfully used by Vuille (2000) and Vuille & Brassard (2000) for the pulsating white dwarf star G 29-38. We show the relative amplitudes and phases of the combination frequencies in Fig. 7.

Several interesting features can be noted in this graph. First, the harmonic $2f_8$ has a relative amplitude almost two orders of magnitude larger than the other combinations. The second largest relative amplitude is due to $f_3 + f_A$, still a factor of at least three larger than the others.

Considering the relative phases, two combinations are again markedly different from the others: $f_3 + f_A$ and $2f_1$. The

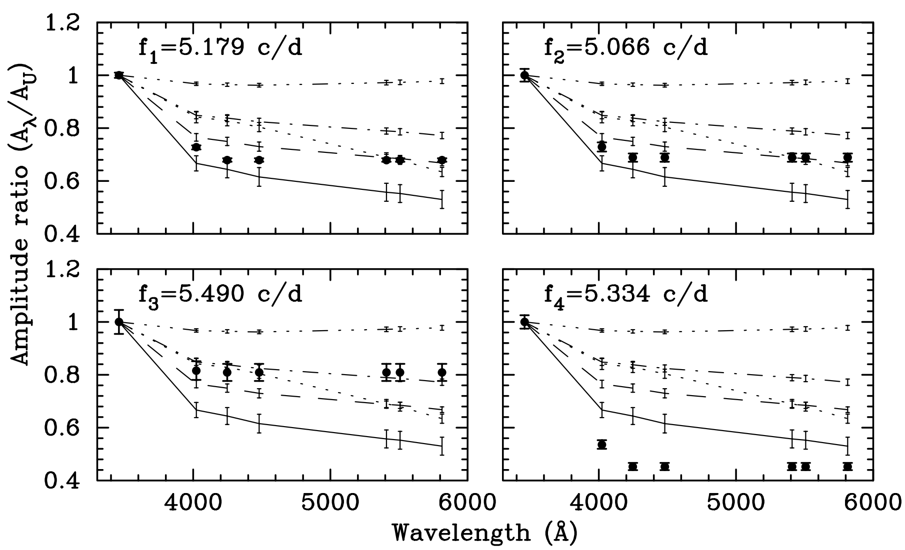

Figure 5. Identifications for the four strongest modes of 12 Lac from a comparison of observed and theoretical amplitude ratios in the Geneva system, normalized to unity at U. The filled circles with error bars are the observed amplitude ratios. The full lines are theoretical predictions for radial modes, the dashed lines for dipole modes, the dashed-dotted lines for quadrupole modes, the dotted lines for $\ell = 3$ modes and the dashed–dot–dot–dotted lines are for $\ell = 4$. The thin error bars denote the uncertainties in the theoretical amplitude ratios.

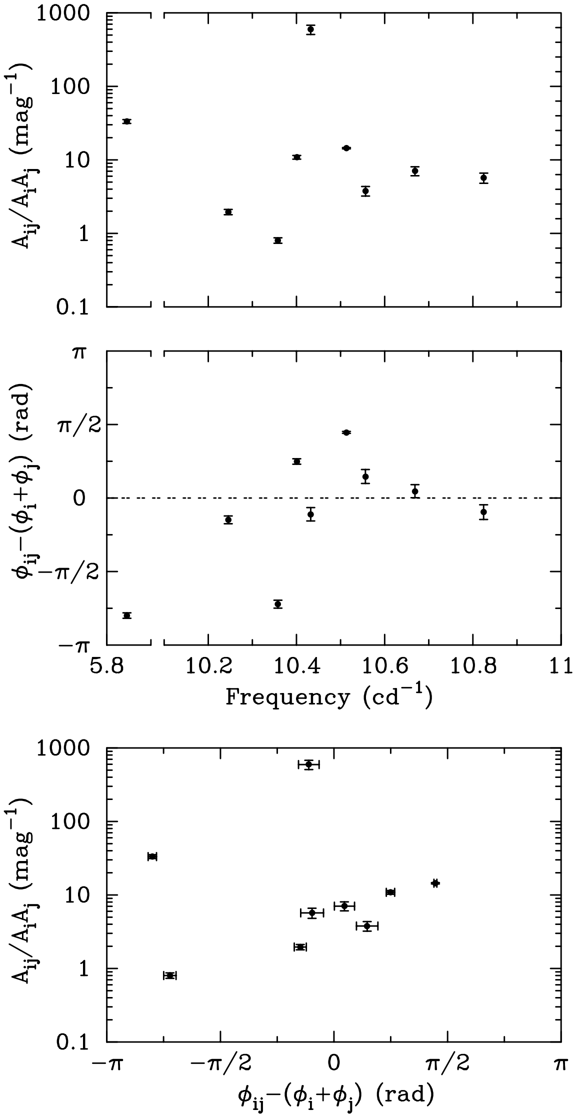

Figure 7. Relative amplitudes (upper panel) and phases (middle panel) of the combination frequencies with respect to their parent modes. The dotted line in the middle panel connects points of zero phase shift. The lower panel shows the relative amplitudes versus relative phase. Note the logarithmic scale for the relative amplitudes.

relative phase of $2f_1$ indicates that the pulse shape of this mode has a descending branch steeper than the rising branch, and that the light maxima are flatter than the light minima. Given the small amplitude of this harmonic, the effect is however minimal. In the remaining cases, the relative phases of the combinations indicate a mixture of different pulse shapes. Some have a rising branch steeper than the descending branch (positive relative phase), some behave the opposite way (negative relative phase). Pulse shapes with descending branches steeper than the rising branches are unusual for pulsating variables and have to our knowledge only been found in a few δ Scuti stars (e.g. see Rodríguez et al. 1997; Musazzi et al. 1998).

The lowest panel of Fig. 7 shows the relative amplitudes with respect to the relative phases. Again, $2f_8$ and $f_3 + f_A$ stand out, whereas the other combination frequencies seem to follow a trend. Given that there is a 2π ambiguity in the determination of the relative phases, $f_3 + f_A$ may actually follow this trend.

In any case, there are two parallel sequences of points along the trend. Under the hypothesis of light-curve distortion, this can be understood at least partly: as the spherical harmonic of these combinations is defined by the product of the spherical harmonics of its parents, their photometric amplitudes are subject to geometrical cancellation, including the effect of inclination. This is consistent with the observations. Besides $2f_8$ and $f_3 + f_A$, the combinations with the highest relative amplitude involve the radial mode f_4, whereas the lower-amplitude combinations, which should have higher spherical degree and thus suffer stronger geometrical cancellation, are between non-radial modes.

Coming back to the nature of the unusual combination frequencies, we have one more statement to make: if $2f_8$ were an independent mode, it would extend the domain of mode frequencies considerably – and there is already a problem with driving the frequency range spanned by the other modes!

For all the reasons given above, we can then only explain the occurrence of $2f_8$ by non-linear mode coupling (Dziembowski 1982). In other words, $2f_8$ is pushed to visible amplitude via a 2:1 resonance with f_8. This would explain the anomalously high amplitude of $2f_8$, and it would also give us further clues on pulsational mode identifications. If f_8 were indeed due to an $\ell = 4$ mode, it would only be able to interact with photometrically detectable modes of $\ell = 0$, 2, 4 with the 2:1 resonance (see Dziembowski 1982). Since we were able to rule out $\ell = 0$ or 4 for $2f_8$ (Fig. 4 and Table 3), it can only be a quadrupole mode under this hypothesis. As the azimuthal order of the resonantly excited oscillation must be twice the azimuthal order of the exciting mode, we are only left with the identifications $|m| =$ 0 or 1 for f_8 and $|m| = 0$ or 2 for $2f_8$.

A similar situation was found for the β Cephei star KK Vel: its strongest mode has $\ell = 4$, $m = 0$. This mode shows a harmonic whose photometric amplitude ratios are consistent with $\ell = 0$ (see the discussion by Aerts, Waelkens & de Pauw 1994).

We note in passing that the low photometric amplitude of f_8 is not an argument against it being able to excite another mode via resonant-mode coupling: geometrical cancellation reduces the amplitude of an $\ell = 4$ mode by one order of magnitude more than that of an $\ell = 2$ mode (Daszyńska-Daszkiewicz et al. 2002). Therefore, the intrinsic amplitude of f_8 would be about a factor of 10 higher than that of $2f_8$.

Concerning $f_3 + f_A$, we are less certain if it would also be resonantly excited. Its properties are not as extreme as those of $2f_8$, although its amplitude is still unusually high. We would just like to conclude with another speculation: maybe it is not $f_3 + f_A$ that is a resonantly excited mode. The occurrence of a single self-excited mode at a low frequency is also not easy to understand. Consequently, it can be hypothesized that in fact f_A is resonantly excited by f_3 and by an independent mode at $f_3 + f_A$.

The behaviour of all the other combination frequencies is consistent with the hypothesis of light-curve distortion, including $f_1 + f_4$ that has previously been suggested to be a resonantly excited mode (Aerts 1996).

6 CONCLUSIONS

The analysis of our extensive photometric observations of the β Cephei star 12 Lac had a number of interesting surprises to offer. We added five new independent modes to the five already known, which may suffice for asteroseismic modelling of the stellar interior. In particular, one radial mode has been found, which is of great benefit in restricting the parameter space in which a seismic model is to be located.

Our mode identifications showed that the previously suspected rotationally split mode triplet was pure coincidence; it actually consists of three modes of different spherical degree. In this context, it is interesting to note that the δ Scuti star 1 Mon also exhibits an equally spaced frequency triplet (Shobbrook & Stobie 1974), but that the central triplet component is a radial mode (Balona & Stobie 1980; Balona et al. 2001), the same situation as found here.

The two pulsation modes of 12 Lac that were suspected to be radial from their frequency ratio both turned out to be non-radial. These results are a warning against performing mode identification by just looking for 'suspicious' structures within the pulsation modes, such as equally spaced frequencies, and against mode identification by 'magic numbers' such as the expected frequency ratios of radial modes.

The mode spectrum of 12 Lac consists of a mixture of pulsation modes with spherical degrees between 0 and 4 over a large range of radial overtones. This is good and bad news for asteroseismology. The good news is that many modes that sample different regions of the stellar interior are potentially available. On the other hand, pulsational mode identification becomes more difficult as the ratio between the number of observed and theoretically predicted modes is smaller compared to other β Cephei stars. A unique identification of all detected pulsation modes is therefore not possible from photometry only.

We must therefore put our hopes on to the spectroscopic mode identifications to follow. Spectroscopic techniques can reveal the azimuthal order of the modes, making them complementary to the photometric method. During a spectroscopic analysis, it is possible to fix the spherical degree of the modes to the values following from unique photometric identifications and to only derive m from the spectroscopy. Such an approach is probably more robust compared to having to identify both ℓ and m from spectroscopy, and was already successful in the case of θ Oph (Briquet et al. 2005).

Another interesting result from our study is the detection of a signal that could correspond to a linearly stable mode excited by a 2:1 resonance via non-linear mode coupling. This is probably the best case for such a mode to be present in a main-sequence pulsator, and it can further be tested by deriving more stringent mode identifications from an even larger set of photometric measurements. In addition, it may be possible to infer the inclination of the pulsation axis of the star from the relative amplitudes of the 'normal' combination frequencies.

Finally, we pointed out that the range of excited pulsation frequencies of 12 Lac may be larger than reproducible by standard models. We therefore suspect that the interior chemical structure of the star is not homogeneous and that there is probably an increased heavy element abundance near the pulsational driving zone due to diffusion, as was already postulated by Pamyatnykh et al. (2004) for ν Eri. Such an interior compositional stratification could also explain the presence of β Cephei stars in the Large Magellonic Cloud (Kolaczkowski et al. 2004).

ACKNOWLEDGMENTS

This work has been supported by the Austrian Fonds zur Förderung der wissenschaftlichen Forschung under grant R12-N02. MJ's participation in the campaign was supported by KBN grant 5P03D01420. ER, PJA and RG are grateful for the support by the Junta de Andalucand the Dirección General de Investigación (DGI) under projects AYA2003-04651 and ESP2004-03855-C03-01. DEM acknowledges his work as a part of research activity of the Astrophysical Research Center for the Structure and Evolution of the Cosmos (ARCSEC), which is supported by the Korean Science and Engineering Foundation. MJ would also like to acknowledge a generous allotment of telescope time and the hospitality of Lowell Observatory. JPS and LP acknowledge the Instituto de Astronomia UNAM and the staff at SPM Observatory for their continued help. GH wishes to express his thanks to Lou Boyd and Peter Reegen for their efforts in maintaining and controlling the Fairborn APTs and to Wojtek Dziembowski for helpful discussions. We thank the following students of the University of Hawaii for their assistance during some of the observations: Moses David, Anne Michels, Don McLemore, Tom Chun, Elizabeth Hart, Erin Brassfield, Robert Knight, David Plant, Thomas Pegues, Ken Plant, Paul Sherard, Alanna Garay, John Rader and Jason Barnes.

REFERENCES

Abt H. A., Levato H., Grosso M., 2002, ApJ, 573, 359
Adams W. S., 1912, ApJ, 35, 163
Aerts C., 1996, A&A, 314, 115
Aerts C., Waelkens C., de Pauw M., 1994, A&A, 286, 136
Aerts C. et al., 2004, A&A, 415, 241
Asplund M., Grevesse N., Sauval A. J., Allende Prieto C., Kiselman D., 2004, A&A, 417, 751
Ausseloos M., Scuflaire R., Thoul A., Aerts C., 2004, MNRAS, 355, 352
Balona L. A., Evers E. A., 1999, MNRAS, 302, 349
Balona L. A., Stobie R. S., 1980, MNRAS, 190, 931
Balona L. A. et al., 2001, MNRAS, 321, 239
Barning F. J. M., 1963, Bull. Astr. Inst. Netherlands, 17, 22
Breger M. et al., 1993, A&A, 271, 482
Breger M. et al., 1999, A&A, 349, 225
Briquet M., Lefever K., Uytterhoeven K., Aerts C., 2005, MNRAS, 362, 619
Crawford D. L., 1978, AJ, 83, 48
Crawford D. L., Warren W. H., 1976, PASP, 88, 930
Daszyńska-Daszkiewicz J., Dziembowski W. A., Pamyatnykh A. A., Goupil M.-J., 2002, A&A, 392, 151
de Jager C., 1963, Bull. Astr. Inst. Netherlands, 17, 1
de Zeeuw P. T., Hoogerwerf R., de Bruijne J. H. J., Brown A. G. A., Blaauw A., 1999, AJ, 117, 354
Dziembowski W. A., 1982, Acta Astr., 32, 147
Dziembowski W. A., Jerzykiewicz M., 1999, A&A, 341, 480
ESA, 1997, The Hipparcos and Tycho Catalogues, ESA SP-1200
Flower P. J., 1996, ApJ, 469, 355
Guthnick P., 1919, AN, 208, 219
Handler G. et al., 2004, MNRAS, 347, 454
Handler G., Shobbrook R. R., Mokgwetsi T., 2005, MNRAS, 362, 612
Jerzykiewicz M., 1978, Acta Astr., 28, 465
Jerzykiewicz M. et al., 2005, MNRAS, 360, 619
Joshi S. et al., 2003, MNRAS, 344, 431
Kolaczkowski Z. et al., 2004, in Kurtz D. W., Pollard K. R., eds, ASP Conf. Ser. Vol. 310, Variable Stars in the Local Group. Astron. Soc. Pac., San Fransisco, p. 225
Künzli M., North P., Kurucz R. L., Nicolet B., 1997, A&AS, 122, 51
Ledoux P., 1951, ApJ, 114, 373
Mathias P., Aerts C., Gillet D., Waelkens C., 1994, A&A, 289, 875
Montgomery M. H., O'Donoghue D., 1999, Delta Scuti Star Newsletter, 13, 28 (University of Vienna)
Musazzi F., Poretti E., Covino S., Arellano Ferro A., 1998, PASP, 110, 1156
Napiwotzki R., Schönberner D., Wenske V., 1993, A&A, 268, 653
Niemczura E., Daszyńska-Daszkiewicz J., 2005, A&A, 433, 659
Pamyatnykh A. A., 1999, Acta Astr., 49, 119
Pamyatnykh A. A., Handler G., Dziembowski W. A., 2004, MNRAS, 350, 1022
Pinsonneault M. H., Stauffer J., Soderblom D. R., King J. R., Hanson R. B., 1998, ApJ, 504, 170

Rodríguez E., González-Bedolla S. F., Rolland A., Costa V., López-González M. J., López de Coca P., 1997, A&A, 328, 235
Sareyan J. P., Chauville J., Chapellier E., Alvarez M., 1997, A&A, 321, 145
Shobbrook R. R., Stobie R. S., 1974, MNRAS, 169, 643
Smith M. A., 1980, ApJ, 240, 149
Sperl M., 1998, Master's thesis, Univ. of Vienna
Stankov A., Handler G., 2005, ApJS, 158, 193
Stebbins J., 1917, Pop. Astr., 25, 657
Vuille F., 2000, MNRAS, 313, 179
Vuille F., Brassard P., 2000, MNRAS, 313, 185

This paper has been typeset from a TEX/LATEX file prepared by the author.

5.7 Photometric studies of three multiperiodic β Cephei stars: β CMa, 15 CMa and KZ Mus

Original paper:

R. R. Shobbrook, **G. Handler,** D. Lorenz, D. Mogorosi, 2006, MNRAS 369, 171

Mon. Not. R. Astron. Soc. **369,** 171–181 (2006) doi:10.1111/j.1365-2966.2006.10289.x

Photometric studies of three multiperiodic β Cephei stars: β CMa, 15 CMa and KZ Mus

R. R. Shobbrook,[1*] G. Handler,[2*] D. Lorenz[2*] and D. Mogorosi[3*]

[1]*Research School of Astronomy and Astrophysics, Australian National University, Canberra, ACT, Australia*
[2]*Institut für Astronomie, Universität Wien, Türkenschanzstrasse 17, A-1180 Wien, Austria*
[3]*Department of Physics, University of the North-West, Private Bag X2046, Mmabatho 2735, South Africa*

Accepted 2005 July 17. Received 2005 August 13; in original form 2005 September 10

ABSTRACT

We have carried out single and multisite photometry of the three β Cephei stars β and 15 CMa as well as KZ Mus. For the two stars in CMa, we obtained 270 h of measurement in the Strömgren *uvy* and Johnson *V* filters, while 150 h of time-resolved Strömgren *uvy* photometry was acquired for KZ Mus. All three stars are multiperiodic variables, with three (β CMa) and four (15 CMa, KZ Mus) independent pulsation modes. Two of the mode frequencies of 15 CMa are new discoveries and one of the known modes showed amplitude variations over the last 33 yr. Taken together, this fully explains the diverse behaviour of the star reported in the literature.

Mode identification by means of the amplitude ratios in the different passbands suggests one radial mode for each star. In addition, β CMa has a dominant $\ell = 2$ mode while its third mode is non-radial with unknown ℓ. The non-radial modes of 15 CMa, which are $\ell \leqslant 3$, form an almost equally split triplet that, if physical, would imply that we see the star under an inclination angle larger than 55°. The strongest non-radial mode of KZ Mus is $\ell = 2$, followed by the radial mode and a dipole mode. Its weakest known mode is non-radial with unknown ℓ, confirming previous mode identifications for the pulsations of the star.

The phased light curve for the strongest mode of 15 CMa has a descending branch steeper than the rising branch. A stillstand phenomenon during the rise to maximum light is indicated. Given the low photometric amplitude of this non-radial mode this is at first sight surprising, but it can be explained by the aspect angle of the mode.

Keywords: stars: early-type – stars: individual: β CMa – stars: individual: 15 CMa – stars: individual: KZ Mus – stars: oscillations – stars: variables: other.

1 INTRODUCTION

The β Cephei stars are a group of early B-type stars with masses between 9 and 17 $M_\odot$ that exhibit light, radial velocity and line-profile variability on time-scales between 2 and 8 h (Stankov & Handler 2005). The cause of their variability is pulsation in pressure and gravity modes of low radial order. About 110 definite members of this group are known in our Galaxy (Handler 2005; Pigulski 2005; Stankov & Handler 2005), but a large number of candidates was also revealed in the Large Magellanic Cloud (Kołaczkowski et al. 2004).

One of the major astrophysical applications of the β Cephei stars is asteroseismology, the determination of the interior structure of pulsating stars via theoretical modelling of their normal-mode spectra. All main-sequence pulsators more massive than the Sun that have been studied asteroseismically so far, and where unambiguous results on stellar structure could be obtained (e.g. see Pamyatnykh, Handler & Dziembowski 2004), belong to the β Cephei stars.

The main prerequisite for an asteroseismic study is that a number of pulsation modes large enough is known to remove any ambiguities concerning the position of the star in the Hertzsprung–Russell (HR) diagram, and that these modes are unambiguously identified with their pulsational quantum numbers, *k*, the radial overtone of the mode, the spherical degree ℓ, and the azimuthal order *m*. Even among the β Cephei stars, such objects are not easy to find, which can often be traced to insufficient data that are incapable of providing the required mode frequency resolution and number of mode detections.

Consequently, it is worthwhile to select potentially promising targets and to obtain reasonably large amounts of time-resolved photometric and/or spectroscopic data so that a reliable assessment of their asteroseismic promise can be made. For the present work, we have chosen three stars that seemed to justify such an effort.

The conspicuous naked-eye star ($V = 1.98$) β CMa is known as a radial-velocity variable for more than a hundred years (see Struve 1950). Shobbrook (1973a) obtained the first extensive photometric

*E-mail: rshob@tpg.com.au (RRS); handler@astro.univie.ac.at (GH); lorenz@astro.univie.ac.at (DL); dipsymogorosi@hotmail.com (DM).

data set for this star and analysed it together with the radial velocities previously published. He found three pulsation periods for the star, and suggested that all of them changed somewhat over the years. As his measurements were taken in the V filter only, no photometric mode identification could be made, but the different light-to-radial-velocity amplitudes of the two strongest modes noticed by Shobbrook (1973a) suggest that they have different ℓ. However, we should note that this conclusion is based on the assumption that both modes had the same intrinsic amplitude at the different epochs of the photometric and spectroscopic measurements.

15 CMa ($V = 4.80$) shows notoriously difficult variability according to the literature. This began with the first claim of its radial velocity variability (Campbell 1911) that was later retracted (Moore 1936). Among the successive studies of its variability, the photometric investigation by Shobbrook (1973b) was the most extensive. He identified the period of the dominant variation in his light curves, and noted its non-sinusoidal shape, but could not push the analysis further. Heynderickx (1992) suggested the presence of at least two pulsation modes, which were later identified with $\ell = 2$ and 0, respectively, on the basis of multicolour photometry (Heynderickx, Waelkens & Smeyers 1994).

KZ Mus ($V = 9.1$) has been studied during a two-site photometric effort by Handler et al. (2003). These authors also review the (short) history of the investigations of its variability. They found four independent modes in the stellar light variations, where the strongest of these have $\ell = 2$, 0 and 1, respectively, and the radial mode is either the fundamental or the first overtone. The presence of additional pulsation modes was suspected by Handler et al. (2003), who also pointed out the importance of an identification of the spherical degree of the fourth known mode.

2 OBSERVATIONS AND REDUCTIONS

We acquired time-resolved differential photoelectric photometry of all the three targets. The bright stars β and 15 CMa were measured with respect to the comparison stars HR 2271 ($V = 5.8$, B3II/III) and 17 CMa ($V = 5.8$, A2V), that were observed alternating with the targets. No evidence for variability of the latter two stars within a limit of 1.5 mmag was found.

This group of four stars was observed from three observatories in the time-span in 2004 November to 2005 February. 35 nights of Strömgren uvy data were obtained at Siding Spring Observatory, Australia, with the 0.6-m telescope. 18 nights were acquired with the 0.5-m telescope at the South African Astronomical Observatory. The Johnson V filter was used for the first five nights; the remaining 13 nights consist of Strömgren uvy data, but the u filter was not used for β CMa at this site. Finally, 10 nights of measurement were performed with the 0.75-m Automated Photometric Telescope T6 at Fairborn Observatory, USA, again using Strömgren uvy filters. Neutral density filters were used in all cases to avoid photomultiplier destruction, owing to the extreme brightness of β CMa; the same neutral density filters were applied to all stars at each site. The total of 63 nights of observation has a time-base of 111.95 d, corresponding to 272.7 h of measurements of β CMa and 265.4 h of measurements for 15 CMa, respectively.

KZ Mus was measured with the same observational technique. The comparison stars were HD 110022 ($V = 7.8$, B8III/IV), which was replaced by HD 109082 ($V = 8.1$, B9IV) after the first few nights when we found evidence for variability of the former object. The second comparison star was HD 111876 ($V = 7.1$, B9.5/A0V). HD 109082 was constant during the observations. However, HD 111876 showed a small ($\sim$0.01 mag in all three filters) mean magnitude drift during the total time-span of observations.

This group of stars was observed from 2005 March to 2005 June, but with the 0.6-m telescope at Siding Spring Observatory only. Data were acquired during 27 nights, giving a total time-span of 98.9 d, and 154.3 h of measurement resulted. Again the Strömgren uvy filters were used, but no neutral density filters had to be employed.

Data reduction comprised a correction for coincidence losses, subtraction of sky background and extinction determination and correction. Whenever possible, nightly extinction coefficients were determined with the classical Bouguer method (fitting a straight line to a plot of magnitude versus airmass) from the measurements of the two comparison stars. For the remaining nights, mean coefficients from the adjoining nights were used.

The magnitudes of the comparison stars were adjusted to their mean differences, and were then combined into a curve that was assumed to reflect the effects of sky transparency and detector sensitivity changes only. Subsequently, these combined time series were binned into intervals that would allow good compensation for the above-mentioned non-intrinsic variations in the target star time series and were subtracted from the measurements of the variables. The binning minimizes the introduction of noise in the differential light curves of the targets.

The timings for the differential light curves were heliocentrically corrected as the next step. Finally, the photometric zero-points of the different instruments were compared between the different sites and were adjusted if necessary. Measurements in the Strömgren y and Johnson V filters were treated as equivalent due to the similar effective wavelengths of these filters, and were analysed jointly after a correction for differential colour extinction in V. Some example light curves of our three targets together with multifrequency solutions to be discussed in the following are shown in Figs 1–3, respectively.

3 FREQUENCY ANALYSIS

Our frequency analysis was mainly performed with the program PERIOD98 (Sperl 1998). This package applies to single-frequency power spectrum analysis and simultaneous multifrequency sine-wave fitting. It also includes advanced options such as the calculation of optimal light-curve fits for multiperiodic signals including harmonic, combination, and equally spaced frequencies. Our analysis will require some of these features.

3.1 β CMa

We started by computing the Fourier spectral window of the u filter data. It was calculated as the Fourier transform of a single noise-free sinusoid with a frequency of 3.979 cycles per day (cd^{-1}) (the strongest pulsational signal of β CMa) and an amplitude of 12 mmag, sampled in the same way as our measurements. The upper panel of Fig. 4 contains the result. The alias structures in this window are sufficiently suppressed to allow easy and unique determinations of the frequencies of the stellar light variations.

We proceeded to compute the amplitude spectra of the data themselves (second panel of Fig. 4). The signal designated f_1 dominates. We pre-whitened it by subtracting a synthetic sinusoidal light curve with a frequency, amplitude and phase that yielded the smallest possible residual variance. We then computed the amplitude spectrum of the residual light curve, which is shown in the third panel of Fig. 4.

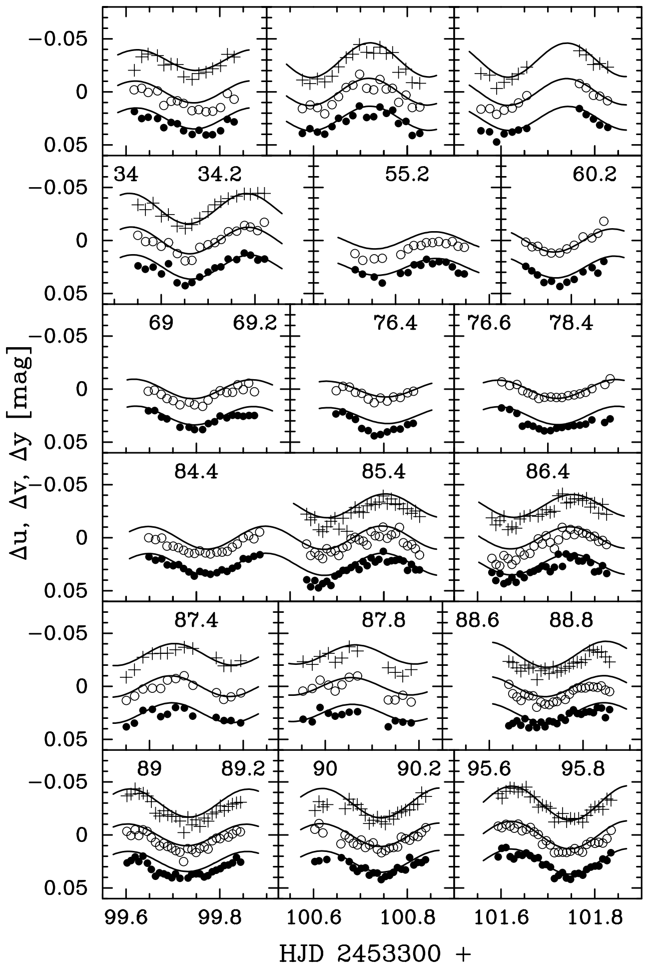

Figure 1. Some of our observed light curves of β CMa. Plus signs are data in the Strömgren u filter, open circles are our v measurements and filled circles represent Strömgren y data. The full line is a fit composed of all the periodicities detected in the light curves (Table 2). The amount of data displayed is approximately one-third of the total.

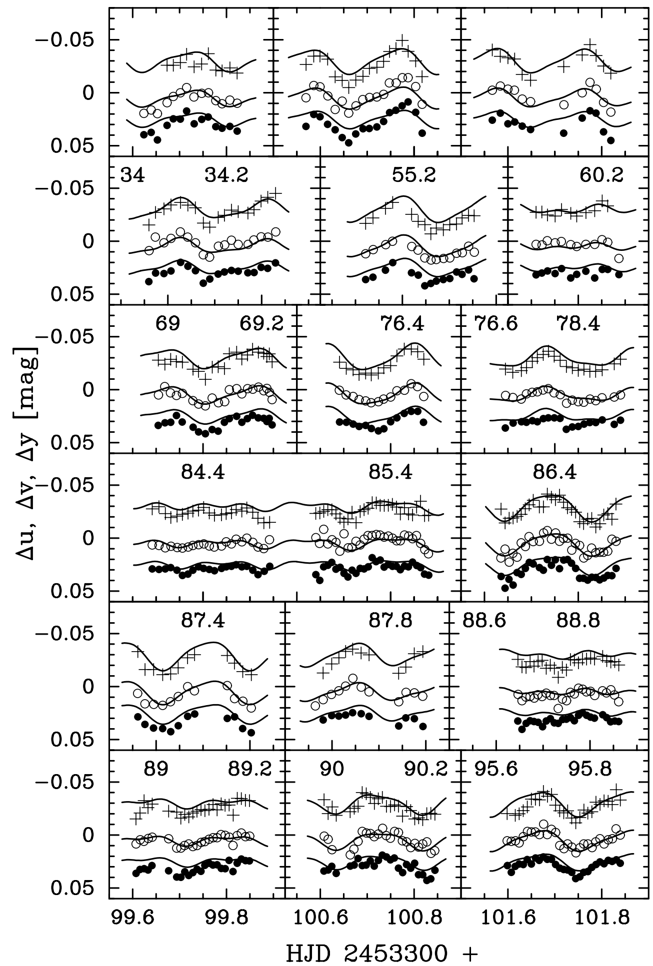

Figure 2. Some of our observed light curves of 15 CMa. Plus signs are data in the Strömgren u filter, open circles are our v measurements and filled circles represent Strömgren y data. The full line is a fit composed of all the periodicities detected in the light curves (Table 3). The amount of data displayed is approximately one-third of the total.

A second signal (f_2) can clearly be seen in this graph. Pre-whitening it leaves no further significant periodicities in the u data alone. At this stage, we pre-whitened the data from the v and y filters by the f_1 and f_2 frequencies, then combined these residuals with those from the u filter data divided by 1.2. This 1.2 factor scales the u data to the same amplitude as that found for f_1 in the v and y data. This procedure is valid because the light curves of β Cephei stars have the same phase at all optical wavelengths.

The residual amplitude spectrum of the *uvy* data combined in this way is shown in the lowest panel of Fig. 4. We note the presence of another signal, f_3, and include it in our frequency solution for β CMa. Pre-whitening by this variation as well, we find no further significant periodicity in our combined residual amplitude spectrum.

We consider an independent peak statistically significant if it exceeds an amplitude signal-to-noise ratio (S/N) of 4 in the periodogram; combination signals must satisfy $\mathrm{S/N} > 3.5$ to be regarded as significant (see Breger et al. 1993, 1999; for a more in-depth discussion of this criterion). The noise level was calculated as the average amplitude in a $5\,\mathrm{c\,d^{-1}}$ interval centred on the frequency of interest.

We are now in a position to determine a final multifrequency solution for our light curves of β CMa. To this end, we first computed a weighted average for the frequencies derived from the data of the individual filters, where the weight corresponded to the S/N of the signals. The results were adopted as our final frequency values. We then fitted these frequencies to the *uvy* data and determined their amplitudes and phases (that were, as assumed previously, found to be the same for all filters within the errors). The final solution is listed in the upper part of Table 1.

The error estimates we give are the formal values for the amplitudes (Montgomery & O'Donoghue 1999). We note that such formal error bars are expected to underestimate the real errors by about a factor of 2 (Handler et al. 2000; Jerzykiewicz et al. 2005). For the frequencies themselves, we computed both the formal errors, and the deviation of the mean of the values from the individual filters; we then adopted the larger of the two values. For frequencies f_1 and f_3 the two results agreed quite well (within 10 per cent). However, the error of the mean was a factor of 2 larger for f_2.

This result can be easily understood: within the time-span of our data, f_2 is not fully resolved from a possible variation of 4 cycles per sidereal day. Such a variation could be present in our light curves due to residual (colour) extinction effects, despite our careful data reduction. This interpretation is supported by the observation that the value of f_2 is closest to 4 cycles per sidereal day in the u band

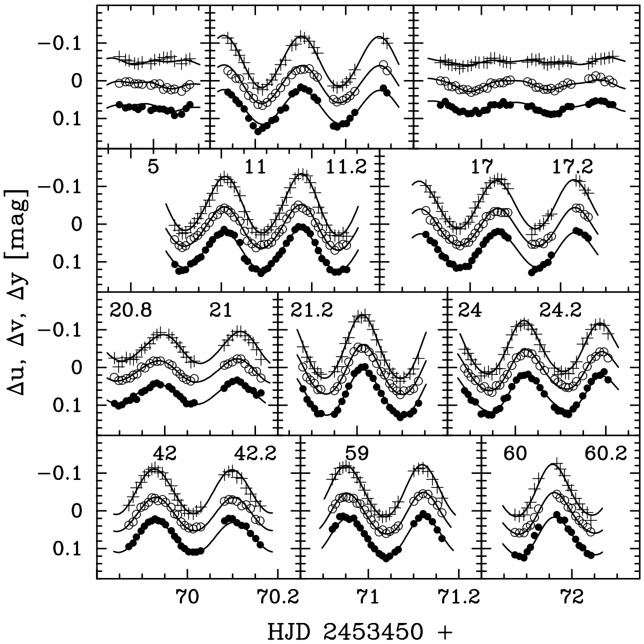

Figure 3. Some of our observed light curves of KZ Mus. Plus signs are data in the Strömgren u filter, open circles are our v measurements and filled circles represent Strömgren y data. The full line is a fit composed of all the periodicities detected in the light curves (Table 4). The amount of data displayed is approximately half the total.

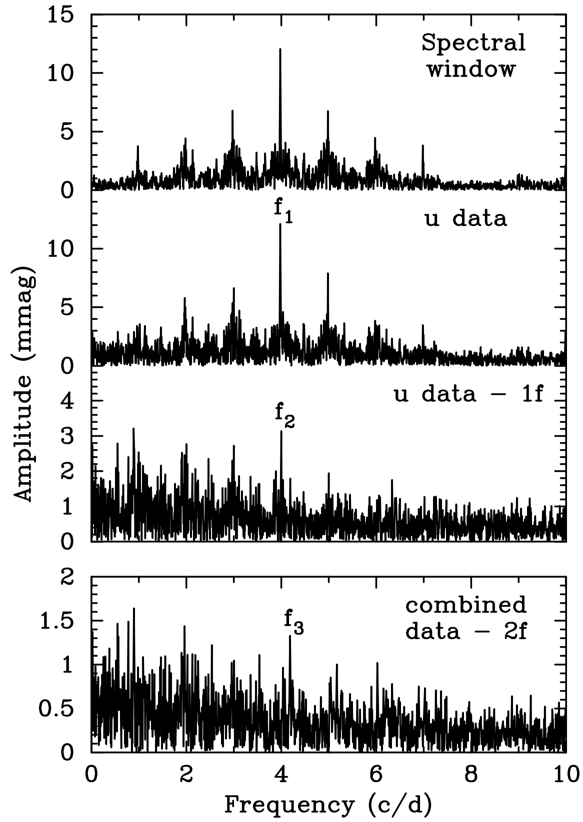

Figure 4. Amplitude spectra of β CMa. The uppermost panel shows the spectral window of the data, followed by the periodogram of the data. Successive pre-whitening steps are shown in the following panels; note their different ordinate scales.

where possible residual extinction effects are expected to be largest. We must therefore be careful in the interpretation of the frequency and *uvy* amplitudes of f_2.

3.1.1 Reanalysis of archival data

One of us (RRS) has digitized his archival V filter photometry of β and 15 CMa taken in the early 1970s. We can therefore analyse these measurements with our frequency analysis methods, allowing a direct comparison of the results.

For β CMa we confirm the findings by Shobbrook (1973a; see lower part of Table 1): we obtain the same three frequencies as he did. Given the probable underestimation of the real errors of the frequencies and amplitudes (especially for mode f_2), we are reluctant to claim the presence of amplitude and/or frequency variability for the star.

On the other hand, we note that there seems to be some low-frequency variability, for which we are unable to determine a period, remaining in the residuals, similar to what can be discerned in the lowest panel of Fig. 4. We find this behaviour in all independent data sets we have for β CMa, but not in the differential light curve of the two comparison stars. Because we can exclude an extinction effect for its origin, we are inclined to believe that this variation is intrinsic to our target star.

We attempted to obtain an improved frequency solution and to check for amplitude and frequency variability of the stellar pulsation modes by analysing the combined visual photometric data by Shobbrook (1973a), Balona et al. (1996) and the *HIPPARCOS* satellite (ESA 1997) together with our measurements. Regrettably, the amount and temporal separation of the data render this investigation inconclusive: we derive a best-fitting frequency for the strongest mode of $3.979\,3334 \pm 0.000\,0009\,\mathrm{cd}^{-1}$ that is slightly variable in amplitude and phase, but we cannot be certain whether or not this is a numerical artefact due to beating with the close mode at $3.9994\,\mathrm{cd}^{-1}$ when unresolved in certain subsets of data.

3.2 15 CMa

The frequency analysis for this star was carried out in a similar way as that for β CMa and is illustrated in Fig. 5. This time we use the v data for display as they resulted in the light curves of best S/N. In the case of 15 CMa, the spectral window had a single noise-free

Table 1. Multifrequency solutions for photometric data of β CMa. Error estimates (following Montgomery & O'Donoghue 1999) on the amplitudes are ± 0.4 mmag in u and ± 0.3 mmag in v and y, respectively. The S/N ratio was computed following Breger et al. (1993) and is quoted for the v filter.

ID	Frequency (cd^{-1})	u amplitude (mmag)	v amplitude (mmag)	y amplitude (mmag)	S/N
		New photometry			
f_1	3.9793 ± 0.0001	12.0	10.6	10.0	25.5
f_2	3.9994 ± 0.0007	3.8	1.7	1.3	4.1
f_3	4.1857 ± 0.0007	1.7	1.7	1.4	4.2
		Archival data			
f_1	3.9792 ± 0.0001			10.3 (V)	28.5
f_2	3.9999 ± 0.0007			1.9 (V)	5.2
f_3	4.1821 ± 0.0009			1.4 (V)	4.0

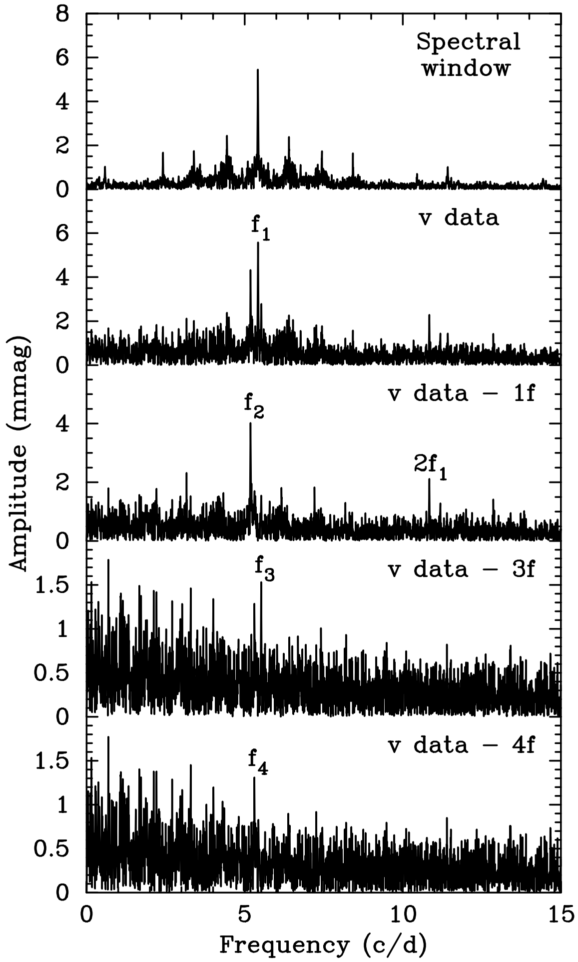

Figure 5. Amplitude spectra of 15 CMa. The uppermost panel shows the spectral window of the data, followed by the periodogram of the data. Successive pre-whitening steps are shown in the following panels; note their different ordinate scales.

sinusoid with a frequency of 5.419 cd^{-1} and an amplitude of 5.4 mmag as input (upper panel of Fig. 5). The amplitude spectrum of the data themselves (second panel) already makes it clear that more than one frequency is present in the light curves. Pre-whitening the strongest signal (f_1) leaves two conspicuous peaks in the residual amplitude spectrum. One of these is the first harmonic of f_1. Further pre-whitening with these three signals indicates the presence of another periodicity, and pre-whitening that one as well reveals a fourth independent frequency in the light curves. Pushing the analysis further, also by combining the residuals for the u, v and y data, as we did for β CMa, did not result in the detection of additional periodicities.

The final multifrequency solution for 15 CMa was determined in the same way as for β CMa: by computing S/N-weighted averages of the frequencies determined from the data of the individual filters. We note that, for reasons of better accuracy, we fixed the frequency of the harmonic signal to exactly twice the value of the parent mode with PERIOD98.

We then recomputed the *uvy* amplitudes with these 'best' frequencies and list the result in Table 2. Again, the adopted error estimates on the frequencies correspond to the larger of the two values derived from analytic formulae and rms deviations of the mean of the frequencies.

Table 2. Multifrequency solution for time-resolved photometric data of 15 CMa. Error estimates (following Montgomery & O'Donoghue 1999) on the amplitudes are ±0.3 mmag in u and ±0.2 mmag in v and y, respectively. The S/N ratio was computed following Breger et al. (1993, 1999) and is quoted for the v data.

ID	Frequency (cd^{-1})	u amplitude (mmag)	v amplitude (mmag)	y amplitude (mmag)	S/N
		New photometry			
f_1	5.4187 ± 0.0002	6.2	5.4	4.6	16.0
f_2	5.1831 ± 0.0003	5.4	3.9	2.9	11.2
$2f_1$	10.8374	2.4	2.1	2.1	7.2
f_3	5.5212 ± 0.0008	2.0	1.6	1.3	4.7
f_4	5.3085 ± 0.0012	1.6	1.4	1.1	4.2
		Archival data			
f_1	5.4180 ± 0.0003			4.8 (V)	12.3
$2f_1$	10.8359			1.9 (V)	6.2
f_2	5.1845 ± 0.0009			1.5 (V)	3.8
f_3	5.5253 ± 0.0007			1.9 (V)	4.9
f_4	5.3103 ± 0.0008			1.6 (V)	4.3

3.2.1 Reanalysis of archival data

We analysed the V measurements of 15 CMa by Shobbrook (1973b; also digitized by RRS), who also detected our signal f_1 and its first harmonic. However, he could not continue to search for further frequencies because the residual amplitude spectrum was too complicated.

Thanks to our multisite measurements, we know four pulsation frequencies of the star without aliasing ambiguities, and we can use this information in our reanalysis. This helps us to solve the puzzle that the data by Shobbrook (1973b) provided: we first detect f_1 and its harmonic. The three other frequencies detected in our new measurements are also present in the older photometry, and all three are required to explain the observations, as proven by different pre-whitening trials. We list the result of this analysis in the lower part of Table 2. We point out that f_2 has an S/N below 4, but since it is known to be an intrinsic signal from our new measurements, we only require S/N > 3.5 to accept this frequency as real in the old data.

In this case, f_2 can be safely claimed as having varied in amplitude, whereas no such statement can be made for the other signals. In this context, it is interesting to revisit the discussion of the Geneva data by Heynderickx (1992), who also observed 15 CMa. He detected our f_1 and its harmonic, but then encountered two closely spaced signals around f_2, where the frequency difference of these signals is close to the inverse time-span of his data set. Consequently, it can be suspected that these two apparent signals near f_2 could in fact be due to a single mode with amplitude variability during Heynderickx's observations. We note that an attempt to refine the pulsation frequencies of the star by analysing the measurements by Shobbrook (1973b) and the *HIPPARCOS* satellite (ESA 1997) together with ours did not bear fruit due to aliasing problems.

We also note that, just as for β CMa, some slow aperiodic variability seems to be left in the residuals of both the archival and the new measurements. This slow variability is not correlated with the one of β CMa (neither in the old nor in the new data), which is further support for the idea that it is intrinsic to the stars and is not an instrumental effect.

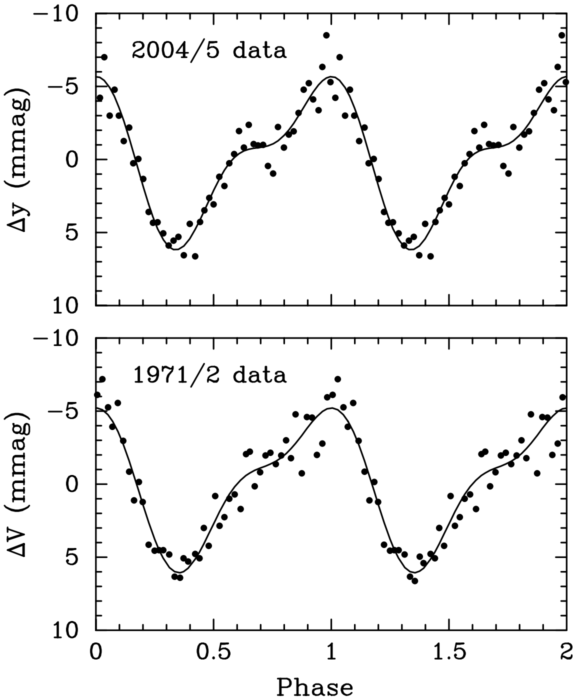

Figure 6. Phase diagram of light curves of 15 CMa with respect to f_1 (full dots), compared to a fit computed with f_1 and $2f_1$. Two cycles of the variation are shown. The rising branch of this light variation is flatter than the descending branch, and there seems evidence for a stillstand before light maximum.

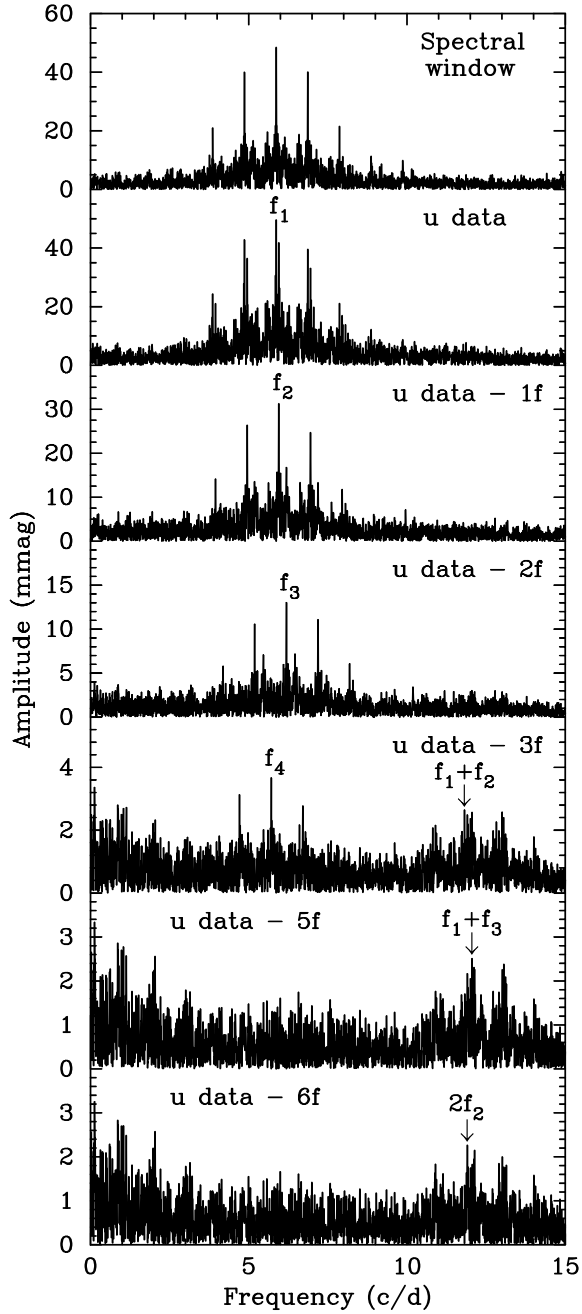

Figure 7. Amplitude spectra of KZ Mus. The uppermost panel shows the spectral window of the data, followed by the periodogram of the data. Successive pre-whitening steps are shown in the following panels; note their different ordinate scales.

3.2.2 The light-curve shape of f_1

The amplitude of the harmonic frequency of f_1 is unusually high given the amplitude of the independent mode to which it is connected. We have therefore examined the shape of the light curve due to this mode. We fitted the five known frequencies of 15 CMa to the archival data and to our new measurements and then prewhitened the fit composed of the resulting parameters for f_2, f_3 and f_4. We then phased the residuals with f_1 and show the results in Fig. 6.

The phase diagrams obtained in this way appear odd for a pulsating star: the rising branch of the light curve is less steep than the descending branch. When computing a fit to these phase diagrams composed of f_1 and $2f_1$, or when averaging the two-phase diagrams, it even seems possible that there is a 'stillstand' phenomenon in the rising branch. We would however like to see more data on the star before coming to a definite conclusion on this matter.

It is interesting to note that the scatter in the two-phase diagrams are very similar: although smaller in number, the precision of the measurements taken in the 1970s is slightly better than that of our present data.

3.3 KZ Mus

The frequency analysis for this star was carried out in a similar fashion as for the others. We determined individual frequencies step-by-step and found four independent modes (see Fig. 7) plus three combination frequencies. Again, the frequencies were first determined for each individual filter, using PERIOD98 to fix the frequencies of combination signals to the exact sums predicted by those of parent modes. Then, S/N-weighted averages of the frequencies determined from the data of the individual filters were computed and adopted as our final frequency values. Our multifrequency solution obtained this way is listed in Table 3.

Comparing our results to those by Handler et al. (2003), we cannot find significant evidence for amplitude or frequency variability, but we do note the occurrence of a new combination frequency, $f_1 + f_3$. This signal is actually present in the older measurements, but we were not convinced about its reality during the previous analysis.

On the other hand, the combination signal $f_2 - f_1$ detected by Handler et al. (2003) is not present in our new measurements. This is likely due to the increased low-frequency noise in the new data

Table 3. Multifrequency solution for our new time-resolved photometry of KZ Mus. Error estimates (following Montgomery & O'Donoghue 1999) on the amplitudes are ±0.4 mmag in u and v, and ±0.3 mmag in y. The S/N ratio was computed following Breger et al. (1993, 1999) and is quoted for the u-filter data.

ID	Frequency (cd^{-1})	u amplitude (mmag)	v amplitude (mmag)	y amplitude (mmag)	S/N
f_1	5.86400 ± 0.00004	47.2	41.0	38.4	85.4
f_2	5.95059 ± 0.00007	35.0	20.6	17.3	63.4
f_3	6.18774 ± 0.00013	16.1	12.4	11.6	29.3
f_4	5.7094 ± 0.0005	4.0	3.2	3.6	7.1
$f_1 + f_2$	11.81459	1.7	1.7	1.7	3.2
$f_1 + f_3$	12.05174	2.3	1.8	1.7	4.3
$2f_2$	11.90118	2.2	1.6	1.8	4.1

caused by the variability of the comparison star HD 111876, which we were not able to remove satisfactorily.

3.3.1 *Refining the determination of the pulsation frequencies*

Although the photometry by Handler et al. (2003) was taken 3 yr before the measurements presented in this paper, the frequency determinations of both works are accurate enough that we can link the previous V and the present y data to obtain more accurate pulsation frequencies. The effective wavelengths of these two bands are also sufficiently similar to render such an approach valid.

Consequently, we performed a joint frequency analysis with PERIOD98, where we could also reveal the presence of one more combination signal. The result is given in Table 4. We have confirmed that the frequencies of the three strongest modes and their combination frequencies are alias-free by including the *HIPPARCOS* photometry of the star (ESA 1997) as well. We could not make a similar check for mode f_4 due to its low amplitude. In any case, the residual amplitude spectrum after pre-whitening our joint solution contains no evidence that measurable amplitude or frequency variations have occurred within the 3.4-yr time-base of our observations. We have also determined the Strömgren v amplitudes given this frequency solution for the combined 2002 and 2005 data. However, we could not do the same for the Johnson U and Strömgren u bands because their wavelength responses are sufficiently different that the calculated amplitudes of the strongest modes do not correspond within the errors.

Table 4. Multifrequency solution for the combined ground-based time-resolved V and y, as well as v photometry of KZ Mus. The error estimates (Montgomery & O'Donoghue 1999) on the amplitudes are ±0.2 mmag. The S/N ratio was computed following Breger et al. (1993, 1999).

ID	Frequency (cd^{-1})	v amplitude (mmag)	V or y amplitude (mmag)	S/N
f_1	5.864016 ± 0.000005	41.2	38.4	109.5
f_2	5.950693 ± 0.000011	20.4	16.5	47.2
f_3	6.187472 ± 0.000016	12.3	10.9	31.4
f_4	5.70935 ± 0.00006	3.1	3.0	8.4
$f_1 + f_2$	11.814709	1.9	1.9	6.2
$2f_2$	11.901386	1.5	1.5	5.0
$f_1 + f_3$	12.051489	1.3	1.3	4.4
$f_2 + f_3$	12.138165	1.2	1.2	4.0

4 MODE IDENTIFICATION

The spherical degree ℓ of the pulsation modes of our three target stars can be identified by comparing their observed *uvy* amplitudes with those predicted by theoretical models. Required input for these models are the mass and effective temperature of the stars, from which their luminosity obviously follows as well.

For KZ Mus, we simply adopt the values given by Handler et al. (2003), who derived $T_{\mathrm{eff}} = 26000 \pm 700$ K and $\log L/\mathrm{L}_{\odot} = 4.22 \pm 0.20$. For the two stars in Canis Major, the calibrations by Crawford (1978) applied to the standard Strömgren photometry by Crawford, Barnes & Golson (1970) results in $E(b-y) = 0.027$ for β CMa and $E(b-y) = 0.031$ for 15 CMa, respectively. The Strömgren system calibration by Napiwotzki, Schönberner & Wenske (1993) then yields $T_{\mathrm{eff}} = 25600 \pm 1000$ K for β CMa and $T_{\mathrm{eff}} = 26300 \pm 1000$ K for 15 CMa.

With the Geneva colour indices of the two stars obtained from the Lausanne Photometric Database, the calibrations by Künzli et al. (1997) provide $T_{\mathrm{eff}} = 25100 \pm 1100$ K and $\log g = 3.3 \pm 0.6$ for β CMa, and $T_{\mathrm{eff}} = 26000 \pm 1500$ K and $\log g = 3.8 \pm 0.6$ for 15 CMa.

The analysis of *International Ultraviolet Explorer* spectra of a number of β Cephei stars by Niemczura & Daszyńska-Daszkiewicz (2005) results in $T_{\mathrm{eff}} = 24700 \pm 800$ K and $\log g = 3.74$ for β CMa and $T_{\mathrm{eff}} = 24600 \pm 1000$ K and $\log g = 3.81$ for 15 CMa.

The *HIPPARCOS* parallax of β CMa is 6.53 ± 0.66 mas. With $V = 1.98$ and the reddening as determined before, we obtain $M_v = -4.1 \pm 0.2$. The parallax of 15 CMa (2.02 ± 0.70 mas) is too inaccurate to be useful. However, 15 CMa is a member of the young open cluster Collinder 121, whose distance was determined as 592 ± 28 pc (de Zeeuw et al. 1999), which is in reasonable agreement with the usually quoted distance to the cluster in the pre-*HIPPARCOS* era, 630 pc (Feinstein 1967). Using the most recent distance to Collinder 121, we determine $M_v = -4.2 \pm 0.2$ for this star, given that $V = 4.80$ and again adopting the amount of reddening suggested by Strömgren photometry.

Summarizing the temperature determinations quoted before, we arrive at final values of $T_{\mathrm{eff}} = 25100 \pm 1200$ K for β CMa and 25600 ± 1200 K for 15 CMa. According to Flower (1996), these effective temperatures correspond to bolometric corrections of $\mathrm{BC} = -2.2 \pm 0.3$ mag and $\mathrm{BC} = -2.3 \pm 0.4$ mag, respectively. Consequently, the bolometric luminosities of the two stars are -6.3 ± 0.4 mag (β CMa) and -6.5 ± 0.4 mag (15 CMa), respectively.

Fig. 8 shows the positions of our three targets in a theoretical HR diagram. The two stars in Canis Major have very similar properties there, indicating that both are massive and are approaching the end of their main-sequence life. This is somewhat in contrast with their distinctly different pulsation periods. KZ Mus appears to just have entered the instability strip and has lower mass than the two other pulsators.

For the purpose of mode identification, we computed theoretical photometric *uvy* amplitudes for the $0 \leqslant \ell \leqslant 4$ modes of models with masses between 13.0 and 16.0 $\mathrm{M}_{\odot}$ in steps of 1.0 $\mathrm{M}_{\odot}$, and in a temperature range of $4.38 \leqslant \log T_{\mathrm{eff}} \leqslant 4.43$ for β and 15 CMa. For KZ Mus, we investigated a range of 11.5–14.0 $\mathrm{M}_{\odot}$ in steps of 0.5 $\mathrm{M}_{\odot}$, and $4.395 \leqslant \log T_{\mathrm{eff}} \leqslant 4.435$, therefore applying a generous interpretation of the derived error bars. All models had an assumed metallicity of $Z = 0.02$. This approach is similar to that by Balona & Evers (1999).

Theoretical mode frequencies between 3.7 and 4.5 cd^{-1} were considered for β CMa, between 4.8 and 5.9 cd^{-1} for 15 CMa and

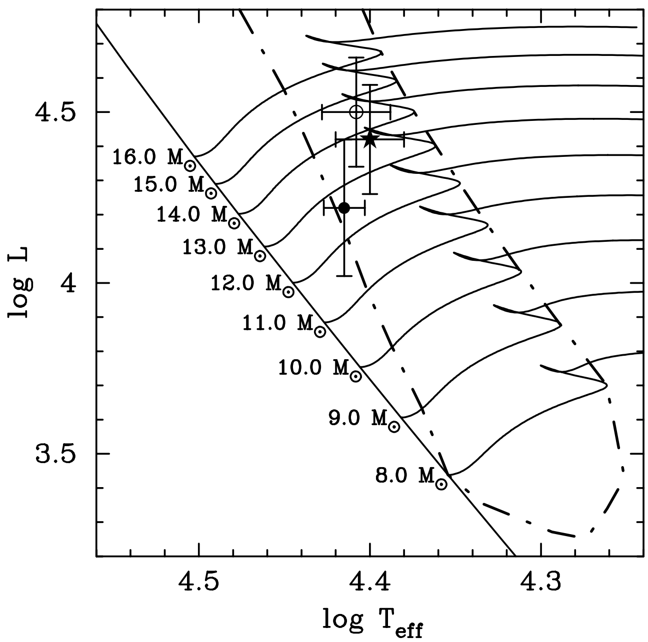

Figure 8. The positions of our three targets in the theoretical HR diagram. The filled circle denotes KZ Mus, the star symbol is for β CMa, and the open circle represents 15 CMa. Error estimates on the effective temperatures and luminosities of the stars are indicated. Some stellar evolutionary tracks, for a metal abundance of $Z = 0.02$, labelled with their masses (full lines) are included for comparison. We also show the theoretical borders of the β Cephei instability strip (Pamyatnykh 1999; dashed–dotted line).

between 5.4 and 6.5 cd^{-1} for KZ Mus. The frequency ranges chosen are somewhat larger than the ones excited in the stars to allow for some rotational m-mode splitting. We compare the theoretical photometric amplitude ratios to the observed ones in Figs 9–11 for all independent modes of all three stars.

Starting with β CMa, it is clear that its strongest mode has a spherical degree of $\ell = 2$. The second mode seems radial, although its measured amplitude versus wavelength dependence is considerably steeper than theoretically predicted. However, we believe that this is caused by problems with differential colour extinction, which artificially increases the measured u amplitude, as discussed in Section 3. In any case, no mode identification other than $\ell = 0$ is possible for this mode. The lowest-amplitude pulsation mode is non-radial, but its spherical degree cannot be constrained due to its small amplitude.

Continuing with 15 CMa, we see that the strongest mode is non-radial with $\ell = 1, 2$ or 3, but no distinction between these hypotheses can be made. The second strongest mode is most likely radial, and no mode identification is possible for the two weakest modes. However, due to their proximity to the radial mode in frequency, they must be non-radial.

Turning to KZ Mus, one immediately sees that its strongest mode is $\ell = 2$. The second strongest mode is suggested to be radial, although again the observed amplitude ratios indicate a steeper wavelength dependence of the amplitudes than theoretically predicted. The third mode of KZ Mus is a dipole, $\ell = 1$, and the fourth is non-radial. These results are in perfect agreement with the mode identifications by Handler et al. (2003).

5 DISCUSSION AND CONCLUSIONS

We have observed the three β Cephei stars because we aimed at new and improved mode identifications and because we wanted to check

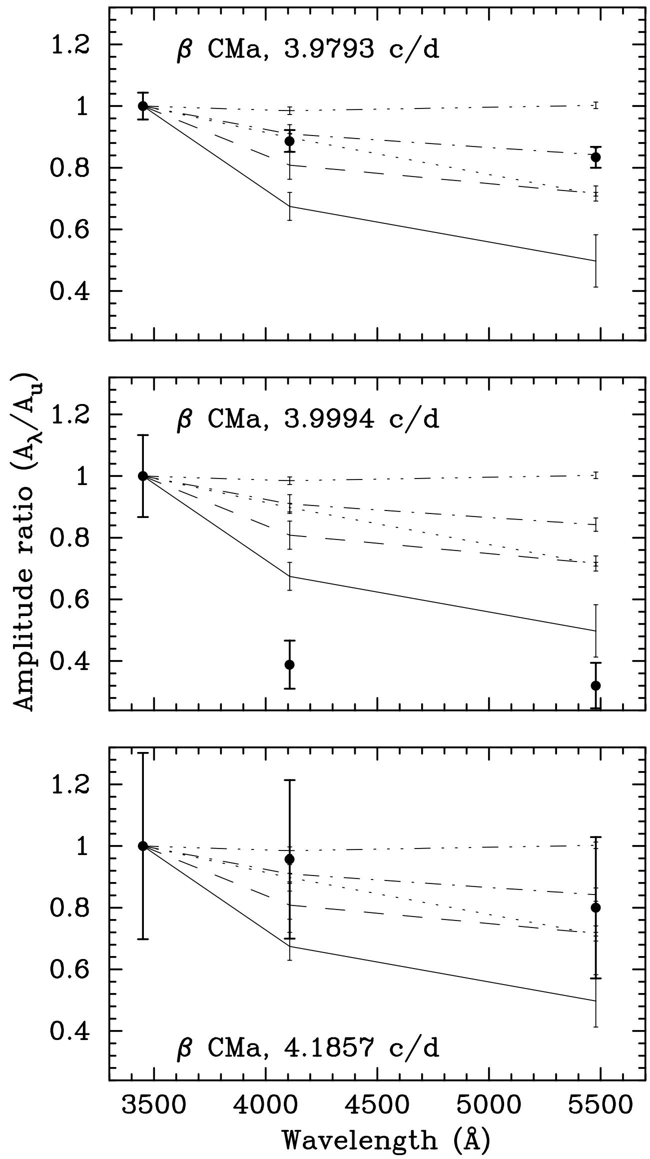

Figure 9. Mode identifications for β CMa from a comparison of observed and theoretical uvy amplitude ratios, normalized to unity at u. The filled circles with error bars are the observed amplitude ratios. The full lines are theoretical predictions for radial modes, the dashed lines for dipole modes, the dashed–dotted lines for quadrupole modes, the dotted lines for octupole ($\ell = 3$) modes, and the dashed–dot–dot–dotted lines are for $\ell = 4$. The thin error bars denote the uncertainties in the theoretical amplitude ratios.

whether these objects would justify a larger observational effort for asteroseismic purposes. We have reasonably succeeded in providing the mode identifications.

One point that appears problematic, however, is that the theoretically predicted u/v and u/y amplitude ratios for radial modes are smaller than the measured ones for β CMa and KZ Mus. Whereas the reason for this discrepancy may be incorrect differential colour extinction coefficients for β CMa that directly affect the measured amplitudes of the 3.9994 cd^{-1} mode, we cannot invoke this explanation for the 5.951 cd^{-1} mode of KZ Mus as its frequency is too different from an integer multiple of one cycle per sidereal day. In addition, the theoretical and observed $UvBV$ amplitudes derived by Handler et al. (2003) are in perfect agreement for a radial mode in

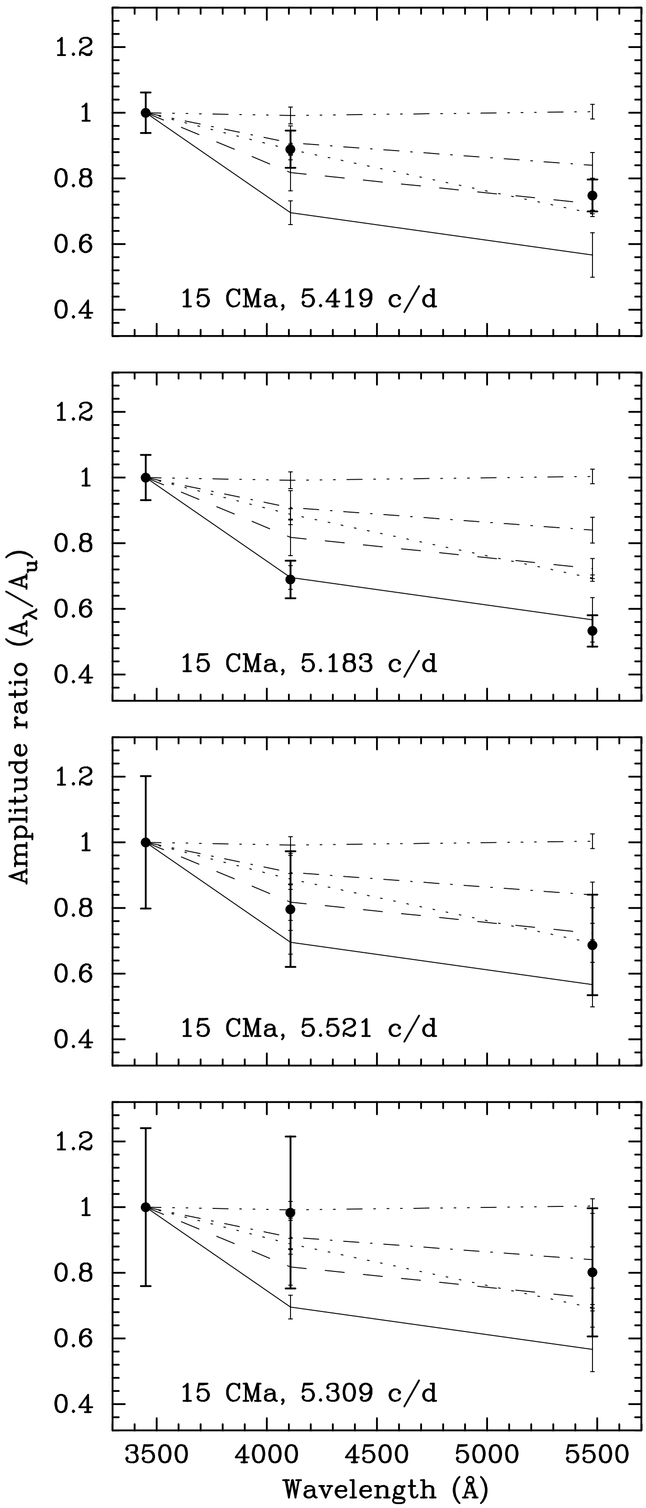

Figure 10. Mode identifications for 15 CMa from a comparison of observed and theoretical *uvy* amplitude ratios, normalized to unity at *u*. The filled circles with error bars are the observed amplitude ratios. The full lines are theoretical predictions for radial modes, the dashed lines for dipole modes, the dashed–dotted lines for quadrupole modes, the dotted lines for $\ell = 3$ modes, and the dashed–dot–dot–dotted lines are for $\ell = 4$. The thin error bars denote the uncertainties in the theoretical amplitude ratios.

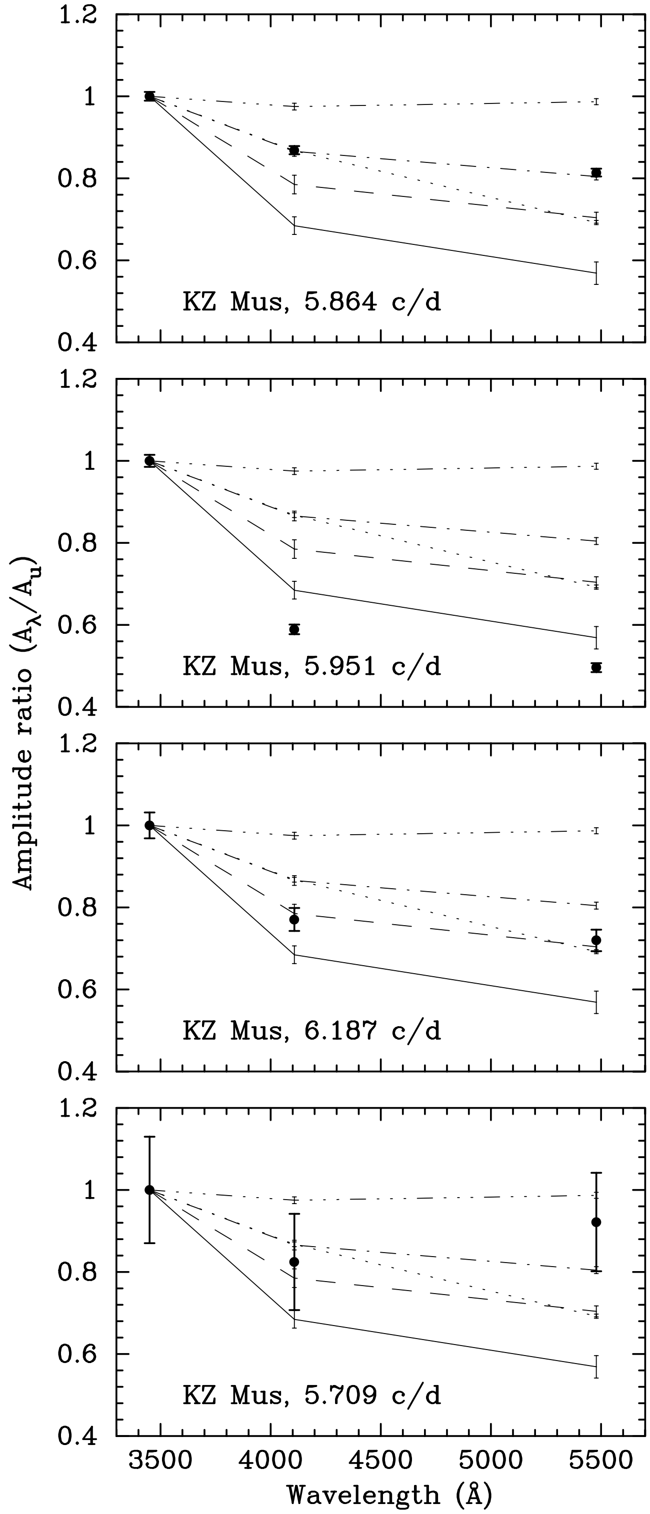

Figure 11. Mode identifications for KZ Mus from a comparison of observed and theoretical *uvy* amplitude ratios, normalized to unity at *u*. The filled circles with error bars are the observed amplitude ratios. The full lines are theoretical predictions for radial modes, the dashed lines for dipole modes, the dashed–dotted lines for quadrupole modes, the dotted lines for octupole modes, and the dashed–dot–dot–dotted lines are for $\ell = 4$. The thin error bars denote the uncertainties in the theoretical amplitude ratios.

this star. We note that we have used the same differential colour extinction correction for β and 15 CMa, which was derived from the 15 CMa data only. These two stars were measured simultaneously, and have very similar colours, which is why this procedure was soundest.

Returning to the mode identifications of the individual stars, the two strongest modes of β CMa are a quadrupole and likely a radial mode. Given the effective temperature, luminosity and thus mass inferred in Section 4, we can compute the pulsation 'constant' for such a radial mode. The result of this calculation is $Q = 0.035 \pm 0.009$ d, indicating that this mode may be the radial fundamental, although the possibility that it is the first overtone cannot be ruled out this way.

We were also able to locate a radial mode in the pulsation spectrum of 15 CMa, whose pulsation constant would be $Q = 0.027 \pm 0.007$ d. This suggests that we deal with the first radial overtone in this case, although the fundamental mode or the second overtone can also not be excluded. We note, however, that no convincing detection of a radial mode in a β Cephei star other than the fundamental has been made to date.

Three of the non-radial pulsation modes of 15 CMa are almost equally spaced in frequency. Regrettably, we cannot be sure whether these modes are $\ell = 1, 2$ or 3. Independent of the ℓ value, we can still assume that these modes do correspond to rotationally split components of the same mode to check whether this leads to reasonable results.

Doing so, and further assuming that the observed splitting corresponds to the surface rotational frequency of 15 CMa, we derive a rotation period of 9.35 d, which translates into an equatorial rotational velocity of $49 \pm 8\,\mathrm{km\,s^{-1}}$. The measured $v \sin i$ of 15 CMa is $40\,\mathrm{km\,s^{-1}}$ (Uesugi & Fukuda 1982), making it possible that the three non-radial modes of the star indeed belong to the same k and ℓ.

For KZ Mus we confirmed the mode identifications by Handler et al. (2003). Unfortunately, the ℓ value of the weakest-known independent mode of the star can still not be uniquely constrained. Repeated observations in the future may help to solve this problem as measurements from different years can be analysed together, if homogeneous filter sets (particularly bluewards of the Balmer jump) are used. If a mode identification of f_4 can be derived, we believe it is likely that theoretical asteroseismic investigations can be undertaken. Of course, additional measurements in the future may also help to reveal modes beyond our present detection limit (1.5 mmag).

To our regret, the asteroseismic prospects of β CMa do not seem to be very high. With only three modes photometrically detected and only two identified with their ℓ value, a detailed exploration of its inner structure seems unlikely. Perhaps this bright star is better studied by means of spectroscopy, for instance as done by Briquet et al. (2006).

15 CMa seems more worthwhile for further study. We have proven the existence of a radial mode, which is of tremendous importance for restricting the location of the star in the HR diagram. We have also found evidence that the remaining three non-radial modes may form a rotationally split triplet, which can be the starting point for an asteroseismic study. What still needs to be done is to prove that this is indeed a mode triplet and to determine its ℓ value.

An independent clue towards the spherical degree of this possible triplet may come from its frequency asymmetry due to the second-order effect of rotation, which is different for different ℓ. Following the definition of the asymmetry of a frequency triplet $f_- < f_0 < f_+$ by Dziembowski & Jerzykiewicz (2003):

$$A_{\rm obs} = f_- + f_+ - 2f_0,$$

we obtain $A = -0.0077 \pm 0.0015\,\mathrm{cd^{-1}}$ from our measurements and $A = -0.0004 \pm 0.0011\,\mathrm{cd^{-1}}$ from the archival data. These two values are inconsistent (perhaps due to systematic frequency errors in the single-site archival data) and can therefore not be interpreted; more time-resolved measurements are needed.

An unusual feature in the light curves of 15 CMa is that the descending branch of pulsation of the strongest mode is steeper than its rising branch. In fact, even a 'stillstand' phenomenon is indicated. This has been found in only one β Cephei star, BW Vul, to date (e.g. see Sterken et al. 1986) and is usually interpreted as a shock phenomenon in the atmosphere due to the vicious acceleration of the stellar material due to pulsation (e.g. Fokin et al. 2004).

However, there are two differences between the pulsations of BW Vul and 15 CMa: BW Vul pulsates in a single radial mode, and with much higher photometric amplitude than 15 CMa, whose mode showing the unusual light-curve form is non-radial. The small photometric amplitude can be explained under the assumption that the strongest mode of 15 CMa is the $m = 0$ component of a rotationally split multiplet. The possible range in the inclination of the pulsation axis to the line of sight may lead to heavy geometrical cancellation of such a mode (e.g. see Pesnell 1985). In other words, this mode could have high intrinsic amplitude and its low photometric amplitude is just a projection effect.

The unusual light-curve form of this mode naturally gives rise to a harmonic frequency with high relative amplitude compared to the mode causing it. Combination frequencies with abnormally high amplitudes could in some cases also be caused by resonant-mode coupling (see Handler et al. 2006, for a more detailed discussion), whereas other combination frequencies may be simple light-curve distortions caused by a non-linear response of the flux to a sinusoidal displacement due to pulsation. The sum frequencies we found in the amplitude spectra of KZ Mus seem to be such 'normal' combinations. Their relative amplitudes are in the same range as those of the 'normal' combinations of the β Cephei stars 12 Lac (Handler et al. 2006) and ν Eri (Handler et al. 2004; Jerzykiewicz et al. 2005), keeping in mind inclinational effects. Resonant-mode coupling is therefore not required to explain the combination frequencies of KZ Mus.

Finally, we noticed the occurrence of slow intrinsic variability in our residual light curves for β and 15 CMa. Such variations have been reported for several other β Cephei stars (see the discussion by Handler et al. 2006), and seem to be a fairly common phenomenon. Despite the existence of very extensive data sets, its physical cause remains unknown.

ACKNOWLEDGMENTS

This work has been supported by the Austrian Fonds zur Förderung der wissenschaftlichen Forschung under grants R12-N02 and P18339-N08.

REFERENCES

Balona L. A., Evers E. A., 1999, MNRAS, 302, 349
Balona L. A., Bregman L., Letsapa B. A., Magoro B. T., Walsh S. E., 1996, IBVS, 4313
Breger M. et al., 1993, A&A, 271, 482
Breger M. et al., 1999, A&A, 349, 225
Briquet M., Mazumdar A., Desmet M., Aerts C., 2006, A&A, submitted
Campbell W. W., 1911, Lick. Obs. Bull., 6, 140

Crawford D. L., 1978, AJ, 83, 48
Crawford D. L., Barnes J. V., Golson J. C., 1970, AJ, 75, 624
de Zeeuw P. T., Hoogerwerf R., de Bruijne J. H. J., Brown A. G. A., Blaauw A., 1999, AJ, 117, 354
Dziembowski W. A., Jerzykiewicz M., 2003, in Balona L. A., Henrichs H. F., Medupe R., eds, ASP Conf. Ser. Vol. 305, International Conference on Magnetic Fields in O, B and A Stars. Astron. Soc. Pac., San Francisco, p. 319
ESA, 1997, The Hipparcos and Tycho Catalogues, ESA, SP-1200
Feinstein A., 1967, ApJ, 149, 107
Flower P. J., 1996, ApJ, 469, 355
Fokin A., Mathias P., Chapellier E., Gillet D., Nardetto N., 2004, A&A, 426, 687
Handler G., 2005, IBVS, 5667
Handler G. et al., 2000, MNRAS, 318, 511
Handler G., Shobbrook R. R., Vuthela F. F., Balona L. A., Rodler F., Tshenye T., 2003, MNRAS, 341, 1005
Handler G. et al., 2004, MNRAS, 347, 454
Handler G. et al., 2006, MNRAS, 365, 327
Heynderickx D., 1992, A&AS, 96, 207
Heynderickx D., Waelkens C., Smeyers P., 1994, A&AS, 105, 447
Jerzykiewicz M., Handler G., Shobbrook R. R., Pigulski A., Medupe R., Mokgwetsi T., Tlhagwane P., Rodríguez E., 2005, MNRAS, 360, 619
Kołaczkowski Z. et al., 2004, ASP Conf. Ser., 310. Astron. Soc. Pac., San Francisco, p. 225
Künzli M., North P., Kurucz R. L., Nicolet B., 1997, A&AS, 122, 51
Montgomery M. H., O'Donoghue D., 1999, Delta Scuti Star Newsletter, 13, 28 (Univ. Vienna)
Moore J. H., 1936, Lick. Obs. Bull., 18, 1
Napiwotzki R., Schönberner D., Wenske V., 1993, A&A, 268, 653
Niemczura E., Daszyńska-Daszkiewicz J., 2005, A&A, 433, 659
Pamyatnykh A. A., 1999, Acta Astr., 49, 119
Pamyatnykh A. A., Handler G., Dziembowski W. A., 2004, MNRAS, 350, 1022
Pesnell W. D., 1985, ApJ, 292, 238
Pigulski A., 2005, Acta Astr., 55, 219
Shobbrook R. R., 1973a, MNRAS, 161, 257
Shobbrook R. R., 1973b, MNRAS, 162, 25
Sperl M., 1998, Master's Thesis, Univ. Vienna
Stankov A., Handler G., 2005, ApJS, 158, 193
Sterken C. et al., 1986, A&AS, 66, 11
Struve O., 1950, ApJ, 112, 520
Uesugi A., Fukuda I., 1982, Catalogue of stellar Rotational Velocities (revised), Univ. Kyoto

This paper has been typeset from a TEX/LATEX file prepared by the author.

Chapter 6

Pulsating white dwarf stars

6.1 Introduction

When a white dwarf star cools, it passes three pulsational instability strips: the hottest are the GW Virginis stars, which are pulsating DO white dwarfs, the second hottest are the V777 Herculis stars that comprise helium-atmosphere DB white dwarf stars, and the coolest are the ZZ Ceti stars, DA white dwarfs whose atmospheres are dominated by hydrogen. All pulsating white dwarfs vary with periods between about 3 to 20 minutes.

Section 6.2 looks at a peculiar GW Virginis star, HS 2324+3944. This star has a significant admixture of hydrogen in its atmosphere, which according to some model computations should cause it to be pulsationally stable. However, it does pulsate, but with time scales much longer than the "normal" GW Virginis stars, and in a very complicated way.

The V777 Herculis stars are the focus of Sect. 6.3, that starts with the discovery of only the ninth member known at the time[1], immediately permitting a determination of this star's rotation period. Section 6.3.2 reports on an extended study of two further pulsating DB white dwarf stars, and points out their interest for asteroseismology. In particular, some constraints on the helium layer mass and the $^{12}C(\alpha,\gamma)^{16}O$ nuclear reaction rate could be obtained. Section 6.3.3 is devoted to a study of amplitude variability of two V777 Herculis stars, which is shown to occur on a time scale of only a few days. Finally, Sect. 6.3.4 reports an attempt to define the instability strip of the pulsating DB white dwarfs, and to answer the important question of whether or not there are nonpulsators inside this instability region.

Two example studies of individual ZZ Ceti stars are the content of Sect. 6.4. First, a "classical" asteroseismic study of such a pulsator is presented on the basis of an extended Whole Earth Telescope run on a star with many pulsation modes. Section 6.4.2 discusses the pulsation spectrum of another ZZ Ceti star whose mode

[1]Meanwhile, the results of the Sloan Digital Sky Survey have nearly doubled this number, see Nitta et al. (2007).

frequencies are arranged in a peculiar sequence of ratios of small integer numbers and whose combination frequencies are used to constrain the physical properties of its surface convection zone.

Finally, Sect. 6.5 reports an attempt to repeat something that white dwarf asteroseismology is famous for: the V777 Herculis stars were first predicted by theory, and only later observationally confirmed. A similar prediction was made for the existence of pulsating DAO white dwarf stars of low mass. Consequently, a search for such objects was undertaken - unfortunately with no success. Is this an observational problem or are there deficiencies in the theory?

6.2 Pulsating DO white dwarfs

6.2.1 Complex light variations of the "hybrid" PG 1159 star HS 2324+3944

Original paper:

G. Handler, A. Kanaan, M. H. Montgomery, 1997, A&A 326, 692

Astron. Astrophys. 326, 692–697 (1997)

ASTRONOMY
AND
ASTROPHYSICS

Research Note

Complex light variations of the "hybrid" PG 1159 star HS 2324+3944

G. Handler[1], **A. Kanaan**[3,4], **and M.H. Montgomery**[3]

[1] Institut für Astronomie, Universität Wien, Türkenschanzstraße 17, A-1180 Wien, Austria (gerald@procyon.ast.univie.ac.at)
[2] Department of Astronomy and McDonald Observatory, University of Texas, Austin, TX 78712, USA
[3] Instituto de Fisica, Universidade Federal do Rio Grande do Sul, 90049 Porto Alegre-RS, Brazil

Received 11 March 1997 / Accepted 15 April 1997

Abstract. We present 17.36 hours of new time-series photometric observations of the variable "hybrid" PG 1159 star HS 2324+3944. These data allow us to demonstrate the presence of four frequencies in the light variations with evidence for more. The dominating time scale of the variability (around 35 minutes) is much longer than that of GW Vir pulsators.

Binarity is not likely to cause the object's light variations. A pulsational origin of the variability seems more attractive. Recent theoretical investigations suggest that pre-white dwarf pulsations can be excited despite the presence of hydrogen in the model's driving region.

Key words: stars: oscillations – stars: individual: HS 2324+3944 – stars: white-dwarfs

1. Introduction

HS 2324+3944 is one of only four "hybrid" PG 1159 stars. The latter objects are a subgroup of DO white dwarfs, whose spectra are dominated by He II, C IV and O VI (Sion et al. 1985). On the other hand, the spectra of "hybrids" show an He II/C IV absorption trough similar to the "classical" PG 1159 stars, but also strong Balmer lines (Napiwotzki & Schönberner 1991).

About 30% of the PG 1159 stars are multiperiodic nonradial g-mode pulsators (the GW Vir stars). Driving of these pulsations is believed to be caused by the κ-γ-mechanism in the region of partial ionisation of carbon and oxygen (Starrfield et al. 1985).

Analyzing two weeks of almost continuous data gathered with the Whole Earth Telescope network, Winget et al. (1991) identified more than 100 pulsation modes in PG 1159-035. This allowed an unprecedented investigation of the object's inner structure by means of precision asteroseismology. Similar analyses of other GW Vir stars have been performed in the recent years (e. g. Kawaler et al. 1995).

However, according to model calculations, the efficiency of the above κ-γ-mechanism seems to be very sensitive to the chemical composition in the driving region, which is located very close to the stellar surface. In particular, the presence of hydrogen in the driving zone is believed to inhibit pulsations (Stanghellini et al. 1991). Regrettably, asteroseismological investigations were not helpful in constraining the structure of the driving regions, since the eigenfunctions of the observed modes have little weight in these parts of the models.

The spectral analysis by Dreizler et al. (1996) places HS 2324+3944 in the GW Vir instability strip. However, their analysis shows the presence of hydrogen as well. Dreizler et al. suggested that HS 2324+3944 should be observed photometrically to look for pulsational variability. This, they suggested, would provide a test for Stanghellini et al.'s (1991) models which predict no pulsations when the partial ionization zone is contaminated by hydrogen.

Silvotti (1995, 1996) obtained two nights of time-series photometric data of HS 2324+3944. He discovered the star to be variable with a period of about 35 minutes and suggested this is due to high-order g-mode pulsations. However, such a period is a factor of 3–4 larger than the periods of GW Vir pulsators.

There is a second possibility to explain the light variations of HS 2324+3944: binarity. The AM CVn stars (see Provencal (1994) and Warner (1995) for detailed discussions) are helium-transferring double-degenerate binaries with orbital periods of the same order as the time scale of the variations of HS 2324+3944 reported by Silvotti (1995, 1996). Hence, it should not be ruled out without further scrutiny that HS 2324+3944 be a related object, although spectroscopic observations (Dreizler et al. 1996) did not show evidence of mass transfer.

Send offprint requests to: G. Handler

Table 1. Journal of the observations

Telescope	Observer(s)	Detector	Date (UT)	Start (UT)	Length (hrs)
McD 2.1 m	GH	PMT	13 Dec 95	2:18:28	1.90
McD 2.1 m	GH	PMT	15 Dec 95	1:11:44	2.71
McD 0.9 m	GH, AK, MHM	CCD	16 Dec 95	2:29:02	3.60
McD 0.9 m	GH, AK, MHM	CCD	17 Dec 95	2:38:05	3.05
McD 0.9 m	GH	CCD	20 Dec 95	1:05:06	1.08
McD 0.9 m	GH	CCD	21 Dec 95	3:13:18	0.50
McD 0.9 m	GH	PMT	27 Dec 95	1:22:54	1.64
McD 0.9 m	GH	PMT	28 Dec 95	1:24:33	2.88
				Total	17.36

Earlier observations of ours (of a quality too low to publish) confirmed the unusual variability. Therefore, and because Silvotti's data set was too small to determine whether the variations are multiperiodic or not, we carried out a more extensive photometric study of HS 2324+3944.

2. Data acquisition and reduction

In December 1995, we acquired eight time-series photometric runs of HS 2324+3944 during a time span of 15 days. Three different telescope/instrument combinations at McDonald Observatory were used: the 2.1 m telescope with a two-channel photoelectric photometer (no filter), the 0.9 m telescope with a CCD (B filter) and the 0.9 m telescope with the two-channel photometer (no filter). This choice of the filters ensures measurements at approximately the same effective wavelength for both the photoelectric and CCD data. An observing log is given in Table 1.

2.1. CCD observations

For our CCD observations we used a Tektronics 2048×2048 CCD with 27μm pixels binned 2×2. The full width at half maximum through most of the measurements was about $3''0$. Each observation consisted of a 60 second exposure; we attempted to observe as many comparison stars on the same frame together with HS 2324+3944. By reading out only part of the chip we decreased the readout time as far as possible. In this way, we acquired one observation each 70 seconds.

The frames were corrected for bias and flat field effects using the standard IRAF procedures. Photometric reductions were then accomplished using the IRAF APPHOT task. We extracted the magnitudes of HS 2324+3944 plus 7 or 8 comparison stars and selected the aperture size giving the lowest scatter for the comparison star data. We double-checked the constancy of the comparison stars by calculating amplitude spectra of their magnitudes relative to the brightest comparison star and relative to the mean of all comparison stars. No evidence for variability of any of these objects was found within the 4 nights of CCD observation. Final synthetic comparison star magnitudes were computed by adopting a weighted mean of the measurements of the individual objects.

These synthetic comparison star data were subtracted from the measurements of HS 2324+3944 on a point-by-point basis and a correction for differential extinction was applied (since HS 2324+3944 is much bluer than its comparison stars). Finally, all the times of measurement were converted into Heliocentric Julian Date (HJD) and the data were subjected to further analysis.

We also note that the nightly mean magnitudes of HS 2324+3944 relative to the comparison stars did not change during the observations.

2.2. Photoelectric observations

Since the variability of the target object happens on time scales at which slow variations in sky transparency can already occur, we checked the quality of the nights by means of the Channel 2 comparison star. The latter was assumed to be photometrically constant, since it was also one of the comparison stars used during the CCD measurements and not found to be variable in these data. Since we had only two channels available and could thus not check the stability of the sky background, we chose a Channel 2 star with star/sky count ratio similar to that of the variable. In this way, we could roughly test for possible sky background variations (and did not find any during our measurements).

We started the reductions with discarding bad data. Consequently, we performed sky subtraction by a piecewise linear or spline fit to our sky measurements (which were obtained by interrupting the target light curves each 20 – 30 minutes). Then we corrected the data for extinction. The mean magnitude of each run was set to zero. If some systematic trends in the data not attributable to intrinsic variations of HS 2324+3944 remained, we removed them by fitting a straight line to the data. Finally, we summed the photoelectric measurements in 70-second bins to give them equal weight to the CCD data, and we calculated the HJD of each observation. Fig. 1 shows our reduced light curves together with a four-frequency fit to be derived in Sect. 3, where we will further comment on this plot.

3. Frequency analysis

Our final time series was analysed with a period-finding package (Breger 1990), using single-frequency Fourier and multiple least-squares sine wave fitting methods. These programs allow us to search for promising peaks and prewhiten the data by calculating simultaneous n-frequency fits[1].

In this way three frequencies can easily be revealed in the light variations of the program star (Fig. 2). As can be seen in the third lowest panel of Fig. 2, there may still be more periodicities hidden in the data. However, special care must be taken

[1] During our prewhitening process we do not necessarily choose the highest peak in our successive power spectra as the next frequency to be included in our solution. Because of the aliasing present we rather select the frequency combination yielding the lowest residuals between the observed light curves and the calculated fit. We consider this approach to be more reliable.

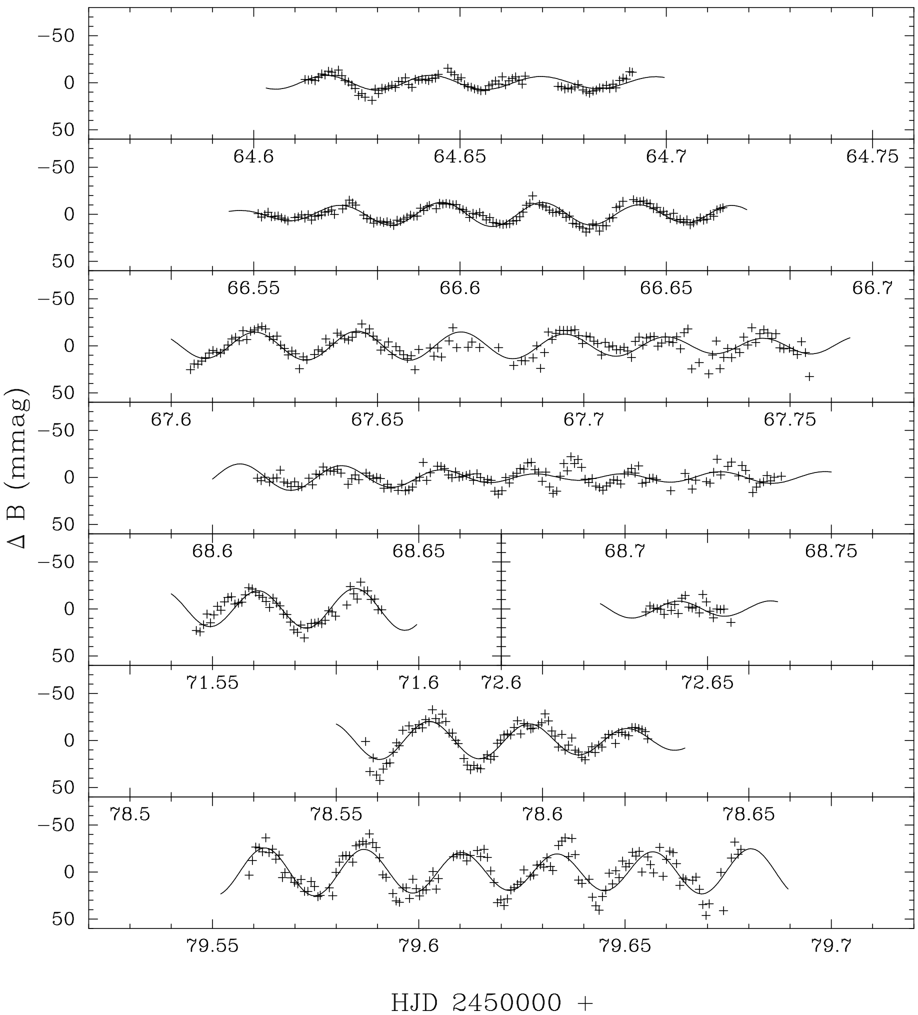

Fig. 1. B-light curves and the corresponding 4-frequency fit (derived in Sect. 3) for our data of HS 2324+3944

when trying to identify them. Therefore, we estimated a detection threshold for intrinsic variations by analysing high-speed photometric observations of constant stars, reduced and sampled in the same way as our data of HS 2324+3944. The nightly scatter was scaled to the same level as the residuals between the program star's light curve and our fit. Using this method we concluded that we may detect signals with an amplitude of about 3 mmag at frequencies around 200 μHz, and 2.5 mmag signals around 1000 μHz. We note that in the presence of strong aliasing like in our data the adoption of signal-to-noise criteria or false alarm tests is less safe.

The next promising frequency to consider is near 408.8 μHz. Its amplitude is almost 4 mmag, and by dividing our data in different subsets (e.g. using the three different telescope/detector combinations), we found out that this signal has constant amplitude and phase throughout the whole data set. On the other hand, adopting the daily alias of this frequency (which is stable throughout the data set as well) at 420.4 μHz for a four-frequency fit, the residual scatter of the light curve is only 0.03% larger. Hence, we cannot decide which of the two peaks is real, and we must consider both as a possible solution.

Including this fourth frequency in our fit and removing the improved fit from our data, a further signal at 368.6 μHz (or 379.3 μHz, when the 420.4 μHz frequency is assumed) becomes conspicuous (second lowest panel of Fig. 2). This signal is present in the whole data set with constant amplitude and phase as well, but its low amplitude of about 2.5 mmag prevents us from suggesting it is intrinsic to the star.

There is further power between 750 and 950 μHz (lowest panel of Fig. 2), which exceeds our detection threshold as estimated above. However, when testing these variations for amplitude and phase stability, they are very prominent in only a few of the nights (mostly December 17 and 27, see below for more). Moreover, the dominating peaks in this frequency region do not correspond to linear combinations or harmonics of the already detected frequencies (Fig. 3). Hence we cannot reliably include them in our frequency solution and we are left with four secure frequencies in the light curves of HS 2324+3944. These are summarized in Table 2. The errors in frequencies, amplitudes and phases as listed in Table 2 are formal errors determined following Kovacs (1981) and should be taken only as estimates.

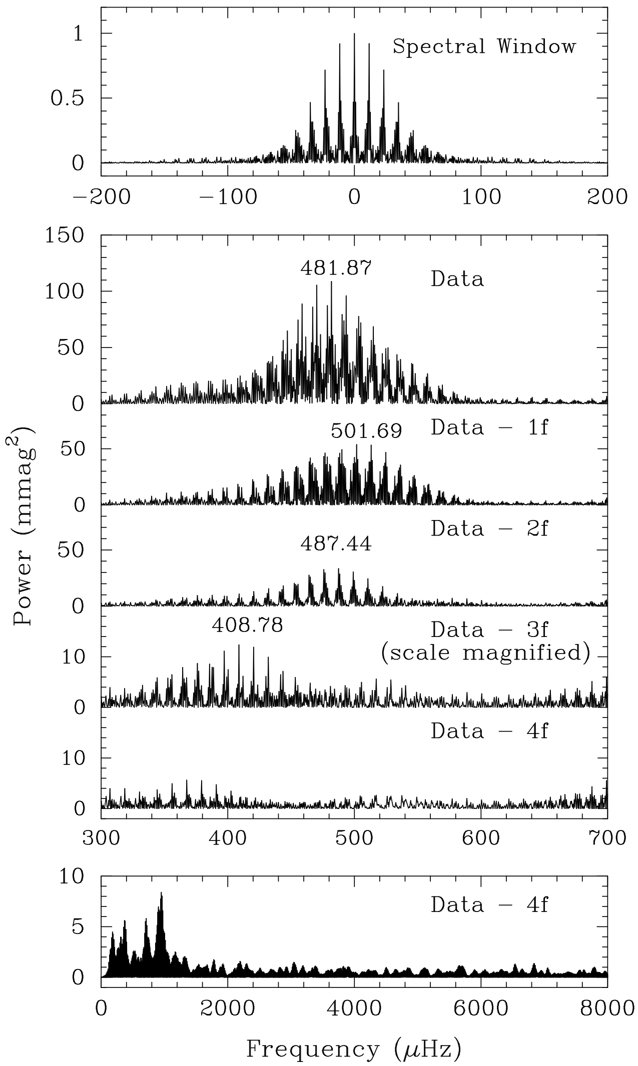

Fig. 2. Power spectra of HS 2324+3944. Four frequencies are detected in the star's light variations

Of course, due to the aliasing present and despite our great care, the frequency values are not definite. They may differ from the values in Table 2 by their daily aliases. It may be suspected that f_2 and f_4 (f_{4a}, respectively) are aliases of each other. However, when calculating residual power spectra of our light curves after removing the variations due to f_1 and f_3, both f_2 and f_4 (f_{4a}) are present, and no alias of either of these frequencies can account for the presence of both maxima in our power spectra.

Our synthetic light curves calculated with the parameters in Table 2 fit the light curves well, except the second half of the run obtained on HJD 2450068. It seems that in this night the variability of the star suddenly switched to a faster time scale. We do not think that this is a sign of inaccurate measurements, since our comparison star data for that night did not show any suspicious behavior. It rather seems likely that further presently undetected frequencies are active in HS 2324+3944.

On the other hand, we are unable to fit these variations when including some promising frequencies near 900 μHz. We are careful to note that the excess power near 900 μHz is present (but it is less strong) when we exclude the Dec 17 run from the analysis; hence it cannot originate from this night only. Its cause remains unexplained.

Table 2. The 4-parameter fit calculated for our light curves of HS 2324+3944

	Frequency (μHz)	Amplitude (mmag)	Epoch (HJD 2450000 +)
f_1	481.87 ± 0.01	11.6 ± 0.5	64.5726 ± 0.0002
f_2	501.69 ± 0.02	6.8 ± 0.5	64.5911 ± 0.0003
f_3	487.44 ± 0.03	6.9 ± 0.5	64.5822 ± 0.0004
f_4	408.78 ± 0.04	3.8 ± 0.5	64.5855 ± 0.0008
(f_{4a})	(420.41 ± 0.04)	(3.8 ± 0.5)	(64.5873 ± 0.0008)

Since we used three different telescope/detector combinations during our observations, it is interesting to compare the accuracy of these measurements. We find that the photoelectric observations with the 2.1 m telescope show a residual scatter between light curve and fit of less than 5 mmag per 70-second integration, while the 0.9 m CCD measurements are accurate to about 8 mmag per integration and the 0.9 m photoelectric observations have an rms error of about 10 mmag. This may suggest that CCD observations are to be preferred for a star of a magnitude and time scale of light variation similar to HS 2324+3944 (V = 14.8). We note, however, that the 0.9 m photoelectric data had a large contribution of moonlight, and thus their quality suffered from this influence.

4. Discussion

Our analysis shows that HS 2324+3944 is very likely a multiperiodic variable. In principle, this can be explained by both a pulsation and a binary hypothesis. Before we start discussing these two possibilities, let us note that Ciardullo & Bond (1996) - during their survey for variability among O VI central stars of Planetary Nebulae - observed the three other "hybrid" PG 1159 stars and reported suspected variations of two of those objects (A 43 and NGC 7094) with periods near 40 minutes and 2 hours, respectively. For the fourth, much fainter "hybrid" (Sh 2-68), their data was not conclusive.

Considering a binary hypothesis, it has to be pointed out that AM CVn stars may show complicated power spectra. These usually contain two independent frequencies (believed to be the orbital frequency and the rotational period of the accretor), which are different by only a few percent. Furthermore, linear combinations and harmonics of these frequencies may be present, as well as sidebands to the fundamental and harmonic periods (the frequency difference of these sidebands to the central frequency is believed to be the inverse precession period of the necessarily elliptical accretion disc). Comparing these features to our frequency solution, it is easy to see that the three close frequencies near 500 μHz we found in our data of HS 2324+3944 can be explained by such a binary hypothesis. However, the presence of the fourth frequency near 410 μHz

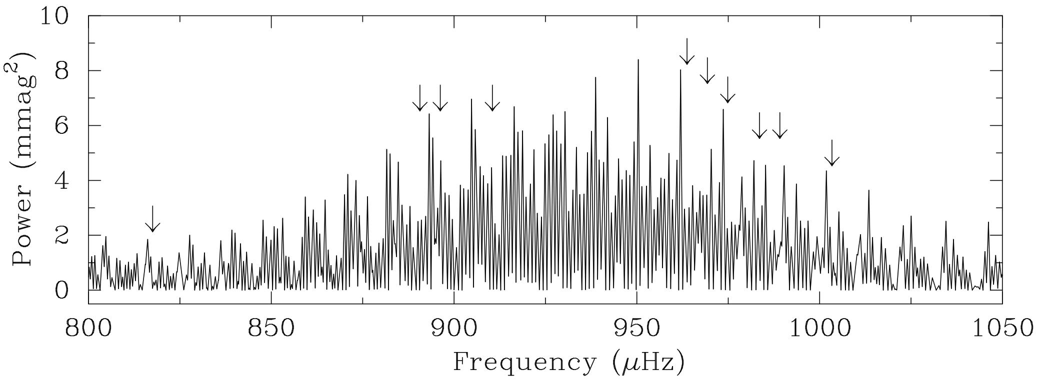

Fig. 3. Power spectra of HS 2324+3944 in the range where linear combinations or harmonics of the four detected frequencies may be present. The ten possible combinations are indicated with arrows. No agreements with the dominating peaks are visible.

does not fit into this scheme and argues against a binary origin of all the different periodicities.

Moreover, there is no spectroscopic correspondence between AM CVn stars and "hybrid" PG 1159-type stars. AM CVn stars have no hydrogen in their spectra; those of HS 2324+3944 show no evidence for mass transfer.

Consequently, the explanation of the variability of HS 2324+3944 in terms of high-order g-mode pulsations becomes attractive. The (nearly) sinusoidal light curves, the photometric amplitudes of the variations and the multiperiodicity point towards the excitation of pulsations.

Another interesting speculation can be made on the possible presence of two "magic numbers" in our frequencies. Firstly, the pulsating PG 1159 central star of NGC 1501 (Bond et al. 1996) shows frequency ratios very close to $\sqrt{3}/2$. These are interpreted in terms of trapped modes (see the paper cited above for more information). Interestingly, the ratio of our frequency f_{4a} to f_2 is within 1% of $\sqrt{3}/2$ as well as the ratio of the suspected signal at 368.6 μHz and f_{4a}. Secondly, mean period spacings of 20– 23 seconds (used to determine the masses) are present in the $\ell = 1$ modes of several GW Vir pulsators. The period difference of the two closest frequencies we determined for HS 2324+3944 is 23.7 seconds.

As mentioned in the Introduction, the efficiency of the driving mechanism for GW Vir pulsators has originally been found to be very sensitive to the chemical composition of the driving region of the models used. However, recent theoretical investigations provided several clues to resolve this difficulty:

In their detailed investigation of pulsation driving in GW Vir models, Bradley & Dziembowski (1996) could only duplicate the observed frequency range with oxygen-rich compositions in the driving region. Furthermore, the surface abundances of some pulsating and nonpulsating PG 1159 stars are so identical, that they are sometimes called "spectroscopic twins". Consequently, Bradley & Dziembowski (1996) suggested that no GW Vir star has a driving region with photospheric abundances. This can of course also be taken as a reason why a "hybrid" PG 1159 star may pulsate.

The periods we found for HS 2324+3944 are between 1990 and 2450 seconds. Bradley & Dziembowski (1996) could only match the maximum unstable periods for the hotter GW Vir stars (e.g. about 1000 seconds for PG 1159-035 itself[2]) by using models with a combination of oxygen-rich driving regions and artificially increased radii. This implies that Bradley & Dziembowski models used to fit the periods of HS 2324+3944 would require even larger radii.

Saio (1996) presented model calculations for pulsations of hydrogen-deficient stars by using new OPAL opacities. These models suggested that the sensitivity of the driving mechanism to the chemical composition in the driving region of pre-white dwarfs is not as strong as previously assumed.

Gautschy (1997) computed envelope models for GW Vir stars and HS 2324+3944. His results disagreed with those of Bradley & Dziembowski (1996). Gautschy's instability domains matched the observed frequency distributions of GW Vir stars well, except for the short period modes. He did not need to postulate chemical compositions in the driving region differing from the photospheric compositions and he did not require artificially increased radii for a good match to the observed frequency ranges.

Another result of Gautschy's (1997) explorations is that the existence of hydrogen in the driving zone does not necessarily influence the pulsational instability of HS 2324-like envelope models. He obtained unstable modes even with a hydrogen admixture of 20% in mass and he suggested that the differences between his results and those of Bradley & Dziembowski (1996) may simply be a consequence of differences in the numerical treatment of the nonadiabatic oscillations.

Anyway, theoretical approaches to possible pulsations of HS 2324+3944 still need refinement. A larger observational database to improve our knowledge of the variability of "hybrid" PG 1159 stars is also required. To this end, a multisite campaign of HS 2324+3944 is being planned.

[2] This may be an observational long-period cutoff because of the observing and analysis techniques used by Winget et al. (1991).

Acknowledgements. This research was partially supported by the Austrian Fonds zur Förderung der wissenschaftlichen Forschung under grant No. S-7309 as well as the Austrian Zentrum für Auslandsstudien.

GH also thanks the vice-director of McDonald Observatory, Thomas G. Barnes, for the generous allocation of telescope time. Stefan Dreizler, Darragh O'Donoghue, Klaus Werner and Roberto Silvotti provided helpful discussions.

References

Bond, H. E., Kawaler, S. D., Ciardullo, R., et al., 1996, AJ 112, 2699
Bradley, P. A., Dziembowski, W. A., 1996, ApJ 462, 376
Breger, M., 1990, Communications in Asteroseismology No. 20 (University of Vienna)
Ciardullo, R., Bond, H. E., 1996, AJ 111, 2332
Dreizler, S., Werner, K., Heber, U., Engels, D., 1996, A&A 309, 820
Gautschy, A., 1997, A&A, in press
Kawaler, S. D., O'Brien, M. S., Clemens, J. C., et al., 1995, ApJ 450, 350
Kovacs, G., 1981, Ap&SS 78, 175
Napiwotzki, R., Schönberner, D., 1991, A&A 249, L16
Provencal, J. L., 1994, PhD thesis, University of Texas
Saio, H., ASP Conf. Ser. 96, 361
Silvotti, R., 1995, IBVS 4265
Silvotti, R., 1996, A&A 309, L23
Sion, E. M., Liebert, J., Starrfield, S. G., 1985, ApJ 292, 471
Stanghellini, L., Cox, A. N., Starrfield, S. G., 1991, ApJ 383, 766
Starrfield, S. G., Cox, A. N., Kidman, R. B., Pesnell, W. D., 1985, ApJ 293, L23
Warner, B., 1995, Ap&SS 225, 249
Winget, D. E., Nather, R. E., Clemens, J. C., et al., 1991, ApJ 378, 326

This article was processed by the author using Springer-Verlag LaTeX A&A style file *L-AA* version 3.

6.2.2 The photometric behaviour of the peculiar PG 1159 star HS 2324+3944 at high frequency resolution

Original paper:

R. Silvotti, S. Dreizler, **G. Handler,** X. J. Jiang, 1999, A&A 342, 745

Astron. Astrophys. 342, 745–755 (1999)

ASTRONOMY
AND
ASTROPHYSICS

The photometric behaviour of the peculiar PG 1159 star HS 2324+3944 at high frequency resolution*

R. Silvotti[1], **S. Dreizler**[2], **G. Handler**[3], **and X.J. Jiang**[4]

[1] Osservatorio Astronomico di Capodimonte, via Moiariello 16, I-80131 Napoli, Italy
[2] Institut für Astronomie und Astrophysik, Waldhäuser Strasse 64, D-72076 Tübingen, Germany
[3] Institut für Astronomie, Universität Wien, Türkenschanzstrasse 17, A-1180 Wien, Austria
[4] Beijing Astronomical Observatory and United Laboratory of Optical Astronomy, CAS, Beijing 100012, P.R. China

Received 6 August 1998 / Accepted 9 November 1998

Abstract. We present the results from 135 hours of nearly continuous time series photometry on the "hybrid" (H-rich) PG 1159 variable star HS 2324+3944, obtained in August–September 1997. The power spectrum of the data shows several frequencies (about 20 or more), concentrated in three narrow and very crowded regions near 475, 390 and 950 μHz in decreasing amplitude order. Most (if not all) of the peaks in the latter region are linear combinations of the high-amplitude frequencies between 455 and 500 μHz. If we divide the data set into two equal parts, the power spectra are different. This is probably due to a not sufficiently long (and therefore not completely resolved) light curve; nevertheless an alternative hypothesis of a single damped oscillator may not be completely ruled out. If we adopt the first hypothesis, the high concentration of peaks between 455 and 500 μHz suggests the presence of both l=1 and l=2 high-overtone nonradial g-modes. The insufficient frequency resolution of our data does not allow to obtain definite precision asteroseismology results. Nevertheless a spacing of the signals is observed, probably due to stellar rotation with a period of 2.3 days. If the signal spacing was due to the successive overtones, the period spacings would be equal to 18.8 (l=1) and 10.4 (l=2) s.

Key words: stars: individual: HS 2324+3944 – stars: oscillations – stars: AGB and post-AGB

1. Introduction

1.1. Pulsating and nonpulsating PG 1159 stars

The stars of the PG 1159 spectral class (31 members) constitute the intermediate evolutionary phase between the end of the constant luminosity phase – at the tip of the asymptotic giant branch (AGB) – and the beginning of the white dwarf (WD) cooling phase. Probing their interior structure provides direct constraints on both classes of stars and may help to understand better the transition from AGB to WDs and the nuclear burning turn off process. A powerful method to probe the interior structure of the pre-WD stars and to determine some of their basic stellar parameters is given by asteroseismology. This is possible because 15 PG 1159 stars and central stars of planetary nebulae (CSPN) of type [WC], called GW Vir stars from the prototype (PG 1159-035), show multiperiodic luminosity variations which have been interpreted as nonradial g-mode pulsations. Among them, ten are CSPN, while five appear not to be surrounded by a nebula (Bradley 1998). The nature of the luminosity variations of the GW Vir stars was first proven to be stellar pulsation in the case of PG 1159-035 itself (Winget et al. 1991). Nevertheless, and despite the successful results from adiabatic models to which we will refer to below, the pulsation mechanism of the GW Vir stars is still not well understood. Although almost all authors agree that the pulsations should be driven by the κ–γ mechanism, based on the C/O cyclic ionization (Starrfield et al. 1984), a good agreement between spectroscopic abundances and observed pulsation periods has not been found yet (Bradley & Dziembowski 1996). A new element in this picture was recently added by Dreizler & Heber (1998): their results suggest that the GW Vir pulsations could be related to the nitrogen abundance. On the other hand, in the adiabatic pulsation field, theory may explain several observed phenomena as frequency splitting due to rotation and/or magnetic fields, period spacing of successive overtones, and variations around the average period spacing caused by mode trapping in the outer layers of the star (Kawaler & Bradley 1994 and references therein). However, the measurement of frequency and period spacing, which leads to accurate determination of rotation, weak magnetic fields, stellar mass, external layer masses, and even luminosity and distance, needs power spectra with low noise and high frequency resolution. For these reasons it is necessary to obtain long and nearly continuous data sets, such as those obtained by the Whole Earth Telescope network (Nather et al. 1990).

1.2. HS 2324+3944

The star HS 2324+3944 (hereafter HS 2324) is one out of four peculiar members of the PG 1159 spectral class showing strong H Balmer absorption in their spectra (Dreizler et al. 1996), called

Send offprint requests to: R. Silvotti (silvotti@na.astro.it)

* Based on observations obtained at the McDonald, Loiano and Beijing Observatories and at the German-Spanish Astronomical Center, Calar Alto, operated by the Max-Planck-Institut für Astronomie Heidelberg jointly with the Spanish National Commission for Astronomy.

Table 1. Journal of the observations

Telescope	Instrument	Observer	Date (UT)	Start Time (UT)	Run Length (hours)
McDonald 2.1 m	PMT	GH	26 Aug 1997	07:31:20	3.55
McDonald 2.1 m	PMT	GH	27 Aug 1997	04:45:00	6.33
Loiano 1.5 m	PMT	RS	27 Aug 1997	20:19:16	3.54
McDonald 2.1 m	PMT	GH	28 Aug 1997	03:16:00	7.66
McDonald 2.1 m	PMT	GH	29 Aug 1997	03:10:30	7.59
Loiano 1.5 m	PMT	RS	29 Aug 1997	23:32:57	1.00
Loiano 1.5 m	PMT	RS	30 Aug 1997	21:57:57	4.84
McDonald 0.9 m	PMT	GH	31 Aug 1997	03:49:30	0.58
Loiano 1.5 m	PMT	RS	31 Aug 1997	22:01:01	5.00
Beijing 0.85 m	PMT	JX	01 Sep 1997	16:17:20	1.03
Calar Alto 2.2 m	CCD	SD	01 Sep 1997	19:58:51	8.98
Loiano 1.5 m	PMT	RS	01 Sep 1997	21:30:01	5.49
Beijing 0.85 m	PMT	JX	02 Sep 1997	11:59:40	8.39
Loiano 1.5 m	PMT	RS	02 Sep 1997	20:05:19	4.29
Calar Alto 2.2 m	CCD	SD	02 Sep 1997	22:16:23	6.20
McDonald 0.9 m	PMT	GH	03 Sep 1997	02:39:40	8.73
Beijing 0.85 m	PMT	JX	03 Sep 1997	12:04:20	8.27
Calar Alto 2.2 m	CCD	SD	03 Sep 1997	20:30:41	8.29
Beijing 0.85 m	PMT	JX	04 Sep 1997	16:03:30	4.10
Loiano 1.5 m	PMT	RS	04 Sep 1997	19:23:35	5.77
Calar Alto 2.2 m	CCD	SD	04 Sep 1997	19:32:06	9.28
McDonald 0.9 m	PMT	GH	05 Sep 1997	05:31:30	1.76
Calar Alto 2.2 m	CCD	SD	05 Sep 1997	19:32:18	8.82
McDonald 0.9 m	PMT	GH	06 Sep 1997	02:39:10	8.77
McDonald 0.9 m	PMT	GH	07 Sep 1997	06:05:00	5.38
McDonald 0.9 m	PMT	GH	08 Sep 1997	02:25:40	9.10

"hybrid PG 1159 stars" (Napiwotzki & Schönberner 1991) or lgEH PG 1159, following the notation scheme of Werner (1992). It has an effective temperature of $(130\,000 \pm 10\,000)$ K and a surface gravity $\log\,g$=6.2 $\pm$ 0.2 (Dreizler et al. 1996). Recent new analysis of the HST-GHRS spectrum of HS 2324 show that the C/He and O/He ratio (0.4 and 0.04 by number) is as high as in ordinary PG 1159 stars (Dreizler 1998). Therefore only the hydrogen abundance (H/He=2 by number) makes it unusual. HS 2324 does not show direct signs of on-going mass loss from P Cygni shaped line profiles, like several other luminous PG 1159 stars (Koesterke et al. 1998). However, detailed line profiles from high resolution Keck spectroscopy show evidence of mass loss in the order of roughly $10^{-8}\ M_{\odot}/yr$ (Dreizler et al., in preparation). Regarding effective temperature and gravity, it belongs to the subgroup of luminous PG 1159 stars which are in general Central Stars of Planetary Nebulae. However, differently from all the other known hybrid PG 1159 stars, no nebula is detected around HS 2324 (Werner et al. 1997).

HS 2324 was discovered to be variable by Silvotti (1996). Handler et al. (1997), with more extensive observations, showed that at least four different frequencies were active and therefore that the GW Vir hypothesis was the most likely. For other two hybrid PG 1159 stars, the nuclei of A 43 and NGC 7094, periodic light variations are only suspected (Ciardullo & Bond 1996). The interest for the variability of HS 2324 is enhanced by its hydrogen abundance. The presence of H was generally considered as a inhibitor of pulsations (Stanghellini et al. 1991). First steps to test the effects of the presence of H in the driving regions have been undertaken by Saio (1996) and Gautschy (1997). The models of Saio (1996) do pulsate with 3% of H mass fraction. The models of Gautschy (1997) are able to reproduce the observed periods of HS 2324, with a very similar H abundance of 20% by mass.

For all the reasons stated above, HS 2324 is a very interesting star: the analysis of its photometric behaviour at high frequency resolution may give important results not only for a detailed study of the star itself, but also for more general questions regarding the GW Vir pulsation phenomenon. Therefore we decided to carry out a multisite photometric campaign on HS 2324, which may be considered as a first step for successive more extensive campaigns.

2. Observations

The multisite campaign on HS 2324 was performed during 2 weeks in August–September 1997, centered on new Moon. The journal of observations in Table 1 gives information on the observatories involved, telescopes and instruments used, and duration of the single runs. Most observations were obtained using two or three channel photometers with bialkali photomultipliers (EMI9784QB for Loiano, Hamamatsu R647 for Beijing and McDonald), no filters, and an integration time of 10 s, which was subsequently merged to 90 s. The leak of sensitivity to periods shorter than 180 s did not give us any trouble because no

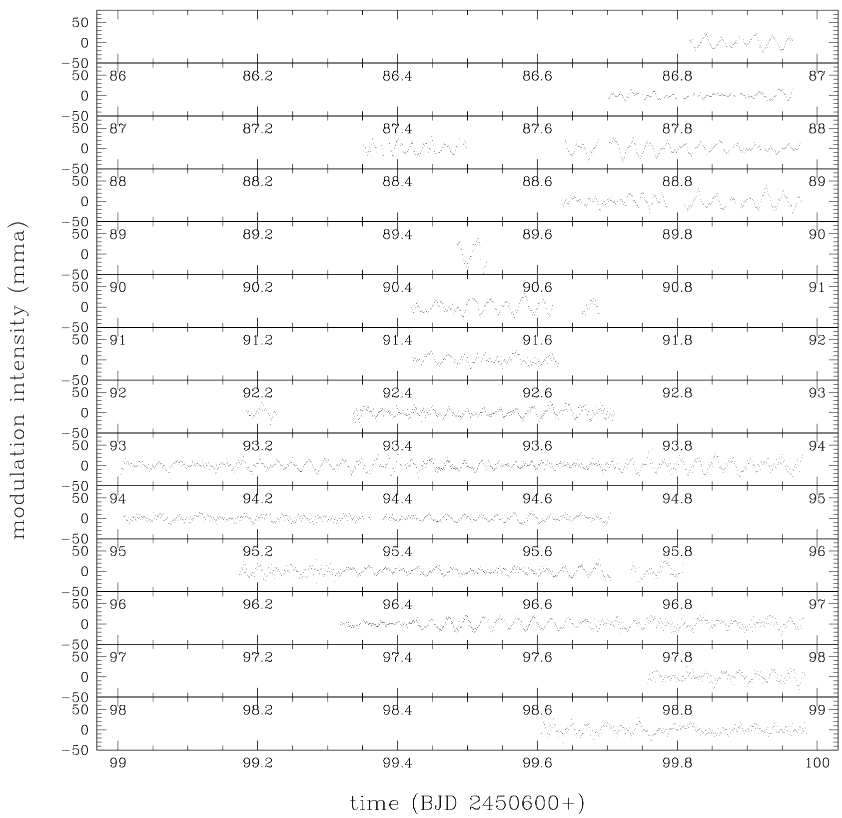

Fig. 1. The complete light curve of HS 2324; each panel represents 24 hours.

signals were detected in that range from a preliminary analysis of the photometer data alone. Only the Calar Alto data were collected using a SITe#1d CCD, B filter, and an exposure time of about 20 s (first two nights) or 40 s (following three nights) for each datum; the times between successive data points vary between about 70 and 100 s. The error introduced by the different effective wavelengths of each detector has been evaluated to be not more than 5% in amplitude.

Despite the small number of participants in the campaign, only four, we obtained a good coverage, comparable with other multisite campaigns, thanks to the good weather conditions in most nights at the different sites. The complete (and combined) light curve is shown in Fig. 1; it has a total duration of 134.9 hours, with an overall duty cycle of 43%. In the central part of the run (40.8 hours), the duty cycle is 98%.

2.1. Details on data acquisition and reduction

We followed basically the same data reduction procedure as described in Handler et al. (1997). Here we summarize this procedure and give some detail on a few differences.

For the Beijing and McDonald photoelectric data, we chose the same comparison star already used by Handler et al. (1997), which was also one of the comparison stars used in the Calar Alto CCD measurements. For the Loiano photoelectric data this was not possible because the box of channel 2 is more distant from channel 1: therefore we used the same comparison star already used by Silvotti (1996). Both comparison stars were tested again for photometric constancy and found not to be variable.

We then turned to sky subtraction. For the Beijing measurements, where a third channel was available, the sky background could be monitored simultaneously. In this case we subtracted the sky counts on a point by point basis. To reduce the scatter of the background measurements, some smoothing was applied whenever possible. At McDonald and Loiano only two channels were available. In this case sky was measured using channel 1 and 2 for about 1 min at irregular intervals of typically 20–90 min, depending on sky stability and presence of the Moon. The sky counts were then interpolated linearly and subtracted. In a few cases we used a cubic spline for the sky interpolation, when it was clear that this procedure was giving better results than the linear fit. All the PMT data were then corrected for extinction. Afterwards, they were used to examine possible transparency variations. In a few cases of high sky instability, the count ratio between channel 1 and channel 2 was used instead of channel 1 counts only. Some smoothing of the channel 2 data was applied when possible. Systematic long time scale trends ($>$ 2 hours), probably due to tube drifts and/or to residual extinction, were finally compensated by means of linear or cubic spline interpolation.

For the Calar Alto CCD data, 10 comparison stars were selected, after having been tested for photometric constancy. Their average magnitude was subtracted from the HS 2324 measurements on a point by point basis. Differential extinction was corrected by means of a cubic spline.

Finally all the single data sets (PMT + CCD) were set to a mean value of zero. The times of all data were then converted to Barycentric Julian Date using the algorithm of Stumpff (1980).

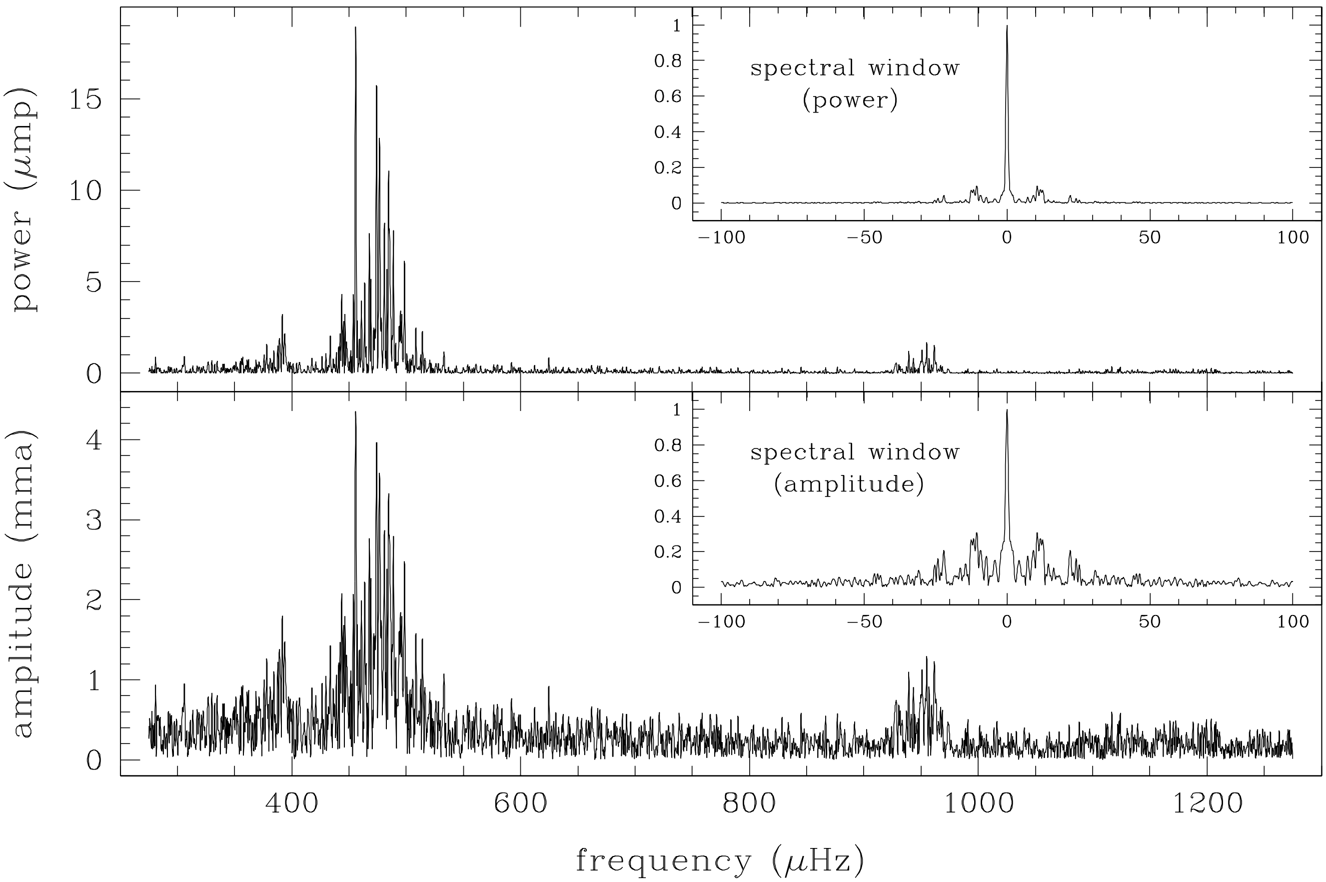

Fig. 2. Power spectrum (*top*) and amplitude spectrum (*bottom*) of the entire data set. The DFT of the window function (spectral window) is also reported both in power and in amplitude; we can note that the 1 cycle/day sidelobes have maxima at $\pm$ 10.6 μHz, corresponding to a period of 1.09 days.

The accuracy of the original times was of the order of $\pm$ 0.3 s (Beijing), $\pm$ 0.01 s (Loiano), $\pm$ 0.2 s (McDonald) and $\pm$ 1 s (Calar Alto). For Calar Alto 1 s is also the time accuracy of each measurement. Moreover, to have a more homogeneous data set, we have binned the PMT data to an effective integration time of 90 s. The value of 90 s has been chosen because it corresponds to the mean distance between consecutive CCD observations. When more than one site was active at the same time, in the overlap regions, we applied a weighted average of the data obtained at the different sites. In this way even lower quality data can be used to improve the S/N ratio (see Moskalik 1993). In its final form, the data set is constituted by the time of each integration, the fractional departure of the count rate from the mean (modulation intensity), and the error.

3. Temporal spectroscopy

3.1. Spectral window and power spectrum

We computed a single sine function with unit amplitude at the same sample times of the entire data set (window function). The discrete Fourier transform of the window function gives the spectral window, which is shown in Fig. 2. For more completeness, both the amplitude and the power (amplitude squared) spectra of the window function are presented. The only structures which may give troubles for the unambiguous identification of the modes are the 1 cycle/day aliases, with a relative amplitude of about 0.3 (relative power of 0.09).

Using the same discrete Fourier transform (DFT), based on the Deeming (1975) method and Kurtz (1985) algorithm, we computed the transform of the entire reduced data set. In Fig. 2 both amplitude and power spectrum are shown in units of millimodulation amplitude (mma) and micromodulation power (μmp), following the suggestion of Winget et al. (1994). We clearly see that the signals are concentrated in three main regions near 390, 470 and 950 μHz. These regions are highlighted in Fig. 3. The tested frequency resolution of our data set is 1.4 μHz, according to Loumos & Deeming (1978); such a value corresponds to obtain a half amplitude separation of two close peaks with equal amplitude.

Looking at Fig. 3, some structures appear to be not completely resolved, suggesting that the light curve could be too short that we can resolve all the present frequencies. To test this crucial point, we divided the data set into two equal parts and computed the Fourier transform of each part. The two power spectra, presented in Fig. 4, show strong differences not only in amplitude, but also in frequency. The first interpretation of such differences is simply that the data set is not long enough

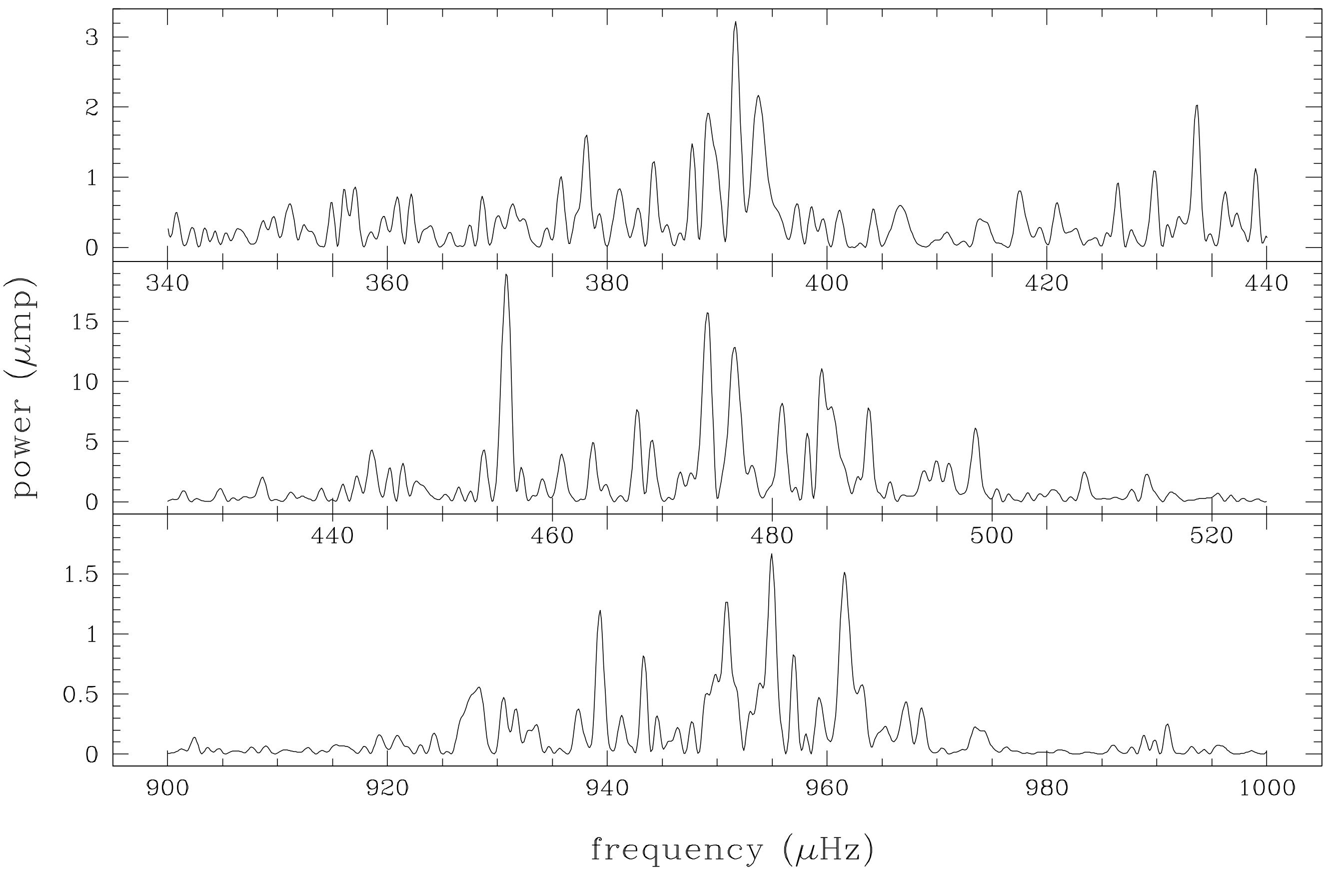

Fig. 3. Detailed power spectrum of the entire data set. Note that different vertical scales have been used.

to “stabilize” the Fourier transform. In other words, the light curve is not completely resolved. The reliability of this hypothesis is increased by the fact that our best multisinusoidal fit of the entire data set (see next section and Table 2) gives good results also when applied only to the first or the second half of data (Fig. 4). If the DFT apparent instability is actually due to the insufficient coverage, most of the analyses reported in Sects. 3.2, 4.1 and 4.2, and based on the assumption that the DFT of HS 2324 is not time dependent on time scales shorter than our run, will need further confirmation from a new longer observational campaign.

On the other hand, if the DFT time instability was real, we would need a different explanation for such peculiar behaviour. An alternative hypothesis of a fast damped oscillator has been considered and is reported in Sect. 5.

3.2. Frequency identification

Looking at Fig. 2 and 3, it is immediately evident that determining the active frequencies from the power spectrum of HS 2324 will be more difficult than in most other GW Vir stars for several reasons: the power is concentrated in only 3 crowded regions; the amplitudes are very low; the low frequencies imply that the frequency and the period spacing expected may have about same values. The high frequency region does not help much because it seems to be constituted only by linear combinations of the low-frequency peaks. Moreover we know that the frequencies are not completely resolved and therefore we certainly have errors both in frequency and in amplitude.

To distinguish the real frequencies present in the HS 2324 data from the artifacts introduced by the spectral window, we proceeded as follows. First we selected the highest peak in each of the three “active regions” near 390, 470 and 950 μHz. The separation of the three active regions guarantees that the aliases of each frequency have almost zero influence in the other two regions. Second we applied a least-squares multisinusoidal fit to the data to determine accurate amplitudes and phases of the three selected sine waves. Third we created an artificial signal adding together the three sinusoids and using the same sampling times as the data. This artificial signal was then subtracted from the data (prewhitening), and the residuals were analyzed again. Three (or less) new frequencies were selected and the whole procedure was repeated n times until the power of the prewhitened data was near the level of the noise. At each iteration we selected first those frequencies which were not coincident with the one day aliases of the strongest signals. At the end of the whole process, the frequencies, amplitudes and phases were optimized with a final least-squares fit with all the frequencies found. The resulting best fit parameters are listed in Table 2. It is important to emphasize, however, that the solution in Table 2 is not the only one. After having performed the prewhitening of 7 frequencies (marked with an asterisk in Table 2), different solutions become

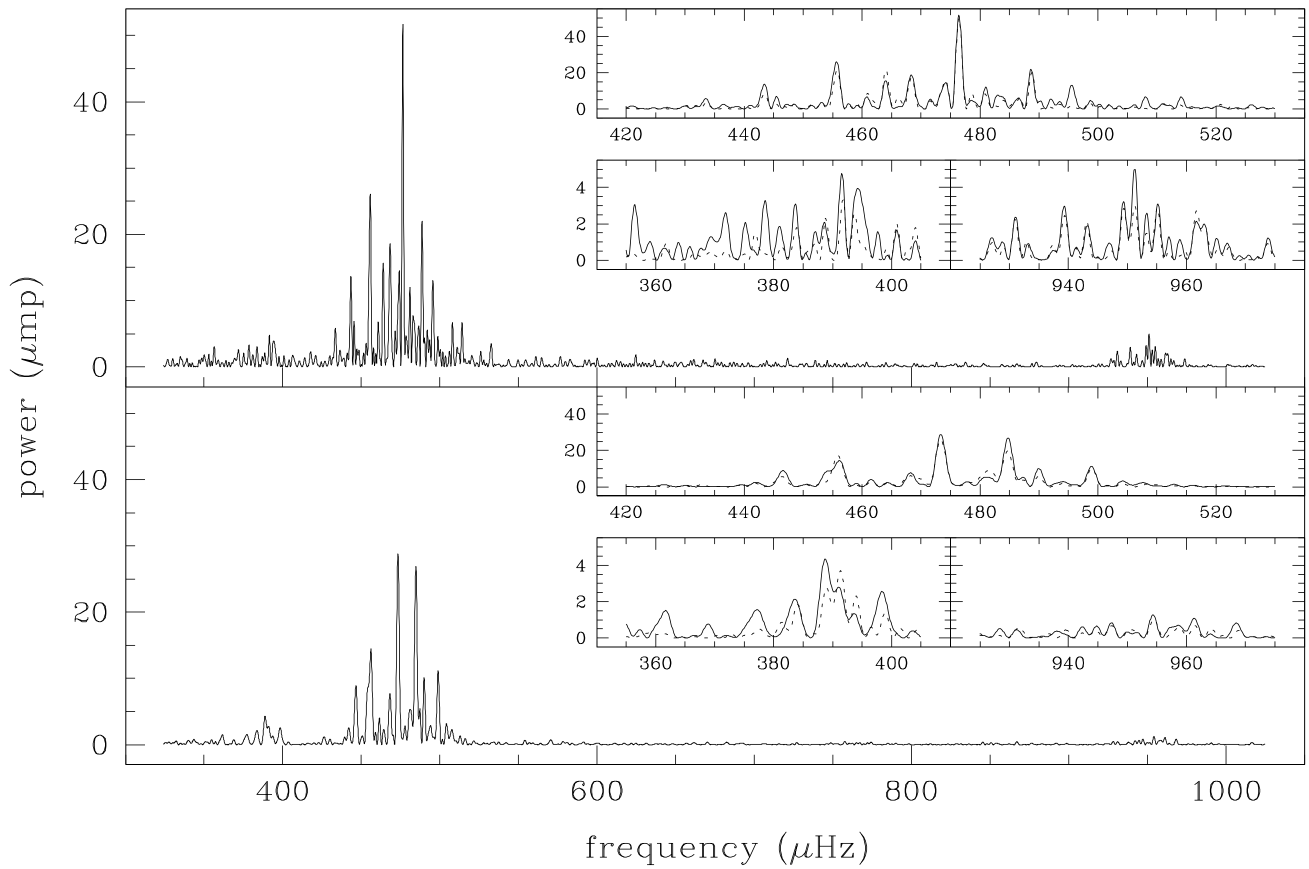

Fig. 4. Power spectrum of the first half of data (*top*) versus second half (*bottom*). Note the strong differences both in power and in frequency. In the small panels the regions of interest are highlighted; the dotted lines represent the spectra of the first and second half of a synthetic light curve obtained summing the 19 sinusoids listed in Table 2 and having same time sampling as the HS 2324 data. No noise was added to the synthetic light curves.

possible. The frequencies selected in Table 2 represent the result of several attempts. The solution that we have chosen has the advantage that it produces small residuals with a relative small number of frequencies (Fig. 5). Looking at Table 2, we can note that most (if not all) of the high frequency signals correspond to linear combinations of the high-amplitude frequencies.

4. "Classical" seismological interpretation

4.1. Frequency splitting

In the power spectrum of HS 2324 there is not any clear direct sign of frequency splitting. This may be due to different reasons. A very small rotation rate, with secondary (m$\neq$0) modes below the frequency resolution, seems quite unlikely because it would require a rotation period longer than about 9 days. A more realistic possibility is that the star has a low inclination, so that the amplitudes of the m$\neq$0 modes are near the level of the noise. A third possibility is that the concentration of the peaks is so high that we are simply not able to recognize the modes splitted by the rotation.

If a direct identification of the rotational splitting is not possible, the high number of peaks allows one to make use of statistical methods. First we constructed an histogram of the frequency separations between the signals listed in Table 2, excluding the linear combinations. The result was not significant: no preferred frequency spacings appeared. Another attempt was done using all the peaks of the power spectrum higher than a fixed level; we selected 49 frequencies and made the histogram. Here also we did not get any significant result apart that all the peaks were never higher than the one day alias near 10–11 μHz.

At this point we invoked a third method: we computed the DFT of the amplitude spectrum, using two different subsets spanning 350–1000 μHz (all signals) and 440–500 μHz (only high power signals). The resulting power spectra are shown in Fig. 6 (left panels). Considering the lower panel, the highest peaks are at 10.1 and 4.2 μHz; a third peak at 2.5 μHz is clearly visible and more evident in the upper panel. Let us focus our attention to the latter two (for the first one we will give an interpretation below): their ratio, equal to 0.594 (or 0.589), is very close (1% level) to the canonical value of 0.6 predicted by asymptotic theory for the ratio between l=1 and l=2 rotational frequency splitting. Therefore the 4.2 and 2.5 μHz peaks might correspond to the frequency separation between m and m$\pm$1 (l=2 and l=1) modes. The corresponding rotation period of the star would be $P_{ROT} = 2.31 \pm 0.15$ days. This result may not be considered definitive because the method used is very sensitive to noise. Moreover the signal that we are looking

Table 2. Results of the sinusoidal fit

Frequency (μHz)	Period (s)	Amplitude (mma)	T^1_{MAX} (BJD 2450686.+)	Comments
389.27±0.06	2568.89±0.41	1.33±0.15	0.82337±0.00145	f1
* 391.64±0.06	2553.38±0.37	1.50±0.15	0.84665±0.00135	f2
393.51±0.06	2541.25±0.37	1.45±0.15	0.82707±0.00133	f3
* 455.74±0.02	2194.23±0.10	4.27±0.15	0.83075±0.00041	f4
460.68±0.06	2170.70±0.27	1.84±0.16	0.83464±0.00117	f5
472.90±0.05	2114.63±0.23	3.28±0.23	0.82214±0.00098	f6
* 473.87±0.05	2110.29±0.24	3.29±0.22	0.82515±0.00097	f7
476.13±0.04	2100.25±0.19	4.69±0.45	0.84137±0.00089	f8
* 476.64±0.04	2098.02±0.17	5.20±0.45	0.84039±0.00078	f9
480.95±0.04	2079.22±0.18	2.25±0.15	0.83641±0.00077	f10
485.11±0.03	2061.37±0.14	3.13±0.17	0.83581±0.00061	f11
498.78±0.04	2004.91±0.18	1.98±0.15	0.82382±0.00082	f12
930.49±0.11	1074.71±0.13	1.02±0.21	0.82086±0.00109	(f4+f7)
931.71±0.12	1073.29±0.13	0.94±0.20	0.82618±0.00111	f4+f8 (f4+f9)
* 939.42±0.11	1064.49±0.13	1.08±0.21	0.81967±0.00105	(f4+f11)
949.25±0.16	1053.46±0.17	0.76±0.22	0.82672±0.00144	f6+f8 (f6+f9)
* 955.04±0.10	1047.07±0.11	1.22±0.20	0.82392±0.00091	f7+f10 (f4+f12)
* 961.71±0.12	1039.82±0.13	1.04±0.22	0.81880±0.00120	f9+f11 (f10+f10)
963.15±0.13	1038.26±0.14	0.96±0.21	0.82792±0.00120	

(1) Time of the first maximum inside the data set.
(*) These frequencies are the most reliable (see the text).

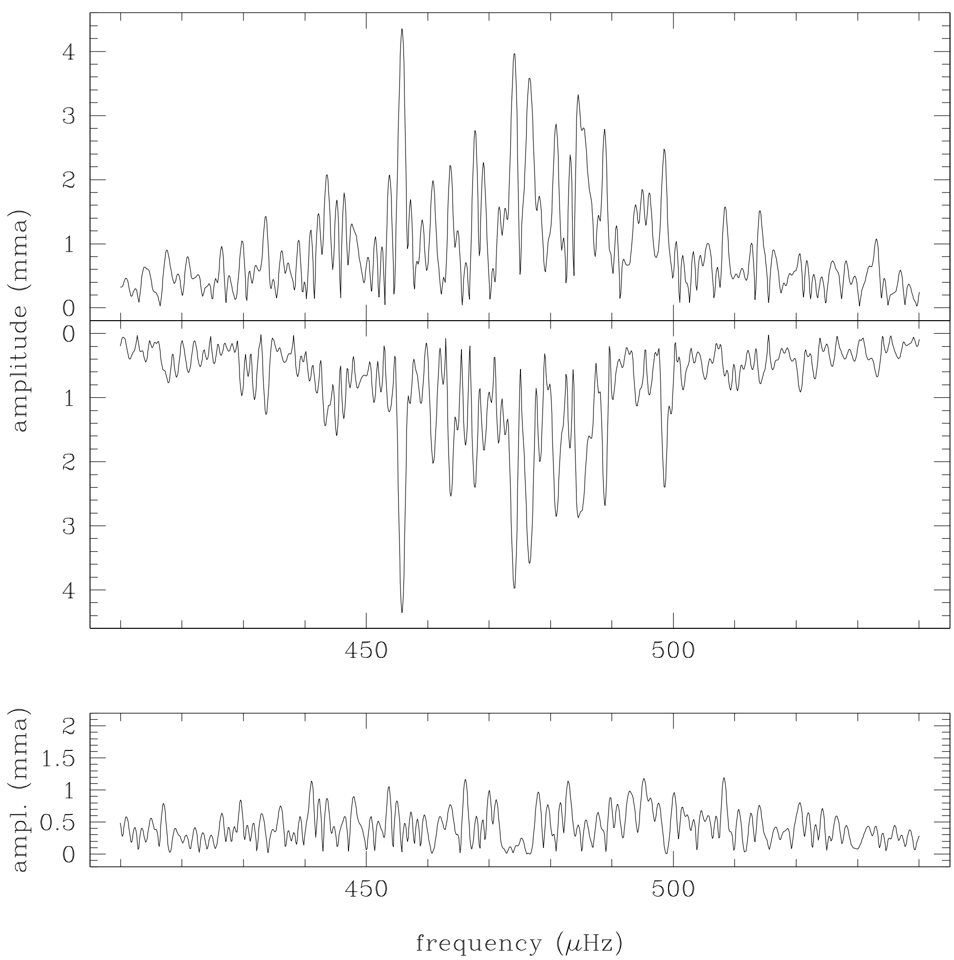

Fig. 5. *Upper panels:* amplitude spectrum of the entire data set (*top*) compared with the spectrum of the 19-frequency fit (*bottom*) having the same time sampling as the data. No noise was added to the synthetic data. *Lower panel:* spectrum of the residuals. Note that the vertical scale is the same in all panels.

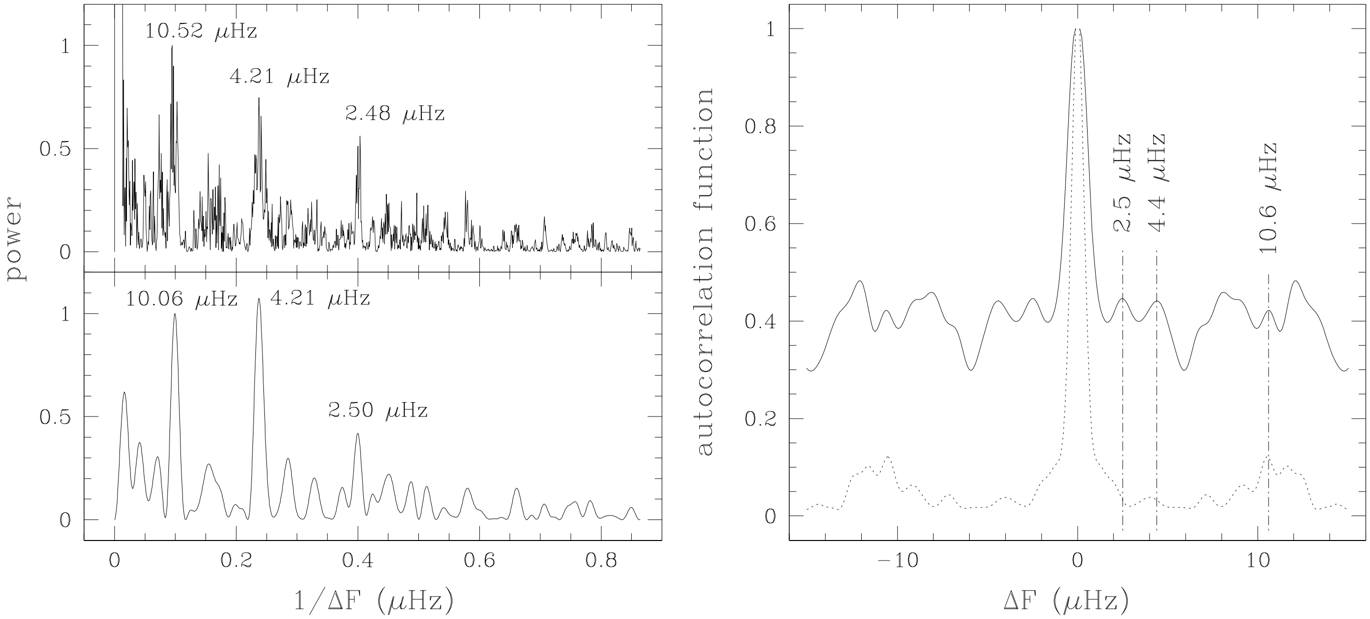

Fig. 6. Search for the frequency spacing. *Left panels:* power spectrum of the data amplitude spectrum using two different subsets of the DFT: $350 \leq f \leq 1000\,\mu$Hz (all the signals, *top panel*) or $440 \leq f \leq 500\,\mu$Hz (only high-power signals, *bottom panel*). The power is normalized to the peak at 10.52 (10.06) μHz, which is partially due to the one day aliases (see the text). *Right panel:* autocorrelation function of the data DFT using the same subset as in the *left bottom panel.* The peaks between about 8 and 13 μHz are partially due to the spectral window, as it is highlighted by the autocorrelation of the spectral window (dotted line).

for is not actually coherent: the constant frequency separation between the modes of the same overtone splitted by the rotation does not correspond, in general, to the separation between successive overtones, which is not constant in frequency (but almost constant in our particular case, due to the narrowness of the high-power region). From this point of view a more appropriate – but not much less noisy – method to measure the frequency spacing is given by the autocorrelation of the DFT (Press et al. 1992). The results of the DFT autocorrelation, reported in Fig. 6 (right panel), are less significant than, but do not contradict, those obtained from the DFT of the amplitude spectrum.

Looking now at the peak near 10 μHz of Fig. 6, its frequency separation is very close to that of the one day alias; therefore we could conclude that it is actually produced by all the aliases of the signals. This conclusion would give more confidence in the rotational origin of the two peaks at 4.2 and 2.5 μHz. Moreover comparing the power of these two peaks with that of the one day alias, we could suppose that the weakness of the m$\neq$0 modes is actually due to the low inclination of the star. But with a deeper analysis (testing the variations of the three peaks of Fig. 6 (left panels) when we subtract different signals from the HS 2324 data (prewhitening)), we can easily demonstrate that the peak at about 10 μHz has at least two components: one at 10.6 μHz actually related to the one day alias and another one related to the separation between the two signals at about 474 and 485 μHz in the data DFT. Therefore it is more difficult to derive any consideration about the weakness of the m$\neq$0 modes and the low inclination hypothesis does not have any support. On the other hand, we can also demonstrate that the origin of the 2.5 and 4.2 μHz peaks is strongly related to the separation between a few large amplitude signals. Conclusion: if the frequency spacings of 2.5 and 4.2 μHz are actually due to the stellar rotation, the low inclination hypothesis can not be longer followed. The new even more simple picture would be the following: there are five l=1 triplet component candidates (474.1 [1] and 476.6 μHz plus 389.1, 391.7 and 393.8 μHz) and there are three l=2 quintuplet component candidates (480.9, 484.5 and 488.8 μHz). If we derive the frequency spacing from these values we obtain a rotation period of the star $P_{ROT} = 2.41 \pm 0.22$ days, slightly different from the previous one. Other possible multiplets might be present at 483.2 and 485.4 μHz (l=1), and 463.7 and 467.7 μHz (l=2).

In this context we can also try to estimate the inclination of the star using the l=1 modes. Following Pesnell (1985)[2] we obtain an indication for $i \simeq 50°$.

4.2. Period spacing and mode trapping

The two peaks in the amplitude spectrum DFT, described in the previous section, could also be due to the period spacing between modes with successive overtones. In Fig. 7 (left panels)

[1] The frequencies reported here are not taken from Table 2; we prefer to use the values found in the data DFT, as Table 2 may contain errors.

[2] These equations require two strong assumptions, certainly not completely – if not at all – realistic for low gravity GW Vir stars: the m$\neq$0 modes should be all excited at the same amplitude level; the amplitude variations during the run must be excluded. Therefore this estimate of the inclination of the stellar rotational axis must be considered very tentative.

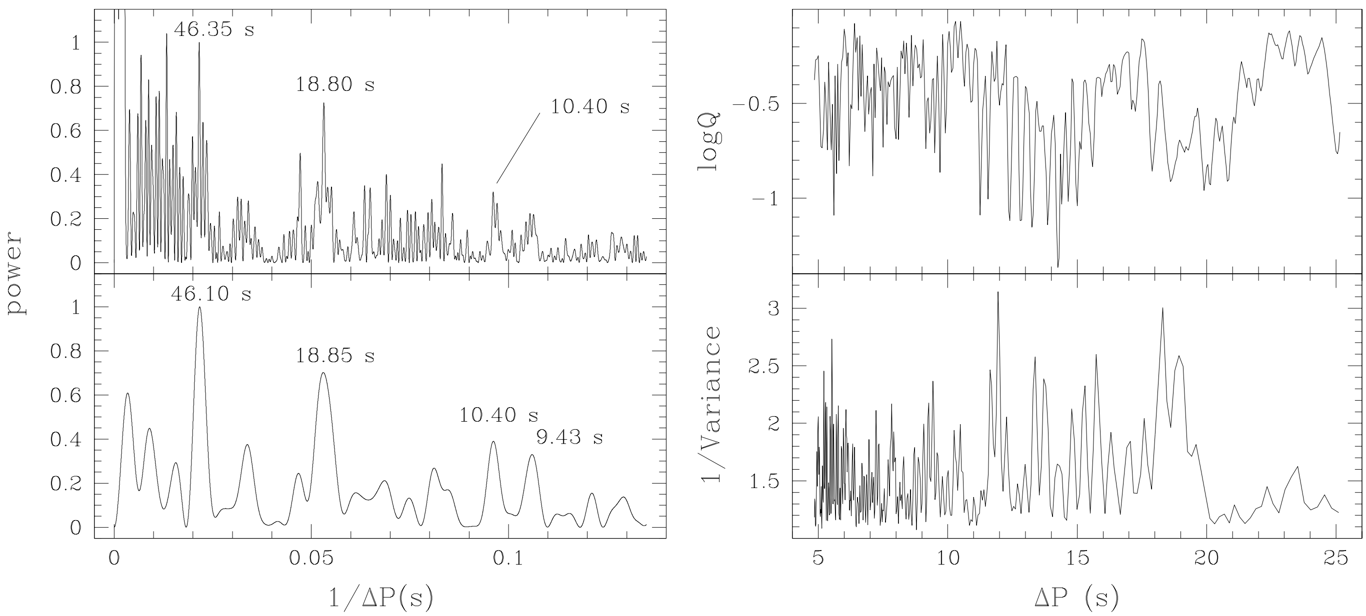

Fig. 7. Search for the period spacing. *Left panels:* Fourier transform of the period spectrum (amplitude spectrum in the period domain) in the period range $1000 \leq P \leq 2857$ s (*top*) and $2000 \leq P \leq 2273$ s (*bottom*). The power is normalized to the peak at 46.3 (46.1) s, which is mainly due to the one day aliases in the main power region between 2000 and 2273 s. The peaks at 18.8 and 10.4 s might be due to the l=1 and l=2 period spacing. The peak at 9.4 s is the first harmonic of the 18.8 s signal. *Right panels:* Kolmogorov-Smirnov test (*top*) and Inverse Variance test (*bottom*) applied to the first 12 frequencies listed in Table 2 (excluding the linear combination region). Both tests do not show any significant value for the period spacing.

we show the DFT of the period spectrum (amplitude spectrum in the period domain). For the upper panel we used a subset of the period spectrum with periods between 1000 and 2857 s, while for the lower panel we used a narrower part with periods spanning 2000 – 2273 s. Excluding the peak at about 46 s, which is related to the one day alias as discussed in the previous section, the most significant period spacings are 18.8 s and 10.4 s (at least in the lower graph; in the upper graph the 10.4 s peak appears more uncertain). Their ratio is close (accuracy better than 5%) to the asymptotic value of $\sqrt{3}$, suggesting that 18.8 and 10.4 s might correspond to the l=1 and l=2 period spacings. In this hypothesis, the differences between the two left panels of Fig. 7 suggest that the l=2 modes might be present only (or mainly) in the high-amplitude region between 2000 and 2273 s.

An attempt to confirm the hypothesis that the modes of HS 2324 are equally spaced in period (and not in frequency) has been done applying the Kolmogorov-Smirnov (K-S) test (Kawaler 1988) and the Inverse Variance technique (O'Donoghue 1994) to the first 12 periods listed in Table 2 (excluding the linear combinations). The results, reported in Fig. 7 (right panels), do not confirm that the modes are equally spaced in period. Moreover, the lack of any significant period spacing further indicates that the period list is not complete[3].

[3] Note that these methods, which are in general much more reliable than the DFT of the period spectrum, can completely fail when they are applied to a period list erroneous and/or incomplete, as it can be in our case. For this reason the hypothesis that the signals are equally spaced in period (and not in frequency) can not be completely ruled out.

Nothing may be said about the trapped modes phenomenon apart the following. The ratio between the frequencies of the highest peaks in the 380 and 475 μHz regions gives $\sqrt{3}/2$ with an accuracy better than 1%. This number was found in other GW Vir stars, as RXJ 2117+3412 and the central star of NGC 1501 (Bond et al. 1996), and is compatible with calculated trapping coefficients (Kawaler & Bradley 1994).

5. The damped oscillator hypothesis

When we discovered that the DFT was unstable, we also tried to explain such apparent time dependence of the DFT with a completely different quasi-periodic approach. We considered the hypothesis that the DFT temporal instability was real and due to a very short life time of the oscillations, which were continuously excited and damped.

We therefore applied to the HS 2324 data the Linear State Space model developed by Michael König for the analysis of X-ray variability of AGN (König & Timmer 1997, König et al. 1997). The current version of this program requires uninterrupted and equally spaced datasets. Moreover, in order to provide reliable results, the time scales to be investigated must be sampled at least ten times. The only part of our light curve which fulfills these criteria (JD 94 – 94.9, after rebinning with 200 s) can be actually fitted with a period of 2134 s and a damping time of approximately 3.5 periods. A further attempt has been done using a larger nearly uninterrupted part of the light curve (JD 94 – 95.7), filling the small gaps with white noise or with synthetic data (both techniques give same results). The results are slightly different in this case: 2154 s and 3.1 periods. In

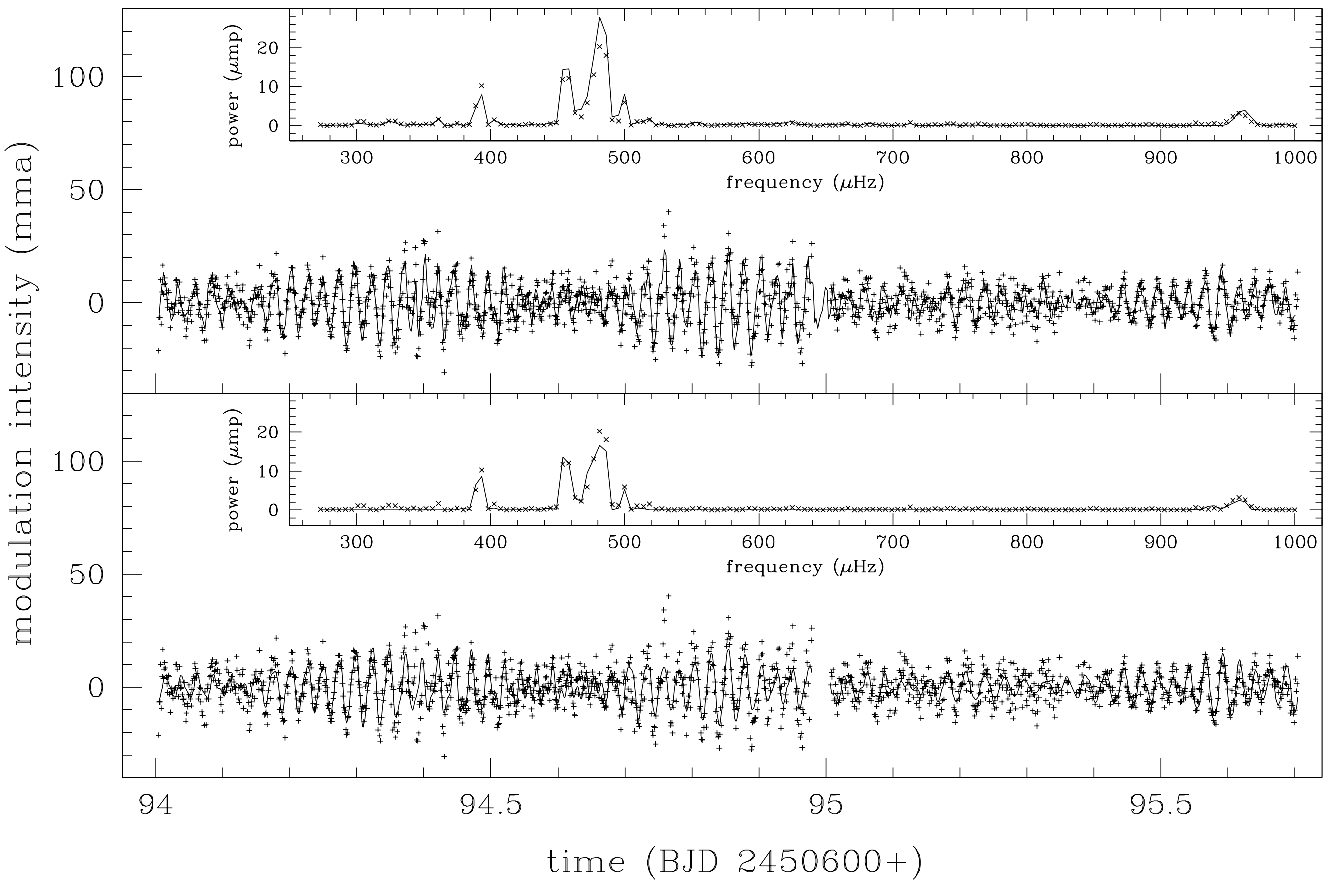

Fig. 8. Damped oscillator (*up*) vs 19 sinusoids function (*down*) in the best part of the light curve (BJD 94.0 – 95.7). Both the synthetic light curves (main panels) and DFTs (window panels) are shown and compared with the HS 2324 data (crosses).

both cases from a K-S test the residual is white noise with over 90% probability. If we try to find a secondary period the results are unreliable (damping time longer than the dataset), but in any case the inclusion of more frequencies does not improve the fit.

In Fig. 8 the fit from the Linear State Space model is compared with the multisinusoidal fit: the quality is comparably good. Despite this partial success, we cannot demonstrate that the damping time found is really a fundamental quantity, constant over at least some days. We would need several datasets (ideally, but not necessarily coherent) of at least one day length to reject or corroborate this hypothesis. Moreover, the excitation time-scale obtained from the Linear State Space model appears to be very short respect to the growth rates obtained from GW Vir non-adiabatic models. For these reasons the present results are not convincing enough to abandon the DFT results. On the other hand, the inviting advantage of the quasi-periodic approach is the small number of parameters required to describe the light curve. Unstable power spectra have been found also in other luminous PG 1159 stars (e.g. RXJ 2117+3412) and [WC] CSPN (e.g. NGC 1501) variables. Changes were observed down to the time resolution of several days (Bond et al. 1996, Table 6).

6. Summary and discussion

The results of our multisite campaign clearly show that the power spectrum of HS 2324 contains several periodic signals (about 20 or more). We therefore may exclude binarity to explain its variability, as already suggested by Handler et al. (1997). The frequencies and amplitudes are comparable with those of the GW Vir stars. If we consider also that HS 2324 is spectroscopically classified as a PG 1159 star, the immediate interpretation is that its variability is due to high overtone g-mode pulsations.

The high H abundance detected in HS 2324, about 17% in mass (Dreizler 1998), is a very interesting and unique (up to now) element, which might help to shed light upon the driving mechanisms of the GW Vir stars. As discussed in the introduction, the presence of H was generally considered as an inhibitor of pulsations (Stanghellini et al. 1991). But this result was rather speculative because, until a few years ago, no H-rich PG 1159 stars were known. With HS 2324 this question has gained importance. Presently the real effects of the presence of H appear to be less severe from preliminary models of H-rich GW Vir stars (Saio 1996, Gautschy 1997). On the other hand, the detection of hydrogen in the atmosphere of HS 2324 does not necessarily imply that hydrogen is present also in the driving regions. However, HS 2324 belongs to the subclass of luminous PG 1159 stars which still show mass loss effects in strong UV/FUV lines (Koesterke & Werner 1998, Koesterke et al. 1998). It is highly probable that HS 2324 is also affected by mass loss which would inhibit an abundance gradient due to gravitational settling. It is therefore plausible that the atmospheric composition is also representative for the driving region. An unambiguous detection of mass loss and the determination of the mass loss rate has to await FUSE (Far Ultraviolet Spectroscopic Explorer) observations of the O VI resonance lines.

However, the asteroseismological analysis is hampered by the fact that the DFT appears to be unstable in time. In principle this is not a new phenomenon: it has been observed in the light curve of all luminous PG 1159 and [WC] variables (the term "variable variables" was therefore coined by S. D. Kawaler). But in our case, as discussed in Sect. 3.1, this fact is probably due to a poor frequency resolution caused by an insufficient coverage.

If this interpretation is correct, it is not possible to obtain definite precision asteroseismology results from our data set. Nevertheless a spacing of the signals is probably present in the DFT and can be explained in two different ways. The most likely hypothesis is that we see the frequency spacing produced by the stellar rotation with a period $P_{ROT} = 2.31 \pm 0.15$ days. The second possibility, which can not be completely excluded, is that we see the period spacing between successive overtones. In this case the period spacings, equal to 18.8 (l=1) and 10.4 (l=2) s, would imply a stellar mass of 0.67 (l=1) and 0.70 $M_\odot$ (l=2) using the interpolation formula of Winget et al. (1991). This asteroseismological mass would be higher than the 0.59 $M_\odot$ value, found from spectroscopy plus evolutionary tracks (Dreizler et al. 1996). But this discrepancy would not be very significant as it is possible that the interpolation formula of Winget et al. (1991) needs some adjustment because of the peculiar composition of HS 2324.

In an alternative interpretation we assumed that the DFT instability was real and we applied the Linear State Space model (König & Timmer 1997) to investigate the quasi-periodic nature of these variations. As discussed in Sect. 5, this approach is also partially successful, but it also requires new longer observations to be confirmed. At the moment we can only speculate about the physical interpretation. Do we see the coupling time between different g-modes or the damping of a single mode? In principle, the quasi-periodic nature of HS 2324 could even endanger the interpretation as g-mode pulsations.

In conclusion both possible interpretations of the apparent DFT instability need a new bigger observational effort, which could be realized only with a larger number of telescopes in a WET-like campaign. If we adopt the hypothesis that the DFT instability is only apparent, it is also possible to estimate the duration needed for such a campaign in order to be able to separate all the frequencies. If all the l=1 and l=2 frequencies were excited in the region between 450 and 500 μHz, where most power is concentrated, the average frequency separation would be about 0.4 μHz. In a more realistic case, if only 50% of the frequencies were excited (as in PG 1159, which is the GW Vir star with the largest number of detected modes), a frequency resolution of about 0.8 μHz would be enough. Therefore we would require a data set with a time base of about 1.7 times the data set analyzed in this paper.

Acknowledgements. This research was partially supported by the Italian "Ministero per l'Università e la Ricerca Scientifica e Tecnologica" (MURST) and by the EU grant ERBFMMACT980343; by the Deutsche Forschungs Gemeinschaft under travel grant DR 281/8-1; by the Austrian Fonds zur Förderung der wissenschaftlichen Forschung under grant S7304-AST; and by the Chinese National Science Foundation. S.D. would like to thank Ralf Geckeler (University of Tübingen) for providing his excellent CCD-photometry analysis program package as well as Katja Potschmidt (University of Tübingen) for her introduction to the time series analysis package of M. König and for her fruitful discussions. R.S. would like to thank Steven Kawaler (Iowa State University, Ames), Thomas Strauss (Astronomical Observatory of Capodimonte, Naples), Pawel Moskalik (Copernicus Astronomy Center, Warsow) and Scot Kleinman (University of Texas at Austin) for interesting discussions, and Adalberto Piccioni (University of Bologna) for the availability of the Loiano photometer. R.S. and S.D. are grateful to the Vienna Delta Scuti Network Group for their kind hospitality during the short stay in April–May 1998, in which part of this work has been done. The same applies to G.H.'s stay at the University of Tübingen in December 1997.

References

Bond H.E., Kawaler S.D., Ciardullo R., et al., 1996, AJ 112, 2699
Bradley P.A., 1998, Baltic Astronomy vol.7, 355
Bradley P.A., Dziembowski W.A., 1996, ApJ 462, 376
Ciardullo R., Bond H.E., 1996, AJ 111, 2332
Deeming T.J., 1975, Ap&SS 36, 137
Dreizler S., 1998, Baltic Astronomy vol.7, 77
Dreizler S., Werner K., Heber U., Engels D., 1996, A&A 309, 820
Dreizler S., Heber U., 1998, A&A 334, 618
Gautschy A., 1997, A&A, 320, 811
Handler G., Kanaan A., Montgomery M.H., 1997, A&A 326, 692
Kawaler S.D., 1988, in Advances in Helio and Asteroseismology, Proc. IAU Symp. 123, eds. J.J. Christensen-Dalsgaard and S. Frandsen (Reidel:Dordrecht), 329
Kawaler S.D., Bradley P.A., 1994, ApJ 427, 415
Koesterke L., Dreizler S., Rauch T., 1998, A&A 330, 1041
Koesterke L., Werner K., 1998, ApJ 500, L55
König M., Timmer J., 1997, A&AS 124, 589
König M., Staubert R., Wilms J., 1997, A&A 326, L25
Kurtz D.W., 1985, MNRAS 213, 773
Loumos G.L., Deeming T.J., 1978, Ap&SS 56, 285
Moskalik, P., 1993, Baltic Astronomy vol.2, 485
Nather R.E., Winget D.E., Clemens J.C., Hansen C.J., Hine B.P., 1990, ApJ 361, 309
Napiwotzki R., Schönberner D., 1991, A&A 249, L16
O'Donoghue D., 1994, MNRAS 270, 222
Pesnell W.D., 1985, ApJ 292, 238
Press W.H., Teukolsky S.A., Vetterling W.T., Flannery B.P., 1992, Numerical Recipes, (Cambridge Univ. Press: Cambridge)
Saio H., 1996, in Hydrogen-Deficient Stars, eds. U.Heber and C.S.Jeffery, ASP Conf. Series 96, 361
Silvotti R., 1996, A&A 309, L23
Stanghellini L., Cox A.N., Starrfield S., 1991, ApJ 383, 766
Starrfield S., Cox A.N., Kidman R.B., Pesnell W.D., 1984, ApJ 281, 800
Stumpff P., 1980, A&AS 41, 1
Werner K., 1992, in Atmospheres of Early-type Stars, eds. U. Heber and C.S. Jeffery, Lecture Notes in Physics 401, (Springer-Verlag: Heidelberg), 273
Werner K., Bagschik K., Rauch T., Napiwotzki R., 1997, A&A 327, 721
Winget D.E., Nather R.E., Clemens J.C., et al., 1991, ApJ 378, 326
Winget D.E., Nather R.E., Clemens J.C., et al., 1994, ApJ 430, 839

6.3 Pulsating DB white dwarfs

6.3.1 Discovery and asteroseismological analysis of a new pulsating DB white dwarf star, PG 2246+121

Original paper:

G. Handler, 2001, MNRAS 323, L43

Mon. Not. R. Astron. Soc. **323**, L43–L47 (2001)

Discovery and asteroseismological analysis of a new pulsating DB white dwarf star, PG 2246+121

G. Handler*

South African Astronomical Observatory, PO Box 9, Observatory 7935, South Africa

Accepted 2001 March 21. Received 2001 March 21; in original form 2001 February 19

ABSTRACT

We report 36.6 h of time-resolved CCD photometry of the DB white dwarf star PG 2246+121 and the discovery that it is a new pulsating variable. Analysis of our compact single-site data set allowed the detection of three mode multiplets, two triplets at 256 and 329 s, respectively, and one doublet at 286 s. The frequency splitting within those structures is exactly the same within the length and accuracy of our data set.

We argue that these multiplets are the result of non-radial g-mode pulsations, most probably of spherical degree $\ell = 1$, which then yields a formal stellar rotation period of 2.00 ± 0.12 d. We suggest that the excited modes are three consecutive radial overtones of order 3–7, most likely $k = 4, 5, 6$. This discovery's impact on the understanding of pulsating DB white dwarfs is discussed.

Key words: stars: individual: PG 2246+121 – stars: individual: ZZ Ceti – stars: oscillations – stars: variables: other.

1 INTRODUCTION

At first glance, the only technique that allows us to explore the deep interior structure of stars – asteroseismology – seems quite successful for the pulsating helium-atmosphere DB white dwarf (DBV) stars. The prototype DBV GD 358 is among the objects for which the most pulsation frequencies were detected (Winget et al. 1994; Vuille et al. 2000), which prompted detailed theoretical studies (Bradley & Winget 1994; Kawaler, Sekii & Gough 1999).

Understanding the DBV stars as a group is difficult. For a long time, all DBVs were believed to show large-amplitude ($A \approx 0.2$ mag) light variations on time-scales around 10 min, with the presence of many pulsation periods (the exception is PG 1351+489: Winget, Nather & Hill 1987).

This viewpoint has changed somewhat with the latest discovery, only the eighth DBV, EC 20058−5234 (Koen et al. 1995), which shows short periods ($\approx$5 min) and low amplitudes ($<$0.05 mag). This is interesting as the coolest class of pulsating white dwarf, the hydrogen-atmosphere DAV stars, show a period–temperature relation (e.g. Bergeron et al. 1995) as expected from the changes of the star's interior structure as it cools through the instability trip. The same should be valid for the DBV stars; EC 20058−5234 may therefore not be an unusual example of its class.

In any case, an important step towards the understanding of the DBV stars as a class has been made by Beauchamp et al. (1999) who presented homogenous model-atmosphere analyses of a set of hot DB white dwarf stars, including all DBVs. Besides many other interesting results, they showed that EC 20058−5234 is most probably the hottest DBV and that in some temperature range all DB white dwarfs seem pulsationally unstable. The only exception would be the star PG 2246+121, which had however apparently never been tested for variability before. We took this as a motivation to perform this test and we indeed obtained a positive result.

In this paper we report the discovery of pulsations of PG 2246+121, dedicated follow-up observations and their analysis and interpretation.

2 OBSERVATIONS AND REDUCTIONS

We first observed PG 2246+121 with the University of Cape Town CCD camera (O'Donoghue 1995) on the 0.75-m telescope at the South African Astronomical Observatory's Sutherland station for approximately 1 h during two nights in 2000 April/May. The measurements were taken at the very end of the nights at high air mass and partly during morning twilight and are therefore not of outstanding quality. However, the amplitude spectra of both runs showed good evidence for short-term variability (Fig. 1).

Consequently, we re-observed the star during one week in 2000 October, with the same instrument, but on the 1.0-m telescope. We obtained data on six nights. During these observations, the CCD was operated in frame-transfer mode, which allows continuous integrations on the field of choice; integration times of 10 s were used (the discovery observations were taken as 20-s integrations in full-frame mode with a readout time of 3 s).

In 2000 October, PG 2246+121 was observed together with four comparison stars in the same CCD field; in April/May we could use six comparison stars because of the larger field of view.

* E-mail: gerald@saao.ac.za

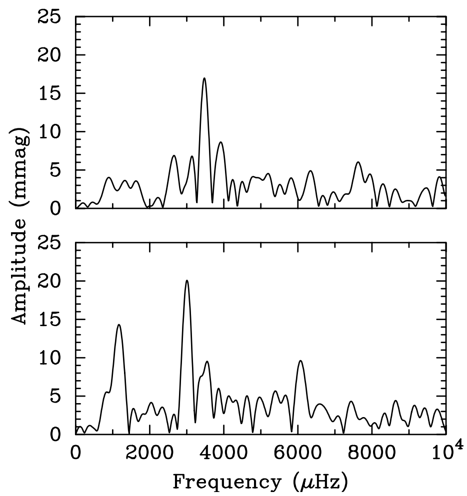

Figure 1. Amplitude spectra of the discovery observations of PG 2246+121; pulsational signals around 3000–4000 μHz are strongly suspected.

Table 1. Time-series photometry of PG 2246+121.

Telescope	Date (UT)	Start (UT)	Run length (h)
0.75-m	2000 Apr 30	03:00:38	1.22
0.75-m	2000 May 1	03:05:44	1.16
1.0-m	2000 Oct 3	18:03:19	6.45
1.0-m	2000 Oct 4	17:39:39	6.78
1.0-m	2000 Oct 5	17:28:26	7.00
1.0-m	2000 Oct 6	20:34:42	2.93
1.0-m	2000 Oct 8	17:33:38	6.61
1.0-m	2000 Oct 9	18:16:14	4.46
Total			36.61

No filter was employed. In every clear night, sky flat-fields were taken during twilight. Because of the efficient operation of the instrument, this resulted in more than 100 flat-fields per clear night. A detailed overview of our observations is presented in Table 1.

Data reduction was started with correction for bias and flat-field; a mean flat-field was used for each night separately. If no flats could be obtained in a given night, the correction was performed with the combined flat closest in time. Photometric measurements on these reduced frames were made with the program MOMF (Kjeldsen & Frandsen 1992). MOMF firstly performs iterative point-spread function fitting (PSF) photometry (determination of initial empirical PSF, initial sky determination, then improving the PSF and sky background measurement). A good determination of sky background is important for stars as faint as PG 2246+121 ($y = 16.73$, Wegner 1983) in particular, as we had a considerable contribution from moonlight on the last two nights; we used a fully local sky determination. The PSF photometry is followed by an aperture correction on the star-subtracted frames. The aperture sizes scale with the full width at half-maximum (FWHM) of the stellar images and the aperture yielding the lowest point-to-point scatter for the variable star measurements was chosen. The relative photometry is calculated with respect to a user-defined ensemble of comparison stars, the contributions of which are weighted with the inverse rms scatter of their measurements. In this way, very precise differential photometry can be obtained. All comparison stars proved to be constant within the accuracy of our data set.

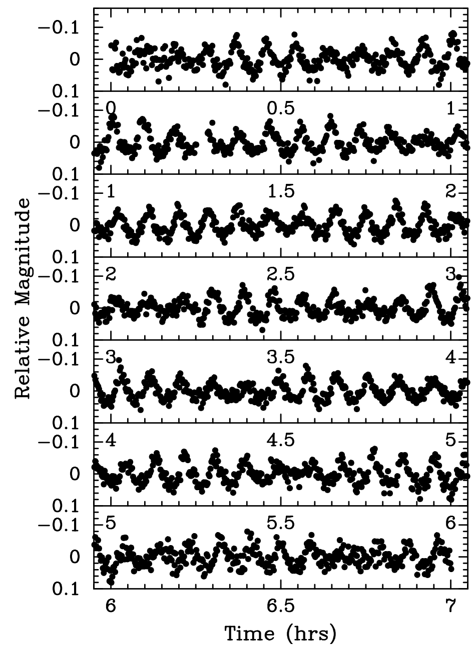

Figure 2. The reduced light curve of PG 2246+121 from the measurements obtained on 2000 October 5. Several features can be discerned: a typical light curve shape of a pulsating white dwarf (sharp peaks, flat bottom), some amplitude modulation resulting from beating and varying data quality caused by the effects of air mass and twilight.

We tested the resulting time series of PG 2246+121 for correlations with some observational parameters, such as air mass, seeing and (x, y) position of the star on the chip. We found a strong linear trend with air mass (differential extinction – the variable is much bluer than its comparison stars) and some correlation with x position (residual flat-field errors – the flat-fields showed some roughly vertical 'ridges'), but no correlation with seeing or y position. The data were hence detrended with air mass and x position.

As the last two steps, residual low-frequency trends in the data were removed by means of low-order polynomials, and the times of measurement were transformed to a homogeneous time base. We chose Terrestrial Time (TT) as our reference for measurements on the Earth's surface and applied a correction to account for the Earth's motion around the barycentre of the Solar system. As this barycentric correction varied by about −1 s throughout the duration of a typical run, we applied it point by point. Our final time base therefore is Barycentric Julian Ephemeris Date (BJED). The final time series was subjected to frequency analysis; we show an example light curve in Fig. 2.

3 FREQUENCY ANALYSIS

Our frequency analysis was performed with the program PERIOD98 (Sperl 1998), which applies single-frequency Fourier analysis and simultaneous multifrequency sine-wave fitting. PERIOD98 can be used to calculate optimal solutions for multiperiodic signals including harmonic, combination, and equally spaced frequencies, which are often found in the analysis of the light curves of pulsating white dwarf stars; the program is therefore ideal for our analysis. We will focus on our data set from 2000 October in what

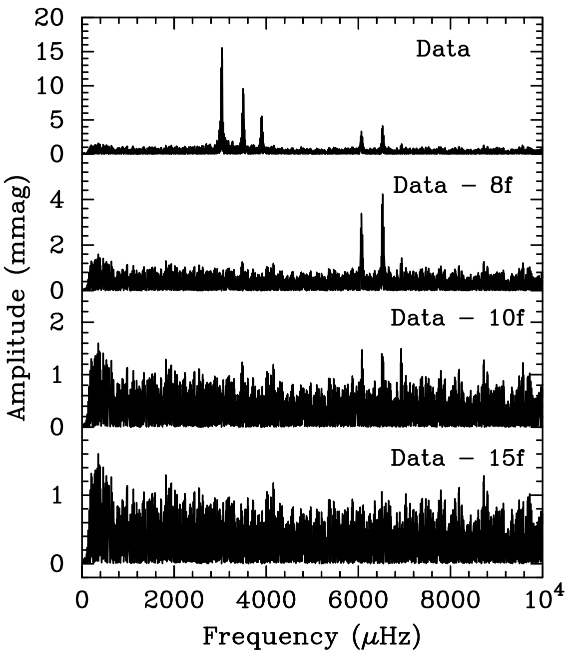

Figure 3. Results of consecutive prewhitening in our data for PG 2246+121. Uppermost panel: amplitude spectrum of the 2000 October data. Second panel: residuals after prewhitening of the features dealt with in Fig. 4. Third panel: residuals after prewhitening of these signals as well as their two strongest frequency combinations. Fourth panel: residuals after including all detected and suspected signals.

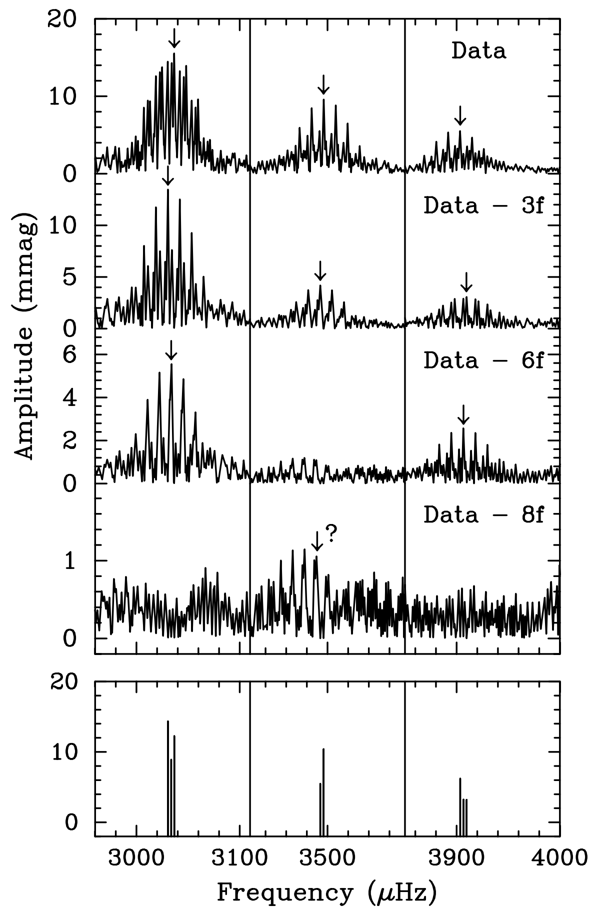

Figure 4. Amplitude spectra of our PG 2246+121 data in the vicinity of the dominating features (upper four panels). The lowest panel shows the detected frequencies with the corresponding amplitudes schematically.

follows; the measurements from 2000 April are too few to be of much astrophysical interest. We merely comment here that they are consistent with the results reported below.

We started by calculating nightly amplitude spectra of our data. The amplitude spectra of the individual nights are different in appearance: the dominating peaks seem to occur at the same frequencies, but their amplitudes vary. The question naturally arises whether this is due to beating of multiple modes or caused by some other phenomenon; we will examine it in what follows.

We combined all our runs and calculated amplitude spectra for the resulting data set. The full amplitude spectrum is displayed in the upper panel of Fig. 3. One can discern three strong features between 3000 and 4000 μHz, and it appears that frequency combinations are present as well. We now concentrate on these three strongest structures.

In Fig. 4, we show consecutive prewhitening steps within these features by simultaneous optimization of the frequencies, amplitudes and phases of all the detected signals. In two cases we could remove three signals from the structures; in one case we found it to be composed of two frequencies and their alias patterns. We simply adopted the highest peak in each panel as the next frequency to be included; we marked these frequencies with arrows for clarity. In the second-to-lowest middle panel we marked another peak with an arrow and a question mark; we will return to it later.

In the lowest panel of Fig. 4, a schematic amplitude spectrum composed of the detected signals is shown. Two structures seem to be equally spaced triplets and the third one is a close doublet. The frequency spacings of the closely spaced consecutive peaks are the same within the errors.

We took this result as a motivation to test whether this spacing is indeed the same within the three mode groups. Consequently, we fixed it within PERIOD98, but allowed it to be optimized together with its parent frequencies, i.e. we fitted a function

$$f(t) = \sum_{k=-1}^{1} a_k \sin[2\pi(f_A + k\nu_{\rm sp})t + \phi_k] + \sum_{k=0}^{1} b_k \sin[2\pi(f_B + k\nu_{\rm sp})t + \psi_k] + \sum_{k=-1}^{1} c_k \sin[2\pi(f_C + k\nu_{\rm sp})t + \xi_k]$$

to the data, where the a_k, b_k, c_k are the amplitudes of the multiplet components, f_A, f_B, and f_C denote the frequencies of the central components, ϕ_k, ψ_k and ξ_k are the phases of the individual signals, t is time and $\nu_{\rm sp}$ is the splitting frequency.

Tests (checking for residual peaks in the amplitude spectrum after prewhitening the fixed solution, applying the Bayes Information Criterion) showed that our data are perfectly consistent with the hypothesis that this splitting frequency is the same for all its parent signals, which are themselves constant in frequency, amplitude and phase within the length and accuracy of our data set. We therefore adopt this fixed-frequency solution for the rest of this paper.

We then searched for further frequencies in the residual amplitude spectrum after removing the eight signals detected so far from the data (second panel of Fig. 3). Two peaks clearly stand out, and they can be easily identified with sums of some of the eight original frequencies. Prewhitening these 10 signals from the light curve (by fixing the combination frequencies to the exact sum of those of their parents), some further peaks are discernible (third panel of Fig. 3). Many of them are consistent with 1 cycle d^1 aliases of combinations of the previously detected frequencies. One relatively high residual peak near 3500 μHz (the one labelled with a question mark in Fig. 4) would actually complete the doublet in this domain to a third equally spaced triplet. However, the application of Breger et al.'s (1993) amplitude signal-to-noise ratio criterion (requiring that the detection of an independent signal is secure if its amplitude exceeds four times the noise value in its frequency domain; signals the frequency of which can be predicted require $S/N > 3.5$) argues against a detection of this signal.

However, for some of the combination frequencies more than one identification is possible. These are frequency sums of different multiplets that are 'degenerate' because of the constant splitting within them; we adopted the one that has the simplest combination of parent modes. We therefore caution that some identifications in Table 2 may be incorrect.

In any case, we finally arrived at a 15-frequency solution. Prewhitening it from our data, only noise seems left behind (fourth panel of Fig. 3). The noise is however somewhat dependent on frequency. We compared our observational noise level with that expected from random noise with the same distribution as ours. We created several data sets consisting of our residual magnitudes shuffled in time and calculated the amplitude spectrum of those. We found that the level of random noise is only reached for frequencies larger than ≈5000 μHz; for frequencies lower than this the observational noise is enhanced.

Table 2. The multifrequency solution for our observations of PG 2246 + 121. Individual error estimates are quoted for the independent frequencies; those of the periods are then easy to infer. The amplitude uncertainty is ±0.3 mmag for all signals.

ID	Frequency (μHz)	Ampl. (mmag)	Period (s)	S/N
Directly detected signals				
$f_A - \nu_{sp}$	3030.57 ± 0.02	14.4	329.971	37.4
f_A	3033.65 ± 0.04	8.9	329.636	23.3
$f_A + \nu_{sp}$	3036.73 ± 0.03	12.3	329.302	32.5
f_B	3493.05 ± 0.06	5.1	286.283	13.8
$f_B + \nu_{sp}$	3496.13 ± 0.03	10.5	286.031	28.3
$f_C - \nu_{sp}$	3903.53 ± 0.05	6.1	256.179	20.3
f_C	3906.60 ± 0.10	3.1	255.977	10.3
$f_C + \nu_{sp}$	3909.68 ± 0.10	3.1	255.775	10.5
$2f_A$	6067.30	3.4		7.7
$f_A + f_B$	6526.70	4.2		10.2
Indirectly detected signals				
$f_A + f_C$	6940.25	1.5		4.7
$2f_A + f_B + \nu_{sp}$	9563.43	1.2		3.9
Suspected signals				
$f_B - \nu_{sp}$	3489.97 ± 0.27	1.1	286.535	3.0
$2f_A + \nu_{sp}$	6070.38	1.4		3.1
$f_A + f_B + 2\nu_{sp}$	6532.85	1.3		3.2
Splitting frequency				
ν_{sp}	3.078 ± 0.012			

Finally, we determined the error estimates for our multifrequency solution. We adopted them by applying the formulae of Montgomery & O'Donoghue (1999). However, we caution that such formal error bars are almost always underestimates, but we believe that the values we quote are reliable within about 50 per cent. Our complete multifrequency solution is summarized in Table 2; the error estimate for the splitting frequency is the error of the mean of all the splittings within the three 'parent' modes, if their frequencies were left as free parameters.

4 ASTROPHYSICAL IMPLICATIONS

It is clear that the light variations of PG 2246+121 are due to stellar pulsation: their complexity leaves no room for alternative hypotheses, and the frequency distribution shows the typical behaviour of a non-radially pulsating star. The lengths of the periods also indicate non-radial gravity (g) mode pulsations, and we identify the eight frequencies between 3000 and 4000 μHz as resulting from independent pulsation modes.

These eight signals consist of two equally split frequency triplets and one doublet with the same splitting. We think that they are due to pulsation modes of spherical degree $\ell = 1$. Modes of $\ell > 2$ would suffer from a large amount of geometrical cancellation because of averaging over the visible disc of the star (Dziembowski 1977), and should therefore not be seen in photometric data of distant stars. The only remaining possibilities for the spherical degrees of the modes are therefore $\ell = 1$ or $\ell = 2$ or a mixture of these.

However, the exact equal spacing of the triplets and the doublet rules out that we see a mixture of $\ell = 1$ and $\ell = 2$: asymptotic theory predicts, and observations confirm (Winget et al. 1991), that frequency splittings resulting from rotation are different for such modes; they have a ratio $R_{1,2} = 0.6$. The resolution and precision of our data is sufficient to detect such discrepancies reliably, but there is not even a trace of them. The modes must therefore be either $\ell = 1$ or $\ell = 2$.

We think that the $\ell = 2$ interpretation is unlikely. Aside from the fact that $\ell = 2$ modes are rarely seen in pulsating white dwarfs (e.g. Winget et al. 1991; Robinson et al. 1995; Fontaine et al. 1996; Clemens, van Kerkwijk & Wu 2000; Kepler et al. 2000), it would require some mode selection mechanism or serendipity that $\ell = 2$ modes produced the observed consistent frequency pattern, whereas an explanation with $\ell = 1$ modes is quite natural.

Under this assumption one can infer a formal rotational timescale of the star from the multiplet splitting. The result is 2.00 ± 0.12 d (the error estimate is caused by the unknown first-order rotational splitting coefficient $C_{k\ell}$, see Brassard et al. 1992b), which is quite typical for pulsating white dwarfs with an asteroseismologically determined rotation period. This result must however still be taken with some caution because of the unknown rotation curve in the stellar interior (Kawaler et al. 1999).

In principle, the pulsation periods of pulsating white dwarfs should allow an identification of the radial overtone number and an estimate of the stellar mass. This is, however, problematic for PG 2246+121, as it only has three radial overtones excited, because pulsation modes of DBV and DAV stars predominantly sample their outer regions, and because white dwarf models show severe mode trapping, which affects the mode eigenfrequencies (see Brassard et al. 1992a for extensive results and Bradley, Winget & Wood 1993 for some examples of DBV models). This means that we cannot put tight constraints on the radial overtone and stellar mass. We only note that the period spacing of the three multiplets is consistent with that of $\ell = 1$ model frequencies of three consecutive radial overtones between $k = 3$ and 7 (Bradley et al. 1993), most likely $k = 4, 5, 6$.

Concerning the impact of this discovery on the understanding of DBV pulsations in general, we first note that PG 2246+121 fills a 'gap' in its instability strip (Beauchamp et al. 1999), in the sense that in a certain temperature range (the theoretical boundaries of which depend on the composition of the model atmospheres) it now seems that all DB stars are pulsationally unstable.

After EC 20058−5234, PG 2246+121 is the DBV pulsator with the shortest dominating pulsation periods and it has a rather low amplitude, which implies that EC 20058−5234 is probably not an exception among the DBV stars. We also note that the pulsation periods of the three excited multiplets are very close to those of prominent modes of EC 20058−5234 (257, 281 and 333 s, Koen et al. 1995). These authors also raised the question of whether there exists a period–amplitude relation such as for the DAV stars (Clemens 1994), and found no clear trend. Adding PG 2246+121 to the ensemble does not change this picture.

It is also conceivable that the DBV stars show very similar pulsational behaviour as a group, like the DAVs. The similarities of the periods of PG 2246+121 to some of those of EC 20058−5234 can be taken as a first clue. The origin of the DB white dwarfs, and thus DBVs, is however a matter of debate. One scenario assumes that different evolutionary 'channels' exist (e.g. see Nitta & Winget 1998) for single and binary star evolution. In that case one would expect a mixed set of DBVs coming from both 'channels'. On the contrary, spectroscopically determined mass distributions (Beauchamp et al. 1996) suggest that the DB white dwarf stars are quite homogenous. Asteroseismological investigations will be able to address this problem from a different viewpoint.

Regrettably, many DBVs are still poorly observed, which is an obstacle to the studies mentioned above. We have therefore started a systematic investigation securing time-resolved CCD photometry of these stars in the hope of answering at least some of these open questions.

ACKNOWLEDGMENTS

This study would never have been performed without the collaboration of Atsuko Nitta, who pointed out the paper of Beauchamp et al. to me. I am grateful to SAAO for the sensible allocation of telescope time that made the success of this project possible. Chris Koen provided helpful comments on a draft version of this paper, and the referee is thanked for constructive criticism, which improved the quality of this work and made its presentation more balanced.

REFERENCES

Beauchamp A., Wesemael F., Bergeron P., Liebert J., Saffer R. A., 1996, in Jeffery C. S., Heber U., eds, ASP Conf. Ser. Vol. 96, Hydrogen-Deficient Stars. Astron. Soc. Pac., San Francisco, p. 295
Beauchamp A., Wesemael F., Bergeron P., Fontaine G., Saffer R. A., Liebert J., Brassard P., 1999, ApJ, 516, 887
Bergeron P., Wesemael F., Lamontagne R., Fontaine G., Saffer R. A., Allard N. F., 1995, ApJ, 449, 258
Bradley P. A., Winget D. E., 1994, ApJ, 430, 850
Bradley P. A., Winget D. E., Wood M. A., 1993, ApJ, 406, 661
Brassard P., Fontaine G., Wesemael F., Hansen C. J., 1992a, ApJS, 80, 369
Brassard P., Fontaine G., Wesemael F., Tassoul M., 1992b, ApJS, 81, 747
Breger M. et al., 1993, A&A, 271, 482
Clemens J. C., 1994, PhD thesis, Univ. Texas
Clemens J. C., van Kerkwijk M. H., Wu Y., 2000, MNRAS, 314, 220
Dziembowski W. A., 1977, Acta Astron., 27, 203
Fontaine G., Brassard P., Bergeron P., Wesemael F., 1996, ApJ, 469, 320
Kawaler S. D., Sekii T., Gough D. O., 1999, ApJ, 516, 349
Kepler S. O., Robinson E. L., Koester D., Clemens J. C., Nather R. E., Jiang X.-J., 2000, ApJ, 539, 379
Kjeldsen H., Frandsen S., 1992, PASP, 104, 413
Koen C., O'Donoghue D., Stobie R. S., Kilkenny D., Ashley R., 1995, MNRAS, 277, 913
Montgomery M. H., O'Donoghue D., 1999, Delta Scuti Star Newsletter, 13, 28 (Univ. Vienna)
Nitta A., Winget D. E., 1998, Baltic Astron., 7, 141
O'Donoghue D., 1995, Baltic Astron., 4, 519
Robinson E. L. et al., 1995, ApJ, 438, 908
Sperl M., 1998, Master's Thesis, Univ. Vienna
Vuille F. et al., 2000, MNRAS, 314, 689
Wegner G., 1983, AJ, 88, 109
Winget D. E., Nather R. E., Hill J. A., 1987, ApJ, 316, 305
Winget D. E. et al., 1991, ApJ, 378, 326
Winget D. E. et al., 1994, ApJ, 430, 839

This paper has been typeset from a TEX/LATEX file prepared by the author.

6.3.2 The asteroseismological potential of the pulsating DB white dwarf stars CBS 114 and PG 1456+103

Original paper:

G. Handler, T. S. Metcalfe, M. A. Wood, 2002, MNRAS 335, 698

Mon. Not. R. Astron. Soc. **335,** 698–706 (2002)

The asteroseismological potential of the pulsating DB white dwarf stars CBS 114 and PG 1456+103

G. Handler,[1]★ T. S. Metcalfe[2] and M. A. Wood[3]

[1]*South African Astronomical Observatory, PO Box 9, Observatory 7935, South Africa*
[2]*Theoretical Astrophysics Centre, Institute of Physics and Astronomy, Aarhus University, DK-8000 Aarhus C, Denmark*
[3]*Department of Physics and Space Sciences & SARA Observatory, Florida Institute of Technology, Melbourne, FL 32901, USA*

Accepted 2002 May 2. Received 2002 May 2; in original form 2002 April 12

ABSTRACT

We have acquired 65 h of single-site time-resolved CCD photometry of the pulsating DB white dwarf star (DBV) CBS 114 and 62 h of two-site high-speed CCD photometry of another DBV, PG 1456+103. The pulsation spectrum of PG 1456+103 is complicated and variable on time-scales of approximately 1 week and could only partly be deciphered with our measurements. The modes of CBS 114 are more stable in time and we were able to arrive at a frequency solution somewhat affected by aliasing, but still satisfactory, involving seven independent modes and two combination frequencies. These frequencies also explain the discovery data of the star, taken 13 yr earlier.

We find a mean period spacing of 37.1 ± 0.7 s significant at the 98 per cent level between the independent modes of CBS 114 and argue that they are caused by non-radial g-mode pulsations of spherical degree $\ell = 1$. We performed a global search for asteroseismological models of CBS 114 using a genetic algorithm, and we examined the susceptibility of the results to the uncertainties of the observational frequency determinations and mode identifications (we could not provide m values). The families of possible solutions are identified correctly even without knowledge of m. Our best-fitting model suggests $T_{\mathrm{eff}} = 21\,000$ K, $M_* = 0.730$ $\mathrm{M}_{\odot}$ and $\log(M_{\mathrm{He}}/M_*) = -6.66$, $X_{\mathrm{O}} = 0.61$. The latter value of the central oxygen mass fraction implies a rate for the $^{12}\mathrm{C}(\alpha, \gamma)^{16}\mathrm{O}$ nuclear reaction near $S_{300} = 180$ keV b, consistent with laboratory measurements.

Key words: stars: individual: CBS 114 – stars: individual: PG 1456+103 – stars: oscillations – stars: variables: other.

1 INTRODUCTION

The helium-atmosphere DB white dwarf stars are very interesting from the standpoint of stellar structure and evolution. The chemical evolution of their atmospheres cannot be satisfactorily explained to date (see Shipman 1997 for a review). In particular, the presence of the so-called DB gap, the absence of DB white dwarfs between temperatures of ∼30 000–45 000 K (Liebert 1986), is poorly understood. It is also not clear whether DBs are mostly produced by single-star evolution or whether a significant fraction of them originates from binary progenitors.

The examination of these problems can be aided by asteroseismology – the study of the interiors of pulsating stars via the analysis of their normal-mode spectra. Fortunately, a class of pulsating DB white dwarf stars (hereinafter DBVs) exists, and their prototype, GD 358, is one of the classical examples for the successful application of asteroseismological methods (Winget et al. 1994; Vuille et al. 2000).

Compared with other classes of pulsating star, the DBVs seem quite promising candidates for asteroseismology: their mode spectra are shown or believed to be rich, and pulsation theory for these stars is quite advanced and well tested. For instance, the central oxygen abundance of the models has been shown to have a measurable effect on the pulsation frequencies (Metcalfe, Winget & Charbonneau 2001), and the possible presence of a $^3\mathrm{He}/^4\mathrm{He}$ transition zone caused by chemical diffusion has also been shown to produce a measurable effect (Montgomery, Metcalfe & Winget 2001), although recent observations have ruled out this possibility (Wolff et al. 2002). In addition, the recently developed application of genetic-algorithm-based model fitting to DBV mode spectra (Metcalfe, Nather & Winget 2000) allows an objective and effective exploration of parameter space to find an optimal model for the observations.

The application of these methods to DBVs other than GD 358 is, however, hampered by a lack of suitable observational data. Most of these stars are rather faint (around 16th magnitude), which requires

★ E-mail: handler@astro.univie.ac.at

the use of 2-m class telescopes to acquire suitable data with photomultiplier detectors. However, time on these telescopes is generally oversubscribed and long runs are difficult to obtain. With the advent of CCD detectors and with the development of systems capable of acquiring measurements of high time resolution, the DBVs are now in reach of smaller telescopes. We have therefore started to acquire measurements aiming to make as many DBVs as possible accessible to asteroseismology.

The pulsations of the DB white dwarf star CBS 114 were discovered by Winget & Claver (1988, 1989), who reported multiperiodic oscillations with peak-to-peak light variations up to 0.3 mag and with a time-scale of approximately 650 s. PG 1456+103 (hereinafter referred to as PG 1456) was reported as a DBV by Grauer et al. (1988). These authors reported multiperiodic pulsations with dominant periodicities of between 420 and 850 s and maximum peak-to-peak amplitudes around 0.15 mag. As no further observations of either of these stars have been published, we deemed it worthwhile to obtain larger data sets to study the pulsations of CBS 114 and PG 1456 in more detail.

2 OBSERVATIONS

Most of our measurements were acquired as differential CCD photometry with the 0.75-m telescope at the Sutherland station of the South African Astronomical Observatory (SAAO), at which we had been allocated 3 weeks of observing time.

We used the University of Cape Town CCD camera (O'Donoghue 1995). Its CCD was operated in full-frame mode to acquire a maximum number of local comparison stars. We used 2×2 or 3×3 pre-binning depending on seeing, which results in readout times of approximately 2–3 s. For the faint CBS 114 ($B \approx 17.2$ as estimated from our CCD frames compared with PG 1456+103), we used integration times of 27 or 28 s to obtain one frame per 30 s, and we used 20-s integrations for PG 1456. No filter was used to maximize the number of photons detected. In every clear night, sky flat-fields were taken during twilight.

In addition, we acquired measurements of PG 1456 with the 0.9-m SARA telescope at Kitt Peak National Observatory (Arizona), to reduce the aliasing problem in the frequency analysis. The CCD used is an Apogee AP7p, with a back-illuminated SITe SIA-502AB 512×512 detector. The pixels are 24 μm square, or 0.75 arcsec pixel^{-1}. Read noise for the camera is 12.2 electrons rms, and the gain is 6.1 electrons ADU^{-1}. We used integration times of typically 30 s, and our readout time was approximately 7 s. Again, we took sky flats during each twilight. Our measurements are summarized in Table 1.

We started data reduction with the corrections for bias, dark counts (SARA measurements only) and flat-field. Mean weekly flat-fields were used for the SAAO data sets and combined nightly flats for the SARA frames. Photometric measurements on these reduced frames were made with the program MOMF (Kjeldsen & Frandsen 1992), which applies a combination of point spread function (PSF) and aperture photometry relative to a user-specified ensemble of comparison stars. No variability of any star other than the targets in the different CCD fields was found, and the comparison star ensemble resulting in the lowest scatter in the target-star light-curves was chosen.

The resulting differential light curves were corrected for differential colour extinction and for correlations with seeing. For CBS 114, it was sometimes also found necessary to de-trend the data with (x, y) position of the star on the chip because of flat-field errors. Residual low-frequency trends in the data (not found to be coherent over the time-span of the observations, hence judged not to be intrinsic to the stars) were removed by means of low-order polynomials.

Table 1. Journal of the observations. The SARA measurements were obtained between JD 245 1987 and 2451990; the remainder are SAAO data. *N* is the number of frames taken.

CBS 114			PG 1456+103		
Run start JD 245 0000	Length (h)	*N*	Run start JD 245 0000	Length (h)	*N*
1940.421	3.32	403	1940.570	1.44	225
1941.400	3.74	450	1941.609	0.55	87
1942.394	4.00	446	1942.570	1.49	219
1943.446	1.30	143			
1944.427	3.40	404	1944.573	1.51	233
1945.397	4.25	484	1945.577	1.44	209
1946.386	4.17	435	1946.567	1.75	267
1954.379	0.68	80			
1955.359	4.20	382	1955.539	2.50	410
1956.357	4.30	513	1956.539	2.62	400
1957.353	4.25	495	1957.533	2.74	442
1959.346	4.38	464	1959.530	2.93	449
1960.346	4.30	511	1960.530	0.55	81
			1987.929	2.71	251
			1988.898	3.34	277
			1989.882	3.60	349
1996.249	4.17	497	1996.426	5.83	897
1997.239	4.32	511	1997.423	5.88	909
1998.235	4.36	520	1998.422	4.37	617
1999.355	1.37	156	1999.416	4.99	692
2001.319	1.38	107	2001.415	4.42	681
2002.252	2.77	324	2002.373	6.94	808
Total	64.66	7325		61.60	8503

Finally, the times of measurement were transformed to a homogeneous time base. We chose terrestrial time (TT) as our reference for measurements on the surface of the Earth and applied a correction to account for the motion of the Earth around the barycentre of the Solar system. As this barycentric correction varied up to ±1 s throughout a run, we applied it point by point. Our final time base therefore is barycentric Julian ephemeris date (BJED). The reduced time series were subjected to frequency analyses; we show example light curves in Figs 1 and 2. The typical rms scatter per single data point is around 40–50 mmag for CBS 114, and for PG 1456 approximately 15 mmag (SAAO data) and 11 mmag (SARA data).

3 FREQUENCY ANALYSIS

Our frequency analysis was performed with the program PERIOD98 (Sperl 1998). This package applies single-frequency power spectrum analysis and simultaneous multifrequency sine-wave fitting, but also has some advanced options. In particular, it can be used to calculate optimal solutions for multiperiodic signals including harmonic, combination and equally spaced frequencies, which are often found in the analysis of the light curves of pulsating white dwarf stars.

3.1 CBS 114

A frequency analysis of single-site data of a multiperiodic variable in the presence of noise is difficult because of aliasing; extreme caution is required. However, the structure and extent of our data set aids us in this effort.

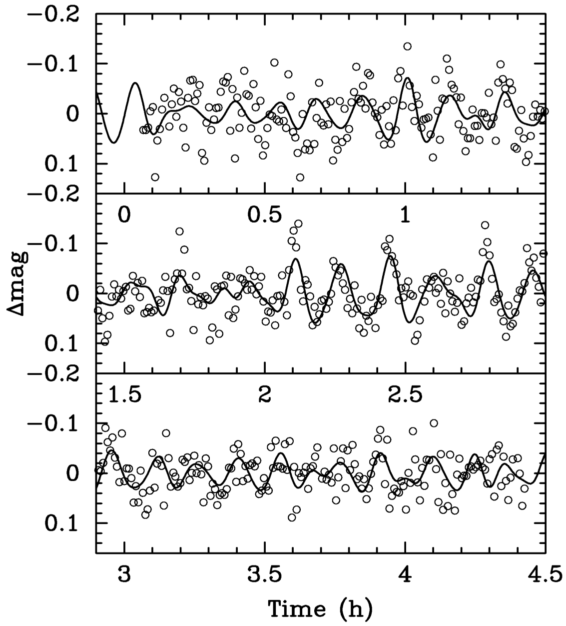

Figure 1. An example light curve of CBS 114; a multifrequency fit is included as well. Although the data are not of impressive quality caused by the faintness of the star, the multiperiodic pulsations are clearly visible.

We started by calculating nightly amplitude spectra of our data. The amplitude spectra of the individual nights were quite similar, with a number of dominant peaks always occurring at similar frequencies. However, some variations in the individual amplitudes were noted.

As the next step, we combined the three 1-week data sets (which are very similar in length and extent) and we computed their amplitude spectra and that of all 3 weeks combined. They are shown in Fig. 3, which shows six dominant structures between 1.4 and 2.6 mHz and some further signals that could be combination frequencies.

Some trial pre-whitening within the strongest features convinced us that all of them are dominated by one signal each. Consequently, we determined their frequencies by examining the combined, the weekly and the average of the weekly amplitude spectra and by least-squares fitting to the light curves. In this way, we could rule out a number of alias frequencies because they gave unreasonable results if adopted. However, in some cases, no unambiguous decision could be made.

Having determined the best set of frequencies, we refined their values by calculating an optimal solution for the whole data set, prewhitened it from the data and calculated the amplitude spectrum of the residuals (upper panel of Fig. 4). Because of the temporal changes in the weekly amplitude spectra, it is not surprising that some residual mounds of amplitude remained near the dominant frequencies.

We examined the frequencies of these features and their aliases and performed trial pre-whitening to check for any multiplet structure possibly present. No such evidence was found. We then fitted our best frequencies to the individual nights longer than 3 h

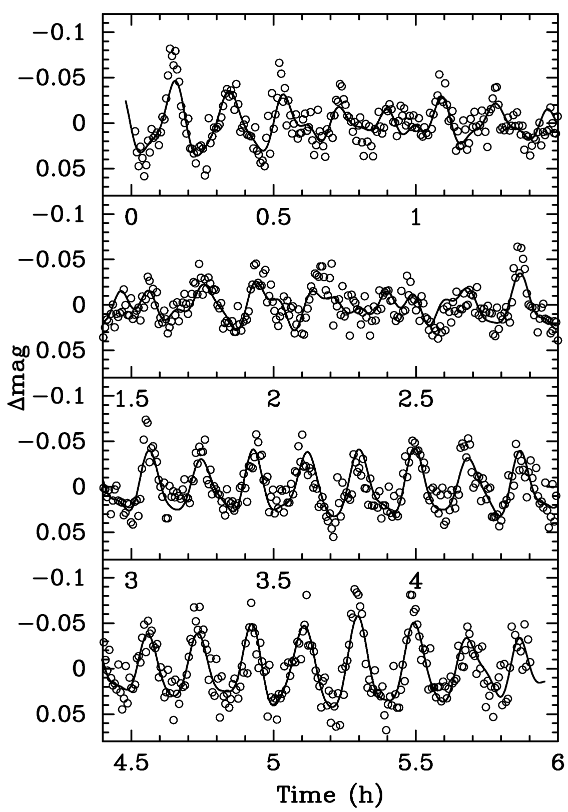

Figure 2. An example light curve of PG 1456+103 with a multifrequency fit. As the star is 1.3 mag brighter than CBS 114, the data are of much better quality; the multiperiodic pulsations are readily visible as well.

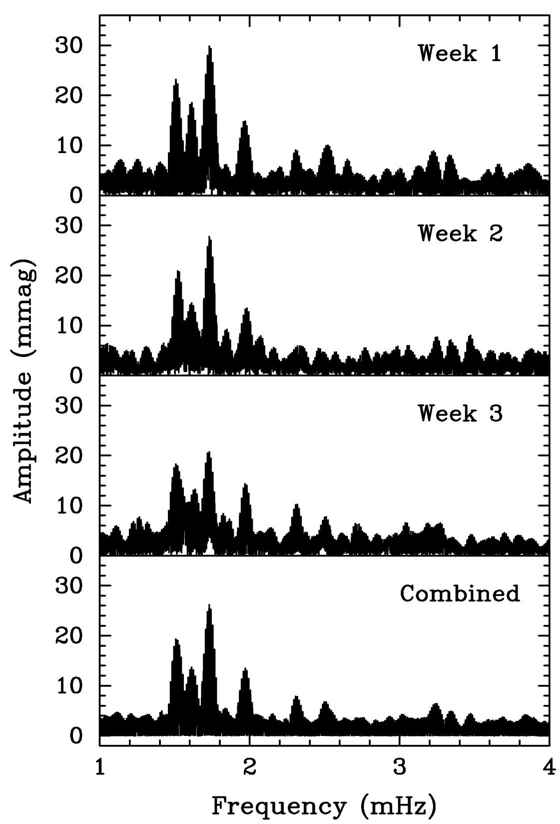

Figure 3. Weekly and combined amplitude spectra of our CBS 114 data. The same peaks are always present, but with somewhat variable amplitudes.

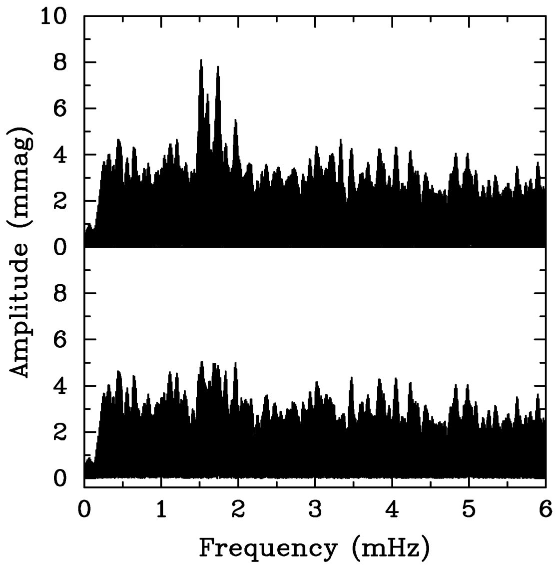

Figure 4. Upper panel, residual amplitude spectrum after pre-whitening the best multifrequency solution for our measurements of CBS 114, assuming constant amplitudes and phases over the whole data set. Lower panel, residual amplitude spectrum after pre-whitening the same frequency solution, but allowing for amplitudes and phases to vary over half-week intervals.

(ensuring that the dominant structures are resolved) and determined their amplitudes, phases and corresponding error estimates (following Montgomery & O'Donoghue 1999). We found that significant amplitude and phase changes occurred over time-scales of 3–4 d, and that either amplitude or phase variability alone is not sufficient to explain the observations – both are present.

As we cannot determine the cause of these variations, we treated them phenomenologically and calculated our final multifrequency solution with constant frequencies as determined previously, but with amplitudes and phases variable over half-week periods. In this way, we can determine ranges of the amplitudes of the dominant signals, and most of the residual mounds in the amplitude spectrum are thus removed (lower panel of Fig. 4). In Table 2, we list the best multifrequency solution determined with this method.

Table 2. Multifrequency solution for CBS 114. For frequencies labelled with a minus sign, the negative daily alias ($f_i - 11.60\,\mu$Hz) may be the correct frequency, and for frequencies labelled with a plus sign, the positive daily alias ($f_i + 11.60\,\mu$Hz) cannot be ruled out as the correct value. Amplitudes are listed in the ranges they assumed during the observations.

ID	Freq. (μHz)	Period (s)	Amp. (2001) (mmag)	Amp. (1988) (mmag)
f_1	1518.75^-	658.43	16–33	33
f_2	1613.12	619.91	10–17	15
f_3	1729.73	578.13	22–37	18
f_4	1969.60	507.71	11–17	<5
f_5	2306.38^+	433.58	4–12	13
f_6	2509.89^-	398.42	4–10	9
f_1+f_3	3248.48	–	5–7	<7
f_2+f_3	3342.85	–	2–8	<6
f_7	1835.64^{+-}	544.77	<4.2	13

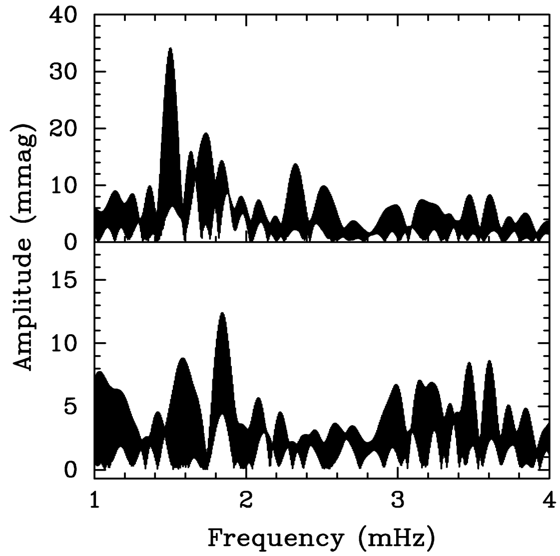

Figure 5. Upper panel, amplitude spectrum of the measurements by Winget & Claver (1988, 1989). Lower panel, residual amplitude spectrum after pre-whitening the first six frequencies determined from our observations.

3.1.1 *Re-analysis of Winget & Claver's data*

Although the measurements by Winget & Claver (1988, 1989) only comprise 5.2 h of data obtained over two nights, we can still use them for a comparison with our results. The amplitude spectrum of these measurements (upper panel of Fig. 5) shows dominant features at frequencies agreeing very well with those determined from our data. Consequently, we fitted the first six frequencies from Table 2 to these measurements and noticed that they were consistent with the older data. We therefore determined corresponding frequencies, amplitudes and phases, subtracted this fit from the data and calculated a residual amplitude spectrum, which is shown in the lower panel of Fig. 5, revealing the presence of yet another signal.

A variation at this frequency is also present in our new observations, although its amplitude is below our detection threshold. Consequently, we include it in our final frequency solution for the combined data sets (Table 2). We note some more suspected signals in the lower panel of Fig. 5, but owing to the small amount of data we do not push the analysis further. We have therefore detected altogether seven independent pulsation frequencies and two combination signals in the available light curves of CBS 114.

3.2 PG 1456

Owing to our two-site coverage of the light variations of PG 1456, the frequency analysis should be comparatively easy. However, initial trials showed that the pulsational amplitudes and frequencies of this star are also somewhat variable, and as our light curves from the first 2 weeks are rather short, they complicate the analysis if the total data set is used. Consequently, we used the JD 245 1987–JD 245 2002 two-site measurements as our primary data set for the frequency analysis; the remaining data were used for comparison purposes and consistency checks. Fig. 6 shows some pre-whitening steps in these two main subsets of data.

A signal (f_B) not present in the early SAAO observations reached considerable amplitude in the combined two-site data obtained

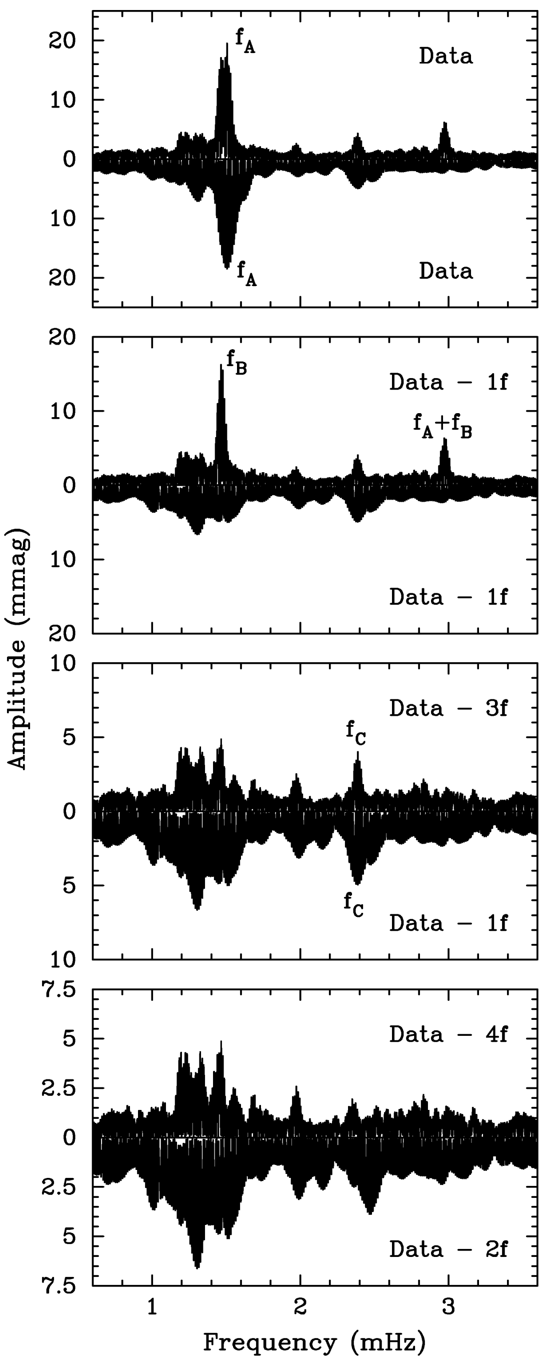

Figure 6. Amplitude spectra of our measurements of PG 1456. The upper halves of the panels are for the two-site JD 245 1987–JD 245 2002 data, whereas the lower, mirrored, halves originate from the preceding single-site observations. Uppermost panel, original data. Second panel, data after pre-whitening of the dominant frequency. Another frequency and a combination are detected only in the two-site data. Third panel, another mode is found in all the data. Lowest panel, the residual amplitude spectra; more signals are clearly present.

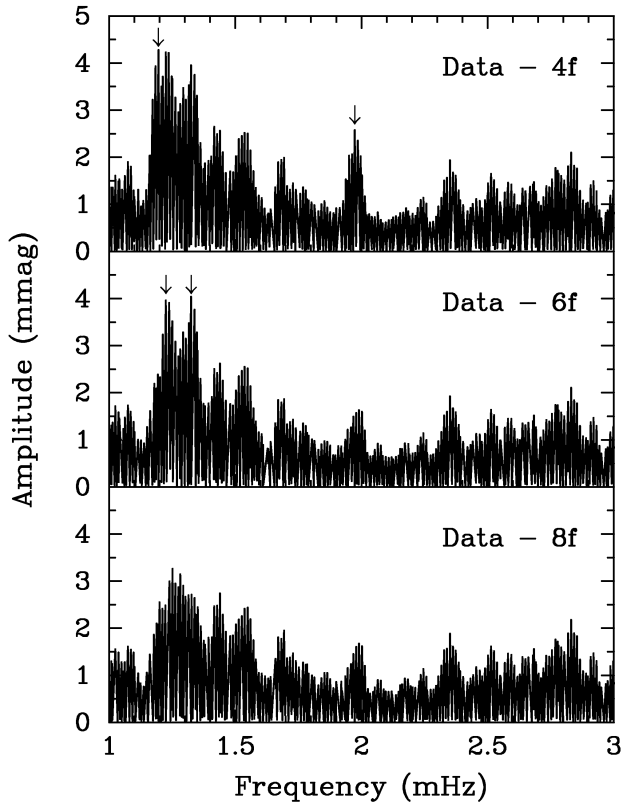

Figure 7. Pre-whitened amplitude spectra of our measurements of PG 1456. The arrows in the individual panels indicate further possible signals that are pre-whitened in the following panels.

approximately 7 weeks later; we note that this is not caused by an aliasing problem. As a matter of fact, the amplitude of this signal was still increasing during the latter measurements. It had approximately 12 mmag in the SARA data, but 18 mmag in the last set of SAAO measurements, in which it also showed a significant phase variation. A combination frequency ($f_A + f_B$) not present initially also appeared in the two-site data. On the other hand, the signal f_C was found to be constant in amplitude and phase over the whole data set, and f_A was constant in amplitude but showed a slight frequency shift of approximately 0.4 μHz between our two subsets of data.

The residual amplitude spectra in the lowest panel of Fig. 6 still show a number of interesting peaks, several of which may be real. To estimate the richness of the frequency spectrum of PG 1456, we performed further pre-whitening in the two-site data (still checking with the early SAAO measurements), taking the temporal variations of f_B into account. The resulting amplitude spectra are shown in Fig. 7.

It becomes clear that the light variations of PG 1456 are quite complicated and that our data set is not sufficient for finding all the frequencies present. A preliminary multifrequency solution is given in Table 3.

A few comments are still necessary. Signals in the region around 1970 μHz are present in both data sets with similar amplitude (e.g. the 1973.4 μHz signal in Table 3), but their frequencies are different by 5 μHz, even taking aliasing into account. The dominant frequency region in the residual single site-data is around 1304 μHz, but neither this frequency nor its aliases are present in the two-site data. It seems that only intensive multisite observations will make a good understanding of the frequency spectrum of PG 1456 possible.

The periods we determined are in very good agreement with those detected by Grauer et al. (1988). Regrettably, a detailed comparison

Table 3. Preliminary multifrequency solution for PG 1456. Whereas we are sure about the frequencies f_A to f_C, the other values may be affected by aliasing. Amplitudes are given for both the two-site measurements (left-hand column) and the preceding single-site SAAO data. Because of amplitude and frequency variability, error estimates are only given for amplitudes of apparently constant signals.

ID	Freq. (μHz)	Period (s)	Amp. (mmag)	Amp. (mmag)
		Certain detections		
f_A	1505.9	664.1	18.9 ± 0.3	18.5 ± 0.6
f_B	1465.4	682.4	$11.7 - 18.4$	–
$f_A + f_B$	2971.3	–	$5.7 - 6.8$	–
f_C	2387.9	418.8	4.0 ± 0.3	5.0 ± 0.6
		Possible further signals		
	1195.9	836.2	4.4 ± 0.3	4.4 ± 0.6
	1973.4	506.7	2.7 ± 0.3	–
	1224.8	816.5	3.9 ± 0.3	–
	1324.9	754.8	3.9 ± 0.3	–

of these periods is impossible as the discovery data are no longer available (Grauer, private communication).

4 INTERPRETATION OF THE OBSERVATIONAL RESULTS

4.1 CBS 114

The independent pulsation periods of CBS 114 as listed in Table 2 seem to have similar spacing. We therefore searched for and determined their mean spacing by calculating the Fourier power spectrum of the period values with unit amplitude (Handler et al. 1997), which we show in Fig. 8. A mean period spacing (significant at the 98 per cent level) is indicated, amounting to 37.1 ± 0.7 s. This result is corroborated by a Kolmogorov–Smirnov test (not shown).

We interpret this preferred period separation as a sign of the excitation of a number of pulsational radial overtones with the same spherical degree ℓ. Some small deviations around its mean value (see Fig. 9 in Section 5) are an indication of mode trapping. The presence of a preferred period separation is predicted by asymptotic theory (Tassoul 1980), and was already observed within, for example, the $\ell = 1, m = 0$ modes of GD 358 (Winget et al. 1994; Vuille et al. 2000), for which a mean period spacing of 39.2 s was found. In addition, Bradley & Winget (1994) showed that the systematic deviations from this mean spacing were caused by mode trapping.

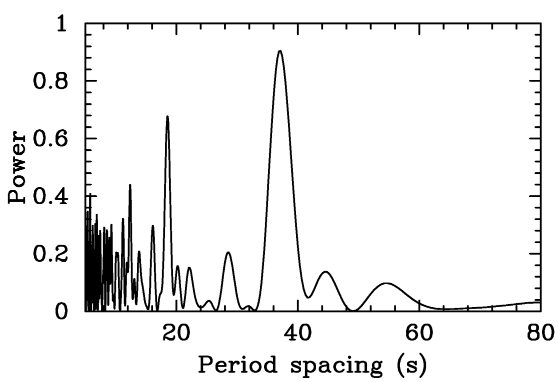

Figure 8. Search for a preferred period separation within the independent signals in the light curves of CBS 114. A spacing of 37.1 s and its harmonics dominate this diagram.

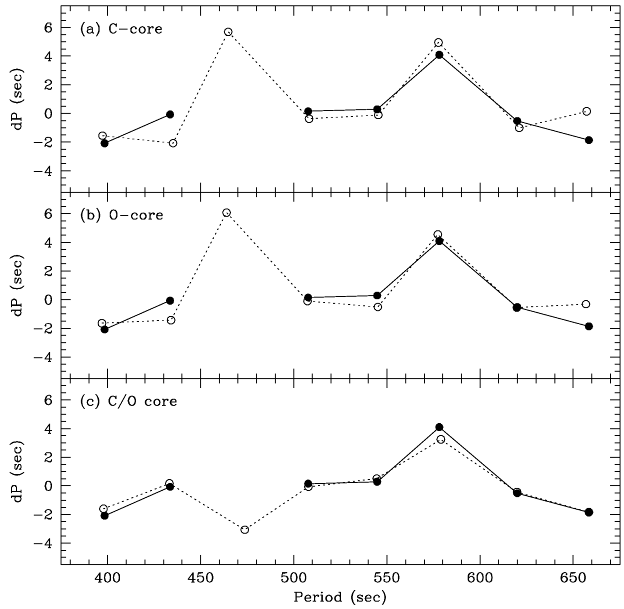

Figure 9. The observed periods of CBS 114 (solid) and the optimal model periods found by the genetic algorithm (open) plotted against the deviations from the mean period spacing, assuming a core of (a) pure C, (b) pure O and (c) mixed C/O (see the text for complete details).

We cannot directly identify the ℓ, m values of the modes we observed in CBS 114 because of the lack of any rotational m-mode splitting in our frequency spectra. However, it seems very likely that the independent modes of CBS 114 are all $\ell = 1$: if we saw a mixture of ℓ values, we would not expect to find such a significant mean period spacing. Therefore, the modes we observed must originate exclusively (or at least predominantly) from the same ℓ. They should be $\ell = 1$ or 2 as the effects of geometrical cancellation (Dziembowski 1977) are expected to render modes of higher ℓ photometrically undetectable.

The mean period spacing between consecutive overtones of a pulsating white dwarf star is a measure of its mass (Kawaler 1987). If the modes of CBS 114 were $\ell = 1$, their mean period spacing would be consistent with the star being a bit more massive than GD 358. However, if the modes were all $\ell = 2$, CBS 114 would need to have a mass below 0.3 $M_\odot$ (see Bradley, Winget & Wood 1993). Such a low mass is inconsistent with the spectroscopic gravity of the star (Beauchamp et al. 1999) and would be quite unusual in the light of the mass distribution of the DB white dwarf stars (Beauchamp et al. 1996).

Based on these arguments, we suggest that CBS 114 is a DBV star pulsating predominantly in non-radial g-modes of spherical degree $\ell = 1$. We note that its individual pulsation periods, especially that of longer period modes, are very similar to that of GD 358.

4.2 PG 1456

The interpretation of the frequency spectrum of PG 1456 is more difficult. A search for a mean period spacing such as in the previous section did not give a significant result. This suggests that the modes we detected are not of the same ℓ or that the star is a fast rotator. The modes of $m \neq 0$ would then mask the possible patterns of equally spaced periods.

Approximately half of the independent periods we detected or suspect are similar to periods of GD 358, but the others are not. We are therefore unable to interpret the mode spectrum of PG 1456 at this stage. Extensive multisite observations, e.g. with the Whole Earth Telescope (Nather et al. 1990), are required to understand the pulsations of this star.

5 ASTEROSEISMOLOGY OF CBS 114

Using the optimization method developed by Metcalfe et al. (2000, 2001), we performed a global search for the optimal model parameters to fit the seven independent pulsation periods for CBS 114 listed in Table 2. The method uses a parallel genetic algorithm to minimize the root-mean-square (rms) differences between the observed and calculated periods for models with effective temperatures ($T_{\rm eff}$) between 20 000 and 30 000 K, total stellar masses (M_*) between 0.45 and 0.95 $M_\odot$, and helium layer masses with $-\log(M_{\rm He}/M_*)$ between 2.0 and ~7.0. This technique has been shown to find the globally optimal set of parameters consistently among the many possible combinations in the search space, but requires between ~10 and 4000 times fewer model evaluations than an exhaustive search of parameter space to accomplish this (depending on the number of free parameters), with a failure rate $<10^{-5}$.

We assumed that all of the observed modes had spherical degree $\ell = 1$ (as suggested in Section 4.1) and azimuthal order $m = 0$. The latter assumption can bias our determination of the *particular* set of model parameters that produces the optimal fit to the data, but if the rotation period is ~1 d, any set of periods drawn from $m = (-1, 0, +1)$ will produce essentially the same overall picture of the parameter space. We demonstrated this general behaviour by generating C-core fits to 100 data sets for GD 358 that used randomly selected m-components from those identified in Winget et al. (1994), and the $m = 0$ values for $k = 12, 18$ (for which no triplet structure was found). In every case, the optimal set of model parameters fell within the same families of good solutions that were identified using the $m = 0$ modes. Thus, when the spherical degree of the modes is known, the model-fitting procedure correctly identifies the *families* of possible solutions even when the values of m are unknown. Furthermore, we found that the optimal solutions fell into the various families within parameter space in proportion to the relative fitness of that family when only $m = 0$ modes were used for the fit. For example, if a family has a peak fitness in the $m = 0$ case that is 3σ better than any other family, then the use of $m \neq 0$ modes will identify an optimal solution in this same family with ~50 per cent probability. This means that if one of the families produces much better solutions than the others, we can be reasonably confident that we have at least identified the correct family of solutions.

5.1 Carbon-core fit

Assuming a pure C core extending to a fractional mass of $0.95m/M_*$, the optimal set of model parameters found by the genetic algorithm were

$T_{\rm eff} = 24\,600$ K

$M_* = 0.655\ M_\odot$

$\log(M_{\rm He}/M_*) = -3.96$,

with rms period residuals $\sigma_P = 1.02$ s. The observed and calculated periods are shown in the top panel of Fig. 9 plotted against the deviations from the mean period spacing (dP), which were calculated using the same set of periods in both cases. Each point in this representation of the data is independent of the others, unlike a period spacing diagram using ΔP ($\equiv P_{k+1} - P_k$; cf. Bradley & Winget 1994). Note that the genetic algorithm only fits the periods of the pulsation modes, and the agreement between the deviations from the mean period spacing is simply a reflection of the overall quality of the match.

As noted in Table 2, the daily aliases of several of the identified modes in CBS 114 cannot be ruled out entirely. We can assess the impact of this uncertainty on the final set of optimal model parameters by repeating the fitting procedure using one or more of the alias periods. However, since the genetic algorithm fitting method with three free parameters is only approximately 10 times more efficient than calculating the entire grid of models, it is better to calculate the pulsation periods of all 10^6 models if we intend to repeat the procedure more than a few times. As there are four periods with a total of five possible aliases, we chose to calculate the entire grid of models. This allows us to check the answer that resulted from the genetic algorithm fit, and will enable us to generate C-core fits very quickly in the future for any additional data sets on DBV white dwarf stars.

All C-core models with rms period residuals smaller than 2.22 s are shown in the top half of Fig. 10, which includes front and side views of the entire search space. Each point in the left-hand panel corresponds to a point in the right-hand panel, and the darkness of a point indicates the relative quality of the match with the observations. Black points are within $\Delta\sigma_P = 0.03$ s of the optimal model, and the four progressively lighter shades of grey correspond to models within 3, 10, 25 and 40 times this difference. The

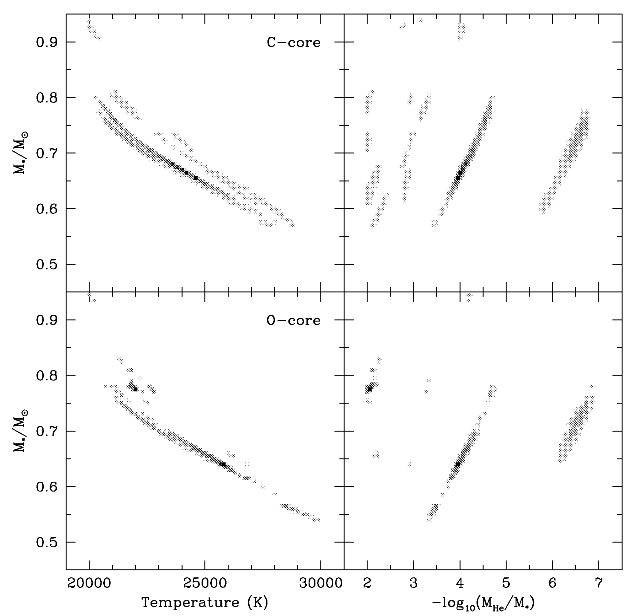

Figure 10. Front and side views of the search space assuming a C-core (top panels) and an O-core (bottom panels). Square points mark the location of models that yield a reasonable match to the periods observed for CBS 114. The darkness of a point indicates the relative quality of the match (see the text for complete details).

parameter correlations explained by Metcalfe et al. (2000) are clearly visible, causing the good models to fall along lines in the plot rather than on a single point.

As expected, the optimal parameters from comparison of the observations to the complete grid of models were identical to those found using the genetic algorithm method. In fact, the identified periods led to lower rms residuals than any set of periods that included one of the possible aliases. Of the combinations with two periods replaced by their aliases, fits with lower residuals were achieved in three cases: (i) $f_1 \rightarrow f_1^-$ and $f_7 \rightarrow f_7^+$, (ii) $f_1 \rightarrow f_1^-$ and $f_7 \rightarrow f_7^-$ and (iii) $f_6 \rightarrow f_6^-$ and $f_7 \rightarrow f_7^-$. When either three or four periods were replaced with aliases, only one combination led to lower residuals: $f_1 \rightarrow f_1^-$, $f_5 \rightarrow f_5^+$ and $f_7 \rightarrow f_7^+$. Note that aliases of f_1 and f_7 appear in most of these alternative period lists, implying that they are relatively important to the outcome of the fit. Although lower residuals were possible using these various combinations of two or more alias periods, the optimal models in every such case are too massive and too cool to be reconciled with the spectral line fits for CBS 114 by Beauchamp et al. (1999).

5.2 Oxygen-core fit

The optimal set of model parameters found by the genetic algorithm for a pure O core extending to 0.95m/M$_*$ had a mass that was inconsistent with the measurements of Beauchamp et al. (1999) and a helium layer mass at the edge of our search range, near the theoretical limit before nuclear burning will occur at the base of the envelope. The second-best model had residuals only ~0.03 s higher and was similar to the optimal C-core model. The parameters of this model were

$$T_{\rm eff} = 25\,800\,{\rm K}$$

$$M_* = 0.640\,{\rm M}_\odot$$

$$\log(M_{\rm He}/M_*) = -3.96,$$

with rms period residuals $\sigma_P = 0.91$ s. The middle panel of Fig. 9 shows the calculated periods of this model along with the observations, plotted against the deviations from the mean period spacing. The fit is only slightly better than the C-core model, and is qualitatively similar.

The O-core models that were calculated by the genetic algorithm during the optimization process with rms period residuals smaller than 2.08 s are shown in the bottom half of Fig. 10. Although this is not a complete sampling of the parameter space, it is heavily sampled in regions where models produce better than average residuals. Again, the shade of each point indicates the relative quality of the match with black points within $\Delta\sigma_P = 0.03$ s of the optimal model, and the shades of grey at 3, 10, 25 and 40 times this difference. Note that because the optimal O-core model has residuals ~0.1 s lower than the optimal C-core model, the darkest grey points in the bottom half of Fig. 10 are actually better than the black points in the top half.

5.3 C/O-core fit

Since it may seem dubious to fit the seven observed periods of CBS 114 using a model with five free parameters, we proceed cautiously. To allow a systematic exploration of models with various internal C/O profiles, Metcalfe et al. (2001) used a simple parametrization that explored a general class of profiles similar to those used by Bradley et al. (1993). The parametrization fixes the oxygen mass fraction to its central value ($X_{\rm O}$) out to some fractional mass (q) where it then decreases linearly in mass to zero oxygen at $0.95m/M_*$.

Using this method, the optimal model parameters for the observed pulsation periods of CBS 114 were

$$T_{\rm eff} = 21\,000\,{\rm K}, \quad M_* = 0.730\,{\rm M}_\odot,$$

$$\log(M_{\rm He}/M_*) = -6.66, \quad X_{\rm O} = 0.61, \quad q = 0.51,$$

with rms period residuals $\sigma_P = 0.43$ s. All models within $\Delta\sigma = 0.03$ s of this fit had the same mass, temperature and helium layer mass at our sampling resolution of 0.005 M$_\odot$, 100 K and 0.05 dex, respectively. Only models with a central oxygen mass fraction within $\Delta X_{\rm O} = \pm 0.01$ and the optimal value of q had rms residuals within this range.

The calculated periods of this model are shown in the bottom panel of Fig. 9 along with the observed periods, plotted against the deviations from the mean period spacing. To evaluate whether or not this fit is better by an amount that justifies the addition of two free parameters, we can use the Bayes information criterion (BIC, following Koen & Laney 2000):

$$\mathrm{BIC} = N_{\rm p}\left(\frac{\log N_{\rm obs}}{N_{\rm obs}}\right) + \log\sigma^2,$$

where $N_{\rm p}$ is the number of free parameters, $N_{\rm obs}$ is the number of observed periods and σ is the rms period residual of the optimal fit. The value of BIC must be lower for a decrease in σ to be considered significant. Our best three-parameter fit was the O-core model, which leads to a value of BIC = 0.28. This leads us to expect the residuals of a five-parameter fit to decrease to 0.69 s without being considered significant. The rms residuals of our five-parameter fit are substantially lower than 0.69 s, so the addition of the extra parameters seems to be justified, and the C/O fit is significantly better than the O-core model.

Even so, we might worry that our optimal model parameters may be less accurate than the values obtained for GD 358, owing to the smaller number of observed pulsation periods. To determine the magnitude of any systematic uncertainties owing to the smaller number of observed modes, we performed a new fit to the pulsation periods of GD 358, but using only the seven modes corresponding to those observed in CBS 114: $k = 8$, 9 and 11–15. When we compared the result of this fit with that using all 11 modes observed in GD 358, we found only small shifts to the optimal model parameters:

$$\Delta T_{\rm eff} = -500\,{\rm K}, \quad \Delta M_* = +0.015\,{\rm M}_\odot,$$

$$\Delta\log(M_{\rm He}/M_*) = -0.05, \quad \Delta X_{\rm O} = -0.02, \quad \Delta q = -0.01.$$

By analogy, we might expect our five-parameter fit to CBS 114 to represent a slight underestimate of the temperature and overestimate of the mass. Both potential biases help to explain part of the discrepancy between the mass and the temperature of our optimal model and the values inferred from the spectroscopic analysis of Beauchamp et al. (1999) ($T_{\rm eff} = 23\,300$; $\log g = 7.98$). Additional differences are expected since we have used different mixing-length parameters (ML3) from those of Beauchamp et al. (ML2/$\alpha = 1.25$). Metcalfe, Salaris & Winget (2002) quantified the offsets between fits to GD 358 using ML3 and ML2, and found them to be approximately the same size as the shifts owing to the smaller number of data points. Unfortunately, CBS 114 does not have a published parallax, so an independent constraint on the mass and temperature from the luminosity is not presently available.

6 CONCLUSIONS

We have presented time-resolved CCD photometry of the pulsating DB white dwarf stars CBS 114 and PG 1456+103. Our data, obtained with telescopes of only 0.75 and 0.9-m apertures, are sufficient for the extraction of useful asteroseismological information even for a star as faint as CBS 114 ($B \approx 17.2$). We have also shown that it is possible to understand the mode spectra of multiperiodic pulsating white dwarf stars from single-site observations in suitable cases (see Handler 2001 for another example). In other cases, such as PG 1456, this is not possible, and worldwide observing campaigns, e.g. with the Whole Earth Telescope, are necessary.

The frequency analysis of our measurements of CBS 114 resulted in the discovery of a mean period spacing of 37.1 ± 0.7 s in the independent modes of the star. Although no convincing evidence for rotational splitting within the modes was detected, we argued that the star pulsates in non-radial $\ell = 1$ g-modes.

We used our data set to check the sensitivity of the newly developed asteroseismological genetic algorithm methods (Metcalfe et al. 2000) to artefacts of data analysis, such as aliasing problems and our lack of assignments of the azimuthal order m to the observed modes. Encouragingly, our results are hardly affected by these shortcomings.

The most significant result from this work is based on the fact that the optimal mass and central oxygen mass fraction of CBS 114 can provide an independent measurement of the astrophysically important rate for the $^{12}C(\alpha, \gamma)^{16}O$ reaction, as was recently done for GD 358 (Metcalfe et al. 2002). In general, higher-mass white dwarfs are expected to have a lower central oxygen mass fraction, because the 3α rate rises faster with increasing density than the $^{12}C(\alpha, \gamma)^{16}O$ rate. Our optimal model for CBS 114 has a higher-mass and a lower central oxygen mass fraction than the optimal model for GD 358 (Metcalfe et al. 2001), thus being consistent with this general trend. A model of the internal chemical profile with the same mass as our fit to CBS 114 requires a rate for the $^{12}C(\alpha, \gamma)^{16}O$ reaction near $S_{300} = 180$ keV b to produce a central oxygen mass fraction of 0.61 (M. Salaris, private communication). This value is close to the rate derived from recent high-energy laboratory measurements ($S_{300} = 165 \pm 50$ keV b; Kunz et al. 2002). In contrast, the rate derived from the optimal model of GD 358 by Metcalfe et al. (2002) was significantly higher ($S_{300} = 370 \pm 40$ keV b). This suggests either that presently unknown sources of systematic uncertainty in our models must affect the analysis of GD 358 and CBS 114 in different ways, or that the two stars have different evolutionary origins, or both. An asteroseismological determination of the central oxygen mass fraction for additional DBV white dwarfs will help us to decide which of these scenarios is most likely.

ACKNOWLEDGMENTS

We thank Don Winget and Chuck Claver for permission to use their data of CBS 114, Maurizio Salaris for providing a new internal chemical profile to match our optimal model and Mike Montgomery for carefully reading a draft version of this paper.

REFERENCES

Beauchamp A., Wesemael F., Bergeron P., Liebert J., Saffer R.A., 1996, in Jeffery C.S., Heber U., eds, Hydrogen-Deficient Stars. ASP Conf. Ser. 96. Astron. Soc. Pac., San Francisco, p. 295
Beauchamp A., Wesemael F., Bergeron P., Fontaine G., Saffer R.A., Liebert J., Brassard P., 1999, ApJ, 516, 887
Bradley P.A., Winget D.E., 1994, ApJ, 430, 850
Bradley P.A., Winget D.E., Wood M.A., 1993, ApJ, 406, 661
Dziembowski W.A., 1977, Acta Astron, 27, 203
Grauer A.D., Bond H.E., Green R.F., Liebert J., 1988, AJ, 95, 879
Handler G., 2001, MNRAS, 323, L43
Handler G. et al., 1997, MNRAS, 286, 303
Kawaler S.D., 1987, in Cox A.N., Sparks W.M., Starrfield S.G., eds, Stellar Pulsations. Springer, Berlin, p. 367
Kjeldsen H., Frandsen S., 1992, PASP, 104, 413
Koen C., Laney D., 2000, MNRAS, 311, 636
Kunz R., Fey M., Jaeger M., Mayer A., Hammer J.W., Staudt G., Harissopulos S., Paradellis T., 2002, ApJ, 567, 643
Liebert J., 1986, Proc. IAU Coll. 87. D. Reidel Publishing Co., Dordrecht, p. 367
Metcalfe T.S., Nather R.E., Winget D.E., 2000, ApJ, 545, 974
Metcalfe T.S., Winget D.E., Charbonneau P., 2001, ApJ, 557, 1021
Metcalfe T.S., Salaris M., Winget D.E., 2002, ApJ, 573, 803
Montgomery M.H., O'Donoghue D., 1999, Delta Scuti Star Newslett., 13, 28, Univ. Vienna
Montgomery M.H., Metcalfe T.S., Winget D.E., 2001, ApJ, 548, L53
Nather R.E., Winget D.E., Clemens J.C., Hansen C.J., Hine B.P., 1990, ApJ, 361, 309
O'Donoghue D., 1995, Baltic Astron. 4, 519
Shipman H., 1997, in Isern J. et al., eds, White dwarfs: Proc. 10th European Workshop on White Dwarfs. Kluwer, Dordrecht, p.165
Sperl M., 1998, Master's thesis, Univ. Vienna
Tassoul M., 1980, ApJS, 43, 469
Vuille F. et al., 2000, MNRAS, 314, 689
Winget D.E., Claver C.F., 1988, IAU Circ. 4595
Winget D.E., Claver C.F., 1989, in Wegner G., ed., White dwarfs. Proc. IAU Colloq. 114, Springer, Berlin, p. 290
Winget D.E. et al., 1994, ApJ, 430, 839
Wolff B., Koester D., Montgomery M.H., Winget D.E., 2002, A&A, 388, 320

This paper has been typeset from a TEX/LATEX file prepared by the author.

6.3.3 Amplitude and frequency variability of the pulsating DB white dwarf stars KUV 05134+2605 and PG 1654+160 observed with the Whole Earth Telescope

Original paper:

G. Handler, D. O'Donoghue, M. Müller, J.-E. Solheim, J. M. Gonzalez Perez, F. Johannessen, M. Paparo, B. Szeidl, G. Viraghalmy, R. Silvotti, G. Vauclair, N. Dolez, E. Pallier, M. Chevreton D. W. Kurtz, G. E. Bromage, M. S. Cunha, R. Østensen, L. Fraga, A. Kanaan, A. Amorim, O. Giovannini, S. O. Kepler, A. F. M. da Costa, R. F. Anderson, M. A. Wood, N. Silvestri, E. W. Klumpe, R. F. Carlton, R. H. Miller, J. P. McFarland, A. D. Grauer, S. D. Kawaler, R. L. Riddle, M. D. Reed, R. E. Nather, D. E. Winget, J. A. Hill, T. S. Metcalfe , A. S. Mukadam, M. Kilic, T. K. Watson, S. J. Kleinman, A. Nitta, J. A. Guzik, P. A. Bradley, K. Sekiguchi, D. J. Sullivan, T. Sullivan, R. R. Shobbrook, X. Jiang, P. V. Birch, B. N. Ashoka, S. Seetha, V. Girish, S. Joshi, T. N. Dorokhova, N. I. Dorokhov, M. C. Akan, E. G. Meistas, R. Janulis, R. Kalytis, D. Alisauskas, S. K. Anguma, P. C. Kalebwe, P. Moskalik, W. Ogloza, G. Stachowski, G. Pajdosz, S. Zola, 2003, MNRAS 340, 1031

Mon. Not. R. Astron. Soc. **340,** 1031–1038 (2003)

Amplitude and frequency variability of the pulsating DB white dwarf stars KUV 05134+2605 and PG 1654+160 observed with the Whole Earth Telescope

G. Handler,[1,2]⋆ D. O'Donoghue,[1] M. Müller,[3] J.-E. Solheim,[4] J. M. Gonzalez-Perez,[4] F. Johannessen,[4] M. Paparo,[5] B. Szeidl,[5] G. Viraghalmy,[5] R. Silvotti,[6] G. Vauclair,[7] N. Dolez,[7] E. Pallier,[7] M. Chevreton,[8] D. W. Kurtz,[7,9] G. E. Bromage,[9] M. S. Cunha,[10,11] R. Østensen,[12] L. Fraga,[13] A. Kanaan,[13] A. Amorim,[13] O. Giovannini,[14] S. O. Kepler,[15] A. F. M. da Costa,[15] R. F. Anderson,[16] M. A. Wood,[17] N. Silvestri,[17] E. W. Klumpe,[18] R. F. Carlton,[18] R. H. Miller,[19] J. P. McFarland,[19] A. D. Grauer,[20] S. D. Kawaler,[21] R. L. Riddle,[21] M. D. Reed,[22] R. E. Nather,[23] D. E. Winget,[23] J. A. Hill,[23] T. S. Metcalfe,[23,24] A. S. Mukadam,[23] M. Kilic,[23] T. K. Watson,[25] S. J. Kleinman,[26] A. Nitta,[26] J. A. Guzik,[27] P. A. Bradley,[27] K. Sekiguchi,[28] D. J. Sullivan,[29] T. Sullivan,[29] R. R. Shobbrook,[30,31] X. Jiang,[32] P. V. Birch,[33] B. N. Ashoka,[34] S. Seetha,[34] V. Girish,[34] S. Joshi,[35] T. N. Dorokhova,[36] N. I. Dorokhov,[36] M. C. Akan,[37] E. G. Meištas,[38] R. Janulis,[38] R. Kalytis,[39] D. Ališauskas,[39] S. K. Anguma,[40] P. C. Kalebwe,[41] P. Moskalik,[42] W. Ogloza,[42,43] G. Stachowski,[42] G. Pajdosz[43] and S. Zola[43,44]

[1]*South African Astronomical Observatory, PO Box 9, Observatory 7935, South Africa*
[2]*Present address: Institut für Astronomie, Universität Wien, Türkenschanzstraße 17, A-1180 Wien, Austria*
[3]*Department of Astronomy, University of Cape Town, Rondebosch 7700, South Africa*
[4]*Institutt for Matematiske Realfag, Nordlysobservatoriet, Universitet i Tromsø 9000 Tromsø, Norway*
[5]*Konkoly Observatory, Box 67, H-1525 Budapest XII, Hungary*
[6]*Osservatorio Astronomico di Capodimonte, via Moiariello 16, I-80131 Napoli, Italy*
[7]*Observatoire Midi-Pyrénées, CNRS/UMR5572, 14 av. E. Belin, 31400 Toulouse, France*
[8]*Observatoire de Paris-Meudon, LESIA, 92195 Meudon, France*
[9]*Centre for Astrophysics, University of Central Lancashire, Preston PR1 2HE*
[10]*Centro de Astrofísica da Universidade do Porto, Rua das Estrelas, 4150-762 Porto, Portugal*
[11]*Instituto Superior da Maia, Lugar de Vilarinho, 4470 Castelo da Maia, Portugal*
[12]*Isaac Newton Group of Telescopes, 37800 Santa Cruz de La Palma, Canary Islands, Spain*
[13]*Departamento de Física, Universidade Federal de Santa Catarina, CP 476-CEP 88040-900 Florianópolis, SC-Brazil*
[14]*Departamento de Física e Química, Universidade de Caxias do Sul, 95001-970 Caxias do Sul, RS-Brazil*
[15]*Instituto de Física, UFRGS, Campus do Vale, C.P. 15051 Porto Alegre, RS, Brazil*
[16]*Department of Physics and Astronomy, University of North Carolina, Chapel Hill, NC 27599-3255, USA*
[17]*Department of Physics & Space Sciences and SARA Observatory, Florida Institute of Technology, Melbourne, FL 32901, USA*
[18]*Department of Physics and Astronomy, Middle Tennessee State University, Murfreesboro, TN 37132, USA*
[19]*Department of Physics and Astronomy, Georgia State University, Atlanta, GA 30303, USA*
[20]*Department of Physics and Astronomy, University of Arkansas at Little Rock, Little Rock, AR 72204, USA*
[21]*Department of Physics and Astronomy, Iowa State University, Ames, IA 50011, USA*
[22]*Department of Physics, Astronomy and Material Science, SW Missouri State University, 901 S. National, Springfield, MO 65804 USA*
[23]*Department of Astronomy and McDonald Observatory, University of Texas at Austin, Austin, TX 78712, USA*
[24]*Harvard-Smithsonian Centre for Astrophysics, 60 Garden Street, Cambridge, MA 02138, USA*
[25]*Information Technology Services Department, Southwestern University, Georgetown, TX 78626, USA*
[26]*Sloan Digital Sky Survey, Apache Pt. Observatory, PO Box 59, Sunspot, NM 88349, USA*
[27]*Los Alamos National Laboratory, X-2, MS T-085, Los Alamos, NM 87545-2345, USA*
[28]*Subaru Telescope, National Astronomical Observatory of Japan, 650 North A'ohōkū Place, Hilo, HI 96720, USA*
[29]*School of Chemical and Physical Sciences, Victoria University of Wellington, PO Box 600, Wellington, New Zealand*
[30]*PO Box 518, Coonabarabran, NSW 2357, Australia*
[31]*Research School of Astronomy and Astrophysics, Australian National University, Weston Creek PO, ACT 2611, Australia*
[32]*National Astronomical Observatories and Joint Laboratory of Optical Astronomy, Chinese Academy of Sciences, Beijing 100012, China*
[33]*Perth Observatory, Walnut Rd, Bickley, Western Australia 6076, Australia*

⋆E-mail: handler@astro.univie.ac.at

[34]Indian Space Research Organization, Vimanapura PO, Bangalore 560 017, India
[35]State Observatory, Manora Peak, Naini Tal 263 129, India
[36]Astronomical Observatory, Odessa State University, Shevchenko Park, Odessa 270014, Ukraine
[37]Ege University, Science Faculty, Department of Astronomy and Space Sciences, Bornova 35100 Izmir, Turkey
[38]Institute of Theoretical Physics and Astronomy, Goštauto 12, Vilnius 2600, Lithuania
[39]Astronomical Observatory of Vilnius University, Čiurlionio 29, Vilnius 2009, Lithuania
[40]Department of Physics, Mbarara University of Science and Technology, PO Box 1410, Mbarara, Uganda
[41]Physics Department, The University of Zambia, PO Box 32379, Lusaka, Zambia
[42]Copernicus Astronomical Centre, ul. Bartycka 18, 00-716 Warsaw, Poland
[43]Mount Suhora Observatory, Krakow Pedagogical University, ul. Podchorążych 2, 30-084 Cracow, Poland
[44]Astronomical Observatory, Jagiellonian University, ul. Orla 171, 30-244 Cracow, Poland

Accepted 2002 December 17. Received 2002 December 13; in original form 2002 September 10

ABSTRACT

We have acquired new time series photometry of the two pulsating DB white dwarf stars KUV 05134+2605 and PG 1654+160 with the Whole Earth Telescope. Additional single-site photometry is also presented. We use all these data plus all available archival measurements to study the temporal behaviour of the pulsational amplitudes and frequencies of these stars for the first time.

We demonstrate that both KUV 05134+2605 and PG 1654+160 pulsate in many modes, the amplitudes of which are variable in time; some frequency variability of PG 1654+160 is also indicated. Beating of multiple pulsation modes cannot explain our observations; the amplitude variability must therefore be intrinsic. We cannot find stable modes to be used for determinations of the evolutionary period changes of the stars. Some of the modes of PG 1654+160 appear at the same periods whenever detected. The mean spacing of these periods (≈40 s) suggests that they are probably caused by non-radial gravity-mode pulsations of spherical degree $\ell = 1$. If so, PG 1654+160 has a mass around 0.6 $M_\odot$.

The time-scales of the amplitude variability of both stars (down to two weeks) are consistent with theoretical predictions of resonant mode coupling, a conclusion which might however be affected by the temporal distribution of our data.

Key words: stars: individual: KUV 05134+2605 – stars: individual: PG 1654+160 – stars: oscillations – stars: variables: other.

1 INTRODUCTION

In recent times it has become clear that amplitude and frequency variations are common amongst pulsating stars. Various mechanisms for their explanation have been proposed. For example, resonant mode interaction (Moskalik 1985) is consistent with observations of this phenomenon in δ Scuti stars (e.g. Handler et al. 1998, 2000), whereas frequency changes of rapidly oscillating Ap stars may be attributed to variations in the magnetic field (Kurtz et al. 1994, 1997).

Time-resolved photometric observations of pulsating (pre-)white dwarf stars revealed that they are no exception in this respect. This bears a potentially enormous astrophysical reward: although these stars may only make part of their pulsation spectra observable to us at a given time, they may reveal their complete mode spectrum when observed persistently. Kleinman et al. (1998), Bond et al. (1996) and Vauclair et al. (2002) took advantage of this possibility and could then make seismic analyses for a pulsating DA white dwarf (G29-38) and two pulsating central stars of planetary nebulae (NGC 1501, RXJ 2117+3412). Without their amplitude variability, these stars would still be poorly understood.

Published reports of amplitude and frequency variations are still sparse for the helium-atmosphere pulsating DB white dwarf stars (DBVs, see Bradley 1995, for a review), but so are their time-series photometric observations, mainly due to their faintness (most DBVs are around 16$^{\text{th}}$ magnitude). The glaring ($B = 13.5$) exception is the prototype DBV GD 358 for which a plethora of measurements, including three Whole Earth Telescope (WET, Nather et al. 1990) runs, is available. Although the mode amplitudes of GD 358 vary, the associated pulsation frequencies seem reasonably stable (Kepler et al. 2003). Very recently, some amplitude and frequency variations have also been reported for the DBVs CBS 114 and PG 1456+103 (Handler, Metcalfe & Wood 2002).

We have started a systematic observing program to obtain reliable frequency analyses of the mode spectra of all pulsating DB white dwarfs. Our measurements consist of extensive single-site observations, which can suffice for very simply-behaved objects (Handler 2001), or low-priority WET observations (this paper), or even full worldwide multisite campaigns.

2 OBSERVATIONS AND REDUCTIONS

The pulsating DB white dwarf stars KUV 05134+2605 and PG 1654+160 were chosen as secondary target stars for the WET runs Xcov20 and Xcov21 during 2000 November and 2001 April,

Table 1. Time-series photometry of KUV 05134+2605. The first part of the table contains the WET measurements, the second part lists additional single-site observations, and the third part contains the available discovery data (Grauer et al. 1989). Runs marked with asterisks were obtained with a CCD.

Run name	Obs./Tel.	Date (UT)	Start (UT)	Length (h)
asm-0080	McD 2.1m	2000 Nov 20	11:32:40	0.90
asm-0082	McD 2.1 m	2000 Nov 21	10:35:30	1.78
joy-003	McD 2.1 m	2000 Nov 23	10:20:00	2.16
joy-013	McD 2.1 m	2000 Nov 26	08:52:16	3.55
joy-017	McD 2.1 m	2000 Nov 27	10:08:40	2.38
joy-021	McD 2.1 m	2000 Nov 28	07:16:20	5.10
joy-026	McD 2.1 m	2000 Nov 29	09:48:50	2.77
sara-0054*	SARA 0.9 m	2000 Nov 30	04:53:00	8.49
joy-029	McD 2.1 m	2000 Nov 30	09:51:20	2.50
joy-032	McD 2.1 m	2000 Dec 01	09:10:00	3.44
sara-0055*	SARA 0.9 m	2000 Dec 03	05:18:20	8.01
sara-0057*	SARA 0.9 m	2000 Dec 05	03:21:00	5.47
tsm-0088	McD 2.1 m	2000 Dec 05	09:46:00	2.67
KU1229OH	OHP 1.9 m	1992 Dec 29	18:23:00	5.00
KU1230OH	OHP 1.9 m	1992 Dec 30	17:50:00	4.50
gh-0484*	SAAO 1.0 m	2000 Oct 04	00:45:26	2.55
gh-0486*	SAAO 1.0 m	2000 Oct 05	00:42:07	2.02
gh-0488*	SAAO 1.0 m	2000 Oct 06	00:36:43	2.76
gh-0492*	SAAO 1.0 m	2000 Oct 09	00:15:49	3.03
gh-0493*	SAAO 0.75 m	2001 Jan 30	19:01:40	2.40
gh-0496*	SAAO 0.75 m	2001 Jan 31	18:57:10	2.40
gh-0499*	SAAO 0.75 m	2001 Feb 01	18:40:15	2.62
adg-0076	MtB 1.5 m	1988 Oct 12	09:37:20	2.43
adg-0077	MtB 1.5 m	1988 Oct 13	08:23:10	1.67
adg-0080	MtB 1.5 m	1988 Oct 14	06:52:30	1.10
adg-0081	MtB 1.5 m	1988 Oct 14	10:19:20	1.86
adg-0082	MtB 1.5 m	1988 Oct 16	09:45:10	2.48
adg-0084	MtB 1.5 m	1988 Oct 18	07:26:00	1.98
Total WET				49.22
Grand total				88.02

Observatory codes: McD = McDonald Observatory (USA), SARA = Southeastern Association for Research in Astronomy Observatory (USA), OHP = Observatoire de Haute-Provence (France), SAAO = South African Astronomical Observatory, MtB = Steward Observatory (Mt. Bigelow site, USA).

Table 2. Time-series photometry of PG 1654+160. The first part of the table contains the WET measurements, the second part lists additional single-site observations, and the third part reports the available discovery data (Winget et al. 1984). Runs marked with asterisks were obtained with a CCD.

Run name	Obs./Tel.	Date (UT)	Start (UT)	Length (h)
sara-0081*	SARA 0.9 m	2001 Apr 17	10:53:30	1.36
luc02a	LNA 1.6 m	2001 Apr 20	04:36:10	0.36
luc03a	LNA 1.6 m	2001 Apr 20	05:51:10	1.13
luap21c	LNA 1.6 m	2001 Apr 21	03:12:00	2.48
luap21d	LNA 1.6 m	2001 Apr 21	05:43:40	2.32
sara-0083*	SARA 0.9 m	2001 Apr 21	06:52:25	5.33
mdr160	CTIO 1.5 m	2001 Apr 21	08:38:50	1.56
luap22c	LNA 1.6 m	2001 Apr 22	07:10:40	1.11
mdr163	CTIO 1.5 m	2001 Apr 22	09:05:20	1.05
luap23b	LNA 1.6 m	2001 Apr 23	06:42:00	1.75
sara-0085*	SARA 0.9 m	2001 Apr 23	09:48:50	2.26
luap24c	LNA 1.6 m	2001 Apr 24	02:58:00	1.35
luap24d	LNA 1.6 m	2001 Apr 24	04:29:00	0.89
mdr166	CTIO 1.5 m	2001 Apr 24	07:50:30	2.33
luap25b	LNA 1.6 m	2001 Apr 25	03:27:00	2.13
mdr169	CTIO 1.5 m	2001 Apr 25	06:37:00	3.45
gh-0508	SAAO 1.9 m	2001 Apr 26	02:06:40	1.94
luap26b	LNA 1.6 m	2001 Apr 26	03:01:00	5.40
NOTkd25b*	NOT 2.6 m	2001 Apr 26	03:29:00	2.46
mdr172	CTIO 1.5 m	2001 Apr 26	09:03:40	1.14
gh-0509	SAAO 1.9 m	2001 Apr 27	00:59:40	2.83
NOTkd26c*	NOT 2.6 m	2001 Apr 27	01:17:20	4.49
luap27b	LNA 1.6 m	2001 Apr 27	03:12:00	3.49
luap27c	LNA 1.6 m	2001 Apr 27	06:52:00	1.46
mdr175	CTIO 1.5 m	2001 Apr 27	09:05:20	1.06
sara-0092*	SARA 0.9 m	2001 Apr 28	06:22:50	5.73
mdr178	CTIO 1.5 m	2001 Apr 28	07:51:40	2.30
sara-0095*	SARA 0.9 m	2001 Apr 29	06:05:25	5.96
gh-0517	SAAO 1.9 m	2001 May 01	02:07:30	1.90
NOTkd30c*	NOT 2.6 m	2001 May 01	03:49:40	1.84
NOTke02a*	NOT 2.6 m	2001 May 02	23:08:50	5.11
NOTke03d*	NOT 2.6 m	2001 May 04	02:22:42	3.33
r3076	McD 2.1 m	1985 Jun 21	03:39:00	6.61
sjk-0317	McD 0.8 m	1994 Apr 06	06:40:30	5.14
sjk-0319	McD 0.8 m	1994 Apr 07	06:28:00	5.42
pi-001*	PO 1.0 m	2001 May 14	21:27:53	4.59
pi-002*	PO 1.0 m	2001 May 16	22:21:34	3.61
pi-003*	PO 1.0 m	2001 Jun 25	19:49:39	1.89
pi-004*	PO 1.0 m	2001 Jun 26	20:47:06	4.01
pi-005*	PO 1.0 m	2001 Jun 27	20:51:02	2.50
r2817	McD 2.1 m	1983 Aug 02	05:32:46	1.43
r2819	McD 2.1 m	1983 Aug 04	03:27:13	0.47
r2822	McD 2.1 m	1983 Aug 07	03:16:00	3.49
Total WET				81.30
Grand total				120.46

Observatories: SARA = Southeastern Association for Research in Astronomy Observatory (USA), LNA = Observatório do Pico dos Dias (Brazil), CTIO = Cerro Tololo Interamerican Observatory (Chile), SAAO = South African Astronomical Observatory, NOT = Nordic Optical Telescope (Tenerife), McD = McDonald Observatory (USA), PO = Piszkestetö Observatory (Hungary).

respectively. Such secondary programme stars are observed by the network if the primary target is not observable or if two telescopes are on line and the larger one already measures the primary or if the observing method at a certain site is not suitable for the primary (e.g. CCDs are not proper instruments for very bright stars). Although the temporal coverage of the variations of a secondary target is usually considerably poorer than that of the primary, the resulting data sets are often quite valuable (see Handler et al. 1997 for an example).

In addition to the WET measurements, we acquired single-site observations of KUV 05134+2605 and PG 1654+160 before and/or after the main data stream. In an effort to understand these two stars to the limits currently possible, we also (re)analysed all available published and unpublished measurements. The time-series photometric data at our disposal are listed in Tables 1 and 2.

Most of the observations consisted of multichannel high-speed photoelectric photometry with 10-s integrations (see Kleinman, Nather & Philips 1996, for more information). Channel 1 measured the programme star, channel 2 measured a local comparison star, and channel 3 simultaneously recorded sky background. If no third channel was available, the measurements were irregularly interrupted to measure sky. Data reduction was performed with a standard procedure, as e.g. described by Handler et al. (1997).

Our CCD measurements were acquired with a number of different photometers – which we do not describe in detail here. The observations were optimized to acquire at least two local comparison stars in the same field as the target by minimizing the readout time, ensuring a duty cycle as high as possible. In this way, consecutive data points were obtained in 10–30 s intervals, depending on the instrument.

CCD data reduction comprised correction for bias, dark counts and flat-field. Photometric measurements on these reduced frames were made with the programs MOMF (Kjeldsen & Frandsen 1992) or RTP (Østensen 2000), and differential light curves were created. No variability of any star other than the targets in the different CCD fields was found, and the comparison star ensemble resulting in the lowest scatter in the target star light curves was chosen.

At this point it should be noted that PG 1654+160 has a companion star (Zuckerman & Becklin 1992) at a separation of about 4″ distance that may affect our measurements. Fortunately for us, this companion is very red. Consequently, we used red-cutoff filters, e.g. a Schott BG 39 glass, which suppressed the companion's contribution sufficiently (it then was ∼2 mag fainter than the target), but did not waste too many photons of the target star. This also means that the companion's flux did not affect the amplitudes of the photoelectrically measured target star light curves significantly, as all our photomultipliers are blue-sensitive.

Finally, the times of measurement were transformed to Barycentric Julian Ephemeris Date (BJED); the barycentric correction was applied point by point. Finally, some overlapping portions of the combined light curves were merged, and the reduced time series were subjected to frequency analyses.

3 FREQUENCY ANALYSIS

Our frequency analyses were mainly performed with the program PERIOD 98 (Sperl 1998). This package applies single-frequency power spectrum analysis and simultaneous multifrequency sine-wave fitting. It also includes advanced options, such as the calculation of optimal light-curve fits for multiperiodic signals including harmonic, combination, and equally spaced frequencies, which are often found in the analysis of the light curves of pulsating white dwarf stars.

In one case to be indicated later, this method was supplemented by a residualgram analysis (Martinez & Koen 1994), which is based on a least-squares fit of a sine wave with *M* harmonics. One advantage of this method is that alias ambiguities can be evaluated more reliably by the simultaneous inclusion of the information in the Fourier harmonics.

3.1 KUV 05134+2605

We first analysed the WET measurements of KUV 05134+2605 with PERIOD 98. We computed the spectral window of the data (calculated as the Fourier Transform of a noise-free sinusoid with a frequency of 1.902 mHz and an amplitude of 9.7 milli-modulation amplitudes[1] (mma)) followed by the amplitude spectrum itself. The results are shown in the upper two panels of Fig. 1. As the WET measurements were only acquired from North American observatories (a result from the star having second priority), the window function is poor.

[1] One milli-modulation amplitude is the Fourier amplitude of a signal with a fractional intensity variation of 0.1 per cent; it is a standard unit for WET data analysis.

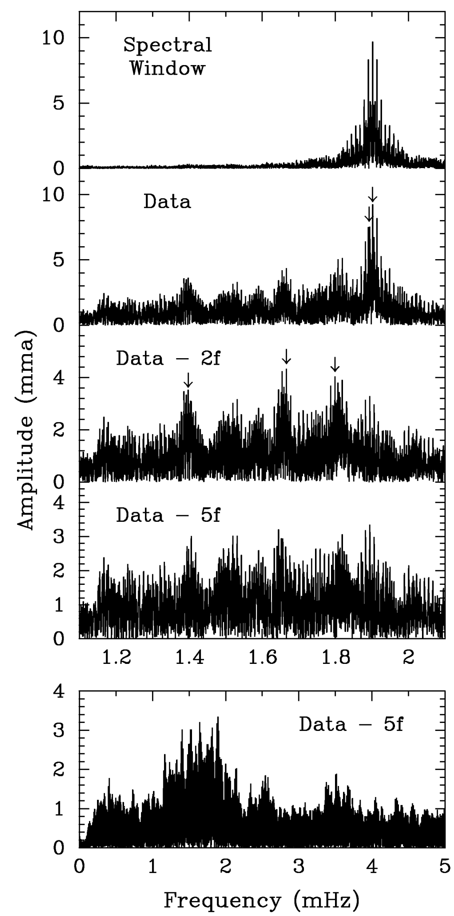

Figure 1. Spectral window and amplitude spectra of the WET measurements of KUV 05134+2605. Some trial prewhitening of the signals indicated with arrows to demonstrate the richness of the frequency spectrum is shown in consecutive panels. Due to the poor spectral window, no frequency can be determined with certainty, but many signals are definitely present in the light curves, as best seen in the lowest panel which shows an extended frequency range.

Still, we show some prewhitening steps in consecutive panels in Fig. 1. This has been done to indicate the main regions in which pulsational signals are present, but definite periods cannot be determined. In any case, it is suggested that KUV 05134+2605 has a rich pulsation spectrum.

This is not the only interesting feature of the pulsations of the star: in the discovery paper (Grauer et al. 1989) it was found to be of much higher amplitude and longer period compared to its pulsational state during the WET run. The star has changed from showing dominant pulsations with time-scales of 710 s and peak-to-peak amplitudes up to 0.2 mag to less than 0.1 mag and a dominant 530-s time-scale (Fig. 2).

We have therefore calculated amplitude spectra of all the available data (Fig. 3). Interestingly, the amplitude spectrum of the star was different every time it was observed. Besides the data discussed before, the measurements from 1992 show a dominant variability time-scale of around 650 s, and the 2001 February data have a prevailing time-scale of 570 s. Only the light curves from October 2000 appear similar to those acquired by the WET some 6 weeks later, but this actually only applies to the signal of highest amplitude. We conclude that KUV 05134+2605 shows notable amplitude variability

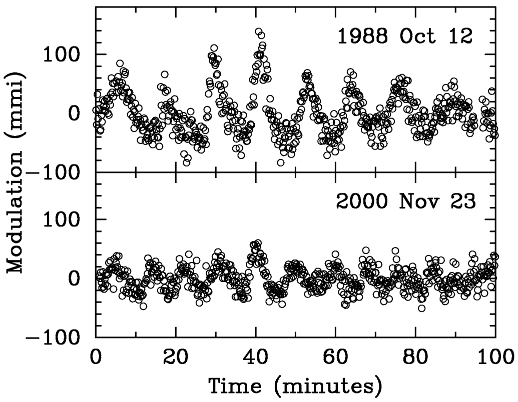

Figure 2. Upper panel: the discovery light curve of KUV 05134+2605. Lower panel: one of the light curves acquired during the WET run on the star. Note the change in the pulsational time-scales and amplitudes.

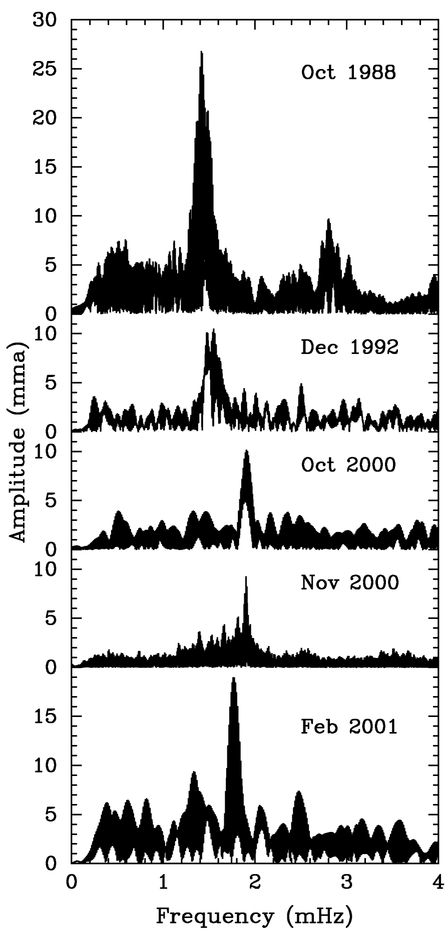

Figure 3. Amplitude spectra of all available measurements of KUV 05134+2605. The frequencies and amplitudes of the dominant signals are different in almost every data set.

on time-scales as short as 6 weeks. We cannot make any statement about frequency/phase variability as our data sets are too small to distinguish this hypothesis from the effects of beating between several signals.

We can attempt to construct the complete mode spectrum of the star by combining the results of the different observing seasons.

Table 3. Dominant signals in the light curves of KUV 05134+2605 in our data. The error estimates in the periods include alias ambiguities, and amplitudes are listed for completeness.

Month/Year	Period (s)	Amplitude (mma)
Oct 1988	707 ± 6	25
	665 ± 7	16
	777 ± 8	10
Dec 1992	645 ± 9	10
	678 ± 11	9
Oct 2000	525 ± 7	9
Nov 2000	526 ± 3	9
	556 ± 4	4
	600 ± 4	4
	716 ± 5	3
Feb 2001	567 ± 8	18
	757 ± 14	8

Of course, all the data sets are affected by aliasing and no definite periods can be determined, but approximate periods in the different regions of power in the Fourier spectra that are separated by more than the width of the envelope of the corresponding spectral window, can be estimated. We summarize these results, omitting possible combination frequencies, in Table 3. The amplitudes in this table must be taken with some caution, as they could be affected by insufficient frequency resolution in some of the data sets.

As already noted, there is no correspondence between the period of the dominant modes in each of the subsets of data except for the two closest in time (2000 October/November). It almost appears that we looked at a different star every time KUV 05134+2605 was observed!

In any case, we tried to find the signatures of non-radial gravity (g)-mode pulsations from Table 3, also with the help of Fig. 4, where we plot the detected periods over the different observing seasons. However, equally spaced periods suggestive of the presence of a number of radial overtones of the same ℓ or equally spaced frequencies that might be due to rotational m-mode splitting were not detected.

We can therefore summarize the frequency analysis of KUV 05134+2605 as follows: it has a very rich mode spectrum and its pulsation amplitudes are highly variable. We cannot find a stable pulsational signal which would allow us to estimate an evolutionary period change. Only a dedicated multisite campaign would help to understand this star.

3.2 PG 1654+160

We again start the frequency analysis with the WET measurements. The spectral window and amplitude spectrum of these data are shown in Fig. 5. Although the amplitude spectrum does not appear very complicated, attempts to determine the underlying variations by prewhitening result in a large number of signals that seem to be present.

However, assuming that we deal with normal-mode pulsations of the star, the number of signals becomes unrealistically large, and some of the frequencies found that way are too closely spaced to be resolved within our data set. All this suggests that the amplitude spectrum of PG 1654+160 was not stable throughout the observations.

Consequently, we attempted to follow the suspected amplitude and frequency variability throughout the data set with various

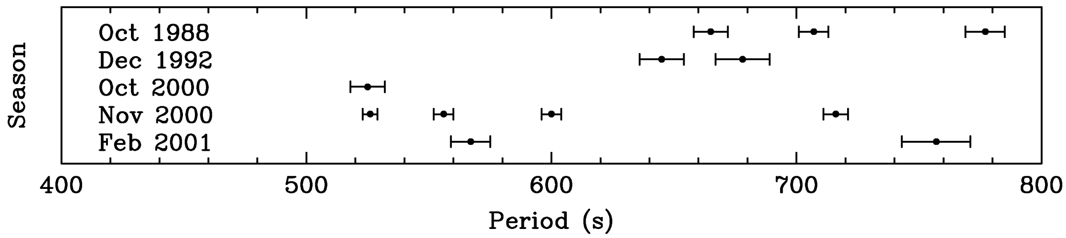

Figure 4. The variability periods of KUV 05134+2605 as listed in Table 3.

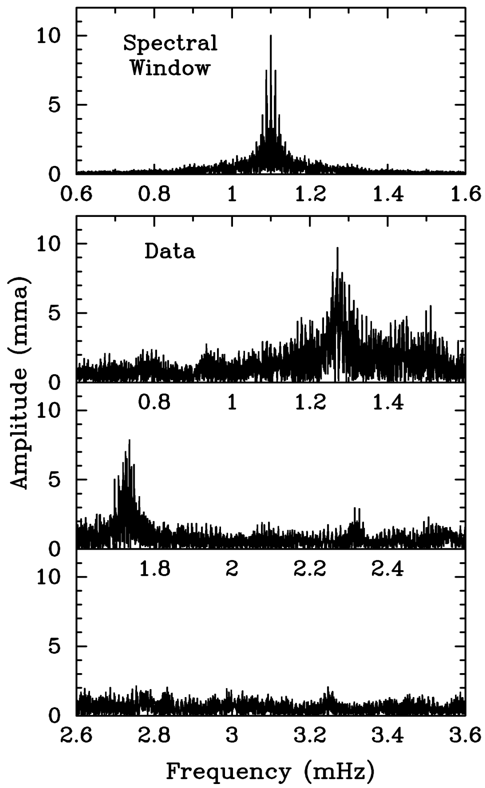

Figure 5. Spectral window and amplitude spectra of the WET measurements of PG 1654+160.

methods but again had to realize that our temporal coverage is insufficient for a detailed analysis. Some results can however be obtained.

(i) The longer period pulsations ($P \gtrsim 700$ s) show a larger degree of instability.
(ii) The amplitude spectrum was more stable during the second part of the run (beginning with April 25).
(iii) Amplitude variability alone is insufficient to account for the observed variations; the pulsation frequencies also appear somewhat variable.
(iv) The periods of the strongest signals can be determined, albeit with large errors due to the instability and aliasing.

The periods we could determine are listed in Table 4, together with the results from the other data sets to which we now turn.

In the same fashion as in the previous section, we computed amplitude spectra of all our data sets over the years. We show them in Fig. 6 which demonstrates that the pulsational behaviour of PG 1654+160 is also highly variable in time; a comparison of light curves is shown in Fig. 7. The time-scales of the amplitude variations of PG 1654+160 can be as short as two weeks: the strong 913-s signal in the May 2001 data was absent in the previous WET data.

Table 4. Dominant signals in our light curves of PG 1654+160. The error estimates in the periods include alias ambiguities, and amplitudes are listed for completeness.

Month/Year	Period (s)	Amplitude (mma)
Aug 1983	577 ± 6	24
	842 ± 13	15
June 1985	777:	14
	756:	11
	705 ± 6	10
	878 ± 8	10
	817 ± 7	8
	656 ± 5	6
Apr 1994	927 ± 10	31
	854 ± 16	12
Apr/May 2001 (WET)	781 ± 6	10
	579 ± 3	8
	662.0 ± 0.5	5
	700 ± 1	4
	833 ± 4	4
	431 ± 1	3
May 2001	791 ± 15	21
	575 ± 6	20
	913 ± 15	19
June 2001	697 ± 5	19
	658 ± 5	12

We determined the dominant periods in the different data sets, and summarize them in Table 4. Again, the amplitudes may be affected by resolution problems, and possible combination frequencies were excluded. In addition, there is good evidence for more signals being present in several of the data sets, but it is not possible to determine their periods and amplitudes reliably.

Some comments are necessary: the two strongest modes in the single-night data set from 1985 June are not resolved, which is why we cannot determine error estimates for their periods and thus disregard them for the following analysis. The errors on the other frequencies in this data set were assumed to be $1/4T$, where T is the length of the run. For the other data sets, the errors on the periods include some possible alias ambiguities. In the 1994 April data, the $2f$ harmonic of the dominant periodicity is also present. We therefore used the residualgram method (as described before) with $M = 2$ to obtain a more reliable determination of this period before searching for more signals.

It is interesting to note that some periodicities in Table 4 occur in more than one data set. We have displayed these results graphically in Fig. 8, where we again show the detected periods over the different observing seasons. We note that the shorter periods ($P <$

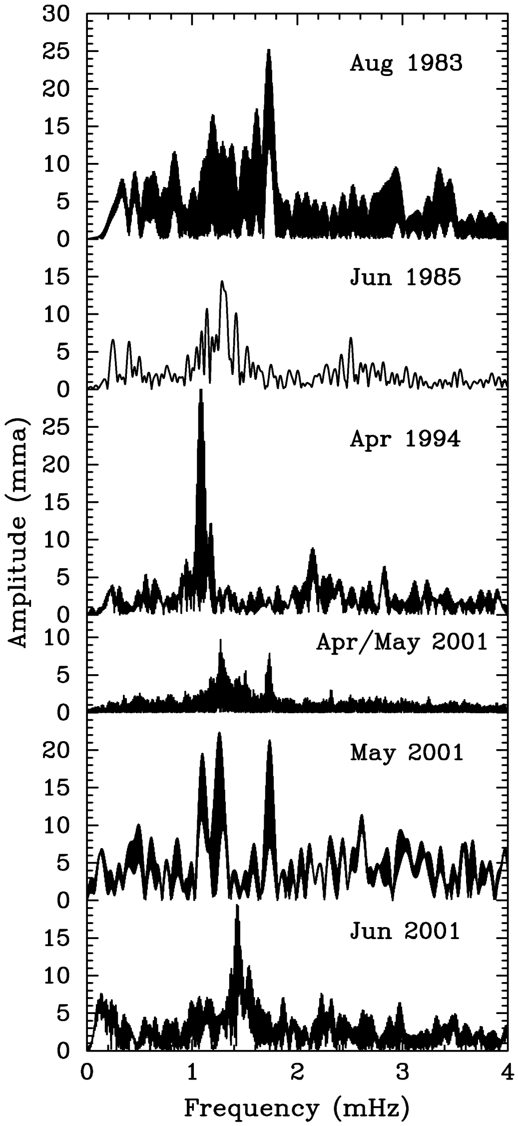

Figure 6. Amplitude spectra of all available measurements of PG 1654+160. This star also shows conspicuous amplitude variability.

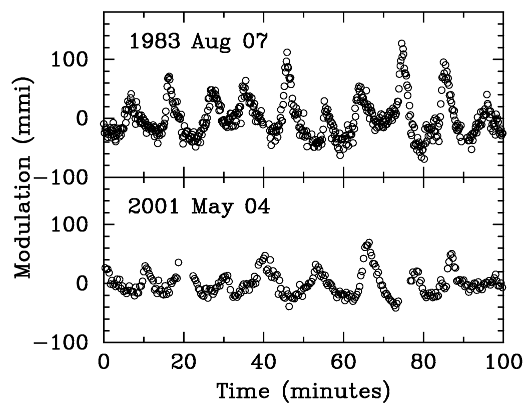

Figure 7. Upper panel: the discovery light curve of PG 1654+160. Lower panel: one of the light curves acquired during the WET run on the star. Again, the pulsational time-scales and amplitudes changed considerably.

800 s) in the light curves of PG 1654+160 appear very consistently in the same regions, whereas the longer periods do not show that much regularity. However, the errors in the determination of those periods are also larger. Finally, the previously mentioned shorter-period signals seem to have an approximately equidistant spacing of about 40 s, and again our data show no sufficiently stable modes to estimate the evolutionary period change rate.

4 DISCUSSION

We have shown that the amplitude spectra of both KUV 05134+2605 and PG 1654+160 are variable in time. Whereas we cannot find an underlying pattern in the periods of KUV 05134+2605, the roughly equidistant spacings within the shorter periods of PG 1654+160 suggests the presence of a number of radial overtones of g-modes. The size of this average period separation (≈40 s) is consistent with the expected mean period spacing of a normal-mass (≈0.6 $M_\odot$) DBV white dwarf pulsating in $\ell = 1$ modes (see, e.g. Bradley, Winget & Wood 1993).

A comparison of the individual mode periods of the known $\ell = 1$ pulsator GD 358 (Winget et al. 1994; Vuille et al. 2000) and those of another DBV, CBS 114 (Handler et al. 2002), with that of PG 1654+160 also supports this interpretation. However, the number of available observed modes of PG 1654+160 is insufficient for seismic model calculations, and the uncertainties of their periods are too large.

What may be the cause of the amplitude (and possibly also frequency) variability in the two stars? As neither has been reported to be magnetic in the literature, interaction between the different pulsation modes remains the most promising hypothesis for an explanation.

In this case, the time-scale of the amplitude variability is expected to be of the order of the inverse growth rates of the affected modes. Growth rates are not very well known for pulsating white dwarfs, but it is clear that longer-period modes have larger growth rates than shorter-period ones. Detailed growth-rate calculations (Dolez & Vauclair 1981) imply that amplitude variability may occur on time-scales down to about one week.

These theoretical predictions are consistent with our observations, at least as far as we can tell. The longer-period modes of PG 1654+160 indeed seem to vary more rapidly in amplitude than the ones at shorter period [it is interesting to note that Kepler et al. (2003) made the same observation for GD 358], as implied by our attempts to trace these variations. The time-scale of the amplitude variability of both stars also appears to be of the expected order of magnitude. However, we must admit that the temporal distribution of our data is such that we can only detect variations on just these time-scales. Hence, the agreement we find can at best be regarded as qualitative.

5 SUMMARY AND CONCLUSIONS

We have carried out new Whole Earth Telescope measurements of the two pulsating DB white dwarf stars KUV 05134+2605 and PG 1654+160 which were supplemented by single-site data. We also re-analysed all available archival measurements of the two stars.

We showed, for the first time, that both have rich pulsational mode spectra, and that the pulsation amplitudes of both stars are highly

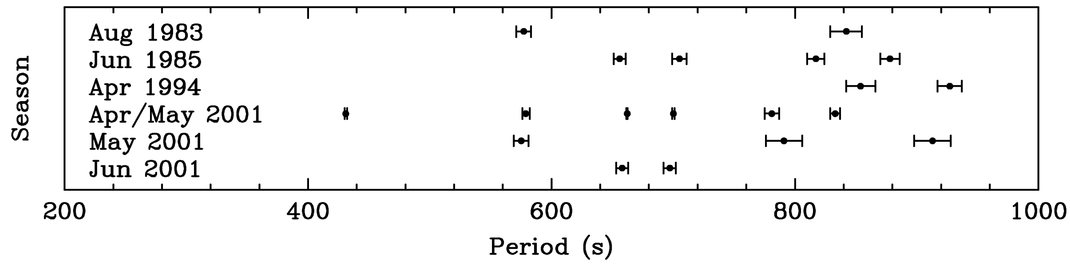

Figure 8. The variability periods of PG 1654+160 as listed in Table 4. Signals with periods below 800 s occur at the same frequencies whenever detected, and they are spaced by integer multiples of about 40 s.

variable in time; PG 1654+160 may show some frequency variability in addition. Beating of multiple pulsation modes cannot explain all our observations, as the observed amplitude and frequency variability is too complex for such an interpretation; hence it must be intrinsic. The pronounced amplitude variations made it impossible to find stable modes to determine the evolutionary period change rates of the two stars.

Whereas there seems no systematic pattern in the periods of KUV 05134+2605 we measured, some of the modes of PG 1654+160 appear at the same periods whenever detected. The spacing of these periods, around 40 s, suggests that they are probably caused by non-radial gravity-mode pulsations of spherical degree $\ell = 1$ in a normal-mass DBV white dwarf.

The amplitude variabilities of both stars could be followed by means of the pre- and post-WET observations that were therefore essential for this work. Their time-scales are consistent with theoretical predictions of resonant mode coupling. This conclusion is however weakened by the temporal distribution of our data, which favour the detection of just those variability time-scales.

Before a more detailed investigation of the amplitude variations of these two stars can be performed (e.g. to guide theoretical work in this direction, Buchler, Goupil & Serre 1995), mode identifications and an improved sampling of the temporal behaviour of the pulsations through continued single-site measurements are desirable. Given the qualitative similarity of PG 1654 and the 'typical' DBV GD 358, we expect that the same nonlinear mode coupling and amplitude modulation mechanisms are at work in both stars. Having very rich mode spectra, both KUV 05134+2605 and PG 1654+160 are also attractive targets for future extensive multisite campaigns.

ACKNOWLEDGMENTS

We acknowledge support from Iowa State University, in part through NSF Grant AST-9876655. MSC is supported through the grants PD/18893/98, of FCT-Portugal, and POCTI/1999/FIS/34549 approved by FCT and POCTI, with funds from the European Community programme FEDER. PM acknowledges partial financial support by the Polish KBN grant 5 P03D 012 20.

REFERENCES

Bond H. E. et al., 1996, AJ, 112, 2699
Bradley P. A., 1995, Baltic Astron., 4, 311
Bradley P. A., Winget D. E., Wood M. A., 1993, ApJ, 406, 661
Buchler J. R., Goupil M.-J., Serre T., 1995, A&A, 296, 405
Dolez N., Vauclair G., 1981, A&A, 102, 375
Grauer A. D., Wegner G., Green R. F., Liebert J., 1989, AJ, 98, 2221
Handler G., 2001, MNRAS, 323, L43
Handler G. et al., 1997, MNRAS, 286, 303
Handler G., Pamyatnykh A. A., Zima W., Sullivan D. J., Audard N., Nitta A., 1998, MNRAS, 295, 377
Handler G. et al., 2000, MNRAS, 318, 511
Handler G., Metcalfe T. S., Wood M. A., 2002, MNRAS, 335, 698
Kjeldsen H., Frandsen S., 1992, PASP, 104, 413
Kleinman S. J., Nather R. E., Philips T., 1996, PASP, 108, 356
Kleinman S. J. et al., 1998, ApJ, 495, 424
Kurtz D. W., Martinez P., van Wyk F., Marang F., Roberts G., 1994, MNRAS, 268, 641
Kurtz D. W., van Wyk F., Roberts G., Marang F., Handler G., Medupe R., Kilkenny D., 1997, MNRAS, 287, 69
Martinez P., Koen C., 1994, MNRAS, 267, 1039
Moskalik P., 1985, Acta Astron., 35, 229
Nather R. E., Winget D. E., Clemens J. C., Hansen C. J., Hine B. P., 1990, ApJ, 361, 309
Østensen R., 2000, PhD thesis, Univ. Tromsø
Sperl M., 1998, Master's thesis, Univ. Vienna
Vauclair G. et al., 2002, A&A, 381, 122
Vuille F. et al., 2000, MNRAS, 314, 689
Winget D. E., Robinson E. L., Nather R. E., Balachandran S., 1984, ApJ, 279, L15
Winget D. E. et al., 1994, ApJ, 430, 839
Zuckerman B., Becklin E. E., 1992, ApJ, 386, 260

This paper has been typeset from a TEX/LATEX file prepared by the author.

6.3.4 Analysis of helium-rich white dwarf IUE spectra

Original paper:

B. G. Castanheira, S. O. Kepler, **G. Handler,** D. Koester, 2006, A&A 450, 331

A&A 450, 331–337 (2006)
DOI: 10.1051/0004-6361:20054221

Astronomy & Astrophysics

Analysis of IUE spectra of helium-rich white dwarf stars*

B. G. Castanheira[1], S. O. Kepler[1], G. Handler[2,3], and D. Koester[4]

[1] Instituto de Física, Universidade Federal do Rio Grande do Sul, 91501-900 Porto-Alegre, RS, Brazil
e-mail: barbara@if.ufrgs.br
[2] Institut für Astronomie, Universität Wien, Türkenschanzstrasse 17, 1180, Wien, Austria
[3] South African Astronomical Observatory, PO Box 9, Observatory 7935, South Africa
[4] Institut für Theoretische Physik und Astrophysik, Universität Kiel, 24098 Kiel, Germany

Received 17 September 2005 / Accepted 30 December 2005

ABSTRACT

We studied the class of DB white dwarf stars, using re-calibrated UV spectra for thirty four DBs obtained with the IUE satellite. By comparing the observed energy distributions with model atmospheres, we simultaneously determine spectroscopic distances (d), effective temperature ($T_{\rm eff}$), and surface gravities ($\log g$). Using parallax measurements and previous determinations of $T_{\rm eff}$ and $\log g$ from optical spectra, we can study whether the atmospheres of eleven DB stars are consistent with pure He or have a small amount of H contamination. We also report on our observations of seventeen stars with $T_{\rm eff}$ close to the DB instability strip through time series photometry and found them to be non variable within our detection limits.

Key words. stars: white dwarfs – stars: variables: general – stars: oscillations – ultraviolet: stars

1. Introduction

Among all known white dwarf stars, around 20% have a helium (He) dominated atmosphere, and are thus assigned the spectral type DB. Most of these stars are believed to be result of the born again or a very late He thermal pulse during the early planetary nebula cooling phase (e.g. Althaus et al. 2005). In this event, the residual hydrogen (H) is completely burnt, the star returns quickly to AGB phase and again to planetary nebula, this time, without H. As they stars cool down, DBs cross an instability strip, where they are seen as multi-periodic pulsators. Beauchamp et al. (1999) determined its boundaries as $27\,800 \geq T_{\rm eff} \geq 22\,400$ K from a comparison of their pure He model atmosphere grid with ML2/α = 1.25 to optical spectra, and $24\,700 \geq T_{\rm eff} \geq 21\,800$ K, if undetectable traces of hydrogen (H) are allowed in the models.

The study of the instability strip of the DBs is still a challenge because of the small number of known pulsators; only seventeen are known to date (Nitta et al. 2005). Another difficulty is that the determinations of $T_{\rm eff}$ and $\log g$ from spectra are degenerate as, in general, these two parameters are correlated. Working with optical spectra is even more problematic, as possible contamination with even trace amounts of hydrogen that are undetected in the spectra can decrease the resulting effective temperatures by up to 3000 K and $\log g$ by up to 0.05 dex (Beauchamp et al. 1999). The uncertainty in $T_{\rm eff}$ derived from the published optical spectra is thus comparable to the width of the instability strip.

The DBs have been studied since the 1960 s, but especially after the discovery of a pulsator, GD 358, based on theoretical predictions (Winget et al. 1982). This star is the brightest and one of the best studied variable He atmosphere white dwarf (DBV) stars. Because pulsation theory gives detailed predictions of DBV properties, these stars can be used to study neutrino rates probing the electro-weak theory (Winget et al. 2004; Córsico & Althaus 2004), the C(α,γ)O cross section (Metcalfe 2003, 2005), and the He^3/He^4 separation (Wolff et al. 2002; Montgomery & Winget 2000) which cannot be achieved in any terrestrial laboratory. Pulsations in DBs are predicted to exist in a narrow temperature range, ~3000 K wide, but it has been difficult to measure $T_{\rm eff}$ with sufficient accuracy to determine the edges of the instability strip.

Considerable interest is focused on the accurate determination of atmospheric parameters for DB white dwarfs, for yet another reason, the so called "DB gap", where there are no observed DB stars. It occurs between 45 000 and 30 000 K in the cooling sequence (e.g. Hansen & Liebert 2003). The physical reason of the DB gap is still not understood. However, many theories attempt to explain why there would be no DBs within this range of temperature. One possibility is that DBs would turn into DAs (white dwarf with pure H atmospheres) by dragging H to the surface of the star, blocking the atmosphere. In this scenario, we expect to find more H in the hot DBs than

* Partially based on observations at Observatório do Pico dos Dias/ LNA.

in the cooler ones. We also investigate that possibility in this paper, but we do not confirm this theory.

2. Fitting the ultraviolet spectra

To study the DBs as a class and the characteristics of their instability strip, we used ultraviolet spectra because they are less affected by possible trace amounts of H that plague the optical determination of the effective temperature (Beauchamp et al. 1999). The data we use to determine the distance (d), effective temperature ($T_{\rm eff}$), and surface gravity ($\log g$) are the recalibrated ultraviolet spectra for DB stars, obtained with the International Ultraviolet Explorer (IUE) satellite and published by Holberg et al. (2003). The spectra were re-calibrated with the New Spectroscopic Image Processing System (NEWSIPS) data reduction by NASA, and in the low-dispersion spectral mode with a resolution of ~6 Å.

One of the major motivations to use the archive of IUE low-dispersion spectra, besides it comprising an homogeneous sample, is to work with spectra of which the absolute calibration is based on a synthetic model atmosphere energy distribution for the white dwarf star G191-B2B (WD 0501+527). The models we fit are the same kind used in the flux calibration.

We used a new grid of Koester's model atmospheres, with input physics and methods similar to those described in Finley et al. (1997), consisting of models with $T_{\rm eff}$ from 12 000 K to 28 000 K, and a step of 500 K, and $\log g$ from 7.0 to 9.0, with 0.1 dex step. We used two sets of model atmospheres: pure He and He contaminated with a small amount of H [$\log y \equiv \log(N{\rm He}/N{\rm H}) = -3.0$]. This is the the upper limit for the amount of H contamination for a star not show discernible H lines in the optical spectra, i.e., to be classified as a DB and not as a DBA. All models were calculated with ML2/α = 0.6 mixing length theory, considering that Bergeron et al. (1995) and Koester & Vauclair (1997) have shown this choice of mixing length gives consistent results in the UV and optical, for the DAs. There is no reason to expect the mixing length description to be different for DBs. These models were used to simultaneously fit $T_{\rm eff}$, $\log g$ and d to the available IUE spectra.

We calculated the minima in χ^2 between the observed spectra and the models, allowing the three parameters, $T_{\rm eff}$, $\log g$, and d, to vary. We used the model radii described in Althaus & Benvenuto (1997), available in `http://www.fcaglp.unlp.edu.ar/evolgroup/tracks.html`.

Our determinations of $T_{\rm eff}$, $\log g$ and the distance for all DB stars with IUE spectra available are shown in Table 1. In Cols. 3−5, we show the values derived using pure He models, and in Cols. 6−8, the same parameters using He/H models.

3. Comparison of results

Our determinations are still degenerate with respect to the contamination of H in the He atmosphere. To minimize this effect, we used external measurements, like: optical spectra, parallax measurements, and V magnitudes, if available.

3.1. Distance moduli

To test the reliability of our spectroscopic distances, we used our determinations of $T_{\rm eff}$ and $\log g$, Bergeron's et al. (2001) absolute magnitude, and the published V magnitude to estimate the distance moduli. In Table 2 we show the derived distances from this method and the distances after cross correlating both solutions.

In almost all cases, both spectroscopic and magnitude derived distances agree, even though we used independent model grids.

3.2. Parallax measurements

For six stars of our sample, parallax measurements are available (van Altena et al. 2001). Comparing these distances with the ones derived spectroscopically, the better agreement, in general, is the solution derived using pure He models. There are two stars, GD 358 and GD 408, for which we could not distinguish the atmospheric composition. Feige 4 is an exception, for which both spectroscopic solutions do not agree with the published parallax. However, this is the faintest star in our sample with parallax measurement, with magnitude close to the limit of the catalog. In Table 3, we show the parallax distance and the best stellar composition cross correlating the solutions.

The IUE spectra of Feige 4 (full line) is shown in Fig. 1 in comparison to the models. The best models derived from the spectra are with $T_{\rm eff}$ = 19 000 K, $\log g$ = 8.50, d = 61 pc, and pure He (dashed line) and with $T_{\rm eff}$ = 18 000 K, $\log g$ = 7.50, d = 112 pc, and He/H grid (dotted line). Using the distance derived from parallax, d = 33 pc, the best models are not only much cooler, $T_{\rm eff}$ = 14 000 K for pure He models (dotted-dashed line) and $T_{\rm eff}$ = 17 000 K for He/H models (long dashed line), but they also do not fit the slope of the observed spectra. Another argument to claim the parallax measurement is not correct is that this star has apparent magnitude V = 15.3, too faint for such a large parallax, unless the radius is extremely small, i.e., high mass, incompatible with the observed spectra.

3.3. Comparison with optical spectra results

Beauchamp et al. (1999) studied the optical spectra of eight known DBVs together with fifteen other DB and DBA stars with temperatures above 20 000 K. For DBs, including DBVs, they used a pure He atmosphere composition, or a homogeneous H/He ratio with only traces of H, at the detection threshold – defined as that which would produce barely visible Hβ or Hγ features, two lines included in their spectra. The influence of small, spectroscopically invisible amounts of H in the DB's atmospheres is an important issue in the definition of the temperature scale in the optical, because $T_{\rm eff}$ determined using He models with small admixture of H are often lower by a few thousand of K, than those determined with pure He models.

The instability strip Beauchamp et al. (1999) derived from the analysis of optical spectra contains non-variable stars. Its $T_{\rm eff}$ is also uncertain due to the possible presence of trace amounts of H in the stellar atmospheres. In Table 4, we compare our determination for $T_{\rm eff}$ from UV spectra, described

Table 1. Atmospheric parameters and distance determined from IUE spectra, using pure He models (He) and He contaminated with a small amount of H (He/H) models. An asterisk indicates a DBA star, for which our determinations are not adequate.

Name	WD	He $T_{\rm eff}$ (K)	He $\log g$	He d (pc)	He/H $T_{\rm eff}$ (K)	He/H $\log g$	He/H d (pc)
G 266-32	0000-170	$16\,000 \pm 600$	8.50 ± 0.60	39 ± 12	$14\,000 \pm 270$	8.00 ± 0.02	46 ± 3
GD 408	0002+729	$14\,000 \pm 40$	8.50 ± 0.04	26 ± 1	$14\,000 \pm 40$	7.50 ± 0.07	54 ± 2
Feige 4	0017+136	$19\,000 \pm 170$	8.00 ± 0.17	61 ± 5	$18\,000 \pm 60$	7.50 ± 0.06	112 ± 7
G 270-124	0100-068	$20\,500 \pm 130$	8.40 ± 0.23	34 ± 4	$19\,000 \pm 100$	7.00 ± 0.15	69 ± 5
PG 0112+104	0112+104	$27\,000 \pm 110$	7.50 ± 0.03	136 ± 2	$27\,000 \pm 130$	8.50 ± 0.06	71 ± 2
GD 40	0300-013	$15\,000 \pm 420$	7.50 ± 0.21	104 ± 11	$15\,000 \pm 310$	8.50 ± 0.16	58 ± 5
BPM 17088	0308-565	$21\,500 \pm 190$	7.70 ± 0.08	58 ± 2	$21\,000 \pm 280$	8.00 ± 0.14	49 ± 3
BPM 17731	0418-539	$20\,000 \pm 140$	8.00 ± 0.14	83 ± 6	$19\,000 \pm 110$	7.50 ± 0.06	110 ± 3
BPM 18164	0615-591	$16\,000 \pm 50$	8.50 ± 0.17	26 ± 2	$16\,000 \pm 40$	7.00 ± 0.04	64 ± 1
Ton 10	0840+262	$21\,000 \pm 90$	7.50 ± 0.09	96 ± 4	$18\,000 \pm 100$	7.00 ± 0.15	103 ± 8
L748-70	0845-188	$18\,000 \pm 140$	7.50 ± 0.14	129 ± 9	$18\,000 \pm 60$	7.50 ± 0.06	135 ± 4
PG 0853+163*	0853+163	$21\,000 \pm 450$	7.70 ± 0.18	126 ± 11	$20\,000 \pm 650$	7.50 ± 0.65	137 ± 44
PG 0948+013	0948+013	$19\,000 \pm 280$	8.20 ± 0.19	92 ± 9	$18\,000 \pm 150$	7.00 ± 0.15	173 ± 13
GD 303	1011+570	$18\,000 \pm 140$	7.50 ± 0.14	75 ± 5	$18\,000 \pm 60$	7.50 ± 0.03	78 ± 1
PG 1115+158	1115+158	$23\,000 \pm 500$	8.50 ± 0.10	137 ± 7	$22\,000 \pm 500$	7.00 ± 0.25	321 ± 40
PG 1149-133*	1149-133	$20\,500 \pm 440$	7.60 ± 0.57	161 ± 46	$19\,000 \pm 260$	7.00 ± 0.19	196 ± 19
PG 1311+129*	1311+129	$26\,500 \pm 450$	7.70 ± 0.05	249 ± 6	$27\,000 \pm 280$	7.50 ± 0.14	298 ± 14
PG 1326-037	1326-037	$21\,500 \pm 290$	8.40 ± 0.35	81 ± 14	$20\,000 \pm 100$	8.00 ± 0.10	100 ± 5
GD 325	1333+487	$16\,000 \pm 40$	8.20 ± 0.01	34 ± 0.2	$15\,000 \pm 120$	7.00 ± 0.06	61 ± 2
PG 1351+489	1351+489	$22\,500 \pm 190$	7.60 ± 0.15	194 ± 14	$22\,000 \pm 150$	7.00 ± 0.07	266 ± 10
PG 1411+218	1411+218	$15\,000 \pm 70$	7.80 ± 0.01	49 ± 0.3	$14\,000 \pm 70$	7.00 ± 0.03	66 ± 1
G 200-39	1425+540	$15\,000 \pm 110$	7.70 ± 0.09	74 ± 3	$15\,000 \pm 310$	8.50 ± 0.31	47 ± 7
PG 1445+152	1445+152	$21\,500 \pm 120$	8.40 ± 0.12	91 ± 5	$21\,000 \pm 120$	8.50 ± 0.06	86 ± 3
PG 1456+103*	1456+103	$24\,000 \pm 190$	8.50 ± 0.27	110 ± 15	$24\,000 \pm 290$	9.00 ± 0.14	76 ± 5
G 256-18	1459+821	$16\,000 \pm 50$	8.00 ± 0.03	53 ± 1	$15\,000 \pm 310$	7.00 ± 0.05	83 ± 2
GD 190	1542+182	$22\,500 \pm 90$	8.50 ± 0.11	48 ± 3	$21\,000 \pm 60$	7.00 ± 0.06	106 ± 3
GD 358	1645+325	$24\,500 \pm 130$	8.50 ± 0.10	29 ± 1	$24\,000 \pm 50$	8.50 ± 0.03	30 ± 0.4
PG 1654+160	1654+160	$25\,000 \pm 550$	7.50 ± 0.11	237 ± 13	$26\,000 \pm 1100$	7.00 ± 0.55	331 ± 91
L 7-44	1708-871	$23\,000 \pm 610$	8.30 ± 0.42	55 ± 12	$21\,000 \pm 680$	7.00 ± 0.34	106 ± 18
GD 378	1822+410	$17\,000 \pm 60$	8.20 ± 0.04	39 ± 1	$16\,000 \pm 80$	7.00 ± 0.08	70 ± 3
L 1573-31	1940+374	$17\,000 \pm 50$	7.60 ± 0.05	62 ± 1	$17\,000 \pm 40$	7.00 ± 0.07	86 ± 3
BPM 26944	2034-532	$17\,000 \pm 390$	8.50 ± 0.39	34 ± 7	$17\,000 \pm 80$	7.00 ± 0.12	86 ± 5
G 26-10	2129+000	$13\,000 \pm 60$	7.50 ± 0.06	50 ± 2	$13\,000 \pm 40$	7.50 ± 0.02	54 ± 1
LTT 9031	2224-344	$19\,000 \pm 160$	7.50 ± 0.16	72 ± 6	$18\,000 \pm 130$	7.00 ± 0.13	88 ± 6

in Sect. 2, with those derived from optical spectra. The optical spectra also give two solutions, with or without trace H. For seven DB stars, the best agreement in $T_{\rm eff}$ in both UV and optical range is for atmospheres consistent with a small amount of H instead of none. The exception is the star GD 358, which has a higher probability of having a pure He atmosphere in agreement with Provencal et al. (2000) determination of $\log(N{\rm He}/N{\rm H}) \leq -5$ for this star. In Fig. 2, we show a comparison between UV (x-axis) and optical (y-axis) spectroscopic determinations of $T_{\rm eff}$, for a pure He atmosphere and a He/H atmosphere. The closer a given data point is to the dashed line (1:1 correspondence between UV and optical spectra), the better the solution for the atmosphere composition becomes. The dotted lines link the two atmosphere determinations for a given star, showing that He/H atmospheres are more likely for this sample.

GD 358 is the only star in our sample which both parallax measurement and optical spectra determination is available. We cannot distinguish the best atmosphere composition from the parallax, but a pure He atmosphere is still consistent with the optical spectra determination.

For the star GD 190, even though we get a better agreement with the optical spectra for a contaminated atmosphere, Provencal et al. (2000) obtained an upper limit of $\log(N{\rm He}/N{\rm H}) \leq -6.5$, consistent with a pure He atmosphere.

An important consideration is that we fitted all stars using DB models, never with DBA models. From the IUE spectra, we cannot determine if a star is a DBA or not. The optical spectra of PG 0853+163, PG 1149-133, PG 1311+129, and PG 1456+103 do show H, which has been taken into account by Beauchamp et al. (1999) by using models with a considerable amount of H. Our temperatures for DBA stars are

Table 2. Distance determined from distance modulus (Cols. 2–3) using IUE $T_{\rm eff}$ and $\log g$, compared to absolute magnitude models and available V magnitudes. We used both pure He models (He) and He contaminated with a small amount of H (He/H) models. The last 2 columns are the distances after cross correlating these values and the spectroscopic distances (see values in Table 1).

Name	He d (pc)	He/H d (pc)	He $d_{\rm cross}$ (pc)	He/H $d_{\rm cross}$ (pc)
G 266-32	36^{+22}_{-16}	45 ± 2	37^{+13}_{-10}	46 ± 2
GD 408	26 ± 1	51 ± 2	26 ± 1	53 ± 1
Feige 4	81 ± 7	108^{+4}_{-3}	71 ± 4	110 ± 4
G 270-124	35^{+7}_{-6}	88^{+10}_{-9}	34 ± 4	78^{+6}_{-5}
PG 0112+104	144^{+28}_{-20}	71^{+3}_{-4}	140^{+14}_{-10}	71 ± 2
GD 40	100^{+20}_{-15}	50^{+3}_{-8}	102^{+11}_{-9}	54^{+3}_{-5}
BPM 17088	61^{+4}_{-3}	50 ± 5	60 ± 2	50 ± 3
BPM 17731	82 ± 6	109^{+4}_{-3}	83 ± 4	109 ± 2
BPM 18164	27 ± 4	79^{+10}_{-9}	27 ± 2	71^{+5}_{-4}
Ton 10	81^{+4}_{-2}	104^{+9}_{-8}	89^{+3}_{-2}	104 ± 6
L748-70	122^{+14}_{-12}	122^{+6}_{-5}	125^{+8}_{-7}	128^{+4}_{-3}
PG 0853+163*	135^{+18}_{-16}	150^{+95}_{-56}	131^{+11}_{-10}	144^{+52}_{-36}
PG 0948+013	92^{+15}_{-13}	205^{+25}_{-23}	92^{+9}_{-8}	189^{+14}_{-13}
GD 303	119^{+14}_{-11}	119^{+7}_{-3}	97^{+7}_{-6}	98^{+3}_{-1}
PG 1115+158	95^{+8}_{-9}	260^{+53}_{-45}	116^{+5}_{-6}	291^{+35}_{-30}
PG 1149-133*	178^{+92}_{-57}	258^{+42}_{-36}	169^{+51}_{-37}	227^{+23}_{-21}
PG 1311+129*	187 ± 9	218^{+29}_{-22}	218 ± 5	258^{+16}_{-13}
PG 1326-037	82^{+23}_{-22}	103^{+7}_{-8}	82 ± 13	101^{+4}_{-5}
GD 325	$33^{+0.2}_{-0.3}$	70 ± 3	$33^{+0.1}_{-0.2}$	66 ± 2
PG 1351+489	194^{+21}_{-36}	293^{+17}_{-15}	194^{+13}_{-19}	280^{+10}_{-9}
PG 1411+218	$48^{+0.5}_{-0.6}$	76 ± 2	48 ± 0.3	71 ± 1
G 200-39	69^{+5}_{-4}	39^{+11}_{-10}	72 ± 3	43^{+7}_{-6}
PG 1445+152	77 ± 7	71 ± 4	84 ± 4	78 ± 2
PG 1456+103*	87 ± 18	57^{+8}_{-7}	98 ± 12	66 ± 4
G 256-18	60^{+1}_{-2}	111 ± 7	56 ± 1	97 ± 4
GD 190	49^{+4}_{-5}	134 ± 6	49 ± 3	120 ± 3
GD 358	30 ± 2	30 ± 1	30 ± 1	$30^{+0.3}_{-0.4}$
PG 1654+160	196^{+22}_{-16}	302^{+192}_{-113}	216^{+13}_{-10}	317^{+106}_{-73}
L 7-44	57^{+14}_{-12}	133^{+28}_{-22}	56^{+9}_{-8}	119^{+17}_{-14}
GD 378	42 ± 1	90 ± 6	40 ± 1	80 ± 3
L 1573-31	67 ± 2	103 ± 4	64 ± 1	95 ± 3
BPM 26944	34^{+13}_{-11}	101^{+10}_{-9}	34^{+7}_{-6}	93^{+6}_{-5}
G 26-10	58^{+3}_{-2}	58 ± 1	54 ± 2	56 ± 1
LTT 9031	78^{+10}_{-8}	108^{+12}_{-11}	75^{+6}_{-5}	98 ± 6

therefore not reliable, but differences in $T_{\rm eff}$ from our models with or without trace H are the same order as our uncertainties.

We did not compare $\log g$ values, as their uncertainties are too large from both UV and optical spectra.

4. Looking for new pulsators

Robinson & Winget (1983) reported a search for pulsating DB white dwarf stars, classifying twenty nine stars as non-variable. Expanding this search, we acquired time-series photometric observations of another thirteen DB white dwarf stars, which have $T_{\rm eff}$ close to the edges of the DB observed instability strip, plus one DA (H atmosphere white dwarf) during two observing runs at the South African Astronomical Observatory (SAAO), and four DBs at the Observatório Pico dos Dias (OPD) in other three runs, to search for variability. At SAAO, one of us (GH) used the 0.75-m telescope in

Table 3. Using the distance determined by parallax measurements (second column), we study the best agreement with our fits, deriving the atmosphere composition (third column).

Star	d (pc)	Atmosphere
GD 408	35 ± 6	undetermined
Feige 4	33 ± 10	undetermined
GD 325	35 ± 4	He/H
G 200-39	58 ± 13	pure He
GD 358	37 ± 4	undetermined
L 1573-31	49 ± 7	pure He

Table 4. Atmospheric parameter determinations from UV spectra in comparison to those derived by Beauchamp et al. (1999) using optical spectra. The last column shows the best agreement in atmosphere composition using both independent determinations.

Name	UV He	UV He/H	Optical He	Optical He/H	Atmosphere
G 270-124	20 500 ± 130	19 000 ± 100	22 500	20 500	He/H
PG 0112+104	27 000 ± 110	27 000 ± 130	31 500	28 300	He/H
PG 1115+158	23 000 ± 500	22 000 ± 500	25 300	21 800	He/H
PG 1351+489	22 500 ± 190	22 000 ± 150	26 100	22 600	He/H
PG 1445+152	21 500 ± 120	21 000 ± 120	23 600	22 200	He/H
GD 190	22 500 ± 90	21 000 ± 60	21 500	21 000	He/H
GD 358	24 500 ± 130	24 000 ± 50	24 900	24 700	He
PG 1654+160	25 000 ± 550	26 000 ± 1100	27 800	24 300	He/H

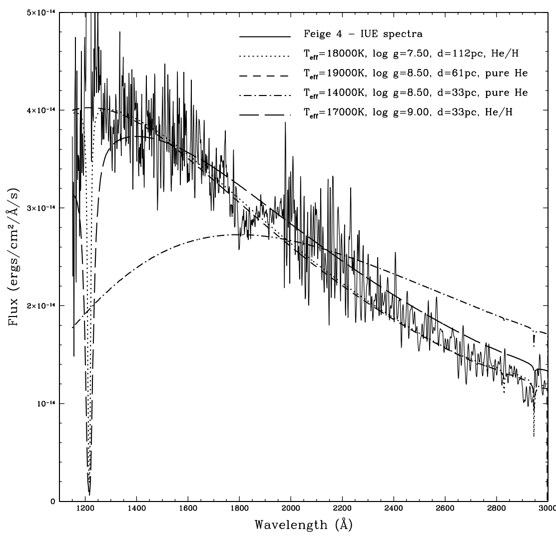

Fig. 1. IUE spectra obtained for Feige 4 (full line) compared with the best models derived leaving all parameters free for a pure He grid (dashed line) at $d = 61$ pc, with $T_{\rm eff} = 19\,000$ K and $\log g = 8.50$, for a a DB contaminated with H (dotted line), at $d = 112$ pc, with $T_{\rm eff} = 18\,000$ K and $\log g = 7.50$. Using the parallax distance, ($d = 33$ pc) for pure He grid (dotted-dashed line), the best solution is for $T_{\rm eff} = 14\,000$ K and $\log g = 8.50$, and for a DB contaminated with H (long dashed line), the atmospheric parameters are $T_{\rm eff} = 17\,000$ K and $\log g = 9.00$.

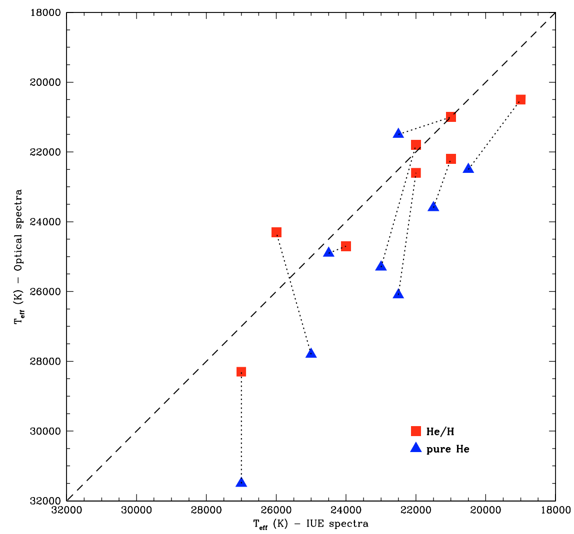

Fig. 2. Comparison between the UV (x-axis) and optical (y-axis) determinations for $T_{\rm eff}$ using pure He models (blue triangles) and DB models contaminated with H (red squares). The dotted lines correspond to the same star. The dashed line delineates 1:1 correspondence between UV and optical spectra.

April/May 2000 and the 1.0-m telescope in December 2001. At both telescopes, a high-speed CCD photometer (O'Donoghue 1995) was employed. It was operated in full-frame mode on the 0.75-m telescope with 20-s integrations and 3−4 s readout during the measurements in 2000, but in frame-transfer mode with 10-s integrations in 2001. At OPD, we used the 1.6-m telescope in 1986, with a single channel photometer and 5-s integration time. We also observed at OPD in 2004, using the 0.6-m telescope and CCD 101, with 30-s integration, and 7−8 s readout. No filters were used in order to maximize the received light and considering that g-mode pulsations should have the same phase at different wavelengths (e.g. Kepler et al. 2000). We show the observing log in Table 5.

We reduced the SAAO CCD data with the standard software for this instrument, and carried out photometry by using the program MOMF (Kjeldsen & Frandsen 1992) which uses a combined approach of PSF fitting photometry and aperture corrections on the star-subtracted frames, giving optimal results. Fourier amplitude spectra of the resulting light curves are shown in Fig. 3. For the OPD runs, the detection limits are 3 mma for BPM 17088 and GD 270-124, 2 mma for BPM 17731, and 1.4 mma for L 7-44.

All the seventeen stars are constant within our detection limit. The detection limits are satisfactory for all stars except PG 0949+094, WD 1415+234 (run terminated by cloud) and PG 2234+064, which should be re-observed. WD 1445+152 may also require some additional observations; the highest peak in its amplitude spectrum is somewhat outside the typical range for pulsating white dwarf stars

Table 5. Journal of observations. ΔT is the length of the corresponding observing run.

Star	Run start (UT)	ΔT (h)	# points
BPM 17088	09/09/86, 05:18	1.24	890
BPM 17731	11/09/86, 04:11	3.17	2282
GD 270-124	31/10/86, 22:54	3.37	2423
WD 0853+163	26/04/00, 17:46	1.13	173
WD 1311+129	27/04/00, 21:23	1.51	230
PG 1445+152	28/04/00, 21:18	1.33	195
PG 0949+094	29/04/00, 17:00	1.25	193
PG 1026-056	29/04/00, 18:19	1.15	175
L 151-81A	29/04/00, 23:53	1.61	250
WD 1134+073	30/04/00, 18:15	1.41	213
WD 1332+162	01/05/00, 18:29	1.79	260
WD 1336+123	01/05/00, 20:19	1.43	222
WD 1444-096	01/05/00, 21:48	1.10	168
WD 1415+234	01/05/00, 22:57	0.57	88
PG 2354+159	16/12/01, 18:38	1.07	386
PG 2234+064	17/12/01, 18:57	0.91	326
L 7-44	15/08/04, 00:33	2.61	233

Table 6. Variability classification of the DB stars in our sample. The V is used for variables, NV for non-variables and NO for not observed for variability.

	Stars
V	PG 1115+158, PG 1351+489, PG 1456+103, GD 358, PG 1654+160
NV	Feige 4, G270–124, PG 0112+104, GD 40, BPM 17731, Ton 10, PG 0853+163, GD 303, PG 1311+129, GD 325, PG 1445+152, G 256-18, GD 190, L 7-44, GD 378, G 26-10, LTT 9031 BPM 17088
NO	G 226-32, GD 408, BPM 18164, L 748-70, PG 0948+013, PG 1149-133, PG 1326-037, PG 1411+218, G 200-39, L 1537-31, BPM 26944

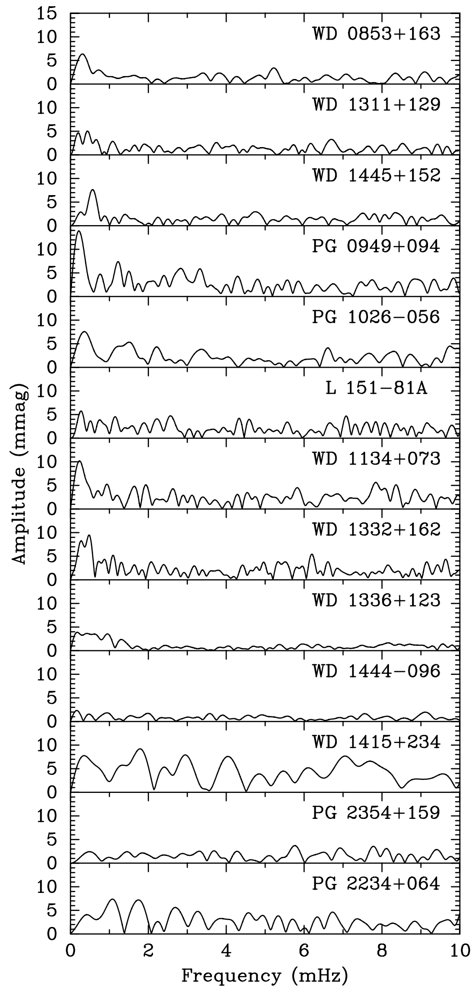

Fig. 3. Fourier amplitude spectra of the null results of a search for pulsation among DB white dwarf stars.

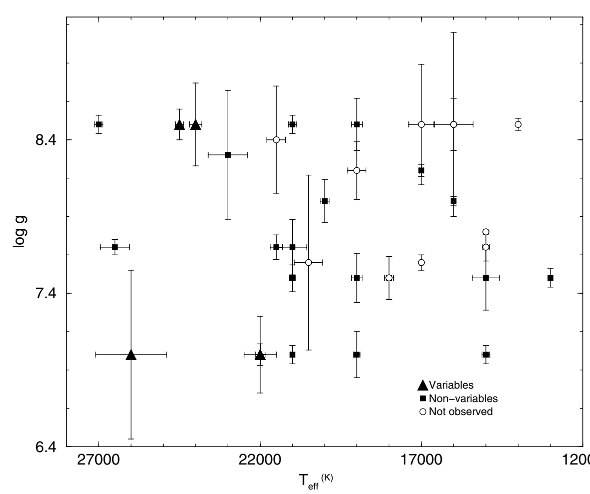

Fig. 4. DB instability strip using pure He models for the stars for which we cannot determine atmosphere composition: variables (filled triangle), non-variables (filled squares), and not observed for variability (open circles). There are 2 stars close to the instability strip that have not been observed for variability.

but we cannot rule out that it is intrinsic to the star from the present data. We also note that we could not detect variability of the DA white dwarf L 151-81B, but our detection limit (~8 mma) is poor. On the other hand, we suspect that the star 2MASS 14581310-6317340, (~8 arcsec East of L 151-81AB) is a δ Scuti star, with a 1.3-h period and 23 mmag semi-amplitude.

The variability classification of DB stars is shown in Table 6, where V is used for variables, NV for non-variables, and NO for not observed for variability reported.

Having derived the physical parameters from ultraviolet spectra, and the atmosphere composition for thirteen stars, we are ready to determine the DB instability strip for this homogeneous sample. In Figs. 4 and 5, we show the final determination

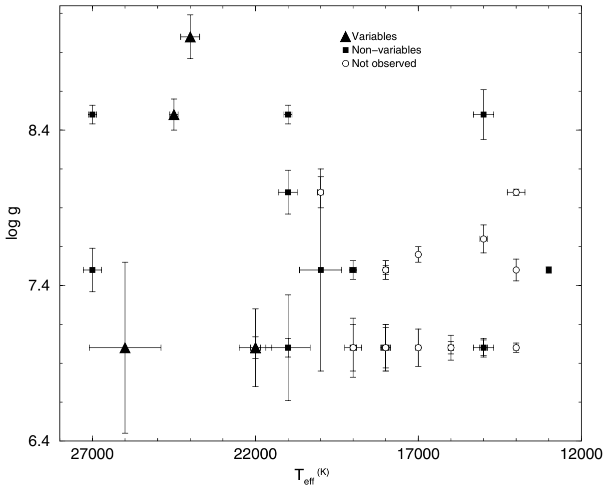

Fig. 5. DB instability strip using H contaminated He models for the stars for which we cannot determine atmosphere composition: variables (filled triangle), non-variables (filled squares), and not observed for variability (open circles). There are 2 stars close to the instability strip that have not been observed for variability.

for $T_{\rm eff}$ and $\log g$ for variables (filled triangle), non-variables (filled squares), and so far not observed by time series photometry (open circles) DB stars. This diagram shows that DBs pulsate in a well-defined temperature range, from $26\,000 \geq T_{\rm eff} \geq 22\,000$ K. For the stars which we could not determine their atmosphere composition, we used both pure He models and He/H models, respectively. There is a 97% chance that the DB instability strip contains only variable stars. Even if the error bars in $T_{\rm eff}$ were three times larger, there is only a 4% probability of contamination. This probability was calculated by adding the probability of all variables that fall inside the instability strip and all non-variables outside, using Gaussian distributions for our $T_{\rm eff}$ determinations only (no consideration for $\log g$). There are still stars close to the instability strip that have not been searched to our knowledge for variability, and which are crucial for the study of the instability strip.

However, Beauchamp et al.'s (1999) optical spectra fitting found non-variables inside the instability strip. In this sense, for a true determination of the DB instability strip it is necessary to fit the optical and UV spectra simultaneously, to analyze the possible differences to convection prescription.

5. Concluding remarks

We used model atmospheres with ML2/α = 0.6 to derive atmospheric parameters ($T_{\rm eff}$ and $\log g$) and distances for thirty four DB stars with available IUE re-calibrated spectra. Our model grid fit well the spectra. Another important conclusion is that atmospheric contamination with H is not directly proportional to $T_{\rm eff}$ for DB stars, based on our determination for eleven stars, which has been a suggestion to explain the DB gap by convection dragging H upwards. We also find no DB stars inside the DB gap.

Acknowledgements. Financial support: CAPES/UT grant, CNPq fellowship.

References

Althaus, L. G., & Benvenuto, O. G. 1997, ApJ, 477, 313
Althaus, L. G., Serenelli, A. M., Panei, J. A., et al. 2005, A&A, 435, 631
Beauchamp, A., et al. 1999, ApJ, 516, 887
Bergeron, P., Saumon, D., & Wesemael, F. 1995, ApJ, 443, 764
Bergeron, P., Leggett, S. K., & Ruiz, M. T. 2001, ApJS, 133, 413
Corsico, A. H., & Althaus, L. G. 2004, A&A, 428, 159
Finley, D. S., Koester, D., & Basri, G. 1997, ApJ, 488, 375
Hansen, B., & Liebert, J. 2003, ARA&A, 41, 465
Holberg, J. B., Barstow, M. A., & Burleigh, M. R. 2003, ApJS, 147, 145
Kepler, S. O., Robinson, E. L., Koester, D., et al. 2000, ApJ, 539, 379
Kjeldsen, H., & Frandsen, S. 1992, PASP, 104, 413
Koester, D., & Vauclair, G. 1997, White dwarfs, ASSL 214, 429
Metcalfe, T. S. 2003, ApJ, 587, L43
Metcalfe, T. S. 2005, MNRAS, 363, L86
Montgomery, M. H., & Winget, D. E. 2000, Baltic Astron., 9, 23
Nitta, A., et al. 2005, in prep.
O'Donoghue, D. 1995, Baltic Astronomy, 4, 519
Provencal, J. L., Shipman, H. L., Thejll, P., & Vennes, S. 2000, ApJ, 542, 1041
Robinson, E. L., & Winget, D. E. 1983, PASP, 95, 386
van Altena, W. F., Lee, J. T., & Hoffleit, E. D. 2001, VizieR Online Data Catalog, 1238, 0
Winget, D. E., Robinson, E. L., Nather, R. D., Fontaine, G. 1982, ApJ, 262, L11
Winget, D. E., Sullivan, D. J., Metcalfe, T. S., Kawaler, S. D., & Montgomery, M. H. 2004, ApJ, 602, L109
Wolff, B., Koester, D., Montgomery, M. H., & Winget, D. E. 2002, A&A, 388, 320

6.4 Pulsating DA white dwarfs

6.4.1 Whole Earth Telescope Observations of the ZZ Ceti star HL Tau 76

Original paper:

N. Dolez, G. Vauclair, S. J. Kleinman, M. Chevreton, J. N. Fu, J.-E. Solheim, J. M. Gonzalez Perez, A. Ulla, L. Fraga, A. Kanaan, M. Reed, S. Kawaler, M. S. O'Brien, T. S. Metcalfe, R. E. Nather, D. Sanwal, E. W. Klumpe, A. Mukadam, M. A. Wood, T. J. Ahrens, N. Silvestri, D. Sullivan, T. Sullivan, X. J. Jiang, D. W. Xu, B. N. Ashoka, E. Leibowitz, P. Ibbetson, E. Ofek, D. Kilkenny, E. G. Meistas, D. Alisauskas, R. Janulis, R. Kalytis, P. Moskalik, S. Zola, J. Krzesinski, W. Ogloza, **G. Handler,** R. Silvotti, S. Bernabei, 2006, A&A 446, 237

A&A 446, 237–257 (2006)
DOI: 10.1051/0004-6361:20053149

Astronomy & Astrophysics

Whole Earth telescope observations of the ZZ Ceti star HL Tau 76⋆,⋆⋆

N. Dolez[1], G. Vauclair[1], S. J. Kleinman[2], M. Chevreton[3], J. N. Fu[1,20], J.-E. Solheim[4,21], J. M. González Perez[4,22], A. Ulla[5], L. Fraga[6], A. Kanaan[6], M. Reed[7,23], S. Kawaler[7], M. S. O'Brien[7], T. S. Metcalfe[8,24], R. E. Nather[8], D. Sanwal[8], E. W. Klumpe[8,25], A. Mukadam[8], M. A. Wood[9], T. J. Ahrens[9], N. Silvestri[9,26], D. Sullivan[10], T. Sullivan[10], X. J. Jiang[11], D. W. Xu[11], B. N. Ashoka[12], E. Leibowitz[13], P. Ibbetson[13], E. Ofek[13], D. Kilkenny[14], E. G. Meištas[15], D. Alisauskas[15], R. Janulis[15], R. Kalytis[15], P. Moskalik[16], S. Zola[17], J. Krzesinski[17], W. Ogloza[17], G. Handler[18,14], R. Silvotti[19], and S. Bernabei[19]

(Affiliations can be found after the references)

Received 29 March 2005 / Accepted 12 September 2005

ABSTRACT

This paper analyses the Whole Earth Telescope observations of HL Tau 76, the first discovered pulsating DA white dwarf. The star was observed during two Whole Earth Telescope campaigns. It was a second priority target during the XCOV13 campaign in 1996 and the first priority one during the XCOV18 campaign in 1999. The 1999 campaign reached 66.5% duty cycle. With a total duration of 18 days, the frequency resolution achieved is 0.68 μHz. With such a frequency resolution, we were able to find as many as 78 significant frequencies in the power spectrum, of which 34 are independent frequencies after removal of all linear combinations. In taking into account other frequencies present during the 1996 WET campaign and those present in earlier data, which do not show up in the 1999 data set, we find a total of 43 independent frequencies. This makes HL Tau 76 the richest ZZ Ceti star in terms of number of observed pulsation modes. We use those pulsation frequencies to determine as much as possible of the internal structure of HL Tau 76. The pulsations in HL Tau 76 cover a wide range of periods between 380 s and 1390 s. We propose an identification for 39 of those 43 frequencies in terms of $\ell = 1$ and $\ell = 2$ non-radial g-modes split by rotation. We derive an average rotation period of 2.2 days. The period distribution of HL Tau 76 is best reproduced if the star has a moderately "thick" hydrogen mass fraction $\log q_{\rm H} \geq -7.0$. The results presented in this paper constitute a starting point for a detailed comparison of the observed periods with the periods calculated for models as representative as possible of HL Tau 76.

Key words. stars: interiors – stars: individual: HL Tau 76 – stars: oscillations – stars: white dwarfs

1. Introduction

There are 71 pulsating DA white dwarfs presently known (the ZZ Ceti or DAV stars). This number is composed on one hand of the 36 ZZ Ceti stars published prior to the first release of the Sloan Digital Sky Survey (SDSS) and includes the ZZ Ceti stars recently discovered on the basis of their location in the $\log g - T_{\rm eff}$ diagram: G30-20 (Mukadam et al. 2002), MCT 0145-2211 and HE 0532-5605 (Fontaine et al. 2003), LP133-144 and HE1258+0123 (Bergeron et al. 2004). They lie well inside the ZZ Ceti instability strip as defined by Bergeron et al. (1995). On the other hand, 35 new ZZ Ceti stars have been discovered from the first release catalog of the SDSS (Mukadam et al. 2004a; Abazajian et al. 2003; Harris et al. 2003; Kleinman et al. 2004). The 36 previously published ZZ Ceti stars define a narrow instability strip in the H-R diagram (or in the $\log g - T_{\rm eff}$ diagram) of trapezoidal form due to the mass dependence of its blue and red edges. Its location in $T_{\rm eff}$ depends on the adopted prescription for the convection. Bergeron et al. (1995) have shown that within the framework of the mixing lenght theory (MLT), the choice of the ML2 version with a mixing length equals to 0.6 pressure height scale optimizes the Balmer lines profiles and the energy distribution from the UV to the visible wavelength range. For the average DA mass, it ranges from 12 460 ± 200 K for the hottest (G226-29) to 11 070 ± 200 K for the coolest (G30-20 and BPM24754), according to Bergeron et al. (1995), Fontaine et al. (2003) and Bergeron et al. (2004). According to Bergeron et al. (2004), the instability strip for these ZZ Ceti

⋆ Based on data obtained at the Haute-Provence Observatory, INSU/CNRS, France, the Teide Observatory, Tenerife, Spain, the Laboratorio Nacional de Astrofisica/CNPq, Brazil, the Cerro Tololo Interamericain Observatory, Chili, the McDonald Observatory, Texas, USA, the Kitt Peak National Observatory, Arizona, USA, the Mauna Kea Observatory, University of Hawaii, USA, the Beijing Observatory, China, the Naini Tal Observatory, India, The South Africa Astronomical Observatory, South Africa, the Moletai Observatory, Lituania, the Wise Observatory, Israel, the Suhora Observatory, Poland and the Loiano Observatory, Italy.

⋆⋆ Table 2 is only available in electronic form at
`http://www.edpsciences.org`

white dwarfs is a "true" instability strip, which means that all the DA white dwarfs falling inside this region of the H-R diagram do pulsate (no non-pulsating DA has yet been found within the instability strip in this sample). This is in disagreement with the instability strip derived from the SDSS newly discovered ZZ Ceti stars. Mukadam et al. (2004b) suggest that it is not pure. Whether this results from a genuine cohabitation of pulsators and non-pulsators within the instability strip or from larger uncertainties in the atmospheric parameters derived from the SDSS needs to be examined. The DA white dwarfs of the SDSS sample falling within the instability strip are fainter than those analyzed by Bergeron et al. (2004). Their atmospheric parameters are derived from lower *S/N* spectra: for instance, the *S/N* of the spectrum for the brighest non variable star (WD 1338-0023, $g = 17.1$) in the Mukadam et al. (2004b) sample is 35 (Kleinman et al. 2004), while all the DA spectra analyzed by Bergeron et al. (2004) have a $S/N \geq 80$. It suggests that the location of the SDSS DA white dwarfs in the $\log g - T_{\rm eff}$ diagram suffers larger uncertainties. This may explain the overlap between pulsators and non-pulsators within the Mukadam et al. (2004b) instability strip.

Whether the instability strip is pure or not pure is an important issue since, if the instability strip is a "pure" one, then it is an indication that the internal structure of the ZZ Ceti white dwarfs as derived from asteroseismology is representative of the DA white dwarfs as a whole group. DA white dwarfs represent 80% of the total white dwarf population (Fleming et al. 1986). As the white dwarfs are the last evolutionary stage of low and intermediate mass stars, which form the vast majority of all stars, it is important to know their internal structure as precisely as possible.

The white dwarf cooling sequence could potentially be used as a powerful cosmochronological tool (Winget et al. 1987). One finds most of the known white dwarfs in the solar neighbourhood, but they are also present in both open and globular clusters, and some have been identified as potential galactic halo members. In each case, calibrating the corresponding cooling sequence would provide an age determination, independent from other methods, and hopefully more precise. This goal is not yet achieved however, due to various uncertainties in the models. Among those uncertainties, the unknown proportion and distribution of C and O in the core and the incomplete understanding of the way they crystallize at the low luminosity end of the cooling sequence affect the estimate of the total thermal energy reservoir, while the unknown helium and hydrogen content and thickness of the envelope affects the estimate of the rate at which this energy is released through radiation and/or convection. They introduce an uncertainty on the derived age of the coolest white dwarfs on the order of 2 Gyr (Winget & Van Horn 1987; see Fontaine et al. 2001 for a recent review).

The asteroseismological study of the ZZ Ceti white dwarfs can help in reducing part of these uncertainties by constraining the stars' total mass and hydrogen mass fraction. The difficulty in determining these values from asteroseismology comes from two main sources: 1) they show generally few modes, in contrast with the theoretical calculations which predict many more unstable modes than observed; and 2) the pulsation amplitudes become increasingly variable as the ZZ Ceti stars become closer to the red edge of the instability strip so that some of the modes may have amplitude below the detection limit during a given observing season, which implies that more than one observing season is necessary to recover a useful power spectrum. Both effects make it difficult to find enough modes to apply the standard method of asteroseismology which needs a sufficient number of pulsation modes to be observed and identified.

Most of the ZZ Ceti stars close to the instability strip blue edge show constant pulsation amplitude. But in this case, very few modes are unstable since the stars are just entering the instability strip. In those stars, the κ–γ mechanism due to hydrogen partial ionization is responsible for the instability since the fraction of the flux conveyed by convection is negligible (Dolez & Vauclair 1981; Winget et al. 1982). However, as they show too few modes for traditional pattern matching analysis, one can only rely on a direct comparison of the frequencies computed in white dwarf models with the observed frequencies to constrain the model, or a set of plausible models, which best reproduce the observations. There is generally no unique solution. As the white dwarfs cool within the instability strip, convection carries an increasing fraction of the flux as $T_{\rm eff}$ decreases. Brickhill (1983, 1990, 1991a,b) found that since the convection zone responds almost instantaneously to the pulsations, it can drive the pulsations. The convective driving in ZZ Ceti stars was further analyzed by Goldreich & Wu (Wu & Goldreich 1999, 2001; Goldreich & Wu 1999a,b; Wu 2001). As the ZZ Ceti cool and the convection zone deepens, more and more modes are driven and the convection give them increasing energy (and so more power). Since the depth of the convection zone varies in response to the variations of the physical conditions induced by the pulsations (temperature and pressure) non linearities occur in the surface flux perturbations which show up through an increasing complexity of the power spectra, variability of the amplitudes, non-sinusoidal pulse shapes, linear combinations of frequencies, etc. Closer to the red edge, almost all the flux is carried by convection. The strong feedback of convection on the pulsations now results in the damping of many of the modes, so that again fewer modes are available for asteroseismological diagnosis. So, the determination of the hydrogen mass fraction for individual ZZ Ceti stars has been attempted in very few cases. This led Clemens (1993) to consider the pulsation properties of the ZZ Ceti stars as a group. From the similarities in the period distribution observed in the hot ZZ Ceti stars, he concluded that they should also have a somehow similar internal structure and estimated that their hydrogen mass fraction should be around $M_{\rm H}/M_* = 10^{-4}$, the value predicted by stellar evolution theory.

Looking for the ZZ Ceti stars for which a hydrogen mass determination has been proposed, one can check that in most cases those determinations rely on a small number of detected modes whose identification remains often ambiguous. Table 1 summarizes the results on the hydrogen mass fraction determined from asteroseismology. Except for G29-38, which is the best studied ZZ Ceti star up to now and in which 19 multiplets have been identified as possible $\ell = 1$ modes, the number of available modes is small. In 5 of the ZZ Ceti stars listed, out of 8 total, the hydrogen mass fraction is estimated

Table 1. Derived M_H/M_{WD} in ZZ Ceti stars.

Object	Number of modes	$M_H \times 10^{-4}\ M_{WD}$	Ref.
G 226-29	3	≈1.0	1
L 19-2	11	≈1.0	2
R 548	7	1.5	3
GD 165	8	≈2.0	4
G 29-38	19	0.005	5
G 117-B15A	3	≈1.0	6
GD 154	3	2×10^{-6}	7
BPM 37093	8	0.02–0.6	8

Notes: The number of modes is obtained after subtracting the linear combinations and harmonics from the power spectra. Its does include multiplet components induced by rotational splitting (except in the case of G 29-38 where the indicated number is the total number of multiplets). This number is the sum of all the modes observed during various observing seasons. References: 1) Kepler et al. (1995); 2) Bradley (1993, 2001); 3) Bradley (1998); 4) Bergeron et al. (1993), Bradley (2001); 5) Kleinman et al. (1998); 6) Robinson et al. (1995), Bradley (1998); 7) Pfeiffer et al. (1996); 8) Kanaan et al. (2005), Metcalfe et al. (2004), but see also Fontaine & Brassard (2004).

to be $\approx 10^{-4} M_{WD}$, where M_{WD} is the white dwarf mass. These estimates rely mostly on the assumption that the shortest observed periods are correctly identified as the periods of the lowest order $\ell = 1$ modes calculated in DA white dwarf models. In some of those models, the effects of varying the helium mass fraction has been included in the analysis, while in others models a standard value of 10^{-2} has been adopted as in the Wood's (1995) evolutionary sequences. In the other three cases, G29-38, GD154 and BPM37093, it is smaller. However, it must be emphasized that in the case of G29-38, there is not yet a convincing model so that the quoted value is only a preliminary estimate. In the case of GD 154, the estimate is based on the assumption that the three independent modes seen during the WET campaign were trapped modes, an assumption which may not be generally true since in the pulsating white dwarfs which show more modes, the largest amplitude ones are not necessarily trapped. For BPM37093, the hydrogen mass fraction is not strongly constrained since the possible models which fit equally well the observed periods cover a rather large range.

Since the hydrogen mass fraction estimate largely relies on a proper identification of the modes, which is often difficult even from long time-series photometric data, two alternative methods have been devised. In the first case, the wavelength dependence of the pulsation amplitudes has been used to select the ℓ degree of the modes (Robinson et al. 1995; Kepler et al. 2000b). The method requires data covering a large enough wavelength range, including preferably the UV where the amplitudes vary most significantly. It also requires high S/N ratio to distinguish between $\ell = 1$ and $\ell = 2$ modes whose predicted amplitude variations are quite close. The second method uses time-dependent spectrophotometry (van Kerkwijk et al. 2000; Clemens et al. 2000; Kotak et al. 2002a; Thompson et al. 2003, 2004). The variations in the line profile during the pulsation cycle contain information on the ℓ degree of the modes. This method implies the use of large telescopes since it relies on high resolution spectroscopy with good enough S/N on time scale which should be a fraction of the typical periods. However, both methods would also require long enough time-series to resolve the close frequencies of rotationally split multiplets or of overlapping modes of different ℓ degrees, a condition which cannot be easily satisfied.

To summarize, the question of whether the DA white dwarfs all have the same hydrogen mass fraction is presently unsettled. A hydrogen mass fraction of $10^{-4}\ M_{WD}$ is adopted as a "standard" value in most models used in computing cooling sequence (the so called "thick" hydrogen models). If a large dispersion in the hydrogen mass fraction in DA white dwarfs was found to be real, it would introduce an equivalent dispersion in the age of white dwarfs of a given luminosity and increase the uncertainty in the age calibration of the white dwarf luminosity function.

So, trying to determine the hydrogen mass fraction in DA white dwarfs from the asteroseismology of the ZZ Ceti stars is worthwhile. HL Tau 76 is a ZZ Ceti star of particular interest in this respect. It shows a large number of pulsation frequencies whose hopefully a significant fraction should be independent pulsation modes. As a result, the model is expected to be rather strongly constrained and its main parameters, including its hydrogen mass fraction, well determined.

The star was the primary target of a Whole Earth Telescope (WET, Nather et al. 1990) campaign whose results are described in the present paper. In Sect. 2, the observations and the data reduction are presented. Section 3 gives a global description of the power spectrum while Sect. 4 offers a detailed analysis of the power spectrum and a discussion of its variations compared to previous observations. Section 5 is devoted to the asteroseismological interpretation of our data. Section 6 summarizes our results.

2. Observations and data reduction

2.1. Summary of previous work

With a $T_{\rm eff} = 11\,440 \pm 350$ K (Bergeron et al. 1995), HL Tau 76 is part of a group of ZZ Ceti stars located in the cool part of the instability strip, the red edge being defined by G30-20 and BPM24754 at $T_{\rm eff} = 11\,070 \pm 200$ K. Its $\log g = 7.89 \pm 0.05$ translates to a mass of $M/M_\odot = 0.55 \pm 0.03$ assuming it has a pure carbon core, a helium layer fractional mass $M_{He}/M_{WD} = 10^{-2}$ and a "thick" hydrogen layer fractional mass $M_H/M_{WD} = 10^{-4}$, according to Bergeron et al. (1995) from the models of Wood (1995). However, since the hydrogen and helium mass fraction are not known, the derived total mass cannot be tightly constrained by spectroscopy alone.

HL Tau 76 = V411 Tau is the very first discovered pulsating white dwarf (Landolt 1968). In the original discovery data set, Landolt identified a quasi-periodic variation of about 12.5 min with a large amplitude of 0.14 mag. This discovery was confirmed by observations of Warner & Nather (1970, 1972) and the main period was more precisely determined as 12.437 min. The light curve of Warner & Nather (1972) was reanalysed by Page (1972) who established for the first time the multiperiodicity of HL Tau 76 in finding three periods: 748.5 ± 2 s, 665 ± 2 s and 628 ± 2 s. Later, Fitch (1973) obtained new observations confirming the multiperiodicity of HL Tau 76. However, while the largest amplitude was still at a period of 748.5 s, another period of 494 s was present in the light curve, while the periods previously detected at 665 s and 628 s were absent, thus revealing the amplitude variations of HL Tau 76. Such amplitude variations were commonly found in many other ZZ Ceti stars discovered later on. HL Tau 76 has been further observed, either from single-site or from multi-site photometric campaigns, including a WET campaign (XCOV13) in February 1996, where it was a secondary target. A preliminary analysis of the data available until 1997 has been presented by Dolez & Kleinman (1997). The available single-site data include those obtained at the 1.5 m telescope of the Tenerife Observatory in November 1989, at the 1.9 m telescope of the Haute Provence Observatory in December 1989 and at the 36-in telescope of the McDonald Observatory in October 1990. A short description of those observations is given in Dolez & Kleinman (1997). In this paper, we will use those results when necessary. The frequency resolution achieved by these observations are ≈1.1 μHz in November 1989, ≈9 μHz in December 1989, ≈5.4 μHz in October 1990 and 2.6 μHz during XCOV13. In addition, a short run of time-resolved spectroscopy is described by Kotak et al. (2002b).

2.2. The observations

The observations described in this paper result from the Whole Earth Telescope multisite fast photometry campaign (XCOV18) organized in November 1999. During that campaign, HL Tau 76 was the first priority target.

The data have been obtained mostly with 3-channel photometers all equipped with blue sensitive photomultipliers (Hamamatsu R647-04 or similar) and used without a filter (white light). These instruments fulfill the specifications and requirements as prescribed by Kleinman et al. (1996). The sampling time was either 5 s or 10 s. The sky background is continuously monitored by the third channel, with the target and comparison stars placed in the other two channels. Some data have been obtained with CCD photometers. Table 2 gives the Journal of the observations. The CCD data are identified in the last column.

During that campaign, the non-overlapping data resulted in a 66.5% duty cycle. The total duration of the campaign was 18 days. The data of 17 days were used for the computation of the power spectrum which leads to a frequency resolution in the Fourier Transform of the corresponding light curve ≈0.68 μHz.

2.3. Data reduction

The photomultiplier (PMT) photometer data have been reduced in a now standard way (Nather et al. 1990; Kepler 1993). In 3-channel photometers, the sky background is measured at the beginning and at the end of each run in all channels. These data are used to determine the sensitivity ratios of the channels. The sky background is subtracted point by point from the target and comparison star channels, after application of the proper sensitivity ratios. Each star channel is then corrected for extinction and normalized. When conditions show evidence for transparency variations, the normalized target star channel counts are divided by the smoothed comparison star channel counts. Subtracting unity from the resulting time series gives the time series on which the barycentric correction to the time base is applied. The exposure times of the PMT data were 5 or 10 s while in the case of the CCD data they were close to 30 s. We performed some simulations to estimate the consequence of adding data sampled at different rates, which is the case for our data (PMT + CCD). We considered different combinations of parts of a noise free single sinusoidal light curve, with gaps, sampled at different rate (5 s, 10 s, 20 s) and calculated the corresponding window functions. This always results in a degraded window function showing higher amplitude aliases compared to the window function computed from the same light curve sampled at a uniform rate. As a result, we decided to homogenize the sampling rate by summing the PMT data to 30 s, after having checked that there was no signals with periods shorter than 60 s.

A few runs have been rejected where the noise level was too high, which was usually due to clouds or instrumental problems. In case of overlapping data, we tried to use the additional data to improve the signal/noise ratio. If a signal S_1, whose noise is b_1, overlaps with a signal S_2, whose noise is b_2, the weighted sum S of these signals is given by:

$$S = S_1 \times b_2^2(b_1^2 + b_2^2)^{-1} + S_2 \times b_1^2(b_1^2 + b_2^2)^{-1}.$$

The resulting noise b is theoretically lower than the individual data noise by:

$$b = b_1 b_2 / \sqrt{(b_1^2 + b_2^2)}.$$

This shows that by adding two signals of similar noise, the resulting noise may be improved by $\sqrt{2}$. Similarly, doing the weighted sum of signals whose noise differs by a factor of 3 improves the resulting noise by only 5%. This is only true in the ideal case where both signals are sampled at the same rate. Practically, we performed such a weighted sum only for data whose noise differs by no more than a factor of 3. Otherwise, we kept only the best signal/noise ratio data. The resulting normalized light curve is shown in Fig. 1.

3. The amplitude spectrum

The amplitude spectrum of the time series is obtained by performing a Fourier Transform. As the amplitude spectrum of HL Tau 76 is somewhat complex, it is shown on a large scale in three parts in Figs. 2–4 for the frequency intervals 0–2000 μHz, 2000–4000 μHz and 4000–6000 μHz respectively. The amplitude spectrum above 6000 μHz is not shown as it is mainly noise and shows only very low amplitude insignificant signal. Each figure is formed of 5 panels, each covering a 400 μHz frequency interval. The corresponding window function is shown in Fig. 5 in full size and on a larger scale for a better visibility of the remaining aliases.

Fig. 1. Normalized light curve of HL Tau 76 during the 1999 WET campaign (XCOV18). All the runs used in the power spectrum computation are shown. We subtract unity to the normalized light curve so that its average value is 0. The fractional modulation intensity (mi) is plotted as a function of time (UT)(left side scale). Each panel corresponds to one day (right side scale).

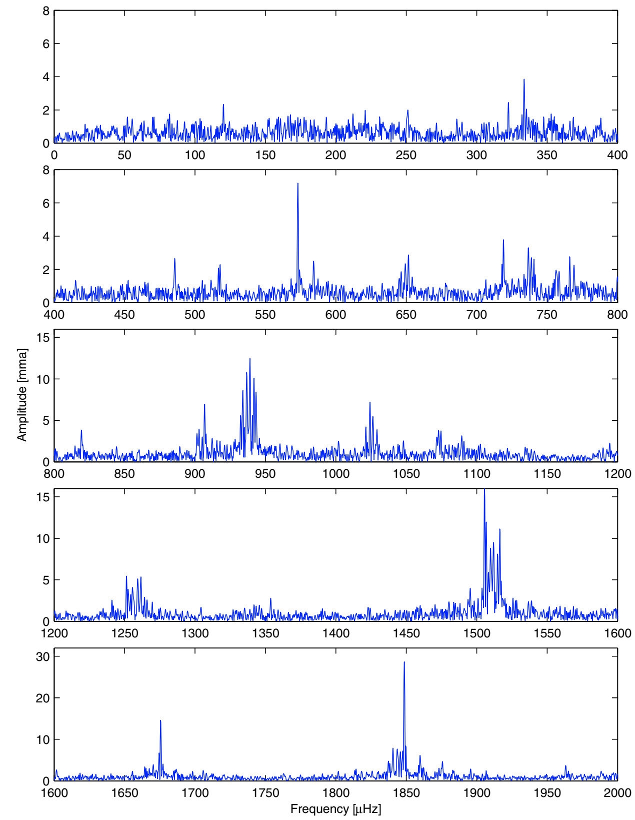

Fig. 2. Fourier amplitude spectrum of HL Tau 76 in the range 0 to 2000 μHz. The amplitude expressed in milli-modulation amplitude (mma) is plotted as a function of the frequency expressed in μHz. Note that the vertical scale for the amplitude varies for each panel.

The peaks in the amplitude spectrum are extracted by successive non-linear least squares fits followed by prewhitening The significance of the peaks is determined in the following way. For each peak, we estimate the average noise σ on a frequency interval of 100 μHz centered on the peak frequency. The False Alarm Probability (FAP) (Scargle 1982) for that peak to be due to noise on such a frequency interval is estimated. As a first step, all peaks with a FAP $\leq 10^{-3}$ are considered as significant, which is equivalent to considering as significant all peaks with amplitude larger than $3.4 \times \sigma$. Each of these frequencies was then subtracted from the light curve in successive steps of pre-whitening, the whole FT being recomputed at each step.

An illustration of the frequency iterative extraction process is shown in Fig. 6 for the first 6 frequencies. We can see in the panel hl07 that after the extraction of the 6 largest amplitude peaks, a large number of significant peaks are still present. The last panel shows the residuals after pre-whitening by the first 52 frequencies. The remaining peaks are all linear combinations of the previously extracted frequencies. This procedure extracts a total number of 85 significant peaks which are listed in Table 3. However, as a second step, one increases the detection limit to $4.1 \times \sigma$. This is equivalent to estimate as significant all peaks with a FAP $\leq 10^{-3}$ on the total frequency range of the FT up to the Nyquist frequency. This more severe selection criterion eliminates 7 of the peaks previously selected whose significance is consequently dubious. Those peaks are noted by a colon (:) in Table 3. Five of them will be identified as linear combinations below. Their elimination does not affect the following discussion. This is not the case for the remaining two (peaks 13 and 26 in Table 3) which were considered as independent frequencies after the first step. To be conservative, we will not use them in the proposed asteroseismological interpretation. We are then left with 78 significant peaks.

Table 3 gives the list of the frequencies in Col. 2. The third column gives δf, the formal error on the frequencies derived from the least-squares analysis. The fourth and fifth columns give the corresponding periods and their uncertainties. The sixth column gives the amplitude in units of milli-modulation amplitude (mma). The phases derived from the least-squares fits are given in the seventh column (between 0 and 1 for the interval 0 to 2π). The formal errors estimated in this way are lower limits to the true uncertainties. Another way of estimating the uncertainty on the frequency determination consists in using the frequencies of the linear combination peaks. As discussed below, a number of peaks in the Fourier spectrum are linear combinations of higher amplitude peaks. The differences Δf between the observed frequency of these combination peaks and the frequency resulting from the sum or the difference of their "parent" peaks frequency is a

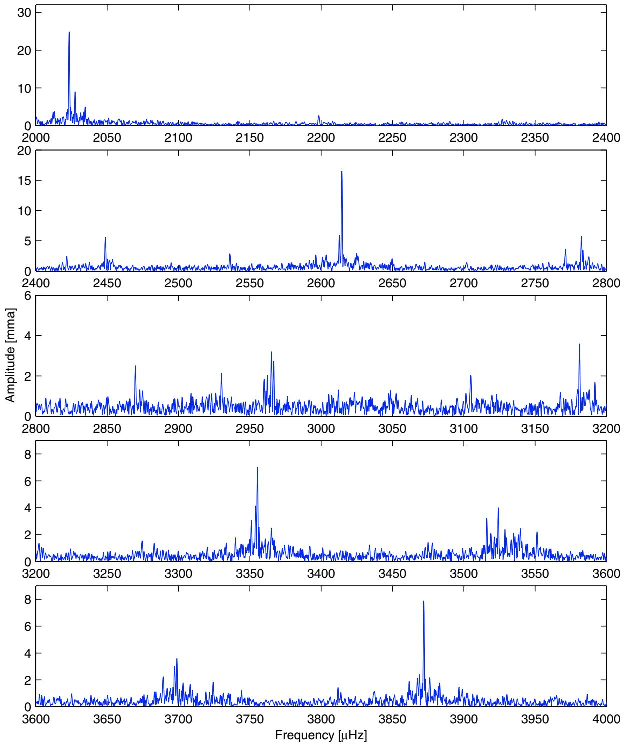

Fig. 3. Same as Fig. 2 for the frequency range 2000 to 4000 μHz.

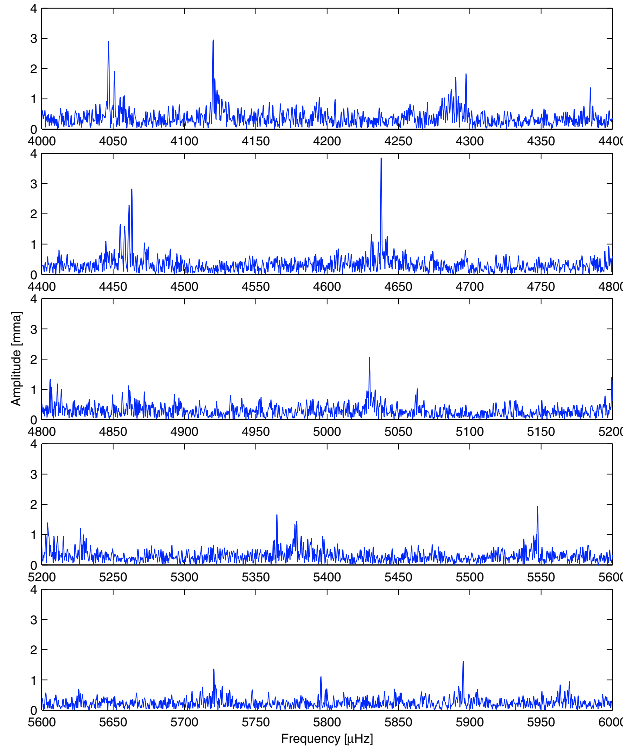

Fig. 4. Same as Fig. 2 for the range 4000 to 6000 μHz.

measure of the "true" uncertainty on the frequency determination. The linear combinations are identified in the eighth column and Δf is given in the last column of Table 3. The average δf is 0.028 μHz and the average Δf is 0.038 μHz.

The amplitude spectrum is characterized by a small number of large amplitude peaks, with amplitudes exceeding 10 mma, plus a large number of smaller amplitude peaks. It is immediately clear that many of these small amplitude peaks are linear combinations and/or harmonics of the large amplitude ones. These frequency combinations reflect the nonlinear response of the flux perturbations at the level of the photosphere to the sinusoidal perturbations at the bottom of the convection zone. This is a consequence of the variations of the depth of the convection zone and of the correlated convective flux during the pulsations. These nonlinearities induce the non-sinusoidal nature of the pulse shapes, which in turn materialize in the Fourier spectrum by the occurence of combination frequencies and harmonics. This is a frequent property of the cool DAV Fourier amplitude spectra. As always in such cases, one finds frequency combinations such that:

$$f_1 \pm f_2 = f_3,$$

with no a priori knowledge of which are the "parent" frequencies and which is the "combination".

To select which are the most probable linear combinations, we used the following arguments: i) the comparison with other epochs of data to check that modes may show up without their linear combinations while the contrary is excluded; ii) the combination of two multiplets results in a much different fine structure than each parent multiplet; iii) the amplitude of the combinations is generally smaller than the amplitude of their parent modes; iv) combinations of combinations are less likely than "first order" combinations; and v) if one knows the period spacings one can check whether a mode is at the expected frequency, which is an indication that it may rather be a real mode. We made use of these criteria to select the linear combinations in the list of frequencies given in Table 3.

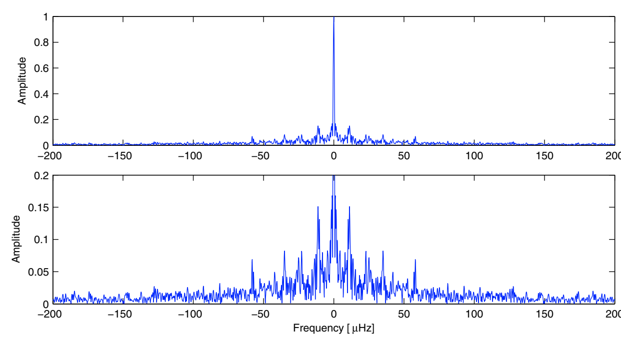

Fig. 5. Window function obtained during the 1999 WET campaign. The window function is shown on the same frequency scale than the Fourier amplitude spectrum. The upper panel shows the window function normalized to an amplitude of unity at maximum. The lower panel shows the same window function truncated at an amplitude of 0.2 for a better visibility of the remaining aliases

We started our search for linear combinations by looking for peaks whose frequency corresponds to the sums or the differences of frequencies of other peaks within ≈two formal errors of the frequency determination as obtained from the

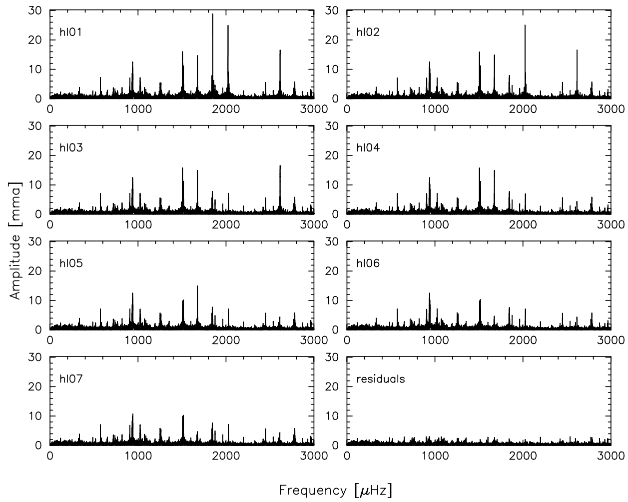

Fig. 6. Illustration of the frequency extraction process. The successive steps of prewhitening are shown for the first six frequencies. Each panel shows the Fourier amplitude spectrum, in unit of mma, in the frequency interval 0−3000 μHz. The panels are labelled from hl01 to hl07. The panel hl01 is the full Fourier spectrum. The next panel, hl02, is the Fourier spectrum after prewhitening by the largest amplitude peak at 1848 μHz. The next panel, hl03 is the Fourier spectrum after prewhitening by the two largest amplitude peaks at 1848 μHz and 2023 μHz, etc. The last panel shows the residuals after prewhitening by the first 52 largest amplitude frequencies. All the remaining low amplitude but still significant peaks are linear combination of the previously extracted largest amplitude peaks.

least-squares fit. By applying these rules, we find more than one set of two "parent" frequencies for almost every linear combination. To select the most probable "parent" combination, we used one or more of the following additional criteria: i) the sum (difference) of the "parent" frequencies is the closest to the frequency of the resulting combination; or ii) the selected "parent" peaks have a larger amplitude than the other "parent" candidates; or iii) a quadratic linear combination of two frequencies is more probable than a higher degree combination involving more than two parent frequencies (cubic and higher). The first harmonics of the four largest amplitude peaks are also found but, with one exception, they overlap with another linear combination so that the resulting frequency does not match exactly the expected harmonics frequency. That is case for the peak 62 which is at 1.75 μHz of the first harmonics of the peak 44 and is also the combination of peak 39 and 48. The exception is the peak 67 which is exactly the first harmonics of the peak 48. The peak 79 is at 1.95 μHz of the first harmonics of the peak 53 but is also the (less probable) cubic linear combination of the peaks 11, 39 and 53. Finally, the peak 59 is at 2.7 μHz of the first harmonics of the peak 39, but is also the quadratic linear combination of the peaks 29 and 44. It must be noted that some linear combinations resulting from large amplitude peaks do have themselves an amplitude large enough to produce higher order linear combinations with their former "parent" peaks or with other large amplitude peaks. It is one of the reasons why the power spectrum has such a complex structure. One example of such a hierarchical series of linear combinations is the combination of the two largest amplitude modes at 1848.58 μHz (44) and at 2023.36 μHz (48) which produces a quadratic linear combination at 3871.96 μHz (65) of 8.0 mma amplitude. This resulting frequency combines with the fourth largest amplitude peak (39) to produce the cubic linear combination at 5547.46 μHz (peak 79). Another interesting case is the peak 83 resulting from a combination of the first harmonics of the largest amplitude peak (44) with the second largest amplitude peak (48). Table 3 lists the selected most probable linear combination in Col. 7. As a summary, among the listed 85 significant peaks (below 6000 μHz) we find 31 quadratic combinations, of which 4 are also first harmonics of the largest amplitude peaks, and 19 cubic combinations.

Since the non-linear least squares fit used to derive the frequencies and amplitudes from the light curve also gives the phases, one could anticipate using the analytical relation between the phases of the parent modes and the phase of their linear combination (Wu 2001) to check whether the combinations have been correctly identified. The theory developed by Wu (2001), after Brickhill, relies on the assumption that the convective turn-over time-scale is much shorter than the pulsation periods. It describes how the flux perturbations at the photosphere is related to the flux perturbations at the bottom of the convection zone. In the case of a linear combination of two modes, the phase delay between the two parent modes and their linear combination implies a thermal time constant τ_{c0} which is related to the thermal relaxation time scale of the convection zone and to the characteristic time scales of the response of the photosphere and of the superadiabatic region towards gravity-mode pulsations. With the adopted ML2/α = 0.6 version of the mixing-length theory, after Bergeron et al. (1995), the thermal relaxation time scale of the convection zone in HL Tau 76 is of the same order, ≈300 s, than the pulsation periods. The response of the photosphere to the flux perturbations at the bottom of the convection zone is not straightforward in this case. The potentially useful informations given by the phases of the linear combinations compared to the phases of their parent modes is not easy to interpret in the case of HL Tau 76. It is why, while those phases are given in Table 3, they are not used in the present paper to check the validity of our linear combination identification.

4. Analysis of the amplitude spectrum

Having eliminated the doubtful peaks and the linear combinations, one is left with 33 frequencies which have to be considered as independent frequencies present in the star. This makes HL Tau 76 the next richest pulsator after PG 1159−035 (Winget et al. 1991), GD 358 (Winget et al. 1994; Kepler et al. 2003) and RX J2117+3412 (Vauclair et al. 2002). These frequencies appear in 10 separated groups between 718.99 μHz and 2614.55 μHz. All the higher frequency peaks in XCOV18 are identified as linear combinations (quadratic and higher) of lower frequency peaks. In their analysis of the XCOV13 data Dolez & Kleinman (1997) also conclude that all the peaks with frequency above 2614 μHz are linear combination peaks.

Table 3. List of the frequencies identified in HL Tau 76.

n	Frequency [μHz]	δf [μHz]	Period [s]	δP [s]	$A \pm 0.26$ [mma]	Phase	linear combination	Δf [μHz]
1	333.68	0.026	2996.88	0.234	3.83	0.7481	44−35	0.01
2	572.99	0.015	1745.23	0.045	7.02	0.7008	30−10	0.03
3	718.99	0.028	1390.84	0.054	3.62	0.1139		
4	736.67:	0.033	1357.46	0.061	3.14	0.3150	37−10	0.09
5	765.96	0.036	1305.55	0.060	2.68	0.3277	53−44	0.01
6	819.34	0.029	1220.49	0.043	3.48	0.4134	41−17	0.06
7	901.44	0.030	1109.33	0.036	3.31	0.0941	41−14	0.23
8	906.72	0.017	1102.87	0.020	6.22	0.2139	44−14	0.05
9	932.40	0.019	1072.50	0.021	5.19	0.2807	15 + 29−36	0.08
10	933.87	0.010	1070.81	0.011	9.61	0.5495		
11	936.73	0.010	1067.54	0.011	9.74	0.1600		
12	938.99	0.009	1064.97	0.011	11.30	0.7761	53−39	0.05
13	941.09:	0.030	1062.60	0.033	3.23	0.2608		
14	941.80	0.009	1061.80	0.010	11.44	0.3381		
15	943.20	0.012	1060.22	0.013	7.67	0.5337		
16	1021.26	0.024	979.18	0.022	4.34	0.3558		
17	1024.19	0.016	976.38	0.015	6.46	0.0317		
18	1026.23	0.020	974.44	0.019	4.96	0.4627		
19	1029.23	0.026	971.60	0.024	3.89	0.1976		
20	1071.58	0.032	933.20	0.027	3.22	0.3445		
21	1074.52	0.028	930.64	0.024	3.62	0.3974		
22	1089.33:	0.034	917.99	0.028	3.09	0.6275	48−10	0.156
23	1251.40	0.020	799.10	0.012	5.19	0.4890		
24	1252.64	0.025	798.31	0.016	4.04	0.1624		
25	1255.69	0.027	796.37	0.017	3.74	0.3478		
26	1256.69:	0.029	795.74	0.018	3.55	0.2307		
27	1259.31	0.020	794.08	0.012	5.10	0.5619		
28	1261.50	0.025	792.70	0.016	4.08	0.1001		
29	1505.54	0.007	664.21	0.003	14.99	0.3064		
30	1506.83	0.008	663.64	0.003	11.90	0.8742		
31	1508.71	0.027	662.81	0.011	3.49	0.6391		
32	1509.83	0.009	662.32	0.004	10.84	0.5580		
33	1510.77	0.013	661.91	0.005	7.61	0.1502		
34	1511.96	0.011	661.39	0.005	9.30	0.0849		
35	1514.91	0.013	660.10	0.005	7.35	0.7732		
36	1516.26	0.009	659.51	0.004	10.71	0.9114		
37	1670.45	0.029	598.64	0.010	3.55	0.4324		
38	1674.63	0.022	597.14	0.008	4.48	0.9758		
39	1675.61	0.007	596.79	0.002	14.60	0.2749		
40	1840.56	0.018	543.31	0.005	5.57	0.8478	10−14 + 44	0.04
41	1843.48	0.015	542.45	0.004	6.95	0.9503		
42	1844.61	0.025	542.12	0.007	3.99	0.7636	30 + 44−33	0.03
43	1845.74	0.013	541.78	0.004	8.05	0.5639		

Table 3. continued.

n	Frequency [μHz]	δf [μHz]	Period [s]	δP [s]	$A \pm 0.26$ [mma]	Phase	linear combination	Δf [μHz]
44	1848.58	0.003	540.95	0.001	28.45	0.1751		
45	1849.87	0.022	540.57	0.006	4.40	0.7465	30 + 44−29	0.00
46	1875.77	0.025	533.11	0.007	3.98	0.4290	10 + 14	0.10
47	1963.15	0.030	509.38	0.008	3.40	0.2265	14 + 16	0.08
48	2023.36	0.004	494.22	0.001	4.42	0.8567		
49	2027.53	0.014	493.21	0.003	7.12	0.7159		
50	2198.32:	0.035	454.89	0.007	2.78	0.3055	11 + 28	0.07
51	2448.74	0.018	408.37	0.003	5.62	0.7558	15 + 29	0.00
52	2612.58	0.022	382.76	0.003	4.50	0.7803	11 + 39	0.23
53	2614.55	0.006	382.47	0.001	16.47	0.5812		
54	2782.47	0.018	359.39	0.002	5.69	0.7640	10 + 44	0.02
55	2965.17:	0.030	337.24	0.003	3.18	0.6527	14 + 48	0.01
56	3104.91	0.044	322.07	0.003	2.04	0.0194	28 + 41	0.08
57	3181.10	0.033	314.35	0.004	3.68	0.9605	29 + 39	0.05
58	3274.64	0.049	305.37	0.005	1.60	0.1444	23 + 48	0.12
59	3353.96:	0.033	298.15	0.003	3.60	0.8302	29 + 44	0.15
60	3355.37	0.015	298.03	0.001	7.08	0.4778	30 + 44	0.04
61	3524.18	0.023	283.75	0.001	4.06	0.8590	39 + 44	0.01
62	3698.91	0.033	270.35	0.002	3.73	0.5215	39 + 48	0.06
63	3724.34	0.047	268.50	0.003	1.74	0.0055	11 +15 + 41	0.92
64	3811.80	0.054	262.34	0.004	1.35	0.4416	13 + 16 + 44	0.86
65	3871.96	0.014	258.26	0.001	8.00	0.5168	44 + 48	0.02
66	3876.06	0.049	257.99	0.003	1.62	0.2944	44 + 49	0.05
67	4046.80	0.034	247.10	0.002	2.84	0.2555	2×48	0.08
68	4050.98	0.046	246.85	0.003	1.84	0.1111	48 + 49	0.09
69	4120.14	0.034	242.71	0.002	2.88	0.4000	29 + 53	0.05
70	4292.04	0.058	232.98	0.003	1.06	0.1166	14 + 38 + 39	0.01
71	4297.37	0.040	232.70	0.003	1.82	0.3944	10 + 35 + 44	0.01
72	4455.00	0.048	224.46	0.003	1.66	0.2486	13 + 37 + 41	0.03
73	4458.02	0.050	224.31	0.002	1.52	0.4555	41 + 53	0.01
74	4461.19	0.038	224.15	0.002	2.42	0.4500	43 + 53	0.90
75	4637.91	0.025	215.61	0.001	3.96	0.8972	48 + 53	0.00
76	5029.76	0.044	198.81	0.002	2.06	0.1555	29 + 39 + 44	0.02
77	5199.63	0.052	192.32	0.002	1.37	0.3944	30 + 41 + 44	0.73
78	5204.10	0.052	192.15	0.002	1.36	0.1236	32 + 43 + 44	0.05
79	5227.15	0.056	191.30	0.002	1.24	0.3805	11 + 39 + 53	0.24
80	5364.76	0.048	186.40	0.001	1.70	0.1972	39 + 41 + 43	0.08
81	5378.73	0.052	185.91	0.001	1.40	0.2750	30 + 44 + 48	0.05
82	5547.46	0.045	180.26	0.001	1.90	0.1069	39 + 44 + 48	0.09
83	5720.65	0.055	174.80	0.001	1.34	0.2166	2 x 44 + 48	0.13
84	5795.72	0.060	172.54	0.002	1.06	0.4875	29 + 39 + 53	0.01
85	5895.42	0.049	169.62	0.001	1.60	0.4000	26 + 48 + 53	0.81

4.1. Time variations

The observations of the HL Tau 76 pulsations span a total interval of 35 years between their discovery and the present WET campaign. They provide some information on the star's amplitude and/or frequency variations. Such information is of interest to understand the physics underlying the excitation mechanism. It is also important to check whether there are pulsations modes stable enough in amplitude and frequency to be suitable for $\dot{P}$ measurements. Such $\dot{P}$ measurements can be used to estimate the cooling time and constrain the core composition (see Kepler et al. 2000a).

The available observations consist in part of: the original discovery of the HL Tau 76 variability by Landolt (1968), the observations themselves having been carried out in 1964; the confirmation data and additional data by Warner & Nather (1970, 1972), the later ones reanalysed by Page (1972); the data published by Fitch (1973). It seems that the star was forgotten for some time until new observations, making use of 3-channel photometers, were undertaken through single-site or multi-site campaigns. These new observations, including a WET campaign (XCOV13) during which HL Tau was a second priority target, have been analysed by Dolez & Kleinman (1997).

Landolt's discovery light curve was dominated by a 746 s period (1340 μHz frequency) of 0.14 mag amplitude. Later on, Page (1972) identified three frequencies in the Warner & Nather (1972) light curve, at 1341 μHz (746 s), 1504 μHz (665 s) and 1592 μHz (628 s). In his data, Fitch (1973) found two frequencies at 1340 μHz (746 s) and 2023 μHz (494 s). During these early days, HL Tau 76 was pulsating with a preferred frequency around 1340 μHz. This frequency, as well as the 1592 μHz, have not been observed since, or at least had amplitudes below detection limits. From the frequencies observed in those early data, only those at 1504 μHz and 2023 μHz are still detected in the data analysed by Dolez & Kleinman (1997) and in the present WET data.

Because the amplitude spectrum of HL Tau 76 is so rich, one must be careful when comparing spectra of different frequency resolutions to infer amplitude and/or frequency variations. As can be seen from Table 3, some frequency regions contain a number of closely-spaced frequency peaks which could not be resolved in short data sets. For instance, the time-resolved spectroscopy observations presented by Kotak et al. (2002b) are too short to resolve most of the complex structures seen in the amplitude spectrum. While this method is supposed to be insensitive to the azimuthal degree, yet it is necessary to resolve the modes of different ℓ degrees which may overlap in frequency. This case occurs in HL Tau 76 as discussed in the next section. The only comparison one can attempt here is with the data of the 1996 WET campaign (XCOV13). The frequency resolution of the amplitude spectrum achieved by XCOV13 is about 2.6 μHz. The formal error on the frequencies of the largest amplitude peaks, derived from the least-squares fit, is of the order of 0.01 μHz. By comparison, the frequency resolution achieved by the present XCOV18 data set is 0.65 μHz, 4 times better. Considering the frequency differences of the peaks listed in Table 3, one concludes that most of them, if present during XCOV13, should have been resolved. So, it is meaningful to compare both WET campaigns. This comparison gives us some information on the variability of the power spectrum's fine structure on a 3.7 year time scale. The amplitudes and frequencies of the modes in common between XCOV13 and XCOV18 are given in Table 4. Some cases require specific comments.

The 741.9 μHz peak seen in XCOV13 and not detected in XCOV18 and the 736.7 μHz marginally detected in XCOV18 are probably two components of a same multiplet (see discussion in 5.2.4 below).

Table 4. Amplitude variations in HL Tau 76 between XCOV13 and XCOV18.

Frequency [μHz] XCOV13	Amplitude [mma] XCOV13	Frequency [μHz] XCOV18	Amplitude [mma] XCOV18
741.9	9.2	736.7	3.1
939.4	18.3	939.0	11.3
1072.4	23.2	1071.6	3.2
1255.5	8.9	1255.7	3.7
1280.3	9.1	abs	abs
1521.0	10.3	1516.3	10.7
1675.0	14.4	1675.6	14.6
1848.3	37.3	1848.6	28.4
2023.4	27.8	2023.4	24.4
2223.3	6.7	abs	abs
2614.6	20.1	2614.5	16.5

Dolez & Kleinman (1997) considered the peak at 939.4 μHz as a linear combination between their 2614 μHz and 1675 μHz peaks. We also suggest that this peak may be a linear combination of the same peaks but on a different basis; namely, in XCOV18, both the 1675.61 μHz and the 2614.55 μHz peaks are present and have amplitudes larger than the 938.99 μHz peak (14.6 mma, 16.47 mma and 11.30 mma respectively). On this argument we suggest that 938.99 μHz peak may be a linear combination of the two other peaks. In contrast, during XCOV13, the 939.4 μHz peak amplitude was intermediate between the amplitudes of the two other peaks. Applying the selection rule used in the present paper to the XCOV13 data, we would have concluded that it is the 1675 μHz peak which is a linear combination of the two others. This illustrates the ambiguous identification of the "true" stellar independent pulsation frequencies versus their linear combinations. In this particular case, one sees that the amplitude of the 1675 μHz peak did not change from XCOV13 to XCOV18 (14.4 mma and 14.60 mma respectively) while the 2614 μHz peak decreased its amplitude from 20.1 mma during XCOV13 to 16.47 mma during XCOV18. The 939 μHz peak decreased in amplitude also from 18.3 mma during XCOV13 to 11.30 during XCOV18. If the 1675 μHz was the resultant linear combination, one would not expect its amplitude to remain constant while its two presumable "parent" peaks decreased in amplitude. To solve the puzzling nature of this 939 μHz frequency, we looked back into the unpublished earlier single-site data taken in November and December 1989 and in October 1990. We find that the three frequencies are always detected except the 939 μHz peak in December 1989. This suggests that the two other frequencies must be independent modes. In the other runs, both the 939 μHz and the 2614 μHz peaks had the highest amplitude in turn. These data suggest that the three frequencies may correspond to three independent modes. In that case, they would not be simply linked through a linear combination but could form a true resonance. We will check below whether there are modes expected by the asymptotic theory at those frequencies.

The peak at 1072 μHz experienced a spectacular decrease of its amplitude. In XCOV18, this peak is resolved into a doublet, but both components have much lower amplitude: 3.22 and 3.62 mma respectively, than the peak seen during XCOV13. One of the peaks, at least, must have changed significantly in amplitude between the two runs. The 1255.5 μHz peak seen in XCOV13 with a 8.9 mma amplitude, is seen in XCOV18 at 1255.69 μHz, within a complex structure of low-amplitude peaks. The fact that this complex structure was not seen in the XCOV13 data may result from a combination of a lower S/N ratio and lower frequency resolution.

The 1521 μHz peak seen in XCOV13 and the 1516.26 μHz peak seen during XCOV18 are suggested to belong to the same multiplet (see Sect. 5.2.5).

We note that the peaks at 741.86 μHz and 1280.30 μHz, seen only in XCOV13, and 2023.4 μHz, seen in all the data, are close to form a linear combination (741.86 μHz + 1280.30 μHz = 2022.16 μHz). It is intriguing, and may be meaningful, that this combination was "active" during XCOV13 and "inactive" during XCOV18. While the 2023.4 μHz frequency must be an independent "parent" mode, it is not possible to know from the WET data alone which of the two other frequencies is the other "parent" mode and which results from their linear combination, since they had the same amplitude during XCOV13 and none was seen during XCOV18. To solve this, we looked back again in the 1989 and 1990 single-site data. We see that the 2023 μHz peak is always present in the data. A peak at 738.72 μHz with an amplitude of 7.2 mma is seen in the October 1990 data. It cannot be the same peak as the one seen at 741.86 μHz during XCOV13 but could be a component of a same multiplet. This peak is not detected in the other runs, unless it could be associated to the peak at 736.67 μHz suspected in the XCOV18 data (see Table 3) and considered as an insignificant linear combination. The 1280 μHz peak is never seen. We conclude that the other parent mode should be the 741.86 μHz one and that the 1280.30 μHz peak may be the linear combination seen only during XCOV13, unless it could be another example of a true resonance. As far as the peaks at 741.86 μHz, 738.72 μHz and 736.67 μHz are concerned, they could be components of a same multiplet. We come back to theses points later.

We also looked for amplitude variations on shorter time scales by dividing the XCOV18 time series in two halves and comparing the amplitudes of the two corresponding FTs. Restricting ourselves to the independent modes of larger amplitudes, we find some variations for all except one mode: the 1675.61 μHz peak kept a constant amplitude. One finds large variations for the peaks at 1505.54 μHz and 1516.26 μHz which increased by 25% and 45% respectively. It is noteworthy to mention that the peak at 938.99 μHz, considered as forming a resonance with the 2614 μHz mode and the 1675 μHz mode, shows the largest amplitude change during the two halves of the run (50%) while its "companion" modes changed their amplitudes by only 12% for the 2614 μHz peak and by 0% for the 1675 μHz peak.

It is finally worthwhile to emphasize once more that the peak at 1675.61 μHz had the same amplitude in XCOV18 and XCOV13, and that its amplitude did not change on the approximately one week time scale separating the two halves of XCOV18. One may wonder whether this mode could be a potentially interesting candidate for a measurement of $\dot{P}$ in HL Tau 76. However, as this frequency might be involved in a resonance with two other modes or a result of their linear combination, any $\dot{P}$ measurement would not be unambiguously interpretable. The value of $\dot{P}$ in those cases could rather be dominated by other mechanisms than the cooling of the degenerate core. Furthermore, we checked that on the longer time scale involved when one takes into account earlier data, the amplitude of this mode is no longer constant. For instance, while it was at 14.8 mma in October 1989, it increased to 21.8 mma in December 1989 and was back to 15.6 mma in October 1990, to decrease during the two WET campaigns to the same value as observed in October 1989. Furthermore, in the time-resolved spectroscopy performed in October 1997, Kotak et al. (2002b) find that the peak at 1675 μHz was insignificant in the velocity power spectrum. So, our conclusion is that we do not find any mode with a stable enough amplitude whose $\dot{P}$ measurement could unambiguously measure the evolutionary time scale.

4.2. Fine structure, multiplets

In this section we look for closely spaced (in frequency) modes with the hope that triplets (or quintuplets) of equal splittings will reveal the ℓ values for a number of modes. However, given our confident estimate of the mass and temperature of HL Tau 76, another diagnostic – the period spacings – can provide a reliable estimate of ℓ as we discuss in the next section.

Recognizing rotationally split modes not only helps in identifying the degree ℓ but also leads to an estimate of the rotation period of the star. In the case of HL Tau 76, this exercise is made difficult by the complexity of the power spectrum which does not show clear structures. We nevertheless attempted a mode identification by adopting the following procedure.

We started by looking at closely spaced frequencies in the low frequency part of the amplitude spectrum, in the asymptotic regime where the rotationally split modes should show a uniform frequency separation. However, the only clearly isolated triplet present in the FT which could safely be identified as an $\ell = 1$ rotationally split mode is in the "high" frequency part of the FT. It is formed by the peaks 41−43−44 around 1848 μHz. For this triplet, the average rotational splitting is 2.55 μHz.

Now, we can go back to the low frequency part of the FT and check that any fine structure identified in this part is compatible with similar signatures found at higher frequency, keeping in mind that the modes in the higher frequency part of the FT may not be in the asymptotic regime. In performing this exercise, we start by examining the region between 933.87 μHz and 943.20 μHz. It contains 5 significant frequencies but the interpretation depends on whether one considers the 938.99 μHz as a real mode in resonance with the 1675.61 μHz and the

2614.55 μHz ones or as a linear combination. In the previous section, we gave arguments in favor of the first hypothesis. In the following discussion, we will consequently consider these three frequencies as corresponding to real modes. One finds then in this group three doublets of comparable frequency separation formed by the peaks 10−11 (933.87 μHz and 936.73 μHz), 11−12 (936.73 μHz and 938.99 μHz) and 12−14 (938.99 μHz and 941.80 μHz) separated by 2.86 μHz, 2.26 μHz and 2.81 μHz, respectively, with the peak 15 (943.20 μHz) 1.4 μHz from peak 14. A possible interpretation is that a ℓ = 1 triplet formed by the peaks 11, 12 and 14 overlaps with three components formed by the peaks 10, 12 and 15 of a $\ell = 2$ quintuplet. It is known that in the slow, solid body rotation limit, the pulsation frequencies of a mode of degree ℓ and order k for a rotating star, $\sigma_{l,k,m}$, are related to the frequencies in the non rotating case $\sigma_{l,k}$ by:

$$\sigma_{l,k,m} = \sigma_{l,k} + m(1 - C_{l,k})\Omega + o(\Omega)^2$$

where $C_{l,k}$ takes a simple form in the asymptotic regime: $C_{l,k} \approx 1/\ell(\ell + 1)$. We expect the rotational spitting for $\ell = 1$ and for $\ell = 2$ modes to be in the ratio:

$$\delta f_{\ell=1}/\delta f_{\ell=2} = 0.6.$$

This has been observationally verified in the PG 1159 pulsator PG 1159-035 (Winget et al. 1991).

The average frequency shift in the triplet 11−12−14 is 2.53 μHz. As it is almost similar to the value derived for the triplet 41−43−44, we consider that it is due to rotational splitting. The frequency separation within the quintuplet is 5.1 μHz on one side and 4.2 μHz on the other side. The average value, 4.65 μHz, compares satisfactorily with the value (4.22 μHz) expected in the asymptotic regime for the rotational splitting of $\ell = 2$ modes if the average rotational splitting for the $\ell = 1$ modes is ≈2.53 μHz in this frequency range. But the ratio $\delta f_{\ell=1}/\delta f_{\ell=2} = 0.544$ instead of the expected 0.6. The peak 12 in this case results from the superposition of the $m = 0$ component of the triplet and of one component of the quintuplet, which could be either $m = +1$, 0 or −1.

In the following groups of peaks, one sees four doublets formed by the peaks 16−17 (1021.26 μHz and 1024.19 μHz), 17−18 (1024.19 μHz and 1026.23 μHz), 18−19 (1026.23 μHz and 1029.23 μHz), separated by 2.93 μHz, 3.0 μHz and 2.04 μHz and 20−21 (1071.58 μHz and 1074.52 μHz), separated by 2.94 μHz. We consider that the 20−21 doublet is formed by two components of consecutive m values of a ℓ = 1 mode split by rotation. Since the doublets 16−17, 17−18 and 18−19 are too close to each other to be consecutive order $\ell = 1$ modes, we suggest that the group of frequencies 16 to 19 could be formed by a $\ell = 1$ triplet overlapping with components of a $\ell = 2$ mode. The combination 16−19 could then result from the overlap of an asymmetric triplet formed by the peaks 16−17−18, with a frequency separation of 2.93 μHz on one side and of 2.04 μHz on the other side, with two components of a quintuplet formed by the peaks 17 and 19, separated by 5.04 μHz. An alternative combination would be a triplet formed with peaks 17−18−19, also asymmetric with frequency separation of 2.04 μHz on one side and 3.0 μHz on the other side, with two components of a quintuplet formed by peaks 16 and 18, with a frequency separation of 4.97 μHz. In both cases one component of the triplet coincides exactly with one component of the quintuplet. The $m = 0$ component of the triplet could be either peak 17 or peak 18. However, in forming the ratio $\delta f_{\ell=1}/\delta f_{\ell=2}$ in the two options, one finds 0.493 in the first case and 0.507 in the second case, instead of the value 0.6 expected in the asymptotic regime. This weakly favors the second case as a better interpretation. Another argument based on the asymmetry of the triplets, which we will discuss in Sect. 5.4 below, could also favor this second case. However we will conservatively consider the two alternatives as possible solutions in the following discussion. We derive an average rotational splitting of 2.525 μHz for this triplet.

In the high frequency part of the FT, one finds the triplet mentioned earlier composed by the peaks 41−43−44 (1843.48 μHz, 1845.74 μHz and 1848.58 μHz). One also finds a doublet formed by the peaks 37−39 (1670.45 μHz and 1675.61 μHz). The triplet is slightly asymmetric and the total frequency difference between its two extreme components is 5.10 μHz. As the frequency separation between the doublet is 5.16 μHz, we interpret this doublet as the two extreme components of a triplet whose the central component is not detected. The peak 38 seen in between the components of the doublet, 0.98 μHz away from peak 39, cannot be the central component of the triplet. It is a small amplitude peak (4.5 mma) compared to peak 39 (14.6 mma) which is the fifth largest amplitude peak of the FT. The determination of its frequency may have been affected by this large amplitude neighbour. As a consequence, the $m = 0$ component of this triplet may not coincide with peak 38 but should be at ≈1673.0 μHz (597.7 s). From this triplet and this doublet, we derive an average rotational splitting of 2.56 μHz. Finally, one finds a doublet formed by the peaks 48−49 (2023.36 μHz and 2027.53 μHz), with a frequency separation of 4.17 μHz, a value which is difficult to reconcile with the one derived from the doublets and triplets discussed above but in good agreement with the expected rotational splitting for the $\ell = 2$ modes. We will argue later about the $\ell = 2$ identification for this doublet. The rotational splitting derived for the $\ell = 1$ modes from the low and high frequency parts of the FT are in satisfactory agreement. The weak difference between the values derived from the low frequency multiplets (2.525 μHz) and the higher frequency triplets (2.56 μHz) is insignificant given the frequency resolution of our data set. In the following discussion we will use the average value, 2.54 μHz, for the rotational splitting of $\ell = 1$ modes.

5. Asteroseismology of HL Tau 76

5.1. Period spacing

Having tentatively identified doublets and triplets as possible $\ell = 1$ modes, one looks for a uniform period spacing in their period distribution. For the same reason that the lower frequency multiplets must be closer to the asymptotic regime than the higher frequency ones, we look for periods difference between the low frequency multiplets first. On the assumption that the doublets are two successive components of triplets, we do not know which of the components is the $m = 0$ mode. Considering first the period differences between the triplet 11−12−14 and the central mode of the next triplet, 17 or 18, we can form two different values for that difference, according to which mode, 17 or 18, is considered as the $m = 0$ in the second triplet: 88.59 s (corresponding to period of mode 12 − period of mode 17 ($P_{12} - P_{17}$), and 90.53 s ($P_{12} - P_{18}$). The average period difference between these two multiplets is 89.56 s.

Doing the same between the components 17 and 18 of the triplet and the doublet 20−21, one finds four values: 43.2 s ($P_{17} - P_{20}$), 45.8 s ($P_{17} - P_{21}$), 41.2 s ($P_{18} - P_{20}$) and 43.8 s ($P_{18} - P_{21}$), with an average period difference of 43.5 s. We note that the 89.56 s average difference between the first multiplets is 2×44.78 s, a value very close to twice the average period difference between the triplet and the doublet 20−21. We conclude that the period spacing for the $\ell = 1$ long period modes should be ≈44.1 s and that there should be a missing multiplet between the triplet 11−12−14 and the triplet 16−17−18 or 17−18−19, centered at a period of ≈1020 s.

For the doublet and the triplet at higher frequencies, the period difference between the middle of the peaks 37−39 and the period of the mode 43 is 55.92 s, a value in satisfactory agreement with the value derived at lower frequency, considering that those multiplets may correspond to modes which are not in the asymptotic regime and/or that their period spacing may be affected by mode trapping.

5.2. Mode identification

5.2.1. Search for $\ell = 1$ modes

Adopting an average period spacing deduced from both the low and high frequency multiplets, $\Delta P = 48.0 \pm 3.9$ s, one can roughly estimate the predicted periods of the $\ell = 1$ successive orders, under the assumption of the asymptotic regime.

In the following, we take the period of the mode 43 (the presumably $m = 0$ component of this $\ell = 1$ triplet) as the reference for the period estimate. The estimated values are shown in Table 5-1. They are listed in the first column. The next three columns give the periods observed during XCOV18, XCOV13 and earlier single-site observations. The last column indicates the relative order difference, Δk, with the order of the reference mode which is defined as $\Delta k = 0$. We should keep in mind that the average period spacing is estimated with a large uncertainty and may formally take any value between 44.2 s and 52.0 s. The cumulative uncertainty on the predicted period becomes comparable to the period spacing for $\Delta k = 48.0$ s/3.9 s ≈ 12. It means that we cannot predict periods for Δk larger than 12. We add a question mark in Table 5-1 for $\Delta k \geq 12$. However, since with an average period spacing of 48.0 s one mode is predicted at 1309.8 s which nicely fit the period of 1308.7 s observed in archival data (see Sect. 5.2.4) it suggests that the period distribution should not depart much from the one predicted in using this value of the average period spacing up to at least $\Delta k = 16$. In cumulating these data, one finds 14 modes, or groups of modes, whose periods may be compared to the expected periods of the $\ell = 1$ modes. We find a satisfactory agreement, better or equal to 1%, between the observed and predicted periods for 11 modes. It does not mean that those 11 modes are all $\ell = 1$ modes since we have to check whether they could also be explained as well by $\ell = 2$ modes, which is discussed in the next section.

It is also possible that the modes whose periods do not fit exactly the distribution predicted by the asymptotic regime for $\ell = 1$ are indeed $\ell = 1$ modes since the period distribution may not follow exactly the distribution expected in the asymptotic regime. That may be the case for the low order modes. In addition, the periods may be altered by mode trapping, whatever is the hydrogen mass fraction responsible for the trapping. We check a posteriori that the $\ell = 1$ mode predicted at 1069.8 s is quite close to the observed 1064.97 s one (939 μHz) which we suspected to be a mode in resonance with the 1675 μHz and the 2614 μHz modes rather than a linear combination. This reinforces our identification of this frequency as a real mode and increases the number of independent modes to 34. It must be noticed that among the 22 expected $\ell = 1$ modes in the period range ≈380−1400 s, we detected only 11 potential $\ell = 1$ modes in the cumulative data.

5.2.2. Search for $\ell = 2$ modes

The next step consists in using what has been derived about the period spacing and the rotational splitting for the $\ell = 1$ modes to predict the period distribution of the possible $\ell = 2$ modes. The rotational splitting of $\ell = 1$ and $\ell = 2$ modes are in the ratio 0.6 in the asymptotic regime. The period spacing for a series of modes of degree ℓ, given by (Tassoul 1980)

$$\Delta P_\ell = \Pi_0/[\ell(\ell+1)]^{1/2}$$

where Π_0 is related to the structure of the star, implies that the ratio of the period spacings

$$\Delta P_{\ell=2}/\Delta P_{\ell=1} = 1/\sqrt{3}.$$

Since the average period spacing is 48.0 ± 3.9 s and the average rotational splitting is 2.54 μHz for the $\ell = 1$ modes, the corresponding values for the $\ell = 2$ modes should be 27.7 ± 2.2 s and 4.23 μHz. We also need to identify at least one $\ell = 2$ mode to be used as a reference value for the period distribution.

The average period spacing for the $\ell = 1$ modes derived in the previous section, $\Delta P = 48.0$ s, is quite consistent with the average spacing of 44.98 s in one of the models with a thick hydrogen layer by Brassard et al. (1992) whose parameters are close enough to HL Tau 76 (see for instance their model 60204). Very similar values are found by Corsico et al. (2002). Furthermore, in considering the periods of the modes in many of the models computed by Brassard et al. (1992) as well as in those computed by Bradley (1993) and Corsico et al., one finds many examples of $\ell = 1$ and $\ell = 2$ modes which overlap in frequency. For instance, in the Brassard et al. (1992) model 60204, there are 6 such coincidences of modes $\ell = 1$ and $\ell = 2$ differing in frequency by less than 11 μHz, within the frequency range 1100−4300 μHz. In examining the frequency list in Table 3 one finds regions with series of close frequency peaks which cannot be explained as $\ell = 1$ triplets

Table 5. 1. Search for $\ell = 1$ modes in HL Tau 76 with $\Delta P_{\ell=1} = 48.0$ s.

Predicted Period (s)	Observed periods (s) (XCOV18)	Observed periods (s) (XCOV13)	Observed periods (s) Archival data	Δk
1405.8	1390.8			+18?
1357.8		1347.9	1353.7	+17?
1309.8			1308.7	+16?
1261.8				+15?
1213.8				+14?
1165.8				+13?
1117.8				+12?
1069.8	1070.8, 1067.5, 1065.0	1064.5		+11
1021.8				+10
973.8	979.2−971.6			+9
925.8	933.2, 930.6	932.5		+8
877.8				+7
829.8				+6
781.8	799.1−792.7	796.5, 781.0		+5
733.8			748.5	+4
685.8			689.3	+3
637.8	659.5	657.4	628	+2
589.8	598.6, 597.1, 596.8	597.0		+1
541.8	542.4, 541.8, 540.9	541.0		0
493.8	493.2, 494.2		494	−1
445.8		449.8		−2
397.8	382.5	382.5		−3

nor by $\ell = 2$ quintuplets alone. We suggest that they should result from such multiplets overlapping. If we exclude the presence of $\ell = 3$ modes on visibility arguments, one is left with this only explanation to interpret the 5 peaks seen between 933 and 943 μHz, the 5 close frequencies detected between 1251 and 1261 μHz, as well as the series of frequencies detected between 1505 and 1516 μHz.

As there is no complete quintuplet identified, we do not have a solid reference $\ell = 2$, $m = 0$ mode to start with to predict the $\ell = 2$ modes period distribution. Any suspected $\ell = 2$ mode in our data is a component of an incomplete multiplet of unknown m value. In the search for fine structures in the frequency spectrum, it was implicitely assumed that the rotational splitting does not change within the range of the periods observed in HL Tau 76. That is consistent with the hypothesis that the rotation law in HL Tau 76 must be close to uniform rotation. In this case, since the frequency shift induced by the rotational splitting is fixed for a given ℓ, the uncertainty on the period scale is smaller if we can identify a high frequency peak as a $\ell = 2$ mode. Fortunately, we have such a possible $\ell = 2$ candidate with the high amplitude doublet at 2023.36 and 2027.53 μHz. This identification is based on the frequency separation of these two peaks, 4.17 μHz, which is in good agreement with the expected rotational splitting for $\ell = 2$ modes. Considering this doublet as two components of an $\ell = 2$ mode and the adopted rotational splitting, there are 4 possible values for the period of the $m = 0$ component of the quintuplet: 495.3 s, 494.2 s, 493.1 s and 492.1. So the central mode period of this incomplete multiplet is known within a 3.2 s interval. The center of this interval is at 493.7 s while the high amplitude component (peak 48 in Table 3) is at 494.2 s. We consider the mode 48 as a good enough reference point for the period distribution of the $\ell = 2$ modes. In addition, it is the second highest amplitude mode, so its period is quite precisely determined.

Table 5-2 shows the corresponding period distribution for $\ell = 2$ modes, assuming the asymptotic regime, a period spacing of 27.7 s and the period of mode 48 as the reference value. The first column shows the predicted periods. The following three columns list the periods present in XCOV18, XCOV13 and earlier single-site observations, respectively. The last column indicates again the relative order difference with the reference mode, which is $\Delta k = 0$. Regions of the spectrum where none of the observed periods fits close enough with any predicted values are not listed. Since the average period spacing is known with a statistical error of 2.2 s for the $\ell = 2$ modes, we cannot formally predict the periods and the relative Δk for $\Delta k \geq 27.7$ s/2.2 s = 12−13, since the uncertainty on the period becomes comparable to the period spacing. For this reason all predicted periods larger than 800 s ($\Delta k \geq 12$) are followed with a question mark. However, since we argued in the previous section that the true period distribution for the $\ell = 1$ modes should

Table 5. 2. Search for $\ell = 2$ modes in HL Tau 76 with $\Delta P_{\ell=2} = 27.7$ s.

Predicted Period (s)	Observed periods (s) (XCOV18)	Observed periods (s) (XCOV13)	Observed periods (s) Archival data	Δk
1380.6	1390.8			+32?
1352.9		1347.9	1353.7	+31?
.	.	.	.	.
.	.	.	.	.
1075.9	1060.2–1070.8	1064.5		+21?
.	.	.	.	.
.	.	.	.	.
965.1	979.2–971.6			+17?
937.4	930.6–933.2	932.5		+16?
.	.	.	.	.
.	.	.	.	.
798.9	792.7–799.1	796.5, 781.0		+11
.	.	.	.	.
.	.	.	.	.
743.5			748.5	+9
688.1			689.3	+7
660.4	659.5–664.2		665	+6
632.7			628	+5
605.0	596.8, 597.1, 598.0	597.0		+4
577.3				+3
549.6	540.9, 541.7, 542.4	541.0		+2
521.9				+1
494.2	493.2, 494.2	494.2	494	+0
466.5				−1
438.8		449.8		−2
411.1				−3
383.4	382.4	382.5		−4

not depart much from the one predicted with the average period spacing of 48.0 s, this should be true also for the period distribution of the $\ell = 2$ modes, if the reference period is a true $\ell = 2$ mode. We also point out that the predicted $\ell = 2$ mode with period 1380.6 s is close to the observed one at 1390.8 s, which should be $\Delta k = 32$. It suggests that the period distribution for the $\ell = 2$ modes does not depart much from the one predicted with the average period spacing of 27.7 s even up to $\Delta k = 32$.

Again comparing the observed periods with the predicted periods, one sees that among the 15 groups of observed periods, 12 fit satisfactorily with $\ell = 2$ modes, with less than 1% difference in period.

From Tables 5-1 and 5-2, one finds that at least 9 modes or groups of modes have periods within 1% of the period of either an $\ell = 1$ or an $\ell = 2$ mode. They very probably result from the overlap between $\ell = 1$ and $\ell = 2$ modes.

Comparing the periods detected during the two WET campaigns, one finds three modes which were seen during XCOV13 and are not present during XCOV18. Since the arguments used to estimate the periods of the modes are based on the period spacing deduced from the XCOV18 data alone, it is worth checking whether and how precisely these additional modes fit the proposed identification. They are the periods 1347.9 s (741.86 μHz), 781.0 s (1280 μHz) and 449.8 s (2223 μHz).

The first one at 1347.9 s (741.86 μHz) fits satisfactory, within 5 s, the period of the predicted $\ell = 2$ mode at 1352.9 s ($\Delta k = +31$ in Table 5-2). But it is also at 10 s of the predicted mode $\ell = 1$ at 1357.8 s ($\Delta k = +17$ in Table 5-1).

We already argued that the second one at 781.0 s (1280 μHz) probably results from the linear combination of the 741.86 μHz mode with the 2023 μHz one. We consequently would not consider it as an independent mode unless there is one predicted mode at this period. That is precisely the case since there is a predicted mode at 781.8 s in the $\ell = 1$ series (Table 5-1). It suggests that this period could correspond to a real mode and points to the possibility that it is another example of a true resonance between the three modes. The third one has a period of 449.8 s (2223 μHz). The closest predicted period is a $\ell = 1$ mode (Table 5-1) at 445.8 s. So, the three additional modes present in XCOV13 and not seen in XCOV18 fit satisfactorily with the periods predicted by the period spacing deduced from XCOV18 data.

5.2.3. Back to the XCOV18 amplitude spectrum

We used the asymptotic period distribution to predict the periods of the expected $\ell = 1$ and $\ell = 2$ modes. It is worth reexamining the best amplitude spectrum obtained for HL Tau 76, from the XCOV18 WET campaign, to check whether we could identify some additional modes not selected by our significance criterion, but whose periods are close enough to the predicted ones to suggest that they could be real modes. In that case, they would not have been selected because their amplitudes were below, or close to the adopted detection limit during XCOV18. We also check whether those modes were detected in previous observations.

Visual inspection of the XCOV18 amplitude spectrum (Figs. 2 and 3) reveals 2 such peaks. The first one at 1353.7 μHz (738.7 s) has a low amplitude of ≈2.6 mma. This peak is quite close to the one found in the early observations of Warner & Nather (1970, 1972) as reanalysed by Page (1972) at 1336.0 μHz (748.5 s). We note that there is one $\ell = 2$ mode predicted at 743.5 s (Table 5-2). Taken at face value as the $m = 0$ component of a $\ell = 2$ quintuplet, and using the rotational splitting of 4.23 μHz for $\ell = 2$ modes, that would predict the $m = -2$ component at 1336.5 μHz and the $m = +2$ component at 1353.4 μHz. We consider this excellent agreement with the observed frequencies as strong evidence that the suspected peak at 1353.7 μHz is real and corresponds to a component of an $\ell = 2$ mode whose other component at 1336.0 μHz happened to be the largest amplitude mode in the early observations of HL Tau 76.

The other one is at 2536.06 μHz (394.3 s) and has an amplitude of 2.9 mma. It has not been observed before. The closest observed frequency is the 2614 μHz (382 s) one of large amplitude seen in all the observing seasons. This small amplitude peak is close to the predicted $\ell = 1$ mode at 397.8 s (Table 5-1) and may possibly be identified with that mode.

In the following, we will keep both the 738.7 s and the 394.3 s periods as real modes according to the above mentioned argument. However, we will keep in mind that they are below the detection limit in XCOV18 by marking them with a colon (:) in the identification list proposed below (Table 6).

5.2.4. Back to archival data

The same checking operation can be performed with the earlier data. Looking back in the early observations of HL Tau 76, we already mentioned that among the dominant periods at 748.5 s, 665 s, 628 s and 494 s (Warner & Nather 1970, 1972; Page 1972; Fitch 1973) only two were seen at a significant level in the XCOV13 and XCOV18 data, the ones at 665 s and at 494 s. It is interesting to check whether the two missing ones can be predicted by the asymptotic extrapolation at their correct values. We have shown in the previous section that the mode at 748.5 s, which had the largest amplitude in the original discovery data, may be associated with the 738.7 s which is present in the XCOV18 data below detection limit. They are both probable components of the $\ell = 2$ mode predicted at 743.5 s ($\Delta k = +9$ in Table 5-2). For the mode at 628 s, the closest $\ell = 1$ mode would be at 637.8 s ($\Delta k = +2$ in Table 5-1) while the closest $\ell = 2$ mode would be at 632.7 s ($\Delta k = +5$ in Table 5-2). This suggests that this mode is also better fit as an $\ell = 2$ mode.

In the data obtained in 1989 and 1990, we also find a few significant peaks in their respective amplitude spectra which are not seen at significant levels in XCOV13 or in XCOV18. In the October 1990 data, we find a peak at 738.72 μHz (1353.7 s) with an amplitude of 7.2 mma. This frequency is quite close to the 736.67 μHz (1357.5 s) listed in Table 3 after the first step of the selection process and rejected as insignificant after the second step. It was anyway considered as a linear combination. However, considering that there is an $\ell = 1$ mode predicted at 1357.8 s (736.5 μHz) and an $\ell = 2$ mode predicted at 1352.9 s it is quite possible that it corresponds to a real mode rather than to a linear combination. A 764.1 μHz (1308.7 s) was seen in the December 1989 data with a small amplitude (3.6 mma). It could be a linear combination between the 2614.5 μHz and the 1847.7 μHz modes seen in the same data (they correspond to the 2614.55 μHz and 1848.58 μHz seen in XCOV18). There is also in this case an $\ell = 1$ mode predicted at 1309.8 s. This frequency could consequently be a linear combination as well as a real mode. Finally, in the November 1989 data, we find a peak at 1450.8 μHz (689.3 s) with an amplitude of 8.2 mma. Examination of Tables 5-1 and 5-2 shows that there is an $\ell = 1$ mode predicted at 685.8 s and an $\ell = 2$ mode predicted at 688.1 s. It suggests that this frequency may be identified with the $\ell = 2$ mode. These three periods present in archival single-site data are included in Tables 5-1 and 5-2. However, for the final identification we conservatively exclude the two ambiguous cases which could be either a real mode or a linear combination but keep the mode at 689.3 s.

5.2.5. Conclusions

To summarize: from XCOV18, we find 36 independent modes. This includes the mode at 939 μHz, considered as a mode in resonance with two other modes, and the two modes at 1353.7 μHz and 2536.06 μHz because the first one coincides with a period observed in the early data and the second one coincides with a mode predicted by the asymptotic period distribution. XCOV13 provides 11 modes of which 4 are not present in XCOV18. Among these four, we discussed the case of the two modes at 742 μHz and 1280 μHz which form a linear combination with a third independent mode at 2023 μHz. We showed that they probably form a resonance and are real modes. For this reason we add these four modes as independent modes from XCOV13. Finally, the archival data provide 5 modes, among which only 2 are present in XCOV18 and/or XCOV13, which adds another 3 independent modes. The total number of independent modes found in the cumulative data sets is 43.

In comparing the periods observed with the ones predicted by the period spacing and taking into account the rotational splitting, we make a preliminary identification of the modes. From Tables 5-1 and 5-2, which list the predicted periods for $\ell = 1$ and $\ell = 2$ modes, one sees a number of cases were the observed periods could be identified as either $\ell = 1$ or as $\ell = 2$ modes.

For some of those cases, we offered a tentative identification above, which lifts the degeneracy between the $\ell = 1$ and $\ell = 2$ identification. On the basis of the period differences between the observed values and the expected values from the asymptotic relation and from the rotational splitting, we can choose one solution rather than another one. The preliminary identification of the modes observed in HL Tau 76 is listed in Table 6. We discuss some remaining difficult or ambiguous cases below.

The five modes between 799.1 s and 792.7 s could correspond to the $\ell = 2$ mode predicted at 798.9 s. However, their frequency separation does not fit the expected rotational splitting. They all show a small amplitude (≤5.2 mma) during XCOV18 so that their frequencies may not be very precisely determined. The closest predicted $\ell = 1$ mode is at 781.8 s and is seen in the XCOV13 data (at 781 s). Could this group of periods results from the overlap of an $\ell = 1$ and an $\ell = 2$ multiplet? Considering the value of the rotational splitting associated to $\ell = 1$ modes, ones does not expect a component of the $\ell = 1$ triplet at a period longer than 784 s, which is the extreme case if the observed 781.0 s is the prograde ($m = +1$) component of the triplet. The multiplets should not overlap within the period range covered by this group. Considering the predicted mode at 798.9 s at face value as an $\ell = 2$, $m = 0$ mode and applying the rotational splitting for $\ell = 2$, one predicts the periods of the other components of the quintuplet at 804.3 s, 801.6 s, 796.2 s and 793.5 s for $m = -2, -1, +1$ and $+2$ respectively. We note that 793.5 s falls between the observed periods at 792.7 s and 794.1 s and that 798.9 s falls between the observed periods at 798.3 s and 799.1 s. It suggests that both double-peaks at 792.7−794.1 s and 798.3−799.1 s could in fact be single peaks incorrectly resolved by the extraction algorithm because of their low amplitudes and correspond to the two components $m = +2$ and 0 of the $\ell = 2$ mode of which the $m = +1$ component corresponds to the 796.4 s period. The other two components of the quintuplet are missing. For these cases, we conservatively list all the periods in Table 6 but identify the two double-peaks as single modes.

The group of modes 29 to 36, from 1505.5 μHz to 1516 μHz, forms the next complex region in the FT as shown in Table 3. As there are exactly 8 peaks in the FT of XCOV18 in this frequency range, it suggests that they could correspond to the superposition of a complete triplet and a complete quintuplet. However, we remark that Dolez & Kleinman (1997) found a peak at 1520.96 μHz during XCOV13 while a peak at 1516.26 μHz (36 in Table 3) was present during XCOV18. They cannot be the same peak because their frequency difference, 4.7 μHz, is 7 and 4 times the frequency resolution of the WET run where they were detected and both are large amplitude peaks (10.7 mma and 10.3 mma respectively), i.e. their frequencies are determined with a much better accuracy

Table 6. Proposed Identification of the modes in HL Tau 76.

Periods (s) (XCOV18)	Period (s) (XCOV13)	Period (s) Archives	ℓ
1390.8			2
	1347.9	1353.7	2
		1308.7	1
1070.8			2
1067.5			1
1065.0	1065.0		1,2
1061.8			1
1060.2			2
979.2			1,2
976.4			1,2
974.4			1,2
971.6			1,2
933.2	932.5		1
930.6			1
799.1			2
798.3			2
796.4	796.5		2
794.1			2
792.7			2
	781.0		1
		748.5	2
738.7:			2
		689.3	2
664.2		665.0	2
663.6			?
662.8			?
662.3			2
661.9			?
661.4			2
660.1			?
659.5			2
	657.4		2
		628.0	2
598.6			1
597.1	597.0		1
596.8			1
542.4			1
541.8			1
540.9	541.0		1
494.2	494.2	494.0	2
493.2			2
	449.8		1
394.3:			1
382.5	382.5		2

than the formal frequency resolution. Such a difference suggests that they could be two consecutive components of an $\ell = 2$ quintuplet. In this case, we get 9 frequencies in this frequency interval that cannot be fit by the overlap of a triplet and a quintuplet. However, one may question the reality of mode 31 (at 1508.71 μHz) whose amplitude (3.49 mma) is small compared to its close neighbours with 11.90 mma amplitude for peak 30 at 1.88 μHz and with 10.84 mma amplitude for peak 32 at 1.12 μHz. It is not certain again that our extraction algorithm can disantangle such a small amplitude peak from such a complex and crowded frequency region. But, even if one rejects the peak 31 as insignificant, one is left with a difficult identification problem for the remaining 8 peaks. Four or five of them could be the components of an $\ell = 2$ mode. That could be either the peaks 30 (1506.83 μHz), 34 (1511.96 μHz), 36 (1516.26 μHz) and the 1520.96 μHz peak seen in XCOV13, separated by 5.1, 4.3 and 4.7 μHz respectively or the peaks 29 (1505.54 μHz), 32 (1509.83 μHz), 34 (1511.96 μHz), 36 (1516.26 μHz) and the 1520.96 μHz of XCOV13, separated by 4.3, 2.1, 4.3 and 4.7 μHz respectively. In the last case one would have a complete quintuplet, rather asymmetrical, with the central component at 1511.96 μHz which fits almost perfectly the predicted $\ell = 2$ mode at 660.4 s. We give a preliminary identification of $\ell = 2$ for those five modes in Table 6. However, there is no $\ell = 1$ mode predicted in this period range able to overlap with the quintuplet. The closest $\ell = 1$ modes are at 1458.1 μHz and 1567.9 μHz far from the frequency range covered by this group of modes, even if one takes into account the rotational splitting. The assumption of an overlap between $\ell = 1$ and $\ell = 2$ modes does not work for this group, at least in the limit of the assumptions made in this paper that the period distribution follows the asymptotic regime. This tentative identification leaves at least 3 modes unexplained which are not small amplitude peaks (12 mma, 7.6 mma and 7.3 mma). They are left with a question mark in Table 6. It should be pointed out that large amplitude variations were observed during XCOV18 in this region (Sect. 4.1). The peaks at 1505.54 μHz (29) and at 1516.26 μHz (36) showed the largest amplitude variations. These variations may explain why we find one close companion to each of these large amplitude peaks (30 and 35). That may be the reason why this frequency domain cannot be satisfactorily interpreted. The two modes below the detection limit of XCOV18 added according to the discussion presented in 5.2.3 are marked with a colon (:).

Kotak et al. (2002b), in their analysis of time-resolved spectroscopy of HL Tau 76, suggest that most of the modes for which they detect a significant peak in the velocity power spectrum are $\ell = 1$ modes (for the periods 657 s, 597 s, 541 s, 494 s and 382 s) while the last one at 781 s would be better identified as an $\ell = 2$ mode. Their proposed identification relies on the value of the parameter R_v, the relative velocity to flux amplitude ratio, after van Kerkwijk et al. (2000). Their identifications are consistent with the values of R_v that they find. Our identifications for the 6 modes we have in common agree for the two modes at 597 s and 541 s, which we also identify as $\ell = 1$ modes, but disagree for the remaining modes. The modes at 657.4 s, 494.2 s and 382.5 s, which we rather identify as $\ell = 2$ modes, should have been detected with a larger relative velocity to flux amplitude ratio than the values they report. We do not offer presently any explanation for this disagreement.

Finally, it is worth comparing the periods found in HL Tau 76 with those of G 29-38 (Kleinman et al. 1998). There are both some similarities and differences. The periods observed in G 29-38 covers also a large range from 110 s to 1240 s, comparable to the range observed in HL Tau 76, from 380 s to 1390 s, but shifted towards shorter periods. Since G 29-38 is both hotter and more massive than HL Tau 76 (11 820 K and 0.69 $M_{\odot}$, according to Bergeron et al. 2004), such a global shift to shorter periods is expected. The main difference is that while all the periods seen in G 29-38 may be attributed to $\ell = 1$ modes, HL Tau 76 exhibits a more complex mixture of $\ell = 1$ and $\ell = 2$ modes, with some overlapping between both as discussed above. Among the modes identified as $\ell = 1$ in HL Tau 76, we find many similarities with the periods found in G 29-38: for instance the period at 933 s, 781 s, 597 s, 542 s and 394 s in HL Tau 76 are close to the periods at 915 s, 771 s, 610 s, 552 s and 400 s, respectively, in G 29-38. But all the other similar periods do not correspond to similar ℓ values in both stars.

5.3. Rotation rate

From the multiplets identified in HL Tau 76 we can derive the average rotation period of the star. In averaging the frequency separation of the doublets and the triplets, all considered as $\ell = 1$ modes split by rotation, we have obtained an average rotational splitting $\delta f = 2.54$ μHz. The average rotation period derived from the rotational splitting is 2.2 days. This rotational period for HL Tau 76 is in the range of rotation periods derived from asteroseismology for other pulsating white dwarfs. It confirms that low and intermediate mass stars lose most of their angular momentum during their evolution from the main sequence to the white dwarfs. There is no significant signature of a dependence of the rotational splitting on the period, which is compatible with a uniform rotation but does not prove it (Kawaler et al. 1999). However, since there are quite few rotationally split modes detected in the data analysed here, we cannot exclude a more complex rotation law.

5.4. Search for weak magnetic field

The fine structure of the Fourier amplitude spectrum reveals only three probable complete triplets and no quintuplets. The triplets are formed by the peaks 41−43−44, 16−17−18 or 17−18−19 and 11−12−14, in the order of increasing period. These triplets are interpreted as $\ell = 1$ modes split by rotation. Rotation by itself would produce symmetric triplets in the limit of slow rotation. However none of the observed triplets is symmetrical. The asymmetry could result from second order rotation effects or from magnetic field. With an average rotation period of 2.2 days, we do not expect the second order effects of rotation to have any detectable consequence on rotational splitting. The influence of weak magnetic fields on the g-modes in white dwarfs has been analysed by Jones et al. (1989). Their effect is to shift the frequencies to higher values proportionally to m^2B^2 and the frequency shifts increase with the order of the mode, i.e. with the period. This produces an asymmetry in the triplets, $\Delta f_m = [(f_{m=+1} - f_{m=0}) - (f_{m=0} - f_{m=-1})]/2$, the retrograde component $m = -1$ being closer to the central component $m = 0$ than the prograde component $m = +1$. The two triplets 41−43−44 and 11−12−14 are very similar in their asymmetry with $f_{m=0} - f_{m=-1} = 2.26\ \mu$Hz in both cases and $f_{m=+1} - f_{m=0} = 2.84\ \mu$Hz and 2.81 μHz respectively. In the case of the third triplet, we discussed the two plausible solutions where the triplet could be formed by the peaks 16−17−18 or 17−18−19. If the triplet is formed by the peak 16−17−18, the observed asymmetry cannot be due to the effect of magnetic field since $f_{m=0} - f_{m=-1} = 2.93\ \mu$Hz and $f_{m=+1} - f_{m=0} = 2.04\ \mu$Hz, i.e. the $m = \pm1$ would be shifted in the wrong direction. If the triplet is 17−18−19 we find $f_{m=0} - f_{m=-1} = 2.04\ \mu$Hz and $f_{m=+1} - f_{m=0} = 3.0\ \mu$Hz. If we assume that the asymmetry in the triplets is due to a weak magnetic field, this rules out the solution 16−17−18 for the third triplet. The asymmetry ($\Delta f_m = 0.29\ \mu$Hz) observed in the best identified triplet (41−43−44) centered at the period of 541 s could be explained with a weak dipole field of $\approx 1-2 \times 10^3$ G, from the results of Jones et al. (their Fig. 1). However, when we consider the other two triplets we do not find the expected variation of the frequency shift with increasing period: $\Delta f_m = 0.48\ \mu$Hz at 974 s for the triplet 17−18−19 but $\Delta f_m = 0.28\ \mu$Hz at 1065 s for the triplet 11−12−14. If there is a hint for the presence of a weak magnetic field in HL Tau 76, as inferred from the asymmetrical triplets, there is no conclusive evidence. Since there is no complete $\ell = 2$ quintuplets, it is not possible to check the effect of the m^2 dependence on the frequency shift.

5.5. Mass of the H outer layers

The average period spacing for $\ell = 1$ modes derived from the present study is $\Delta P = 48.0$ s. This value translates to $\Pi_0 = 67.9$ s. A detailed comparison of the periods of observed $\ell = 1$ and $\ell = 2$ modes with the periods of modes calculated in a grid of models will be presented in a forthcoming paper. It should provide the model or series of models best fitting the observed periods. With a total of $\approx$40 observed modes, the model should be rather well constrained if the pulsations of HL Tau 76 are still well described by linear nonradial pulsation theory. As HL Tau 76 shows this large number of modes on an extended range of periods, from 382 s to 1390 s, there are very few modes of consecutive orders for a given degree. Due to this unfortunate circumstance, one cannot build the period spacing-Period (ΔP-vs.-P) diagram which would have provided a useful tool to search for evidence of mode trapping. Considering Table 5-1 for $\ell = 1$ modes, one finds only few modes of consecutive order separated by a number of missing modes. While the data are compatible with a distribution of periods covering as much as 23 orders, one finds 14 possibly consecutive order modes. The situation is similar for the $\ell = 2$ modes (Table 5-2) where the entire period range covers 37 orders but where one finds only 9 possibly consecutive order modes. Hopefully, future observations may reveal additional modes which could fill the gaps so that a period spacing-vs.-period diagram could eventually be built.

In comparing with the published models, those of Brassard et al. (1992) for instance, one finds a series close enough to HL Tau 76 with a total mass of 0.6 $M_\odot$, effective temperature of $\approx$12 000 K, and a range in hydrogen mass fraction $-14 \leq \log q_{\rm H} \leq -4$ and helium mass fraction $-8 \leq \log q_{\rm He} \leq -2$. The sensitivity of the period spacing to the various stellar parameters may be estimated from those results. For HL Tau 76, the total mass is $.55 \pm 0.03\ M_\odot$ and $T_{\rm eff} = 11\,440 \pm 350$ K (Bergeron et al. 1995). Within this small range of total mass and effective temperature, the dominant effect on the period spacing is due to the hydrogen mass fraction. In comparing with the various models of this sequence of Brassard's models (their Tables 2−5), one finds that HL Tau 76 period distribution is compatible with their moderately "thick" hydrogen models with $\log (q_{\rm H}) \geq -7.0$. A precise constraint on the stellar parameters of HL Tau 76 must await a detailed comparison of the periods calculated for realistic models of HL Tau 76 with the observations described here. This is out of the scope of the present paper and will be presented in a forthcoming publication.

6. Summary

We have analysed the light curve of HL Tau 76 obtained during the WET XCOV18 campaign. We found as many as 78 peaks in the power spectrum. After eliminating the linear combinations, we are left with 36 significant independent modes. That is the richest spectrum found in any of the ZZ Ceti white dwarfs studied so far. The range of periods present in HL Tau 76 is exceptionally large, from 380 s for the shortest period to 1390 s for the longest. HL Tau 76 belongs to the group of ZZ Ceti stars close to the red edge of the instability strip which show both short and long periods. The presence of short periods in HL Tau 76, which belong to modes which seem to be still in the asymptotic regime, suggests that HL Tau 76 must have a moderatly "thick" hydrogen layer. We identified a few multiplets, doublets and triplets, which we interpret as $\ell = 1$ modes split by rotation. From these multiplets we have derived an average period spacing of 48.0 s for the $\ell = 1$ modes. By assuming that the modes observed in HL Tau 76 are in the asymptotic regime, we estimated the expected periods for consecutive order $\ell = 1$ modes. The comparison with the observed periods leads to the identification of other $\ell = 1$ modes. Some complex regions of the power spectrum are interpreted as due to overlapping $\ell = 1$ and $\ell = 2$ modes of close periods. We found some cases of doubtful identification since overlapping $\ell = 1$ and $\ell = 2$ modes are not rare. We also identify a number of $\ell = 2$ modes which do not overlap with $\ell = 1$ modes.

Having identified $\ell = 1$ and $\ell = 2$ modes in the XCOV18 data, we looked back in earlier data, the WET XCOV13 and earlier archival data, to check that the periods extracted from those data do fit satisfactorily the $\ell = 1$ and $\ell = 2$ identifications proposed here. In doing this, we found 7 more independent modes which fit nicely the expected period distribution. We propose a preliminary identification for most of the 43 modes detected in HL Tau 76.

The rotation period derived from the rotational splitting is 2.2 days. There is no evidence for a dependence of the rotational splitting on the periods, which is compatible with the assumption that HL Tau 76 is rotating as a solid body at least in the outer layers.

Assuming the total mass and effective temperature well determined from spectroscopy, the period spacing may be used to estimate that the hydrogen mass fraction must be $\log(q_{\rm H}) \geq -7.0$. In spite of the large number of modes present in HL Tau 76, their distribution within an extended range, between 380 s and 1390 s, does not allow to build a period spacing-vs.-Period diagram (ΔP-vs.-P diagram) because of the large number of missing modes and the small number of consecutive order modes. As a consequence, it is not possible from the available data to derive information on potential mode trapping which would give another way to estimate the hydrogen mass fraction.

A detailed comparison between the observed periods determined in the present work and the periods of realistic models representative of HL Tau 76 should constrain more precisely the stellar parameters and the internal structure of HL Tau 76.

Acknowledgements. The WET acknowledges support from the U.S. National Science Foundation, through Grants AST-0205983 and AST-9877665 to Iowa State University. We thank Paul Bradley for his carefull reading of an earlier version of the manuscript and an anonymous referee whose recommendations helped improving a first version of this paper.

References

Abazajian, K., Adelman-McCarthy, J. K., Agüeros, M. A., et al. 2003, AJ, 126, 2081
Bergeron, P., Fontaine, G., Brassard, P., et al. 1993, AJ, 106, 1987
Bergeron, P., Wesemael, F., Lamontagne, R., et al. 1995, ApJ, 449, 258
Bergeron, P., Fontaine, G., Billères, M., Boudreault, S., & Green, E. M. 2004, ApJ, 600, 404
Bradley, P. A. 1993, Ph.D. Thesis, University of Texas at Austin
Bradley, P. A. 1998, ApJS, 116, 307
Bradley, P. A. 2001, ApJ, 552, 326
Brassard, P., Fontaine, G., Wesemael, F., & Tassoul, M. 1992, ApJS, 81, 747
Brickhill, A. J. 1983, MNRAS, 204, 537
Brickhill, A. J. 1990, MNRAS, 246, 510
Brickhill, A. J. 1991a, MNRAS, 251, 537
Brickhill, A. J. 1991b, MNRAS, 252, 334
Clemens, J. C. 1993, Baltic Astron., 2, 407
Clemens, J. C., van Kerkwijk, M. H., & Wu, Y. 2000, MNRAS, 314, 220
Corsico, A. H., Althaus, L. G., Benvenuto, O. G., & Serenelli, A. M. 2002, A&A, 387, 531
Dolez, N., & Vauclair, G. 1981, A&A, 102, 375
Dolez, N., & Kleinman, S. J. 1997, in White Dwarfs, ed. I. Isern et al. (Kluwer Academic Publishers), 437
Fitch, W. S. 1973, ApJ, 181, L95
Fleming, T. A., Liebert, J., & Green, R. F. 1986, ApJ, 308, 176
Fontaine, G., & Brassard, P. 2004, 14th European Workshop on White Dwarfs, ed. D. Koester, & S. Moehler, 565
Fontaine, G., Brassard, P., & Bergeron, P. 2001, PASP, 113, 409
Fontaine, G., Bergeron, P., Billères, M., & Charpinet, S. 2003, ApJ, 591, 1184
Goldreich, P., & Wu, Y. 1999a, ApJ, 511, 904
Goldreich, P., & Wu, Y. 1999b, ApJ, 523, 805
Harris, H., Liebert, J., Kleinman, S. J., et al. 2003, AJ, 126, 1023
Jones, P. W., Hansen, C. J., Pesnell, W. D., et al. 1989, ApJ, 336, 403
Kanaan, A., Nitta, A., Winget, D. E., et al. 2005, A&A, 432, 219
Kawaler, S. D., Sekii, T., & Gough, D. 1999, ApJ, 516, 349
Kepler, S. O. 1993, BaltA, 2, 515
Kepler, S. O., Giovannini, O., Wood, M. A., et al. 1995, ApJ, 447, 874
Kepler, S. O., Mukadam, A., Winglet, D. E., et al. 2000a, ApJ, 534, 185
Kepler, S. O., Robinson, E. L., Koester, D., et al. 2000b, ApJ, 539, 379
Kepler, S. O., Nather, R. E., Winget, D. E., et al. 2003, A&A, 401, 639
Kleinman, S. J., Nather, R. E., & Phillips, T. 1996, PASP, 108, 356
Kleinman, S. J., Nather, R. E., Winget, D. E., et al. 1998, ApJ, 495, 424
Kleinman, S. J., Harris, H. C., Eisenstein, D. J., et al. 2004, ApJ, 607, 426
Kotak, R., van Kerkwijk, M. H., Clemens, J. C., & Bida, T. A. 2002a, A&A, 388, 219
Kotak, R., van Kerkwijk, M. H., Clemens, J. C., & Bida, T. A. 2002b, A&A, 391, 1005
Landolt, A. U. 1968, ApJ, 153, 151
Metcalfe, T. S., Montgomery, M. H., & Kanaan, A. 2004, ApJ, 605, L133
Mukadam, A., Kepler, S. O., Winget, D. E., & Bergeron, P. 2002, ApJ, 580, 429
Mukadam, A., Mullaly, F., Nather, R. E., et al. 2004a, ApJ, 607, 982
Mukadam, A., Winget, D. E., von Hippel, T., et al. 2004b, ApJ, 612, 1052
Nather, R. E., Winget, D. E., Clemens, J. C., et al. 1990, ApJ, 361, 309
Page, C. G. 1972, MNRAS, 159, 25
Pfeiffer, B., Vauclair, G., Dolez, N., et al. 1996, A&A, 314, 182
Robinson, E. L., Mailloux, T. M., Zhang, E., et al. 1995, ApJ, 438, 908
Scargle, J. D. 1982, ApJ, 263, 835
Tassoul, M. 1980, ApJS, 43, 469
Thompson, S., Clemens, J. C., van Kerkwijk, M. H., & Koester, D. 2003, ApJ, 589, 1001
Thompson, S., Clemens, J. C., van Kerkwijk, M. H., et al. 2004, ApJ, 610, 921
van Kerkwijk, M. H., Clemens, J. C., & Wu. Y. 2000, MNRAS, 314, 209
Vauclair, G., Moskalik, P., Pfeiffer, B., et al. 2002, A&A, 381, 122
Warner, B., & Nather, R. E. 1970, MNRAS, 147, 21
Warner, B., & Nather, R. E. 1972, MNRAS, 156, 1
Winget, D. E., & Van Horn, H. M. 1987, IAU Coll. 95, The Second Conference on Faint Blue Stars, ed. A. G. Davis Philip, D. S. Hayes, & J. W. Liebert (New York: L. Davis Press Inc., Schenectady), 363
Winget, D. E., Van Horn, H. M., Tassoul, M., et al. 1982, ApJ, 252, L65
Winget, D. E., Hansen, C. J., Liebert, J. W., et al. 1987, ApJ, 315, 77
Winget, D. E., Nather, R. E., Clemens, J. C., et al. 1991, ApJ, 378, 326
Winget, D. E., Nather, R. E., Clemens, J. C., et al. 1994, ApJ, 430, 839
Wood, M. A. 1995, in White Dwarfs, ed. D. Koester, & K. Werner (Berlin: Springer), 41
Wu, Y. 2001, MNRAS, 323, 248
Wu, Y., & Goldreich, P. 1999, ApJ, 519, 783
Wu, Y., & Goldreich, P. 2001, ApJ, 546, 469

[1] Université Paul Sabatier, Observatoire Midi-Pyrénées, CNRS/UMR5572, 14 Av. E. Belin, 31400 Toulouse, France
[2] Sloan Digital Sky Survey, Apache Point Observatory, PO Box 59, Sunspot, NM 88349, USA
[3] Observatoire de Paris-Meudon, LESIA, 92195 Meudon, France
[4] Department of Physics, University of Tromsø, 9037 Tromsø, Norway
[5] Departamento de Fisica Aplicada, Universidade de Vigo, 36200 Vigo, Spain
[6] Universidade Federal de Santa Catarina, Florianopolis, SC, Brazil
[7] Department of Physics and Astronomy, Iowa State University, Ames, IA 50011, USA
[8] Department of Astronomy and McDonald Observatory, Texas University at Austin, Austin, TX 78712, USA
[9] Department of Physics and Space Sciences and SARA Observatory, Florida Institute of Technology, Melbourne, FL 32901, USA
[10] School of Chemical and Physical Sciences, Victoria University of Wellington, PO Box 600, Wellington, New-Zealand
[11] National Astronomical Observatories, Chinese Academy of Sciences, 20A, Datun Road, Beijing 100012, PR China
[12] Indian Space Research Organization, Airport Road, Vimanapura PO, Bangalore 560 017, India
[13] Wise Observatory, Tel Aviv University, Tel Aviv 69978, Israel
[14] South African Astronomical Observatory, PO Box 9, Cape Town, 7935 South-Africa
[15] Vilnius University Research Institute of Theoretical Physics and Astronomy, A. Gostauto 12, 01108 Vilnius, Lithuania
[16] Copernicus Astronomical Center, Ul. Bartycka 18, 00-716 Warsaw, Poland
[17] Mt. Suhora Observatory, Cracow Pedagogical University, Ul. Podchorazych 2, 30-084 Cracow, Poland
[18] Institut für Astronomie Universität Wien, Tükenschanzstrasse 17, 1180, Austria
[19] Osservatorio Astronomico di Capodimonte, via Moiariello 16, 80131, Napoli, Italy
[20] Astronomy Group, Vrije Universiteit Brussel (VUB), Pleinlaan 2, 1050 Brussel, Belgium
[21] Institute of Theoretical Astrophysics, University of Oslo, P. Box 1029, 0315 Oslo, Norway
[22] Present address: Instituto de Astrofisica de Canarias, Tenerife, Spain
[23] Present address: Department of Physics, Astronomy, and Material Science, SW Missouri State University, Springfield, MO 65804, USA
[24] Present address: High Altitude Observatory, PO Box 3000, Boulder, CO 80307-3000, USA
[25] Present address: Department of Physics and Astronomy, Middle Tennessee State University, Murfreesboro, TN 37132, USA
[26] Present address Department of Astronomy, Box 351580, University of Washington, Seattle, WA 98195-1580, USA

Online Material

Table 2. Journal of observations: 1999 WET (XCOV18).

Run name	Telescope	Date (UT)	Start time (UTC)	Run length (s)
suh-79	Suhora 0.6 m	30 Oct. 99	20:52:00	15 440
jxj-9935	BAO 0.85 m	1 Nov. 99	13:36:40	28 480
suh-80	Suhora 0.6 m	1 Nov. 99	18:24:20	32 240
tsm-0050	McDonald 2.1 m	2 Nov. 99	04:39:30	21 810
sara-016	KPNO SARA 0.9 m	2 Nov. 99	05:11:08	19 010 CCD
jxj-9937	BAO 0.85 m	2 Nov. 99	13:53:00	28 030
suh-81	Suhora 0.6 m	2 Nov. 99	17:48:30	32 800
teide01	IAC 0.8 m	3 Nov. 99	02:10:30	14920
sara-017	KPNO SARA 0.9 m	3 Nov. 99	04:09:35	6210 CCD
tsm-0052	McDonald 2.1 m	3 Nov. 99	04:40:00	26 760
jxj-9938	BAO 0.85 m	3 Nov. 99	13:41:00	28780
teide02	IAC 0.8 m	3 Nov. 99	23:45:50	23830
sara-018	KPNO SARA 0.9 m	4 Nov. 99	03:51:13	32 700 CCD
jxj-9939	BAO 0.85 m	4 Nov. 99	13:23:20	30 010
suh-82	Suhora 0.6 m	4 Nov. 99	17:21:00	34 900
HL1104OI	OHP 1.9 m	4 Nov. 99	21:45:00	24 240
tsm-0054	McDonald 2.1 m	5 Nov. 99	04:21:30	28 110
sara-019	KPNO SARA 0.9 m	5 Nov. 99	05:16:28	28 280 CCD
suh-83	Suhora 0.6 m	5 Nov. 99	17:57:00	31 850
sara-020	KPNO SARA 0.9 m	6 Nov. 99	03:12:32	9910 CCD
tsm-0056	McDonald 2.1 m	6 Nov. 99	04:42:30	26 250
N49-0423	Naini Tal 1.0 m	6 Nov. 99	19:51:30	14 060
HL1106OJ	OHP 1.9 m	6 Nov. 99	22:01:00	22 820
tsm-0058	McDonald 2.1 m	7 Nov. 99	04:17:30	28 650
jxj-9940	BAO 0.85 m	7 Nov. 99	13:30:30	30 700
n49-0424	Naini Tal 1.0 m	7 Nov. 99	17:25:00	23 010
hl1107oi	OHP 1.9 m	7 Nov. 99	20:09:00	27 040
teide04	IAC 0.8 m	8 Nov. 99	01:30:10	17 750
mdr073	CTIO 1.5 m	8 Nov. 99	04:39:10	14 570
no0899q1	Hawaii UH 0.6 m	8 Nov. 99	08:48:40	24 110
jxj-9941	BAO 0.85 m	8 Nov. 99	13:15:30	30 490
wccd-001	Wise, 1 m	8 Nov. 99	18:30:00	27 580 CCD
HL1108OJ	OHP 1.93 m	8 Nov. 99	20:53:00	27 160
teide05	IAC 0.8 m	9 Nov. 99	00:06:30	22 360
sara-021	KPNO SARA 0.9 m	9 Nov. 99	03:38:30	32 200 CCD
mdr076	CTIO 1.5 m	9 Nov. 99	04:37:50	6130

Table 2. continued.

Run name	Telescope	Date (UT)	Start time (UTC)	Run length (s)
no0999q1	Hawaii 0.6 m	9 Nov. 99	07:54:40	27 440
tsm-0059	McDonald 2.1 m	9 Nov. 99	09:04:00	11 160
wccd-005	Wise 1.0 m	9 Nov. 99	18:57:00	16 990 CCD
HL1109OI	OHP 1.93 m	9 Nov. 99	21:11:00	28 230
teide06	IAC 0.8 m	9 Nov. 99	21:26:30	26 500
lo09-1.dat	Loiano 1.5 m	9 Nov. 99	22:32:40	20 660
sara-022	KPNO SARA 0.9 m	10 Nov. 99	03:05:29	14 100 CCD
tsm-0061	McDonald 2.1 m	10 Nov. 99	03:25:30	30 600
no1099q1	Hawaii 0.6 m	10 Nov. 99	07:54:00	27 350
N49-0429	Naini Tal 1 m	10 Nov. 99	17:52:30	21 470
wccd-008	Wise 1.0 m	10 Nov. 99	18:49:10	27 970 CCD
HL1110OJ	OHP 1.9 m	10 Nov. 99	20:35:00	29 470
teide07	IAC 0.8 m	10 Nov. 99	23:12:30	25 260
tsm-0063	McDonald 2.1 m	11 Nov. 99	03:20:00	32 400
no1199q3	Hawaii 0.6 m	11 Nov. 99	11:26:40	14 690
jxj-9942	BAO 0.85 m	11 Nov. 99	17:23:20	2140
wccd-013	Wise 1.0 m	11 Nov. 99	18:54:20	28 500 CCD
teide08	IAC 0.8 m	11 Nov. 99	21:12:30	29 850
tsm-0066	McDonald 2.1 m	12 Nov. 99	03:25:30	20 200
no1299q1	Hawaii 0.6 m	12 Nov. 99	07:20:10	28 140
jxj-9943	BAO 0.85 m	12 Nov. 99	13:12:20	11 920
suh-84	Suhora 0.6 m	12 Nov. 99	17:08:10	40 000
mdr085	CTIO 1.5 m	13 Nov. 99	04:29:20	13 850
no1399q1	Hawaii 0.6 m	13 Nov. 99	07:09:30	24 390
tsm-0067	McDonald 2.1 m	13 Nov. 99	07:29:30	16 830
suh-86	Suhora 0.6 m	13 Nov. 99	17:04:10	19 720
tsm-0069	McDonald 2.1 m	14 Nov. 99	03:13:30	31 100
no1499q2	Hawaii 0.6 m	14 Nov. 99	11:31:10	14 450
edrim01	Moletai 1.65 m	14 Nov. 99	19:18:20	4450
edrim02	Moletai 1.65 m	15 Nov. 99	01:23:20	3510
tsm-0070	McDonald 2.1 m	15 Nov. 99	02:53:00	32 820
no1599q3	Hawaii 0.6 m	15 Nov. 99	11:44:50	13 340
suh-87	Suhora 0.6 m	15 Nov. 99	21:00:10	27 230
tsm-0072	McDonald 2.1 m	16 Nov. 99	03:43:00	29 910
no1699q2	Hawaii 0.6 m	16 Nov. 99	11:20:00	14 700
suh-88	Suhora 0.6 m	16 Nov. 99	16:40:00	17 620
no1799q1	Hawaii 0.6 m	17 Nov. 99	09:43:00	19 810

6.4.2 The unusual pulsation spectrum of the cool ZZ Ceti star HS 0507+0434B

Original paper:

G. Handler, E. Romero-Colmenero, M. H. Montgomery, 2002, MNRAS 335, 399

Mon. Not. R. Astron. Soc. **335,** 399–409 (2002)

The unusual pulsation spectrum of the cool ZZ Ceti star HS 0507+0434B

G. Handler,[1★] E. Romero-Colmenero[1] and M. H. Montgomery[2]

[1] *South African Astronomical Observatory, PO Box 9, Observatory 7935, South Africa*
[2] *Institute for Astronomy, Madingley Road, Cambridge CB3 0HA*

Accepted 2002 April 26. Received 2002 April 22; in original form 2002 February 8

ABSTRACT

We present the analysis of 1 week of single-site high-speed CCD photometric observations of the cool ZZ Ceti star HS 0507+0434B. 10 independent frequencies are detected in the light variations of the star: one singlet and three nearly equally spaced triplets. We argue that these triplets are caused by rotationally split modes of spherical degree $\ell = 1$. This is the first detection of consistent multiplet structure in the amplitude spectrum of a cool ZZ Ceti star and it allows us to determine the rotation period of the star: 1.70 ± 0.11 d.

We report exactly equal *frequency*, not period, spacings between the detected mode groups. In addition, certain pairs of modes from the four principal groups have frequency ratios that are very close to 3 : 4 or 4 : 5; while these ratios are nearly exact (within one part in 10^4), they still lie outside the computed error bars. We speculate that these relationships between different frequencies could be caused by resonances. One of the three triplets may not be constant in amplitude and/or frequency.

We compare our frequency solution for the combination frequencies (of which we detected 38) to Wu's model thereof. We obtain consistent results when trying to infer the convective thermal time and the inclination angle of the rotational axis of the star. Theoretical combination-frequency amplitude spectra also resemble those of the observations well, and direct theoretical predictions of the observed second-order light-curve distortions were also reasonably successful assuming the three triplets are caused by $\ell = 1$ modes. Attempts to reproduce the observed combination frequencies adopting all possible $\ell = 2$ identifications for the triplets did not provide similarly consistent results, supporting their identification with $\ell = 1$.

Key words: stars: individual: HS 0507+0434B – stars: oscillations – stars: variables: other.

1 INTRODUCTION

Asteroseismology is the only observational method that permits the exploration of the deep interior structure of stars. Just as we know about the interior of the Earth from the analysis of earthquakes, the oscillations of pulsating stars are used to probe stellar interiors. Pulsating white dwarf stars are well suited for asteroseismology, as they often show a large number of excited normal modes, each of them carrying a different part of the information. Asteroseismology has therefore been quite successful for some of these objects. The interior structures of the DO star PG 1159-035 (Winget et al. 1991) and the DB white dwarf GD 358 (Winget et al. 1994) were constrained with unprecedented accuracy.

However, this task proved to be more difficult for the coolest known white dwarf pulsators of spectral type DA, the ZZ Ceti or DAV stars (see Kleinman 1999 for a review). They can be separated into two groups, hot and cool ZZ Ceti stars, which show different pulsation properties. The hot ZZ Ceti stars have only a few excited modes of short period (2–5 min) and low amplitude (<0.05 mag), and can, in principle, be understood as a group (Clemens 1994). The cool ZZ Ceti stars, on the other hand, have higher amplitudes (>0.1 mag) and longer periods (≈10 min) than their hotter counterparts and their pulsation spectra are generally variable in time. This, together with their few independent pulsation modes, left them as a mystery for a long time.

The first cool ZZ Ceti star that can be regarded as reasonably well understood is G29-38. Kleinman et al. (1998) finally managed to decipher its pulsational mode structure after 24 different monthly observing runs, including two Whole Earth Telescope (WET, Nather et al. 1990) campaigns! Consequently, it seems that large amounts of data are necessary to understand the pulsations of such stars and, therefore, few cool ZZ Ceti stars are well observed (given their complexity) in terms of time-series photometry.

In the case of HS 0507+0434B, the secondary component in a doubly degenerate DA binary system (Jordan et al. 1998), only a 3-h discovery light curve demonstrating the presence of multiperiodic pulsations was available. The analysis of these data showed

★E-mail: handler@astro.univie.ac.at

Table 1. Time series photometry of HS 0507+0434B.

Run no	Date (UT)	Start (UT)	Run length (h)
1	2000 January 4	22:20:02	2.61
2	2000 January 5	20:00:37	4.65
3	2000 January 6	20:54:23	3.60
4	2000 January 7	19:12:53	4.52
5	2000 January 8	19:13:16	5.31
6	2000 January 9	18:52:58	5.32
7	2000 January 10	18:39:15	6.04
Total			32.05

clear signs of the pulsations of a cool ZZ Ceti star: a few pulsation modes with a number of combination frequencies. However, as HS 0507+0434B is a member of a wide binary system where both components can be assumed to have evolved as single stars, further constraints aiding its modelling can be utilized (see Jordan et al. 1998), which makes HS 0507+0434B of increased interest. Consequently, we decided to study the star in more detail to explore its asteroseismological potential.

2 OBSERVATIONS AND REDUCTIONS

HS 0507+0434B was observed with the University of Cape Town CCD camera (O'Donoghue 1995) on the 0.75-m telescope at the Sutherland station of the South African Astronomical Observatory for seven consecutive nights in 2000 January. The instrument was operated in frame-transfer mode, which allows continuous integrations on the field of choice; integration times of 10 s were used. HS 0507+0434B ($V = 15.36$) and three comparison stars (including HS 0507+0434A, a hotter DA white dwarf) of similar brightness were observed. No filter was used. In every clear night, sky flat-fields were taken during twilight. The journal of our observations is presented in Table 1.

Data reduction was started with correction for bias and flat-field. After examining the nightly mean flat-field images for possible variations (and not finding any), we formed a mean flat-field for the whole run by which each science frame was divided. The stellar magnitudes were determined through point spread function (PSF) fitting with a modified version (O'Donoghue, private communication) of DOPHOT (Schechter, Mateo & Saha 1993). No evidence for variability of any of the comparison stars was found.

We then corrected for differential colour extinction ($k_C \approx 0.04$), indicating that the target is bluer than the ensemble of comparison stars. A correlation of the differential magnitudes of HS 0507+0434B with seeing was not found.

Finally, some low-frequency trends in the data were removed by means of low-order polynomials, and the times of measurement were transformed to a homogeneous time base. Terrestrial time (TT) served as our reference for measurements on the surface of the Earth and a barycentric correction was calculated. As this barycentric correction varied by approximately −1 s throughout a typical run, we applied it point by point. Thus our final time base is barycentric Julian ephemeris date (BJED). The final time series was subjected to frequency analysis. Fig. 1 shows an example light curve.

3 FREQUENCY ANALYSIS

Our frequency analysis was performed with the program PERIOD98 (Sperl 1998). This package applies single-frequency Fourier analysis and simultaneous multifrequency sine-wave fitting. PERIOD98 can also be used to calculate optimal fits for multiperiodic signals including harmonics and combination frequencies at values fixed relative to the 'parent' modes. Such fixed-frequency solutions increase the stability of the results as a result of decreasing the number of free parameters in the fit and by its smaller vulnerability to aliasing and noise problems.

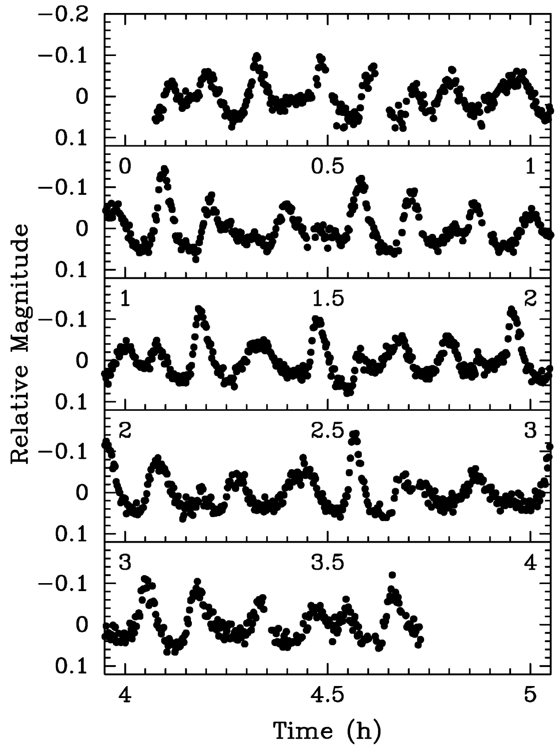

Figure 1. The reduced light curve of HS 0507+0434B from 2000 January 5. Note the multiperiodic variability.

We calculated nightly amplitude spectra of our data; they are shown in Fig. 2. The amplitude spectra of the individual nights are different, but the dominant peaks seem to occur at the same frequencies. Their amplitudes vary, however, and there is no obvious correspondence between the variations of the different peaks. For instance, the peak near 2800 μHz appears to vary less in amplitude than that near 1800 μHz.

As the next step, we combined all the different runs and calculated amplitude spectra for the resulting data set. The full amplitude spectrum is displayed in Fig. 3, which contains a number of dominant features and combination frequencies. Some of the structures are more complicated than a single frequency convolved with the spectral window. We will now concentrate on the three strongest features.

In Fig. 4, we show pre-whitening within these features by simultaneous optimization of the frequencies, amplitudes and phases of all the detected signals. We consecutively removed one, two and three signals from each structure. We adopted the location of the highest peak in each panel as the next frequency to be included in the following fit; we verified that this was indeed the best choice by evaluating the residuals. In the lowest panel of Fig. 4, schematic amplitude spectra composed of the detected signals are shown. All three structures are equally spaced triplets with the central component being lowest in amplitude. The frequency spacings within these triplets are very similar.

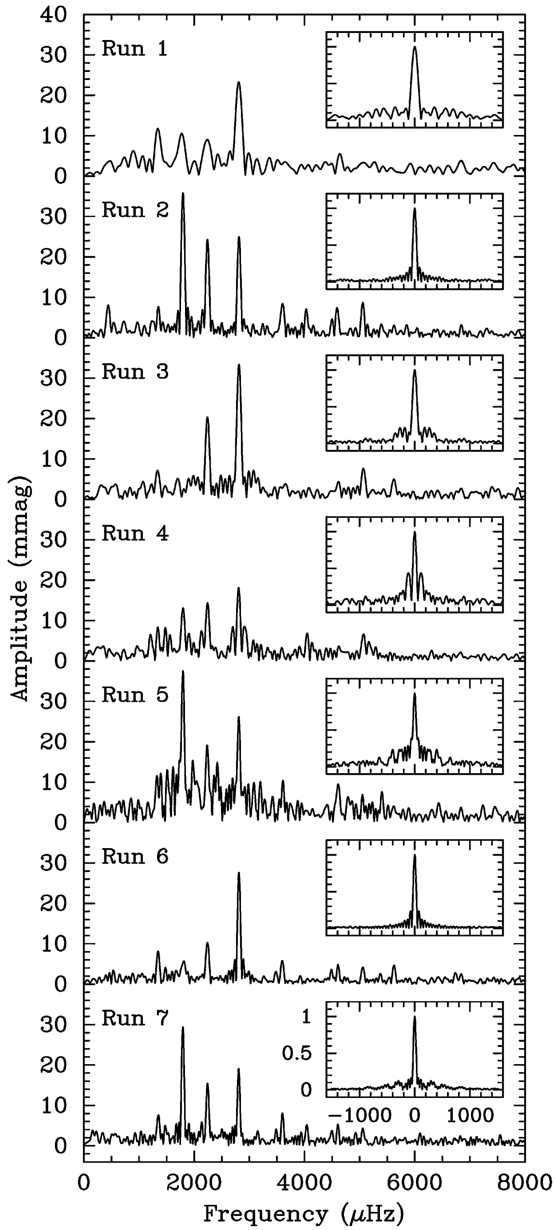

Figure 2. Nightly amplitude spectra of HS 0507+0434B; the corresponding spectral window patterns are shown as insets. There seem to be three dominant signals ('regions of power') which are variable in amplitude. The presence of combination frequencies can also be suspected.

The residual amplitude spectrum after pre-whitening the data with the three triplets is displayed in the upper panel of Fig. 5. Several of the highest peaks were recognized as combinations $m \times f_i \pm n \times f_j$ of these nine frequencies. Using PERIOD98 we verified that this was indeed the case. Consequently, we fixed those frequencies to their exact value predicted from the parent frequencies. We also suspected that more combination frequencies were present in the residuals. We searched for them using the program LINCOM (Kleinman 1995), which finds all possible combinations automatically.

We detected many more combination frequencies clearly exceeding the noise level in the amplitude spectrum. For some of these more than one identification is possible. In such cases, for example, frequency sums or differences of different multiplets that are 'degenerate', we adopted the most plausible one. This would be the one matching best in frequency, the one yielding the lowest residual between the light curve and the fit or the one that would be generated by the highest-amplitude parent modes. Thus we caution that some matches must be regarded as being formal, especially where higher-order combinations are concerned; some of these can have many different potential combinations of parent modes.

After identification and pre-whitening of all detectable combination frequencies of the components of the three triplets, we calculated the residual amplitude spectrum (second panel of Fig. 5). One dominant peak and a few other signals are visible. Including this highest peak and its combinations with previously detected signals into the multifrequency solution and pre-whitening it from the data results in the new residual amplitude spectrum shown in the third panel of Fig. 5. Some peaks still exceed the noise level in this amplitude spectrum considerably; thus their frequencies and amplitudes were determined as well. The final residual amplitude spectrum can be found in the lowest panel of Fig. 5.

The multifrequency solution we derived is summarized in Table 2 together with 1σ error estimates calculated with the formulae from Montgomery & O'Donoghue (1999). The detected signals are ordered in the following way: corresponding to increasing frequency, the independent modes are listed first, then two-mode frequency sums followed by two-mode frequency differences, three-mode frequency combinations, then fourth-order combinations and finally further signals, some with suggested identifications.

As mentioned previously, the frequency spacing of the three triplets among the 10 'fundamental' frequencies is very similar. Consequently, we examined whether this spacing can be assumed to be exactly the same by calculating a forced fit with PERIOD98, but residual amplitude spectra then showed conspicuous mounds of power in the frequency domains of the triplets. This suggests that either the spacing between their components is not exactly the same, or that (some of) the triplet components are not constant in amplitude and/or frequency over the whole data set, or that the light variations require a more complicated description than the frequency triplets provide.

Our results depend strongly on the correctness of the determination of the independent frequencies. To check their reliability, we repeated the frequency analysis, removing single nights from the total data set, thus restricting ourselves to six nights of data only. We independently recovered the correct frequencies in all seven possible subsets. Although light curves of pulsating white dwarf stars are in most cases only decipherable with observations from many sites, as used, for example, by the WET, in this special case we think we were fortunate enough to do so with single-site data only.

4 DISCUSSION AND INTERPRETATION

The discussion of the pulsation spectrum of HS 0507+0434B is separated into several sections. Section 4.1 deals with the interpretation of the 10 'fundamental frequencies', in Section 4.2 we attempt an interpretation of the 'further' signals (cf. Table 2), and in Section 4.3 we will examine the combination frequencies.

4.1 The 10 'fundamental frequencies'

4.1.1 Mode identification

The pulsation spectrum of HS 0507+0434B is reminiscent of a cool ZZ Ceti star: there are a few independent frequencies and many combinations of these. A very important finding based on the 10

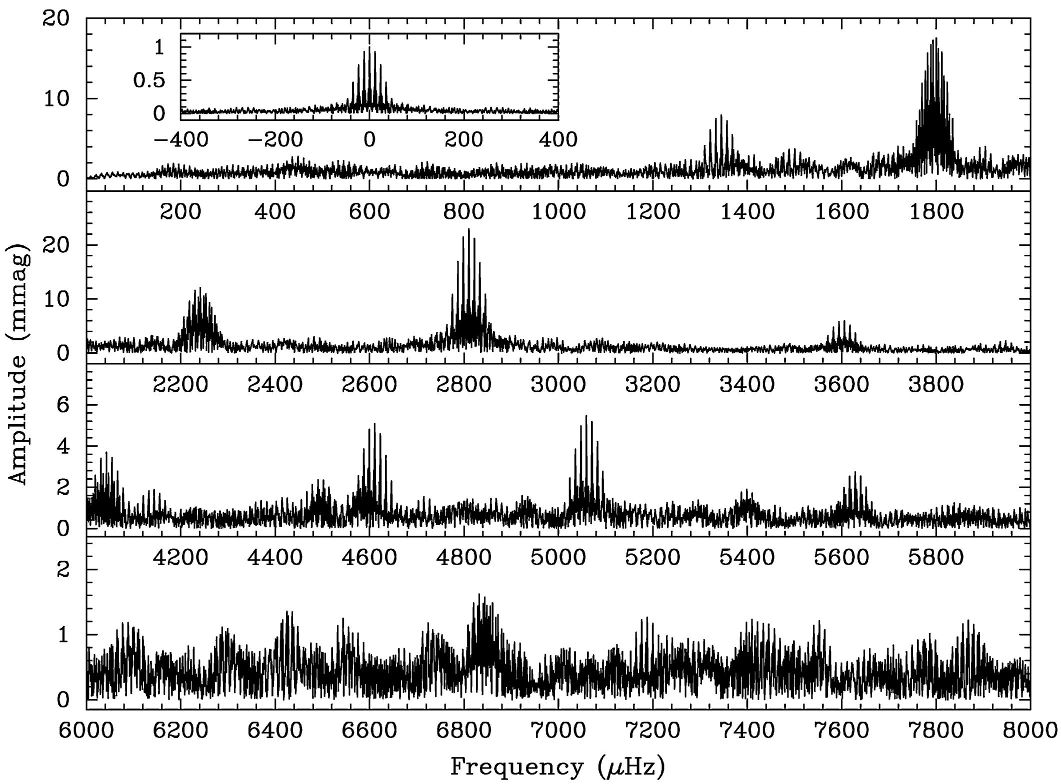

Figure 3. Amplitude spectrum of our combined HS 0507+0434B data. The inset is the spectral window of the data. As our data were taken from a single site only, aliasing is present. Note the different ordinate scale of each panel.

'fundamental' frequencies is that three equally spaced triplets are among them. Moreover, all three triplets have the same basic structure in amplitude: the central component is the weakest.

We suggest that these three independent frequency triplets are caused by non-radial gravity (g) mode pulsations: the appearance and complexity of the pulsation spectrum leaves pulsation as the only explanation for the light variations. Since the fundamental radial mode of a ZZ Ceti star has a period of only a few seconds, but the observed time-scales of the pulsations are much longer, they must be caused by g-modes, which are normal-mode pulsations.

We now attempt to constrain the spherical degree ℓ of the pulsations. Modes of $\ell > 2$ are not expected to be detectable owing to geometrical cancellation of the variations over the visible stellar disc (Dziembowski 1977). We are therefore left with the possibilities of modes of $\ell = 1$ only, $\ell = 2$ only, or a mixture of these. We restrict the following discussion to the three nearly equally spaced triplets, as we have no means to constrain the ℓ value of f_1 at this point.

For the three triplets, an explanation in terms of $\ell = 2$ modes only is unlikely, as one would need to invoke some mode selection mechanism, a specific inclination of the stellar pulsation axis to the line of sight, or chance, to produce the more or less consistent triplet structure observed.

A more natural explanation of the three triplets is that they are all caused by $\ell = 1$ modes. The frequency splitting within the triplets is very similar, and no special effects need to be assumed to produce such structures with $\ell = 1$ modes.

The presence of a mixture of $\ell = 1$ and 2 cannot conclusively be ruled out, although it would be contrived. The different amount of rotational splitting (with a ratio of approximately 0.6, see Winget et al. 1991) within mode groups of $\ell = 1$ and 2 would be immediately obvious, unless single modes intruding into multiplets of the other ℓ would have just the right frequency to fit into the pattern. We consider this unlikely. In any case, if a mixture of both spherical degrees was observed, it is more likely that most of the detected frequencies are caused by $\ell = 1$ modes because of the arguments given previously.

Consequently, we believe that the most likely mode identification for the observed triplets in the amplitude spectra of HS 0507+0434B is that they are all caused by rotationally split modes of spherical degree $\ell = 1$. From experience with other ZZ Ceti stars we must, however, be somewhat cautious with arguments based on this identification.

4.1.2 Pulsation periods

Kleinman (1999) summarized the preferred pulsation periods of ZZ Ceti stars, with particular focus on the cooler variables. He found concise groupings of modes from 350 to 650 s, with a typical spacing of 50 s. Our three presumed $\ell = 1$ triplets fit this pattern nicely (they are close to the 'preferred' periods of 359, 454 and 546 s), which supports our mode identification further. Conversely, if the pulsation modes of HS 0507+0434B were not predominantly $\ell = 1$, this would represent a challenge for Kleinman's (1999) identifications (if HS 0507+0434B is a normal ZZ Ceti star), which we, however, believe to be on solid ground.

Using the periods listed by Kleinman (1999) as a template, we note that there are gaps within the frequencies of the triplets of HS 0507+0434B where additional $\ell = 1$ modes would be expected, suggesting that some possible radial overtones are not excited to

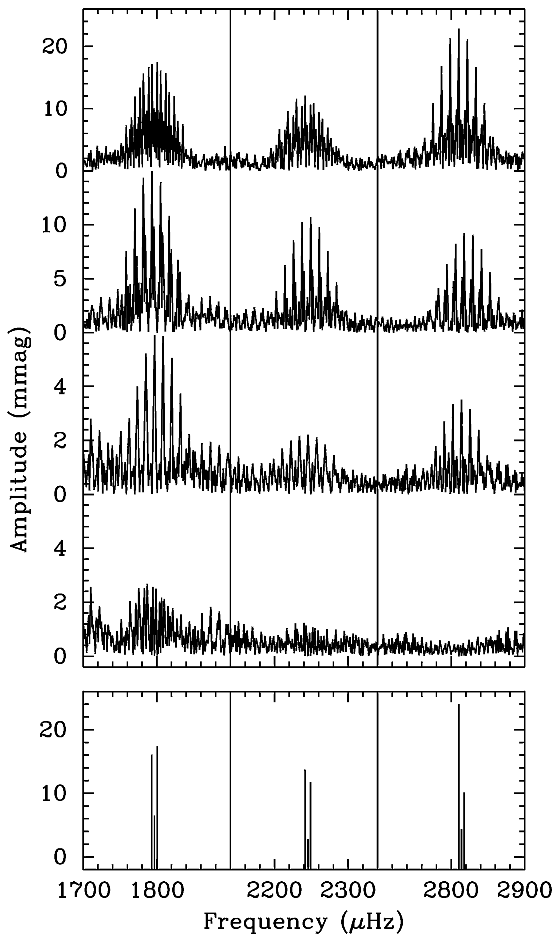

Figure 4. Amplitude spectra of our HS 0507+0434B data in the vicinity of the dominant features. Upper panel, original data; second panel from top, amplitude spectrum after pre-whitening of one frequency in each section; third panel, after pre-whitening of two frequencies each; fourth panel, three frequencies each pre-whitened. The lowest panel shows the detected frequencies with the corresponding amplitudes schematically. Note the change of the ordinate scale between the different panels.

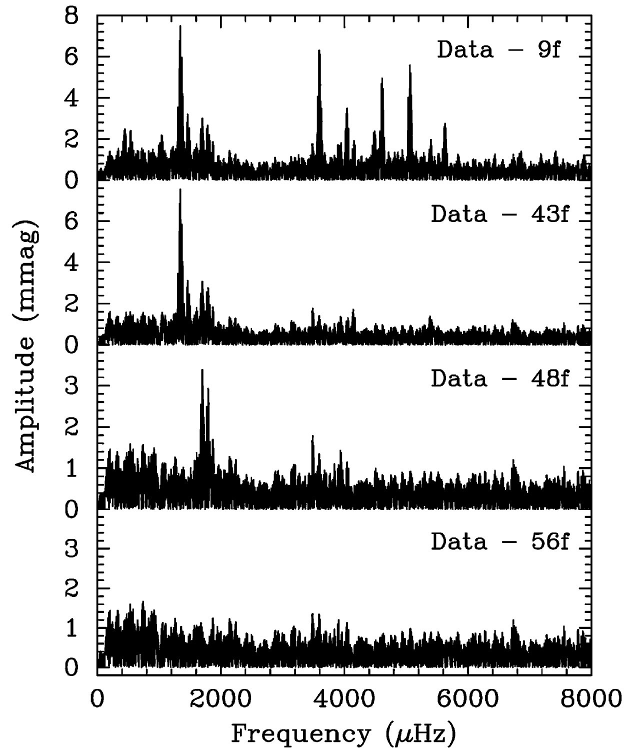

Figure 5. Residual amplitude spectra of HS 0507+0434B with consecutive pre-whitening of detected signals. Uppermost panel, residuals after pre-whitening of the three triplets decomposed in Fig. 4. Second panel, residuals after pre-whitening these triplets and their frequency combinations. Third panel (ordinate scale magnified), residuals after subtracting one more signal plus its combinations. Lowest panel, residuals after including seven more (partly suspected) periodicities.

detectable amplitudes. In addition, the 743-s singlet falls into a period region where no clear groupings of modes are observed in the ensemble of cool ZZ Ceti stars investigated by Kleinman (1999).

The gaps in the suspected $\ell = 1$ mode pattern of HS 0507+0434B, combined with the effects of mode trapping in ZZ Ceti star pulsation models (Brassard et al. 1992a), also preclude an asteroseismological mass estimate based on our data. More independent modes need to be detected.

4.1.3 Rotation of HS 0507+0434B

We use the frequency spacings within the three triplets to determine the rotation period of HS 0507+0434B. The average frequency separation between the outer two components of the triplets is 7.48 ± 0.07 μHz. Assuming that all modes are $\ell = 1$, that the star rotates uniformly and adopting first-order rotational splitting coefficients $C_{k,\ell}$ from Brassard et al. (1992b, for masses around 0.6 $M_\odot$ and radial overtones corresponding to the observed period range), this leads to a rotation period of $P_{\rm rot} = 1.70 \pm 0.11$ d. The main contribution to the uncertainty in $P_{\rm rot}$ comes from the poorly constrained $C_{k,\ell}$. The dependence of $C_{k,\ell}$ on the radial overtone may be one of the reasons why the triplets do not show exactly the same spacing. Our estimate of the rotation period is perhaps the most reliable for any cool ZZ Ceti star to date: consistent multiplet structure has never been observed in these objects before.

We can also derive the inclination angle Θ from the relative amplitudes within the triplets, but this requires several questionable assumptions, the most important of which is equal physical

Table 2. Our multifrequency solution for HS 0507+0434B. Individual error estimates are quoted for the independent frequencies and periods; the amplitude uncertainty is ±0.2 mmag. Frequencies are given in μHz, amplitudes in mmag and periods in seconds. Combinations marked with asterisks were detected outright.

	Independent signals		
ID	Frequency	Amplitude	Period
f_1	1345.22 ± 0.03	7.6	743.373 ± 0.017
f_2	1793.31 ± 0.02	16.0	557.628 ± 0.005
f_3	1796.81 ± 0.03	7.2	556.542 ± 0.010
f_4	1800.70 ± 0.01	16.6	555.341 ± 0.004
f_5	2241.47 ± 0.02	13.9	446.136 ± 0.003
f_6	2245.63 ± 0.08	2.8	445.309 ± 0.017
f_7	2249.01 ± 0.02	11.9	444.641 ± 0.004
f_8	2810.37 ± 0.01	24.0	355.826 ± 0.001
f_9	2814.00 ± 0.05	4.3	355.366 ± 0.007
f_{10}	2817.89 ± 0.02	10.2	354.875 ± 0.003

Table 2 – *continued*

Combination frequencies			
ID	Combination	Frequency	Amplitude
f_{11}	$f_1 + f_4$	3145.92	0.9
f_{12}^*	$f_2 + f_4$	3594.01	6.4
f_{13}	$f_3 + f_4$	3597.51	1.1
f_{14}	$2f_4$	3601.40	1.6
f_{15}	$f_2 + f_5$	4034.78	1.1
f_{16}	$f_3 + f_5$	4038.28	1.7
f_{17}^*	$f_4 + f_5$	4042.17	3.3
f_{18}	$f_1 + f_8$	4155.59	1.6
f_{19}^*	$f_5 + f_7$	4490.48	2.5
f_{20}	$f_2 + f_8$	4603.68	2.6
f_{21}^*	$f_4 + f_8$	4611.07	5.2
f_{22}^*	$f_5 + f_8$	5051.84	2.3
f_{23}^*	$f_7 + f_8$	5059.37	5.9
f_{24}	$2f_8$	5620.73	1.8
f_{25}^*	$f_8 + f_{10}$	5628.26	2.9
f_{26}	$2f_{10}$	5635.79	1.0
f_{27}	$f_5 - f_4$	440.77	2.2
f_{28}^*	$f_5 - f_2$	448.16	2.4
f_{29}	$f_8 - f_5$	568.90	1.7
f_{30}	$f_8 - f_4$	1009.67	1.3
f_{31}	$f_8 - f_2$	1017.05	2.2
f_{32}^*	$f_8 - f_1$	1465.14	3.2
f_{33}	$f_3 + f_5 - f_8$	1227.91	1.4
f_{34}	$f_7 + f_8 - f_4$	3258.67	1.4
f_{35}	$f_1 + f_4 + f_5$	5387.40	1.5
f_{36}	$f_2 + 2f_4$	5394.71	1.2
f_{37}	$3f_4$	5402.10	1.0
f_{38}	$f_3 + f_4 + f_5$	5838.98	1.2
f_{39}	$f_3 + f_5 + f_7$	6287.28	0.9
f_{40}	$f_8 + 2f_4$	6411.76	0.9
f_{41}	$f_4 + f_5 + f_8$	6852.54	1.4
f_{42}	$f_3 + f_7 + f_8$	6856.18	0.8
f_{43}	$f_4 + f_7 + f_8$	6860.07	1.4
f_{44}	$2f_7 + f_8$	7308.38	1.1
f_{45}	$f_4 + 2f_8$	7421.43	1.2
f_{46}	$f_5 + 2f_{10}$	7877.26	1.0
f_{47}	$2f_2 + 2f_{10}$	6404.52	1.0
f_{48}	$3f_2 + f_3$	7176.74	1.3
Further signals			
ID	Frequency	Amplitude	Period/Comb.
f_{49}	1698.59 ± 0.07	3.6	588.73 ± 0.023
f_{50}	1712.80 ± 0.16	1.5	583.84 ± 0.053
f_{51}	3491.89	1.6	$f_{49} + f_2$
f_{52}	3495.39	1.0	$f_{49} + f_3$
f_{53}	3947.59	1.4	$f_{49} + f_7$
f_{54}	4516.48	1.0	$f_{49} + f_{10}$
f_{55}	1786.91 ± 0.09	2.5	559.62 ± 0.029
f_{56}	1794.60 ± 0.08	2.9	557.23 ± 0.025

amplitudes within a multiplet. We mainly list the resulting Θ for completeness: it would be $\Theta = 78^\circ \pm 3^\circ$, i.e. we would see the star almost equator-on.

4.1.4 *Frequency differences and ratios*

Asymptotic theory (e.g. Tassoul 1980) predicts that the pulsation periods of high-order g-modes, such as those excited in HS 0507+0434B, should be equally spaced. This is roughly true (allowing for other effects, e.g. mode trapping to operate), but Table 2 holds a number of surprises. The modes f_1, f_2 and f_5, and hence f_3, f_6 and f_4, f_7 are, within the errors of frequency determination, equally spaced in *frequency*. The combination peak at the corresponding frequency difference is also clearly detected.

The second interesting result from Table 2 concerns the frequency ratios of the 'fundamental' modes: the ratio of f_1/f_2 is 0.750132 ± 0.000018 and the frequency ratio f_2/f_5 amounts to 0.800060 ± 0.000011, i.e. the frequencies of these modes relate almost exactly as 3 : 4 : 5! In addition, the frequency ratio of f_7/f_8 is 0.800254 ± 0.000008, very close to 4 : 5 as well, but there is no frequency difference $f_7 - f_8$ within the detected combination peaks. We found a combination peak at $f_8 - f_5$, but the frequency ratio of the corresponding parent modes is 0.797543 ± 0.000008, which is not as close to the 3 : 4 and 4 : 5 ratios exhibited by the other modes.

Despite the close coincidence of these frequency ratios with integer-number ratios, they are still different from the exact values by several σ. However, we also bear in mind that the errors quoted in Table 2 assume white noise and are therefore likely to be underestimates. In particular, as we will argue in detail later, at least some of the fundamental modes appear to exhibit temporal frequency or amplitude variations, which increases our error estimates severely.

We checked whether it is justifiable to assume that exact integer-fraction frequency ratios are present. Using PERIOD98, we fixed the above-mentioned frequency ratios to exactly 3/4 or 4/5 and examined the quality of such a fit with the Bayes information criterion (e.g. see Handler et al. 2000, for a description) and by computing amplitude spectra of the residuals. Both tests strongly suggested that exact 3/4 or 4/5 frequency ratios (between any of the mode groups) are not an acceptable solution.

In any case, similar 'magic numbers' were found among the frequencies of other pulsating white dwarfs, e.g. the cool ZZ Ceti stars GD 154 (Robinson et al. 1978), G 191-16 (Vauclair et al. 1989) and BPM 31594 (O'Donoghue, Warner & Cropper 1992) or the pulsating DB white dwarf PG 1351+489 (Winget, Nather & Hill 1987), but their agreement with fractions of integers was much poorer than in the present case. The majority of pulsating white dwarfs do not show integer-fraction frequency ratios between their mode frequencies.

The explanation of these frequency ratios between the pulsation modes of HS 0507+0434B is not straightforward. We speculate that resonances could be involved; this could reproduce the observed frequency ratios (e.g. see Buchler, Goupil & Hansen 1997). However, to our knowledge, the possibility of 3 : 4 or 4 : 5 resonances in pulsating stars has not yet been explored, perhaps because the coupling is expected to be weak (Moskalik, private communication).

4.2 The meaning of the remaining signals

Having finished the discussion of the 10 fundamental frequencies, we will now try to explain the signals in the light curves of HS 0507+0434B listed at the bottom of Table 2.

The frequency f_{49} may correspond to a further independent mode. After pre-whitening of the 10 fundamental frequencies and their combinations, it is the highest peak in the residuals, and it is not explicable with a reasonable combination frequency. Furthermore, some of the highest peaks in the residual amplitude spectrum ($f_{51} - f_{54}$) can be explained by combinations of f_{49} and one of the 10 fundamental frequencies.

After pre-whitening of f_{49}, a peak separated by 14.22 ± 0.17 µHz (f_{50}) remains in the residuals. Assuming that our $\ell = 1$

identifications for $f_2 - f_{10}$ are correct, f_{49} cannot be $\ell = 1$, as it is too close to the $f_2 - f_4$ triplet. If f_{49} were part of an $\ell = 2$ quintuplet, then f_{50} could be explained as another rotationally split component of it: the separation between modes of $|\Delta m| = 2$ would be 12.5 μHz, which is consistent with the observed spacing as it could be blended with the 1 c/d alias of f_{49}.

The previous hypothesis does not, however, account for the number of peaks in the 3500-μHz region in the lowest panel of Fig. 5, assuming they are all combinations of f_{49} or f_{50} with $f_2 - f_4$. It is interesting to note that $\ell = 1$ pulsation modes around frequencies of 3500 μHz are frequently present in pulsating DA white dwarfs (Kleinman 1999). The power in this frequency region could therefore be due to such a mode, to combination frequencies or to a combination of both. We can therefore not determine whether the signals around 1700 μHz are combinations of such modes with $f_2 - f_4$ or represent independent modes.

We now turn to the signals at f_{55} and f_{56}, which are located in the same frequency domain as the modes $f_2 - f_4$. It is immediately obvious that they cannot be independent pulsation modes of $\ell = 1$ or 2, as their frequencies do not result in consistent multiplet structure. We suggest that these peaks are manifestations of amplitude and/or frequency variations of $f_2 - f_4$. f_{56} is unresolved from f_2 and f_{55} is unresolved from the 1-d alias of f_4; f_2 and f_4 are the strongest components of this multiplet. Regrettably, our data set is too small to investigate the temporal behaviour of the $f_2 - f_4$ multiplet in detail. Some support for this interpretation comes from the combination frequencies of $f_2 - f_4$, as signals suggestive of these temporal variations are also present in the corresponding frequency range.

Temporal variability of the pulsation spectra of cool ZZ Ceti stars is not uncommon; it is rather the rule than the exception (see Kleinman 1995), and it is consistent with theory (e.g. Wu & Goldreich 2001). Therefore, the presence of f_{55} and f_{56} does not lead us to doubt our mode identification. On a longer time-scale, however, the amplitudes of HS 0507+0434B seem remarkably stable compared with other cool ZZ Ceti stars: the results from the discovery observations (Jordan et al. 1998) and spectrophotometric light curves (Kotak & van Kerkwijk 2001), both obtained years apart from each other and from our measurements, seem to be adequately reproduced by our frequency solution. There is also no evidence for temporal variations of the $f_5 - f_7$ and $f_8 - f_{10}$ triplets.

4.3 Combination frequencies

Combination frequencies potentially contain a wealth of astrophysical information, which we are only just beginning to explore (e.g. see Wu 1998; Vuille 1999). As a further step in this direction, we will make a detailed comparison of our observations with the model by Wu (1998, 2001, hereinafter 'Wu's model').[1] This model is based on Brickhill's (1992) argument that the combination frequencies are generated by the surface convection zone as the eigenmodes pass through them (see Vuille 2000, for a summary). The combination frequencies are thus a manifestation of the distortion of the light curve generated by the convection zone, which means that a quantification of these distortions can be used to infer physical properties of the convection zone. These can, in turn, yield other constraints, such as the relative temperatures of ZZ Ceti stars over their instability strip. The form of some of the distortions also depends on the spherical degree ℓ and azimuthal order m of their parent modes, which holds the promise of achieving a mode identification for the parents by making use of their combinations.

HS 0507+0434B is ideally suited for the application of Wu's model. Owing to the triplet structures observed within the pulsation modes, assignments of ℓ, m are possible. This is a definite asset for combination frequency study, which we will take advantage of in what follows.

Wu's model provides analytical formulae, which bring the observable parameters in direct connection with the theoretical quantities to be inferred. It can therefore be immediately applied without the use of specific model calculations. However, the model is built on a perturbation analysis, which means it can only be used within certain limits of the pulsational amplitude of the star. Ising & Koester (2001) examined these limits by means of numerical model calculations and found that it is only valid for variations with photometric amplitudes smaller than approximately 4 per cent (a necessary but not sufficient condition). All the modes of HS 0507+0434B detected by us have amplitudes smaller than that.

In what follows, we will apply Wu's model step by step to assess its potential. We rewrite Wu's equations so that the results from the frequency analysis of the photometric data can be used directly as input. We restrict ourselves to the second-order combinations, which are the most numerous and have the best signal-to-noise ratio of all the combination frequencies.

4.3.1 *Convective thermal time* τ_c

This is the first parameter of Wu's model to be tested. It can be inferred from the amplitudes and frequencies of combinations where both the difference and sum frequencies are observed. We rewrite equation (21) from Wu (2001) as

$$\tau_c = \frac{1}{2\pi \left| f_i^2 - f_j^2 \right|} \sqrt{\frac{[r A_{i-j}(f_i + f_j)]^2 - [A_{i+j}(f_i - f_j)]^2}{A_{i+j}^2 - r^2 A_{i-j}^2}}, \quad (1)$$

where

$$r \equiv \frac{c(m_i, m_j)}{c(m_i, -m_j)},$$

where A_{i-j} is the amplitude of the difference frequency, A_{i+j} is the amplitude of the sum frequency, f_i and f_j are the frequencies of the parent modes, and values for $c(m_i, m_j)$, a constant depending on the values of the azimuthal order m of the parent modes, are listed in Table 3. The amplitudes can be given in any (consistent) units, but the frequencies need to be in Hz for τ_c to result in units of seconds.

The application of equation (1) requires a mode identification. This means we have to assume the three triplets are rotationally

Table 3. m-dependent constants for determining the amplitudes of a combination peak, adapted from Wu (2001). Θ is the inclination of the pulsational axis to the line of sight of the star. The results are for $\ell = 1$.

m_1	m_2	$c_{(m_i,m_j)}$
0	0	$0.65 + 0.45/\cos^2\Theta$
0	+1	0.65
0	−1	0.65
+1	+1	0.65
+1	−1	$0.65 + 0.90/\sin^2\Theta$
−1	−1	0.65

[1] We have also tested the model by Brassard, Fontaine & Wesemael (1995), but found it to underestimate the observed combination frequency amplitudes by more than an order of magnitude. We will therefore not discuss it further.

Table 4. Amplitude ratios and phase differences of the two-mode combinations relative to their parent modes. Signals indicated with an asterisk (∗) were used for determining τ_c, those marked with a diamond (◇) were utilized to determine $|2\beta + \gamma|$; their amplitudes are independent of the inclination angle Θ. Frequencies denoted with a plus sign (+) were also used to derive $|2\beta + \gamma|$, but their relative amplitudes depend on Θ. $A_{i\pm j}$ is the amplitude of the combination peak of the modes with frequencies f_i and f_j, and A_i and A_j are the corresponding amplitudes of the parents. Similarly, $\phi_{i\pm j}$ is the phase of the combination of modes f_i and f_j, and ϕ_i and ϕ_j are phases of the parents. f_{51} to f_{54} are only listed for completeness. Note, however, that their amplitude ratios are larger than those of the combinations of the other modes.

ID	$A_{i\pm j}/A_i A_j$ (mag)$^{-1}$	$\Delta\phi = \phi_{i\pm j} - (\phi_i \pm \phi_j)$ (rad)
$f_{11}{}^{*}$	6.9 ± 1.8	0.35 ± 0.26
$f_{12}{}^{*+}$	23.9 ± 1.0	-0.03 ± 0.04
$f_{13}{}^{*\diamond}$	9.6 ± 1.9	0.13 ± 0.20
$f_{14}{}^{*\diamond}$	5.9 ± 0.8	0.52 ± 0.14
$f_{15}{}^{*\diamond}$	4.8 ± 1.0	0.77 ± 0.21
f_{16}	17.2 ± 2.3	-0.35 ± 0.14
f_{17}	14.3 ± 1.0	0.39 ± 0.07
$f_{18}{}^{*}$	8.9 ± 1.3	0.12 ± 0.14
$f_{19}{}^{*+}$	14.8 ± 1.4	0.89 ± 0.10
$f_{20}{}^{*\diamond}$	6.6 ± 0.6	0.52 ± 0.09
f_{21}	13.1 ± 0.6	1.40 ± 0.05
$f_{22}{}^{*\diamond}$	6.9 ± 0.7	0.62 ± 0.10
f_{23}	20.8 ± 0.9	0.70 ± 0.04
$f_{24}{}^{*\diamond}$	3.1 ± 0.4	0.24 ± 0.13
$f_{25}{}^{*+}$	11.8 ± 1.0	0.54 ± 0.08
$f_{26}{}^{*\diamond}$	9.6 ± 2.2	0.10 ± 0.23
$f_{27}{}^{*+}$	9.4 ± 1.0	0.16 ± 0.11
f_{28}	10.9 ± 1.0	0.93 ± 0.09
f_{29}	5.0 ± 0.7	1.01 ± 0.14
$f_{30}{}^{*+}$	3.3 ± 0.6	0.78 ± 0.17
f_{31}	5.6 ± 0.6	2.33 ± 0.10
$f_{32}{}^{*}$	17.4 ± 1.3	1.23 ± 0.08
f_{51}	27.1 ± 4.3	2.67 ± 0.16
f_{52}	38.5 ± 9.2	-2.97 ± 0.24
f_{53}	32.0 ± 5.7	0.28 ± 0.18
f_{54}	26.2 ± 6.4	-0.01 ± 0.25

split m-components of $\ell = 1$ modes. Consequently, we used the five mode pairs f_4/f_5, f_2/f_8, f_4/f_8, f_5/f_8 and f_2/f_5 for which equation (1) can be applied. Whereas the combinations involving f_8 implied a range of $\Theta > 45°$ and $60 < \tau_c < 120$ s, the other two-mode pairs gave unphysical results. Thus we refrain from determining τ_c in this way.

An alternative possibility to determine τ_c uses the observed phase differences of the combination frequencies relative to those of the parent modes. We have therefore calculated these parameters from our observations for the second-order combinations; these are listed in Table 4 together with other parameters required later on.

We can now estimate τ_c using equation (15) of Wu (2001), for which we find the following form most practical:

$$\Delta\phi = \pi/2 - \arctan(2\pi(f_i \pm f_j)\tau_c), \qquad (2)$$

where the meaning of $\Delta\phi$ is given in the caption of Table 4, and the other parameters were explained previously (equation 1).

As some of the combination signals have more than one potential set of parent modes caused by degeneracy of their frequencies, we only used combinations that have unique parents or where one pair of parents strongly dominates possible others. Thus we only included combinations where the product of the amplitudes of one pair of parents exceeds that of all potential others by at least a factor of 4. These signals are indicated with an asterisk in Table 4. The application of equation (2) does not require a mode identification.

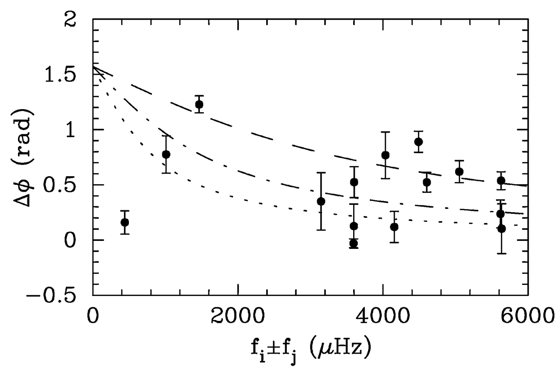

Figure 6. A comparison of the relative phases of the two-mode combination frequencies (filled circles with error bars) with theoretical predictions for different values of τ_c by means of equation (2). The dashed line is for $\tau_c = 50$ s, the dashed-dotted one for $\tau_c = 110$ s (best fit) and the dotted line for $\tau_c = 200$ s. Except for one outlier, the theoretically predicted trend is roughly followed, but an accurate determination of τ_c is not possible.

In Fig. 6, the measured values of $\Delta\phi$ are compared with the predictions of equation (2). Theory and observations are roughly consistent. A best fit to the observed phase differences results in $\tau_c \approx 110$ s, but every τ_c between 80 and 150 s seems to give an acceptable fit.

Within the framework of the same convection model, the condition $2\pi f_i \tau_c > 1$ needs to be fulfilled for pulsation modes to be driven (Goldreich & Wu 1999). The best-fit $\tau_c = 110$ s yields $2\pi f_1 \tau_c = 0.93$, which is marginally consistent with these stability considerations. It also becomes clear that reliable results for the difference frequencies are vital for determinations of τ_c.

Unfortunately, the low frequencies of difference signals makes their amplitudes and phases observationally harder to determine, as they are more affected by variations in sky transparency and extinction. The use of CCD detectors, such as in our case, helps in this respect, but does not fully eliminate this problem. From the theoretical point of view, Wu (2001) noted that the combinations of lowest frequency are also the least reliable, which may be caused by the assumption of a dynamically and thermally coherent convection zone breaking down. This may explain the discrepancies we have noted, but we conservatively do not reject certain measurements based on these arguments.

4.3.2 $|2\beta + \gamma|$ and inclination angle Θ

The parameter $|2\beta+\gamma|$ describes the response of the stellar material to the pulsations, and Θ is the inclination of the pulsational axis to the line of sight of the star, which is assumed to coincide with the stellar rotation axis.

To determine these parameters, we rewrite equation (20) of Wu (2001) as

$$c_{(m_i,m_j)}|2\beta + \gamma| = 1.086\frac{A_{i\pm j}}{A_i A_j}\frac{4\alpha_V\sqrt{1+(2\pi(f_i \pm f_j)\tau_c)^2}}{n_{ij}2\pi(f_i \pm f_j)\tau_c}, \qquad (3)$$

where $A_{i\pm j}$ is the amplitude of the combination peak at frequency $f_i \pm f_j$, A_i and A_j are the amplitudes of the parent modes, 1.086 is the scalefactor between magnitude and intensity variations, $c_{(m_i,m_j)}$

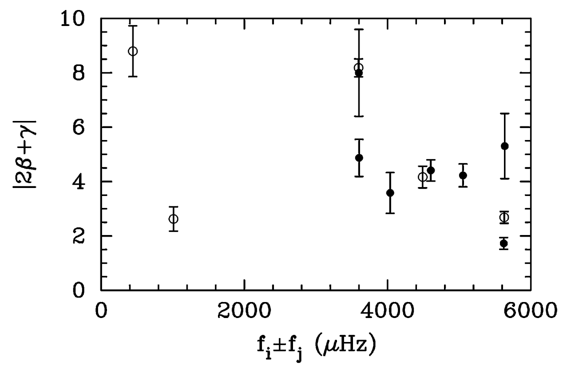

Figure 7. Values of $|2\beta + \gamma|$ from the relative amplitudes of the two-mode combinations (equation 3), assuming $\Theta = 80°$. Filled circles are for combinations where $c_{(m_i,m_j)}$ is independent of the inclination angle Θ; open circles denote Θ-dependent combinations.

was again taken from Table 3, n_{ij} is the number of possible permutations of i and j ($n_{ij} = 2$ if $i \neq j$, $n_{ij} = 1$ otherwise), theoretical values of $|2\beta + \gamma|$ are around 15 (see Wu (2001)), τ_c is again the convective thermal time and α_V is a scalefactor from bolometric luminosity variations to those in the observational passband (our data can be considered as being obtained in a 'wide V filter', which leads us to adopt $\alpha_V = 0.72$). The amplitudes used in equation (3) need to be in magnitudes, the frequencies are in units of Hz and τ_c is in seconds.

We can now constrain $|2\beta+\gamma|$. We start by applying equation (3) to the combinations marked with diamonds (Θ-independent $c_{(m_i,m_j)}$ values) and plus signs (Θ-dependent $c_{(m_i,m_j)}$ values) in Table 4. These combinations have, as previously, a unique or at least one dominant pair of parents, and we assign an m value to these parents by assuming all triplets are generated by rotationally split $\ell = 1$ modes.

The mean value of $|2\beta + \gamma|$ from the Θ-independent combinations is 4.6 ± 0.7, lower than predicted by theory. The Θ-dependent combinations show a mean $c_{(m_i,m_j)}$ $|2\beta + \gamma|$ of 8.3 ± 2.1. They are all combinations of parents identified with $(m_i, m_j) = +1, -1$. Assuming $|2\beta + \gamma| = 4.6$, we then obtain $\Theta > 48°$. We show the individual values of $|2\beta + \gamma|$ for $\Theta = 80°$ in Fig. 7.

4.3.3 *Theoretically predicted amplitude spectra*

We now check how well Wu's model can reproduce the amplitude spectrum of the second-order combination frequencies. We used our best frequency solution (Table 2), and took the frequencies, amplitudes and phases of all detected second-order combinations to create a synthetic light curve (hereinafter SLC), sampled in exactly the same way as the observational data, to which the model results were compared. This was done for clarity of presentation, as it disregards the observational noise. However, the basic results including noise are the same.

We then used Wu's model to predict the amplitudes and phases of the combination frequencies, varying the three free model parameters within reasonable limits ($80 < \tau_c < 150$ s, $5 < |2\beta + \gamma| < 25$ and $\epsilon < \Theta < \pi/2 - \epsilon$ for $\epsilon > 0$) and computed the amplitude spectra of these theoretical light curves. We did not compare the theoretically predicted parameters directly to those of the SLC as our data set has finite temporal resolution and gaps, which will cause some of the computed signals to interact either through their aliases or because some will not be resolved.

We attempted to find amplitude spectra that resembled that of the SLC closely. We computed a series of theoretical light curves varying the parameters in the intervals given above, calculated their amplitude spectra, subtracted those from the amplitude spectrum of the SLC and used the resulting residual scatter as a criterion for the adoption of a set of parameters. Values of $|2\beta + \gamma| = 10.0 \pm 1.5$, $80 < \tau_c < 110$ s and $\Theta = 80° \pm 2°$ resulted in the best representation of the SLC. Disregarding the combination frequency differences because of the reasons given at the end of Section 4.3.1 does not change the results significantly; best-fitting parameters would be $|2\beta + \gamma| = 11.3 \pm 1.0$, $80 < \tau_c < 110$ s and $\Theta = 79° \pm 1°$. We show the observed amplitude spectrum of the SLC and a theoretical one, which resembles it well in Fig. 8.

The left-hand panels of Fig. 8 show the overall amplitude spectra of the SLC and the theoretical second-order combination light curve. The global agreement is quite good. In the right-hand panels of

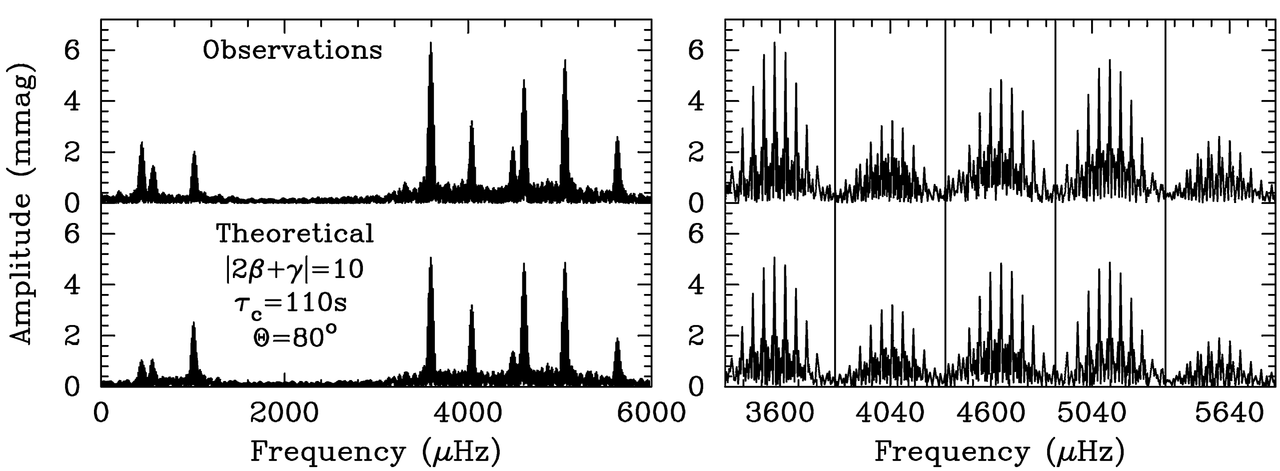

Figure 8. Upper half, the amplitude spectrum of the two-mode combinations in the SLC of HS 0507+0434B. Lower half, theoretical amplitude spectrum computed with Wu's model and the parameters given in the left half. The panels on the left-hand side show the predicted amplitude spectrum globally, whereas those on the right-hand side present zoom-ins on the five strongest sum frequencies.

Fig. 8 we show the dominant structures with better resolution. The intermultiplet structures also seem well reproduced.

4.3.4 Direct light-curve fitting

The previous comparison did not make full use of the phase information contained in the light curves and predicted by Wu's model. As a final test we therefore compared the SLC and the theoretically predicted combination light curve directly. We again computed theoretical light curves for a wide set of free parameters and evaluated the rms residual between the SLC and theoretical light curves as our criterion.

The result of this test was very similar to that of the previous one. The best fits were obtained with the following parameter values: $|2\beta + \gamma| = 9.7 \pm 1.0$, $80 < \tau_c < 110$ s and $\Theta = 79° \pm 1.5°$, and $|2\beta + \gamma| = 11.7 \pm 1.0$, $80 < \tau_c < 110$ s, $\Theta = 79° \pm 1.0°$ disregarding the frequency differences. These light-curve fits resembled the observations well, but not as well as our frequency solution.

We conclude from our applications of Wu's model that it is possible to obtain plausible values for the convective thermal time τ_c, but with large uncertainties. Our results for $|2\beta + \gamma|$ also appear reasonable, but the small values obtained in Section 4.3.2 suggest caution. The parameter that seems to be best constrained is the inclination angle Θ; its preferred values were around 80°. This is consistent with the Θ-determination from the relative amplitudes of the components of the three-mode triplets (Section 4.1.3).

We do not want to overemphasize this consistency, as we believe the results on the value of Θ from Section 4.1.3 and that of the application of Wu's model are not fully independent. Hence, we do not dare to base further interpretations on this result.

The results from Sections 4.3.1 and 4.3.2 are somewhat different from those of Sections 4.3.3 and 4.3.4. This may be caused by the stronger influence of the combination frequency differences on the general results in the first two investigations. We think that the outcome of Sections 4.3.3 and 4.3.4 is more meaningful as it is dominated by the best-determined frequency sums and because we have used more of the information in the observed light curve.

4.3.5 Application to $\ell = 2$ modes

Having shown that Wu's model yields consistent results under the assumption that all the triplet components detected in Section 3 are caused by modes of $\ell = 1$, we now examine whether we can reproduce the observations assuming the triplets are caused by $\ell = 2$ modes. To this end, we first computed $c_{(m_i,m_j)}$ for the $\ell = 2$ case, and we list them in Table 5.

We applied direct light-curve fitting (Section 4.3.4) as it uses most of the light-curve information and as its consistency has already been demonstrated. We performed the fits for all 28 possible m assignments to the triplet components for $\ell = 2$, and we did so with and without considering the combination frequency differences.

Our best fits were obtained for m values of $(-1, 0, 1)$ for all three triplets and the parameters $|2\beta + \gamma| = 3.1$, $\tau_c = 90$ s and $\Theta = 46°$, which produced residuals that were 3 per cent higher than that for the best fit with $\ell = 1$ combinations. Disregarding the difference frequencies, the best fits resulted from the same m assignments as above and $|2\beta + \gamma| = 3.5$, $\tau_c = 110$ s and $\Theta = 46°$. The corresponding residuals were 20 per cent higher than those for the best $\ell = 1$ solution. Only those fits with m assignments of either $(-1, 0, 1)$ or $(-2, 0, 2)$ gave nearly as good results as those for the $\ell = 1$ case.

However, the best-fitting values for $|2\beta + \gamma|$ are much smaller than predicted by theory and thus appear unreasonable. This is easy to understand (e.g. see Wu 2001) as $\ell = 2$ modes suffer a larger amount of geometrical cancellation (Dziembowski 1977), and thus the photometric amplitudes of their combinations are higher than those of the combinations of $\ell = 1$ modes.

Table 5. Same as Table 3, but for $\ell = 2$ modes.

m_1	m_2	$c_{(m_i,m_j)}$
2	2	-0.197
1	2	-0.197
0	2	$\frac{-3.939-0.592\cos(2\Theta)}{1+3\cos(2\Theta)}$
-1	2	$-0.197 + 1.871/\sin^2\Theta$
-2	2	$[4.457 - 1.772\cos(2\Theta) - 0.02465\cos(4\Theta)]/\sin^4\Theta$
1	1	$[0.369 - 0.0986\cos(2\Theta)]/\cos^2\Theta$
0	1	$\frac{1.674-0.592\cos(2\Theta)}{1+3\cos(2\Theta)}$
-1	1	$\frac{1.342+0.234\cos(2\Theta)+0.02465\cos(4\Theta)}{(\sin(\Theta)\cos(\Theta)^2}$
-2	1	$-0.197 + 1.871/\sin^2\Theta$
0	0	$\frac{33.584+10.042\cos(2\Theta)-0.8876\cos(4\Theta)}{[1+3\cos(2\Theta)]^2}$
-1	0	$\frac{1.674-0.592\cos(2\Theta)}{1+3\cos(2\Theta)}$
-2	0	$\frac{-3.939-0.592\cos(2\Theta)}{1+3\cos(2\Theta)}$
-1	-1	$[0.369 - 0.0986\cos(2\Theta)]/\cos^2\Theta$
-2	-1	-0.197
-2	-2	-0.197

The combination of the small $|2\beta + \gamma|$ values with the poorer fits that resulted despite the larger (by a factor of 28) number of possibilities for matches provided by possible $\ell = 2$ modes, leads us to suggest that the three triplets detected in Section 3 are indeed pulsation modes of $\ell = 1$.

As noted in Section 4.1.1, it may be possible that one or the other $\ell = 2$ mode disguised itself in a predominant $\ell = 1$ pattern, which cannot be confirmed or disproven by the analysis of the combination frequencies, but again we believe such an interpretation would be contrived.

4.3.6 Mode identification for f_1 by means of its combination frequencies?

Having obtained support for $\ell = 1$ for the three triplets, it is now tempting to try a mode identification for the singlet f_1. Unfortunately, only three two-mode combinations of f_1 are observed, which is less than expected considering its amplitude. Indeed, the light-curve fitting did not result in acceptable solutions for any m value, assuming f_1 was caused by an $\ell = 1$ mode; more combination signals than actually observed should be present.

We are left with the possibility that f_1 is caused by a mode of $\ell = 2$. Consequently, we computed $c_{(m_i,m_j)}$ constants for combinations of $\ell = 1$ and 2 modes, which we list in Table 6. The examination of this hypothesis with the direct light-curve fitting method yielded inconclusive results, although the solutions were generally better under the $\ell = 1$ assumption. This is not surprising as the $c_{(m_i,m_j)}$ coefficients in Table 6 are generally smaller than those in Table 3. A mode identification of f_1 by means of its combination frequencies is, however, not possible at this point.

5 SUMMARY AND CONCLUSIONS

We obtained 1 week of time-resolved CCD photometry of the cool ZZ Ceti star HS 0507+0434B. We were able to detect 10 'fundamental frequencies', 38 combinations of these, and eight more signals.

Table 6. Same as Table 3, but for modes where $\ell_1 = 1$ and $\ell_2 = 2$.

m_1	m_2	$c_{(m_i,m_j)}$
1	2	0.271
0	2	0.271
−1	2	$0.271 + 2.244/\sin^2\theta$
1	1	0.271
0	1	$0.271 + 0.561/\cos^2\theta$
−1	1	$0.271 + 1.122/\sin^2\theta$
1	0	$\frac{-1.973+0.814\cos(2\theta)}{1+3\cos(2\theta)}$
0	0	$\frac{4.760+0.814\cos(2\theta)}{1+3\cos(2\theta)}$
−1	0	$\frac{-1.973+0.814\cos(2\theta)}{1+3\cos(2\theta)}$
1	−1	$0.271 + 1.122/\sin^2\theta$
0	−1	$0.271 + 0.561/\cos^2\theta$
−1	−1	0.271
1	−2	$0.271 + 2.244/\sin^2\theta$
0	−2	0.271
−1	−2	0.271

This frequency solution explains the observed light variations satisfactorily. Even though light curves of multiperiodic variables, such as pulsating white dwarf stars, usually can only be deciphered with multisite observations, we believe that in this case we were fortunate enough to achieve just that.

The fundamental frequencies we detected consist of one singlet and three almost equally spaced triplets. The frequency spacings within the individual triplets are very similar, which leads us to suggest that they are caused by rotational m-mode splitting. This is the first clear detection of rotationally split triplets in a cool ZZ Ceti star. Assuming they are caused by $\ell = 1$ modes, we infer a rotation period of 1.70 ± 0.11 d for HS 0507+0434B.

The periods of the three triplets support the identification with $\ell = 1$ modes by comparison with other cool ZZ Ceti stars. The pulsational spectrum of the star determined by us is too poor for a detailed asteroseismological analysis.

We reported the curious detection that three of the basic four structures (one singlet, three triplets) are exactly equally spaced in frequency, not in period as predicted by asymptotic theory. In addition, these three structures show frequency ratios very close to (within 10^{-4}), but still significantly different from, 3 : 4 : 5. The fourth basic structure also shows a frequency ratio close to 4 : 5 with its neighbour. We speculate that resonances, perhaps together with mode trapping, are responsible for these frequency ratios.

Among the features in the pulsation spectrum of the star that could not be easily explained are two more signals, together with some of the combinations of one with other mode frequencies. These frequencies could correspond to components of an $\ell = 2$ multiplet. We have also found evidence for temporal amplitude and/or frequency variations of the longest-period 'fundamental' triplet.

We used the detected combination frequencies to test the predictions of Wu's (1998, 2001) model. We were able to arrive at a believable-looking estimate of the convective thermal time, but the result has large uncertainties. Our determination of the inclination angle Θ appears plausible. Theoretical predictions of the observed amplitude spectra of the combination signals were reasonably successful as were attempts to fit the observed light curves directly. They also supported the identification of the three triplets with $\ell = 1$.

We believe that the application of Wu's model is promising, but requires further testing. This could be done, for instance, using well-resolved WET data or by confrontation with numerical models such as those by Ising & Koester (2001), in particular, if the latter could be extended to multiperiodic pulsations. A comparison of the numerical computations with observations would then become very interesting.

ACKNOWLEDGMENTS

We are indebted to the referee, Yanqin Wu, for her insightful report on the manuscript that led to considerable improvements in this paper. GH thanks Noel Dolez for drawing his attention to this star, Steve Kawaler and Chris Koen for useful discussions and Scot Kleinman for supplying his LINCOM code that was essential for this analysis. The constructive and critical comments of Atsuko Nitta on an early draft version of this paper are appreciated. ERC would like to thank S. Potter, D. Romero and E. Colmenero for their support. MHM thanks D. E. Winget and A. Mukadam for useful discussions.

REFERENCES

Brassard P., Fontaine G., Wesemael F., Hansen C.J., 1992a, ApJS, 80, 369
Brassard P., Fontaine G., Wesemael F., Tassoul M., 1992b, ApJS, 81, 747
Brassard P., Fontaine G., Wesemael F., 1995, ApJS, 96, 545
Brickhill A.J., 1992, MNRAS, 259, 519
Buchler J.R., Goupil M.-J., Hansen C.J., 1997, A&A, 321, 159
Clemens J.C., 1994, PhD thesis. Univ. Texas
Dziembowski W.A., 1977, Acta Astron., 27, 203
Goldreich P., Wu Y., 1999, ApJ, 511, 904
Handler G. et al., 2000, MNRAS, 318, 511
Ising J., Koester D., 2001, A&A, 374, 116
Jordan S. et al., 1998, A&A, 330, 277
Kleinman S.J., 1995, PhD thesis. Univ. Texas
Kleinman S.J., 1999, ASP Conf. Ser. Vol. 169. Astron. Soc. Pac., San Francisco, p. 116
Kleinman S.J. et al., 1998, ApJ, 495, 424
Kotak R., van Kerkwijk M.H., 2001, in Provencal J.L., et al. eds, 12th European Conf. on White Dwarfs, p. 320
Montgomery M.H., O'Donoghue D., 1999, Delta Scuti Star Newsletter, 13, 28 Univ. Vienna
Nather R.E., Winget D.E., Clemens J.C., Hansen C.J., Hine B.P., 1990, ApJ, 361, 309
O'Donoghue D., 1995, Baltic Astron., 4, 519
O'Donoghue D., Warner B., Cropper M., 1992, MNRAS, 258, 415
Robinson E.L., Stover R.J., Nather R.E., McGraw J.T., 1978, ApJ, 220, 614
Schechter P.L., Mateo M., Saha A., 1993, PASP, 105, 1342
Sperl M., 1998, Master's thesis. Univ. Vienna
Tassoul M., 1980, ApJS, 43, 469
Vauclair G., Goupil M.J., Baglin A., Auvergne M., Chevreton M., 1989, A&A, 215, L7
Vuille F., 1999, PhD thesis. Univ. Cape Town
Vuille F., 2000, Baltic Astron., 9, 33
Winget D.E., Nather R.E., Hill J.A., 1987, ApJ, 316, 305
Winget D.E. et al., 1991, ApJ, 378, 326
Winget D.E. et al., 1994, ApJ, 430, 839
Wu Y., 1998, PhD thesis. California Institute of Technology
Wu Y., 2001, MNRAS, 323, 248
Wu Y., Goldreich P., 2001, ApJ, 546, 469

This paper has been typeset from a TEX/LATEX file prepared by the author.

6.5 A search for pulsations among low-mass DAO white dwarfs

Original paper:

G. Handler, 1998, A&A 339, 170

Astron. Astrophys. 339, 170–172 (1998)

ASTRONOMY AND ASTROPHYSICS

Research Note

A search for pulsations among low-mass DAO white dwarfs

G. Handler[⋆]

Institut für Astronomie, Universität Wien, Türkenschanzstrasse 17, A-1180 Wien, Austria

Received 29 June 1998 / Accepted 27 July 1998

Abstract. We performed a search for periodic light variations among low-mass DAO white dwarfs. These objects have theoretically been predicted to exhibit low-order g-mode pulsations due to a potent ϵ mechanism in hydrogen-burning shells according to model calculations of Charpinet et al. (1997).

No pulsations were detected in any of our nine candidate stars. This can be attributed to the very narrow instability strip predicted or to the fact that pulsationally unstable modes are not necessarily excited, a common phenomenon among pulsating stars. It may also be the case that hydrogen-burning shells in the stars are too small to drive pulsations or not present.

Key words: white dwarfs – stars: oscillations

1. Introduction

Pulsational driving via nuclear burning (the ϵ-mechanism) has been suspected to be present in a number of different classes of star. Some examples are Wolf-Rayet stars (Maeder 1985), where the driving region is located in the stellar core, or hot central stars of Planetary Nebulae and hot white dwarfs with hydrogen surface layers (Kawaler et al. 1986, Kawaler 1988), whose pulsations are to be powered by nuclear-burning shell sources.

For the latter objects Kawaler (1988) theoretically predicted pulsationally unstable nonradial g-modes under the condition that the stars still contain an active hydrogen-burning shell. Hine (1988) carried out an extensive optical search for such pulsators and did not find any. Kawaler (1988) suggested that this may be due to a fundamental problem in the standard hydrogen-burning models of central stars of Planetary Nebulae. In any case, no class of star whose pulsations are driven by the ϵ mechanism has been observationally detected yet.

Recently, Charpinet et al. (1997) discovered a potent ϵ mechanism operating in their models of post-extreme horizontal branch stars with active hydrogen-burning shells. They predicted luminosity variations with periods in the range 40–125 s in low-mass DAO white dwarfs, suggested to search for such pulsations in these objects and particularly recommended six objects which seem to be the most promising candidates.

In an effort to discover pulsations in low-mass DAO white dwarfs, we photometrically observed five of the stars recommended by Charpinet et al. (1997) plus four further DAO white dwarfs (partly of presently unknown mass). The results of this survey are reported below.

2. Observations, reductions and analysis

Time-series photometric measurements of our targets were acquired during two observing runs at McDonald Observatory, Fort Davis, Texas. Both the 2.1m and 0.9m telescopes were used together with a standard two-channel photoelectric photometer. Continuous integrations on the target star and a comparison star in the field were obtained, only interrupted by sky measurements. No filter was used to maximize the number of photons counted.

Reductions were started with sky subtraction using a piecewise linear or spline fit to our background measurements. Then the data were corrected for extinction. The mean magnitude of each run was set to zero. Remaining long-period variations in the data were removed by low-order polynomial fits, since we were only interested in variations occurring on time scales of 10 minutes and less. Finally, the HJD of each observation was calculated.

These reduced data were subjected to frequency analysis using a modified version of the program PERIOD (Breger 1990). Amplitude spectra of each run were calculated out to the Nyquist frequency of the respective data set, and are shown in Fig. 1 together with some further information.

3. Interpretation of results

We did not detect any coherent periodic variations in the light curves of any of our targets. The detection levels we achieved are generally between 0.7 and 1.5 mmag for each star except for PG 0134+181, where it is about 5 mmag. This star should be re-observed, but its faintness (V=16.12 mag) requires a long run on a fairly large telescope. Ton 353 is the only object suggested to be observed (Charpinet et al. 1997), where we could not acquire

Send offprint requests to: gerald@dsn.astro.univie.ac.at

⋆ Visiting Astronomer, The University of Texas and McDonald Observatory

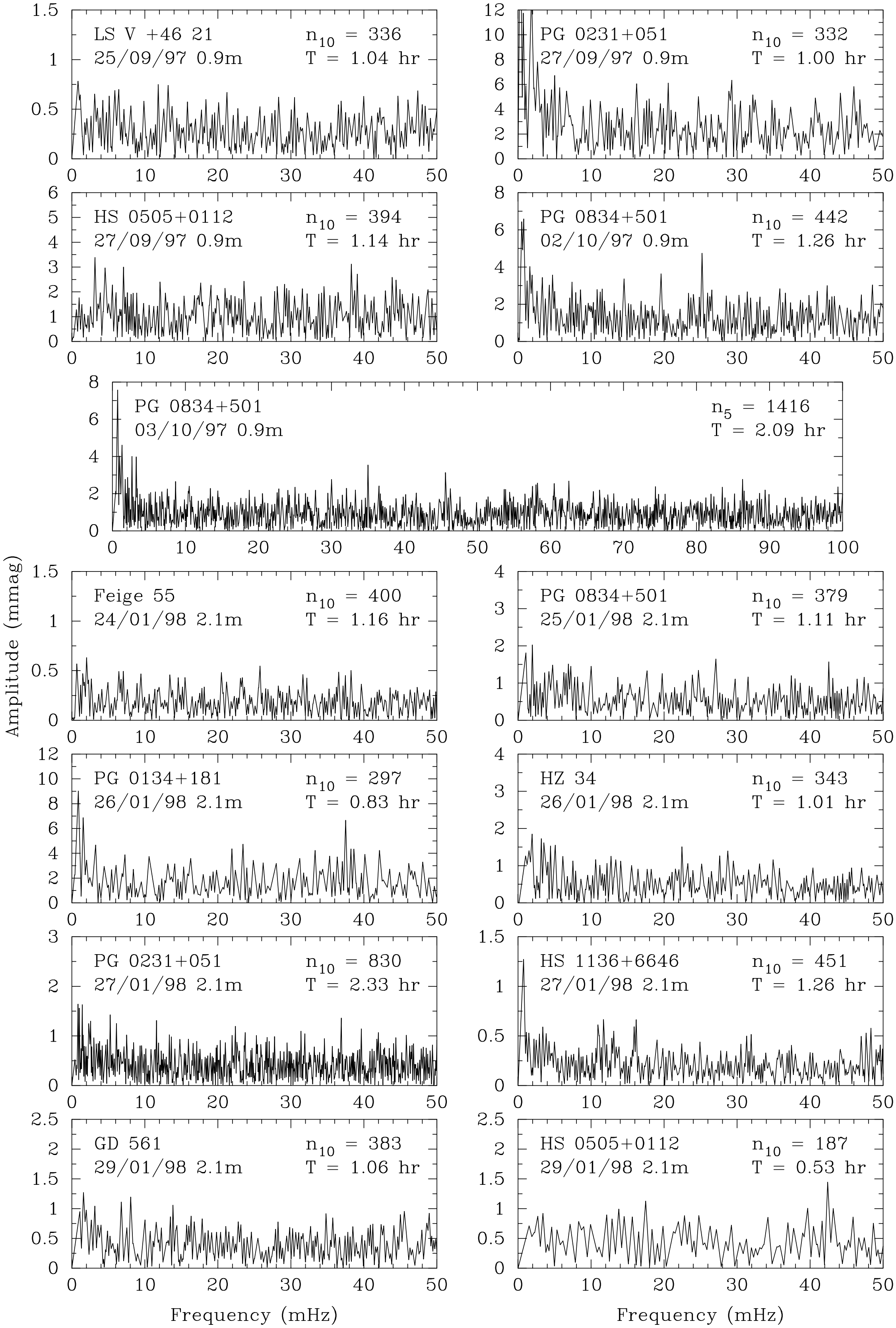

Fig. 1. Amplitude spectra for all our runs in chronological order. They are calculated out to the corresponding Nyquist frequency. The latter is usually 50 mHz, except for the October 3, 1997 observations of PG 0834+501, where it is 100 mHz. Informations about the targets, the telescope, the number of k-second integrations (n_k) on the stars themselves and about the run lengths (T) are also given.

any data. This faint, southern object should be examined for light variations as well.

The only star where one could suspect periodic light variations in the frequency region of interest is PG 0834+501, whose amplitude spectrum of the first run showed some higher peaks. There are also higher peaks in the amplitude spectrum of the second run, but at different frequencies. A combined analysis of both runs (which were taken in consecutive nights) does not show any significant peak. The third run taken on the 2.1m telescope confirms this conclusion.

We can think of three possible explanations of this absence of observed pulsations. First, the instability strip determined by Charpinet et al. (1997) is very narrow. It may simply be the case that all our target stars do not fall into the predicted instability region and hence cannot pulsate. Second, it is a well-known fact that not all stars inside a given instability strip are necessarily pulsators; only a small number of promising objects was available. Mode-selection mechanisms may be at work or our noise levels were too high that we would be able to detect the light variations.

Third, and astrophysically most interesting, it is possible that the evolutionary history of the models used by Charpinet et al. (1997) is different from that of the real stars. The hydrogen layer masses of the progenitors may be too small for a driving region being efficient enough to generate pulsational instabilities. Furthermore, no model is perfect. As an example, stellar winds which may be present in the stars might be sufficient to remove enough hydrogen that a driving region cannot develop.

To conclude, still no class of pulsating star definitely being driven by an ϵ mechanism is known. Pulsating low-mass DAO white dwarfs may exist, but the number of promising objects is still small. Spectroscopic observations will reveal further candidates to be examined for pulsational light variations. This will both increase the chances to find pulsators and contribute to a better understanding of this phase of stellar evolution, even if no variables are found.

Acknowledgements. This research was partially supported by the Austrian Fonds zur Förderung der wissenschaftlichen Forschung under grant No. S-7304. The author thanks Stefan Dreizler for background informations about objects of interest for this study discovered by the Hamburg-Schmidt survey.

References

Breger, M., 1990, Communications in Asteroseismology No. 20 (University of Vienna)

Charpinet, S., Fontaine, G., Brassard, P., Dorman, B., 1997, ApJ 489, L149

Hine, B. P., 1989, PhD thesis, The University of Texas

Kawaler, S. D., 1988, ApJ 334, 220

Kawaler, S. D., Winget, D. E., Hansen, C. J., Iben, I., 1986, ApJ 306, L41

Maeder, A., 1985, A&A 147, 300

Bibliography

Asplund M., Grevesse N., Sauval A. J., Allende Prieto C., Kiselman D., 2004, A&A 417, 751
Baglin A., 2003, Advances in Space Research, 31, 345
Baker N., Kippenhahn R.: 1962, Zeitschrift für Astrophysik 54, 114
Balona L. A., 2000, MNRAS 319, 606
Breger M., Huang L., Jiang Sh.-Y., Guo Z.-H., Antonello E., Mantegazza L., 1987, A&A 175, 117
Breger M. et al. 1998, A&A 331, 271
Breger M. et al. 2004, A&A 419, 695
Christensen-Dalsgaard J., 2002, Rev. Mod. Phys. 74, 1073
Cox J. P. 1980, Theory of Stellar Pulsation (Princeton: Princeton University Press)
Dziembowski W. A., 1977, Acta Astr. 27, 203
Handler G., 1994, Master's Thesis, University of Vienna
Handler G., et al., 2000, MNRAS 318, 511
Hatzes A. P., 1998, MNRAS 299, 403
Henry G. W., Fekel F. C., Kaye A. B., Kaul A., 2001, AJ 122, 3383
Henry G. W., Fekel F. C., 2003, AJ 126, 3058
Henry G. W., Fekel F. C., Henry S. M., 2005, AJ 129, 2815
Henry G. W., Fekel F. C., Henry S. M., 2007, AJ, in press
de Jager C., 1963, Bull. Astr. Inst. Netherlands 17, 1
Kazarovets E. V., Kireeva N. N., Samus N. N., Durlevich O. V., 2003, IBVS 5422
Kurtz D. W., 1982, MNRAS 200, 807
Ledoux P., 1951, ApJ 114, 373
Nather, R. E., Winget, D. E., Clemens, J. C., Hansen, C. J., Hine, B. P., 1990, ApJ 361, 309
Nitta A., et al., 2007, Comm. Asteroseismology Vol. 150, in press
Paunzen E., 2003, Habilitationsschrift, University of Vienna
Tassoul M., 1980, ApJS 43, 469
Unno W., Osaki Y., Ando H., Saio H., Shibahashi H., 1989, Nonradial Oscillations of Stars, University of Tokyo press, 2nd edition
Walker G. et al., 2003, PASP 115, 1023
Winget D. E. et al., 1991, ApJ 378, 326
Winget D. E. et al., 1994, ApJ 430, 839